NASA SP-492

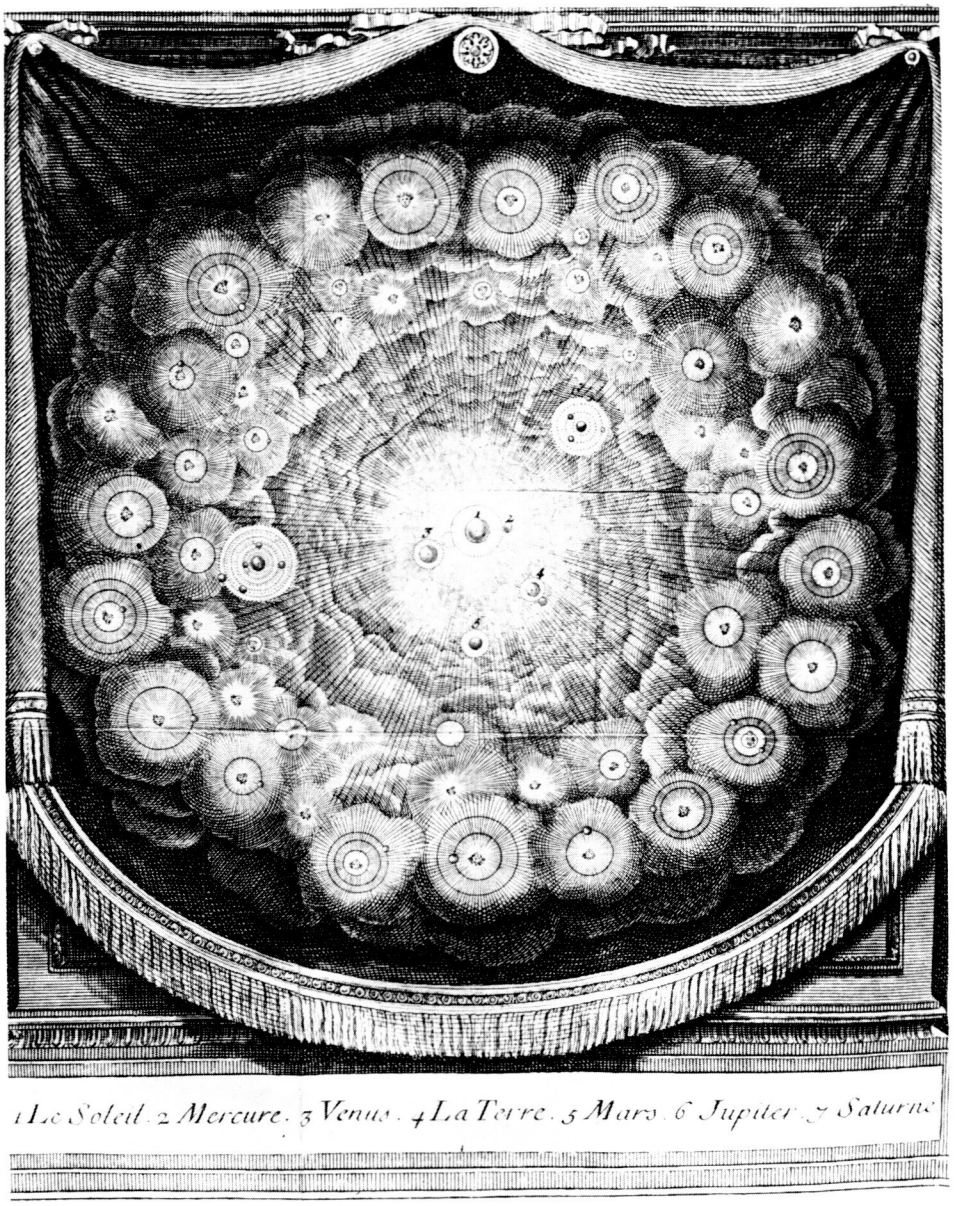
THE M-TYPE STARS

MONOGRAPH SERIES ON NONTHERMAL PHENOMENA
IN STELLAR ATMOSPHERES



NASA

THE M-TYPE STARS



. . . Assurons-nous bien du fait, avant que de nous inquiéter de la cause. Il est vrai que cette méthode est bien lente pour la plupart des gens, qui courent naturellement à la cause, et passent par dessus la vérité du fait; mais enfin nous éviterons le ridicule d'avoir trouvé la cause de ce qui n'est point.

. . .

. . .

. . . De grands physiciens ont fort bien trouvé pourquoi les lieux souterrains sont chauds en hiver, et froids en été; de plus grands physiciens ont trouvé depuis peu que cela n'était pas.

–Fontenelle, Histoire des Oracles
Chapitre IV, pp. 20 et 23

ORIGINAL PAGE IS
OF POOR QUALITY

NASA SP-492

MONOGRAPH SERIES ON NONTHERMAL PHENOMENA
IN STELLAR ATMOSPHERES

THE M-TYPE STARS

Hollis R. Johnson
Francois R. Querci

Stuart Jordan, Solar Physics
Editor/Organizer and American Coordinator

Richard Thomas, Stellar/Solar
Editor/Organizer and European Coordinator

Leo Goldberg
Senior Adviser to NASA

Jean-Claude Pecker
Senior Adviser to CNRS



Centre National de la
Recherche Scientifique
Paris, France

1986

National Aeronautics and
Space Administration
Scientific and Technical
Information Branch
Washington, D.C.

Library of Congress Cataloging-in-Publication Data

The M-type stars.

(Monograph series on nonthermal phenomena in stellar atmospheres) (NASA SP-492)
Includes index.
1. M stars. I. Johnson, Hollis R. (Hollis Ralph), 1928-
II. Querci, François R. III. Centre national de la recherche scientifique (France) IV. Series. V. Series: NASA SP ; 492.
QB843.M16M89 1987 523.8'7 87-11340

For sale by the Superintendent of Documents, U.S. Government Printing Office, Washington, DC 20402

DEDICATION

in grateful appreciation
we dedicate this series and these volumes

to *Cecilia Payne-Gaposchkin*, who, with Sergei, set the spirit of empirical-theoretical atmospheric modeling by observing:

> "All true variable stars have variable atmospheres, but a variable atmosphere is probably the property of all stars, whether obviously variable in brightness or not [as witness the solar envelope]";

and who, by her intimate knowledge of particular stars, pioneered in the recognition of the fundamental importance of "individuality of stellar atmospheric characteristics."

to *Daniel Chalonge*, who sought, by ingenious meticulous observations, to make quantitative the features of qualitative classical taxonomy, thereby laying the foundations of showing the inadequacy of its two-dimensional, single-region atmospheric, character;

and who always opposed the spirit of a distinguished theoretical colleague's remark:

> "Don't show me those new observations of yours; they inhibit the range of my speculations."

PERSPECTIVE

Publication of Volume 4 (December 1983) marked the halfway point for the projected eight volumes sponsored by NASA and CNRS in our series of monographs on nonthermal phenomena in, and structures of, stellar atmospheres. The interlude of nearly 3 years between the publication of that volume and of the present Volume 5 arose from a variety of circumstances beyond our control, but the delay and its causes make appropriate a restatement of a Perspective on the series and its objectives. We divide it into three parts: a science perspective on the series as a whole, a science perspective on this particular M-star volume, and an organizational perspective on the series. We introduced each of the first four volumes by a short, general, continuing sequential preface to put the volume into perspective relative to the preseries environment. In each of the remaining four volumes, we begin with a Perspective on the contribution of that volume to the currently evolving pictures of stellar atmospheres—to which these volumes seem to be contributing, judging by their reviews. We stress not only the evolution of stellar atmospheric modeling, but also its relation to the thermodynamic character, and eventual modeling, of the whole star. We also try to draw on the perspective gained from editing the entire series, to suggest to editors/authors of a particular volume those questions/problems which we hope that the volume, focusing on only a few stellar types, might clarify. But we emphasize that we can hardly dictate their response in this observationally centered monograph series. Hopefully, our authors know better than anyone else what the data demand and where their present incompleteness leaves ambiguity. But we have found the interaction stimulating and educational. The reader can judge its productivity.

SCIENCE PERSPECTIVE ON THE SERIES

The combination of eclipse, coronagraphic, high-resolution limb, and rocket-borne studies of the Sun during the 1940's through the 1960's made unambiguously clear for the Sun what a century of studies of various kinds of peculiar stars—including the Sun—had implied for all these stars called peculiar. While the great majority of stars appeared to have atmospheres dominated by quasi-thermal photospheric phenomena and structure, when studied by only low-resolution disk spectra, there were strong exceptions. Since the 1860's, the Be stars had joined the Sun in revealing the existence of outer atmospheres many radii in extent. The Wolf Rayet stars had exhibited the same, together with evidence for a dynamic mass outflow which could provide both that atmospheric extent and an aerodynamic energy dissipation to produce the superionization observed in their spectra. Successively, as observations improved over the years, these particular types of peculiar stars had been joined by others, enlarging the observed classes of stars showing extended, nonradiatively heated atmospheres with mass outflow—phenomena all contrary to accepted stellar atmospheric theory.

PRECEDING PAGE BLANK NOT FILMED PAGE VI INTENTIONALLY BLANK

The classical, speculative theoretical, thin, static, quasi-equilibrium model of a stellar atmosphere was, historically, far from reality for such peculiar stars generally. Just how to modify the theory to include such peculiarity was, however, uncertain. In the 1940–1960's, this increasing variety of solar data exhibited in detail precisely what were the speculative theoretical misconceptions for at least that star—which is peculiar essentially because of its proximity. These data showed grossly that the Sun is not a closed thermodynamic system (i.e., one with no mass outflow), nor has it a radiatively controlled, thermal outer atmosphere. All these now broadly observed thermodynamic properties are forbidden by the then-current speculative theoretical models. Therefore, obviously, theory must be modified to permit at least some stars to be open—as opposed to closed—thermodynamic systems, with nonthermal energy modes. The central question is whether all or only some (e.g., the peculiar) stars are to be allowed this freedom, and is such freedom the mark of peculiarity? We needed more observational detail on a variety of stars, both normal and peculiar. Obviously, empiricism, not speculation, must guide the reformation of theory, thus returning the function of theory to its historic, pragmatic role: first, to represent real-world observations, and second, to "explain" the phenomena.

The Sun is peculiar because its proximity allows detection of small-amplitude phenomena that are unobservable in more distant stars. For these phenomena to be seen in other stars, with comparable instruments, their amplitudes must be much larger. The basic question was/is whether stellar "peculiarity" represents exceptional phenomena not common to all stars or simply exceptionally large amplitudes of common phenomena that are anomalous only in the magnitude of their departure from the predictions of classical theory. Indeed, more modern observations with more sensitive detectors and covering different spectral regions increasingly showed the Sun's community of anomaly with more strikingly peculiar stars. The simple common anomaly of the 1860's was greatly extended atmospheres, that of the 1940's was nonradiative heating, and that of the 1950–1960's was aerodynamic mass loss: all these features, found first in the stars and then detailed in the Sun, have enlarged observationally to include even finer details. Such empirical orientation and guidance, impossible to obtain under only low-resolution visual spectral study, stands out under the high-resolution, time-resolved, panspectral capability of modern ground plus spatial facilities. So in asking how general are such small-amplitude solar anomalies and large-amplitude stellar peculiarities, one can only be guided by increasingly refined systematic observations, not simply by speculation from a few "snapshot observations."

Thus, for a normal star—as the Sun would be classified at normal stellar distances—the required *observational, not speculative*, details are not only those on such gross nonthermal phenomena as strictly radial pulsation and catastrophic or nova-like mass ejection. They also include the observed small-amplitude photospheric motions, the not-always small-sized inhomogeneities and the sometimes associated magnetic fields—both small and large. All these are symptomatic of nonthermal phenomena, which amplify nonlinearly in the upper stellar atmosphere to produce that anomalous exophotospheric structure that so strongly contrasts with the predictions of classical thermal theory: a sequence of thermodynamically distinct regions instead of the only single-region quasi-thermal upper photosphere.

In principle, it is those almost inconspicuous photospheric anomalies in a quasi-thermal photosphere—not a pulsating or nova-ejected photosphere—that demand the most widespread change in "theory." Quasi-thermal, pulsating, or ejected photospheres alike demand a basic change in the thermodynamics postulated in classical atmospheric modeling. "Peculiar" stars may demand more extensive varieties of change from classical modeling, but there are simply

many more stars having quasi-thermal, rather than blatantly nonthermal, photospheres. Therefore, any changes required in normal star modeling are felt more sweepingly. They cannot be simply dismissed as "peculiar"—star or phase of stellar evolution.

To understand the thermodynamics of such quasi-thermal photospheres and the regional exophotosphere they produce, we must delineate the details of structure of, and phenomena in, those photospheres which are *only quasi*-thermal, not fully nonthermal. Then we ask what kind of subatmospheric structure—and its thermodynamic state—can produce the quasi-thermal photosphere. But we recognize that we are able to observe directly only these *atmospheric* phenomena and structures. A knowledge of subatmospheric and deep interior structure and thermodynamic state can come only by inward, theoretical extrapolation from surface conditions. As evidenced by the inability of existing theory to predict atmospheric structure, one had/has little confidence in its completeness. So we recognize that it, also, must be modified, in parallel with our observational modification of the picture of a real-star atmosphere. It is too often not understood that an observed anomalous atmospheric structure implies an erroneous thermodynamic basis for that theory of the subatmosphere and interior relative to whose atmospheric predictions the observations are anomalous. *So while we can observe only the atmosphere, and thus obtain empirical guidance in making a theory for its modeling, it is not only atmospheric theory which needs reexamination/modification*, and in this aspect, we have no direct empirical guidance. But we do recognize that demands for such expanded theory focus more on a broadened basic thermodynamics—nonlinear, nonequilibrium thermo*dynamics*—than on studies of linearized nonequilibrium thermo*statics*, programmed in endless arithmetic, but not thermodynamic, detail. And these nonlinear effects are most evident in the boundary and, hence, observable regions. Therefore, we have indirect methods to study interior conditions—a focus on nonlinear effects toward the boundary. We study the quasi-thermal photospheric regions directly by studying linear effects there, and we probe the subphotosphere by studying the breakdown of linearity in the upper photosphere.

The need for thermodynamic/aerodynamic rather than thermostatic studies in stellar atmospheres had been put into perspective by a decade of Workshops, jointly between aerodynamicists and astronomers, extending the theme of the previous decade's focus on such phenomena in the interstellar medium. Topics discussed, initiated by expanded observations, had ranged from solar atmospheric oscillations to stellar pulsations, from the solar wind to low-velocity mass loss from M giants, from adiabatic mixing-length modeling of convection to radiation-dominated gas dynamics, from spectroscopic diagnostics based on "astrophysical turbulence" to those focused on systematic mass motions, ranging from pulsation to simple outflow.

The 1972 Goddard Space Flight Center (GSFC) conference on stellar chromospheres put into clear perspective the realization that leadership in delineating the variety of extended, nonthermal, exophotospheric structure of stellar atmospheres generally—not simply of peculiar stars—would not come from then-accepted theory. The same realization applied to phenomena of mass outflow and nonradiative heating. What theory had been developed to try to represent the existence of chromospheres/coronae and of mass outflows called "winds" focused on solar-like stars alone. Similar phenomena of atmospheric extent and mass outflow in much hotter stars were treated as something completely different from the solar case. In each of the two extremes—cool stars and hot stars—interest focused on exceptional circumstances.

For cool stars, a convective instability was assumed to produce acoustic waves, which dissipate to produce chromospheres/coronae, thence the hot wind by thermal expansion of the hot corona. Winds in hot stars were/are assumed to produce cool winds by a radiation-pressure origin and acceleration. The super-hot Wolf Rayet stars were dismissed as simply too peculiar to warrant discussion by theoreticians. The 1976 reunion on the less hot Be stars reaffirmed that their conjectured, equatorial only mass outflow to produce the observed subionized exophotospheric envelope is caused by rotational instability. Cyclically occurring symposia on planetary nebulae reiterated that these cool distant envelopes—long ago regarded as extreme examples of Be envelopes by McLaughlin—were the last gasp of late-stage stellar evolution, a one-time mass ejection that prevented the star from becoming a supernova. The various kinds of mass outbursts from the variety of nova-like objects were conjectured to originate in a mass transfer in close binaries, one of which is degenerate. All this was dogma imposed by the inadequate speculative theory of the early and mid-1970's. The spatial observations of the 1960–1970's showed how profoundly fact contradicted theory. The solar-wind velocity varies and at times greatly exceeds thermal theoretical values. Hot-star winds were as hot as the solar. All B stars, not just Be, have mass outflow; the distinguishing characteristic of Be-star winds is their variability, not their existence. Presently existing mass-outflow patterns in Be and planetary-nebular stars show close resemblance. Wolf Rayet stars are not unique in the existence of mass outflow or superionization but in size of mass loss, that size ensuring that their photospheres are nowhere quasi-thermal.

The spatial observations of the 1960–1970's gradually demonstrated the pervasiveness of extended multiregional, nonradiatively heated, mass-outflowing exophotospheric atmospheric structure. The earliest spatial observations—from rockets, hence observing only the brightest stars—had echoed the Wolf Rayet paradigm: superionized, superthermal, and superescape mass outflow from hot supergiants. But many features of supergiants had long relegated them to quasi-peculiar status.

Probably the most abruptly shocking result was the observation of mass outflow in superionized lines at superescape velocities in what had been a standard reference star in classical thermal atmospheric modeling: τ Sco, a normal B0 main-sequence star. This observation, via the Copernicus satellite, was followed rapidly by similar identifications of mass outflow in superionized spectral lines across the HR plane. So apparently those gross thermodynamic features of many peculiar stars, including the Sun—which demand the removal from stellar theory of the conditions of being closed thermal systems—were more prevalent than generally admitted among even normal stars. Nonradiative heating and nonthermal mass loss were apparently prevalent across the HR plane. But "theoretical" modeling remained peculiar to each stellar type, its own peculiarity in understanding why classical theory failed. The "solar/stellar connection" referred only to the similarity between the Sun and cool stars later than about spectral type F. And one would understand models of such stars by studying how the Sun predicted stars to be, not by studying the stars to delineate phenomena not exhibited by the Sun (e.g., the cool exocoronal envelope exhibited by Be, T Tauri, and an increasing number of other varieties of peculiar stars). Stellar peculiarity as a key to understanding the breadth of stellar atmospheric structure was still suspect unless it were that variety of peculiarity exhibited by the Sun.

Again, after spatial observations of all stars just as before them, when only peculiar stars were considered anomalous relative to theory, it was clear that revision of modeling

theory would not come from simply "bending" current theory by its practitioners, not even solar-stimulated modified theory. Only much more data—high resolution, panspectral, time-sequenced—could stimulate the search for unifying features and, hence, empirical theory all across the HR plane. Fortunately, at this epoch, the IUE was on the threshold, and many observing astronomers were poised to exploit it on the basis of the tantalizing rocket observations on the one hand, Copernicus results on the other, and many years of accumulated visual/spectral data that emphasized discord and anomaly with classical speculative theoretical models. We had no great problem convincing NASA—with much thanks to GSFC's Scientific Directorate (George Pieper, Jack Brandt) and Headquarters support (Harold Glaser; later, Dave Bohlin and Ed Weiler)—of the utility of assembling the best modern ground-based, space-based, visual, far-infrared, radio, and far-ultraviolet data in a series of monographs, and then comparing these data to the results of current theoretical prediction. Hopefully, such comparison would both put into focus just how large is the discrepancy between speculative and real worlds and suggest how theory might be modified. Even more important, there should be a continuous process of data compilation, then preliminary examination to assess its adequacy, and the institution of new observational programs to fill in the gaps—preparatory to next-approximation assessment of how to construct better theory—or at least empirical/theoretical modeling algorithms. Clearly, such an effort should not be parochial, and clearly, the European-U.S.A. collaboration on IUE had been a major factor in its fruition. The French CNRS agreed to cosponsor with NASA some volumes in our proposed monograph series. Their focus was to be precisely as stated: a critical compilation of the best and most modern observations over as broad a spectral region as possible from the X ray to the radio. All these observations were to be encradled in the century-long accumulation of data on stellar "normality and peculiarity," inspired by the solar/stellar connection, asking if the stellar/solar were not the most productive future orientation.

The first four monographs have appeared and have been reviewed. Readers can judge for themselves the project's present success in terms of its objectives. We first make a few comments on the overall situation, as it seems to us, mainly to place future work in perspective. We do not comment on the remaining four volumes only, but also on future observational programs and the state of "theory" capable of representing the data. Then we try to place the present M-star volume into this same perspective.

Overall, we recognize progress in clarifying three gross questions in this program of exploring nonthermal, nonlinearly nonequilibrium phenomena and structures of stellar atmospheres: first, the generality of the historic atmospheric three-fold peculiarity; second, the adequacy of the Sun in exhibiting the full range of exophotospheric structures among stars having quasi-thermal photospheres; third, the relation between stars with, and those without, quasi-thermal photospheres.

First, there is finally a general recognition of the ubiquitous character of the historically outstanding features characterizing some bright peculiar stars, including the Sun: extended exophotospheres, nonradiative heating, mass outflow. Thermodynamically, these are all related: given a mass outflow (i.e., an open system, gravitationally bound) the others follow. This thermodynamic generalization, however, is not yet generally accepted. However, observationally, all three features seem generally present to some degree in all stars. The literature is full of debates on whether all stars can be considered to have chromospheres/coronae, but such controversy is essentially semantics. To many, a chromosphere/corona must have the solar range of T_e to be such. To insist on some stellar exophotospheric regions being

solar-identical before calling them chromosphere/corona simply confuses community of thermodynamic class with identical thermodynamic state. The same remarks hold on the practice of considering mass outflow from hot stars as "cool winds" because "theory" places their origin in radiative acceleration, while "hot solar-type winds" originate, again in theory, via a thermal expansion of a corona. Both "types" of wind are observed to be superthermal, superescape, and superionized, but sometimes in some stars, *all* these wind characteristics hold only in *some* exophotospheric regions. This distinction, not differences in thermal state, implies an atmospheric structural pattern differing from the solar and one that cannot be studied empirically from an observational focus on solar-type stars alone.

Second, therefore, the monographs thus far have demonstrated that the full range of exophotospheric regional structure in stars with quasi-thermal photospheres is indeed not exhibited by study of only the cool-star part of the solar/stellar connection. At least one variety of such atmospheres was brought into focus via the Be stars, but seems common to many other stellar types once called peculiar. These include the T Tauri and symbiotic stars, both to be summarized in detail in forthcoming volumes. These stars have in common postcoronal regions in which the mass outflow seems to be decelerated and becomes subionized. The term Local Stellar Environment (LSE) has been applied to such subionized postcoronal regions, and via the Be stars, theirs is a long observational history. The planetary nebulae appear to be included among them. When we ask the distinction between stars with and without a prominent LSE, we appear to find the distinction linked to the presence of a variability in the mass outflow. All stars have winds to some degree, but not all have strongly variable winds. The extreme example of such will be treated in the eighth volume of the series—The Cataclysmic Stars, which, from the IUE observations, are now recognized to have a continuous mass outflow as well as one abruptly larger at some epochs. As we prepare to read the discussion of M stars in the present volume, therefore, we recognize several aspects in which these stars may help to clarify this distinction between solar-type and nonsolar-type postcoronal regions: the great atmospheric extent of regions so cool as to produce dust, their often-identified evolutionary parentage of the planetary nebulae, and their dominating characteristics of variability. We return to these aspects below. Here, we simply stress the unambiguous establishment of classes of stars for which the Sun cannot be taken as an empirical thermodynamic model. At the same time, we stress the greater range of stars—cold *and* hot—for which the solar atmospheric structural pattern can be a guide if one does not confuse identity of thermal state with community of thermodynamic character.

Third, stimulated by solar observations, the first attempts at quantitative thermodynamic modeling of exophotospheres were for stars with quasi-thermal photospheres. On one hand, for chromospheric/coronal accelerated expanding regions, one models solar-similar stars. On the other hand, for stars with extended cool postcoronal regions, one models Be stars. Even current radiative-acceleration models of hot stars—ms, g, sg, but excluding Wolf Rayet—join the other two types in having very small velocities in photospheric regions producing the visual continuum. Apparently, all models of such stars converge in representing the subthermal outflow as amplification of an initial small velocity by the density gradient of a hydrostatic-equilibrium photosphere. We recognize, however, that some of the strongest examples of stellar peculiarity—relative to adequacy of classical modeling—were stars with pulsating or abruptly ejected photospheres. In such stars, very large photospheric velocities occur. At least first-approximation treatments of the motion of an equivalent photosphere to represent the behavior of the visual continuum exist. Treatments of nonradiative energy

dissipation from large differential velocity gradients, including shock waves, are less complete. Indeed, in such stars, especially the pulsating ones, one can say that nonthermal modeling of the subatmosphere is more complete than that of the atmosphere, but again stimulated by far-ultraviolet observations, one would expect an improvement in the situation. Since the compilation in our B–Be star volume, such observations of the β Ceph stars have already stimulated tentative models that differ from the photosphere-only ones and emphasize comparison between superionized and photospheric spectral lines. We hope that this problem of photospheric and exophotospheric structure and behavior in stars with distinctly nonthermal photospheres can be clarified in this and following volumes. When we consider the M and the cataclysmic stars—even the symbiotic, often linked to the M stars—we recognize that the photospheres are not obviously quasi-thermal and that exophotospheric structure is controversially vague. We hope for clarification. The increasing focus on nonradial pulsation—ranging from solar to hot-star studies—provides a transition from quasi-thermal to strongly nonthermal, as one considers the transition from nonradial to radial pulsation modes. And we note the shift in source of nonradiative energy fluxes to nonradial pulsational from turbulent convective nonthermal modes among those theorizing in the field equally in solar-like and solar-different stars. In abstract, while we have many examples of nonthermal photospheres and some observations and exploratory theory on what kinds of exophotospheric regions may result, we have, as yet, no really good picture of either photospheric or exophotospheric thermodynamics for such stars.

We recognize this M-star volume as the first in the series, apart from the preceding general volume, in which at least some of the considered stars may have nonthermal, rather than only quasi-thermal, photospheres. That is, some of the stars have photospheres in which macroscopic velocities are already so large as to invalidate hydrostatic equilibrium to determine the density distribution and/or differential velocities may be such as to introduce a nonradiative energy dissipation invalidating radiative equilibrium. So, for such stars, we must be prepared to find a quite thermodynamically different set of atmospheric regions—photospheric and exophotospheric—than those existing in stars with quasi-thermal photospheres. We simply must be prepared to identify such regions operationally in terms of thermodynamic definitions that are as equally based on empirical properties as those introduced for stars having quasi-thermal photospheres.

We emphasize that the operational definition of the lowest atmospheric region—the photosphere—has nothing to do with its thermodynamic character or state, only with its opacity; it is the deepest stellar region from which a photon of some wavelength can escape directly to the observer. Only in trying to model its thermodynamic and spectroscopic states do the various assumptions on these states, which characterize the model, enter. And the basic series objective is to use the best modern data to test such models and, hence, such assumptions, and to try to infer what can better replace them in terms of better representations of data and more thermodynamic consistency.

An example of such evolution of models begins with the historic attempts to represent the photospheres of pulsating cepheids by classical hydrostatic- and radiative-equilibrium models of supergiants, but with phase-dependent effective gravity and effective temperature. These static-atmosphere boundary regions—"tacked on" to the sinusoidally pulsating subatmosphere, which provided the effective radii, gravity, and luminosity—were then "diagnosed" to compare observation and theory, as well as to infer chemical composition. But conceptually, in sequence, one recognized that: (1) such standing-wave pulsation must become

running waves in the upper atmospheric regions, with such waves steepening into shocks for sufficiently extended (nonclassical) atmospheres, both extending and nonradiatively heating the atmosphere; and (2) these phenomena provide the possibility of mass ejection. Not only does the classical thermal caricature of the atmosphere suppress observable photospheric phenomena, it thermodynamically excludes the development of exophotospheric features. Therefore, one tried to explore the physics of these suppressed effects by replacing the "top" of the subphotospheric pulsation by an equivalent piston and studying the outward propagation of its compression/rarefaction-wave interaction with the overlying atmosphere. Much useful insight has resulted, but sometimes the origin of the phenomenon is forgotten in its identification as a "shock-wave model" of the atmosphere. The various shock waves arising in various phases and at various locations in such a pulsation/piston model are derivative, not causative, features of such a representation. Observationally, identifying their presence, location, and particular characteristics provides valuable diagnostic information on the pulsation/equivalent piston that produces them.

We emphasize, especially in the study of stars with nonthermal photospheres, that the major objective of these monographs is: (1) to collect sufficient data to ask whether some particular model reproduces them with sufficient accuracy, and (2) to ask whether any thermodynamc inconsistency of the representation suppresses some of the consequences of a nonthermal photospheric configuration on exophotospheric structure. For example, does it suppress nonradiative heating, mass outflow, acceleration or deceleration of such outflow, supercooling and "snowing" (i.e., particle condensation), or any other potentially important nonthermal phenomena?

SCIENCE PERSPECTIVE ON THIS M-STAR VOLUME

In the preceding, we emphasized a distinction between solar-like and solar-unlike stars, which is not based on cool versus hot photospheres, but on exophotospheric structural pattern: absence or presence of a cool, decelerated, very extended postcoronal region. In this empirical picture, chromosphere and corona are similar in being nonradiatively heated and dissimilar in being effectively hydrostatic versus significantly expanding, respectively. The solar-unlike postcoronal cool region is variable in existence and appears to be associated with variable mass outflow. The situation for photospheres more nonthermal than "quasi" remains to be explored for both chromosphere/corona and any cool postcorona. That nonradiative heating exists somewhere in the atmosphere is clear; the question is how low it begins. The same question holds for a hydrostatic versus aerodynamically controlled density distribution and for a monotonic outward acceleration of any mass outflow versus an eventual deceleration. All these questions remain to be put in perspective and resolved. Hopefully, some of the M stars can help.

The M stars exhibit a mélange of all the observational phenomena/anomalies stimulating the above-summarized reexamination of stellar atmospheric modeling. It is not simply that their range in luminosity and radius exceeds that in any other spectral class: the brightest M supergiant has absolute visual magnitude about -8, the faintest M dwarf about +17; photospheric radius—if such is meaningful—can reach $4.10^4\ R_\odot$ for an M-sg and descend to $0.1\ R_\odot$ for an M-d. But what is provocative is the range of quasi-thermal and strongly nonthermal photospheres and exophotospheric structures encompassed by the M stars. There are apparently mildly varying sg whose atmospheres exhibit both nonradiative heating and very extended cold, dusty external regions, pulsating M-g include the long-period and

semiregular variables, as well as the R CorBor stars with apparently abruptly ejected or collapsing dust envelopes, and M-d characterized by superflares. In addition, there are apparently "quiet" stars. We make a few remarks of perspective on what detailed study of particular kinds of these stars may ultimately contribute to our empirical/theoretical mapping of real-star atmospheric structural patterns and to understanding whence they arise. The reader can evaluate our perspective and assess how much the present volume contributes toward that objective—or toward something else.

One kind of star, called "Miras" after their prototype Mira Ceti, M7 IIIe, is a peculiar star, as equally historic as those discussed above because of its variable luminosity. It was the prototype long-period variable, interpreted as pulsating, thus with nonthermal photosphere. Like the Be stars and some other variable stars representing yet other kinds of nonthermal photospheres—like the dwarf nova SS Cyg—it is rich in long-time coverage of its visual-region behavior. To these data, the far ultraviolet and far infrared contribute another dimension of knowledge. An empirical determination of its atmospheric structural pattern, and those of other stars like it, should give us guidance on how at least this variety of pulsation perturbs both the photosphere and the exophotospheric pattern over what we have found them to be in stars with quasi-thermal photospheres.

We note that, although the Mira-type variables occupy a fairly definite region in the HR diagram, there are also a number of other stars (giants in luminosity class) in that same region which do not show such variable luminosity. Therefore, just as we proceed in trying to understand the thermodynamic distinction between other pairs of differing stars lying in a common HR region (e.g., the B and Be stars and those pulsating and nonpulsating stars lying in the Cepheid instability strip), we seek any empirical delineation in atmospheric structural patterns between pulsating and nonpulsating stars in this M-star region.

This distinction between pulsating and nonpulsating stars lying in the same region of the HR diagram should be more useful than in simply delineating *atmospheric* structure as such. Presumably, the particular type of nonthermal mode that occurs, or does not occur, reflects the subatmospheric structure/thermodynamic state. So *the presence of these two apparently different kinds of stars in the same HR region implies that its two-dimensional specification—luminosity and spectrum—is insufficient to specify the star.* The problem is not novel; witness the Be and Cepheid examples cited above. The question is whether the particular situation reflects a particular circumstance of origin, state of evolution, or something else. As we have stressed repeatedly (cf. the frontispiece of each volume), the first essential is to specify in as much detail as possible precisely *what* is the phenomenon, which again explains our focus on the directly observable—the atmosphere. We always try, however, to keep the various "explanations" in mind simply to ask whether some particular atmospheric observation might be particularly illuminating in deciding between them.

Then we note that the question of internal structure and evolution has always been a major focus in interpreting why such a large variety of stars are grouped in the spectral class M and what does the great difference between M-d and the M-g, M-sg reflect. Presumably, the M-d, the faintest stars on the main sequence, simply represent the smallest masses that can exist as stars with nuclear energy generation. Their dominant number among stellar types presumably reflects the long time they spend in the hydrogen-burning evolutionary phase because of their low central temperatures. On the other hand, the M-g and M-sg are thought to represent the late stages of stellar evolution for *essentially* all stellar masses: hydrogen shell, He, et seq burning. Without a significant mass expulsion, the above statement applies to all of these stars; late-evolutionary-stage stars should remain in this M-star domain until

they leave it to enter white-dwarf or supernova stages, depending on their particular mass. Therefore, it was conjectured, even before it was observed, that some mass loss must occur, given the observed supernova and white-dwarf frequency of occurrence. The planetary nebulae were considered as the graphic evidence of a drastic mass ejection. An M-g that, by losing about one-fourth of a solar mass, could end up as a hot subdwarf of less than a solar mass was a possible candidate for the process. Presumably, more massive stars must either become supernovae or find other mass-ejection processes.

Again, the modern far-ultraviolet observations, with their demonstration of the universality of some size of mass loss everywhere on the HR diagram, change the picture very drastically. One does not need such "catastrophic" single-event mass loss for either the evolutionary picture or for the production of the planetary nebulae. At the same time, however, one is not at all sure as to the relative roles of a slowly varying mass flux of moderate size versus one enhanced for limited time intervals. A combination of these has been suggested for both the origin of planetary nebulae and for the distinction between Be and B stars. Its significance for the M stars lies in its making less clear what role the planetary nebulae can play as evidence for something in regard to those late stages of evolution conventionally associated with the M stars. The several "active" late-type stars, such as V1016, sometimes interpreted as "incipient" planetary nebulae, may eventually cast light on this problem of a continuous mass outflow, perturbed by an enhanced mass outflow, in its relation to all these questions.

For all the preceding reasons, evolutionary theorists have rushed to compute evolutionary tracks with mass loss. Unfortunately, mass-loss rates determined from observations are presently crude, and only statistical values seem to be trusted—even these being represented by crude empirical formulae based on the assumption that mass loss can be specified in terms of the gross parameters of thermal modeling: mass, radius, luminosity, effective temperature, etc. The validity of this assumption has never been established; the increasing evidence for variability of mass-loss rate in a given star and wide differences between stars in the same HR location put it strongly in question. Clearly, much remains to be done both observationally and diagnostically to clarify this empirical stellar-atmospheric contribution to "theoretical" modeling of interior and its evolution. At present, we can only realize that evolutionary models with mass loss are completely tied to thermal models; those attempts at representing the origin of mass loss in nonthermal modes are not yet integrated with structural modeling and its evolution. Clearly, the process of such integration will result in changes at the interface between subatmosphere and atmosphere, and thus in the details of how deep in the atmosphere the mass outflow has an effect, as well as in the details of the variety of atmospheric regions and the structural patterns in which they occur.

Finally, the observational demonstration of mass loss at all evolutionary stages—and the uncertainty as to its possible enhancement at certain evolutionary phases and nonevolutionary epochs—has introduced other changes in ideas on late-stage evolution. And these changes strongly link the contents of this M-star volume to the following one on the hot early stars, O and Wolf Rayet, in that part of the book edited by Conti (to whom, and to Kudritski, we are much indebted for orientation on these evolutionary questions). For a sufficiently large mass outflow/expulsion, it is argued that the star can be stripped to an He, even carbon, core and leave the M region, to return as an OB-sg to the hot-star HR regions. The dividing line between remaining in the M-star region or returning to the OB is currently set at some 30–40 $M_{\odot}$. But for the reasons mentioned—mass-losing evolutionary models are still thermal—this limiting mass seems highly uncertain at this moment. The proponents

of these ideas cite, as observational support, the presence of blue sg with much larger luminosity (presumably reflecting higher mass) than is found for the brightest red sg. One recalls current discussions on the upper mass limit under which stars can exist and the arguments that, instead of radiative disruption, one simply obtains pulsational instability, with amplitudes limited by aerodynamic dissipation in chromospheric-like exophotospheres. Unless one proposes to restrict such supermassive stars to the main-sequence evolutionary phases, the presence of such pulsational instability from a radiative instability should be an observational discriminator in precisely these hot sg. So again, we come to examples in which differential atmospheric behavior between hot and cold extremes of the HR diagram should provide insight into nonthermal, subatmospheric, and atmospheric structure.

Under these evolutionary arguments and caricature, the difference between M-g, M-sg, and M-d is therefore mainly that they do not refer to stars of the same mass, whereas in the OB regions, those stars on the MS have essentially the same initial masses as the g and sg stars. Any discrepancies reflect an aerodynamic mass loss. This does not mean, of course, that stars initially on the OB–MS always remain in the OB region as they evolve. Giants and supergiants in the regions between OB and M reflect a mélange of evolutionary phases and, hence, masses. In principle, under such evolutionary modeling, one should search for the origin of discrepancies between two unlike stars in the same HR region in terms of intersecting evolutionary tracks. Obviously, substituting nonthermal evolutionary models for thermal should broaden the range of such intersecting tracks. But at present, all such interpretations are largely speculative, mainly due to the great uncertainty in the correct values of mass loss for any given star in any stage of evolution, but also strongly—and linked—is the uncertainty of just what are the nonthermal modes of importance for a given star. And we recognize that the best hope, today, to obtain more correct mass-loss rates and to identify nonthermal modes is observational. Our theoretical understanding of the broad structure of nonlinear, nonequilibruim thermodynamics of open systems is still miniscule.

Therefore, a very profound linkage exists between the major contemporary problems of atmospheric structure and those of subatmospheric and internal structure and evolution for stars generally, but particularly for these M-type stars because of the wide range of stars they embrace. Always the atmosphere's exophotospheric structure, and sometimes its photospheric structure, are fixed by the particular details of the mass outflow. In turn, this is linked to the nonthermal modes of the photosphere and subphotosphere, probably to those of the interior. We also know that, in some stars, it is the time history of the mass outflow which controls the structure of the cool outermost layers. While the planetary-nebular, Be, and T Tauri stars are the most unambiguous examples, the symbiotic stars and presumably some of the extended-atmosphere M stars are also examples, even if as yet less well defined.

One set of observations, on the Mira χ Cyg by Hinkle, Hall, and Ridgway, merits particular comment in this connection; it is mentioned several times in this volume's chapters; it is suggestive of the general picture emerging from both Be and β Ceph modeling as abstracted in the preceding section *Science Perspective on the Series*. The Mira observations are diagnosed as suggesting four atmospheric regions: (1) a pulsating nonthermal photosphere; (2) a nonradiatively heated infalling region lower bounded by a shock formed as outgoing material from the current pulsation ejection collides with material infalling from previous ejection phases; (3) an effectively static cool reservoir layer—the source for both the infalling material of layer (2) and that of an "escaping" layer; and (4), which is a much colder layer expanding at a velocity of 0.5–0.25 the pulsation value. The common possibility of a cool "quasi-static reservoir layer" existing in both quasi-thermal (Be) and pulsating nonthermal (Mira, and maybe Cepheid) photosphered stars, whose existence and structure depends on interaction

between present and previous phases of lower-atmosphere mass outflow and which serves as a "mass-loss valve," is intriguing.

The linkage between mass and nonradiative energy fluxes is presently ill-defined, although we know we cannot have the former without some size example of the latter. But again, the controversy over cool-but-large versus hot-but-small mass outflows, which erupts already in the K stars, carries over strongly into the M stars. All these problems of the mass outflow are ultimately linked to subatmospheric structure, and, as mentioned above, the problems of the origin and the effect of such mass loss are completely coupled. Today, we continue to live under empirical iteration in regard to modeling and understanding. In the following chapters, the authors explore these problems for the M stars. We trust that many of the above points, on which we have commented very naively, will be clarified.

A few comments on the organization of this volume, essentially coming from the mentioned variety of stars covered, follow. For each monograph in the series, we aim at an overall structure that broadly consists of three parts: an extensive survey of the observational material for all kinds of stars covered in the volume; an attempt to place existing theoretical modeling of such stars into perspective—what are the models, and how well do they represent the observations; some attempt to improve the model and/or instigate further observational programs to guide such improvement. Overall, given that existing modeling across the HR diagram is largely thermal and that we focus on improving such modeling, we try to put into perspective the observational evidence for nonthermal phenomena and what kind of quasi-thermal and nonthermal modeling features they suggest exploring. When such nonthermal models are already being explored for some stellar types—as already mentioned for pulsating stars in the preceding discussion—we hoped the authors would equally explore their promise.

Then relative to the approach adopted in earlier volumes, in which normal MS stars were discussed first, the present volume considers first the g and sg population of this M-star class; a discussion of the M-d comes only in the last two chapters. The focus is on those stars which are M type, not because they were "born" there, but because they are its most striking members. They are striking not only because they are the most luminous and most easily observed, but also because of their nonthermal characteristics—greatly extended atmospheres, variability, pulsation, strong individuality in nonradiative heating, and mass loss. So it is that the first two chapters, summarizing the observational background, focus exclusively on the giants and supergiants. The same focus holds for the following four chapters on circumstellar radio molecular lines, grain formation in circumstellar shells, mass loss, and circumstellar chemistry, respectively, each summarizing another aspect of the observational situation, reviewed in the context of the adequacy of current modeling. The discussion of thermal modeling in Chapter 7 again focuses on its application to stars whose atmospheres may or may not be distended simply by low-gravity but thermal effects. The following Chapter 8 discusses both thermal non-LTE effects and quasi-thermal, as well as broader nonthermal effects on such modeling. Not until Chapter 9 do we turn to the observational situation with respect to native-born low-mass M stars, which are difficult to observe because of their low intrinsic luminosity, but nonthermally striking because of the large number that exhibit flaring-type luminosity enhancement. Chapter 10 concludes the volume with a summary of the relation between classical thermal and nonclassical modeling of such M-d and MS stars in other parts of the HR plane. Again, it stresses unique features of the M-type stars: that they should be the outstanding example of convective effects and that the "neoclassical" production of nonradiative energy fluxes by such convection is inadequate. The chapter explores current thinking on alternatives. The focus of the volume really rests on

nonclassical stars as the norm, not the exception—a viewpoint gradually emerging all across the HR diagram.

SOME ORGANIZATIONAL PERSPECTIVE

As mentioned above, the possibility of organizing, writing, publishing, and diffusing this series of monographs arose from: (a) the enthusiastic collaboration of a number of colleagues, and (b) the generous commitment to support the project by NASA and CNRS. Our primary objective was a homogeneous collection of observations—both within and outside the visual/spectral range—sufficient to provide a sound empirical basis for a critical look at the adequacy of present-day stellar atmospheric modeling over the entire HR diagram. Such an examination of the thermodynamic adequacy of atmospheric models also raises questions on the adequacy of present models for interiors and evolution.

Because, in the decade preceding the monograph project, it was already becoming clear how basic were spectral observations in the far ultraviolet to such a program, a parallel objective of our monograph project was the use of its results, as they became available, toward planning observing programs from space. Clearly, such planning requires a consideration of the necessary characteristics of space vehicles, the instruments they can carry, and the kinds of observing programs they can support in order to conduct the specific programs on particular stars that the results of our project suggest. Moreover, as the results of this program accumulate, one increasingly appreciates the need for coordinated ground and space programs. Any surprise at the new thermodynamic characteristics exhibited by real stars becomes equaled in considering the new kinds of observing programs required to detail them.

An excellent example of this is immediately obvious in the continuous stream of results in all fluxes, for a variety of stellar types, both hot and cold, that exhibit the importance of stellar variability. In the early days of the IUE, variable stars were a priori excluded from observing programs to avoid tying up too much observing time. By contrast, "snapshot" surveys of a large variety of stars were favored. Indeed, so unexpected to most of the astronomical community were many of the results that the catchword became "serendipitous" exploration. However, as the observations multiplied, it became clear that variability is a common, rather than a peculiar, property of stars. The focus is now shifting to establishing its details, especially simultaneously in different spectral and, hence, different atmospheric, regions. Many of us involved in these monographs, hence increasingly conscious of thermodynamic similarities across the HR diagram, advocate future space vehicles adopted for, and programs focused on, just these problems of stellar variability over very long times, a decade or more, accompanied by dedicated ground-based instruments to ensure simultaneity of observations across the accessible spectrum.

Therefore, it is that our own outlook as organizers and editors of the monographs rests on applying literally the Fontenelle maxim featured on the frontispiece of each volume as the prime focus of the project and as the objective of collecting the data. We remain equally committed to an empirical/theoretical, as opposed to a speculative, approach to the use of these data in revising the thermodynamic basis for modeling and to revising the models themselves. We also hold the viewpoint that a major goal of the monograph project should be its use in planning and demanding new observing facilities and programs oriented around this continuous iteration between new data and new theory.

Finally, we wish to thank the respective agencies, NASA and CNRS, for their continuing help in completing the volumes of this series. Any project of this duration is exposed

to changes in personnel and sometimes policies and procedures inevitable in government agencies. There have indeed been some problems and delays in the production of this volume and its immediate successor on O and Wolf Rayet Stars. Hopefully, these have now been resolved, and we are confident that the final four volumes will be written in the spirit under which the series was concluded. Throughout, we have enjoyed the steadfast commitment of several key individuals to this project. For this support and the constructive attitude toward science that it reflects, we are grateful.

R. N. Thomas
Boulder, Paris, December 1986

ACKNOWLEDGMENTS

When this volume was undertaken, we had no idea that its completion would be almost as complicated as the atmospheres of the cool stars this book describes. Difficulty of communicating with some of our authors and the vastly different completion dates of the chapters have caused numerous problems, with the net result of a substantial delay in publication. There is no book of this scope and subject anywhere, and we earnestly hope that it was worth waiting for!

As editors, we are deeply grateful to each chapter author. Researching and writing a chapter is a task of several tough man-months (perhaps stretching over several years), the reward for which can only be the knowledge gained and the contribution made in sharing the knowledge. They deserve our continuing applause.

Some indication of the interest in this field can be gauged from the size of this book, and rapid advances will probably fill another volume within a few years. Eager scientists researching the fascinating M, S, and C stars the world over will, we hope, make good use of these chapters, and to them we dedicate this volume.

Hollis R. Johnson
François Querci

October 1986

CONTENTS

Chapter		*Page*
Perspective		vii
Acknowledgments		xxi
Résumé		xxv
Summary		lvii
1	Basic Properties and Photometric Variability *François Querci*	1
2	Spectroscopy and Nonthermal Processes *Monique Querci*	113
3	Circumstellar Radio Molecular Lines *Nguyen-Quang-Rieu*	209
4	Circumstellar Shells, the Formation of Grains, and Radiation Transfer *Jean Lefèvre*	225
5	Mass Loss *Leo Goldberg*	245
6	Circumstellar Chemistry *Alfred E. Glassgold and Patrick J. Huggins*	291
7	Thermal Atmospheric Models *Hollis R. Johnson*	323

PRECEDING PAGE BLANK NOT FILMED

PAGE XXII INTENTIONALLY BLANK

Chapter *Page*

8 Quasi-Thermal Models 373
Ramiro de la Reza

9 The Atmospheres of M Dwarfs: Observations 409
Marcello Rodonò

10 M Dwarfs: Theoretical Work 455
Dermott J. Mullan

Subject Index 481

Star Index 493

Contributing Authors 501

RÉSUMÉ

D'une certaine manière, l'atmosphère d'une étoile comprend la totalité de la région qui s'étend entre le noyau producteur d'énergie et l'espace interstellaire. De ce point de vue, l'atmosphère comporte précisément ce que l'on appelle d'habitude l'enveloppe, la photosphère, la chromosphère, la couronne, la totalité de la région circumstellaire, et la matière quittant l'étoile; est seulement exclue de cette liste la matière qui a quitté réellement l'étoile et qui est devenue partie intégrante du milieu interstellaire. Garder à l'esprit cette perspective permet de mettre en valeur l'unité de ces régions qui sont quelquefois traitées comme des parties séparées d'une étoile. Une telle insistance est particulièrement nécessaire pour les étoiles étudiées dans ce volume, qui ont une tendance à présenter une si large variété de phénomènes et de dimensions que la compartimentalisation s'impose plus facilement.

L'une des caractéristiques distinctives des étoiles M, S, et C est en fait l'étendue très large des phénomènes variables avec le temps qu'on peut y observer. Même les étoiles naines de type M, décrites dans les chapitres terminaux, apparaissent, vu l'importance de leur chromosphère et la violence de leurs éruptions, être plus que simplement les contres-parties plus froides des étoiles du haut de la série principale. Les géantes froides montrent, de façon fréquente, des aspects aussi fascinants que des raies d'émissions, des raies d'absorptions déplacées ou multiples, un excès d'émission infrarouge du aux poussières, des émissions d'ondes radio dues à l'effet maser ou thermiques—et souvent ces caractéristiques varient de façon périodique ou irrégulière. Au point de vue de l'étoile, ces phénomènes doivent être caractérisés par une zone convective profonde, et une photosphère relativement calme, à travers laquelle passe néanmoins l'énergie mécanique nécessaire à alimenter la chromosphère en énergie. L'énergie nécessaire à la pulsation de la photosphère est produite dans les profondeurs de l'étoile elle-même. Pourtant, beaucoup de ces étoiles varient seulement de façon semi-régulière, ou même d'une façon erratique. Tout mouvement organisé dans la photosphère doit donner lieu à des ondes de choc qui, lorsqu'elles traversent l'immense atmosphère extérieure, produisent du rayonnement à partir des gaz excités au fur et à mesure de leur dissipation lente, et soutiennent peut-être les gaz en une région stagnante, localisée à plusieurs rayons solaires au dessus de la surface de la photosphère. Des grains doivent se former quelque part peut-être sous la forme de grains "propres" dans certaines des photosphères les plus froides, et ceux-là sont alors poussés vers l'extérieur par la pression de radiation, entraînant avec eux les gaz et devenant "sales" au fur et à mesure de leur progression. Peut-être les grains se forment-ils au contraire dans la région des gaz stationnaires, très

au-dessus de la photosphère, et leur effet, en alimentant le flot matière vers l'extérieur de l'étoile, commence-t-il là. De toute façon, de très grandes pertes de masse sont observées, suffisantes pour contaminer l'espace interstellaire par l'atmosphère (qui est peut-être actuellement enrichie en éléments lourds), et peut-être aussi suffisante pour modifier l'évolution ultérieure de l'étoile. Dans les gaz éloignés de l'étoile, des émissions de micro-ondes (aussi bien thermiques que produites par l'effet Naser issu du radical OH et de la molécule H_2O) sont fréquemment observées dans celles des variables riches en oxygène de type Mira, qui ont la période la plus grande et l'amplitude la plus importante. L'émission de type maser produite par le radical SiO se produit beaucoup plus près de l'étoile, peut-être même dans la photosphère. Enfin un certain nombre d'étoiles, parmi les plus froides, aussi bien des étoiles riches en oxygène que riches en carbone, sont entourées par des enveloppes de poussières ou par des nuages optiquement épais dans l'infrarouge; et ces nuages sont des sites favorables à la richesse d'une chimie moléculaire et atomique.

Un autre aspect des étoiles les plus froides nous apparaît quelquefois surprenant, c'est l'étendue des conditions physiques. Il est facile d'oublier qu'un changement de température effective de 4000 K à 3000 K est en fait un changement énorme, et que des étoiles ayant ces températures effectives peuvent ne pas être du tout semblables entre elles. Il pourrait être utile de *classer les étoiles* en trois groupes: les étoiles *chaudes*, les étoiles *tièdes* et les étoiles *froides*. Les étoiles chaudes sont les étoiles O, B, et A; les étoiles tièdes sont les étoiles solaires F, G, et K et les étoiles froides sont les étoiles de type M, S, et C, celles qui sont concernées par cet ouvrage. Cette division correspond grossièrement à la forme la plus abondante sous laquelle se trouve l'hydrogène, celle qui domine la thermodynamique de l'objet: dans le cas des étoiles chaudes, l'hydrogène est sous la forme H II (hydrogène ionisé), dans les étoiles tièdes, c'est de l'hydrogène neutre (H I) et dans les étoiles froides c'est la molécule d'hydrogène (H_2) qui domine.

Après cet examen d'ensemble des étoiles M, S, et C (auxquelles nous nous réfèrerons simplement sous le nom de géantes rouges ou encore étoiles GR (en anglais RG)), on rappelle au lecteur les observations qui constituent la base de notre discussion.

Le volume débute par un Chapitre sur *Les Propriétés de Base et la Variabilité des étoiles géantes et supergéantes M, S, et C*. Ce chapitre insiste surtout sur la variabilité de ces étoiles, d'autant plus que la variabilité est due à des processus non thermiques.

Les *proprietes fondamentales* des variables M, S, et C sont décrites. On expose d'abord les principes de la classification des différents objets; une rapide description des principaux types d'étoiles est donnée, en réservant la description de données plus spécifiques pour le paragraphe suivant. La classification courante est basée sur des rapports d'abondance: le rapport C/O (<1, $=0$, >1) indique le type spectral de la majeure partie des étoiles (M, S, et C respectivement). Les abondances des métaux et/ou des éléments issus du processus s distinguent des types plus particuliers–les étoiles aux fortes bandes moléculaires de CN ou aux fortes raies du Ba II, les étoiles déficientes en hydrogène, etc. Pour mieux comprendre la grande variété de ces étoiles rouges qui sont si voisines dans le diagramme HR, plusieurs autres classifications basées sur d'autres critères physiquement significatifs sont proposées. La plus connue repose sur l'amplitude et le profil des courbes de lumière des variables.

Les propriétés intrinsèques des géantes rouges sont ensuite résumées. En bref, ces étoiles sont caractérisées par des températures telles que $3.3 \leqslant \log T_{\text{eff}} \leqslant 3.5$, des luminosities telles que $3 \leqslant \log L/L_0 \leqslant 5$ ou encore $-7 \leqslant M_{bol} \leqslant +3$, des âges d'environ 10^7 à 10^{10} ans, et par une échelle étendue en masses d'environ 1 $M_\odot$ à $\geqslant 20$ $M_\odot$.

Les mouvements et la distribution dans l'espace des géantes froides sont décrits. La distribution apparente et la distribution spatiale au voisinage du Soleil sont bien connues

grâce aux anciennes revues sur la question. Les recherches plus récentes étudient la distribution des géantes rouges dans la direction des régions centrales de notre Galaxie et d'autres galaxies proches (par exemple, le Grand et le Petit Nuage de Magellan). Le rapport du nombre d'étoiles C au nombre d'étoiles M est longuement discuté à cause de son importance dans les études d'évolution stellaire sur la branche asymptotique des géantes et dans la compréhension des propriétés fondamentales galactiques.

Le paragraphe suivant développe le sujet principal du Chapitre 1 par *une revue des observations et des interprétations des différents types de variabilité* des géantes et supergéantes rouges. Toutes ces étoiles peuvent être assimilées soit à des variables pulsantes, soit à des variables éruptives. Dans le groupe des étoiles pulsantes, trois types sont reconnus. (1) Les Miras sont des étoiles à longue période: de façon générale elles ont une périodicité bien exprimée et une bonne régularité (elles sont aussi appelées variables à longue période, soit LPV en anglais). (2) Les variables semi-régulières (ou encore SR) ont des variations en amplitude visible plus faibles et des courbes de lumière plus irrégulières que les Miras. (3) Les vraies variables irrégulières sont appelées Lb (ce sont des géantes) ou Lc (ce sont des supergéantes). Les étoiles RCB forment le groupe éruptif; elles sont de classes spectrales F, G, K, et R. La classe R concerne les étoiles carbonées chaudes, les seules étoiles éruptives qui nous intéressent dans ce volume. La distribution trés différente des divers types de variabilité au sein des trois classes spectrales M, S, et C est commentée.

Les caractéristiques de chaque groupe de variables sont ensuite décrites. Par "*Miras*", c'est un type de courbe de lumière qui est distingué et non un type spectral stellaire, comme la confusion existe souvent dans la littérature. Des généralités sont notées. Dans quelques étoiles, l'amplitude de la variation dand le visible avec la phase est trés forte (par exemple dans χ Cyg). La plupart des changements sont cycliques avec une période égale à celle de la courbe visible. Cependant, quelquefois la période des cycles de lumière individuels diffère de la période moyenne stellaire par quelques pour-cent, et les propriétés observables ne se répètent pas exactement d'un cycle à l'autre. Le flux de quelques Miras dévie d'un corps noir de façon significative au-delà de 8 μm en présentant un grand excès infrarouge dû à une enveloppe de poussière; ces étoiles sont appelées Miras IR. On trouve les masers OH parmi les Miras de type spectral M; quelques exemples de changements du type OH I au type OH II sont décrits (R Leo et U Ori).

Notre description des Miras se continue par l'exposé des propriétés spécifiques à leur variabilité. Le phénomène de *retard de phase* est discuté en premier. Il s'agit d'un décalage en phase entre les courbes de lumière de différentes couleurs (on stipule que l'époque de la phase zéro se rapporte au maximum visuel). De façon typique, le maximum en infrarouge est en retard de 0.1 à 0.2 périodes sur le maximum visible. Des décalages de phase sont aussi observés entre les courbes de lumière radio (raies OH, SiO, H_2O) et infrarouges. Le comportement du retard de phase n'est pas le même dans toutes les Miras et, de plus, son comportement avec la phase peut ne pas être exactement le même au cours des différents cycles d'une même étoile.

L'amplitude des variations de lumière change dans les Miras d'une longueur d'onde à l'autre. Elle est beaucoup plus grande dans le visible que dans l'infrarouge. Généralement, les amplitudes de variation $[F_{max}/F_{min}]$ décroissent dans l'infrarouge avec les longueurs d'onde croissantes de 1.2 à 3.5 μm et sont à peu prés constantes entre 3.5 et 10 μm. Dans de nombreuses Miras les différences d'un cycle à l'autre ne sont pas erratiques: brillants et faibles maxima tendent à alterner, et les maxima brillants tendent à se produire avant la date prédite. Dans tous les cas, le minimum ne peut pas être considéré comme l'état normal d'une Mira.

Les courbe de lumière des Miras présentent un grand choix de profils dans le visible (forme en dents de scie ou en sinusoïdale lissée, présence d'épaulements, de points d'inflexion, etc.). Dans les courbe de lumière des étoiles M et S, trés semblables, la montée vers le maximum est quelque peu plus rapide que le déclin vers le minimum. Les courbes de lumière des étoiles C sont plus graduelles et plus symétriques. Toutes ces courbes de lumière aux formes différentes pourraient être le reflet des variations de l'opacité et de la densité dans les différentes couches atmosphériques, variations causées par la propagation d'ondes de choc. Des exemples montrent que la forme de la courbe de lumière visible est conservée dans d'autres longueurs d'onde. Quelques étoiles ont des courbes de lumière avec deux maxima et deux minima par période; ce curieux comportement a aussi été trouvé théoriquement lors d'un essai pour produire une forte valeur de la vitesse d'aprés-choc dans le cas d'un modèle pulsant isotherme.

Pendant le cycle d'une Mira, *des variations dans les indices de couleur* apparaissent. De façon générale, l'étoile devient plus rouge lorsqu'elle devient plus faible en V (elle va vers le minimum). Puisque l'index moléculaire (TiO+VO) autour de 1 μm est corrélé à la température observée, chaque Mira M se déplace sur le plan [index de couleur/température] au cours de la période. On montre aussi que le type spectral de chaque Mira varie pendant la période. De nombreux effets contribuent à la variation temporelle des indices de couleur: la température, l'opacité moléculaire, etc.—quelques uns d'entre eux ne sont pas complètement indépendants.

On a déjà parlé de quelques changements dans la forme des courbes de lumière entre deux ou plusieurs périodes consécutives. D'autres sortes de changements de période sont observées dans les Miras: (1) une évolution séculaire par une augmentation ou une décroissance régulière de la longueur de la période ou bien par une variation sinusoïdale de cette dernière, (2) des changements de la forme de la courbe de lumière entre deux ou plusieurs périodes consécutives, (3) un changement soudain de la longueur de la période et des décalages soudains du maximum (fluctuations de phase). Quelques-uns de ces changements de période sont utilisés comme confirmation observationnelle directe de la théorie du "flash" de l'hélium. Dans la majorité des Miras observées, on détermine des *périodes multiples*. En général, la période la plus courte P_1 est associée avec la plus grande amplitude de la variation. Il est suggéré que cette période principale P_1 est la période de pulsation, alors que la période de modulation P_2 peut être due à un mode non radial ou à des taches froides sur la surface stellaire. D'autres interprétations sont proposées, tel le temps de retournement convectif de cellules géantes. La valeur du rapport P_2/P_1 est d'environ 9 pour les variables de type M et de 12 pour les étoiles de type C.

Dans les Miras, des fluctuations à courte échelle de temps sont illustrées par: (1) une évolution rapide de la température effective de *o* Cet sur 12 jours, (2) des effets remarquables de dépendance de phase dans la forme et l'intensité des raies d'émission maser SiO, (3) des variations sur une nuit des vitesses radiales de raies d'absorption et d'émission, interprétées comme le résultat de l'intéraction d'ondes de choc avec des couches atmosphériques non uniformes ou d'éventuelles éruptions ("flares").

Des *corrélations entre les différentes quantités* décrites, telles la longueur de la période, la forme de la courbe de lumière, l'excès infrarouge, les diagrammes de couleur (visible et IR), sont ensuite discutées. Les relations les plus significatives sont résumées. (1) Une relation statistique existe entre la forme de la courbe de lumière d'une Mira et la période. (2) Une corrélation est notée entre la différence en magnitude de deux maxima successifs et l'intervalle de temps qui sépare les deux maxima. (3) Les variables Miras ayant les périodes les plus courtes sont des étoiles de la Population II, alors que celles de périodes plus longues

appartiennent à des populations plus intermédiaires: ceci suggère que l'amplitude de la période d'une Mira peut être une fonction de l'abondance métallique. (4) Le lien entre la longueur de la période et la variation d'amplitude a été étudié. On vérifie que les étoiles qui ont les périodes les plus longues, ont les amplitudes les plus grandes, et ceci dans de nombreuses longueurs d'onde. Des relations sont aussi observées entre l'amplitude de la période et les différents index de couleur IR; quelques conclusions en sont tirées, telles que la hauteur du fait spectral à 10 μm, dû aux silicates, paraisse augmenter avec l'amplitude de la période, ou bien que la relation entre l'index [8.7 μm]-[11.4 μm] et la période indique que la masse de poussière observée dans une thermosphère donnée est presque une fonction linéaire de la période. D'autres corrélations impliquent des raies radio. (1) Les masers OH à 1612 MHz et les variations IR montrent une corrélation compatible avec un pompage radiatif des masers vraisemblablement à 2.8 - 35 - 53 - 80 et 120 μm. (2) Le maser H_2O à 1.35 cm et le flux IR à 2.2 μm peuvent être liés soit par une relation exponentielle, soit par une relation linéaire une fois que le flux infrarouge a atteint son seuil. (3) La vitesse d'expansion donnée par les Miras OH de types I et II est en corrélation directe avec la variation d'amplitude à 1.04 μm et en corrélation inverse avec la longueur de la période.

Le paragraphe se continue par les *semi-régulières*. On donne d'abord quelques généralités sur ces variables. Trois groupes sont définis: (1) les variables dites SRa sont des géantes et en général ne diffèrent des Miras que par l'amplitude des variations de lumière qui est plus faible; néanmoins, leur courbes de lumière montrent fréquemment de fortès variations d'un cycle à l'autre; (2) les variables dites SRb, aussi des géantes, présentent une piètre périodicité avec des variations irrégulières lentes que, par moment, remplacent des changements périodiques; (3) les variables dites SRc sont des supergéantes avec un comportement de SRb; les variations de lumière visible sont en général de l'ordre d'une magnitude ou même moins. Presque la moitié des semi-régulières connues sont des étoiles N, le reste étant de classe M; trés peu de semi-régulières de types S et R sont connues.

Différentes échelles de temps dans les variations de lumière des semi-régulières ont été découvertes à partir d'estimations visuelles de la brillance. Les courbes visuelles sont tout à fait individuelles, c'est à dire ne présentent pas la forte similarité notée pour les courbes des Miras. Elles pourraient être caractérisées par une sorte de périodicité cachée par des variations irrégulières en brillance. Parmi les semi-régulières, les variables SRa sont le plus semblables aux Miras (émission Balmer autour de quelques maxima, changements de période, etc.). Les étoiles SRb sont plus irrégulières que les SRa. Dans ces étoiles, des variations sur une échelle de temps d'environ une heure ont été détectées, comme dans R Crt. L'exemple de l'étoile C, TW Hor, analysée par photométrie à larges bandes, montre que l'indice U-B varie de façon opposée aux indices $V-R$, $V-I$ et $B-V$; il présente de fortes oscillations rapides entre les phases 0.8 et 0.9, probablement en relation avec l'intéraction d'ondes de choc avec la matière inhomogène de la chromosphère. Sur un siècle, quelques SRc ont leur éclat au maximum qui décroit jusqu'à 2 magnitudes; comme les amplitudes de variation de lumière des supergéantes sont à leur maximum à la limite de Hayashi du diagramme HR, on en conclut que les étoiles SRc ne restent pas plus d'une centaine d'années prés de cette limite. Des variables SRc appelées hypergéantes (ou super-supergéantes) sont vraiment trés étendues; elles peuvent avoir une magnitude bolométrique de -7 à -9. Elles présentent des perturbations à long terme (sur plusieurs années), avec de grandes variations en luminosité et en classes spectrales (par exemple, ϱ Cas), probablement dues à une forte quantité de matière éjectée. De plus, on observe des variations d'une nuit à l'autre, dont la cause est peut-être l'éjection de petites bouffées de matière ou des mouvements locaux dans l'atmosphère.

Des corrélations entre les quantités telles que les pseudo-périodes, les magnitudes absolues, les classes spectrales et les retards de phase sont moins évidentes dans *les variables SR* que dans les Miras. Néanmoins, des relations sont mentionnées: (1) plus longue est la pseudo-période, plus rouge est le spectre; (2) aucun couplage mécanique ne semble exister entre la photosphère qui endure quelques variations périodiques, et les régions des masers qui ont des vitesses radiales tout à fait constantes (seules des variations photosphériques plus fortes qu'un certain seuil induisent des variations masers); (3) une étude de plusieurs étoiles SRc de types Ia, Iab et II dans le filtre V montre que, pour un type spectral donné, plus l'amplitude de brillance est grande, plus lumineuse est la supergéante; (4) et encore, plus la luminosité de la supergéante est importante, plus jeune est le type spectral; (5) une relation entre la période et la luminosité a été établie pour des supergéantes rouges dans le Grand Nuage de Magellan. Finalement, on insiste sur la nécessité de longues séries d'observations interrompues, par satellites, de variables choisies, qui aideraient efficacement à débrouiller les phénomènes présents sur différentes échelles de temps dans ces étoiles. En fait, il s'agit de décider si les *courbes de lumière des semi-régulières sont multipériodiques, chaotiques ou réellement aléatoires.* Dans les dernières décades, des analyses sur les multipériodes ont été développées, et de nombreuses irrégularités apparentes sont expliquées par un mélange complexe de deux ou plusieurs oscillations individuelles, généralement identifiées par une analyses sur les multipériodes ont été développées, et de nombreuses irrégularités apparentes sont expliquées par un mélange complexe de deux ou plusieurs oscillations individuelles, généralement identifiées par une analyse harmonique des observations. Aujourd'hui, des techniques mathématiques utilisées pour expliquer le comportement des courbes de lumière des semi-régulières et des irrégulières sont proposées: (1) un procédé dit de hasard où les évènements sont en grande partie indépendants les uns des autres et où les prédictions d'un ensemble quelconque de variations sont impossibles, (2) un procédé dit chaotique où les variations observées reflètent les mouvements instables produits par le comportement collectif et coopératif de la matière soumise à des forces agissantes amplifiées.

Quant aux *variables irrégulières*, les étoiles Lb et Lc (respectivement géantes et supergéantes), elles varient lentement sans qu'il y ait trace de périodicité. Les irrégulières M sont en majorité concentrées aux types M5 et M6; aucune d'entre elles n'est plus tardive que M7. De nombreuses variables irrégulières de la classe M sont rattachées aux associations d'étoiles 0 jeune de Population I. On trouve les carbonées irrégulières surtout dans les sous-classes les plus jeunes. Comme l'intervalle de temps entre les maxima successifs est trés long (de quelques centaines de jours à quelques milliers), il n'est pas facile d'affecter une supergéante soit à la classe SRc, soit à la classe Lc. Un critère basé sur l'amplitude des variations est appliqué. Dans les supergéantes à faible amplitude, le maximum moyen est d'environ 1.1 magnitudes au-dessus du minimum et la dispersion d'environ 0.2 à 0.3 magnitudes. Des exemples de supergéantes à grande amplitude montrent un maximum à environ 4.2 magnitudes du minimum et une dispersion d'environ 1.1 magnitude.

Des variations de lumière sur différentes échelles de temps sont observées dans les irrégulières. Quelques étoiles ont des changements rapides de brillance (sur quelques jours); d'autres ont des variations périodiques sur quelques intervalles de temps, suivies d'une période pendant laquelle la brillance est tout à fait constante. Leurs variations peuvent beaucoup plus résulter de processus chaotiques ou dûs au hasard (conséquences d'irrégularités de surface telles des taches ou des boucles magnétiques, etc.) que de processus harmoniques. Cependant, ce point de vue est discutable; la supergéante μ Cep est un bon exemple dans lequel certains attribuent les variations de lumière de l'étoile à des perturbations temporaires

et distribuées au hasard à la surface stellaire et où d'autres les expliquent par la superposition de termes périodiques. Dans α Ori observée pendant prés de soixante ans, les courbes de lumière sont caractérisées par des variations de lumière à long terme avec une période d'environ 5.8 ans et une amplitude moyenne d'environ 0.4 magnitudes, sur lesquelles sont superposées des variations irrégulières à court terme avec des ascensions ou des déclins sur des échelles de temps de quelques semaines à quelques mois. Dans le procédé chaotique appliqué aux irrégulières, les éruptions ("flares") qui sont observées dans ces étoiles, pourraient représenter les variations à plus courtes périodes.

On décrit ensuite *les étoiles carbonées déficientes en hydrogène*, brièvement nommées étoiles HdC. Elles constituent une classe d'étoiles complètement différente des autres étoiles carbonées (des types R et N). Ce sont des supergéantes (M_{bol} = –4 à –6) et leur abondance en hydrogène est déficiente d'un facteur pouvant aller jusqu'à 10^5 ou plus, comparée au rapport solaire H/Fe. Elles ont un excès de carbone (d'un facteur 3 à 10) et d'hélium en comparaison avec le soleil. Elles se partagent en trois sous-classes: les étoiles dites RCB, les étoiles HdC non variables et les étoiles à hélium.

Les étoiles RCB, les plus connues et les plus nombreuses parmi les étoiles HdC, sont pour la plupart des étoiles R caractérisées par des baisses abruptes de brillance suivies par une remontée plus lente, baisses que l'on suppose être dues à une éjection soudaine de matière fortement absorbante. À l'occasion, on les a imaginées progéniteurs de supernovae de type I, de novae, de nébuleuses planétaires, d'étoiles à hélium et de naines blanches! L'étoile prototype est R CrB. Comme dans les autres variables, le type spectral change pendant les variation de brillance. L'échelle de température couverte par toutes les étoiles RCB est tout à fait étendue (des températures des étoiles F aux étoiles R). Bien que les variations dans le spectre et les couleurs de ces étoiles éruptives soient trés complexes, un comportement général est décrit. La perte de masse se continue pendant le maximum de lumière à travers une chromosphère permanente. De nombreux modèles ont été proposés pour donner une illustration cohérente du phénomène RCB. Le modèle de base actuellement accepté est le suivant. Le gaz est éjecté radialement du sommet de cellules convectives au travers d'une partie importante de la surface stellaire et traverse les couches profondes de l'atmosphère. Le gaz s'étend, se refroidit et des particules de graphite se condensent. Les nuages ou les condensations de poussière qui en résultent, s'étendent poussés par la pression de radiation, et obscurcissent la lumière photosphérique permettant de voir les raies étroites d'émission chromosphérique. Quand ces nuages (éjectés à haute vitesse) rencontrent l'enveloppe circumstellaire, de larges raies d'émission apparaissent sur le spectre. La collision a lieu avec un retard de phase de 30 à 70 jours qui permet, également avec l'aide des vitesses radiales des raies circumstellaires, d'estimer la distance de l'enveloppe de grains et de gaz à environ 4 à 8 Unités Astronomiques de l'étoile.

Quelques étoiles RCB ont un excès d'émission infrarouge. Cette émission est de 40% à 60% de la luminosité totale de l'étoile. Une explication possible de cette émission infrarouge est que les particules éjectées sont des particules de Platt de dimensions de 3 à 30 A. De telles particules absorberaient la radiation visible beaucoup mieux que les particules de graphite, mais ne la re-rayonnerait pas dans l'infrarouge. L'émission IR est observée quand les particules grossissent par accrétion jusqu'à des dimensions de 10^{-6} à 10^{-5} cm, ce qui correspond au temps nécessaire à la croissance des particules.

Aprés cette vue générale sur les étoiles RCB, l'accent est mis sur leurs courbes de lumière. Etonnamment, les étoiles RCB sont les seules variables dont l'état normal est la brillance au maximum de lumière. La durée de cet état est variable, jusqu'à atteindre plusieurs années. Il existe aussi des moments où le maximum n'est jamais atteint. La vitesse du déclin (c'est à

dire dm/dt) est aussi variable. Cependant, les déclines sont toujours beaucoup plus abrupts que les montées vers le maximum, bien qu'une même forme de la courbe ne soit pas conservée à chaque minimum. L'amplitude, la fréquence et la durée des minima sont imprévisibles.

Des variations sur différentes échelles de temps sont connues dans les étoiles RCB. D'abord, le fait frappant est le déclin sur plusieurs magnitudes, appelé aussi déclin "d'obscurité", d'une durée imprévisible. Ensuite, il y a des oscillations semi-régulières, appelées oscillations "pulsationnelles", avec une pseudo-période entre 19 et 120 jours. Elles ont une amplitude visible de 0.2 à 0.4 magnitudes. De plus, des oscillations trés courtes, non permanentes, sur des échelles de temps de une à deux heures, sont détectées dans quelques RCB et peuvent alterner avec des phases stellaires calmes. Finalement, une périodicité à long terme (c'est à dire avec une pseudo-période de 1100 jours) apparait dans l'excès IR, généralement dans le filtre *L*, peut-être due à une pulsation naturelle de l'enveloppe de poussière circumstellaire.

Pour finir, le paragraphe sur les étoiles RCB traite de quelques corrélations entre les quantités observées. L'étoile RY Sgr donne de bons exemples de corrélations. Nous notons que le début du déclin "d'obscurité" est autour de la phase 0.8 de la pulsation, qui est une phase stratégique dans les Miras; cette coincidence suggère que le minimum "d'obscurité" est le résultat d'une oscillation pulsationnelle plus forte que les autres. L'indication la plus importante pour comprendre le phénomène RCB pourrait être le fait que, pendant que l'étoile descend vers le minimum profond, l'excès IR n'est pas affecté: on ne note ni changement dans le flux émis par l'enveloppe de poussière, ni changement sur la phase de la courbe *L*. L'enveloppe circumstellaire et l'atmosphère stellaire semblent être déonnectées dynamiquement.

Les étoiles carbonées déficientes en hydrogène sont considérées habituellement comme des *étoiles HdC non variables*. Cependant, cette conclusion pourrait n'être que la conséquence d'observations sur des échelles de temps insuffisamment courtes (l'échelle de temps explorée est la semaine). On doit remarquer que ces étoiles ne possèdent pas un quelconque excès IR et que l'étoile HdC chaude, non variable, HD 182040 n'a pas d'enveloppe, ce qui suggère l'absence d'un phénomène de forte perte de masse; de plus, dans cette étoile, aucune raie d'émission chromosphérique n'est détectée.

Le dernier sous-groupe d'étoiles HdC concerne *les étoiles à hélium*. De façon générale, elles sont aussi considérées comme non variables. Cependant, comme pour les étoiles HdC "non variables", la cause pourrait en être un manque d'observations. En fait, l'exemple de HD 160641 qui a montré une brillance évidente d'environ 0.1 magnitude pendant 7 heures d'observation, démontre que des variations à courte échelle de temps existent dans les étoiles à hélium.

Quelques étoiles apparaissent comme un lien d'évolution entre deux classes d'étoiles, telle MV Sgr avec ses variations de lumière semblables à celles des RCB, et son spectre semblable à celui de l'étoile à hélium HD 124448.

Quelques mots sont dits sur les étoiles "réellement" non variables ou encore normales parmi les étoiles M et S: une preuve des plus valables qu'on a affaire à une étoile M normale, est la non variabilité de la force des bandes d'absorption moléculaires et des raies atomiques, ainsi que des maxima adjacents du flux. Ces étoiles vont des types M0 à M8 avec des classes de luminosité de Iab à III. Quelques étoiles jeunes R sont aussi des étoiles non variables.

Le dernier paragraphe du Chapitre 1 se propose d'étudier *les changements irreversibles et l'évolution rapide* qui se produisent dans les variables rouges. D'abord, on s'attache à considérer les *Miras* à travers l'exemple de l'objet complexe, évolué, *R Agr*, longuement commenté. C'est une étoile binaire qui est formée d'une Mira (M7e) et d'un compagnon bleu

(dont le type n'est pas fermement défini) et qui baigne dans une nébuleuse dense, compacte, à haute excitation. Le tout définit l'objet central spatialement non résolu. Celui-ci est entouré par une nébuleuse en forme de lentille convexe de 2 arc-minutes. Un jet interne avec une structure apparente changeante et des noeuds discrets variables est observé à 10 arc-secondes de l'étoile. L'éventualité d'un contre-jet est à considérer. Les spectres de la nébuleuse la plus interne montrent de remarquables variations temporelles et reflètent une activité continue dans l'objet central.

On donne ensuite des *exemples de changements irréversibles dans les étoiles SR et L.* De nombreuses étoiles des classes M et C montrent des changements rapides et définitifs en une ou plusieurs décades. V1016 Cyg est un système binaire avec une variable à longue période et une étoile chaude qui excite une nébuleuse. L'analyse du spectre UV, riche en raies d'émission, amène à conclure à une éjection soudaine de l'enveloppe et à la formation d'une nébuleuse planétaire de trés grande excitation. L'étoile carbonée HD 59643 est un autre exemple d'évolution irréversible et rapide. L'examen de données spectroscopiques obtenues depuis plusieurs décennies suggère que l'activité de l'étoile est d'origine récente. L'émission UV ne peut pas venir de la photosphère, mais doit émaner d'une enveloppe chaude circumstellaire. Entre 1979 et 1983, les raies UV d'ions de trés différentes ionisations ont variées et le continu de 2200 à 1200 Å a baissé de façon significative. Une autre étoile carbonée, la variable SRb, UU Aur, a vraisemblablement subi une augmentation de la profondeur optique des couches absorbantes situées au minimum de température, qui atténue tous les faits spectraux en absorption venant de couches plus basses et qui laisse l'émission chromosphérique apparaitre.

L'évolution irréversible des différentes étoiles RCB est propre à chaque étoile. On détaille l'évolution d'étoiles choisies. L'étoiles RY Sgr évolue lentement. Elle a le comportement d'une céphéide, à ceciprès qu'une décroissance de la longueur de la période de pulsation (1.1 jour en 80 ans) a été confirmée par plusieurs études. Cependant, il apparait une modulation dans le taux linéaire de changement de la période de pulsation, sur une échelle de temps de 100 à 200 périodes. Ce taux est à rapprocher du taux prédit pour une étoile déficiente en hydrogène de 1 $M_\odot$ et de 6900 K de température effective, qui évoluerait rapidement de l'étape de géante rouge vers celle de naine blanche.

Au contraire de RY Sgr, l'étoile RCB, S Aps, change rapidement de période. Entre 1922 et 1960, la période était de 120 jours. Aprés le minimum "d'obscurité" de 1967, la période de pulsation instantanée passe à 135 jours; ensuite, aprés le déclin d'obscurité suivant de 1971, l'étoile développe de façon surprenante une oscillation de période de pulsation moyenne de 37.5 jours. Lors du maximum de 1979, la période était d'environ 40 jours. Un tel phénomène est-il lié à un changement du mode de pulsation (du mode fondamental à quelque harmonique)? Il n'existe pas de modèle d'évolution d'étoiles déficientes en hydrogène autorisant un tel changement rapide de la période, bien que l'évolution d'une étoile déficiente en hydrogène vers une naine blanche soit rapide. Quelques étoiles RCB qui subissent de tels changements de leur période de pulsation, montrent en plus un amortissement de l'amplitude des variations de la pulsation.

La variabilité des étoiles M, S, et C dont le Chapitre 1 nous a montré l'incidence sur les courbes de lumière en particulier, se manifeste à l'évidence sur les faits spectraux (sur leur intensité, leur forme, leur vitesse radiale). Le *Chapitre 2* a pour principal but *de décrire les faits marquants en relation avec les processus non thermiques.* Pour trois des premiers paragraphes, les raies spectrales sont passées en revue par type de raies, comme un observateur peut les découvrir d'un coup d'oeil sur des spectres de l'ultraviolet à l'infrarouge: nombreuses raies d'absorption, quelquefois des raies d'émission, et aussi des raies d'absorption au

profil P-Cygni ou assymétrique ou aux multiples composantes. Chaque type de raies est le résultat des conditions d'excitation qui règnent dans les couches stellaires où il se forme. Aussi, en fin de chaque paragraphe, on tire des enseignements qualitatifs sur la région de formation des raies—par exemple sur sa structure, sa dynamique—qui pourront servir de contraintes à une modélisation. De façon générale, chacun des paragraphes successifs viendra naturellement compléter les enseignements du précédent.

Parmi les remarques préliminaires, la plus importante pour la compréhension de la dynamique stellaire est la notion de vitesse radiale du centre de masse du système (tirée de raies radio thermiques), vitesse constante par définition et, par conséquent, base de référence des vitesses radiales de raies, c'est à dire du sens des mouvements de matière (en expansion vers le milieu interstellaire ou retombant vers l'étoile).

Les variations, avec la phase, des intensités et des vitesses radiales *des raies d'absorption* qui peuvent être qualifiées de "classiques", c'est à dire formées sans ambiguité dans la photosphère de l'étoile, sont décrites. Les examples les plus abondants concernent les Miras M et S. Le fait le plus frappant est qu'une distinction apparait entre les vitesses radiales des raies atomiques ou moléculaires de faible potentiel d'excitation χ ($\sim$1 eV) et celles de χ élevé ($\sim$2.5 eV ou plus). Les premières ne présentent pas de changements significatifs avec le cycle de lumière, alors que les deuxièmes présentent une courbe discontinue en forme de "S", d'amplitude totale d'environ 25–30 km/s, avec un doublement des raies autour du maximum de lumière. Ce sont là les caractéristiques de l'influence du passage d'une onde de choc à travers les couches de formation des raies du haute excitation. En notant que dans la photosphère des étoiles froides plus le potentiel d'excitation de la raie est élevé, plus sa couche de formation est profonde, ce sont les couches profondes de la photosphère qui sont ainsi perturbées par une pulsation radiale de l'étoile variable. Cette pulsation est liée à des ondes acoustiques qui développent des ondes de choc dès leur émergence dans la photosphère de la Mira. Les raies de faible excitation, aussi bien les raies infrarouges que les raies bleues, ne subissent pas cette influence. On peut dire que les raies de haute excitation appartiennent pleinement à la photosphère de l'étoile (la partie pulsante), alors que les raies de plus faible excitation appartiennent aux couches supérieures de la photosphère ou plutôt à des couches intermédaires vers les couches circumstellaires. En fait, les raies infrarouges de divers potentiel d'excitation révèlent plusieurs couches stellaires ou composantes de l'atmosphère d'une Mira, par exemple pour χ Cygni (à partir de raies IR du CO): (1) la photosphère pulsante dont nous venons de parler, dans laquelle la température d'excitation des raies peut varier de 2200 à 4000 K par le passage du front d'onde de choc, (2) une composante à 1500 K dont la matière tombe sur l'étoile, (3) une couche de vitesse stationnaire (au centre de masse) d'environ 800 K formée rapidement et disparaissant en 3 cycles, (4) une composante avec $T \sim 300$ K appartenant à une couche circumstellaire en expansion. D'autres couches de l'atmosphère peuvent être mises en évidence par l'étude d'autres molécules IR que CO, telles H_2O et OH, et des raies IR atomiques. Par exemple, dans la Mira R Leo, à côté de la photosphère ($3000\ K < T > 4500\ K$) on distingue: (1) une couche de transition photosphère-enveloppe circumstellaire ($T \sim 1700$ K) plus faiblement pulsante que la photosphère, montrant un couplage mécanique plus faible avec la pulsation profonde, (2) une couche à 1100 K dont la variation de vitesses radiales duplique celle d'une couche à 1000 K de 16 km/s d'amplitude totale, à la limite interne de la couche circumstellaire, avec un couplage mécanique encore significatif avec la photosphère. Quant au spectre visible—région bleue-violette à 4000 Å—formé surtout de raies d'absorption de faibles χ, il ne présente pas de changement significatif en vitesses radiales. Dans χ Cygni, sa vitesse radiale moyenne est en

accord avec celle de la couche de CO tombant sur l'étoile: ceci suggère que les raies d'absorption atomiques visibles ne se forment pas dans la photosphère pleinement pulsante, mais au-dessus d'elle. Il devrait y avoir un léger doublement des raies au maximum de lumière; cependant, le continuum au-delà de 6000 Å est tel qu'il empêche d'observer la composante en expansion et donne l'illusion que les couches gazeuses responsables du spectre dans le bleu retombent constamment sur l'étoile. Quelques données sur des Miras de type C montrent que leur photosphère se comporte comme celle des Miras M ou S, sauf que l'amplitude de la courbe des vitesses radiales en fonction de la phase est moins importante (15–20 km/s).

Intéressantes sont les rares observations sur des semi-régulières M et C dont la photosphère présente le même phénomène de pulsation que les Miras, avec cependant des amplitudes plus faibles ($\leqslant$10 km/s).

Le paragraphe se termine par la présentation d'histogrammes de vitesses radiales de raies d'absorption dans des Miras; ils soulèvent le problème de la présence d'un ou deux chocs au même moment dans l'atmosphère de l'étoile pour expliquer les observations.

Les raies d'émission atomiques sont le fait primordial des spectres de Miras M, S, et C autour du maximum de lumière. Il apparait que ces raies, aussi bien dans le visible que dans l'ultraviolet observé par satellite, varient en intensité (jusqu'à disparaître pour certaines autour du minimum de lumière) et en vitesse radiale au cours du cycle. Une sélection de raies d'émission caractéristiques est présentée et leur profil étudié pour des Miras et des semi-régulières. Chaque raie (d'éléments neutres ou ionisés, de fluorescence, etc...) formée dans des conditions physiques particulières apporte sa contribution à la connaissance de la structure de l'atmosphère stellaire.

Dans le cas des Miras, on montre comment les raies d'émission viennent s'insérer dans le modèle d'onde de choc mis clairement en évidence par les raies d'absorption infrarouges et le conforter. Les vitesses radiales des différentes raies d'émission sont un indicateur des vitesses à l'arrière du choc. La question de la présence d'un seul choc au maximum de lumière dans l'atmosphère de l'étoile ou de la présence de deux chocs au même moment (l'un localisé dans la basse photosphère, l'autre dans les couches plus hautes) pour rendre compte de l'excitation des raies d'émission observées et de leur vitesse radiale, pourrait être résolue par l'étude de la structure du front d'onde lui-même et des conditions d'excitation différentes qui y règnent.

Dans le cas des géantes et supergéantes semi-régulières, trois exemples sont commentés. Dans la supergéante M μ Cep, une série d'observations indique que les raies de Balmer se comportent comme dans une Mira, suggérant une onde de choc produite dès les couches les plus basses de la photosphère. D'autres observations à des dates différentes semblent dénier un tel comportement et être expliquées par le développement de chocs seulement quand l'onde atteint les hautes couches de l'atmosphère de l'étoile (il s'agit de la chromosphère de l'étoile), et la théorie de Ulmschneider et de ses collaborateurs s'appliquerait alors. Ce sont ces chocs qui excitent l'émission de raies telles que Mg II h and k ou Fe II autour de 3280 Å. La semi-régulière carbonée TW Hor illustre pleinement ce mécanisme dans lequel l'amortissement radiatif de l'énergie des ondes pendant leur trajet dans la photosphère joue un role prépondérant. Enfin, la supergéante M, α Ori, possède sans ambiguité une chromosphère étendue jusqu'à 1.8 R_* avec une température d'excitation moyenne d'environ 8500 K. Alors que sa photosphère pulsant à la manière d'une Mira, mais avec une amplitude totale faible (~6 km/s) caractéristique des semi-régulières, prouverait le passage d'ondes acoustiques, les raies d'émission seraient excitées par la dissipation de leur énergie sous forme d'ondes de choc au niveau chromosphérique, comme dans les deux exemples précédents, μ Cep et TW Hor. Cependant, le mouvement de lévitation de la matière puis sa retombée dès

l'amortissement de l'onde, dont on s'attend qu'il soit grossièrement régulier dans le temps, est perturbé par la présence d'un compagnon observé à environ 2.5 R_* de l'étoile. En effet, la variation temporelle des vitesses radiales de raies d'émission prouve l'influence de ce compagnon sur les hautes couches chromosphériques: la matière est attirée par un effet de marée et retombe à vitesse supersonique dès que le compagnon n'a plus d'influence sur les couches observées, si bien que les raies d'émission sont vues non seulement dans du gaz en éjection, mais encore dans du gaz retombant sur la surface stellaire. Les vitesses radiales d'une sélection de raies montrent que les mouvements de matière dûs au compagnon ne semblent pas atteindre la couche appelée intermédiaire (au-dessus de la photosphère) par analogie avec les Miras, ni la photosphère elle-même, dans la limite des erreurs de mesure.

Pour conclure sur *la cinématique de l'atmosphère*, un mécanisme de chauffage des couches stellaires commun aux étoiles froides, quelque soit leur type de variabilité, est suggéré par les observations: il s'agit d'ondes acoustiques produites dans la zone convective profonde, qui se transforment en ondes de choc à des niveaux géométriques différents de l'atmosphère de chaque étoile et même à des niveaux variables dans le temps pour une étoile donnée (même les Miras peuvent voir l'amplitude de leurs ondes tellement amortie dans la photosphère que les raies d'émission de l'hydrogène peuvent ne pas être excitées, cas exceptionnel il est vrai). Ces ondes acoustiques sont évidemment responsables de la pulsation de l'étoile avec une amplitude plus ou moins large. La question est posée de comprendre la cause physique qui expliquerait pourquoi, dans les Miras, les ondes se dissipent sous forme de choc en général dès leur entrée dans la photosphère, alors qu'un tel comportement semble exceptionnel dans les semi-régulières. L'amortissement radiatif dans la photosphère joue un rôle, mais il ne semble pas être le seul élément de discrimination.

Les trois derniers paragraphes du Chapitre 2 concernent les enveloppes des étoiles froides. Un paragraphe traite des *raies circumstellaires* (en bref, raies CS) et en conséquence des *propriétés des couches gazeuses circumstellaires*. Les raies CS montrent un profile P-Cygni ou un coeur en absorption déplacé vers le bleu. Leur potentiel d'excitation est bas (<1 eV); ce sont souvent des raies de résonance. La variation dans le temps du profil d'une sélection de raies est présentée, ainsi que leur variation avec les types spectraux et les classes de luminosité. La haute résolution spectrale a permis de détecter dans le coeur des raies CS des composantes multiples. L'étude de ces composantes sont à la base de notre connaissance des couches circumstellaires, en particulier de leur vitesse d'expansion, de leur température, de leur distance. Cependant certaines hypothèses sont en général adoptées dont les plus douteuses sont les suivantes: (1) les vitesses sont en général reliées à une vitesse photosphérique et non à la vitesse du centre de masse de l'étoile, (2) les températures d'excitation ne sont souvent pas des températures cinétiques, puisque les processus radiatifs dominent sur les processus collisionnels, (3) les écarts à l'ETL ne sont pas pris en compte dans la détermination du ces températures, (4) l'interprétation des températures d'excitation des couches en terme de leur distance à l'étoile est entachée d'erreur à cause de l'hypothèse d'équilibre du gaz et de la poussière dans la couche. En gardant ces hypothèses présentes à l'esprit et en se basant sur les étoiles pour lesquelles un ensemble d'observations sur le domaine optique, proche-IR et radio existe—c'est à dire la supergéante α Ori, des Miras dont χ Cyg et aussi la carbonée enveloppée de poussière IRC + 10216, on met en évidence différentes couches qui composent l'enveloppe circumstellaire (couches en expansion). Par exemple, une couche à 200 K qui est aussi bien détectée par des raies atomiques optiques que par des raies CO infrarouges, semble commune à ces étoiles. Pour les Miras, un échantillon probant montre la présence d'une couche stationnaire à 800 K. Dans le cas de χ Cyg couvert par un large nombre d'observations sur plusieurs années, cette couch s'est constituée rapidement pour dispar-

aître doucement en trois cycles: elle est une candidate valable pour être un réservoir de matière à la fois pour la formation de couches plus froides en expansion, sous l'impulsion de la pression de radiation sur les grains de poussière qui pourraient s'y former, et aussi pour la formation de matériel retombant sur la photosphère. La question rests intacte quant à la présence formelle d'une telle couche dans les supergéantes, même pour α Ori. Davantage d'observations sont nécessaires.

La présence de couches multiples pour lesquelles il n'y a pas de corrélation entre leur vitesse d'expansion, la quantité d'hydrogène ou de CO ou de poussière, peut laisser penser que la matière subit des éjections multiples, épisodiques. Cependant, une distribution continue de matière peut aussi produire une telle structure multiple à condition que la vitesse du flux change lentement avec la distance. Le cas d'IRC +10216 présenté à la lumière d'observations récentes, est un exemple.

Dans le courant du paragraphe, sont mentionnées quelques méthodes d'analyse des profils circumstellaires et sont revues les mesures d'extension de l'enveloppe circumstellaire par cartographie directe qui détecte la lumière émise par l'enveloppe dans une raie CS, l'étoile centrale étant occultée. L'étoile-type est α Ori. Des écarts à la symétrie sphérique sont mis en évidence.

L'exploration des enveloppes stellaires se poursuit par l'étude de *la poussière circumstellaire*. Sa détection se fait soit par les mesures d'excès infrarouges, soit par celles de polarisation. En premier lieu est décrite la distribution d'énergie spectrale dans les étoiles M et les étoiles C, ainsi que les signatures des excès d'émission, soit principalement les silicates et le graphite respectivement. Quant à la variabilité temporelle des excès IR, elle n'est pas significative, semblant prouver que la quantité de grains dans les enveloppes circumstellaires ne change pas beaucoup dans le temps. Néanmoins, sur l'exemple de la Mira M, o Cet, l'émission IR et en particulier l'excès à 10 μm sont clairement dépendants de la phase: la poussière est vraisemblablement chauffée cycliquement par les changements périodiques de la luminosité stellaire. Un ensemble d'étoiles M, S, et C de tout type de variabilité et décrivant un large spectre en taux de perte de masse montre que le rapport poussière/gaz est pratiquement constant dans les enveloppes circumstellaires. Ce résultat est en accord avec un mécanisme de perte de masse par pression de radiation sur les grains.

La présence de poussière est aussi détectée par les observations en polarisation optique, la polarisation linéaire intrinsèque est caractérisée par la variabilité dans le temps du pourcentage et de l'angle de polarisation, ainsi que de leur dépendance en longueur d'onde. Quelques corrélations entre la polarisation et d'autres paramètres sont revues. Une remarque importante est qu'il n'y a pas de relation entre la variation de la polarisation et les changements de la courbe de lumière avec la phase, en particulier dans les Miras. Quant au lien avec le flux infrarouge, on conclut que: (1) pour un excès IR donné, une forte ou faible polarisation peut apparaître suivant l'étoile considérée, (2) aucune variation temporelle du flux IR n'est observée dans les étoiles où la polarisation varie beaucoup. La polarisation pourrait produire des effets localisés plutôt que globaux dans des nuages épars de poussière. Il a été trouvé que la lumière bleue dans le continu est linéairement polarisée de 550 à 3300 R_* autour de la supergéante α Ori.

Les propriétés caractéristiques de la polarisation sont décrites sur l'exemple de quelques étoiles spécifiques telles la Mira o Cet, la semi-régulière V Cvn, les supergéantes μ Cep et α Ori, en mettant l'accent sur les observations à bandes étroites. Par exemple, la variation temporelle du pourcentage est liée ou non liée à la variation de l'angle de rotation, la dépendance de la polarisation (du taux et de l'angle) avec la longueur d'onde est complexe,

quelquefois avec une croissance du taux dans certaines raies atomiques ou bandes moléculaires et une décroissance dans d'autres faits spectraux au même moment. Des changements temporels de la polarisation sur des échelles de temps courtes (de l'ordre du mois) ont été détectés dans la majorité des étoiles, indiquant une grande anisotropie prés de l'étoile.

Les interprétations actuelles des faits observés sont ensuite indiquées. La dépendance en longueur d'onde ainsi que les variations dans le temps de l'angle et du pourcentage de polarisation sont considérées comme pouvant être dues à la combinaison de plusieurs mécanismes actifs dans la même étoile, à la condition de la présence concomittante d'une atmosphère assymétrique. Les modèles théoriques expliquent l'origine de la polarisation par les propriétés diffusantes soit de grains circumstellaires distribués assymétriquement et/ou du gaz photosphérique. C'est le mérite des observations à haute résolution d'avoir mis en relief la contribution possible du gaz de la photosphère à la polarisation. Le modèle généralement retenu pour expliquer les variations de la polarisation photosphérique à travers les bandes moléculaires (TiO) ou les raies d'absorption atomiques (Ca I à 4427 Å) est basé sur le fait que la radiation émise sur la ligne de visée prés du limbe stellaire de l'atmosphère en pulsation est polarisée par diffusion Rayleigh. Une augmentation ou une diminution de la polarisation dans les faits spectraux est liée à la profondeur optique à laquelle la diffusion Rayleigh (par hydrogène atomique et moléculaire) domine sur l'absorption (par TiO et H^-). Une polarisation variant à la fois en degré et angle à travers chacune des bandes TiO (par exemple dans μ Cep) suggère, à côté de la diffusion Rayleigh photosphérique, une diffusion de Mie par les grains circumstellaires. Cependant, dans le cas de la Mira o Cet, le haut degré de polarisation continue ne semble pas pouvoir être expliqué par la diffusion de Mie dans une enveloppe assymétrique, car il semble que les écarts à la symétrie sphérique de l'enveloppe ne soient pas suffisants. Un champ magnétique est préféré pour obtenir l'orientation des particules avec un changement systématique dans l'alignement des grains en fonction de la distance à l'étoile conduisant à un changement dans la géométrie de la diffusion. La présence possible de champs magnétiques dans les étoiles froides est revue dans un contexte général. Une autre source d'assymétrie due à l'effet dynamique d'un système binaire est illustrée par la supergéante α Ori.

Le Chapitre 2 se termine par l'examen de la mesure "directe" du *diametre angulaire* des étoiles et/ou de *la cartographie de la distribution de la poussière et du gaz circumstellaire* par occultation lunaire ou par les diverses techniques d'interférométrie. Deux prototypes d'étoiles sont plus particulièrement étudiées: la supergéante M, α Ori, et l'étoile carbonée enveloppée de poussière, IRC +10216.

Au sujet d'α Ori, de nombreuses mesures à différentes longueurs d'onde optiques donnent une estimation du diamètre apparent photosphérique, par exemple à environ 0.037 quand on observe dans le continu à 5350 Å. Les longueurs d'onde infrarouges sont, elles, appropriées à la détermination de l'extension de l'enveloppe circumstellaire; des écarts à la symétrie sphérique sont évidents, comme ils avaient déjà été mentionnés à partir des profils de raies CS obtenus en occultant l'étoile centrale. Bételgeuse (α Ori) est l'étoile pour laquelle la structure des couches circumstellaires proches de sa surface et leur dynamique ont été directement observées: le disque stellaire est accompagné d'un nuage brillant assymétrique, en forme de croissant de lune, situé à 2.5 R_* (soit 0".05) du centre stellaire et large d'environ 1 R_*. De plus, l'image reconstituée de Février 1982 révèle la présence d'un compagnon situé à 0".4 - 0".5 (soit 20–25 R_*) à 80° (modulo 180°) par rapport au Nord, vers l'Est. Un autre compagnon, plus proche de l'étoile (situé à environ 2 R_*, c'est à dire à environ 0".04 en Novembre 1980) aurait une orbite excentrique avec une période d'environ 2.1 ans d'aprés les interprétations de mesures de polarisation. On peut suggérer que le nuage de poussière en

forme de croissant de lune est dû à un effet de marée du compagnon proche. D'aprés la théorie de Draine, des grains de poussière "propres" sont capables de se former trés proche de l'étoile, vraisemblablement dans la basse chromosphère où la température est relativement peu élevée. Ensuite, ils pourraient être éjectés par pression de radiation et être alors responsables de l'émission IR détectée à 45 R_* (0".9) de la photosphère d'α Ori.

Au sujet de l'étoile carbonée poussièreuse, IRC +10216, un résumé des mesures d'extension spatiale de cet objet à diverses longueurs d'onde est présenté. Le nuage de poussière a été détecté jusqu'à un rayon de 1200 R_* (soit 27") autour de l'étoile. Les couches sont assymétriques et leur degré d'assymétrie varie avec la longueur d'onde et le rayon de la couche; des contour elliptiques sont évidents. La région gazeuse (en CO) émet jusqu'à un rayon d'au moins 8000 R_* (soit 3') autour de l'étoile; elle présente une géométrie sphérique. Le mélange de morphologie–un disque à faible inclinaison pour rendre compte de la géométrie des nuages de poussière, plus une sphère–s'expliquerait par la présence d'un compagnon proche, parmi d'autres interprétations. D'autres structures composites observées dans des étoiles C extrêmes, constituées par un tore équatorial poussiéreux et des lobes polaires diffusant la lumière, pourraient être un lien évolutif avec les nébuleuses bipolaires.

Complétant la description des faits observés commencée dans les chapitres précédents, le *Chapitre 3* traite des *raies radio moléculaires* qui sont des raies circumstellaires. En fait, les enveloppes étendues des étoiles froides rouges (les étoiles identifiées dans le domaine visible comme celles qui n'ont pas de contre-partie visible) émettent aussi des raies d'émission moléculaires aux longueurs d'onde centimétriques et millimétriques. Des transitions moléculaires appropriées qui ont lieu à différents rayons stellaires (des masers SiO dans les couches proches de l'étoile, aux émissions du CO thermique ou des cyanopolynes dans les couches circumstellaires lointaines) peuvent échantillonner les diverses couches et servir de révélateur de leurs conditions physiques.

Les premières détections radio de *molécules circumstellaires* conduisirent à la découverte de raies masers OH et H_2O dans des étoiles des derniers types riches en oxygène, principalement des Miras et des supergéantes rouges. On donne une liste des molécules circumstellaires connues de nos jours dans les étoiles froides (environ une soixantaine). Leurs raies sont caractérisées par des largeurs importantes qui reflètent l'expansion à grande échelle de l'enveloppe (d'environ 5 à 50 km s^{-1}).

Les émissions radio de OH, H_2O, SiO, et SiS présentent des caractéristiques de processus non thermiques. Les masers sont des sources variables dont les intensités sont corrélées avec celles observées dans le proche infrarouge. Ils ont un haut degré de polarisation (par exemple OH, SiO). Une inversion de population peut être obtenue par un pompage par la radiation infrarouge, de grains de poussière circumstellaires "tièdes" ou de l'étoile centrale. Des détails sur les mécanismes de pompage sont donnés dans la théorie simplifiée d'un maser à deux niveaux et dans la théorie du transfert radiatif pour un maser à plusieurs niveaux.

Ensuite sont définies les caractéristiques des masers circumstellaires. L'émission maser est souvent caractérisée par un spectre à double pic (par exemple OH). Cette forme peut s'expliquer par un modèle sphérique dans lequel le parcours d'amplification est maximum dans la direction de la ligne de visée. On montre des exemples de spectres de masers et on discute le pompage approprié à un maser donné.

L'émission thermique par SiO, CO, CN, et CS et leurs isotopes est détectée dans les étoiles M, S, et C. Il existe aussi des molécules à chaîne carbonée linéaire (HNC, HCN, $HC_{2n+1}N$, etc.) dans les enveloppes stellaires riches en carbone. Les spectres d'émission

thermique s'étendent sur l'enveloppe entière et donnent des informations sur ses paramètres physiques (perte de masse, densités de gaz et de poussière, etc.). L'excitation moléculaire met en jeu des processus collisionnels et radiatifs. Les collisions, essentiellement avec H_2, tendent à thermaliser les raies. Les différents *profils de raie* (rectangulaires, paraboliques, à pics doubles, etc.) s'expliquent en relation avec la nature de l'enveloppe circumstellaire (optiquement épaisse ou mince, résolue ou non résolue, etc.). Une *asymétrie des raies* est observée (l'aile déplacée vers le bleu est plus faible que l'aile déplacée vers le rouge): comme l'enveloppe la plus interne est davantage excitée et plus chaude que l'enveloppe plus externe, il en résulte que, le long de la ligne de visée, dans l'hémisphère frontal la matière extérieure froide absorbe la radiation émise par les couches internes plus chaudes, alors qu'une telle absorption n'affecte pas l'hémisphère arrière. Dans ce cas, la température de brillance de la source doit être calculée séparément pour l'hémisphère frontale et pour l'hémisphère arrière.

Des variations temporelles de la lumière infrarouge influencent aussi la forme des raies moléculaires masers. Au maximum de la courbe de lumière infrarouge, les photons IR qui s'échappent de la source de chaleur centrale agissent sur l'enveloppe externe et font élargir les ailes des raies.

Les conclusions du Chapitre 3 soulignent combien les raies radio moléculaires sont utiles pour sonder l'environnement stellaire, du voisinage immédiat de la photosphère stellaire aux enveloppes externes.

Comme un chapitre précédent (Chapitre 2) le montre, l'astronomie infrarouge établit la présence indubitable de poussières autour d'un grand nombre de géantes et supergéantes rouges. Le *Chapitre 4* détaille *la formation de grains et le transfert radiatif dans les enveloppes circumstellaires*.

En ce qui concerne *la formation des grains*, le formalisme généralement adopté dans la littérature est la théorie de la *nucléation homogène*. On en rappelle les idées de base et les résultats principaux. On donne les définitions de quantités importantes comme le rayon critique du noyau, le taux de nucléation et le rapport de supersaturation. Comme le gaz circumstellaire est un mélange complexe où de nombreuses espèces sont capables de se condenser et où des nuages de toutes sortes peuvent agir comme noyaux de condensation pour d'autres matériaux, la nucléation hétérogène est mentionnée et un exemple évoqué.

Les équations de la théorie de nucléation homogène impliquent l'équilibre thermodynamique dans lequel gaz, nuages et grains ont la même température. Dans les enveloppes circumstellaires, la présence d'une *forte radiation stellaire* et d'une densité gazeuse basse sont des contraintes à la théorie. Ses principes sont décrits. Le cas particulier de l'influence d'une chromosphère sur l'existence et la condensation des grains (en particulier les silicates propres) est soulevé.

La structure amorphe ou cristalline des grains circumstellaires peut-elle être prédite par la théorie de nucléation et de croissance? La structure des nuages contenant de quelques atomes à plusieurs dizaines d'atomes n'est pas connue. Les arguments en faveur de graphite amorphe ou cristallin dans les étoiles froides carbonées sont analysés.

Le problème de la formation des grains ne peut être résolu que si la densité et la température du gaz, la composition et la température des nuages sont connues en chaque point de l'enveloppe et à chaque moment. *Une nucléation et une croissance dependant du temps* sont nécessaires. C'est l'échelle de temps de saturation qui gouverne la situation. Des scénarios de l'évolution dynamique de l'enveloppe influencée par la pression de radiation sur les grains sont présentés.

Les conclusions du paragraphe sur la formation des grains mettent l'accent sur les déficiences de la théorie de nucléation homogène appliquée aux enveloppes circumstellaires

réelles: (1) incertitudes sur les paramètres physiques des solides et sur la croissance des grains dans un gaz en expansion; (2) hypothèse erronée de l'équilibre thermodynamique dans un gaz contenant un grand nombre d'espèces capables de se condenser ou de se déposer sur d'autres grains; (3) possibilités de condensations locales ou de fortes variations en densité permettant à la nucléation de commencer, alors que la densité moyenne semblait trop basse; (4) température des grains liée à un rayon stellaire photosphérique bien défini et à la radiation du corps noir à la température effective de l'étoile, bien qu'il soit connu que la radiation à différentes longueurs d'onde ne vienne pas des mêmes niveaux photosphériques.

Le paragraphe suivant du Chapitre 4 concerne *le transfert radiatif dans les enveloppes de poussière circumstellaires* qui est en général traité indépendamment de la formation des grains.

La résolution de l'équation de transfert dans une enveloppe sphérique (atmosphère étendue) tente de décrire correctement le champ de radiation en chaque point de l'enveloppe. Pour définir un modèle, il est nécessaire de fixer les caractéristiques stellaires (température effective, rayon), la géométrie de l'enveloppe (rayon interne et rayon externe, densité) et les propriétés des grains (dimension, propriétés optiques). Les limites de l'enveloppe sont plus particulièrement discutées. Le modèle de grains utilisé est la source principale d'incertitude. Par exemple, les propriétés optiques des grains de graphite qui entrent dans les modèles d'enveloppes d'étoiles carbonées, ne sont pas toujours correctement décrites.

Avant de considérer la construction de modèles pour différents types d'étoiles, on rappelle des résultats généraux. (1) La loi d'extinction circumstellaire n'a pas la forme de la loi d'extinction interstellaire aux longueurs d'onde où la diffusion est efficace. (2) On note l'existence théorique d'un maximum étroit du flux d'énergie dans la direction de la frontière interne de l'enveloppe. Cet anneau brillant correspond au maximum d'abondance des grains qui est atteint quand le paramètre d'impact est égal au rayon interne de l'enveloppe. Si l'anneau était détecté par les mesures à haute résolution angulaire, la limite interne de l'enveloppe pourrait être fixée et l'équilibre radiatif des grains mieux compris.

Différents modèles d'enveloppes d'étoiles oxygénées sont passés en revue. Parmi eux, un modèle, largement utilisé par la suite, implique les silicates "sales" pour rendre compte de la courbe de flux théorique et du profil des bandes d'émission entre 0.25 et 8 μm; d'autres modèles étudient le profil de la bande à 10 μm dans un ensemble de géantes et de supergéantes et montrent la possibilité d'une augmentation du rayon des grains avec la latitude galactique, alors qu'une grille étendue de modèles d'enveloppes sphériques en expansion (avec de petits grains de silicates et une densité en r^{-2}) conduit, dans la plupart des cas, à une température des grains les plus internes supérieure à 1000 K. Quelques autres modèles sont développés pour un objet particulier, comme α Ori. On présente ensuite des modèles d'enveloppes d'étoiles carbonées dans lesquels les grains introduits sont des grains de graphite. Une bonne représentation de la courbe de flux est obtenue avec une enveloppe sphérique en expansion et de petits grains de graphite; les grains les plus chauds sont à 1000–1300 K. Quelques modèles qui tentent de rendre compte de l'étoile particulière carbonée, IRC +10216, sont résumés.

Finalement, les *enveloppes non sphériques* sont discutées; elles sont nécessaires, comme il est mentionné dans le Chapitre 2, pour interpréter les taux de polarisation intrinsèque des étoiles. Le traitement complet du transfert de la radiation stellaire diffusée dans une enveloppe ellipsoïdale a été fait sans approximation. La simulation numérique souligne plusieurs ponts. (1) Une enveloppe à densité constante ne peut pas produire un taux de polarisation supérieur à 12 pour-cent. (2) Même si l'opacité est modifiée, la rotation de 90° de l'angle

de polarisation à une longueur d'onde fixée est maintenue. En fait, il s'agit d'une propriété individuelle des grains. La rotation disparaît quand les grains sont de forts absorbants, comme le graphite. (3) On ne peut obtenir des taux importants de polarisation et la variation abrupte observée de l'angle de polarisation que si la lumière stellaire directe est atténuée le long du plan équatorial et diffusée principalement prés des régions polaires de l'enveloppe (on parle de modèle de nébuleuse bipolaire).

Quant aux mécanismes physiques responsables de la perte de symétrie sphérique, on invoque le plus souvent la rotation et les champs magnétiques. Cependant, la forme de l'enveloppe peut aussi être en rapport avec les processus qui induisent l'éjection de matière à la surface stellaire.

L'importance de l'hypothèse de sphéricité sur plusieurs quantités physiques est évaluée en traitant le transfert de la radiation infrarouge émise dans une enveloppe ellipsoïdale, dans le cas de densité constante. De plus, des simulations numériques ont montré que la répartition spatiale du flux est trés asymétrique à chaque longueur d'onde quand l'opacité est faible.

Dans le futur proche, le problème du transfert devrait être fortement lié à l'étude de l'évolution dynamique de l'enveloppe.

La perte de masse, discutée en détail au *Chapitre 5*, a été remarquée il y a un demi-siècle, mais le développement de ce domaine dut attendre des instrumentations plus modernes; et la quasi-totalité de nos connaissances sur la perte de masse et ses conséquences pour l'évolution stellaire et la pollution interstellaire, s'est mise en place seulement au cours de la dernière décennie. Une vue d'ensemble générale du développement historique des idées, aussi bien de celles liées à l'observation que de celles basées sur la théorie et concernant la perte de masse stellaire, constitue la base de notre compréhension actuelle du phénomène. La nouveauté du domaine, et le caractère très incomplet des modèles théoriques actuellement disponibles de la perte de masse, sont ainsi mis en évidence d'une façon très naturelle.

Des déterminations empiriques des taux de pertes de masse, déduites des spectres du domaine de 0.2 à 5 microns, pour différents types d'étoiles, sont ensuite considérées dans leurs détails. Les spectres eux-mêmes sont d'abord décrits, et nous somme conduits, pas à pas, dans l'analyse des raies pour en déduire la densité columnique et les vitesses d'expansion. Les incertitudes considérables liées aux calculs de l'équilibre d'ionisation nécessaires pour obtenir la densité columnique des atomes d'un élément particulier sont discutées, et les contradictions sévères entre les résultats obtenus, par différents auteurs, et pour différents éléments, sont mis en évidence.

Le taux de perte de masse dépend bien entendue de la densité, du carré du rayon, et de la vitesse. Si la densité décroît vers l'extérieur comme l'inverse du carré de la distance, la perte de masse dépend directement de la densité columnique, de la vitesse terminale, et du rayon intérieur de l'enveloppe circumstellaire.

Les difficultés bien connues rencontrées dans la déduction du rayon intérieur de l'enveloppe circumstellaire, sont décrites, ainsi que le sont aussi les méthodes utilisées par les différents chercheurs et les résultats obtenus. Les estimations conduisent à des résultats raisonnables dans le cas de quelques étoiles, et à des résultats médiocres pour d'autres. Reste la question naturellement plus sérieuse, qui est de savoir s'il y a généralement un rayon intérieur bien défini pour l'enveloppe circumstellaire dans toutes les étoiles. Dans l'étoile α Ori, par exemple, il y a au moins deux enveloppes bien définies. Dans de nombreuses étoiles, il est clair que la perte de masse a un caractère épisodique, ce qui rend tout-à-fait incertain tout effort pour déduire des observations, la perte de masse sous la forme d'un processus supposé stationnaire. Au moins quelques-unes des incertitudes rencontrées dans l'estimation

du rayon intérieur de l'enveloppe circumstellaire, peuvent être évitées, en principe, grâce à l'observation de systèmes binaires; de nombreux systèmes bien connus ont été étudiés de cette façon, notamment les systèmes du type ζ Aurigae.

De nombreuses idées nouvelles sont issues de l'étude *des variables de type Mira* au cours de leur cycle de variation. En particulier, quatre régions circumstellaires séparées ont pu être observées dans l'étoile Mira (de type S) χ Cyg: (1) une photosphère en pulsation, (2) un gaz froid (1500 K) retombant sur la photosphère, (3) une région stagnante encore plus froide (800 K), et (4) un gaz très froid (350 K) en mouvement vers l'extérieur, l'enveloppe circumstellaire elle-même. La même structure semble avoir été trouvée aussi dans la cas d'autres étoiles de type Mira. Ces observations complètent et amplifient les observations qui indiquent une enveloppe semblable, stationnaire dans α Ori, ce qui suggère un mécanisme de perte de masse commun aux Mira et aux supergéantes. La région stationnaire, vraisemblablement soutenue par la dissipation de l'énergie d'un choc, constitue en réservoir de matière pour la formation de grains (les calculs montrent que les grains pourraient se former là), et pour la matière que l'on observe en chute vers l'étoile.

Il est maintenant bien connu qu'une perte de masse de 0.2 masse solaire sur la branche des géantes rouges, et une autre de 0.1 masse solaire sur la branche asymptotique des géantes, sont nécessaires pour que la distribution calculée des étoiles sur le diagramme HR soit en accord avec les observations menées dans les amas globulaires. La présence de la raie Hα dans le spectre des géantes rouges des amas globulaires, a été considérée comme l'indication de l'existence d'une perte de masse, et de nombreux calculs de perte de masse, basés sur l'idée que cette émission provient d'une enveloppe circumstellaire, ont été menés. Il est cependant encore douteux que l'émission en Hα vienne nécessairement d'une enveloppe circumstellaire, ou exige nécessairement une perte de masse.

La fréquence d'un excès d'émission à 10 microns dans les étoiles riches en hydrogène, et à 11 microns dans les étoiles riches en carbone, est comprise de façon générale en l'attribuant à la température de la poussière (par conséquent à sa distance à l'étoile, si elle est en équilibre thermique), à sa profondeur optique et à sa composition. Ces trois paramètres ne peuvent pas être déterminés de façon unique et quelques hypothèses sont faites d'habitude en ce qui concerne la composition des grains, ou la profondeur optique. Une région spectrale plus favorable pour ce genre d'étude est le domaine submillimétrique, où la poussière devient optiquement mince, et où le rayonnement se forme dans la portion Rayleigh-Jeans du spectre. Les observations dans ce domaine en sont juste à leur commencement.

Des observations de profils de raies moléculaires, notamment d'oxyde de carbone CO dans les domaine millimétrique, apportent une information complémentaire et plusieurs études de telles données sont décrites. Il est tenu compte des écarts par rapport à l'équilibre thermodynamique local (ETL). Les modèles supposent que la perte de masse est provoquée par la pression de radiation dans une géométrie à symétrie sphérique. Ces études relativement sophistiquées ont quelquefois été combinées avec l'information issue d'autres régions spectrales.

Dans les étoiles infrarouges OH (OH-IR), comportant des enveloppes poussiéreuses épaisses, les équations usuelles prennent des formes nettement plus simples et les taux de perte de masse pour ces objets sont déterminés avec une bonne précision, au-moins dans quelques cas. L' un des développements les plus intéressants au cours des récentes années est la découverte des liens entre les étoiles de type Mira, et les étoiles OH-IR, et l'indication qu'il s'agit d'une séquence évolutive conduisant à la formation de nébuleuses planétaires.

Une table des taux de pertes de masse, pour des étoiles choisies de tous les types, est ensuite donnée et discutée; on espère que ceci constituera une liste de références commodes

pour tous les chercheurs travaillant dans ce domaine. On notera que: (1) parmi les étoiles de type M les moins froides, le taux de perte de masse pour les supergéantes excède d'un ordre de grandeur celui correspondant aux géantes; (2) les taux de perte de masse pour les nébuleuses planétaires et les étoiles Mira sont comparables à ceux affectant les supergéantes chaudes; (3) les étoiles M et S montrent une dispersion beaucoup plus large dans leur vitesse d'expansion que ne le font les étoiles carbonées C.

Des arguments continuent à s'accumuler en faveur du caractère épisodique de la perte de masse d'au moins quelques étoiles; des cas nombreux sont examinés. Une fois de plus α Ori est l'exemple le mieux connu.

De nombreux mécanismes ont été proposés pour rendre compte de la perte de masse; il semble improbable qu'un seul mécanisme puisse suffire à rendre compte de la perte de masse pour toutes les étoiles. Les mécanismes usuels d'une perte de masse stationnaire sont passés en revue: pression thermique gazeuse (qui semble être trop faible pour les étoiles froides en général), pression de radiation sur les grains de poussière, onde de choc (particulièrement dans les étoiles de type Mira), et onde d'Alfvén. Un flot entraîné par la poussière est la solution la plas populaire, et a été aussi la plus intensément étudiée et appliquée. Les traitements de plus en plus élaborés de ce mécanisme sont décrits. Quelques auteurs ont commencé en utilisant la région stationnaire découverte par l'observation des étoiles de type Mira, pour le calcul de la formation des grains, et sa position comme une valeur initiale de la distance à partir de laquelle le gaz est poussé vers l'extérieur par la pression de radiation sur les grains, et le transfert de moment au gaz qui s'en suit. Les résultats que l'on trouve dépendent fortement du modèle, et les modèles les plus élaborés tendent à donner les taux les plus bas de perte de masse.

Souvent l'hypothèse à été faite que *toute* la perte de masse trouvait son origine dans la pression de radiation excercée sur les grains; ceci est pourtant loin d'être prouvé. Des arguments maintenant disponibles indiquent que ce mécanisme est presque certainement responsable de la perte de masse dans les géantes les plus froides de type M et S et dans les supergéantes, y compris les étoiles de type Mira; mais ceci n'est pas prouvé, et semble quelque peu douteux dans le cas des supergéantes les plus chaudes de type M et des étoiles carbonées. Les ondes de choc ont attiré une attention considérable comme l'un des processus susceptibles de déclencher une perte de masse dans les étoiles de type Mira. Il semble qu'une combinaison de chocs (isotherme, et adiabatique) puisse jouer un rôle essentiel, au-moins en soutenant l'atmosphère et peut-être même en provoquant la perte de masse elle-même, au-moins jusqu'à la distance de formation des grains. Les ondes de Alfvén ont reçu une attention relativement moindre, bien que quelques auteurs aient attiré l'attention sur de nombreux aspects très séduisants de cette théorie. Certainement ils peuvent soutenir par chauffage des atmosphères étendues. Qu'ils puissent apporter une énergie suffisante pour soutenir l'atmosphère sans provoquer simultanément l'émission d'une quantité de rayonnement beaucoup plus grande que ne l'indiquent les observations, cela semble pour l'instant assez incertain.

Plusieurs mécanismes de perte de masse épisodique sont aussi passés en revue; mais ce domaine est beaucoup moins bien développé que celui de le perte de masse stationnaire.

Ce chapitre se termine par une discussion *des conséquences évolutives de la perte de masse*. Quatre aspects sont passés en revue: (1) l'évolution et la fréquence des supernovae, (2) le diagramme HR des amas globulaires, (3) la composition de la matière interstellaire, et (4) la formation des nébuleuses planétaires.

La chimie circumstellaire décrite dans le *Chapitre 6* est un domaine nouveau et très actif de l'astrophysique. En fait, ceci est l'une des premières études d'ensemble du progrès

accompli dans ce domaine. En liaison étroite avec l'étude des nuages moléculaires interstellaires, la chimie circumstellaire traite des réactions moléculaires atomiques se produisant dans la matière expulsée par l'étoile, qui forme une enveloppe circumstellaire étendue et en expansion. Il est à noter que les enveloppes circumstellaires, sont à bien des égards, plus faciles à traiter que les nuages moléculaires interstellaires, et quelque compréhension de ce dernier problème peut donc être acquise par l'étude des enveloppes circumstellaires.

Après une introduction à l'histoire brève de la recherche sur la chimie circumstellaire, des considérations générales sont données sur *les domaines de température, de vitesse, de dimensions, de densité* pertinentes à l'étude de la chimie circumstellaire. Les vitesses des vents sont basses, +10 km/s, les dimensions sont grandes, jusqu'à 10^{18} cm par rapport au rayon stellaire, et les taux de perte de masse sont substantiels (10^{-7} à 10^{-4} masse solaire/an). A cette distance, les densités vont de 10^{6} cm^{-3} à 10^{2} cm^{-3}. Puisque ces valeurs sont si profondément différentes de celles qui caractérisent les photosphères et les chromosphères des étoiles en considération, il est clair que la matière doit passer par un grand intervalle de conditions physiques dans son mouvement de la photosphère à l'enveloppe circumstellaire. En conséquence, nous devons nous attendre à ce que différents processus physiques l'emportent à différentes distances de l'étoile. Bien que les processus thermiques puissent dominer au voisinage de l'étoile (et il y a quelque bons arguments en faveur de cette conclusion), la matière doit s'éloigner des conditions d'équilibre à mesure que la densité s'effondre à une certaine distance de l'étoile; d'autres processus peuvent devenir alors importants. La photodissociation et la photoionisation dues au rayonnement galactique ultraviolet doivent l'emporter dans les confins de l'enveloppe circumstellaire.

Comme c'est naturel dans un nouveau domaine, ce sont *les observations* qui montrent le chemin. Comme peut-être dans aucun autre domaine, la chimie stellaire profite d'une façon vitale de l'information déduite de l'étude de chaque région spectrale. Les observations, d'une extrémité du spectre à l'autre, ont pourtant été faites seulement pour un très petit nombre d'objets, et il vaut mieux en discuter individuellement, tout spécialement puisqu'il n'y a pas de preuve que ces objets proches et bien observés soient typiques, en tant que groupe cohérent d'objets, des enveloppes circumstellaires.

Bien que l'hydrogène soit l'élément le plus abondant, il n'a pas été détecté, ni sous la forme neutre, ni sous la forme moléculaire dans une enveloppe circumstellaire entourant une étoile centrale froide. La sensibilité des limites supérieures est tout juste suffisante pour permettre d'envisager l'étude astrophysique d'un ou deux objets. Dans IRC +10216, la limite de l'abondance fractionnelle de l'hydrogène atomique, déterminée par l'absence de la raie à 21 cm, commence à avoir une certaine influence sur les prédictions théoriques. Dans α Ori, la limite supérieure au taux de perte de masse, impliquée par l'absence d'un rayonnement à 21 cm, est proche du taux de perte de masse total prédit par quelques uns des modèles. L'hydrogène est naturellement observé dans les nébuleuses planétaires, et ces objets constituent une condition limite utile pour les recherches concernant la matière circumstellaire.

Un grand intérêt s'attache aux observations des molécules contenant du carbone, de l'azote et de l'oxygène dans les enveloppes circumstellaires, mais les observations sont très ponctuelles, sauf peut-être pour un ou deux objets. Est particulièrement bien étudié l'objet IRC +10216, où plus de 20 molécules ont été détectées. Des tables d'abondance sont disponibles, et l'on en donne dans ce chapitre un résumé; mais elles sont incertaines par un facteur de l'ordre de 3, même dans les meilleurs cas, en raison des difficultés de l'interprétation d'une observation donnée. L'accroissement significatif de la molécule HCN par rapport à ce qui se passe dans les nuages moléculaires et la grande abondance de radicaux tels que CN et C_2H, posent d'intéressants problèmes et donnent des indices significatifs.

Dans les enveloppes circumstellaires d'étoiles M et S, les observations les plus intensives ont été celles des raies de OH, H_2O, et SiO susceptibles de provoquer un effet maser. L'interprétation de ces observations concerne seulement en partie la chimie circumstellaire. Alors qu'il n'y a pas de contrepartie à l'objet 10216 pour les étoiles M, les molécules CO, H_2O, SiO, OH, et NH_3 sont observées dans quelques sources. Des observations étendues de K I, à de grandes distances de l'étoile α Ori, ont permis dans certaines mesures une modélisation, comme il est décrit dans le Chapitre 6.

Des idées très valables sur les processus impliqués dans les enveloppes circumstellaires peuvent être déduites de la comparaison entre les échelles de temps dynamiques, et celles caractérisant les processus radiatifs, les réactions chimiques ordinaires, et les collisions à 3 corps. Il semble clair que, sauf au voisinage immédiat de l'étoile, ces processus peuvent l'emporter sur les conditions d'équilibre. Dans les régions extérieures de l'enveloppe, c'est la photochimie qui l'emporte.

Deux modèles de chimie circumstellaire ont généralement été appliqués: *l'équilibre thermique et la photochimie.* L'équilibre thermique est appliquable seulement au voisinage de l'étoile, et semble décrire de façon adéquate (à un facteur 2 à 5 près) l'abondance de molécules aussi simples que CO, C_2H_2, HCN, et CH_4. Le modèle échoue dans le cas de NH_3 qui est observé comme surabondant, par un très grand facteur. SiS et SiO sont observés comme sous-abondants, peut-être parce qu'ils sont incorporés dans les grains de poussière. Tous les radicaux sont surabondants par de grands facteurs, les cas les pires étant ceux de CN et de C_2H. Même les succès apparents des modèles en équilibre thermique, doivent être considérés avec quelque réserve, puisque la formation de poussières n'y a pas encore été incluse. Les réactions chimiques, influençant aussi bien les atmosphères riches en oxygène que les atmosphères riches en carbone, sont discutées. Bien que des solutions soient disponibles pour les atmosphères riches en oxygène, aucune ne convient encore pour les atmosphères riches en carbone.

Des chocs sont observés dans les étoiles variables de type Mira, et peuvent être importants aussi dans d'autres types d'étoiles variables. Généralement, ils ont été discutés comme une source d'énergie et de moment dans le processus de perte de masse. Mais cependant ils causent aussi une excitation supplémentaire, et pourraient bien avoir une certaine importance dans le diagnostic des régions qui en sont affectées.

La photochimie peut être importante partout dans le nuage circumstellaire, car si le rayonnement ultraviolet de la chromosphère peut être une source voisine de l'étoile, le champ de rayonnement galactique sera en revanche important à grande distance. L'attention, jusqu'à présent, a surtout été apportée aux molécules abondantes H_2 et CO, et à la formation de radicaux lourds à partir des molécules parentes correspondantes. Les modèles photochimiques démontrent cependant que les molécules ne peuvent plus survivre dans les portions extérieures des enveloppes circumstellaires. Ceci est en contradiction avec ce qui se passe pour les grains qui peuvent parfaitement survivre au voyage à travers l'enveloppe circumstellaire.

Les observations remarquables des étoiles géantes rouges décrites dans les chapitres précédents sont un défi à l'imagination du plus audacieux des constructeurs de modèle d'atmosphère. Pourtant, dans le *Chapitre 7*, l'on discute *les modèles* beaucoup plus simples, *thermiques, et statiques.*

Les principes physiques des atmosphères stellaires classiques sont rassemblés et décrits: l'équilibre hydrostatique, dans une géométrie plan-parallèle et horizontalement homogène. Des généralisations possibles de ces modèles sont envisagées, bien que l'addition d'une con-

vection dans le cadre de la théorie de la longueur de mélange et de la géométrie sphérique soient les seules généralisations probables dans un avenir proche.

En liaison avec une discussion de l'opacité des atmosphères des géantes rouges, on décrit spécialement les effets des raies spectrales. Toute raie spectrale, indépendamment de son mode de formation, ou de la situation dans le spectre, ou de la région de formation, bloque le rayonnement, et ce phénomène est appelé le "bloquage" dans les raies (line blocking). Puisque nous exigeons que le flux d'énergie soit conservé à chaque profondeur, l'énergie bloquée dans la raie doit apparaître dans quelque autre partie du spectre. Transporter ces flux supplémentaires à travers l'atmosphère exige un gradiant de température légèrement plus rapide et cette modification est appelée l'effet de "serre" (backwarming). Que la raie refroidisse ou chauffe les régions extérieures de l'atmosphère est discuté à la fois à partir d'une intuition physique et d'un traitement mathématique, en tenant compte des écarts par rapport à l'équilibre thermodynamique et de l'effet des mécanismes divers de formation des raies.

Dans les étoiles les plus chaudes, les raies spectrales, relativement peu nombreuses, peuvent être traitées individuellement, alors que dans les géantes rouges, des millions de raies spectrales doivent être traitées collectivement ou statistiquement. Les méthodes statistiques de traitement de cette forêt de raies sont décrites, depuis les méthodes relativement grossières, telle la moyenne linéaire ou la moyenne harmonique utilisée pour le calcul des opacités, jusqu'aux méthodes modernes les plus puissantes, telles que celles utilisant une fonction de distribution de l'opacité ou un échantillonnage d'opacité. Après une revue rapide de chacune de ces méthodes, y compris la méthode VAEBM (un développement de la méthode de fonction de distribution des opacités), les avantages et désavantages relatifs de chacune de ces méthodes sont décrits. Une fois qu'une fonction de distribution de l'opacité est construite, des modèles sont obtenus rapidement. Cependant, la fonction de distribution des opacités doit être calculée à nouveau pour chaque changement important des paramètres du modèle. Cette méthode est donc particulièrement bonne lorsque l'on dispose de grilles de modèles pour lesquels tous les paramètres du modèle sont connus dès le départ. Par contraste, puisque la méthode de l'échantillonnage d'opacité n'utilise pas de moyenne des opacités, de quelque nature que ce soit, elle est tout à fait flexible et peut facilement prendre en compte toutes les modifications jugées désirables des paramètres initiaux. Cette flexibilité signifie cependant que le calcul de chaque modèle est relativement lent. Un travail récent fait par le groupe suédois, et qui permet de combiner les fonctions de distribution des opacités pour différentes molécules, résout avec précision et rapidité une difficulté majeure de la fonction de distribution des opacités. Nous admettons à priori que les deux méthodes sont capables de développements ultérieurs, et nous prévoyons que le calcul de grilles d'atmosphères prenant en compte beaucoup d'opacités moléculaires nouvelles, et des millions de raies supplémentaires, sera un développement important dans l'avenir.

Les modèles publies pour les étoiles géantes rouges sont présentés, et discutés en deux catégories, les étoiles riches en oxygène et les étoiles riches en carbone. Les modèles BEGN largement utilisés sont discutés dans la mesure où les étoiles les plus froides sont concernées par ces modèles. Basée sur une fonction de distribution des opacités des molécules CO, CN, CH, NH, OH, MgH et des raies atomiques, la grille couvrait le domaine, en température effective, de 3750–6000 K, en log g de 0.75–3.00, et, en abondances métalliques, de la valeur solaire à 1% de cette valeur. La convection est prise en compte. En tant que fonction de distribution des opacités simplifiées, Tsuji a introduit la méthode VAEBM et l'a utilisée pour calculer une grille de modèle d'étoiles rouges supergéantes. Ces modèles ont été alors utilisés pour une discussion de l'étoile Bételgeuse. Un jeu de 22 modèles a été ensuite calculé pour

des géantes rouges. Tsuji a trouvé que la distribution du flux prédite par lui dans l'infrarouge suffit à représenter les données photométriques et spectrophotométriques disponibles des géantes K et M assez bien pour qu'une calibration de l'échelle de température de ces étoiles soit possible. Ultérieurement, afin de mieux exploiter les modèles, Tsuji les a utilisés avec la photométrie dans la bande L de 22 étoiles géantes de type K et M, pour en déterminer la température effective par la méthode de la photométrie infrarouge.

Sur la base d'un programme d'ordinateur ATLAS 5 et d'opacités OS pour un grand nombre de molécules, mais en traitant la molécule H_2O en utilisant les opacités SM, le groupe de l'Indiana a calculé 40 modèles, pour des étoiles géantes rouges et supergéantes rouges. On peut être rassuré par l'accord de bonne qualité entre les modèles issus des trois groupes.

Pour des modèles d'étoiles carboneés, nous commencerons avec les modèles obtenus par le groupe français. Sur la base des fonctions de distribution de l'opacité, ce groupe calcule un total de 35 modèles, avec des compositions différentes, de façon à inclure à la fois les processus d'élaboration des éléments selon le cycle CNO, selon les réactions du type triple-alpha. Ces modèles n'ont été utilisés qu'avec un succès modéré, dans la déduction de la température effective et des abondances de carbone et d'azote, dans le cas des étoiles UU Aur et TX Psc.

Un jeu de 27 modèles des étoiles M, S et C a été établi par Johnson; il est présenté et discuté. Comme ces modèles forment un ensemble uniforme, ils sont utilisés pour étudier la variation de la structure atmosphérique lorsqu'on modifie le rapport carbone/oxygène. Un modèle où le rapport carbone/oxygène est égal à l'unité est semblable dans sa structure à un modèle solaire, où l'on n'a pas tenu compte de l'effet de serre, et caractérisé par les mêmes paramètres, ce qui souligne la faiblesse de l'opacité dans les étoiles S.

Des modèles nouveaux encore non publiés, calculés par le groupe suédois, sont décrits; ils incluent pour la première fois l'opacité des molécules HCN et C_2H_2.

Enfin, des modèles d'étoiles R ont été calculés à la fois par le groupe suédois, et par le groupe de l'Indiana; ils sont en excellent accord.

Des modèles sphériques sont vraisemblablement nécessaires pour la description de certaines étoiles supergéantes, et de certaines étoiles de type Mira. Bien que les modèles actuellement disponibles aient été calculés avec des opacités très simplifiées (d'habitude des opacités SM), certaines caractéristiques de sphéricité sont déjà évidentes. Il est montré par exemple (par des groupes de chercheurs en Allemagne, au Japon et en Lettonie) qu'une extension de l'atmosphère conduit toujours à une décroissance de la température et de la densité dans les régions extérieures de l'atmosphère. On montre aussi que la plupart des étoiles de masse m = 1 passeront par une étape d'extension atmosphérique, à un moment ou à un autre durant leur vie. Ces conclusions ont été confirmées, et se sont généralisées, au fur et à mesure que l'on a disposé d'opacités plus précises. Par exemple on peut noter que, bien que la densité de la plupart des molécules suivent la décroissance générale de la densité dans l'atmosphère, certaines d'entre elles, par exemple H_2O, se comportent d'une façon différente. Le rayon de l'étoile aussi a augmenté de façon significative dans celles de ces bandes moléculaires sensibles à une telle extension. Un troisième paramètre de l'observation a été donc cherché et des suggestions intéressantes de telles observations sont données: ainsi la couleur, entre 1 et 4 microns, pourrait fournir la température effective, certaines raies d'ions métalliques pourraient donner la gravité superficielle, et les raies rouges TiO peuvent être sensibles à l'extension atmosphérique. Enfin nous passons en revue les effets des abondances de métaux et de C, N, et O, sur la structure atmosphérique, toujours dans le cadre de l'étude des étoiles M. Pour finir, nous décrivons le premier modèle calculé d'étoiles riches en carbone, et nous exposons la découverte selon laquelle, à cause de la plus grande sensibilité à la

température de la composition des étoiles riches en carbone, l'étoile carbonée est moins étendue qu'une étoile M par ailleurs comparable.

La convection, qui constitue une autre généralisation possible des équations de base de l'atmosphère stellaire classique, est rapidement discutée. De nombreux essais de construire une meilleure théorie que la théorie de la longueur du mélange, sont décrits. Il semble que quelques progrès soient accomplis, mais même une théorie cohérente, opérationnelle, peut encore appartenir à un futur lointain. Pendant que l'on attend cette théorie, les chercheurs essaient de déterminer d'une meilleure façon les paramètres de la théorie de la longueur de mélange. On remarque que la convection ne devrait pas être importante dans la détermination de la structure des photosphères des géantes rouges, au contraire, elle peut être importante pour de nombreux autres problèmes dont la liste est donnée. Les hétérogénéités restent un problème à l'horizon de ces recherches. Alors que leur existence même est généralement encore en question, quelques effets possibles en sont soulignés.

Les comparaisons sont faites entre les prévisions du *modèle* théorique et les *observations*, lorsque celles-ci sont disponibles. Pour les étoiles M, la prévision correcte de la relation empirique entre la température effective et la température de couleur mesurée sur le système Wing, grâce à des modèles théoriques, par trois groupes indépendants de chercheurs, a permis d'établir une solide base de confiance dans le fait que, pour des étoiles M aussi froides que M5, des modèles précis sont disponibles.

Pour les étoiles S et pour les étoiles carbonées, la situation n'est pas aussi rassurante. Les observations à large bande sont représentées de façon modérément satisfaisante par des modèles de QQT, bien que l'on s'en soit servi, en liaison avec la photométrie dans la bande L, dans les méthodes infrarouges pour en déduire la température des étoiles carbonées, qui est en accord raisonnable avec les quelques températures que l'on peut déduire et de la mesure des diamètres angulaires. Représenter correctement des spectres stellaires est une opération dont on montre qu'elle n'est pas un critère très fort de la qualité d'un modèle d'atmosphère. Pour les étoiles S, les modèles conviennent suffisamment bien pour établir une échelle de température, à la fois par l'adaptation du modèle au données spectrophotométriques et par la méthode de la photométrie infrarouge.

Nous terminons ce chapitre par la discussion des caractéristiques spectrales qui pourraient être particulièrement sensibles à des variables telles que la température effective, la structure thermique, la gravité superficielle, la composition, la pression, l'étendue de l'atmosphère, les chromosphères et la perte de masse.

A la suite de cette étude des modèles strictement thermiques du chapitre précédent, qui étaient basés sur les concepts de *l'équilibre hydrostatique*, de *l'équilibre radiatif* (quelque fois en tenant compte de la convection) et de *l'équilibre thermodynamique local*, nous examinons dans le *Chapitre 8 des théories et des modèles qui renoncent ces hypothèses.* Après une courte introduction, nous analysons: (a) les écarts à l'équilibre thermodynamique local dans les photosphères thermiques, (b) la chromosphère des étoiles géantes rouges, (c) l'aérodynamique du choc et l'application de cette étude à ces étoiles.

Les atmosphères des étoiles géantes rouges sont tout à fait différentes des atmosphères des étoiles plus chaudes et plus compactes. Les densités et les températures, plus basses garantissent une formation abondante de molécules. La photosphère surmonte une zone convective profonde, où de l'énergie mécanique sous différentes formes, est disponible, et peut se dissiper dans l'atmosphère extérieure. Les échelles de hauteur sont fréquemment très grandes et les effets de la sphéricité sont souvent importants. Les hétérogénéités, peut-être liées à la convection, peuvent être assez communes. Toutes les étoiles géantes rouges

sont variables de quelque façon, et des ondes de chocs sont souvent liées aux pulsations qui doivent sous-tendre la variabilité. La perte de masse est un phénomène banal.

Il est commode de commencer par *la photosphère*, qui est aussi la région la plus étudiée. Les écarts par rapport à l'équilibre thermodynamique dans une photosphère thermique donnée sont discutés d'abord. Les équations de l'équilibre statistique et du transfert radiatif sont décrites afin de rappeler au lecteur quels sont les termes importants et la nature des couplages. La nature exploratoire du travail dans le domaine des fascinantes étoiles géantes rouges, est soulignée avec éloquence par le petit nombre de recherches poursuivies dans cette direction. La formation de la raie de Li I, diagnostic très sensible de l'histoire thermique et convective de la matière, est décrite dans les étoiles géantes M comme dans les étoiles carbonées, et liée aux abondances. Dans les étoiles M, aucun effet d'écarts à l'ETL plus grands que 0.1 dex n'a pu être trouvé. Dans les étoiles carbonées, les écarts à l'ETL, qui seraient beaucoup plus sensibles à l'abondance que le champ de rayonnement ultraviolet (d'ailleurs mal connu) produisent des raies quelque peu plus faibles que dans le cas de l'équilibre thermodynamique local.

Un intérêt considérable s'attache à la formation des raies moléculaires, puisque la plupart de notre information vient de l'analyse de ces raies. Pour les bandes de vibration rotation, au sein d'un état fondamental électronique (ce que l'on trouve usuellement dans les plus importants des spectres moléculaires infrarouges), les raies sont formées en "absorption pure", en raison de la dominance des processus collisionnels; cependant que les transitions électroniques excitées sont généralement contrôlées par le rayonnement et que les raies correspondant aux transitions entre ces états et l'état fondamental sont essentiellement formées par "diffusion". La fluorescence de nombreuses raies de la molécule CO, provoquée par des raies atomiques de l'ultraviolet lointain, est mentionnée.

Une examen plus général des écarts à l'ETL dans les photosphères implique la solution des équations de l'équilibre statistique pour les principaux fournisseurs d'électrons (Na, Mg, Al, K, et Ca), combinées avec les équations d'équilibre atmosphérique pour de nombreuses étoiles froides. Bien que la température des modèles "hors-ETL" diffère peu de celle des modèles ETL qui ont constitué le point de départ, la densité électronique est plus basse, et de façon significative, dans les modèles hors-ETL pour les étoiles les plus froides (un facteur 14, à 2500 K). Des valeurs comparables, préliminaires, sont données pour les étoiles carbonées.

Il est clair que la plupart des étoiles froides ont *des chromosphères "tièdes"* et sont affectées par une perte de masse. Mais il n'existe aucune trace de raies issues de la région de transition entre couronne et chromosphère, et aucune trace de couronne non plus. Au lieu de ces régions plus chaudes, de nombreuses géantes froides semblent avoir des chromosphères "tièdes" énormes. Comment ces régions ont elles été créées? Comment sont-elles soutenues, et chauffées? A cause des températures basses impliquées, un soutien thermique est certainement inefficace, et il faut faire appel à d'autres mécanismes générateurs de pression, comme la turbulence, le magnétisme, ou les ondes de choc; -peut-être couplées aux pulsations. L'argument en faveur de l'existence de ces régions étendues vient des estimations relatives aux régions responsables des raies d'émission de C II. Les effets géométriques de ces zones étendues ont une influence importante sur le traitement de la formation des raies.

D'autres problèmes sont mentionnés. Il semble possible que l'hydrogène soit sous-abondant dans certaines de ces géantes rouges et assez froides. Peut-être ces étoiles ont-elles communément des atmosphères inhomogènes ou à structure double, dans lesquelles une matière "tiède" responsable de l'émission de raies d'atomes ionisés coexisterait avec une matière froide produite par des agents refroidissants, par exemple la molécule CO.

Bien q'une activité intense de recherche ait été consacrée aux étoiles géantes G et K, très peu d'efforts ont été faits en ce qui concerne les étoiles les plus froides, à l'exception possible de α Ori. La plupart de ce travail a été d'une nature semi-empirique, c'est-à-dire que les profils des raies Mg II et Ca II ont été calculés pour un jeu de chromosphères arbitraires, et les modèles adéquats ont été choisis de manière à rendre le meilleur compte des observations. Un travail de nature purement théorique est encore dans le futur. Les modèles de α Ori–l'étoile froide qui a les faveurs de tous–sont présentés et décrits. Ils sont discutés également dans le Chapitre 5.

Les étoiles carbonées de type N, montrent aussi des raies d'émission de Fe II, Mg II et C II, ce qui prouve la présence d'une inversion de température et des chromosphères "tièdes". Dans le spectre de quelques étoiles, ces raies sont variables. A partir des observations à basse résolution, il semble que les chromosphères des étoiles N soient, beaucoup plus faibles que celles des étoiles M correspondantes, et cette différence constitue un problème fascinant mais non résolu. La première façon simple de construire des modèles de chromosphère des étoiles carbonées a commencé par des modèles produisant au moins l'émission en Mg II, mais sans exciter les raies de Balmer, qui ne sont pas observées. Prédire les raies de C II sera un défi encore plus difficile à tenir. Les modèles prédisent aussi une caractéristique forte d'absorption due à Mg I, à 2850 Å, qui n'est pas observée. On pense que cette structure pourrait être naturellement compensée, dans le spectre de l'étoile, par l'émission issue d'une région froide, extérieure et étendue.

Un choc peut jouer un rôle significatif dans *les étoiles Mira* (peut-être même dans toutes les étoiles géantes rouges), et ces effets sont discutés en détail. Les équations de Rankine-Hugoniot sont établies, et appliquées à des cas simples. On prend en considération les conditions régnant dans les régions antérieures et postérieures aux chocs. Les raies d'emission dans les étoiles Mira sont classées en groupes, les raies primaires et les raies secondaires. Les raies primaires, Mg II, Ca II, Fe II, et Ti II, sont vraisemblablement formées dans la région postérieure au choc, et les raies secondaires dans la région antérieure au choc, par des phénomènes de fluorescence associés aux raies primaires.

L'influence des chocs sur la structure thermique de l'atmosphère pourrait être considérable, mais aucun calcul suffisamment détaillé n'est actuellement disponible pour permettre d'élucider complètement ce point.

Une discussion des caractéristiques de pulsation des étoiles M conclut ce chapitre. Les arguments en faveur d'une pulsation, soit dans le mode fondamental, soit dans le premier harmonique, sont décrits. De toute évidence, cette question est encore en pleine controverse.

Dans les deux derniers chapitres, nous quittons les fascinantes étoiles géantes rouges et rattachons le "stellaire au solaire" par une analyse *des étoiles M naines. Le Chapitre 9 résume les très nombreuses observations des dernières années*, en particulier celles obtenues par *satellite*, et *décrit les phénomènes, prévus et imprévus*, que manifestent à la fois les étoiles naines M *normales* (appelées dM) et celles qui *présentent des raies d'émission* (appelées dMe et qui se distinguent plus spécifiquement des précédentes par la présence de la raie Hα en émission).

La plupart des naines M qui ont été suffisamment observées, sont tout à fait proches; par conséquent, leurs parallaxes trigonométriques sont sûres et leur luminosités absolues précises. Comme de nombreuses étoiles dM et dMe sont aussi des membres de systèmes binaires, leurs masses peuvent souvent être déterminées: elles vont d'environ 0,06 masses solaires (la limite inférieure pour la combustion de l'hydrogène) à environ 0,60 masses solaires. (Dans le cas des étoiles CM Dra et YY Gem, les rayons et les masses peuvent être déterminés avec précision, car elles sont des binaires à la fois spectroscopiques et à éclipse.) Ces objets

de faible masse subissent une forte convection; cette dernière doit fournir l'énergie qui donne aux étoiles dMe leurs caractéristiques inhabituelles. Sont passés en revue: les méthodes et les résultats afférents à la détermination des masses des naines M, leur situation et leur densité dans la Galaxie, leur âge, leur température effective, leur rayon, leur gravité superficielle, et les phénomènes plus exotiques révélés par les données sur les domaines de l'ultraviolet, des rayons X et radio. Plusieurs corrélations rigoureuses entre la température effective, la correction bolométrique, la magnitude absolue visuelle, et plusieurs indices de couleur, sont décrites.

Bien que la masse d'une étoile M naine soit faible, ces étoiles sont si abondantes qu'elles constituent une composante substantielle de la masse de la Galaxie; en fait, de toutes les étoiles, elles pourraient y contribuer le plus. Leur contribution au gaz interstellaire est encore sujette à débat, mais il est possible qu'elles contribuent aussi de façon importante à la perte de masse des étoiles.

A cause des températures extrêmement basses des naines M, leur spectre optique est dominé par de fortes bandes moléculaires de TiO et de CaOH; de nombreux autres faits plus faibles, tant moléculaires qu'atomiques, sont présents. La molécule H_2O produit aussi de fortes bandes, en particulier dans l'infrarouge, bandes dont l'intensité augmente fortement et de façon monotone avec une décroissance de la température. Dans de nombreuses étoiles dMe non binaires, la raie Hα montre un renversement central trés étroit que l'on suppose dû à des phénomènes présents en surface.

Environ 75% des étoiles naines M sont des objets à raies d'émission. La fraction d'étoiles dMe croît d'autant plus que le type spectral est tardif, jusqu'à atteindre presque 100 pourcent au type M5. Cependant, il y a quelques étoiles des types spectraux les plus tardifs qui ne présentent pas de raies d'émission: ce fait pourrait être en relation avec un phénomène, encore inconnu, se produisant dans l'atmosphère externe.

Une analogie pertinente entre les étoiles dM et dMe est la plage solaire. Comme les étoiles dM sont caractérisées par un fort flux magnétique, on suppose qu'il en est de même pour les étoiles dMe. La source de flux nonradiatif et le champ magnétique pourraient, tous les deux, être renforcés dans les naines M, avec, pour conséquence, la forte émission qui y est observée. Une dynamo auto-excitée dans la zone convective est, en général, acceptée comme mécanisme de base de la génération du champ magnétique dans les étoiles actives. La dynamo est actionnée par la rotation différentielle qui est due, à son tour, à l'intéraction de la convection et de la rotation. Ceci est compatible avec le fait que les étoiles dMe paraissent avoir des vitesses rotationnelles plus élevées que les naines M n'en ont en général. Ces dernières sont alors supposées avoir leur chromosphère et leur couronne plus froides et plus énergétiques que dans le Soleil. Les chromosphères des étoiles dMe sont moins étendues, plus chaudes et plus denses, et montrent des inhomogénéités en surface plus importantes que dans le Soleil. Les températures électroniques des chromosphères des étoiles dMe se situent entre 10000 et 140000 K.

Les observations dans l'ultraviolet ont révélé un ensemble de fortes raies d'émission qui permettent de mieux pénétrer la physique des atmosphères des naines rouges. Les résultats d'observation les plus importants sont les suivants. (1) Les pertes radiatives dans les seules raies d'émission du Ca II sont trop fortes pour rendre compte de la dissipation des flux acoustiques. (2) Les flux du Mg II et les émissions coronales de rayons X mous sont indépendants de la gravité et de la température effective, à l'inverse de ce que l'on attend d'un chauffage par dissipation d'ondes acoustiques; des ondes magnétohydrodynamiques de faible mode, dans des tubes de force, pourraient pallier cette difficulté. (3) Les flux de raies d'émission provenant de la surface de l'étoile, rapportés aux températures de formation des

raies dans des naines calmes G à M se comportent qualitativement comme dans le Soleil calme, alors que dans les étoiles dMe ils sont comparables ou d'un ordre de magnitude supérieurs à ceux des régions trés actives du Soleil. (4) Les étoiles qui montrent des régions actives de transition chromosphère-couronne, ne sont situées que dans des parties restreintes du diagramme HR; on les distingue par l'existence de nombreux tubes fermés de flux magnétique. (5) L'augmentation bien connue des pertes radiatives chromosphériques avec la vitesse de rotation et leur décroissance avec la racine carrée de l'âge sont vérifiées aussi bien pour les flux de la région de transition chromosphérique que pour ceux de la couronne. (6) Les luminosités des rayons X mous sont proportionnelles aux températures coronales et inversement proportionnelles à la gravité superficielle de l'étoile. (7) Une émission radio d'étoiles calmes a été détectée sur des étoiles actives dMe avec un trés grand radiotélescope (en anglais, VLA).

Des variations de flux photométriques à larges bandes, de basse amplitude, périodiques ou quasi-périodiques ont été observées dans plusieurs naines et sous-géantes proches de types K à M à raies d'émission, dont la plupart sont membres de systèmes binaires. Il apparaît que ces variations sont dues à des taches ou autres inhomogénéités, qui, de façon typique, couvrent 10 à 40 pourcent du disque stellaire apparent et sont plus froides de 400 à 1500 K que la photosphère. De plus, ces taches stellaires immenses demandent une dynamo étonnamment efficace. Les hétérogénéités apparaissent se continuer dans la chromosphère et la couronne. Plusieurs programmes sont en cours pour rechercher la période et les caractéristiques des cycles d'activité stellaire et de la modulation rotationnelle.

Les phénomènes les plus proéminents de l'activité stellaire sont *les éruptions*. Bien que ces dernières soient détectables à travers toute la région spectrale, c'est seulement dans le domaine optique qu'elles ont été suffisamment observées pour qu'une étude significative soit engagée. La marque usuelle d'une éruption est la forte intensification des raies de H I, Ca II, et He I. Dans l'ultraviolet, on observe un continu élevé et les raies de la région de transition relativement plus intenses. Pour comprendre les éruptions stellaires, les efforts portent sur des observations conjuguées en longueurs d'onde optiques, ultraviolettes et radio, plus particulièrement sur des étoiles trés actives commes les étoiles RS CVn. Si le niveau d'activité des éruptions solaires suit de prés le cycle solaire, il semble qu'il n'en soit pas de même dans les étoiles dMe.

La Chapitre 10 propose *un examen d'ensemble* soigneux *des essais d'interprétation des phénomènes d'activité et des cycles d'activité dans les étoiles naines M*, grâce soit à *des modèles thermiques*, soit à *des modèles non thermiques.*

En raison des densités élevées de l'atmosphère des étoiles naines M (par comparaison aux géantes), des modèles thermiques y sont construits, incorporant la double complexité introduite par la formation des molécules et par la convection dans des gaz de profondeur optique faible. Bien que ces problèmes ne soient pas nouveaux, ils ont été en fait discutés en quelque détail dans un chapitre antérieur sur les modèles thermiques des étoiles géantes rouges (Johnson, même volume), leur difficulté, qui a considérablement gêné le calcul des modèles, et la construction de meilleurs modèles thermiques est encore un but dont on attend beaucoup dans le futur.

Les meilleurs modèles disponibles tiennent compte de l'opacité H_2O comme d'une sorte d'opacité moyenne, et traitent la convection dans le formalisme usuel de la longueur de mélange. Les ailes observées de certaines raies fortes et les couleurs à large bande RIJHKL, peuvent être reproduites relativement bien, au moins pour quelques-unes des étoiles naines M normales. Des observations à des longueurs d'onde plus courtes et plus grandes ne sont

pas, elles, représentées correctement par ces modèles. Une autre question bien gênante concerne la vitesse microturbulente qu'il faut introduire dans les modèles pour comprendre la convection qui s'y développe.

Des observations établissent l'existence de *taches obscures* (*taches stellaires*) sur au moins la photosphère des étoiles M à émission (dMe). Ces taches sont suffisamment froides, et couvrent une surface suffisamment grande de l'étoile, pour affecter le spectre observable de l'étoile. Alors qu'aucun modèle à deux composantes n'est encore disponible, quelques unes des caractéristiques des taches ont été déduites de l'observation, et l'on a étudié le rôle possible de ces taches dans le stockage ou la redistribution des énergies radiatives stellaires.

Bien qu'aucun argument direct ne soit disponible, les arguments indirects, déduits de la polarisation circulaire des émissions radio, suggèrent la présence de champs magnétiques de l'ordre du kilogauss à la surface des naines M, et l'on décrit l'étude des effets des tubes de flux magnétique sur la structure thermique de l'atmosphère d'une naine M et sur les bilans d'énergie qui la caractérise. L'adaptation des modèles d'atmosphère aux modèles de l'intérieur stellaire est particulièrement importante dans le cas des naines M, où c'est par une convection complète que l'on peut caractériser l'étoile. Ces divers aspects sont résumés.

La puissance d'interprétation des modèles thermiques est bien entendu limitée aux courbes de flux continu émergent et à certaines raies d'absorption. Les modèles comprennent *une augmentation de température chromosphérique* permettant de rendre compte de l'émission caractéristique dans les raies de H I et de Ca II. Nous visions à mettre en oeuvre une théorie cohérente qui *decrirait* la structure chromosphérique à partir des propriétés disponibles des flux mécaniques. Mais, jusqu'à ce qu'une telle théorie soit disponible, nous devons nous limiter à une technique semi-empirique de construction de modèles. Des modèles limités à une couche isotherme, ou à deux plateaux de température, sont décrits. Si le plateau le plus élevé est à 20000 K, les noyaux des raies d'émission du Ca I sont en accord avec les observations dans un domaine relativement limité de densité électronique. Aux densités plus élevées des chromosphères des étoiles M naines, les processus collisionels peuvent dominer les processus radiatifs, et la raie Hα peut être observée en émission à des températures relativement basses. Si les taux de chauffage chromosphérique restaient sans subir de modification le long de la série principale, les raies de Balmer apparaîtraient inévitablement en émission dans les étoiles les plus froides.

Quelques modèles plus détaillés, permettant de prendre en considération un chauffage de la photosphère élevée et un plateau de température à 8000°, ont réussi à rendre compte des profils de la raie K du Ca, mais sont moins heureux avec les raies de Balmer. Une étude plus détaillée des raies de Balmer, prenant en compte un atome à 5 niveaux, sont capables de reproduire ces profils. Il est intéressant de noter qu'alors qu'on ajoute la chromosphère, l'absorption dans la raie Hα commence à augmenter, et c'est seulement ensuite que la raie devient une raie d'émission. On doit être très prudent en considérant la distinction entre les étoiles dM et dMe comme celle qui sépare les étoiles sans chromosphère des étoiles à chromosphère. Ce résultat pourrait être utilisé comme un argument en faveur du fait que les chromosphères des étoiles dM sont moins denses que celle des étoiles dMe.

Contrairement au cas du Soleil, il semble, au moins dans le cas des étoiles M les plus chaudes, que la fraction de flux issue de la couronne est plus grande que celle de la chromosphère. C'est-à-dire que le problème de chauffage coronal est le problème majeur, la chromosphère pouvant en revanche être chauffée à partir de la couronne.

Les modèles d'éruption sont très nombreux, et, au cours des ans, on a pu observer une croissance régulière dans l'élaboration de ces modèles. Pourtant ils ne sont pas encore complètement cohérents, et restent semi-empiriques: on suppose simplement qu'une nouvelle

entité a fait son apparition dans l'atmosphère des étoiles M, et l'on essaie de calculer la(les) signature(s) empirique(s) d'une telle entité. Cette entité, dans quelques modèles, est le volume du gaz "coronal" chaud, à des températures de plusieurs millions de degrés. Dans quelques autres modèles, il s'agit seulement d'une entité "chromosphérique" à des températures de l'ordre de 10^4 degrés. Dans d'autres modèles encore, c'est une région de la photosphère qui est considérée comme chauffée de "seulement" quelques centaines ou milliers de degrés, et la signature spectroscopique est alors dominée par les propriétés optiques de l'ion négatif H^-. Dans tous les cas, l'hypothèse est que la création de cette "entité" est due, de toutes façons à la libération d'une énergie non thermique, quelque part dans l'atmosphère de l'étoile et avec une constante de temps très courte. Mais, dans aucun des modèles connus jusqu'à présent, les détails de ce processus n'ont été encore élaborés avec une précision suffisante pour que l'on puisse garantir qu'il s'agit de modèles réalistes, "vrais" d'une éruption stellaire. Les efforts futurs à mener pour améliorer cette situation dépendront très profondément de la relation entre les étoiles et le Soleil.

Alors que les estimations du chauffage acoustique dans les étoiles naines M sont relativement grossières, il nous semble que le flux acoustique est certainement moindre que dans le Soleil. Pourtant le flux chromosphérique, seul, est égal à celui du Soleil et le flux coronal est 10 à 100 fois plus grand. D'autres prévisions issues de la théorie des ondes acoustiques sont également en désaccord avec les observations. A moins qu'il n'y ait une erreur fondamentale dans notre compréhension de la production d'énergie par les ondes acoustiques, on peut en conclure que celles-ci doivent être éliminées comme la source de l'énergie chromosphérique et coronale dans les étoiles dM.

De nombreux chercheurs ont examiné la façon dont *les effets magnétiques* pourraient être incorporés aux équations d'énergie s'appliquant aux chromosphères d'étoiles M. Une possibilité est celle d'ondes à mode lent. En imposant un flux donné à la base de l'atmosphère, et en équilibrant les gains et les pertes d'énergie à tous les niveaux, on peut aboutir à une structure thermique. D'autres recherches ont pris en considération des ondes de magnétohydrodynamique (MHD). La plupart de ces travaux sont basés sur une analogie avec le Soleil. Si les densités dans les couronnes et les chromosphères d'étoiles M sont dix fois plus grandes que dans le Soleil, le taux de dissipation par effet Joule est cent fois plus grand, et ceci peut aider à expliquer la rapide croissance de l'éclat des éruptions stellaires. Une étude soigneuse du chauffage des boucles magnétiques coronales par des ondes, soulève des questions intéressantes en ce qui concerne les fréquences adéquates. Dans le Soleil la période des ondes convectives est de l'ordre de 500 s, alors que la période typique de résonance des boucles est de l'ordre de 5 s. Dans les étoiles dM, cependant, les périodes convectives peuvent être beaucoup plus courtes que 500 s, alors que les périodes de résonance des boucles peuvent être, elles, plus longues que 5 s. Par conséquent, il semble qu'une intersection puisse avoir lieu entre ces 2 groupes de périodes, peut-être dans les plus chaudes des étoiles dM. Si c'est le cas, on doit s'attendre à un chauffage fortement accru, pour ces étoiles, et il semble bien que l'observation vienne à l'appui de cette prévision. Malheureusement, il peut y avoir d'autres processus, encore inconnus, qui affecteraient la production d'énergie, sa propagation et sa dissipation.

SUMMARY

In some sense, the atmosphere of a star comprises the entire region that connects the energy-producing core to interstellar space. From this viewpoint, the atmosphere properly includes what is usually called the envelope, photosphere, chromosphere, corona, the entire circumstellar region, and the outflowing matter, excluding only that which has escaped the star and become part of the interstellar medium. Keeping this perspective in mind emphasizes the unity of what are sometimes treated as separate parts of a star. Such emphasis is more necessary for the stars discussed in this book, which tend to be so large in variety of phenomena and size that compartmentalization comes more easily.

One of the distinguishing characteristics of the M, S, and C stars is, in fact, the wide-ranging, time-varying phenomena they display. Even the M dwarf stars described in the final chapters, appear, in the strength of their chromospheres and the violence of the flares, to be more than simply cooler counterparts of earlier main-sequence stars. The cool giants commonly display such fascinating features as emission lines, shifted or multiple absorption lines, excess infrared dust emission, and microwave maser and thermal emission—and these often vary periodically or irregularly. From the point of view of the star, it must be characterized by a deep convective zone and a relative quiet photosphere through which nevertheless passes the mechanical energy to power the chromosphere. Energy for the pulsating photospheres arises deep within the star itself, yet many of these stars vary only semiregularly or even erratically. Any organized motion in the photosphere must give rise to shock waves that then traverse the immense outer atmosphere, producing radiation from excited gases as they slowly dissipate and perhaps levitating gases to a stagnant region several stellar radii above the photospheric surface. Grains must form somewhere, perhaps as clean grains in certain of the coolest photospheres, and these are then pushed outward by radiation pressure, dragging the gases along and becoming "dirty" as they flow. Perhaps the grains form in the region of stationary gases far above the photosphere, and their effect in powering outflow of matter begins there. In any case, large outflows of mass are observed—sufficient to contaminate interstellar space with the atmosphere (possibly now enriched with an extra load of heavy elements) and perhaps sufficient to alter the future evolution of the star. In the gases far from the star, microwave emission—both thermal and maser—from OH and H_2O are commonly seen in the oxygen-rich Mira variables of longest period and largest amplitude. Maser emission from SiO arises much nearer the star, perhaps even in the photosphere. Finally, a number of the coolest stars, both oxygen-rich and carbon-rich, are surrounded by dust shells or clouds optically thick in the infrared, and these clouds are sites for rich molecular and atomic chemistry.

PRECEDING PAGE BLANK NOT FILMED

PAGE IV I INTENTIONALLY BLANK

Another feature of the coolest stars sometimes surprises us—the range of conditions. It is easy to forget that a change of effective temperature from 4000 to 3000 K is an enormous change, and stars with these effective temperatures may not be at all similar. It might be helpful to classify stars into three groups: *hot*, *warm*, and *cool*. The hot stars are the O, B, and A stars, the warm stars are the solar types of F, G, and K, and the cool stars are the stars of M, S, and C types (the stars discussed in this book).

This volume begins with a chapter on the *basic properties* and the *variability* of the giant and supergiant M, S, and C stars. Because of the diversity of these objects, several classification schemes have been used—by spectra, chemical composition, photometry, or variability type. Each of the recognized groups—M, MS, S, SC, C, R, Ba, and others—is identified and described. The current classification is based on abundance ratios, the C/O ratio (<1; 0; >1) indicating the spectral type of the bulk of the stars (M, S, and C, respectively). The metal and/or the s-process abundances distinguish more particular types: stars with strong CN molecular bands or with strong Ba II lines, hydrogen-deficient stars, etc. To better understand the large variety among these stars, which lie so close together in the HR diagram, several other classifications based on other criteria are proposed with the aim to be physically meaningful. The most famous of these leans on the light-curve amplitude and profile of the variables.

One of the goals in delineating the properties of red-giant stars is the desire to understand the fascinating evolutionary history behind them. Each of these objects was once a main-sequence star, and its interesting color, luminosity, variability, and composition arose as a consequence of its fascinating past. In a similar way, most of these stars will eventually become planetary nebular and white dwarfs.

Broadband photometry serves to outline the energy-flux curve, and narrowband photometry provides a sharper tool. Results for M, S, and C stars are described. Newer results from ultraviolet studies are already yielding important insights into the chromospheres of these objectives, which lie on the warm chromosphere and mass-loss side of the famous chromospheric dividing lines.

The space motions and space distribution of the cool giants are described. The apparent and the space distribution in the solar neighborhood are well known through the early reviews on the question.

More recent investigations study the distribution of late-type red giants in the direction of the central regions of our Galaxy and other nearby galaxies (e.g., Large Magellanic Cloud (LMC) or Small Magellanic Cloud (SMC)). The number density of C stars relative to the number density of M stars is specifically discussed due to the importance of this ratio for asymptotic giant-branch evolutionary purposes and for understanding fundamental galactic properties. Values of such intrinsic properties as temperature, radius, and luminosity of these stars are given. In brief, these stars are characterized by temperatures such as $3.3 \leqq \log T_{\text{eff}} \leqq 3.5$; luminosities, $3 \leqq \log L/L_0 \leqq 5$ or $-7 \leqq M_{bol} \leqq 3$; ages, $\sim 10^7$ to 10^{10} yr; and a broad range of masses from ~ 1 to $\geqq 20\ M_\odot$.

Chapter 1 concludes with a summary of observations of M, S, and C stars in the LMC and SMC. There the supergiants are distinguished from the long-period variables, and the latter are observed up to the theoretical luminosity limit. The evolutionary sequence M → S → C is clearly delineated. A complete HR diagram can be obtained.

The next section emphasizes the main topic of Chapter 1 through *a survey of observations and interpretations of the various variability types* of the red giants and supergiants. All these stars can be identified either as pulsating or eruptive variables. In the pulsating group, three types are recognized: (1) Miras are long-period stars—generally, they have a

well-expressed periodicity and a good regularity (they are also called long-period variables (LPV's)); (2) the semiregular (SR) variables have smaller visible amplitude variations and more irregular light curves than Miras; and (3) the true irregular variables are called Lb (giants) or Lc (supergiants). The RCB stars constitute the eruptive group; they are of spectral classes, F, G, K, and R. The latter concerns the hot carbon stars, the only eruptive stars of interest in this volume. The very different distribution of the different types of variability for the three spectral classes M, S, and C is noted.

The general characteristics of each group of variables is then described. By "Miras" is meant a distinctive type of light curve and not a stellar spectral type, as is often confused in the literature. Some generalities are noted. In some stars, the amplitude of the variation in the visible with phase is very large (e.g., χ Cyg). Most of the changes are cyclic with a period equal to that of the visual curve. However, the period of individual light cycles sometimes differs from the mean period of the star by several percent, and the observable properties are not exactly repeated from cycle to cycle. Fluxes of some Miras show a significant deviation from a blackbody beyond 8 μm with a great IR excess due to the presence of a dust envelope; they are called IR Miras. OH masers are found among Miras of M spectral type. Some examples of changes from OH type I to OH type II Miras are described (e.g., R Leo and U Ori).

Our descriptions of Miras continues with properties specific to their variability. First of all, *the phase lag* phenomenon is discussed. It is a phase delay (or shift) between light curves of various colors, setting that the epoch of zero phase refers to the visual maximum. Typically, the IR light maximum lags the visual by 0.1 to 0.2 period. Phase delays are also observed between radio (OH, SiO, and H_2O lines) and infrared light curves. The behavior of the phase lag is not the same in all observed Miras; moreover, the behavior with phase may not be exactly the same in all the cycles of the same star.

The amplitude of light variations differs in Miras from one wavelength to another. It is much larger in the visible than in the infrared. Generally, the amplitudes of variations $[F_{max}/F_{min}]$ decrease in the infrared spectral range with increasing wavelengths from 1.2 to 3.5 μm and are roughly constant between 3.5 and 10 μm. For many Miras, the cycle-to-cycle differences are not erratic; bright and faint maxima tend to alternate, and bright maxima tend to occur before the predicted date. In all the cases, the Mira minimum cannot be considered as the normal state of the Miras.

Mira light curves present a great choice of visual *profiles* (sawtooth or smoothed sinusoidal shape, humps, inflection points, etc.). In M and S star light curves, both very similar, the rise to maximum is somewhat more rapid than the decline to minimum. The C light curves are more gradual and more symmetric. All the differently shaped light curves might reflect the interaction of the opacity and density variations in the different atmospheric layers caused by the propagation of shock waves. Examples show that the shape of the visible light curve persists in other wavelengths. Some stars have light curves with two maxima and two minima per period; this curious behavior has also been found theoretically in an attempt to produce a large postshock velocity maximum in an isothermal pulsation model.

During the Mira light cycle, *variations in color indices* appear. Generally, as the star becomes fainter in V (as it moves toward the minimum), it becomes redder. Because the molecular (TiO + VO) index around 1 μm is correlated to the observed temperature, each M Mira moves on the color index/temperature plane during the period. Also, the spectral type of each Mira is shown to vary during the period. Numerous effects contribute to the variation of the color indices during the period: temperature, molecular opacity effects, etc.; some of them are not fully independent.

That the shape of some of the light curves changes between two or several consecutive periods has already been noted. Other kinds of Mira period changes are observed: (1) a secular evolution by smooth increasing or decreasing of the length of the period or by a sine or cosine variation of the latter, (2) shape of light-curve changes between two or several consecutive periods, (3) an abrupt change of period length and abrupt shifts of maximum (fluctuations of phase). Some of these period changes are used to provide direct observational confirmation of the theory of helium shell flashes. For the majority of the observed Miras, *multiple periods* are determined. In general, the shorter period, P_1, is associated with the larger amplitude of variation. It is suggested that the primary period P_1 is the pulsational period, while the modulating period P_2 may be derived from a nonradial mode or from cold spots on the surface. Other interpretations are investigated—such as convective turnover time of giant cells. The ratio P_2/P_1 is around 9 for the M-type variables and 12 for the N-type stars.

In Miras, some short-term fluctuations are illustrated by: (1) a rapid evolution in the o Cet effective temperature on 12 days, (2) outstanding phase-dependence effects in line shape and intensity of SiO maser emission lines, and (3) nightly variations in emission and absorption-line radial velocities, interpreted as the interaction of shock waves with nonuniform atmospheric layers or as linked to eventual flares.

Correlations between the various quantities previously described, such as period length, light-curve shape, IR excess, and visible and IR color diagram, are then discussed. The most significant relationships are summarized as follows: (1) A statistical relationship exists between the shape of the Mira light curve and the period. (2) A correlation is noted between the difference in magnitude of two successive maxima and the time interval separating the two maxima. The outward propagating shock wave takes more or less time to reach the star surface, this time being a function of the energy carried. (3) The shorter period Mira variables are Population II stars, while those of longer periods belong to more intermediate populations; this suggests that the period amplitude of Miras may be a function of the metal abundance. (4) The link between period length and amplitude variation has been investigated. A tendency for larger period stars to have greater amplitudes is verified in many wavelengths. Relations are also observed between the period, amplitude, and various IR color indices. Some conclusions are drawn, such as that the height of the silicate feature at 10 μm appears to increase with the period amplitude or the [8.7 μm]–[11.4 μm] index versus period relation indicates that the observed mass of dust in a given thermosphere is an almost linear function of the period. Other correlations involve radio lines: (1) The OH 1612-MHz masers and the IR variations show a correlation consistent with a radiative pumping of the masers, possibly at 2.8, 35, 53, 80, and 120 μm. (2) The 1.35-cm H_2O maser and the 2.2-μm IR flux may be related either by an exponential rate or by a linear relation above a threshold of the IR flux value. (3) The expansion velocity given by the type I and II OH Miras directly correlates with the amplitude variation at 1.04 μm and inversely with the period length.

The section continues by looking at the *semiregulars* and firstly by giving some generalities about these variables. Three groups are defined: (1) SRa variables are giants and generally differ from the Miras only in the smaller amplitude of light variations; nevertheless, they frequently show strong variations in their light curve from one cycle to another; (2) SRb variables, also giant stars, have a poorly expressed periodicity with slow irregular variations that temporarily replace the periodic changes; and (3) SRc variables are supergiants with a SRb behavior; the visual light changes are generally of the order of 1 magnitude or less. Almost half of the known semiregulars are N stars, the remainder being of M class; very few semiregulars of S and R classes are known.

Different time scales in SR light variations have firstly been secured from visual estimates of the brightness. Visual curves are quite individual (i.e., without the strong similarity found in Mira curves). These may be characterized by a form of periodicity hidden by irregular variations in brightness. Among the semiregulars, SRa variables are most similar to Miras (Balmer emission around some light maxima, changing period, etc.). The SRb stars are more irregular than the SRa. In these stars, variations with a time scale of about 1 hour have been detected, as in R Crt. On the example of the C star, TW Hor, analyzed by broadband photometry, the U–B index varies oppositely to V–R, V–I, and B–V; it presents strong and rapid oscillations between $\psi = 0.8$ and $\psi = 0.9$, probably connected with the interactions of the shock waves and the inhomogeneous matter of the chromosphere. Over a century, some SRc may exhibit changes up to 2 mag. As at the Hayashi limit in the HR diagram that the amplitudes of light variation of the supergiants are at their maximum, it may be concluded that the SRc stars stay no more than 100 years near the limit. Some SRc stars, called hypergiants (or super-supergiants), are really very extended; they may have M_{bol} around –7 to –9. They present long-term disturbances over several years with large variations in luminosity and spectral classes (e.g., ϱ Cas), probably due to large amounts of ejected matter. Moreover, night-to-night variations are observed, perhaps caused by small puffs or local motions in the atmosphere.

Correlations between quantities such as periods, absolute magnitudes, spectral classes, and phase lags are less obvious in the *SR variables* than in Miras. Nevertheless, some relationships are reported such as: (1) the longer the period, the redder the spectrum; (2) no mechanical coupling seems to exist between the photosphere, which suffers some periodic variations, and the masing regions, which have definitely nonvariable radial velocities and are induced only when the photospheric variations become stronger than a certain threshold; (3) an investigation of several SRc of type Ia, Iab, and II in the V filter shows that, for a given spectral type, the larger the brightness amplitude, the more luminous the supergiant; (4) also, the higher the luminosity of the supergiant, the earlier the spectral type; and (5) from surveys of red supergiants in the LMC, a period-luminosity relation is deduced. Finally, it is stressed that long series of uninterrupted observations of selected variables by satellites should be an enormous step to disentangling the various time-scale phenomena involved in these stars. In fact, the question is raised to decide if the *semiregular light curves are multiperiodic, random, chaotic, or truly unpredictable.* In the last decades, multiperiodic analyses have been developed, and many apparent light-curve irregularities are explained by a complex mixing of two or more individual oscillations, generally separated by a harmonic analysis of the observations. Today, mathematical techniques are used to explain the behavior of the semiregular and irregular light curves: (1) the random process where the events are largely independent of each other and where predictions of any range of variations are impossible, and (2) the chaotic process where the observed variations reflect the unstable motions produced by a collective and cooperative behavior of the matter submitted to amplified acting forces.

As for the *irregular variable Lb and Lc stars* (i.e., giants and supergiants, respectively), they are slowly varying without any trace of periodicity. The M irregulars are mainly concentrated at M5 and M6 types, with none later than M7. Many M-class irregular variables are connected with young O-associations of Population I. The carbon irregulars are chiefly found in the earlier subclasses. As the time interval between successive maxima is very long (from a few hundreds to a few thousands of days), it is not easy to decide if a supergiant belongs to class SRc or Lc. Another criterion based on the amplitude variations have been investigated. In the small-amplitude supergiants, the mean maximum is ~ 1.1 mag, and the

dispersion is about 0.2 to 0.3 mag. Examples of large-amplitude ones show a mean maximum amplitude of $\sim$4.2 mag and a dispersion of $\sim$1.1 mag.

Different time-scale light variations are observed. Some stars have rapid changes of brightness (over a few days); other stars have periodic variations during some intervals of time, and just after, they show a very constant brightness. Their variations may result more from chaotic or random than harmonic processes (surface irregularities: spots, loops, etc.). However, this point of view is debatable; the supergiant, μ Cep, is a good example, in which a few workers ascribe the starlight variations to temporary and random surface disturbances and others explain them by the superposition of periodic terms. In α Ori, monitored over 60 years, the light curves are characterized by long-term light variations with a period of about 5.8 years and a mean amplitude of $\sim$0.4 mag, on which is superposed short-term irregular variations with rise or decline time scales of a few weeks to some months. In the chaotic scheme applied to the irregulars, flares which are observed in these stars should represent the shortest time variations.

The *hydrogen-deficient carbon stars*, concisely named HdC stars, are reviewed. They form a class of stars completely different from the other carbon stars (R and N types). They are supergiants (M_{bol} = -4 to -6), and their abundance of hydrogen is deficient by a factor up to 10^5 or more compared to the H/Fe ratio in the Sun. They have a surplus of carbon (by a factor 3 to 10) and of helium compared to the Sun. They split into three subclasses: the RCB stars, the nonvariable HdC stars, and the helium stars.

The *RCB stars*, the most well known and numerous among the HdC stars, are mostly R stars characterized by abrupt drops in brightness followed by a longer climb back to normal light, suggested to be due to the sudden ejection of highly absorbent matter. Occasionally, they are thought to be progenitors of type I supernovae, novae, planetary nebulae, helium stars, and white dwarfs. The prototype star is R CrB. As in the other variables, the spectral type changes during the brightness variations. The temperature range covered by all the RCB stars is quite large (from F to R stellar temperatures). Although the changes in spectra and colors of these eruptive stars are very complex, a general pattern is described in detail. The mass loss continues during the maximum light through a permanent chromosphere. Many models have been stressed to give a coherent picture of the RCB phenomenon. The currently accepted basic model is as follows. The gas is radially ejected at the top of 10 to 100 convective cells through a fairly large area of the stellar surface and crosses the deeper layers of the stellar atmosphere. The gas expands and cools and graphite particles condense. The resultant dust clouds or dust blobs expand, moved away by radiation pressure, and obscure the photospheric light, allowing the sharp chromospheric emission lines to be seen. When the new shell (ejected at high velocity) collides with the circumstellar envelope material, broad emission lines are formed. The collision happens with a phase lag of 30 to 70 days that allows, when taken together with the radial velocities of the circumstellar lines, an estimate of the distance of the shell of gas and grains of about 4 to 8 AU from the star. Some RCB stars have an excess of infrared emission. The IR emission is up to 40 to 60 percent of the star's total luminosity. A possible explanation of the infrared emission might be that the ejected particles have the form of Platt particles of 3 to 30 Å size. Such particles would absorb the visible radiation better than graphite particles, but would not reradiate in the IR. The IR emission is observed when the growth of particles by accretion leads to a size of 10^{-6} to 10^{-5} cm, which corresponds to the time elapsed from the visual minimum by the growth period of the particles.

After this general view on the RCB stars, focus is put on the RCB light curves. Surprisingly, the RCB stars are the only class of variables for which maximum brightness is the

normal state. The duration of this normal state is variable, up to several years. Epochs also exist where the maximum is never reached. The speed of the decline (i.e., dm/dt) is also variable. However, the declines are always much more abrupt than the rises to the maximum, although their respective shape is not kept the same at each minimum. The amplitude, the frequency, and the duration of minima are unpredictable.

Different time-scale variations are known in RCB stars. First, the decline of many magnitudes, also called "obscurational" decline, with an unpredictable duration, is a striking feature. Then, there are semiregular oscillations, called "pulsational" oscillations, with a pseudoperiod between 19 and 120 days. They have a visual amplitude of 0.2 to 0.4 magnitudes. Further, very short nonpermanent oscillations with time scales of 1 or 2 hours are detected in some RCB stars and may alternate with quiet stellar phases. Finally, a long-term periodicity (e.g., with a pseudo-period of 1100 days) is noted in the IR excess, generally in the *L* filter, perhaps due to a natural pulsation of the circumstellar dust shell.

Finally, the RCB star section looks at some correlations between observed quantities. The star, RY Sgr, gives good examples of correlations. We note that the beginning of the RY Sgr obscurational decline might be around phase 0.8, which is a "strategic" phase in Mira variables, coincidence raising the suggestion that the obscurational minimum is the result of one pulsational oscillation stronger than the others. The most important clues to the RCB phenomenon might be that, when the star drops into the deep minimum, the infrared excess is not affected: no change in the emitting flux of the dust shell and no change on the phase of the L curve. The CS envelope and the stellar atmosphere seems to be dynamically disconnected.

The hydrogen-deficient carbon stars are usually considered as *nonvariable HdC stars*. However, this conclusion might be linked to insufficient short time-scale observations (shorter than the explored week time scale). It is to be remarked that these stars do not possess any infrared excess and the hot, nonvariabe HdC star, HD 182040, has no envelope, suggesting no large mass-loss phenomenon; in addition, no chromospheric emission lines are detected in this star.

The last HdC subgroup concerns the *helium stars*. Generally, they are also considered as nonvariable stars. However, as for the "nonvariable" HdC stars, this might be an observational defect. In fact, the example of HD 160641 showing an evident brightening of the star by about 0.1 mag during 7 hours of observation demonstrates that short time-scale variations exist in helium stars.

Some stars appear as an evolutionary link between two classes of stars, such as MV Sgr with its light variations like those of RCB stars and its spectrum similar to the helium star, HD 124448.

Some words are given on "really" *nonvariable* or normal stars among M and C stars. One of the most valuable proofs that we are dealing with a normal M star is the nonvariability of the strength of the absorption molecular bands and atomic lines and of the adjacent flux peaks. They extend from M0 to M8 types with a luminosity class going from Iab to III. Some *early R Stars* are also nonvariable stars.

The last section of Chapter 1 proposes to study *irreversible changes and rapid evolution* in red variables. Firstly, *Miras* are considered through the example of the evolved complex object, *R Agr*. It is a binary star formed by a Mira (M7e) and a blue companion (the type of which is not conclusively resolved) and imbedded in a dense compact high-excitation nebula. This defines the spatially unresolved central object. The latter is surrounded by a convex lens-shaped nebula of 2 arc-minutes. An inner jet with an apparent changing structure and discrete variable knots is observed within 10 arc-seconds of the star. A counterjet is also

possible. The spectra of the inner nebula show striking changes in time and reflect a continuing activity in the central object.

Examples of irreversible changes in the SR and L stars are then given. Many M and C class stars showed rapid and definitive changes in one or more decades. V1016 Cyg is a binary system with a long-period variable and a hot star exciting a nebula. The analysis of the UV-rich emission-line spectrum indicates a sudden shell ejection and the formation of a planetary nebula with a very large excitation. The carbon star, HD 59643, provides another example of nonreversing and rapid evolution. Spectroscopic data examined over several decades suggest that the star activity is of recent origin. The UV emission cannot come from the photosphere; rather the radiation must emanate from a hot circumstellar envelope. From 1979 to 1983, UV lines from ions of a great range in ionization varied, and the continuum from 2200 to 1200 Å decreased significantly.

Another carbon star, the SRb variable, UU Aur, likely suffered an increase of the optical depth of the absorbing layers located at the temperature minimum, which smears out all the absorption features coming from layers situated beneath, and the chromospheric emission appears.

The *irreversible evolution of the various RCB stars* is not exactly the same. The detailed evolution of some selected stars is presented. The star, RY Sgr, is a slowly evolving one. It has a cepheid-like behavior, but a decrease of the pulsational period length (1.1 day in 80 years) has been confirmed by several studies. However, there appears to be some modulation in the linear rate of change of the pulsational period, with a time scale of 100 or 200 pulsational periods. This rate is close to that expected for a hydrogen-deficient star with $M = 1\ M_{\odot}$ and $T_{\text{eff}} = 6900$ K, evolving rapidly from the red-giant to the white-dwarf stage. Contrarily to RY Sgr, the RCB star, S Aps, is rapidly changing its period. From 1922 to 1960, the period is about 120 days. After the 1967 obscurational minimum, the instantaneous pulsational period becomes about 135 days; then surprisingly, after the next obscurational decline in 1971, the star develops an oscillation of a 37.5-day mean pulsational period. At the 1979 maximum, the period was about 40 days. Is such a phenomenon linked to a change of pulsational mode from the fundamental tone to some overtone? There is no model of evolution of hydrogen-deficient stars allowing such a rapid period change, although the evolution of a hydrogen-deficient star to a white-dwarf stage is rapid. In addition, it appears that a fading of the amplitude of the pulsational variations occurs in some RCB stars suffering such changes in pulsational period.

Variability in M, S, and C stars of which Chapter 1 shows the consequence particularly on light curves, evidently manifests itself on the spectral features (on their intensity, their shape, and their radial velocity). The main aim of *Chapter 2* is *to describe striking features in relation to nonthermal processes*. For three of the first sections, the spectral lines are reviewed by line type as an observer may discover them by glancing on spectra from the UV to the IR range: numerous absorption lines, sometimes emission lines, and also P Cygni or asymmetric, or multiple component absorption-line profiles. Each type of line results from the excitation conditions in the stellar layers in which it forms. Therefore, at the end of each section, qualitative results are drawn on the line-forming region (e.g., on its structure and its dynamics) that could serve to constrain a modeling. Generally speaking, each successive section naturally completes what is learned from the previous ones.

Among the preliminary remarks, the most important for understanding the stellar dynamics is the notion of center-of-mass velocity of the star (drawn from thermal radio lines), a constant velocity by definition and consequently the basic reference for line radial velocities inferring material motions (outfall to the interstellar medium or infall to the star).

Absorption lines that can be termed "classical" (i.e., unambiguously formed in the stellar photosphere) are described for their intensity and radial velocity variations with phase. The most numerous examples concern M and S Miras. The most striking feature is the distinction appearing between the radial velocities of atomic or molecular lines of low excitation potential χ (~ 1 eV) and of high χ (~ 2.5 eV at least). The first do not show significant change with the light cycle, whereas the last show a discontinuous S-shaped curve and a line doubling around the light maximum.

There are the characteristics of a shock wave crossing through the high-χ line-forming region. In the cool-star photosphere, the higher the line excitation potential, the deeper the line-forming layer is. Therefore, there are the deep photospheric layers which are disturbed by the stellar radial pulsation linked to acoustic waves that develop shock waves as soon as they emerge in the photosphere of the Mira. The low-χ molecular infrared, as well as blue atomic lines, do not suffer such an influence. It can be said that the high-χ lines definitely belong to the stellar photosphere (the pulsating part), while the low-χ lines belong to higher photospheric layers or rather to intermediate circumstellar layers. In fact, infrared lines of various excitation potentials reveal several stellar layers or atmospheric components in a Mira, as for example, in χ Cyg (from IR CO lines): (1) the pulsating photosphere we just discussed, in which the line excitation temperature varies from about 2200 to 4000 K because of the shock front running through it; (2) a 1500 K component, the material of which is observed falling down the star; (3) a layer at a stationary velocity (i.e., at the center-of-mass velocity) and of about 800 K, rapidly formed and vanishing; and (4) a 300 K component belonging to an outfalling circumstellar layer.

Other atmospheric layers can be shown by IR molecules other than CO, such as H_2O and OH, or by IR atomic lines. For example, in the Mira, R Leo, besides the photosphere ($3000\ \text{K} < T < 4500\ \text{K}$), there appears: (1) a layer intermediate between the photosphere and the circumstellar layers, with $T_{ex} \sim 1700$ K, more weakly pulsating than the photosphere (i.e., showing a weaker mechanical coupling with the deep pulsation); and (2) a layer at 1100 K, the radial velocity variations of which duplicate those of a 1000 K layer located at the inner limit of the circumstellar shell and showing a 16-km/s total amplitude, which still shows significant mechanical coupling with the photosphere. As for the visible spectrum—the blue-violet region around 4000 Å—chiefly presenting low-χ atomic absorption lines, it does not show significant radial-velocity changes. In χ Cyg, its mean radial velocity agrees with that of the CO infalling layer; this suggests that the visible atomic absorption lines do not form in the fully pulsating photosphere, but above it. There ought to be a slight line-doubling at maximum light; however, the effect of the continuum beyond 6000 Å is such that it obscures the outfalling component and gives the illusion that the gaseous layers responsible for the blue spectrum are always infalling. A few data on C-type Miras show that their photospheres behave like those of the M or S Miras, but the amplitudes of the radial-velocity curves in the function of phase are weaker (15 to 20 km/s).

Interesting are the scarce observations on the M and C semiregulars in which the photosphere shows the same pulsation phenomenon as that in the Miras, but with still weaker amplitudes ($\leqslant$10 km/s).

The section ends by displaying absorption-line radial-velocity histograms in Miras; they raise the question of whether one or two shocks present at the same time in the stellar atmosphere explain the observations.

The atomic emission lines are the outstanding features in the spectra of M, S, and C Miras around the maximum light. It appears that these lines, in the visible as well as in the ultraviolet observed by satellites, change their intensity (even disappearing in some cases around

the light maximum) and their radial velocity during the cycle. Selected characteristic emission lines are introduced and their profiles studied in Miras and semiregulars. Each line (from the neutral or ionized state, or fluorescent line, etc.) is formed in particular physical conditions and contributes to the understanding of the stellar atmospheric structure. *In the case of Miras*, it is shown how the emission lines fit into the shock-wave model clearly suitable to the infrared absorption lines and confirm it.

The radial velocities of the various emission lines are indicative of the velocities behind the shock. The question raised in the section *Absorption Lines* about the presence of only one shock at the maximum light in the stellar atmosphere or of two shocks at the same time (one located low in the photosphere, another in higher layers) to account for the excitation of the observed emission lines and for their radial velocity should be resolved by looking at the shock-front structure itself and at the different excitation conditions found there. *In the case of giant and supergiant semiregulars*, three examples are discussed. In the M supergiant, μ Cep, time-series observations indicate that the Balmer lines behave as in a Mira with a shock wave effective right from the lower photospheric layers. Other observations on other dates seem to contradict such behavior and to be explained by shocks that develop only when the wave reaches the highest layers of the stellar atmosphere. (This is really the chromosphere of the star, and the theory of Ulmschneider and coworkers is then valid.) There are such shocks that excite the emission of lines such as Mg II h and k or 3200 Å Fe II. The semiregular carbon star, TW Hor, nicely illustrates this mechanism in which the radiative damping of the waves occurs preponderantly while they are progressing through the photosphere. Finally, the M supergiant, α Ori, unambiguously shows a chromosphere extended up to about 1.8 R_* with a mean excitation temperature of about 8500 K. Although its photosphere pulsates as a Mira but with a weaker total amplitude ($\sim$6 km/s) characteristic of the semiregulars and one would expect acoustic waves progressing through it, the emission lines are excited by the energy dissipated as shock waves at the chromospheric level such as in the previous examples of μ Cep (at times) and TW Hor. However, the levitating motion of the matter, followed by its infalling as soon as the wave fades, is disturbed by the presence of a close companion observed at about 2.5 R_* from the α Ori center. The temporal variation of the emission-line radial velocities proves such a presence on the high chromospheric layers: material is attracted by a tidal effect and falls down at supersonic velocities as soon as the companion has no more effect on the observed layers, so that the emission lines are seen not only in outfalling gas but also in infalling gas. The radial velocities of selected lines show that the material motion caused by the companion does not seem to reach the layer called intermediary (above the photosphere) by analogy with Miras, or the photosphere itself in the limit of the measurement errors.

To summarize *atmospheric kinematics*, a heating mechanism common to cool stars, whatever their variability type, is suggested by the observations. That is, acoustic waves generated in the deep convective layer are transformed into shock waves at geometric atmospheric levels that are different in each star and even variable with time in a given star—even Miras may have their wave amplitudes so damped in the photosphere that the Balmer emission lines are not excited, an exceptional case in fact. It is obvious that the acoustic waves are responsible for the pulsation of the star with a more or less large amplitude. The question is raised as to why the waves in the Miras usually dissipate in shocks as soon as they enter the photosphere, although such behavior seems exceptional in the semiregulars. Although the radiative damping in the photosphere plays a role, it might not be the only discriminating element.

The last three sections of Chapter 2 concern the envelopes of cool stars. A section deals with *circumstellar (CS) lines*, and consequently with the *properties of the gaseous circumstellar layers*. The CS lines show a P Cygni profile or a blue-shifted absorption core. Their excitation potential is low (<1 eV); often they are resonance lines. The temporal variation of selected line profiles is displayed, as well as the line-profile variations with spectral types and luminosity classes. The high spectral resolution allows one to detect multiple components in the CS-line cores. The modeling of these components is at the root of our knowledge of circumstellar layers, particularly of their expansion velocity, their temperature, and their distance. However, some assumptions are usually adopted, the most drastic of which are the following: (1) the velocities are generally linked to a photospheric velocity and not to the stellar center-of-mass velocity, (2) the excitation temperatures are often not kinetic temperatures since the radiative processes dominate over collisional processes, (3) non-LTE effects are not taken into account to determine these temperatures, and (4) interpreting the excitation temperatures in terms of layer distances is erroneous due to the hypothesis that the gas and the dust are at equilibrium in the layer. Keeping these hypotheses in mind and looking at stars for which many observations are available over the optical, the near-infrared, and the radio ranges—such as the supergiant, α Ori, Miras such as χ Cyg, and the dust-enshrouded carbon star, IRC + 10216, various layers (expanding layers) forming the circumstellar envelope are described. For example, a 200 K layer detected through optical atomic lines as well as through infrared CO lines appears to be common to these stars. For the Miras, a convincing sample shows a stationary layer at 800 K. In the case of χ Cyg, a star carefully observed over several years, this layer has been rapidly built to vanish quietly in three cycles: it is a valuable candidate for a reservoir of matter both to form cooler expanding layers upon the impulsion of radiation pressure on dust grains that should be formed there and to form material infalling on the photosphere. The question is not fully resolved as for the presence of such a stationary layer in supergiants, even for α Ori. More observations are needed.

The multiplicity of the layers, for which there is no relationship between their expansion velocity, their hydrogen, or CO or dust rate, should lead us to believe that the material suffers multiple episodic ejections. However, a continuous distribution of matter can also produce such a structure, on the condition that the flux velocity slowly changes with the distance. Recent observations of IRC + 10216 show that this star is indeed such a good example.

The section mentions some methods of analysis of the CS-line profiles and reviews the measurements of extension of the circumstellar envelope by direct mapping from light emitted by the envelope in a given CS line, the central star being occulted. The typical star is α Ori. Deviations from spherical symmetry are evident.

The description of stellar envelopes is carried on through the *circumstellar dust*. The latter is detected by either the infrared excesses or the polarization measurements. First, the spectral energy distribution is described in M and C stars, emphasizing the excess emission signatures, mainly silicates and graphite, respectively. The temporal variability of the IR excesses is not significant, meaning that the grain rate in the circumstellar envelopes does not change very much with time. Nevertheless, the M Mira, *o* Cet, shows that the IR emission and particularly the 10-μm excess are clearly phase-dependent: dust is likely cyclically heated by periodic changes in stellar luminosity. Observations of many stars from M, S, and C spectral types and all variability types, covering a wide range in mass-loss rate, indicate that the dust-to-gas ratio is roughly constant in the circumstellar envelopes. This result is in agreement with a mass-loss mechanism by radiation pressure on grains.

The presence of dust is also detected from optical polarization observations. The linear intrinsic polarization is characterized by the change with time of its percentage and the rotation of its position angle, as well as of its wavelength dependence. Some correlations between the polarization and other parameters are looked for. An important remark is that there is no relationship between the polarization variations and the light changes, particularly in the Miras. As for the link to the infrared excess, it is concluded that: (1) for a given IR excess, either a weak or a strong polarization may appear, according to the considered star, and (2) no time variation of IR flux is observed in stars in which the polarization varies greatly. The polarization should produce localized rather than global effects in clumpy dust regions. Linearly polarized blue continuum light has been found from 550 to 3300 R_* around the supergiant, α Ori.

Characteristic properties of polarization are described in the case of specific stars, emphasizing narrowband observations, in the Mira, o Cet, the semiregular, V CVn, and the supergiants, μ Cep and α Ori. For example, the time change in percentage is either related or not related to the rotation angle variation—the wavelength dependence of the percentage and position angle of polarization is complex—sometimes with an increase in percentage across some atomic lines or molecular bands and a decrease across other spectral features at the same time. Temporal variability of polarization on short time scales (months) has been detected in the majority of stars, indicating considerable anisotropy near the star.

Present interpretations of the polarization features are then reviewed. The wavelength dependence, as well as temporal changes of the position angle and of the percentage of polarization, suggests that these could be caused by several active competing mechanisms in the same star, providing that a concomitant asymmetric envelope is present. The theoretical models explain the origin of polarization by the scattering properties either of asymmetrically distributed CS grains and/or of photospheric gas. The merit of the higher wavelength resolution observations has been to emphasize the possible contribution of the photospheric gas to the polarization. The model generally favored to explain the variation of photospheric polarization across the molecular bands (TiO) or atomic absorption lines (Ca I at 4227 Å) rests on the fact that the radiation emitted into the line of sight from near the stellar limb of the pulsating atmosphere is polarized by Rayleigh scattering. An increase or a decrease of the polarization in the molecular bands is related to the optical depth at which the Rayleigh scattering (by atomic and molecular hydrogen) dominates over the absorption (by TiO and H^-). A polarization varying in both degree and position angle across each of the TiO bands (e.g., in μ Cep) suggests Mie scattering from circumstellar grains besides the photospheric Rayleigh scattering. However, in the case of the Mira, o Cet, the high degree of continuum polarization does not appear to be explained by Mie scattering in an asymmetric envelope because departures from spherical symmetry are low. A magnetic field is invoked to orientate the particules; a systematic change in the grain alignment with a distance from the star is needed to obtain a change in the scattering geometry. The possible presence of magnetic fields in cool stars is discussed in a general scheme. Another source of asymmetry due to the dynamic effects of a binary system is depicted by the supergiant, α Ori.

Chapter 2 closes by surveying the "direct" approach to measure the *angular diameters* of stars and/or *to map the distribution of circumstellar dust and gas* by lunar occultation techniques or by the numerous interferometry techniques. Two prototype stars are studied: the M supergiant, α Ori, and the dusty carbon star, IRC + 10216.

For α Ori, multimeasurements at various optical wavelengths evaluate the photospheric apparent angular diameter (e.g., to be about 0″037) when observing in the continuum at 5350 Å. Infrared wavelengths are suited for determining the excitation of the circumstellar

shell and for showing departures from spherical symmetry, previously mentioned from CS-line profiles off the stellar disk. Betelgeuse is a star for which the structure of the circumstellar layers near its surface has been directly observed: the stellar disk is surrounded with a bright half-moon asymmetric cloud located at about 2.5 R_* (i.e., 0″05) from the stellar center and about 1 R_* large. Moreover, the reconstructed image observed in February 1982 indicates the presence of a companion located at 0″4 to 0″5 (i.e., 20 to 25 R_*) at 80° (modulo 180°) with respect to the North in the East direction. Another companion, closer to the star (located at about 2 R_* (i.e., ~0″4 in November 1980) would have an eccentric orbit with a period of about 2 years according to interpretations of polarization measurements. It may be suggested that the patchy dust cloud is caused by a tidal effect by the close companion. Following Draine's theory, "clean" dust grains are able to form near the star, probably in the low chromosphere where the temperature is relatively low. They should then be ejected by radiation pressure, so that they are responsible for the IR emission detected at 45 R_* (0″9) from the α Ori photosphere.

Data on multispectral spatial mapping of the dusty carbon star, IRC + 10216, are summarized. The dust cloud has been mapped up to a radius of 1200 R_* (27″); it is quite asymmetric, with the amount of asymmetry varying with wavelength and radius. Elliptic contours are evident. The gaseous (CO) emitting region has been mapped up to a radius of at least 8000 R_* (3′); the cloud is circularly symmetric about the center of the star. We deal with a mixed morphology (a disk viewed at low inclination to account for the circumstellar dust geometry plus a sphere) that might be explained by a close binary system, among other interpretations. Other mixed structures observed in extreme C stars formed by a dusty equatorial torus and polar scattering lobes might show their evolutionary link with bipolar nebulae.

Completing the description of observed features begun in the previous chapters, *Chapter 3* deals wth *circumstellar radio molecular lines*. In fact, the extended shells of both visible and unidentified infrared cool stars also emit molecular emission lines at centimeter and millimeter wavelengths. Appropriate molecular transitions occurring at various stellar radii (from SiO masers near the star to thermal CO or cyanopolyne emissions in the outermost circumstellar layers) can sample different shell layers and serve to probe their physical conditions.

The first radio detections of *circumstellar molecules* were of OH and H_2O maser lines in oxygen-rich late-type stars, mainly Miras and red supergiants. A list of the presently known circumstellar molecules in cool stars is given (about 60). Their lines are characterized by their broad line width, which reflects the large scale expansion of the shell (~5 to 50 km/s).

The radio emission from OH, H_2O, SiO, and SiS presents characteristics of nonthermal processes. Masers were variable sources whose intensities are correlated with those observed in the near-infrared. They present a high degree of polarization (e.g., OH and SiO). Population inversion can be achieved through pumping by infrared radiation from warm circumstellar dust grains or from the central stars. Details of the pumping mechanisms are illustrated by a simplified maser theory in a two-level maser and by the description of radiative transfer for a multilevel maser.

Characteristics of circumstellar masers are then defined. The maser emission is often characterized by a double-peaked spectrum (e.g., OH). This shape is explained in terms of a spherical model in which the amplification path is maximum in the direction of the line of sight that intersects the central star. Examples of maser spectra are shown, and the pumping appropriate to a given maser is discussed.

Thermal emission from SiO, CO, CN, and CS and their isotopes is detected in M, S, and C stars. Linear carbon chain molecules (HNC, HCN, $HC_{2n+1}N$, etc.) also exist in the

carbon-rich stellar shells. Thermal emission spectra extend over the whole envelope and give information on the physical parameters of the entire shell (mass loss, gas and dust densities, etc.). Molecular excitation involves collisional and radiative processes. Collisions, essentially with H_2, tend to thermalize the lines. The various *line profiles* (rectangular, parabolic, double-peaked, etc.) are explained in relation to the nature of the circumstellar shell (optically thick or thin, resolved or not, etc.). *Line asymmetry* (blue-shifted wing weaker than red-shifted one) is observed: because the inner shell is more excited and hotter than the outer shell, the result is that, along the line of sight, the outer colder material is absorbing emission from the hotter inner layers in the front hemisphere but such absorption does not affect the back hemisphere. In this case, the brightness temperature of the source must be calculated separately for the front and back hemispheres.

The time variation of infrared light also influences the maser molecular line shape. At the IR light-curve maximum, infrared photons escaping from the central heating source can affect the outer shell and enhance the line wings.

The conclusions of Chapter 3 emphasize how the radio molecular lines are useful as probes into the stellar environment, from the immediate vicinity of the stellar photosphere to the external envelopes.

As shown in a previous chapter (Chapter 2), infrared astronomy firmly established the presence of dust around a large number of red giants and supergiants. *Chapter 4* details *the formation of grains and radiation transfer in the circumstellar shells.*

Concerning *the grain formation*, the formalism generally adopted in the literature is the theory of homogeneous nucleation. Its basic ideas and main results are recalled. Definitions are given for important quantities such as the critical nucleus radius, the rate of nucleation, and the supersaturation ratio. Because the circumstellar gas is a complex mixture in which many species are able to condense and clusters of one kind can act as condensation nuclei for another material, the heterogeneous nucleation is mentioned, and an example of this complicated problem is evoked.

The equations of the homogeneous nucleation theory imply thermodynamic equilibrium in which gas, clusters, and grains have the same temperature. In the circumstellar shells, the presence of a *strong stellar radiation* and a low gas density constrains the theory, and its principles are described. The particular case of the influence of a chromosphere on the existence and the condensation of grains (particularly clean silicates) is also raised.

Is the structure of the circumstellar grains (amorphous or crystalline) predictable by the theory of nucleation and growth? The structure of clusters containing few atoms or several tens of atoms is not known. Arguments in favor of amorphous or crystalline graphite in cold carbon stars are analyzed.

The problem of the formation of grains can be solved only if the density and the temperature of the gas and the composition and the temperature of the clusters are known at every point in the shell and at each moment. *A time-dependent nucleation and growth* is needed. It is the saturation time scale which governs the situation. Scenarios are presented for a dynamic evolution of the shell influenced by radiation pressure on the grains.

Conclusions of the section *Grain Formation* emphasize the deficiencies of the theory of homogeneous nucleation applied to real circumstellar shells: (1) uncertainties in the physical parameters of the solids and the kinetics of the growth of grains in the expanding gas; (2) the erroneous hypothesis of thermodyanmic equilibrium in a gas containing a wide number of species able to condense or deposit onto other grains; (3) possibilities of local condensations or strong variations in the density allowing nucleation to begin even where the average density seems too low; (4) propagation of shock waves in the shells, perhaps influencing the

evolution of grains; and (5) temperature of grains linked to a well-defined photospheric stellar radius and to the blackbody radiation at the stellar effective temperature, although it is known that the radiation at different wavelengths does not arise from the same photospheric levels.

The next section is about *the radiative transfer in circumstellar dust shells*, which is generally treated independently of the formation of grains.

The solution of the transfer equation in a spherical shell (extended atmosphere) attempts to correctly describe the radiation field at each point in the shell. To define a model, it is necessary to fix the stellar characteristics (effective temperature and radius), the geometry of the shell (inner and outer radii and density), and the properties of grains (size and optical properties). The shell boundaries are discussed in more detail. The model of grains used is the main source of uncertainty. For example, optical properties of graphite grains entering in carbon-star shell models are not always correctly described.

Before considering models built for various type stars, some general results are noted: (1) the circumstellar extinction opacity law does not have the shape of the interstellar extinction law at wavelengths where scattering is efficient; and (2) the theoretical existence of a sharp maximum of the energy flux from the direction of the shell inner boundary is pointed out. This bright ring corresponds to the maximum of the column density of grains reached when the impact parameter is equal to the internal radius of the shell. If it is detected through measurements of high angular resolution, the inner limit of the shell can be fixed, and the radiative equilibrium of grains can be better understood.

Various models of shells around oxygen stars are reviewed. Among them, a model involving dirty silicates, widely used afterward, fits the theoretical flux curve and the profile of the emission bands between 0.25 and 8 μm, and another model fits the 10-μm-band profile in a set of giants and supergiants, showing the possibility of an increase in the radius of the grains with the galactic latitude. An extended grid of expanding spherical shell models (with small silicate grains and a density in r^{-2}) gives inner grains hotter than 1000 K in most cases. Some other models are developed for a particular object, as for α Ori. Models of shells around carbon stars are then presented, in which the involved grains are carbon grains. A good representation of the flux curve is obtained with an expanding spherical shell and small carbon grains. The hotter grains are at 1000 to 1300 K. Some models attempting to fit the particular carbon star, IRC +10216, are summarized.

Finally, *nonspherical shells* are discussed; as mentioned in Chapter 2, they are needed to interpret efficient, intrinsic polarization of stars. The complete treatment of the transfer of the scattered stellar radiation in an ellipsoidal shell has been done without approximation. The numerical simulation highlights several points:

1. A shell with a constant density cannot produce a polarization higher than 12 percent.
2. Even if the opacity is modified, a rotation of 90° of the polarization angle at a fixed wavelength is maintained. In fact, it is an individual property of grains. The rotation disappears when the grains are strong absorbers, such as the graphite.
3. High polarization rates and the observed steep variation of the polarization angle can be obtained only if the direct stellar light is attenuated along the equatorial plane and scattered mainly near the polar regions of the shell (bipolar nebula model).

Concerning the physical mechanisms responsible for the loss of spherical symmetry, rotation and magnetic fields are most often invoked. However, the shell shape can also be related to processes that induce the ejection of matter at the stellar surface. The importance of the hypothesis of sphericity on several physical quantities is evaluated through the transfer of

infrared emitted radiation in an ellipsoidal shell in the constant density case. Numerical simulations have shown that the spatial repartition of flux is very asymmetric at every wavelength when the opacity is low.

In the near future, the problem of transfer must be tightly linked with the study of the dynamic evolution of the shell.

Mass loss, discussed in detail in *Chapter 5*, was noted 50 years ago, but the development of the field had to await modern instrumentation, and almost our entire knowledge of mass loss and its consequences for stellar evolution and interstellar pollution has arrived in the past 10 years. A general overview of the historical development of both observational and theoretical ideas on stellar mass loss lays the foundation for our present understanding. The newness of the field and the incompleteness of our present theoretical modeling of mass loss are set forth in a straightforward fashion.

Empirical determinations of rates of mass loss from spectra in the range 0.20 to 5.0 μm for various types of stars are considered in detail. The spectra themselves are first described, and we are led step by step through the analysis of the lines to infer column densities and the expansion velocities. The considerable uncertainties attached to the calculations of ionization equilibrium to obtain the total column density of atoms of a particular element are discussed, and the severe contradictions between results for different workers and different elements are displayed.

The rate of mass loss depends on the density, the square of the radius, and the velocity. If the density falls off as the inverse square of the distance, the mass loss depends on the column density, the terminal velocity, and the inner radius of the CS shell.

Well-known difficulties in deducing the inner radius of the CS shell are described, as are the methods used by various workers and their results. The estimates lead to reasonable results in some stars and poor results in others. There is the more serious question, of course, as to whether there is generally a well-defined inner radius in all stars. In α Ori, for example, there are at least two well-defined shells. In several stars, evidence exists for episodic mass loss, which renders quite uncertain any attempt to infer mass loss in terms of a steady process. At least some of the uncertainties in estimating the inner radius can, in principle, be avoided by considering binary systems, and several well-known systems have been studied in this way, including systems of the Zeta Aur type.

Several *new insights* have come from a study of *Mira variables* over their cycle. In particular, four separate CS regions could be seen in the S Mira, Chi Cyg: (1) a pulsating photosphere, (2) a cool gas (1500 K) falling back onto the photosphere, (3) a cooler (800 K) stagnant region, and (4) a very cool (350 K) outflowing gas, the CS shell itself. The same structure is apparently found in other Miras as well. The observations complement and amplify observations indicating a similar stationary shell in α Ori, which suggests a common mechanism for mass loss in both Miras and supergiants. The stationary region, presumably supported by dissipated shock energy, provides a reservoir of material for grain formation (calculations show grains would form here) and for the infalling material observed.

It is by now well known that a mass loss of 0.2 solar mass on the red-giant branch (RGB) and another 0.1 solar mass on the asymptotic giant branch (AGB) are necessary to bring the calculated distribution of stars on the HR diagram into agreement with the observations for globular clusters. The presence of Hα in the spectra of globular-cluster red giants has been taken as indicative of mass loss, and several calculations of mass loss based on the idea that this emission arises in a CS shell have been made. There is some doubt, however, that the Hα emission necessarily comes from a CS shell or necessarily requires mass loss.

The common occurrence of excess emission at 10 μm in oxygen-rich stars and at 11 μm in carbon-rich stars is understood to arise from CS dust, and its shape and strength depends on the temperature of the dust (hence, its distance from the star if in thermal equilibrium), its optical depth, and its composition. All three parameters cannot be found uniquely, and some assumptions are usually made regarding grain composition or optical depth. A more favorable spectral region for study—just now being explored—is the submillimeter range, in which the dust becomes optically thin and its radiation is in the Rayleigh-Jeans part of the spectrum.

Observations of molecular line profiles, notably CO, in the millimeter wavelength range provide additional information, and several studies of such data are described. Allowance for departure from LTE is made. Models assume that mass loss is by radiation pressure in spherical symmetry. These relatively sophisticated studies have sometimes been combined with information from other wavelength regions.

In OH-IR stars with thick dust shells, the usual equations assume somewhat simpler forms, and mass-loss rates for these objects are often fairly accurate. One of the more interesting developments of recent years is the uncovering of the links between the Miras and OH-IR stars, and the indication that they constitute an evolutionary sequence leading to the formation of planetary nebulae.

A *tabulation* of *mass-loss rates* for selected stars of all types is given and discussed. It is hoped this will provide a convenient reference list for all workers in the field. It is noted that: (1) among early M stars, rates for supergiants exceed those for giants by a factor of 10, (2) rates for planetary nebula and Miras are comparable to those of early-type supergiants, and (3) M and S stars show a much larger scatter in their expansion velocities than that of carbon stars.

Evidence that at least some mass loss is episodic continues to accumulate, and several examples are given. Again, α Ori is the best studied.

Many *mechanisms* have been proposed to account for *mass loss*, and it seems unlikely that one mechanism is responsible in all stars. The usual mechanisms for steady mass loss are reviewed: thermal gas pressure (which appears too weak for cool stars in general), radiation pressure on dust grains, shock waves (especially in Miras), and Alfvén waves. Dust-driven flow, the popular favorite, has been extensively studied and applied. The increasingly sophisticated treatments of this mechanism are described. Some workers have begun using the stationary region found by observation in Miras for calculations of grain formation and as a starting value of the distance from where the gas is driven outward by radiation pressure on the grains. The results are found to be strongly model-dependent, and more sophisticated models tend to give lower rates of mass loss.

Although the assumption that *all* outflow is driven by radiation pressure on grains is often made, it is far from proven. Evidence now available indicates that this mechanism almost certainly is responsible for mass loss in the coolest M and S giants and supergiants, including Miras. It is unproven, and seems somewhat doubtful, for the warmer M supergiants and for the carbon stars. Shock waves have received considerable attention as a means for generating mass loss in Miras. It appears that some combination of isothermal and adiabatic shocks can play a major role, at least in levitating the atmosphere and perhaps in driving the mass loss itself, as least out to the point of grain formation. Alfvén waves have received relatively less attention, although some authors have pointed to their several attractive features. Certainly, they can levitate outer atmospheres by heating. Whether they can supply enough energy to lift the atmosphere without simultaneously producing more emission than is observed

appears uncertain at present. Several mechanisms for episodic mass loss are also reviewed, but this field is far less developed than that of steady mass loss.

This chapter closes with a discussion of the *evolutionary consequences* of *mass loss*. Four aspects of mass loss are reviewed: (1) the evolution and frequency of supernovae; (2) the HR diagram of globular clusters; (3) the composition of interstellar matter; and (4) the formation of planetary nebulae.

Circumstellar chemistry, described in *Chapter 6*, is an active new field of astrophysics. In fact, this is one of the first reviews of progress in the field. Closely allied with the study of interstellar molecular clouds, CS chemistry treats the molecular, atomic, and ionic reactions occurring in matter expelled from the star, which forms an extended, expanding CS envelope. It is pointed out that CS shells are in some ways more tractable than interstellar molecular clouds, and some insight into the latter may be gained by studying CS envelopes.

After an introduction to the short history of research on circumstellar chemistry, general considerations of the *regimes* of *temperature*, *velocity*, *sizes*, and *densities* relevant to the study of circumstellar chemistry are given. Wind speeds are low (~ 10 km/s), dimensions are large (up to 10^{18} cm) compared to the stellar radius, and the mass-loss rates are substantial (10^{-7} to $10^{-4}\ M_\odot$/yr). Densities at these distances range from 10^6/cm^3 down to 10^2/cm^3. Because these values are so vastly different from those in the corresponding stellar photospheres or chromospheres, it is clear that the matter must pass through a great range in physical conditions in moving from the photosphere to the CS shell. As a consequence, we must expect different physical processes to dominate at different distances from the star. Although thermal processes may dominate close to the star (and there is some evidence that they do), the material must come out of equilibrium as the density falls away from the star, and other processes may become important.

Photodissociation and photoionization due to the galactic UV radiation must dominate in the outer reaches of the CS envelope.

As is natural in a new field, *observations* lead the way. As in perhaps no other field, CS chemistry profits in a vital way from information from every spectral region. Yet observations across the spectrum have been made for only a very few objects, and these are best discussed individually, especially since there is no proof that these nearby, best-observed objects are typical of CS shells as a group.

Although hydrogen is the most abundant element, it has not been detected either as H I or as H_2 in a CS envelope with a cool central star. The sensitivity of these upper limits is just reaching astrophysical interest for one or two objects. In IRC +10216, the limit on the fractional abundance of atomic hydrogen determined by the lack of detectable 21-cm-line radiation begins to impinge on theoretical predictions. In α Ori, the upper limit to the mass-loss rate implied by the lack of detectable 21-cm radiation is close to the total mass-loss rate predicted by some models. Hydrogen is, of course, seen in planetary nebulae, and these objects constitute a useful boundary condition for investigations of CS material.

Much interest attaches to the observations of molecules containing C, N, and O in CS shells, but the observations, except for one or two objects, are spotty. Particulary well studied is IRC +10216, where over 20 molecules have been detected. Tables of abundances are available and a summary is given here, but these are uncertain to a factor of 3 even in the best cases because of the difficulties in interpreting the observation. The significant enhancement of HCN compared to molecular clouds and the great abundance of such radicals as CN and C_2H are interesting problems and clues.

In the CS shells of M and S stars, the most extensive observations are those of the masing lines of OH, H_2O, and SiO. Interpretations of these observations are only partially relevant for CS chemistry. Although no counterpart to +10216 for M stars is known, the molecules CO, H_2O, SiO, OH, and NH_3 are observed in some sources. Extended observations of K I at great distances from α Ori have allowed some modeling, as described in Chapter 5.

Valuable insight into the processes involved in CS shells can be gained by comparing dynamic time scales with those for photoprocesses, ordinary chemical reactions, and three-body reactions. It seems clear that, except close to the star, these processes can dominate over equilibrium. In the outer parts of the shell, photochemistry will dominate.

Two models of CS chemistry have generally been applied: *thermal equilibrium* and *photochemistry*. Thermal equilibrium is applicable only close to the star and appears to describe adequately (within a factor of 2 to 5) the abundances of such simple molecules as CO, C_2H_2, HCN, and CH_4. The model fails for NH_3, which is observed to be overabundant by a large factor. SiS and SiO are observed to be underabundant, perhaps because they are incorporated into grains. All radicals are overabundant by large factors, the most extreme cases being CN and C_2H. Even the apparent successes of the thermal equilibrium model must be viewed with some reservation because dust formation has not yet been included. Relevant chemical rections for both oxygen-rich and carbon-rich atmospheres are discussed. Although solutions are available for oxygen-rich atmospheres, none are yet available for carbon-rich atmospheres.

Shocks are observed in Mira variable stars and may be important in other types of variable stars as well. Generally, these have been discussed as a source of the energy and momentum for mass loss. At the same time, however, they cause additional excitation and could be important for diagnostic purposes.

Photochemistry may be important everywhere in the CS cloud, for the ultraviolet radiation from the chromosphere may be a source near the star, and the galactic radiation field will be important farther out. Most attention to date has been given to the abundant molecules H_2 and CO and to the formation of heavy radicals from the corresponding parent molecules. The photochemical models demonstrate, however, that molecules cannot long survive in the outer portions of CS shells. This is in contrast to grains, which can well survive the journey through the CS shell.

The marvelous observations of red-giant stars assembled in Chapters 1 and 2 challenge the imagination of the boldest maker of atmospheric models. In *Chapter 7*, we examine the current state of knowledge of *thermal static models*. The physical principles of the classic stellar atmosphere—constancy of total (radiative plus convective) energy flux, local thermodynamic equilibrium, and hydrostatic equilibrium in a plane-parallel, horizontally homogeneous geometry—are assembled and displayed. Possible generalizations of these are envisioned, although the addition of convection in the local mixing-length theory and spherical geometry are the only generalizations that seem likely in the immediate future.

In discussing the opacities of red-giant atmospheres, we pay particular attention to the effects of spectral lines. Any spectral line, irrespective of its mode of formation, location in the spectrum, or region of formation blocks radiation, and this is called line-blocking. Since energy flux conservation is imposed at every depth, the energy blocked by the line must appear in some other part of the spectrum. To drive this extra flux through the atmosphere requires a slightly steeper temperature gradient, and this change is called backwarming. Whether the line cools or heats the outer part of the atmosphere is discussed on the basis of both physical intuition and mathematical formalism, including departures from LTE and the effects of various mechanisms of line formation.

In hotter stars, the relatively few spectral lines can be treated individually, while in red giants, the millions of spectral lines must be treated collectively or statistically. Statistical methods for treating this forest of lines are described, starting from relatively crude methods such as the straight mean and the harmonic mean opacities to the powerful modern methods such as the opacity distribution function (ODF) and opacity sampling (OS). After a brief review of each of these, including the Voight-Analog-Elsasser-Band model (VAEBM), an offshoot of the ODF, the relative advantages and disadvantages of each are described. Once an ODF is computed, models are quickly computed. However, the ODF must be recomputed for each important change in input parameters. Thus, it excels in grids of models for which all input parameters are known at the outset. By contrast, since the OS method uses no averaging whatever of the opacities, it is entirely flexible and can easily accommodate any desirable changes in input parameters. This flexibility means, however, that the calculation of each model is relatively slow. Recent work by the Swedish group that allows ODF's for different molecules to be combined quickly and accurately overcomes a major drawback of the ODF. We speculate that both methods are capable of further development and foresee the calculation of grids of atmospheres including many additional molecular opacities and millions of additional lines.

Published models for *red-giant stars* are presented and discussed in two categories: oxygen-rich and carbon-rich. The widely used BEGN models are discussed because the coolest are of interest here. Based on ODF opacities of CO, CN, CH, NH, OH, MgH, and atomic lines, the grid covered the range in $T_{\rm eff}$ from 3750 to 6000 K, in log g from 0.75 to 3.00, and from solar to 0.001 solar in metal abundance. Convection is treated. As a simplified ODF, the VAEBM method was introduced by Tsuji and used by him to compute a grid of red supergiant stars. These models were then used for a discussion of Betelgeuse. A set of 22 models were later computed for red giants. Tsuji found that his predicted emergent flux curve in the infrared sufficiently matched the available photometry and spectrophotometry of K and M giants to allow a calibration of the temperature scale for these stars. Later, to better exploit the models, Tsuji used the models and L-band photometry of 22 K and M giant stars to infer their effective temperatures by the method of infrared photometry. Based on the ATLAS5 computer program and OS opacities for several molecules, but treating H_2O by straight mean (SM) opacity, the Indiana group computed 40 models for red giant and supergiant stars. We are reassured by the good agreement between models from these three groups.

Models for carbon stars begin with the French group. Based on ODF opacities, they computed a total of 35 models with various compositions to include both CNO processing and triple-alpha material. These were used, with only fair success, to deduce effective temperatures and abundances of C and N for UU Aur and TX Psc. A set of 27 Indiana models of M, S, and carbon stars is discussed. Because these form a uniform set, they are used to study the variation of the atmospheric structure as the ratio C/O is changed. A model with C/O = 1.0 is similar in structure to an unblanketed solar model with the same parameters, emphasizing the lack of opacity in the S stars. New, unpublished models by the Swedish group are described. These include for the first time the opacity of HCN and C_2H_2. Finally, it is noted that models for R stars computed by both the Swedish group and the Indiana group are in excellent agreement.

Spherical models are probably necessary for some supergiant stars and most Mira stars. Although models available at present have been computed with very simple opacities, usually SM, certain features of sphericity already are clear. It is shown, for example, by groups in Germany, Japan, and Latvia, that an extension of the atmosphere always leads to a decrease in the temperature and density in the outer layers of the atmosphere. It is also shown that

most stars of mass $M = 1\ M_\odot$ will pass through a stage of atmospheric extension sometime during their lifetime. These conclusions have been confirmed and extended in work with increasingly more accurate opacities. For example, it is noted that, although the density of most molecules follow the general decrease of the atmospheric density, certain ones (e.g., H_2O) behave oppositely. The radius of the star also increases significantly in the molecular bands that are sensitive to the extension. An observational third parameter has been sought, and the interesting suggestion has been given that 1- to 4-μm color might give T_{eff}, certain metal-ion lines can give surface gravity, and the red TiO lines may be sensitive to atmospheric extension. The effect of metal and CNO abundance on the M-giant atmospheres is reviewed. Lastly, we describe the first crude carbon-rich model calculated and the finding that, because of the greater sensitivity of the carbon-rich composition to the temperature, the carbon star was less extended than a comparable M star.

Convection, another possible generalization of the basic equation of the classic stellar atmosphere, is briefly discussed. Several attempts to build a better theory than the local-mixing-length theory are described. It appears that some progress is being made, but a self-consistent workable theory may still be in the future. While waiting for that theory, workers are attempting to better determine the parameters of the mixing-length theory. It is pointed out that convection is not expected to be important for determining the structure of red-giant photospheres, but may well be important for several other applications that are listed. Inhomogeneities remain a miserable problem on the horizon. Although their existence generally is an open question, some possible effects are pointed out.

Comparisons are made between the predictions of the theoretical *models* and available *observations*. For the M stars, the correct prediction of the empirical relation between effective temperature and color temperature (on the Wing system) with theoretical models by three independent groups establishes a cornerstone of assurance that, for M-giant stars as cool as M5, accurate models are available. For S stars and carbon stars, the situation is not as comforting. Broadband observations are fit only moderately well by the French models, although these have been used in conjunction with L-band photometry in the IR method to deduce temperatures for carbon stars that are in fair accord with the few available from angular diameters. Fitting a segment of stellar spectra is shown not to be a strong criterion of the goodness of a model atmosphere. For S stars, models fit sufficiently well to establish a temperature scale both by model fitting to spectrophotometry and by the method of IR photometry; further improvement depends on a better knowledge of the CNO composition.

We close with a discussion of spectral features that might be particularly sensitive to such variables as effective temperature, temperature structure, surface gravity, composition, pressure, atmospheric extension, and chromospheres and mass loss.

Following the strictly thermal models of the last chapter, which were based on the concepts of *hydrostatic equilibrium*, *radiative equilibrium* (sometimes with convection), and *local thermodynamic equilibrium* (LTE), we examine in *Chapter 8 theories and models that relax these assumptions*. After a short introduction, we analyze: (1) departures from LTE in thermal photospheres, (2) chromospheres of red-giant stars, and (3) the gas dynamics of shock and its application to these stars.

Atmospheres of red-giant stars are quite different from the atmospheres of hotter and more compact stars. Lower densities and temperatures guarantee abundant formation of molecules. The photosphere overlies a deep convective zone from which mechanical energy in various forms is available for dissipation in the outer atmosphere. Scale heights are frequently very large, and effects of sphericity are often important. Inhomogeneities, perhaps linked to convection, may be common. All red-giant stars are variable in some way, and

shock waves are often linked to the pulsations that must underlie the variability. Mass loss is a common phenomenon.

It is convenient to begin with the *photosphere*, which is also the best studied region. Departures from LTE in a given thermal photosphere are first discussed. The equations of statistical equilibrium and radiative transfer are displayed to remind us of the important terms and the nature of the coupling. The pioneering nature of work in the fascinating red giants is eloquently emphasized by the paucity of previous research. The formation of the Li I line, a sensitive diagnostic of thermal and mixing history of the material, is described in both oxygen stars and carbon stars and is related to the abundance. In M stars, no effects of departures from LTE larger than 0.1 dex in Li I could be found. In carbon stars, departures from LTE, which were more sensitive to the abundance than the (poorly known) UV radiation field, produced somewhat weaker lines than in LTE.

Considerable interest attaches to molecular line formation, since much of our information comes from analyses of these lines. Vibration/rotation lines within the ground electronic state (found in the infrared for most molecules) are formed in pure absorption due to the dominance of collisional processes, whereas excited electronic transitions are generally radiatively controlled, and lines connecting these states to the ground state are mostly scattering. Fluorescence of many CO lines by atomic lines in the far-UV is mentioned.

A more general attack on departures from LTE in photospheres consists of solutions of the statistical equilibrium equations for the principal electron donors—Na, Mg, Al, K, and Ca—along with the atmospheric equations for several cool stars. Although the temperatures of the "non-LTE" models differ little from the LTE models that formed the starting point of the calculation, the electron density is significantly lower in the non-LTE models for the coolest stars—a factor of 14 at 2500 K. Similar, exploratory values for carbon stars are shown.

It is clear that most cool stars have *warm chromospheres* and mass loss, but no trace of transition-region lines and no indication of coronae. Instead of these hotter regions, many late-type giants appear to have enormous warm chromospheres. How are these extended regions created, supported, and heated? Due to the low temperatures involved, thermal support will certainly be insufficient, and such other pressure-producing mechanisms as turbulence, magnetic fields, or shockwaves—perhaps coupled to pulsations—must be invoked. Evidence for the existence of those extended regions comes from estimates of the C II-emitting regions. Geometrical effects of these extended zones have important influences in problems of line formation.

Other problems are mentioned. There is evidence of a possible hydrogen deficiency in some of these cool red-giant stars. Perhaps these red-giant stars commonly have inhomogeneous or bifurcated atmospheres in which a warm material producing ionic emissions coexists with a cool material produced by important coolants, such as the CO molecule.

Although intensive research has been focused on the G and K giant stars, very little has been done on any cooler stars, with the possible exception of α Ori. Most of this work has been semiempirical in nature. That is, profiles for Mg II and Ca II have been calculated for a set of arbitrary chromospheres, and the appropriate model has been chosen as that giving the best fit to the observations. A purely theoretical approach is still in the future. Models for α Ori—everyone's favorite cool star—are presented and described. (These are also discussed in Chapter 5.)

N-type carbon stars also display emission lines of Fe II, Mg II, and C II, indicating the presence of a temperature inversion and a warm chromosphere. In some stars, these lines are variable. From low-resolution observations, it appears that the chromospheres are much

weaker, however, than those of corresponding M stars, and that difference presents a challenging but unsolved problem. The first simple modeling of carbon-star chromospheres has begun with models that at least produce the Mg II emission but without exciting the Balmer lines, which are not observed. Predicting the C II lines will be more difficult. Models also predict a strong absorption feature due to Mg I at 2850 Å, which is not observed, and it is speculated that this feature is filled in in the star by emission from a cool extended outer region.

Shocks may play rather significant roles in *Mira stars* (perhaps in all red-giant stars), and these are discussed in detail. The Rankine-Hugoniot equations are derived and applied to simple cases. Consideration is given to conditions in the preshock and postshock regions. Emission lines in Miras have been classified into two groups: primary lines and secondary lines. The primary lines—Mg II, Ca II, Fe II, and Ti II—are supposedly formed in the postshock region, and the secondary lines are formed in the preshock region by fluorescence from the primary lines. The influence of shocks on the thermal structure of the atmosphere could be considerable, but sufficiently detailed calculations are not presently available to elucidate this point fully.

A discussion of the mode of pulsation of Mira stars concludes the chapter. The evidence for either a fundamental-mode pulsation or a first-overtone pulsation is displayed. Apparently, the matter is still in dispute.

In the final two chapters, we turn from the fascinating red-giant stars to the "solar/stellar connection" and a discussion of M-dwarf stars. *Chapter 9 summarizes* the flood of *new observations*, especially from *spacecraft*, over the past few years and *describes* the *expected* and *unexpected phenomena* displayed by both the *normal* (dM) and *emission-line* (dMe) *stars*, the latter distinguished by the appearance of Balmer alpha in emission.

Most well-observed M dwarfs are quite near, and their trigonometric parallaxes are therefore quite reliable, so that accurate absolute luminosities are known. Since many dM and dMe stars are also members of binary systems, masses can often be determined, and these range from about 0.06 solar masses (the lower limit for hydrogen burning) up to about 0.60 solar masses. For CM Dra and YY Gem, reliable radii and masses can be determined because they are both spectroscopic and eclipsing binaries. These low-mass objects support vigorous convection, and this must be the source of the energy that gives the dMe stars their unusual characteristics. Methods and results of determinations of mass, location, and density in the galaxy, age, effective temperature, radius, surface gravity, and the more exotic phenomenon that are revealed through ultraviolet X-ray and radio data are reviewed. Several tight relations involving effective temperature, bolometric correction, absolute visual magnitude, and several color indices are displayed.

Although the mass of an individual M dwarf is small, these stars are so abundant that they constitute a substantial mass component of the galaxy; among stars, in fact, they may be the largest contributors of mass! Although their contribution to interstellar gas is still a matter of debate, it is possible that they also contribute a substantial amount of the mass loss from stars.

Due to the extremely low temperatures of M dwarfs, their optical spectra are dominated by strong molecular bands of TiO and CaOH with many fainter atomic and molecular contributors. H_2O also contributes strong bands, especially in the infrared, and these bands increase strongly and monotonically as temperature decreases. In many single dMe stars, the Balmer alpha line also has a very narrow central reversal, for which a number of surface features have been suggested as being responsible.

Approximately 75 percent of all M-dwarf stars are emission-line objects. The fraction of dMe stars increases with advancing spectral type until it reaches almost 100 percent at

M5. However, a few stars of even later spectral type do not show emission lines, and this must be related to some as yet unknown feature of the outer atmosphere.

An apt analogy for dM and dMe stars appears to be a solar plage. Since these are characterized by an enhanced magnetic flux, it is assumed that the same will be true for dMe stars. Both the source of the nonradiate flux and the magnetic field may be stronger in the M dwarfs, leading to the enhanced emission observed there. A self-excited dynamo in the convection zone is generally accepted as the basic mechanism for magnetic field generation in active stars. The dynamo is driven by differential rotation, which arises in turn from the interaction of convection and rotation. This is consistent with the fact that dMe stars appear to have higher rotational velocities than those of M dwarfs generally. The M dwarfs are thus assumed to be cooler and more energetic analogies of the Sun in their chromospheres and coronas. The chromospheres of dMe stars are less extended, hotter, and denser and show larger surface inhomogeneities than the Sun. The electron temperatures of the chromospheres of dMe stars appear to be somewhere between 10000 and 14000 K.

Ultraviolet observations have revealed an array of strong ultraviolet emission lines that allow considerable insight into the physics of red-dwarf atmospheres. Major observational results include the following:

1. Radiative losses in the Ca II emission lines alone are too great to be accounted for by the dissipation of acoustic fluxes.
2. The Mg II fluxes and the coronal soft X-ray emissions are independent of gravity and effective temperature, contrary to the expectation of heating by acoustic wave dissipation. Slow-mode magnetohydrodynamic (MHD) waves in flux tubes may overcome the difficulty.
3. A plot of emission-line surface fluxes versus temperatures of line formation in quiescent G–M dwarfs shows qualitative trends similar to the quiet Sun, but in dMe stars, the emission lines are comparable to or up to an order of magnitude greater than the very active regions of the Sun.
4. Stars with active chromosphere/corona transition regions are located only in restricted parts of the HR diagram, and they may be distinguished by the existence of many closed magnetic flux tubes.
5. The well-known increase of chromospheric radiative losses with rotational velocity and decrease with square root of age apply as well to chromospheric transition region and coronal fluxes.
6. Soft X-ray luminosities are positively correlated with coronal temperatures and are negatively correlated with stellar surface gravity.
7. Quiescent microwave emission has been detected with the very large array from active dMe stars.

Periodic or quasi-periodic, low-amplitude, wide-band photometric flux variations are observed in several nearby K–M emission-line dwarfs and subgiants, most of which are

members of binary systems. These variations are apparently due to star spots or other inhomogeneities. Typically, these areas cover 10 to 40 percent of the projected stellar disk and are cooler than the photosphere by 400 to 1500 K. Moreover, these huge star spots require a surprisingly efficient dynamo. The inhomogeneities appear to continue outward into the chromosphere and the corona. Several programs are now under way to search for and determine the period and characteristics of stellar activity cycles and rotational modulation.

The most prominent phenomena of stellar activity are *flares*. Although these occur across the spectral region, only in the optical domain have sufficient events been observed for meaningful study. Flares are marked by the usual strong intensification of H I, Ca II, and He I lines. In the ultraviolet region, a strong UV continuum and a stronger relative enhancement of transition-region lines are observed. Comprehensive efforts are under way to investigate stellar flares by correlated observations at optical, ultraviolet, and radio wavelengths, especially in such very active stars as the RS CVn stars. Although the flare activity level on the Sun closely follows the solar cycle, this does not appear to be the case in dMe stars.

A careful *overview* of *attempts* to *interpret* the *activities* and *activity cycles* of *M dwarfs* with both *thermal* and *nonthermal models* is presented in *Chapter 10*. Because of the high densities in the atmospheres of M-dwarf stars (compared to giants), thermal models there are beset with the double complexities of molecular formation and of convection in an optically thin gas. Although these problems are not new, both having been discussed in some detail in Chapter 7, their difficulty has greatly hindered the calculation of models, and the computation of better thermal models is still a greatly anticipated future goal.

The best available models include H_2O opacity as some sort of a mean opacity and treat convection in the usual mixing-length formalism. The observed wings of certain strong lines and the broadband colors *RIJHKL* can be matched fairly well, at least for some normal M-dwarf stars. Observations at shorter and longer wavelengths are not well matched. Another troublesome question regards the microturbulent velocity to be used in understanding convection in these stars.

Observations establish the existence of *dark spots* (*starspots*) on the photospheres of at least the dMe stars. These spots are cool enough and cover a sufficiently large area to affect the emergent spectrum of the star. Although no two-component models are yet available, some of the characteristics of the spots have been deduced from observation, and the possible role of the spots in storing or redistributing the stellar radiative energy have been investigated.

Although no direct evidence is available, indirect evidence from circular polarization of radio emission suggests the presence of kilogauss magnetic fields on the surfaces of M dwarfs, and the investigation of the effects of magnetic flux tubes on the thermal structure and energy balance of the M-dwarf atmosphere is described. Fitting of model atmospheres to interior models is particularly important in M dwarfs, where complete convection may characterize the star. These aspects are summarized.

The interpretive power of thermal models is, of course, limited to emergent flux curves and certain absorption lines. Models that include a *semiempirical chromospheric temperature rise* to account for the characteristic emission lines of H I and Ca II are described. Ultimately, one seeks a self-consistent theory, which would *predict* the chromospheric structure from the properties of the mechanical fluxes available. Until such a theory appears, semiempirical modeling must be done. Models with one isothermal slab or two temperature plateaus are described. If the hottest plateau is at 20000 K, Ca I emission cores agree with the observations for a restricted range of electron density. At the high densities of M-dwarf chromospheres, collisional processes may dominate radiative processes, and H alpha may be driven

into emission at relatively low temperatures. If chromospheric heating rates remain unchanged along the main sequence, the Balmer lines would inevitably go into emission in the coolest stars.

More detailed models, allowing some heating in the upper photosphere and a temperature plateau of 8000 K, are successful in matching the Ca K profiles, but are less successful with the Balmer lines. More intensive investigation of the Balmer lines with a five-level atom are more successful in matching those profiles. Interestingly, as the chromosphere is added, Balmer alpha first goes more deeply into absorption and only later into emission. Thus, one must be cautious of viewing the division of dM and dMe as "nonchromospheric" and "chromospheric." This result might be used to argue that chromospheres of dM are less dense than dMe stars.

Contrary to the Sun, it appears that, at least in the warmer M-dwarf stars, the fractional flux in the corona is greater than that for the chromosphere. That is, the coronal heating problem is the major problem, and the chromosphere may, in turn, be heated from the corona.

Flare models abound, and the years have naturally seen a steady growth in the sophistication of these models, yet they are not yet self-consistent, but are semiempirical; one simply assumes that a new entity has made its appearance in the atmosphere of the M dwarf, and one attempts to calculate the spectroscopic signature(s) of such an entity. The entity is in some models a volume of hot "coronal" gas at temperatures of many millions of degrees; in some models, only a "chromospheric" entity is considered, with temperatures of the order of 10^4 degrees; in still others; a region of the photosphere is considered to be heated up by only a few hundred or a few thousand degrees, and the spectroscopic signature is dominated by the optical properties of the H^- ion. In all cases, the assumption is that the creation of the "entity" is eventually due to the release of nonthermal energy somewhere in the atmosphere of the star on a short time scale, but the details of this process have not been specified with sufficient precision in any of the models published to date to warrant the title of a true model of a stellar flare. Future efforts to improve the models will probably rely heavily on the solar/stellar connection.

Although estimates of acoustic heating in M-dwarf stars are relatively crude, it appears that the acoustic flux is certainly less than that in the Sun. Yet the observed chromospheric radiative flux alone is equal to that in the Sun, and the coronal flux is 10 to 100 times as large. Other predictions from the acoustic theory are also in disagreement with observations. Unless there is a basic misunderstanding of the energy generation by acoustic waves, therefore, these are ruled out as the source of the chromospheric/coronal energy in dM stars.

Several investigators have examined how *magnetic effects* might enter the energy equations for M-star chromospheres/coronae. One possibility is slow-mode waves. A prescribed flux at the base of the atmosphere and a balance of energy gains and losses at every level yields a thermal structure. Other investigations have considered MHD waves. Much of the work is based on analogy with the Sun. If the densities in M-dwarf chromospheres/coronae are 10 times those in the Sun, the Joule dissipation rate is 100 times greater, and this may help explain the rapid rise time of stellar flares. Careful consideration of the heating of coronal magnetic loops by waves raises interesting questions regarding matching frequencies. In the Sun, convective-wave periods are 500 seconds, while loop resonance periods are 5 seconds. In dM stars, however, the convective periods may be much shorter than 500 seconds, and loop resonance periods may be longer than 5 seconds. It therefore appears that a crossover may take place, perhaps in the early dM stars. If so, one might expect strongly increased heating in that case, and there is some evidence for this prediction. Unfortunately, other, as yet unknown, processes may be affecting the energy generation, propagation, and dissipation.

N88-11593

1

BASIC PROPERTIES AND VARIABILITY

François R. Querci

INTRODUCTION TO GIANT AND SUPERGIANT M, S, AND C STARS

The most diverse of any spectral class, M stars range from tiny objects barely able to burn core H—and some which probably cannot—to dust-enshrouded supergiants. In mass, they range from a few hundredths of a solar mass to several tens of solar masses and, in radius, from hundreds of thousands of km to several AU. Spanning the evolutionary spectrum, M stars range from pre-main-sequence dwarfs to stars ready to end their asymptotic giant branch (AGB) stage with a transition to a supernova or planetary nebula. Atmospheres of M stars likewise include a wide range of conditions and phenomena described in this and subsequent chapters. As unevolved low-mass stars, main-sequence M stars form a class quite distinct from the red-giant stars that occupy most of our attention, and *these dwarfs are treated exclusively in Chapters 9 and 10.*

Because of the unusual variety of structures and processes that appear near the end of nuclear burning and the additional complications of binarity, it is not easy to find common characteristics of the M giant and supergiant stars and their numerous relatives of peculiar chemical composition. The authors prefer to reserve the term "cool" for these objects, even though that term is also sometimes applied to the F, G, and K stars, which are so different that we would call them by comparison "warm" or "intermediate" stars. Among these cool giant and supergiant stars—distinguished firstly by spectroscopy into the classes M, MS, S, SC, C, R, N-type, CH, Ba, mild (or marginal) Ba, J stars, and more—are objects with a wide range in mass, composition, size, and evolutionary history. Collectively they are called red giants. They are red because they are cool (among the coolest stars known); their photospheres range in effective temperature from perhaps 5000 K for the warmest R stars to less than 2000 K for the coolest Mira-type variables, and some dust-enshrouded stars may be cooler still. Many reasons for their becoming giants have been elaborated in the scientific literature, but most of these have been shown to be wrong, and the discussion of that phenomenon continues (cf. Eggleton and Faulkner, 1981; Renzini, 1984).

Red-giant stars are of considerable interest for several reasons. Their unusual evolutionary states provide both a unique means to test, and a unique reason to generalize, stellar evolutionary theory (cf. Scalo, 1981; Iben and Renzini, 1983; Wood, 1985; Iben, 1984, 1985).

Their chemical composition is important to our understanding of nucleosynthesis and mixing and, coupled with mass loss, to the enrichment of the interstellar medium. Their outer atmospheres contain unusual regimes of temperature and pressure that provide a series of nice challenges to theories of stellar atmospheres, both static and dynamic. Eventually, such processes as grain formation, chromospheric heating, circumstellar chemical reactions, and mass loss must be quantitatively understood; the current state of affairs in these areas is reviewed in Chapters 2, 3, 4, 5, 6, and 8.

Ultimately, one would hope to be able to point to a red-giant star—Betelgeuse or χ Cyg or IRC +10216—and describe in detail its characteristics and evolutionary history. Although this desirable goal is presently still out of reach, some broad outlines and details of specific processes and phases are available. Sometime after hydrogen core exhaustion, almost all stars, except the most massive, become red giants or supergiants. Although the exact cause of this transformation is still a matter of some dispute, there is no doubt that such stars develop an inflated atmosphere (including envelope) around a compact core.

Most or all of the red giants of interest in this book are intermediate-mass ($1 \leqq M \leqq 9$ $M_\odot$) stars of Population I, and these are also the best studied. As core hydrogen is exhausted and the main-sequence stage ends, a compact helium core develops, and stars move rapidly to the right in the HR diagram (toward lower temperatures at approximately constant luminosity) and then upward on the red-giant branch (RGB). For the first time, some mixing to the surface of nuclearly processed material occurs in all stars (the "first dredge-up"). Rather specific predictions of the results of this first mixing episode on the observed surface abundance are available (Iben and Renzini, 1983; Iben, 1984), and observations confirm the general correctness of these predictions (Lambert, 1981).

At some epoch, helium ignites in the core, either by a "helium core flash" in the degenerate cores of lower mass stars (M less than 2.3 $M_\odot$) or quietly in the nondegenerate core of more massive objects. Additional mixing (second dredge-up) may occur upon core helium ignition in more massive (4 to 9 $M_\odot$) stars. In any case, core helium ignition lifts the degeneracy, if any, and the star moves rapidly leftward on the HR diagram to a "helium burning main sequence." After core helium is burned and a compact, electron degenerate core of carbon and oxygen is formed, helium burning continues in a shell, and the star again moves coolward and then sharply upward toward higher luminosities—the AGB phase of a star's life. It is now powered by double-shell burning—an outer shell of hydrogen burning and an inner shell of helium burning. As the helium shell burns outward, it narrows and flickers (pulses), driving intermittent convection and leading to a third dredge-up. Cool S- and N-type carbon stars are presumably formed during this AGB phase (Iben and Renzini, 1983; Iben, 1984; Wood, 1985), which is also marked by dredge-up of heavy metals (s-process elements) in many stars. Inferring the details of these remarkable events by careful studies of elemental and isotopic abundances for all types of peculiar red-giant stars is presently an area of intense interest (Lambert, 1981, 1985; Tsuji, 1985b).

Of more direct connection to this series, mass loss becomes general in AGB stars (see Goldberg, this volume; Dupree, 1986). Finally, part or all of the AGB stars develop a superwind (Iben and Renzini, 1983) that leads to rapid mass loss, and the star becomes a planetary nebula. Exactly which stars become planetaries is, however, presently unclear. After the ejection of a planetary nebula, the remnant compact core is a white dwarf that simply continues to cool (forever), although some energy is released by hydrogen burning in the base of the atmosphere. A small fraction (25 percent) of white dwarfs undergo a final helium pulse and briefly return to the red-giant region of the HR diagram, perhaps as RCB stars (Iben, 1984, 1985).

Certain red-giant stars do not fit the above simple scheme for single intermediate-mass

Population I stars. The most notable mysteries are the barium (or Ba II) stars, so-called because of the enhanced line of barium at 4554 Å in their spectrum, for their low luminosity indicates an insufficiently advanced evolutionary stage to have mixed to the surface the observed excess of carbon and s-process elements. The discovery of their binary nature (McClure, 1983) neatly solved the problem; the barium stars were contaminated with mass thrown onto the star by its present white-dwarf companion at the time that companion was itself an AGB star. But at least some of the white dwarf companions have cooling times longer than the red-giant lifetime of these stars, and the situation is presently unclear. R stars pose a similar but tougher problem (Iben, 1984 and discussion by Wing). As with the barium stars, R stars are insufficiently luminous to have dredged up sufficient carbon to become carbon rich (C/O > 1). Yet these show no more than average binarity (McClure, 1985), which would appear to eliminate that otherwise attractive hypothesis. Certain S and MS stars also may prove to be challenges to the present theory (Iben, 1985).

Important questions about red giants are: What is the source of neutrons for heavy element formation? What are the various correlations between these physical properties and others such as their galactic distribution, their spatial velocity, their age, their periods of variability, and the shape of their light curve? Is their mass loss steady, periodic, or sporadic? What mechanisms are responsible? How can mass loss be measured? What are the main criticisms of such measurements? How to progress about the evolution of these various types of stars that are concentrated on the right side of the top of the HR diagram? What fundamental physical data are necessary for improving the model of evolution? Are these data sufficiently accurate? What confidence can we have in such models? What is the place of these stars in present-day astrophysics?

Clearly, answers to all of these questions are not yet available, and of the remainder, we must carefully select our material. In this chapter, after a general overview, we stress the variability because virtually all the stars that are discussed are variable, and all the more since the variability is due to nonthermal processes, the subject of this series of Monographs. This chapter will mainly discuss *photometric variability*; spectroscopic variability is presented in the following chapter by M. Querci.

Particular questions that are addressed on variability include the following: What are the various characteristic times of the observed variations? Are they correlated with any other characteristic period intrinsic to the given object? To what radial or nonradial motions of matter do such variations correspond? How are the irreversible changes explained? Are the latter a sure sign of the stellar evolution of these stars which suffer them?

What should we recommend to people who want to help to disentangle these fundamental questions? In the present exploratory state of our knowledge of the red giants and supergiants and because the observed variations are so complex, every feature found to be variable must be noticed and analyzed, and all correlations must be tested in an attempt to list better the various motions of matter suffered by the different stellar layers. Simultaneously, we must endeavor to find the pulsational frequencies with methods adapted to the necessarily intermittent ground-based observations. Also, theoretical studies of the periodic phenomena of Miras, which seem to be replaced by chaotic or aperiodic phenomena in the semiregular and irregular variables, are to be pursued. To analyze the variability both observationally by monitoring some characteristic stars and theoretically by developing red-giant hydrodynamics (just beginning) would help to clarify the evolutionary problems raised in this part of the HR diagram, where many apparently diverse objects are found.

Basic properties of the M, S, and C variables—more specifically, abundance classification, luminosity, mass, radius, surface gravity, extension of the outer layers, effective temperature, abundances, space distribution, period or pseudoperiod, and shape of the light

curves and their variations—have been described in the past by many reviews: Bidelman (1956), Blanco (1965), Hack (1967), Beeckmans (1969), Spinrad and Wing (1969), Fujita (1970 and references therein), Vardya (1970), Alksne and Ikaunieks (1971, updated by Baumert in 1981), Baumert (1972), Rybski (1973), Wallerstein (1973), Barbaro and Dallaporta (1974), Boyarchuk (1974), Ikaunieks (1975), Keenan and McNeil (1976), Johnson (1978), Keenan and Boeshaar (1980), de Jager (1980), Fujita (1980), Feast (1981), Scalo (1981), Duerbeck and Seitter (1982), Alksne et al. (1983), McClure (1984), Jaschek (1985), and Wing (1985). Even this list is far from being exhaustive. Some reviews are especially devoted to C stars, and others are restricted to M stars, each author favoring a particular point. A few recent colloquia or workshops are completely devoted to such stars: "Physical Processes in Red Giants," Erice in 1980; "Cool Stars with Excesses of Heavy Elements," Strasbourg in 1984; and "Mass Loss in Red Giants," Los Angeles in 1984.

In the following, we present the various classifications of these red-giant stars, their photometry and colors, their space motion and space distribution, and their intrinsic properties. I must apologize for showing my own biases and for omitting many important studies and reviews.

Classifications

Much more varied than warmer stars, the M, S, and C stars can be classified in several ways. Classification by *spectra* is the most obvious and most common scheme. For the varied objects found among the red giants, classification by *chemical composition* or key *abundance ratios* is important. These objects can also be classified by *photometry* and *color*. Finally, since almost all red giants are variable in light, they are classified by *type of variability*. All of these must be considered to form a complete picture of a red-giant star.

Even before a clear understanding of their nature was available, red-giant stars were classified on the basis of their *spectra*. The normal red giants—the M stars—were classified according to the increasing strength of the TiO bands. In contrast, other stars have spectra dominated by such carbon-rich molecules as CN and C_2. Quite early, it was realized that the tightly bound molecule CO controls the spectra because CO forms in cool-star atmospheres until the less abundant of either carbon or oxygen (which are in turn the most abundant elements after hydrogen and helium) is used up. Whichever of the two elements is more abundant is then left over to form other molecules, which dominate the spectrum. The ratio of these two—the C/O ratio—thus becomes a crucial determinant of red-giant spectra. Other abundance parameters such as metallicity and enhancement of s-process elements (those heavy elements—Sr, Y, Zr, and Ba—produced primarily by slow neutron capture and beta decay) are also key classification criteria easily determined from spectra.

A didactic presentation of the M, S, and C stars and related objects and their classification through *abundance ratios* is given in Jaschek (1985). The relative position of the different groups of stars can be easily visualized in the tridimensional representation (Figure 1-1) based on the C/O ratio, the metal abundances, and the s-process abundances. The C/O abundance ratio is the primary criterion differentiating the oxygen-rich M (C/O $<$ 1) and the S stars (C/O $\approx$ 0.8 to 1) from the carbon-rich stars (C/O $>$ 1). The second gives the cool stars that are metal-deficient, such as the CH stars or the HdC stars, and the third distinguishes the degree of enhancement in the abundance of s-process elements.

Before giving a description of the main types of stars mentioned in Figure 1-1, let us recall that these stars are located between the Hayashi lines for fully convective stars of various solar masses (see Figure 40 in de Jager, 1980, adapted from published HR diagrams: e.g., from Scalo, 1976). Wood (1985) found an evolutionary sequence up to the AGB in the M $\rightarrow$ S $\rightarrow$ C, but the quantitative agreement between the theory of shell-flash mixing and observations is still

ORIGINAL PAGE IS
OF POOR QUALITY

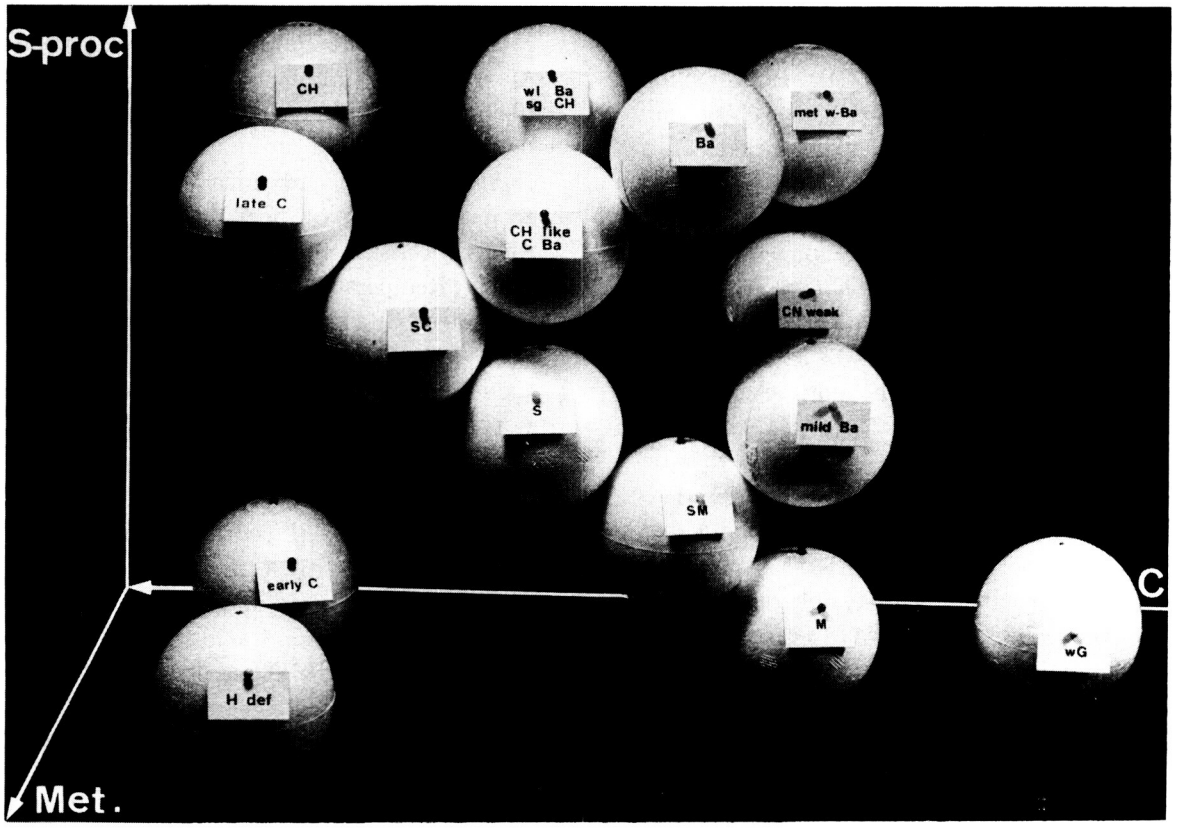


Figure 1-1. Main varieties of red giants, according to the three-dimensional representation described in the text (from Jaschek, 1985).

not satisfactory. Additional insight into the observational constraints on theories of mixing and nucleosynthesis during the advanced red-giant stages of evolution can be gleaned from several recent reviews (Scalo, 1981; Iben and Renzini, 1983; Iben, 1984, 1985). Although we have chosen not to discuss in detail the red giants in other galaxies, conclusions drawn from these stars in the Magellanic Clouds are illuminating, particularly with respect to their evolution, and a later section provides an overview.

The *M stars*, also called oxygen stars in parallel with carbon stars because the composition is basically oxygen-rich (solar C/O $\approx$ 0.6), are characterized by molecular absorption bands of such oxygen-rich molecules as TiO and VO in the visible. These bands are very weak in M0 stars; their strength increases with later (cooler) types. In fact, M stars are classified from M0 to M8 primarily by the increasing strength of the bands of the alpha system of TiO from 4350 to 4950 Å (e.g., Keenan and McNeil, 1976; Wing, 1979; Keenan and Pitts, 1980). A few stars have even been classified M9 or M10. In the infrared, M stars are characterized by CO, OH, SiO, and H_2O absorption bands. The 10-μm region shows the emission of silicate grains, which are discussed in Chapters 2, 4, and 5. Maser lines of CO, OH, H_2O, and SiO are observed in the coolest M Mira stars.

Among the M variables, some belong to the regularly pulsating group of cool stars, the Miras (see the section on *Variability Types*). Although the Miras change their spectral subtype and magnitude during their light cycle, they occupy a rather distinct zone around the

giant and subgiant tracks. However, nonvariable M giants (see the section *Nonvariable Stars*), such as β And (M0 III), also fall in this region of the HR diagram. The OH/IR stars (i.e., very red objects with double-peaked 1612-MHz OH maser emission) are a continuation of M Mira stars to lower temperatures, larger masses and luminosities, and longer periods of pulsation (Duerbeck and Seitter, 1982). Their evolution is discussed by de Jong (1983); the most luminous ones (8 to 13 $M_\odot$) are to be identified with the core helium-burning supergiant stars, while those of 3 to 8 $M_\odot$ are AGB stars. Some of them are OH objects with undetected IR counterparts (Jones et al., 1982). They pulsate only weakly or not at all, and their mass-loss rate is as large as $10^{-4}\ M_\odot$/yr (Baud and Habing, 1983); they possibly reach the end of their evolution on the AGB (Herman, 1983). This is consistent with the very red colors observed by IRAS (Olnon et al., 1984). If our current ideas of stellar evolution are right, these stars soon produce planetary nebulae (Olnon et al., 1984).

The *C stars* (carbon stars) are distinguished by the presence of C_2 Swan bands in their spectra (Keenan and Morgan, 1941; Keenan and McNeil, 1976; Fujita, 1980). They are further divided into *R-type stars* (the hotter ones) and *N-type stars* (the cooler ones), the criterion being the strength of the violet flux, which is very weak in N-type stars (Shane, 1928)—weaker than in corresponding M stars and weaker than blackbodies at the effective temperature. Historically, the R and N types were initially used in the HD catalog. The first to observe N stars was Secchi (1868). Later, Pickering (1898) identified a small group of C stars that differed from the N stars in displaying sensible flux shortward of 4500 Å, and Espin (1889, 1898) remarked that none of the stars observed by Secchi were from this group. In 1908, Pickering defined the R subtype (i.e., the present R type) by the extension of the continuum shortward of 4700 Å, the earlier stars having the larger extension. This deficiency of flux in N-type stars continues into the ultraviolet. Finally, the R and N types were unified by the Cx,y classification of Keenan and Morgan (1941). Let us note that, in the Keenan-Morgan classification, (Cx,y), the first figure (0–9) following the "C" is a temperature index obtained from atomic lines; the second figure (0–9) is a carbonicity index obtained from the strength of the C_2 bands. Underlying the Cx,y classification was the assumption that x and y (temperature and carbonicity) were independent. If so, the Cx classification would have arrayed the carbon stars in a temperature sequence parallel to that of M stars. Nature is not so simple, however, and the ambiguity of this classification has been amply demonstrated (e.g., Fujita, 1980) both observationally from variability studies (Eggen, 1972b), infrared broadband colors (Mendoza and Johnson, 1965), near-infrared narrowband colors (Baumert, 1972), and infrared spectrophotometry (Goebel et al., 1978) and theoretically from calculations of the effect of carbon enhancement on opacities (Scalo, 1973) and atmospheric structure (Johnson, 1982) and on effective temperatures (Tsuji, 1981c).

The *early R stars* (R0 to R4) are termed "ordinary R stars" because their hydrogen lines have strengths similar to those in normal G9 to K2 giants of the same effective temperature. Vandervort (1958) gives the criteria for the classification of the R stars between R0 and R8.

In the carbon stars, the visible spectrum contains bands of the carbon-rich molecules CN, C_2, C_3, SiC_2, and CH instead of the oxide bands that characterize the M stars spectra, and these bands dominate the spectra of cooler stars—the late R (R5 to R9) and the N stars. Apart from the CO bands seen in all cool stars (though unexpectedly weak in the R0 to R4 stars), the infrared (1 to 5 μm) is increasingly chopped up by bands of CN, C_2, HCN, and C_2H_2 toward later spectral types. Emission at 11 μm due to graphite and SiC grains is often seen. In the radio frequencies, CO, CN, SiO, CS, C_2H, HNC, HCN, C_3N, and complicated molecules such as the cyanopolyyne family ($HC_{2n+1}N$) or CH_3CN are detected in the extreme dust-enshrouded C stars.

The s-process elements are stronger in late carbon stars than in M stars (Utsumi, 1970), but the ^{13}C-rich carbon stars (J stars) apparently show little or no enhancements of s-process elements with respect to Fe (Utsumi, 1985).

The spectra of N-type stars show a stronger absorption in the blue and the ultraviolet than do the R-type spectra. This classic problem, termed the "violet opacity," is discussed further under *Photometric Observations*. It seems that this degree of faintness in the ultraviolet region of N-type spectra is not entirely due to their lower temperature (de Jager, 1980). The absorption by molecular bands (particularly C_3) and graphite and silicon carbide particles could be an important contributor to this observed faintness. Stars redder than $B-V$ = 3 are nearly always carbon stars, of which the reddest are the cool N types with $B-V \approx 5$ or 6 (Wing, 1985); for comparison, the solar $B-V$ value is 0.62, and M0 to M6 giants have $B-V \approx 1.55$ (Johnson, 1966).

The early R stars, extensively described by Dominy (1982, 1984), have an abnormal oxygen/carbon ratio relative to the M stars by 0.7 dex; the nitrogen and oxygen are enhanced by only 0.2 dex. The iron abundance is near the solar value, except in HD 100764, which has an iron abundance 0.6 dex lower than the solar one. The s-process elements such as Y, Zr, Mo, Ba, La, Ce, Nd, and Sm are not enhanced in these hotter carbon stars. A bright member of this class, HD 156074, was well analyzed by several authors: Greene et al. (1973) for the Fe abundance, Wyller (1966), Gordon (1967), and Fujita and Tsuji (1976) for the C^{12}/C^{13} ratio, and Yorka (1981) for the N abundance. The elemental abundances in the early R stars are interpreted as products of mixing during the helium flash (Dominy, 1982; Wood, 1985). On the other hand, due to uncertainties both in observations (mainly in luminosity) and in evolution theory, Tsuji (1981c) remarks that it is difficult to decide whether N stars (N-type Miras are not considered) are produced just after the onset of He-shell flash. The carbon-star evolutionary "mystery," paraphrasing Iben (1981b), has been studied specifically by this author (Iben, 1984) and by Lucy et al. (1986).

Beside these "classical" carbon stars, a class of stars that are carbon-rich but have the additional peculiarity of hydrogen deficiency—the so-called *hydrogen-deficient carbon (HdC) stars*—group together, following the convenient classification of Richer (1975): (a) the R Coronae Borealis (RCB) stars; (b) the helium (He) stars; and (c) a few supergiant R stars (e.g., HD 182040) (see the section *Intrinsic Properties*) that appear to be nonvariable (McKellar and Buscombe, 1948; Bidelman, 1953; Warner, 1963, 1967) and are called the nonvariable HdC stars.

The group of HdC stars is deficient in hydrogen by a factor up to 10^5 or more compared to the H/Fe ratio in the Sun. The dominant constituent of their atmosphere is helium, although it is not spectroscopically dominant in all the HdC stars. Because no HdC star is known to be a close binary, the observed abundances can only be due to the ejection of the outer layers during the natural course of evolution. The lifetime of the HdC stage appears to be $\sim 10^3$ years; if so, secular changes should be observable. It is proposed that these supergiants (see below) quickly evolve to white dwarfs (Iben, 1981a, 1985,).

The *RCB stars* are characterized, at maximum light, by narrow and sharp absorption lines of metals and very strong molecular absorptions such as CN in R CrB and RY Sgr, and C_2 in S Aps and HV 5637. During minimum light and the subsequent increase, emission lines of helium (e.g., Querci and Querci, 1978) and metals usually appear in the spectrum. These stars have a surplus of carbon (by a factor of 3 to 10 (Warner, 1967)), as well as a surplus of helium, compared to the Sun. Earlier, Ludendorff (1906), Berman (1935), and Herbig (1949) remarked on these peculiar abundances in R CrB, and Bidelman (1948) showed these peculiarities in XX Cam. They are believed to be due to the loss of the hydrogen envelope (Sackmann-Juliana et al., 1974). Some differences exist between them; in XX

Cam, carbon is a little more abundant and hydrogen more deficient than in RY Sgr (Rao et al., 1980)—log $[(C/H_{RY\ Sgr}/\ (C/H)_{XX\ Cam}) \sim -1.16$. Schonberner (1975) has estimated this ratio to be -0.9. The abundance in oxygen is also slightly different; it is 3 times more abundant in R CrB than in RY Sgr. Most RCB stars are members of the R type; some of them are known to have earlier type spectra, including the prototype star itself, which is of spectral class cGOep. In the HdC group, they are called cool HdC stars. The RCB are eruptive stars (and not pulsating stars, such as the "classical" C stars; see the section *Types of Variability*) with long periods; moreover, they are the only eruptive stars in which the quiescent state is the state of maximum brightness. Their minima are interpreted by ejections of obscuring matter (soot, particles of graphite, etc.).

Helium stars and RCB stars have several common properties, although the He stars have a higher temperature (leading to their being also called hot hydrogen-deficient stars, like BD +13°3224 (Kilkenny and Lynas-Gray, 1982)), a larger gravity, and a smaller pulsational period than the RCB stars. MV Sgr appears to be a possible evolutionary link between these two classes (Hill, 1967) with its light variations like those of RCB stars and its spectrum like that of the helium star, HD 124448. Tutukov and Iben (1985) show theoretical evolutionary connections between them. Herbig (1964) noted that the strongest lines in the spectrum of MV Sgr are from He I and C II. The latter is somewhat weaker than He I lines, whereas in BD +10°2179, the lines of the two atoms are of the same strength. Warner (1967) analyzed some nonvariable helium stars and found abundance characteristics like those of the nonvariable HdC stars. Envelopes around the helium stars were suspected by Hill (1964), such as around HD 168476, which appears like an A-type star with many lines of ionized elements of the iron group. This star shows that the excitation temperature for the ionized elements is much lower than that for the other elements, leading Hill to suggest that they are formed in a low-temperature shell. The immediate progenitors of the helium stars are believed to be RCB stars (Schönberner, 1975). However, nothing is really known about their common origin and by what mechanism they have lost their initial hydrogen-rich atmosphere.

As for the *nonvariable HdC stars*, the stars HD 137613, HD 173409, HD 175893, and HD 182040 are hydrogen-deficient by factors of more than 10^5 compared to the H/Fe ratio in the Sun. The deficiency is around a factor of 50 in HD 148839; this last star shows C_2 and C I enhancement, while CH and Balmer lines are absent. It represents "an intermediate type between normal C stars and the more extreme hydrogen-deficient stars" (Warner, 1967). In all these stars, the carbon is overabundant by factors of 3 to 10, but C^{13} is not observed at all. All elements heavier than oxygen have a roughly solar abundance relative to iron.

Among carbon-rich stars, we note other particular stars such as the *CH stars*, which are G5–K5 giants with strong CH molecular bands (G band at 4300 Å) and enhanced lines of s-process elements in their carbon-rich and metal-poor spectrum. They have high radial velocities and can be considered Population II carbon stars. Stars with a strong G band and low spatial velocity are also observed; they are called *CH-like stars*. Bidelman and McConnell (1973) identified a large number of stars with a very weak or absent G band, the so-called *weak G-band stars*; no correlation was found between the CH faintness and the line strength of metallic lines. The *CN-strong stars* are carbon stars with a metal overabundance and a slight enhancement of carbon (Schmitt, 1971).

Jaschek (1985) stated that "The *S-stars* constitute a natural bridge between M and C stars with all kinds of intermediates." They are late (K5–M8) giants. These stars contain metals with roughly the same abundances as the M stars, but the enhancement of the heavy elements, including Zr, Y, Sr, Ba, and La, is very strong and consequently the ZrO bands are much more prominent than those of TiO. Oxides of yttrium, lanthanum, and vanadium are affected by the change in C/O between M and C stars.

The C and O atoms are fully trapped in CO; this reduction in the free oxygen supply as carbon is enhanced explains the presence of many atomic hydrides in the S star spectra. Their $B-V$ colors are between -2 and -3.

The presence of unstable isotopes such as $^{99}T_c$ in the stellar spectrum of some S and C stars (Little-Marenin and Little, 1979; Smith and Lambert, 1985), indicates that the rising to the surface of the interior material has occurred less than about 10^6 years ago, which corresponds to a few half-lives of the Tc^{99} isotope, the longest lived of the Tc isotopes, under conditions representative of interiors of AGB stars (Iben and Renzini, 1983).

A very few C and S stars (T Sgr, WZ Cas, HR 8714, WX Cyg, T Ara, etc.) present a very strong absorption resonance line of lithium at λ6707 (see the surveys of Torres-Peimbert and Wallerstein, 1966, and Boesgaard, 1969). These stars are named *lithium-rich stars* (LRS). The derived abundance of lithium is up to 10^5 times the solar value in WZ Cas. To obtain the Li formation or destruction processes in such stars, two difficulties must be solved (Scalo, 1981): to infer the Li/Fe ratio and to infer the $^6Li/^7Li$ ratio. The first ratio is only tentatively estimated (Merchant-Boesgaard, 1970; Wallerstein, 1977; de la Reza and Querci, 1978) because the λ6707 line is largely blended by CN red-system lines. The knowledge of the second ratio is not easy to obtain through the analysis of the lithium resonance atomic line because, besides the CN blending, the isotopic shift is smaller than the observed Doppler width of the stellar line. Some efforts have been made in the direction of the molecular isotopic shift by the development of computations of molecular abundances of LiH, LiOH, and LiO (Merchant, 1967; Querci and Querci, 1977) and of wavelength measurements in the laboratory (Plummer et al., 1984). Stellar observations of lithium hydride must be made to provide the desired ratio.

Hybrid objects are also observed; for example, the *CS and SC stars* have characteristics of both C and S stars (Stephenson, 1967b; Catchpole and Feast, 1971), and the *MS stars* are intermediate between M and S types. Keenan and Boeshaar (1980) provide reference stars in the sequence MS through S and SC (sometimes called D-line stars (Gordon, 1967)) to C stars with weak C_2 bands.

We conclude this description of the main types of cool stars by the *Ba II stars* (also named Ba or barium stars) that constitute another family of anomalous giant stars with strong Ba II features (especially the λ4554 line). They share with the early R stars (R0 to R4) the fact of being "warm" or "intermediate-temperature" stars (see the section on *Intrinsic Properties*). Most Ba stars have strengthened CN absorption (Wing, 1985) relative to normal G and K stars, although not as strong as in carbon stars. The s-process elements, especially those with $38 < Z < 56$, are enhanced (McClure, 1984; Smith, 1984). An estimate of the strength of the barium lines was added to the spectral type by Warner (1965). This group has no sharp boundaries (Jaschek, 1985). So-called semi-barium stars have s-process element abundances intermediate between those seen in the pure Ba II stars and the M stars. The stars for which the enhancement is not obvious are named "marginal barium stars." To designate the strength of the Ba II characteristics, Keenan and Pitts (1980) give a decimal scale that is often used. Catchpole et al. (1977) and Yamashita and Norimoto (1981) have reobserved the Ba II sample of MacConnell et al. (1972) and conclude that about one-third of these stars are weak-line objects, such as the subgiant CH stars defined by Bond (1974).

The lack of luminosity determinations is the main difficulty in placing the Ba stars on the HR diagram, but they are generally believed to have luminosities of normal giants. Until the recent discovery of their binarity (McClure et al., 1980; McClure, 1983), the evolutionary status of the barium stars was a puzzle because such apparently low-mass stars should not have been able to have mixed to the surface nuclearly processed material. It now appears fairly certain that the abundance anomalies seen in the real Ba stars are the result of mass transfer from

formerly more massive companions when the companions were in the asymptotic giant branch stage of evolution (Smith, 1984; Lambert, 1985). Whether the same holds true for mild or marginal barium stars is, however, still an open question (McClure, 1985). Wood (1985) suggests that the Ba II stars (and CH stars) are probably the result of mass transfer from an N-type star to a white-dwarf companion in a binary system.

To understand better the large variety of these giants and supergiants, which lie on the right side of the HR diagram and cover a large range on absolute visual magnitude (see the section on *Intrinsic Properties*), several other classifications based on criteria other than abundance ratios or temperatures are proposed (Eggen, 1972b; Feast, 1981; Feast et al., 1982). The importance of finding physically meaningful, significant classifications dividing the objects into homogeneous subgroups is stressed. Of the various attempts to classify these stars, the most famous classification, based on type of light variation, is the *General Catalogue of Variable Stars* (GCVS) (Kukarkin et al., 1958, 1976), which essentially divides the late-type variables into Miras, semiregulars (SR), and irregulars (L) according to their light-curve amplitude and profile. This point will be discussed in the section on *Variability Types*. As noted by Eggen (1972b), the GCVS is a poor guide to the type of variation of the N-type red variables, maybe because of their extreme $(B-V)$ colors. This author, from an extensive study of red giants, suggests a subdivision of the variables on the basis of their place in the luminosity/temperature plane (i.e., $(M_{bol}, R-I)$-plane, adopting Johnson's (1966) relation between $R-I$ and log T_e) and from their space motions linked to their age.

Feast (1981) sorts out the variables by a spectroscopic argument—the strength of the emission lines: (1) the variables with strong emission lines, called Xe stars, are Miras (i.e., large-amplitude variables); (2) the variables with weak emssion lines at some phases, called X(e), are semiregulars (i.e., small-amplitude variables); and (3) the variables that do not show emission lines, called X variables, are semiregulars or irregulars, where X denotes the spectral type M, S, C, CS, SC, etc. The basic idea is that the emission-line strength is linked to the extent to which the stellar layers are disturbed by the variability (see M. Querci, this volume). Feast et al. (1982) relate this division to mean infrared colors and define two reddening-free parameters b_1, b_2. The b_1, b_2 colors suggest an evolutionary sequence M-M(e)-Me that is in fact a sequence of increasing light amplitude and decreasing temperature. The Mira variables that show OH or H_2O maser emission are at the cold end of the b_1 - b_2 plot, while the carbon stars show a large scatter that is also seen in the infrared photometric indices (Tsuji, 1985). The SC stars form a tight group, whereas the CS stars are scattered more widely. The main sources of infrared opacity, different in each stellar type, evidently have a strong effect on the infrared colors and cause the difference as to the region occupied by each type, as demonstrated by Feast et al. (1982).

The main purpose of establishing such empirical relationships is to provide a norm with which red variables in other galaxies (e.g., the Magellanic Clouds) or in other regions of our Galaxy than in the neighborhood of the Sun (e.g., in the galactic bulge) might be compared.

Photometric Observations

After the pioneer astronomers who were fascinated by the red stars—let us note Espin, Hale, Kirch, Koch, Maraldi, Pickering, Secchi, Schjellerup, Shane, and Sidgraves—the first sustained observations of visual light curves of red stars began in the late 1930's at the Harvard College Observatory (Campbell, Hughes, Payne, Sterne, etc.). For more than 50 years, amateur astronomers (working together in such groups as AAVSO, AFOEV, GEOS, etc.) have joined their observational efforts to those of the professionals. More recently, the UBV system and its extension into the infrared have been extensively used for determining such physical parameters of the red giants and supergiants as

energy distribution, effective temperature, and infrared excesses and for showing correlations among them at various phases of the light curves (e.g., color/magnitude relation, variations of various indices such as $(B-V)$, $(I-K)$, and (8 μm–11 μm) indices with spectral class; see below). Astronomers who made important investigations in broadband photometry include: Bahng, Bergeat, Bessel, Bidelman, Blanco, Catchpole, Eggen, Feast, Johnson, Landolt, Leighton, Mendoza, Morgan, Neugebauer, Nicolet, Price, Smak, Stephenson, Walker, Westerlund, and Wood.

Table 1-1 gives broadband magnitudes and colors from the ultraviolet to the infrared for characteristic stars of different spectral and variability types. For χ Cyg, an S Mira, it is worth noting that the magnitude variations are much larger in the ultraviolet than in the infrared region. (A specific example of variations in ultraviolet flux for χ Cyg is shown in Figure 1-7, and other examples in the visual are given in Figure 1-8.) With the advent of more sensitive infrared detectors, broadband photometry across the entire spectrum became possible, and this material has been published and discussed in detail. Although readers are probably already familiar with these observations and it is impossible to review them here in any case, we note a few of those papers containing fundamental broadband photometric data for M giants (Johnson, 1966; Eggen, 1967; Johnson and Mitchell, 1975), carbon stars (Mendoza and Johnson, 1965; Eggen, 1972; Walker, 1979; Bergeat and Lunel, 1980; Noguchi et al., 1981), and Mira variable stars of all types (Mendoza, 1967; Catchpole et al., 1979). A useful review of photometry of all types of peculiar red giants is that of Wing (1985).

A persistent problem threading its way through the astrophysical literature is the violet flux deficiency of carbon stars. A normal M6 giant has a value of $(U-V) = 2.43$ (Johnson, 1966), while α Ori (M2 Iab) has $(U-V) = 3.96$ (Table 1-1). By contrast, a warmer N-type carbon star such as TX Psc has $(U-V) = 6.11$ (Table 1-1), and many carbon stars have even larger values. This rapid drop of flux toward the violet was noticed long ago and became the basis for the distinction between the carbon stars with sensible flux shortward of 4700 Å (R stars) and those with no short wavelength flux (N-type stars) (e.g., Shane, 1928). On the basis that the flux deficiency was due to an unknown violet opacity, the phenomenon is termed the "violet opacity" problem, which is still unsolved. Among several suggestions for the agent responsible, the leading candidates are the molecule C_3 in the photosphere (McKellar and Richardson, 1955; Bregman and Bregman, 1978) or SiC grains in a circumstellar shell (Gilra, 1973; Walker, 1976). Observations with IUE demonstrate that the violet opacity extends into the ultraviolet as well (Querci et al., 1982; Johnson and O'Brien, 1983).

The widths of these broadband filters are too large ($\geqq$ 1000 Å), however, for the analysis of the time behavior of the various bands of TiO, VO, ZrO, CO, CN, C_2, CH, and HCN in the visible and the near-infrared, and the observed variations are difficult to interpret quantitatively in terms of energy dissipated in the various stellar layers submitted to acoustic/shock waves. Consequently, intermediate-band photometries (with filter bandwidths in the range 200 to 500 Å), initially developed for investigations on A to G stars (i.e., with filters adapted to their spectral features), are used for the analysis of the warmer stars among M, S, and C giants and supergiants; such systems are: DDO, Strömgren, Geneva, and Vilnius systems.

In 1966, Wing (1967a) pointed to a spectral band of 30 Å width near 1.04 μm that was free from serious atomic and molecular blanketing in M, S, and C stars. A new epoch was born: the variations of the continuum of these late-type stars could be followed. Narrowband filters adapted to the M star molecular bands appeared (Wing, 1971; Lockwood and McMillan, 1971). White and Wing (1978) classified M supergiants; Baumert (1972) used the Wing system to measure the CN absorption versus the continuum of C stars; Wing and Stock (1973) identified carbon stars in stellar

Table 1-1
Broadband Magnitudes for Characteristic Stars

		0.36 μ	0.45 μ	0.56 μ	0.67 μ	0.87 μ	1.20 μ	2.3 μ	3.3 μ	4.8 μ	8.6 μ	10.8 μ	12.2 μ	18.0 μ
M stars:														
R LMi	(1)	11.50	11.12	9.42	5.40	2.24	0.82	-0.48	-1.12	---	---	---	---	---
Mira, M7e-M8e	(2)	---	---	---	---	---	---	-0.7	-1.4	-1.8	-2.2	-3.0	-2.8	-3.2
α Ori														
SRc, M1-2lab	(3)	4.36	2.29	0.40	-1.19	-2.47	-2.93	-4.01	-4.43	---	---	---	---	---
	(2)	---	---	---	---	---	---	-4.2	-4.5	-4.3	-4.8	-5.7	-5.5	-5.7
BC Cyg	(3)	16.17	13.23	9.97	6.22	3.44	2.03	0.17	-0.44	---	---	---	---	---
Lc, M4	(2)	---	---	---	---	---	---	0.4	-0.2	-0.1	-1.0	-3.2	-2.7	-3.5
C stars:														
U Cyg	(4)	16.30	11.78	8.47	6.32	4.54	3.21	1.05	0.05	---	---	---	---	---
Mira, C7,2e-C7,9	(2)	---	---	---	---	---	---	1.5	0.7	0.0	-0.3	-1.5	-1.0	-1.3
V Hya	(5)	---	---	8.36	5.33	3.67	---	---	---	---	---	---	---	---
SRc, C6,4e	(2)	---	---	---	---	---	---	-0.9	-2.1	-2.5	-3.6	-4.2	-4.2	-4.2
TX Psc	(6)	11.15	7.65	5.04	3.17	1.82	0.92	-0.56	-0.89	---	---	---	---	---
Lb, C6,2	(2)	---	---	---	---	---	---	-0.7	-1.2	-0.9	-1.1	-1.7	-1.3	---
	(7)	---	---	---	---	---	0.73	-0.23	-0.66	-1.02	---	---	---	---
S stars:														
	(8)	7.01	6.05	4.23	1.81	0.01	-0.91	-2.43	-2.98	-2.97	---	---	---	---
χ Cyg	(1)	12.53	12.19	10.26	5.55	1.99	-0.05	-1.84	-2.60	---	---	---	---	---
Mira, S7le-S10le	(8)	15.49	14.68	13.00	6.90	2.75	0.22	-1.73	-2.32	-2.9	-3.3	---	---	---
	(2)	---	---	---	---	---	---	-2.5	-3.1	-3.1	-3.5	-4.5	-4.3	-4.6

(1) Mendoza (1968), (2) Hackwell (1972), (3) Lee (1970), (4) Mendoza and Johnson (1965), (5) Olson and Richer (1975), (6) Johnson et al. (1966), (7) Walker (1980), (8) Mendoza (1967).

fields, Piccirillo (1977, 1980) investigated the S stars with the ZrO and LaO filters, and Yorka (1983) published data on R stars. However, let us note that some of the filters adapted to selected molecules are weakly contaminated by other molecules.

Unfortunately, the observations on the other spectral intervals such as X rays and far-UV, far-IR, and radio frequencies are scarce.

The fingers of one hand suffice to count the Einstein *X-ray* satellite *observations* of red giants and supergiants (Ayres et al., 1981). For the M supergiants, α Ori (M2 Iab) and α Sco (M1 Ib + B), values of f_x/f_{bol} are respectively $<0.03 \times 10^{-7}$ and $<0.02 \times 10^{-7}$, and for the bright giant, β Peg (M1 II–III), this ratio is $<0.2 \times 10^{-7}$. This is consistent with the IUE observations and demonstrates that there is no stellar coronal ($T \geqq 10^6$ K) radiation observed from such stars. In this frame, perhaps the most important result of the observations of soft X rays is the discovery, with the Einstein spacecraft, of a rather sharp dividing line in the HR diagram. For giants, those stars hotter than about $V-R = 0.80$ (K0 III) emit soft X rays in detectable amounts, while those cooler do not (Ayres et al., 1981). This coronal dividing line (the X rays are presumed to arise from a hot corona) falls close to the temperature dividing line defined by the appearance in the ultraviolet spectra of giant stars warmer than approximately K0 of lines of C IV, indicating the presence of a plasma with $T \geqq 10^5$ K. EXOSAT detections are actually made on Miras with a hot companion (R Aqr and CH Cyg), individual nonvariable M giants (β And), Miras (RS Aqr), and protoplanetary nebulae (V1016 Cyg, HM Sge, and RR Tel). It was demonstrated by Viotti et al. (1985) that the weak X-ray emission at Mira maximum is not correlated with the Mira-type variations. Detection of X-ray emission in any single M, S, and C star would certainly warrant further investigation, since it would clearly be an exception and so little is presently known about the chromospheres of these objects.

Only disparate attempts on *far-UV* flux measurements exist. The Orbiting Astronomical Observatory (OAO-2) UV spectrometer observed only the M supergiant, α Ori: no variations were detected on the seven scans (Code and Meade, 1979). On the other hand, Code et al. (1980) gave UV magnitude between 1330 and 4250 Å for five M variable and nonvariable giants and supergiants. Unfortunately, the large bandwidth required for OAO-2 photometry by the rapidly decreasing fluxes toward the ultraviolet and the complex spectra of these stars made the flux determination ambiguous. With the Astronomical Netherlands Satellite (ANS), Wesselius et al. (1982) have observed eight M giants and supergiants, some of them many times. The star α Ori, registered six times, appears to be variable; however, as the pointing prevision was 1 arc-minute, two or more stars could be present in the field of view, and the observed variability cannot be conclusive. On the basis of three observations, the authors conclude that HD 100029 (M0 III) is not variable. A probable hot UV-bright companion was found on HD 216131 (M2 III).

In their comparison between the current UV photometric and spectrophotometric systems used for late-type stars, Kjaergaard et al. (1984) point out: (a) a strong nonlinearity at low flux level for the TD1 2635 Å band; (b) a strong color effect on the TD1 2740 Å band, as well as on the OAO-2 2950 Å band, due to red leaks in the sensitivity functions; and (c) a strong influence of the scattered light of the late-type stars on OAO-2 spectrophotometry. Only the ANS photometry and the International Ultraviolet Explorer (IUE) LWR spectrophotometry are found to be without large systematic errors. Their Table 2 gives several $(UV-V)$ indices for stars of various spectral types and luminosity classes. Unfortunately, this table gives no data for giants with $(B-V) > 1.5$ (K5) and for supergiants with $(B-V) > 1.8$; therefore, it is applicable only for the hotter R and Barium stars, keeping in mind uncertainties in the data as commented by the authors. Moreover, the presence of emission lines such as Si II λλ1808, 1817 or the Mg II doublet may cause uncertainties in these indices. Only the three M giants or supergiants, HD 6860 (M0 III), α Ori (M1

Ia), and HD 217906 (M2.5 II–III), are observed with the satellites TD1, OAO-2, and ANS; the accuracy of the measurements does not permit quantitative comparisons.

A new era in research on outer atmospheres and chromospheres dawned with the launch of IUE, for it made possible fairly routine observations of ultraviolet spectra in either a short-wavelength (1150 to 2050 Å) or a long-wavelength (1800 to 3250 Å) band. Most studies of IUE spectra have focused, naturally enough, on the emission lines, and these results are discussed in Chapter 2 (observations) and Chapter 8 (chromospheric modeling). It became clear from the earliest ultraviolet observations that, in the cooler part of the HR diagram, spectra of giants and supergiants were of two distinct types, depending on the presence or absence of lines of stages of high ionization. All stars show emission lines from such easily ionized elements as Mg II and Fe II (the archetypal line being Mg II λ2800), which are representative of a warm chromosphere (6000 to 15000 K). Those stars to the left of an almost vertical line near K0 also show lines from highly ionized elements (the archetypal line being C IV λ1550 Å) representative of a hot ($\sim 10^5$ K) plasma; those to the right of this "temperature" dividing line show no high-ionization lines (Linsky and Haisch, 1979). The asymmetry of the emission lines (Mg II h and k) further indicates an outflow of material in the cooler giants (Stencel and Mullan, 1980), and this "mass-loss" dividing line lies close to the temperature dividing line. As described above, observations with the Einstein spacecraft of X rays reveal a similar dividing line in the HR diagram between stars with (to the left) and without (to the right) soft X-ray emission (Ayres et al., 1981), which X-ray dividing line is also close to the temperature dividing line and the mass-loss dividing line.

These observations accord with and greatly expand previous knowledge that violet emission lines of Fe II (multiplets 1, 6, and 7) are practically ubiquitous in the spectra of M giant stars (Boesgaard and Boesgaard, 1976) and are even seen in N-type carbon stars (Bidelman and Pyper, 1963), but are not seen in warmer stars, while the high-excitation 10830 Å line of He I is almost universally absent from single red-giant stars (Zirin, 1982). The common interpretation of these results, supported by many observations and based on a fair amount of modeling, is that giant stars warmer than about K0 are solar-like in having warm chromospheres and hot coronae, while cooler giants have warm chromospheres and outflowing matter (Linsky, 1980, 1982; Brown, 1984; Linsky, 1985). Except for binary stars, then, we expect the red giants of interest here, all of which, except perhaps for the warmest R stars, lie clearly to the right of the dividing lines in the HR diagram, generally to show Mg II in emission in some strength and evidence of mass loss but no spectral lines from several-times-ionized elements.

Stickland and Sanner (1981) observed the far-ultraviolet continua of 15 late K and M giant and supergiant stars (as late as M6) with IUE and obtained radiation temperatures at 1850 and 1250 Å. Remarkably, the radiation temperature at 1850 Å of all stars was close to 3400 K. They also demonstrated that this flux originates in the chromosphere. Several studies have found a general decrease in the fraction of ultraviolet flux in both emission lines and continuum, relative to bolometric flux, as one goes to later spectral types among the M giants. IUE has confirmed and delineated this trend down to M6 for stars with angular diameters from lunar occultation (Steiman-Cameron et al., 1985).

Along with numerous G and K giants, several M giants and supergiants have been observed with IUE. Representative spectra of three M giants and one supergiant (α Ori) are shown in the valuable atlas by Wing et al. (1983). When line profiles of Mg II are available, the usual procedure is to construct a temperature profile through the chromosphere. Even then, no attempt has yet been made to reproduce by any empirical or theoretical model the flux of other lines or the continuum. Average properties of the chromospheres can be deduced from lines of Fe II and C II. A study

of 14 noncoronal G8–M3 giants, for example, leads to temperatures of 7000 to 9000 K and electron densities of $\sim 10^8$ cm^{-3}, and these appear to be independent of spectral type (Carpenter et al., 1985). Most of the effort in warmer (F, G, and K) stars has been directed toward linking the observed line emission to other stellar parameters such as mass, luminosity, age, or rotational velocity. Although the M, S, and C stars of interest here have often been neglected, progress can best be judged from several recent reviews (Linsky, 1980, 1982, 1985; Brown, 1984; Böhm-Vitense and Querci, 1986).

More attention has been given to Betelgeuse than any other star of interest here; it is often taken as the archetype red giant. Although *spectral lines* are discussed more fully in Chapter 2, we mention here some of the results so far derived. Analyses of the Mg II h and k lines, along with the Ca II H and K lines, leads to a temperature profile of the upper photosphere and lower chromosphere (Basri et al., 1981). Chromospheric densities can be deduced from the relative strengths of the lines in the C II (UV 0.01) multiplet (Stencel et al., 1981; Carpenter, 1984). The extent of the chromosphere can then also be deduced from the absolute intensities of the C II lines. For Betelgeuse, the chromosphere has a temperature of 6000 to 8000 K and a thickness on the order of the radius of the star. The variation of relative velocity within the chromosphere can be obtained from a study of the line shifts of the numerous Fe II lines (Carpenter, 1984).

Ultraviolet observations of other M, S, and C stars we summarize briefly. Barium stars show strong emission lines of Mg II similar to K giants of the same temperature. Early R stars show no ultraviolet chromospheric indicators, while later R stars (R8) have weak emission lines of Mg II and Fe II (Eaton et al., 1985). S stars apparently show a large range in strength of chromospheric emission, but very little has been published. One special use of IUE is to search for hot companions to M, S, and C stars. Several types of these peculiar red giants have been observed in the short-wavelength region for possible white-dwarf companions, and a few have been discovered (Dominy and Lambert, 1983; Böhm-Vitense and Johnson, 1985).

The first attempt to observe N-type carbon stars was negative (Querci et al., 1982): neither emission lines nor continuous flux were recorded; the observed flux was lower than $\approx 10^{-16}$ erg/cm^2 Å (3σ flux limit). Later observations with IUE detected weak UV spectra, with some continuum down to at least 2850 Å, for seven bright N-type carbon stars (Johnson and O'Brien, 1983; Querci and Querci, 1985; Johnson and Luttermoser, 1986). Longward of 2850 Å, the spectrum is basically an absorption spectrum—apparently the ultravioletward extension of the photospheric spectrum; shortward of 2850 Å, only emission lines (C II, Mg II, Al II, and Fe II) are detected. The continuous flux is, however, much weaker than in M giants, which implies either that the cool C stars have weak chromospheres (low temperatures or densities) or that an important opacity source is located above the emission-line-forming region (see the conclusions obtained in this sense in Chapter 2). Yet the strength of the chromosphere (e.g., L_{Mg}/L_{Bol}) decreases rapidly with spectral type among the M giants. Will M7 or M8 giants, which have effective temperatures as low as those of N-type carbon stars, have chromospheres as weak? Why are chromospheres of carbon stars so weak? Is it due to lower temperatures or different chemical composition or more overlying absorbing material? *Observation time on the Space Telescope* is necessary to observe these stars with enough light signal and at various phases to make decisive progress on this problem.

A violet-ultraviolet color-color diagram (Mg II–V vs. IUE–V) has been developed and used to compare spectrophotometric aspects of IUE-LWR observations for K, M, S, and C stars (Eaton et al., 1985), as is shown in Figure 1-2 (see also the section on *Intrinsic Properties*). As anticipated, red giants and supergiants have low UV continuous fluxes and display lines from only such low ionization stages as Mg II and

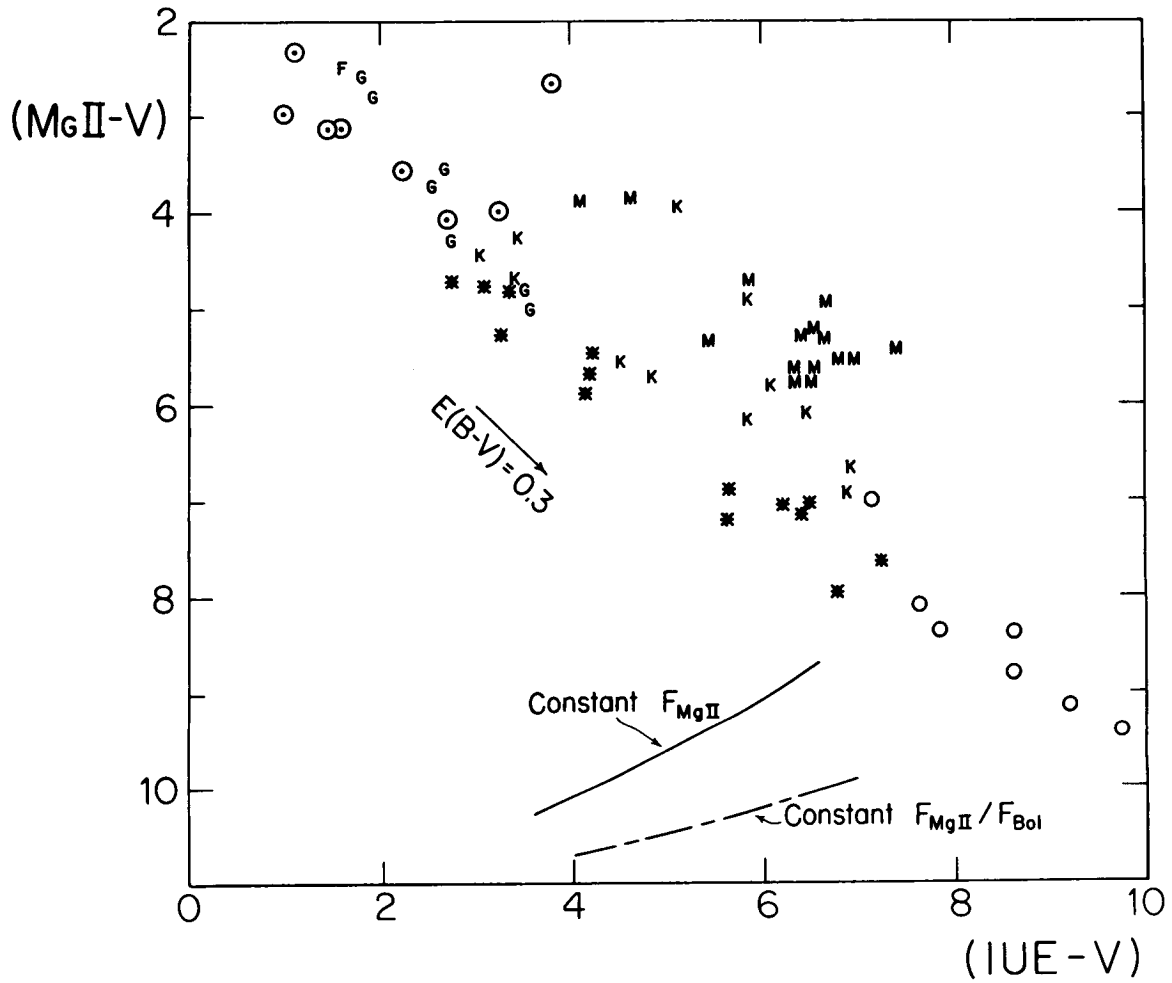


Figure 1-2. A two-color diagram for stars showing an Mg II index (measuring ratio of the flux in a 30 Å band at 2800 Å to the flux at V) against an IUE color (the ratio of flux between 2585 and 3200 Å (Mg II omitted) to the flux at V). G and K dwarf stars are shown as circled dots, G, K, and M giants and supergiants as letters, R stars as asterisks, and N stars as open circles (from Eaton et al., 1985).

Fe II (see Chapter 2), indicating the *lack of a transition region*.

On the low-energy side, (i.e., the *far-IR*), the opaqueness of the terrestrial atmosphere necessitates the use of satellites. The outstanding of these—the Infrared Astronomical Satellite (IRAS), a joint project of the United States, the Netherlands, and the United Kingdom—produced a wealth of valuable data during 1 year of use (Neugebauer et al., 1984). Another one, the Infrared Space Observatory (ISO), is planned to be launched by the European Space Agency (ESA) in 1992 to perform imaging, spectroscopic, photometric, and polarimetric investigations in the IR spectral range from 3 to 200 μm during an operational lifetime of about 18 months.

The data of IRAS are presently under reduction; the first results on cool giants were presented at the University of California at Los Angeles, meeting, "Mass Loss from Red Giants," held in June 1984, and at the Calgary Workshop in 1986. Physical parameters of the stellar outer layers are deduced. The low-resolution spectrometer (LRS) made spectra

between 8 and 22.5 μm with a spectral resolution varying between 15 and 30. A continuous sequence is found by Olnon et al. (1984) from classical Miras to the very red Miras like OH 17.7 - 2.0 or OH 26.5 + 0.6, which are very cool objects (Werner et al., 1980); only the outermost dust shell is visible at all LRS wavelengths, and no absorption features are observed. As it is already known from the radio observations (Smolinski et al., 1977), Stickland (1985) found no contribution to the IR excess from free-free radiations on hypergiants. Analyzing the IRAS data of many RCB stars, Schaefer (1985) finds a bimodal distribution among them (see the section *Eruptive Variables: The RCB Stars*). Maps at 60 and 100 μm around M supergiants are also obtained with IRAS. For α Ori, "shells" appear that are not centered on the star. Are these shells ejected remnants or parent cloud to α Ori (Wesselius, 1984)?

Long-term monitoring of a few oxygen-rich Mira variables has already begun to provide information about the temporal variation of the peak intensity and the shape of some radio maser lines (Barcia et al., 1985); their profile and their three-peak structure are in agreement with theoretical calculations (Zhou and Kaifu, 1984). Moreover, the mean intensity ratio between the $v = 1$ and $v = 2$ SiO lines seems to agree qualitatively with the theoretical predictions of Bujarrabal and Nguyen-Q-Rieu (1981). Let us also point out some scarce radio flares detected on o Cet (Boice et al., 1981), on R Aql (Woodsworth and Hughes, 1973; Bowers and Kundu, 1981), on V Cyg (Querci et al., 1979), and on α Ori (Kellermann and Pauliny-Toth, 1966; Seaquist, 1967). We stress the importance of monitoring radio, visible, and far-UV continuum for the detection of such nonthermal flares and the analysis of their energy distribution. The radio continuum spectrum of α Ori obtained with the very large array (VLA) was fitted by a power law $S_v \sim v^{\alpha}$ with $\alpha = 1.32$ (Newell and Hjellming, 1982). A model of chromosphere has been deduced with an electron temperature of 10000 K and an extension of 4 R_*.

In this brief review, we have summarized the first photometric attempts made in the far-UV and X rays and in the far-IR and radio frequencies to show the relative lack of monitoring in these spectral ranges and the urgency in fostering such observations. The reasons for the paucity of observations are mainly that: (a) the stellar flux is very low, and it can be registered with current instruments for only a few bright stars; and (b) the flux may be strongly variable (why not?), and the phase of the star's maximum has not always been considered.

Space Motion and Space Distribution

Although detection of M, S, and C stars has mainly been due to objective-prism surveys, new techniques involving photoelectric spectral scanners or photography of star fields through narrowband filters are adopted to identify cool stars in crowded fields such as the fields of rich star clusters (Palmer and Wing, 1982). These filters are selected from Wing's (1971) eight-color photometry previously used to identify carbon stars (e.g., Wing and Stock, 1973) or to classify M supergiants (White and Wing, 1978).

In the solar neighborhood, only 1 percent of all the stars are giants, and the G, K, M, and correlated types of giants make up at most 5 percent of this 1 percent (Jaschek, 1985). The apparent and space distributions in the solar neighborhood are well known through early reviews on the question. M stars are found in large numbers in the galactic center direction (2000 per square degree according to Blanco, 1965), while the C stars avoid this direction. On the other hand, the C stars are strongly concentrated toward the galactic equator, compared to the late M stars. The majority of carbon stars appear to be spiral-arm objects. Among the carbon stars, the R stars have smaller concentration toward the galactic plane than the N stars; moreover, the R stars are found in great numbers where no N stars are present. The dispersion of the early R stars above the galactic plane indicates that they are representative of a population that is older and less massive than the

C - 2

N stars (Stephenson, 1973). Alksne and Ikaunieks (1971) note an apparent concentration of later (R5–R9) stars toward the galactic equator similar to that for Mira and semiregular C stars, while type Lb (irregular variations of light) variables are concentrated more to the equator. The radial distribution and hydrogen deficiency appear to be correlated: R stars such as HD 100764 have low radial velocity (5 km/s) and do not suffer the severe hydrogen deficiency seen in supergiant R stars such as the high-velocity star, HD 182040, in which the Balmer lines are absent (Sanford, 1944).

The nonvariable HdC stars have strong similarities with the RCB (variable HdC stars): chemical composition, space distribution ($|\mu_\alpha|$ from 0.008 to 0.024 and $|\mu_\delta|$ from 0.010 to 0.035). These values of radial velocities and proper motions are the characteristics of high-velocity stars. With space velocities in excess of 400 km/s, these stars are members of the halo population. The He stars (hotter HdC stars) seem to be spread out farther from the galactic plane than the cooler ones, as is also indicated by their somewhat larger radial velocities (Warner, 1967). In summary, all the cool nonvariable HdC stars appear to be closely concentrated to the galactic center, whereas the RCB stars are not noticeably concentrated toward the galactic plane and galactic center. The He stars are widely distributed.

As for the M stars, if the late types (M7–M10) are concentrated in directions close to the galactic center, as quoted above, M5–M6 types are not as concentrated, and M2–M4 types are nearly equal in number in the galactic center and the anticenter directions. Moreover, the early M types present local groupings along the galactic equator. It is concluded by several authors (quoted by Alksne and Ikaunieks, 1971) that half or more of early M-type stars are members of the galactic spiral arms, while late M types belong to the disk population. An illustration is provided by the careful study of 722 M giant stars (with a few S and C stars) in the Perseus spiral arm (Ichikawa, 1981). As pointed out by Gehrz et al. (1981), OH/IR stars are strongly confined to the galactic plane and are usually found at such large distances (6 to 8 kpc) (Baud et al., 1981; de Jong, 1983) that interstellar extinction at infrared wavelengths cannot be neglected. Space densities (n_o) and effective heights of the space distribution (z_e) from the galactic plane of late-type M giants in the solar neighborhood observed by various authors are listed by Mikami and Ishida (1981; see their Table 3). These authors compare them with their statistical estimates based on the Two-Micron Sky Survey data (Neugebauer and Leighton, 1969) and find them to be in good agreement; moreover, they determine the space density and distribution of M supergiants (Table 1-2).

S stars are as numerous in the direction of the galactic center (like the late M stars) as they are concentrated in the galactic spiral arms.

Discussing the kinematics and stellar population of the Ba II stars, Eggen (1972a) concludes that their space motions resemble those of an old disk population of 1.0 to 1.5 $M_\odot$ stars. In their sample of Ba II stars, Catchpole et al. (1977) found a difference in velocity dispersion from Ba-strong versus Ba-weak stars, which is explained by Rocca-Volmerange and Audouze (1979) as a reflection of an age-versus-abundance correlation.

Other investigations studied the distribution of late-type red giants in the direction of the central regions of our Galaxy and of other nearby galaxies, the Large and Small Magellanic Clouds, and other galaxies such as M31. Blanco et al. (1978, 1984) survey Baade's Window (that surrounds the globular cluster, NGC 6522), which constitutes a uniquely complete sample of the red-giant population of the galactic nuclear bulge. The striking feature is a very large number of M giants, but no C or S stars were found, even though they should have been detected had they existed. Such a result confirms a previous survey in the Sagittarius I region (Baade, 1951), in a direction closer to the galactic center than Baade's Window. Therefore, the ratio of the number density of carbon stars to the number density of M giants—the C/M ratio—is negligibly small in the galactic bulge.

Table 1-2
Space Densities and Distributions of Nearby M Giants and Supergiants*

Spectral Type	Member Density (10^{-6} stars/pc^3)	Effective Height (pc)
K0–K4	40.0	170
K5–M1	3.5	200
M2–M4	3.1	310
M5–M6	0.9	390
≥M7	0.6	380
M supergiants	0.054	210

*Adapted from Mikami and Ishida (1981).

The distribution of carbon and M-type giants in the Magellanic Clouds (Aaronson, 1984) and nearby galaxies is important for interpreting AGB evolution (e.g., Iben, 1984; Wood, 1985) and for understanding fundamental galactic properties, such as the metal abundance (C/M is strongly correlated with this quantity (e.g., Scalo, 1981)), the distance to the galaxy, and the full AGB luminosity function for the galactic field studied. Outstanding is the lack of late-type M stars in the central regions of the Small Magellanic Cloud (SMC), reminding us of the almost complete lack of C stars in the bulge of our Galaxy (Blanco et al., 1978). Also, differences in the C/M ratio between the SMC and the Large Magellanic Cloud (LMC) are noticeable. A survey of high degree of completeness for carbon stars and M-type giants in the Magellanic Clouds (Blanco and McCarthy, 1983) indicates that the ratio of the surface density of carbon stars and that of giants of type M6 or later in the SMC varies from 19.2 ± 0.8 at the center to 4.7 ± 0.4 in the periphery, while the C/M ratio is 2.2 ± 0.1 throughout the LMC. It is suggested that the mixture of stellar populations is roughly uniform across the LMC, but not in the SMC. Recalling the negligible value of the C/M ratio in the galactic nuclear regions, Blanco and McCarthy (1983) note that their population includes older and less massive red giants than those observed in the Magellanic Clouds. A recent review of the distribution and motions of red giants in the Magellanic Clouds is by Catchpole and Feast (1985).

A field in M31 has been investigated by Richer, Crabtree, and Pritchet as quoted by Richer (1985) in which C/M is about 0.12, implying a metal abundance higher than that in either the LMC or NGC 300, but lower than that in the galactic center. In addition, there appears to be a deficiency of luminous AGB stars as in the LMC.

To conclude on the spatial distribution, we note that carbon stars have been discovered in all dwarf spheroidal galaxies (Aaronson et al., 1983).

Intrinsic Properties

Red giants and supergiants (M, S, C, Ba II, MS, CS, CH, and CN stars, etc.) occur in a large range of stellar masses and ages because they are found in halo, old disk, and young disk populations. The observational data indicate that they have mixed nuclearly processed material from the core to the atmosphere for

luminosities such as $-10 \leqq M_{bol} \leqq +3$, ages from $\sim 10^7$ to 10^{10} yr, and a broad range of masses from $\sim 1\ M_\odot$ to $\geqq 20\ M_\odot$, with a mean mass of $1.2\ M_\odot$ (Scalo, 1976, 1984). A summary of the physical properties (luminosities, temperatures, masses, abundance of elements, population types, etc.) of red giants of the disk population, as well as their characteristic spectral features, is given in Table 1-3 (from Scalo, 1981).

Absolute Magnitudes and Colors. The N-type stars and the various S-, MS-, and CS-type stars belong to luminosities $-4 > M_{bol} > -6$ (Richer, 1981; Bessel et al., 1983; Lloyd-Evans, 1983). They are asymptotic giant branch (AGB) stars where the helium shell flashing occurs in the intermediate mass stars. Ishida (1960) gives an M_v of -1.5 to -2.0 for the N-type stars. The R5-R8 stars are also very bright but probably not well classified (Eggen, 1972a). The hotter R stars (R0 to R4 types), the Ba II and CH stars, fall in a fainter range of luminosity ($+3 \leqq M_{bol} \leqq -3$); they are not so high on the AGB as the N-, S-, MS-, and CS-type stars quoted above. They are probably older, lower mass stars. With the well-known relation among the emission core of Ca II H and K lines and the luminosity of late-type stars (Stratton, 1925; Wilson, 1959; Wilson and Bappu, 1957; Warner, 1969), Richer (1975) obtains the range in M_v between -0.1 and +1.1 for the hot R stars. Bright members of this class are HD 182040 with $V = 6.99$, $B-V = 1.07$, $U-B = 0.65$, $R-I = 0.55$, and $I-L = 0.44$ and HD 156074 with $V = 7.61$, $B-V = 1.1$, $R-I = 0.3$, and $I-L = 2.2$.

Although the great majority of these stars are variable, we must keep in mind that some are considered nonvariable, such as the early R stars, which are predominantly nonvariable giants (see the section *Nonvariable Stars*). Distinctions in absolute magnitudes or in colors are noted between variables and nonvariables of the same type or same class. The variable R stars are redder than the latest R nonvariables (Vandervort, 1958). The nonvariable R and N stars both have a continuum I104 magnitude M(104) $\geqq$ -1.2 (Baumert, 1974); they are approximately 1.5 to 5 mag fainter than the variables, while the early nonvariable R stars are 2 mag fainter than the late R nonvariable stars. Baumert (1974) notes that the brightness increases in the sequence nonvariables, irregular Lb giants, semiregular SRb giants, Miras, and semiregular SRa giants. (See the section *Variability Types of Giants and Supergiants* for the definition of these various variables.) No clear correlations were observed between absolute magnitude and CN strength or temperature.

To conclude on the "classical" carbon stars, we stress that the early R stars are physically distinct from the later carbon stars. Such a dichotomy is not only striking from visible indices, as mentioned above, but also from the $(R-I)$ index (Eggen, 1972b) and from a far-UV index (Eaton et al., 1985). From the latter, the carbon stars seem to be separated into three groups in the color diagram (Mg II-V)/(IUE-V) (Figure 1-2). Early R stars fall into two groups among the late G and early K giants; late R stars (R5 to R8) distinctly overlap with the reddest K and M giants, joining smoothly with the N stars at their bluer end. The N sequence extends 2.5 mag farther to the red. On the other side, Figure 1-2 illustrates the relation between color and chromospheric emission for C stars and other giants: the fraction of stellar luminosity radiated in the chromospheric Mg II lines decreases with effective temperature. Low chromospheric emission characterizes the N and R stars (also the G dwarfs) and a few K stars, whereas most of the K and M giants are located above the carbon sequence by up to 2 mag.

All the properties of the HdC stars are well summarized by Warner (1967), Wallerstein (1973), and Hunger (1975).

The atmospheric parameters of the RCB stars indicate high luminosity; they are as luminous as other HdC stars (Warner, 1967). These stars are supergiants (Orlov and Rodriguez, 1977). Herbig (1958) gives $M_{bol} \sim -4.0$ to -6.0 for the prototype star, R CrB. In his Table 20, Glasby (1968) gives 25 RCB stars

Table 1-3
Physical Properties and Characteristic Spectral Features of Disk Population Red Giants*,**

Spectral Type	Distinguishing Spectra	C/O	s-process	Tc	$^{12}C/^{13}C$	Li	Relative Numbers	M_{bol} Range	Mass Range ($M_\odot$)	Mean Mass ($M_\odot$)
K	---	0.3	N	A	---	--	7×10^4	+1 – –3?	1 – 5:	1.2
Ba	Ba II λ4554 CH, C_2, CN	≳0.6	+	A	N	N	10^3	+1 – –3	1 – 5:	1.2
R0–R4 (C0–C4)	Strong C_2, CH, CN	>1	N	A	~10	N?	10^3:	~0	1 – 1.7:	~1
M	TiO, VO	0.3 – 0.7?	(+)	+	?	N	10^3	–3 – –6	1 – 10?	1.2
MS	TiO, weak ZrO	0.5? – 0.80	+	+	?	N	10^2?	–3 – –6	?	~1.2:
S	Weak or absent TiO; ZrO, LaO	0.80 – 0.99	+	+	?	(++)	10	–3 – –6	1 – >10	1.2
SC	Very weak ZrO and C_2	0.99 – 1.01	+	+	?	(++)	1	?	?	1.2:
N (C5–C9)	Very strong C_2, CN, CH	>1.01 – 2?	+	+	(--)	(++)	10^2	–3 – –6	1 – >10	1.2 – 1.5

*From Scalo (1981).

**K type is given for comparative purposes.

Symbols: N = K giant normal abundance, A = Absent, + or – = somewhat enhanced or deficient with respect to normal K giants, ++ or –– = strongly enhanced or deficient, ? = unknown or uncertain, ( ) = only a small fraction of the spectral type possess the anomaly.

The straight line across the table delineates the "hot" stars, early R and Ba II stars (above the line) for which $\sim 4000 < T_{color} < 5500$ K, and the cooler ones (below the line) for which $\sim 2000 < T_{color} < 3800$ K.

with maximum and minimum magnitudes and spectral types. Alksne and Ikaunieks (1971) show the spectral class, Howarth (1976) shows the maximum magnitude and spectral class, and Sherwood (1976) adds some stars to Glasby's list. Among them, four are observed in the Large Magellanic Cloud: W Men, SY Hyi, HV 5637, and HV 12842, with the absolute magnitude at maximum being -4.8, -6.6, -3.2, and -4.9, respectively. Duerbeck and Seitter (1982) give a list of RCB stars with their spectral type, their V, $B-V$, and $U-B$ values, and their pulsational period.

Various estimates have been made concerning the helium stars; they are based on the strength of interstellar lines and proper motions. For MV Sgr, Klemola (1961) gives $M_v \approx -2.0$ to -4.0, and consequently, $M_{bol} \approx -4.0$ to -6.0; Herbig (1964) gives a value of -5.0 for M_{bol}.

The analysis of the interstellar D lines of the typically hydrogen deficient C (HdC) nonvariable star, HD 182040, shows that this R star is highly luminous and confirms Warner's (1967) conclusion that the HdC stars are supergiants (Utsumi and Yamashita, 1971). From observations of the Ca II K emission cores and the Wilson-Bappu effect, Richer (1975) gives $M_v \approx -4.1$ for the three nonvariable HdC stars: HD 137613, HD 173409, and HD 182040. Because their atmospheric parameters indicate high luminosity, they are as luminous as their variable analogs (Warner, 1967). The hydrogen-deficient (supergiant) R stars are physically distinct from the N and "classical" giant R stars. The He, RCB, and nonvariable HdC stars have a common range in values of mean M_v value -2.0 to -5.0.

MacConnell et al. (1972) estimate that 1 percent of the G and K giants are Ba II stars; therefore, the Ba II are Population I giants (classical and very weak line objects), and their absolute magnitudes are similar to those of G and K giants (Baumert, 1974). The classical Ba II stars are all binaries, but this may not be true for the mild Ba stars. Bond and Neff (1969) and Gow (1976) showed the excess absorption in the violet region of the Ba II stars: a controversy developed about the reality and the identity of this feature (McClure, 1984, and references therein). The difficulty in placing the Ba II stars in the HR diagram is mainly one of determining their luminosities and Morgan-Keenan spectral classification. From his analysis of many studies, McClure (1984) concludes that most Ba II stars have "normal or slightly above normal ($<M_v> \approx 0.0$ mag) G and K giant luminosities." However, the classical bright Ba II star, ξ Cap, has a very high luminosity: $M_v \approx -3$. This implies that the star has a large mass or that it could be in a helium shell flashing stage of evolution on the second AGB (McClure, 1984).

For the CH stars, we have M(104) = -3.9 as derived by Baumert (1974), who believes that the CH stars measured by Wing and Stock (1973) are at the extreme tip of the red-giant branch.

Among the brightest stars are early M-type supergiants (M0 to M4 types) with $-8 \leqq M_v \leqq -5$. Stothers and Leung (1971), Humphreys (1978, 1979), and Cowley and Hutchings (1978) collected such bright objects in clusters, nearby galaxies, and the Large Magellanic Cloud. Their M_{bol} would be -7 to -10 (Glass, 1979), like the M supergiant near 30 Doradus, the carbon stars in NGC 1783 or NGC 2477, or ϱ Cas and VX Sgr (Sargent, 1961). The most luminous of the nearby supergiants is μ Cep. With its $M_v \approx -8$ and its $M_{bol} \approx -10$, it is about one million times brighter than the Sun. All these stars are also considered to be super-supergiants, a term introduced by Feast and Thackaray (1956), otherwise called hypergiants (Van Genderen, 1979).

For the M Miras, Clayton and Feast (1969) conclude that the absolute magnitudes vary smoothly within the period: $M_m = -3.0$ to -1.0 at maximum light and $M_1 = -1.5$ to 0.1 at mean light intensity, with periods varying from ~ 180 to ~ 500 days. The shorter period Miras (~ 130 days) deviate from this period/luminosity relation. They have $M_m = -1.6$ and $M_1 = 0.1$. Robertson and Feast (1981) show that the stellar luminosity decreases with period for the galactic Miras, and Glass and

Lloyd-Evans (1981) reach the same conclusion for the Miras in the Large Magellanic Cloud.

Information on colors and luminosities are best displayed as an observational HR diagram, and several attempts to construct such diagrams for galactic red giants have been made (e.g., Scalo, 1976; Tsuji, 1981c). A better result comes from the Magellanic Clouds, where the known distance permits absolute luminosities to be determined (Wood et al., 1983). (See the section *Aspects of Evolution of Long-Period Variables (LPV's) in the Magellanic Clouds.*)

Effective Temperatures. Effective temperatures can be measured or estimated for at least a few stars from the relation $F = \sigma T_{\text{eff}}^4$, where F is the integrated energy flux at the stellar surface. This flux can in turn be derived by any of several means, all depending on some variation of the relation between observed energy flux (f), emitted flux (F), and angular diameter (θ): $f = F(\theta^2/4)$, where the flux is either monochromatic or integrated. That is, the effective temperature can be inferred for any star for which the angular diameter and total integrated (bolometric) flux (outside the Earth's atmosphere) can be measured. This latter quantity is often difficult to obtain for late-type stars since the bolometric correction is so large. In fact, the desired information—complete spectrophotometry—is seldom available for the M, S, and C stars (Strecker et al., 1979, for M stars; Goebel et al., 1980, for a carbon star; and Augason et al., 1986, for S stars), and fluxes obtained from broadband colors are used instead (e.g., Ridgway et al., 1980a).

Angular diameters are measured or inferred by several means:

1. They can be directly measured by lunar occultation for stars near the ecliptic, and this is the principal source of our current data (e.g., Ridgway et al., 1980; Beavers et al., 1982).
2. For a few stars, values of angular diameters are available from Michelson interferometry or from speckle interferometry (e.g., Balega et al., 1982; Bonneau et al., 1982; see also Chapter 2).
3. Angular diameters can be indirectly inferred from the relation between visual surface brightness and unreddened (V–R) color (Barnes and Evans, 1976; Barnes et al., 1978; Eaton and Poe, 1984) although the validity of this relation for the coolest giant stars has not been established beyond doubt.
4. Substitution of the monochromatic flux from an appropriate model for the flux at the stellar surface allows one to infer the angular diameter of any selected star for which the monochromatic flux can be observed (see above formula).

If the integrated flux can be observed, the effective temperature can also be calculated. Since the infrared region is often least influenced by molecular bands, it offers the best choice for application, and the method is generally called the method of infrared photometry (Blackwell and Shallis, 1977; Blackwell et al., 1980). For the coolest red giants generally, this method provides the best present information and has been used to define a temperature scale for M giants (Tsuji, 1981a), for S stars (Augason et al., 1986), and for N-type carbon stars (Tsuji, 1981b).

A final method of determination of effective temperature, that of model fitting, does not depend on the angular diameter. Instead, one directly compares computed and observed flux curves and chooses the effective temperature of the best-fitting model. Widely used in hot and intermediate stars, the method has not been much used in cool stars (e.g., Querci et al., 1974; Bouchet et al., 1983; Steiman-Cameron and Johnson, 1986) because of the lack of complete spectrophotometry and the deficiencies of the models, although it has been applied to calibrate a scale of effective temperatures for M giants (Tsuji, 1978). As these deficiencies are corrected, this method will assume greater importance. In this scope, the comparison between observed and synthetic spectra should give an effective temperature (e.g., Querci and Querci, 1976). However, it remains the problem of uniqueness of the solution.

Table 1-4
Effective Temperatures (T_{eff}) for M Giant Stars*

Spectral Type	T_c (K)	$V-K$ Color	T_{eff} (K)[1]	T_{eff} (K)[2]	T_{eff} (K)[3]
M0	3750	3.78	3895	3900	3800
M1	3640	4.02	3810	3800	3865
M2	3530	4.30	3730	3700	3800
M3	3400	4.64	3640	3600	3640
M4	3250	5.10	3560	3500	3460
M5	3000	5.96	3420	3300	3310
M6	2600	6.84	3250	3200	3280
M8	---	---	---	2300	---

1. Effective temperature from broadband colors and lunar occultation angular diameters (Ridgway et al., 1980a,b).
2. Effective temperature from model fitting (Tsuji, 1978).
3. Effective temperature by method of infrared photometry (Mira variables are not considered) (Tsuji, 1981a).

*Color temperature is on the Wing system (Ridgway et al., 1980).

In the past, a rough method was to use a spectroscopic temperature or excitation temperature for the effective temperature.

Results for M giant stars are collected in Table 1-4. Although these are the best current values, there is still considerable uncertainty, and much more work is needed. A graphic comparison of the results obtained for M stars by lunar occultation (Ridgway et al., 1980a, b), by infrared photometry (Tsuji, 1981a), and by the method of model fitting (Steiman-Cameron and Johnson, 1986) is shown in Chapter 7 (Figure 7-14). As yet, there is no reliable temperature scale for M giants or supergiants later than M6, where most stars are Mira variables, the very red ones being OH-IR objects.

Several obstacles hinder the decisive determination of effective temperatures for the R stars. No angular diameters are available, molecules distort all broadband colors, the method of infrared photometry fails because of an excess of flux in the L band compared to G-K giants, blackbody colors are inconsistent, and insufficient spectrophotometry is available for model fitting. These and other problems have been exhaustively discussed by Dominy (1982, 1984), who finds that effective temperatures for three R0 stars lie in the range $4500 \leqq T_{eff} \leqq 4850$ K. However, some R0 stars may be even hotter. Dominy finds that R5 stars are nearly as hot as R0 stars. The temperature scale for the later R stars is presently quite uncertain, and these stars may not be closely related to the early R stars.

Effective temperatures for N-type carbon stars have been notoriously difficult to obtain,

and even now they are uncertain except for a few stars. Angular diameters have been measured for six non-Mira N-type carbon stars, of which five (TX Psc, X Cnc, AQ Sgr, SZ Sgr, and TW Oph) are irregular variables and one (Y Tau) is an SRa variable (Ridgway et al., 1977; Walker et al., 1979; Ridgway et al., 1980b; Ridgway et al., 1982). Although one star (TW Oph) is so heavily reddened that the effective temperature is unreliable, values for the other stars form the cornerstone of any further effort.

Tsuji (1981b) has obtained values of effective temperatures of 31 N-type carbon stars (SRb and Lb variables) by the method of infrared photometry (Blackwell et al., 1980). Angular diameters were deduced from previously published models (Querci et al., 1974; Querci and Querci, 1975) and L band photometry (Noguchi et al., 1977), corrected for the effects of molecular bands (however, see discussion by Bouchet, 1984a). Combined with complete broadband photometry, these yield effective temperatures. For the stars in common, the results of Tsuji agree with those obtained from measured angular diameters, and we believe that these are the best values currently available. The effective temperatures are all confined within the range $2400 \leqq T_{\rm eff} \leqq 3200$ K, and most fall between 2600 and 3100 K. It is well known that the "temperature classes" of the C star classification are not well correlated with effective temperatures (e.g., Tsuji, 1981b); Tsuji (1985a) presents arguments to explain this situation.

A scale of effective temperature for non-Mira S stars has been deduced (Augason et al., 1986) both by model fitting and by the method of infrared photometry, and the complicating effect of the unknown C/O ratio is revealed. There is also no temperature scale for S or C Mira variables.

Once fundamental effective temperatures have been determined for a sufficient number of calibrating stars, it will be useful to calibrate a color temperature derived from a carefully chosen set of filters (Wing, 1985). When this is possible for all types of peculiar red giants, values of effective temperature can be routinely obtained. Many effective temperature indicators are presently taken into account among the cool stars. Since the bolometric flux is very sensitive to temperature variations and the infrared monochromatic flux is not, the color index, m_{bol}-L, can be used as a temperature indicator (proportional to $T_{\rm eff}^3$) (Tsuji, 1981a, 1981b, 1985a). Another is the I(104)–L(400) index by Wing and Rinsland (1981) because the two spectral regions, 104 (1.04 μm) and 400 (4.00 μm), are free from molecular absorptions in the cooler stars.

For cool carbon stars, Tsuji (1981c) shows that all broadband photometric colors correlate fairly well with his effective temperature scale. Interestingly, although the intrinsic $(R-I)$ color is nearly the same for the N-type irregular stars, these have a range of temperature, and $(R-I)$ is therefore an indicator, not of temperature, but of interstellar reddening. The $(I-L)$ color is suggested by Tsuji as the best temperature discriminant for both carbon stars and M giant stars. Wing (1985) also suggests the use of the $I-K$ index.

Although the intrinsic infrared colors, $(J-K)$ and $(H-K)$, for cool carbon stars correlate with effective temperature and have been used to infer effective temperature, the range in both colors is relatively small (~ 0.6), and the scatter in $(J-K)$ is large. These colors do not appear to be reliable temperature indicators. One reason for the scatter might be the imprecision of the effective temperatures. On the other hand, the claim has been made, on the basis of comparative studies of carbon stars in the Magellanic Clouds and the Galaxy, that the infrared colors of carbon stars are primarily determined by strengths of molecular bands and only secondarily by effective temperatures (Cohen et al., 1981). Perhaps the answer lies somewhere between; infrared colors may well be influenced both by effective temperature and by chemical composition.

The temperature range covered by the RCB stars as a group is very large. For example, RS Tel has a spectral class as late as R8 with a surface temperature of 2500 K. Two very hot

stars—the B star, MV Sgr, and the 09 star, V348 Sgr—are also considered as RCB stars because of their variability behavior.

Radii. The giants, and chiefly the supergiants, are enormously distended. Most of them have sizes approaching that of our solar system. Some examples follow. If we adopt an effective temperature of 3000 K for μ Cep, one of the most luminous supergiant M stars, we find a radius of some 1590 times the solar value; this means that the photospheric layers of the star fill in our planetary system out to the orbit of Saturn! The extent of the μ Cep outer envelope layers are not yet measured nowadays. The photosphere of the supergiant Betelgeuse (α Ori: M2 Iab) is roughly the size of Jupiter's orbit ($R \approx 650\ R_\odot$). Polarimetric observations give a radius of the α Ori outer envelope of roughly 3700 $R_\odot$. (Our planetary system would be filled out to the Uranus orbit!) Observed from the Earth, the outer envelope of α Ori has an apparent diameter equal to 1/10 of that of the Sun. When we consider the HR diagram, we have to bear in mind that two supergiants of the same luminosity but with different temperatures do not have the same diameter. For example, the M, S, and C stars have radii 100 times that of a main-sequence B star. The cool hypergiants are still more extended stars. Finally, the S Mira, χ Cyg, has a photospheric radius $R \sim 240\ R_\odot$ (Hinkle et al., 1982).

The direct measurement of angular diameter of single stars uses the lunar occultation technique (e.g., Ridgway et al., 1980a, 1980b; Beavers et al., 1982) and numerous interferometric techniques such as speckle interferometry (e.g., see the review of Dainty, 1981, and references therein), as noted in the previous section. A photometric approach may also furnish the stellar radius; if one knows the absolute bolometric magnitude, M_{bol} (or the luminosity), and the effective temperature, $T_{\rm eff}$, the radius of the star comes from: $L = 4\ \pi\ R^2\ \sigma\ T_{eff}^4$.

Description of the geometrical shell extension is given by M. Querci (this volume). As an example, let us add that, using the very long baseline interferometer (VLBI), Bowers et al. (1980) found some masing regions in OH/IR stars from $> 0.5''$ to $> 0.04''$. The extent of the 1612-MHz region can be quite large, from 1000 to 10000 AU. The apparent diameter is consistent with the general predictions of the maser models (Goldreich and Scoville, 1976).

From the knowledge of the stellar radius and mass, the acceleration of gravity in a stellar atmosphere may be determined. In these stars, the $g_{\rm eff}$ values are rather badly known since the masses are linked to an uncertain evolution theory (Wood, 1985); they are considered to be $0.1 < g_{\rm eff} < 10$. Determination of the surface gravity for these peculiar red-giant stars remains a pressing unsolved problem. Much insight can be gained by examining the exhaustively discussed parallel problem for the well-observed K2 giant, Arcturus (Trimble and Bell, 1981). (Examples of indirect methods of estimating the surface gravity of late-type giants are given in Chapter 7.)

Aspects of Evolution of Long-Period Variables (LPV's) in the Magellanic Clouds

Studying long-period variables (i.e., the most extreme—in luminosity—red giants and supergiants) in the Magellanic Clouds releases us from the problem of distance determinations (hence, absolute magnitude determinations) in comparison to LPV's in the galactic disc for which existing distance determinations are generally based on statistical parallaxes (since they are not known to be related to open clusters). Also, the LPV's in the Magellanic Clouds cover a wide range in mass and luminosity and are generally free from significant interstellar reddening (Wood, 1982).

Wood et al. (1983) obtain IR photometry (*JHK*) and low-dispersion red spectra of 90 LPV's in the Small Magellanic Cloud (SMC) and the Large Magellanic Cloud (LMC), completing the IR photometry data of Glass and Feast (1982 and references herein) on Miras in the LMC. Their results, which are summarized below, largely contribute to progress in the knowledge of the red-giant or supergiant phase

of evolution that ends by drastic events such as planetary nebula ejection or supernova explosions. One must also recall that these observations include the brightest and, hence, most massive stars, some considerably more massive than the intermediate-mass stars that form the bulk of the M, S, and C stars.

Evolutionary calculations show that the LPV's fall into two distinct groups: (1) non-degenerate core helium (or carbon) burning supergiants with mass $M \geqq 9\,M_{\odot}$ on their first appearance as red giants; (2) asymptotic giant branch (AGB) stars (among them Miras) with degenerate carbon/oxygen cores and hydrogen- and helium-burning shells, climbing up the giant branch for the second time. Relevant properties of the AGB stars must be noted: (1) theoretical maximum possible luminosity for an AGB star is $M_{bol} \sim -7.1$; (2) their main-sequence masses are $\leqq 9\,M_{\odot}$; and (3) they are able to dredge up carbon and s-process elements to the surface through undergoing helium shell flashes, so that they participate in the enrichment of the interstellar medium in these elements at the onset of current loss of their envelopes by stellar winds.

Observational data of LPV's in the Magellanic Clouds confirm the division of these stars in supergiants and AGB's: (1) An absolute K-magnitude (M_K) against period (P) plot (see Figure 2 in Wood et al., 1983) shows that the stars fall into two sequences separated by the theoretical AGB limit in M_K: below this limit, stars are AGB stars, whereas above the limit, they are supergiants. (2) In this plot, carbon (N) stars and S stars (rich in s-process element Zr) are located in AGB sequence only, as expected from theoretical evolution calculations for which C and s-process elements are dredged up to the surface during helium shell flashes suffered by AGB stars. (3) K light curves indicate that the AGB stars have pulsation amplitudes of 0.5 to 1.0 mag, whereas the supergiants have smaller K amplitudes (<0.25 mag). (4) Finally, the mean J-K colors are rather similar for the supergiants whatever the period, while they become redder with period for the AGB stars.

Wood et al. (1983) discuss the evolution and physical properties of the LPV's in the Magellanic Clouds through the ($< M_{bol} >$, P)-diagram (Figure 1-3) on which the two regions occupied by the supergiants and the AGB stars are again clearly delimited (by dotted lines on the figure). For each bolometric luminosity, the core mass, M_c, of the AGB stars is indicated (theoretically, a linear relation exists between these quantities), as well as the main-sequence mass, M_{MS}, for the supergiants. (These quantities are related regardless of subsequent mass loss.) Theoretical lines of constant mass (the pulsation mass) are also plotted assuming the LPV's are first-overtone pulsators (see details in the section *Modes of Pulsation of the Long-Period Variables*). From Figure 1-3, Wood et al. note that the pulsation masses: (1) for the supergiants, range from ~ 7 to $\sim 30\,M_{\odot}$, with a strong concentration from ~ 10 to $\sim 25\,M_{\odot}$; (2) for the AGB oxygen-rich stars, tend to range from ~ 0.7 to $7\,M_{\odot}$; and (3) for the carbon stars in their sample (mainly in the field of NGC 371 and, hence, perhaps coeval), tend to concentrate from 1.0 to $1.5\,M_{\odot}$. The evolutionary implications of Figure 1-3 are as follows.

The supergiants (including some galactic supergiants) describe a continuous band from (P, M_{bol}) $\sim$ (100 days, -6.5) to (850 days, -8.2), with all but three of the Magellanic Cloud objects having $P > 400$ days. On the other hand, the initial main-sequence masses in this range of luminosities and $P > 400$ days go from ~ 16 to $23\,M_{\odot}$. The pulsation masses, which are present-day masses, indicate that the supergiants have lost up to half their mass since the main-sequence phase: the more luminous and the initially more massive the supergiants, the more mass they have lost in previous evolutionary phases. The supergiant evolution results from: (1) the decrease in mass, causing P to increase ($P \propto M^{-1/2}$), and (2) the change in radius with evolution ($P \propto R^{3/2}$).

As AGB stars evolve, they increase their luminosity with time, and correspondingly, they increase their periods, P. It is worth noting that, for the first time, stars on the upper AGB (i.e., with luminosity right up to the AGB limit

($M_{bol} \sim 7.1$)) have been identified. The arrows on the constant mass lines for AGB's in Figure 1-3 indicate that these lines are approximate evolutionary tracks. (Mass-loss effects are shown to be qualitatively unimportant.) To each luminosity corresponds an observed maximum period, the approximate position of which is given on the dotted line. As discussed by Wood et al. (1983), the normal evolution of an AGB variable evolving on an evolutionary track with $M < 3.5\ M_{\odot}$ stops when its track crosses the dotted line (maximum period reached); at this moment, the total mass of the star is still greater than the core mass, showing that the envelope hydrogen and helium has not yet been fully destroyed by nuclear-burning shells. The authors suggest that the evolution is terminated by the loss of the stellar envelope, followed by the formation of a planetary nebula, with nebula mass they estimate to be from $\sim 0.1\ M_{\odot}$ (for the oldest evolved stars) to $2.1\ M_{\odot}$ (for stars of initial mass $5\ M_{\odot}$). The mechanism they suggest for ejection of the envelope is the switch in mode of pulsation from first overtone to fundamental. This suggestion is supported by theoretical pulsation models, indicating that, as an AGB star increases its luminosity, it pulsates in modes of lower and lower order until the fundamental one—thought we have to keep in mind that the mode of pulsation remains a disputed question (see the section *Modes of Pulsation of Long-Period Variables*).

The galactic OH/IR stars (see the section *Classification*) with $P \sim 1000$ days are a good example of these stars pulsating in the fundamental mode and being in a transition phase between LPV and planetary nebula. When the evolution track of a more massive AGB star with $M > 3.5\ M_{\odot}$ reaches the AGB maximum luminosity limit, such a massive star will produce a supernova by the ignition of carbon in the degenerate core.

Finally, Wood et al. (1983) discuss further important points related to nucleosynthesis on the AGB. During helium shell flashes, ^{12}C and s-process elements are dredged up to the stellar surface. Carbon stars have dredged up sufficient carbon to be characterized by $C/O > 1$. The S stars, located on the AGB between M and C stars, have not yet dredged up sufficient carbon to have $C/O > 1$, but they have dredged up sufficient Zr, an s-process element, so that ZrO bands are observed to be enhanced in these stars. Carbon stars in the Magellanic Clouds were already known to have their higher luminosity at $M_{bol} \sim -6$. This is confirmed by Figure 1-3, in which all the more luminous AGB stars are noncarbon stars, among them S stars. It is clear that s-process elements are dredged up in these upper AGB stars, but C/O remains less than unity. An explanation favored by Wood et al. to the fact that some AGB stars of type S are found above the most luminous C stars is that the ^{12}C dredged up is converted to ^{14}N during quiescent evolution between shell flashes by CNO cycling at the base of the envelope convection zone; therefore, the AGB stars are the source of primary nitrogen (since ^{14}N is synthesized from the hydrogen and helium in the star at its birth), as well as s-process and carbon elements.

VARIABILITY TYPES OF GIANTS AND SUPERGIANTS: A SURVEY OF OBSERVATIONS AND INTERPRETATIONS

The brightness fluctuations of these intrinsic or physical variable stars are caused by geometrical and physical factors: fluctuations in diameter, temperature, pressure, molecular and dust opacity strengths, etc. Apparently, complex phenomena make up their entire unstable atmosphere: shock waves, strong coupling of convection and pulsation, and certainly motions of clouds of matter from the photosphere to the circumstellar layers (if any) and infalling of this matter at other phases of the variation, perturbation in the layers due to companion tidal effect.

The *visual* light curves tend to be regular, with large amplitudes for the Miras; they tend to be less regular and/or erratic, with much smaller amplitudes for the semiregular and irregular variables. Among all these variables, we

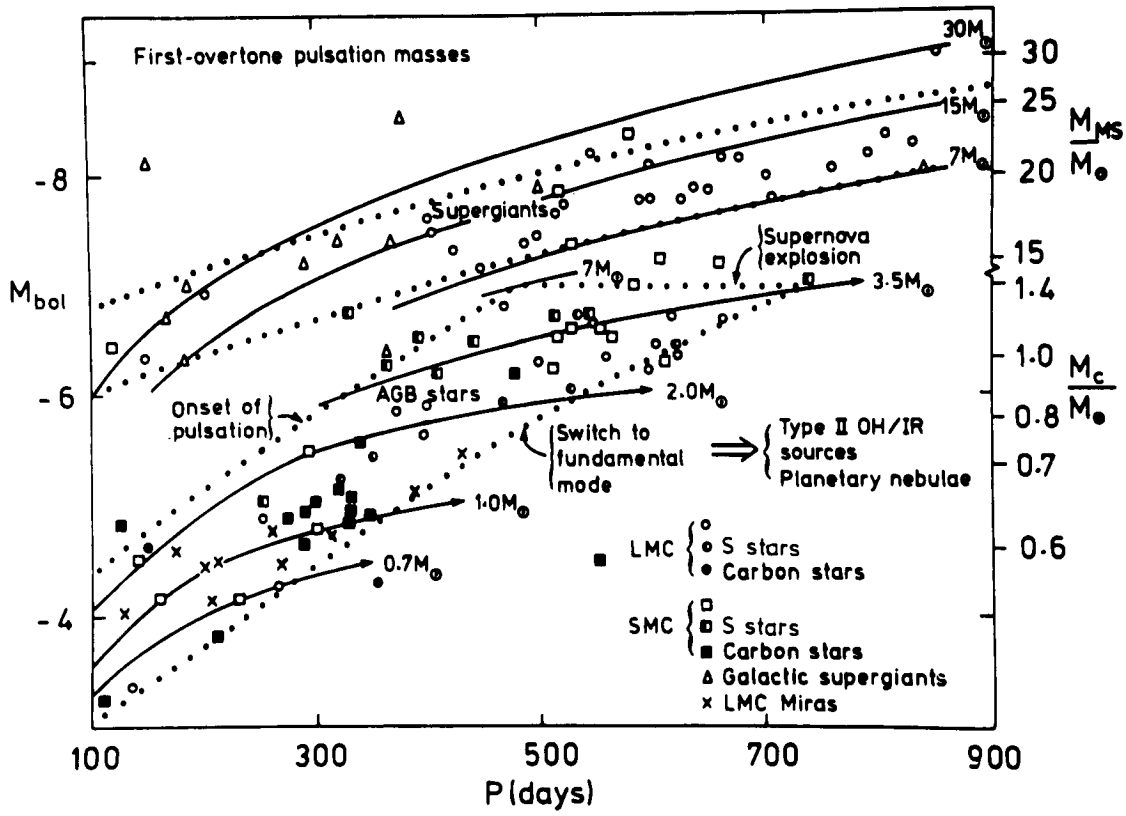


Figure 1-3. Bolometric luminosity (M_{bol}) plotted against period (P) for long-period variables (LPV's) in the Magellanic Clouds (SMC and LMC). Also included are some galactic supergiant variables. Stars labeled "LMC Miras" are LPV's studied by Glass and Feast (1982). Dotted lines delineate the regions occupied by supergiants and AGB stars. Continuous lines are lines of constant mass assuming that LPV's are first-overtone pulsators. Also indicated are theoretical values of the core masses (M_c) of AGB stars and the initial main-sequence masses (M_{MS}) of supergiants. See text for comments (from Wood et al., 1983).

find stars with all different values of the ratio C/O (<1 for M-type stars, ≤ 1 for S-type stars, and >1 for C stars). They may be either giants or supergiants (Kukarkin et al., 1958). All these stars can also be identified as pulsating or eruptive variable stars (Strohmeier, 1972).

In *the pulsating group*, we recognize three types—Miras, semiregulars (SR), and irregulars (L)—as follows:

1. The Mira Ceti-type stars are long-period stars with visible amplitude variation over 2 magnitudes (and for some cases up to 5 and larger), with well-expressed periodicity, good regularity, and periods from 2 months to 1 year or more. (They belong to the AGB long-period variables (LPV); see Figure 1-3.) Around the maximum, characteristic emission spectra are observed, mainly the hydrogen Balmer series. They occupy the tip of the AGB. Representative stars are o Cet, R Lep, χ Cyg, etc.
2. The semiregular variables are further classified SRa, SRb, and SRc. Their visible amplitude variations are smaller than those of the Miras. The SRa light curves are not regular and have strong variations from one period to another. Different durations of cycles with irregularities and some constancy of brightness are observed in the SRb light curves. The SRa and SRb variables are giants; the SRc's are supergiants with SRb behavior. Some of the giants are

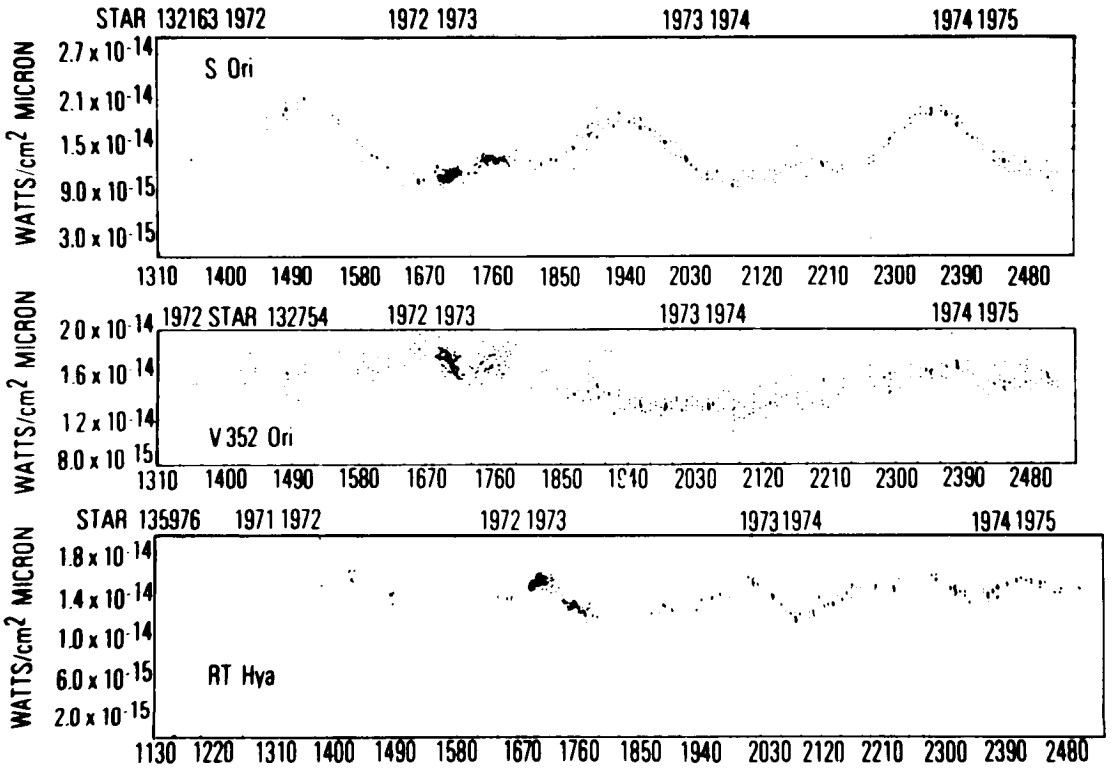


Figure 1-4. 2.7-μm light curves: Top: S Ori is a Mira-type variable with a period of 419 days; bottom: RT Hya is an SRa-type variable; center: the irregular (Lb) variable V352 Ori shows a small flux variation on a time of 2 years (from Maran et al., 1977).

probably on the AGB, others on the first ascent of the red-giant branch (RGB). Typical representatives are WZ Cas, ϱ Per, S Per, etc.

3. The true irregular variables are called Lb or Lc. The former are giants; among them, β Peg, CO Cyg, and V Aql are the typical representatives. The latter are supergiants; the best known is TZ Cas.

Figure 1-4 shows the three characteristic curves of Mira, SRa, and Lb stars (Maran et al., 1977).

R CrB is the typical representative of the RCB stars, *the eruptive group*. These stars are of spectral classes, F, G, K, and R (hot carbon stars) and have a very high luminosity, as described in the previous section. They are characterized by slow nonperiodic drops in brightness of different amplitudes (1 to 9 magnitudes) and of different duration (up to several hundred days for some). The increase in brightness is generally rapid (a few days). Besides R CrB, other representative stars are XX Cam, RY Sgr, and SU Tau. The star, ϱ Cas, is one of these stars which appear in the literature as pulsating (SRc) or eruptive (RCB) stars.

Let us remark that we do not intend to study here certain peculiar but rare types of variables, mainly among the carbon spectral-type stars such as Isb (V374 Aql, UX Cas, and DY Aur), RVa (AC Her, etc.), or the cepheids with carbon molecular bands (RU Cam, etc.). These types of variables are described by various authors (e.g., Payne-Gaposchkin, 1954a).

In the late-type star family, the carbon stars are not only different by the C/O ratio, which is greater than one, but also by the behavior of their light curves (i.e., perhaps by specific reactions of their atmospheres to mechanical energy transport). First of all, the distribution

Table 1-5
Percentage of Variability Types in M, S, and C Stars*

Spectral Type	Type of Variability(%) Mira	SR	Lb
M	46	29	25
S	58	23	19
C	20	38	42

*From Alksne and Ikaunieks (1971).

of the different types of variability is very different for the three spectral classes, M, S, and C. Table 1-5 (Alksne and Ikaunieks, 1971) shows that the number of semiregular and irregular stars increases sharply as one goes to carbon stars. This might be partially due to a selection effect, since these stars are faint and their light variations are not so easily followed as in the M stars. Half of the variable stars of M and S classes are Mira variables. For carbon stars, only 20 percent are Mira variables, 40 percent are SR, and 30 percent are Lb. The Mira and semiregular carbon stars have the largest mean periods; carbon Miras have the smallest photographic amplitude variations among all the Mira variables, whereas the irregular carbon stars have the largest ones among all the Lb variables.

The study of the cool star variability is at present based on visible and IR photometric data: Far-UV and far-IR data are too rare (see the section on *Photometric Observations*) to study the photometric variability. The present data are borrowed from a large number of papers, and consequently, they suffer from too many inhomogeneities like observations at different phases, use of different photoelectric systems (*UBV*, *DDO*, etc.), and data reduction method not always being adapted to cool stars. To achieve homogeneous data covering several periods, Bouchet (1984b) carried out a photometric analysis (from the blue to far-infrared ranges) of a sample of galactic carbon stars at ESO-La Silla during 4 years. This work is an example of a long set of data for Mira, SR, and L carbon stars made under the same observational conditions. It will be a good sample for testing the evolution and/or dynamical pulsation theories. Another extensive example concerning infrared photometry on M, S, and C stars comes from Catchpole et al. (1979).

Before describing the general characteristics of each group of variables, we focus on two important remarks:

1. The Mira variables, as well as the SRb, Lb, or HdC stars, have microvariations with a duration much smaller than the length of the period or the pseudoperiod generally known (some hours or days compared to several months or years).

2. In the HR diagram, some stages of the evolution of the variables can be followed during a human life. For example, some of these stars become apparently planetary nebulae in less than 10 years (e.g., HD 59643, HM Sge, or V1016 Cyg). (See the section *Irreversible Changes in SR and L Stars*.)

The Miras

By "Miras," we distinguish a type of light curve, not a spectral type of stars. Many papers have confused the term and sometimes speak about Miras without any definition of the spectral type of the stars; this can occasionally be confusing for a nonspecialist. Therefore, we have to be clear: we point out that the Mira variable-type stars exist among the three spectral types: M (R Aqr, R Aql, R Cae, R Cen, o Cet, R Hya, U Ori, etc.), S (R And, R Cyg, χ Cyg, etc.), and C (U Cyg, V Cyg, T Dra, R Lep, SS Vir, etc.). Moreover, the chemical equilibrium of the elements inside the atmosphere of these later stars shows that it is impossible to find OH in carbon stars. Consequently, the papers on OH masers usually refer to the spectral-type M stars. This is meaningful when looking for eventual correlations among the observed features.

The Miras are the most observed and best known among the intrinsic variable stars. The earlier curves of light were recorded during the 18th century:

> During the autumn of 1596, the shepherd David Fabricius discovered a variable star in the constellation of the Whale, a star of the 3rd magnitude. In 1603, the astronomer Bayer added this star, which was of the 4th magnitude, onto his famous atlas and labeled it with the letter *o*. In 1635, Dutch astronomers Holwarda and Fullenius likewise showed that this star is variable, and in 1638, Holwarda gave the amplitude of variation to be from the 2nd to the 10th magnitude. Hevelius observed this star during 50 consecutive days and determined its period: 331 days. At that time, this star was the sole variable known in the sky. It was therefore named "Mira Ceti" or the "magic star of the Baleen constellation" (Jacchia, 1933). In 1839, Argelander, the German astronomer who is often called the father of variable star astronomy, observed a maximum of 2.2.
>
> χ Cyg was discovered by G. Kirch in 1681, R Hya by G.P. Maraldi in 1704, and R Leo by Koch in 1782. In the following century, Baxendell discovered, among many stars, S Aql (1863) and U Boo (1880); Pogson discovered R Cyg in 1852 and R Cas, R UMa, and S UMa in the following year. R Car was discovered at Cordoba in 1871.
>
> Let us quickly describe the famous work of Padre Angelo Secchi. In 1868, he observed nearly 100 red stars with the 9-inch Merz refractor of the Collegio Romano and a small direct-vision spectroscope. Among them, he included 15 long-period variables from Schjellerup's catalog (1866). The first slit spectrogram of LPV stars could indeed be this of *o* Cet taken by J. Wilsing with the Potsdam refractor in February 1896. Vogel (1896) remarked on the great intensity of the bright hydrogen lines and the absence of Hϵ. In 1897, the Reverend Walter Sidgreaves (1897) pointed out the rapid variation of *o* Cet during a week, "but a marked change in the relative intensities of the yellow-green and the blue radiation appears to have taken place during the cloudy week between December 2 and December 11." He confirmed the absence of Hϵ noted by Vogel the previous year: "Of the hydrogen lines Hϵ is still absent, lost, or much weakened in the calcium absorption." The notion of stellar envelope is already contained here, 100 years ago....

Nearly all photoelectric V magnitudes of *o* Cet and T Cas at bright phases lie above the curves given by the American Association of Variable Star Observers (AAVSO) and may indicate a systematic difference between the AAVSO and the V magnitude (Lockwood and Wing, 1971). Stanton (1983) gives an experimental relation between the visual magnitude (m_v) and the photometric measurements V and $B-V$.

The Mira light variations with phase are sometimes very large in the visible. For example, the Mira, χ Cyg (spectral type S), has a visual amplitude variation that is about 9 magnitudes (4000 times brighter at maximum light than at minimum). Consequently, UV and visual spectrograms can hardly be obtained, especially near the light minimum of the Mira stars (Maehara, 1971). The Mira stars were analyzed mainly by the Japanese group (Maehara, 1968; Yamashita and Maehara, 1977, 1978; Yamashita et al., 1978; and others).

Most of the Mira changes are cyclic, with a period equal to that of the visual light curve. Some obvious inconsistencies appear in the observational data, as well as phase lags between light curves in different colors, which are caused by the actions of the cyclical temperature variations on the various layers of their very extended atmospheres. Joshi et al. (1980) give the evolution of the effective temperature during 12 days for *o* Cet: on October 6, 1979, Mira was an M5.5 III star with 2470 K, and on October 18, 1979, it reached M4.5 III with 2760 K. Because the period of individual light cycles sometimes differs from the star's mean period by several percent, the observable properties are

not repeated exactly from cycle-to-cycle (Barnes, 1973; Wing, 1980).

Fluxes of some M Miras show a significant deviation from a stellar blackbody beyond 8 μm due to the presence of a cold thin dust shell (10-μm excess radiation), whereas some have a great excess of infrared (see M. Querci, this volume) due to the presence of a thick circumstellar dust envelope (Epchtein et al., 1980). Among the M Miras with the largest infrared excess at 10 μm, we know: IRC +10011, IRC +50137, and IRC -10529. Some of them have masers; the OH satellite line at 1612 MHz is seen in many sources, representatives of which are IRC +10011, WX Sgr, R Aql, NML Tau, IRC +50137, VY CMa, and NML Cyg. U Her and U Ori are known to be 1665-MHz emitters. The M star, RV Hya, has no OH microwave emission (Zuckerman, 1980). For the first time in a carbon-star envelope, Henkel et al. (1983) found a maser line in IRC + 10216. Like OH, the observed SiS maser has two horn features.

Some changes from OH type I to OH type II Miras were observed during recent years, such as on R Leo, for which Lesqueren (1983) reports an unusual intensity variation: the flux at 1667 MHz has steadily decreased from 1.5E-22 W/m^2, reached during the 1980 cycle, to a smaller value 0.1E-22 W/m^2 at the maximum of the 1982 cycle. Another striking example is U Ori. Pataki and Kolena (1974a, 1974b) found a bright 1612-MHz flash up to 22 Jy and a disappearance of the 1667-MHz line below the 0.4-Jy detection level on May 28, 1974 (the 1612-MHz line is characteristic of the OH type II maser star), whereas before 1974, particularly on July 28 and November 26, 1973, only the main lines (at 1667 and 1665 MHz, characteristic lines of OH type I maser stars) are present in emission. Moreover, on May 28, 1974, no radical change is registered in the output of the 1665-MHz main line. Coincidentally, the 43.122-GHz SiO maser line was not detected on June 2, 1974, by Snyder and Buhl (1975), but it was detected exactly two U Ori periods later by Balister et al. (1977) with an energy level of 89 Jy. On the basis of these observations, Cimerman (1979) develops a monitoring that shows no variation on the 1667-MHz main line until May 1977. On January 25, 1978, this line appears with 0.8 Jy and -42 km/s. The 1665-MHz line was not observed as often as the 1612-MHz line because of its weakness. On March 1, 1978, the 1612-MHz line has a flux peak of 2.2 Jy, which is about one-half of that observed by Pataki and Kolena (1974b) in May 1974. On July 15, 1975, the spectrum of 1612 MHz consists of a sharp feature at -42 km/s and a group of blended lines peaking at -46 km/s. This large blend evolves to a sharp feature at -47 km/s, and the -42-km/s peak remains constant (spectrum of January 25, 1978). Besides the variation of the line profile, a variation on the intensity of the 1612-MHz line occurs: the average level of 45.E-22 W/m^2 detected by Pataki and Kolena (1974a, 1974b) remains constant until the beginning of 1976, when it drops to one-half its previous level in 100 days and continues to decline (see correlations with visible variations below). This decline is confirmed by Jewell et al. (1979; see their Figure 15). The main-line emission has exhibited highly circular polarized components and large semiperiodic variations (Fix, 1979). Cimerman (1979) attributes the origin of these events to the central star; this assumption is corroborated by the coincidence in velocity between one of the 1612-MHz lines and the optical emission lines. All these lines are interpreted as the outcome of a shock or magnetohydrodynamic (MHD) wave originating under the photosphere of U Ori (Merrill, 1960; Wallerstein, 1973). The model of Elitzur et al. (1976), which explains the 1612-MHz maser in sources with a thick shell like IRC +10011, seems to be inadequate for U Ori, where the dust shell is very thin. In this case, another pumping process for the 1612-MHz line may exist in addition to the one that uses the dust grains (Cimerman, 1979). A mapping of the U Ori neighborhood was made by the VLBI on the principal and satellite frequencies. Unfortunately, the variations on 1665-MHz lines (Fix et al., 1980) were made 3 years after the 1612-MHz ones (Reid et al., 1977), and comparisons are therefore hazardous.

Phase lag. Since their discovery, the Miras have attracted generations of astronomers until the present day; the pioneers are Herschel, Secchi, Pettit and Nicholson, Hetzler, Hoffleit, Campbell, Stern, Joy, Merrill, and others. Occasionally, astronomers of more recent times have made the same discoveries as those of their forerunners for want of looking at their old publications. The study of the phase delay between the visible, photographic, and near-infrared light curves illustrates this fact to perfection.

Traditionally, the epoch of zero phase refers to the visual maximum. The phase lag (or shift or delay) of the maximum of an infrared or radio curve is the epoch of this maximum, minus the epoch of the visible maximum coming immediately before it. The first correlations between the variations at different wavelengths were made by Pettit and Nicholson (1933). As an example, they have shown that *o* Cet, R LMi, R Leo, R Hya, R Aql, and χ Cyg have a real maximum of energy shifted by a phase lag of about 0.14 after the visual maximum. Hetzler (1936) has monitored 30 Mira variables with photographic plates at an effective wavelength of 8500 Å ($\Delta\lambda$ = 100 Å). His light curves have a much smaller amplitude than the corresponding visual light curves because of the longer wavelength effect and the decreased blanketing by TiO bands. Hetzler showed that the maxima of the infrared and the visual curves are reached at about the same time, but the infrared maximum persists longer. R Lyn and R Cam are two characteristic examples of simultaneity. R Hya is an exception; the infrared maximum precedes the visual one. In this case, the IR phase lag is negative. This phenomenon is to be confirmed by careful monitoring of many Mira-type stars at several wavelengths. Generally speaking, the infrared light maximum typically lags the visual by 0.1 to 0.2 period, agreeing with all the previous quoted observations and with those of Mendoza (1967), Lockwood and Wing (1971), and Frogel (1971).

An analysis of the spectrum of the spectral M class Miras allowed the astronomers of the late 1960's to distinguish the behavior of the continuum from that of the absorption lines. With the I104 filter, Wing (1967a) showed that the I(1.04-μm) magnitude of χ Cyg was brighter at phase +49 days than at 0 day by 0.1 magnitude; this is very similar to the phase lag noted in radiometric curves obtained with the vacuum thermocouple by Pettit and Nicholson (1933). He explains this phase lag by a two-layer model. The infrared magnitude measured at a continuum point refers to the photosphere, while the heavily blanketed visual magnitudes presumably refer to the upper layers of the atmosphere. He concluded that the temperature variations of the two regions appear to be out of phase. At present, such an explanation must be viewed in the context of shock-wave interpretation (see M. Querci, this volume).

Fillit et al. (1977) have analyzed the time variation of some type I OH Mira sources and the correlation with their visual magnitude. More than 2-year monitoring of seven OH/IR stars was done on six Miras (R LMi, R Cas, Y Cas, RS Vir, U Her, and S CrB) and on an SRc variable (S Per). Even allowing for experimental uncertainties, a systematic phase lag of about 20 days between OH lines and visible light is observed on S CrB (Figure 1-5). These authors implicitly assume that the shape of the radio and visible curves are the same. This assumption must be proved.

The phase delay of the [V = 1, J = 2–1] SiO curve on R Leo, is greater than that of the 2.7-μm curve, whereas the 2.7-μm and SiO curves have the same lag as on *o* Cet. The SiO masers observed by Spencer et al. (1981) are interpreted as collisional pumping by Bujarrabal and Nguyen-Q-Rieu (1981). This requires high temperatures and densities in the SiO layers ($T_K \sim 2000$ K, $n_H \sim 10^{10}$ cm^{-3}), and consequently these layers are close to the star ($R \sim 1.5\, R_*$). Hinkle et al. (1976) indicate that the SiO strength in Miras varies markedly with phase (see also Nguyen-Q-Rieu, this volume).

The behavior of another maser line, H_2O at 1.35 cm, and of lines at 2.2 μm and in the visible were compared (Schwartz et al., 1974) for some Mira stars (U Her, S CrB, U Ori, R Aql, and

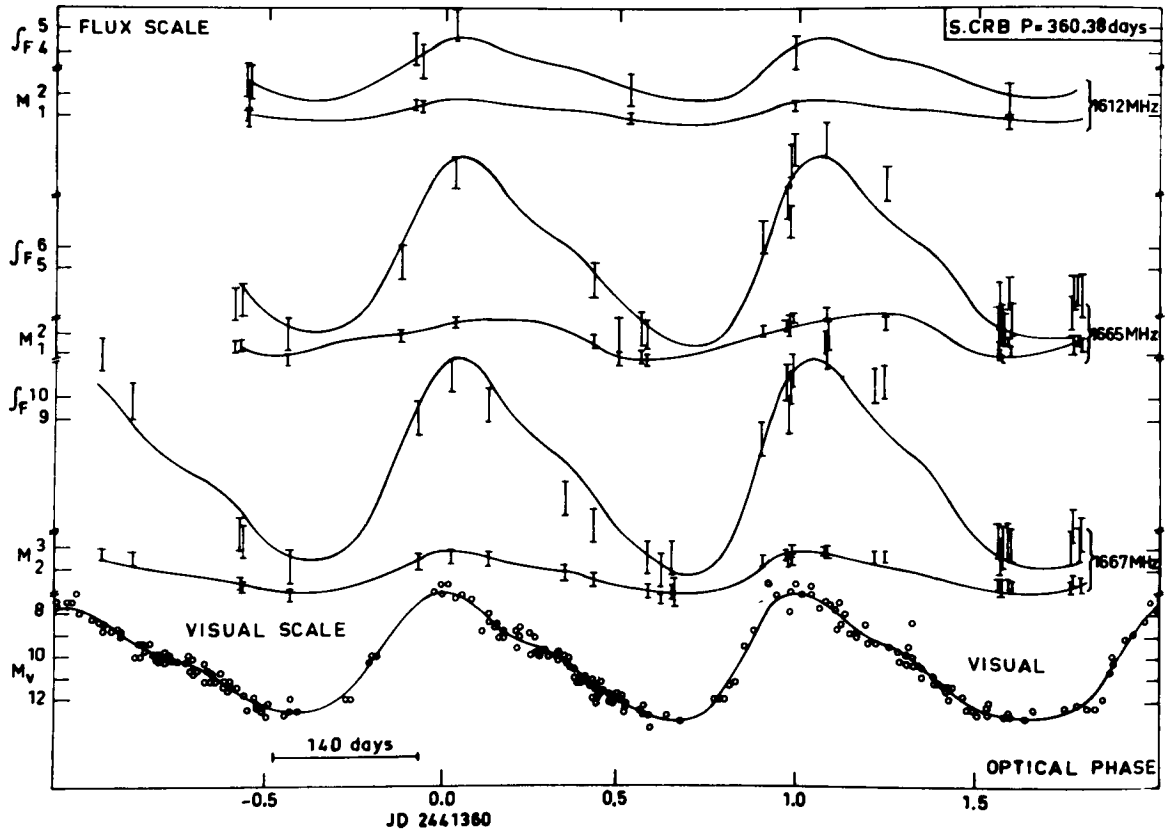


Figure 1-5. The flux and the magnitude for each of the OH maser lines: 1612 MHz, 1665 MHz, and 1667 MHz lines of S CrB were fitted by least squares using the visual light curve (from Fillit et al., 1977).

W Hya; see their Figures 1 through 5). The mean curves show the phase lags of radio and infrared curves relative to visual ones. These lags are characteristic on U Her and S CrB. Some stars do not have the usual phase lags (e.g., the H_2O maser curve of U Ori has a large lag compared to the infrared curve at 2.2 μm). Although the IR curve of R Aql has a phase lag of 0.2 compared to the visual curve, the 1.35-cm curve has the same phase as the visual one. W Hya shows an analogous behavior. This nonconventional behavior requires comment. Is it real? Yes, if the observed values at the different wavelengths are obtained simultaneously; no, if there is a time lag between them: in this case, we find the presence of large amplitude variations during small intervals of time (a small percentage of the period). If the quoted values are from different cycles, another interpretation is possible: the behavior of the maser lines with the phase is not exactly the same in all the cycles. This was already demonstrated by Wing (1967b). Cox and Parker (1979) demonstrate that the H_2O was often not stable for more than a few cycles of stellar brightening. (A more comprehensive description of the nature of the different maser pumps is made by Nguyen-Q-Rieu in this volume.)

From 1972 onward, observations of some M Miras were obtained by using the satellites of the U.S. Air Force (Maran et al., 1977). Because the spectral interval on the water-vapor bands around 2.7 μm was chosen, correlations with the H_2O maser should be possible without the perturbations introduced by the variable telluric water vapor. Figure 1-6 shows the 2.7-μm infrared and the visual curves of two Miras, S CMi and *o* Cet.

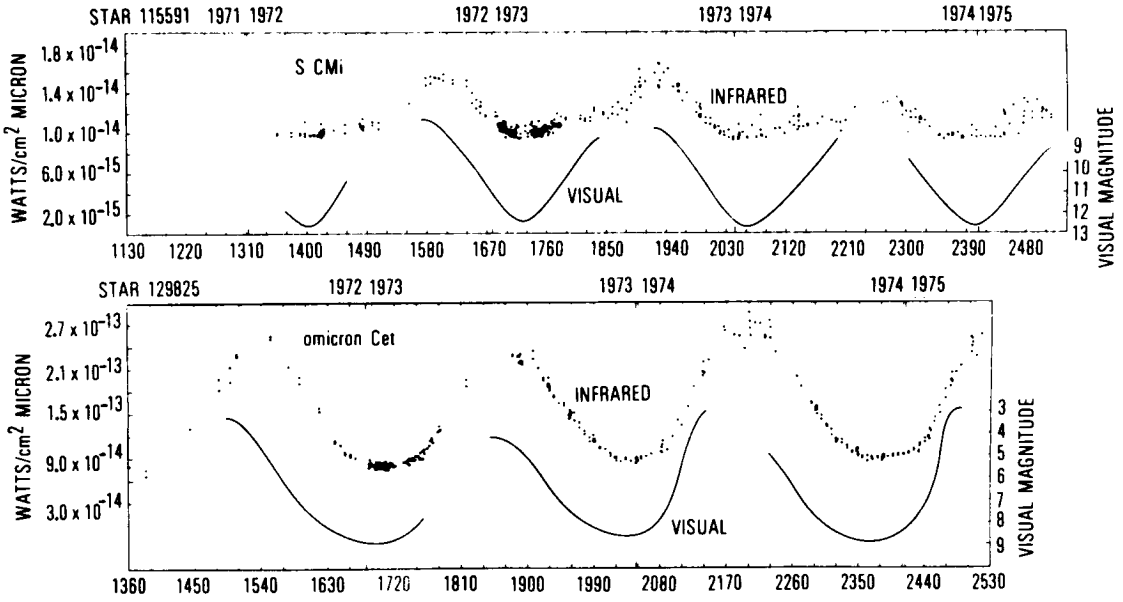


Figure 1-6. 2.7-μ infrared curve (top) and AAVSO visual curve (bottom) for two Mira variables, S CMi and o Cet. The left ordinates are the infrared fluxes and the right ones are for the visual magnitude (from Maran et al., 1977).

Amplitude of Light Variations at Different Wavelengths. The S Mira, χ Cyg, is a very good example for this purpose. Maehara (1971) observed a visual amplitude variation of about 9 magnitudes, whereas the photographic infrared variation was only about 2 magnitudes. Although similar data for the ultraviolet region is incomplete, some information on the variability of the energy distribution of χ Cyg from 2500 to 3350 Å at two different phases is shown on Figure 1-7. The flux longward of about 3050 Å becomes considerably fainter at phase 0.18 than at the light maximum (phase 0.04). The total energy emitted in the range from 2000 to 3240 Å is 4.5 E-11 erg/cm^2 s at phase 0.04 and is lower by a factor of 3.53 at phase 0.18. The stellar continuum is even more depressed at phase 0.22 on a high-resolution spectrum. This remarkable change is mainly due to a change in the temperature of the region of continuum-formation (Cassatella et al., 1980).

Lockwood and Wing (1971) show examples of some M Miras for which the curves of the filters, V, 78, 87, and 88, are depressed by TiO, and the filter-105 curve by VO. These curves are strongly correlated with the differential temperature effect, the local continuum, and the variation of diameter of the forming layers, so that these curves are the best reflection of the physical parameter variations of the atmosphere along the period. Figure 1-8 describes the curves of two Miras, *o* Cet and T Cas, in which the minima appear to occur at the same phase. The behavior of R Aql is different from that of *o* Cet and T Cas because the visual minima of these two stars have a phase lag relative to the infrared minima. This is shown on the 2.7-μm curve obtained with the U.S. Air Force satellite (Maran et al., 1977, 1980). When one considers the infrared spectral range, one sees that the amplitudes of variation $[F_{max}/F_{min}]$ decrease with increasing wavelengths from 1.2 to 3.5 μm and are roughly constant between 3.5 and 10 μm. The amplitudes of the 1612-MHz OH masers which are linked with the IR fluxes are significantly less than, or at most equal to, the infrared amplitudes (Harvey et al., 1974). Herman (1983) followed OH/IR Miras during a period

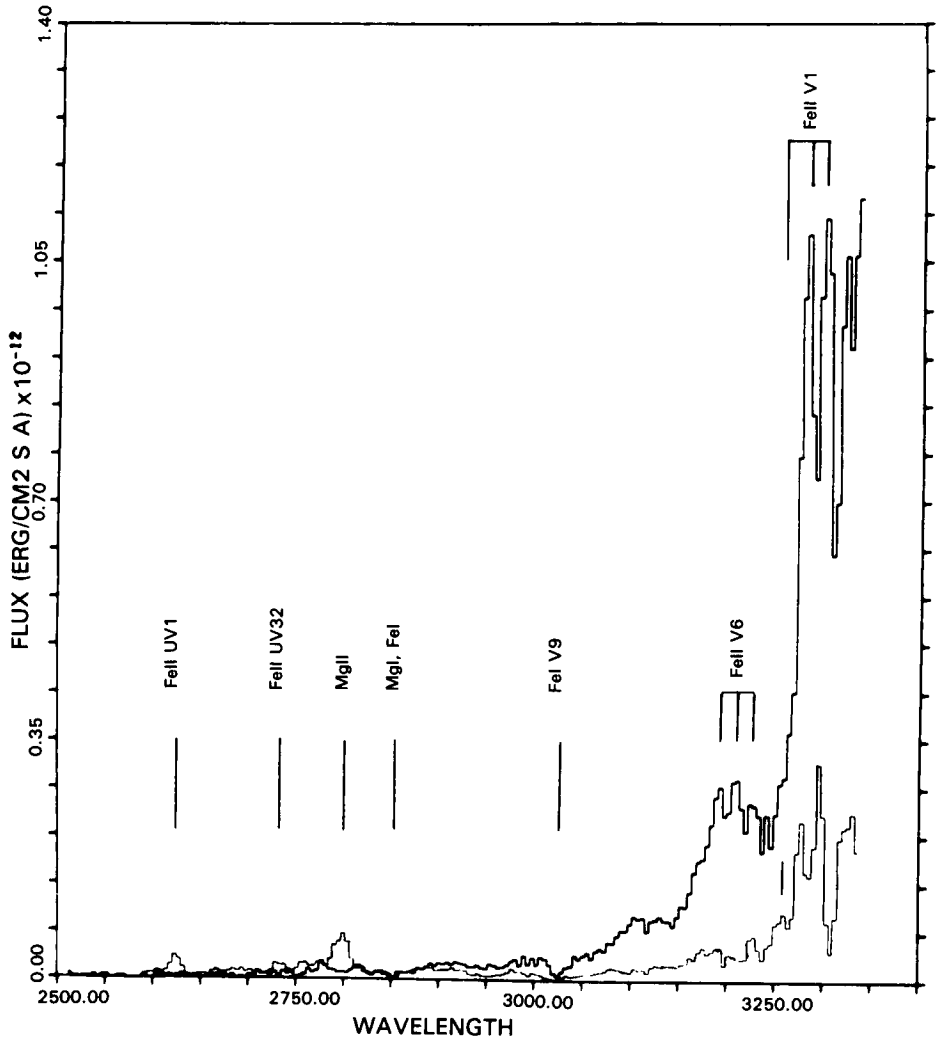


Figure 1-7. Ultraviolet energy distribution of the S Mira variable χ Cyg from 2500 to 3350 Å at phases 0.04 (thick line) and 0.18 (thin line). The total energy flux in this spectral region is less at the latter phase by a factor 3.53 (see text) (from Cassatella et al., 1980).

of 3 to 5 years with the 25-m Dwingeloo radiotelescope in order to study their variability.

After considering the amplitude variations in visible, infrared, radio, and ultraviolet wavelengths, we now follow the amplitude variation at one wavelength and point out the characteristic behavior of the Miras. Maran et al. (1980) show five well-observed minima of S CMi (with the U.S. Air Force satellite), where we note the agreement of flux density level at all five minima. The flux of S CMi is remarkably representative of all minima. The authors emphasize that the minimum is the "normal state of a long-variable star." However, there has been a good deal of controversy about the reproduction of Mira minima. Glasby (1968) said that *o* Cet has variable minima: "on occasion [the minimum] has only been as faint as magnitude 8.0 while at other times it has sunk as low as 10.2 magnitudes." Campbell and Payne (1930) show variation of magnitude of the minima of S Pav. On the other hand, we sometimes observe a strong contrast between consecutive

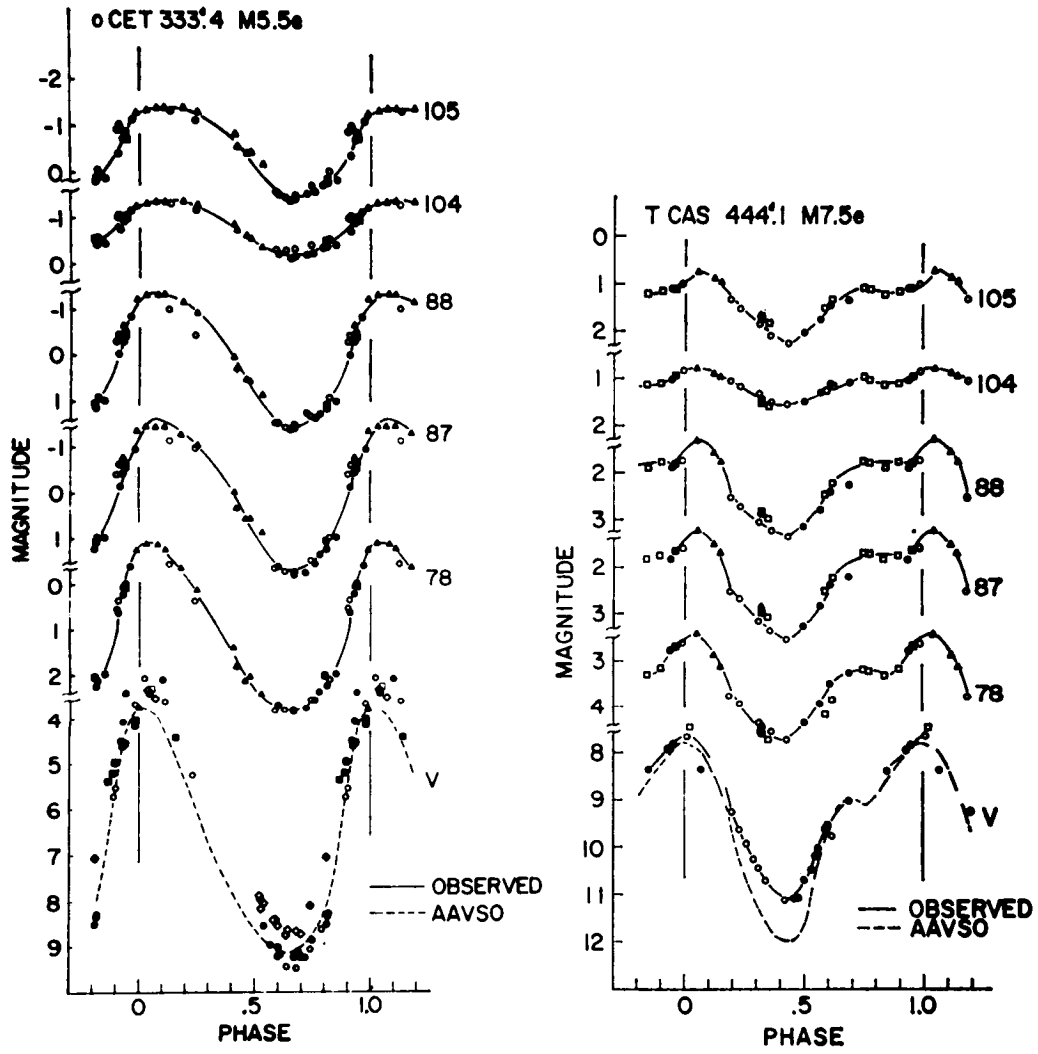


Figure 1-8. Light curves of o Cet (Mira) at left and T Cas at right, in V and at five infrared wavelengths. The wavelength designations to the right of the curves are defined in Lockwood and Wing's (1971) Table 1. The observed cycles of the stars are numbered serially; the IR observations start with cycle 1 in 1965 and are coded as follows: -1 = ◆, 0 = ◇, 1 = ●, 2 = O, 3 = ■, 4 = □, 5 = ▲, 6 = △, 7 = ▼, 8 = ▽, 9 = ◆, and 10 = ◇ (from Lockwood and Wing, 1971).

maxima of Mira stars, such as the two maxima of R Aql in 1972–1973 and those of S CMi in 1973 and 1974 (Maran et al., 1977). In the late 18th century, the irregularity of the maximum light was already noticed by William Hershel on *o* Cet, where it is extremely well pronounced in the visual curve. In 1779, it attained the first magnitude, being equal to Aldebaran in brightness. For many Miras, the cycle-to-cycle differences are not erratic; bright and faint maxima tend to alternate, and bright maxima tend to occur before the predicted date (Harrington, 1965; Keenan, 1966). This could be correlated with the intensity of the pulse (i.e., the size of the energy reservoirs in the cycle). RS Cen, R Cet, V Cen, T Gru, R Vir, RT Cen, and SS Her are Miras with alternative bright and faint maxima.

Different Profiles of Light Curves. The AAVSO report 38 (1983) gives many visual light

curves of Mira variables. We warmly congratulate all the AAVSO members for their arduous and comprehensive work; we are convinced of its usefulness to professional astronomers.

The light curves of carbon stars are more gradual and more symmetrical than those of M class stars (Figure 37 in Alksne and Ikaunieks, 1971). Campbell (1955) shows that the S star light curves are very similar to those of M stars. As a rule in M and S spectral types, the rise to maximum is somewhat more rapid than the decline to minimum. In general, D ~ 0.44, with D = (epoch of maximum–epoch of minimum)/period. However, some exceptions exist, such as: o Cet (D = 0.62) and R Cyg (D = 0.7). (Because D is always larger than zero, it represents the fraction of the period needed to go from the minimum to the maximum.)

All the Mira light curves do not have the same shape (Figure 1-9). They can present:

1. A rapid rise to the maximum and a slow decline to the minimum: the majority of the Mira light curves have this shape, with D ~ 0.45 (R Gem, U Her, and U Ori).

2. A slow and long rise to the maximum with a rapid decline with D ~ 0.7 (S CMi and U CMi).

3. A narrow and sharp maximum with a large minimum (R Aqr, R Cas, Z Cas, U Cet, T Col, R Crv, R For, R Pav, T Sgr, RU Sgr, and R UMa).

4. A large and round maximum and a narrow and deep minimum (Z Cap, S Car, RT Cen, X Cet, T Hor, and S UMa). These stars have a period P $\leqslant$ 225 days (Celis, 1977) so that the magnitude varies rapidly around the minimum.

5. A sawtooth shape with sharp maxima and minima with D ~ 0.5 (RT Cyg and V Oph). The variations between their extremes are rectilinear segments. These stars have periods shorter than 150 days (SS Her, W Pup, and R Vir; Celis, 1977).

6. A smoothed sinusoidal shape (SS Vir, R Dra, W Cas, and U UMi).

7. Two maxima of the same intensity and two minima with different depths per cycle (R Cen and R Nor, both discovered by Gould at Cordoba in 1871). The main maximum is followed by the main minimum. This curious light curve was reproduced theoretically by Wood (1979) in an attempt to produce a larger post-shock velocity maximum in an isothermal pulsation model. It appears that this situation is apparently stable (over 75 cycles) where shocks with different velocities alternate. This visual curve also shows variation from cycle to cycle in the rate of rise and fall, in the amplitude and in the height of the maxima, and in the depth of the minima (Marino et al., 1979). CR Mus shows a scatter of approximately one magnitude in the level of the V light curve; the shape of this maximum varies extensively from cycle to cycle.

8. A hump on the rising branch, around the phase 0.7, so that the minimum is moved at earlier phase (R Lep, T Tuc, and S Vol). Such a hump is also observed by Hetzler (1936) on R Tri, R Vir, R Hya, T Cep, and χ Cyg. For R Tri (Figure 1-10a) and R Vir (Figure 1-10b), the shoulder (or hump) is much more important in the photographic infrared (λ = 8500 Å and $\Delta\lambda$ = 100 Å) than in the visible, whereas for T Cep (Figure 1-10c), the shoulder rises in proportion to the brightness variation in the 8500 Å region and in the visible. To explain the 8500 Å behavior of R Tri and R Vir, Wing (1967b) suggests that the effective wavelength of Hetzler's photographic infrared agrees well with his curves 87 and 88, which are likewise affected by moderately strong TiO absorption. For these stars, it therefore seems that the visible region is less affected by the TiO opacity. The humps on the rising branch of the light curve are generally centered at ϕ = 0.7

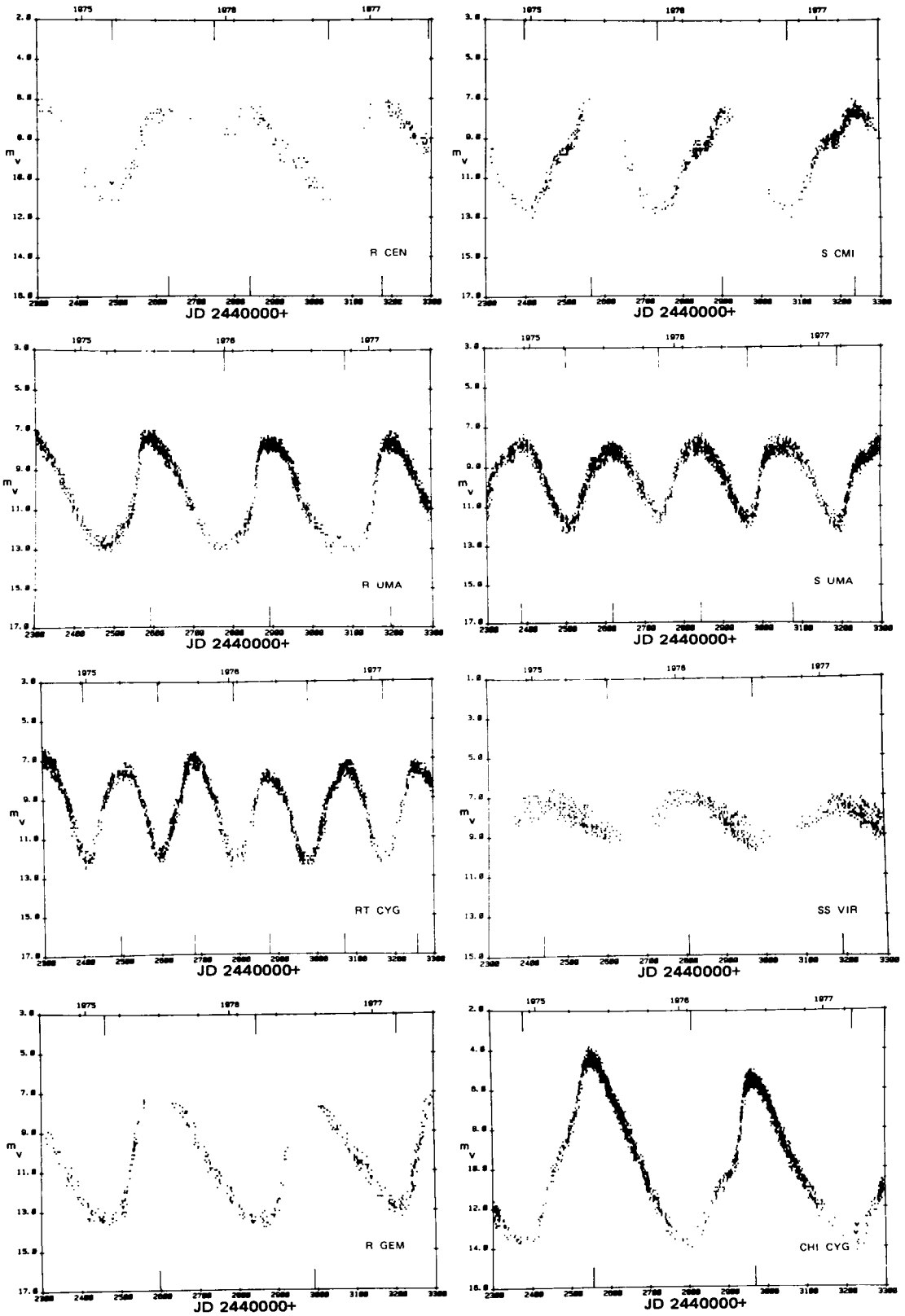


Figure 1-9. Various shapes in the Mira light curves (from AAVSO, 1983).

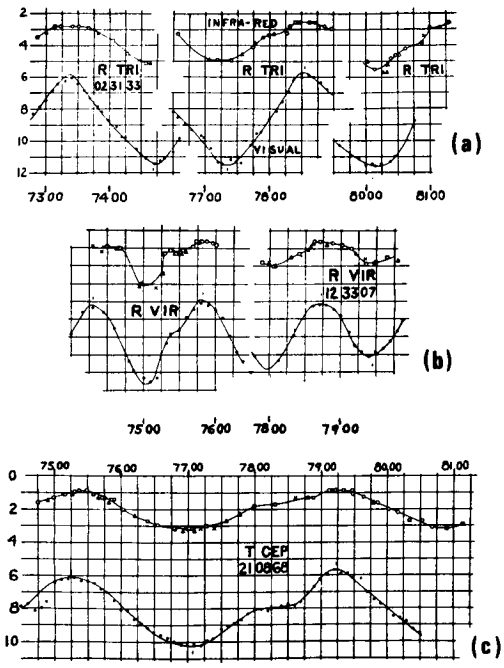


Figure 1-10. Mira light curves illustrating humps on the rising branch (from Hetzler, 1936).

(e.g., T Cas in Figure 1-8). The majority of the stars studied by Lockwood and Wing (1971) show evidence of humps in at least a few cycles. In some of these stars, the humps have reoccurred (R Cam and T Cep), but in some stars, the humps are spread out during the phase interval 0.6 to 0.8. Glasby (1968) indicates the presence of humps in the descending branch of the light curves. Vernon-Robinson (1929) observed secondary oscillation on the descending branch of XY Cas. The hump phenomenon is present in some Miras and not in others, and it comes and goes in some of them. The visual curve of χ Cyg is a good example of a hump on the ascending branch (Figure 1-9). T Cas has a hump on the ascending branch of the light curve; its maxima and minima and the size of the hump vary from one cycle to the following one (Leung, 1971). The humps are considered as a rapid drop of the radius of the star (Lockwood and Wing, 1971).

9. Inflection points in the increasing and decreasing parts of the light curves (R Cha, T Hya, R Ind, V Mon, T Nor, and RT Sgr); their periods range from 200 to 350 days (Celis, 1977).

Nearly all the short-period stars (less than 150 days) do not have very constant elements p and q with respect to the length of a given period P (Celis, 1977). As an example, T Gru (P = 136.6 days, M1 Iae-M2 Ibe) has P periods between 121 and 138 days, Q periods from 124 to 145 days, and partial period p from 54 to 83 days. The amplitudes go from 1.80 to 3.05, and the light minima differ up to 1.5 mag.

All these light curves might reflect the interaction of the opacities and density variations of the different atmospheric layers and the propagation of shock waves (see M. Querci, this volume).

Are light curves at other wavelengths similar to the visual ones? The two stars in Figure 1-8 have V light variations of a strikingly different nature, which is preserved at the different observed wavelengths. The hump on the rising branch of the AAVSO curve for T Cas also appears on the infrared curves, including the continuum curve, I104.

Variation in Colors During Mira Light Cycles. All the observed Miras (for M, S, and C spectral types) show variations in color during their cycles of light, which are first indicated by the analysis of color indices obtained from visual observations (generally from AAVSO or Association Française des Observateurs d'Etoiles Variables (AFOEV)) and broadband photometry U, B, V, I, K, etc. Narrowband photometry with adapted filters for characteristic atomic (He I, Hα, and Na I) and molecular (TiO, ZrO, VO, etc.) features is proposed, at first by Wing (1967b). Spectrophotometry is also a good technique for investigating the variation in colors during the Mira phases. We will not elaborate here on the variations of line intensity or profile; they are dealt with by M. Querci, this volume.

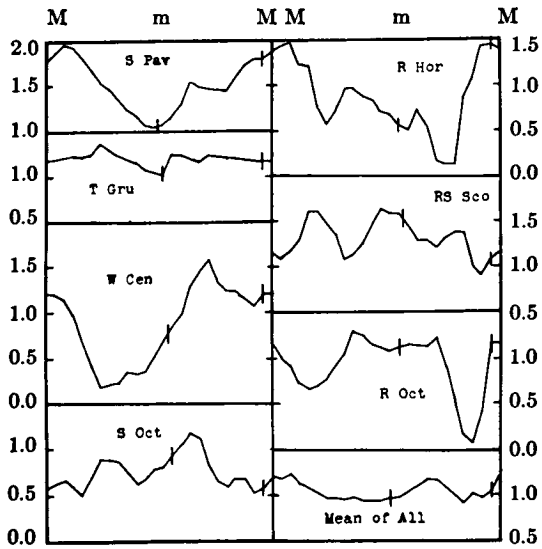


Figure 1-11. Mean color curves of seven Mira variables: S Pav, R Hor, T Gru, RS Sco, W Cen, R Oct, and S Oct. Ordinates and abscissas are color index and phase, respectively, all periods being reduced to the same horizontal scale. Maxima and minima are marked with short vertical lines and labeled "M" and "m" (from Campbell and Payne, 1930).

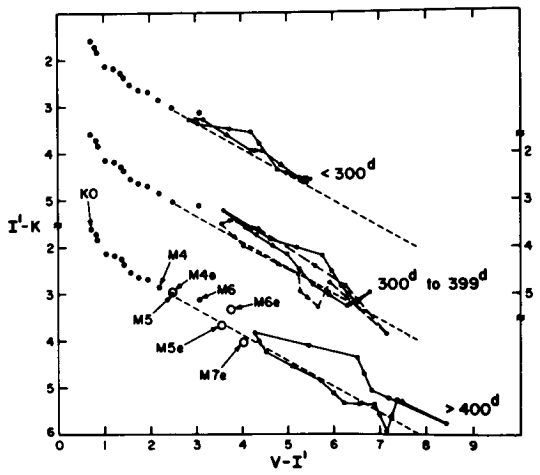


Figure 1-12. Color-color curves for luminosity class III nonvariable stars and Mira stars of spectral type M and S. Ordinates, in (I'-K) magnitudes; abscissas, in (V-I') magnitudes. Heavy dots (plotted three times on shifted scales of ordinates) = nonvariable stars from K0 to M6; smaller dots = loops described during the cycle of variation for stars of average period 239, 350, and 456 days, class Me; broken lines = Se stars, mean period 380 days; dotted lines extend the relation for nonvariable stars through points corresponding to the fall from maximum. On the lowest curve, points corresponding to K0 III, M4 III, M5 III, and M6 III are identified. Circles show the relation between maximal colors for Mira stars of classes M4e, M6e, and M7e (from Payne-Gaposchkin, 1975).

As early as 1930, Cannon (1930) showed that the color index (difference between the photographic and photometric magnitudes) is at its greatest about 40 days before maximum and at its minimum for 100 to 150 days after maximum. Campbell and Payne (1930) obtained photographic light curves and used the AAVSO visual ones to give the color indices from observations assembled into 10-day means; these are obtained by subtracting the visual magnitude from the photographic one (Figure 1-11). Two opposite effects contribute to the photographic minus visual index: (1) the great strengthening of TiO absorption, which cuts down the red part of the spectrum and diminishes the visual brightness more than it reduces the photographic light; and (2) during the fall, the decrease of the temperature of the photographic and visual forming layers which should strengthen the red end of the spectrum.

During the Mira light variations, the $B-V$ values vary and the spectral classes usually change, the earliest spectral class appearing near the visual maximum light.

It is interesting to compare the color indices of Miras during their cycles with the indices of the nonvariable stars of the same spectral type and luminosity class. Payne-Gaposchkin (1975; Figure 1-12) shows color/color curves for Mira stars and nonvariable stars of luminosity class III. During the decline from the visual maximum and a little later, the representative points of the Miras follow the relation shown by the nonvariable stars of the same spectral type. The I′ filter used in Figure 1-12 is related to the Johnson system by (I-K) = 0.745(I′-K) - 0.13. Two remarks will be made about this figure: the length and the maximum width of the loop

(I′–K), and consequently, its area versus (V–I′) seem to be correlated with the period/amplitude relation of the M Mira stars; secondly, during the maximum phase, the stars are bluer than during the minimum. This was also obtained by Mendoza (1967), using his multicolor photometry. The analyzed set of stars indicates that, with the light variation in V, the B–V index and the other color indices change. Typically, as the star becomes fainter in V (it is running to the minimum), it becomes redder; however, the C star, LW Cyg, is an exception.

Spinrad and Wing (1969) demonstrate that the variation of the molecular (TiO + VO) index around 1 μm is correlated to the observed temperature (Figure 1-13). On the other hand, the nonvariables and small amplitude variables are represented by their mean line running from near the origin to the box labeled RX Boo in Figure 1-13. (This box contains all five scans of the semiregular variable, RX Boo.) Each Mira moves on the color index/temperature

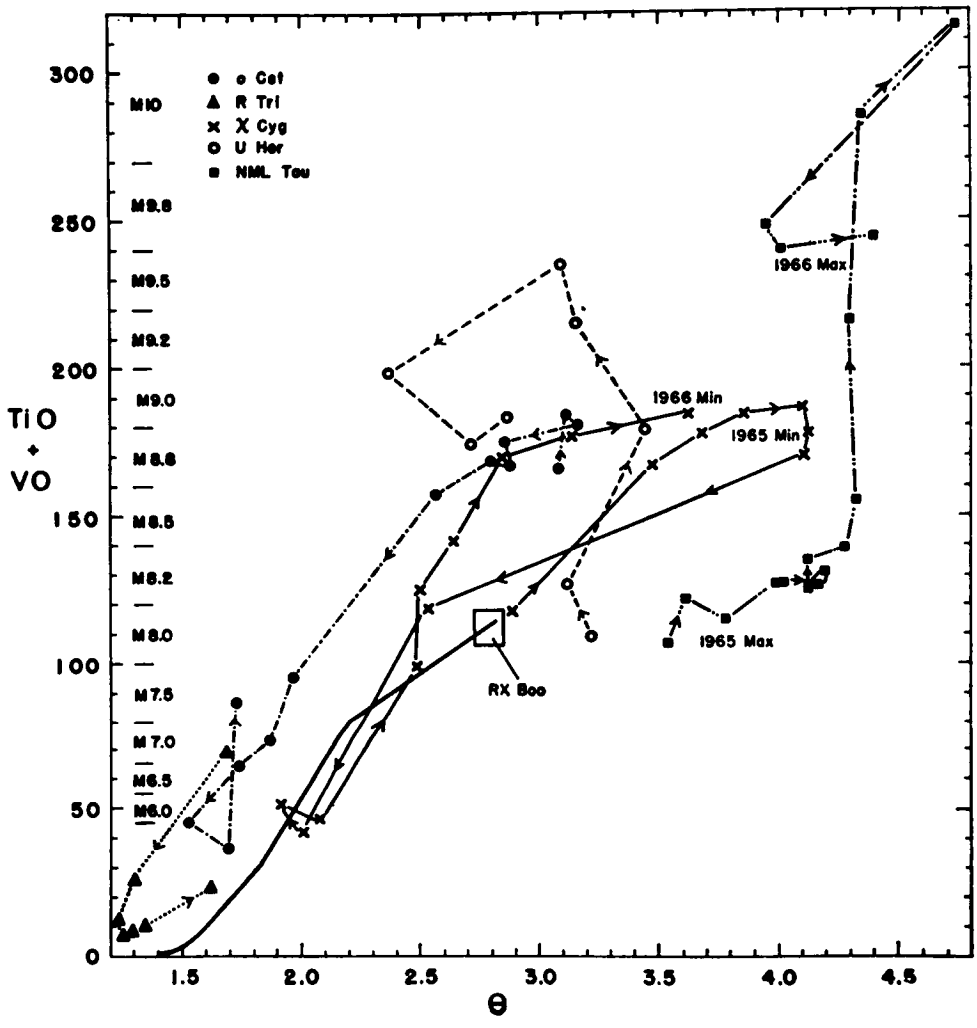


Figure 1-13. The relations between band strength and temperature are obtained from observations in the 1-μm region. The ordinate is the sum of TiO and VO indices (unit = 0.01 mag) and is calibrated in terms of spectral type. The abscissa is θ = 5040/T, where temperature T is obtained from a blackbody fit to the continuum. Observations are connected in chronological order (from Spinrad and Wing, 1969).

plane along the period:

1. R Tri (▲) is a relatively early-type Mira; its earliest spectral type was M3, obtained at its 1965 maximum, but its corresponding temperature was that of a normal K4 giant.
2. χ Cyg (×) was observed during a large part of two successive cycles, and its minimum approach paths were seen to be different in the two cycles.
3. *o* Cet (●) is shown from minimum to the post-maximum in the 1965 cycle. Its molecular index is much stronger than in non-Miras of the same temperature; consequently, this star is much hotter than the temperature obtained from its spectral type.

Another extensive project is from Maehara and Yamashita (1978), who use a photoelectric scanning spectrophotometer. The wavelength region covered is 3700 to 5500 Å with 13 Å resolution. They give the energy distribution measured at flux peaks for a suitable sample of stars of luminosity class Iab to III and spectral range from M0 to M8 stars. Three S stars (V Cnc, R And, and W And) and one carbon star (SS Vir) are also included. The comparison of these curves with those of nonvariable M stars gives the spectral type variation of each Mira star during the period: *o* Cet ranges from M5 to M8, R Aur from M6 to M8, R Cnc from M6 to M8, etc. The S stars have an M-star behavior in the spectral region of this investigation because they suffer from TiO absorptions. The C-type Mira, SS Vir (C6,3e), shows an entirely different distribution. The flux is too small to be measured shortward of λ4250. The variations of the color indices in the spectral range 4250 to 5000 Å are very small compared to those of M and S stars; the variation of the C_2 band head at λ4737 is also relatively small.

Krempec (1975) shows changes of the central depth in spectral features, such as in C_2 and CN molecular bands and in atomic D-lines, with the light phase.

A comparison of the color changes observed on two prototype stars with two maxima per period (R Cen and BH Cru) shows differences: (1) the two $U-B$ curves have reversed shapes, and (2) on the R Cen curve, the color index decreases at the second maxima, while in BH Cru, a sharp increase is observed. The $B-V$ curves of these two stars show only small differences.

To conclude this study on the variations of color indices, we point out that there is a large variation in the color index for stars of the same spectral subclass; the strength of the hypothetical shock wave that causes the variability should not be correlated with the spectral subclass. The same remark applies to the SRa variables according to Alksne and Ikaunieks (1971). In their review of carbon stars, these authors emphasize that the mean values of $B-V$ and $V-I$ indices decrease somewhat in the sequence Mira, SR, L.

Period Changes. Little is known about the frequency of period changes in Mira-type stars because a long-time base of observations is required and the different shape and amplitude of successive cycles make the inferences more doubtful. Nevertheless, three kinds of period changes are listed:

1. A secular evolution by smooth increasing or decreasing of the length of the period or by a sine or cosine variation of the latter.
2. Some shape changes of the light curve between two or several consecutive periods.
3. An abrupt change of period and an abrupt shift of epoch.

From a 20-year survey, Hoffleit (1976) shows that log ($\Delta P/P$) is spread around a linear function of log P, where ΔP is the maximum difference between the various periods of the same star and P is the mean period. This observed relationship holds for Miras, SR variables, W Vir stars, classical cepheids, and RR Lyr stars.

Hoffleit (1979) has drawn a catalog of 356 stars that have, at one time or another, been recorded as having changing periods; these stars

were selected in the *General Catalogue of Variable Stars* (Kukarkin, 1976), in the *Geschicht und Literarur des Lichtwechsels* (Prager and Schneller, 1934, 1963), and in some *Information Bulletins of Variable Stars* (IBVS). Among 332 Miras, 273 individual increases in period (e.g., for V Cas and U Her) and 290 decreases (e.g., for T Cep) were noted. This catalog is available on request to its author. To have some idea as to the number of variable stars with different kinds of changing period, we must refer to the 108 Sagittarius stars examined in sufficient detail by Hoffleit (1979). The observations could not be suitably represented by a constant period over 50 years, but the O–C plots for a constant period are best represented by one *abrupt change*. Three stars have the O–C curve represented by a parabola, indicating that the period is progressively increasing or decreasing. One star has its O–C curve represented by a sine-term, which suggests that the period is alternatively increasing and decreasing.

The four stars, V462 Cyg, V734 Cyg, HO Lyr, and MV Sgr, have cyclical changes in period. The O–C curves are represented by sine or cosine terms (Hoffleit, 1979). U Boo and S Ser have sinusoidally changing periods (Sterne and Campbell, 1937), as well as six others (R And, RS Cen, Z Cyg, TU Cyg, W Her, and W Hya) given by Prager and Schneller (1934). However, this kind of ephemeris is a very simple mathematical representation of very complex physics, and also it breaks down during 50 years. Thus, several later catalogs dropped these representations in favor of listing discrete periods for successive time intervals.

The conclusions of Nudjenko (1974) about the period changes are noticeably different from those of Hoffleit (1979). Forty-three (O-C) curves of the former demonstrate that the changes appear to be smoothly continuous rather than abrupt like these observed by Hoffleit. Investigations of all of the data are required. Table 1-6 summarizes the number of stars that have changed their period n times (Hoffleit, 1979).

Sterne and Campbell (1937) and Hoffleit (1979) come to the same conclusion that the stars, R Cnc, R Cen, and X Lib, have changed periods.

Table 1-6
Number of Stars Having Changed Period* n Times

n	No. Stars	n	No. Stars
2	146	7	1
3	110	8	0
4	46	9	1
5	15	10	0
6	4	≥10	2

*From Hoffleit (1979).

Some examples of stars that have a progressively decreasing period length are:

1. HS Aql, with its period ranging from 267 days in the 1930's, through 263.8 days in the late 1950's, to approximately 260 days in 1970's (Thompson, 1981). This star might be climbing the asymptotic branch.
2. W Tau, with its period ranging from 273 days in 1887 to 253 days in 1956 (Schneller, 1965).
3. R Aql, with its regularly decreasing period (Hoffleit, 1979; Schneller, 1965) in a sinusoidal steady manner (Payne and Campbell, 1930).
4. R Hya, with its period of about 500 days in the 18th century to about 390 days as noted by Merrill (1946). These period changes are used by Wood and Zarro (1981) to provide direct observational confirmation of the theory of helium flash shell (see their Figure 3).

A list of such stars may be found in Hoffleit's catalog (1979).

On the other hand, some stars, like V Cas and U Her, have increasing period length (Lockwood and Wing, 1971). Again, Hoffleit's

catalog (1979) lists stars with likely smooth varying periods.

It is useful to know that the prototype star, *o* Cet,was noted in Prager and Schneller (1934) to have 12 discrete periods ranging from 322.5 to 335.4 days. For a total of 335 epochs of maxima, the best constant period is 331.7 days, giving a *nonsystematic* spread in O–C of 82 days and $\Delta(O-C)/P = 0.247$. Consequently, Hoffleit (1979) concludes that "this star is no longer considered as having a significantly changing period."

In 1936, Hetzler (1936) shows some small variations on consecutive light curves of Miras. The perturbation appears in the visible AAVSO light curves and in the infrared ones at λ8500. The latter wavelength is affected moderately by strong TiO absorption (Wing, 1971). Figure 1-10b shows two light curves (IR on the top and visual on the bottom) for two periods of R Vir separated by a period which is not indicated. The hump shown in the first period is not present in the second one (or is much less noticeable).

R Car is an astonishing star; it shows a wide maximum cycle followed by a narrow maximum one (Celis, 1977).

Abrupt changes of period (rapid fluctuations of the length of period) appear in some Miras; they are visible from the differences (O–C) between the observed epoch of maximum and the computed dates derived from formulas ($JD_{Max} = P \times E$). This phenomenon was observed on T Phe and U Tuc by Campbell (1926) and on RT Eri (Payne and Campbell, 1930); it is not correlated with the length of the next cycle, such as the shift of maximum described in the next paragraph.

Abrupt shifts of epoch (fluctuations of phase) are also pointed out by Ludendorff (1928) on R Lup and by Shapley (1929) on Z Aqr. For the latter, the (O–C) curve demonstrates that the period remains constant over the interval covered by observations (1896 to 1929), although there appears to be a jump in epoch of about -55 days near JD 2420900. This change seems to take place within about two periods, but the observations are not spaced closely enough to determine whether the change is due to an abnormal lengthening of a maximum or a minimum. New photometric and spectroscopic observations are needed on such stars.

Multiple Periods. The light curves can also be analyzed by other means, such as the superposition of two or more distinct periodic light curves. Payne-Gaposchkin (1954b) notes that the ratio P_2/P_1 is approximately the same for the stars of a given spectral type, but it differs from one spectral type to another. She gives $P_2/P_1 \approx 9.4$ for the M stars and 12.2 for N stars. The frequency distribution of P_2/P_1 for M-type variables has a rather flat maximum between 7.5 and 10, with a slight peak between 9 and 10 (Houck, 1963). With a small sample of N-type stars, Houck shows a maximum frequency of P_2/P_1 between 12 and 13. These values agree well with Gaposchkin's earlier results. Houck (1963) gives six Mira variables with secondary periods: SV And, U Per, V Hya, V545 Cen, Y Per, and V1280 Sgr. Among the variables with M-type spectra, there are five with P_2/P_1 ratio in the range 22.5 to 51.5 and one N star with this ratio about 45.4. In these quoted papers, P_2 should be interpreted in terms of a beat frequency phenomenon resulting from interference between two slightly different periods within the atmosphere of the stars.

Leung (1971) describes a method of analysis of superposition of two or more nonsinusoidal period components. Leung (1980) applies this method to 50-year observations on six selected M and S Miras: *o* Cet, R And, T Cep, T Cas, R Hya, and S CrB. Two components were determined for the majority of the observed Miras (Figure 1-14). For five variables, the period ratios, P_2/P_1, of the two individual nonsinusoidal period components are around the value, 1.04 ± 0.01. In general, the shorter period P_1 is associated with the larger amplitude of variation, and the amplitude ratios, A_2/A_1, range from 0.15 to 0.28. The amplitude and period ratios of period components of S CrB do not fit into the general behavior pattern described

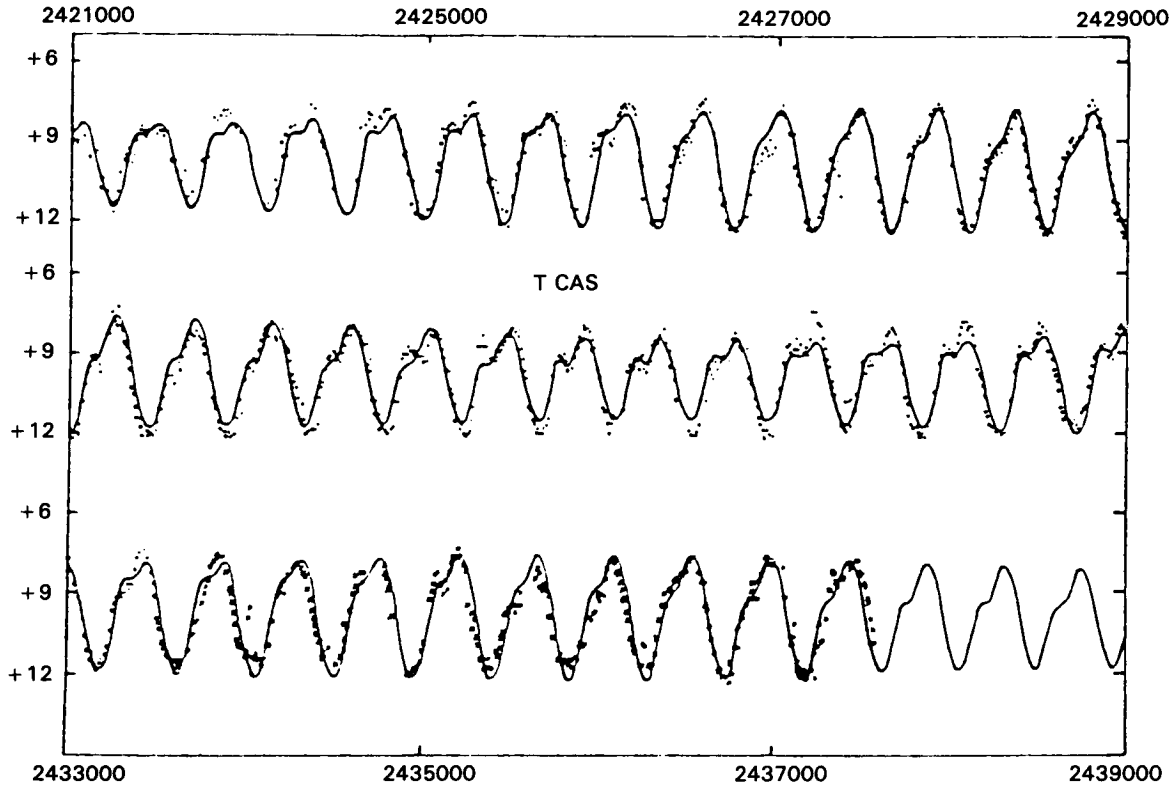


Figure 1-14. AAVSO observations of T Cas (10-day mean). The computed light curve (smooth curve) is based on two period components. The observations not included in the determination of period components are denoted as crosses. The abscissa is Julian Day (from Leung, 1980).

here. The *o* Cet light curve needs the superposition of three periodic components.

Houck (1963) gives two periods for the C star, V Hya: P_1 = 533 days and P_2 = 6500 days (beat frequency). These values are of the same order as those of Campbell (1943), who finds P_1 = 539 days and P_2 = 18 years. The latter period gives extra-deep minima reached in 1889, 1908, 1925, and 1943. Analyzing the data gathered by AAVSO from 1860 to 1968 and using the method of analysis of Leung (1971), Leung (1973) points out one period of 6670 days with an amplitude of about 3.5 magnitude. The other component has a period of 530.7 days, an amplitude variation of 1.1 magnitude, and a shape close to sinusoidal, so that the larger period component has the larger amplitude. Note that the opposite holds for the red supergiant variables (Leung, 1973). He concludes that V Hya may be a late Mira of Ib type, for which the long-period component is not due to a normal mode of radial pulsation, and that the dip preceding the minimum is probably due to nonlinear effects or cold spots on the star surface. Reanalyzing the data of V Hya, Leung (1980) concludes that this carbon star has an extremely peculiar light variation and proposes four distinct period components.

To conclude, we recall Leung (1980), who suggests that the primary period, P_1, is the pulsational period and that the modulating period, P_2, may be derived from a nonradial mode. The multiple periodicity may reveal information on the modes of oscillation of these stars.

Short-Term Fluctuations. In addition to the rapid evolution in the *o* Cet effective temperature on 12 days reported by Joshi et al. (1980), we want to detail some scarce observations

which seem to indicate short-term fluctuations in the Mira variables.

The J = 1→0, v = 1, and v = 2 SiO maser emission lines of the Mira variable, R Leo, show phase-dependence effects in both line shape and intensity. At the premaximum phases, they are strong narrow features of decreasing intensity. Around the visual maximum (φ = 0.98, 0.02, 0.04), they appear to be respectively about 30 and 15 percent broader without any trace of narrow features (Clark et al., 1982). The effective duration of these changes continues up to $\varphi \approx 0.40$.

With the Griffin-type radial-velocity spectrometer and masks especially designed for Mira spectra, Pierce et al. (1979) find nightly variations of radial velocity of emission and absorption lines in the spectra of Miras. More precisely, the range in the measurements for each night is larger than the average uncertainty for a set of observations covering 7 nights between φ = 0.9 and φ = 0.2. For example: on T Cep, the nights at φ = 0.02 and φ = 0.12 show a variable behavior of the absorption lines (the emission lines are too faint to be measured); on χ Cyg, the nights at φ = 0.07, φ = 0.11, and φ = 0.13 show a variable behavior of the emission lines; and on o Cet, the radial velocity is variable in the absorption lines for the nights around φ = 0.76 and φ = 0.21 and in the emission lines for the nights at φ = 0.12. The range of these nightly radial-velocity variations is between -2 and -13 km/s. These short-term variations should be interpreted by the *interaction of shock waves with nonuniform atmospheric layers*. Also, they should be linked to eventual flares such as those observed in R Aql (Woodworth and Hughes, 1973, 1977) or V Cyg (Querci et al., 1979); however, simultaneous observations are not available. Finally, it might be that these variations in radial velocity are a consequence of matter swept along magnetic tubes (see M. Querci, this volume).

Correlations Between Different Observed Quantities. Numerous correlations between the observed quantities such as period length, light-curve shape, IR excess, visible and IR color diagram, and OH radio-line separation exist in the literature. Apparently, some of them are surprising, because we do not understand for the moment why they happen. However, we shall note in detail here those of the greatest importance and shall endeavor to draw conclusions on the relationships between the derived physical parameters.

The first correlations between the observed quantities were made at the Harvard Observatory. Campbell (1925) first demonstrated that a statistical relationship exists between the shape of the light curve and the period. The asymmetry becomes gradually more pronounced as the period increases. In all three spectral classes (M, S, or C), Mira light amplitudes are smaller for shorter periods and greater for longer periods. This was again explained by J.G. Garcia (1980).

Using the data of Kukarkin et al. (1958), Merrill (1960) found that the period of M, S, and C stars is distributed in a broad maximum around 300 days for M stars, 360 days for S stars, and 400 days for C stars. Consequently, the C Miras have, on the average, the longest periods.

Using two groups of Miras, one in which emission lines have low radial velocities (<20 km/s) and another in which they have high radial velocities (>80 km/s; from Merrill's catalog, 1941), Ahnert (1969) finds that the larger the scattering of cycles in percentage of periods, the earlier the subgroup of Me stars. A corresponding relation exists between the scattering and the period length, a relation which seems trivial because it is a well-known fact that the longer the period, the later the Me subgroup (Glasby, 1968).

Harrington (1965) investigated 165 Miras from among the data of Campbell (1955) and found a correlation between the difference in magnitude of two successive maxima and the time interval separating the two maxima. When the interval is under the average value, the second maximum is brighter (45 percent of the considered stars show this correlation with a significance of at least 95 percent). These light curves may be interpreted by the outward propagating disturbances taking more or less time

to reach the star surface, this time being a function of the energy carried.

The kinematic studies of Feast (1962) imply that the shorter period Mira variables are Population II stars, while those of longer periods belong to more intermediate populations. These conclusions suggest that the period amplitude of the Mira stars may be a function of their metal abundance.

To determine the difference in metal abundances between short and long-period Mira variables, DeGioia-Eastwood et al. (1981) used the relationship derived between |W|, the velocity of the star perpendicular to the galactic plane, and $\delta(U-B)$, the ultraviolet excess, given by Eggen et al. (1962). To calibrate the relationship between [Fe/H] and the kinematic properties, they use Carney's (1979) relation between $\delta(U-B)$ and [Fe/H]. They have examined two groups of Mira variables: the stars with periods $149 < P \leq 200$ days were found to be deficient in [Fe/H] by more than 1 dex, compared to the group with $350 < P \leq 410$ days. The metal deficiencies in the short-period Mira variables are substantial, and consequently, the mass lost is proportional not only to the outflow velocity and the mass of the shell, but also to the abundance of heavy elements contained in the ejected matter.

Eggen (1973) shows that the periods and colors of small-amplitude red variables are not related. Eggen (1975) deduces a linear relation in the plane $(\log P, (R-I)_0)$ for the Miras, the index $(R-I)_0$ being measured at phase 0.25 (approximately medium light). This linear relation is given by:

$$(R-I)_0 = -0.45 \text{ mag} + 0.90 \log P$$

It is probable that this relation becomes nonlinear for stars with periods longer than 500 days that are redder than $R-I = 1.8$ mag (Eggen, 1975); although the number of such stars is not important, observations are needed to determine the $((R-I)_0, \log P)$ relationship. The halo Mira variables have no correlation between the period and the color $R-I$ at phase 0.25 (medium light). Feast (1980) points out that Miras show a slow rise in brightness with period, from $M_{bol} \sim -4.1$ at 200 days to $M_{bol} \sim -4.6$ at 400 days. The short-period (~ 135 days) Miras do not follow this law and are quite fainter.

The extension of the visible to the red and radio spectral ranges, and consequently, the detection of the IR excess and of the maser lines, leads to many correlations for an improved knowledge of the Mira behavior. Moreover, the analysis of M, S, and C stellar spectra using model atmosphere synthetic spectra is very useful because it shows that the stellar continuum could be reached in small intervals around 1.04, 3.6, and 8 μm (see H.R. Johnson, this volume).

Lockwood and Wing (1971) and Wing and Lockwood (1973) find a direct correlation between the period length and the amplitude variation at 1.04 μm for a large sample of M stars, whereas Keenan et al. (1974) find a direct correlation between the mean spectral type at maximum light and the period for the Me stars. Ukita (1982) shows (Figure 1-15) this relationship for the Mira stars with strong OH emission, weak OH emission, non-OH Miras, and Miras which have not been observed in OH. Frogel (1971) established a correlation between the variation of the [1.2 μm]-[3.5 μm] color index and the amplitude variation at 2.2 μm for stars with little or large excess 10-μm radiation. A tendency for larger period stars to have longer amplitudes and larger [0.8 μm]-[2.2 μm] or $[I-K]$ color indices was noted by Hyland et al. (1972). The continuum amplitude variations can be explained by variations in the effective temperature, whereas both the effective temperature and molecular opacities act together on other spectral ranges. Using the 2.2-μm spectral range, Harvey et al. (1974) again found the period-amplitude relation previously obtained in the visible and at 1.04 μm; they also established a relation between the variation of the [3.5 μm]-[10.0 μm] color index and the period amplitude. DeGioia-Eastwood et al. (1981) found that the [8.7 μm]-[11.4 μm] color augments monotonically with increasing period for a sample of 41 Mira variables of M spectral type. However, since the photometric phase at the time of each measurement had not been

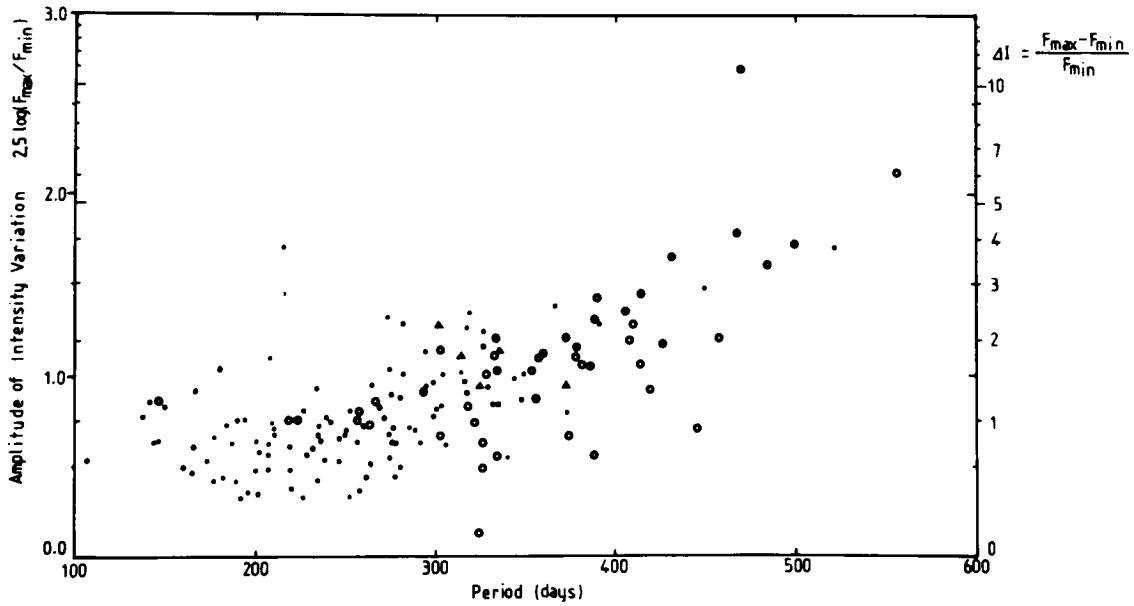


Figure 1-15. Plot of the 1.04-μm intensity variations against stellar period for oxygen-rich Mira variables: filled circles represent OH Miras in which OH emission was detected [OH luminosity $\equiv SD^2 \geq 0.1$ *Jy (kpc)^2]; filled triangles are OH Miras with weak OH emission [*$SD^2 < 0.1$ *Jy(kpc)^2]; open circles are non-OH Miras; dots are Miras not having been observed in OH or for which upper limits are poorer than the above criterion (from Ukita, 1982).*

taken into account (of course, how could it?), some of the scatter may be due to intrinsic variability. We conclude that the height of the silicate feature increases with the period amplitude, and consequently, the ratio of mass loss and dust formation, as well as the temperature of the silicate emitting layers, are directly linked to the stellar parameters which dictate the period amplitude. The height of the silicate feature does not seem to be due to a stochastic process in any Mira variable.

Like DeGioia-Eastwood et al. (1981), we point out that the IR excess is not indicative of the total amount of mass in the shell, which is governed by the mass loss, but only of the mass of dust (and not gas) contained in the *thermosphere*, which extends to that radius in the shell where the dust is sufficiently warm to radiate significantly at 10 μm. Therefore, the [8.7 μm]–[11.4 μm] versus period relation can be interpreted as an indication that the observed mass of dust in a given thermosphere is an almost linear function of the period.

Bearing in mind that the Population II stars have a short period and that they are metal-deficient, we assume that two stars are equal in mass and luminosity and differ only in period; the previous correlation permits us to conclude that the Population II stars are also infrared-excess-deficient, and consequently, that dust formation may be a function of the metal abundance.

In some stars, Wilson (1970) noted that the OH 1612-MHz masers and the IR variations are clearly correlated. Harvey et al. (1974) developed a monitoring program to measure, at monthly intervals, the maser at 1612 MHz and the broadband infrared fluxes at six wavelengths for OH/IR sources. They essentially confirm the observed correlation between the infrared and the 1612-MHz variability of the OH/IR stars and the OH clouds. This coupling mechanism is consistent with a radiative pumping of the masers, possibly at 2.8, 35, 53, 80, and 120 μm (Litvak, 1969; Litvak and Dickinson, 1972; Elitzur, 1978; Elitzur et al., 1976; Bujarrabal et al., 1980; Epchtein et al., 1980).

A monitoring of OH maser emission from the M-type stars, IRC +10011, NML Tau, U Ori, S CrB, WX Ser, U Her, R Aql, and R Cas is made by Jewell et al. (1979). The maser emission is observed in the 1612-, 1665-, and 1667-MHz lines of OH and 22-GHz line of H_2O. They conclude that, in most cases (their Figures 7 through 13), for all main and satellite lines, the maser pumping mechanism must be radiative in nature. For the satellite line, this has already been established with some certainty by Harvey et al. (1974). The data presented by Fillit et al. (1977) also suggest a radiative pumping for the satellite line and, with less certainty, for the main lines. For these latter lines, the work of Jewell et al. (1979) establishes conclusively that the main lines are also related to the optical flux of the star (see later for controversy). Schwartz et al. (1974) suggest two possible correlations between the 1.35-cm H_2O maser and the 2.2-μm infrared flux, either an exponential rate which fits the intensity of the maser versus the IR flux at 2.2 μm, or a linear relation between them after a threshold of the infrared flux value (which is probably correlated with some processes quenching the maser at low level of infrared flux or a possible collisional deexcitation of H_2O molecules). The pump may be linearly proportional to the infrared flux above the threshold if the maser is saturated.

Werner et al. (1980) simultaneously monitored far-IR, near-IR, and radio observations on five very red objects with 1612-MHz emissions. The direct comparison of these data strongly supports the hypothesis that the maser emission is pumped by 35-μm photons (see also Nguyen-Q-Rieu, this volume).

In the case of U Ori, the comparison of different line velocities produces three velocity groups (Cimerman, 1979). The most important is the group at -42 km/s, which includes the zero-volt optical absorption lines, one line of the SiO transitions, and an OH line of each frequency seen in all observations. The second group includes the optical emission lines and one line of the 1612-MHz features at -47 km/s. Lines scattered around the velocity of -36 km/s form the last group. Garrigue (1980) attempts to correlate the OH maser emission with the observed visible light curve. In his U Ori monitoring, he finds an entire period of light shifted by 2 mag above its usual mean value for each phase, whereas the light curve of this Mira is usually very regular. Garrigue and Mennessier (1980) point out that the beginning of this epoch of higher brightness began approximately 650 days before the 1612-MHz flare discovered by Pataki and Kolena (1974b) in November 1974 and that the lifetimes of both visual brightness and 1612-MHz satellite increases have 550-day durations. This confirms that the OH emission in the satellite line is due to a perturbation which propagates throughout the stellar atmosphere. The proposed scenario is as follows:

1. An overbrightening perturbation occurs in the photosphere, disturbing the visual light curve during 550 days.
2. It propagates thoughout the stellar atmosphere with a mean velocity of 20 km/s (Slutz, 1976).
3. After about 650 days, the perturbation reaches the dust shell and disturbs the IR radiation emitted by it (at about 10^{14} cm; from Gehrz and Woolf, 1971).

The shell IR radiation reaches the U Ori OH-emitting region (10^{15} cm; from Reid et al., 1977) in 1 day, and "by OH radiation coupling, is responsible to the maser effect during 550 days" (Garrigue and Mennessier, 1980). This interpretation is a little different from the one proposed by Cimerman (1979), who does not take account of the 650-day delay between the beginning of the visible and the radio variations.

Four papers (Dickinson et al., 1973; Harvey et al., 1974; Dickinson et al., 1975; Morris et al., 1979) argue in favor of a direct correlation between the expansion velocity given by the OH maser circumstellar lines and the period. Lépine et al. (1976) show that this correlation is doubtful for their Mira sample. Using the relationship of Figure 1-15 and the hypothetical correlation expansion velocity versus period

amplitude, one might conclude that a direct correlation exists between the OH expansion velocity and the amplitude variation on the I104 filter. Research in this way was attempted by Ukita (1982), who confirms the uncertainty stressed by Lépine et al. (1976). With data of type I and II OH Miras (Figure 1-16), he finds that the expansion velocity has a direct correlation with the amplitude variation at 1.04 μm and an inverse correlation with the period length. Knowing that the type II OH/IR Mira stars have larger color indices than the OH Miras and, consequently, have thicker envelopes (Harvey et al., 1974; Dickinson et al., 1975; Olnon, 1977), Ukita (1982) assumes that the mass-loss rates increase in the order: non-OH Miras, OH Miras, and type II OH/IR stars. Ukita interprets his result in terms of a dust-driven wind enhanced by pulsation, a hybrid model of mass loss (Wood, 1979; Deguchi, 1980).

Looking for the SiO masers in a large sample of Miras, SRb, and supergiants, Spencer et al. (1981) conclude that no global properties of these stars correlate with the SiO luminosity; this indicates that the SiO masers are located very close to the stars, where the local conditions affect the maser intensity much more than the global properties of the photosphere, such as the stellar temperature, affect it. The local conditions could be governed by clumps of gas, convective cells, or turbulent eddies. The variation of the SiO maser intensity and profile pointed out by Clark et al. (1982a, 1982b) in the Mira, R Cas, is a good example (see their Figures 1 through 5). Moreover, in Miras, the SiO maser flux is correlated with the bolometric flux (Cahn and Elitzur, 1979; Cahn, 1981) and with the infrared flux (Hjalmarson and Olofsson, 1979). (Let us remark that, when the lines are weak, broad, and roughly parabolic, they are due to nonmaser emission formed in a thick expanding envelope (Robinson and Van Blerkom, 1981).)

Using VLBI observations, Bowers et al. (1980) correlate the mass-loss rates with the size

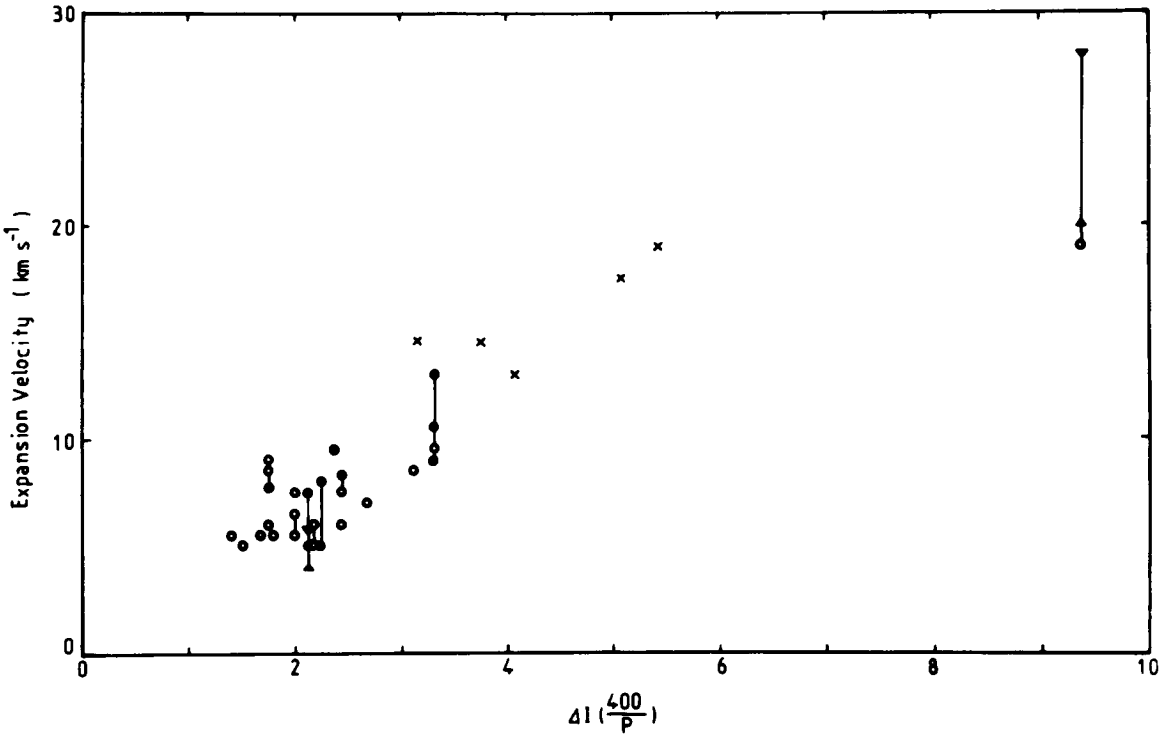


Figure 1-16. Plot of expansion velocity versus the quantity $\Delta I \times 400/P$, for oxygen-rich Mira variables. (ΔI and marks are defined in Figure 1-15.) The crosses represent type II OH/IR stars (from Ukita, 1982).

of the masing regions; stars with mass-loss rates less than $10^{-5}\ M_\odot\ \mathrm{yr}^{-1}$ have masing regions <1000 AU in extent, while stars with stronger mass-loss rates have larger masing regions.

Wolff and Carlson (1982) point out a "general tendency of both line width and integrated intensity of SiO thermal emission lines to increase with infrared color excess."

Scharlach and Woolf (1979) look for a correlation between the maser activity and the amount of ejected matter, which is correlated with the subphotospheric activity (Thomas, 1973) as indicated by the hydrogen emission. They therefore searched for a correlation between the maser activity and the Hδ emission line (which is the only Balmer line not disturbed by TiO absorptions); no correlation was found.

Modes of Pulsation of Long-Period Variables. Miras are radial pulsators and are driven mainly by hydrogen ionization effects (e.g., Cox, 1984). The real germane problem is to know which radial mode is the primary mode of pulsation, the fundamental or the first overtone. Both modes have been proposed by different groups through comparisons between observational values of the pulsation constant Q and theoretical Q-values.

The pulsation constant Q (in days) relates the period P (in days) and the density ϱ by: $Q = P(\varrho/\varrho_\odot)^{1/2}$, otherwise:

$$Q = P\,(M/M_\odot)^{1/2}\,(R/R_\odot)^{-3/2},$$

with M, the mass, and R, the radius (i.e., a period-mass-radius (PMR) relation exists).

A primordial observational constraint to the Q determination concerns the knowledge of radii. Their evaluation by direct methods (giving angular diameters) such as occultation technics or speckle interferometry, or by photometry is debated by Wood (1981) and Willson (1982). (See also the section on *Radii.*) In the direct method, it is shown that radii vary from one spectral region to another; also distances to individual objects must be known. The photometric approach involves the luminosity definition:

$$L = 4\pi R^2 \sigma T_{\mathrm{eff}}^4$$

The radius may be expressed in the function of L, hence the absolute bolometric magnitude M_{bol}, and of T_{eff}. Therefore, knowing observationally the $M_{\mathrm{bol}}/\log P$ relation and the $\log T_{\mathrm{eff}}/P$ relation for LPV's, we get observational $Q\ M^{-1/2}/P$ relations. However, the uncertainty in the effective temperature determination (hence, in the radius determination) for the Miras remains the major problem in estimating Q-values from observations. (See the extensive discussions in Willson, 1982, and in Wood, 1981, 1982.) This is shown in the summary of observed Q-values given by Fox and Wood (1982, and references herein): (1) for the Population II small-amplitude variables (e.g., in globular clusters 47 Tuc, M4, M22, and ω Cen), using the Ridgway et al. (1980) temperature scale (an extension to Miras of a scale based on nonvariable M giants), the pulsation mode is the first overtone for stars in the two first-quoted clusters, and the fundamental for stars in the two latter, without clear explanation; (2) for Miras in the solar neighborhood, using a blackbody temperature scale based on lunar occultation angular diameters, the mode is the first overtone, whereas the use of the Ridgway et al. T_{eff} scale might lead to the fundamental mode; (3) in the Magellanic Clouds, for the two groups of long-period variables (see the section *Aspects of Evolution of Long-Period Variables in the Magellanic Clouds*), the pulsation mode appears to be first overtone if blackbody temperatures are used, or fundamental mode if the Ridgway et al. T_{eff} are favored. In fact, one can have confidence in the blackbody color temperatures for LPV's of large amplitude that are linked to infrared lunar occultation diameters of Mira variables (as described in Glass and Feast, 1982); therefore, first-overtone pulsations are favored.

Pulsation models, as well as linear nonadiabatic models (Fox and Wood, 1982), have been calculated as nonlinear nonadiabatic models (Wood, 1974; Tuchman et al., 1979; Ostlie et al., 1982). In the extensive grid of linear nonadiabatic pulsation models of Fox and Wood (1982), theoretical values of the

pulsation constant are derived for the first three radial pulsation modes in red giants (galactic disc and Population II) and supergiants. Main results are as follows:

- In the standard models, for Miras in the galactic disc, Q is not constant for either mode. Q-values for the first overtone asymptotically approaches $Q_1 \sim 0.04$ at low luminosity or high mass, and short P, but Q_1 may take values up to about 0.075 (see Figure 3 in Fox and Wood, 1982); no simple period-mass-radius relation exists. For the fundamental mode, Q-values increase with P, and the relation $P M^a R^{-b} = Q$ with a $\sim$ 1.0 and b $\sim$ 2.0 holds.

- The ratio P_0/P_1 can take values from $\sim$2 to 3 for values of $P_1 \leqslant 630$ days; $P_0/P_1 \sim 7$ occurs when $P_0 \sim$ 2000–5000 days in some massive luminous stars. Beat periods exist between P_1 and P_2 of $\sim 3\, P_1$ to $\sim 20\, P_1$ (Wood, 1982); some observed beat periods are given in the section *Multiple Periods*.

Note that, for the LPV's in Magellanic Clouds (models with slightly decreased metal abundances), the Q-values for the first overtone tend to cluster around Q (days) = 0.38.

Therefore, although the ratio of P_0/P_1 seems to be well determined theoretically, determination of the mode of pulsation itself of the Miras requires more than the Q-value determination. Wood (1981) suggests that the strongest evidence in favor of the *first-overtone pulsation mode* is the presence of secondary periodicities caused by resonant coupling between the first-overtone (corresponding to the primary mode of pulsation) and the fundamental mode (the secondary mode of pulsation) when the latter has a period *almost twice* that of the first overtone. In fact, Wood (1982), among various examples, quotes massive supergiants (see Figure 1-3) which present secondary periods with $P \sim$ 2000–7000 days (i.e., about seven times the length of the primary pulsation period) in agreement with the $P_0/P_1 \sim 7$ found in supergiant models of Fox and Wood (1982). Also, carbon stars among AGB variables are known to have such an observed P_0/P_1 ratio. Another support to the first-overtone primary mode of pulsation comes from Figure 1-3. As commented in the section *Aspects of Evolution of Long-Period Variables in Magellanic Clouds*, an AGB LPV switches from the first-overtone mode to the fundamental mode when crossing the dotted line corresponding to the long-period edge of the AGB region, to subsequently form a planetary nebula. If the primary mode is the fundamental one, the event that could suddenly stop the AGB evolution of an LPV still having substantial envelope mass is not clear. Evidence for the fundamental mode of pulsation in Miras has been given by Willson (1981, 1982, and references herein). Again, the controversy comes mainly from the used radii. Also, Willson analyzes shock propagation in Mira atmospheres to determine Q-values indicating the fundamental mode of pulsation. Wood (1981, 1982) extensively discussed her arguments and did not find them convincing.

The SRa-SRb-SRc Variables

Sir Williams Hershel discovered the first two variable stars of this type: μ Cep in 1782 and α Her in 1796, with their magnitude varying in a "random" manner between 4–6 and 3–4, respectively. John Hershel attributed these irregularities to some periodic veiling effects caused by interposing dark nebulous matter.

The amplitudes of SR variables are smaller than those of Miras, and the lengths of their cycles are generally smaller than the period of the Miras, except for certain supergiants in which periods of many years are observed (e.g., α Ori).

It is very difficult to define a period for stars in which the random brightness fluctations are more marked than the regular period. The duration of the observed cycle often varies by more than 1 month, and the individual maxima by more than a magnitude. However, the classification into the three following groups

(more or less arbitrary) is generally accepted:

1. The semiregulars of late spectral class (M, S, and C), denoted SRa, are giants. Many of these stars differ from the Mira types only in the smaller amplitude of light variations. Frequently, their curves have strong variations from one cycle to another. Typical representative stars are RU And, S Aql, Z Aqr, T Cnc, WZ Cas, T Cen, RS Cyg, RS Gem, and R UMi.

2. The SRb-type semiregulars have a poorly expressed periodicity. Different periods of the individual cycles prevent the prediction of the epochs of minimum and maximum brightness. These stars sometimes temporarily replace periodic changes by slow irregular variations or even by the constancy of the brightness. Typical stars are V Aqr, V Boo, RX Boo, UU Aur, X Cnc, Y CVn, TT Cyg, R Dor, RY Dra, UX Dra, T Ind, R Lyr, VY Leo, W Ori, L_2 Pup, ϱ Per, SW Vir, and S Sct. The SRb stars are giants.

3. The SRc-type semiregulars are supergiants with an SRb behavior. The visual light changes are generally of the order of a single magnitude or less (Maeder, 1980). Typical representatives of the SRc type are VY CMa, μ Cep, RS Cnc, RW Cyg, TV Gem, Y Lyn, α Ori, S Per, and VX Sgr.

It appears that we find a larger fraction of semiregular variables among the carbon stars (C spectral class) than among the M and S stars. Almost half of the known semiregulars are N stars, the remainder being of M class; very few of S and R classes are known. Moreover, it is of interest to note that the N-type stars have larger primary and secondary cycles than the M class stars (for example, see Table 9 in Glasby, 1968).

The frequency-distribution curve of class C Mira and SR stars are very different. The former has a large maximum between 350 and 450 days, while the latter has two maxima around 150 and 400 days, clearly separated by a minimum around 270 days (Alksne and Ikaunieks, 1971). Analyzing this minimum in the distribution, Guzeva Yakimova (1960) noted the absence of carbon stars with periods (Miras) or cycles (SRa) between 250 and 285 days. With observations based on 316 stars (mainly spectral class M), Glasby (1968) uses the shortest cycle for SR stars (cycle intrinsically related to a possible pulsation of the star itself) and constructs a frequency-distribution curve for the cycle length. Two maxima are detected, around 85 and 135 days, on a period range from about 30 to 1000 days or more.

Different Time-Scale Light Variations of Semiregular Variables. The first approach to these stars could be light curves obtained by a visual estimate of the brightness; such tasks are well suited to amateur observers. Visual curves of semiregular stars do not have the strong similarity among them as do the Miras, but are quite individual. Moreover, instead of the mean periods of the Miras, the SR variables may be characterized by a form of periodicity which is hidden by irregular variations in brightness (Glasby, 1968).

Among the semiregular variable stars, the SRa are most similar to the Miras, with which we find many common characteristics such as Balmer emission around some light maxima as in WZ Cas, changing periods (Hoffleit, 1979), and other characteristics.

As for the SRb stars, there is often an erroneous classification between them and the irregular variables, Lb, because the observations are not continued for a sufficient duration. Maran et al. (1980) give a good example with VY Leo (56 Leo), which clearly shows the slow irregular variations that temporarily replace the periodic changes. Two groups of Brazilian astronomers have separately detected variations with a time scale of about 1 hour on the M8 II star, R Crt: Gomes Balboa et al. (1982) in the 22-GHz H_2O line and Livi and Bergmann (1982) in the DDO magnitudes and colors (over TiO bands and Ca I lines). R Crt is the first SRb

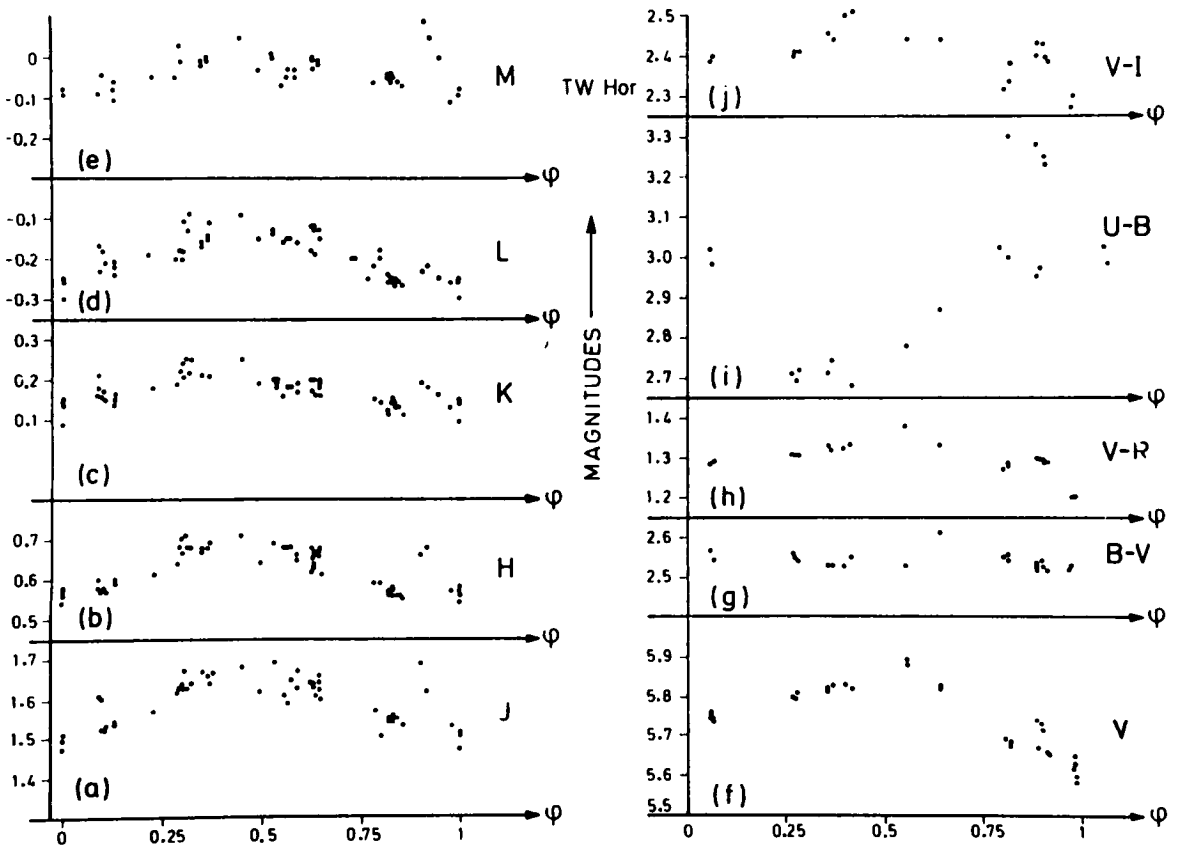


Figure 1-17. Photometric light curves of the SRb variable, TW Hor (from Bouchet, 1984a).

variable to show such rapid variations.

Bouchet (1984a) analyzes the C star, TW Hor, by broadband photometry from the U band to 30 μm (i.e., using U, B, V, R, I, J, K, L, M, N, Q, and P filters; Figure 1-17) carried out over a 4-year period and by spectrophotometry from 1 to 13 μm. The variations of brightness are similar in the J, H, L, and V bands. They are less pronounced in the K and M bands. The *V–R* and *V–I* indices vary slightly in phase with the V-magnitude. The *B–V* index remains nearly constant over the period, but the *U–B* varies oppositely to the other colors and magnitudes. Strong and rapid oscillations on *U–B* are pointed out between $\varphi = 0.80$ and $\varphi = 0.90$ (see his Figure 2); they are probably connected with the λ3280 Fe II V1 emission-line variations (Bouchet et al., 1983; see also M. Querci, this volume). These oscillations should duplicate rapid temperature or opacity variations due to *nonthermal chromospheric excitation* (Querci and Querci, 1983, 1985a). Surely, important scientific information is contained in these variations, but many opacity contributors such as C_3, violet CN, SiC, or graphite are included in the flux of each filter, and the restoration of each one is impossible. A new photometric system for carbon stars is needed (Querci and Querci, 1985b). A feature noted in the Bouchet's (1984a) paper is the variation on the N flux where SiC particles may form, which is either due to the variation of the amount of emitting SiC or to the fading of the exciting emission. Moreover, the time-scale variations over a week on N and P filters are not quoted, but they are not negligible. At phase 0.25, the N flux varies from 8.1 to 6.3 $\times$ 10^{-25} Wm^{-2} Hz^{-1}, while Q varies from 2.8 to 5.7 $\times$ 10^{-25} Wm^{-2} Hz^{-1}.

Lastly, we describe the supergiants (SRc). Because the time interval between two consecutive maxima for the supergiants is between

several hundred and several thousand days with amplitude variations which are generally small (≤ 1.5 mag), several years of observations are needed to decide whether a supergiant such as ϱ Cas belongs to the SRc class or to the Lc class (Smith, 1976). Maeder (1980) observed on the Geneva photometry file that the cyclical amplitude variations of the SRc stars decrease by several tenths of magnitude over some years; he concludes that "over half a century or more they may exhibit changes up to 2 magnitudes." Moreover, he points out that the limit in the HR diagram where the light variation amplitudes of the G–M supergiants become important coincides very closely with the limit of appearance of very deep convective zones in these stars. Using these two observations, we may conclude that the SRc supergiants stay no more than 100 years near the Hayashi limit because, in this area of the HR diagram, the amplitude variations are at their maximum and the observations show that the light maxima decrease about 2 magnitudes in one century.

The hypergiant, ϱ Cas, shows large variations in luminosity and spectral class. Before 1930, it had a K class spectrum; in 1943, Morgan et al. (1943) classified it as F8Ia,b, and during 1946–1947, the star underwent a deep light minimum ($\Delta m_v \sim 2.0$), probably because of the large amount of ejected matter, and consequently, the spectrum looked like that of an M star. In 1948, Greenstein (1948) pointed out signatures of matter falling back on the star a day after a sudden expansion. Joshi and Rautela (1978) found that the color temperature of ϱ Cas was higher than that of δ CMa (a non-variable star of the same spectral class) by about 650 K in 1920 and 100 K in 1974. As quoted by Glasby (1968): "One marked peculiarity of the light curve of ϱ Cas is the apparent existence of three fairly distinct modes with quite abrupt changes occurring from one to the next. Such changes have been observed in 1911, 1922, and 1946 when a very deep minimum occurred which was well followed visually and photoelectrically."

Some other observational proofs of long-term variations have been made by the analysis of the variable polarization. For example, Tinbergen et al. (1981) interpret the yearly variations of α Ori and α Sco by very large eddies (size about 1.5×10^8 km) with a lifetime of 1 year. One, or at most two or three, of these large moving elements are seen at the same time; this agrees with Schwarzschild's (1975) estimate that a cell moving up and down in the stellar atmosphere with a sonic speed (supposedly constant and equal to 5 km/s) crosses the whole stellar diameter in 1 year. In α Ori, Goldberg (1979) finds random fluctuations on the time scales of 1 year or less noted above. He also finds a cycle of about 5 years with both brightness and photospheric radial-velocity variations, which demonstrates the correctness of the period of 5.781 years of Jones (1928), Sanford (1933), and Pettit (1945). (However, see the discussion by M. Querci, this volume.)

In addition to these long-term disturbances, night-to-night variations are observed in some super or hypergiants. In ϱ Cas (Figure 1-18), Joshi and Rautela (1978) show variations in the slope of the Paschen continua and the Balmer jump and suggest that they are brought about by the circumstellar cloud surrounding the star. The daily disturbances are probably due to local interaction between the photosphere and surrounding matter in small puffs or to local motions in the atmosphere itself, leading to irregular variations of brightness and polarization. Sargent (1961) suggested that the weak Balmer absorption lines of ϱ Cas during the late 1950's are probably filled in by emission lines, and he argued that there is no deficiency of hydrogen in the irregular variables. We conclude that a monitoring with high-resolution spectroscopy could clarify the problem.

Looking for the middle-term color changes shown by ϱ Cas (Beardsley, 1961), Landolt (1968) concludes that "such a very long-term project as this color change problem is one to which serious amateur-astronomers using standard UBV filters, a photoelectric cell, and a small reflector could usefully contribute."

The above variabilities remind us of those observed in the hotter supergiants, from A to

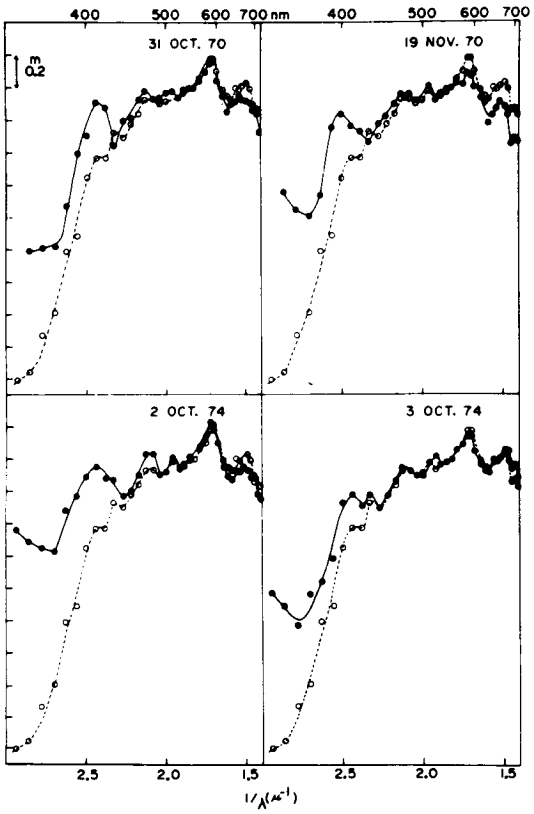


Figure 1-18. Energy distribution curves of ϱ Cas and S CMa: filled circles = ϱ Cas; open circles = S CMa (from Joshi and Rautela, 1978).

G spectral classes, with the three different time scales: (1) the nightly variations, (2) the cyclic variations of several hundred days, and (3) the long-term variations of several years which are sometimes quasi-catastrophic for the star.

Correlations Between Observed Quantities. Definite correlations between periods, absolute magnitudes, spectral classes, and phase lags are less obvious in the SR variables than in Miras. Generally, the clouds of points in the figures (Feast et al., 1980) are scattered around the mathematical relation deduced from these figures. However, efforts have been made to rectify the situation: Glasby (1968) reports studies from Palmer which conclude that, statistically, the amplitude variations may be accepted as constant. Or rather, he points out that the behavior of the maximum and minimum apparent brightness is virtually the same in the SRa stars, whereas it is very different in the Miras, in which two successive maxima could vary appreciably while the minima show very little variation. Moreover, he notes that the longer the period, the redder the spectrum—an association also noted by Strohmeier (1972).

Although the monitoring of H_2O microwave (Schwartz et al., 1974) on the SR variables, RX Boo (SRa), NML Cyg, and VX Sgr (SRc), was of such low signal-to-noise ratio that no correlation between microwave variations and visual luminosity was possible, Cox and Parker (1979) found a steady increase of the H_2O line with no sign of cyclic variation seen at optical wavelength in RX Boo (SRb). Moreover, sharp maxima appear in the maser strength with no apparent correlation with the visible. The monitoring of the two H_2O peaks of the SRb star, R Crt, gives a different behavior of these two features against the visual brightness. Spencer et al. (1981) conclude that the SiO maser intensities are correlated not with the stellar properties but with local conditions in the stellar atmosphere of the SRa, SRb, and SRc stars (like the Miras). When the visual brightness of VX Sgr (SRc) monotonically increases by about 3 magnitudes (Schwartz et al., 1974), the 2.2-μm flux increases by a factor 2. Then, and then only, does the H_2O microwave emission appear. It seems that the masering regions and the photosphere of the star are not usually coupled mechanically because the stellar photosphere suffers some periodic variations, but the masers have quite nonvariable radial velocities.

In his investigation on the SRa carbon star, Y CVn, with photoelectric B, V, and R filters and spectroscopic observations, Vetesnik (1982b, 1982c) gives a C_2 Swan radial-velocity oscillation of ± 2 km/s. Although a gap exists in the photometric observations, he suggests a likely relationship between the light variations and the radial-velocity oscillations. Moreover, he gives the light elements of the minima by $JD_{Min} = 2436097.3 + 251.6E$. However, this new period disagrees with the mean period

given in the GCVS (P = 158 days); the changing period is quite evident unless there is a mistake in the GCVS.

Another SRa carbon star, UX Dra, shows a light curve with a marked regularity, alternating one deep and one shallow minimum, which suggests the light curve of a photometric binary (Vetesnik, 1982a). On the other hand, the radial velocity deduced from the C_2 Swan has a half-amplitude of 2.2 km/s and a period of 340 days, which is double the mean period obtained with the light curves. Confirmation by continuous observations is needed.

Referring to 20-year observations in the Geneva photometry, Maeder (1980) gives the V amplitude variations for several SRc supergiants of type Ia, Iab, and II. For a given spectral type, the larger the brightness amplitude, the more luminous is the supergiant; however, Strohmeier (1972) argues that the cycle length has no apparent correlation with the luminosity. This apparent contradiction indicates that a very high quality of measurement is necessary for investigating SR stars. (The Geneva photometry is a good example.) Moreover, Maeder (1980) points out a new observed correlation for the G–M supergiants; for the same amplitude variation, the higher the luminosity, the earlier the spectral type is. Observations of numerous supergiants are necessary to confirm Maeder's conclusions because he has used only three Ia supergiants, nine Iab and three II supergiants of M0–M2 class, and three Iab and two Ib supergiants for spectral classes later than M2. Because the irregular variable stars are generally poorly monitored by ground-based observers, numerous observations are needed to contribute to the understanding of these stars.

Nevertheless, from 24 red supergiant variables in the LMC, Feast et al. (1980) deduce a period-luminosity relation. The measurements of Glass (1979) come close to a theoretical P–L relationship derived from the work of Stothers and Leung (1971).

The satellites hail a new epoch. Maran et al. (1980) demonstrate that VY Leo is clearly an SRa variable with a period of about 1 year, although it was classified Lb in the GCVS. Thus, this star can no longer be used as a normal giant (Wing, 1980). Consequently, it is urgent to use satellites for long series of uninterrupted observations of selected variable stars; such sustained observations will help to point out the various time-scale phenomena involved in these star atmospheres.

Superposition of Periods, Chaos, or Randomness in Light Curves. A primal question is: are the semiregular stars multiperiodic, chaotic, or truly random?

In the last decades, astronomers have mainly developed multiperiodic analysis, and many apparent light-curve irregularities may be explained by a complex mixing of two or more oscillations, each of which is more or less regular and varies independently. Harmonic analysis of the observations must be employed to identify the individual oscillations. RS Gem (SRb, M II) is a representative star, with a secondary variation which is observed as a second maximum progressing along the light curve relative to the primary cycle (Figure 1-19). UZ Per is one of the SRa variables which has been studied in depth over several years; it apparently has three cycles of different length: a short period of 90.8 days, a longer period of 922 days, and a third one which is estimated to be more than 5000 days long (Glasby, 1968).

Variable stars with a double period are more often observed among C stars than among M and S stars. A list of those stars are given in Table 26 of Alksne and Ikaunieks (1971). Values of the ratio of the secondary to the primary periods (P_2/P_1) are quoted in the works of Payne-Gaposchkin (1954b), Houck (1963), and Alksne and Ikaunieks (1971), in which the majority of the stars are SRa or SRb of both M and C classes. We will not discuss it again. Leung (1980) found that this period ratio (secondary to primary) is about 10 for the M supergiants (SRc). Stothers and Leung (1971) suggest two possible explanations for these two periods. First, the primary period is connected to the radial fundamental mode of pulsation, and the long secondary period is tentatively interpreted as the convective turnover time of

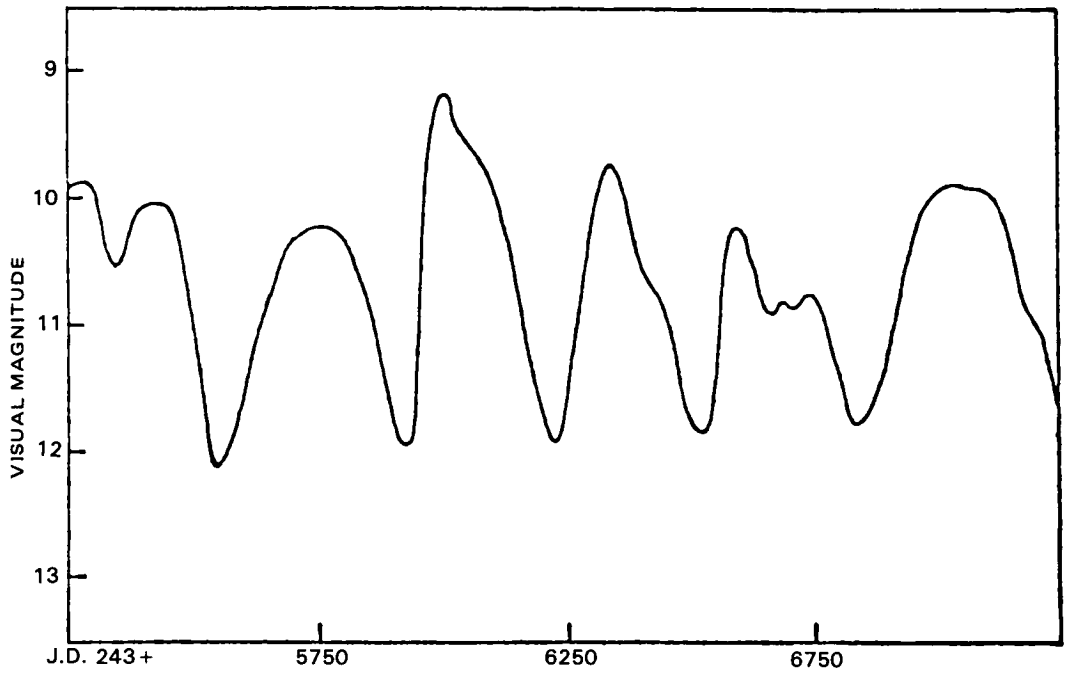


Figure 1-19. Light curve of RS Gem, a typical semiregular variable (from Glasby, 1968).

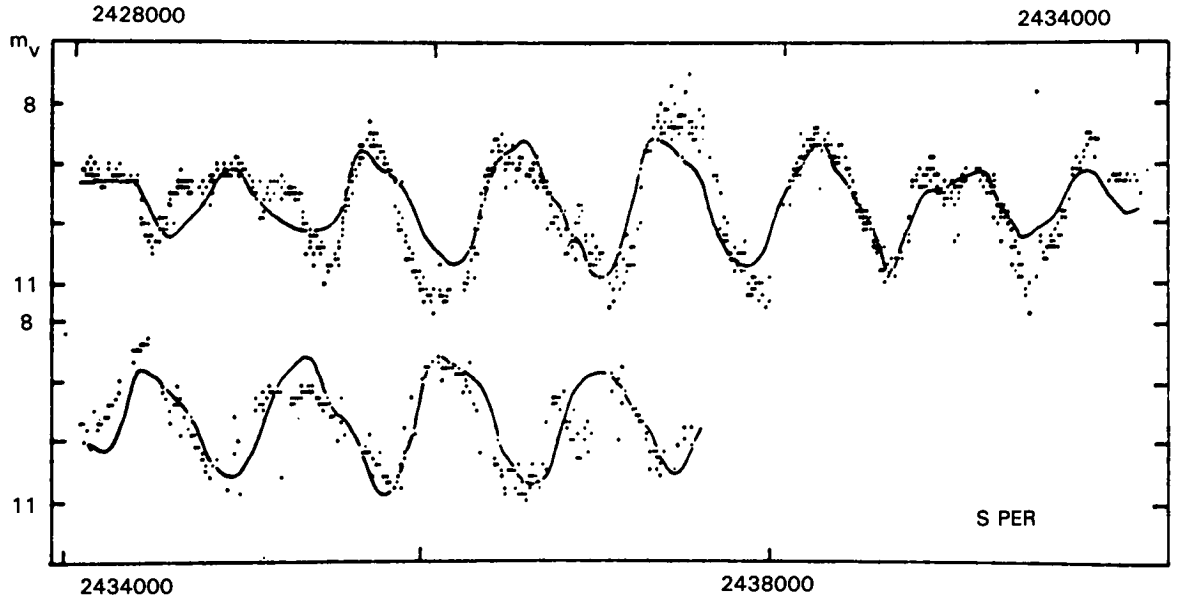


Figure 1-20. AAVSO observations of the supergiant semiregular variable (SRc), S Per. Each point is a mean of 6-day observations. The computed light curve (smooth curve) is based on two period components. The abscissa is in Julian days (from Leung, 1980).

giant cells in the stellar envelope. A second possible interpretation is that the primary period may represent the first radial overtone, while the secondary period may represent the fundamental mode itself. Stothers (1972) prefers the first explanation, while Fox and Wood (1982) argue in favor of the second one and give a period ratio of about 7 (see the section *Modes of Pulsation of Long-Period Variables* and de la Reza, this volume). Figure 1-20 shows the S Per light curve and the computed two-component light curve from Leung (1980).

Nowadays, two other types of physical explanations for the behavior of the semiregular and irregular stars are proposed: the randomness and the chaos. In the randomness process, the events are largely independent of each other, and it is impossible to make accurate predictions of any range of variations with certainty. However, in a chaotic process, which has been mainly analyzed in mathematics and physics, the observed variations reflect the unstable motions which are produced by a collective and cooperative behavior of the matter when some acting forces are largely amplified (Whitney, 1984). Nonlinear equations are used to investigate such behavior.

Here, we make two observational remarks:

1. The analysis of semiregular and irregular variables requires a much longer series of uninterrupted observations than have been done until now; only very few stars (Houck, 1963; Glasby, 1968; Hoffleit, 1980; Leung, 1980) have been monitored to this extent.
2. Although observations of new periods in cepheids or binaries with improved accuracy permit us to obtain more precise quantitative parameters of these stars, the accuracy of the observations on the semiregular stars may determine the nature of the variations amidst the processes described above and may allow us to choose between two competing physical theories (Whitney, 1984). Observations with improved accuracy are crucial for semiregular and irregular stars.

As we know, there are many more irregular variables among the carbon stars than among the M stars. Let us give some examples of semiregular C stars with apparent behavior changes in their light curve, illustrating chaotic variations. First, we quote the SRa star, S Cam. This star was observed from the beginning of the 20th century. Ludendorff (1923) derived a period of 325.5 days and a light amplitude of 2.8 mag from his 1911–1912 observations. Later, Campbell (1941, 1947) and Payne-Gaposchkin (1944) indicate a period of 326.5 days and a light amplitude of 2.5 mag. Nielsen (1952) obtained a period of 324 days. All these results seem homogeneous. However, Mayall (1960a, 1964, 1966) suggests that S Cam light amplitudes decreased to 2.0 mag, and Romano (1950) points out time intervals with constant brightness and other ones *with additional waves* on the light curve. From her 1966–1971 observations, Krempec (1973) deduces a period of 326.4 days and a variable behavior in the light amplitude. During some time intervals, the light amplitude is above 1.3 mag, and during some other ones (presenting very flat minima), the light amplitude is only about 0.8 mag. During the Krempec's observational period (1966–1971), the SRb star, RV Aur, presented regular time variations with a period of 229 days, but the behavior of this star was sometimes quite irregular. UV Cam is another SR star with an apparent period (294 days) and considerable irregularities (Krempec, 1973). U Cam is one of the SRb stars with multiple periods. Payne-Gaposchkin (1944) finds three periods for this star (223, 435, and 3000 days). Kukarkin (1949) confirms the two periods of Jacchia (1933): 419 days (as the period of fundamental oscillations) and a superposed wave of 3000 days. Krempec (1973) shows that the period of 400 days is probable. The light variations were often irregular.

As quoted by Krempec (1973), there is no regularity in the light variations of the SRb star, X Cnc, and the observations give considerably different periods, such as 970 or 365 days. The light amplitude does not exceed a few tenths of magnitude, but Mendoza (1967) and Eggen

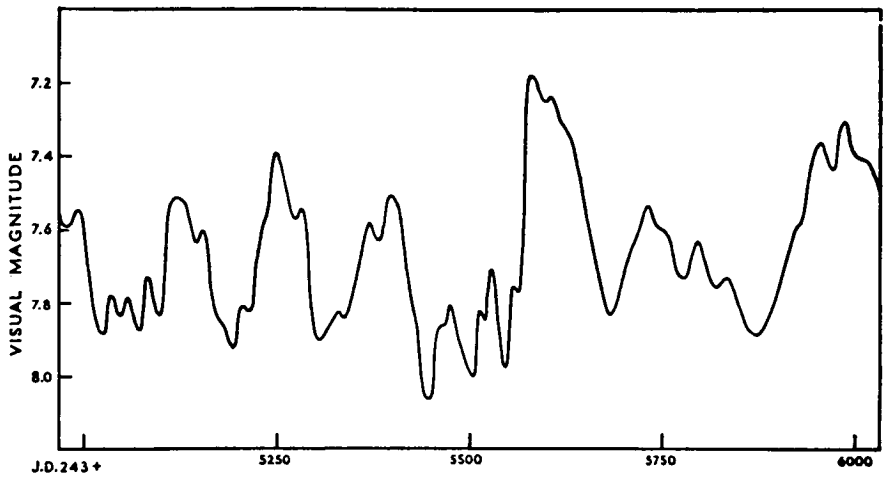


Figure 1-21. Light curve of V Aql (from Glasby, 1968).

(1967) stated that the photometric color index, $B-V$, ranges from 2.9 to 3.4 and 3.0, respectively. Hagen (1925) notes that X Cnc is imbedded in a dark symmetric cloud of size 0°8. This cloud is confirmed by a strong continuous ultraviolet absorption (Mendoza, 1967) and a strong continuous infrared emission (Gillett et al., 1971). TT Cyg, also an SRb carbon star, is an astonishing object; it shows very rapid irregular light variations during the 1923–1924 and 1928–1929 observations of Parenago (1938). During other time intervals, it has a period of 118 ± 18 days (Payne-Gaposchkin, 1944; Krempec, 1973).

To conclude this analysis of the semiregular stars, we emphasize some occasional striking behavior like the one observed by Garcia et al. (1977) on the SRb star, R Dor. On the basis of 455 visual observations, these authors show the occasional appearance of an 8-day harmonic period besides the 332-day fundamental period. At the present time, it is difficult to give a physical explanation to the excitation of the 8-day mode.

The Lb and Lc Stars

Generalities. The Lb and Lc stars, giants and supergiants, respectively, are slowly varying without any trace of periodicity and with small amplitude (<1.5 mag). Deep minima appear at irregular intervals. The light curves seem to be composed by slow waves of varying amplitude. Strohmeier (1972) notes that an extremely weak periodicity occasionally appears.

Some variables are initially classified Lb or Lc and are later shifted to other variability classes as new observations reveal unsuspected periodicity. Therefore, the red irregular stars with unknown spectral class and luminosity are first assigned to the irregular star class while awaiting new observations.

Few such stars are regularly observed by spectroscopy. Even today the presence of Balmer emission lines has not been successfully demonstrated in these variable stars.

Although the Miras of spectral class M are scattered over a large spectral range—M2 to M10—the irregular stars, as well as the semiregulars, are concentrated at M6 and M6.5, with none later than M7 (Cameron and Nassau, 1956); the latest should be RX Boo (M7–M8). Joy (1942) showed that the concentration of irregular M stars occurs at M5 and M6. This discrepancy occurs because a small difference appears between the Mt. Wilson (Joy) and Case (Cameron and Nassau) systems of classification. We must keep in mind that these differences are partially due to the variation of

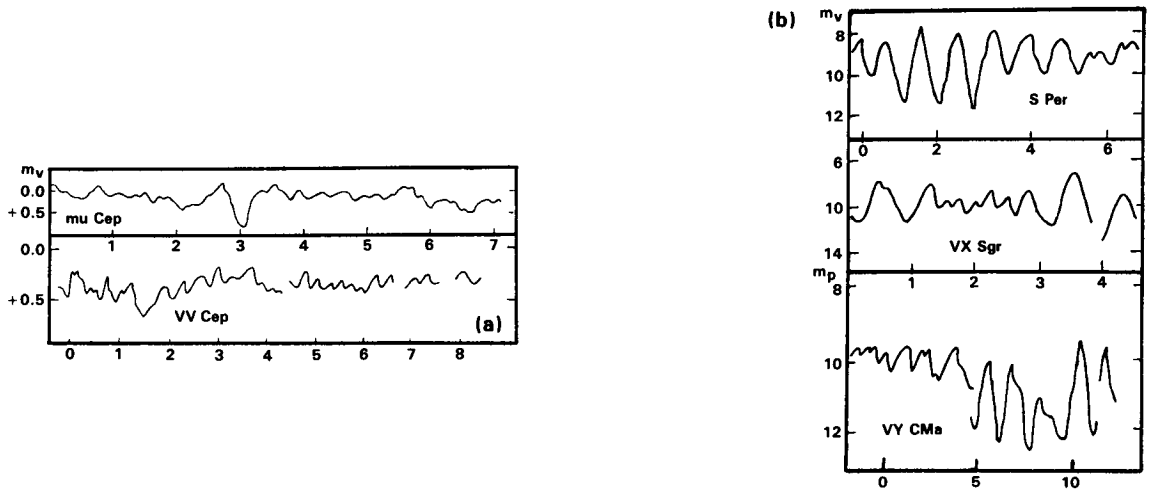


Figure 1-22. (a) Portions of the visual light curves of two supergiant variables of small amplitude. The ordinates are in magnitudes, and the abscissas are in thousands of days from an arbitrary zero-point. Note that the scales for the two variables are not the same. The curve for μ Cep is from Hassenstein (1938), and that of VV Cep is from Fredrick (1960). (b) Portions of the light curves of three red supergiant variables of large amplitude. The ordinates of S Persei and VX Sagittarii are in units of visual magnitude, while photographic magnitudes are given for VY Canis Majoris. The abscissas are in thousands of days from an arbitrary zero-point. The visual light curves are based on AAVSO observations, and the photographic curve was determined by Robinson (1970) from Harvard plates (from Smith, 1976).

spectral class of the star during its light variations. Wilson and Merrill (1942) give a long list of irregular variables with M spectral types. They add two S spectral-type stars: SU Mon and AD Cyg. The stars μ Cep, α Ori, α Her, and α Sco are also classified irregular by Strohmeier (1972). Many M class irregular variables are connected with young O-associations of Population I (Crawford et al., 1955).

The carbon Mira variables are found in the low-temperature C6–C7 subclasses, while the semiregular and irregular variables are chiefly found in the earlier subclasses (Alksne and Ikaunieks, 1971). Typical representative Lb carbon stars are V Aql (Figure 1-21), W CMa, V460 Cyg, U Hya, V Hya, T Lyr, BL Ori, TX Psc, and VY UMa.

In any case, it is generally difficult to decide whether a supergiant belongs to class SRc or class Lc because the time interval between successive maxima is very long. This time varies from a few hundreds to a few thousands of days, and extensive observations are needed before a conclusion can be reached. This raises the question that another kind of distinction between the supergiants must be investigated. Smith (1976) suggests a much more physical splitting among the supergiants: those with small amplitude variations and those with large amplitude variations (Figure 1-22a, b). In the first group, we find μ Cep and VV Cep, the latter being an eclipsing binary. Their mean maximum amplitude is 1.1 mag with a dispersion of about 0.2 to 0.3 mag. The second group includes stars like S Per, VY CMa, and VX Sgr. Using the published line curves of Robinson (1970), Dinerstein (1973), and Smith (1974), Smith (1976) found a mean maximum amplitude of 4.2 visual magnitudes with a dispersion of 1.1 mag among these three stars. The light curves of μ Cep and VV Cep suggest that they have something in common, but they are different from the other three supergiants which are rather inhomogeneously classified in GCVS: S Per as SRc, VY CMa as Lc, and VX Sgr as SRb.

It seems to be necessary to support this division into small and large amplitude variables by studying other stellar properties and observations of other stars. Humphreys (1974) found that the three stars, S Per, VY CMa, and VX Sgr, share a few peculiarities, such as large excess radiation between 0.7 and 1.5 μm and between 1.5 and 8 μm. This last excess has a slope like that of free-free emission in VX Sgr and S Per. Moreover, these stars show absorption-line weakening in their near-infrared spectra, silicate emission features between 10 and 20 μm, and strong OH and H_2O emissions. S Aur and Y Lyn can be added to this group of large amplitude variables.

Among the observed variable supergiants, the number of large amplitude variables is very limited. Then, if we suppose that the supergiants cross through the small and large amplitude phase, we could conclude that the latter phase is very short. Moreover, no theoretical works give any information on the order and the duration of these two phases; only observations on the cluster, h and χ Per, suggest that S Per (large amplitude variable) may lie at the tip of the red supergiant branch in the HR diagram because it appears redder than the small amplitude supergiants of the same cluster (Smith, 1976).

Different Time-Scale Light Variations of Irregular Variables. Visual or photoelectric photometry monitoring of a few irregular stars (e.g., VY CMa, and VX Sgr) indicates that their variations result more from chaotic or random processes than from harmonic processes. This could be interpreted as irregular surface features—spots, loops, or cells—that should have an effect on the light variation larger than have the pulsational effects. Spectroscopic observations in support of random variations in these stars appear in literature. As an example, we quote the variability in the emission lines in the IUE low-resolution spectra of the Lb carbon star, TX Psc, over a 3-year period, reported by Baumert and Johnson (1984). These authors show a probable time variation of the Mg II λ2800 lines by a factor of 3 to 25 and the possible variation of the C II λ2325 line by 25 percent in the spectra of this object. On the basis of these data, Avrett and Johnson (1983) attempted to model a chromosphere for cool carbon stars (see de la Reza, this volume). A monitoring during 4 years (1981–1984) was jointly developed by the Bloomington and Toulouse groups on the low-resolution and long-spectral observations of TX Psc (Johnson et al., 1986). The intensity variations of Mg II, C II, and Fe II emission lines were confirmed with a factor of variability of 6 to 15, 5, and 8 to 80, respectively. Moreover, all the lines appear to vary together. The possible mechanisms for the production of these emission lines are reviewed: shock waves such as in Miras, magnetic fields associated with plages, heating by short-period acoustic waves, and changes in absorbing overlying clouds by their own motion. However, the continuous flux in the long-wavelength spectral range (LWR) is essentially constant. A recent high-resolution LWP spectrum of TX Psc confirms unusual profiles and line strengths for h and k lines. These lines are heavily absorbed by overlying Mg II, Mn I, and Fe I absorption features (Eriksson et al., 1985).

As in semiregular variables, changes in light-curve shapes are observed:

1. Some irregular stars, like W CMi, have an irregular light curve, but during some periods of time, their light curve suggests a regular light period and during other periods a very constant brightness (Krempec, 1973). Some other stars have periodic variations during some intervals of time, and shortly thereafter, are not variable at all. BM Gem is a good example pointed out by Krempec (1973); RX Lep is the typical representative star.

2. Some stars have rapid changes of brightness. Krempec (1973) notes a change of 0.80 mag during 30 days on UY And and "very rapid light variations of the order of a few tenths of magnitude during a few days" on the light curve of SV Cyg.

3. Other stars, such as TT CVn, have a period approximately defined at different epochs (Wendel, 1913; Krempec, 1973); however, during some time intervals, the brightness varies rather irregularly (Krempec, 1973).

Ashbrook et al. (1954) describe the light curve of the SRc–Lc star, μ Cep, by a second stochastic chain. "The light variation is not explicable by a simple pulsation; rather, it may be interpreted as arising from temporary, random surface disturbances on the star." Sharpless et al. (1966) found that the light curve is the result of the sum of periodic terms, with 4836 days of fundamental period. Its light variations have short-period components and at least four different periods between 700 and 14000 days (Polyakova, 1983). By spectral analysis, Mantegazza (1982) shows that the light variation of μ Cep may be explained by the superposition of two periodic terms and their nonlinear couplings, the longer term having a cepheid-like shape. The results of Mantegazza tend to support the second hypothesis of Stothers and Leung (1971; see below) and are in agreement with the theoretical ones obtained by Uus (1976), who demonstrates that some red supergiants are pulsating in the radial fundamental and first-overtone modes.

In general, the Lb and Lc stars have not been sufficiently observed. To have a global point of view of their variations, some of them must be followed individually during many years. However, the analysis of the light curves of many of them should give indications to ascertain if chaotic variations are really possible in the Lb stars. More observations are urgently needed to confirm this suggestion.

Finally, we point out the observations of flares in these stars. In the chaotic point of view of the irregular star variations, flares should represent the shortest time variations. However, they are not really used in the analysis of the star behavior because, at present, a permanent followup is impossible with the conventional telescopes, photoelectric equipment, and adapted filters, which prevent the study of consecutive flares and their correlation with other variations. As an example of flares on such variable stars, we describe the recent event recorded on μ Cep by Arsenijevic (1985). A sudden fast (20-second duration) brightening of 0.034 magnitude on V was observed on August 3, 1981, at 0h 31.9 mn UT, with a standard deviation in the measurements of ± 0.011 mag; simultaneously, a shallow minimum in the polarization position angle appeared. The declining phase was 28 mn long. The similarity of this phenomenon with the red-dwarf flares strongly favors a stellar flare in the supergiant, μ Cep, although the declining phase was longer than in red dwarfs, maybe being correlated with a larger amount of irradiated energy. The flare appeared during the minimum light, such as in the case of the solar ones which are due to a large number of spots at the stellar surface. The total energy irradiated by the μ Cep flare is about 10^{32} joules, fitting flare energies observed in the Sun and in stars.

We also note flare activities in the radio wavelength range, for example, in α Ori and α Sco (Hjellming and Gibson, 1980; see also the section on *Photometric Observations*); they infer the presence of magnetic fields (see M. Querci, this volume).

To conclude the discussion on irregular stars, we mention the light variability of the brightest and the most famous irregular variable star, which has been observed more or less regularly over 60 years—α Orionis.

The M2 Iab supergiant, α Ori (Betelgeuse), was monitored by photoelectric photometry in the visual quite regularly from 1916 to 1931 by Stebbins (1932). Occasionally, Johnson et al. (1966) and Rucinski (as quoted by Goldberg, 1984) have also made some observations. In recent years, Krisciunas (1982) systematically observed α Ori in B and V filters from 1979 to 1982, and Guinan (1984) began measurements (around Hα and in the blue at λ4530) in 1981 that have continued to the present. Besides these data, AAVSO has recorded regular measurements for the last 60 years, and this extensive temporal coverage makes them very useful, especially in the absence of professional works.

However, these data must be viewed with great caution because the scatter is very large in a single measurement. All the above-quoted data are shown on Figures 1 and 3 through 5 in Goldberg (1984) and on Figure 2 (upper panel) in Guinan (1984). The characteristics of the α Ori light curves, particularly clearly seen on Guinan's Figure 2, are long-term light variations with a period of about 5.78 years, and with a mean amplitude of about 0.4 mag, and short-term irregular variations with rise or decline time scales of a few weeks to some months superposed on the long-term periodic light variations. The following systematic trends are noted:

1. 1916–1931: Stebbins (1932) found a period of 5.4 years after the use of a drastic smoothing process which cancels all the short-term fluctuations (see his Figure 1). From radial velocity data, Jones (1928) and Sanford (1933) obtain a period of 5.78 years.
2. 1934–1938: The photoelectric data of α Ori show no evidence of periodicity, the points scatter widely, and the radial velocities are not connected to the 6-year period throughout the period of Adams's (1956) observations: 1937–1947.
3. 1939–1965: The brightness variations seem to follow the 5.78-year period and between 1949 and 1961, a phase lag relative to the mean curve previously found by Stebbins (1932) seems to be observed.
4. 1965–1975: Random variations on brightness and radial velocities appear again.
5. 1975–1980(?): The 6-year period was followed surprisingly well by the radial-velocity measurements of Boesgaard (1979) and Goldberg (1979).

Moreover, short-lived abrupt drops in brightness are evident in 1926, 1934, 1942, 1943, 1947, 1951, 1971, 1974, and 1981 and very short time variations appear in the 10-μm region; the intense infrared emission surrounding α Ori varies in shape, size, and intensity from night to night during September and December 1966. The stars μ Cep and α Tau have the same behavior (Low, 1965).

As noted by M. Querci (this volume), the atomic lines giving the radial velocities are not listed in the text of some of the papers mentioned above. Consequently, we suppose that the lines used are from various excitation potentials (i.e., from atmospheric layers of different behavior). Therefore, many possible correlations between the radial-velocity variations and drops or declines of brightness in large bandwidth filters, like UBV, cannot be fully inferred and exploited because we are unable to locate the layers from which the light variations come. Some examples of such unexploitable data are:

1. Between Julian days 2424538 and 2424598, the radial velocity decreases by nearly 4 km/s, while the brightness increases by 0.2 mag in the same time (visual brightness). After 200 days, the radial velocity was found to be lower by 3.5 km/s and the brightness was also declining during this time.
2. On Julian day 2431400, α Ori suffers a steep drop in radial velocity, followed some days later by a fall in brightness by about 0.6 mag. Goldberg (1984) argues that this rapid change takes place soon after the minimum of the "mean velocity curve" like the changes seen in 1925, and shows that some other large disturbances follow the two velocity minima of 1972 and 1978.

During the short-term variations, the change on the linear polarization of the visible light variation varies with the same time scale as the brightness. This suggests a high degree of asymmetry and a local origin in the features involved in these variations (Tinbergen et al., 1981). Hayes (1981) suggests that the change of polarization follows the formation and growth of the local features on the surface of the star (lower chromosphere) and progressive changes

in their orientation. Viewing the entire phenomena described by Goldberg (1984), it seems "equally possible that a sharp drop in radial velocity was accompanied by an initial brightening followed by rapid fading," which can be explained by a gaseous matter ejected from the star which diffuses and condensates into grains and becomes optically thick in the visible region (Goldberg, 1984).

To conclude, it appears that the long-term light variations probably arise from the radial pulsation of the star, the short-term variations having been believed to be caused by large-scale photospheric convective cells (Schwarzschild, 1975). Hayes (1982), Goldberg (1984), and Antia et al. (1984) favor such an explanation, the two first authors for explaining polarization changes. However, Roddier and Roddier (1983, 1985), Petrov (1983), Roddier et al. (1984), and Karovska (1984) argue against it (see M. Querci, this volume), and Guinan (1984) notes a lack of correlation between the short-term variations in the TiO band strength and the short-term light changes. This fact suggests that "the mechanism responsible for the short-term light enhancement is not linked to temperature increases as would be expected from ascending giant convective cells... and that the brightness enhancements are produced above the stars's surface."

The problem might be resolved if the recently claimed companion objects to α Ori are confirmed. That circumstance would also seem to explain some variations in chromospheric emission-line radial velocities, as well as circumstellar dusty clumps (see M. Querci, this volume). (Anecdotally, Bottlinger (1910) mentions α Ori as a binary star for which he finds a 6-year period. Other authors (Wilson and others) as reported by Karovska (1984), also classified α Ori as a binary star.)

Eruptive Variables: The RCB Stars

Generalities. The main characteristics of the eruptive RCB stars are the abrupt drops in brightness, followed by a longer climb back to normal light, probably due to the sudden ejection of highly absorbent matter. They are occasionally thought to be the progenitors of type I supernovae (Wheeler, 1978), novae (McLaughlin, 1935), planetary nebulae (Webster and Glass, 1974), or helium stars (Tutukov and Iben, 1985), and white dwarfs (Schönberner, 1977).

In 1795, E. Piggott discovered the variability of R CrB, the prototype of the well-known RCB stars. In the southern hemisphere, a few random observations of RY Sgr have been made since 1751 (Lacaille, 1847). From 1895 to 1908, the brightness of UV Cas dropped twice by 1 to 1.5 mag (Florya, 1949); its variability was recognized with the 4-mag fall of 1913 (Shenavrin, 1979). Innes (1903, 1907) published the first series of observations of some RCB stars. After monitoring R CrB for several years, Sterne (1935) concluded that this star is a "perfect irregular" with its visual variation from 5.8 at maximum to 14.8 for the deepest minimum, whereas the light of SU Tau falls almost annually.

As in the other variables, the spectral type of the RCB stars changes during their brightness variations, and accordingly, changes in the spectra and colors of the RCB stars are noted. The latter are extremely complex because the star waxes and wanes. A general behavior of the stellar spectrum during one of the abrupt drops in brightness and recovery may be described as follows, mainly on the basis of R CrB and RY Sgr observations.

At maximum, the spectrum is very similar to that of a supergiant of spectral type F or R, with narrow and sharp absorption lines, the main differences being in the weakness or absence of the Balmer lines and in the strong lines due to carbon. The cooler stars have strong molecular absorption bands of CN and C_2.

As the star dims, we continue to see the absorption spectrum, but it is veiled. However, in general, the molecular spectrum becomes more and more intense as the minimum is reached. There is a *sharp* emission spectrum which appears during the fall and suffers

gradual changes. Some of these narrow emission lines sometimes replace the atomic absorption lines (Herbig, 1949). First, the sharp lines of Fe II appear (Payne-Gaposchkin, 1963). As the fading continues, the spectrum becomes dominated by Ti II lines. Occasional anomalies are detected. For example, Alexander et al. (1972) found the same intensity for the two Sc II lines at 4354.61 and 4320.75 Å as in the laboratory. Spite and Spite (1979) showed that, in the next drop of RY Sgr, the 4354.61 Å line has disappeared and the 4320.75 Å line is approximately 500 mÅ. In general, this sharp emission spectrum is slightly displaced to the blue (3 to 10 km/s) relative to the absorption lines at maximum. Its intensity increases rapidly during the initial part of the drop and then grows weaker as the star continues to fade. It is likely produced by an expanding region (chromosphere or large envelope), with decreasing expansion as the star approaches minimum. In the decline of RY Sgr during 1977, Spite and Spite (1979) note that the narrow emission lines and the absorption lines of the atmosphere itself have the same radial velocity. The behavior of this emission spectrum is apparently not related to the absolute magnitude of the star (Feast, 1975), but seems to depend on the time from initial decline (Payne-Gaposchkin, 1963). During the 1948 minimum of R CrB (Herbig, 1949), only the second part of the narrow emission spectrum was seen (Ti II). Perhaps this is connected to the observed low initial rate of decline.

A very *broad* emission spectrum appears some days after the brightness begins to fade (40 days in the case of R CrB in 1948 and 70 days in the case of RY Sgr). In the spectrum of R CrB, the lines of He I 3889, Ca II H and K, and Na I D appear with different widths (Rao, 1975). Using narrowband filters, Wing et al. (1972) discovered the presence of a strong He I 10830 emission line during the minimum of R CrB. As the minimum progresses, the profile of these lines changes, and the intensity remains constant at first, then increases, and finally decreases. In the spectrum of the cooler RCB stars, these broad emission lines are sometimes accompanied by absorption components with velocities of -250 to -130 km/s (Querci and Querci, 1978; Rao, 1980b). (See M. Querci, this volume, for details on observations of the He I 10830 Å line in red giants and the implied constraints to future modeling.) Because the UV spectrum fades much less than the visible and red spectrum, additional sources of emission shortward of 4000 Å have to be taken into account. As the star approaches minimum light, the relative intensity of the emission lines of each element changes gradually (implying variations in the conditions of excitation). Also, a variable polarization with variable wavelength dependence is observed in stars like R CrB and RY Sgr (Serkowski and Kruszewski, 1969; Coyne and Shawl, 1973). At the end of minimum phase, P Cygni profiles develop (Payne-Gaposchkin, 1963; Querci and Querci, 1978; Rao, 1980b). The bands of CN are observed in emission at this time (Wing et al., 1972). Seeds and Ignatuk (1973) have shown changes in strength of the C_2 emission bands in the R CrB minimum. These changes are probably due to the filling in of the photospheric absorption bands by chromospheric emission. Taking into account the numerous atomic lines in the violet, the chromospheric contribution to the total observed light increases to shorter wavelengths; consequently, the dependence of polarization with wavelength is not linked to the particle size only.

As the star brightens again, the absorption lines gradually come back, while the emission spectrum fades with a varying rapidity in the various lines. Finally, the maximum spectrum is reached approximately 2 magnitudes before the light maximum itself; in R CrB, Rao et al. (1981) observe h_3 and k_3 Mg II components, which demonstrate that this star also has a continuous mass loss during the maximum light through a permanent chromosphere (Payne-Gaposchkin, 1963; Rao, 1974, 1975).

Can we draw a coherent qualitative modeling of the RCB phenomenon?

Many models have been proposed during the past 20 years. Payne-Gaposchkin (1963) suggested that the particles are formed in the

upper photosphere of the star, because the emission lines observed at minimum light are not themselves obscured. Wing et al. (1972) propose that there is a quasi-permanent blotchy cloud orbiting around the star. Humphreys and Ney (1974) associate the particle cloud with the atmosphere of a probable cool LPV companion. These last two models are attractive, but pose problems in so far as they fail to explain why the decline is rapid and the rise is slower.

Nowadays, it appears that the initial hypothesis of Loreta (1934) and O'Keefe (1939), in which the light minimum of the RCB stars is due to dust obscuration, gives the best account of the observed features. Feast (1979), sustaining this basic model of ejection of thick dust clouds, explains how it might act. The gas is ejected at the top of one or some of the large convective cells, and it crosses the deeper layers of the star's atmosphere. This ejection is made radially through a fairly large area of the stellar surface in a semiangle of $\sim 20°$ and roughly at 20 km/s. If the material is ejected along our line of sight, a major visual luminosity minimum occurs, whereas, if it is ejected at an angle to our line of sight, it causes a minor minimum (e.g., Forrest et al., 1972). The gas expands and cools, and the graphitic carbon condenses. The resultant dust clouds expand and cause an eclipse which allows the chromospheric sharp lines to be seen. The particles move away by radiation pressure. When the new cloud collides with the circumstellar shells, strong and broad emission lines are produced. Because the speed of the collision is greater than the escape velocity, the matter is: (1) partially ejected in space with a drop in density and in optical depth of the medium causing the emission lines to fade, (2) partially replenishing the circumstellar patchy envelope of dust and gas, giving rise to the infrared excess observed in some RCB stars (e.g., in RY Sgr and R CrB). Recent IUE data confirm the Loreta-O'Keefe cloud ejection model and are consistent with the dust to be composed of carbon (Hecht et al., 1984). In addition, they show that 5 to 60 nm glassy or amorphous carbon rather than graphite is formed around the RCB stars.

It is now worth turning to some observations that argue in favor of this model and complete it.

Patterson et al. (1976) showed that their spectrophotometric measurements made on different nights during the R CrB climb in 1974 were consistent with extinction of particles that they thought to be spherical graphite ones of about 0.07-μm radius, expanding by radiation pressure. No variations of the particle size were detected.

Orlov and Rodriguez (1974, 1981) find a microturbulent velocity of 8.9 km/s in XX Cam and 11 km/s in UV Cas, which supports the idea suggested by Howarth (1976) that the initial condensation may be due to turbulent motions (seed creation).

Forrest, as quoted by Rao (1980a), points out that the extinction during the decreasing light tends to be neutral without any color changes, but that the colors redden during the climb back to maximum. Using these confirmations and the electron pressure computed from the broad emission lines, Rao (1980a) suggests that the gas that produces these broad emissions also produces the neutral extinction by electron scattering during the decreasing light. The grains appear later, and the circumstellar shell is replenished by ejecta at minimum light. Consequently, the light from the photosphere is obscured, and the chromosphere (Payne-Gaposchkin, 1963; Alexander et al., 1972) or the circumstellar gas shell (Hartmann and Apruzese, 1976) is the obvious source of the narrow emission spectrum. As pointed out by Herbig (1949), the emitting gas has a relatively low level of excitation.

The radial velocity of the chromosphere is the same as that of the star itself (Spite and Spite, 1979). When the emission region is suddenly cut off from its source of excitation, it would be an ideal place for the production of an electron recombination spectrum. Feast (1969) suggests that the CN molecule is reasonably abundant in these stars and that its spectrum has a longward edge at 4000 Å. This could explain the blue and UV continuum anomalies by: $CN + e \rightarrow CN^- + h\gamma$. The

emission excess on the V band observed by Shenavrin (1979) on UV Cas tallies with this explanation. Moreover, this model supports the changes in the wavelength-dependent polarization, showing that different particle sizes exist successively.

As noted above, some RCB stars have an excess of infrared. The first observations are recorded by Stein et al. (1969), who find the infrared emission much brighter than the expected emission from the star itself, and who conclude that 40 percent of the star's total luminosity is in the infrared; Shenavrin (1979) finds 60 percent for SU Tau. An excess of infrared is also found by Lee and Feast (1969) in RY Sgr. However, XX Cam and UV Cas have no infrared excess at all (Shenavrin, 1979; Rao et al., 1980), and sometimes R CrB does not have any IR excess during some minima, as in 1972 (Rao et al., 1980). Either the physical conditions are not favorable for grain formation in XX Cam and UV Cas or these stars are between the RCB and the nonvariable HdC stars. To explain the infrared emission, Herbig (1949) believes that grains have to condense far from the stellar surface, whereas Maron (1974) suggests the following way: the freshly ejected particles could have the form of "Platt" particles of 3 to 30 Å; they would absorb the visible radiation better than graphite particles but would not reradiate in the infrared. Then, these particle grow by accretion up to sizes between 10^{-6} and 10^{-5} cm (the classical grain nuclei size). Therefore, the occurrence of the infrared emission waits for the growth of the particles. This growth period is a function of the physical conditions in the shell, mainly low density and velocity of escape, which vary from minimum to minimum.

The broad emission lines which are observed after the beginning of the decline are due to matter which is ejected at high velocity and collides with the circumstellar envelope material with a phase lag of 30 to 70 days. From the radial velocity of the circumstellar lines and this phase lag, we conclude that the shell of gas and grains is at about 4 to 8 A.U. from the star. This agrees more or less with Lee and Feast (1969), giving 5 to 10 A.U., and with Pecker (1976), giving a dust-cloud envelope of approximately 350 R_* at the IR maximum brightness to 600 R_* at the minimum. Moreover, Pecker estimates the total mass of the envelope to 5.10^{-7} solar mass. The broad emission lines are noted violet-displaced by Payne-Gaposchkin (1963). However, during the end of the decline of RY Sgr observed by Spite and Spite (1979), the broad emission lines seem slightly displaced to the red relative to the star. (They extend from -100 to +240 km/s.) This last observation is explained by an ejection of matter in which only a small amount is ejected toward the observer and a larger one is ejected backward. Wdowiak (1975) assumes that 10 to 100 convection cells are responsible for the formation of dust blobs that are ejected by radiation pressure. Rao (1980a) indicates that the broad emission lines are formed in a gas with Ne $\approx 10^{11} - 10^{12}$ per cm^3 and Te $\approx 10^4$K.

High-velocity shells and/or clumps are observed in MV Sgr at -200 km/s with a temperature of 800 to 900 K (Krishna Swamy, 1972), although the star has a hotter shell about 1300 K (Feast and Glass, 1973).

The presence of the circumstellar shell in some RCB stars is also pointed out by IRAS. It discovers a bimodal distribution of RCB stars: (1) the majority of the RCB stars have a flux such as $F_\nu \sim \nu^{1.6}$; they have an IRAS spectrum that can be understood as the spectrum of a star with a constant ejection rate of dust where the emission is proportional to the frequency (Schaefer, 1985); (2) a fifth of RCB stars exhibit a qualitatively different IRAS spectrum with a flux such as $F_\nu \sim \nu^{-1}$ and a peak flux at 100 μm or beyond; they are brighter than the majority of the RCB's. Their IRAS spectrum is undistinguishable from normal planetary nebulae (known to have a large amount of dust at a great distance from the central star (Schaefer, 1985)). This fact is in agreement with one of Iben and Tutukov's (1984) evolutionary scenarios that place the RCB stars in planetary nebulae.

Light Curves. Surprisingly, the RCB stars are the only class of eruptive variables for which

maximum brightness is the normal state. The duration of this state is variable (up to several years). In addition, epochs exist in which the full maximum is not reached. For example, from 1898 to 1948, XX Cam had only one minimum in 1939–1940 (Yuin, 1948); R CrB gave flat maxima from 1925 to 1935, 1936 to mid-1938, 1953 to 1956, 1969 to 1972, etc. The latter also shows a series of minima without full maxima being reached in the 1860's (Mayall, 1960b) and from mid-1962 to 1965. Howarth (1977) defines fades and minima, respectively, "as an initial drop of one magnitude from maximum" and "a fall of one magnitude relative to local sub-maxima." The events appear to obey Poisson's statistics. For R CrB and SU Tau, the mean intervals between minima are 532 ± 57 and 625 ± 104 days, respectively, and between fades, they are 1026 ± 156 and 1140 ± 220 days, respectively. The cooler star, S Aps (R3), has a mean time between fades of 1249 days (Howarth, 1976). This should suggest a trend of decreasing activity with later spectral type. However, observations of more stars are needed to confirm this correlation.

The speed of the decline has also been investigated. In R CrB, Oberstatter (1972) points out a drop of 0.5 visual magnitude per day during the 1972 decline; amateurs have observed 0.3 visual magnitude per day during the decline in 1983 (Proust and Verdenet, 1983), while the "normal" fade is about $dm/dt \approx 0.1$ mag per day (Howarth, 1976).

The amplitude, the frequency, and the duration of minima are unpredictable. The declines are much more abrupt than the rises to the maximum. However, the shape of the decline and the rise is not the same for each minimum of the RCB stars; sometimes, "a star may rise halfway to maximum only, to fall again to an even deeper minimum" (Howarth, 1976). This could be caused by many ejection centers.

Superposition of Light Curves. Different timescale variations are very well defined in the RCB variable stars. They are:

1. The unpredictable decline of many magnitudes (already described) called "obscurational" minimum.
2. The semiregular oscillations with a visual amplitude of 0.2 to 0.4 magnitudes and with a pseudoperiod between 19 and 120 days according to the star, called "pulsational" oscillations.
3. The very short nonpermanent oscillations with a time scale of 1 or 2 hours detected in some RCB stars and probably originating from the star itself.
4. A long-term periodicity in the infrared excess, perhaps due to a natural pulsation of the circumstellar dust shell.

Semiregular oscillations over a 38.6-day period were detected by Jacchia (1933) on RY Sgr. Many observations of RCB stars reveal that these small fluctuations appear at each phase of the variation cycle (Bateson, 1978). Mendoza (1978) detected them photometrically in Hα and OI (λ7774) filters. Pugach (1977) concludes from observations of RY Sgr that these pulsational variations do not depend on light fading. First, these oscillations are observed during the brightest, largest observable phase (i.e., the maximum). Fernie et al. (1972) report a visual variation of R CrB with an amplitude of 0.15 mag and a period of 45 days. Totochava (1973a) confirms this amplitude variation, but deduces a variation period of 40 days from her 1971–1973 observations. Alexander et al. (1972) confirm the oscillations of RY Sgr with a 0.5-mag average amplitude and a 38.6-day period observed by Jacchia (1933); the light and color curves (Figure 1-23a, b) show smooth variations: $\Delta V \approx 0.5\,\Delta(B-V) \approx 0.3\,\Delta(U-B) \approx 0.5$ mag. Sherwood (1976) finds tentative periods from 19 to 54 days for some RCB stars and a period greater than 90 days for S Aps, whereas Waters (1966) suggests 120 days and 0.3 mag of amplitude variation for this star. Later, Kilkenny and Flanagan (1983) find evidence for a rapid period decrease, and Kilkenny (1983) shows that S Aps changes from the 120-day periodicity (present in 1960) to one near 40 days (around 1971). Bateson and Jones

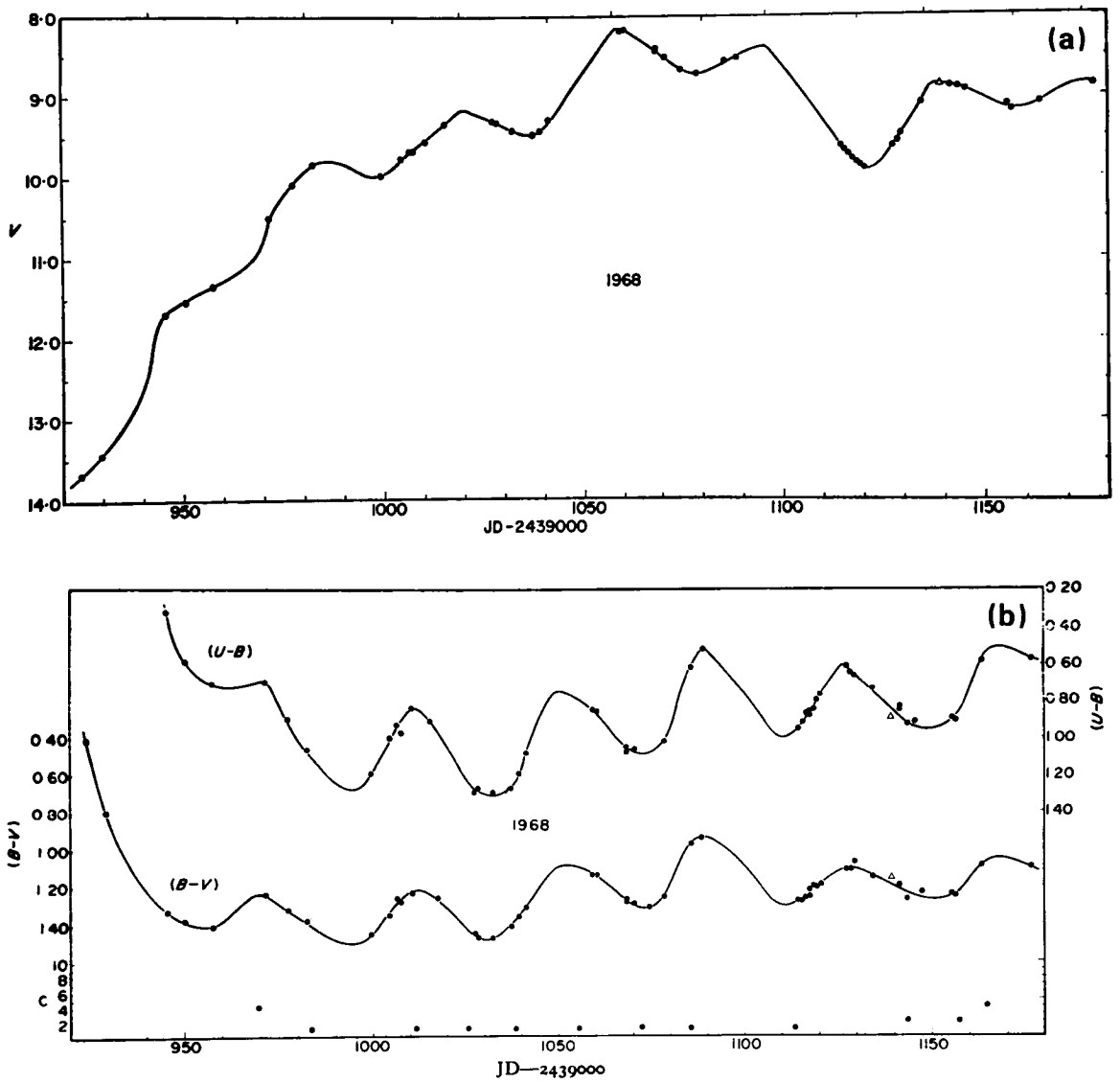


Figure 1-23. RY Sgr (a): V light curve for 1968 plotted against JD. The open triangle is an observation from Lee and Feast (1969). The predicted maxima and minima in V are shown at the top of the diagram. (b): (U-B), (B-V), and spectral classification for 1968 plotted against JD. The same remarks as stated previously apply for the open triangles, maxima and minima. For the spectra, absorption (C) types are shown by filled circles (from Alexander et al., 1972).

(1972) find such semiregular variations in two stars, UW Cen and GU Sgr, with 0.5 mag and 42 days and 0.4 mag and 38 days of amplitude and pseudoperiod, respectively. (See the section *Irreversible Changes in HdC Stars* for details.)

During the deep decline and the rise to maximum, R CrB also has semiregular oscillations with a time scale of 40 days (Oberstatter, 1972). Isles (1973) confirms that this star occasionally displays oscillations, the amplitude of which decreases as the star brightens. Another RCB star, RY Sgr, shows oscillations during the climb back to maximum, similar to those detected during its maximum; these oscillations

support the idea that no major physical changes took place in the star itself during the minima. The greatest amplitude of the UW Cen variations seems to be when the star is brightening (Bateson and Jones, 1972); it persists along the light curve except during the sudden falls to deep minima (Bateson, 1972). During maximum light, XX Cam varies with the same amplitude as that of R CrB, but the period of the former is more or less shorter than those of the latter (Totochava, 1973b). The light, color, and radial velocity of the RCB's demonstrate that these stars pulsate.

Research on light fluctuations with a smaller time scale requires continuous observations of the light. Herbig (1967) reports that Miskin observed rapid oscillations in R CrB near minimum, but very high frequency pulsations in R CrB were not detected by Horowitz et al. (1971) in 1969. Interesting observations were also made by Totochava (1975) on XX Cam from 1972 to 1974. At first, Totochava conducted her observations with a single-channel photometer, alternatively in U, B, and V. Some variations appear in the yellow filter, with an amplitude of about 0.1 mag over several minutes. Fluctuations alternate with quiet stellar phases (e.g., no light variations are observed during the 1973 autumn). The observations are simultaneously obtained with a three-channel spectrophotometer in the following ranges: 3350 to 3650 Å, 4155 to 4280 Å, and 5120 to 5320 Å. The observed curves obtained in this way show several synchronous fluctuations in the violet and blue regions during certain nights (Figure 1-24a, b). The amplitude of the UV fluctuations are a little larger than in the blue; they amount to approximately 0.1 mag and last for about 2 hours. During a period of several nights, the fluctuations become much less visible in all the colors. At the quiescent phase of XX Cam, Kolotilov et al. (1974) find interstellar polarization characteristics, but a higher value of P than

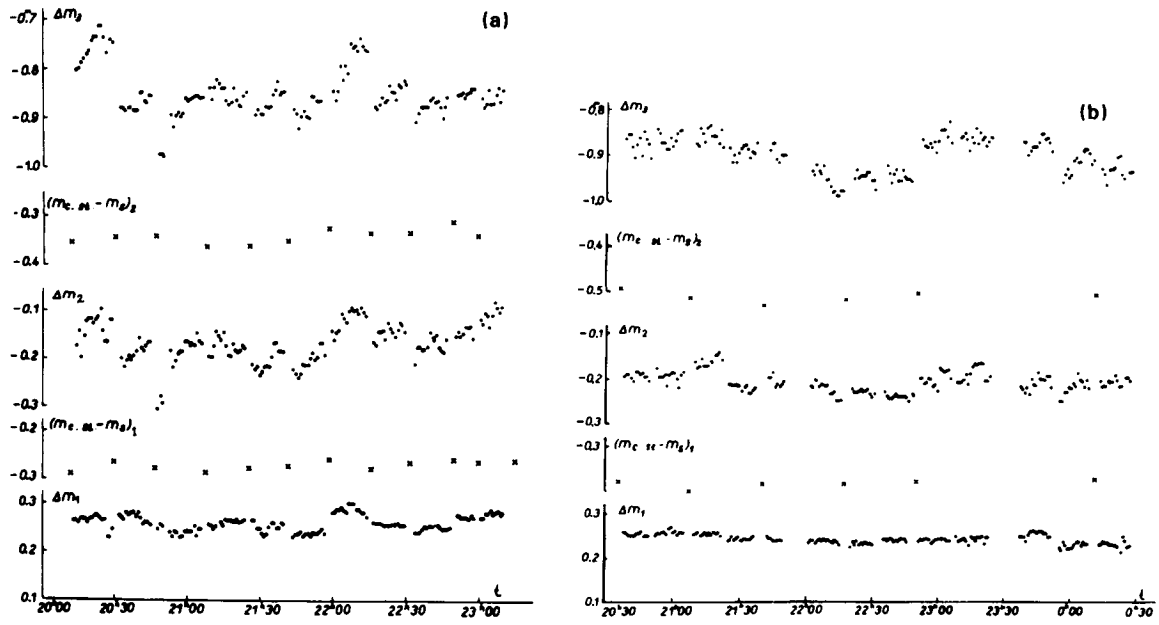


Figure 1-24. Light curves of XX Cam obtained from simultaneous three-color observations (see text): (a) on December 23–24, 1973, where the fluctuations are visible only on the violet (top) and blue (middle) curves; (b) on February 15–16, 1974, where the fluctuations are visible in the three colors. The crosses show the difference between the reference stars (from Totochava, 1975).

for neighboring stars, suggesting that an intrinsic polarization of the star makes some contribution.

Following R CrB itself, Humphreys and Ney (1974) and Strecker (1975) observed a smooth variation between 1.4 and 3.0 mag at L (3.5 μm) with a pseudoperiod of about 1100 days. (The monitoring was done only between JD 2440000 and 2442360.) In RY Sgr, besides the 38-day variation, Feast et al. (1977) also detected a long period variability at L, which is related to the variation of the star itself. They found a long-term change of 1.5 mag, but the period was not well analyzed for lack of observations. Feast and Glass (1973) and Feast (1975) show how the star can make only a minor contribution at L, and Feast et al. (1977) testify that 70 to 80 percent of the L flux is due to the infrared excess (in the case of RY Sgr), with an estimated dust shell radius of 5 to 10 A.U. (Lee and Feast, 1969). "It seems natural to suppose that this is due to pulsation of the circumstellar dust shell itself" (Feast et al., 1977).

It is useful to remember that Bergeat and Lunel (1980) state that "the contribution of shell emissions to the J values is usually small" for the Miras, SR, and L stars, while Walker (1980) concludes that there is no evidence of dust thermal emission in the near infrared for most of the N-type irregular variables, and Tsuji (1981c) uses the L flux for his temperature-effective determination of SRb and Lb carbon stars. Consequently, although the C spectral type Mira, SRb, Lb variables, and the RCB stars are all carbon stars, the effectiveness of the circumstellar dust shells is very different at L wavelength among them.

Additional observations are required to improve our knowledge of the RCB circumstellar dust shells. For example, the phase lag between V, I104, and L magnitude curves could help us to define the thickness of the envelope. Some cool variable stars with extensive dust shells have already shown such long-term variability.

Correlations Between Observed Quantities. The observations of the RCB stars at different epochs indicate that, in general, the infrared excess compensates for the loss of light in the visible and UV wavelengths (Alexander et al., 1972); however, this is not true for all the stars.

The oscillations of brightness of RY Sgr during the climb back to maximum, and during the maximum itself, are correlated with the radial-velocity variations of the absorption lines (Figure 1-25) and have 38.6 and 39.0 days of period, respectively (Alexander et al., 1972), confirming that RY Sgr pulsates as a helium star of two solar masses.

The emission lines of RY Sgr do not have the same behavior pattern as the absorption lines (Alexander et al., 1972). We are not able to decide whether the emission lines follow the 38.6-day pulsation or not; large differences on radial velocity between absorption and emission lines are nevertheless observed.

Pugach (1977) found that the beginning of the obscurational decline appears between phases 0.24 and 0.37, and he chose the origin φ_0 of the pulsational phase φ at the minimum light of pulsation. If we suppose that these pulsational oscillations are roughly sine waves and if we change the origin φ_0 to the maximum, we see that the beginning of the obscurational decline is around the phases 0.74 and 0.87. This reminds us of the famous phase 0.8 of the Mira variables. Can we conclude that the obscurational decline is a result of one pulsational oscillation being stronger than the others? Pugach (1977) concludes that "the serial number of cycles when declines occur, is probably accidental," which seems erroneous today. For the decline of RY Sgr in 1967, the pulsational phase of the drop of light does not confirm the Pugach phase. Howarth (1976, 1977) notes that "the 1967 fade of RY Sgr took place at the time of minimum of the secondary variation."

The occurrence of pulsational minima in RY Sgr can be well represented by a quadratic solution of the cycle number n ($JD_{min} = T_o + nP_o + n^2k$). The (O-C) residuals are shown in Figure 1-26a. The value of k is $\sim(-51 \pm 2) \times 10^{-5}$ day per cycle. This value is in agreement with theoretical models for the evolution of

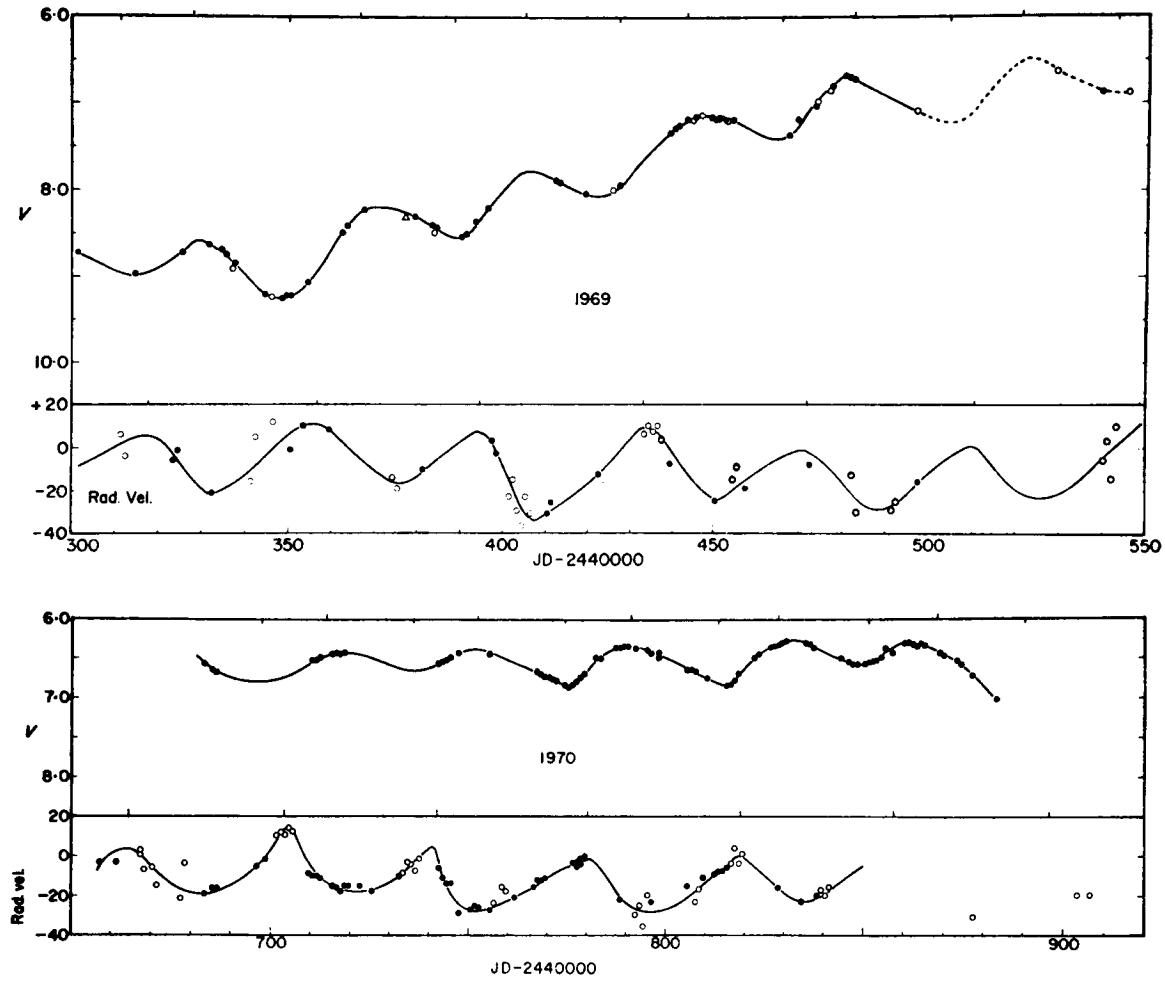


Figure 1-25. RY Sgr (a): V light curve and radial velocity (km/s) curve during the rising of 1969; (b): during the maximum of 1970. Predicted maxima and minima in V and predicted maxima in radial velocities are marked above the curves (from Alexander et al., 1972).

HdC stars (Schönberner, 1977). The comparison of the RY Sgr light curve (Figure 1-26b) and the depth estimates of pulsational minima observed on the same time scale (Figure 1-26c), shows that the deeper pulsational minima tend to occur on or near rising branches of the obscurational minima.

Bateson (1972) has noted a similar effect on UW Cen. This behavior remains unexplained (Kilkenny, 1982). Forrest et al. (1972) were the first to stumble on one of the most important clues to the RCB phenomenon: when the star drops into the deep minimum, the infrared excess is not affected (no change in the emitting flux of the dust shell and no change in the phase of the *L* curve; Figure 1-27). The envelope and the atmosphere of these stars seem to be dynamically disconnected. This restricts the model of obscuration, and Hartmann and Apruzese (1976) suggest that the dust is formed above a small region of the stellar surface and is blown away by the radiation pressure. Consequently, comparative studies of the visible and infrared light curves come to the same conclusions as those of the foregoing investigations. Glass (1978) argues in the same vein

about the 1975/1976 visual minimum of S Aps: when J, mainly due to the star itself, drops to minimum, L is not so strongly affected.

There is a pressing need to summon observers' help in making observations during light fades of different amplitude and duration to find correlations between observed features and to conclude which parameters are linked together and which are not.

Nonvariable Stars

After this extensive review of all the types of cool variable giants and supergiants and their probable connections with white dwarfs, planetary nebulae, or supernovae, we have to discuss stars which—though located in the same area of the HR diagram as the red variables—are surprisingly mentioned as nonvariable or normal stars.

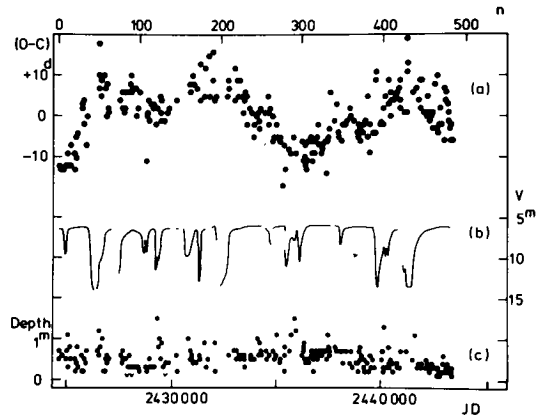


Figure 1-26. RY Sgr (a): (O–C) residuals from the quadratic formula of the pulsational minima plotted against cycle n and Julian date for ephemeris with decreasing period; (b): sketch occurrence of obscurational minima on same time scale as (a); (c): estimates of depths of pulsational minima on same time scale as (a) (from Kilkenny, 1982).

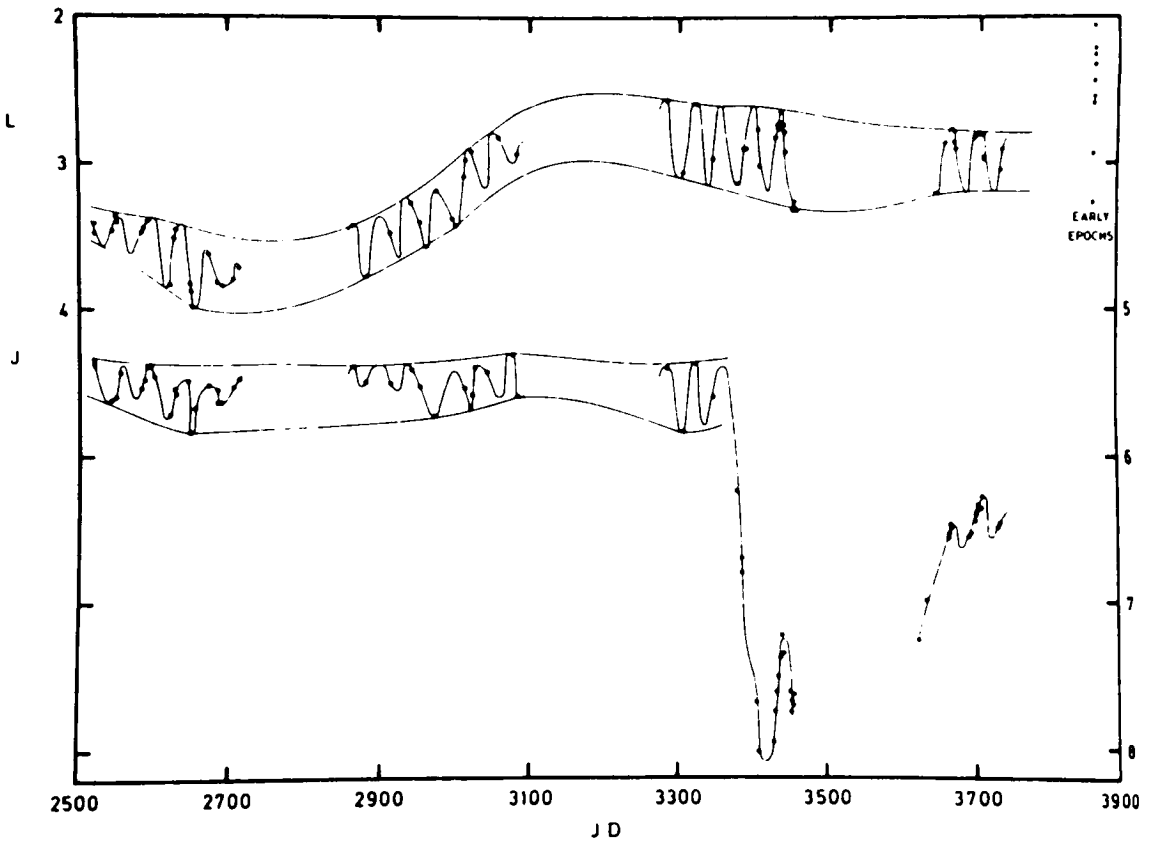


Figure 1-27. SAAO observations of RY Sgr at L(3.5 μm) and J(1.2 μm) (from Feast, 1979).

Nonvariable HdC Stars. Knowing that the RCB stars have fluctuations of brightness around 0.1 mag or more with periods as large as 40 days (38.9 for RY Sgr and 44 for R CrB), Rao (1980b) searched for variability in the nonvariable HdC stars. He observed the cool HdC star, HD 137613, eleven times in *UBV* during 85 days and detected no periodic variations greater than 0.1 mag in *V*. This variation range is larger than the expected RMS error (± 0.025 in *V*, ± 0.020 in *B–V*, and ± 0.025 in *U–B*), which may indicate a real variability in cool HdC stars. However, we conclude that this number of observations is too low to point out clearly any kind of variability. The total range of 0.1 mag in *V* encourages new observations with a time scale shorter than the week time scale used by Rao. As an example, such a long time scale should prevent us from discovering the short time-scale fluctuations in XX Cam by Totochava (1975), as well as the suspected nonradial-connected phenomena as discussed above.

Feast and Glass (1973) demonstrate that the nonvariable HdC stars do not possess any IR excess, and Rao (1980a) points out that the nonvariable star, HD 182040, has no envelope. This should be correlated with the low evidence for large mass loss on the nonvariable hot HdC stars (Schönberner and Hunger, 1978; Herber and Schönberner, 1980). The high-dispersion IUE observations of HD 182040 show no emission lines (i.e., chromospheric indicators; Johnson et al., 1984).

Helium Stars. Although all the following helium stars are known to be nonvariable: BD +37°442, BD +10°2179, HD 124448, HD 160641, and HD 168476, Herbig (1967) stressed that possible long-period variations exist. Landolt (1968) made intensive observations over periods of a few nights on two or three occasions each year for detecting short-term and middle-term variations; the set of stars are those given above, plus HD 264111 (Stephenson, 1967a) and BD +13°3224 (Berger and Greenstein, 1963). Only short-term variations are noted on BD +10°2179: on February 3, 1968, the star changed by 0.04 mag in *V* between two consecutive nights, a change greater than the probable error of a single measurement. Rao (1980b) also analyzed the variability of this star with 13 observations made on 100 consecutive days. The star does not seem to have any periodic variations in light greater than 0.1 mag in *V*. These variations are in agreement with those observed at the same epoch by Landolt (1973), who gives a total range of 0.09 mag in *V*. Here also, the observations are too few and lead to the same conclusions made for the low-temperature HdC stars.

Observations like these made by Landolt (1973) must be carried out: the large scatter in the data of HD 160641 and the evident brightening of the star by ~ 0.1 mag during 7 hours of observation demonstrate that short time-scale variations exist in helium stars as well as in the cooler HdC stars (Figure 1-28). On the other hand, Herbig (1964) concluded that: "A survey of the bright helium stars on a long-time series of ordinary patrol photographs would appear to be the more promising approach." Today, we endeavor to collaborate with the IAPPP or GEOS members or to use automatic telescopes with automatic photometers or satellites to do such surveys. Correlations between brightness and radial velocity are also seen in the extremely hydrogen-deficient hot star, BD + 13°3224, by Hill et al. (1981). The correlations between observations and evolutionary models (Schönberner, 1977; Hill et al., 1981) are to be analyzed carefully (Tutukov and Iben, 1985).

Early R Stars. There are no systematic studies on the relative number of variables and nonvariables among carbon (R and N) stars, such that it has been necessary to gather such information from catalogs. For example, among the 122 carbon stars that are brighter than 10.0 mag in the DDO catalog (Lee et al., 1940, 1947; Lee and Bartlett, 1945), 68 percent are variable.

Looking at the early R stars, we discover that only some are variables. (The variability is everywhere!) Among these early R variables, some, like BD +20°5071 and BD +69°417

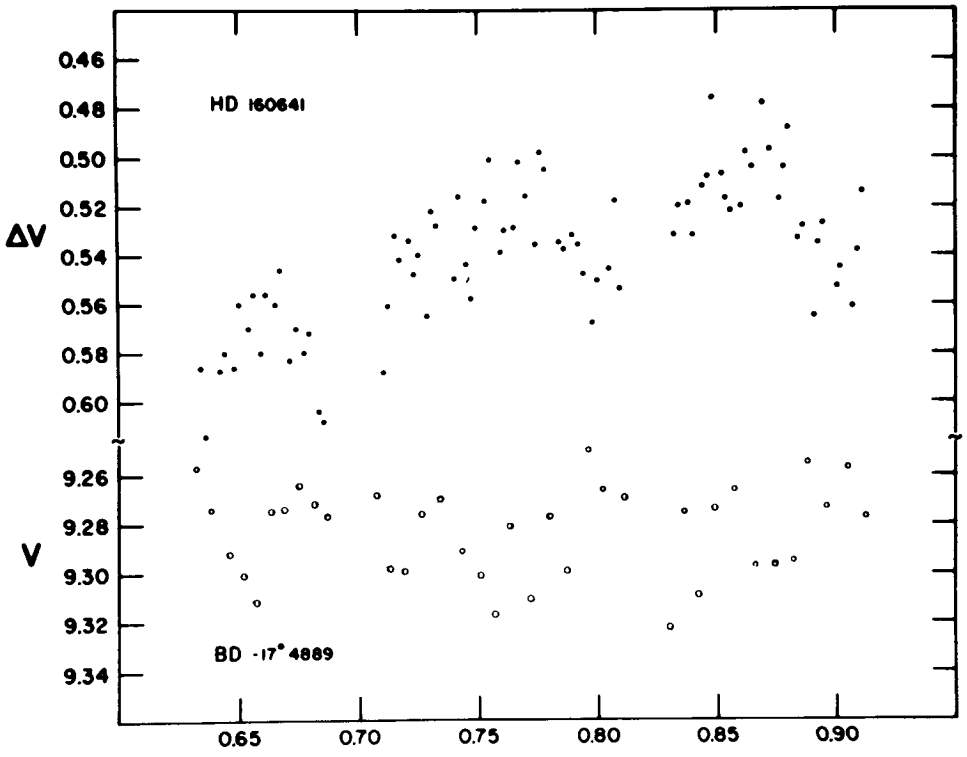


Figure 1-28. Top: plot of the differential V magnitude for HD 160641 (the gap in data at JD-2441452.70 and 452.83 occurs at times when UBV standard stars were observed); bottom: V magnitude plot for the comparison star BD-17°4889. For the 7-hour observing run, the large scatter in comparison star data is due to technical difficulties. The observations are made on May 15, 1972 UT (from Landolt, 1973).

(RU Cam), are bluer than the nonvariables. RU Cam has a period of 22 days (W Virginis type). Its spectrum varies from R0 at minimum to K0 at maximum. BD +57°2161 is also suspected to be variable, but it is redder than the nonvariable R stars. A few further photometric analyses should be undertaken for a better knowledge of these stars. Among the R2 stars, BD +19°3109 and BD +02°3326 are variable and have a higher color index than the normal stars.

Nonvariable M-Type Stars. Only a few papers are devoted to normal M stars. Generally, these stars are discussed in papers in which their characteristics are used as reference to the Mira, SR, or L variable stars. One of the most valuable proofs that we observe a normal M star is the nonvariability of the strength of absorption molecular bands and atomic lines and of the adjacent flux peaks.

The nonvariable M-type stars extend from M0 to M8, with a luminosity class from Iab to III. On the following stars, β And, π Aur, α Cet, μ Gem, ψ Peg, 119 Tau, 83 UMa, and δ Vir, Maehara and Yamashita (1978) obtained repeated observations of their fluxes within about 0.05 mag for most wavelengths. The energy distribution varies gradually from class to class. For stars later than M5, the gradient of the 4000 to 5000 Å region is mainly determined by strong TiO absorption bands rather than by temperature effects on the flux peaks.

We will not elaborate further on the nonvariable M stars which are not especially within

the scope of this volume on variability and nonthermal phenomena. However, a red star can be accepted as nonvariable and, consequently, as a photometric standard, only if it is observed to be constant over a sufficient period of time. It often happens that red stars accepted as UBV standard stars (i.e., nonvariable a priori) prove to have highly variable chromospheric lines (Sherbakov, 1979). As a consequence, they cannot be considered as nonvariable stars in narrowband photometric systems (Wings, 1971; Querci and Querci, 1985b).

IRREVERSIBLE CHANGES AND RAPID EVOLUTION

Irreversible Changes in Miras—An Example: R Aqr

Among the Mira variables, one evolved star that illustrates the purpose of this paragraph is the complex object, R Aqr. This binary star—a Mira (M7e) and a blue companion (Ofp, Bep, hot subdwarf, or white dwarf with an accretion disk)—is imbedded in a compact high-excitation nebula (Lampland, 1923a). These three components, which form the spatially unresolved central object of the R Aqr complex, are surrounded by a convex lens-shaped nebula of 2 arc-minutes (Lampland, 1923b) with filamentary and clumpy structures. More recently, an inner jet with an apparent changing structure and discrete variable knots was observed within 10 arc-seconds of the star. A possible counter jet was recently pointed out with radio and optical mappings.

Let us briefly review the main studies looking at the various causes of variability of this object and showing its rapid evolution.

The variability of the classical Mira was discovered by K. L. Harding in 1811, and the first objective-prism spectrograms obtained at Harvard as early as August 1893 show an Me spectrum. One of them, taken on October 17, 1893, shows a faint nebular line at λ5007 and bright hydrogen lines from Hβ to Hξ, with no trace of the Me spectrum (Merrill, 1928). The first slit spectrogram, taken at Mount Wilson in October 1919, shows (superposed on the normal spectrum of the M7e star) several characteristic emission lines of the gaseous nebula, a combination never observed previously.

As pointed out by Merrill (1940), the inner nebulosity is variable in position and brightness. The existence of both inner and outer nebulosities have been confirmed by numerous photographs taken in 1919 by Hubble (1940, 1943) with the Mount Wilson 100-inch refractor. From the measurements of a pair of plates taken at 16-year intervals, Baade (1943, 1944) estimates from the expansion rate that the onset of expansion was about 600 years ago. These observations could confirm the nova-like event noted by the ancient Japanese records in A.D. 930 and which formed the outer extended nebulosity.

During many years, the emission lines of the inner nebula have been photographed repeatedly. Their intensities vary through a large range, apparently without any correlations with the phase of the Mira star. Table 20 in Merrill (1940) describes the behavior of the spectrum of the companion and of the nebular lines from 1919 to 1939, but Merrill neglected the month-to-month variations in his description.

During the 1920–1930 decades, the very high-excitation spectrum marked by bright lines of hydrogen, helium, and iron was ascribed to the companion, which varies in an irregular manner (Merrill, 1935; Campbell, 1938) from the 11th magnitude or fainter to the 8th magnitude in 1933. Slight brightnesses were seen during 1922–1925. In July and September 1925, the nebular lines and the companion spectrum were particularly weak, but by December 1926, a rapid and well-marked increase in brightness occurred; the continuous spectrum of the companion was abnormally strong, and the spectral features were completely different from anything previously seen. The bright hydrogen lines had P Cygni profiles, and numerous ionized iron lines were prominent, whereas the nebular lines, λ4959 and λ5007, of [O III] were just detectable.

In 1927, the continuous spectrum and the nebular lines were much weaker, but the forbidden iron lines were stronger. Until 1933, no

large variation was noticeable; all the lines were slightly diffuse but not of great width. During 1931–1933, Payne-Gapochkin and Boyd (1946) observed an apparent correlation between the extremely bright active companion and the smeared-out light curve of the Mira in which the minima were bright and the maxima were abnormally low.

In July 1934, the combined flux of the Me and hot companion appeared to be fainter than it had been for several years, and the spectrum was very different. The [Fe II] lines in the blue-violet and the [S II] lines near λ4068 were well marked, while the Ca II H and K, the Fe II, and the nebular lines were very weak. After the Mira maximum of August 1934, the Me spectrum became fainter, and in November, the post-maximum Mg I λ4571 line appeared and became rapidly bright. The active companion was close to the 10th magnitude during the summer of 1935, and its forbidden lines dominated the spectrum during the Mira minimum of July 1935. These forbidden lines remained fainter during 1936–1939, few of them were recorded superposed to the Me spectrum.

Some spectral features must be noted for understanding this complex object. For example:

1. The nebular line, λ3967, of [Ne III] is not present (Wright, 1919); it could be absorbed by the Ca II H line and could demonstrate the existence of Ca II in the line of sight (i.e., in the outer nebulosity or in a large absorption shell surrounding it).

2. The P Cygni profile of the companion lines has often varied in intensity and structure, perhaps demonstrating important motions inside the inner nebula.

Between 1936 and 1949, the Me component of R Aqr was varying like a "normal" Mira (Merrill, 1950), while the spectrum of the active companion was subject to changes from an Ofp star spectrum with bright lines of N III and Fe II to the spectrum of a Bep star with numerous Fe II lines and a strong continuous spectrum. Its nebular lines, weak in 1936, increased in intensity until 1940 and remained relatively strong during a decade. On 10 Å/mm spectra, their widths appear variable and sometimes slightly unsymmetrical. Variable motions of matter are thus demonstrated in the forming layers of these lines. Merrill (1950) suggests either a probable orbital interpretation (a spectroscopic binary with 27-year period) or large-scale pulsations in the inner nebulosity to interpret the radial-velocity displacement of the [O III] and [Ne III] nebular lines. However, these variations reflect a continuing activity in the inner nebula.

The spectra obtained by Herbig (1965) in the late 1950's show a very strong nebular spectrum that nearly disappears in the observations of Ilovaisky and Spinrad (1966) made during the 1964 and 1965 minima; present were only the [S II], λ4068, and the doublet, [O II] λλ 3726–3729, from which an electron density $N_e \approx 10^3/cm^3$ was deduced. However, the Mira spectrum at minimum is clearly present, and moreover, there were no traces of the active companion.

The IR emission of R Aqr was detected independently by Woolf (1969) and Stein et al. (1969). The 11-μm emission of R Aqr is not brighter than that of o Cet or μ Cep, but it is much larger (from 8 to 12 μm). It is not as broad in wavelength as that observed in the planetary nebula, NGC 7027 (Gillett et al., 1968). This peak shape should be correlated with the various sizes of the emission grains located in the nebula. Stein et al. (1969) also note a strong and narrow absorption feature at 7.8 μm. Today, the 7.8-μm feature found in HD 44179 is attributed to coronene (C_{24} H_{12}) by Léger and Puget (1984).

The IUE spectra show strong emission lines, which are probably formed in the dense compact nebula located around the binary system and close to it ($d \approx 2 \times 10^{14}$ cm). The spectral type of the active companion is not conclusively resolved; it was identified as a bright white dwarf ($T \geqslant 50000$ K) or a subluminous central planetary-nebula star. Whatever it is, it

would have to be less than $T_{\rm eff} \approx 65000$ K in order to explain the weakness or absence of the He II 1640 Å line as stressed by Michalitsianos et al. (1980). Its brightness is comparable to that of the solar one. As suggested by Merrill (1950), it can produce enough ionizing photons to excite the continuum and the emission lines, but it is relatively faint for direct observations: "Such a star would photoionize the inner, high density nebula, but lacks a sufficient flux to photoionize the entire extended nebulosity." The observed IUE line fluxes, such as those from He II, C II, C II], C III], C IV, [O II], O III, [O III], O IV, S II, Si III], etc., can be used to obtain the general parameters of the ionized nebula ($T_e \approx 15000$ K, $L \approx 2 \times 10^{14}$ cm, $N_e \approx 10^6$ to 10^7 cm^{-3}). The observed UV continuum, essentially flat, is attributed to Balmer recombination. Michalitsianos et al. (1980) conclude that the compact nebula (inner nebula) could be entirely due to a mass-loss phenomenon from the primary M7e star with a mass-loss rate larger than $10^{-7}\ M_\odot$/year. To explain the 1933 brightness of the companion ($m_v \approx 8$ mag), they propose that it was provoked by mass transfer from the primary to the secondary. A set of parameters for the companion was deduced in their Table 3. Moreover, from the emission lines such as O I, Mg II, and Si II, they deduce the presence of a warm chromosphere around the M primary star.

A model of such a transfer of mass was developed by Kafatos and Michalitsianos (1982). In this model, the high brightness could be triggered when the companion accretes matter from the Mira component when it crosses over the periastron of its highly elliptical orbit. This hypothesis was one of the two previously suggested by Wallerstein and Greenstein (1980) to explain the apparent correlation observed by Payne-Gaposchkin and Boyd (1946). As suggested by Usher (quoted by Payne-Gaposchkin and Boyd), the companion's outburst might inhibit the pulsation and suppress the maxima by a change in the boundary conditions of the Mira itself. However, Wallerstein and Greenstein (1980) prefer the possibility of a single Mira star with a flaring region made by complex magnetic fields. During such flares, the pulsation of the Mira is inhibited by the magnetic fields and its maxima are smeared out. Jacobsen and Wallerstein (1975) arrive at the same conclusion by radial-velocity measurements of the nebular lines on plates from 1957–1965 and from 1970–1971. They do not find the 26.7-year period of Merrill (1940), and they conclude that a type of activity takes place in the outer layers of the Mira during the interval 1930–1940.

Using the criterion for Roche formation, the value of the primary radius, $R_1 \approx 2 \times 10^{13}$ cm, and the half-value of the orbit axis, $a \approx 2.5 \times 10^{14}$ cm, Kafatos and Michalitsianos (1982) found $0.84 \leq e \leq 0.92$. With $e = 0.85$, they obtain $M_1 + M_2 \approx 2.5\ M_\odot$, $P \approx 44$ years, a visible brightness of the disk of the order of $\approx \leq 1/5$ the Mira brightness, and a disk optically thick with an external temperature of ≈ 2300 K and $R_d \approx 2\ R_1$. If these values are correct, it is probable that the gravitational field of the secondary could be more important than that of the Mira. Kafatos and Michalitsianos (1982) believe that the disk around the unseen companion is not as large as $2\ R_1$, but has its larger extent at periastron because a moderate dimension of the disk would be more consistent with the expected mass of the secondary ($1\ M_\odot$).

Viewing the visual light curves of the Mira, Willson et al. (1981) suggest that the 1934 and 1978 low maxima are caused by an eclipse of the Mira itself by the accretion disk or by the gas cloud of the system and conclude that the orbital period is 44 years.

The thermal relaxation time of the envelope of the Mira, as well as the free-fall time scale, is about some years. These times are comparable in range to the 8.5-year eclipse duration observed between 1928 and 1935 and to the appearance of the jet between 1970 and 1977, which occurs about 44 years later (i.e., binary period). Such observations may not represent an eclipse at the periastron (≈ 1 year), but they would in fact infer the characteristic dynamical time scale required by the Mira to recover to its preperiastron quiescent state.

The first hypothesis of Wallerstein and Greenstein (1980), quoted previously, is supported by Bath (1977), who proposes that the mass transfer from the Mira envelope to the companion at its periastron orbital phase builds a spatially thick accretion disk at supercritical accretion rates, accompanied by the formation of a jet, possibly driven by radiation pressure. To confirm this hypothesis, Herbig (1980) found such a spike on the inner nebulosity, extending 10 arc-seconds from the star, with an angle position of approximately 22° on direct plates obtained with the Lick telescope. Tapia et al. (1982) reveal an 8'' jet at position angle (P.A.) 26° formed by discrete variable knots and perhaps a diffuse component and apparently a very small extension at the opposite direction not observed before. They suggest that this violent ejection may have taken place during the current minimum of the variable.

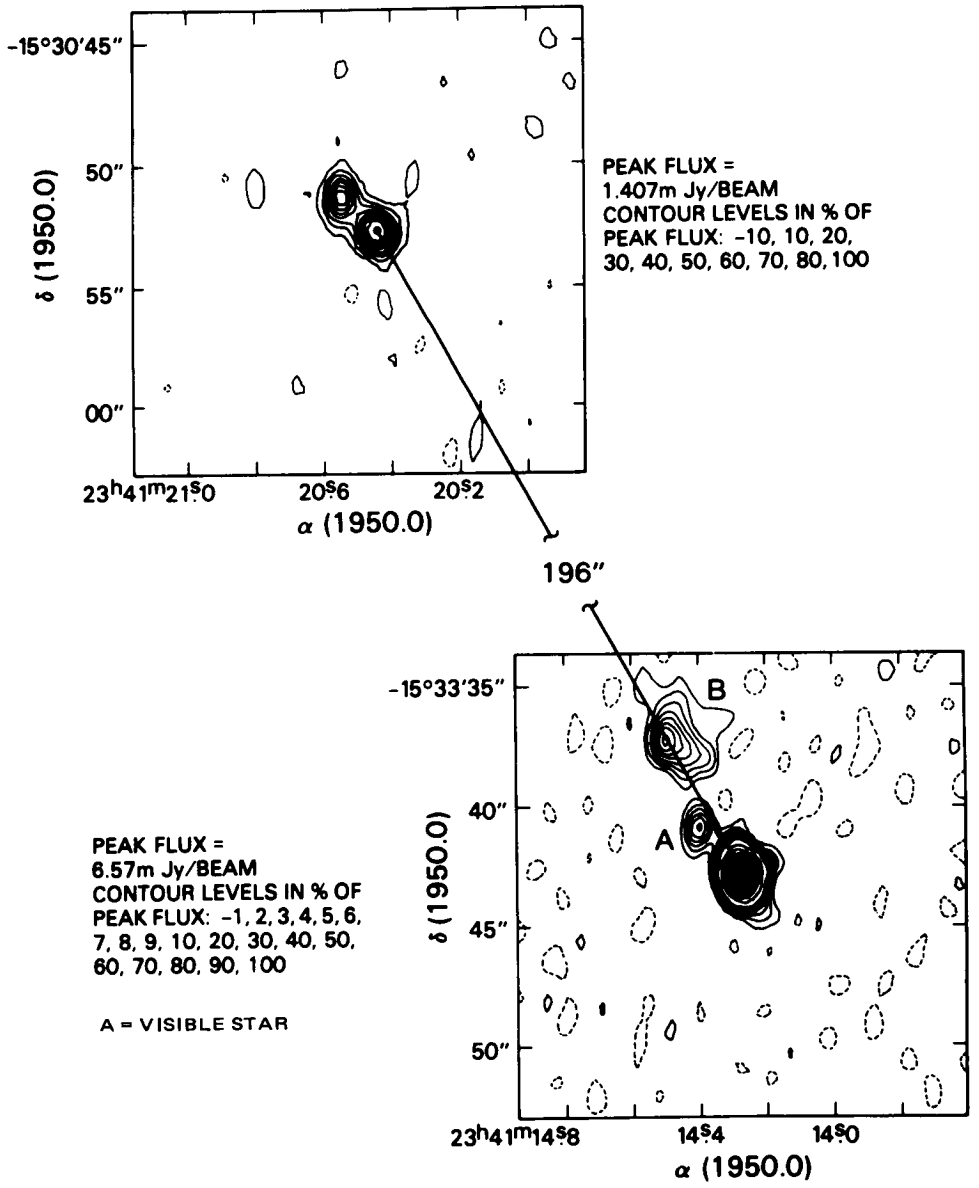


Figure 1-29. A 6-cm map of the R Aqr complex showing the secondary source located at 196 arc-seconds and the neighborhood of the star (from Kafatos et al., 1983).

This optical jet was rapidly confirmed by a radio counterpart. Sopka et al. (1982) describe its observational properties from optical and very large array (VLA) mappings. They found extensions both north and south of the star, at right angles to the outer nebular arcs, and they confirm that the inner nebulosity is variable in both brightness and structure, as already mentioned by Hubble (1940, 1943). These observations must be made again.

The mean radial velocity of the jet is -70 km/s, whereas the mean radial velocity centered on the star is - 44 km/s (Sopka et al., 1982). Kafatos et al. (1983) made VLA observations of the complex R Aqr, with a resolution of 1 arc-second. At 6.4″ from the radio emission of R Aqr itself, they found a peak radio intensity at 29°3 P.A. (jet B on Figure 1-29). An unresolved radio source is also found at ≈196 arc-second away on the line defined by the previous jet and the star itself. This feature may represent matter previously ejected by the complex. Besides these two sharp radio features, a new undetached one has been detected at ≈45° P.A. and ≈2.7 arc-second from the central star.

The near-UV map (Figure 1-30) taken by Mauron et al. (1985) duplicates the 6-cm VLA map made by Kafatos et al. (1983), but the northern knots seem a little more resolved; on this near-UV map, the counterjet located in the opposite side of the jet is well identified (C in Figure 1-30).

The optical and the radio structures of knot B are quite similar, suggesting that we see the same emitting region which produces the Balmer continuum in the near-UV and the free-free radiation at 6 cm.

Knot A seems more radially elongated on the near-UV electronic camera photograph than in the Kafatos et al. (1983) 6-cm map. Moreover, near knot A, on the isophotes of the unresolved inner nebula, a bump is visible (E on Figure 2 in Mauron et al., 1985).

Assuming that the R Aqr distance is about 300 pc (Whitelock et al., 1983), Kafatos et al. (1983) deduce from their VLA observations that knot A is located about 1.2×10^{16} cm and knot B is about 2.9×10^{16} cm from the central cool Mira variable. Since the knot B structure has not changed much in approximately 1 year (from September 1982 to December 1983), if we compare the 6-cm map from Kafatos et al. (1983) to the near-UV direct electronic camera photograph from Mauron et al. (1985), the latter authors deduce that this knot cannot have been ejected later than about 20 years ago. However, the proper motions of the knots obtained by Kafatos et al. (1983) and Mauron et al. (1985) have very poor accuracy; new measurements, chiefly from space, are required.

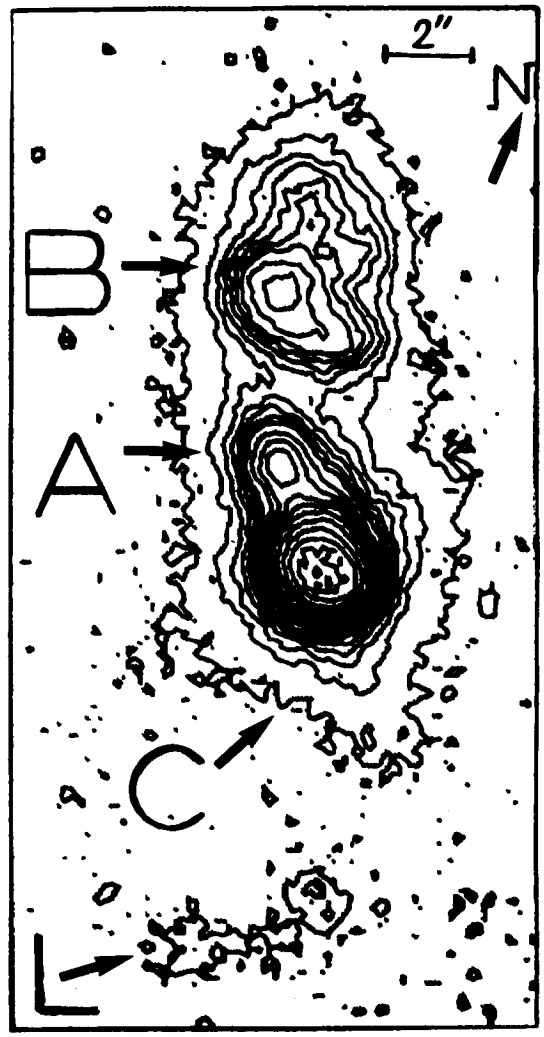


Figure 1-30. The R Aqr inner nebulosity with knots A and B and the possible counter-jet feature (from Mauron et al., 1985).

Taking into account that Si II λ1815 and Si III λ1892 are seen in the spectrum of the central region and are absent in the jet spectrum, Michalitsianos and Kafatos (1982) suggest that the material in the jet is comparatively cooler or less dense than in the central region. Quoting the optical spectra of the O II and O III emission lines of R. Fersen, Kafatos et al. (1983) confirm the cooler temperature of the jet.

In conclusion, these knots may be formed in different ways:

1. In the Mira inhomogeneous stellar wind, being perhaps excited by the UV flux from the orbiting companion when they enter its Strömgren sphere (Spergel et al., 1983), with the pressure radiation on dust in the knots making them move outward.
2. During the periastron phase, when the Mira fills in its Roche lobe (accretion at supercritical rates; Ferland et al., 1982).
3. In a probable polar ejection from the disk, giving them a roughly axial orientation relative to the elliptical outer nebula.

Kafatos et al. (1983) write that: "if the jet and the nearby point source (feature A) are ejecta, their difference in position angles could be interpreted as precession of the system while it expels material. The morphology of the outer $\approx 2'$ nebula could be accounted for in this manner, thus explaining the characteristic lens-shaped filamentary structure." This is to be confirmed by repeated high spatial resolution observations.

The extended nebula has a mass about 0.2 $M_\odot$, a kinetic energy larger than 2×10^{46} ergs. It radiates more than 5×10^{44} ergs/year in Balmer and Lyman emission lines and continua. Its cooling time scale is estimated to be ≈ 2 years. It seems unlikely that the photoionization from the companion star is the power source of the extended nebula for the past 600 years because its excitation requires much more energy than the Eddington limit for a 1 $M_\odot$ star. However, from purely energetic arguments, the jet itself could be the source of the excitation of the outer nebula. The jet parameters estimated by Sopka et al. (1982) are used by Kafatos and Michalitsianos (1982) to conclude to a jet kinetic energy of $\approx 5 \times 10^{45}$ ergs, which the authors estimate in reasonable agreement with the radiation cooling given previously.

The material of the extended nebula is trapped in rings, generally perpendicular to the axis of the jet. Such a structure is favored for the formation of the nebula in a single explosive event hundreds of years ago. This is confirmed by the high content of the nebula in He, and more particularly in N (Wallerstein and Greenstein, 1980), which is also in agreement with models of recurrent novae (Starrfield et al., 1982).

The counterjet feature situated on the opposite side of knot A (C in Figure 1-30) was initially detected by Tapia et al. (1982) on B and V plates taken on September 23–24, 1982. By radio observations, Kafatos et al. (1983) detected a possible counterjet. Using the ratio of the UV C IV to C III] lines at various places on the R Aqr complex, Michalitsianos and Kafatos (1982) found that this ratio at the opposite side of the jet is much different from that elsewhere.

What future projects are now planned for clarifying the R Aqr complex? To study the structure and the evolution of the inner nebula, the knots of the jet, and the counterjet, it is necessary to reach Mira phases and wavelengths when and where the Mira brightness is very low. Observations during the Mira minima and in the UV region could be powerful.

In the aim to diminish or to eliminate the turbulence of the Earth atmosphere usually attached to ground-based observations, observations in good seeing observatories by Speckle interferometry and Space Telescope (ST) investigations are needed. The Faint Object Camera (FOC) was developed especially for high spatial resolution studies. Moreover, the image restoration techniques could help in the analysis of observations which are at the limit of resolution of the ST, such as for the inner

nebula of R Aqr. The proper motions and evolution of the shape of the elements of the inner and outer nebulas could be investigated by this instrumentation. The kinematics of various features of the R Aqr complex could be deduced. High-resolution spectra of the jet and the knots should be made to evaluate the richness of the extended nebula in helium and nitrogen—richness suspected by Wallerstein and Greenstein (1980).

Irreversible Changes in SR and L Stars

Many M and C class stars showed outstanding and nonreversing variations in one or more decades. We shall elaborate here on some examples of these rapid and definitive changes.

V1016 Cyg (MHα 328–116) was classified as a strong Hα emission object (Merrill and Burwell, 1950) with an estimated V magnitude around 15 (Fitzgerald et al., 1966). Between July 1963 and August 1965, this object brightened by ≈ 4 mag (McCuskey, 1965). Since this outburst, its behavior has been monitored optically by Mammano and Ciatti (1975); in the infrared by Harvey (1974), Puetter et al. (1978), and Aitken et al. (1980); in the radio by Purton et al. (1973) and Altenhoff et al. (1976); and in the UV-IUE by Flower et al. (1979) and Carpenter and Wing (1979). In the visible, many lines indicate a very hot source of radiation although some low-excitation lines are also present, and this, together with the absorption bands of TiO and VO, has been taken as evidence of a binary system with an LPV and a hot star exciting a nebula (Mammano and Ciatti, 1975). From their analysis of the IUE spectrum, Carpenter and Wing (1979) conclude that there has been sudden shell ejection with a very large excitation which developed a rich emission-line spectrum, with lines of O I, Fe II, Mg II, C II, N V, O V, [Ne V], and [Mg V]. As these lines are also seen in the spectra of planetary nebulas such as NGC 7027, something like a planetary nebula was probably formed or excited around the star (see also Flower et al., 1979). Nussbaumer and Schild (1981) interpret that spectrum with a single star planetary model, the central star having a temperature of $T = 160000$ K and a radius of $0.06\,R_\odot$. The expansion velocity deduced from the line shape is around 100 km/s. The electron density in the shell is approximately 3×10^6 cm^{-3}, and the electron temperature varies from 8000 to 18000 K. From the reddening determined in the IUE observed UV region, they derive a distance of 2.2 kpc.

The carbon star, HD 59643, provides another example of nonreversing and rapid evolution. Shane (1928) and Keenan and Morgan (1941) considered it as a cool, but otherwise rather ordinary, nonvariable carbon star and classified it as R8 or R9. After reduction of its spectrum, Wildt (1941) considered it as a normal carbon star, with normal excess of heavy elements and with Ca II H and K lines in absorption. After more than 25 years, Gordon (1967) and Yamashita (1967) noticed an increase in the equivalent widths of the absorption lines of the heavy elements Ba, La, Sc, and Sr, as well as a deeper molecular G band. Greene and Wing (1971) examined the plates of HD 59643 taken by Keenan in 1949 and found no evidence of hydrogen emission. Hα was seen in emission for the first time in November 1966 by Gordon (1967), when it was a little brighter than its nearby continuum. In 1969, Utsumi (1970) saw Hβ quite clearly in absorption. These data suggest that the activity is of recent origin but not easy to understand. Greene and Wing (1971) found an abnormal and variable spectrum below 4000 Å with a filling in of the K line and the (0,0) CN violet band. This activity of February 1970 was also observed near the hydrogen emission lines Hδ–Hξ, but the longward spectrum was not significantly different from that analyzed by Wildt (1941). The main difference is that the Ca II H and K lines were completely invisible in 1970, although they were in absorption in 1941. This absence cannot be interpreted as a calcium deficiency because the Ca I λ4226 line appeared to be strong. Another difference is the appearance of a very weak Hα emission line in 1966, along with the strong Hδ–Hξ and the UV

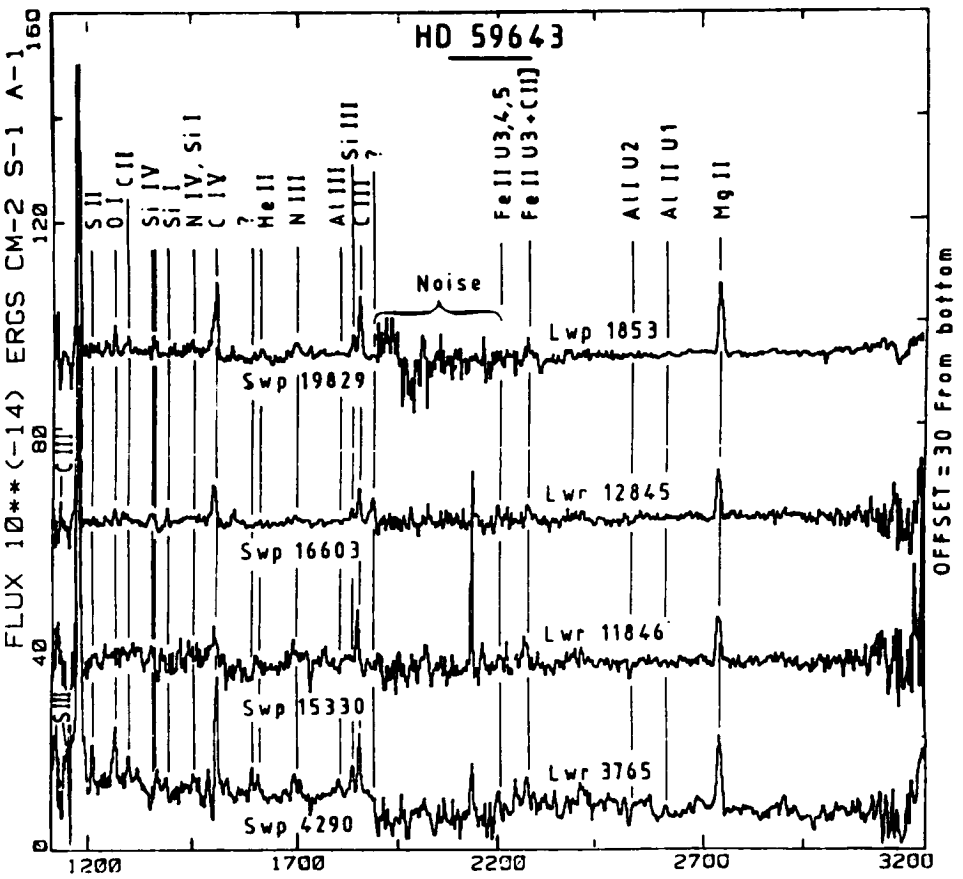


Figure 1-31. Low-resolution IUE spectra of HD 59643. The abscissas are in Angstroms, the ordinates are absolute fluxes. The lower spectra are obtained from the data bank. The observations are made on: Feb. 17, 1979 (SWP 4290); Feb. 14, 1979 (LWR 3765); Oct. 25, 1981 (SWP 15330, LWR 11846); March 23, 1982 (SWP 16603, LWR 12845); April 27, 1983 (SWP 19829, LWP 1853). We note the high level of noise from 2000 to 2200 Å for the LWP spectrum and a spike at 2180 Å in the LWR spectra (from Querci and Querci, 1985b).

continuous emission in 1970. Greene and Wing (1971) conclude that the UV continuous emission does not come from the photosphere; the radiation must emanate either from a hot circumstellar envelope or from the secondary star of the binary system. The latter interpretation disagrees with Wildt's observations, in which no continuum or emission lines are reported. Therefore, the UV emission could be considered to be an activity located above the layers responsible for the violet Ca II H and K lines, giving an IUE spectrum (Carpenter and Wing, 1979) with ions of a great range in ionization: O I, Mg II, C II, and N IV. Querci and Querci (1985b) demonstrate that the emission lines are variable and that the continuum from 2200 to 1200 Å decreased significantly between 1979 and 1983 (Figure 1-31). The Balmer lines in HD 59643 are formed in the same outer layers because the Balmer decrement is very small, whereas it is very steep in the Mira variables and consequently affected by the violet depression. Through IUE and visible high-resolution spectra, the Bloomington and Toulouse groups are following the evolution of this complex object.

The ultraviolet continuum of the SRb carbon star, UU Aur, decreases with time. Shajn and Struve (1947) measured the Ca II H and K lines to be seven times weaker than those of the gM0 comparison star, HD 80943, while the Ca I 4226 Å line is not weakened and the Sr II 4078 Å line seems to be less affected. They suggest that the weakening of the continuous violet background may be attributed to the effect of many overlapping unknown molecular bands rather than to continuous absorption, in any case not to some temperature effect. They also measured the wavelength of emission lines like λλ 4036, 4009, 3959, 3949, 3914, and others, whereas in the regions centered at λλ 3983, 4005, and 4052, there is no apparent emission in the N stars. In the 200-inch plates obtained by Bowen (1951) in January 1951, the H and K lines, as well as the Al I 3944 and 3961.5 Å lines, are not visible on a spectrum which has a very low continuous background without absorption features shortward to Mn I 4030 Å multiplet. Only numerous emission lines are observed, especially at 3982.5 Å, which are identified as Ti I, V I, or Zr I low-excitation lines (Gilra, 1976). We therefore suggest an increase of the optical depth of the absorbing layers situated at the temperature minimum, which smears out all the absorption features coming from layers situated beneath. The very extended layers situated above might give rise to emission lines (low-temperature chromosphere) and narrow absorption lines (extended shell) such as those from Mn I multiplets, which eat away the emission lines. It is suspected that the changes in UU Aur are more in the nature of variations than secular changes.

Irreversible Changes in HdC Stars

The irreversible evolution for the different RCB stars is not exactly the same. In the following, we detail the observed evolutions of only a few chosen RCB stars, all the more so because, unfortunately, the sample of the correctly observed RCB is very poor.

A Slowly Evolving Star: RY Sgr. Using data from 1967 to 1970, Alexander et al. (1972) confirm the cepheid-like behavior of RY Sgr by spectroscopic and photoelectric observations. Yet again, they find the cyclic variations of 0.6-mag amplitude and the 38.6-day period found by Jacchia (1933), with data covering the period 1920–1932. They conclude that "neither evolutionary effects nor mass loss by ejection are of enough importance to significantly change the period on the time scale of 50 years." However, observations with longer time intervals could give slightly different results. Pugach (1977) was the first to point out a shortening of 0.9 days in 40 years, using observations from 1926 to 1977, but with a gap of 168 pulsational cycles. However, he was unable to find a relation between the period shortening and the time. This decrease of the pulsational period length was confirmed by the results of Marraco and Milesi (1980, 1982) and those of Kilkenny (1982). With observations of RY Sgr from 1897 to 1977, Marraco and Milesi (1982) give the instantaneous periods of the pulsational oscillations in 1897, 1926, and 1977 to be 39.3, 39.0, and 38.2 days, respectively. The periods of Jacchia (1933) and Pugach (1977) are again found, and the period decrease of 1.1 day in 80 years is deduced. Kilkenny (1982) reexamines the archive material from 1926 to 1978, material largely due to the efforts of amateur astronomers. He shows that the epochs of the observed minima agree with $JD_{min} = T_0 + P_0 n + kn^2$, where T_0, P_0 are the "zero" epoch and period, respectively, and k represents the linear rate of change of the pulsational period. The decreasing period thus ties in with the general data rather well, but there appears to be some modulation of k, with a time scale of 100 or 200 pulsation periods. Therefore, RY Sgr has $k = -0.0005$ (Kilkenny, 1982), a value which is close to that expected by Schönberner (1977) for a deficient hydrogen star of $M = 1M_\odot$ and $T_{eff} = 6900$ K, evolving rapidly from the red-giant to the white-dwarf stage.

A Star Rapidly Changing Its Period: S Aps. Waters (1966) analyzed the visual observations

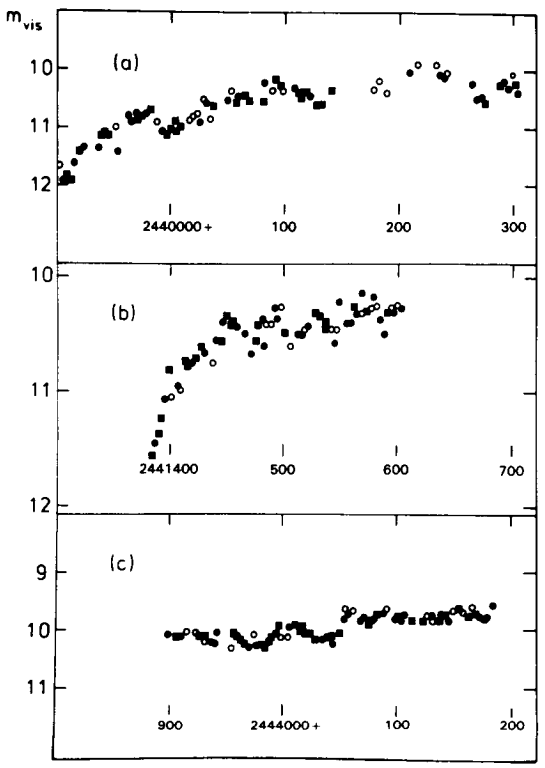


Figure 1-32. Visual observations (3-day means) of S Aps. Abscissas are Julian dates. Symbols indicate the number of observations in the mean: squares have five or more observations; filled circles three or four; and open circles, two; singles observations are omitted (from Kilkenny, 1983).

made during the period 1922–1960 and found a period of about 120 days. Kilkenny (1983) investigates 8000 individual observations covering the interval 1960–1982. After the obscurational minimum of 1967, S Aps shows an instantaneous pulsational period of about 135 days (Figure 1-32a). Surprisingly, after the next obscurational minimum in 1971, S Aps appears to have developed an oscillation of a 37.5-day mean pulsational period (Figure 1-32b). Observations on the 1979 maximum show an instantaneous period of about 40 days (Figure 1-32c). Other observations of such a phenomenon are necessary before we can conclude that the period change is linked to the obscurational minima or if the deep minima facilitate the change of pulsational mode (from fundamental to first or other overtones). We cannot explain this observation in terms of decreasing pulsational rate, and there is no model of evolution of hydrogen-deficient stars which allows such a rapid change of period (Röser, 1975), although the evolution of a hydrogen-deficient star to a white dwarf is rapid. Therefore, any changes in the observational material should be virtually undetectable on a time scale of a few years (Schönberner, 1977). In addition to these changes on pulsational period, there appears to be a fading of the amplitude of the pulsational variations in some RCB stars (Fernie et al., 1972; Kilkenny, 1983).

As for UW Cen, another example, the situation is not as comprehensible as for S Aps because the reduction of the observations gives many solutions with $+0.003 \geqslant k \geqslant -0.006$; consequently, the period could be constant or decreasing/increasing, but at a relatively low rate. We must point out that "if UW Cen has an increasing period, this could mean that it has not yet reached the top of the asymptotic giant branch" (Kilkenny and Flanagan, 1983).

The helium stars could also have irreversible changes. For example, HD 168476 had $V = 9.37$ mag in 1964 (Hill, 1964); the data of 1969–1971 given by Landolt (1973) and communicated to him by Hill in 1973, as well as the observations of mid-1972 made by Landolt (1973), seem to indicate a slight secular brightening over the decade 1964–1973.

The V mean value and the colors of the HdC star, HD 182040, obtained by Rao (1980b), agree with the data deduced from the one observation of this star made 25 years before by Mendoza and Johnson (1965). Consequently, no middle-term variations seem to appear.

PROSPECTS AND CONCLUSIONS

At the end of this description of the slow or rapid, reversible or irreversible phenomena presented by the cool giants and supergiants, we should like to emphasize the observations to be performed for having a necessary solid basis of data to model these hydrodynamical

phenomena, and progress in knowledge of the evolutionary status of these stars.

To evaluate the nonthermal energy variations on various time scales involved in the different layers of the entire stellar atmosphere, simultaneous observations in many spectral ranges are required. Consequently, extensive monitoring must be organized from the ground with the present and new well-adapted instruments and with space facilities that will become more and more available in the not too distant future.

Some of the *ground telescopes* and their focal instrumentation could be used for photometric, high-resolution spectroscopic, and polarimetric analysis, as well as in the visible and infrared ranges and in the radio range.

To stimulate long-term variability observations of the carbon-star energy distribution, today partially followed with non-well-adapted means, Querci and Querci (1985b) propose a photometric system covering the main atomic and molecular features over the largest wavelength range. This system is inspired by their previous studies of N-type spectra from the far-UV to the radio frequencies and by synthetic spectra deduced from their model-atmosphere calculations. Also selected are three points on the continuum: at 1.5 mm, 3.8 μm, and 1.04 μm (Wing's I104 filter). Active observations in the visible are presently made in ESO-Chile by the Sterken group with some of the Querci's filters. Variations in color indices such as in C_2, *CN*, *D–Na*, *Hα*, *I104*, etc., can be followed, and various correlations with the known physical parameters can be shown. Monitoring on *other spectral intervals* is urgently required, such as around *C IV* (if any, possibly at some phases) and *CO* features and at 3.8 μm, 11.3 μm, and 1.5 mm, etc. This should allow a detailed analysis of the behavior of the various stellar layers. In addition, the high spectral resolution presently available, which gives fine details on the structure and dynamics of the red giants (see M. Querci, this volume), should let us envisage the modeling of the entire variable atmosphere.

Collaboration with amateurs on photometric monitoring cannot be neglected. The high instrumental and scientific levels of some of them permit productive cooperation. The International Amateur-Professional Photometric Photometry (IAPPP) members, mainly in the United States, and the Groupe d'Etudes et d'Observations Stellaires (GEOS), mainly in Europe, are experienced in the photoelectric photometry. In the United States, after the first telescopes and photometers that work on semi-automatic control or remote control, some Automatic Photometric Telescopes (APT's) of 40-cm aperture are already operating, mainly at the Fairborn Observatory in Phoenix, Arizona (Boyd et al., 1985). These telescopes are driven by a computer that has on memory the star program and the comparison stars. The tests on sky quality and the night observations are automatically made on-line (i.e., finding the stars and centering them on the aperture, recording the data, etc.). The computer makes decisions such as when to open the dome, in what order the stars should be observed, and when to shut down. The telescope calls for human assistance if some failures appear. The data are reduced at the end of the night. The accuracy of such measurements made with the UBV filters of the Johnson system is of ≈ 0.02 magnitude. An APT service permits anyone to request differential photometry for his own program stars.

Many efforts are also being made in Europe; among them, the twin-telescope technique is being developed by the Section de Photométrie Photoélectrique of GEOS (Gregory and Querci, 1985). Because the sky transparency is rapidly variable during a night in Western Europe and because the GEOS amateurs aim at an accuracy of 0.002 mag in *UBV* filters, human assistance during the night is preferred for various technical and sky-quality controls through the rms of the on-line data on the computer display. In the twin-telescope technique, two telescopes with 28-cm apertures are fixed on the same mounting: one follows the star program, and the other, which is also driven by computer, follows the comparison star. The angle between their optic axes is calculated by the computer, which drives stepper motors for

a differential orientation of the second quoted telescope relative to the first. The two stellar lights are led into the two-channel photometer by liquid optic fibers. This new photometer is the second European Photoelectric Photometer (EPP-2) built by Fontaine (1985). It was derived from the EPP-1 (one-channel photometer) made by Fontaine (1984) and Walker (1985) in a collaboration decided at the IAPPP meeting at Herstmonceux-Castle during the fall of 1984. Full-sky photometry is made by using the standard stars. The *UBV* filters are now being used. Soon, we plan to use narrower filters and larger telescopes.

This photometric monitoring is the basis of research on variability. Narrow-filter photometry with 1-m telescopes and visible and infrared high-resolution spectra with 2.0- or 3.6-m telescopes could be made when interesting phases of variation are detected by photometric monitoring with small telescopes. Larger telescopes, such as VLT's and NNTT's, could be required when the stellar flux is very low.

It is also worth noting that *combined radio and infrared observations* should be developed between radio observatories such as Onsala, IRAM, Eiffelsberg, and ESO and infrared telescopes such as UKIRT, CFHT, and ESO to provide constraints on models describing the molecular excitation mechanisms on the emitting layers, since it is well known that the infrared continuum and lines can excite the radio molecular transitions (see Nguyen-Q-Rieu, this volume). New molecules could be detected in the millimetric wavelength. The very far-UV and submillimetric wavelength ranges (i.e., between 200 and 900 μm) have not been extensively examined. There, photometry, together with spectroscopy, should give insight into the outer layers of the cool stars and special isotopic abundance determinations.

Already, the *space gave a new scope* on the cool giant research through the IUE and IRAS spacecrafts. (See the section *Photometric Observations*.) However, the small aperture of IUE seriously limits the high-resolution analysis to a very small number of cold bright stars.

The first EXOSAT investigations on cool giants and supergiants are presently in progress. (See the section *Photometric Observations*.) It seems to us that X-ray fluxes should be obtained at some phases of Miras (i.e., when the shock waves are the most powerful), and some constraints could therefore be added on the shock-wave interpretation of the Mira variations.

In the near future, new spacecraft will be launched: the Hubble Space Telescope (ST), the largest one with its 2.4-m diameter, by NASA in 1988, the space astrometry satellite, Hipparcos, by ESA in July 1988, and the Infrared Space Observatory (ISO), another ESA spacecraft, foreseen for 1992.

The scientific community has received detailed information on the different focal instruments of the Hubble Telescope via the "Space Telescope Science Institute" in Baltimore, Maryland (The Space Telescope Observatory, 1982). With its planned mission over 15 years, long-term programs on the variability of Miras and semiregular, irregular, and eruptive RCB stars are possible. Such an observational basis could permit great progress in the knowledge of the hydrodynamics of these stars. Many proposals have already been presented on the cool giants and supergiants, some of which are:

- WF/PC observations for the spatial distribution analysis of the clumpy ejected matter around individual stars as a function of star distance (e.g., α Ori),

- WF/PC observations of the R Aqr jet in the direction of the secondary radio source seen on the 6-cm map and analysis of the jet formation,

- FOC observations of the R Aqr complex, mainly the high-excitation nebula surrounding the mass-losing Mira variable, and the compact hot companion with its accretion disk for hydrodynamical modeling of the whole object,

- FOC observations of extended chromospheres for an analysis of the spatial properties of the wind such as asymmetric mass loss, radial variations of density and temperature, interaction of cool wind with the cool companion (e.g., α Ori), or interaction of cool wind with a hot companion (e.g., α Sco and o Cet),

- FOC observations of the rapidly evolving stars such as V1016 Cyg, HM Sge, and HD 59643 to determine the location of the variable high-excitation region pointed out by IUE spectra,

- FOC exploration of the nearby giants for the structure of their own surface (convective cells, spots, etc.) and for the determination of the spatial and particle-size distributions on their nearby neighborhood (e.g., α Ori and o Cet),

- HRS Echelle spectra of supergiants for dynamical analysis of the various layers by the monitoring of radial velocities and profiles of the spectral lines (e.g., δ Vir, α Ori, and R CrB).

Hipparcos (High Precession Parallax Collecting Satellite) was named in memory of Hipparcos, who was the first Greek astronomer to measure a parallax (that of the moon) and who cataloged 800 stars. During the 2.5 years of the Hipparcos mission, any particular point of the sky enters in both fields of the satellite several times a year, making accurate photometry of selected stars possible (Turon-Laccarieu, 1978). The absolute coordinates of each star, its parallax, and each component of its annual proper motion will be measured with a maximum mean error of ± 0.002 arc-seconds (for stars brighter than B = 12). Many astrophysical parameters can be deduced from these astronomical data: (a) with the parallax, we get the distance of the star; (b) with its apparent magnitude and distance, we obtain the absolute magnitude; (c) from already measured apparent angular diameter and distance, we deduce the stellar radius; and (d) with the effective temperature and stellar radius, we have the luminosity and the mass of the stars. During the Hipparcos mission, the period of many Miras could be defined, the calibration of the period-luminosity relation could be improved, and the theory of pulsation of Miras could be checked. Knowing the center-of-mass radial velocity (obtained from the radio thermal lines) and the proper motions, the spatial motion of the various populations of stars could be deduced. Moreover, the satellite will collect a considerable quantity of accurate photometric data on the variability of the Miras and the semiregular and irregular stars; their analysis could provide the various pulsating periods and their temporal changes. Tests on stellar evolution and structure theories could be developed. The variations on various time scales detected on some stars could also be analyzed.

During the 18-month mission of the 60-cm cooled telescope named Infrared Space Observatory (ISO), some interesting programs on late-type giants and supergiants should be developed: (a) temperature distribution on circumstellar material and planetary dust clouds; (b) determination of the shape of various diffuse features (e.g., solid-state spectral features at 11 and 18 μm) and correlation of these shapes with the physical parameters of the star and its envelopes; (c) mapping of the neighborhood (1° by 1°) of some hypergiants and planetary nebulae at 40, 80, 120, and 160 μm and determination of the shell diameters, energy balance, densities, etc.; and (d) determination of mass-loss rates. The problem described by Wesselius (1984) on the origin of the outer envelopes of α Ori should be solved by the ISO high-resolution spectroscopy (Barlow and Storey, 1984).

Finally, a large organized international collaboration on photometry, spectroscopy, and polarimetry both from the ground in the visible, near-IR, and radio ranges and from space in the X-ray, far-UV, near- and far-IR, and submillimetric frequencies seems unavoidable

if we want to effectively progress in the knowledge of these variable cool stars.

Constructive comments by Hollis R. Johnson have improved the first part of this chapter.

REFERENCES

Aaronson, M. 1984, in *Proc. IAU Symp. 108, Structure and Evolution of the Magellanic Clouds*, ed. S. Van den Bergh and K.S. de Boer (Dordrecht: Reidel), p. 183.

Aaronson, M., Olszewski, E.W., and Hodge, P.W. 1983, *Astrophys. J.*, **267**, 271.

Adams, W.S. 1956, *Astrophys. J.*, **123**, 189.

Ahnert, P. 1969, in *Proc. IAU Colloq. 4, Variable Stars, Non-Periodic Phenomena in Variable Stars*, ed. L. Detre (Dordrecht: Reidel), p. 325.

Aitken, D.K., Roche, P.F., and Spencer, P.M. 1980, *Mon. Not. Roy. Astr. Soc.*, **193**, 207.

Alexander, J.B., Andrews, P.J., Catchpole, R.M., Feast, M.W., Lloyd-Evans, T., Menzies, J.W., Wisse, P.N.J., and Wisse, M. 1972, *Mon. Not. Roy. Astr. Soc.*, **158**, 305.

Alksne, Z.K., and Ikaunieks, Y.Y. 1971, *Carbon Stars*, (Riga, Estonia, U.S.S.R.: Pub. House Zitnatne); also, 1981, *Astron. Astrophys. Ser.*, **11**, ed. J.H. Baumert (Pachart Publishing House).

Alksne, Z.K., Alksnis, A., and Dzervitis, U. 1983, *Properties of Carbon Stars of the Galaxy* (Riga, Estonia, U.S.S.R.: Pub. House Zitnatne).

Altenhoff, W.J., Braes, L.L.E., Olnon, F.M., and Wendker, H.J. 1976, *Astron. Astrophys.*, **46**, 11.

American Association of Variable Star Observers, 1983, Report 38, Cambridge, Massachusetts.

Antia, H.M., Chitre, S.M., and Narasimha, D. 1984, *Astrophys. J.*, **282**, 574.

Arsenijevic, J. 1985, *Astron. Astrophys.*, **145**, 430.

Ashbrook, J., Duncombe, R.L., and Van Woerkom, J.J. 1954, *Astron. J.*, **59**, 12.

Augason, G.C., Johnson, H.R., Bregman, J.D., and Witteborn, F.C. 1986, *Astrophys. J.*, submitted.

Avrett, E.H., and Johnson, H.R. 1983, in *Proc. Third Cambridge Workshop on Cool Stars, Stellar Systems, and the Sun*, ed. S.L. Baliunas and L. Hartmann (Berlin, Heidelberg: Springer-Verlag), p. 230.

Ayres, T.R., Linsky, J.L., Vaiana, G.S., Golub, L., and Rosner, R. 1981, *Astrophys. J.*, **250**, 293.

Baade, W. 1943, *Ann. Rept. Dir. Mt. Wilson Obs.*, 1942–1943, p. 15.

Baade, W. 1944, *Ann. Rept. Dir. Mt. Wilson Obs.*, 1943–1944, p. 12.

Baade, W. 1951, *Pub. Ob. Univ. Michigan*, **10**, 7.

Balega, Y., Blazit, A., Bonneau, D., Koechlin, L., Foy, R., and Labeyrie, A. 1982, *Astron. Astrophys.*, **115**, 253.

Balister, M., Batchelor, R.A., Haynes, R.F., Knowles, S.H., McCulloch, M.G., Robinson, B.J., Wellington, K.J., and Yabsley, D.E. 1977, *Mon. Not. Roy. Astr. Soc.*, **180**, 415.

Barbaro, G., and Dallaporta, N. 1974, *Astron. Astrophys.*, **33**, 21.

Barcia, A., Bujarrabal, V., Gomez-Gonzalez, J., Martin-Pintado, J., and Planesas, P. 1985, *Astron. Astrophys.*, **138**, 359.

Barlow, M., and Storey, P.J. 1984, in *Proc. Alpbach Workshop on Infrared Space Observatory*, ed. C.J. Cesarsky, p. 61.

Barnes, T.G. 1973, *Astrophys. J. Supplement*, **25**, 369.

Barnes, T.G., and Evans, D.S. 1976, *Mon. Not. Roy. Astr. Soc.*, **174**, 489.

Barnes, T.G., Evans, D.S., and Moffett, T.J. 1978, *Mon. Not. Roy. Astr. Soc.*, **183**, 285.

Basri, G.S., Linsky, J.L., and Eriksson, K. 1981, *Astrophys. J.*, **251**, 162.

Bateson, F.M. 1972, *Inf. Bull. Variable Stars (IAU Comm. 27)*, No. 661.

Bateson, F.M. 1974, *Pub. Roy. Astr. Soc. New Zealand*, Variable Star Section, No. 2, (C74), 26.

Bateson, F.M. 1978, *Pub. Roy. Astr. Soc. New Zealand*, Variable Star Section, No. 6, 39.

Bateson, F.M., and Jones, A.F. 1972, *Roy. Astr. Soc. New Zealand Circ.*, **185**.

Bath, G.T. 1977, *Mon. Not. Roy. Astr. Soc.*, **178**, 203.

Baud, B., and Habing, H.J. 1983, *Astron. Astrophys.*, **127**, 73.

Baud, B., Herbig, H.J., Matthews, H.E., and Wimmberg, A. 1981, *Astron. Astrophys.*, **95**, 156.

Baumert, J.H. 1972, Ph.D. Thesis, Ohio State Univ.

Baumert, J.H. 1974, *Astrophys. J.*, **190**, 85.

Baumert, J.H., and Johnson, H.R. 1984, in *Proc. NASA/GSFC Conf. on Future of UV Astronomy Based on 6 Years of IUE Research*, April 3-5, 1984.

Beardsley, W.R. 1961, *Astrophys. J. Supplement*, **5**, 381.

Beavers, W.I., Cadmus, R.R., and Eitter, J.J. 1982, *Astron. J.*, **87**, 818.

Beeckmans de West-Meerbeeck, F. 1969, *Étude Spectrale d'Étoiles Variables Infrarouges*, Mémoire de Licence en Sciences Physiques, Institut d'Astrophysique de Liège, Belgium.

Bergeat, J., and Lunel, M. 1980, *Astron. Astrophys.*, **87**, 139.

Berger, J., and Greenstein, J.L. 1963, *Pub. Astron. Soc. Pacific*, **75**, 336.

Berman, L. 1935, *Astrophys. J.*, **81**, 369.

Bessel, M.S., Wood, P.R., and Lloyd-Evans, T. 1983, *Mon. Not. Roy. Astr. Soc.*, **202**, 59.

Bidelman, W.P. 1948, *Astrophys. J.*, **107**, 413.

Bidelman, W.P. 1953, *Astrophys. J.*, **117**, 25.

Bidelman, W.P. 1956, in *Vistas in Astronomy*, vol. 2, ed. A. Beer (London: Pergamon), p. 1428.

Bidelman, W.P., and MacConnell, D.J. 1973, *Astron. J.*, **78**, 687.

Bidelman, W.P., and Pyper, D.M. 1963, *Pub. Astron. Soc. Pacific*, **75**, 389.

Blackwell, D.E., Petford, A.D., and Shallis, M.J. 1980, *Astron. Astrophys.*, **82**, 249.

Blackwell, D.E., Shallis, M.J. 1977, *Mon. Not. Roy. Astr. Soc.*, **180**, 177.

Blanco, V.M. 1965, in *Stars and Stellar Systems, Vol. V*, ed. A. Blaauw and M. Schmidt (Chicago: Chicago Univ. Press), p. 241.

Blanco, V.M., Hoag, A.A., and McCarthy, M.F. 1978, in *Proc. IAU Symp. 80, The HR Diagram*, ed. A.G.D. Philip and D.S. Hayes (Dordrecht: Reidel), p. 33.

Blanco, V.M., and McCarthy, M.F. 1983, *Astron. J.*, **88**, 1442.

Blanco, V.M., McCarthy, M.F., and Blanco, B.M. 1984, *Astron. J.*, **89**, 636.

Boesgaard, A.M. 1969, *Bull. Amer. Astron. Soc.*, **1**, 183.

Boesgaard, A.M. 1979, *Astrophys. J.*, **232**, 485.

Boesgaard, A.M., and Boesgaard, H. 1976, *Astrophys. J.*, **205**, 448.

Böhm-Vitense, E., and Johnson, H.R. 1985, *Astrophys. J.*, **293**, 288.

Böhm-Vitense, E., and Querci, M. 1986, in *Scientific Accomplishments of the IUE*, ed. Y. Kondo, Part III: Stars, Chp. 11, ed. C. de Jager (Dordrecht: Reidel), in press.

Bond, H.E. 1974, *Astrophys. J.*, **194**, 95.

Bond, H.E., and Neff, J.S. 1969, *Astrophys. J.*, **158**, 1235.

Bonneau, D., Foy, R., Blazit, A., and Labeyrie, A. 1982, *Astron. Astrophys.*, **106**, 235.

Bottlinger, C.F. 1910, *Astron. Nachr.*, **187**, 3.

Bouchet, P. 1984a, *Astron. Astrophys.*, **139**, 344.

Bouchet, P. 1984b, in preparation.

Bouchet, P., Querci, M., and Querci, F. 1983, *The Messenger*, **31**, 7.

Bowen, I.S. 1951, private communication.

Bowers, P.F., and Kundu, M.R. 1981, *Astron. J.*, **86**, 569.

Bowers, P.F., Reid, M.J., Johnston, K.J., Spencer, J.H., and Moran, J.M. 1980, *Astrophys. J.*, **242**, 1088.

Boyarchuk, A.A. 1974, in *Proc. IAU Symp. 66, Late Stages in Stellar Evolution*, ed. R.J. Tayler and J.E. Heesser (Dordrecht: Reidel), p. 198.

Boyd, L.J., Genet, R.M., and Hall, D.S. 1985, *Sky and Telescope*, **70**, 16.

Bregman, J.D., and Bregman, J.N. 1978, *Astrophys. J. (Letters)*, **222**, L41.

Brown, A. 1984, in *Cool Stars, Stellar Systems, and the Sun*, ed. S.L. Baliunas and L. Hartmann (New York: Springer-Verlag), p. 282.

Bujarrabal, V., Guibert, J., Nguyen-Q-Rieu, and Omont, A. 1980, *Astron. Astrophys.*, **84**, 311.

Bujarrabal, V., and Nguyen-Q-Rieu 1981, *Astron. Astrophys.*, **102**, 65.

Cahn, J.H. 1981, *Astron. J.*, **86**, 1935.

Cahn, J.H., and Elitzur, M. 1979, *Astrophys. J.*, **231**, 124.

Cameron, D., and Nassau, J.J. 1956, *Astrophys. J.*, **124**, 346.

Campbell, L. 1925, *Harvard Report*, No. 21.

Campbell, L. 1926, *Harvard Bull.*, No. 840, 5.

Campbell, L. 1938, *Pop. Astr.*, **46**, 56.

Campbell, L. 1941, *Ann. Harvard College Obs.*, **110**, 36, 69, 98, 175.

Campbell, L. 1943, *Pop. Astr.*, **51**, 400.

Campbell, L. 1947, *Ann. Harvard College Obs.*, **116**, 61, 181, 252.

Campbell, L. 1955, *Studies of Long-Period Variables* (Cambridge, Massachusetts: AAVSO).

Campbell, L., and Payne, C.H. 1930, *Harvard Bull.*, No. 872, 30.

Cannon, A.J. 1930, *Harvard Bull.*, No. 872, 28.

Carney, B.W. 1979, *Astrophys. J.*, **233**, 211.

Carpenter, K.G. 1984, *Astrophys. J.*, **285**, 181.

Carpenter, K.G., Brown, A., and Stencel, R.E. 1985, *Astrophys. J.*, **289**, 676.

Carpenter, K.G., and Wing, R.F. 1979, *Bull. Amer. Astron. Soc.*, **11**, 419, and private communication.

Cassatella, A., Heck, A., Querci, F., Querci, M., and Stickland, D. 1980, in *Proc. Second European IUE Conf.*, Tubingen, Germany.

Catchpole, R.M., and Feast, M.W. 1971, *Mon. Not. Roy. Astr. Soc.*, **154**, 197.

Catchpole, R.M., and Feast, M.W. 1985, in *Proc. Strasbourg Colloq. on Cool Stars with Excesses of Heavy Elements*, ed. M. Jaschek and P.C. Keenan (Dordrecht: Reidel), p. 113.

Catchpole, R.M., Robertson, B.S.C., and Warren, P.R. 1977, *Mon. Not. Roy. Astr. Soc.*, **181**, 391.

Catchpole, R.M., Robertson, B.S.C., Lloyd Evans, T.H.H., Feast, M.W., Glass, I.S., and Carter, B.S. 1979, *South Africa Astr. Obs. Circ.*, **1**, 61.

Celis, L. 1977, *Astron. Astrophys. Supplement*, **29**, 15.

Cimerman, M. 1979, *Astrophys. J. (Letters)*, **228**, L79.

Clark, F.O., Troland, T.H., and Johnson, D.R. 1982, *Astron. Astrophys.*, **261**, 569.

Clark, F.O., Waak, J.A., and Bologna, J.M. 1982, *Astron. J.*, **87**, 1803.

Clayton, M.L., and Feast, M.W. 1969, *Mon. Not. Roy. Astr. Soc.*, **146**, 411.

Code, A.D., Holm, A.V., and Bottemiller, R.L. 1980, *Astrophys. J. Supplement*, **43**, 501.

Code, A.D., and Meade, M.R. 1979, *Astrophys. J. Supplement*, **39**, 195.

Cohen, J.G., Frogel, J.A., Persson, S.E., and Elias, J.H. 1981, *Astrophys. J.*, **249**, 481.

Cowley, C.R., and Hutchings, J.B. 1978, *Pub. Astron. Soc. Pacific*, **90**, 636.

Cox, A.N. 1984, in *Proc. 25th Liège International Astrophysical Colloq. on Theoretical Problems in Stellar Stability and Oscillations* (Belgium: Institut d'Astrophysique, Liège).

Cox, G.C., and Parker, E.A. 1979, *Mon. Not. Roy. Astr. Soc.*, **186**, 197.

Coyne, G.V., and Shawl, S.J. 1973, *Astrophys. J.*, **186**, 961.

Crawford, D., Nelson-Limer, D., Mendoza, E., Schulte, D., Steinman, H., and Swihart, T. 1955, *Astrophys. J.*, **121**, 24.

Dainty, J.C. 1981, in *Proc. Symp. on Recent Advances in Observational Astronomy*, ed. H.L. Johnson and C. Allen (Ensenada, Mexico), p. 95.

DeGioia-Eastwood, K., Hackwell, J.A., Grasdalen, G.L., and Gehrz, R.D. 1981, *Astrophys. J. (Letters)*, **245**, L75.

Deguchi, S. 1980, *Astrophys. J.*, **236**, 567.

de Jager, C. 1980, *The Brightest Stars, Geophysics and Astrophysics Monographs*, ed. B.M. McCormack (Dordrecht: Reidel).

de Jong, T. 1983, *Astrophys. J.*, **274**, 252.

de la Reza, R., and Querci, F. 1978, *Astron. Astrophys.*, **67**, 7.

Dickinson, D.F., and Chaisson, E.J. 1973, *Astrophys. J. (Letters)*, **181**, L135.

Dickinson, D.F., Kollberg, E., and Yngvesson, D. 1975, *Astrophys. J.*, **199**, 131.

Dinerstein, H. 1973, *Journal AAVSO*, **2**, 52.

Dominy, J.F. 1982, Ph.D. Thesis, Univ. Texas at Austin.

Dominy, J.F. 1984, *Astrophys. J. Supplement*, **55**, 27.

Dominy, J.F., and Lambert, D.L. 1983, *Astrophys. J.*, **270**, 180.

Duerbeck, H.W., and Seitter, W.C. 1982, in *Landolt-Börnstein, Group VI, Vol. 2, Subvolume b, Stars and Star Clusters*, ed. K. Schaifers and H.H. Voigt (Berlin, Heidelberg: Springer-Verlag), pg. 197.

Dupree, A. 1986, *Ann. Rev. Astron. Astrophys.*, **24**.

Eaton, J.A., Johnson, H.R. O'Brien, G.T., and Baumert, J.H. 1985, *Astrophys. J.*, **290**, 276.

Eaton, J.A., and Poe, C.H. 1984, *Acta. Astron.*, **34**, 97.

Eggen, O.J. 1967, *Astrophys. J. Supplement*, **14**, 307.

Eggen, O.J. 1972a, *Mon. Not. Roy. Astr. Soc.*, **159**, 403.

Eggen, O.J. 1972b, *Astrophys. J.*, **174**, 45.

Eggen, O.J. 1973, *Astrophys. J.*, **180**, 857.

Eggen, O.J. 1975, *Astrophys. J.*, **195**, 661.

Eggen, O.J., Lynden-Bell, D., and Sandage, A.R. 1962, *Astrophys. J.*, **136**, 748.

Eggleton, P.P., and Faulkner, J. 1981, *Physical Processes in Red Giants*, ed. I. Iben and A. Renzini (Dordrecht: Reidel), p. 179.

Elitzur, M. 1978, *Astron. Astrophys.*, **62**, 305.

Elitzur, M., Goldreich, P., and Scoville, N. 1976, *Astrophys. J.*, **205**, 384.

Epchtein, N., Guibert, J., Nguyen-Q-Rieu, Turon, P., and Wamsteker, W. 1980, *Astron. Astrophys. (Letters)*, **85**, L1.

Eriksson, K., Gustafsson, B., Johnson, H.R., Querci, F., Querci, M., Baumert, J.H., Carlson, M., and Olofsson, H 1985, *Astron. Astrophys.*, **161**, 305.

Espin, T.E. 1889, *Mon. Not. Roy. Astr. Soc.*, **49**, 364.

Espin, T.E. 1898, *Mon. Not. Roy. Astr. Soc.*, **58**, 443.

Feast, M.W. 1962, *Mon. Not. Roy. Astr. Soc.*, **125**, 367.

Feast, M.W. 1969, in *Proc. IAU Colloq. 4, Variable Stars, Non-Periodic Phenomena in Variable Stars*, ed. L. Detre (Dordrecht: Reidel), p. 253.

Feast, M.W. 1975, in *Proc. IAU Symp. 67, Variable Stars and Stellar Evolution*, ed. V.E. Sherwood and L. Plaut (Dordrecht: Reidel), p. 129.

Feast, M.W. 1979, in *Proc. IAU Colloq. 46, Changing Trends in Variable Star Research*, ed. F.M. Bateson et al. (Hamilton, New-Zealand: Univ. Waikato Press), p. 246.

Feast, M.W. 1980, *Highlights in Astronomy*, ed. P.A. Wayman (IAU, Dordrecht: Reidel), **5**, 493.

Feast, M.W. 1981, *Physical Processes in Red Giants*, ed. I. Iben and A. Renzini (Dordrecht: Reidel), p. 193.

Feast, M.W., Catchpole, R.M., Carter, B.S., and Roberts, G. 1980, *Mon. Not. Roy. Astr. Soc.*, **193**, 377.

Feast, M.W., Catchpole, R.M., Lloyd-Evans, T., Robertson, B.S.C., Dean, J.F., and Bywater, R.A. 1977, *Mon. Not. Roy. Astr. Soc.*, **178**, 415.

Feast, M.W., and Glass, I.S. 1973, *Mon. Not. Roy. Astr. Soc.*, **161**, 293.

Feast, M.W., Robertson, B.S.C., Catchpole, R.M., Lloyd-Evans, T., Glass, I.S., and Carter, B.S. 1982, *Mon. Not. Roy. Astr. Soc.*, **201**, 439.

Feast, M.W., and Thackeray, A.D. 1956, *Mon. Not. Roy. Astr. Soc.*, **116**, 587.

Ferland, G.J., Lambert, D.L., McCall, M.L., Shields, G.A., and Slovak, M.H. 1982, *Astrophys. J.*, **260**, 794.

Fernie, J.D., Sherwood, V., and DuPuy, D.L. 1972, *Astrophys. J.*, **172**, 383.

Fillit, R., Proust, D., and Lépine, J.R.D. 1977, *Astron. Astrophys.*, **58**, 281.

FitzGerald, M.P., Houk, N., McCuskey, S.W., and Hoffleit, D. 1966, *Astrophys. J.*, **144**, 1135.

Fix, J.D. 1979, *Astrophys. J. (Letters)*, **232**, L39.

Fix, J.D., Mutel, R.L., Benson, J.M., and Claussen, M.L. 1980, *Astrophys. J. (Letters)*, **241**, L95.

Florya, N.F. 1949, Tr. Gos. Astron. Inst. Inn. Sternberger, **16**, 187.

Flower, D.R., Nussbaumer, H., and Schild, H. 1979, *Astron. Astrophys. (Letters)*, **72**, L1.

Fontaine, B. 1984, in *Proc. Prèmiere École Européenne de Photométrie Photoélectrique*, Toulouse, April 29—May 2, 1984, ed. F. Querci, p. 66.

Fontaine, B. 1985, in *Proc. Deuxieme École Européenne de Photométrie Photoélectrique*, Toulouse, April 5–7, 1985, ed. F. Querci, p. 127.

Forrest, W.J., Gillett, F.C., and Stein, W.A. 1972, *Astrophys. J. (Letters)*, **178**, L129.

Fox, M.W., and Wood, P.R. 1982, *Astrophys. J.*, **259**, 198.

Fredrick, L.W. 1960, *Astron. J.*, **65**, 628.

Frogel, J.A. 1971, Ph.D. Thesis, California Institute of Technology.

Fujita, Y. 1970, *Interpretation of Spectra and Atmospheric Structure in Cool Stars* (Tokyo: Univ. Tokyo Press).

Fujita, Y. 1980, *Space Science Rev.*, **25**, 89.

Fujita, Y., and Tsuji, T. 1976, *Proc. Japan Acad.*, **52**, 296.

Garcia, J.R. 1980, in *Proc. IAU Colloq. 46, Changing Trends in Variable Star Research*, ed. F.M. Bateson et al. (Hamilton, New-Zealand: Univ. Waikato Press), p. 235.

Garcia, J.R., Galassi, G.A., and Guedes, A.R. 1977, in *Proc. 29e Reunion de la Sociedade Brasileira para o Progresso da Ciencia*, Sao Paulo, 6 al 13 de Julio de 1977.

Garrigue, J.P. 1980, These de 3ième cycle, Faculté des Sciences et des Techniques du Languedoc, Montpellier, France.

Garrigue, J.P., and Mennessier, M.O. 1980, *Astron. Astrophys. (Letters)*, **81**, L13.

Gehrz, R.D., and Woolf, N.J. 1971, *Astrophys. J.*, **165**, 285.

Gehrz, R.D., Grasdalen, G.L., and Hackwell, J.A. 1981, *Bull. Amer. Astron. Soc.*, **13**, 895.

Gillett, F.C., Low, F.J., and Stein, W.A. 1968, *Astrophys. J. (Letters)*, **149**, L97.

Gillett, F.C., Merrill, K.M., and Stein, W.A. 1971, *Astrophys. J.*, **164**, 86.

Gilra, D.P. 1973, in *Proc. IAU Symp. 52, Interstellar Dust and Related Topics*, ed. J.M. Greenberg and H.C. van de Hulst (Dordrecht: Reidel), p. 517.

Gilra, D.P. 1976, *Mém. Soc. Roy. Sci. Liège*, 6th Ser., **IX**, 77.

Glasby, J.S. 1968, *Variable Stars* (Tiptrie, Essex: Ancher Press Ltd).

Glass, I.S. 1978, *Mon. Not. Roy. Astr. Soc.*, **182**, 93.

Glass, I.S. 1979, *Mon. Not. Roy. Astr. Soc.*, **186**, 317.

Glass, I.S., and Feast, M.W. 1982, *Mon. Not. Roy. Astr. Soc.*, **199**, 245.

Glass, I.S., and Lloyd-Evans, T. 1981, *Nature*, **291**, 303.

Goebel, J.H., Strecker, D.W., Witteborn, P.C., Bregman, J.D., and Erickson, E.F. 1978, *Bull. Amer. Astron. Soc.*, **10**, 407.

Goebel, J.H., Bregman, J.D., Goorvitch, D., Strecker, D.W., Puetter, R.C., Russell, R.W., Soifer, B.T., Willner, S.P., Forrest, W.J., Houck, J.R., and McCarthy, J.F. 1980, *Astrophys. J.*, **235**, 104.

Goldberg, L. 1979, *Quart. J. Roy. Astr. Soc.*, **20**, 361.

Goldberg, L. 1984, *Pub. Astron. Soc. Pacific*, **96**, 366.

Goldreich, P., and Scoville, N. 1976, *Astrophys. J.*, **205**, 144.

Gomes-Balboa, A., Lépine, J.R.D., and Pires, N. 1982, private communication.

Gordon, C.P. 1967, Ph.D. Thesis, Univ. Michigan.

Gow, C.E. 1976, *Astron. J.*, **81**, 993.

Greene, A.E., and Wing, R.F. 1971, *Astrophys. J.*, **163**, 309.

Greene, T.F., Peery, J., Snow, T.P., and Wallerstein, G. 1973, *Astron. Astrophys.*, **22**, 293.

Greenstein, J.L. 1948, *Astrophys. J.*, **108**, 78.

Grégory, C., and Querci, F. 1985, private communication.

Guinan, E.F. 1984, in *Proc. Third Cambridge Workshop on Cool Stars, Stellar Systems, and the Sun*, ed. S.L. Baliunas and L. Hartman (Berlin, Heidelberg: Springer-Verlag), p. 336.

Guzeva Yakimova, N.N. 1960, *Kursova Robota*, GAISh.

Hagen, J.G. 1925, *Astron. Nachr.*, **225**, 383.

Hack, M. 1967, *Sky and Telescope*, **33**, 74.

Hackwell, J.A. 1972, *Astron. Astrophys.*, **21**, 239.

Harrington, J.P. 1965, *Astron. J.*, **70**, 569.

Hartmann, L., and Apruzese, J.P. 1976, *Astrophys. J.*, **203**, 610.

Harvey, P.M. 1974, *Astrophys. J.*, **188**, 95.

Harvey, P.M., Bechis, K.B., Wilson, W.J., and Ball, J.A. 1974, *Astrophys. J. Supplement*, **27**, 331.

Hassenstein, W. 1938, *Pub. Astr. Obs. Potsdam*, **29**, Part 1.

Hayes, D.P. 1981, *Publ. Astron. Soc. Pacific*, **93**, 752.

Hayes, D.P. 1982, *Inf. Bull. Variable Stars (IAU Comm. 27)*, No. 2064.

Hecht, J.H., Holm, A.V., Donn, B., and Wu, C.C. 1984, *Astrophys. J.*, **280**, 228.

Henkel, C., Matthews, H.E., and Morris, M. 1983, *Astrophys. J.*, **267**, 184.

Herber, U., and Schönberner, D. 1980, in *Proc. Second European IUE Conference*, ESA SP-157, p. 327.

Herbig, G.H. 1949, *Astrophys. J.*, **110**, 143.

Herbig, G.H. 1958, *Mém. Soc. Roy. Sci. Liège*, **20**, 251.

Herbig, G.H. 1964, *Astrophys. J.*, **140**, 1317.

Herbig, G.H. 1965, *Kleine Veröff. Remeis-Sternwarte Bamberg*, **4**, 164.

Herbig, G.H. 1967, *Trans. IAU*, **A13**, 530.

Herbig, G.H. 1980, *IAU Circ.*, **3535**.

Herman, J. 1983, Ph.D. Thesis, Leiden Univ.

Hetzler, C. 1936, *Astrophys. J.*, **83**, 372.

Hill, P.W. 1964, *Mon. Not. Roy. Astr. Soc.*, **127**, 113.

Hill, P.W. 1967, *Observatory*, **87**, 210.

Hill, P.W., Kilkenny, D., Schönberner, D., and Walker, H.J. 1981, *Mon. Not. Roy. Astr. Soc.*, **197**, 81.

Hinkle, K.H., Hall, D.N.B., and Ridgway, S.T. 1982, *Astrophys. J.*, **252**, 697.

Hinkle, K.H., Lambert, D.L., and Snell, R.L. 1976, *Astrophys. J.*, **210**, 684.

Hjalmarson, Å., and Olofsson, H. 1979, *Astrophys. J. (Letters)*, **234**, L199.

Hjellming, R.M., and Gibson, D.M. 1980, in *Proc. IAU Symp. 86, Radiophysics of the Sun*, ed. M.R. Kundu and T.E. Gergely (Dordrecht: Reidel), p. 209.

Hoffleit, D. 1976, *Inf. Bull. Variable Stars (IAU Comm. 27)*, No. 1131.

Hoffleit, D. 1979, private communication.

Hoffleit, D. 1980, in *Proc. IAU Colloq. 46, Changing Trends in Variable Star Research*, ed. F.M. Bateson et al. (Hamilton, New-Zealand: Univ. Waikato Press), p. 235.

Horowitz, P., Papaliolios, C., and Carleton, N.P. 1971, *Astrophys. J. (Letters)*, **163**, L5.

Houck, N. 1963, *Astron. J.*, **68**, 253.

Howarth, I.D. 1976, *Journal AAVSO*, **5**, 8.

Howarth, I.D. 1977, *Acta Astronomica*, **27**, 65.

Hubble, E.P. 1940, *Ann. Rept. Dir. Mt. Wilson Obs.*, 1939–1940, p. 19.

Hubble, E.P. 1943, *Ann. Rept. Dir. Mt. Wilson Obs.*, 1942–1943, p. 17.

Humphreys, R.M. 1974, *Astrophys. J.*, **188**, 75.

Humphreys, R.M. 1978, *Astrophys. J. Supplement*, **38**, 309.

Humphreys, R.M. 1979, *Astrophys. J. Supplement*, **39**, 389.

Humphreys, R.M., and Ney, E.P. 1974, *Astrophys. J.*, **190**, 339.

Hunger, K. 1975, *Problems in Stellar Atmospheres and Envelopes*, ed. B. Baschek, W.H. Kegel, and G. Traving (New York: Springer-Verlag), p. 57.

Hyland, A.R., Becklin, E.E., Frogel, J.A., and Neugebauer, G. 1972, *Astron. Astrophys.*, **16**, 204.

Iben, I. 1981a, *Physical Processes in Red Giants*, ed. I. Iben and A. Renzini (Dordrecht: Reidel), p. 3.

Iben, I. 1981b, *Astrophys. J.*, **246**, 278.

Iben, I. 1984, in *Obs. Tests of the Stellar Evol. Theory*, ed. A. Maeder and A. Renzini (Dordrecht: Reidel), p. 30

Iben, I. 1985, *Quart. J. Roy. Astr. Soc.*, **26**, 1.

Iben, I., and Renzini, A. 1983, *Ann. Rev. Astron. Astrophys.*, **21**, 277.

Ichikawa T. 1981, *Pub. Astron. Soc. Japan*, **33**, 107.

Ikaunieks, J. 1975, *Pulsating Stars*, ed. B.V. Kukarkin (New York: John Wiley), p. 259.

Ilovaisky, S.A., and Spinrad, H. 1966, *Pub. Astron. Soc. Pacific*, **78**, 527.

Innes, R.T.A. 1903, *Ann. Cape Observatory*, **9**, 135B.

Innes, R.T.A. 1907, *Astr. Nachr.*, **175**, 127.

Ishida, K. 1960, *Pub. Astron. Soc. Pacific*, **12**, 214.

Isles, J.E. 1973, *J. Brit. Astr. Assoc.*, **83**, 368.

Jacchia, L. 1933, *Pub. Astron. Obs. U. Bol.*, **2**, 173.

Jacobsen, T.S., and Wallerstein, G. 1975, *Pub. Astron. Soc Pacific*, **87**, 269.

Jaschek, C. 1985, *Cool Stars with Excesses of Heavy Elements*, ed. M. Jaschek and P.C. Keenan (Dordrecht: Reidel), p. 3.

Jewell, P.R., Elitzur, M., Webber, J.C., and Snyder, L.E. 1979, *Astrophys. J. Supplement*, **41**, 191.

Johnson, H.L. 1966, *Ann. Rev. Astron. Astrophys.*, **4**, 196.

Johnson, H.L., Iriarte, B., Mitchell, R.I., and Wisniewski, W.Z. 1966, *Comm. Lunar and Planetary Obs.*, **4**, 99.

Johnson, H.L., and Mitchell, R.I. 1975, *Rev. Mexicana de Astron. y Astrof.*, **1**, 299.

Johnson, H.R. 1978, *Astrophys. J.*, **223**, 238.

Johnson, H.R. 1982, *Astrophys. J.*, **260**, 254.

Johnson, H.R., Ameen, M.M., and Eaton, J.A. 1984, *Astrophys. J.*, **283**, 760.

Johnson, H.R., Baumert, J.H., Querci, F., and Querci, M. 1986, *Astrophys. J.*, in press.

Johnson, H.R., and Luttermoser, D.J. 1986, preprint (to appear in *Astrophys. J.*).

Johnson, H.R., and O'Brien, G.T. 1983, *Astrophys. J.*, **265**, 952.

Jones, H. S. 1928, *Mon. Not. Roy. Astr. Soc.*, **88**, 660.

Jones, T.J., Hyland, A.R., Wood, P.R., and Gatley, I. 1982, *Astrophys. J.*, **253**, 208.

Joshi, S.C., and Rautela, B.S. 1978, *Mon. Not. Roy. Astr. Soc.*, **183**, 55.

Joshi, S.C., Rautela, B.S., and Sanwal, B.B. 1980, *Inf. Bull. Variable Stars (IAU Comm. 27)*, No. 1754.

Joy, A.H. 1942, *Astrophys. J.*, **96**, 344.

Kafatos, M., and Michalitsianos, A.G. 1982, *Nature*, **298**, 540.

Kafatos, M., Hollis, J.M., and Michalitsianos, A.G. 1983, *Astrophys. J. (Letters)*, **267**, L103.

Karovska, M. 1984, Thèse de 3ième cycle, Université de Nice.

Keenan, P.C. 1966, *Astrophys. J. Supplement*, **13**, 333.

Keenan, P.C., and Boeshaar, P.C. 1980, *Astrophys. J. Supplement*, **43**, 379.

Keenan, P.C., Garrison, R.F., and Deutsch, A.J. 1974, *Astrophys. J. Supplement*, **28**, 271.

Keenan, P.C., and McNeil, R.C. 1976, *An Atlas of Spectra of the Cooler Stars* (Columbus: Ohio State U. Press).

Keenan, P.C., and Morgan, W.W. 1941, *Astrophys. J.*, **94**, 501.

Keenan, P.C., and Pitts, R.E. 1980, *Astrophys. J. Supplement*, **42**, 541.

Kellermann, K.I., and Pauliny-Toth, I.I.K. 1966, *Astrophys. J.*, **145**, 933.

Kilkenny, D. 1982, *Mon. Not. Roy. Astr. Soc.*, **200**, 1019.

Kilkenny, D. 1983, *Mon. Not. Roy. Astr. Soc.*, **205**, 907.

Kilkenny, D., and Lynas-Gray, A.E. 1982, *Mon. Not. Roy. Astr. Soc.*, **198**, 873.

Kilkenny, D., and Flanagan, C. 1983, *Mon. Not. Roy. Astr. Soc.*, **203**, 19.

Kjaergaard, P., Nørgaard-Nielsen, H.U., Cacciari C., and Wamsteker, W. 1984, *Astron. Astrophys.*, **133**, 363.

Klemola, A.R. 1961, *Astrophys. J.*, **134**, 130.

Kolotilov, E.A., Orlov, M.Y., and Rodriguez, M.H. 1974, *Soviet Astr.*, **17**, 615.

Krempec, J. 1973, *Studia Societatis Scientiarum Torunensis (Torun: Polonia)*, **5**, No. 2, Sectio F (Astronomia), p. 19.

Krempec, J. 1975, *Acta Astron.*, **25**, 235.

Krisciunas, K. 1982, *Inf. Bull. Variable Stars (IAU Comm. 27)*, No. 2104.

Krishna Swamy, K.S. 1972, *Pub. Astron. Soc. Pacific*, **84**, 64.

Kukarkin, B.W. 1949, *Trudy Gos. Astr. Inst. Sternberga*, **16**, 128.

Kukarkin, B.V., Kholopov, P., Efremov, Y.U., Kukarkina, N.P., Kuruchkin, N.E., Medvedeva, G.I., Perova, N.B., Federovitch, V.P., and Frolov, M.S.: 1958, *General Catalogue of Variable Stars (GCVS)*, 3rd Supplement, 3rd Ed., 1976.

Lacaille, J. 1847, *Catalogue of the Southern Stars* (London: British Association).

Lambert, D.L. 1981, *Physical Processes in Red Giants*, ed. I. Iben and A. Renzini (Dordrecht: Reidel), p. 115.

Lambert, D.L. 1985, *Cool Stars With Excesses of Heavy Elements*, ed. M. Jaschek and P.C. Keenan (Dordrecht: Reidel), p. 191.

Lampland, C.O. 1923a, *Pub. Amer. Astron. Soc.*, **4**, 366.

Lampland, C.O. 1923b, *Pub. Amer. Astron. Soc.*, **4**, 320.

Landolt, A.U. 1968, *Pub. Astron. Soc. Pacific*, **80**, 318.

Landolt, A.U. 1973, *Pub. Astron. Soc. Pacific*, **85**, 661.

Lee, O.J., Baldwin, R.B., Hamlin, D.W., and Kinnaird, R.F. 1940, *Ann. Dearborn Obs.*, **4**, Part 16.

Lee, O.J., and Bartlett, T.J. 1945, *Ann. Dearborn Obs.*, **5**, Part 3.

Lee, O.J., Gore, G.D., and Bartlett, T.J. 1947, *Ann. Dearborn Obs.*, **5**, Part 7.

Lee, T.A. 1970, *Astrophys. J.*, **162**, 217.

Lee, T.A., and Feast, M.W. 1969, *Astrophys. J. (Letters)*, **157**, L173.

Léger, A., and Puget, J.L. 1984, *Astron. Astrophys. (Letters)*, **137**, L5.

Lépine, J.R.D., Paes de Barros, M.H., and Gammon, R.H. 1976, *Astron. Astrophys.*, **48**, 269.

Lesqueren, A.M. 1983, *IAU Circ.*, No. 3838.

Leung, K.C. 1971, *Bull. Amer. Astron. Soc.*, **3**, 485.

Leung, K.C. 1973, *Bull. Amer. Astron. Soc.*, **5**, 415.

Leung, K.C. 1980, in *Proc. GSFC Conf. on Current Problems in Stellar Pulsation Instabilities*, ed. D. Fischel et al., NASA TM-80625, p. 567.

Linsky, J.L. 1980, *Ann. Rev. Astron. Astrophys.*, **18**, 439.

Linsky, J.L. 1982, in *Advances in Ultraviolet Astronomy: Four Years of IUE Research*, ed. Y. Kondo, J.M. Mead, and R.D. Chapman, NASA CP-2238, p. 17.

Linsky, J.L. 1985, *Solar Physics*, **100**, 333.

Linsky, J.L., and Haisch, B.M. 1979, *Astrophys. J. (Letters)*, **229**, L27.

Livi, S.H.B., and Bergmann, T.S. 1982, *Astron. J.*, **87**, 1783.

Little-Marenin, I.R., and Little, S.J. 1979, *Astron. J.*, **84**, 1374.

Litvak, M.M. 1969, *Astrophys. J.*, **156**, 471.

Litvak, M.M., and Dickinson, D.F. 1972, *Astrophys. J. (Letters)*, **12**, L113.

Lloyd-Evans, T. 1983, *Mon. Not. Roy. Astr. Soc.*, **204**, 985.

Lockwood, G.W., and McMillan, R.S. 1970, in *Proc. Tucson Conf. on Late-Type Stars*, ed. G.W. Lockwood and H.M. Dyck, KPNO Contribution 554, p. 171.

Lockwood, G.W., and Wing, R.F. 1971, *Astrophys. J.*, **169**, 63.

Loreta, E. 1934, *Astr. Nachr.*, **254**, 151.

Low, F.J. 1965, *IAU Circ.*, No. 1884-5.

Lucy, L.B., Robertson, J.A., and Sharp, C.M. 1986, *Astron. Astrophys.*, **154**, 267.

Ludendorff, H. 1906, *Astr. Nachr.*, **173**, 1.

Ludendorff, H. 1923, *Astr. Nachr.*, **217**, 161.

Ludendorff, H. 1928, *Handbuch der Astrophysics*, **6**, 127.

MacConnell, D.J., Frye, R.L., and Upgren, A.R. 1972, *Astron. J.*, **77**, 384.

Maeder, A. 1980, *Astron. Astrophys.*, **90**, 311.

Maehara, H. 1968, *Pub. Astron. Soc. Japan*, **20**, 77.

Maehara, H. 1971, *Pub. Astron. Soc. Japan*, **23**, 503.

Maehara, H., and Yamashita, Y. 1978, *Ann. Tokyo National Obs.*, **17**, Ser. 2, 93.

Mammano, A., and Ciatti, F. 1975, *Astron. Astrophys.*, **39**, 405.

Mantegazza, L. 1982, *Astron. Astrophys.*, **111**, 295.

Maran, S.P., Heinsheimer, T.F., Stocker, T.L., Anand, S.P.S., Chapman, R.D., Hobbs, R.W., Michalitsianos, A.G., Wright, F.M., and Kipp, S.L. 1977, *Infrared Physics*, **17**, 565.

Maran, S.P., Michalitsianos, A.G., Heinsheimer, T.F., and Stocker, T.L. 1980, in *Proc. GSFC Conf. on Current Problems in Stellar Pulsations Instabilities*, ed. D. Fischel et al., NASA TM-80625, p. 629.

Marino, B.F., Walker, W.S.G., Beuning, J.A., and Blow, G. 1979, in *Proc. IAU Colloq. 46, Changing Trends in Variable Star Research*, ed. F.M. Bateson et al. (Hamilton, New-Zealand: Univ. Waikato Press), p. 223.

Maron, N. 1974, *Nature*, **252**, 214.

Marraco, H.G., and Milesi, G. 1980, *Bull. Assoc. Argentina Astron.*, **25**, 32.

Marraco, H.G., and Milesi, G. 1982, *Astron. J.*, **87**, 1775.

Mauron, N., Niéto, J.L., Picat, J.P., Lelièvre, G., and Sol, H. 1985, *Astron. Astrophys. (Letters)*, **142**, L13.

Mayall, M.W. 1960a, *J. Roy. Astr. Soc. Canada*, **54**, 193.

Mayall, M.W. 1960b, *Quart. Reports AAVSO*, **24**.

Mayall, M.W. 1964, *Quart. Reports AAVSO*, **26**.

Mayall, M.W. 1966, *Quart. Reports AAVSO*, **27**.

McClure, R.D. 1983, *Astrophys. J.*, **268**, 264.

McClure, R.D. 1984, *Pub. Astron. Soc. Pacific*, **96**, 117.

McClure, R.D. 1985, *Cool Stars With Excesses of Heavy Elements*, ed. M. Jaschek and P.C. Keenan (Dordrecht: Reidel), p. 315.

McClure, R.D., Fletcher, J.M., and Nemec, J.M. 1980, *Astrophys. J. (Letters)*, **238**, L35.

McCuskey, S.W. 1965, *IAU Circ.*, No. 1916–1917.

McKellar, A., and Buscombe, W. 1948, *Pub. Dominion Astrophys. Obs.*, **7**, 361.

McKellar, A., and Richardson, E.H. 1955, *Mem. Soc. Roy. des Sci. de Liège*, **15**, 256.

McLaughin, D.B. 1935, *Pub. Amer. Astron. Soc.*, **8**, 145.

Mendoza, E.E. 1967, *Bull. Obs. Tonantzintla y Tucabaya*, **4**, 114.

Mendoza, E.E. 1968, *Univ. Chile Pub.*, **7**, 106.

Mendoza, E.E. 1978, *Bull. Amer. Astron. Soc.*, **10**, 615.

Mendoza, E.E., and Johnson, H.L. 1965, *Astrophys. J.*, **141**, 161.

Merchant, A.E. 1967, *Astrophys. J.*, **147**, 587.

Merchant-Boesgaard, A. 1970, *Astrophys. J.*, **161**, 1003.

Merrill, P.W. 1928, *Ann. Harvard College Obs.*, **79**, 205.

Merrill, P.W. 1935, *Astrophys. J.*, **81**, 312.

Merrill, P.W. 1940, *Spectra of Long-Period Variable Stars, Astrophysical Monographs*, sponsored by the Astrophys. J. (Chicago: Univ. Chicago Press).

Merrill, P.W. 1941, *Astrophys. J.*, **94**, 171.

Merrill, P.W. 1946, *Astrophys. J.*, **103**, 6.

Merrill, P.W. 1950, *Astrophys. J.*, **112**, 514.

Merrill, P.W. 1960, *Astrophys. J.*, **131**, 385.

Merrill, P.W., and Burwell, C.G. 1950, *Astrophys. J.*, **112**, 72.

Michalitsianos, A.G., Kafatos, M., and Hobbs, R.W. 1980, *Astrophys. J.*, **237**, 506.

Michalitsianos, A.G., and Kafatos, M. 1982, *Astrophys. J. (Letters)*, **262**, L47.

Mikami, T., and Ishida, K. 1981, *Pub. Astron. Soc. Japan*, **33**, 135.

Morgan, W.W., Keenan, P.C., and Kellman, E. 1943, *An Atlas of Stellar Spectra* (Chicago: Univ. Chicago Press).

Morris, M., Redman, R., Reid, M.J., and Dickinson, D.F. 1979, *Astrophys. J.*, **229**, 257.

Neugebauer, G., Beichman, C.A., Soifer, B.T., Aumann, H.H., Chester, T.J., Gautier, T.N., Gillett, F.C., Hauser, M.G., Houck, J.R., Lonsdale, C.J., Low, F.J., and Young, E.T. 1984, *Science*, **224**, 14.

Neugebauer, G., and Leighton, R.B. 1969, *Two-Micro Sky Survey*, NASA SP-3047.

Newell, R.T., and Hjellming, R.M. 1982, *Astrophys. J. (Letters)*, **263**, L85.

Nielsen, A.V. 1952, *Pub. Mind. Medd. Kobenhavens Obs.*, **157**, 22.

Noguchi, N., Kaware, K., Kobayashi, Y., Okuda, H., and Sato, S. 1981, *Pub. Astron. Soc. Japan*, **33**, 373.

Noguchi, N., Maehara, T., Okuda, H., Sato, S., and Mukai, T. 1977, *Pub. Astron. Soc. Japan*, **29**, 511.

Nudjenko, A.C. 1974, *Russian Variable Stars*, **19**, 381.

Nussbaumer, H., and Schild, H. 1981, *Astron. Astrophys.*, **101**, 118.

Oberstatter, A. (Abbé) 1972, *Bull. de la Société d'Astronomie Populaire de Toulouse*, No. 547, 129.

O'Keefe, J.A. 1939, *Astrophys. J.*, **90**, 294.

Olnon, F.M. 1977, Ph.D. Thesis, Univ. Leiden.

Olnon, F.M., Baud, B., Habing, H., de Jong, T., Harris, S., and Pottasch, S.R. 1984, *Astrophys. J. (Letters)*, **278**, L41.

Olson, R.I., and Richer, H.B. 1975, *Astrophys. J.*, **200**, 88.

Orlov, M.Y., and Rodriguez, M.H. 1974, *Astron. Astrophys.*, **31**, 203.

Orlov, M.Y., and Rodriguez, M.H. 1981, *Soviet Astron. (Letters)*, **7**, 126.

Ostlie, D.A., Cox, A.N., and Cahn, J.H. 1982, in *Proc. Boulder Conf. on Pulsations in Classical and Cataclysmic Variable Stars*, ed. J.P. Cox and C.J. Hansen (Univ. Colorado: JILA), p. 297.

Osvalds, V., and Risley, A.M. 1961, *Pub. Leander McCormick Obs.*, **11**, Part 21.

Palmer, L.G., and Wing, R.F. 1982, *Astron. J.*, **87**, 1739.

Parenago, P.P. 1938, *Trudy Gos. Astron. Inst. Sternberga*, **12**, 1.

Pataki, L., and Kolena, J. 1974a, *Bull. Amer. Astron. Soc.*, **6**, 340.

Pataki, L., and Kolena, J. 1974b, *IAU Circ.*, No. 2680.

Patterson, R.S., Fix, J.D., and Neff, J.S. 1976, *Astrophys. J.*, **204**, 838.

Payne, C., and Campbell, L. 1930, *Harvard Bull.*, **875**, 1.

Payne-Gaposchkin, C. 1944, *Ann. Harvard College Obs.*, **113**, 191.

Payne-Gaposchkin, C. 1954a, *Variable Stars and Galactic Structure*, ed. University of London (The Athlone Press).

Payne-Gaposchkin, C. 1954b, *Ann. Harvard College Obs.*, **113**, 207.

Payne-Gaposchkin, C. 1963, *Astrophys. J.*, **138**, 320.

Payne-Gaposchkin, C. 1975, in *Proc. IAU Symp. 72, Abundance Effects in Classification*, ed. B. Hauck and P.C. Keenan (Dordrecht: Reidel), p. 91.

Payne-Gaposchkin, C., and Boyd, C. 1946, *Astrophys. J.*, **104**, 357.

Pecker, J.C. 1976, *Highlights of Astronomy*, ed. E.A. Muller (Dordrecht: Reidel), **4**, p. 3.

Petrov, R. 1983, Ph.D. Thesis, Université de Nice, France.

Pettit, E. 1945, *Pub. Astron. Soc. Pacific*, **57**, 174.

Pettit, E., and Nicholson, S.B. 1933, *Astrophys. J.*, **78**, 320.

Piccirillo, J. 1977, Ph.D. Thesis, Indiana University.

Piccirillo, J. 1980, *Mon. Not. Roy. Astr. Soc.*, **190**, 441.

Pickering, E.C. 1898, *Harvard Circ.*, No. 9.

Pickering, E.C. 1908, *Harvard Circ.*, No. 145.

Pierce, J.N., Willson, J.A., and Beavers, W.I. 1979, *Pub. Astron. Soc. Pacific*, **91**, 372.

Plummer, G.M., Herbst, E., and De Lucia, F.C. 1984, *Astrophys. J. (Letters)*, **282**, L113.

Polyakova, T.A. 1983, *Trudy Astron. Obs. LGU*, **38**, 91.

Prager, R. 1934, *Geschichte und Literatur des Lichtwechsels der Veränderlichen Sterne*, Zweite Ausgabe, Berlin.

Prager, R., and Schneller, H. 1934–1963, *Geschichte und Literatur des Lichtwechsels der Veränderlichen Sterne*, Z. Ausgabe, Band I-V, Ferd. Dümmler und Akademic-Verlag, Berlin.

Proust, D., and Verdenet, M. 1983, *La Bonne Étoile*, No. 73 (AFOEV).

Puetter, R.C., Russell, R.W., Soifer, B.T., and Willner, S.P. 1978, *Astrophys. J. (Letters)*, **223**, L93.

Pugach, A.F. 1977, *Inf. Bull. Variable Stars (IAU Comm. 27)*, No. 1277.

Purton, C.R., Feldman, P.A., and Marsh, K.A. 1973, *Nature Phys. Sci.*, **245**, 5.

Querci, M., Courtin, R., Querci, F., Coron, N., and Gispert, R. 1979, *Astron. Astrophys.*, **77**, 155.

Querci, F., and Querci M. 1975, *Astron. Astrophys.*, **39**, 113.

Querci, F., and Querci, M. 1977, in *Proc. 21ième Colloq. International d'Astrophysique*, Les Spectres des Molécules Simples au Laboratoire et en Astrophysique, ed. Univ. Liège (Liège: Belgium), p. 206.

Querci, F., and Querci, M. 1983, in *Proc. Japan-France Seminar on Active Phenomena in the Outer Atmosphere of Sun and Stars*, ed. J.C. Pecker and Y. Uchida (Paris: Collège de France), p. 140.

Querci, F., and Querci, M. 1985a, *Astron. Astrophys.*, **147**, 121.

Querci, F., and Querci, M. 1985b, in *Cool Stars with Excesses of Heavy Elements*, ed. M. Jaschek and P.C. Keenan (Dordrecht: Reidel), p. 99.

Querci, F., Querci, M. 1986, in preparation.

Querci, F., Querci, M., and Tsuji, T. 1974, *Astron. Astrophys.*, **31**, 265.

Querci, F., Querci, M., Wing, R.F., Cassatella, A., and Heck, A. 1982, *Astron. Astrophys.*, **111**, 120.

Querci, M., and Querci, F. 1976, *Astron. Astrophys.*, **43**, 443.

Querci, M., and Querci, F. 1978, *Astron. Astrophys. (Letters)*, **70**, L45.

Rao, N.K. 1974, Ph.D. Thesis, Univ. California, Santa Cruz.

Rao, N.K. 1975, *Bull. Astron. Soc. India*, **3**, 51.

Rao, N.K. 1980a, in *Proc. IAU Colloq. 59, Effects of Mass Loss on Stellar Evolution*, ed. C. Chiosi and R. Stalio (Dordrecht: Reidel), p. 469.

Rao, N.K. 1980b, *Astrophys. Space Sci.*, **70**, 489.

Rao, N.K., Ashok, N.M., and Kulkarni, P.V. 1980, *J. Astrophys. Astr.*, **1**, 71.

Rao, N.K., Nandy, K., and Bappu, M.K.V. 1981, *Mon. Not. Roy. Astr. Soc.*, **195**, 71P.

Reid, M.J., Muhleman, D.O., Moran, J.M., Johnston, K.J., and Schwartz, P.R. 1977, *Astrophys. J.*, **214**, 60.

Renzini, A. 1984, in *Obs. Tests of the Stellar Evol. Theory*, ed. A. Maeder and A. Renzini (Dordrecht: Reidel), p. 21.

Richer, H.B. 1975, *Astrophys. J.*, **197**, 611.

Richer, H.B. 1981, *Physical Processes in Red Giants*, ed. I. Iben and A. Renzini (Dordrecht: Reidel), p. 153.

Richer, H.B. 1985, *Inf. Bull. CFHT*, **13**, 14.

Ridgway, S.T., Jacoby, G.H., Joyce, R.R., Siegel, M.J., and Wells, D.C. 1982, *Astron. J.*, **87**, 808.

Ridgway, S.T., Jacoby, G.H., Joyce, R.R., and Wells, D.C. 1980b, *Astron. J.*, **85**, 1496.

Ridgway, S.T., Joyce, R.R., White, N.M., and Wing, R.F. 1980a, *Astrophys. J.*, **235**, 126.

Ridgway, S.T., Wells, D.C., and Joyce, R.R. 1977, *Astron. J.*, **82**, 414.

Robertson, B.S.S., and Feast, M.W. 1981, *Mon. Not. Roy. Astr. Soc.*, **196**, 111.

Robinson, L. 1970, *AAVSO Abstracts*, fall issue, 6.

Robinson, S.E., and Van Blerkom, D.J. 1981, *Astrophys. J.*, **249**, 566.

Rocca-Volmerange, B., and Audouze, J. 1979, *Astron. Astrophys.*, **75**, 371.

Roddier, C., and Roddier, F. 1983, *Astrophys. J. (Letters)*, **270**, L23.

Roddier, F., and Roddier, C. 1985, *Astrophys. J. (Letters)*, **295**, L21.

Roddier, F., Roddier, C., and Karovska, M. 1984, *UCLA Workshop on Mass Loss from Red Giants*, ed. M. Morris and B. Zuckerman (Dordrecht: Reidel).

Romano, G. 1950, *Osservazioni Visuali ed Elementi di Quattrostelle Variabili* (Trieste).

Röser, M. 1975, *Astron. Astrophys.*, **45**, 335.

Rybski, P.M. 1973, in *Proc. IAU Symp. 50, Spectral Classification and Multicolor Photometry*, ed. C. Fehrenbach and B.E. Westerlund (Dordrecht: Reidel), p. 96.

Sackmann-Juliana, I., Smith, L.R., and Despain, K.H. 1974, *Astrophys. J.*, **187** 555.

Sanford, R.F. 1933, *Astrophys. J.*, **77**, 110.

Sanford, R.F. 1944, *Astrophys. J.*, **99**, 145.

Sargent, W.L.W. 1961, *Astrophys. J.*, **134**, 142.

Scalo, J.M. 1973, *Astrophys. J.*, **186**, 967.

Scalo, J.M. 1976, *Astrophys. J.*, **206**, 474.

Scalo, J.M. 1981, *Physical Processes in Red Giants*, ed. I. Iben and A. Renzini (Dordrecht: Reidel), p. 77.

Scalo, J.M. 1984, private communication.

Schaefer, B.E. 1985, *Bull. Amer. Astron. Soc.*, **17**, 598.

Scharlach, W.W.G., and Woolf, N.J. 1979, *Pub. Astron. Soc. Pacific*, **91**, 380.

Schjellerup, H. 1866, *Astr. Nachtr.*, **67**, 97.

Schmitt, J.L. 1971, *Astrophys. J.*, **163**, 75.

Schneller, H. 1965, *Mitt. Ver. Sterne (Sonneberg)*, **3**, 86.

Schönberner, D. 1975, *Astron. Astrophys.*, **44**, 383.

Schönberner, D. 1977, *Astron. Astrophys.*, **57**, 437.

Schönberner, D., and Hunger, K. 1978, *Astron. Astrophys. (Letters)*, **70**, L57.

Schwartz, P.R., Harvey, P.M., and Barrett, A.H. 1974, *Astrophys. J.*, **187**, 491.

Schwarzschild, M. 1975, *Astrophys. J.*, **195**, 137.

Seaquist, E.R. 1967, *Astrophys. J. (Letters)*, **148**, L23.

Secchi, A. (Padre) 1868, *Mon. Not. Roy. Astr. Soc.*, **28**, 196.

Seeds, M.A., and Ignatuk, N. 1973, *Bull. Amer. Astron. Soc.*, **5**, 344.

Serkowski, K., and Kruszewski, A. 1969, *Astrophys. J. (Letters)*, **155**, L15.

Shajn, G., and Struve, O. 1947, *Astrophys. J.*, **106**, 86.

Shane, C.D. 1928, *Lick Obs. Bull.*, **13**, 123.

Shapley, H. 1929, *Harvard Bull.*, No. 868, 14.

Sharpless, S., Riegel, K., and Williams, J. 1966, *J. Roy. Astr. Soc. Canada*, **60**, 15.

Shenavrin, V.I. 1979, *Soviet Astr.*, **23**(6), 696.

Sherbakov, A.G. 1979, *Pisma V. Astron. Zh.*, **5**, 542.

Sherwood, V.E. 1976, in *Proc. IAU Symp. 67, Variable Stars and Stellar Evolution*, ed. V.E. Sherwood and L. Plaut (Dordrecht: Reidel), p. 147.

Sidgreaves, W., S.J. (Rev.) 1897, *Mon. Not. Roy. Astr. Soc.*, **58**, 344.

Slutz, S. 1976, *Astrophys. J.*, **210**, 750.

Smith, H.A. 1974, *Journal AAVSO*, **3**, 20.

Smith, H.A. 1976, *Journal AAVSO*, **5**, 67.

Smith, V.V. 1984, *Astron. Astrophys.*, **132**, 326.

Smith, V.V., and Lambert, D.L. 1985, *Astrophys. J.*, preprint.

Smolinski, J., Feldman, P.A., and Higgs, L.A. 1977, *Astron. Astrophys.*, **60**, 277.

Snyder, L.E., and Buhl, D. 1975, *Astrophys. J.*, **197**, 329.

Sopka, R.J., Herbig, G.H., Kafatos, M., and Michalitsianos, A.G. 1982, *Astrophys. J. (Letters)*, **258**, L35.

Space Telescope Observatory, 1982, ed. D.N.B. Hall, NASA CP-2244.

Spencer, J.H., Winnberg, A., Olnon, F.M., Schwartz, P.R., Matthews, H.E., and Downes, D. 1981, *Astron. J.*, **86**, 392.

Spergel, D.N., Giuliani, J.L., and Knapp, G.R. 1983, *Astrophys. J.*, **275**, 330.

Spinrad, H., and Wing, R.F. 1969, *Ann. Rev. Astron. Astrophys.*, **7**, 249.

Spite, F., and Spite, M. 1979, *Astron. Astrophys.*, **80**, 61.

Stanton, R.H. 1983, *Journal AAVSO*, **12**, 78.

Starrfield, S.G., Sparks, W.M., and Williams, R.E. 1982, in *Proc. NASA/GSFC Conf. on Advances in Ultraviolet Astronomy, Four Years of IUE Research*, ed. Y. Kondo and R.D. Chapman, NASA CP-2238, p. 470.

Stebbins, J. 1932, *Publ. Washburn Obs.* (Univ. Wisconsin), **15**, 177.

Steiman-Cameron, T.Y., Johnson, H.R., and Honeycutt, R.K. 1985, *Astrophys. J. (Letters)*, **291**, L51.

Stein, W.A., Gaustad, J.E., Gillett, F.C., and Knacke, R.F. 1969, *Astrophys. J. (Letters)*, **155**, L3.

Stencel, R.E., and Mullan, D.J. 1980, *Astrophys. J.*, **238**, 221.

Stencel, R.E., Linsky, J.L., Brown, A., Jordan, C., Carpenter, K.G., Wing, R.F., and Czyzak, S. 1981, *Mon. Not. Roy. Astr. Soc.*, **196**, 47p.

Stephenson, C.B. 1967a, *Astrophys. J.*, **149**, 35.

Stephenson, C.B. 1967b, *Astrophys. J.*, **150**, 543.

Stephenson, C.B. 1973, *Pub. Warney and Swasey Obs.*, **1**, No. 4.

Sterne, T.E. 1935, *Harvard Bull.*, No. 896, 16.

Sterne, T.E., and Campbell, L. 1937, *Harvard Reprint*, **23**, 115.

Stickland, D.J. 1985, *The Observatory*, **105**, 229.

Stickland, D.J., and Sanner, F. 1981, *Mon. Not. Roy. Astr. Soc.*, **197**, 791.

Stothers, R. 1972, *Astron. Astrophys.*, **18**, 325.

Stothers, R., and Leung, K.C. 1971, *Astron. Astrophys.*, **10**, 290.

Stratton, F.J.M. 1925, *Astronomical Physics* (London: Methuen), 132.

Strecker, D.W. 1975, *Astron. J.*, **80**, 451.

Strecker, D.W., Erickson, E.F., and Witteborn, F.C. 1979, *Astrophys. J. Supplement*, **41**, 501.

Strohmeier, W. 1972, *Variable Stars*, ed. A.J. Meadows (Pergamon Press).

Tapia, S., Crane, E.R., and Jacoby, G. 1982, *IAU Circ.*, No. 3729.

Thomas, R.N. 1973, *Astron. Astrophys.*, **29**, 297.

Thompson, K.D. 1981, *Journal AAVSO*, **10**, 11.

Tinbergen, J., Greenberg, J.M., and de Jager, C. 1981, *Astron. Astrophys.* **95**, 215.

Torres-Peimbert, S., and Wallerstein, G. 1966, *Astrophys. J.*, **146**, 724.

Totochava, A.G. 1973a, *Astron. Circ. U.R.S.S.*, No. 744.

Totochava, A.G. 1973b, *Astron. Circ. U.R.S.S.*, No. 791.

Totochava, A.G. 1975, in *Proc. IAU Symp. 67, Variable Stars and Stellar Evolution*, ed. V.E. Sherwood and L. Plaut (Dordrecht: Reidel), p. 161.

Trimble, V., and Bell, R.A. 1981, *Quart. J. Roy. Astr. Soc.*, **22**, 361.

Tsuji, T. 1978, *Astron. Astrophys.*, **62**, 29.

Tsuji, T. 1981a, *Astron. Astrophys.*, **99**, 48.

Tsuji, T. 1981b, *J. Astrophys. Astron.*, **2**, 95.

Tsuji, T. 1981c, *J. Astrophys. Astron.*, **2**, 253.

Tsuji, T. 1985a, *Cool Stars with Excesses of Heavy Elements*, ed. M. Jaschek and P.C. Keenan (Dordrecht: Reidel), p. 93.

Tsuji, T. 1985b, *Cool Stars With Excesses of Heavy Elements*, ed. M. Jaschek and P.C. Keenan (Dordrecht: Reidel), p. 295.

Tuchman, Y., Sack, N., and Barkat, Z. 1979, *Astrophys. J.*, **234**, 217.

Turon-Laccarieu, C. 1978, *Colloq. on European Satellite Astrometry*, Padova, June 5-7, 1978, ed. C. Barbieri and P. Bernacca, p. 231.

Tutukov, A., and Iben, I. 1985, *Cool Stars with Excesses of Heavy Elements*, ed. M. Jaschek and P.C. Keenan (Dordrecht: Reidel), p. 345.

Ukita, N. 1982, *Astron. Astrophys.*, **112**, 167.

Utsumi, K. 1970, *Pub. Astron. Soc. Pacific*, **22**, 93.

Utsumi, K. 1985, *Cool Stars With Excesses of Heavy Elements*, ed. M. Jaschek and P.C. Keenan (Dordrecht: Reidel), p. 243.

Utsumi, K., and Yamashita, Y. 1971, *Pub. Astron. Soc. Pacific*, **23**, 437.

Uus, U. 1976, *Pub. Tartu Astron. Obs.*, **44**, 227.

Van Genderen, A.M. 1979, *Astron. Astrophys. Supplement*, **38**, 151.

Vandervort, G.L. 1958, *Astron. J.*, **63**, 477.

Vardya, M.S. 1970, *Ann. Rev. Astron. Astrophys.*, **8**, 87.

Vernon-Robinson, L. 1929, *Harvard Bull.*, No. 872.

Vetesnik, M. 1982a, *Inf. Bull. Variable Stars (IAU Comm. 27)*, No. 2225.

Vetesnik, M. 1982b, *Inf. Bull. Variable Stars (IAU Comm. 27)*, No. 2250.

Vetesnik, M. 1982c, *Inf. Bull. Variable Stars (IAU Comm. 27)*, No. 2271.

Viotti, R., Piro, L., Friedjung, M., and Cassatella, A. 1985, *Exosat Express*, **13**, 13.

Vogel, H.C. 1896, *Slitz.d.k.Preussischen Akad.d.Wissenchaften*, 395.

Walker, A.R. 1976, *Mon. Not. Roy. Astr. Soc.*, **174**, 609.

Walker, A.R. 1979, *South Afr. Astr. Obs. Circ.*, **1**, 112.

Walker A.R. 1980, *Mon. Not. Roy. Astr. Soc.*, **190**, 543.

Walker, N. 1985, in *Proc. Deuxième Ecole Européenne de Photométrie Photoélectrique*, Toulouse, April 5–7, 1985, ed. F. Querci, p. 96.

Walker, A.R., Wild, P.A.T., and Byrne, P.B. 1979, *Mon. Not. Roy. Astr. Soc.*, **189**, 455.

Wallerstein, G. 1973, *Ann. Rev. Astron. Astrophys.*, **11**, 115.

Wallerstein, G. 1977. *Pub. Astron. Soc. Pacific*, **89**, 35.

Wallerstein, G., and Greenstein, J.L. 1980, *Pub. Astron. Soc. Pacific*, **92**, 275.

Warner, B. 1963, *Mon. Not. Roy. Astr. Soc.*, **126**, 61.

Warner, B. 1965, *Mon. Not. Roy. Astr. Soc.*, **129**, 265.

Warner, B. 1967, *Mon. Not. Roy. Astr. Soc.*, **137**, 119.

Warner, B. 1969, *Mon. Not. Roy. Astr. Soc.*, **144**, 333.

Waters, B.H.J. 1966, *Roy. Astr. Soc. New-Zealand*, Var. Star Section Circ. 119.

Wdowiak, T.J. 1975, *Astrophys. J. (Letters)*, **198**, L139.

Webster, B.L., and Glass, I.S. 1974, *Mon. Not. Roy. Astr. Soc.*, **166**, 491.

Wendel, O.C. 1913, *Ann. Harvard College Obs.*, **69**, 118.

Werner, M.W., Beckwith, S., Gatley, I., Sellgren, K., and Berriman, G. 1980, *Astrophys. J.*, **239**, 540.

Wesselius, P.R. 1984, in *Proc. Alpbach Workshop on Infrared Space Observatory*, ed. C.J. Cesarsky, p. 61.

Wesselius, P.R., van Duinen, R.J., de Jong, A.R.W., Aalders, J.W.G., Luinge, W., and Wildeman, K.J. 1982, *Astron. Astrophys. Supplement*, **49**, 427.

Wheeler, J.C. 1978, *Astrophys. J.*, **225**, 212.

White, N.M., and Wing, R.F. 1978, *Astrophys. J.*, **222**, 209.

Whitelock, P.A., Feast, M.W., Catchpole, R.M., Carter, B.S., and Roberts, G. 1983, *Mon. Not. Roy. Astr. Soc.*, **203**, 351.

Whitney, C.A. 1984, *Bull. AAVSO*, **13**, 31.

Wildt, R. 1941, *Astrophys. J.*, **93**, 502.

Willson, L.A. 1981, *Physical Processes in Red Giants*, ed. I. Iben and A. Renzini (Dordrecht: Reidel), p. 225.

Willson, L.A. 1982, in *Proc. Boulder Conf. on Publications in Classical and Cataclysmic Variables Stars*, ed. J.P. Cox and C.J. Hansen, (Univ. Colorado: JILA), p. 269.

Willson, L.A., Garnavich, P., and Mattei, J.A. 1981, *Inf. Bull. Variable Stars (IAU Comm. 27)*, No. 1961.

Wilson, O.C. 1959, *Astrophys. J.*, **130**, 499.

Wilson, O.C., and Bappu, M.K.V. 1957, *Astrophys. J.*, **125**, 661.

Wilson, R.E. and Merrill, P.W. 1942, *Astrophys. J.*, **95**, 248.

Wilson, W.J. 1970, Ph.D. Thesis, Massachusetts Institute of Technology.

Wing, R.F. 1967a, in *Proc. Trieste Colloq. on Astrophysics, Late-Type Stars*, ed. M. Hack (Osservatorio Astronomico di Trieste), p 205.

Wing, R.F. 1967b, Ph.D. Thesis, Univ. California, Berkeley.

Wing, R.F. 1971, in *Proc. Tucson Conf. on Late-Type Stars*, ed. G.W. Lockwood and H.M. Dyck, KPNO Contribution No. 554, p. 171.

Wing, R.F. 1979, in *Proc. IAU Colloq. 47, Spectral Classification of the Future*, ed. M.F. McCarthy, A.G.D. Phillip, and G.V. Coyne, (Vatican Observatory: Vatican City State), p. 347.

Wing, R.F. 1980, in *Proc. GSFC Conf. on Current Problems in Stellar Pulsations Instabilities*, ed. D. Fischel et al., NASA TM-80625, p. 533.

Wing, R.F. 1985, *Cool Stars with Excesses of Heavy Elements*, ed. M. Jaschek and P.C. Keenan (Dordrecht: Reidel), p. 61.

Wing, R.F., Baumert, J.H., Strom, S.E., and Strom, K.M. 1972, *Pub. Astron. Soc. Pacific*, **84**, 646.

Wing, R.F., Carpenter, K.G., and Wahlgren, G.M. 1983, *Perkins Obs. Spec. Pub. 1* (Ohio State Univ.).

Wing, R.F., and Lockwood, G.W. 1973, *Astrophys. J.*, **184**, 873.

Wing, R.F., and Rinsland, C.P. 1981, *Revista Mexicana Astron. Astrof.*, **6**, 145.

Wing, R.F., and Stock, J. 1973, *Astrophys. J.*, **186**, 979.

Wolff, R.S., and Carlson, E.R. 1982, *Astrophys. J.*, **257**, 161.

Wood, P.R. 1974, *Astrophys. J.*, **190**, 609.

Wood, P.R. 1979, *Astrophys. J.*, **227**, 220.

Wood, P.R. 1981, *Physical Processes in Red Giants*, ed. I. Iben and A. Renzini (Dordrecht: Reidel), p. 205.

Wood, P.R. 1982, in *Proc. Boulder Conf. on Pulsations in Classical and Cataclysmic Variable Stars*, ed. J.P. Cox and C.J. Hansen (Univ. Colorado: JILA), p. 284.

Wood, P.R. 1985, *Cool Stars with Excesses of Heavy Elements*, ed. M. Jaschek and P.C. Keenan (Dordrecht: Reidel), p. 357.

Wood, P.R., Bessel, M.S., and Fox, M.W. 1983, *Astrophys. J.*, **272**, 99.

Wood, P.R., and Zarro, D.M. 1981, *Astrophys. J.*, **247**, 247.

Woodsworth, A.W., and Hughes, V.A. 1973, *Nature Phys. Sci.*, **246**, 111.

Woodsworth, A.W., and Hughes, V.A. 1977, *Astron. Astrophys.*, **58**, 105.

Woolf, N.J. 1969, *Astrophys. J. (Letters)*, **167**, L37.

Wright, W.H. 1919, *Pub. Astron. Soc. Pacific*, **31**, 309.

Wyller, A.A. 1966, *Astrophys. J.*, **143**. 828.

Yamashita, Y. 1967, *Pub. Dominion Astrophys. Obs. (Victoria)*, **13**, 67.

Yamashita, Y., and Maehara, H. 1977, *Pub. Astron. Soc. Japan*, **79**, 319.

Yamashita, Y., and Maehara, H. 1978, *Pub. Astron. Soc. Japan*, **30**, 409.

Yamashita, Y., Maehara, H., and Norimoto, Y. 1978, *Pub. Astron. Soc. Japan*, **30**, 219.

Yamashita, Y., and Norimoto, Y. 1981, *Ann. Tokyo Astron. Obs.*, **18**, 125.

Yorka, S.B. 1981, Ph.D. Thesis, Ohio State Univ.

Yorka, S.B. 1983, *Astron. J.*, **88**, 1816.

Yuin, C. 1948, *Astrophys. J.*, **107**, 413.

Zhou, Zhen-pu, and Kaifu, N. 1984, *Astron. Astrophys.*, **138**, 359.

Zirin, H. 1982, *Astrophys. J.*, **260**, 655.

Zuckerman, B. 1980, *Ann. Rev. Astron. Astrophys.*, **18**, 263.

N88-11594

2

SPECTROSCOPY AND NONTHERMAL PROCESSES

Monique Querci

PRELIMINARY REMARKS

This chapter presents observational data, mainly from spectral lines, which imply the existence of nonthermal phenomena—phenomena not expected to occur in hydrostatic thermal atmospheres under radiative equilibrium. Those sections of this chapter following this overview summarize spectroscopic data from the ultraviolet to the infrared; the chapter following covers spectral lines in the radio region. Sequentially, we survey:

1. The variability of those absorption lines whose excitation/ionization levels correspond to photospheric conditions. In some variable red stars, especially the Miras, such absorption lines are those whose velocity shifts are interpreted to be caused by subatmospheric pulsation driving outward compression waves: producing shocks by either wave-steepening or collision with infalling material from a preceding phase, or both. Such photospheres are already nonthermal.

2. The variability of the emission lines, interpreted as arising in higher atmospheric layers and whose diverse spectral characters imply a wide range of physical processes leading to their formation. Such processes that, in the Sun, are mainly interpreted in terms of thermal chromospheres, appear, in some pulsating stars, to reflect more dynamical circumstances such as shocks and extended atmospheres. So we try to survey these emission lines, of varying character, in terms of the different possibilities for their production, to try to infer the kinds of atmospheric regions existing in such stars. In this regard, we summarize recent suggestions offered by Willson and Bowen (1985).

3. The characteristics and variability of those absorption lines considered to be circumstellar because of their low excitation and because of certain characteristics of their profiles. We are particularly interested in the relation of the circumstellar observations, and regions, to mass-loss consequences.

This survey of the line spectrum, and the nonthermal extended structure that it implies for the atmospheres of many red giants and supergiants, leads naturally to asking about the relation between those outermost cool regions found and the source of that observed radiation diagnosed as coming from dust grains. So

C-3

we survey those observations, including data from the continuum as well as from the lines, and the inferences that have been drawn from them.

Finally, we summarize the attempts that have been made to measure directly angular diameters of these stars and to map the distribution of gas and dust in the most exterior atmospheric regions.

In both this chapter's survey of the line spectrum and the preceding chapter's survey of the continuum, variability of all features is stressed. From these discussions, we attempt to depict the dynamic motion of the atmospheric layers. But first, we must clarify certain ideas, as discussed by Wing (1979) in his review on Miras.

First, the radial velocity of the center of mass of the star must be determined. From among various velocities that might represent the motion of the center of mass (e.g., see Wallerstein, 1975), there appears to be a consensus of opinion in the literature (e.g., Hinkle et al., 1982, and references therein) for using the molecular emission of thermally excited SiO or CO. This idea has been stressed by Reid and Dickinson (1976) after the observations of SiO by Buhl et al. (1975) in some Mira stars, while Lambert and Vanden Bout (1978) and Dickinson et al. (1978) found further stars showing SiO and also CO thermal emission. As demonstrated by Morris and Alcock (1977), the thermal emission lines arise in the external layers of an extended low-density region. The velocity, inferred from the center of the emission profile, should then be considered as the velocity of the star center of mass (systemic velocity), because, paraphrasing a comment by Knapp et al. (1980), it is free of shifts caused by pulsation of the photosphere. Also, the stellar center-of-mass velocity may be obtained from the midpoint of the twin OH maser emission feature (see Rieu, this volume). The velocity of expansion of the emitting region is inferred from the width at the base of the SiO or CO line profile.

The second point to be decided is the spectral features indicative of the photospheric velocity. Until recently, the motion of the photosphere was supposed to be represented by an average radial velocity of the absorption lines, mainly those seen in the blue spectral region. Nevertheless, Wallerstein (1977) showed that a discrepancy exists between the changes in photospheric radius derived by means of photometric data and those deduced from the displacement of the line-forming region found from integrating the radial-velocity curve. It has now been proved that high-excitation-potential CO lines exist in the infrared region which unambiguously show the values and the amplitudes of radial velocity expected for the motion of the photosphere (see the sections *Changes in Absorption-Line Radial Velocities with Phase* and *Source of the Visible Spectrum*).

Finally, the measured radial velocities have to be further corrected for projection effects before deciding if the stellar layer is expanding or contracting relative to the center of mass. Although these correction factors for geometry and limb darkening are badly defined (Wallerstein, 1975, 1977), appropriate geometrical correction factors for Miras have been calculated (Willson et al., 1982).

We end these preliminaries with the following miscellaneous remarks:

1. The term "atmosphere" stands for all the stellar layers from the photosphere to the external envelopes.

2. The variability will be mainly dealt with from spectra of Miras, chiefly from some prototypes of M and S types for which the observational data are exhaustive. The phase coverage of C types is as yet too incomplete for detailed discussion.

3. We adopt the convention that "red" and "blue" shifts refer to shifts to longer and shorter wavelengths (or to lower and higher frequencies), respectively. We set the velocities as positive for infalling material relative to the center-of-mass velocity (red-shifted lines) and negative for rising material (blue-shifted lines).

4. The phase of events which occur in the preceding or following cycles is specified by substracting or adding 1.0 to the normal phase convention. When the observation time is given in days before or after the maximum light in the literature, the corresponding phases are calculated on the basis of the periods issued from Kukarkin et al. (1969, 1970).

5. To link radial velocities from optical features, generally given with respect to the Sun, to the center-of-mass velocity (a radio line velocity generally given with respect to the local standard of rest, V_{LSR}), we have to convert the latter to a heliocentric velocity (Lang, 1980).

PHOTOSPHERIC ABSORPTION LINES

Introduction

The spectra of the late-type stars are crowded with absorption lines. For the earlier of these, the atomic lines are quite strong in a relatively molecular-band free spectrum, while in the later types the molecular bands appear and the atomic line-strengths decrease.

Even at high dispersion, only a few regions are suitable for studying the atomic lines. One of these, nearly free of absorption by molecular bands, lies shortward of about 4400 Å; this blue region of the visual was extensively studied by the spectroscopists until the 1960s. Longward of this wavelength, interference by the TiO bands in M stars gradually increases, and the intensities and displacements of atomic lines become difficult to study. The spectra of S stars, in which the ZrO bands are less extended than the TiO bands of M stars, should be more favorable. Unfortunately, as there is little flux in the blue-violet region of these cool stars, only the phases near maximum light have been exploited. Moreover, the blue region contains circumstellar (CS) lines (excitation potential ≤ 0.5 eV) that may alter the conclusions on radial-velocity changes in papers written before these circumstellar components became well known. (See the section *Circumstellar Lines—Properties of Gaseous Shells.*)

Another region in which the depression due to molecular bands is not too strong is in the near-infrared (λλ 7900–8700). In recent years, high-resolution Fourier transform spectroscopy became available in the infrared region from 1.6 to 2.5 μm, making it possible to analyze the behavior of atomic and molecular lines there. The present advanced infrared spectroscopy is well suited to radial-velocity determinations: high resolution up to 0.07 cm^{-1} is practicable at all phases because Miras have relatively small light amplitudes in the infrared. We recall that red giants have their flux peak between 1 and 2 μm and that the 1.65-μm region corresponds to the minimum opacity due to H^-.

Survey of Changes in Absorption-Line Strengths with Phase

Blue-violet spectra of *Miras* extending over many light cycles indicate periodic changes in line intensities. Some examples come from the blue-violet region of *o* Cet, R Leo, R And; Buscombe and Merrill (1952) find that, although the majority of atomic absorption lines are much stronger at maximum light, not all elements show exactly the same variations in equivalent widths with phase. Also, the example of U Ori (Merrill, 1945) shows that changes in atomic-line intensities are not *a fortiori* correlated with great changes in the brightness of the star: while the magnitude of the star increases as much as 2.2 mag from phase -38 days to phase -4 days, changes in the atomic-line spectrum were minor. For molecular bands, numerous examples indicate that the molecular features strengthen with the (cooler) later types and within a type with the declining light phases (i.e., ultimately with a decrease in temperature). For M3–M6 Miras, the depth of the TiO bands at 4584 and 4955 Å becomes smaller near maximum light, and the earlier the type, the smaller the depth (Maehara and Yamashita, 1979). The TiO and VO bands at 1 μm, which appear in stars later than M6, strengthen toward minimum light (Lockwood, 1969). Sanford (1950)

reports on the appearance of strong CaCl bands in the orange and red regions of C stars, but only during minimum light. In the infrared, Hinkle (1978) indicates that the 4400- to 4800-cm^{-1} region in R Leo contains only weak molecular lines near maximum light (allowing for the identification of weak to moderate atomic lines). On the other hand, the strengthening of the water spectrum near minimum light is responsible for reducing the number of unblended lines by well over one half. Hinkle and Barnes (1979a) found that the H_2O column density in R Leo varies by about an order of magnitude with phase, while in χ Cygni (Hinkle et al., 1982), the CO column density strongly changes near maximum light and stays at a constant value from about phase 0.20 to 0.70. Incidentally, using the curve-of-growth/isointensity method (Hinkle et al., 1976), the excitation temperature is found as a function of phase for the various molecular bands; such a quantity is essential when discussing the structure of the atmosphere. (See the section *Photospheric Kinematics—The Shock-Wave Model.*)

Variations in Radial Velocities of Absorption Lines

Dependence of Absorption-Line Radial Velocities on the Excitation Potential. Line shifts of neutral atoms increase monotonically with the excitation potential of the lower atomic-energy level. Clearly deduced from the visual atomic lines in Miras (Merrill and Greenstein, 1956), it is now also shown for the IR atomic lines. As an example, in the blue spectrum of χ Cygni (Merrill, 1947b), Fe I lines with a lower state excitation potential of 1.0 eV, which is the value of most of the visual atomic lines measurable in Miras, are displaced toward longer wavelengths by 2 km/s with respect to the resonance lines; this is confirmed by Maehara (1968), who finds radial velocities from violet and IR absorption lines of Ti I and Fe I in χ Cygni decreasing with decreasing excitation potentials. The low excitation lines are shifted toward short wavelengths with respect to high excitation lines. Moreover, it has been noted from studies of both S Car in the infrared at high dispersion at all phases (Shinkawa, 1973) and χ Cygni (Hinkle et al., 1982) that the phase dependence of the relation between velocity and excitation potential relation varies with phase.

A similar dependence of radial velocity on the excitation potential is also found from molecular lines. Interesting examples are given by the irregular C star, TX Psc, in the visible range with AlH and SiH molecules (Peery, 1979) and in the 2.5-μm region with CO and HF molecules (Peery et al., 1977).

As discussed by Hinkle (1978), the excitation potential is one measure of the depth of formation of a line in the cool star photosphere: the higher the excitation potential, the deeper is the line-forming region (and also the weaker are the lines). The dependence of radial velocities on the excitation potential explains the strong dependence of the velocity of the absorption lines on the line intensity (Maehara, 1971) (i.e., our understanding of the temperature stratification and region of line formation leads directly to the phenomenon of a *velocity gradient* in the atmosphere). Finally, Pilachowski et al. (1979) note a strong correlation between the radial velocity and the ionization potential in several Mira variables.

Changes in Absorption-Line Radial Velocities with Phase

Blue Range in Miras. In his extensive study of the brightest phases over 16 cycles of o Cet's light variation (from 1935 to 1951), Joy (1954) proves that variations in the radial-velocity curves of atomic absorption lines, from λ3770 to λ4290, are evident from cycle to cycle; greater positive velocities correspond to the cycles with a greater brightness at maximum. This author also notes that in other Miras, at post- and pre-maximum, the atomic-line velocities do not repeat regularly from cycle to cycle. However, the typical general trend of the velocities in Miras shows that *the blue-violet atomic lines do not exhibit significant velocity changes with phase.* A striking example is given for R Leo by Hinkle and Barnes (1979b), who collected

data from Merrill (1946, 1952c) and Wallerstein (1975). The velocity is nearly constant at +12 ± 3 km/s from phase 0.8 to 0.3 and then decreases to about 7 km/s at minimum light.

Such a velocity trend of the photospheric absorption lines is inconsistent with the velocity behavior of the emission lines that support a pulsation interpretation, suggested by the periodic variations in brightness to be discussed in the sections *Changes in Emission-Line Radial Velocities with Phase* and *Atmospheric Kinematics* (part on *The Mira Stars): The Shock-Wave Model.* It confused the visual spectroscopists and prevented a deduction of an overall atmospheric structure of these stars until recently, when infrared techniques became available.

Infrared Range—An Example: the Mira χ Cygni. High-resolution Fourier transform IR observations by Hall et al. (1979), Hinkle (1978), Hinkle and Barnes (1979a, 1979b), and Hinkle et al. (1982) led to a real breakthrough in understanding *the Mira phenomenon.* These authors analyze molecular and atomic absorption lines of various excitation energies and strengths at several different phases and give a picture of how the velocity structure and, furthermore, the temperature structure and column densities change along the light cycle.

When summarizing the key observational results, a typical example used is a time-series spectra of χ Cygni (Hinkle et al., 1982). The authors rely on the CO bands from 1.5 to 5 μm in which the Δv = 3, 2, and 1 vibration/rotation bands are found. Figure 2-1, adapted from Hinkle et al. (1982), displays the changes in radial velocities with phase for groups of lines of low, high, or moderate excitation belonging to the second-overtone (Δv = 3) and the first-overtone (Δv = 2) bands. Obviously, χ Cygni has a composite absorption spectra with multiple velocity components.

The Second-Overtone Bands. Discontinuous S-shaped velocity curves with a *double-lined* spectrum for about one fourth of the light cycle, from before φ = 0.90 to about φ = 0.15, are the outstanding features in Figure 2-1 (upper panel). Additional evidence comes from Figure 2-2, which presents an average Δv = 3 line profile at representative phases. As summarized by Hinkle et al. (1982): (1) during the double-line phases, the line to the red (inward flow) fades as the line to the blue strengthens; (2) the absorption lines move to the red with phase; (3) a blue-shifted emission edge develops after phase 0.60 and emerges as a separate emission feature; and (4) the lines weaken during the emission-line and double-line phases.

Instances of absorption-line doubling in Miras near maximum light have been known earlier from near-infrared spectra. It has been reported for χ Cygni by Maehara (1971) from near-infrared atomic lines around 8000 Å. These lines reported on Figure 2-1 behave as the Δv = 3 lines. Not having a complete set of observations along the phase, Maehara could not deduce the discontinuous S-shaped curves. For the first time, Maehara showed that the blue components are formed in a much hotter gas (therefore in deeper layers) than the red ones. This result has been confirmed by Hinkle et al. (1982): given the stellar velocity of −7.5 km/s (Dickinson et al., 1978), the longward component corresponds to cool falling gas, and the shortward component to hot rising gas. We now understand why the blue region has never been detected for double lines: the opacity in the blue is too strong to let the deep layer be seen. Hinkle et al. further establish the run of the excitation temperature with phase; the temperature drops about 2000 K through the light cycle.

The First-Overtone Bands. In the Δv = 2 bands, absorption lines of low, high, or moderate excitation are distinguished. Generally speaking, lines with low rotational quantum numbers J″ are low-excitation lines (e.g., the (2–0) R8 or R10 lines (~0.02 to 0.03 eV)). A 2–0 high-excitation line is R92 (1.98 eV). Moderate-excitation lines are (3–1) R32 to R35 (~0.50 to 0.56 eV); higher excitation (3–1) lines such as R66 and R65 (~1.3 eV) are not shown

in Figure 2-1. The main results from the middle panel of Figure 2-1 devoted to the $\Delta v = 2$ bands follow:

1. The high-excitation (2–0) lines exhibit a large amplitude periodic change in velocity that mimics the second-overtone ($\Delta v = 3$) lines, but they double later in phase due to an assumed increase in continuous opacity from 1.6 μm ($\Delta v = 2$) to 2.3 μm ($\Delta v = 3$).

2. The low-excitation (2–0) lines do not have a periodic change in velocity; rather, they cluster around the center-of-mass velocity,

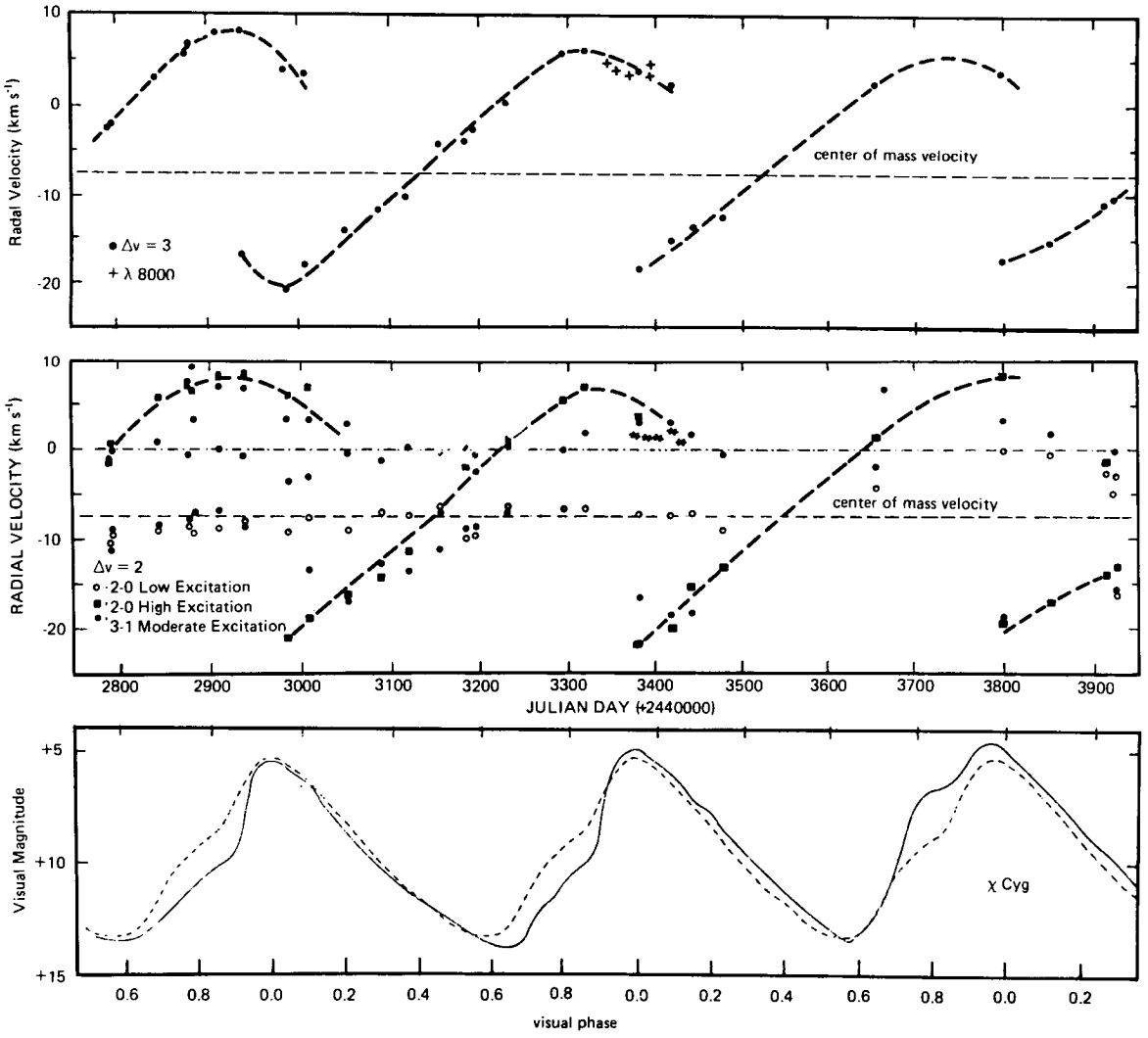


Figure 2-1. The S Mira, χ Cygni, in the infrared range. Upper panel: the mean CO second-overtone velocity as a function of Julian Day number (+ 2440000); crosses = the Maehara's (1971) atomic-line velocities from 8000 Å region. Middle panel: the CO first-overtone velocities for three different groups of lines as a function of Julian Day number; dot-dash line = mean absorption visual (4000 Å) velocity; stars = blue-violet region velocities measured during the same time interval as the CO (3, 1) moderate excitation lines. Lower panel: the visual light curve as a function of Julian Day number; dash line = average light curve; Solid line = actual light curve (adapted from Hinkle et al., 1982).

and one can infer an excitation temperature of the line-forming region of 800 K ± 100 K.

3. The moderate-excitation (3–1) lines exhibit line doubling, conspicuous at phases 0.01 and 0.24; however, extra components may be present (as at $\varphi = 0.04$). The general trend is as follows: one component always matches the (2–0) high-excitation velocity; the other component present is either at the velocity of the low-excitation (2–0) lines or at positively shifted (i.e., infalling) velocities relative to the center-of-mass velocity. Hinkle et al. (1982) add that considerable cycle-to-cycle variation is conspicuous: in some cycles, the infalling line is single; in others, multiple components are likely. The excitation temperature of the infalling lines is around 1500 K.

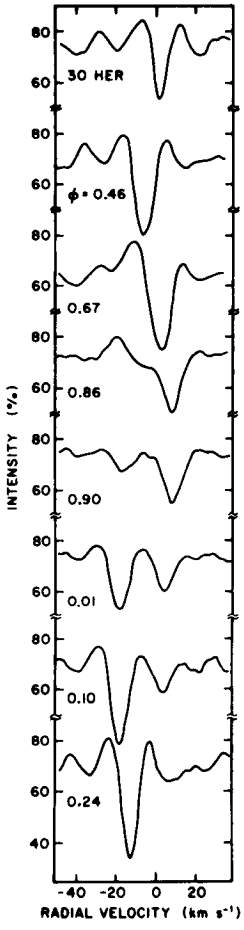


Figure 2-2. The S Mira, χ Cygni: Average CO second-overtone (Δv = 3) line profiles as a function of phase. The M6 III low amplitude variable 30 Her is shown for a comparison profile (from Hinkle et al., 1982).

To complete the description, we note the *fundamental bands* (Δv = 1) in the 4.6-μm region. The (1–0) band is indicative of a cool circumstellar shell. No velocity changes are noted. The excitation temperature is 300 ± 200 K. The circumstellar shells will be fully discussed in the section *Circumstellar Lines—Properties of Gaseous Shells.*

In short, four components have been identified in the spectra by Hinkle et al. (1982):

1. One component consists of second-overtone CO lines and the high-excitation component of the first-overtone lines, together with the atomic lines at 8000 Å. These lines share a discontinuous velocity curve of nearly 30 km s^{-1} amplitude and an excitation temperature change from 4000 to 2200 K. Both properties are indicative of lines formed in a pulsating region traversed by a shock front near maximum light. They are an indisputable indicator of the dynamics of the stellar photosphere.

2. One component deals with first-overtone lines with infall velocities. Hinkle et al. remark that this group of lines persists to at least minimum light and may well be present throughout the entire cycle. Their excitation temperature is about 1500 K.

3. Another component groups low-excitation first-overtone stationary lines (i.e., with the center-of-mass velocity) and with T ~ 800 K. This component is suggested to originate in the inner region of the circumstellar shell.

4. Finally, low-excitation fundamental lines with T ~ 300 K are formed in the expanding circumstellar shell.

The four components are the signatures of different regions in the atmosphere that will now be discussed.

Overall Picture of a Mira Atmosphere from the Absorption Lines (the example of χ Cygni)

Photospheric Kinematics—The Shock-Wave Model. The discontinuous S-shaped radial velocity curves were first observed for another class of pulsating variable stars, the W Virginis stars, for which the line doubling is explained by a shock wave model (e.g., Wallerstein, 1959). In the Mira χ Cygni, Maehara (1968), to account for the line doubling observed at 8000 Å around maximum light, put forward a two-layer model in which a layer of shock-heated gas is rising through a layer of cooler gas. The shape of the radial-velocity curve described by the first group of CO lines investigated by Hinkle et al. (1982) throughout three cycles fully supports the shock-wave model: radial stellar pulsation drives compression waves which develop into shocks *before emergence into the photosphere*. A first qualitative description of the model is given in Hinkle (1978) or Hinkle and Barnes (1979b) and is then updated in Hinkle et al. We rely on their various descriptions for a more comprehensive approach to the model.

> "By about minimum light, maximum radius has been reached and gas [from the outer layers] falls back [under a constant inward acceleration] while the deep layers become compressed and fall less rapidly...[A shock develops when] the photospheric gas moving inward can no longer decelerate smoothly into the underlying gas...that becomes nearly stationary at maximum compression.... [Otherwise], the shock region occurs where the falling photospheric gas of the last-cycle meets the photospheric gas of the present cycle at a velocity difference greater than that of sound... At this shock interface, the gas is heated from ~2000 K to > 4000 K [in χ Cygni] and molecular species are dissociated; atomic hydrogen is probably predominantly ionized.... The first indication of the emergence of the shock into the χ Cygni atmosphere is probably the brightening of the star after minimum light near phase -0.40. Between phases -0.40 and -0.30 the shock propagates through the infrared (1.6 μm) continuum. The infrared line-forming layers are first affected at phase -0.30 when the CO column density (Figure 6 [in Hinkle et al., 1982]) begins to decrease [due to the CO dissociation by the shock]. By about phase -0.10, the expanding gas behind the shock has cooled to the point where a detectable column density of CO can form. From phases -0.10 to 0.15, the CO continues to associate behind the shock zone while CO is simultaneously dissociated by the advancing shock.... The observations. . .[from phases -0.10 to 0.15] record (1) part of the previous photospheric gas falling inward and (2) gas for the next light cycle moving outward.... [Note that] the shock *has already passed through much of the photosphere* when the CO second-overtone spectrum becomes double lined.... By phase 0.15, the CO column density reaches its plateau value and from then until phase 0.7, it remains constant to within the accuracy of measurement. During this interval, the line forming layer expands, stops and falls back towards the stellar surface under a constant inwards acceleration of 0.098 ± 0.005 cm s^{-2}. The CO column density drops an order of magnitude by phase 0.85 and another by phase 1.1. The observed acceleration of the layer changes at phase 0.85 and it reaches an equilibrium infall value of 7.5 km/s which is maintained by a small amount of gas until at least minimum light."

Note that the weak CO emission lines of Figure 2-2 might result from the recombination of the CO behind the shock.

Some estimates of the physical parameters of the χ Cygni photosphere are available from

the foregoing model:

1. From $L \sim R^2 T^4$, where L is the luminosity ($L = 7000\, L_\odot$), T is the mean photospheric CO excitation temperature, and R is the photospheric radius (all quantities reduced to solar units), Hinkle et al. (1982) obtain: $R = 240\, R_\odot$ (i.e., 1.7×10^{13} cm). It is found that the stellar pulsation produces a variation in radius of $\pm 100\, R_\odot$.

2. The thickness of the CO line-forming region is the total thickness of the linearly accelerated part of the atmosphere, obtained from the time the rising shock takes to traverse the falling line-forming region. With some assumption on the shock velocity not directly measurable, Hinkle et al. find that, from phase -0.3 to -0.10, the outward-moving shock covers about 8×10^{12} cm. Concurrently, the infalling gas travels 1.2×10^{13} cm. Finally, the thickness of the CO line-forming region is 2×10^{13} cm, comparable to the radius.

3. The mass of the stellar atmosphere is $M \sim 2.5 \times 10^{31}$ gm (if one assumes $mL = 4200$ gm/cm^2 and an exponential distribution of the mass through the line-forming region).

Source of the Visible Spectrum. Besides the photospheric layers, we described another three atmospheric components seen by Hinkle et al. in χ Cygni from CO observations. These are: (1) a hot ($T \sim 1500$ K) gas infalling at about 8 km/s relative to the center of mass, (2) a cooler ($T \sim 800$ K) stationary shell, and (3) a still cooler ($T \sim 300$ K) gas expanding at 7.5 km/s. The last two components clearly correspond to extended atmospheric layers that will be detailed in the section *Circumstellar Lines—Properties of Gaseous Shells*. The infalling gas deserves further comment. From Figure 2-1 (middle panel, 3-1 CO lines), the infalling CO component velocity appears to be in agreement with the blue-violet absorption-line velocity, rendering plausible the idea of Hinkle et al. that the infalling region is the source of the visible spectrum. In fact, as the blue spectrum does not suffer the pronounced phase-dependent velocity change shown by the $\Delta v = 3$ photospheric lines, it can well be formed *above* this IR line-forming region (i.e., above the photosphere). Consequently, the fact that the visual (blue) atomic absorption lines do not arise in the photosphere removes the discrepancy in the determination of the sizes of the Miras that puzzled the astronomers (e.g., Wallerstein, 1977) when they used a photometric or a visual spectroscopic approach.

Hinkle and Barnes (1979b) explain that the continuum shortward of about 6000 Å, formed in the shock region near maximum phases, permits us to see only the component of the slightly doubled lines formed above the shock, producing illusion of infalling gas in the 4000 Å spectrum. Also, they explain the gross cycle-to-cycle variations of the blue visual velocities by suggesting that the infalling gas might be in clumps or in a layer of uneven thickness. In addition, Hinkle et al. (1982) present some evidence for this material falling back onto the photosphere from the 800 K quasi-stationary layer. Emission lines discussed in the next section will come back to this point.

Further Probes of the Pulsating Photosphere

The Mira M Star, R Leo. R Leo also provides evidence that a Mira variable is radially pulsating. It has been extensively studied in the infrared by Hinkle (1978) and Hinkle and Barnes (1979a, 1979b), as well as in the visual (Merrill, 1946, 1952c) and in the millimeter range (Wallerstein, 1975).

It is interesting to complete the results shown by χ Cygni with the analysis of molecular lines not only by CO, but also of OH and H_2O and of atomic lines in R Leo, by Hinkle (1978) and Hinkle and Barnes (1979a, 1979b).

Large amplitude radial-velocity variations with phase (S-shaped curves) are obtained for:

1. The low excitation OH first-overtone lines, the CO second-overtone lines together with the 2–0 high-excitation CO first-overtone lines and the atomic lines, all formed in the stellar photosphere: the excitation temperature ranges from 4500 to 3000 K. The velocity amplitude of the photospheric spectrum is around 25 km/s.

2. Some lines from the H_2O molecule. Their excitation temperature is about 1700 K, showing that they originate near the boundary layers of the photosphere, in cooler and outer layers. They are expected to move more slowly than the hotter CO and OH forming regions, due to a weaker mechanical coupling to the underlying pulsation.

In addition, still cooler overlying components that might be the inner portion of the circumstellar shell are distinguished, such as a H_2O layer at $\sim$1100 K, the velocity of which duplicates a CO plus OH region at $\sim$1000 K showing radial-velocity variations of $\sim$16 km/s amplitude; it is reasonably to be located at the inner boundary of the CS shell close to the star and still having a significant mechanical coupling with the photospheric layers.

Carbon Stars: Miras and Semiregular Variables. In the literature, a Mira carbon star, R Lep, is known for doubling the CN molecular lines in the 6100 to 6700 Å spectral range near maximum light (Phillips and Freedman, 1969). On the other hand, the radial-velocity curve drawn for R Lep as a function of phase from CN lines over the same spectral region by Sanford (1950; Figure 2-3) is illuminating. We now recognize that this curve has a distinct S-shape, which is also conspicuous in other Miras observed by Sanford (1950): V CrB, V Oph, and U Cyg. Unfortunately, the curves are average curves for several cycles, obliterating a possible line-doubling effect. Nevertheless, the Mira C stars probably behave in the same way that the Mira M stars behave, the pulsation being associated with the photometric variability. The amplitude of the shock is about 20 km/s in U Cyg and R Lep, but only about 15 km/s in V CrB and V Oph, thus lower than in the Mira M or S stars where it can reach up to $\sim$30 km/s.

For such semiregular C stars as RR Her, T Cnc, and V Hya, the characteristic radial-velocity S-curve is also noticeable in Figure 2-3, in particular for the SRb variable RR Her, but the amplitude is low ($\leq$10 km/s). However, such a low-amplitude shock seems able to ionize a sufficient quantity of hydrogen, since Sanford (1950) see Hα in emission in the quoted stars, except in T Cnc. We will return to hydrogen emission in SR variables in the section *Hydrogen Emission Lines*. We note that Hinkle et al. (1984), observing IR CO lines in M semiregular stars, noticed S-shaped radial-velocity curves, but *no* line doubling (e.g., X Oph). The M supergiant, α Ori, which will be fully discussed in the section *Atmospheric Kinematics*, part on *Other Giants and Supergiants*, is another example.

An interesting point to make from these radial-velocity curves is that they might be used to determine the stellar velocity, despite the restrictions noted by Hinkle (1978). This is important for the C stars, still hardly observed for the CO microwave thermal lines. (The SiO thermal lines might be observed only in stars with a high Si abundance.)

Analysis of Absorption-Line Velocity Histograms in Miras. Willson et al. (1982) plot histograms of the radial-velocity distribution of atomic absorption lines in some Mira variables at various phases. Furthermore, they investigate the dependence of velocity on excitation and ionization potential, wavelength, and line strength by a multiple regression technique (Pilachowski et al., 1979). From their analysis, they claim that the histogram of the visual spectra (4000 to 7000 Å), together with the IR molecular lines, is better understood physically

speaking *by assuming two shocks propagating in the atmosphere at any one time*, a large amplitude "lower" shock (at about 1 R_*), plus a smaller amplitude "upper" shock (1.5 to 2.5 R_*). The two-shock model is implied by the theory that one shock is formed per period and persists for more than one period in the atmosphere, becoming gradually weaker with time (Hill and Willson, 1979). Thus, the upper shock is the weakened relic of the lower shock from the previous cycle. Criteria for assigning spectral features to either the upper or lower shocks have been given (Hill and Willson, 1979; Willson et al., 1982). Linked to the lower shock are the visible continuum near maximum, the high-excitation components of the IR molecular lines, and more generally, absorption lines with higher excitation (T_{ex} > 3000 K) and ionization potentials than lines originating in the upper shock. The lines from the lower shock are expected to be weaker because they may be filled in by the continuum from overlying layers; they occur mainly in the red spectral range (≥ 7000 Å), where the strongly wavelength-dependent opacity (assumed due to the Rayleigh scattering) is much smaller. To the upper shock are linked the visible absorption-line spectrum (TiO included for the M Miras), the low-excitation component of the IR molecular lines, features from the blue spectral range, and generally speaking, features with low excitation (T_{ex} < 3000 K).

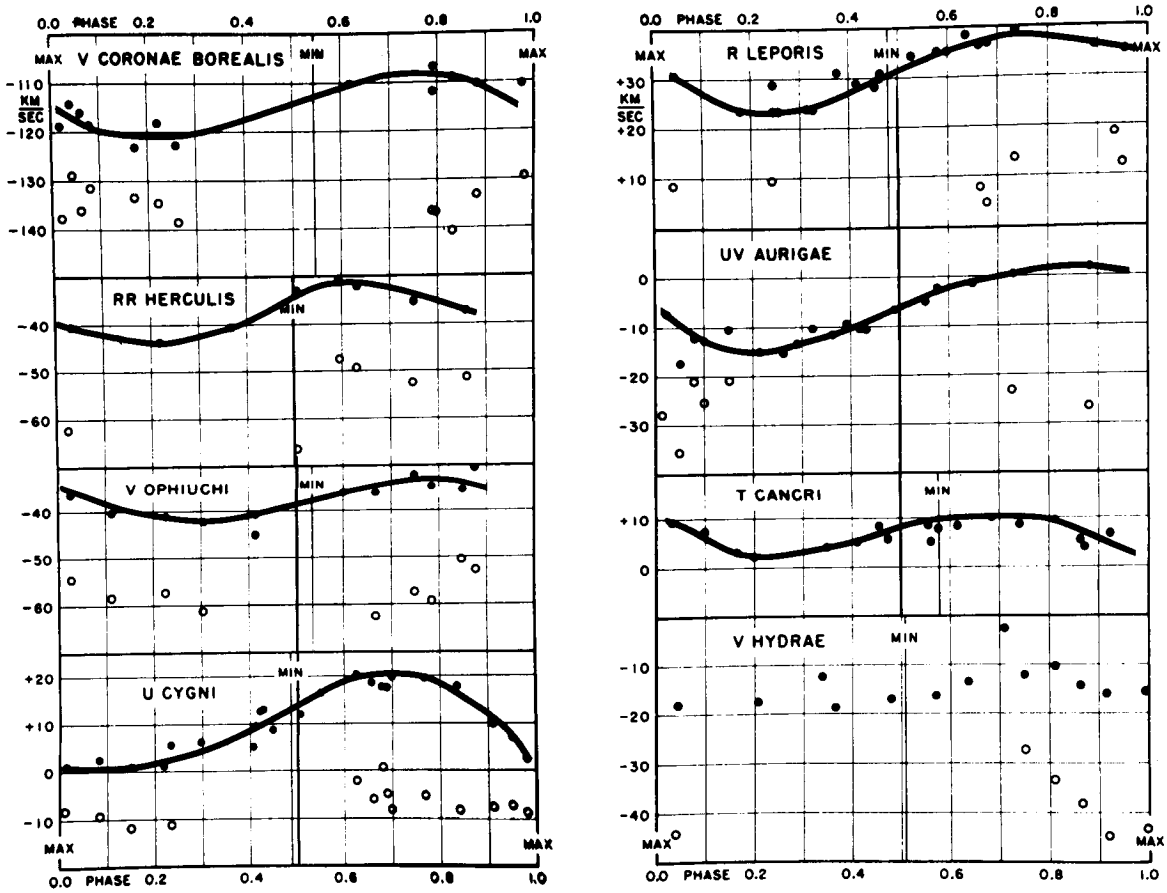


Figure 2-3. The radial velocities in carbon stars as a function of phase. Solid circles = CN absorption-line velocities; open circles = emission Hα velocities (adapted from Sanford, 1950).

Willson (1979) summarizes other criteria for the features assumed to form near the lower shock: (1) they are as regular as the light curve of the IR high-excitation line-velocity curves; (2) they show consistent phasing with the light curves; (3) they show overlying absorption; and (4) they are formed at large continuum optical depths (as are the IR lines). Two regions of line origin arise from each shock: postshocks A and C and preshocks B and D for the lower and upper shock, respectively, implying a four-component velocity (Figure 2-4a).

The main issue is whether there is an alternative interpretation of the observations *involving a single rising shock* (Figure 2-4b). As an example, we report RT Cygni as discussed by

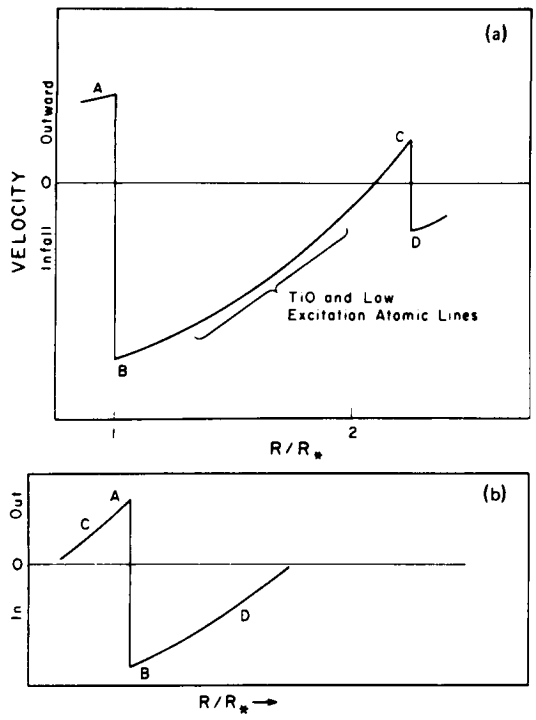


Figure 2-4. Schematic velocity structure in a Mira near maximum light: (a) if two shocks are assumed to propagate in the atmosphere at any one time; (b) if only one shock is assumed; (A) and (C) postshock line-forming regions; (B) and (D) preshock line-forming regions in lower and upper shock, respectively (from Willson et al., 1982).

Willson et al. (1982). On one hand, from their regression coefficients analysis, they conclude that the presence of at least one shock front in the reversing layer can explain the dependence of the velocity on the wavelength, line strength, ionization potential, and excitation potential with complete consistency. From the red and yellow spectral regions especially, it is seen that, as the shock rises through the atmosphere, first the low-lying higher excitation lines are affected, followed by the lower excitation lines that originate higher in the atmosphere. On the other hand, from the histogram analysis, near maximum light (φ = -0.02), the velocity structure might be consistent with a two-shock model (Figure 2-4a and Willson et al.'s Figure 5). For the lower shock, the postshock velocity at A is about +11 km/s, and the preshock velocity at B is about -20 km/s, while for the upper shock, C ~ +6 km/s and D ~ -8 km/s relative to a theoretical stellar velocity (Hill and Willson, 1979) at about -119 km/s. The velocities are corrected for geometrical effects. (See the section *Preliminary Remarks.*)

As emphasized by Willson et al. (1982), the A and C components are difficult to separate from each other (we will refer again to this point when discussing emission lines in the section *Atmospheric Kinematics*, part on *The Mira Stars: The Shock-Wave Model*) and very few lines are available to give the B component since they tend to be weak because of the filling in by the continuum from higher atmospheric layers. Willson et al. continue that, if the A and C lines are combined into a single region of origin and if the B component lines are ignored, using only the D component for the infall velocity, a single shock with a geometrically corrected amplitude of $\Delta v \equiv A - D \sim 19$ km/s is invoked to interpret the histograms. However, with such an amplitude, a shock in a Mira atmosphere is not likely to ionize sufficient hydrogen to produce the strong Balmer lines that are observed. (See the section *Hydrogen Emission Lines.*) An amplitude of at least Δv = 25 km/s seems to be required (Tsuji, 1971). However, as some B component lines are observed (at +8 and +25 days from maximum

in yellow and red ranges), it should be more plausible to consider a single shock, such as that in Figure 2-4b, with an amplitude $\Delta v \equiv A - B \sim 31$ km/s. Such a shock amplitude is inferred from the IR molecular absorption lines and the red atomic lines in χ Cygni (Figure 2-1, from Hinkle et al., 1982) or R Leo. In support of this single-shock model, one should recall (see the above section *Photospheric Kinematics—The Shock-Wave Model*) that the shock is first detected in the infrared (due to a lower opacity than in the blue region), early in phase, through the observed variation in the CO column density; it has passed through a large part of the atmosphere when the IR and red lines become double around maximum light. The D components, issuing mainly from the blue spectrum, appear to be formed well above the shock. This is in agreement with the idea (Hinkle et al., 1982) discussed in the above section *Source of the Visible Spectrum* that the blue absorption lines are no longer representative of the photosphere or the reversing layer of the star as previously thought; rather, they are related to an outer shell and formed relatively high in the atmosphere. Consequently, an upper shock appears to be no longer necessary to explain their nonperiodic fluctuations in velocity. Emission lines (see the section *Atmospheric Kinematics*, part on *The Mira Stars: The Shock-Wave Model*) will provide further arguments in favor of a single shock.

Summary: What information is obtained from the absorption lines?

They tell us that cooler circumstellar layers are present in Miras. In this framework, important results are: (1) the blue-violet absorption lines are linked to an outer layer rather than to the photosphere; and (2) a quasi-stationary shell exists in the Miras.

Infrared absorption lines, mainly molecular lines, prove that the photosphere of M, S, and C *Miras* undergo a shock-pulsation motion of the W Virginis-type linked to the radial global stellar pulsation driving acoustic waves. Generated by turbulence at the top of the hydrogen convective zone, these waves turn into shocks, dissipating energy and heating the stellar layers, as they propagate outward into layers of decreasing density (Stein and Leibacher, 1980). The characteristic of the Mira model is that *a shock is formed just below the visible photosphere*; this is essentially what we mean when speaking later about the photospheric Mira-like shock-wave model. The undisputable indicators of such a mechanism are the S-shaped large-amplitude radial-velocity curves with respect to the stellar phases and the line-doubling effect around maximum light.

For semiregular stars, data are still scarce. However, S-shaped curves from visible CN or IR CO lines are recognized in the few available examples, suggesting that the Mira-like pulsating mechanism might work in these stars. However, the curves have a much lower amplitude than in the Miras, indicating less available energy or larger damping. IR CO line doubling is also absent, meaning that the rising hot gas from deep layers cannot be seen at the same time as the cool infalling gas, but the cause is presently unclear. *Observations are urgently required on semiregular (SR) and irregular (L) stars.*

EMISSION LINES

We exclude here the radio emission lines (see Rieu, this volume) and emission in P Cygni line profiles, which are treated in the section *Circumstellar Lines—Properties of Gaseous Shells.*

In general, all the M, S, and C stars of Mira type show strong emission lines at some epoch, as do some semiregular stars. (See, for example, the compilations by Bidelman, 1954; Meinel et al., 1969; Yamashita, 1972; Stephenson, 1973; Keenan et al., 1974; and Catchpole et al., 1979.) Some additional semiregular variables show weak emission lines at some phases; others show emission lines at some phases in some cycles.

In what follows, the discussion on changes with phase will focus mainly on the Mira stars. Note that, among the 223 Miras reported by Catchpole et al. (1979), only some rare cases

are not mentioned as having emission lines (e.g., the M star, SU Pup, or the C star, RV Cen). However, these stars may not have been observed for a sufficient time.

General Behavior of Emission Lines with Phase

Optical Range of Mira Variables. Variability of the atomic emission lines in the visible spectral range has been known since the beginning of the century, whereas the UV range recently explored by satellites has seldom been used. In the following section, the discussion is based mainly on certain typical stars because the very similar behavior in various Mira spectra of many complicated details is remarkable (Merrill, 1952c).

The emission lines undergo striking modifications with phase. They can have a strong intensity and a broad profile and can appear as the most outstanding features in the spectrum, even at low resolution, or they may be radically altered and partly extinguished by the absorption lines above them or so weakened as to completely disappear. Moreover, this behavior is cyclic in the Mira stars, although some differences are noted in the pattern from cycle to cycle in a given Mira, and from star to star in the same spectral type (Merrill, 1952b). The emission lines are stronger and more numerous in cycles with a high maximum brightness (e.g., Hβ in o Cet is much more intense for the brighter maxima (Joy, 1954)).

Except for about one third of the period just after minimum, emission lines are usually present in the spectra. Roughly speaking, most of the lines are brightest just after maximum. The hydrogen Balmer lines, recognized up to H18 (Merrill, 1947a), characterize the spectra of Mira variables at maximum light when they are very bright, whereas at minimum light, they are weak or absent. With advancing phase, the Fe II(1) emission lines become outstanding features. For a given phase after maximum, the emission spectrum is completely different from the spectrum at the same phase before maximum. As an example, for o Cet, Joy (1954) in his Table 7 gives the phases in which the main lines of various elements in the optical range are just detectable, when they are at their maximum, and finally when they disappear. Some metallic lines appear early in the cycle on the blue part of the absorption lines. After the maximum, the number of emission lines of additional elements and their brightness rapidly increase, beginning with the lines from higher excitation potentials. Common are the main lines from the following neutral atoms: Fe I (in particular, the lines at λ4202 and λ4308 are abnormally strong in emission and indicative of a resonance mechanism), Mg I, Si I, Mn I, In I, and Co I; and from ionized atoms: Fe II, Ti II, Mn II, Ca II (H and K lines and the IR triplet lines), and Sr II. Some lines are so dominant that they obliterate the absorption lines.

An example depicting different behavior from most emission lines in various cycles is given by the S Mira star, R Cyg. In 1951, a large number of sharp metallic emission lines of certain multiplets were stronger a month before maximum light ($\varphi \sim 0.93$) than after it, with an abrupt decrease as maximum light was approached (Merrill, 1952a), contrasting with the classical behavior of the various metallic emission lines in Miras that become strongest after maximum. Further spectra were obtained at two successive maxima in 1957 and 1958 (Deutsch and Merrill, 1959). At the abnormally low maximum in 1957, the spectra show many more metallic emission lines than in 1951. They appear in absorption at the 1958 maximum, whereas in 1957, fewer absorption lines appeared and the resonance lines were much weaker than in 1958.

At minimum light, the striking feature is the high-excitation [Fe II] forbidden lines. Other lines such as [Mn I], [S II], and [O I] are also visible. Note that the forbidden lines are not mutilated by absorption lines (e.g., by the TiO lines which are strong in the M stars spectra); this should imply that they are formed above the TiO layer. Another particular feature of minimum light is the appearance of emission lines due to the AlH molecule identified in S-type spectra such as in χ Cyg (Herbig, 1956) and in U Ori (Wallerstein, 1975), a star which

does not show [Fe II]. Referring to the occurrence of molecular emission, Herbig (1956) also quotes AlO emission in the Mira M star, *o* Cet, at the abnormally low maximum in 1924 and emission by the violet CN molecule in R CrB near minimum light, which was also confirmed by Wing et al. (1972). A search for the AlO emission in spectra of several variables (Kipper and Kipper, 1979) indicates that this emission is an extremely rare event.

UV Range

Example of a Mira Variable, χ Cygni. Variation in emission-line strength with postmaximum phases has been observed for the S Mira star, χ Cyg (Cassatella et al., 1980), with the International Ultraviolet Explorer (IUE) satellite in the low- and high-resolution modes. At phase 0.04, at the limit of the optical spectrum near 3200 Å, the Fe II (V1) and (V6) lines are the only outstanding emission features. Two months later, at phase 0.18, the Mg II h and k doublet appears in emission, together with Fe II (UV 1, 32, 62, and 63) lines, whereas the Fe II (V6) lines are now almost unidentifiable at low resolution and the Fe II (V1) lines are still strong.

Example of a Semiregular C Star, TW Hor. Nine spectra of TW Hor (Figure 2-5) were obtained with IUE in the low-resolution long-wavelength mode during an interval of 3 years (Querci and Querci, 1985a). The striking feature is the variation in intensity of all the emission lines. The most important variations are shown by the Mg II U1 doublet at 2800 Å and by the Fe II V1 lines and the V II V7 lines around 3280 Å. The Fe II V1 + V II V7 blend varies by at least a factor of 10. It is strongest on LWR 7774 on May 16, 1980 ($\varphi \sim 0.72$), and weakest on LWP 1852 on April 27, 1983 ($\varphi \sim 0.70$). This points out a different behavior of the blend for very similar phases in various periods, unlike what is observed in Miras. On the other hand, the Mg II h and k blend varies less strongly than the Fe II V1 blend for nearly similar phases in different periods (LWR 7774, LWR 9049, and LWP 1852 at $\varphi \sim 0.7$).

The other emission lines are mainly other Fe II lines. Lines from the U3, U4, and U5 multiplets around λ2250 are visible in May 1980, absent in December 1982, and again observable 1 month later. They are of similar strength to the Mg II U1 lines on March 23, 1982, but only just detectable a day before (LWR 12834 and 12835). Note that the Fe II V1 + V II V7 blend does not change on such a short time scale. It should be concluded either that the various Fe II lines do not originate from the same chromospheric layers (as it is observed in α Ori by Carpenter, 1984, for example) or that the λ2250 Fe II lines are blended with another element (C II U43, for example).

The Fe II U3 + C II U0.01 blend at λ2325 exhibits a different behavior. It is broader on March 23, 1982, similar on March 22, 1982, and January 1983, and fainter on May 1980, demonstrating the variable contribution of the C II and/or Fe II lines. The Fe II U62 and Fe II U63 lines around λ2750 are sometimes detectable, mainly during March 1982. The Al II U1 lines at λ2670 are not visible on the image LWR 12834, but are suspected 1 hour later on LWR 12835 and, being much stronger 1 day later, on March 23, 1982. Presently, Al II U1 lines are the only lines through which such a short time-scale variation might be inferred; because they are very near the noise level (about 3σ), further observations are needed to confirm this variation.

Variations in Radial Velocities of Emission Lines

Changes in Emission-Line Radial Velocities with Phase—An Example: the Mira Star, *o* Ceti. The variation of radial velocities with phase is obtained from the sharp emission lines of metals in the visible region. In their initial stages, many of the emission lines appear as bright edges on the shortward sides of absorption lines (Merrill, 1940). We shall come back to such profiles in the section *Selected Emission-Line Profiles.* As the phase advances, they

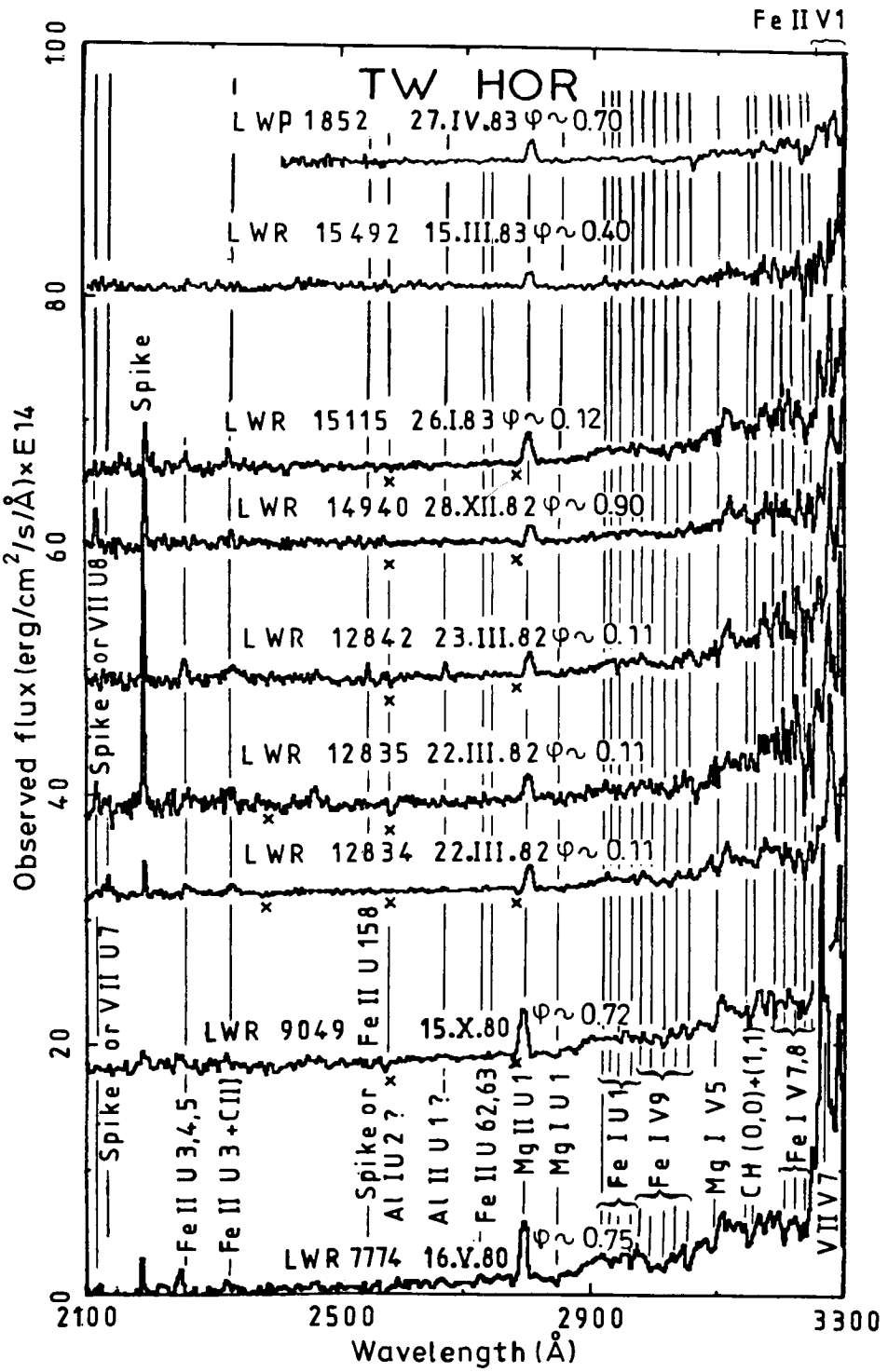


Figure 2-5. IUE spectra of the semiregular carbon star, TW Hor (N0; C7, 2; P ~ 157 days) taken on various dates from 1980 to 1983, illustrating emission-line variations with time. Note the particularly high emission in the Fe II V1 + V II V7 lines around 3250 Å on May 16, 1980, compared to its low level on April 27, 1983. The LWR 12834 and LWR 12835 images are two successive exposures about 1 hour each. The crosses indicate reseau marks (from Querci and Querci, 1985a).

increase in strength, shifting longward and encroaching on the absorption line that is apparently displaced longward. Velocity measurements of the hydrogen lines are possible at all phases if the lines are strongly overexposed. The most complete set of radial-velocity curves over many cycles is given for *o* Cet, from spectra in the region 3770 to 4290 Å obtained over a period of 16 years (Joy, 1954).

Because of differing processes leading to their formation, different spectral lines require particular physical conditions. For instance, the pumped emission lines (in other words, the fluorescent lines) arise in cool tenuous gas, whereas emission lines of singly ionized elements are formed in the hottest regions. Consequently, reliable radial-velocity curves cannot be drawn from emission lines belonging to different classes, as has sometimes been done in the past. Furthermore, it is now known that absorption lines with a low-excitation potential are circumstellar lines; they are blue-shifted and generally present a P Cygni profile. (See the section *Circumstellar Lines—Properties of Gaseous Shells.*) Finally, we discuss Joy's (1954) curves reproduced in Figure 2-6a, b. Also reported in this figure is the center-of-mass velocity of *o* Cet of 56 km/s (heliocentric; Engels, 1979; Knapp et al., 1982), enabling us to update Joy's discussion: *all the lines*, from their appearance to their disappearance around minimum light, *are seen to be formed in rising layers*.

While the ionized metals (Ti II, Sr II, and Fe II) have rather small velocity variations with phase, the neutral metal lines (Si I) show a large amplitude variation (Figure 2-6b). As for the hydrogen lines, Joy measures Hγ and Hδ because, in his spectra, they are visible over the longest time interval and are disturbed less by the overlying absorption than other hydrogen lines. Figure 2-6b shows the course of the velocity variations of the Hγ and Hδ lines in *o* Ceti and, for comparison, Figure 2-6d (i.e., Joy's Figure 4f) reproduces the R Leo, R Hya, and χ Cyg curves from numerous hydrogen lines up to H18. For R Leo, Hinkle (1978) plots the hydrogen velocity curve and a part of the IR CO and OH photospheric S-shaped velocity curves together (Figure 2-6c). The shape of the curves is similar, supporting the idea of a shock wave propagating in the photosphere (as discussed in the section *Photospheric Kinematics—The Shock-Wave Model*) which also excites the hydrogen emission. Moreover, the hydrogen emission-line curve lags in phase by 0.2; this is a further argument for a running wave through the photosphere, as discussed below. (See the section *Atmospheric Kinematics.*)

The shapes of the hydrogen curves of R Hya and *o* Cet might support the radial-velocity behavior with phase in Miras, in spite of the lack of measurements from $\varphi = 0.2$ to 0.4 in *o* Cet and of unpublished data of IR lines for these stars. The χ Cyg hydrogen curve is not representative because one lacks data at maximum light and it has an erratic behavior with phase, perhaps due to some difficulties in the measurements.

Figure 2-6a reports on pumped Fe I emission lines: the 4307.9 line is pumped by Mg II (2795.5 Å), together with the 4202 line, and the 4063 line is excited by Hϵ. The Fe I pumped lines are present at the same phase as the ionized metal lines, Sr II and Ti II. As for Fe II, the lines from multiplets (27) and (28) surprisingly cover all the star's period except for a few weeks after minimum, whereas multiplet (3) lines at 3914 and 3938 Å behave as the other ionized metals. (Note that all the Fe II lines are blended in the velocity curve of Joy, 1954.).

Dependence of Emission-Line Radial Velocities on Excitation Potential. The dependence of the radial velocities on the excitation potential of the upper level appears clearly in the emission lines of the ionized and neutral metals. The high-excitation Fe I lines yield algebraically greater velocities than the low-excitation lines (Merrill, 1952b). An illustration is provided by the Fe I lines in χ Cygni (Maehara, 1971), in which large velocity gradients occur in the emitting layer. In *o* Ceti, Joy (1954) also notes that the Fe I lines with a mean excitation potential of 5.3 volts, such as $\lambda\lambda$ 3852.6 (73), 3949.9 (72),

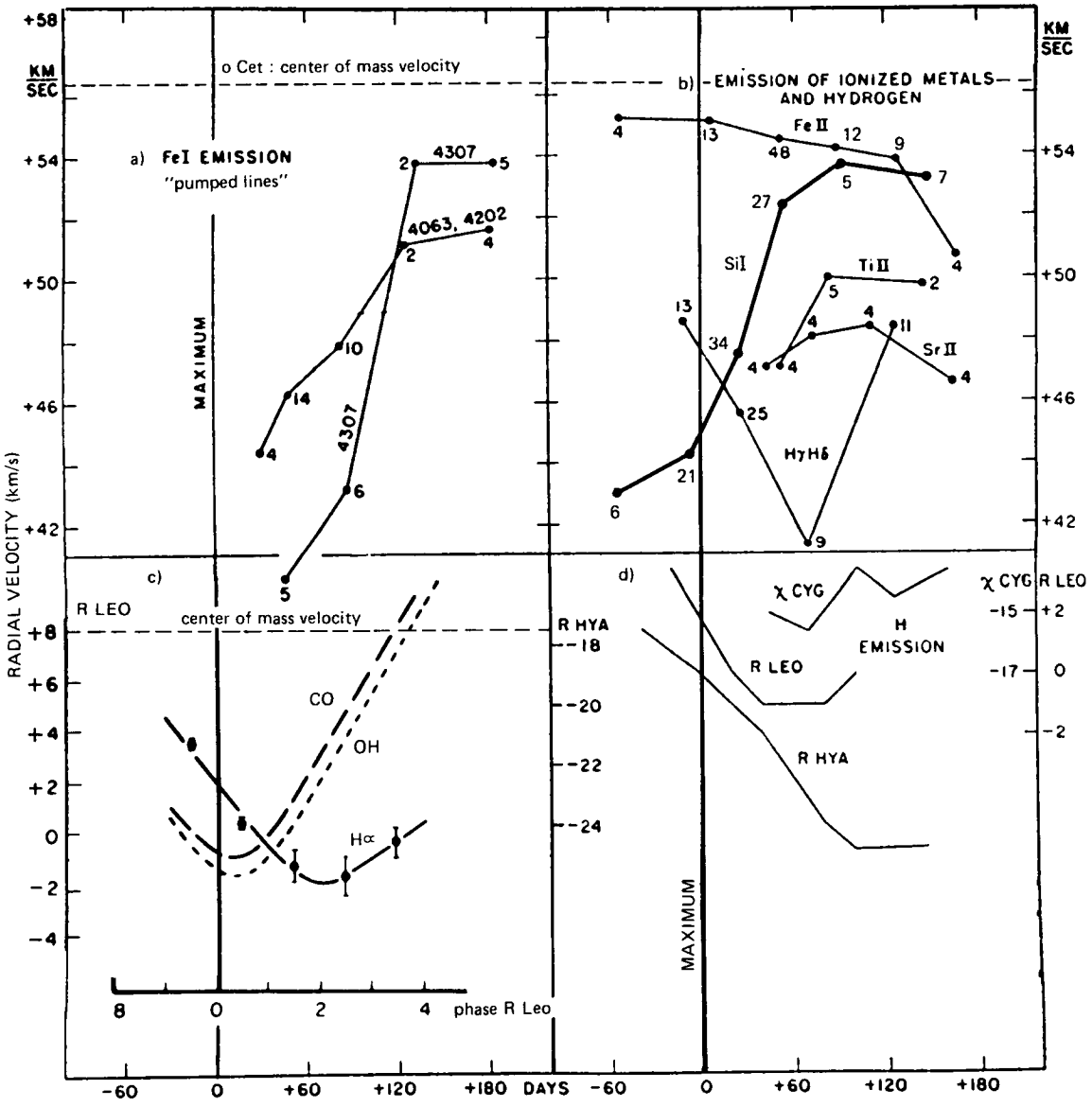


Figure 2-6. Mean radial velocities in M Miras plotted according to phase from maximum light: (a) pumped Fe I emission lines (λ4307 and λλ 4063, 4202) in o Cet (the numerals represent the number of measures included in the means and defined in Joy's (1954) Table 8); (b) emission lines from ionized metals (λλ 3759, 3761 Ti II, λ4077 Sr II, λλ 3938, 4233, 4178 Fe II), from the hydrogen-like neutral metal λλ 3905, 4102 Si I, and from Hγ and Hδ, in o Cet; (c) Balmer emission (solid line) and photospheric components of CO (long dashes) and OH (short dashes) in R Leo; (d) hydrogen emission lines in χ Cyg, R Leo, and R Hya. (a, b, d: adapted from Joy, 1954; c: from Hinkle, 1978).

and 3977.7 (72), give higher velocities than lines with a mean excitation potential of 4.5 volts, such as lines at 4063.6, 4202 (42), or 4307.9 (42) Å. Following the phase, the mean difference between high- and low-excitation lines is 2.5 km/s from +40 to +110 days (φ = 0.12 to 0.33) after maximum and 13.3 km/s from +110 to +170 days (φ = 0.33 to 0.51).

Using the data published by Joy (1954) for the metal lines in *o* Ceti, over eight cycles from -20 to +120 days around the maximum in each cycle (i.e., from φ = 0.06 to φ = 0.36 with a mean period of 331.65 days (Kukarkin et al. (1969)), Maehara (1971) finds the variation of the acceleration (the time derivative of velocity) with the visual magnitude at maximum, assuming a linear relationship between the radial velocity and the phase. From this, the smaller decelerations tend to occur in the brighter cycle.

Selected Emission-Line Profiles—Temporal Changes, Particular Shapes

Hydrogen Emission Lines. Very intense Balmer emission lines are observed in the spectra of the *Mira variables*. At the premaximum phase or shortly after maximum light, the lines appear to be much broader and severely mutilated by several superposed sharp absorption lines. Since the absorbents vary from one type of star to another, this explains the variation in line intensity with stellar type: Hβ is stronger in C stars than in M stars where it is affected by the heavy bands of the TiO molecule. Hα emission is usually disturbed by an absorption band in the M Miras and is absent in other types (Wallerstein, 1975). Examples showing Balmer line profiles in M Miras are given by Joy (1947) and Fox et al. (1984). With advancing phase, the absorptions disappear and the lines become intense and narrow, suggesting that the hydrogen-forming layers have progressed above the absorbing layers.

In the infrared, Paschen γ and Paschen δ are detected (Spinrad and Wing, 1969). A strong emission Paschen β line at 7802 cm^{-1} is found in *o* Ceti with the equivalent width of the line changing by a factor 2 on *a time scale of about 2 days* (Kovar et al., 1972). Because Pβ is not affected by molecular absorption, this might be an intrinsic variation in the strength of the hydrogen line. Kovar et al. confirm these variations in time when quoting the short variations observed in Hγ and Hδ by Odell et al. (1970) in *o* Ceti. Several Miras show a variation in the intensity of the Hδ emission, which also appears relatively free of overlying absorption, over 1 or 2 days, while the brightening of the stars remains constant to within 0.1 magnitude (Keenan, 1966).

Brackett γ is present in emission in *o* Ceti 40 days after maximum and also in R Leo (Johnson and Mendez, 1970). In the latter star, it is strongest at phase 0.94 and also broad (90 km/s across the base) (Hinkle and Barnes, 1979b). Bγ is already undetectable when the Balmer lines first appear at about phase 0.9 and reach their maximum intensity at phase 0.16. The differing lifetimes of the hydrogen lines in the visible and the infrared regions is explained by a continuum intensity in the visible which decreases with phase faster than the line intensity, which keeps the Balmer lines relatively stronger. This effect is reversed in the infrared. A depression of the continuum in R Leo around the Hγ emission is noted by Maehara (1971).

Jennings and Dyck (1972) summarize Balmer emission data for stars of *semiregular and irregular M types*, specifically excluding the Miras. Only five M giants and supergiants are quoted in the literature consulted from 1893 up to 1971 as showing or having shown Balmer emission. The most interesting data (originally from McLaughin, 1946) concern the supergiant, μ Cep, in which Hβ, Hγ, and Hδ emissions appear strongest just before the maximum light and then disappear as the star fades; the hydrogen lines become visible in absorption at minimum light. This is a Mira-like phase behavior. Such a behavior is also observed in the semiregular C stars, RR Her and V Hya (Sanford, 1950), in which Hα is present in emission from 0.25 period before to 0.25 period after maximum light. It is not observed at all in the semiregular C star, T Cnc.

Another different example is given by the semiregular C star, WZ Cas. Bidelman (1950) observes the hydrogen lines in emission on January 2, 1949, and recalls that the only available previous observations showing emission in Hγ goes back to 1903. Yamashita (1972) notes the absence of Hα and Hβ on his spectra taken in January 2–10, 1967. Examination of spectra on file at the Haute-Provence Observatory showed that the best covered year is 1978: hydrogen emission was visible on September 13–16, but no emission was detected on September 17 or on January 1, August 9, October 16–23, and December 16–17. Unfortunately, the available photometric data are too scattered over these periods to determine the corresponding light phase.

Generally speaking, the presence of hydrogen lines in emission, if any, in the SR variables is not likely to be regular from cycle to cycle or within a cycle, as in the Miras. Is it due to some fundamental differences in chemical composition or physical properties or to observational problems? In fact, the SR light-amplitude variations are smaller (see F. Querci, this volume), so that we can expect that the causes of the SR variations (e.g., in the shock-wave mechanism) are weaker than those producing the large-amplitude Mira variations and the emission lines around the Mira maxima. On the other hand, knowing that the cycle of an SRa variable is shorter than the Mira period, the duration of the emission lines may also be shorter. Much more closely spaced observations are needed.

Finally, we note that no emission has ever been observed in the hydrogen lines in the M supergiant, α Ori; they are asymmetric absorption lines (Goldberg, 1979; Dupree et al., 1984).

Violet Fe II Emission Lines. The Fe II lines from multiplets 1, 6, and 7 around 3200 Å were observed as early as 1947 by Merrill in postmaximum spectra of Mira variables (e.g., Merrill 1947b). The upper excitation potential is from 4.8 to 5.6 eV, adding up to a total ionization excitation energy of 13.5 eV from the ground state of Fe I. Multiplet (1) was noted as being remarkably intense. In R And during the postmaximum observed interval (+40 to +103 days (i.e., $\varphi \sim 0.10$ to 0.25)), several lines appear to change in relative intensity, while the radial velocities derived from several multiplets do not vary with phase or with excitation potential (Merrill, 1947a); this behavior also occurs in o Cet (Figure 2-6b).

Strong lines of multiplets (1), (6), and (7) were first seen in the spectra of the two M supergiants, α Herculis and α Scorpii (Herzberg, 1948) and were later detected in many other M stars (Bidelman, 1954; Boesgaard and Boesgaard, 1976) and certain carbon stars, such as the irregular variable, TX Psc (Bidelman and Pyper, 1963), and the semiregulars, TW Hor (Bouchet et al., 1983) and T Ind (Bouchet, 1984, private communication). In fact, Fe II emission is virtually always present in giants and supergiants cooler than M0 (Boesgaard and Boesgaard, 1976).

Fe II line profiles have been best studied in the M supergiant, α Ori (Weymann, 1962; Boesgaard and Magnan, 1975; Boesgaard, 1979). The profiles are broad (20 to 80 km/s). Some appear to be mutilated by overlying absorptions: Boesgaard and Magnan identify most of the absorbers with low-excitation lines of circumstellar origin. Many of the moderate and strong lines show steep-sided emission with a central reversal and are asymmetric (Boesgaard, 1973). The degree of asymmetry changes little with time, but the shortward peak is always stronger (Boesgaard and Magnan). The relative intensities of the lines and the intensity of the central reversal are apparently constant. On the plates taken by Boesgaard and Magnan (1975) and Boesgaard (1979) covering a 5-year period from 1970 to 1975, variations in the velocities of the Fe II emission lines follow the same pattern as those of the absorption atomic lines measured in the same spectral region (see Figure 1 in Boesgaard, 1979), implying that they follow the motions of the absorption-line-forming layer. Furthermore, the Fe II emission lines are red-shifted relative to these absorption

atomic lines. Adopting a center-of-mass heliocentric velocity, $V_* = 19.1 \pm 1$ km/s, for α Ori (Huggins, 1984, improving the Knapp et al. (1980) value of 18.8 ± 2.5 km/s), it appears that in the observing period: (1) the considered absorption atomic-line velocities in the blue-violet region are infalling with extreme red shifts of 6.0 ± 1.5 and 1.7 ± 1.8 km/s, (2) the Fe II emission lines also form in infalling layers with extreme velocities being $+12.5 \pm 2$ and $+6.5 \pm 1.8$ km/s relative to V_*. Boesgaard (1979) notes that the reversals in the Fe II emission lines measured in 1974 and 1975 are redshifted relative to the atomic absorption lines. Thus, the Fe self-reversals are also formed in infalling layers with velocities included between $+23.2 \pm 1.6$ and $+7.3 \pm 1.9$ km/s relative to V_*; they are probably the same layers in which the Fe emission is produced.

However, Van der Hucht et al. (1979) found that all the UV Fe emission lines observed in α Ori on September 16, 1976, with the balloon-borne Ultraviolet Stellar Spectrograph (and in particular, three lines from multiplets 6 and 7 also observed by Boesgaard and Magnan (1975)), are *blue-shifted* by -14 (± 9) km/s with respect to the Adams (1956) adopted "photospheric" radial velocity of $+21$ (± 4) km/s (i.e., $\sim -12 \pm 10$ km/s with respect to the systemic velocity). We conclude that in 1976 the Fe emission lines were correlated to an outflow of material and to an infall during the period 1970 through 1975.

Carpenter (1984) studies Fe II emission lines in the 2300 to 3000 Å region of four high-resolution IUE spectra of α Ori obtained from April 1978 to November 1982. Unfortunately, these line radial velocities are not absolute due to a lack of absolute wavelength calibration during the IUE exposures. It may be possible to correlate the photospheric radial velocities by Goldberg (1984) to the ones drawn by Carpenter from the studied spectra at the dates of the observations. Nevertheless, the average photospheric velocity is defined by Goldberg from IR and near-IR absorption lines, whereas it is measured by Carpenter from UV Fe I lines. Recalling the results from Miras that the IR and blue atomic lines are formed in very different layers (see the section *Source of the Visible Spectrum*), it might be hazardous to combine the two average "photospheric" velocities in α Ori. Rather, adopting a probable radial velocity of 21 km/s for the blue lines (as done by Van der Hucht et al., 1979), it appears that the Fe II emission-line centroids are in infalling layers during the observational period. A correlation of Fe II line asymmetry with intrinsic line strength, indicating velocity gradients inside the line-forming region, is also found (Carpenter, 1984).

The semiregular carbon star, TW Hor, deserves special mention. The Fe II emission lines can appear during only 2 consecutive days as in July 1979 ($\varphi \sim 0.75$) (Figure 2-7) or can last at least 4 consecutive days as in August 1981 ($\varphi \sim 0.7$; Bouchet et al., 1983). In addition, they can vary strongly in intensity over a few days; for example, they were observed on October 15, 1980 (IUE observation), then they nearly disappeared on October 17 and 18, and on October 19, they again became as strong as on October 15. Unfortunately, no radial-velocity data are yet available.

Ca II H and K Lines. The Ca II lines (3933 and 3968 Å) show a complex profile in the late-type stars (Deutsch, 1960), giving information on the atmospheric stratification and on the motion of the layers as a function of the geometric depth. The H line is less well studied than the K line due to a weaker oscillator strength and a possible contamination by the Hϵ hydrogen line. The various components that can be found in a Ca II K (or H) line profile are: the K_1 wings that refer to the broad absorption formed in the "photosphere," the K_2 chromospheric emission core onto which is superimposed a K_3 self-reversed absorption core of chromospheric (non-LTE radiative-transfer) origin, and a K_4 deep and sharp CS component. Moreover, faint emission lines of other elements may appear in the K_1-H_1 wings (Stencel, 1977; Linsky et al., 1979). The profile varies with spectral type, showing either a K_3 component inseparable

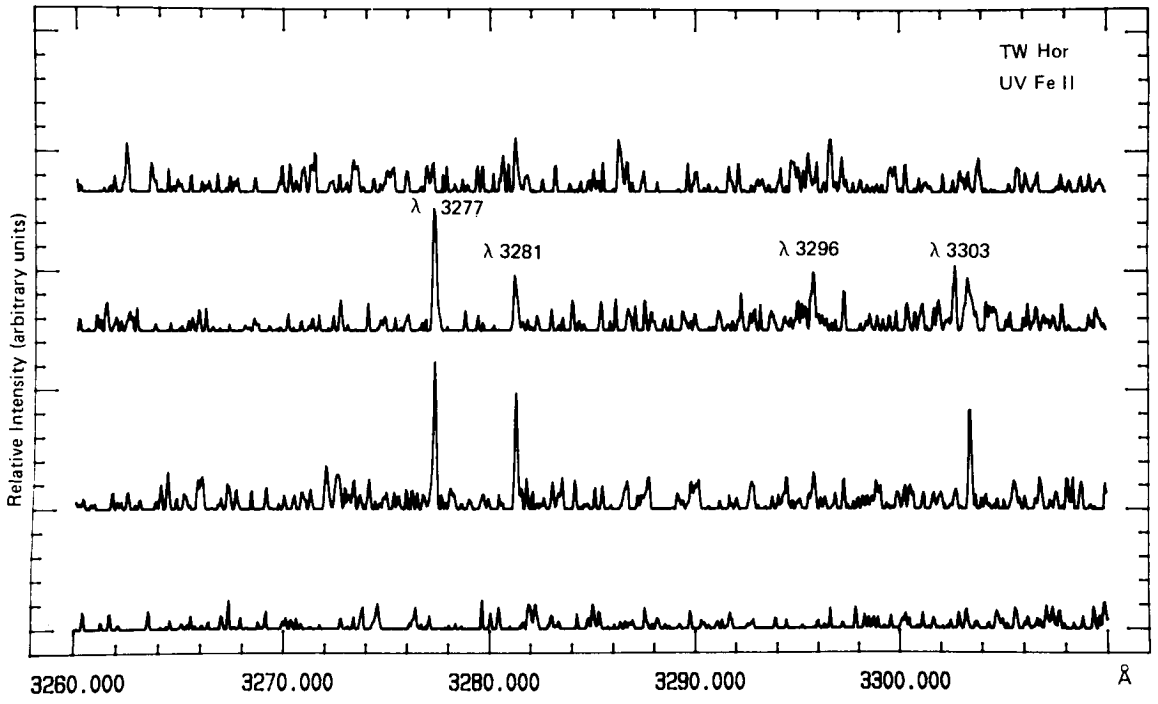


Figure 2-7. Violet Fe II line region in the semiregular carbon star, TW Hor, on four consecutive dates in July 1979 (bottom to top: July 13, 14, 15, and 16, respectively). The ordinates are in arbitrary units (from Bouchet et al., 1983).

from a dominating K_4 component or noticeable asymmetries, as described below. The CS component is discussed in the section devoted to the *Circumstellar Lines*.

The Ca II H and K lines in the *Miras* mimic the metallic emission lines in appearing only on the shortward edge of the H and K absorption cores. Merrill (1960) describes the phase behavior of the Ca II lines in the Mira variables (also see Figure 2 in Merrill, 1952c, which illustrates the line variation with phase in R Leo). In brief, as noted by Hagen et al. (1983), a single blue-shifted feature is seen, rather than the self-reversed absorption core observed in the semiregular and irregular giants (see below and Figure 2-8). These authors also remark that strong and phase-variable emission lines are found in the K_1-H_1 wings at 3938, 3945, and 3969 Å and that they are collisionally excited Fe II (V3) lines. Analogous to R Leo (Merrill, 1952c), o Cet shows pronounced wing emission lines at 3936 and 3938 Å at certain phases; there is a strong contrast variation with phase for the

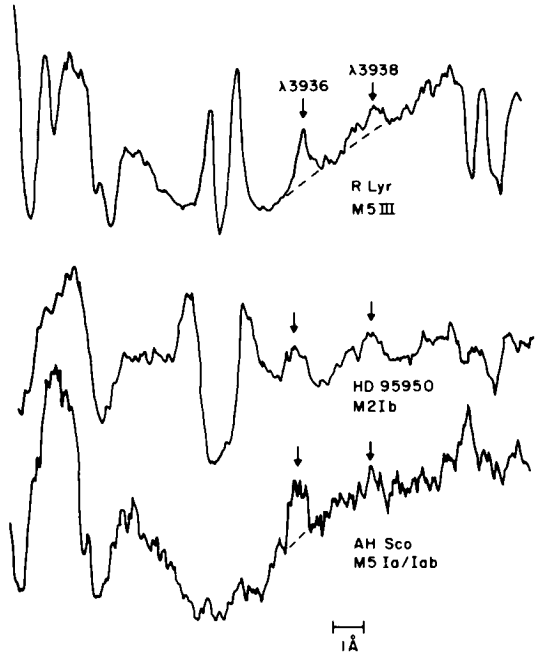


Figure 2-8. Representative Ca II K line profiles in various luminosity class M stars. K_1 wing emission lines are marked by arrows (from Hagen et al., 1983).

3938 Å line, while 3936 Å line maintains an almost unvarying contrast (Stencel, 1977).

A large sample of M *semiregular and irregular giants and supergiants* are observed by Hagen et al. (1983). In all the stars, the K_3 self-reversal component is completely dominated by the deeper CS K_4 component, which is generally blue-shifted relative to the line center. Representative profiles are differentiated (Figure 2-8): (1) the stars of luminosity class III show nearly identical profiles—the long-wavelength emission peak, K_2R, is stronger than the K_2 emission feature on the violet side, K_2V, due to the blue-shift of the narrow K_4 absorption; and (2) the latest giants and most of the supergiants show much broader K_4 features and reduced or no emission: the stars with reduced emission have either $K_2V \sim K_2R$ or $K_2V > K_2R$, depending on the slightly blue-shifted CS component (Stencel, 1978).

Figure 2-8 also mentions emission lines identified in the K_1 wings. All the stars of the sample show one or more of the H–K wing emission lines, even the stars which lack Ca II H_2–K_2 emission. Hϵ in emission is noted in some stars.

The supergiant, α Ori, was observed in the Ca II H and K region in 1974 and 1975 by Boesgaard (1979) with a concentration of six spectra over a 64-day interval. The Ca II K_1 feature is broad, and a deep central absorption reversal is present. The six close spectra show only small changes in the Ca II line profiles due to the position of the deep central absorption minimum. This is in contrast with the high time variation of the Ca II profile shown by Boesgaard (1973) from spectra taken in November 1970 and in December 1971, in which the brightness ratio K_2V/K_2R decreases from 1 to less than 1, and by Kondo (1973) from an undated spectrum in which $K_2V/K_2R > 1$ (compare Figure II-42 from Boesgaard, 1973, and Figure II-18 from Kondo, 1973). Changes in the V/R intensity ratio are common in late-type giants (see discussions in Mullan, 1984; Drake and Linsky, 1983). The measured radial velocities on the 2-year spectra give the following results, obtained by setting the α Ori systemic velocity at 19.1 ± 1 km/s (Huggins, 1984): (1) the absorption-line velocity in the Ca II region fluctuates between +26.0 ± 0.4 and 19.5 ± 0.3, evidencing infalling material (as already found for the absorption lines in the Fe II region); (2) the Ca II emission lines follow the same pattern as the blue-violet absorption lines and are red-shifted relative to the latter (as already noted in the foregoing section for the violet Fe II lines in α Ori during the same observational period) by a mean red shift of +5.9 ± 1.3 km/s; that is more precisely from +14.3 ± 3.9 to +5.1 ± 1.9 km/s with respect to the center-of-mass velocity, depicting *infalling* gas; (3) the position of the central reversals fluctuates around the systemic velocity from +1.4 ± 1.1 to −1.7 ± 1.1 km/s; we are likely dealing with the H_4–K_4 CS component (while the reversals for the Fe II lines are red-shifted, implying that they are formed in the same region as the Fe II emission).

On the other hand, from a series of observations of Ca II H and K lines in α Ori, Linsky et al. (1977) claim that the emission-line velocity with respect to the "photosphere" ranges from −12 to +10 km/s. If we adopt the averaged absorption-line velocity over the Ca II region of 23.8 km/s from Boesgaard (1979) since the authors do not give one, these measurements allow one to interpret the Ca II emission lines as *either infalling or rising material.* (The Fe II measurements in September 1976 by Van der Hucht et al. (1979) put the Fe II lines in rising layers.) If the period of observation of Linsky et al. is supposed to straddle the observations by Boesgaard and by Van der Hucht et al., a change in the dynamical structure of the star is to be taken into account.

Ca II Infrared Triplet Emission Lines. The Ca II infrared lines at 8497.7, 8541.7, and 8661.7 Å have been reported as being strong in emission in Mira stars at maximum and post-maximum phases. All lines are mutilated by TiO absorption in M stars and by CN features in carbon stars, except for the line at 8662 Å. In R Cyg, Tsuji (1971) notes that, for each emission

of the Ca II triplet, there is a shallow absorption feature toward the red that is a leftover part of the wing of the broad Ca II absorption; it is also clearly visible at 8662 Å in χ Cygni (for example, Maehara, 1968). For S Car, Shinkawa (1973) remarks that asymmetries in the absorption-line profiles are present, sometimes when emission is not, and that, in some cases, emission is only observed in one of the three lines of the multiplet, with asymmetries occurring in the other lines. (Her Figure 10 shows how, in S Car near maximum, the Ca II triplet line profiles, with their deep absorption core, differ from the profiles in χ Cygni.) An unidentified emission is also seen in the red wing of the 8662 Å Ca II line (reminiscent of the H-K wing emission lines) in nearly all of the spectra of S Car that exhibit the blue-shifted Ca II emission. However, this never happens in the larger wings of the other Ca II triplet lines (Shinkawa, 1973).

Emission in the Ca II triplet has been observed in the Mira C stars, U Cyg and RZ Peg, just after maximum light (Richer, 1971). Note that the Ca II infrared lines are in emission at maximum light, while the Ca II H and K lines are still in absorption, becoming later in emission (Contadakis and Solf, 1981). This recalls the differing lifetimes of the hydrogen lines in the visible and the infrared regions: the continuum intensity would decrease with phase in the visible faster than the line intensity.

In the supergiant, α Ori, Goldberg (1979) observed no emission in the Ca II triplet lines; rather, a strongly asymmetric absorption core was detected (see Figure 2-17).

Mg II h and k Emission Lines. In M semiregular giants and supergiants, the Mg II resonance doublet lines with the k component at 2795.5 Å and the h component at 2802.7 Å are observed at high resolution as two strong emission lines with a deep central self-reversal (e.g., Wing, 1978; Basri and Linsky, 1979). The reversals are displaced slightly shortward from the centers of the emission components; they are circumstellar absorption features, indicating a cool outer shell expanding at a moderate rate. All the observations of several stars—the M giants such as β And, γ Eri, μ Gem, and γ Cru and the M supergiants such as α Sco and α Her—particularly the numerous observations of the supergiant, α Ori (Kondo et al., 1972; Kondo et al., 1975; Modisette et al., 1973; Bernat and Lambert, 1976a; Wing, 1978; Carpenter and Wing, 1979; Basri and Linsky, 1979; Weiler and Oegerle, 1979; Van der Hucht et al., 1979; Dupree et al., 1984), display k line asymmetries, always observed on the shortward wavelength side of the intrinsic emission, whereas the h line is reasonably symmetric. Theoretically, the k line is expected to be twice as strong as the h line (Modisette et al., 1973). The k line asymmetry has been attributed to a selective absorption by Fe I UV3 (2795.006 Å) resonance transition, occurring in the cool shell surrounding the M star (de Jager et al., 1979, and references therein; also Kondo et al., 1977; Figure 2-9).

The M supergiants have much broader Mg II emission profiles than the M giants. From the survey of Weiler and Oegerle (1979), it appears that the Mg II k line shapes are not unique to a given spectral class. The width-luminosity correlation (the famous Wilson-Bappu effect) analogous to the Ca II one is seen in the Mg II h and k emission cores (e.g., Ayres, 1979).

A comparison of IUE flux obtained in August 1978 for α Ori with previous measurements obtained with the OAO-2 (Orbiting Astronomical Observatory; Doherty, 1972), BUSS (Balloon-borne Ultraviolet Stellar Spectrometer; Kondo et al., 1976), and Copernicus (Bernat and Lambert, 1976; Weiler and Oegerle, 1979) satellites shows that the Mg II flux in α Ori is fairly variable with time (Basri and Linsky, 1979), as also noted by Dupree et al. (1984) from Mg II fluxes measured from 1978 to 1984. Van der Hucht et al. (1979) find the Mg II h emission line (observed on September 16, 1976) to be indicative of an *outflow* velocity ($\sim$-3 km/s with respect to the systemic velocity), as also indicated by the violet Fe II lines they observe at the same epoch. Apparently, a special event occurred in α Ori about 1976, as already mentioned from the Ca II H and K and UV Fe II lines.

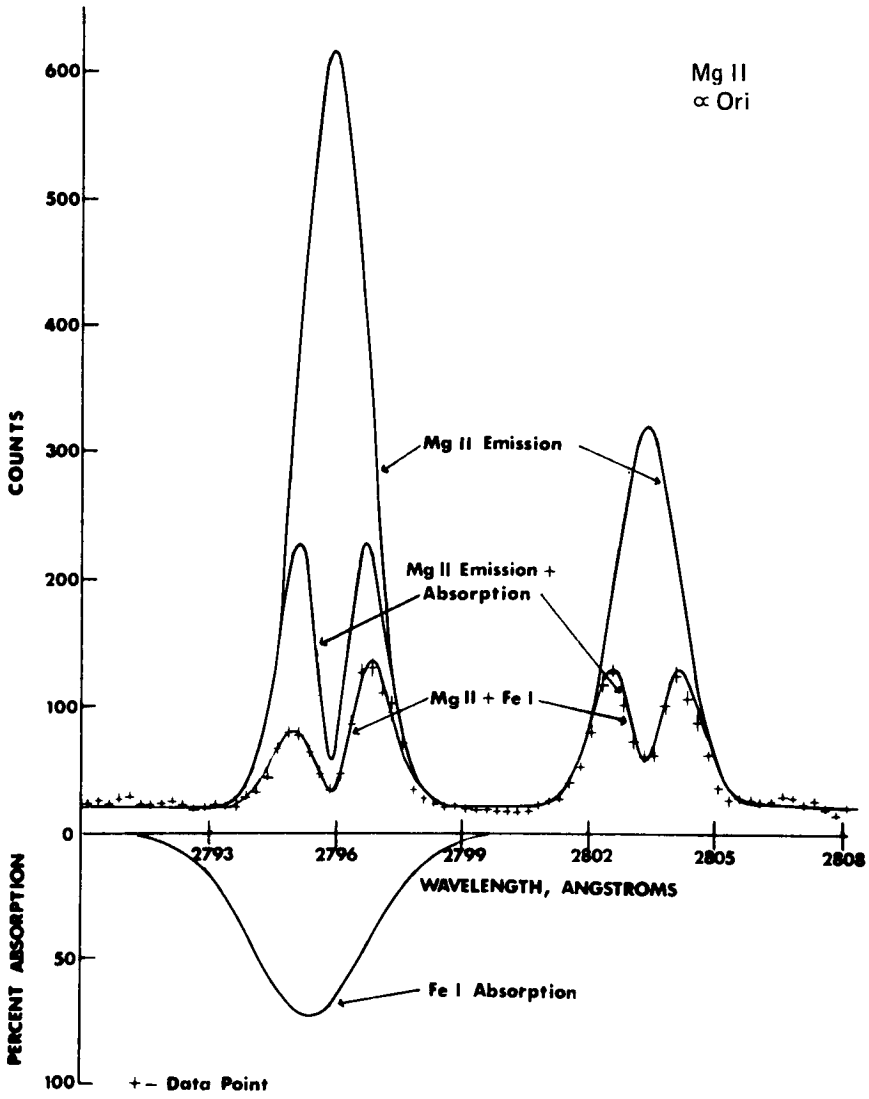


Figure 2-9. Synthetic spectra of the M supergiant, α Ori, in the vicinity of the Mg II h and k lines. The crosses represent the observations of Kondo et al. (1972) (from Modisette et al., 1973).

Figure 2-10 presents Mg II h and k lines from an IUE high-resolution spectrum of the S Mira, χ Cygni, at $\varphi = 0.22$ (Cassatella et al., 1980). The h and k lines are asymmetric with a sharp red edge. The profiles recall the Ca II H and K profiles from the Miras; the red part of the lines is hidden by the overlying circumstellar absorption, giving apparent blue-shifted emission lines. The k line is more blue-shifted than the h line due to the further mutilation on the red edge by the circumstellar Fe I resonance line at 2795 Å. As a result, only the h line is saturated. As noted by Stencel et al. (1980), the wings of the Mg II lines are frequently underexposed because of the limited dynamic range of the IUE detectors. In fact, the absorption core is not recorded in χ Cygni as it is for the Ca II H and K lines.

In addition, for the first time, Mg II h and k high-resolution profiles have been observed

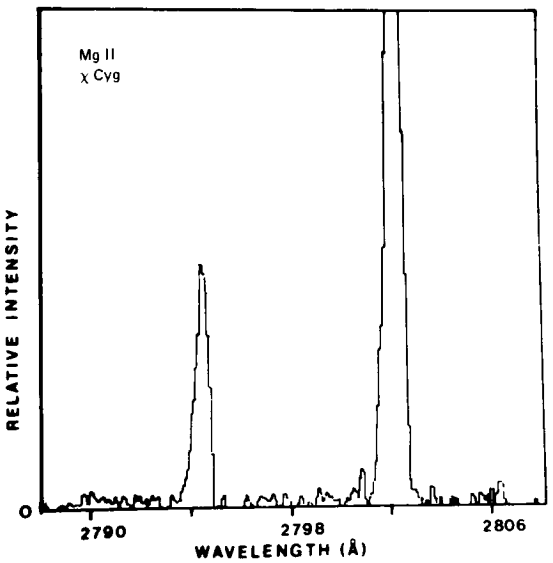


Figure 2-10. Mg II h and k lines from an IUE high-resolution spectrum of the S Mira, χ Cygni, at phase 0.22 (from Cassatella et al., 1980).

for the bright irregular N-type carbon star, TX Psc, suggesting an expanding chromosphere (Eriksson et al., 1985). Let us note that low-resolution profiles for N, R, and S stars have been published (Johnson and O'Brien, 1983; Eaton et al., 1985; Johnson and Ake, 1984; Johnson et al., 1985a; Johnson et al., 1985b; Querci and Querci, 1985a).

Other Emission Lines. Besides the classical emission lines just reviewed, other lines are valuable as additional indicators of the atmospheric structure.

The C II (UV 0.01) intercombination lines near 2325 Å have been observed with the IUE satellite at high resolution in several red giants and supergiants. Stencel et al. (1981) and Stencel and Carpenter (1982) showed that the relative intensities of emission lines within the multiplet are sensitive to electron density in the 10^7 to 10^9 cm^{-3} range, which is appropriate for measuring densities in the low-gravity cool stars. Carpenter (1984) applies the method to α Ori. He finds a mean density of 3.2×10^7 electrons cm^{-3}. A rough estimate of the geometric extent of the C II line-forming region may be predicted on the basis of the electron density, the total multiplet flux, and the temperature in the C II emitting region (Carpenter et al., 1985). So, with a temperature of the C II region set at 8300 K (obtained independently from the ratio of the total flux in the 2325 Å multiplet to that in the 1335 Å resonance-line multiplet by Brown and Carpenter, 1984), the thickness of the C II layer—perhaps close to α Ori chromospheric extent (see the section *Atmospheric Kinematics—Other Giants and Supergiants*)—is estimated to be 7.4×10^{13} cm (i.e., 1.5 R_*). Higher quality spectra and atomic data are needed to improve this conclusion (Carpenter, 1984; Carpenter et al., 1985).

The He I 10830 Å line has been observed in a sample of M, S, and C stars by Zirin (1976, 1982). The line is found in emission in Mira stars. In R Hya, the emission is seen at maximum ($\varphi = 0.93$), but not on the rise at $\varphi = 0.77$; in R And, it is a strong emission feature at $\varphi = 0.77$. However, in χ Cyg, no feature is detected either at a premaximum at $\varphi = 0.8$ or at the postmaximum at $\varphi = 0.16$ of the same cycle, or on the rise to the next maximum at $\varphi = 0.6$. Surprisingly, in R Gem, the emission is observed at minimum light. The He I emission is always accompanied by Pγ in emission, even in R Gem.

The helium line has also been detected in a few supergiants. The 10830 Å emission was observed in α^1 Her (on October 29, 1978) by O'Brien and Lambert (1979); its strength does not appear to vary over 8-month observations. The He I absorption line was detected in α Ori by Zirin (1982) in September 1965 and February 1973, but no detection is reported in February 1966 and December 1979 by this author, nor in November 1978 by O'Brien and Lambert (1979), nor in December 1974 by Sherbakov (1979). In the supergiant, μ Cep, He I absorption is seen in August 1965 (Zirin, 1982). Let us add the observation of a P Cygni profile in the helium line in the RCB carbon-rich star, R CrB, on January 18, 1978, on rise to maximum (Querci and Querci, 1978).

The He I 10830 Å emission demands densities of about 10^{12} electrons cm^{-3}. If the density is less, an absorption line may appear. However, an emission, as well as an absorption, He I line is excited only for temperatures of at least 20000 K (Vaughan and Zirin, 1968). In the solar-type stars, the He I line is excited by coronal X rays. Such an explanation is not valid in the cool stars, where there is an apparent lack of plasma hotter than, say, 20000 K and therefore no corona. Simon et al. (1982) suggest that the line in giants and supergiants is formed in the extended cool chromosphere at low densities by a scattering process. In the Miras, λ10830 emission is probably excited in the shock front progressing in the photosphere. We exclude the term *chromosphere* in discussing Miras; cf. the discussion in the section *Atmospheric Kinematics*, explaining the exclusion.

The emission lines from neutral atoms shortward of 4000 Å must be mentioned. In the M supergiant, RW Cep, numerous narrow emission lines, mainly from Fe I + Ti I, are superposed on the weak continuous spectrum (Merrill and Willson, 1956). Such emission lines from Ti I, V I, and Zr I in the 3900 Å region are also reported for the irregular carbon stars, UU Aur and Y CVn (Gilra, 1976). They are primarily zero-volt lines, assumed to be formed in an extended outer circumstellar shell, where the gas is neutral because the far-UV radiation is insufficient to ionize it (Querci et al., 1982). Similar emission from an extended region may also be responsible for filling in the Mg I absorption line in carbon stars (Johnson and O'Brien, 1983).

Finally, we noted in the section *Changes in Emission-Line Radial Velocities with Phase* that in the Miras some visual (blue) atomic lines first appear with blue-shifted emission (i.e., with inverse P Cygni profiles (P Cygni type profiles are defined in the section *Circumstellar Lines*)). A good example is *o* Cet (Joy, 1954). Also, Hinkle and Barnes (1979b) observe such Ti I, Sc I, V I line profiles in the 2-μm region of R Leo at premaximum phases, which they explain in the following way. The atomic absorption cores come from lower excitation levels of between 1.5 and 2.5 eV and behave with phase as the $\Delta v = 3$ infrared CO lines (as in Figure 2-1), showing an S-shaped curve. They are formed over an extended region of the atmosphere (in comparison to weak atomic lines coming from excitation levels of 4 eV or greater, such as Fe I lines and being therefore excited only in the deepest, hottest photospheric layers). At the phase at which the P Cygni type profiles appear (~0.6 to 0.8), the absorption cores are in infalling cool layers (Figure 2-1, upper panel), in agreement with their red shift with respect to the center-of-mass velocity. Like the IR CO absorption lines observed at such phases, they are produced by the inward-moving gas left over by the preceding rising shock wave. As for the excitation of the emission peak, we are dealing with an extended outer region, all the more as the phase is nearest to the minimum light where the photosphere is at its highest extension. Moreover, Hinkle and Barnes note that there is a large apparent velocity difference between the "stellar" disk (this part limited by the continuum optical depth unity) and off the edge of the disk; such conditions favor emission by scattered light from the stellar radiation field, giving its full meaning to the observed P Cygni type profile.

Ti I inverse P Cygni profiles at 1 μm have also been observed in *o* Cet (Ferlet and Gillet, 1984). The lower excitation level of the lines is 1.9 to 2.1 eV, which is roughly in the same range as the 2-μm metallic lines previously discussed. The difference with R Leo comes from the phase of observation which is just after the maximum ($\varphi = +0.04$). At maximum light, there corresponds a minimum radius of the pulsating photosphere. Consequently, the Ti I line-forming region above the continuum optical depth unity (in other words, the Ti I emitting region) is still sufficiently extended at maximum light in *o* Cet so that scattering effects are still possible. Ferlet and Gillet claim that the Ti I emission might be formed through the ballistic motion of the infalling material.

However, this seems unlikely because the emission peak is at the *o* Cet center-of-mass velocity, which is quite normal when dealing with scattered emission in an extended zone.

In conclusion, it can be found for atomic lines of similar strength from the blue to the IR range, which are formed throughout an extended atmospheric layer.

Atmospheric Kinematics

The Mira Stars: The Shock-Wave Model Resulting from Pulsation Plus Matter Infall. From the above survey of observations of emission-line variability, we are now able to complete the qualitative description of the shock-wave model developed earlier (mainly from the behavior of the infrared molecular lines in the Mira, χ Cygni, following Hinkle et al., 1982). We assume that the emission lines arise as a consequence of the formation of an upward-moving shock by the collision of the outward-moving pulsation wave and the infalling matter from the preceding pulsation cycle, and are thus formed under post-shock conditions (Willson, 1976). The observations of Figure 2-6 place the emission-lines in rising matter. But we consider that the fluorescent lines require different physical conditions for their formation.

Unfortunately, there is not yet a set of data that covers all the spectral range from the UV to the IR wavelengths for a given star. Let us summarize the main data at hand on temporal changes in the emission lines as well as in the absorption lines:

1. We know the behavior of the CO infrared absorption lines and of the blue-violet atomic absorption lines (Figure 2-1) from χ Cygni and that of the CO (and OH) infrared lines and of the hydrogen emission lines from R Leo (Figure 2-6c). The behavior of the hydrogen emission lines, neutral and ionized metallic emission lines, and fluorescent lines from *o* Ceti (Figure 2-6a, b) is also known. Furthermore, data from other stars give additional information (e.g., that from S Car, Figure 2-11).

2. Comparisons between radial-velocity curves give meaningful information on the relative location of the absorption and emission lines. As discussed in the section *Changes in Emission-Line Radial Velocities with Phase* and displayed in Figure 2-6c, the hydrogen radial-velocity curve for R Leo has a shape similar to the IR CO and OH rising component curves, but particularly near maximum light, it lags in phase by 0.2. A wave moving outward from the deepest layers of the star will first disturb the spectral features arising at great optical depths, and their radial velocity will be ahead in phase compared with the radial velocity of features situated at smaller optical depths. Near maximum, the hydrogen emission line-forming region is situated higher in the atmosphere than the CO and OH absorption line layers.

Let us assume a hypothetical Mira star for which all the previous observational information is available, with the radial velocities from the hydrogen and IR lines behaving with phase in *o* Ceti as in R Leo. First, the observations at maximum light could be interpreted in the

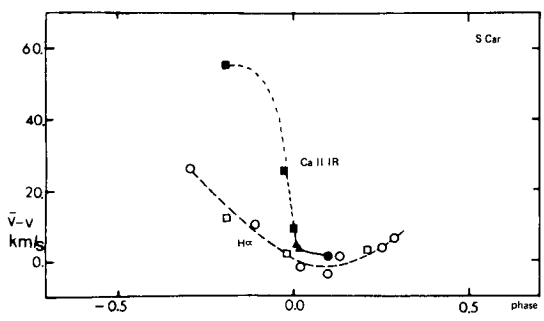


Figure 2-11. Velocities of Ca II infrared triplet emission lines and Hα emission as a function of phase in the M Mira, S Car (adapted from Shinkawa, 1973).

following manner. Hydrogen emission originates in a shock which precedes the layers (kept moving outward due to the outward momentum given by the shock wave), giving rise to the shortward component of the CO (and OH) line-doubling. The Si I emission-line velocity is similar to the hydrogen velocity (i.e., about -10 km/s with respect to the stellar velocity in *o* Ceti), and thus one should expect that both Si I and H lines are excited by the same shock. Similarly, the Ca II IR emission lines which have nearly the same velocity as the Hα lines (from S Car, Figure 2-11; see also Contadakis and Solf, 1981) are also likely to originate from the same shock front. Secondly, the propagation of the shock with phase in such a model would be depicted as follows by implementing the emission-line information into the scheme that describes the absorption lines in the section *Photospheric Kinematics—The Shock-Wave Model*. From the IR absorption lines, the emergence of the shock into the photosphere is at phase -0.3 when the total CO ($\Delta v = 3$) column density begins to decrease. It progresses outward, and at phase -0.2, the emission in Hγ, Hδ, Si I, and Ca II lines is detectable. (Note that Hα emission is seen in S Car as soon as phase -0.3 in Figure 2-11.) From phase -0.10 to 0.15, the CO second overtone becomes double-lined, and the hydrogen emission is at its maximum strength. The shock must have traveled through most of the photosphere because, at phase -0.2, the hydrogen lines are strongly mutilated by overlying absorption (as Ti O in M Miras), while at maximum, they are quite sharp. By means of the emission lines, the rising shock can be followed until minimum light (Hγ, Hδ, and the Si I (2) line at 4102 Å are in emission in *o* Ceti up to $\varphi = 0.65$, 0.57, and 0.60, respectively, from Table 7 in Joy, 1954), and its passage must also account for the CO column density variation.

The ionic emission lines and the fluorescent lines fit the foregoing explanation. Among the first, in *o* Cet at maximum light, the Fe II lines, especially the chief line of multiplet 28 at 4178 Å (that appears in emission and lasts as the hydrogen lines do), have a mean velocity clearly lower by about -3 km/s than the H and Si I lines ($v \sim -10$ km/s; Figure 2-6b). We suggest two possible interpretations: a second shock located higher in the atmosphere and structure within the shock front itself.

The Two-Shock Model. As described in the section *Analysis of Absorption-Line Velocity Histograms in Miras*, Willson et al. (1982, and papers cited therein) favor the coexistence of two shocks, particularly at maximum light, at different altitudes in the stellar atmosphere. An example taken from these authors and involving emission lines is given by the histogram of the velocity distribution in the blue spectrum of RT Cygni 4 days before maximum ($\varphi = -0.02$; Figure 2-12). Emission lines of Si I ($v \sim -14.5$ km/s) and hydrogen ($v \sim -8.5$ km/s) are likely to be assigned to the lower shock (in A), while emission lines of Fe I, V I, and Cr I and of ionized metals ($v \sim -3.5$ km/s) are assigned to the upper shock (in C; see also Figure 2-4a).

Similarly, in *o* Cet, the hydrogen and Si I emission lines, together with the blue-shifted IR molecular absorption lines, should again arise from the lower shock, while the Fe II emission lines, with $v = -3$ km/s at maximum light, would be produced by the upper shock. The aperiodic Fe II velocity curve with phase also supports the idea of an upper shock. The Ti II (13) and Sr II (1) lines (which appear in emission in *o* Cet at $\varphi = 0.03$ and $\varphi = 0.13$, are at their maximum strength at $\varphi = 0.24$, and last up to $\varphi \sim 0.5$ and 0.6, respectively) also show rather small aperiodic velocities and could be related to the upper shock, though their mean velocity ($v \sim -7$ km/s and -9 km/s, respectively) is larger than that inferred from Fe II ($v \sim -3$ km/s). The upper shock is "observationally" lost from phase 0.6 to phase 0.8. In fact, the Ti II and Sr II lines are reminiscent of the ionic emission lines that appear in the RT Cygni histogram (Figure 2-12) between the lower and upper postshock components (A and C) at $v \sim -6$ km/s). As noted by Willson et al. (1982), it is generally rather difficult to separate these postshock components.

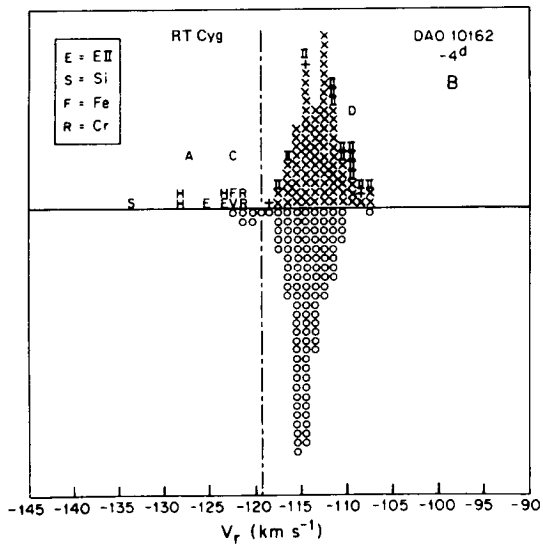


Figure 2-12. Histogram of velocity distribution in the blue spectrum of the M Mira, RT Cygni, just before maximum light (φ = -0.02). Lines of "high excitation" (arbitrarily chosen as χ_{ex} >1 eV) are plotted above the horizontal line; lines of low excitation (<1 eV) are plotted below. Emission lines are indicated by the symbol for the element above the line; ion lines are shown as "II," and emission from ions as "EII." Doubled lines are shown as a pair of dots at the appropriate velocities above or below the line, depending on their excitation class. A "+" sign indicates "very high excitation" ($\geq$ 3 eV) lines (from Willson et al., 1982).

Structure of Shock-Front in Single-Shock Interpretation. When describing the absorption lines in the carbon star, RT Cygni (in the section *Further Probes of the Pulsating Photosphere*), we presented the two-shock model of Willson et al. (1982) and concluded that a single-shock model need not be ruled out. Arguments by Wood (1981, 1982) also sustain this conclusion. From the variations with phase of the Balmer emission-line profile and flux in a sample of nine M Miras, it appears that a simple shock model can account for the velocities and temperatures of the Balmer line-emitting region (Fox et al., 1984).

How can one account for the velocity variations in the various emission lines, such as those observed in *o* Cet, with a single rising shock? The velocity of the emission lines is an indicator of the postshock velocity, and their variability is related to changes in the postshock velocity with phase. Furthermore, the various emission lines might be indicative of the velocity gradient within the shock front.

In the front structure, ionization and excitation processes occur in the relaxation zone behind the outward propagating shock face (for example, Slutz, 1976; Whitney and Skalafuris, 1963), specifically in the zone called "internal" by Whitney and Skalafuris. While Slutz investigates the postshock propagation in the conditions prevailing in a Mira atmosphere, Whitney and Skalafuris detailed the shock-front structure in a long-period Cepheid, W Vir. Both authors recognize that their investigations of shock variation with temperature, density, and velocity as a function of the distance, x, to the shock face or as a function of the face velocity, V_s, is based on simplified assumptions. However, their results provide at least a guide for a qualitative interpretation of the observations. In Whitney and Skalafuris's cepheid "internal" relaxation zone, for a given temperature, density, and velocity at the shock face, and also in Slutz's Mira relaxation zone, the run of the temperature and velocity as a function of x shows that both variables decrease significantly in value as x grows, all the more so because V_s is higher. When traveling down density gradients as in a Mira atmosphere, the shock wave is expected to accelerate. Whitney and Skalafuris find that, for increasing V_s (ΔV_s = 40 km/s) in W Vir, the temperature increases very rapidly at the front of the "internal" zone called "1" ($\Delta T_1 \sim$ 92000 K) and increases gradually at the rear of this zone, called "2" ($\Delta T_2 \sim$ 19000 K). The velocity is rapidly increasing at "1" ($\Delta V_1 \sim$ 9 km/s), while rather gradually increasing at "2" (ΔV_2 = 3.8 km/s); for the lowest V_s, it is nearly constant.

In *o* Ceti, as the shock propagates through the atmosphere (i.e., as it increases in velocity with phase), the Fe II lines are kept at a nearly

constant velocity, indicating that their region of formation might be in the relaxation zone near the rear of the "internal" zone (region "2"), whereas the hydrogen lines would be at the front of this zone (region "1"), in particular at $\varphi = 0$ and 0.2.

As stressed by Wood (1979), a direct interpretation of emission-line velocities in terms of postshock velocities are, in practice, subject to complicating factors because of the unknown optical thickness of the emitting region and geometric and limb-darkening effects. (See the section *Preliminary Remarks.*) Reliable velocities for the postshock region require a model that simulates the emission process, as well as information about the detailed thermal structure of the relaxation zone and the shock-wave kinematics in a Mira atmosphere that lies over several density-scale heights. An encouraging result is given by Wood (1979), who computes a long series of isothermal models covering 92 pulsation periods: the postshock velocity follows the same variation with phase as that of the observational hydrogen emission-line velocities, with a steep rise at maximum followed by a decline. A favorable feature of Wood's models is the inclusion of periodic shock injections into the Mira atmosphere rather than the propagation of an isolated large-amplitude shock, which neglects the periodic nature of the shock, as in Slutz's (1976) model. (See de la Reza, this volume, for details on shock-wave gas dynamics.)

Finally, we conclude by looking at the fluorescent lines. They are selectively excited; for example, the Fe I (42) line at 4307 Å is excited by the Mg II k line. Incidentally, as the Mg II lines are mutilated by overlying circumstellar absorption, they must arise at the upper shock in the two-shock model frame. In the single-shock model, it seems likely that the shock has to be high in the atmosphere when the Mg II lines first appear in emission ($\varphi = 0.18$ (i.e., at +73 days) in χ Cygni from the section *General Behavior of Emission Lines with Phase*). It would be interesting to know if the fluorescent lines are really in emission at the same phases as those of the exciter.

Clearly, the fluorescent lines are located in cool tenuous layers. Their velocities imply that they arise from outwardly moving matter and therefore considerably ahead of the shock itself. (Just above the shock, matter is infalling.) These lines must come from an expanding outer shell, in layers in which the expansion velocity is not yet constant. From the Fe I line at 4307 Å in o Ceti, the velocity changes by about 14 km/s from phase 0.14 to phase 0.40 and then stays constant up to phase 0.56 where no more velocity measurements are available, although the line is visible up to phase 0.78. The layers that produce such a line might be between the low-excitation 800 K CO first-overtone line shell with stationary velocity at the center of mass and the low-excitation 300 K CO fundamental line shell expanding at a constant velocity, as seen in χ Cygni. (See the section *Changes in Absorption Line Radial Velocities with Phase.*)

It is worth noting that the Mira shock-wave model described in this section is related to the most probable phase behavior of the features as generally observed in the life of a Mira. However, we noted on the o Cet example that cycle-to-cycle variations happen (e.g., more intense hydrogen emission is known to be linked to the brighter light maxima ($m_v \sim 2.5$)). This is indisputably confirmed by the absence of Hα emission at $\varphi = 0.04$, just after the June 1983 maximum of o Cet (Ferlet and Gillet, 1984) that appears to be a faint one ($m_v \sim 4$). A weak (i.e., a low shock amplitude) or an overdamped shock wave, preventing sufficient hydrogen to be ionized, could be the explanation. (Such shocks are discussed below in the C star, TW Hor.)

Atmospheric Kinematics—Other Giants and Supergiants. For illustration, we select the most thoroughly documented cases among the red stars: the M supergiants, μ Cep and α Ori, and the C giant, TW Hor, for which cross checks

between features in emission and/or in absorption might give an insight into their mechanism of origin.

Examples of a Mira-like shock wave progressing in the photosphere of irregular variables come from the H I Balmer emission in the supergiant, μ Cep, and in some C stars that show the same phase dependence seen for the Miras. (See the section *Selected Emission-Line Profiles*.) Also, S-shaped velocity curves typical to the presence of photospheric shock waves are observed from absorption lines in semiregulars. (See the section *Further Probes of the Pulsating Photosphere*.)

In μ Cep, a striking feature is the lack of detectable emission in the Ca II H and K lines, while the Fe II and Mg II lines appear strongly in emission. Hagen et al. (1983) assign Mg II emission to a Bowen fluorescence with Lyman β emission. Boesgaard and Boesgaard (1976) conclude that the Fe II emission in μ Cep comes from an outer region with respect to the photosphere, by analogy with α Ori (see below). Quite simply, from rough considerations on their ionization potential, their oscillator strengths, and the (supposed solar) atomic abundances, it may be expected that the Mg II and Fe II cores are formed above the Ca II ones (e.g., Basri et al., 1981). Therefore, they cannot be formed by the shock invoked for the Balmer emission because, if so, the Ca II H and K lines should have an emission component. We could imagine that some cycles see a Mira-like phenomenon, while in other cycles, a rising shock develops only in high layers of the atmosphere such as in TW Hor (discussed below) or in β Peg, in which the Fe II emission lines are seen to be blue-shifted with respect to the systemic velocities. Mira itself suffers exceptions such as at its June 1983 maximum (discussed in the previous section). However, whatever the mechanism, *it will stay speculative as long as temporal correlations between the various features, as well as their radial velocities with respect to the systemic velocity, are not known*. It is remarkable that the Mira-like shock-wave phenomenon can be detected in μ Cep thanks to a series of observations by McLaughin (1946). To our knowledge, no further observations over several other light phases have been done since then.

As for α Ori, the first observations to be regularly spread in time (from 1970 to 1975) concern the Fe II emission lines that are seen in infalling matter with respect to the systemic velocity over the observing period (Boesgaard and Magnan, 1975; Boesgaard, 1979). First, Boesgaard and Magnan show that a model with an extended envelope and a fluid velocity nearly equal to the Doppler velocity is well suited. Then, Boesgaard and Boesgaard (1976) confirm that the Fe II intensities are primary indicators of shell extent. Therefore, Boesgaard models the Fe II lines by adapting the method developed by Kunasz and Hummer (1974) for a spherical moving envelope in which the radial velocity is not more than a few times the Doppler velocity. However, Boesgaard does not specifically solve for the line source function, but parameterizes it to simulate a chromospheric rise in temperature, followed by a subsequent decline due to radiation losses in an extended envelope subject to velocity gradients. The best fit of the model parameters to the observed strong self-reversed Fe II line at 3228 Å in α Ori is obtained for the values shown in Table 2-1. Such values have been verified to fit profiles of other weak and strong Fe II emission lines in the star, with a change in the optical depth only. In brief, *Fe II emission lines are produced in an outer region relative to the α Ori photosphere, called the chromosphere, that is extended up to about 1.8 R_**. Let us recall that the UV C II line-forming region extends up to 1.5 R_* above the photosphere with a mean excitation temperature of 8300 K.

It appears that, to account for the large line breadths in Fe II (FWHM ~ 85 km/s for the 3228 Å line), high velocities are required; the Doppler velocity (microturbulence) is about 9 km/s throughout the Fe II shell, and the large-scale motions (macroturbulence) are about 8 km/s. These velocities are marginally subsonic as the sonic velocity is about 9 km/s at the surface of α Ori. Boesgaard (1979) also recalls how large the breadths are in the Ca II K_2 feature

Table 2-1
Shell Model Parameters* to Match the Fe II λ3228 Line in α Orionis (from Boesgaard, 1979)

Size of Fe II region	1.8 R_*
Optical depth T	500
Fluid velocity near star (km/s)	+60
Fluid velocity, outer edge (km/s)	+18
Doppler velocity near star (km/s)	9
Doppler velocity, outer edge (km/s)	9
Macroturbulence (km/s)	8
Core brightness	0.3
Density distribution exponent	2
S_1†	0.25

*The density distribution within the shell is $\varrho \sim r^{-2}$.
†S_1 is such that $S_1 T$ represents the optical depth at which the line source function reaches its maximum value.

(186 km/s) and in the Mg II k emission line (410 km/s at the base) in α Ori. Such broad features are suggested to reflect *high nonthermal random motions*. Note that no homogeneous chromosphere could reproduce the Mg II k line profile (Basri et al., 1981). Furthermore, to fit the red shifts in the emission and in the central reversal, a gradient in the fluid velocity is required; the material is accelerating inward from 15 to 20 km/s at 1.8 R_* (the outer shell edge) to 60 km/s at the stellar surface. Because the free-fall velocity is 61 km/s, the matter is accelerated by the gravitational field. In addition, the material is *infalling at supersonic speeds and would produce a shock front*. In fact, such a shock front would have the conditions necessary to excite the emission lines. Let us recall that infalling gas in α Ori is also seen from Ca II H and K and UV Fe II emission cores.

On the other hand, *outfalling* material from the Fe II, as well as from the other chromospheric indicators, Mg II, and Ca II H and K emission lines (particularly in September 1976) is observed in α Ori. Another example of fluid velocities indicative of expanding matter from the Fe II emission comes from available data on the giant, β Peg (Boesgaard, 1981). There the material expands from 0 to 25 km/s within the Fe II region, which is 2.0 R_* in size. The Fe II line widths are also very broad, implying a microturbulence of 10 km/s within the Fe II region. However, from the Ca II K_4 circumstellar absorption feature observed in β Peg, also formed over a velocity gradient of 0 to 25 km/s, the turbulence beyond about 2 R_* averages ≤4 km/s.

The extreme broadness of the features and the corresponding high Doppler velocities probably caused by nonthermal motions are explained by Boesgaard (1981) by a turbulent exchange of material between the photosphere and the chromosphere. This author presumes that the chaotic mass motions are attributed to large-scale convective cells which Schwarzschild (1975) assumed to arise in the photosphere of red giants and supergiants.

In this view, how should the emission lines be excited? Boesgaard (1979) stipulates that the matter might be driven upward by photospheric convective overshoot into the chromosphere from the large-scale convective cells, and some of it may then return toward the star at high velocity. These convective cells are often put forward in the literature to explain unexpected observations (for example, Hayes, 1982; Goldberg et al., 1981; Goldberg, 1984; Antia et al., 1984). However, we do not really understand how they could be responsible for driving mass up to 2 R_*. Also, arguments by Karovska (1984) about polarization observations, which will be presented in the section *Interpretations of the Polarization Observations*, question the suggestion by Goldberg et al. that these authors might have observed such a structure in α Ori.

To clarify the atmospheric dynamics of this star, let us highlight the striking features among the relevant available observations from 1970 to 1978—a period during which α Ori has been rather well monitored.

The data on absorption lines are displayed in Goldberg's (1984) Figure 5. First, let us recall

that in the Miras the radial velocities permit one to distinguish beyond objection the phase behavior of the low-excitation-potential absorption lines ($\chi \leq 1$ eV) with no CS component (see the section *Circumstellar Lines*) from that of the high-excitation-potential absorption lines ($\chi \geq 2.5$ eV; e.g., Figure 2-1, middle panel). The low-excitation lines (from the 4000 Å region) which are observed in infalling matter (an artificial effect as explained in the section *Source of the Visible Spectrum*) do not present a significant change in radial velocities with the light cycle, in any case not so striking that the changes shown by the high-excitation lines with their S-shaped discontinuous radial-velocity curve (consequence of the run of a shock wave). Noting that, in the cool star photosphere, the higher the excitation potential of a line, the deeper its layer of formation (see the section *Dependence of Absorption-Line Radial Velocities on the Excitation Potential*), there are the deep photospheric layers which are therefore the most disturbed by the radial pulsation of the star. We propose *to define the stellar "photosphere" as the part of the extended atmosphere in which the high-excitation absorption lines form (i.e., the fully pulsating part)*. The lines of weak or moderate potentials belong to layers just above the photosphere (i.e., layers not as much mechanically coupled with the deep pulsation), we call intermediate layers to chromospheric layers. By analogy with the Miras, let us adopt this picture for the supergiant, α Ori. In fact, IR atomic absorption lines of excitation potentials about 2 eV (Goldberg, 1979), reported from October 1975 to 1981 on Figure 5 in Goldberg (1984), clearly show a pulsational motion around the systemic velocity of 19.1 ± 1 km/s (also see Figure 12 in Goldberg, 1979); they define what we call the photosphere of α Ori. On the other hand, the absorption lines from the blue (Fe II and Ca II H and K) spectral region reported on the Figure from November 1970 to October 1975 (seen infalling over the observational period; see discussion in the sections *Violet Fe II Emission Lines* and *Ca II H and K Lines*) apparently designate the intermediate layers to the chromosphere.

Now, let us add that the fully pulsational atmospheric part may not be as easy to distinguish in the semiregulars for which the total pulsation amplitude is around 10 km/s, as noted in the section *Further Probe of the Pulsating Photosphere*—it is about 6 km/s in α Ori—as in the Miras for which the pulsation is about 20 to 30 km/s amplitude. Accurate Fourier transform spectroscopy measurements in IR are desirable, as is the case for the IR atomic lines quoted above for α Ori.

Rather suddenly, between October 1975 and September 1976, the α Ori chromosphere stopped its infall revealed by observations of Fe II and Ca II H and K emission lines since November 1970, and matter outfalls (from the observations by Van der Hucht et al. (1979) of the Fe II and Mg II h and k cores). This outfalling motion apparently lasts to at least March 25, 1978, when we note the absorption Hα core (Goldberg's (1979) observation), which is also a chromospheric indicator, blue-shifted with respect to the systemic velocity (see discussion in the section *Examples of Time Variation in Various CS Line Profiles*). Finally, on April 22, 1978, the Fe II emission cores are seen again infalling, as well as on August 16, 1978, when the Mg II h and k cores are also in infall (Carpenter's (1984) observations).

In consequence, it might be that an event has perturbed the chromosphere at the end of 1975 or in 1976. Specifically, the Fe II and Mg II h and k emission core-forming regions, as well as the Hα absorption core region, are changing their motion with respect to the center-of-mass velocity, while the "blue" absorption lines and the Hα wings remain infalling, suggesting that they are formed in lower chromospheric layers that are not affected by the event. On the other hand, the self-reversed Mg II h and k lines (Van der Hucht et al. (1979) and Carpenter's (1984) observations), together with the λλ 8542 and 8662 Ca II IR cores (Goldberg, 1979, and discussion again in the section *Examples of Time Variations in Various CS Line Profiles*), are always seen to be outfalling, suggesting that their formation in outer atmospheric layers is also undisturbed. Finally, the self-reversed Ca

II H and K lines (observed only from September 1974 to October 1975) distribute around the center-of-mass velocity, perhaps illustrating a quasi-stationary shell. (A complete diagram of the available observations extended to other periods is in preparation by Querci and Querci (1985b).)

What we have just described might be caused by the tidal effect of the close binary companion discovered by Karovska (1984), located specifically at 2.5 R_* (i.e., at 0.″05) from the α Ori center in Welter and Worden's reconstructed image observed in January 1976. (See the section *Geometrical Shell Expansion*.) In fact, recent characteristics of the companion orbit give $T = 1980.4 \pm 0.1$ and $P = 2.08 \pm 0.05$ years (see Figure 2-35); this means that the presence of the companion might be observed, in 1976, from January or from April or from June, considering the error bars in the T and P data. Once the companion has no more effect on the observed part of the chromosphere, the matter would stop and fall down toward the star as described above through the Fe II lines; it would recover a uniform motion as observed from the Fe II high layers and the "blue" absorption region, which share a common motion (Boesgaard and Magnan, 1975) in the 1970 to 1975 period. Also, at the time when the chromosphere might undergo the influence of the companion, no special effect is detected in the photospheric radial-velocity curve.

Finally, we discuss the C star, TW Hor, which might give a clue to the questions raised above. In this star, no hydrogen is detected either in emission or in absorption, nor Ca II H and K reemission in spectra with 12 Å/mm dispersion covering about 3 years (1979–1981; Bouchet et al., 1983). However, violet Fe II lines around 3200 Å are seen in emission at times by spectroscopic observations over this period and by the IUE satellite up to 1983, together with the Mg II h and k emission. (See Figure 2-5 and the section *UV Range* in *Emission Lines*.) Photospheric Mira-like shock waves (as defined in the *Summary* on *Photospheric Absorption Lines*) seem unlikely in such a star because the shock appears to have a velocity amplitude in the photosphere too low to ionize a significant fraction of hydrogen and to give Balmer emission. (Incidentally, hydrogen absorption lines might be not seen because the H^- continuum opacity is larger than the hydrogen line center opacity (Avrett and Johnson, 1984).) On the other hand, a "chromosphere" that excites the emission lines is more plausible. Such a chromosphere needs a heating mechanism that is inefficient in the Ca II and hydrogen line-forming regions; in other words, the temperature minimum would be so flat that the chromospheric flux would be too small for exciting an identifiable Ca II or H emission, but the heating must be sufficient in higher layers to excite the Mg II and Fe II lines. This could agree with the model chromosphere by Schmitz and Ulmschneider (1981) of low-gravity stars, linked to the short-period acoustic heating theory (see also Bohn, 1984). In short, acoustic waves are generated by turbulence at the top of the hydrogen convective zone, and they propagate outward into the photospheric layers of decreasing density, becoming shock waves around the temperature minimum where they dissipate their energy and heat the chromospheric layers. In some cooler stars, the radiative damping is so extensive that the position of the temperature minimum is shifted to a greater height compared to the shock formation; the models show a flat temperature minimum and a gradual chromospheric temperature rise. Querci and Querci (1985a) attempted to test such a heating theory for TW Hor in estimating the acoustic flux and the chromospheric radiative losses. The total integrated emission-line flux at the Earth from image LWR 7774 in Figure 2-5 (where emission lines Fe II, Mg II, C II, and V II are at their maximum intensity), normalized to the total radiative flux of the star measured at the Earth, is $f(\text{lines})/f(\text{bol}) = 48 \times 10^{-7}$. The main contributor lines to the radiative cooling are the Fe II V1 + V II V7 lines with a flux of 36×10^{-7}, while the Mg II flux is 45×10^{-8}. Table 2-2 gives Mg II emission-line fluxes in several N and M stars. However, from a single high-resolution long-wavelength IUE spectrum of

Table 2-2
Magnesium II Emission-Line Fluxes*

Star	Spectral Type	10^8 f(Mg)/ f(bol)
TW Hor†	N	45
TX Psc	N	10
T Ind	N	22
BL Ori	N	5
HD 37212	R8	<140
HD 52432	R5	<210
α Her	M5 II	130
72 Leo	M3 III	670
β Peg	M2 II–III	360
α Ori	M2 Iab	320

*From O'Brien and Johnson (1982), except TW Hor from Querci and Querci (1985a).
†From image LWR 7774 in Figure 2-5.

the N star, TX Psc, recently obtained (Eriksson et al., 1985), it appears that the Mg II are heavily absorbed by overlying matter and the low values of Table 2-2 may not give a true picture of the strength of the chromosphere in these objects. In spite of uncertainties in the radiative damping rate supported by the waves as they travel through the photospheric layers (up to 99 percent of energy lost by radiative damping (Leibacher and Stein, 1981)) and in the H^- radiative loss rate (no direct measure available), the heating acoustic waves, which are in fact shock waves dissipating their energy high in the outer atmosphere, may account for the emission lines in the cool low-gravity semiregular carbon star. In fact, equivalent acoustic slow magnetic waves should be better suited because they should account for the time variability in the lines in TW Hor, thanks to a variable magnetic field creating plages in the outer chromospheric layers, particularly influencing the Fe II lines. It remains to be verified whether such a mechanism is able to support the full chromosphere of supergiants that might be rather extended, as suspected from the observation of the λ10830 He line in absorption. As suggested by Hartmann and Avrett (1984), Alfven waves might be called for (see de la Reza, this volume).

Atmospheric Kinematics—Summary. What do we learn from the emission lines in addition to the absorption lines?

For the Miras, we were able to give further arguments in favor of a photospheric shock-wave model, previously revealed from the IR absorption lines. We fully discuss it by following the shock progression in the photosphere thanks to the appearence and disappearance of the various emission lines and their radial-velocity variations with phase. The single-shock interpretation (only one shock propagating in the photosphere at any time in the period) is strengthened.

Unlike SR or L giants and supergiants, we never mention the notion of chromosphere when discussing Miras. Naively, as the emission lines can be excited in shock fronts as well when the waves cross through the photosphere as when they reach higher atmospheric layers, the term "chromosphere" appears here questionable in its "solar" meaning. For theoretical grounds, we refer the reader to a recent paper by Willson and Bowen (1985) that explains why these authors entirely avoid using the term "chromosphere" and that defines the convenient zones to distinguish in pulsating stars such as the large amplitude Mira variables. These zones are determined primarily by the dynamics behavior of the star and its atmosphere; in fact, the extent of the atmosphere is linked to its dynamics, not to its temperature structure.

The fluorescent emission lines depict the presence of an outer layer in Miras, as already noted from a few absorption lines. Further data summarized in the next paragraph on circumstellar lines will help to clarify the shell structure finally discussed in the section *Summary: Structure of Expanding Gaseous Envelope.*

For the semiregular giants and supergiants, we attempt to draw general conclusions from the selected cases we have discussed. On one hand, the supergiant, α Ori, shows evidence of an extended chromosphere up to 1.8 R_* (i.e., up to 10^{14} cm, with R_* = 900 $R_\odot$ from Weymann, 1962) clearly depicted by the classical chromospheric indicators such as the Fe II, Ca II, Mg II, and C II emission lines. There,

the temperature is about 8300 K from the C II emission lines and even to 20000 K where the λ10830 He I absorption line is seen. The mean electron density is 3.2×10^7 cm^{-3}, as measured through the UV C II lines. The star is a very attractive object because it might allow us to observe the influence of a binary companion on its high chromospheric layers, mainly through the emission lines. Also, the few observational data we have in hand let us begin to guess how the structure of such an extended atmosphere (the photosphere as defined above, the intermediate layers, and the low and high chromosphere) might be, without speaking of the outer circumstellar shells.

The other supergiant, μ Cep, might be a more "classical" star (not a priori suspected to be a binary). From the behavior of the Balmer emission lines, it teaches us that shock fronts can indeed form in the stellar photosphere in the same manner as in the photospheres of Miras. Inversely, TW Hor might prove that shock waves are really able to dissipate their energy only at the chromospheric level. Depending on the physical parameters (mainly temperature and gravity) introduced in the modeling, a more or less flat temperature minimum followed by a more or less gradual temperature rise is obtained. Such shocks, issuing from short-period acoustic waves, are drastically damped in the photospheric layers. Note that the longer the wave period, the higher in the atmosphere the waves dissipate.

As a general synoptic conclusion, the observational results hint to us that a basic common heating mechanism might be at work in the atmosphere (at this step we do not look after the CS shells) of the various "red giants," Miras, or semiregular giants and supergiants. In fact, it appears that the efficiency in the line excitation is a question of the ability of the shock acoustic waves to heat the layers through which they propagate; high efficiency occurs at a different atmospheric level from one star to another and changes with time in a given star. In the Miras, the waves turn into shocks generally before emerging in the photosphere. However, it may happen, as in the Mira prototype, *o* Cet, that the wave crosses over the photosphere without dissipating energy. In the semiregulars, the waves may also turn into shocks in the photosphere as in the carbon stars, RR Her and V Hya, or in the M supergiant, μ Cep (from Hα emission-line behavior). However, there are several examples in which the waves dissipate high in the atmosphere of the semiregular giants or supergiants, creating a stellar chromosphere (e.g., μ Cep at times, β Peg where outfalling Fe II emission lines are observed, and TW Hor). We put the supergiant, α Ori, in this category. However, it is a case in which emission lines are seen not only in outfalling matter, but also in infalling matter. This star is not the prototype we took because it is a star with companions. It might be that, because of suffering the influence of a close companion, the matter is able to fall down with supersonic velocities.

Finally, we reemphasize the importance of *simultaneously monitoring temporal variations* in selected lines, such as Fe II and λ2335 C II violet lines, Mg II h and k, Balmer, Ca II H and K, λ10830 He lines, Ca II IR triplet lines, and molecular IR absorption lines, along the stellar period to progress in understanding the dynamical structure of a particular star and in atmospheric/chromospheric modeling. Until now, the interpretations are by far intuitive and qualitative.

Editorial Comment: In discussing the He I λ10830 line, as well as in the above summary on *Atmospheric Kinematics*, the author remarks that she does not use the term *chromosphere* in Miras, deferring to the suggestions by Willson and Bowen (1985) that, for pulsating stars, other atmospheric regions than those used for quasi-thermal stars are more appropriate. It is useful to abstract their suggestions, detailed in the cited references, here. The first reference discusses a number of regions; the second amalgamates them to four. The lower two focus on what replace photosphere and subphotosphere; the outer two, the exophotosphere. The lowest region, termed *undulosphere*, represents the locus of quasi-standing pulsation waves becoming progressive waves and steepening into

shocks. Its upper boundary is where the shock amplitude takes a value (assumed to be) fixed by the condition of periodicity. In the *agitosphere*, an (assumed) isothermal and radiative-equilibrium shock, with an amplitude limited and decreasing outward, still distends the atmosphere over any hydrostatic-equilibrium value. Emission coming from mechanical dissipation may vary, but its emission-measure $\ll$ volume of the region. Phenomena of a nonradiative energy dissipation significantly perturbing its thermal state lie in the *calorisphere*, which embraces the solar-type chromosphere-corona, they not being strictly applicable here. The densities are too low to permit rapid cooling. This region ends at the (conventional) *sonic* point. All the atmosphere above the thermal point is simply called *wind*. The authors emphasize that any given star may have all or only some of these regions, depending on the particular circumstances. The wind may be hot or cold. They suggest that, for rapidly rotating stars such as the Be, there may be a hot polar wind and a cool equatorial one. They stress the need for many more detailed observations to test their suggestions, which are based on their long-time efforts on numerical modeling. Certainly, these suggestions go beyond a preoccupation with solar-type, and even broader quasi-thermal, variable-mass-loss, stars. One continues to be impressed by the need for—or depressed by the lack of—far-ultraviolet data on the higher energy-shock phenomena and far-infrared and radio data on the coolest outer atmosphere. One also remains bemused by the search for hot polar and cold equatorial regions in rapidly rotating stars in the face of little evidence for their existence—which lack, of course, may again simply reflect insufficient observations.

CIRCUMSTELLAR LINES—PROPERTIES OF GASEOUS SHELLS

Appearance of Circumstellar Lines and Their Implication

The circumstellar (CS) absorption lines are characterized either by a P Cygni line profile defined as a line with a deep absorption core displaced toward the violet and bordered on its red wing by an emission component, or by a simple blue-shifted absorption line with one or more components. In the main, CS lines have excitation potentials less than 1 volt—often resonance lines—implying a shell excitation temperature of less than 1000 K (Goldberg, 1979). Known for some years in the blue spectral region, P Cygni lines have been detected in recent years in UV spectra through satellite observations (Van der Hucht et al., 1979) and in the infrared by Fourier transform spectroscopy at high resolution (Bernat et al., 1979; Bernat, 1981). Figure 2-13 gives examples of such line profiles.

Certain CS profiles, such as the CS H and K components of Ca II, can be seen in the spectra of all giants and supergiants later than M0 (Deutsch, 1960). Other lines, such as Na D, Sr II 4078, Ca I 4226, etc. appear in the M5 giants and are easily seen in all supergiants (Reimers, 1975). The best-studied star is the supergiant, α Ori, observed since about 1935 to the present with increasingly higher resolution; we will refer constantly to this star in the following paragraphs. For example, striking CS features, mainly in the blue range, are noted by Adams (1956) and Weymann (1962). Note that today, the interpretation of Adams' observations is in the recognition of P Cygni line profiles, whereas Adams himself mentioned line doubling, seeing violet and red-shifted absorption features. This comment pertains to all papers on CS lines before, say, 1960. Because dispersions of at least 10 A/mm are required to detect the CS components, prohibitively long exposures have been necessary for most red-giant stars. Only one C star, TX Psc, is reported to show such absorption cores in the blue atomic resonance lines (Deutsch, 1956). However, astronomical sites with good violet transparency and large telescopes raise hopes for obtaining sufficiently exposed spectra for these stars with reasonable exposures.

As early as 1935, Adams and McCormack (1935)—the first to discover absorption-line

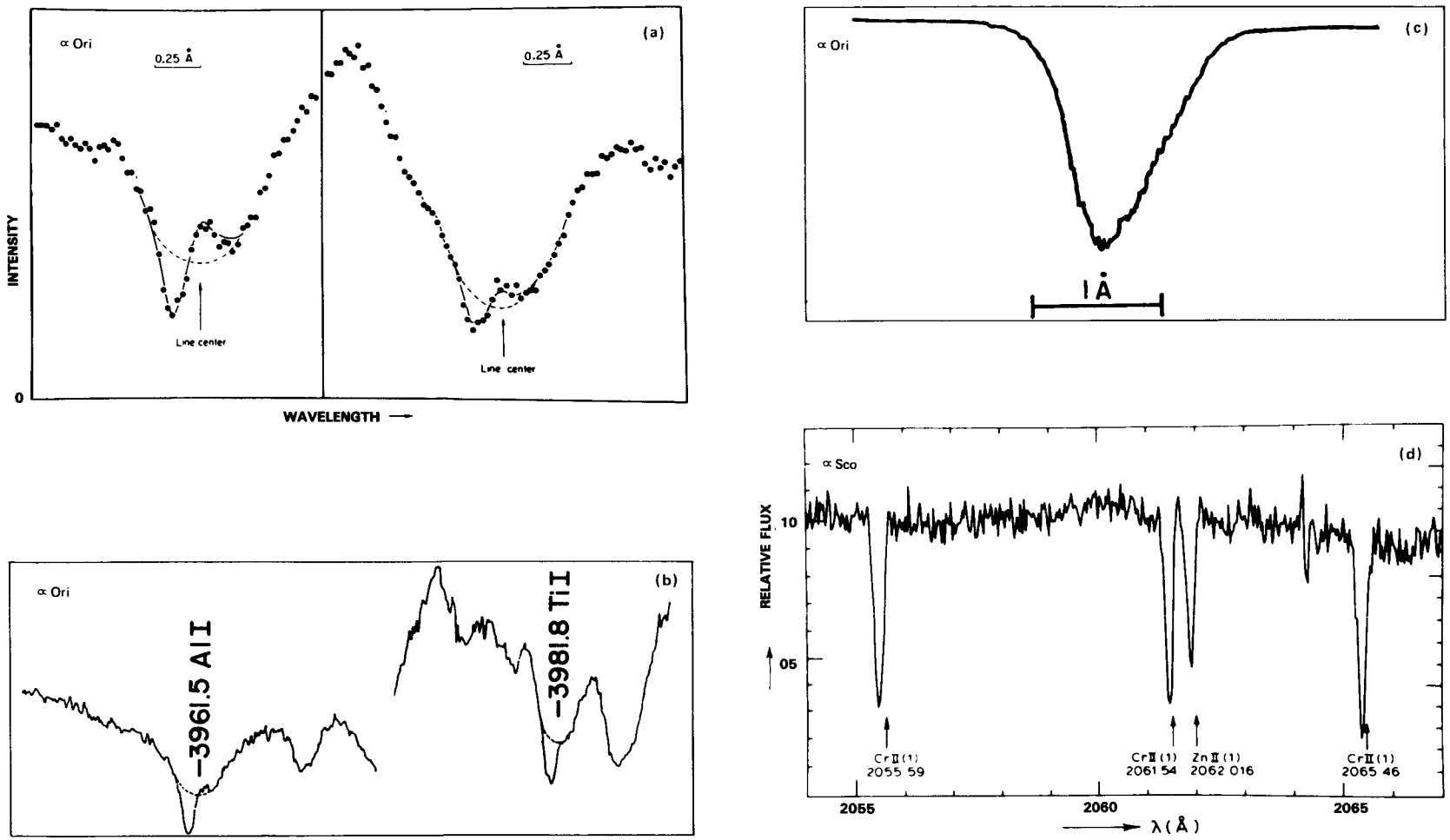


Figure 2-13. Selected circumstellar lines in the M supergiant, α Ori: (a) Mn I resonance lines at λ4030.8 (left) and λ4033.1 (right), showing a P Cygni type profile. The interpolated core of the photospheric line is shown by the dashed line, while the predicted shell absorption core with redward emission is shown by the solid line (from Bernat and Lambert, 1976a); (b) λ3961.5 Al I and λ3981.8 Ti I CS lines (from Weymann, 1962); (c) asymmetric core in Hα (from Weymann, 1962); (d) CS absorption lines of Cr II near λ2060 in the M supergiant, α Sco (from de Jager et al., 1979).

cores from atoms and ions in zero-volt levels invariably displaced blueward from the lines of the photosphere in the spectrum of M stars (α Ori, α Sco, α^1 Her, and o Cet)—attributed them to an extended expanding atmosphere. Today, it is well known (Rottenberg, 1952; Mihalas, 1978, p. 472) that a blue-shifted absorption line originating in an idealized spherical symmetric expanding envelope will be bordered on the red by an emission component, representing scattered radiation reemitted by the shell. In fact, as Reimers (1978) remarks: (a) owing to a sufficiently low density in the envelope, line scattering dominates over true absorption, and (b) because the scattering shells are dimensionally large in relation to the star, the P Cygni profiles end up being superimposed on the photospheric absorption lines.

Figure 2-13a shows clearly that the emission component is a blend of shell emission and the broad underlying photospheric absorption line (Bernat and Lambert, 1976a). Moreover, Sanner (1977) found that the circumstellar emission component in the Miras, χ Cyg and R Leo, is shifted longward of the "stellar" emission lines, thereby denying any common origin with these lines. The strongest CS features take the form of a "pure" P Cygni profile, especially when they lie in the cores of relatively narrow photospheric lines (Sanner, 1976).

The envelopes extend several stellar radii above the region in which the local continuum (and usually the photospheric absorption lines as well) is formed. We shall return to this topic later. Here, we simply note that the extent of the circumstellar shells was first suspected around 1956. Deutsch (1956, 1960) reported on the α Herculis system, a visual binary composed of an M supergiant star and of a giant G star which is a spectroscopic binary. He found that the strongest of the shifted absorption CS lines in α^1 Her were also present in the spectrum of its companion, α^2 Her. Because a G-type star never shows such zero-volt lines, he concluded that the extended envelope of the M star incorporates the G star. Furthermore, the deep absorption CS component Ca II K_4 visible in the spectrum of the companion is the only motionless feature, while all other components of the Ca II K line display normal orbital Doppler shifts. The Ca II K_4 line does not share the orbital motion and therefore obviously originates in the CS gas that extends outside the orbit of the G star. The angular separation of the visual pair is 4".7, about 360 times the radius of the M star (Reimers, 1975). Similar observations of CS absorption lines in the spectra of other visual near companions and stationary CS lines in spectroscopic binaries among red giants, implying that the shell is decoupled from the photosphere, prove that the CS gas is in fact lost to the interstellar medium. The CS lines are the spectroscopic signature of mass loss. The mass loss itself—its rate and its mechanisms—is reviewed by Goldberg (this volume).

Temporal Changes in CS Line Profiles

General Behavior. Generally speaking, these variations must be discussed in relation to the photospheric radial velocity. As an example, the general behavior of CS features in optical spectra of α Ori shows (Adams, 1956) that: (1) numerous lines have a variable violet asymmetry, (2) well-marked emission in the P Cygni profiles becomes ill-defined with time, and (3) a wing may emerge on the violet edge of the blue-shifted strong absorption lines and disappear in about 2 years. Its appearance and its behavior are associated with that of the red-emission peaks; when the latter is faintest, it is strongest and widest. Clearly, it appears that the intensity of the emission component is correlated to the photospheric velocity (Bernat and Lambert, 1976a). When the photosphere-envelope velocity difference is at its greatest, the emission component is at its strongest.

Sanner (1976) indicates from a sample of 11 M late giants and supergiants that several P Cygni profiles vary on a time scale of a few months or less. In Mira stars, P Cygni profiles are pointed out in the K I and Na D resonance lines at maximum and postmaximum phases (χ Cygni: Bretz, 1966; Sanner, 1977—R Leo: Lambert and Vanden Bout, 1978). Nevertheless, the strong variations in radial velocity with

phase for the circumstellar optical lines as shown for o Ceti in Figure 5 of Joy (1954), which are normally expected to be found at a constant velocity (see the section *Physical Conditions in Gaseous Shells*), are caused by the relatively strong variations in radial velocities of the photospheric spectrum during a cycle.

Circumstellar line-strength variations may have causes other than the photospheric variations—perhaps a time-dependent ionizing UV radiation field, which, one suspects, could explain the variations of the Ca II H and K lines in early M giants (Figure 2-14) or discrete shell ejections, giving rise to multiple shell components.

Examples of Temporal Variations in Various CS Line Profiles. Goldberg et al. (1975) and Goldberg (1976, 1979) observed the *K I resonance line at 7699 Å* in α Ori at high resolution, as shown in Figure 2-15. The component labeled "λ_{ph}" that denotes the position of the photospheric line center is determined relative to the position of photospheric lines with excitation potential ≥ 2 eV. It is clear that the smaller the radial velocity of the photosphere (V), the deeper the absorption profile and the fainter the red emission. These effects are correlated to the photospheric line, which is strongly displaced to the violet at low radial velocity. Sanner (1977) notes also that the emission component was absent on April 9, 1976, corresponding to a low value of V. Besides α Ori, the emission component in the CS K I line is also variable in the supergiants 119 Tau and α^1 Her (Sanner, 1976). Figure 2-15 also shows that two absorption components are present in the K I profile. We shall report on such line-profile features in the section *Evidence of Multiple Absorption Components in CS Lines.*

Sanner (1976) emphasizes the variability of the *Ca II infrared line profile at 8542 Å* in spectra observed with a resolution of 4 km/s. In α Ori, the line profile over 3 years shows net blueward absorption of up to 70 mÅ and, for several scans, a net redward absorption. Once again, these variations, occurring over a time scale of several months or less, might be caused by variations in the radial velocity of the underlying photospheric line. Sanner notes

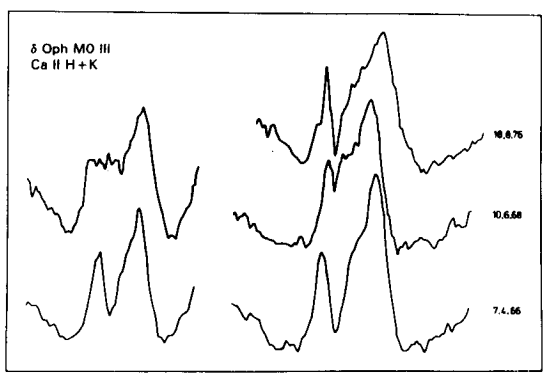


Figure 2-14. Variable circumstellar Ca II H and K lines in the early M giant, δ Oph (from Reimers, 1981).

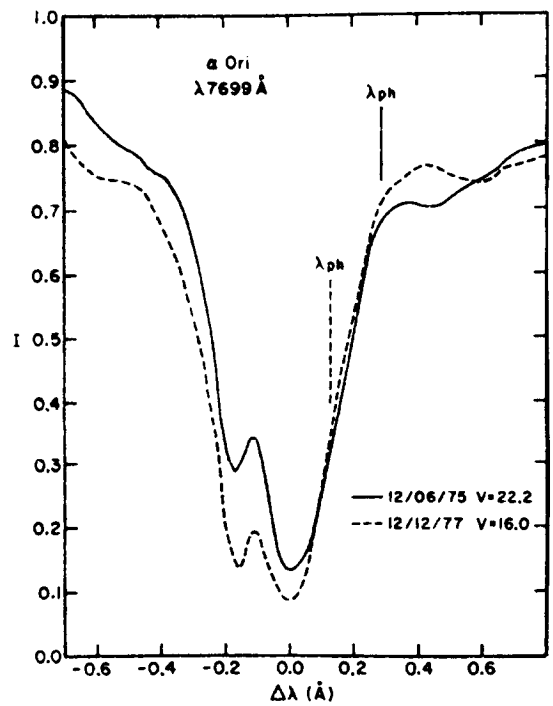


Figure 2-15. K I line profiles in the M supergiant, α Ori, on two different dates when the photospheric radial velocity was V = 16.0 and 22.2 km/s, respectively. λ_{ph} denotes the position of the photospheric line center (from Goldberg, 1979).

similar variations for the semiregular giant stars, R Lyr and β Peg. The Ca II line profile is also given for a few supergiants by Bernat (1977): the line appears to be definitely asymmetric in α Sco at 0.12 Å resolution (Figure 2-16).

In α Ori, Goldberg (1979) recorded the three IR triplet lines simultaneously (for example, Figure 2-17) from October 1975 to February 1979. The radial velocities averaged for the 8542 and 8662 Å cores are outfalling relative to the α Ori systemic velocity of 19.1 $\pm$ 1 km/s (Huggins, 1984). As for the line wings, the bulk of the data suggests that they belong to infalling matter because their radial velocity remains above 19.1 km/s. However, the red shifts are scattered from 0 ($\sim$5 values over 20) to +3 km/s. Is the infall artificial, due to difficulties in the measurements (though the observations are accurate Fourier transform spectrometer ones)? Is the forming layer to be considered rather stationary at the center-of-mass velocity, as claimed by Goldberg (1979)? (In fact, this author presumes the systemic velocity to be at 21 to 22 km/s.) More data are necessary to judge.

Goldberg (1976, 1979) reports observations of the *Na D lines* in α Ori, using the same techniques as for the K I line at 7699 Å. These lines are heavily saturated. In Figure 2-18, showing the Na D profiles on different dates, it appears that about the top third of each profile follows the motion of the photosphere, whereas the lower portion is static. From observations of the Mira, χ Cygni, on July 10, 1976, Sanner (1977) remarks that the emission feature is more pronounced in the D_1 line at 5896 Å than in the D_2 line at 5890 Å, while the photospheric absorption D_2 line is known to be deeper than the D_1 line; he explains this inversion in line strength by the fact that the amount of radiation scattered by the envelope depends partly on the intensity of the underlying photospheric line.

Finally, concerning the *Balmer lines*, we hesitated to range them in a section dealing with

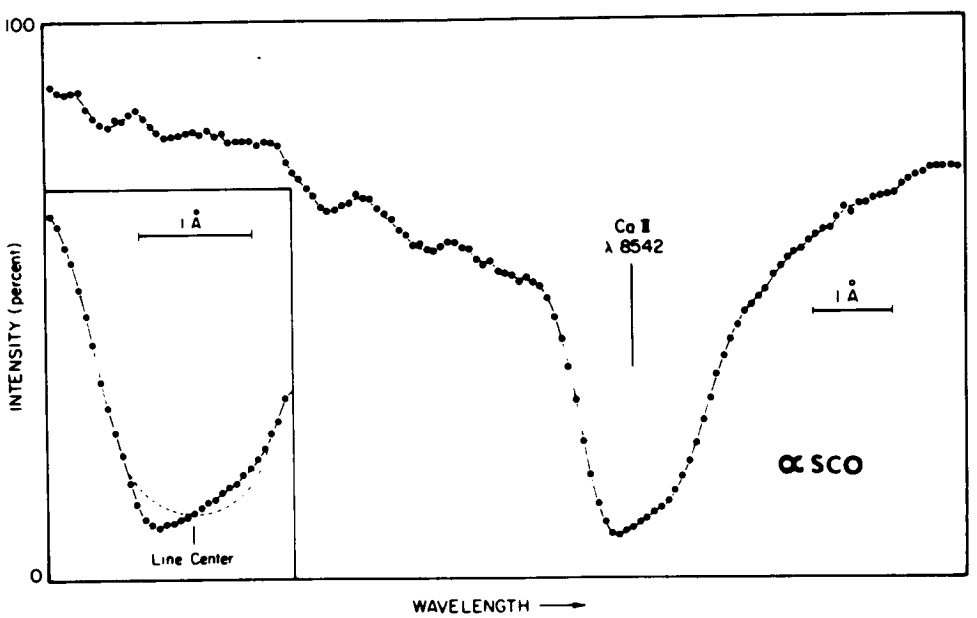


Figure 2-16. Ca II λ8542 line profile in the M supergiant, α Sco, illustrating the asymmetry of the core (better displayed in the inset). Broken line shows estimated photospheric line profile by a reflection about the line center (from Bernat, 1977).

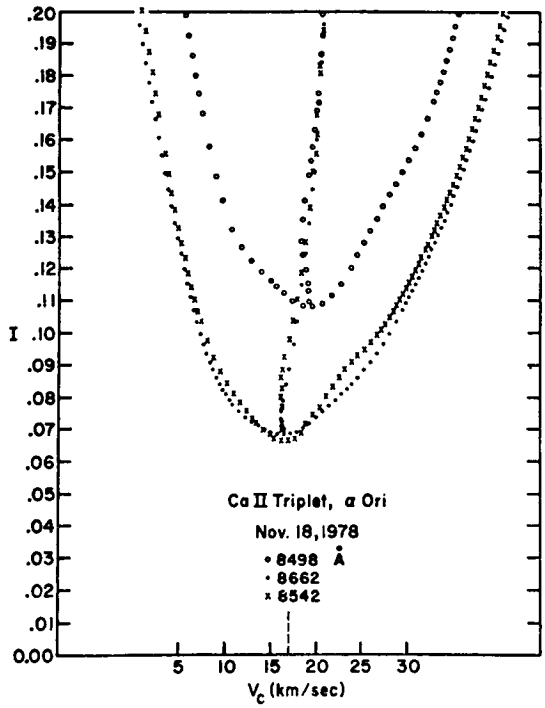


Figure 2-17. Ca II triplet line profiles in the M supergiant, α Ori. The loci of the bisectors are plotted. The vertical dashed line marks the phototospheric radial velocity (from Goldberg, 1979).

CS lines. In fact, because of the excitation conditions they need, these lines are rather chromospheric indicators. However, because they are asymmetric absorption lines in numerous giants and supergiants, we present them in this section. In α Ori, the core in the Balmer line Hα and/or Hβ (e.g., Figure 2-13c) appears to be asymmetric (Weymann, 1962; Goldberg, 1979, 1981; Dupree et al., 1984). We note that they may be either blue- or red-shifted relative to the systemic velocity. For example, Goldberg's Hα core velocities recorded on March 25, October 23, and December 15, 1978, give a blue shift of -3.7 ± 1.1 km/s and then no shift at all, respectively. On the other hand, we find the following red shifts: +1.5, +8.9, and +10.2 km/s from the three measurements of Dupree et al. on August 26, 1983, and January 23 and February 26, 1984, respectively. It is obvious that the Hα core region changed velocity relative to the center-of-mass velocity between 1978 and 1984. The same sources of data provide evidence of an infalling forming region from the Hα wings.

Asymmetric Hα lines and violet-displaced or, in some cases, red-displaced emission components have been observed in 16 red supergiants of the I Per association, some of which show time variations in the Hα line (Gahm and Hultquist, 1971). For example, on August 19, 1969, the Hα line in the supergiant, BD + 56°595, is broad with a central reversal (Figure 2-19), and the violet absorption component is displaced by about 20 km/s. On September 24, 1969, the Hα line is narrower; a reverse P Cygni profile with a strong violet-shifted emission is observed, but no obvious change is seen on the red side of the absorption line. The authors note that the mean radial velocity of the photospheric lines is similar during both observations. The light curve of the star for the period of observation is not known.

Variation of CS Lines with Spectral Types and Luminosity Classes

Particularly well studied in M stars are the CS components of the *Ca II* resonance lines at 3934 and 3968 Å—henceforth called K_4 and H_4 (Boesgaard and Hagen, 1979). The appellation H_3 and K_3 is reserved for the chromospheric absorption, particularly important in the G and K giants. (See the section *Selected Emisson-Line Profiles*.) In the M giant stars, the K_4 component superimposed on the chromospheric K_2 emission dominates K_3 completely. In early M giants, it is narrow and deep with very steep sides, reaching zero at the blue-shifted central intensity (see Figure 1 in Vaughan and Skumanich, 1970). In fact, the contribution of the H_3-K_3 components might not be significant because it appears to be very weak in those M0 giants in which no CS component is to be seen. (Note that only certain M0 III stars, such as β And, show a CS component.) In the coolest giants and most of the supergiants, the K_4 absorption is much broader (see Figure 2-8). The H and K lines are the most

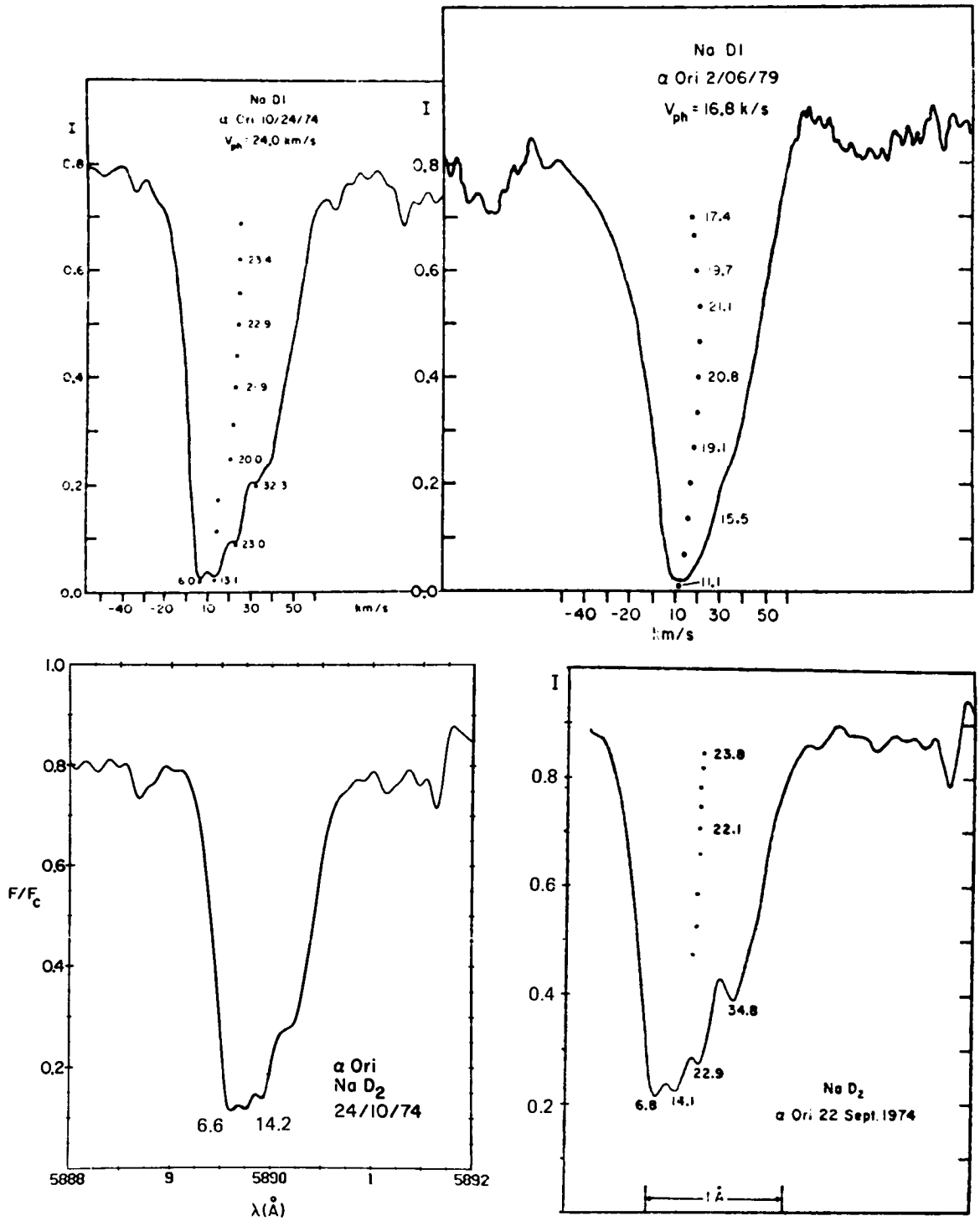


Figure 2-18. Na D line profiles in the M supergiant, α Ori, on different dates: Top: Na D_1 profile when the photospheric radial velocity was 16.8 and 24.0 km/s, respectively (from Goldberg, 1979). Bottom: Na D_2 profile when the photospheric radial velocity was 24 km/s (right, from Goldberg, 1979; left, from Goldberg, 1976, and private communication, 1980, for the noted values of velocities).

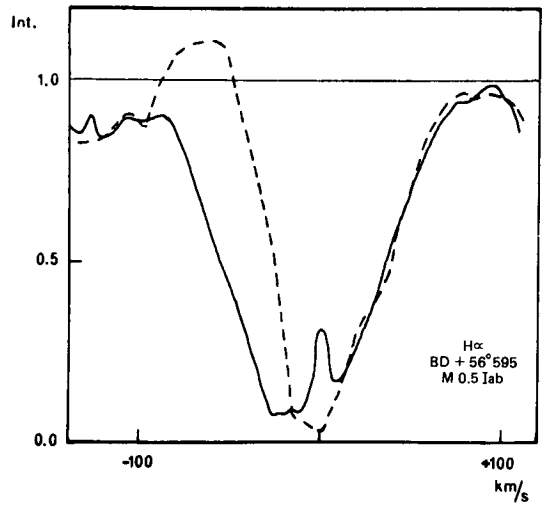


Figure 2-19. Hα *profile in the M supergiant, BD + 56°595 (M0.5 Iab) on August 19 (solid line) and September 24 (dashed line), 1969. The radial velocity in abscissa is given with respect to the mean velocity of the photospheric lines (from Gahm and Hulquist, 1971).*

obvious CS feature in giants and supergiants (Deutsch, 1960; Reimers, 1975; Boesgaard and Hagen, 1979; Hagen et al., 1983). At dispersion of 4.5 Å/mm, the CS H and K lines can be seen in the spectra of all giants of types later than M0.

In spite of their diversity, the CS H and K line profiles correlate with spectral type. The following correlations have been established in the M giants by Boesgaard and Hagen (1979) through about 60 spectrograms intentionally heavily exposed to reveal the deep CS cores:

1. A correlation exists between the spectral type and line strength. The Ca II K_4 feature shows a marked regular increase in strength toward late spectral type due to a widening of the feature. (The violet edge of the profiles remains fairly stationary, while the red edge moves redward toward later spectral types.) The average line width of the K_4 line (a good indicator of the line strength) varies from about 120 ± 70 mÅ at M1 to 600 mÅ at M7. Modeled K_4 line profiles in M giants reveal that the changes in width of the profiles are produced by an increase in the turbulence velocity and/or line formation over a velocity gradient (Boesgaard and Hagen, 1979; see also the section *Physical Conditions in Gaseous Shells*). In the supergiants, the strength of the CS H and K lines also increases with advancing spectral type and augments rapidly with greater luminosity (Reimers, 1975). The width of the absorption H and K cores in later giants and in supergiants might be caused by large velocity gradients combined with a double ionization of Ca in the inner parts of the shell.

2. A correlation exists between the expansion velocity (given by the displacement from line center in km/s) and the spectral type (or line strength). The later the spectral class, the lower the velocity. The average K_4 line displacement varies from about -20 km/s at early M to about -10 km/s by M6. Moreover, there is considerable scatter in the velocities for a given spectral type, perhaps revealing intrinsic variations in the CS shells from star to star (Boesgaard and Hagen, 1979).

The correlation between the spectral type and the expansion velocity shows much more scatter for the supergiants than for the giants (Reimers, 1975). The CS Ca II H and K cores, strong in supergiants and late M giants, do not show reemission (Reimers, 1978). The scattered photons are captured by CS dust at these short wavelengths and at these great line optical depths.

Sanner (1976) shows the behavior of the strong resonance lines of *Na I* at 5890 and 5896 Å for four early M giants and five supergiants (M2–M5) at resolutions of 2 and 4 km/s. From this sample, he notes the strengthening of the CS asymmetry with later spectral type and increasing luminosity, and the marked breadth of the lines in the supergiants. Boesgaard and

Hagen (1979) study a sample of 61 M giant stars (M0–M7) with a dispersion of 8 or 6.7 Å/mm. They confirm that the asymmetry becomes more apparent toward later types (Figure 2-20, left). None of their M0–M1 giants shows CS cores, but the M0-type supergiant, σ CMa, does (complementing the sample of Sanner for supergiants of early types). The increase in strength and velocity is minimal toward cooler M giant stars (i.e., the core displacement from the photospheric line center varies around –7 km/s at M2 to –11 km/s at M6). Boesgaard and Hagen (1979) also indicate an average equivalent width of 230 ± 75 mÅ for the CS Na I components. They propose that the low velocities could result from the formation of these lines of moderate optical depth in an envelope involving a gradient velocity.

The *Hα* line appears to be asymmetric in about one-half the stars of the sample of Boesgaard and Hagen (1979; Figure 2-20, right), including stars of all M subtypes. Their cores are blue-shifted with respect to the photospheric velocity determined from a sample of photospheric lines. In no way does this allow one to speak of a shell expansion beginning within the chromosphere of these stars because the radial velocities are not related to the systemic velocity. The equivalent width of the Hα core and its displacement from line center does not vary much with spectral type. The authors note an average equivalent width of the CS component of 27 ± 10 mÅ and an average displacement of –3.8 ± 1.6 km/s. The average concerns the stars of the same spectral type. From a larger sample of M0–M4 stars, including some supergiants listed by Merchant (1967), Boesgaard and Hagen (1979) point out that Hα is asymmetric whenever CS cores are visible in the Na D line. On the spectrum of α Ori, Weymann (1962) notes that the hydrogen lines are abnormally strong with equivalent widths of about 1 Å for Hα and Hβ. Hα shows a marked asymmetry (Figure 2-13c).

Besides the Na I D lines already mentioned, Sanner (1976) studies several atomic lines (i.e., Sr II λλ 4078 and 4216, Ba II λλ 4554 and 4934, K I λ7699, and the lines of the Ca II infrared

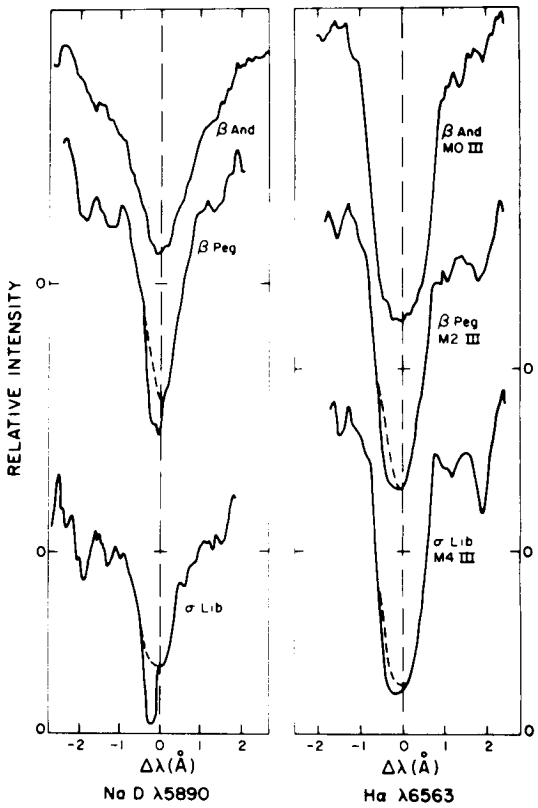


Figure 2-20. Line profile variations in representative M giants, Na I λ5890 line (left), Hα line (right). The dotted lines outline the "effective continuum" (from Boesgaard and Hagen, 1979).

triplet (λλ 8498, 8542, and 8662) in about 10 giant and supergiant stars. The line K I λ7665 was observed exclusively in the supergiant, μ Cep, because of severe O_2 telluric interference there. We quote Sanner:

- *Sr II lines*: "The strengthening of the CS asymmetry with later spectral type and increasing luminosity can be seen in both lines, in spite of severe blending in λ4078." (See Figure 1 in Sanner, 1976.)

- *Ba II, K I lines*: "The lines of both Ba II and K I are symmetric in the giants, CS components not appearing in stars with M_v fainter than about –2."

- *Ca II lines*: "The CS Ca II triplet features are generally comparable in strength to those in the Ba II line. In the giants, the asymmetries in these lines weaken progressively along the sequence λλ 8542, 8662, 8498; λ8498 is generally symmetric. In the supergiants, the asymmetries in λ8542 and 8662 are comparable, while that in λ8498 is weaker.... The triplet lines do not show marked CS emission, in contrast to the profiles of the metal [Sr II and Ba II] and trace [Na I D and K I] lines."

Evidence of Multiple Absorption Components in CS Lines

At high resolution (≥2 km/s), the CS cores of some lines are resolved into multiple components. As noted by Sanner (1976), in the Na and K lines, these components appear either as fine structure in the absorption lobe of the P Cygni profile or as sharp isolated lines blueward of it. The optical components are named by velocities obtained by simple measurements of the absorption minima with respect to the photospheric velocity generally known from lines with no shell contribution (e.g., from lines with excitation potentials of 2 eV or more (Goldberg, 1976)). For the lines of the fundamental (1–0) vibration/rotation band of CO around 4.6 μm, note that Bernat (1981) gives minima relative to the center-of-mass velocity, which he assumes to be equal to the time average of the photospheric radial velocities as taken from Abt and Biggs (1972). The determination of the expansion velocities of the shells will be discussed in the following paragraph. Temperatures are sometimes assigned to the components; these will be explained in more detail below.

Figure 2-15 shows the presence of two absorption components in the K I λ7699 line profile of α Ori. Goldberg (1979) plots the heliocentric velocities of the deeper component recorded from about 1974 to 1979, which are remarkably constant around a mean value of 10.9 ± 0.3 km/s. The blue component of the K I line, likewise plotted on Figure 2-15, shows an apparent increase from 4.2 ± 0.2 to 5.0 ± 0.2 km/s, beginning in March 1977. The author wonders if this increase is real or not. The K I line observations of Sanner (1976) emphasize the importance of a sufficiently high resolution for the detection of the components; the blue component is not seen at low resolution (4 km/s) in Sanner's Figure 11i, while a strong and wide component, together with a weak and narrow one, is clearly identified at 2 km/s resolution (cf. same figure).

Another example of double components is given by the Na D lines at λ5890 and λ5896 in α Sco, where they are at the same heliocentric velocities (Table 3 in Sanner, 1976).

The fine structure of the Na D lines in α Ori observed by Goldberg (1976, 1979) shows four absorption features (Figure 2-18). Multiple components are striking in the λ7699 K I line in α Sco (Figure 2-21) and also in μ Cep, an extreme case in which up to six components are detected (Sanner, 1976; see also Figure 1 in Bernat, 1981).

High-resolution spectra in the infrared also show multiple components in the low-excitation lines of the fundamental CO band near 4.6 μm. For example, line profiles in *o* Cet (Hall, 1980) display a complex structure (Figure 2-22) with three clearly resolved circumstellar components: one, the reddest, at a heliocentric velocity of 62.7 km/s, possibly similar to the center-of-mass velocity, and two others expanding at 7.5 km/s, corresponding to the velocities of the OH, H_2O, and SiO masers. The rotational temperatures are 200 and 70 K, respectively. The number of components in a CO line of the fundamental band depends on the luminosity; the most luminous star (μ Cep) has five components, intermediate stars such as α Ori or α Her show two, and class III stars show only one (Bernat, 1981). Note that objects such as IRC + 10216 show two components in the CO fundamental lines (Ridgway and Hall, 1980; Keady et al., 1984), components which are also recognized in the CO first overtone (2.3 μm), along with a further component at 2.5 km/s. In α Ori (Bernat et al., 1979), the two components are

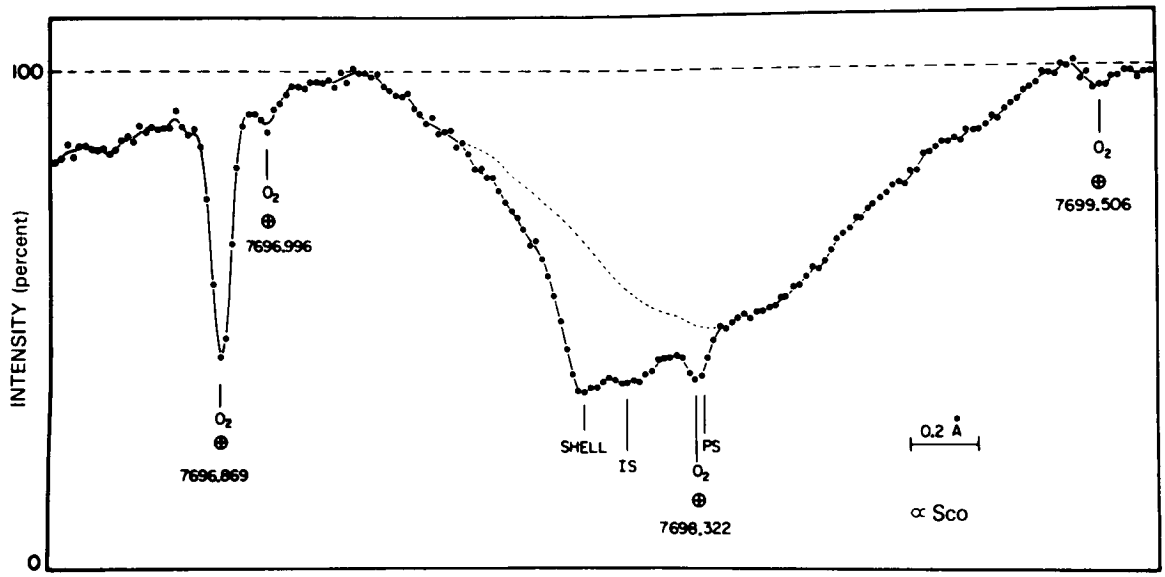


Figure 2-21. K I λ7699 profile in the M supergiant, α Sco (resolution 0.05 Å). Telluric O_2 lines, a possible interstellar component (IS) and the center of the photospheric line (PS) are shown. The broken line is a reflection of the observed line about the photospheric line center (from Bernat and Lambert, 1975).

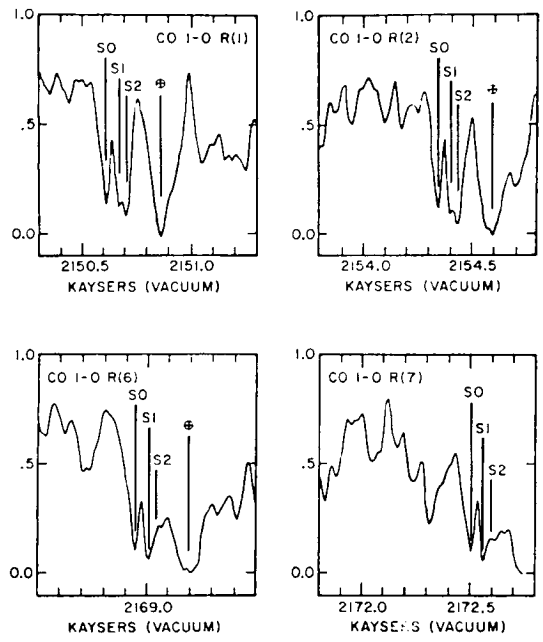


Figure 2-22. Selected CO (1–0) vibration/rotation lines from a 0.6-km/s resolution spectrum of the M Mira star, o Ceti. Components (S0, S1, S2) due to three CS shells and telluric absorption are noted (from Hall, 1980).

S_1 at ~11 km/s (T ~ 200 K +50, -10) and S_2 at ~4.8 km/s (T ~ 70 ± 10 K) relative to the center-of-mass velocity, assumed equal to a mean photospheric radial velocity from Abt and Biggs (1972). S_2 corresponds to the velocity of the blue component distinguished in the K I line (5.0 km/s; Goldberg, 1979) and also in the CO (2–1) radio emission line (Huggins, 1984).

Table 2-3 summarizes such multiple velocity structure from infrared CO lines in some typical stars. Goldberg (1976) and Hagen et al. (1983) note that, besides the K I line, doubling of the CS absorption features has been observed only in Na D, Ca II, and CO lines.

Concerning the origin of the components, the weak blue component in the K I λ7699 line in α Ori is unambiguously circumstellar since it is associated with the radio CO emission line. As for the Na D lines in the same star (Figure 2-18), the minima at 6 or 7 and 13 or 14 km/s might correspond to the two different shells expected for the K I line; they have higher values than the K I line because they are not as much affected by the redward emission. The origin

Table 2-3
Multiple Shell Components from Infrared Vibration/Rotation CO Observations in Selected Stars*

α Ori[a]			o Cet[b]		χ Cyg[c]			IRC + 10216[d]		
T (K)	v km/s	D R_*	T (K)	v km/s	T (K)	v km/s	D R_*	T (K)	v km/s	D R_*
70	4.8[e]	2000 (~55″)	70	12.2	60±20	10		450–200	14	15–30[f] (0″35–0″7)
200	11	150 (~4″)	200	7.5	300±200	7.8	100	1000–500	11	4–11 (0″09–0″3)
			(800)	0	800	0	10	1800–1200	2.5	1–3 (0″02–0″07)
					1500	Infall				

*All the velocities refer to outfalling matter, otherwise noted.

Notes:
[a]From Bernat et al (1979).
[b]From Hall (1980); components also detected in mm-wave CO spectra (Knapp et al., 1982).
[c]From Hinkle et al. (1982).
[d]From Keady et al. (1984).
[e]Also detected in K I λ7699 line and in mm-wave CO spectra (Knapp et al., 1980; Huggins, 1984).
[f]Also measured by Dyck et al. (1983); see Table 2-5.

of the apparent components at about 23 and 32 or 35 km/s is not fully understood. Goldberg (1979) suggests that they must be the emission counterpart of P Cygni profiles, having their absorption part at 6 or 7 and 13 or 14 km/s, respectively. On the other hand, Goldberg (1976) points out that "the structure could be accounted for if there were a single-peaked emission combined with interstellar absorption near the center of the photospheric component." Bernat and Lambert (1975) account for one of the multiple components in the scan of the K I line in α Sco (Figure 2-21) as having a possible interstellar origin. An irrefutable example of interstellar origin is given by one of the double components in the Na D lines in the carbon star, T Lyr (Utsumi, 1971).

As for the fundamental lines of CO in α Ori, Bernat et al. (1979) were able to detect lines arising from transitions of ^{13}CO. The $^{12}C/^{13}C$ ratios they derive prove that the two components observed in the CO lines arise in matter ejected from the photosphere and confirm their circumstellar origin, particularly for the cooler component (~70 K) that could be suspected to be interstellar. Bernat (1981) assumes that all absorption features seen in the fundamental CO lines in his sample of nine M giants and supergiants are CS, although ^{13}C lines are not technically observable. However, arguments described by Bernat (1981), such as the nondetection of 4.6-μm CO lines in the interstellar medium, the inconsistency of the CO velocities with velocities derived for nearby stars from optical lines, and the temperatures of some components which are too excessive to be alloted an interstellar origin, render the assumption justifiable.

Double absorption components are not seen exclusively in late giants and supergiants. In some early M giants, such as β And, the Ca II H and K lines show two distinct components. In other early giants such as α Vul and α Lyn, Reimers (1978) notes that the CS Ca II H and

K lines may consist of weak multiple velocity components.

Quantitative Analysis of CS Lines: Shell Characteristics

Methods. As Bernat (1977) successfully shows, difficulties for an accurate interpretation of the CS features come from unknown quantities, particularly the shell geometry and the velocity field. Some evidence that the flows in α Ori are not spherically symmetric is presented, and multiple absorption features in the line could be caused by episodic ejections that negate the steadiness of the flows. However, to make the transfer of radiation tractable, constant expansion velocity and spherical symmetry are assumed. A notable advance in the interpretation of CS line profiles for these highly idealized spherical atmospheres came with the application of the observer's frame method of Kunasz and Hummer (1974); that is, the formal solution of the transfer equation in an expanding extended spherical atmosphere in the low-velocity regime (comprehensively explained by Kunasz (1974) and Mihalas (1978, p. 459) as well). It was first adopted by Bernat (1977) and Hagen (1978) for the fitting of the theoretical line profiles to high-resolution data in M stars. Later, the method was often used in the various studies on the circumstellar envelopes (e.g., Boesgaard and Hagen, 1979; Boesgaard, 1979, 1981; Bernat, 1981). However, Keady et al. (1984) favor the comoving frame formalism of Mihalas et al. (1975; see also Mihalas, 1978, p. 503) to calculate the line radiative transfer in the flow, whereas Sahai and Wannier (1985) use the Sobolev escape probability method.

To determine the effect of shell parameters on the line profiles, Hagen (1978) calculated a series of line profiles, varying the optical depth (around unity), the expansion velocity (around 10 km/s), and the turbulent velocity (from 3 to 10 km/s; cf. her Figure 3), which are the only variables that significantly affect the resultant line profile. For this theoretical test, the author determines the underlying photospheric line by a gaussian fit to the Al I λ3944 line of μ Cep. As the optical depth increases, the P Cygni profile becomes progressively clearer: the absorption core becomes sharper and the red emission comes more into focus. The greater the value of the expansion velocity, the greater the violet shift of the CS absorption core. As the turbulent velocity mounts, the P Cygni profile disappears to give an asymmetric profile with a broader, shallower, and less blue-shifted absorption core. However, the turbulence has a negligible effect on the equivalent width of the absorption core and hence on the column densities. Hagen (1978) emphasizes that:

1. The profile is sensitive to the amount of matter in the shell rather than to its distribution within the shell.

2. The outer shell radius has no more influence on the emergent profiles than the inner radius, as long as both are significantly larger than the stellar radius.

3. The change of the power in the power-law density distribution has only a small effect on the emergent line profile.

Another difficulty in the analysis of line profiles comes from a lack of knowledge about the profile of the underlying photospheric line. A common method for inferring this profile (Weymann, 1962; Hagen, 1978; Bernat, 1977; Figure 2-23) assumes equal emission and absorption, so that a symmetric underlying profile can be hand-drawn. Bernat notes the uniqueness of this profile. Generally, the position of the line center of the photospheric component is inferred from nearby photospheric lines with high excitation potential. This empirical method gives the basic quantities for the absorption component of the CS line, displayed in the resultant shell line profile of Figure 2-23: the expansion velocity, v_e, the line center depth, and the width at half-maximium (WHM). The method is excellent for the strong lines. For the lines with a sharp CS core (i.e., lines with sufficient optical depths as shown by

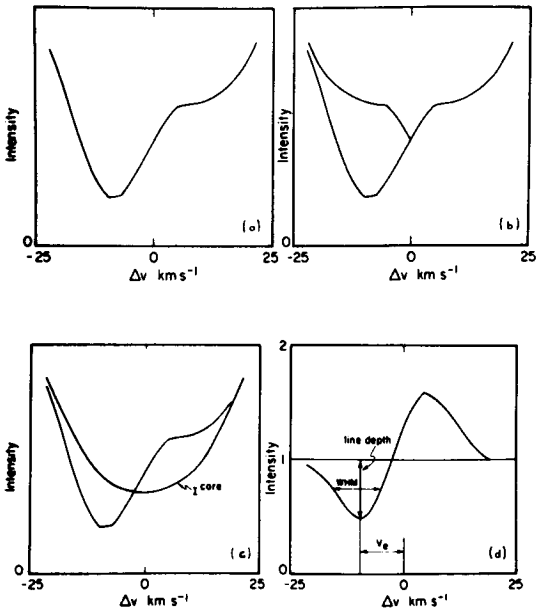


Figure 2-23. The determination of the shell line profile: (a) the original profile; (b) the flip assuming that both line wings are purely photospheric; (c) the drawn-in smooth photospheric profile; (d) the resultant shell line profile (from Bernat, 1977).

the theoretical line modeling), the radiative-transfer calculations show that the position of line minimum is determined by the expansion velocity, and vice versa. Note the remark made by Hagen (1978) and Bernat (1977) that the shell optical depths or the derived column densities are not very sensitive to the photospheric line profile. However insufficient knowledge of the photospheric radiation field lamentably prevents the modeling of the shell line profile (Bernat, 1981).

Another important quantity, in addition to the expansion velocities, is the gas-column density, which is related to the optical depth (Sanner, 1976; Hagen, 1978) and which influences the mass-loss rate (Goldberg, this volume). The method for obtaining them is clearly described by Hagen (1978). Briefly, the equivalent width of the absorption core in the resultant line profile of Figure 2-23 is measured. Then, given the expansion velocity (as easily determined from sharp CS cores), a series of theoretical line profiles are calculated with different shell optical depths. Theoretical equivalent widths are plotted against corresponding optical depths, and observed equivalent widths are converted to line-center optical depths. Finally, column densities along the line of sight are calculated. In order to relate them to the total abundances, the relative abundances in the different ionization stages must be determined. A linear fit in a plot of the derived column densities versus the excitation potential of the line level implies that the populations may be described by a single excitation temperature (Bernat, 1981).

Physical Conditions in Gaseous Shells. In what follows, we mainly refer to studies by Bernat (1977), Hagen (1978), or Sanner (1976), giving a summary of the results of the column densities, the shell temperatures, and the velocities. Other details can be found in Goldberg (this volume), in particular, a discussion on the shell inner radius which is so vital for determining the mass-loss rate. The section ends on shell distances inferred through the CS line profiles.

The observed *column densities* derived by Hagen (1978) from visual lines in some M giants, supergiants, and Miras are given in Table 2-4 as an example. In these gaseous envelopes, lying over warmer layers, the dominant ionization state of most metals is probably the singly ionized state. This is the case with Ca II, Sr II, and Ba II. However, most of the resonance lines arise from neutral metals (i.e., from a trace ionization state). As Bernat (1977) and Hagen (1978) show, the ionization balance within the CS shells is uncertain, and total abundances are better determined by using lines arising from the dominant stage of ionization. The Sr II resonance lines, unsaturated in these stars, are often chosen (Sanner, 1976; Hagen et al., 1983). The amount of CS matter in the line of sight assumes cosmic abundances, a point that could be open to criticism (Hagen et al., 1983). A scheme of determination of the hydrogen column density is given by Tanabé and Kamijo (1981). Inferred column densities of hydrogen atoms in the shell of some supergiants (in cm^{-2}) are: α Ori, 1.3×10^{22}; α

Table 2-4
Observed Gas Column Densities (cm^{-2})*

Ion	μ Cep	α Ori	α Sco	α Her	X Her	RX Boo	HD 207076	W Hya	R Leo
Fe I	1.3 (15)	9.1 (14)	7.5 (14)	4.9 (14)	2.5 (14)	2.2 (15)	1.0 (15)	6.6 (14)	<2.5 (14)
Al I	3.4 (13)	1.7 (13)	1.4 (13)	2.6 (13)	...	...	...	...	...
Mn I.....	1.5 (13)	1.3 (13)	3.2 (12)	1.0 (13)	1.8 (13)	1.3 (14)	4.0 (13)	2.8 (14)	1.8 (14)
Sr II.....	1.9 (12)	3.7 (12)	9.7 (11)	1.1 (12)	1.6 (11)	1.9 (11)	2.7 (11)	<1.6 (11)	3.4 (11)
Ba II	7.2 (11)	2.1 (11)	4.7 (11)	...	...	...	...	...	...
Sc II.....	2.3 (13)	1.9 (12)	9.7 (12)	4.4 (12)	...	...	...	...	...
Cr I	8.3 (12)	2.2 (13)	9.2 (12)	9.3 (12)	4.0 (12)	2.0 (13)	8.7 (12)	1.0 (12)	<1.0 (12)
Ti I	2.2 (13)	8.5 (14)	8.4 (12)	1.6 (13)	4.0 (13)	3.0 (13)	3.1 (13)	1.3 (13)	<8.4 (12)

*From Hagen (1978).

Sco, 1.9×10^{22}; α Her, 6.6×10^{21}; and μ Cep, 7.3×10^{21} (Bernat, 1977).

From observations of the fundamental 4.6-μm CO band in nine red giants and supergiants, Bernat (1981) derives column densities and demonstrates that there is no correlation of total CO column density with total gas (hydrogen) column density. We will discuss later what this result might imply for the shell structure.

Bernat (1977) indicates that radiative rates are orders of magnitude larger than collisional ones for the atomic species in the circumstellar envelope of α Ori. Consequently, the derived *excitation temperatures* do not give the kinetic temperatures in the shells. In the case of lines of the fundamental CO band, however, Bernat et al. (1979) show that collisional processes dominate and, therefore, the excitation temperatures are indeed electron temperatures, such as the temperatures of 200 and 70 K derived for the observed shells in α Ori (see also Ridgway, 1981a).

As shown earlier, *the expansion velocity of the shells* (otherwise known as the stellar wind velocity) is inferred from the blue shift of the CS lines, generally related in the literature to a mean photospheric velocity. Again, we emphasize that the expansion velocity must be finally related to the systemic velocity to be meaningful. In α Ori, through the Mn I and Cr I CS lines observed over 25 years, Weymann (1962) finds that the heliocentric radial velocity of the absorption-line cores varies over a range of only 2 km/s around an average value of +10.4 km/s. This near-perfect constant radial velocity is also confirmed by Goldberg (1979) from measurements of the K I deepest component at 7699 Å (see the section *Evidence of Multiple Absorption Components in CS Lines*) and by Linsky et al. (1977) on various optical CS lines. Hall (1980) reports that, at spectral resolutions of the order of 10 km/s, the observed 4.6-μm spectra of M supergiants and Miras show sharp CO lines with expansion velocities of about 10 km/s, which are totally consistent with the visible atomic resonance-line values. A constant expansion velocity is expected if the CS lines are produced in a quasi-steadily expanding envelope, many times larger than the star itself and well separated from it.

From a survey of the expansion velocities drawn from the core shift of metal lines, Reimers (1977) finds a continuous transition, on the average, of stellar wind velocities from luminous M supergiants (10 km/s), to late M giants (15 km/s), to medium M giants (20 km/s), and to early giants (25 km/s). As pointed out by Goldberg (1979), the direct measurement of the line shift gives a smaller velocity than the true velocity because the red side of the absorption profile is filled in with emission. Goldberg quotes the model calculations by Bernat (1977) and Sanner (1976) that predict errors of about 25 percent. For example, the corrected heliocentric velocity of the inner shell of α Ori (from

the K I deepest component) is 13.5 km/s (Goldberg, 1981) instead of the apparent value of about 10. Bernat (1977) remarks that the expansion velocities show no dependence on optical depth, excitation potential, or ionization state, further proof of a constant outflow velocity for the matter. (The Ca II H and K lines that show a variable expansion velocity are exceptional, coming from perturbations by chromospheric effects.)

The expansion velocities are always much lower than the surface escape velocity $v_{esc} = (2\ MG/R)^{1/2}$ (for example, Deutsch, 1960). Reimers (1977) notes that there seems to be a shaky correlation between stellar wind velocities and velocities of escape at the stellar surface. At any rate, the expansion velocity of the matter at several hundred stellar radii is greater than the escape velocity there, further demonstrating that the matter is really lost to the interstellar medium.

Shell expansion velocities are also inferred from the half-line width of thermal CS, SiO, or CO emission. A measurement such as this in CO J = 2–1 line in α Ori by Huggins (1984) gives a velocity of 14.1 ± 1 km/s. Is a previously detected shell implied? The question is open. For a sample of red giants, supergiants, and Miras, there is no relation between expansion velocity and radius (as measured by the temperature), such as larger radii correlated with higher expansion velocities (Bernat, 1981). The supergiant, α Ori, is another example (Table 2-3).

It could be expected that *velocity gradients* in the envelope produce a difference in radial velocity among the CS lines of the various neutral and ionized elements. Weymann (1962) emphasizes that, owing to the greater optical depth in H_4 and K_4 cores in relation to the other lines, velocity gradients could affect the CS H and K lines. In fact, these lines give convincing evidence for velocity gradients in the wind acceleration region (very inner shells) of M giants, depending on the stellar type, as we have discussed in the section *Variation of CS Lines with Spectral Types and Luminosity Classes*. According to Reimers (1975) and confirmed by Boesgaard and Hagen (1979), at spectral type M1, the expansion velocity given by the H_4 and K_4 lines is larger by 15 km/s than the velocity of the other line elements. This difference then decreases to zero at M5 and, with the later types, shows lower expansion velocities of about 5 km/s than the CS lines of other elements. This velocity gradient is the cause of the wider Ca II H and K lines and less blue-shifted core as the spectral type advances.

From modeling of the K_4 feature, Boesgaard and Hagen (1979) find that, in the earliest M giants, the narrow entirely blue-shifted core cannot have been formed over a great velocity gradient. Moreover, as these authors find no evidence for a Ca II K_4 feature at zero velocity (their Figure 4), they infer that the acceleration to a terminal velocity occurs very rapidly. They show that the broadening of the K_4 feature with the simultaneous advancement of the type is indicative of a large turbulence and/or velocity gradients in the shell. In fact, in modeling the K_4 profile, these authors find that a minimum velocity (inner shell velocity) affects the red edge of the profile only, whereas a maximum velocity (outer shell velocity) affects the blue edge. This confirms the conclusion of Reimers (1975, 1981) that the inner radius of the observed shell decreases with later types in the wind acceleration region. It is interesting to note Reimers' (1975) observations that some individual stars having CS Ca II lines which are variable in time (Figure 2-14) map the line-strength/velocity relation of Ca II K, intrinsically showing the various regimes of the wind acceleration. Reimers (1975) supports Deutsch's (1960) model in which the line-strength/velocity relation among the various classes of the M giants would be due to a Ca ionization structure.

As for the M supergiants, in α Ori, Weymann (1962) detects no significant velocity gradients among the CS lines over 25 years of observation, except for a small average deviation of about 1.7 km/s noted for the Ca II H and K lines; we recall that, from September 1974 to October 1975, these lines distribute around the systemic velocity (+2, −1

km/s). A general observation is that, in all M supergiants, only the CS Na D and the strong Ca II H and K cores (up to 1 Å) have very low expansion velocities (2 to 5 km/s). From IR CO observations in α Ori, α Her, and α Sco, Brooke et al. (1974) notice occasional large velocity gradients.

Finally, there is observational evidence of *shell turbulent velocities* (i.e., microturbulence defined as nonthermal velocities with an assumed gaussian distribution (Reimers, 1981)). From measurements quoted by Reimers (1981) for the supergiants α Her, α Sco, and α Ori, this author states that, on the average, the microturbulence is found to be one half the expansion velocity. Boesgaard and Hagen (1979) derive limits on the turbulent velocities in M giant stars; they increase from the order of 2 km/s or less for M0 giants to 4 km/s or more for M6 giants. Reimers (1981) notes that "if the microturbulence is caused mainly by wind velocity variations on a time scale short compared to typical flow times in the observed shell (10 to 10^3 years), the relative amplitudes of these variations are then similar to those in the solar wind."

A direct approach to the *shell extension* involves the detection of CS line emission off the star. We recall that the emission results from resonance-line scattering of photospheric radiation by neutral atoms in the shell. The λ7699 K I line is most often used for this purpose, with α Ori as the favorite star once again. However, let us mention an attempt on the supergiant, μ Cep, by Munch et al. (1979), using the Na I D_2 line.

The first such direct mapping of the α Ori shell was obtained by detecting the presence of K I emission out to 4–8" from the disk center by Bernat and Lambert (1975). In further series of observations, Bernat and Lambert (1976b) and Lynds et al. (1977) observe the K I emission out to 5" (i.e., 200 R_*) at numerous position angles around the star. The northwest quadrant shows more intense K I emission. Bernat et al. (1978) spatially extended the observations up to 30" (600 R_*) by using a two-dimension television detector, which was adequate to explore regions of the shell at large radius which were too faint to be detected by the single-channel scanner of the previous experiments. Honeycutt et al. (1980), using the same system with a narrowband filter, detected the gas shell surrounding α Ori out to a radius of 50". They confirm that the northwest quadrant is brighter by a factor of about 2. They suggest that this might be due either to an asymmetrical mass ejection giving a denser shell or to an asymmetrical stellar surface intensity giving more K I photons to be scattered. The authors state that the 50" radius corresponds to 9500 AU or 55 light days, if a distance of 190 pc is accepted for α Ori (Weymann, 1962). With a constant expansion velocity of 10 km/s, the outermost potassium would have been ejected 4500 years ago. In March 1981, Mauron et al. (1984) mapped the α Ori shell at the K I line up to 63", using a Fabry-Pérot etalon and a CCD camera. They found a slight asymmetry of the brightness distribution but not in the same direction as Honeycutt et al. (1980), who observed in March 1977: it is the southwest quadrant that appears to be brighter, while the southeast quadrant is fainter than the average.

Usually, the physical mean distances of the various shells to the photosphere are determined on the assumption that the dust and the gas are in equilibrium in the shell. The relation between the excitation temperature and the radius for the gas is directly obtained from a dust-shell model (for example, Tsuji's (1979) α Ori dust model; also see Lefèvre, this volume). Such distances are shown in Table 2-3. The equilibrium hypothesis appears to be badly in error. Bernat (1981) comments on the microwave CO emission from α Ori observed by Knapp et al. (1980), which leads to the cooler (70 K) shell detected through the CO fundamental; the mm-wave spectra give a shell distance five times smaller than the classical equilibrium assumption applied to the fundamental CO lines (see also a discussion by Goldreich, 1980). We shall not elaborate further on this highly difficult question: the correct interpretation of excitation temperatures in terms of physical distances needs detailed

theoretical models, themselves linked to a better understanding of the mass-loss mechanism, as Bernat (1981) emphasizes. This author also hints that CO may certainly be present in the entire velocity space between the multiple components, but at low densities, high temperatures, or both, and is unobservable.

Direct measures of stellar diameters by different techniques (lunar occultation, interferometry, speckle, etc.) will be discussed elsewhere.(See the section *Geometrical Shell Expansion*.)

Summary: Structure of Expanding Gaseous Envelope

Discrete velocity components in the circumstellar material are commonly observed in M giants, supergiants, and Miras. Table 2-3 summarizes such velocity structures from infrared CO observations in some typical stars.

A component at 200 K is common both to the supergiant, α Ori, and to the Mira stars and even to the dust enshrouded carbon star, IRC + 10216. This component characterizes the classical expanding shell detected in the optical range of the unobscured stars (e.g., in the K I line of α Ori). Assuming that decreasing temperature corresponds to increasing distance from the photosphere, a more extreme outer shell ($T \sim 70$ K) is clearly resolved at high spectral resolution (i.e., at 0.6 km/s, Hall, 1980). The Mira stars (not only χ Cygni and R Leo, but 10 other Miras observed by Hinkle et al., 1982) show another component around 800 K which is stationary at the center-of-mass velocity. (See the section *Changes in Absorption-Line Radial Velocities with Phase*.) At present, such a CO component is not observed in giants and supergiants. Is it unique to Miras? As noted by Hall (1980), such circumstellar features are difficult to separate from their photospheric counterparts because the photospheric motions are far too small in the late-type supergiants. Nevertheless, this author states that, in supergiants, some fundamental CO lines of low rotational number have a line strength corresponding to a radiation (brightness) temperature of $\leq$1000 K. However, in the case of the CO fundamental lines, there can be marked departures from local thermodynamic equilibrium (LTE) in the vibrational levels though not in the rotational levels (Carbon et al., 1976; Heasley et al., 1978), which leaves open to question the relation between the radiation and the electron temperature. Bernat (1981) notes that such a component may be present at too high a temperature, too low a density, or too large a turbulent velocity to be observable. As Clegg (1980) points out, if such a layer exists around the M supergiants, "this observation will be of extreme importance for mass-loss theories, because a cool, almost stationary layer of gas outside the star but interior to the CS flow would be incompatible with any theory predicting a flow sonic point in the stellar chromosphere (e.g., Mullan, 1978)."

In the Mira, χ Cyg, it is interesting to mention that the 800 K stationary layer was rapidly built up late in 1975, as described by Hinkle et al. (1982). Bearing in mind that the shock-wave model works well in the Mira stars (see part *Atmospheric Kinematics* in the section *Emission Lines*), it is quite feasible that the 800 K layer represents gas ejected from the star, either by a particularly violent oscillation or by the pulsation degenerating into a relaxation oscillation during which mass loss occurs (for example, see discussions by Wood, 1981; and Willson and Hill, 1979). Thus, it could provide a reservoir for any outflowing material driven possibly by radiation pressure on dust grains formed there (Tielens, 1983). Hinkle et al. (1982) find support for this point of view in the temperature of 800 K suitable for dust condensation and in the total mass they estimate for the layer ($>10^{-5} M_{\odot}$), which is large enough to explain the classical $10^{-6} M_{\odot}$/yr mass-loss rate in these stars. Moreover, in χ Cyg, the stationary layer is observed to weaken steadily over the three cycles following its creation. It appears to provide a source for material infalling to the photosphere, particularly the source of the visible spectrum, as previously discussed in the section *Photospheric Absorption Lines*. The authors add that the 800 K shell

might be the source of SiO maser emission observed in χ Cygni, a hypothesis which could be confirmed by correlating long-term variations in SiO maser characteristics with the formation and dissipation of the 800 K shell.

In the outermost CS shells, the multiple layers in many semiregular M variables present no correlation between expansion velocity, hydrogen column density, CO column density, or dust column density (Bernat, 1981). The absence of correlations favors multiple episodic ejections, according to Bernat, giving rise to individual shells formed under different physical conditions at various times. However, such a component structure does not necessarily imply the ejection of discrete shells. A continuous distribution of matter may produce it; the condition is that the flow velocity changes relatively slowly with distance (Mihalas, 1979). This condition is fulfilled if several distinct dust condensation events occur in the envelope, producing regimes of rapid acceleration by radiation pressure on grains, separated by regions of quasi-constant velocity in the gas flow, as emphasized by Keady et al. (1984). These authors apply such a distribution to the dusty C star, IRC + 10216 (Table 2-3). Because the observations indicate the presence of gas and dust, they assume that various grain species (described in the section *Circumstellar Dust*) may condense at different places in the envelope due to different physical characteristics, and they present the following scenario. First, SiC condenses close to the photosphere, and it results in the gas being accelerated to $\sim$2 km/s; then carbon soot condensation meets favorable conditions to begin at 3 R_*, resulting in a gas acceleration to $\sim$11 km/s; finally another condensation event, possibly from Mg S, occurs at 11 R_* and accelerates the gas to $\sim$14 km/s.

Jura (1984) also comes to the conclusion of a hybrid model for the mass loss, in connection with the spectral appearance of the CS lines; although very dusty stars (such as IRC + 10216) with multiple CS components as broad troughs experience continuous outflow of matter, stars (such as α Ori and o Cet) with distinct sharp CS components experience impulsive discontinuous mass loss. In fact, for α Ori, multiple episodic ejections seem best adapted to the presence of companion objects. (See the section *Geometrical Shell Expansion*.)

Finally, it is worth noting that shells of cool stars have characteristics similar to planetary nebula envelopes (Table 1 in Ridgway, 1981a), suggesting the possibility of a common mechanism of origin.

CIRCUMSTELLAR DUST

Detection of Circumstellar Dust

In some infrared wavelength intervals, late-type stars radiate an excess above the blackbody radiation expected for the assumed effective temperature or measured color temperature of the star. Such infrared excesses can be attributed to circumstellar dust: grains absorbing starlight are heated and then reradiate in the infrared, causing the excess. For example, the excess observed between 8 and 14 μm in the M stars was found to be identical to the energy distribution expected from an optically thin cloud of silicate grains. Additional evidence comes from these color temperatures, which are less than 1000 K in stars in which most of the energy longward of 3 μm is due to infrared excess (e.g., Forrest et al., 1975). Because this temperature is less than the effective temperature of the star, longward radiation has to come from a cooler additional source. Moreover, these stars show that, shortward of 3 μm, the radiation is consistent with radiation weakened by dust absorption. In fact, a weakening of photospheric absorption bands due to a veiling by thermal emission from a circumstellar dust shell is currently observed. In carbon stars, the strength of the CO band at 2.2 μm is seen to vary with the infrared color; the thicker the shell, the redder the colors and the weaker the bands. Note that the systematic weakening of the CO band in Mira variables is normal at maximum light where the photospheric temperature is higher. (See the section *Survey of Changes in Absorption-Line Strengths with Phase*.) Another example of thermal emission

acting to fill in the absorption bands and giving an increasingly featureless spectrum as the shell's thickness grows concerns the carbon star, V Cyg, with its smooth spectrum longward of the 4.6-μm CO band (Puetter et al., 1977). The circumstellar nature of the excess emission longward of 8 μm has been confirmed by spatially resolving the shells from the stars. (See the section *Geometrical Shell Expansion.*)

Finally, the reality of dust shells is proved through linear polarization due partly to the scattering and absorption of the stellar radiation by small grains. These grains need not be the same grains responsible for the infrared excesses; nevertheless, this may be the case in favorable envelope geometry and optical depth.

Infrared Excesses

The shape of the infrared excess depends on whether the cool star is oxygen-rich (M star) or carbon-rich (C star). Silicates are expected in the first case (e.g., bands at 9.7 and 18 μm); silicon carbide, which exhibits a distinctive resonance at 11.2 μm, and graphite, which presents a featureless spectrum and is thought to be responsible for the extinction encountered from the optical to the far-infrared, are expected in the C stars. Infrared excesses are recognized from infrared spectrophotometry or infrared photometry.

Let us remark that the quoted observations do not include the data from 8 to 22 μm collected by the Infrared Astronomical Satellite (IRAS), launched in January 1983, and not yet available at this time. Preliminary results should be found in the Proceedings of the Meeting on "Mass Loss from Red Giants" held in June 1984 at California State University, Los Angeles.

Spectral Energy Distribution of Excess Emission. Reviews of the infrared excesses shown through moderate spectral resolution infrared spectrophotometry for M and C giants and supergiants have been given by Merrill (1977).

Some examples of energy distributions from 2 to 14 μm are reproduced in Figure 2-24. The signature of silicate grains in the M stars is clearly visible through the emission feature at 9.7 μm. It is stronger in supergiants in class Ia than in class Ib. In the M giants with very thick dust shells, the feature is seen in absorption. In several M-type Mira stars, the spectral energy distribution over the 8- to 14-μm wavelength range observed by Forrest et al. (1975) is clearly seen to be different: "Some appear to show a somewhat more sharply increasing distribution in the 8–9.5 μm range and a more slowly decreasing distribution at wavelengths larger than 11 μm (e.g. R. Leo)." In carbon stars, SiC emission at 11.2 μm appears in all the stars shown in Figure 2-24, being strong in the semiregular late C star, UU Aur, and in the Mira, R Lep. Forrest et al. (1975) note that the amount of blackbody excess is much stronger from carbon Miras than from semiregular variables. Among a sample of 25 irregular carbon stars, none appear to have infrared excess at wavelengths shorter than 3.4 μm (Walker, 1980).

Forrest et al. (1979) observe the 16- to 39-μm spectra of many M stars (supergiants and Miras) known to have a 10-μm excess; they confirm the presence of an excess emission due to a silicate material in this region (first detected around 20 μm by Treffers and Cohen (1974) in α Ori) "in the form of a broad hump peaking near 18 μm and falling smoothly to longer wavelength" as a blackbody continuum. That no sharp structure is observed in the spectra is indicative of a silicate in an amorphous disordered form. Hagen et al. (1975) report on a possible silicate emission band at 33 μm in some M stars, although this is not confirmed by Forrest et al. (1979) in μ Cep. However, Hagen (1982), by broadband photometry, concludes that there are infrared excesses not only at 33 μm, but also at 20 and 25 μm for stars that show a 10-μm silicate emission feature; such excesses are explained by radiation from silicate dust. Epchtein et al. (1980) also detect 30-μm emission in Mira M stars. Incidentally, they show that the 35-μm emission is strong enough to pump the OH circumstellar masers in the thin envelope of Mira variables. Hagen (1982) also

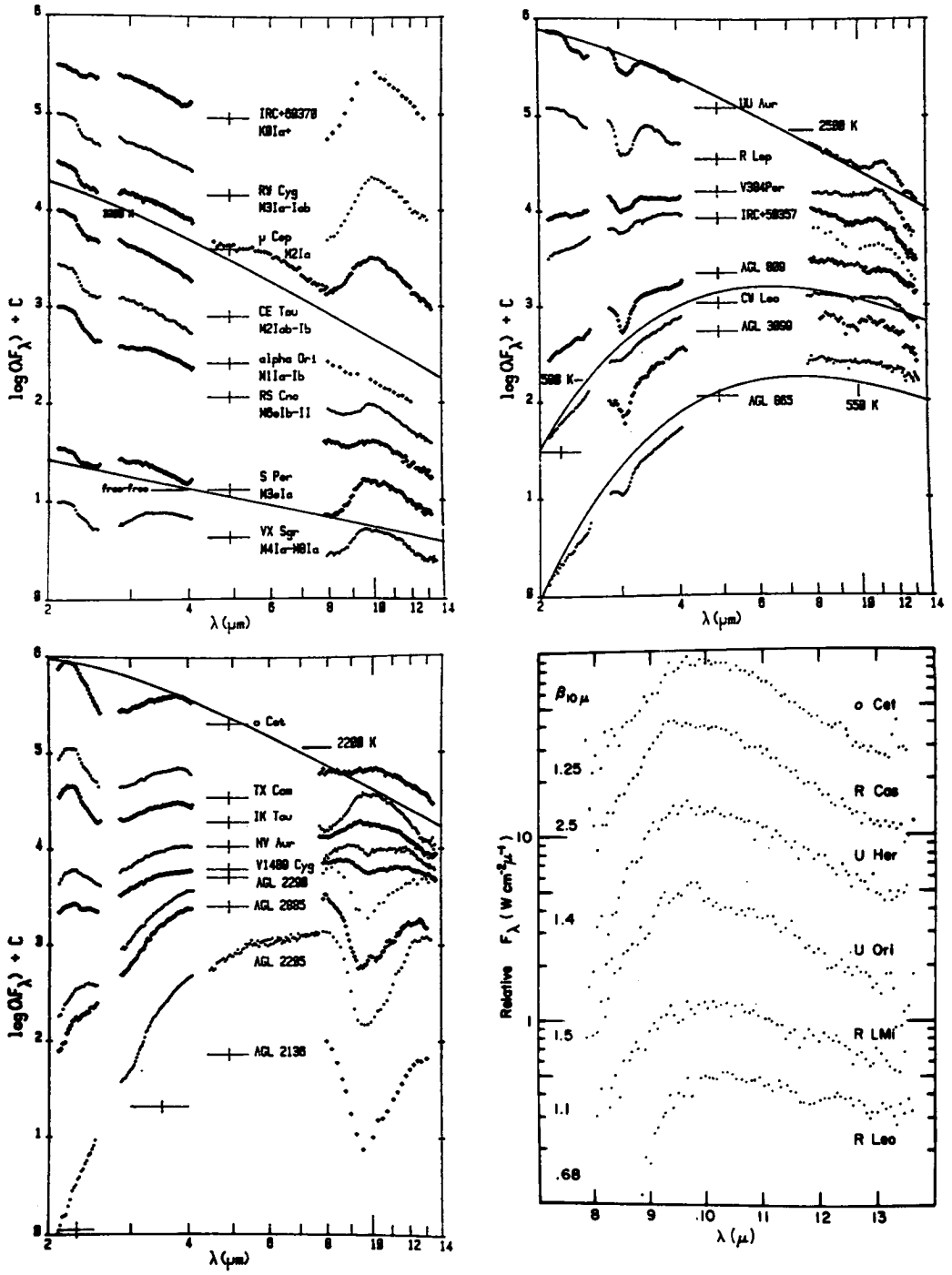


Figure 2-24. Spectral energy distribution of IR excess emission. Top left: in representative luminous M supergiants as examples of optically thin shell emission (a 3300 K blackbody and a free-free slope are included for comparison). Bottom left: in M stars and top right, in C stars, to illustrate the observed range in total optical depth in dusty CS shells (from Merrill, 1977). Bottom right: in several M-type Miras (the "relative flux" represents the actual flux normalized by an arbitrary constant for convenient display); $\beta_\lambda \equiv \{ F_\lambda \text{ (total)} - F_\lambda \text{ (continuum)} \} F_\lambda^{-1}$ (continuum), calculated with appropriate blackbody temperatures (from Forrest et al., 1975).

shows that there is sufficient 35-μm flux to pump the 1612-MHz OH masers for all the stars she observes—Miras, giants, and supergiants—except for the Mira, R Aql. An emission feature beginning at 24 μm and extending to at least 37 μm is identified in dusty carbon-star spectra, including IRC + 10216 (Forrest et al., 1981; Herter et al., 1982). It is interpreted as resulting from a solid-state resonance in the dust grains which have condensed around this star. The grain material causing this feature is MgS (Goebel and Mosely, 1985; Nuth et al., 1985).

The N-type carbon star, Y CVn, deserves special attention. It has been observed over a complete IR wavelength coverage from 1.2 to 30 μm by spectrophotometry at high resolution by Goebel et al. (1980). The particulate emission band of SiC at 11.2 μm, well known in several carbon stars, is also present in Y CVn. By superposing the emission of an optically thin shell with the dust temperature, $T = 1600$ K, on a blackbody spectrum of $T = 2750$ K, the authors show that a mixture of SiC crystalline forms fits the 11.5-μm band better than amorphous SiC, in agreement with the conclusion by Friedemann et al. (1981). The latter estimate that the column density of SiC grains is 7.0×10^{-5} g cm^{-2} and the total mass of SiC grains in the shell is 10^{24} g (if the star's photospheric radius and the radius of the envelope are evaluated according to Cohen, 1979).

As for graphite, its lack of distinct spectral features in the infrared makes its identification difficult. However, the photospheric C_3 molecule, the main vaporization product of graphite, is observed and is particularly strong at 5.2 μm. Its strength constrains the degree of veiling present (i.e., the amount of graphite in the circumstellar shell). It appears that there is little or no graphite in the CS shell about Y CVn.

Generally speaking, apart from the 11.5-μm SiC band, the photosphere in Y CVn is dominant over circumstellar emission to 30 μm. The conclusion is also valid for the violet range, in which the cause of the opacity in carbon stars has been debated at length for years (e.g., Gilra, 1973; Hartmann and Dolan, 1974; Bregman and Bregman, 1978; Walker, 1980). For Y CVn, Goebel et al. (1978) show that reradiation by circumstellar SiC is inadequate and that the violet opacity is primarily due to photospheric C_3, as was also concluded by Bregman and Bregman (1978). The dominance of the photospheric light might imply a limit to the amount of graphite ejected through the mass-loss process by such early N-type stars as Y CVn.

In contrast with Y CVn, the bright infrared object, IRC + 10216, a late-type carbon star, shows a substantial infrared excess emission. The overall flux distribution is similar to a blackbody, indicative of gray grains. This star is one of those extreme carbon stars, embedded in thick dusty CS shells that efficiently convert starlight into thermal emission. The overall featureless infrared excess is assumed to be predominantly due to graphite grains (soot) by Cohen (1979), who also discusses 16 other carbon stars (AFGL infrared sources from 10-μm sky surveys, Price and Walker, 1976). Mitchell and Robinson (1980) ascribe the infrared excess mainly to an optically thick extended graphite shell that contains 1 to 2 percent per number of SiC particles. Nevertheless, due to the inverse greenhouse effect, SiC is expected to condense close to the star, while graphite condenses much farther out, as developed by McCabe (1982; see also Lefèvre, this volume).

A feature similar to the MgS emission feature at about 30 μm appears in the spectra of the planetary nebulae, NGC 6572 and IC 418 (Forrest et al., 1981); the presence of the same type of dust indicates a possible evolutionary link between carbon stars and some planetary nebulae. Remember that gaseous shells of cool stars and planetary nebulae also have common properties (Ridgway, 1981a). Zuckerman et al. (1976) have previously described a sequence leading from extreme carbon stars to planetary nebulae. However, about the 11.2-μm SiC feature observed in NGC 6572 and IC 418, Kwok (1981) asks if the SiC grains are left over from the preceding red-giant phase or not. In

fact, it appears that some properties of planetary nebulae may be explained if their progenitors are red giants with extensive circumstellar envelopes, but the transition from red giants to planetary nebulae is not yet completely resolved.

It is worth noting the observation of an unexpected high peak in the flux energy distribution at 1.5 mm in the Mira carbon star, V Cyg (Querci et al., 1979). This star is known to be so dusty that emission in the dust shell provides more than 90 percent of the total flux for $\lambda > 5.5$ μm (Puetter et al., 1977). The flux at 1.5 mm is about four times larger than the flux measured at 1 mm by Campbell et al. (1976) from IRC + 10216. A flare-like event is suggested. Let us note that a radio flare at 2.8 cm has also been observed on the M Mira, R Aql (Woodsworth and Hughes, 1973, 1977). For the M supergiant, α Ori, Oster (1971) reports a flux variation at 10 μm from night to night supporting a flare-type origin.

An interesting point in carbon stars concerns the relationship between SiC dust and the SiC_2 molecules that are a vaporization product of solid SiC: the strength of the SiC_2 molecular bands investigated from the Merrill-Sanford bands observed in the visible part of carbon-star spectra should be correlated with the strength of the ultraviolet absorption feature (Walker, 1976) and the infrared SiC emission feature (e.g., Mitchell and Robinson, 1980).

An additional contribution to the infrared excess might arise from chromospheric free-free emission. A modeling of the observed infrared flux in some cool stars, including free-free emission, has been attempted by Gilman (1974) and Lambert and Snell (1975). Nevertheless, further observations by Fawley (1977) and Hagen (1982) of stars common with Gilman favor an additional grain species rather than free-free emission.

Time Variability of Infrared Excesses. Forrest et al. (1975) investigate the possibility of a temporal variation of the excess infrared radiation by observing M stars with broadband photometry at effective wavelengths of 3.5, 4.9, 8.4, and 11 μm. As stressed by Gehrz and Woolf (1971), at 3.5 μm the optical depth of the silicate envelope is minimal for both its absorption and emission effects; at 11 μm, silicates have their peak emissivity, but are often optically thick, whereas at 8.4 μm, the emission has a low optical depth but is rarely saturated. Therefore, designating $[\lambda_n]$ as the observed magnitude of the wavelength λ_n, the color [8.4 μm]–[3.5 μm] measures silicate emission, and the color [11 μm]–[8.4 μm] is indicative of the optical depth of the envelope of the excess dust emission. An example of such a color-color diagram as a function of phase is given for R Cas (Figure 2-25). Although visual light and light at 3.5 μm vary by a large amount, the infrared colors appear to show no significant changes throughout the cycle. This conclusion applies to the 25 program stars of all kinds of variability types (including Miras), except for R Gem (S Mira star), in which the [11 μm]–[3.5 μm] color changes significantly. Considering the large number of stars observed, the authors conclude that the total abundance of grains surrounding these stars does not change by a large amount with time.

The same authors also show spectra of o Cet, R Cas, and μ Cep obtained at several times (Figure 2-26). Very little change is seen in the spectral energy distribution from 8 to 14 μm over 4 years for the Mira, R Cas, and over 6 years for the supergiant, μ Cep. In o Cet, a large change is observed in the excess emission strength at 9.7 μm between 1967 and 1973, with a slow decrease from 1971 to 1973. For the authors, this would represent a secular decrease by about a factor 1.5 to 2 in the amount of dust around o Cet from 1967 to 1971. Infrared observations are also reported for o Cet by McCarthy et al. (1978) at various wavelengths around the December 18, 1977, maximum light. Between phases 0.76 and 0.92, the 10.2-μm flux density increased by a factor of 1.7. At the same time, both the [10.5 μm]–[3.5 μm] and [8.4 μm]–[3.5 μm] color indices increase by 0.50 mag relative to those observed between $\varphi = 0.25$ and $\varphi = 0.8$ by Forrest et al. (1975). During the light cycle (from $\varphi = 0.76$ to $\varphi = 0.28$),

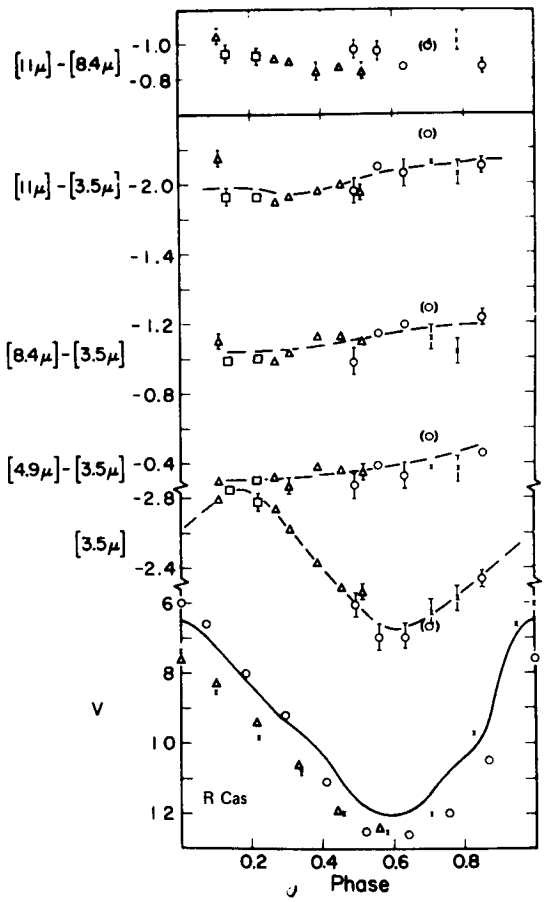


Figure 2-25. Color-color diagram as a function of phase for the M Mira, R Cas (from Forrest et al., 1975).

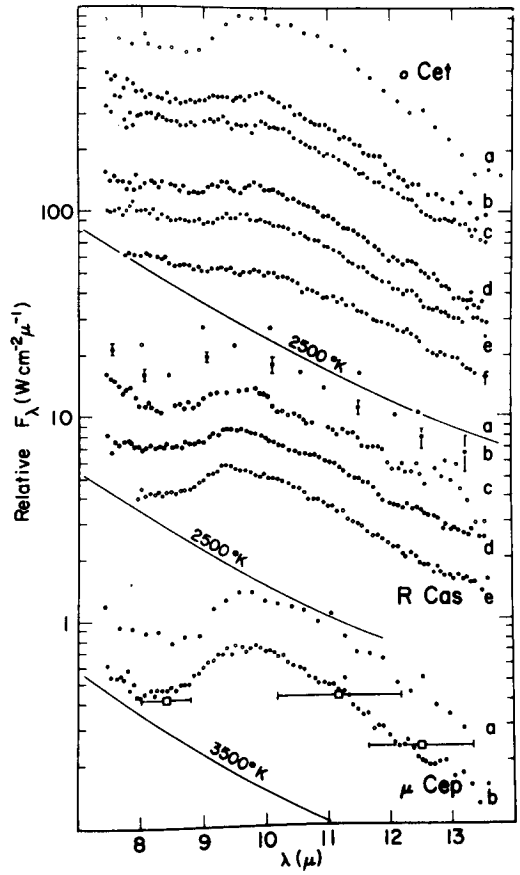


Figure 2-26. Spectral energy distribution as a function of time from o Cet, R Cas, and μ Cep. The blackbody curves are typical assumed stellar continua referring to the spectrum just above. For o Cet: (a) October 17, 1967 (UT), φ = 0.96; (b) December 13, 1971, φ = 0.45; (c) January 10, 1972, φ = 0.54; (d) November 4, 1972, φ = 0.42; (e) December 4, 1972, φ = 0.50; (f) December 18, 1973, φ = 0.64. For R Cas: (a) November 22, 1969 (UT), φ = 0.86; (b) November 13, 1970, φ = 0.71; (c) December 17, 1971, φ = 0.64; (d) November 4, 1972, φ = 0.39; (e) September 21, 1973, φ = 0.14. For μ Cep: October 17, 1967, and June 17, 1973 (UT) (from Forrest et al., 1975).

the 10.2-μm flux varies by a factor ≥3.5 (~1.4 times more than the bolometric flux), the change in 20-μm flux is 2.5 times (like the change in bolometric flux), and the 3.5-μm flux varies by less than a factor of 2. The excess emission at 10 μm is strongly phase-dependent: from $\varphi = 0.6$ to $\varphi = 1.0$, the ratio of photospheric to excess emission at 10 μm changes from 0.50 to 0.26. The authors suspect that existing circumstellar dust must be cyclically heated by periodic changes in stellar luminosity; changes in stellar temperature may produce changes in the contrast of silicate dust emission relative to the stellar continuum, as previously suggested by Forrest et al. (1975). Large contrast changes do occur at 10 μm, as proved by the observations. These probably begin at $\varphi =$ 0.8 in conjunction with increases in the bolometric and visual energy. The possible origin of these temperature changes might be flare-like events as developed in the section *Interpretations of the Polarization Observations.*

Relationships Between Gas and Dust in Circumstellar Envelopes. The amount of CS material from observations of CS dust has been estimated by Gehrz and Woolf (1971), by Dyck and Simon (1975), by Hagen (1978), by Hagen et al. (1983), and by Knapp (1985), who studies not only M stars but also S and C stars. Because the last three authors combine a study on CS gas and dust shells in a sample of stars, the bulk of the results given below is from these sources. (See also Goldberg and Glassgold and Huggins, this volume.)

Hagen et al. (1983) estimate the quantity of dust from the contrast in the 10-μm silicate emission feature through a dust-shell model described in Hagen (1978, 1982). This model calculates the emergent radiation from an optically thin circumstellar dust shell following the code of Dyck and Simon (1975), modified to include the effects of self-absorption by dust. It is shown that the shell parameters that have a strong effect on the appearance of the 10-μm feature (specifically, its height) are: (1) the dust temperature determined by assuming that the grains emit thermally at the same rate at which they absorb starlight (i.e., by the absorption efficiency of the grains shortward of 5 μm where the photosphere emits strongly); (2) the inner radius of the dust shell; and (3) the optical depth of the dust. In Hagen et al. (1983), the inner radius is (somewhat arbitrarily) set to 10 R_*, the grain mixture is "dirty" silicates, and the power-law density distribution, $N(r)$, is proportional to radius $r^{-\alpha}$ with $\alpha = 1.5$. (See Lefèvre, this volume, for a discussion of such a model.) An equal fractional condensation of the elements is assumed (crudely justified by a roughly constant relative abundance of the elements from star to star); therefore, the ratio of the amount of metal in the gaseous state to that condensed on grains is the ratio of the total column density determined from gas to that determined by dust. (See the section *Quantitative Analysis of CS Lines* for the method for determining the column density.)

Knapp (1985) also finds the dust content of the envelopes from the 10-μm feature, but uses the models of Rowan-Robinson and Harris (1982, 1983a, 1983b; see also Lefèvre, this volume). Although the amount of circumstellar gas is estimated through the optical CS line, Sr II λ4077, in Hagen et al. (1983), Knapp uses the CO (1–0) line. The main difference between the two works is that the observations by Hagen et al. cover a small range in mass-loss rate (10^{-6} to 10^{-8} $M_\odot$/yr) and thus any relationship between gas and dust abundances may be altered by uncertainties in the data, as Knapp remarks. In fact, uncertainties are numerous in such approaches (see Goldberg, this volume), and the suggestion by Hagen et al. that the dust-to-gas ratio in the circumstellar envelopes is not constant is dismissed by the results of Knapp, who observes stars over a very wide range in mass-loss rate (10^{-7} to a few $\times$ 10^{-4} $M_\odot$/yr). Clearly, the gas-loss rate is proportional to the dust-loss rate for M, S, and C variables (giants and OH/IR supergiants; Mira or not Mira variables). Consequently, the dust-to-gas ratio is roughly constant over almost 4.5 decades in mass-loss rate, with mean values of $\sim$160 by mass for M and S stars and $\sim$400 by mass for carbon-rich stars. This constancy is expected when the mass-loss mechanism is radiation pressure on grains (Deguchi, 1980). Knapp notes that the value found for the oxygen stars is very close to the value found for the interstellar medium ($\sim$150), suggesting that, in all the studied envelopes with silicate grains, all the available heavy elements condense out as grains.

Hagen et al. (1983) argue that the CS envelopes have clumpy regions of greater density in which the grain formation may be essentially complete, whereas there is little or no grain formation in less dense regions. The possibility of high-density condensations present in the envelope and moving in the line of sight had been raised by Reimers (1978), for example, to explain the weak multiple velocity components present in the CS Ca II H and K lines of early M giants. (See the section *Evidence of Multiple Absorption Components in CS Lines.*)

Intrinsic Polarization of Starlight

As noted in the section *Detection of Circumstellar Dust*, the presence of dust has also been detected from optical polarization observations. The linear intrinsic polarization in red variables is distinguished from the interstellar polarization by its variability with time, by its wavelength dependence, which differs from that of the interstellar polarization, and/or by the rotation of the position angle of polarization with wavelength. At the origin, these properties have been measured over broad spectral ranges; the reviews by Serkowski (1971) and by Shawl (1974) report on these results. On the other hand, the relatively recent review given by Coyne and McLean (1979) emphasizes the results from high spectral resolution. Let us also note King's (1983) didactic article on polarized light in astronomy, intended for the general reader.

First, we shall summarize general results; then we shall study details from high spectral resolution, particularly from well-documented specific stars—Miras and giant and supergiant semiregulars. Finally, we shall resume the interpretations suggested at the present moment for these observations.

Overall Results on Polarization. All the supergiants studied by Dyck and Jennings (1971), as well as the giants later than M2, show intrinsic linear polarization. These authors remark that, among the giants, "the frequency of the phenomenon increases rather abruptly at M4 and remains high in later spectral type." The percentage of polarization may be high, with $P \geq 2$ percent, especially higher than 2 percent in the blue spectral region, as high as 10 percent for extreme red objects (Figure 2-27), and up to 20 percent at 1 μm in IRC + 10216 (Shawl and Zellner, 1970; Cohen and Schmidt, 1982).

In short, quoting Magalhaes (1981) about polarization in red late-type stars: "its amount, position angle and spectral behavior generally vary with time for a given object, as does the polarization wavelength dependence from one star to another." In the Mira variables, these changes are not necessarily in phase with light variations. Temporal variability on short time scales (months) has been detected in the majority of stars and indicates that considerable anisotropy exists near the star.

Although the wavelength dependence of polarization changes its shape with time, there is a general trend toward an increase in the amount of polarization with decreasing wavelength. The increase toward the ultraviolet often follows the Rayleigh λ^{-4} law; an exception is the supergiant, μ Cep, which departs completely from this rule (Figure 2-27). Furthermore, a maximum toward 1 μm is not so rare, such as that for L_2 Pup, showing a peak around 1.6 μm (Shawl, 1975). Secondary ups and downs in the wavelength dependence of polarization appear at times, with their strengths also varying with time (for example, R CrB, Figure 3 in Coyne and Shawl, 1973).

Correlations between the polarization and other parameters have been sought because they should be useful in interpreting the observations.

It appears that there is no general relationship between changes in the polarization and light changes with time. In Mira stars, a decreasing polarization in the yellow, blue, and ultraviolet spectral regions is seen as the visual light increases, with the largest polarization observed halfway between the minimum and maximum light (as we shall detail for *o* Cet below), whereas for the semiregular, V CVn, the largest polarization in the yellow and blue spectral regions is observed at minimum light (Serkowski, 1971). In the case of this latter star, the polarization in the B filter suddenly increases by more than a factor of 1.5 between phases 0.6 and 0.8 (Shawl, 1974).

Shawl (1974) notes that the presence of intrinsic polarization is always associated with emission lines in the stellar spectrum. He quotes that a spectrogram of V CVn at phase 0.68 shows no emission and a low polarization, while another one at phase 0.84 shows strong emission and a high polarization. In fact, Hβ emission increases as the polarization increases.

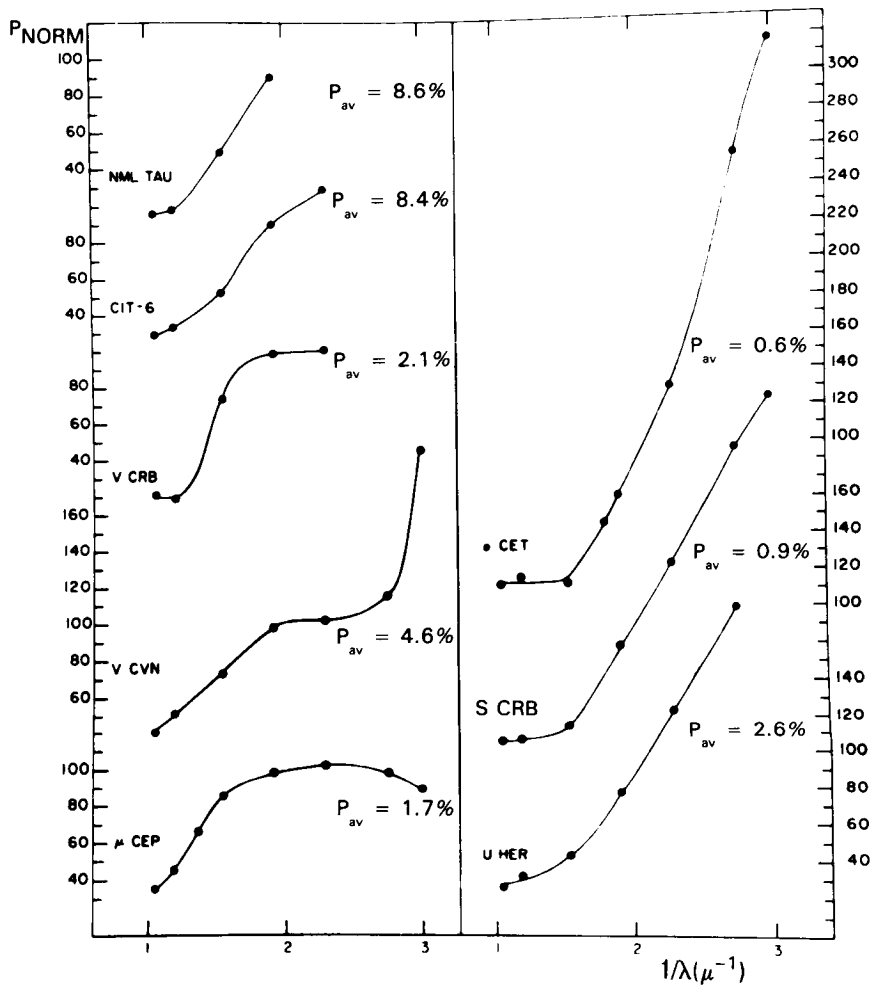


Figure 2-27. Wavelength dependence of polarization for a representative sample of red variables. The observed values were normalized by setting the average polarization through the green and blue filters equal to 100 percent. The actual value of this average is marked to the right side of each curve (from Kruszewski et al., 1969).

In *o* Cet, the polarization begins to increase as soon as the hydrogen lines appear. However, Shawl (1975) reports on L_2 Pup, which presented a very high polarization when the hydrogen emission was barely visible. This is in agreement with Dyck and Jennings (1971), who noted that the existence of intrinsic polarization does not necessarily imply concurrent Balmer emission lines, although it is likely to be found in stars having shown Balmer emission lines.

Dyck et al. (1971) demonstrate a linear relationship between the observed average degree of polarization in the blue and yellow spectral ranges and the amount of excess infrared emission—the latter attributed to reradiation from circumstellar grains (see the section *Infrared Excesses*)—also verified in the near infrared at 1.21 μm (McCall and Hough, 1980). They find that, if the presence of intrinsic polarization is always linked to an infrared excess, the reverse is not necessarily verified, particularly for Miras. In the data of Dyck et al. (1971), some of the Miras show a low mean polarization and

a large infrared excess simultaneously (Landstreet and Angel, 1977). Shawl (1974) discusses that details in the geometrical aspects in the envelope (e.g., clumpy regions of dust) might be the cause of high and low polarization for a given infrared excess in various stars. This is also the opinion of Landstreet and Angel (1977).

The correlation between the intrinsic polarization and the infrared excess (Dyck et al., 1971) is similar for M stars and carbon stars, implying that the polarization mechanism is independent of the chemical composition of grains (Reimers, 1975).

Kruszweski and Coyne (1976) and McCall and Hough (1980) show a clear correlation between the level of polarization and the separation of the 18-cm emission lines in the OH maser stars (i.e., between the expansion velocity and the scattering optical depth of the shell).

Forrest et al. (1975) conclude that there is no evidence that the variations in polarization are caused by a change in the total amount of circumstellar dust. No time variation of infrared flux is observed in stars in which the polarization varies greatly, suggesting a local rather than a global polarization effect (McCall and Hough, 1980). In fact, the infrared excess is interpreted in terms of large-scale emission of grains far around the star, and the variable polarization in terms of more localized scattering and absorption effects in transient regions of gas and dust. However, circumstellar dust at large distances from the star has been brilliantly detected by the discovery of linearly polarized blue continuum light from 15 to 90″ around the supergiant, α Ori (that is, from 550 to 3300 R_* in the frame of reference of Table 2-3), by McMillan and Tapia (1978). Indeed, these authors attribute the polarization to starlight scattered by the dust shell around the central star. The polarization structure is centrosymmetric—except that the polarization map is rather asymmetrical at 15 and 30″ from the star—and is detectable as far as 90″ in the north-east direction. The apparent polarization decreases slowly with angular distance; its directions are generally perpendicular to the radius vectors of the star. Similar, preliminary observations around o Cet reported by Coyne and McLean (1979) show that polarized light extends to at least 30″ (i.e., 1650 R_*) from the central star.

The possibility of observing the circular polarization produced by the scattering of linearly polarized light by circumstellar grains in red supergiants is discussed by Shafter and Jura (1980).

Specific Stars

The Mira, o Ceti. Broadband observations showed that the polarization in the ultraviolet increases abruptly at phase 0.8—coinciding with the first appearance of the hydrogen emission lines (see the section *Emission Lines*)—and then reaches a maximum value at phase 0.9 (Shawl, 1974).

Narrowband observations were obtained around maximum light, from about 3600 to 6200 Å, with additional wavelength regions in the near infrared. They showed small-scale polarimetric structure, detailing a complex dependence of the polarization with wavelength.

McLean and Coyne (1978) studied the phases from 0.94 to 0.97 near the 1977 maximum, with a resolution of about 50 Å. We quote the summary of the most notable features in the polarization spectrum from Coyne and McLean (1979): "(i) virtually no wavelength dependence of θ [less than 10°, but at an unusually high value of 107°]; (ii) increases in the degree of polarization across the Balmer lines, Hα to Hδ [indicating the presence of polarized Balmer-line flux]; (iii) decreases in P across TiO bands, e.g. 4955 Å, 5847 Å, and 7054 Å; and (iv) a general λ^{-4} increase in P into the blue as far as 4500 Å; (v) a wide polarization minimum in the UV at 3775 Å [also called the UV dip] having a sharp rise on the violet side [with no obvious relationship to absorption features in the flux spectrum]" (Figure 2-28, upper panel). Figure 2-29 illustrates the polarization profile at Hβ measured at a spectral resolution of about 0.5 Å; the increase in

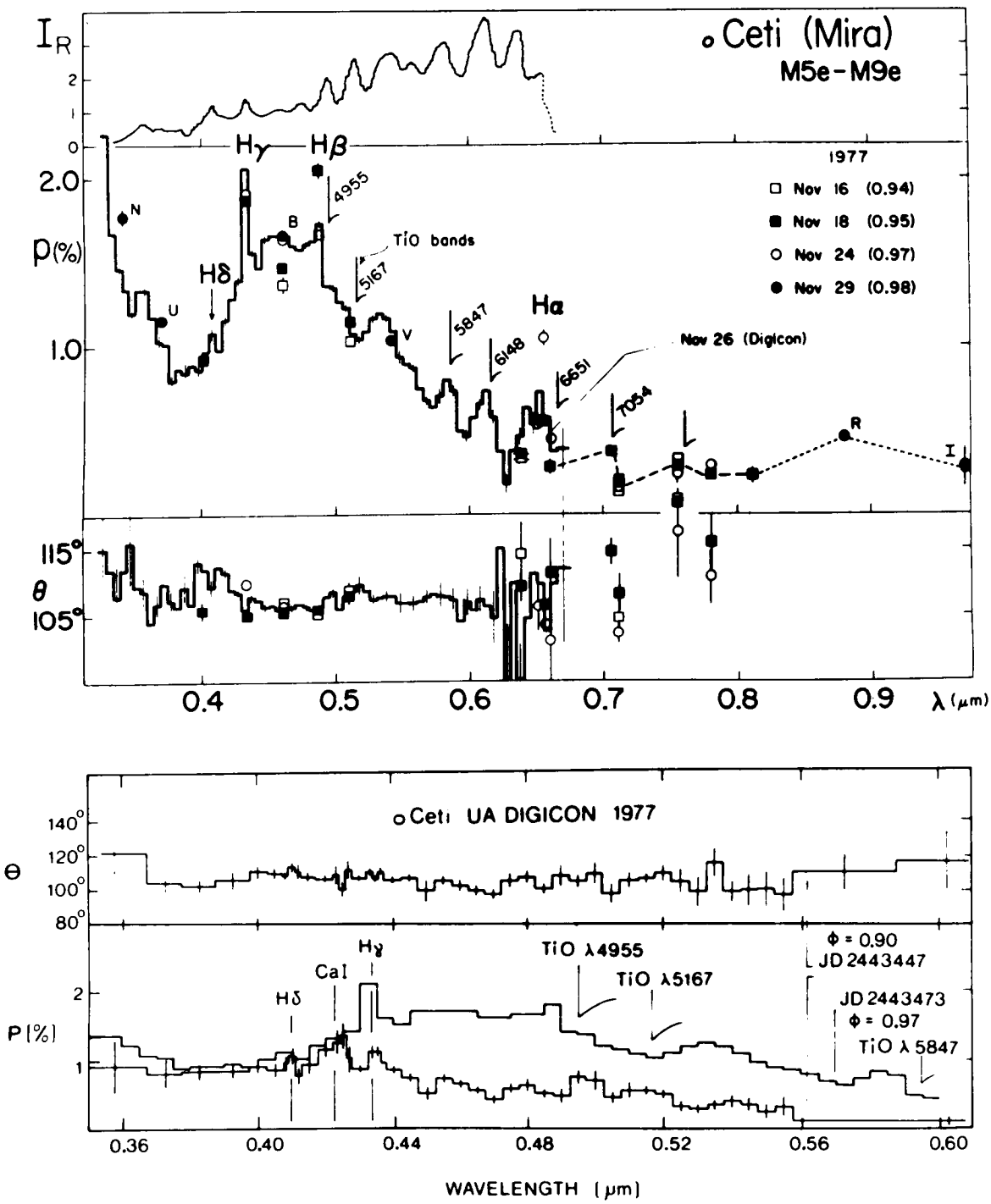


Figure 2-28. Wavelength-dependence of the degree of linear polarization P (in percent) and of the position angle θ for the M Mira, o Ceti, in 1977. Upper panel: around phase 0.95 from data obtained with various technologies (the flux profile I_R is also marked) (from McLean and Coyne, 1978). Lower panel: at phase 0.90 (the polarization data from the upper panel on November 26, 1977, at phase ~0.97 have also been plotted) (from Tomaszewski et al., 1980).

P is up to 6.8 percent, four times the continuum value, although there is no significant change in the position angle across the emission. Figure 2-29 also reports measurements using the 2.3 Å filter that obviously demonstrate the need for very high resolution. With respect to the flux profile, the polarization profile at Hβ is wider and more asymmetric, with its maximum displaced about 0.5 Å to the blue.

At φ = 0.90, 1 month before the 1977 maximum, Tomaszewski et al. (1980) note that they observe a polarization peak at Ca I λ4226 (Figure 2-28, lower panel). No evidence of this peak is seen about 1 month later at φ = 0.97 on McLean and Coyne's (1978) scan, also drawn on Figure 2-29. An earlier phase (around 0.85) reported by Coyne and McLean (1979) showed that the polarization was generally

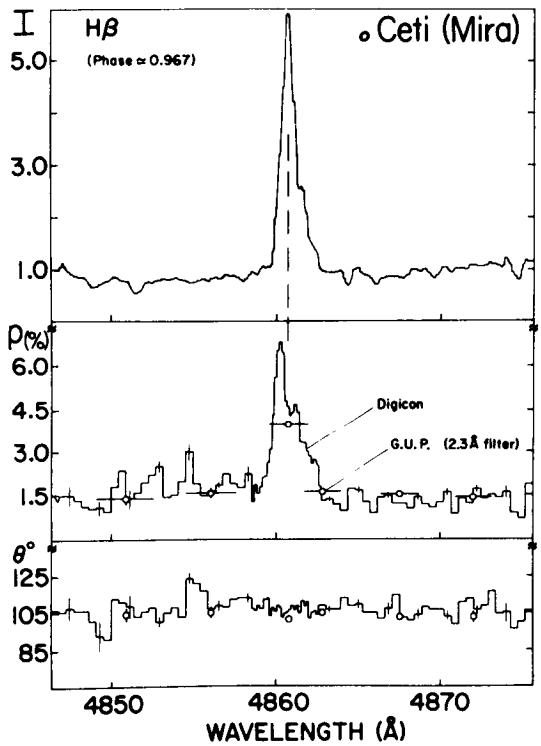


Figure 2-29. Relative flux (I), percentage of linear polarization P, and position angle θ across the Hβ region in the M Mira, o Ceti, on November 24, 1977 (from McLean and Coyne, 1978).

much weaker and that changes across Hβ were not significant. The location of the UV dip varied with respect to its location at phase around 0.95, indicating that the UV dip changes its location with time in the same star.

Around the 1978 maximum (a faint one with $m_v \sim 5.0$), observations at 20 Å resolution are reported by Tomaszewski et al. (1980; Figure 2-30). The conspicuous result is a striking change in the wavelength dependence of the polarization during the rise to maximum. At φ = 0.92, in addition to the general polarization features described by McLean and Coyne (1978) at the 1977 maximum, Tomaszewski et al. again find a peak in the degree of polarization corresponding to the Ca I 4226 Å resonance line, but they do not detect Hβ in either the flux or the polarization spectra. At φ = 1.09 (nearly 1 month after maximum), the sharp polarization peak at Ca I 4226 Å is no longer visible. The peak at Hδ is still visible but reduced. The position angle of polarization is about 45° smaller during the 1978 maximum than during the 1977 one. Shawl (1974) noted from Serkowski's observations that the position angle for o Cet, as well as for R Hya and R Lep, may show alternate high and low values in each cycle, recalling the behavior of the position angle with the light phase in the RV Tauri star, U Mon. However, Landstreet and Angel (1977) comment that most Mira variables show long-term stability of mean position angle, as would be expected if the asymmetries (see the section *Interpretations of the Polarization Observations*) were coupled to a rotation axis.

Around the 1979 maximum, Magalhaes (1980) observes a polarization peak at the Ca I wavelength approximately at phase 0.93 and also at phases 0.08 to 0.09. The striking feature is that the position angle at this wavelength changes dramatically, varying from near 5° at $\varphi \sim 0.93$ to about 170° at φ = 0.08 to 0.09, while staying around 25° in the other wavelengths.

As concerns other Mira variables observed around maximum light, we cite the observations of Landstreet and Angel (1977) about R Boo, RU Her, U Her, and R And; they detect

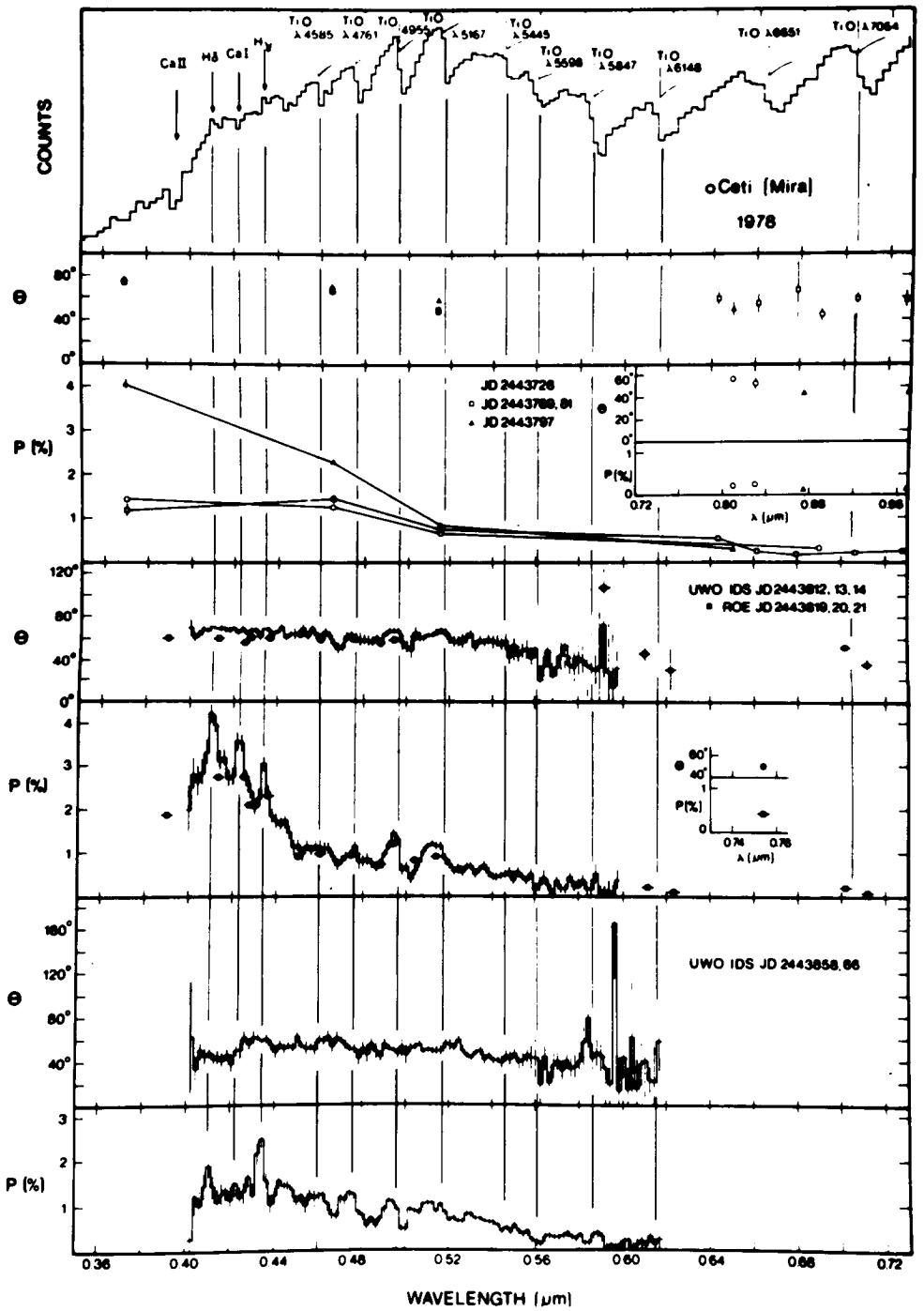


Figure 2-30. Wavelength dependence of the degree of linear polarization P and of the position angle θ for the M Mira, o Ceti, around the 1978 faint maximum. The first section is a flux spectrum in which the positions of the strongest spectral features are indicated by vertical lines. The remaining sections are divided into three panels according to phase—Panel 1: φ = 0.70, 0.80, 0.88; Panel 2: φ = 0.92 (IDS data) and 0.94 (ROE data); Panel 3: φ = 1.09 (from Tomaszewski et al., 1980).

a significant variation in the percentage of polarization peaks coinciding with molecular and atomic absorption features. This behavior has also been studied in the other Mira variables, R Car and R Cen, by Codina-Landaberry and Magalhaes (1980); they see changes across the TiO λ6159 band in R Car and R Cen that are decreases in percentage of polarization *not* accompanied by significant position angle changes. In contrast, in R Boo and U Her, Landstreet and Angel (1977) observe clear variations of about 20 to 30° in position angle across the strongest absorption features longward of 5500 Å. Coyne and McLean (1979) notice that the location of the UV dip varies from star to star.

Because the carbon stars have rarely been subject to polarization measurements, the observation of R Lep, a carbon Mira, is of special interest. This star was observed by Landstreet and Angel (1977) at minimum light (φ = 0.49). The polarization spectrum is nearly featureless, but a sharp change of position angle is observed at the Na I D lines.

The Semiregular Variable, V CVn. Important clues for the interpretation of the observed polarization have been extracted from V CVn, especially through two sets of observations by Coyne and Magalhaes (1977, 1979). In this star, the wavelength dependence of the polarization, $P(\lambda)$, in the blue-violet range strongly varies with time from 2 to 8 percent. The last remarkably large percentage often, but not always, coincides with minimum light. Relevant features of the $P(\lambda)$ curve are: (1) an increase of the polarization near Hβ with a shift of the polarization peak to shorter wavelengths as the polarization in the visual increases from about 2 to 8 percent; (2) a rising of the continuum polarization in the UV at the high-polarization phases, following a wide minimum at about 3800 Å or UV dip (also noted in *o* Cet, see above; Figure 2-31); (3) a change with time of

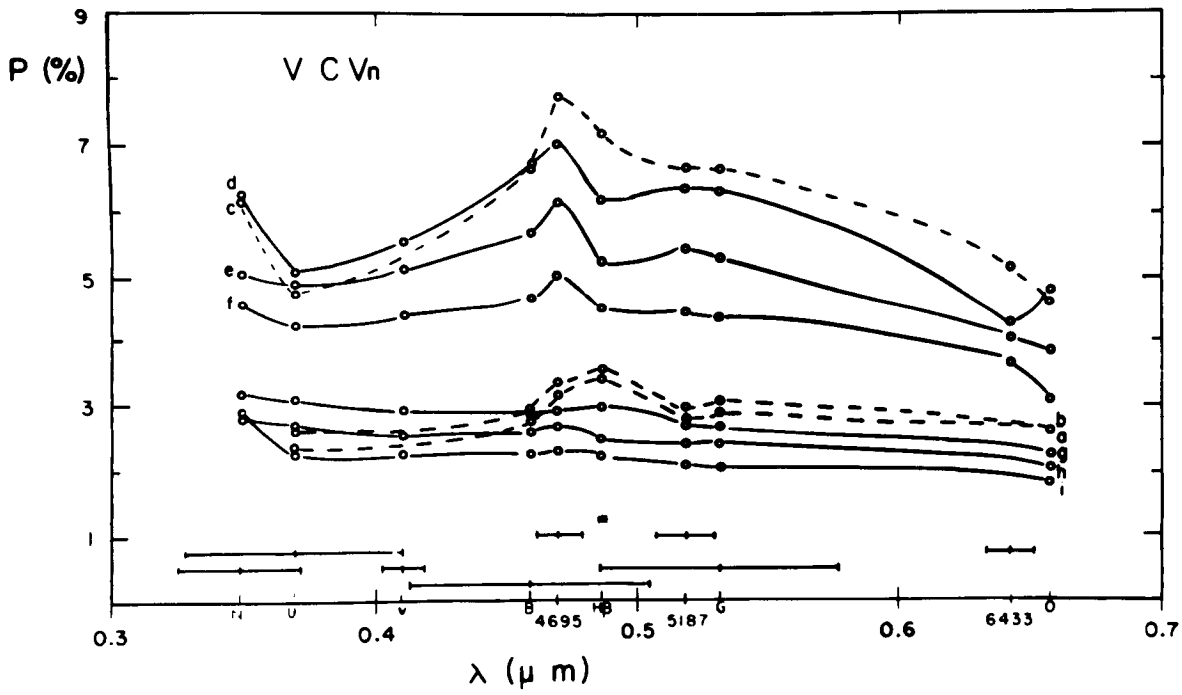


Figure 2-31. Temporal changes in the wavelength dependence of the polarization in the semiregular M star, V CVn, in 1976: (a) February 19–23, (b) February 25–26, (c) April 8–11, (d) April 22–28, (e) May 7–8, (f) May 14–18, (g) June 5, (h) June 13–14, (i) June 23 (from Coyne and Magalhaes, 1977).

the ratio of the polarization in the Hβ region to that in the adjoining continuum; it is less than one at the high-polarization phases and about one at the lower polarization phases; and (4) across the TiO bands, a clear dependence of the change in polarization across the 4955 Å band for which *increases* at times occur (see Figure 1 in Coyne and Magalhaes, 1979) and are seen with smaller amplitude across the 5167 Å band; otherwise, there is no observed change in the polarization greater than ±0.1 percent across any of the other TiO bands. There is virtually *no* change in the polarization angle with time.

Other semiregulars, such as S Lep and L_2 Pup observed by Codina-Landaberry and Magalhaes (1980), are also known to show changes at the time of observation (i.e., decreases) across at least one of the two TiO bands studied. S Lep shows changes across the TiO band at 4761 Å; L_2 Pup shows changes across the TiO bands at 4761 and 6159 Å and across the Ca I 4227 Å line for which the position angle at this wavelength also strongly differs from the one expected from the small gradual rotation position angle with wavelength. On the other hand, there is *no* significant position angle rotation at the TiO bands.

The Supergiant Semiregular Variables, μ Cep and α Ori. For μ Cep, unlike the previous stars, the wavelength dependence of polarization shows variations in *both* degree and position angle across *each* of the observed TiO bands (McLean, 1979; Coyne and Magalhaes, 1979). This makes us expect a different origin of polarization from that found in V CVn, all the more since a λ^{-4} curve never occurs for μ Cep, as already noted in the section *Overall Results on Polarization*. A UV dip is also present in this star (Coyne and McLean, 1979).

Time variation of the change in polarization has proved to be remarkably large in recent years. Prior to 1980, this star was not known to present large-scale polarization. The measurements in wide bands by Coyne and Kruszewski (1968) showed a polarization varying from about 0.2 to 2.5 percent. Narrowband observations in October 1976 (McLean, 1979) also reported an increase in percentage from red to blue of about 0.7 to 1 percent. Furthermore, in June 1979, the polarization measured by Coyne and Magalhaes (1979) belonged to this range of variation. However, from August to December 1980, wideband polarization measurements showed a surprisingly high percentage—around 4 percent (Arsenijevic et al., 1980; Hayes, 1981a). Then, measurements from August (P ~ 2.47 percent) to December (P ~ 1.85 percent) 1981 indicate that a remarkable decrease occurred in the course of about 1 year (Hayes, 1982). The polarization angle did not change significantly in 1980 and in 1981. We are not aware of spectroscopic observations during that time; however, if such observations exist, it would be interesting for the interpretation of such an event to determine whether the hydrogen emission (Balmer alpha is observed near maximum light in μ Cep; see the section *Hydrogen Emission Lines*) was barely visible when the polarization was high at 4 percent, as is the case in L_2 Pup.

For α Ori, we choose to present two sets of data, each being quasi-continuous over several years: (1) multicolor observations from 4250 to 8250 Å during seven observing periods from December 1973 to February 1975 (Tinbergen et al., 1981); (2) wideband (B filter) measurements over four consecutive observing seasons during 1979–1983 (Hayes, 1980, 1981b, 1984); as an example, the 1979–1980 and 1980–1981 observations are reported in Figure 2-32 (upper panel) as plots of the degree and angle polarization against time (Schwarz and Clarke, 1984). Figure 2-32 (lower panel) reports the polarization data as a function of wavelength from 4500 to 8000 Å, by Tinbergen et al. (1981), at various dates, in a presentation again due to Schwarz and Clarke: the degree of polarization shows a monotonous increase with decreasing wavelength from 6600 to 5000 Å, corresponding well to a λ^{-4} law. Furthermore, for a given observing time, when the polarization in the various filters from 6600 to 5000 Å is plotted in the Stokes vector diagram, it falls on a straight line. All these facts suggest that a

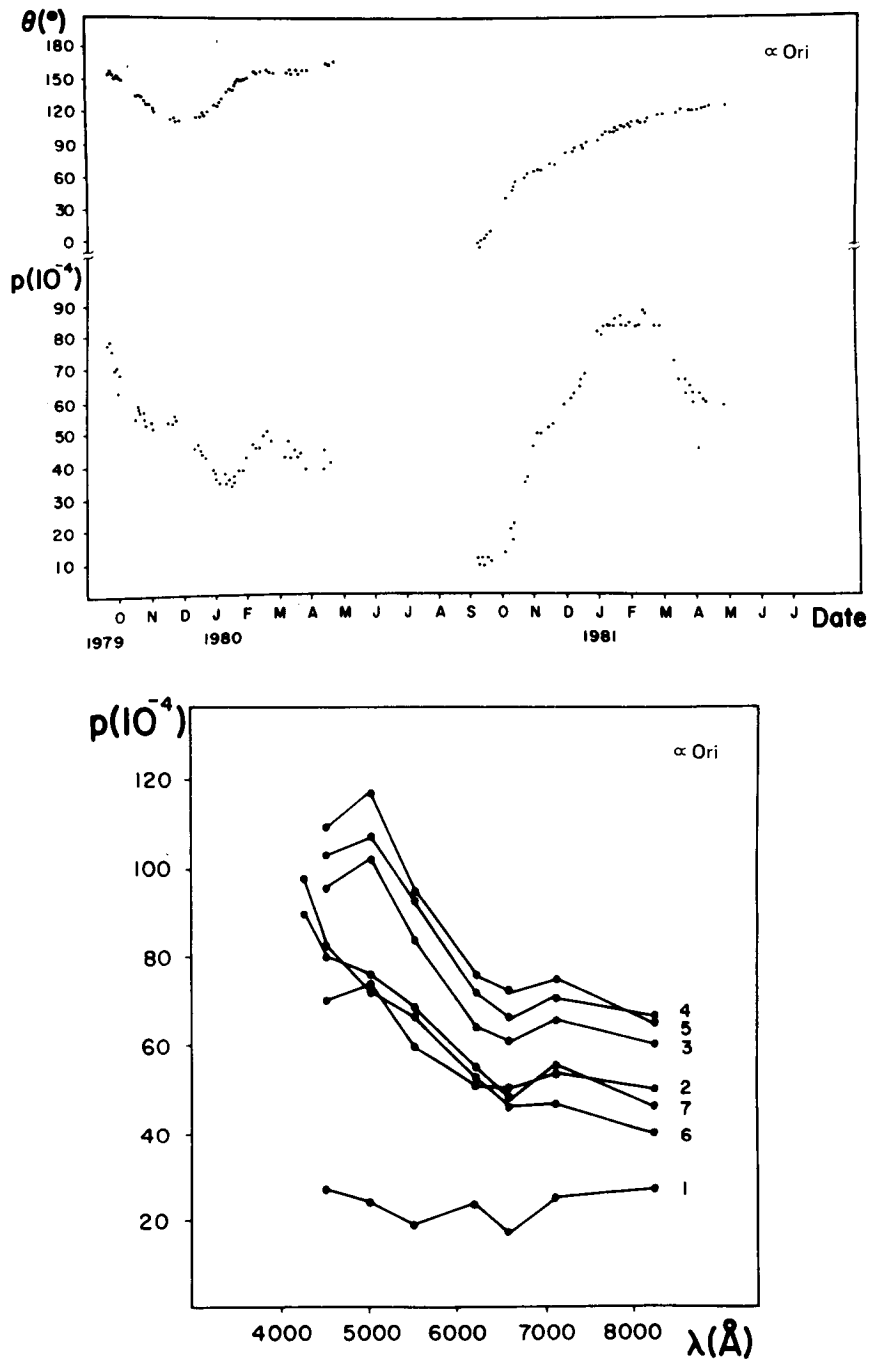


Figure 2-32. The polarization in the M supergiant, α Ori. Upper panel: Hayes's polarimetric data as plots of P and θ_P against time from 1979 to 1981 (the units for P are 10^{-4} (i.e., 0.01 percent) while θ_P is in degrees in the equatorial frame). Lower panel: Tinbergen et al.'s data plotted as P(λ) curves for different dates of observation: (1) 01.12.73; (2) 01.02.74 to 06.02.74; (3) 19.02.74 to 24.02.74; (4) 27.02.74 to 06.03.74; (5) 07.03.74 to 14.03.74; (6) 23.08.74 to 26.08.74; (7) 04.02.75 to 08.02.75 (from Schwarz and Clarke, 1984).

single physical process is responsible for the polarization in the quoted wavelength range.

The observations displayed in Figure 2-32 emphasize time variations. From the upper panel, the important points noted by Hayes (1980, 1981b) are: (1) changes in the position angle; (2) an almost complete reversal of the direction of polarization that happened between October and December 1979; and (3) the occurrence of two distinct events suggested by differences in the morphology of the 1979–1980 and 1980–1981 observations. Significant changes take place on time scales of about one to several months. Also, changes in the stellar brightness distribution over time scales correlated with changes in the Hayes polarization measurements are reported by Goldberg et al. (1981).

Finally, it is worth noting that Coyne and McLean (1979) do not find clear evidence of polarization structure in high-resolution Hβ data and 50 Å scans of the yellow TiO bands in α Ori. In fact, Clarke and Schwarz (1984) obtain a variation of the degree of polarization in the TiO absorption features on 50 Å resolution spectra; the polarization is less than 1 percent.

In addition, we recall that polarization up to 90″ from the central star has been observed by McMillan and Tapia (1978). (See the section *Overall Results on Polarization*.)

Interpretations of the Polarization Observations. The wavelength dependence, as well as the time variations of the position angle and of the percentage, are characteristics of the intrinsic polarization. It is now admitted that their interpretation may require the combination of several mechanisms in the same star; for example, the fact that the observed variations in polarization across absorption features sometimes occur primarily in P and sometimes in θ suggests that in some cases two different polarization mechanisms (having different principal axes) are competing to produce the observed polarization (Landstreet and Angel, 1977). Also, besides the mechanisms of the polarization, intrinsic polarization can be expected only if there is a concomitant asymmetric atmosphere. In brief, even if the physical processes underlying the observations are not yet understood in detail, theoretical models put forward to explain the origin of polarization are linked to "the scattering properties of either asymmetrically distributed circumstellar grains and/or the photospheric gas," as concisely formulated by Magalhaes (1981). The merit of the higher wavelength resolution observations with regard to the large-band data was to show that dust alone is not accountable for the intrinsic polarization, but that a contribution from the photospheric gas may be required.

The various sources of asymmetries for a nonuniform brightness distribution over the photosphere may be: (1) geometrical effects of nonradial pulsation; (2) pole-to-equator temperature gradients or small variations of temperature over the stellar surface; for example, coming from cooler regions of grain formation or from hotter spots at the surface (the excess brightness near the limb breaks the azimuthal symmetry and results in net residual linear polarization); (3) giant convective cells according to the Schwarzschild (1975) hypothesis; and (4) active regions on the stellar surface. As for the envelope, its likely clumpiness would make it appear asymmetric when viewed from any angle. Finally, asymmetries produced by the dynamical effects of a binary system may exist (as is probable for α Ori as discussed below). McCall and Hough (1980) point out that such nonuniformities not only provide highly asymmetric scattering geometries, but also cause anisotropic illumination of the dust envelope.

Details on the origin of the continuum polarization, as well as on the UV dip—probably due to absorption by the numerous lines around 4000 Å—have been thoroughly developed in the Coyne and McLean (1979) review. In the following, we discuss the up-to-date theoretical models favored for explaining some specific observations described above. (It would thus be most interesting to have polarization measurements in the corresponding region in N-type carbon stars which exhibit a more drastic decrease in flux shortward of 4000 Å.)

Causes of Polarization Variations Across Molecular Absorption Bands or Atomic Lines. On the basis of the observations in V CVn, Coyne and Magalhaes (1979) suggested that the time variations in the polarization across TiO absorption bands (with no change in the polarization angle) support the model of Harrington (1969). In this model, the radiation emitted into the line of sight from near the stellar limb of the pulsating atmosphere is polarized by Rayleigh scattering. (The polarization is largest near the maximum expansion.) According to Magalhaes (1981), who combines Tsuji's (1978a) model atmosphere computations for M stars with Harrington's model, it is indeed relatively small changes in the ratio of absorption to scattering due to variations with time in the photospheric optical depth that produce the observed polarization changes, particularly verified across the 4955 Å band in V CVn. Thus, as emphasized by Coyne and Magalhaes (1979): "the time dependence of the polarization in V CVn is fundamentally connected to the pulsation cycle and to photospheric parameters which vary with the pulsation cycle...namely: temperature, extent, ratio of absorption to scattering, variation of source function, molecular constituents and their energy states etc." Increase (such as in V CVn) or decrease (such as in S Lep, L_2 Pup, or *o* Cet) in the bands is related to the optical depths at which the Rayleigh scattering (mainly by atomic and molecular hydrogen) dominates over the absorption (mainly by TiO and H^-). Magalhaes (1981) writes: "In certain cases, this region is situated too deep in the atmosphere [as when later spectral types are considered], in which situation only decreases should be expected. In others, the relevant region may be found nearer to the surface so that either decreases or increases may be expected." Incidentally, Codina-Landaberry and Magalhaes (1980) remark that small solid particles could well exist in the very outer atmospheric layers and partly contribute to scattering in the visible region.

For Coyne and Magalhaes (1979), the more likely source of the asymmetry required to give a net polarization integrated over the disk necessitates the consideration of the star as a rotating one: the asymmetry is produced by systematic pole-to-equator temperature differences due to pole-to-equator gravity differences. An equatorial rotational velocity of about 11 km/s (rotational period ~7 years), which is a reasonable value for red giants (Allen, 1973), is implied.

The high polarization across the Ca I absorption line at 4227 Å in L_2 Pup or *o* Cet would also come in support of the photospheric mechanism as suggested by Codina-Landaberry and Magalhaes (1980). Furthermore, remember that the position angle at this wavelength is very different from the value for the continuum polarization and even from that in the TiO bands. The authors just quoted imagine that the necessary remarkable asymmetry at this wavelength might be caused by an unevenly distributed Ca I across the stellar surface.

An alternative application of Harrington's (1969) model is made to *o* Cet by Tomaszewski et al. (1980). These authors interpret the observed polarization as effects of Rayleigh scattering in an atmosphere which is not uniformly bright, owing to one large-spot region near the limb which is hotter and brighter than the rest of the photosphere. They explain local decreases through the strongest TiO absorption bands and polarization increases in the weakest bands as follows: "At wavelengths where absorption is strong, photons are likely to have last interacted with photospheric material by absorption and reemission (which usually results in no polarization) rather than by scattering. Thus, since local emission is largely unpolarized, the integrated radiation will be as well."

In the supergiant, μ Cep, the polarization varies in both degree and position angle across each of the TiO bands. McLean (1979) suggests two competing polarization mechanisms: a photospheric Rayleigh scattering and Mie scattering from circumstellar grains, the former being suppressed at wavelengths at which strong molecular absorption dominates. However, Coyne and Magalhaes (1979) attribute the polarization only to Mie scattering from grains in

an extended asymmetric envelope; the smaller polarization observed in the continuum with respect to the TiO bands might be due to a depolarization of the light undergoing a larger path length. The authors propose the following model: in the TiO bands are mainly seen the outer regions of an extended asymmetric dust-scattering envelope in which dust and gas are well mixed and which is characterized by given mean grain size and scattering geometry; in the continuum are seen deeper regions of the envelope characterized by different grain sizes and another scattering geometry. In fact, if there is a systematic increase of mean grain size with distance to the star, Mie scattering calculations show that the plane of polarization rotates by 90° beyond a certain grain size for a given wavelength. Moreover, the systematic change in scattering geometry of the envelope with distance might be caused by changes in the alignment of elongated grains.

The drastic rapid change in continuum polarization observed in 1980 in μ Cep helps to specify the source of the polarization. According to Hayes (1982), the observed time scales of variability give evidence that the polarization changes were not linked to a mass-loss event as it traversed the extended circumstellar envelope (1.8 years might be necessary for matter to traverse one stellar radius in μ Cep). Rather, they are consistent with a continuum polarization originating in the lower atmosphere where the survival of grains might be probable (Draine, 1981; Schmid-Burgk and Scholz, 1981). In addition, the polarization variations might be indirectly produced through photospheric processes that control time changes in the anisotropic illumination of the polarizing circumstellar material (e.g., the waxing and waning of one or, at most, a few large-scale convective cells on the stellar surface).

The case of α Ori will be discussed in the following section.

In o Cet, as well as in other Mira variables, the flux is polarized in the Balmer emission lines. These lines originate in the ionization front of the shock wave traveling through the stellar atmosphere. (See the section *Atmospheric Kinematics*.) According to Feofilov (1961), this ionization zone also produces Lyman photons which are the polarizing agents of the Balmer line flux (McLean and Coyne, 1979; Svatos and Solc, 1981). However, the emitting region must not be spherically symmetric about the star. To circumvent this difficulty, Svatos and Solc argue for a magnetic field transverse to the line of sight as a more probable agent of the high polarization degree in the Balmer lines.

The α Ori Case: Is a Binary Nature Accountable for Its Polarization Changes? Ordered (as opposed to stochastic) polarization changes appear over the course of each of four consecutive observing seasons in α Ori (Hayes, 1984). As Hayes already proposed for μ Cep, the time scales of the changes suggest that the latter are a manifestation of the waxing and waning of large-scale convective cells at or near the photospheric surface. Tinbergen et al. (1981) also adopt such an explanation. Schwarz and Clarke (1984) and Clarke and Schwarz (1984) model photospheric Schwarzschild's convection cells (hotspots) to give account for the observations of Hayes and Tinbergen et al. Goldberg et al. (1981), reconstructing the image of α Ori observed by speckle interferometry in 6500 Å continuum radiation on February 3, 1981, find an asymmetry due to an unresolved bright feature near the southwest limb at position angle 208°; they lend support to the Hayes model, assuming the bright feature to be a convective photospheric cell. Since the polarization resumed its variation in October 1980 (see Figure 2-32, upper panel), these authors conjecture that a bright feature developed in September–October 1980 on or near the stellar limb at position angle 208° and grew in luminosity until around the end of December 1980 when the integrated visual light curve begins a steady decline. They support their conjecture that the asymmetry needed for a net polarization is due to a convective cell by the fact that on February 1, 1981, the angle of the plane of polarization was within 5° of being at right angles to the direction of the bright spot. They interpret the

evolution of the cell in relation to the observed polarization degree in the following manner: "The progressive increase in the angle of the plane of polarization before and after February 3 implies either that the bright feature was moving around the limb, which seems unlikely, or that light from the surface feature was being scattered by material in motion above the limb and changing its orientation with respect to the active region." However, Karovska (1984) contests these two interpretations. She remarks that, due to the increase observed in the polarization angle from, say, November 17, 1980, to April 28, 1981 (i.e., $\Delta\theta = 52°$), the bright feature ought to have a proper motion on the stellar disk characterized by a too high velocity. Karovska also applies the remark to an eventual scattering matter in motion above the stationary cell. She suggests that the unresolved bright feature observed by Goldberg et al. (1981) is a companion star near α Ori (see the section *Geometrical Shell Expansion*) that might account for the observed changes in polarization. The Hayes data show that the polarization degree strongly increases from the end of 1980 to the beginning of 1981. During this period, the companion might be embedded in the dusty patch observed by Roddier and Roddier (1983; see the section *Geometrical Shell Expansion*). The scattering dust, together with the companion position, might favor the increase in polarization. We suggest that phase-locked polarization variations in the Stokes parameters (Q, U) frame should help to decide on the α Ori binarity. However, the problem might be confused by the presence of another, farther companion.

The Magnetic Field Hypothesis Applied to Mira Stars. Svatos and Solc (1981) recognize that grains—dirty silicates—exposed to short-wavelength radiation might be responsible for the polarization in *o* Cet. These authors conclude that Mie scattering in an asymmetric envelope cannot explain the observed high degree of continuum polarization because, in particular, only low departures from spherical symmetry (less than 15 percent) have been found by Speckle interferometry by Labeyrie et al. (1977). Thus, just as for explaining the polarized Balmer flux, they call on a magnetic field. Its global value (about 150 gauss) is chosen to be sufficient for obtaining the particle orientation. The transfer of the signal that triggers the polarization is by radiation because it seems more reasonable to the authors that "the location of dust is far from the place where storming processes due to stellar pulsation occur." The source of the grain irradiation energy is surface magnetic flares (or magnetohydrodynamic (MHD) shock waves). The grains irradiated continuously due to flares are responsible for the polarization observed over the entire cycle.

The cyclic variability of the degree of polarization is due to changes in irradiation of the amorphous silicate grains due to changes in their optical properties, linked to chaotic flare-like events (Svatos, 1980). Particularly, enhanced polarization degree is caused by the increase of the imaginary part of the refractive index.

On the other hand, UV emission in the continuum and in lines in *o* Cet is observed from the IUE satellite before the maximum visual light, showing that UV radiation also lies in the ionization front of the shock wave, according to the model of Hinkle and Barnes (1979a). So, this further irradiation acts at phase 0.8 where the shock wave rises in the photosphere, explaining the observed UV sudden enhanced continuum polarization at that time. Incidentally, the temperature of irradiated grains increases, causing the enhanced 10-μm flux at this phase. (See the section *Time Variability of Infrared Excesses*.)

Finally, Svatos and Solc (1981) distinguish three types of polarizing silicate grains by looking to Shawl's (1975) observations in various filters; some particles scatter in N and U colors, others in B, G, and O, and the last ones in R and I colors. Consequently, they propose the model envelope for Miras, shown in Figure 2-33, that completes the model by Hinkle and coworkers from the molecular gas. (See the section *Photospheric Kinematics*.) Three regions

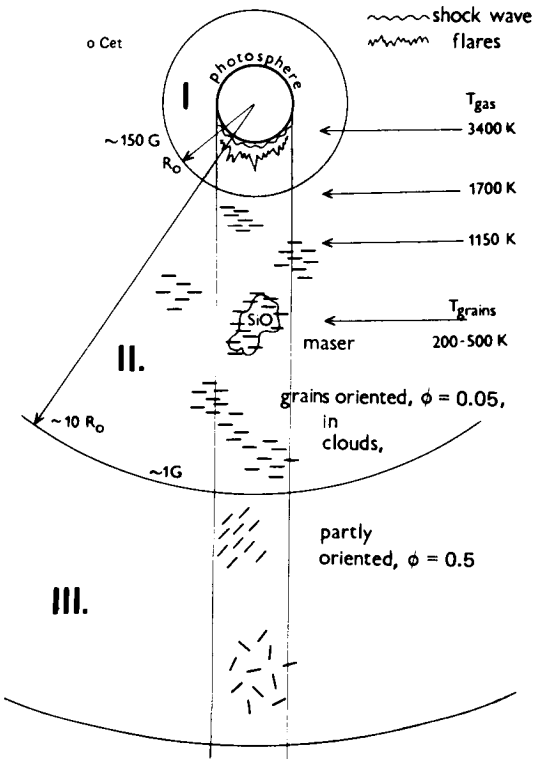


Figure 2-33. Schematic representation of dust in the extended atmosphere of Mira variables submitted to a magnetic dipole field assumed to be perpendicular to the plane of drawing. The various T_{gas} reported on the figure represent the CO, OH, and H_2O gaseous regions described in Hinkle and Barnes's (1979a) shock-wave model applied to R Leo (also see the section, Further Probes of the Pulsating Photosphere). R_o is the measured diameter in the blue color and the TiO bands by Labeyrie et al. (1977); φ is the grain radius in μm (from Svatos and Solc, 1981).

are defined. Region I is the region of gas; regions II and III (which have a cloudy structure, lowering the value of the global magnetic field by enhancing it locally in the dust clouds) mainly contain the silicate grains which become bigger and bigger—by impurities sticking on them as they move away from the star (Draine, 1981)—i.e., more and more efficient from UV to near IR to reproduce the P(λ) behavior. In region II, where the 800 K quasi-stationary gas layer (which is at the origin of grain formation with a resulting outward acceleration) is located (see the section *Summary: Structure of Expanding Gaseous Envelope*), there are "perfectly" oriented elongated grains due to paramagnetic relaxation (Dolginov and Mitrofanov, 1977); these grains are responsible for the relatively large continuum polarization (1 to 4 percent) in the visible. (They polarize at B, G, and O wavelengths mainly with a λ^{-4} law.) In region III, which is far from the star, the grains are partly oriented as they suffer both field and radial orientation and produce less polarization. (They polarize in R and I wavelengths with a nearly λ^{-1} law.)

The systematic change in alignment of elongated grains with distance from the star (i.e., change in scattering geometry) has already been evoked by Coyne and Magalhaes (1979) as a likely cause of the interaction of stellar winds on magnetic fields. Dolginov and Mitrofanov (1977) study the influence of magnetic fields of various strengths on the orientation mechanism of the particles lying in the outflow of gas and dust (either paramagnetic relaxation or the relative motion of the dust and the gas) and, consequently, the percentage of polarization to expect.

Although dust might be the main polarization mechanism in Miras, the polarization structure (decrease) in the TiO bands (without any significant change in θ) shows that at least a part of the polarization originates in the stellar atmosphere, possibly following the photospheric scattering mechanism developed above for V CVn. However, if the grains are outside the region of TiO formation, decreases in polarization across TiO bands might be caused by the great optical depth of these bands (Coyne and McLean, 1979).

Conclusion: The Magnetic Field Frame

To conclude, we comment on the influence of magnetic fields on the outer layers of Miras presented by Svatos and Solc (1981). They propose what likely happens to the dust above the

800 K stationary layer. Let us remember that, concerning o Cet, dust has been detected up to at least 30'' (i.e., 1650 R_*) through polarization measurements (Coyne and McLean, 1979).

Svatos and Solc (1981) superpose flares on the photospheric shock waves. These flares are necessary to produce irradiation of the dust grains and to account for the variable degree of polarization. However, flare-like activity supposes erratic strong intensification of Balmer lines, Ca II lines, and UV continuum (see Rodonò, this volume). Rather, we favor magnetic waves (more precisely, acoustic slow-magnetic shock waves) that travel along magnetic flux tubes (Leibacher and Stein, 1981) and are able to heat magnetic regions, particularly the dust clouds assumed by Svatos and Solc. These waves dissipate higher up in the atmosphere than the photospheric shock waves because they have a longer period. Moreover, it might be that, in the higher layers of the atmosphere, the variability in emergence and decay of the magnetic field dominates (i.e., temporal changes in magnetic field strength are expected there). Such magnetic waves also appear to be very attractive for explaining the erratic behavior of chromospheric emission lines in some carbon stars (Querci and Querci, 1985a; see also the section *Atmospheric Kinematics*).

In support of the magnetic presence, besides the first attempt by Donn et al. (1966, 1968) to explain a few percent visual polarization by a magnetic field of 100 gauss acting on submicron graphite disks, Marcondes-Machado (1979) shows that magnetic grains (Fe_3O_4), which are probably condensing in the envelope of M stars, can be aligned by a minimum magnetic field as low as 1×10^{-5} gauss. (As a purely theoretical example, this author adds that a 10-gauss dipole magnetic field at a stellar surface would give a 0.03-gauss field at 7 R_*.) The produced polarization has a wavelength dependence qualitatively similar to the observed intrinsic continuum polarization; for example, the agreement between the theoretical polarization curve and the g Her observations is striking.

Further support to the presence of a magnetic field might be given by linearly polarized SiO maser emission from R Leo (Clark et al., 1980), where the position angle of polarized emission varies systematically with respect to the spectral-line center. Magnetorotation might be the cause of this change in position angle, with a magnetic field of $9 \times 10^{-3}/\cos\theta$ gauss (where θ is the angle between the magnetic field and the line of sight). Also, magnetic fields are proved by radio flares as observed, for example, on the M supergiant, α Ori (Oster, 1971), on the C giant, V Cyg (Querci et al., 1979), or on the M giants, R Aql (Woodsworth and Hughes, 1973) and α Cet (Boice et al., 1981). Finally, as emphasized by Coyne (1979), polarization might be the best probe of stellar magnetic fields.

Strengths of magnetic fields are poorly known among late-type stars. Direct observations of the Zeeman effect are rare (Babcock, 1958). Nevertheless, there is evidence for time variability in the magnetic fields; this variability may be partially responsible for the difficulty some authors have had in confirming Babcock's work (see comments by Stencel and Ionson, 1979, and Slovak, 1982). In addition, magnetic fields could have very low strength. We mentioned previously that a few gauss should be sufficient to act on the polarization mechanism. It is encouraging that a stellar magnetometer able to measure longitudinal magnetic fields as small as a few gauss has been assembled by Borra et al. (1984).

As for the mechanism-generating fields in red giants and supergiants, it is still debated. Though these stars have deep convective zones, their angular velocity is much lower than a main-sequence star and the radius to pressure scale-height ratio is of the order of unity (Wdowiak, 1977), making a hydrodynamical dynamo unlikely. First proposed by Levy and Rose (1974) and then reviewed by Wdowiak (1977), magnetic fields could be generated in a rapidly rotating core during helium-shell flash instability, with subsequent rise to the surface because of the buoyancy of the magnetic flux tubes.

GEOMETRICAL SHELL EXTENSION—THE DIRECT APPROACH

We discuss here the "direct" approach to measuring the angular diameter of stars and/or to mapping the distribution of dust and gas in their circumstellar shells. In fact, the approach is not really direct because the definitive results must be extracted from geometrical optics through physical optics (Ridgway, 1981b; Wing, 1979).

Generally speaking, the derived apparent angular diameters assume a stellar disk with uniform brightness distribution and/or a linearly fully darkened disk. Information about limb darkening is required to obtain a "true" angular diameter from the apparent one. The correction factor for limb darkening as a function of wavelength can be calculated from model atmospheres (for example, Manduca, 1979); in consequence, it is limited by the inherent assumptions in the models. A possible observational determination of limb darkening might be reached by multiwavelength measurements through the techniques that yield angular diameters.

The spatial scales of dust distribution and, more generally, stellar angular diameters are provided by lunar occultation techniques or by the numerous interferometry techniques—Michelson or heterodyne spatial or speckle or rotation-shearing interferometry. The use of lunar occultations has led to a rapid expansion in the acquisition of angular diameters for numerous giants (e.g., Ridgway et al., 1979, 1980a; White, 1980). Measurements in visible and near-IR wavelengths (say, up to filter K) are suited for stellar photospheric diameters. Longer wavelengths measure circumstellar shells. Let us mention the importance of stellar angular diameters for the interpretation of stellar spectrophotometry, in particular for the calibration of cool-star effective temperatures (Ridgway et al., 1980b).

Reviews about the techniques and/or their results may be found, for example, in Davis and Tango (1979) and in Johnson and Allen (1981). Here, we choose to present two stars that have been observed at length and that display the state of the art in the "direct" knowledge of their size and structure: (1) one of the most frequently studied stars in high angular resolution astronomy, the M supergiant, α Ori, that teaches the most on a spatial stellar structure, and (2) the prototype of very dusty stars, the carbon star, IRC + 10216. We do not intend to discuss the data in terms of radial density and temperature distributions or mass loss (see Goldberg and Lefèvre, this volume).

The M Supergiant, α Ori

Multimeasurements at various optical wavelengths (for example, from the pioneer interferometric observations by Michelson and Pease in 1920, listed in Tsuji, 1976; in Wilkerson and Worden, 1977; and in Welter and Worden, 1980) evaluate *the photospheric* apparent angular diameter and show its *variability*. A mean value is about 0.″050, with a minimum of 0.″034 and a maximum of 0.″069. From the diameter estimates by Bonneau and Labeyrie (1973) and Welter and Worden (1980), the angular diameter appeared to decrease with increasing wavelength, possibly due to decreasing scattering by dust or molecules with wavelength in the stellar atmosphere (also see Tsuji, 1978b). However, the observations by Balega et al. (1982) and Roddier and Roddier (1983) do not really confirm this trend (within the error bars). Also, the diameter measured in the TiO strong absorption bands and their nearby continuum shows a slight excess of about 0.″004 in the TiO band as an effect of their opacity (Lynds et al., 1976; Balega et al., 1982; Roddier and Roddier, 1983). Finally, we have to bear in mind that α Ori is a variable star. Time variability in the diameter is expected, with minimum radius occurring near maximum light when the photospheric layers are at their maximum compression, and vice versa. This statement was called into question by White (1980), who plots angular diameters of α Ori, directly measured at wavelengths between 0.51 and 0.65 μm, against phase. The trend indicates a rapid increase in the diameter to maximum, followed

by a more gradual decrease to minimum. However, Balega et al. (1982) show that such a variation of diameter with time is not meaningful within the range of errors; errors in standard deviations of the fitting at the 1σ confidence level largely overlap when the fit to the data is done through a sine or a serrated curve, as well as a horizontal straight line. Also, arguments of Guinan (1984) that the star attains its maximum radius near the time it is brightest remain speculative, waiting for improvements in the determination of effective temperatures for supergiants and particularly for α Ori (for example, Tsuji, 1976; Scargle and Strecker, 1979; Balega et al., 1982).

Observing by heterodyne spatial interferometry at infrared wavelengths suited for determining the extension of *the dust circumstellar shell*, Sutton et al. (1977) find that the dust exists outside 12 R_* from α Ori, while the density of grains is rather low out to there. Bloemhof et al. (1984), observing at 10 μm in February 1983 with a new spatial array instrument, give an effective outer diameter of the dust radiation of about 2.″5 (i.e., 125 R_*) and detect a shell of dust emission at 0.″9 (i.e., 45 R_*) from the photosphere. We recall that circumstellar dust around α Ori has been detected from 550 to 3300 R_* by polarization measurements (McMillan and Tapia, 1978). *Departure from spherical symmetry* of the circumstellar envelope was apparent in the last-mentioned observations and in the dust distribution found by Bloemhof et al., as well as from line profiles off the stellar disk. (See the section *Physical Conditions in Gaseous Shells.*) Such shell asymmetry is also found by Ricort et al. (1981) observing α Ori by speckle interferometry in October 1979, by Roddier and Roddier (1983, 1985) observing by rotation-shearing interferometry in the visible at 5350 Å in November 1980 (see Figure 3 in Lefèvre, this volume), and by Karovska (1984), also by the same technique, in February 1982 in the continuum at 5350 and 6400 Å and on a TiO band at 6207 Å. This set of observations constituted an enormous advance in knowledge of the morphology and the dynamics of the α Ori atmosphere. The main results of the direct mapping are as follows:

1. The curves representing the azimuthal average of the observed fringe visibilities as a function of spatial frequency indicate an important temporal evolution of the radial distribution of the visibility in the envelope, over 28 months and 15 months with respect to Karovska's observations. (Let us recall that the fringe visibility is a measure of the spatial distribution of the radiation from a given source; generally, this radiation consists partly of stellar photospheric emission and partly of CS dust emission.)

2. None of these curves account for a stellar disk with any limb-darkening coefficient, but rather the curves are consistent with a stellar disk surrounded with an envelope of dust scattering the visible light. The stellar disk diameter is estimated to 0.″035 ± 0.″010 by Ricort et al. and to 0.″037 by Roddier and Roddier (1983; uniform brightness distribution), with 85 and 40 percent of total irradiance coming from the stellar disk, respectively. The light scattered by the envelope therefore increased from 15 to 60 percent, respectively, while Karovska finds a decrease to 30 percent 15 months after Roddier and Roddier's observations (also in agreement with measurements made 9 months later in November 1982 by Petrov, as quoted by Karovska, 1984).

3. The reconstructed image of α Ori from a map of fringe visibilities produced by the star in November 1980 shows a stellar disk surrounded with a bright half-moon asymmetric cloud located at about 2.5 R_* (i.e., 0.″05) from the stellar center and about 1 R_* large (Figure 2-34).

4. The modulation of the fringe visibility produced by α Ori on February 1982 reveals the presence of a companion

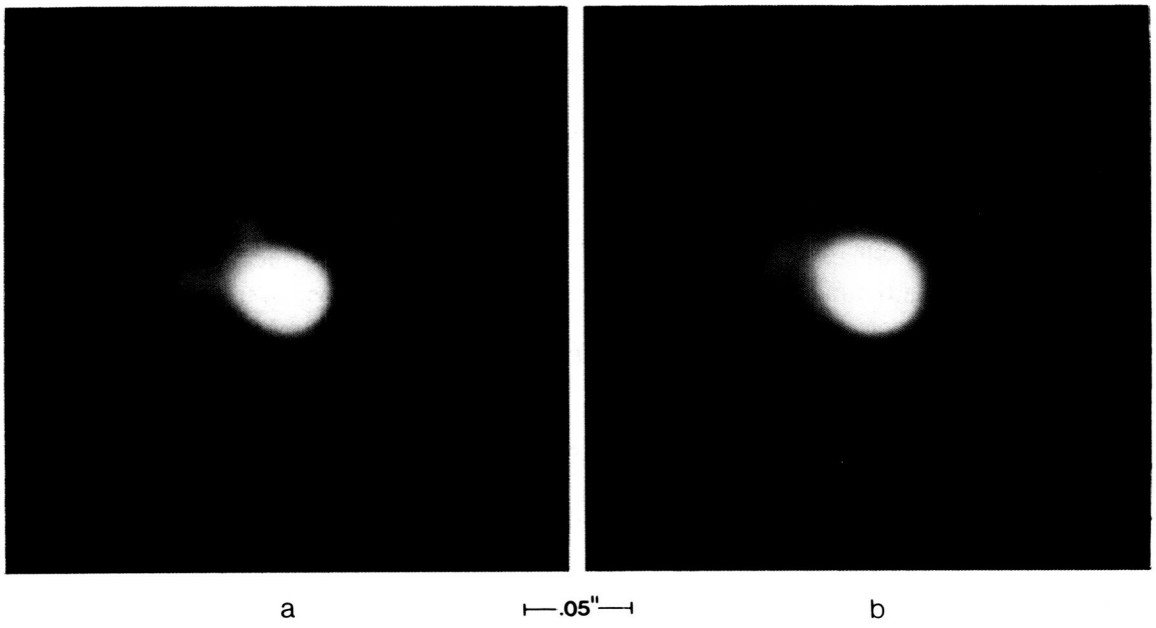


Figure 2-34. Reconstructed images of α Ori from a map of fringe visibilities obtained on November 30, 1980: (a) using the maximum entropy algorithm, (b) with the data extrapolated half-way up to the first zero of the Bessel function (from Roddier and Roddier, 1985).

located at about 0.″4 to 0.″5 (i.e., ~20 to 25 R_*) at 80° (mod 180°) with respect to north in the east direction. The visual magnitude difference is 3.5. The presence of such a companion has also been confirmed by Karovska (1984) on observations by speckle interferometry obtained in November 1982 by another group (C. Aime).

5. A bright feature (much brighter than the envelope) is mentioned by Karovska (1984) to be present in the November 1980 reconstructed image: it is located at 2 R_* from the stellar center (i.e., ~0.″04), at 330° with respect to north (mod 180°). As suspected by Karovska, an identical feature might be present in the reconstructed image observed in January 1976 by Welter and Worden (1980), but at 2.5 R_* and toward the direction 312°5 with respect to north. It may be admitted that this feature is a close companion to the star. In fact, recent analysis of polarization data (Karovska et al., 1985a, 1985b) sustains the existence of such a close companion to α Ori (Figure 2-35). It is also striking that the position angles calculated by Karovska (1984) at the dates of observation by Goldberg et al. (1981; see discussion in the section *Interpretations of the Polarization Observations*) agree with the position angles derived by these authors.

Again, as when interpreting the variability in the chromospheric emission lines (see the section *Atmospheric Kinematics*), we raise the influence of the close companion for explaining the patchy dust shell observed by Roddier and Roddier (1985). Should grains survive at the Lagrangian point L_1? The last is inside the chromosphere, more likely in the low chromosphere where the temperature might allow the Draine (1981) scenario to work to form the dust grains. If the grains are ejected at L_1 at a sufficiently low velocity, a streak of dust might form behind the moving companion during the

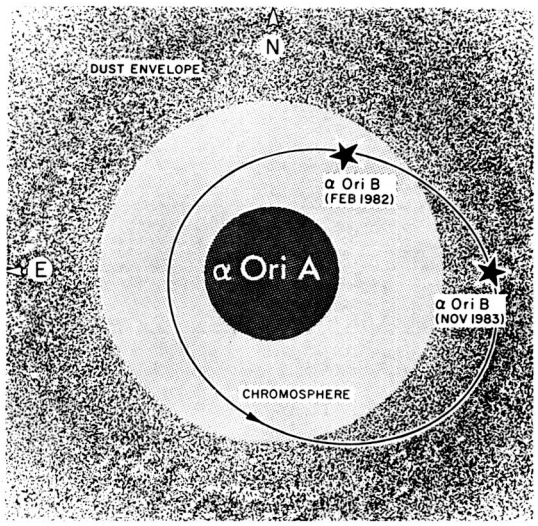


Figure 2-35. Schematic geometry for α Ori system showing the close companion orbiting α Ori. The possible eccentric orbit for the companion is characterized by: P = 2.08 ± 0.05 years, T = 1980.4 ± 0.1; e ~0.35 ± 0.05; i = 30° ± 10°; Ω + ω = 66° ± 10° (from Karovska et al., 1985b).

observed part of its orbit around α Ori and give the half-moon cloud observed by Roddier and Roddier near the stellar surface. The cloud then expands by radiation pressure on the grains such that IR emission is observed at several tens of stellar radii in direct IR mapping by Bloemhof et al. (1984).

The α Ori binary nature is also very attractive for explaining the asymmetries in the shells observed in directions variable with time (see the sections *Physical Conditions in Gaseous Shells* and *Overall Results on Polarization*); it should be the clue to understanding the dust distribution that suggests the involvement of localized and temporary instabilities in the ejection of material from α Ori (Bloemhof et al., 1984). Indeed, more progress in the comprehension of the α Ori dynamic structure is expected, as soon as more information on the companion star(s) is available and more coordinated observations (by spectroscopy, photometry, and polarization) are obtained.

The Dusty Star, IRC + 10216

It is now established that IRC + 10216 is a carbon Mira variable (from 1-μm spectra; e.g., Herbig and Zappala, 1970), nearby (d ~ 200 to 300 pc), luminous (one of the brightest 5- to 10-μm source), heavily enshrouded in an extensive dust envelope of its own making (see Table 1 in Lafont et al., 1982, for the assumed parameters of IRC + 10216). The degree of obscuration is such that all the photospheric stellar radiation is absorbed and reemitted by the dust. Various multiwavelength infrared measurements give indications on the size and shape of the dust envelope and the molecular clouds.

Table 2-5 summarizes data from the literature on the angular extent of the emitting regions. The dust cloud has been mapped up to a radius of 27″ (~1200 R_*), and the CO cloud up to a radius of at least 3′ (8000 R_*). The star is quite asymmetric in its dust shells, with the amount of asymmetry varying with wavelength and radius. *Elliptical contours* are obvious when sufficient position angle coverage is available. At 4.6 μm, the axis ratio b/a is 0.77, while at 0.8 μm, it is equal to 0.4 (Mariotti et al., 1983), with the major axis lying nearly north-south. As for the gaseous emitting regions near the star, we discussed a modeling by Keady et al. (1984) in the section *Summary: Structure of Expanding Gaseous Envelope* (also see Table 2-3). It would be interesting to determine if the scattered light from the gas is as asymmetric as the dust emission by mapping observations in several directions through the center of the star (Beckwith, 1985). Such an available observation, the only one to our knowledge, is from the CO (2–1) emission profile that is circularly symmetric about the center of the star at 6′ (Wannier et al., 1980; Knapp et al., 1982).

It has been suggested that the nonspherical 2.2- to 5.0-μm circumstellar dust geometry could represent a flattened disk viewed at low inclination or be caused by the binary nature

ORIGINAL PAGE IS
OF POOR QUALITY

Table 2-5
Multispectral Spatial Mapping of IRC + 10216

λ	Diameter	R/R_* [a]	R_{cm}	References*
	Dust Emitting Regions			
0.8 μm	φ_{E-W} = 1″	22	1.5×10^{15}	1
	φ_{N-S} = 2″5	55	4×10^{15}	1
2.2 μm	φ_{E-W} = 0″14	3	2×10^{14}	1,2
5 μm	φ_{E-W} = 0″36	8	55×10^{14}	1
2.2 to 5 μm	φ_{N-S} = 0″48	11	7×10^{14}	1,3,4
11 μm	φ [b] = 0″9	20	1.3×10^{15}	1,5
20 μm	φ [b] = <2″5	55	4×10^{15}	1
40 to 250 μm	φ [c] = 0′9	1200	8×10^{16}	6
	Gaseous Emitting Regions			
CO (4.6^{abs}μm)	φ_{N-S} ~1″3	30	2×10^{15}	3
CO (4.6^{em}μm) [d]	φ ~ 4″	90	6×10^{15}	7
HCN (mm)	φ < 40″	<980	$<6 \times 10^{16}$	8
CN (mm)	φ ~ 1′80	2400	1.6×10^{17}	9
CO (1–0)	φ ~ 2′3	3040	2×10^{17}	8,10,11
CO (2–1)	φ_{sph} ~ 6′	8000	5.5×10^{17}	12,13

*References: 1. McCarthy et al., 1980; 2. Selby et al., 1979; 3. Dyck et al., 1983; 4. Mariotti et al., 1983; 5. Sutton et al., 1979; 6. Fazio et al., 1980; 7. Sahai and Wannier, 1984; 8. Wilson et al., 1973; 9. Wootten et al., 1982; 10. Ulich and Haas, 1976; 11. Kuiper et al., 1976; 12. Wannier et al., 1980; 13. Knapp et al., 1982.

Notes:

[a] With d = 200 pc (see comment in Lafont et al., 1982)
(1″ ≡ 3×10^{15} cm ≡ 44 R_* with 1 R_* ~ 970 $R_\odot$ from Keady et al., 1984, and
1 $R_\odot$ = 6.96×10^{10} cm).

[b] Lack of sufficient position angle coverage at high spatial frequencies to investigate an asymmetry.

[c] At a position angle of 151° measured east from north (along the minor axis of the elliptical optical image).

[d] By isolating radiation being scattered resonantly from the gas in the expanding envelope.

of the star (e.g., McCarthy et al., 1980). A close binary system may explain the evidence for a mixed morphology (sphere plus disk) according to Bowers et al. (1983), as well as the large mass-loss rate ($\sim 1.5 \times 10^{-4}$ $M_\odot$ yr^{-1} from Knapp et al., 1982). Also, an ellipsoidal or disk-shaped envelope would generate the larger polarization observed in IRC + 10216 (e.g., Fazio et al., 1980). Such large degrees of polarization have been detected in other dust-enshrouded carbon stars by Cohen and Schmidt (1982). Particularly interesting is the extreme C star, GL 1403, for which these authors find two orthogonally polarized spectral components, implying a dusty equatorial torus and polar scattering lobes. Such a structure favors an evolutionary link between those objects and bipolar nebulae. On the other hand, Bowers et al. (1983) suggest that evolved stars with non-spherical envelopes, which are spatially rare, are influenced by close binary companions, while evolved stars with spherical envelopes (most OH Miras) may be responsible for the optical halos associated with some planetary nebulae.

REFERENCES

Abt, H.A., and Biggs, E.S. 1972, *Bibliography of Stellar Radial Velocities* (Tucson: Kitt Peak National Observatory).

Adams, W.S., and McCormack, E. 1935, *Astrophys. J.*, **81**, 119.

Adams, W.S. 1956, *Astrophys. J.*, **123**, 189.

Allen, C.W. 1973, *Astrophysical Quantities*, 3rd Edition (London: The Athlone Press).

Antia, H.M., Chitre, S.M., and Narasimha, D. 1984, *Astrophys. J.*, **282**, 574.

Arsenijevic, J., Kubicela, A., and Vince, I. 1980, *Inf. Bull. Variable Stars*, IAU Comm. 27, No. 1859.

Avrett, E.H., and Johnson, H.R. 1984, in *Proc. Third Cambridge Workshop on Cool Stars, Stellar Systems, and the Sun*, ed. S.L. Baliunas and L. Hartmann (Berlin, Heidelberg: Springer-Verlag), p. 330.

Ayres, T.R. 1979, *Astrophys. J.*, **228**, 509.

Babcock, H.W. 1958, *Astrophys. J. Supplement*, **3**, 141.

Balega, Y., Blazit, A., Bonneau, D., Koechlin, L., Foy, R., and Labeyrie, A. 1982, *Astron. Astrophys.*, **115**, 253.

Basri, G.B., and Linsky, J.L. 1979, *Astrophys. J.*, **234**, 1023.

Basri, G.B., Linsky, J.L., and Eriksson, K. 1981, *Astrophys. J.*, **251**, 162.

Beckwith, S. 1985, in *Proc. Conf. on Mass Loss from Red Giants*, ed. M. Morris and B. Zuckerman (Dordrecht: Reidel).

Bernat, A.P. 1977, *Astrophys. J.*, **213**, 756.

Bernat, A.P. 1981, *Astrophys. J.*, **246**, 184.

Bernat, A.P., Hall, D.N.B., Hinkle, K.H., and Ridgway, S.T. 1979, *Astrophys. J. (Letters)*, **233**, L135.

Bernat, A.P., Honeycutt, R.K., Kephart, J.E., Gow, C.E., Sandford, M.T., and Lambert, D.L. 1978, *Astrophys. J.*, **219**, 532.

Bernat, A.P., and Lambert, D.L. 1975, *Astrophys. J. (Letters)*, **201**, L153.

Bernat, A.P., and Lambert, D.L. 1976a, *Astrophys. J.*, **204**, 830.

Bernat, A.P., and Lambert, D.L. 1976b, *Astrophys. J.*, **210**, 395.

Bidelman, W.P. 1950, *Astrophys. J.*, **112**, 219.

Bidelman, W.P. 1954, *Astrophys. J. Supplement*, **1**, 225.

Bidelman, W.P., and Pyper, D.M. 1963, *Pub. Astron. Soc. Pacific*, **75**, 389.

Bloemhof, E.E., Townes, C.H., and Vanderwyck, A.H.B. 1984, *Astrophys. J. (Letters)*, **276**, L21.

Boesgaard, A.M. 1973, in *Proc. IAU Colloq. 19, Stellar Atmospheres*, ed. S.D. Jordan and E.H. Avrett, NASA SP-317, p. 158.

Boesgaard, A.M. 1979, *Astrophys. J.*, **232**, 485.

Boesgaard, A.M. 1981, *Astrophys. J.*, **251**, 564.

Boesgaard, A.M., and Boesgaard, H. 1976, *Astrophys. J.*, **205**, 448.

Boesgaard, A.M., and Hagen, W. 1979, *Astrophys. J.*, **231**, 128.

Boesgaard, A.M., and Magnan, C. 1975, *Astrophys. J.*, **198**, 369.

Bohn, H.U. 1984, *Astron. Astrophys.*, **136**, 338.

Boice, D.C., Kuhn, J.R., Robinson, R.D., and Worden, S.P. 1981, *Astrophys. J. (Letters)*, **245**, L71.

Bonneau, D., and Labeyrie, A. 1973, *Astrophys. J. (Letters)*, **181**, L1.

Borra, E.F., Edwards, G., and Mayor, M. 1984, *Astrophys. J*, **284**, 211.

Bouchet, P., Querci, M., and Querci, F. 1983, *The Messenger*, ed. P. Véron, ESO, No. 31, p. 7.

Bowers, P.F., Johnston, K.J., and Spencer, J.H. 1983, *Astrophys. J.*, **274**, 733.

Bregman, J.D., and Bregman, J.N. 1978, *Astrophys. J. (Letters)*, **222**, L41.

Bretz, M.C. 1966, in *Proc. Trieste Colloq. on Astrophysics, Late-Type Stars*, ed. M. Hack, June 1966 (Osservatorio Astronomico di Trieste), p. 166.

Brooke, A.L., Lambert, D.L., and Barnes, T.G. 1974, *Pub. Astron. Soc. Pacific*, **86**, 419.

Brown, A., and Carpenter, K.G. 1984, *Astrophys. J. (Letters)*, **287**, L43.

Buhl, D., Snyder, L.E., Lovas, F.J., and Johnson, D.R. 1975, *Astrophys. J. (Letters)*, **201**, L29.

Buscombe, W., and Merrill, P.W. 1952, *Astrophys. J.*, **116**, 525.

Campbell, M.F., Elias, J.H., Gezari, D.Y., Harvey, P.M., Hoffmann, W.F., Hudson, H.S., Neugebauer, G., Soifer, B.T., Werner, M.W., and Westbrook, W.E. 1976, *Astrophys. J.*, **208**, 396.

Carbon, D.F., Milkey, R.W., and Heasley, J.N. 1976, *Astrophys. J.*, **207**, 253.

Carpenter, K.G. 1984, *Astrophys. J.*, **285**, 181.

Carpenter, K.G., Brown, A., and Stencel, R.E. 1985, *Astrophys. J.*, **289**, 676.

Carpenter, K.G., and Wing, R.F. 1979, *Bull. Amer. Astron. Soc. (Abstract)*, **11**, 419, and private communication.

Cassatella, A., Heck, A., Querci, F., Querci, M., and Stickland, D.J. 1980, in *Proc. Second European IUE Conference*, ESA SP-157, p. 243.

Catchpole, R.M., Robertson, B.S.C., Lloyd Evans, T.H.H., Feast, M.W., Glass, I.S., and Carter, B.S. 1979, *South Africa Astron. Obs. Circ.*, **1**, 61.

Clark, F.O., Johnson, D.R., Troland, T.H., and Heiles, C.E. 1980, in *Proc. IAU Symp. 87, Interstellar Molecules*, ed. B.H. Andrew (Dordrecht: Reidel) p. 543.

Clarke, D., and Schwarz, H.E. 1984, *Astron. Astrophys.*, **132**, 375.

Clegg, R.E.S. 1980, in *Proc. 5th European Regional Astronomy Meeting*, ed. P. Ledoux (Liège, Belgium).

Codina-Landaberry, S.J., and Magalhaes, A.M. 1980, *Astron. J.*, **85**, 875.

Cohen, M. 1979, *Mon. Not. Roy. Astr. Soc.*, **186**, 837.

Cohen, M., and Schmidt, G.D. 1982, *Astrophys. J.*, **259**, 693.

Contadakis, M.E., and Solf, J. 1981, *Astron. Astrophys.*, **101**, 241.

Coyne, G.V. 1979, in *Proc. IAU Colloq. 47, Spectral Classification of the Future*, ed. M.F. McCarthy, A.G.D. Philip, and G.V. Coyne (Citta del Vaticano: Specola Vaticana).

Coyne, G.V., and Kruszewski, A. 1968, *Astron. J.*, **73**, 20.

Coyne G.V., and Magalhaes, A.M. 1977, *Astron. J.*, **82**, 908.

Coyne, G.V., and Magalhaes, A.M. 1979, *Astron. J.*, **84**, 1200.

Coyne, G.V., and McLean, I.S. 1979, in *Proc. IAU Colloq. 46, Changing Trends in Variable Star Research*, ed. F.M. Bateson, J. Smak, and I.H. Urch (Hamilton, New Zealand: Univ. Waikato Press), p. 386.

Coyne, G.V., and Shawl, S.J. 1973, *Astrophys. J.*, **186**, 961.

Davis, J., and Tango, W.J., ed. 1979, *Proc. IAU Colloq. 50, High Angular Resolution Stellar Interferometry* (College Park, Maryland) published by Chatterton Astron. Dept., School of Physics, Univ. Sydney, N.S.W. 2006 Australia.

Deguchi, S. 1980, *Astrophys. J.*, **236**, 567.

de Jager, C., Kondo, Y., Hockstra, R., Van der Hucht, K.A., Kamperman, T.M., Lamers, H.J.G.L.M., Modisette, J.L., and Morgan, T.H. 1979, *Astrophys. J.*, **230**, 534.

Deutsch, A.J. 1956, *Astrophys. J.*, **123**, 210.

Deutsch, A.J. 1960, in *Stars and Stellar Systems, Vol. VI: Stellar Atmospheres*, ed. J.L. Greenstein (Chicago: Univ. Chicago Press), p. 543.

Deutsch, A.J., and Merrill, P.W. 1959, *Astrophys. J.*, **130**, 570.

Dickinson, D.F., Reid, M.J., Morris, M., and Redman, R. 1978, *Astrophys. J. (Letters)*, **220**, L113.

Doherty, L.R. 1972, *Astrophys. J.*, **178**, 495.

Dolginov, A.Z., and Mitrofanov, I.G. 1977, *Sov. Astron.*, **21**(6), 715.

Donn, B., Stecher, T.P., Wickramasinghe, N.C., and Williams, D.A. 1966, *Astrophys. J.*, **145**, 949.

Donn, B., Stecher, T.P., Wickramasinghe, N.C., and Williams, D.A. 1968, *Astrophys. J. (Letters)*, **153**, L143.

Draine, B.T. 1981, in *Proc. Second Workshop on Physical Processes in Red Giants*, ed. I. Iben and A. Renzini (Dordrecht: Reidel), p. 317.

Drake, S.A., and Linsky, J.L. 1983, *Astrophys. J.*, **273**, 299.

Dupree, A.K., Sonneborn, G., Baliunas, S.L., Guinan, E.F., Hartmann, L., Hayes, D.P. 1984, *Future of UV Astronomy Based on 6 Years of IUE Research*, ed. J. M. Mead, R. D. Chapman, and Y. Kondo, NASA CP-2349.

Dyck, H.M., Beckwith, S., and Zuckerman, B. 1983, *Astrophys. J. (Letters)*, **271**, L79.

Dyck, H.M., Forrest, W.J., Gillett, F.C., Stein, W.A., Gehrz, R.D., Woolf, N.J., and Shawl, S.J. 1971, *Astrophys. J.*, **165**, 57.

Dyck, H.M., and Jennings, M.C. 1971, *Astron. J.*, **76**, 431.

Dyck, H.M., and Simon T. 1975, *Astrophys. J.*, **195**, 689.

Eaton, J.A., Johnson, H.R., O'Brien, G.T., and Baumert, J.H. 1985, *Astrophys. J.*, **290**, 276.

Engels, D. 1979, *Astron. Astrophys. Supplement*, **36**, 337.

Epchtein, N., Guibert, J., Nguyen-Quang Rieu, Turon, P., and Wamsteker, W. 1980, *Astron. Astrophys.*, **85**, L1.

Eriksson, K., Gustafsson, B., Johnson, H.R., Querci, F., Querci, M., Baumert, J.H., Carlsson, M., and Olofsson, H. 1985, *Astron. Astrophys.*, in press.

Fawley, W.M. 1977, *Astrophys. J.*, **218**, 181.

Fazio, G.G., McBreen, B., Stier, M.T., and Wright, E.L. 1980, *Astrophys. J. (Letters)*, **237**, L39.

Feofilov, P.P. 1961, *The Physical Basis of Polarized Emission* (New York: Consultants Bureau).

Ferlet, R., and Gillet, D. 1984, *Astron. Astrophys.*, **133**, L1.

Forrest, W.J., Gillett, F.C., and Stein, W.A. 1975, *Astrophys. J.*, **195**, 423.

Forrest, W.J., Houck, J.R., and McCarthy, J.F. 1981, *Astrophys. J.*, **248**, 195.

Forrest, W.J., McCarthy, J.F., and Houck, J.R. 1979, *Astrophys. J.*, **233**, 611.

Fox, M.W., Wood, P.R., and Dopita, M.A. 1984, *Astrophys. J.*, **286**, 337.

Friedemann, C., Gürtler, J., Schmidt, R., and Dorschner, J. 1981, *Astrophys. Space Sci.*, **79**, 405.

Gahm, G.F., and Hultquist, L. 1971, in *Proc. Third Trieste Colloq. on Astrophysics*, ed. M. Hack (Osservatorio Astronomico di Trieste), p. 148.

Gehrz, R.D., and Woolf, N.J. 1971, *Astrophys. J.*, **165**, 285.

Gilman, R.C. 1974, *Astrophys. J.*, **118**, 87.

Gilra, D.P. 1973, in *IAU Symp. 52, Interstellar Dust and Related Topics*, ed. J.M. Greenberg and H.C. Van de Hulst (Dordrecht: Reidel), p. 517.

Gilra, D.P. 1976, *Mém. Soc. Roy. Sci. Liège*, **IX**, Sér. 6, p. 77.

Goebel, J.H., Bregman, J.D., Goorvitch, D., Strecker, D.W., Puetter, R.C., Russell, R.W., Soifer, B.T., Willner, S.P., Forrest, W.J., Houck, J.R., and McCarthy, J.F. 1980, *Astrophys. J.*, **235**, 104.

Goebel, J.H., Bregman, J.D., Strecker, D.W., Witteborn, F.C., and Ericksson, E.F. 1978, *Astrophys. J. (Letters)*, **222**, L129.

Goebel, J.H., and Mosely, S.H. 1985, *Astrophys. J. (Letters)*, **290**, L35.

Goldberg, L. 1976, *Mém. Soc. Roy. Sci. Liège*, **IX**, Sér. 6, p. 387.

Goldberg, L. 1979, *Quart. J. Roy. Astron. Soc.*, **20**, 361.

Goldberg, L. 1981, in *Proc. Second Workshop on Physical Processes in Red Giants*, ed. I. Iben and A. Renzini (Dordrecht: Reidel), p. 301.

Goldberg, L. 1984, *Pub. Astron. Soc. Pacific*, **96**, 366.

Goldberg, L., Hege, E.K., Hubbard, E.N., Strittmatter, P.A., and Cocke, W.J. 1981, SAO Special Report 392, p. 131.

Goldberg, L., Ramsey, L., Testerman, L., and Carbon, D. 1975, *Astrophys. J.*, **199**, 427.

Goldreich, P. 1980, in *Proc IAU Symp. 87, Interstellar Molecules*, ed. B.H. Andrew (Dordrecht: Reidel), p. 522.

Guinan, E.F. 1984, in *Proc. Third Cambridge Workshop on Cool Stars, Stellar Systems, and the Sun*, ed. S.L. Baliunas and L. Hartmann (Berlin, Heidelberg: Springer-Verlag), p. 336.

Hagen, W. 1978, *Astrophys. J. Supplement*, **38**, 1.

Hagen, W. 1982, *Pub. Astron. Soc. Pacific*, **94**, 835.

Hagen, W., Simon, T., and Dyck, H.M. 1975, *Bull. Amer. Astron. Soc.*, **7**, 434.

Hagen, W., Stencel, R.E., and Dickinson, D.F. 1983, *Astrophys. J.*, **274**, 286.

Hall, D.N.B. 1980, in *Proc. IAU Symp. 87, Interstellar Molecules*, ed. B.H. Andrew (Dordrecht: Reidel), p. 515.

Hall, D.N.B., Hinkle, K.H., and Ridgway, S.T. 1979, in *Proc. IAU Colloq. 46, Changing Trends in Variable Star Research*, ed. F.M. Bateson, J. Smak, and I.H. Urch (Hamilton, New Zealand: Univ. of Waikato Press), p. 264.

Harrington, J.P. 1969, *Astrophys. Letters*, **3**, 165.

Hartmann, L.W., and Avrett, E.H. 1984, *Astrophys. J.*, **284**, 238.

Hartmann, L.W., and Dolan, J.F. 1974, *Astrophys. J.*, **187**, 151.

Hayes, D.P. 1980, *Astrophys. J. (Letters)*, **241**, L165.

Hayes, D.P. 1981a, *Inf. Bull. Variable Stars IAU Comm. 27*, No. 1984.

Hayes, D.P. 1981b, *Pub. Astron. Soc. Pacific*, **93**, 752.

Hayes, D.P. 1982, *Inf. Bull. Variable Stars, IAU Comm. 27*, No. 2064.

Hayes, D.P. 1984, in *Proc. Third Cambridge Workshop on Cool Stars, Stellar Systems, and the Sun*, ed. S.L. Baliunas and L. Hartmann (Berlin, Heidelberg: Springer-Verlag), p. 342.

Heasley, J.N., Ridgway, S.T., Carbon, D.F., Milkey, R.W., and Hall, D.N.B. 1978, *Astrophys. J.*, **219**, 970.

Herbig, G.M. 1956, *Pub. Astron. Soc. Pacific*, **68**, 204.

Herbig, G.H., and Zappala, R.R. 1970, *Astrophys. J. (Letters)*, **162**, L15.

Herter, T., Briotta, D.A., Gull, G.E., and Houck, J.R. 1982, *Astrophys. J. (Letters)*, **259**, L25.

Herzberg, G. 1948, *Astrophys. J.*, **107**, 94.

Hill, S.J., and Willson, L.A. 1979, *Astrophys. J.*, **229**, 1029.

Hinkle, K.H. 1978, *Astrophys. J.*, **220**, 210.

Hinkle, K.H., and Barnes, T.G. 1979a, *Astrophys. J.*, **227**, 923.

Hinkle, K.H., and Barnes, T.G. 1979b, *Astrophys. J.*, **234**, 548.

Hinkle, K.H., Hall, D.N.B., and Ridgway, S.T. 1982, *Astrophys. J.*, **252**, 697.

Hinkle, K.H., Lambert, D.L., and Snell, R.L. 1976, *Astrophys. J.*, **210**, 684.

Hinkle, K.H., Scharlach, W.W.G., and Hall, D.N.B. 1984, *Astrophys. J. Supplement*, **56**, 1.

Honeycutt, R.K., Bernat, A.P., Kephart, J.E., Gow, C.E., Sandford, M.T., and Lambert, D.L. 1980, *Astrophys. J.*, **239**, 565.

Huggins, P.J. 1984, in *Proc. Mass Loss from Red Giants*, meeting held in UCLA Faculty Center on June 20-21, 1984.

Jennings, M.C., and Dyck, H.M. 1972, *Astrophys. J.*, **177**, 427.

Johnson, H.L., and Allen, C., ed. 1981, *Proc. Symp. on Recent Advances in Observational Astronomy*, (Ensenada, Baja California: Universidad Nacional Autónoma de Mexico).

Johnson, H.R., and Ake, T.B. 1984, in *Proc. Third Cambridge Workshop on Cool Stars, Stellar Systems, and the Sun*, ed. S.L. Baliunas and L. Hartmann (Berlin, Heidelberg: Springer-Verlag), p. 362.

Johnson, H.R., Ake, T.B., and Eaton, J.A. 1985a, in *Cool Stars with Excesses of Heavy Elements*, ed. M. Jaschek and P.C. Keenan (Dordrecht: Reidel), p. 53.

Johnson, H.R., Baumert, J.H., Querci, F., and Querci, M. 1985b, *Astrophys. J.*, in press.

Johnson, H., and Mendez, M. 1970, *Astron. J.*, **75**, 785.

Johnson, H.R., and O'Brien, G.T. 1983, *Astrophys. J.*, **265**, 952.

Joy, A.H. 1947, *Astrophys. J.*, **106**, 288.

Joy, A.H. 1954, *Astrophys. J., Supplement*, **1**, 39.

Jura, M. 1984, *Astrophys. J.*, **282**, 200.

Karovska, M. 1984, *Thèse de 3e cycle*, U.E.R. Institut de Mathématiques et Sciences Physiques, et Observatoire de Nice (Sept. 1984).

Karovska, M., Nisenson, P., Noyes, R.W., Stachnik, R.V. 1985b, in *Proc. Fourth Cambridge Workshop on Cool Stars, Stellar Systems, and the Sun*, held in Santa Fe, New Mexico, Oct. 16–18, 1985, in press.

Karovska, M., Noyes, R.W., Roddier, F., Nisenson, P., Stachnik, R.V. 1985a, *Bull. Amer. Astrophys. Soc.*, **17**, 598.

Keady, J.J., Hall, D.N.B., and Ridgway, S.T. 1984, preprint to appear in *Astrophys. J.*

Keenan, P.C. 1966, *Astrophys. J. Supplement*, **13**, 333.

Keenan, P.C., Garrison, R.F., and Deutsch, A.J. 1974, *Astrophys. J. Supplement*, **28**, 271.

King, D.J. 1983, *Mercury*, March–April 1983.

Kipper, T.A., and Kipper, M.A. 1979, *Pub. Astrophys. Obs. Tartu*, **XLVII**, p. 222.

Knapp, G.R., 1985, *Astrophys. J.*, **293**, 273.

Knapp, G.R., Phillips, T.G., and Huggins, P.J. 1980, *Astrophys. J. (Letters)*, **242**, L25.

Knapp, G.R., Phillips, T.G., Leighton, R.B., Lo, K.Y., Wannier, P.G., Wootten, A., and Huggins, P.J. 1982, *Astrophys. J.*, **252**, 616.

Kondo, Y. 1973, in *Proc. IAU Colloq. 19, Stellar Atmospheres*, ed. S.D. Jordan and E.H. Avrett, NASA SP-317, p. 122.

Kondo, Y., Duval, J.E., Modisette, J.L., and Morgan, T.H. 1976, *Astrophys. J.*, **210**, 713.

Kondo, Y., Giuli, R.T., Modisette, J.L., and Rydgren, A.E. 1972, *Astrophys. J.*, **176**, 153.

Kondo, Y., Modisette, J.L., Morgan, T.H., de Jager, C., Lamers, H.J., and Van der Hucht, K.A. 1977, *Bull. Amer. Astron. Soc.*, **9**, 365.

Kondo, Y., Morgan, T.H., and Modisette, J.L. 1975, *Astrophys. J. (Letters)*, **196**, L125.

Kovar, R.P., Potter, A.E., Kovar, N.S., and Trafton, L. 1972, *Pub. Astron. Soc. Pacific*, **84**, 46.

Kruszewski, A., and Coyne, G.V. 1976, *Astron. J.*, **81**, 641.

Kruszewski, A., Coyne, G.V., and Gehrels, T. 1969, in *Proc. Second Trieste Colloq. on Astrophysics, Mass Loss from Stars*, ed. M. Hack (Dordrecht: Reidel), p. 42.

Kuiper, T.B.H., Knapp, G.R., Knapp, S.L. and Brown, R.L. 1976, *Astrophys. J.*, **204**, 408.

Kukarkin, B.V., Kholopov, P.N., Efremov, Yu.N., Kukarkina, N.P., Kurochkin, N.E., Medvedeva, G.I., Perova, N.B., Fedorovich, V.P., and Frolov, M.S. 1969, *General Catalogue of Variable Stars*, Third Ed., Vol. I, and Supplements (Moscow).

Kukarkin, B.V., Kholopov, P.N., Efremov, Yu.N., Kukarkina, N.P., Kurochkin, N.E., Medvedeva, G.I., Perova, N.B., Fedorovich, V.P., and Frolov, M.S. 1970, *General Catalogue of Variable Stars*, Third Ed., Vol. II and Supplements (Moscow).

Kunasz, P.B. 1974, Ph.D. Thesis, Univ. of Colorado.

Kunasz, P.B., and Hummer, D.G. 1974, *Mon. Not. Roy. Astr. Soc.*, **166**, 57.

Kwok, S. 1981, in *Proc. Second Workshop on Physical Processes in Red Giants*, ed. I. Iben and A. Renzini (Dordrecht: Reidel), p. 421.

Labeyrie, A., Koechlin, L., Bonneau, D., Blazit, A., and Foy, R. 1977, *Astrophys. J. (Letters)*, **218**, L75.

Lafont, S., Lucas, R., and Omont, A. 1982, *Astron. Astrophys*, **106**, 201.

Lambert, D.L., and Snell, R.L. 1975, *Mon. Not. Roy. Astr. Soc.*, **172**, 277.

Lambert, D.L., and Vanden Bout, P.A. 1978, *Astrophys. J.*, **221**, 854.

Landstreet, J.D., and Angel, J.R.P. 1977, *Astrophys. J.*, **211**, 825.

Lang, K.R. 1980, *Astrophysical Formulae* (Berlin, Heidelberg: Springer-Verlag), p. 535.

Leibacher, J., and Stein, R.F. 1981, in *Proc. Second Cambridge Workshop on Cool Stars, Stellar Systems, and the Sun, Vol. I*, ed. M.S. Giampapa and L. Golub, Spec. Report 392 (Smithsonian Astrophys. Obs.), p. 23.

Levy, E.H., Rose, W.K. 1974, *Astrophys. J.*, **193**, 419.

Linsky, J.L., Basri, G.S., Chiu, H.Y., Chang, S.W., and Maran, S.P. 1977, *Bull. Amer. Astrophys. Soc.*, **9**, 345.

Linsky, J.L., Worden, S.P., McClintock, W., and Robertson, R.M. 1979, *Astrophys. J. Supplement*, **41**, 47.

Lockwood, G.W. 1969, *Astrophys. J.*, **157**, 275.

Lynds, C.R., Harvey, J., and Goldberg, L. 1977, *Bull. Amer. Astron. Soc.*, **9**, 345.

Lynds, C.R., Worden, S.P., and Harvey, J.W. 1976, *Astrophys. J.*, **207**, 174.

Maehara, H. 1968, *Pub. Astron. Soc. Japan*, **20**, 77.

Maehara, H. 1971, *Pub. Astron. Soc. Japan*, **23**, 503.

Maehara, H., Yamashita, Y. 1979, *Annals Tokyo Astron. Obs.*, **XVII**, Ser. 2, p. 93

Magalhaes, A.M. 1980, in *Proc. Colloq. on Phenomena of Mass Ejection*, Cambuquira (Sociedade Astronomica Brasileira: MG Brazil).

Magalhaes, A.M. 1981, in *Proc. Second Workshop on Physical Processes in Red Giants* ed. I. Iben and A. Renzini (Dordrecht: Reidel), p. 231.

Manduca, A. 1979, *Astron. Astrophys. Supplement,* **36**, 411.

Marcondes-Machado, J.A. 1979, in *Proc. IAU Colloq. 46, Changing Trends in Variable Star Research*, ed. F.M. Bateson, J. Smak, and I.H. Urch (Hamilton, New Zealand: Univ. Waikato Press), p. 273.

Mariotti, J.M., Chelli, A., Foy, R., Léna, P., Sibille, F., and Tchountonov, G. 1983, *Astron. Astrophys.*, **120**, 237.

Mauron, N., Fort, B., Querci, F., Dreux, M., Fauconnier, T., and Lamy, P. 1984, *Astron. Astrophys.*, **130**, 341.

McCabe, E.M. 1982, *Mon. Not. Roy. Astr. Soc.*, **200**, 71.

McCall, A., and Hough, J.H. 1980, *Astron. Astrophys. Supplement,* **42**, 141.

McCarthy, D.W., Howell, R., and Low, F.J. 1978, *Astrophys. J. (Letters),* **223**, L1.

McCarthy, D.W., Howell, R., and Low, F.J. 1980, *Astrophys. J. (Letters),* **235**, L27.

McLaughin, D.B. 1946, *Astrophys. J.*, **103**, 35.

McLean, I.S. 1979, *Mon. Not. Roy. Astr. Soc.*, **186**, 21.

McLean, I.S., and Coyne, G.V. 1978, *Astrophys. J. (Letters),* **226**, L145.

McMillan, R.S., and Tapia, S. 1978, *Astrophys. J. (Letters),* **226**, L87.

Meinel, A.B., Aveni, A.F., and Stockton, M.W. 1969, *Catalog of Emission Lines in Astrophysical Objects.*, 2nd ed. (Tucson, Arizona: Optical Sciences Center and Steward Observatory, Univ. Arizona).

Merchant, A.E. 1967, *Astrophys. J.*, **147**, 587.

Merrill, P.W. 1940, *Spectra of Long-Period Variable Stars* (Chicago: Univ. Chicago Press).

Merrill, P.W. 1945, *Astrophys. J.*, **102**, 347.

Merrill, P.W. 1946, *Astrophys. J.*, **103**, 275.

Merrill, P.W. 1947a, *Astrophys. J.*, **105**, 360.

Merrill, P.W. 1947b, *Astrophys. J.*, **106**, 274.

Merrill, P.W. 1952a, *Astrophys. J.*, **116**, 21.

Merrill, P.W. 1952b, *Astrophys. J.*, **116**, 344.

Merrill, P.W. 1952c, *Astrophys. J.*, **116**, 337.

Merrill, P.W. 1960, in *Stars and Stellar Systems, Vol. VI: Stellar Atmospheres,* ed. J.L. Greenstein (Chicago: Univ. Chicago Press), p. 509.

Merrill, K.M. 1977, in *Proc. IAU Colloq. 42, The Interaction of Variable Stars with their Environment*, ed. R. Kippenhahn, J. Rake, and W. Strohmeier (Erlanger-Nurnberg: Astronomisches Institut der Universitat).

Merrill, P.W., and Greenstein, J.L. 1956, *Astrophys. J. Supplement,* **2**, 225.

Merrill, P.W., and Wilson, O.C. 1956, *Astrophys. J.*, **123**, 392.

Mihalas, D. 1978, in *Stellar Atmospheres*, 2nd ed., ed. G. Burbidge and M. Burbidge (San Francisco: W.H. Freeman and Company).

Mihalas, D. 1979, *Mon. Not. Roy. Astr. Soc.*, **189**, 671.

Mihalas, D., Kunasz, P.B., and Hummer, D.G. 1975, *Astrophys. J.*, **202**, 465.

Mitchell, R.M., and Robinson, G. 1980, *Mon. Not. Roy. Astr. Soc.*, **190**, 669.

Modisette, J.L., Nicholas, R.E., and Kondo, Y. 1973, *Astrophys. J.*, **186**, 219.

Morris, M., and Alcock, C. 1977, *Astrophys. J.*, **218**, 687.

Mullan, D.J. 1984, *Astrophys. J.*, **284**, 769.

Mullan, D.J. 1978, *Astrophys. J.*, **226**, 151.

Munch, G., Roesler, F., and Tranger, J. 1979, in *Proc. 4th Trieste Colloq. Astrophysics, High Resolution Spectroscopy*, ed. M. Hack (Osservatorio Astronomico di Trieste).

Nuth, J.A., Moseley, S.H., Silverberg, R.F., Goebel, J.H., and Moore, W.J. 1985, *Astrophys. J. (Letters)*, **290**, L41.

O'Brien, G., and Johnson, H.R. 1982, in *Advances in Ultraviolet Astronomy: Four Years of IUE Research*, ed. Y. Kondo, J.H. Mead, and R.D. Chapman, NASA CP-2238, p. 255.

O'Brien, G., and Lambert, D.L. 1979, *Astrophys. J. (Letters)*, **229**, L33.

Odell, A.P., Vrba, F.J., Fix, J.D., and Neff, J.S. 1970, *Pub. Astron. Soc. Pacific*, **82**, 883.

Oster, L. 1971, *Astrophys. J.*, **169**, 57.

Peery, B.F. 1979, *Pub. Astron. Soc. Japan*, **31**, 461.

Peery, B.F., and Wojslaw, R.S. 1977, *Bull. Amer. Astron. Soc.*, **9**, 365.

Phillips, J.G., and Freedman, R.S. 1969, *Pub. Astron. Soc. Pacific*, **81**, 521.

Pilachowski, C., Wallerstein, G., and Willson, L.A. 1979, in *Proc. Goddard Conf. on Current Problems in Stellar Pulsation Instabilities*, ed. D. Fischel et al., NASA TM-80625, p. 577.

Price, S.G., and Walker, R.G. 1976, *AFGL Infrared Sky Survey*, Environmental Research Papers, No. 576.

Puetter, R.C., Russell, R.W., Sellgren, K., and Soifer, B.T. 1977, *Pub. Astron. Soc. Pacific*, **89**, 320.

Querci, M., Courtin, R., Querci, F., Coron, N., and Gispert, R. 1979, *Astron. Astrophys.*, **77**, 155.

Querci, M., and Querci, F. 1978, *Astron. Astrophys.*, **70**, L45.

Querci, M., and Querci, F. 1985a, *Astron. Astrophys.*, **147**, 121.

Querci, M., and Querci, F. 1985b, in preparation.

Querci, F., Querci, M., Wing, R.F., Cassatella, A., and Heck, A. 1982, *Astron. Astrophys.*, **111**, 120.

Reid, M.J., and Dickinson, D.F. 1976, *Astrophys. J.*, **209**, 505.

Reimers, D. 1975, in *Problems in Stellar Atmospheres and Envelopes*, ed. B. Baschek, W.H. Kegel, and G. Traving (Berlin, Heidelberg: Springer-Verlag), p. 229.

Reimers, D. 1977, *Astron. Astrophys.*, **57**, 395.

Reimers, D. 1978, in *Proc. IAU Colloq. 42, Interaction of Variable Stars with Their Environment*, ed. R. Kippenhahn, J. Rahe, and W. Strohmeier (Erlangen-Nürnberg: Astronomisches Institut der Universität), p. 559.

Reimers, D. 1981, in *Proc. Second Workshop on Physical Processes in Red Giants*, ed. I. Iben and A. Renzini (Dordrecht: Reidel), p. 269.

Richer, H.B. 1971, *Astrophys. J.*, **167**, 521.

Ricort, G., Aime, A., Vernin, J., and Kadiri, S. 1981, *Astron. Astrophys.*, **99**, 232.

Ridgway, S.T. 1981a, in *Proc. Second Workshop on Physical Processes in Red Giants*, ed. I. Iben and A. Renzini (Dordrecht: Reidel), p. 305.

Ridgway, S.T. 1981b, in *Proc. Symp. on Recent Advances in Observational Astronomy*, ed. H.L. Johnson and C. Allen (Ensenada, Baja California: Universidad Nacional Autónoma de Mexico), p. 81.

Ridgway, S.T., and Hall, D.N.B. 1980, in *Proc. IAU Symp. 87, Interstellar Molecules*, ed. B.H. Andrew (Dordrecht: Reidel), p. 509.

Ridgway, S.T., Jacoby, G.H., Joyce, R.R., and Wells, D.C. 1980a, *Astron.J.*, **85**, 1496.

Ridgway, S.T., Joyce, R.R., White, N.M., and Wing, R.F. 1980b, *Astrophys. J.*, **235**, 126.

Ridgway, S.T., Wells, D.C., Joyce, R.R., and Allen, R.G. 1979, *Astron. J.*, **84**, 247.

Roddier, F., and Roddier, C. 1983, *Astrophys. J. (Letters)*, **270**, L23.

Roddier, F., and Roddier, C. 1985, *Astrophys. J. (Letters)*, **295**, L21.

Rottenberg, J.A. 1952, *Mon. Not. Roy. Astr. Soc.*, **112**, 125.

Rowan-Robinson, M., and Harris, S. 1982, *Mon. Not. Roy. Astr. Soc.*, **200**, 197.

Rowan-Robinson, M., and Harris, S. 1983a, *Mon. Not. Roy. Astr. Soc.*, **202**, 767.

Rowan-Robinson, M., and Harris, S. 1983b, *Mon. Not. Roy. Astr. Soc.*, **202**, 797.

Sahai, R., and Wannier, P.G. 1985, *Astrophys. J.*, **299**, 424.

Sanford, R.F. 1950, *Astrophys. J.*, **111**, 270.

Sanner, F. 1976, *Astrophys. J. Supplement*, **32**, 115.

Sanner, F. 1977, *Astrophys. J. (Letters)*, **221**, L35.

Scargle, J.D., and Strecker, D.W. 1979, *Astrophys. J.*, **228**, 838.

Schmid-Burgk, J., and Scholz, M. 1981, *Mon. Not. Roy. Astr. Soc.*, **194**, 805.

Schmitz, F., and Ulmschneider, P. 1981, *Astron. Astrophys.*, **93**, 178.

Schwarz, H.E., and Clarke, D. 1984, *Astron. Astrophys.*, **132**, 370.

Schwarzschild, M. 1975, *Astrophys. J.*, **195**, 137.

Selby, M.J., Wade, R., and Sanchez Magro, C. 1979, *Mon. Not. Roy. Astr. Soc.*, **187**, 553.

Serkowski, K. 1971, in *Proc. IAU Colloq. 15, New Directions and New Frontiers in Variable Star Research* (Erlangen-Nürnberg: Astronomisches Institut der Universität).

Shafter, A., and Jura, M. 1980, *Astron. J.*, **85**, 1513.

Shawl, S.J. 1974, *Planets, Stars and Nebulae Studied with Photopolarimetry*, ed. T. Gehrels (Tucson: Univ. Arizona Press), p. 821.

Shawl, S.J. 1975, *Astron. J.*, **80**, 602.

Shawl, S.J., and Zellner, B. 1970, *Astrophys. J. (Letters)*, **162**, L19.

Sherbakov, A.G. 1979, *Pisma V Astron. Zh.*, **5**, 542.

Shinkawa, D. 1973, *Astrophys. J. Supplement*, **25**, 253.

Simon, T., Linsky, J.L., and Stencel, R.F. 1982, *Astrophys. J.*, **257**, 225.

Slovak, M.H. 1982, *Astrophys. J.*, **262**, 282.

Slutz, S. 1976, *Astrophys. J.*, **210**, 750.

Spinrad, H., and Wing, R.F. 1969, *Ann. Rev. Astron. Astrophys.*, **7**, 249.

Stein, R.F., and Leibacher, J. 1980 in *Proc. IAU Colloq. 51, Stellar Turbulence*, ed. D.F. Gray and J.L. Linsky (Berlin, Heidelberg: Springer-Verlag), p. 225.

Stencel, R.E. 1977, *Astrophys. J.*, **215**, 176.

Stencel, R.E. 1978, Astrophys. J. (Letters), **223**, L37.

Stencel, R.E., and Carpenter, K.G. 1982, in *Advances in Ultraviolet Astronomy: Four Years of IUE Research*, ed. Y. Kondo, J.M. Mead, and R.D. Chapman, NASA CP-2238.

Stencel, R.E., and Ionson, J.A. 1979, *Pub. Astron. Soc. Pacific*, **91**, 452.

Stencel, R.E., Linsky, J.L., Brown, A., Jordan, C., Carpenter, K.G., Wing, R.F., and Czyzak, S. 1981, *Mon. Not. Roy. Astr. Soc.*, **196**, 470.

Stencel, R.E., Mullan, D.J., Linsky, J.L., Basri, G.S., and Worden, S.P. 1980, *Astrophys. J. Supplement*, **44**, 383.

Stephenson, C.B. 1973, *Pub. Warner and Swasey Obs.*, Vol. 1, No. 4.

Sutton, E.C., Betz. A.L., Storey, J.W.V., and Spears, D.L. 1979, *Astrophys. J. (Letters)*, **230**, L105.

Sutton, E.C., Storey, J.W.V., Betz, A.L., Townes, C.H., and Spears, D.L. 1977, *Astrophys. J. (Letters)*, **217**, L97.

Svatos, J. 1980, *Bull. Astron. Inst. Czech*, **31**, 302.

Svatos, J., and Solc, M. 1981, *Astrophys. Space Science*, **77**, 511.

Tanabé, T., and Kamijo, F. 1981, in *IAU Colloq. 59, Effects of Mass Loss on Stellar Evolution* ed. C. Chiosi and R. Stalio (Dordrecht: Reidel).

Tielens, A.G.G.M. 1983, *Astrophys. J.*, **271**, 702.

Tinbergen, J., Greenberg, J.M., and de Jager, C. 1981, *Astron. Astrophys.*, **95**, 215.

Tomaszewski, L., Landstreet, J.D., McLean, I.S., and Coyne, G.V. 1980, *Astrophys. J.*, **238**, 935.

Treffers, R.R., and Cohen, M. 1974, *Astrophys. J.*, **188**, 545.

Tsuji, T. 1971, *Pub. Astron. Soc. Japan*, **23**, 275.

Tsuji, T. 1976, *Pub. Astron. Soc. Japan*, **28**, 567.

Tsuji, T. 1978a, *Astron. Astrophys.*, **62**, 29.

Tsuji, T. 1978b, *Pub. Astron. Soc. Japan*, **30**, 435.

Tsuji, T. 1979, *Pub. Astron. Soc. Japan*, **31**, 43.

Ulich, B.L. and Haas, R.W. 1976, *Astrophys. J. Supplement*, **30**, 247.

Utsumi, K. 1971, *Pub. Astron. Soc. Japan*, **23**, 437.

Van der Hucht, K.A., Stencel, R.E., Haisch, B.M., and Kondo, Y. 1979, *Astron. Astrophys. Supplement*, **36**, 377.

Vaughan, A.H., and Skumanich, A. 1970, in *Proc. IAU Colloq. 2, Spectrum Formation in Stars with Steady-State Extended Atmospheres,* ed. H.G. Groth and P. Wellman, NBS-SP-332, p. 295.

Vaughan, A.H., and Zirin, H. 1968, *Astrophys. J.,* **152**, 123.

Walker, A.R. 1976, *Mon. Not. Roy. Astr. Soc.,* **174**, 609.

Walker, A.R. 1980, *Mon. Not. Roy. Astr. Soc.,* **190**, 543.

Wallerstein, G. 1959, *Astrophys. J.,* **130**, 560.

Wallerstein, G. 1975, *Astrophys. J. Supplement,* **29**, 375.

Wallerstein, G. 1977, *J. Roy. Astr. Soc. Canada,* **71**, 298.

Wannier, P.G., Redman, R.O., Phillips, T.G., Leighton, R.B., Knapp, G.R., and Huggins, P.J. 1980, in *Proc. IAU Colloq. 87, Interstellar Molecules*, ed. B.H. Andrew (Dordrecht: Reidel), p. 487.

Wdowiak, T.J. 1977, *Pub. Astron. Soc. Pacific,* **89**, 569.

Weiler, E.J., and Oegerle, W.R. 1979, *Astrophys. J. Supplement,* **39**, 537.

Welter, G. L., and Worden, S.P. 1980, *Astrophys. J.,* **242**, 673.

Weymann, R. 1962, *Astrophys. J.,* **136**, 844.

White, N.M. 1980, *Astrophys. J.,* **242**, 646.

Whitney, C.A., and Skalafuris, A.J. 1963, *Astrophys. J.,* **138**, 200.

Wilkerson, S., and Worden, S.P. 1977, *Astron. J.,* **82**, 642.

Willson, L.A. 1976, *Astrophys. J.,* **205**, 172.

Willson, L.A. 1979, in *Proc. IAU Colloq. 46, Changing Trends in Variable Star Research*, ed. F.M. Bateson, J. Smak, and I.H. Urch (Hamilton, New Zealand: Univ. Waikato Press), p. 199.

Willson, L.A., and Bowen, G.H. 1985, in *Proc. Third Trieste Workshop on the Relations Between Chromospheric-Coronal Heating and Mass Loss in Stars*, ed. R. Stalio and J. Zirker (Trieste: Tabographs-TS), pp. 127–176.

Willson, L.A., and Bowen, G.H. 1986, in *Proc. Fourth Cambridge Workshop on Cool Stars, Stellar Systems, and the Sun*, ed. M. Zeilik and D.M. Gibson (Heidelberg: Springer-Verlag), p. 385.

Willson, L.A., and Hill, S.J. 1979, *Astrophys. J.,* **228**, 854.

Willson, L.A., Wallerstein, G., and Pilachowski, C.A. 1982, *Mon. Not. Roy, Astr. Soc.,* **198**, 483.

Wilson, W. J., Schwartz, P.M., and Epstein, R.E. 1973, *Astrophys. J.,* **183**, 871.

Wing, R.F. 1978, in *Proc. 4th International Colloq. on Astrophysics, High Resolution Spectrometry*, ed. M. Hack (Osservatorio Astronomico di Trieste), p. 683.

Wing, R.F. 1979, in *Proc. Goddard Conference on Current Problems in Stellar Pulsation Instabilities*, ed. D. Fischel et al., NASA TM-80625, p. 533.

Wing, R.F., Baumert, J.H., Strom, S.E., and Strom, K.M. 1972, *Pub. Astron. Soc. Pacific,* **84**, 646.

Wood, P.R. 1979, *Astrophys. J.,* **227**, 220.

Wood, P.R. 1981, in *Proc. Second Workshop on Physical Processes in Red Giants*, ed. I. Iben and A. Renzini (Dordrecht: Reidel), p. 205.

Wood, P.R. 1982, in *Proc. Conf. on Pulsations in Classical and Cataclysmic Variable Stars*, ed.

J.P. Cox and C.J. Hansen (Boulder, Colorado: JILA), p.284.

Woodsworth, A.W., and Hughes, V.A. 1973, *Nature Phys. Sci.*, **246**, 111.

Wordsworth, A.W., and Hughes, V.A. 1977, *Astron. Astrophys.*, **58**, 105.

Wootten, A., Lichten, S.M., Sahai, R., and Wannier, P.G. 1982, *Astrophys. J.*, **257**, 151.

Yamashita, Y. 1972, *Annals Tokyo Astron. Obs.*, **XIII**, Ser. 2, p. 169.

Zirin, H. 1976, *Astrophys. J.*, **208**, 414.

Zirin, H. 1982, *Astrophys. J.*, **260**, 655.

Zuckerman, B., Gilra, D.P., Turner, B.E., Morris, M., and Palmer, P. 1976, *Astrophys. J. (Letters)*, **205**, L15.

N88-11595

3

CIRCUMSTELLAR RADIO MOLECULAR LINES

Nguyen-Quang-Rieu

INTRODUCTION

Late-type stars radiate most of their energy in the near- and mid-infrared regions. The energy distribution of Mira variables peaks around 2 μm and the well-known infrared source, IRC + 10216, is very bright between 2 and 20 μm. Many infrared stars similar to IRC + 10216 are believed to be long-period variables, their thick circumstellar shell almost totally obscuring the central star. Reemission of stellar radiation by warm dust grains causes the infrared continuum flux. The extended shells of both visible and unidentified infrared cool stars also emit molecular emission lines at centimeter and millimeter wavelengths. Since radio lines can be excited by infrared photons, a combination of infrared and radio observations is very useful in determining molecular excitation mechanisms (Kwan and Scoville, 1974; Deguchi and Iguchi, 1976; Elitzur et al., 1976; Bujarrabal et al., 1980).

Late-type stars are characterized by mass loss (see Goldberg, this volume). Sporadic ejection of matter or modulation of a continuous process may produce stratification of the circumstellar shell (Bernat, 1981; Ridgway, 1981). As a result, molecular lines can serve to probe the physical conditions in different layers. In particular, SiO masers (rotation lines in the ground and excited vibration states) and infrared vibration/rotation molecular lines, which need extreme excitation conditions (i.e., high gas densities and temperatures), occur close to the stellar photosphere. On the other hand, millimeter thermal emission from CO and linear carbon chain molecules—the cyanopolyyne family ($HC_{2n+1}N$)—takes place in the circumstellar envelope at several 10 to 10^3 stellar radii. Different shell layers can therefore be sampled by observing appropriate molecular transitions (Figure 3-1).

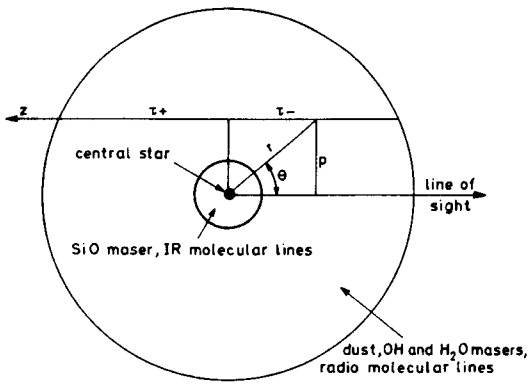


Figure 3-1. Schematic drawing of the circumstellar envelope.

PRECEDING PAGE BLANK NOT FILMED

PAGE 208 INTENTIONALLY BLANK

CIRCUMSTELLAR MOLECULES

Molecules in space were discovered through the ultraviolet absorption lines of CH, CN, and CH^+ in stellar spectra (Swings and Rosenfeld, 1937; McKellar, 1940; Adams, 1941). The first detection of interstellar molecules at radio wavelength, the OH line at 18 cm, was made by Weinreb et al. in 1963. The improvement of radio astronomical techniques resulted later in the detection of polyatomic molecules, NH_3 and H_2O, around 1.3 cm (Cheung et al., 1968, 1969). So far, about sixty molecules and many of their isotopes have been detected, mostly in the millimeter range, in the star-forming region of Orion, in the galactic center (Sgr B2), and in the circumstellar envelope of the carbon star IRC + 10216, as well as in a number of dark clouds.

The first discoveries of circumstellar molecules were made through the detection of OH and H_2O maser lines in oxygen-rich late-type stars, mainly Mira variables and red supergiants (Wilson and Barrett, 1972; Knowles et al., 1969; Schwartz and Barrett, 1970; Robinson et al., 1971; Nguyen-Q-Rieu et al., 1971). SiO maser emission was later detected in these objects (Snyder and Buhl, 1974; Kaifu et al., 1975; Spencer et al., 1981). Subsequent systematic surveys in the 1612-MHz OH line in the galactic plane resulted in the detection of OH sources whose spectra exhibited the characteristics of OH stellar masers (Winnberg et al., 1973; Johansson et al., 1977; Bowers, 1978; Baud et al., 1979a, 1979b). These OH sources, which also have infrared but no visible counterparts (Schultz et al., 1976; Evans and Beckwith, 1977; Glass, 1978; Epchtein and Nguyen-Q-Rieu, 1982), form the so-called "unidentified OH/IR" class of objects. About 300 stars and unidentified IR objects are known to emit at least one of these maser lines (Engels, 1979).

Thermal CO emission has been detected in the envelope of carbon-rich as well as oxygen-rich stars (Solomon et al., 1971; Zuckerman et al., 1977). Other molecules containing carbon, such as HCN, HNC, and HC_3N have also been detected in some carbon-rich stars (Jewell and Synder, 1984; Olofsson et al., 1982b). In particular, 22 molecular species and their isotopes have been found in the envelope of IRC + 10216, including a complex member of the cyanopolyyne family, $HC_{11}N$, which is also the heaviest molecule so far detected in our Galaxy (Bell et al., 1982). Recently, Thaddeus et al. (1984) have identified nine of the previously unassigned lines in IRC + 10216 as those emitted by the SiC_2 radical, which turns out to be a compact symmetric ring molecule. Table 3-1 lists the circumstellar molecules. (See also Glassgold and Huggins, this volume.)

Circumstellar molecular lines are characterized by their broad line width, which reflects the large-scale expansion of the shell ($\sim$5 to 50 km s^{-1}).

MASER EMISSION

The radio emission from OH, H_2O, and SiO presents characteristics of nonthermal processes. The brightness temperature of maser sources can be as high as 10^{14} K. While OH and H_2O masers correspond to transitions in the ground vibration state $v = 0$, SiO masers occur in excited vibration states $v = 1$, 2, and 3. Recently, SiS maser emission in the ground state has also been detected in the envelope of IRC + 10216 (Henkel et al., 1983).

Masers are variable sources whose intensities are correlated with those observed in the near infrared (Hjalmarson and Olofsson, 1979). A high degree of polarization has been observed. Population inversion can be achieved through pumping by infrared radiation from warm circumstellar dust grains (Elitzur et al., 1976; Bujarrabal et al., 1980) or from the central star (Kwan and Scoville, 1974; Deguchi and Iguchi, 1976; Bujarrabal and Nguyen-Q-Rieu, 1981). Details of the pumping mechanisms will be discussed in the following sections.

Two-Level Maser

It is possible to describe a simplified maser theory by representing all details of the pumping mechanism in a two-level maser using the

Table 3-1
Molecules in Stars

Molecule	Transition	Star	Characteristics
OH	Radio	Oxygen-rich	Maser emission
H_2O	Radio	Oxygen-rich	Maser emission
SiO	Radio	Oxygen- and carbon-rich	Maser and thermal emissions
CO	Radio	Oxygen- and carbon-rich	Thermal emission
SiS	Radio	Carbon-rich	Maser and thermal emissions
CN	Radio	Carbon-rich	Thermal emission
CS	Radio	Carbon-rich	Thermal emission
HCN	Radio	Carbon-rich	Thermal emission
HNC	Radio	Carbon-rich	Thermal emission
HC_3N	Radio	Carbon-rich	Thermal emission
HC_5N	Radio	Carbon-rich	Thermal emission
HC_7N	Radio	Carbon-rich	Thermal emission
$HC_{11}N$	Radio	Carbon-rich	Thermal emission
C_2H	Radio	Carbon-rich	Thermal emission
C_4H	Radio	Carbon-rich	Thermal emission
C_3N	Radio	Carbon-rich	Thermal emission
CH_3CN	Radio	Carbon-rich	Thermal emission
SiC_2	Radio	Carbon-rich	Thermal emission
NH_3	Radio and IR	Carbon-rich	Thermal emission
C_2H_2	IR	Carbon-rich	Thermal emission
C_2H_4	IR	Carbon-rich	Thermal emission
CH_4	IR	Carbon-rich	Thermal emission

pump rates (Litvak, 1972). The populations of the upper and lower levels n_u and n_l, are given by the statistical equilibrium equation:

$$n_u (A_{ul} + B_{ul}\,\Omega I/(4\pi) + C_{ul} + P_{ul}) = n_l (B_{lu}\,\Omega I/(4\pi) + C_{lu} + P_{lu}) , \quad (3\text{-}1)$$

where A_{ul}, B_{ul} are the Einstein coefficients for spontaneous and stimulated emissions, B_{lu} is the absorption coefficient, and C_{ul} and C_{lu} are the collision rates. The pump rates, P_{ul} and P_{lu}, correspond to indirect population transfer between levels u and l through other higher levels which are not considered. P_{ul} and P_{lu} are the pump rates which transfer population to the lower and to the upper level, respectively. I is the specific intensity, and Ω is the solid angle of the microwave emission.

To simplify the explanation, we shall ignore spontaneous emission and collisions and assume that the two maser levels have the same statistical weight. The rate of fractional population inversion can then be derived from Equation (3-1):

$$\frac{n_u - n_l}{n_u + n_l} = \frac{\Delta P}{P + B_{ul}\,\Omega I/(2\pi)} , \quad (3\text{-}2)$$

where $P = P_{ul} + P_{lu}$ is the total net pump rate and $\Delta P = P_{lu} - P_{ul}$ is the difference in pump rates to the upper and lower levels.

Population inversion occurs when $\Delta P > 0$. Furthermore, the maser is saturated when the stimulated emission comes very much into evidence, $B_{ul}\,\Omega I/2\pi \gg P$. The population inversion then decreases inversely proportional to the stimulated emission rate. In the saturated

regime, the pumping is the most efficient because the population of the upper level is transferred as fast as possible to the lower level through stimulated emission. The saturation intensity is defined as:

$$I_S = 2\pi P/(B_{ul}\Omega) \quad . \tag{3-3}$$

The population inversion rate $\Delta n = n_u - n_l$ can be expressed in terms of the unsaturated rate Δn_o, which is equal to $(\Delta P/P)\ (n_u + n_l)$:

$$\Delta n = \frac{\Delta n_o}{1 + (I/I_s)} \quad . \tag{3-4}$$

The maser intensity I can be obtained by the one-dimensional radiative transfer equation:

$$\frac{dI}{dx} = -\kappa I + \epsilon \quad . \tag{3-5}$$

The absorption and emission coefficients, $\varkappa$ and ϵ, are defined as:

$$\varkappa = (n_l - n_u)\ B_{ul}\ h\nu/(4\pi\Delta\nu) \quad ,$$

$$\epsilon = n_u\ A\ h\nu/(4\pi\Delta\nu) \quad ,$$

where A is the spontaneous emission coefficient, and $h\nu$ is the level energy separation of the maser transition.

The solution of Equation (3-5) is:

$$I = I_o\, e^{-\kappa x} + \frac{\epsilon}{K}\ (1 - e^{-\kappa x}) \quad . \tag{3-6}$$

When population inversion occurs, $(n_u > n_l)$, $\varkappa$ is negative, and the maser intensity increases exponentially with path length. In the saturated regime, Equation (3-5) gives:

$$\frac{dI}{dx} \simeq \frac{\kappa_o I}{1 + (I/I_s)} \simeq -\kappa_o I_s \quad , \tag{3-7}$$

and

$$I \simeq I_s\ [1 - \varkappa_o\ (x - x_s)] \quad ,$$

where $\varkappa_o = \varkappa\ (1 + I/I_s)$ and x_s is the length where saturation begins to occur.

Equation (3-7) shows that, when the maser becomes saturated, the intensity increases linearly with path length. Litvak (1971) has shown that an unsaturated maser core can be formed at the center of a spherical saturated maser cloud.

Multilevel Radiative Transfer

A detailed study of molecular excitation requires the resolution of the radiative transfer and statistical equilibrium equations, involving many molecular levels. For an expanding spherical circumstellar cloud, the population of a level i at a distance r from the central star is given by:

$$n_i(r)\ \Sigma_j\ (A_{ij} + B_{ij}\bar{J}_{ij} + C_{ij}) = \Sigma_j\ n_j\ (r)\ (A_{ji} + B_{ij}\ \bar{J}_{ij} + C_{ji}) \quad , \tag{3-8}$$

with $A_{ij} = 0$ for $j \quad i$,

and $A_{ji} = 0$ for $j \quad i$.

A and B are the Einstein coefficients, and C represents the collision rates. The mean radiation field J, integrated over the line profile and averaged over the angle, is usually calculated by use of the escape probability formalism (see, for example, Castor, 1970):

$$\bar{J} = \left\{ 1 - \beta(r) \right\}\ S(r) + \beta_c\ (r)\ I_c \quad . \tag{3-9}$$

The source function $S(r)$ is:

$$S(r) = \frac{2h\nu^3}{c^2} \Big/ \left(\frac{n_j(r) g_i}{n_i(r) g_j} - 1 \right) , \tag{3-10}$$

where g_i and g_j are the statistical weights, β is the probability that a photon emitted at r

escapes without being absorbed by the cloud, and β_c is the probability of a photon which escapes at r and strikes the central star. In general, β_c, I_c is the contribution to the intensity of all continuum sources:

$$\beta = \int_0^1 \frac{1 - e^{-\tau(\mu)}}{\tau(\mu)} \, d\mu \quad , \qquad (3\text{-}11)$$

and

$$\beta_c \simeq \frac{\Delta\Omega}{4\pi} \left\{ \frac{1 - e^{-\tau(\mu=1)}}{\tau(\mu = 1)} \right\}, \qquad (3\text{-}12)$$

where μ is the cosine of the angle θ between a radius and the line of sight (Figure 3-2). $\Delta\Omega/4\pi$ is the dilution factor of the stellar radiation field (Bujarrabal and Nguyen-Q-Rieu, 1981).

The opacity is:

$$\tau = \frac{\tau_o}{1 + (\gamma - 1)\mu^2} \quad , \qquad (3\text{-}13)$$

where γ is the logarithmic velocity gradient $d \ln V / d \ln r$, τ_o is related to the population inversion Δn by $\tau_o \propto r\Delta n / V(r)$ (Castor, 1970), and V(r) is the expansion velocity.

The population distribution of the entire set of molecular levels can be calculated by solving Equation (3-8) and using Equations (3-9) through (3-13). In particular, the population inversion of the maser transition $i \rightarrow j$ can be determined, and hence the optical depth, as well as the excitation temperature, T_{ex}:

$$\frac{n_i}{n_j} = \frac{g_i}{g_j} \, e^{-h\nu/\kappa T_{ex}} \, . \qquad (3\text{-}14)$$

The brightness temperature of the maser source can then be calculated by an integration along the line of sight:

$$T_B = \left\{ \hat{T}_{ex} - \hat{T}_{bb} \right\} (1 - e^{-\tau}) \quad , \qquad (3\text{-}15)$$

with

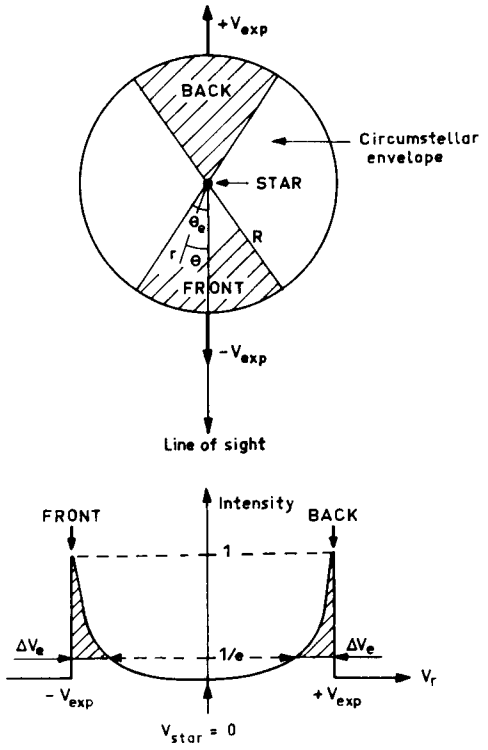


Figure 3-2. Spherical model of an OH circumstellar maser. The maser emission is confined within a double cone (hatched area) whose axis is along the line of sight (top). A schematic maser spectrum is drawn (bottom). The regions of the spectrum emanating from the hatched areas in the circumstellar envelope are also represented (hatched areas).

$$\hat{T} = \frac{h\upsilon}{k} \, (e^{h\upsilon/kT} - 1)^{-1} \quad .$$

T_{bb} is the 3 K cosmic background temperature. The convolution of T_B with the antenna beam will give the observed main-beam brightness temperature. See Equation (3-16).

Characteristics of Circumstellar Masers

Circumstellar maser emission, namely that of OH, is often characterized by a double-peaked spectrum (Figure 3-3). This shape can be explained in terms of a spherical model in which the amplification path is maximum in the direction of the line of sight which intersects

the central star (see Nguyen-Q-Rieu et al., 1979). In an expanding spherical shell for which γ is constant and positive, the velocity field can be expressed as: $V(r) = V_{exp}\,(r/R^{\gamma})$, where V_{exp} is the expansion velocity at the outer radius R. Equation (3-13) shows that the optical depth along the z axis ($\theta = 0$) is τ_0/γ (see Figure 3-1). In the case of an expansion due to radiation pressure, γ is small ($\gamma \ll 1$) and $\tau_{max} \gg \tau_0$. Hence, the maximum amplification, corresponding to the two spikes in the maser spectrum, occurs in a narrow double cone whose apex is the central star and whose axis is the line of sight (Figure 3-2). The emission at the line center corresponds to the part of the envelope outside the cone and perpendicular to the line of sight with the smallest path length. This geometrical effect is illustrated in Figure 3-2, in the case of a circumstellar shell expanding at a nearly constant velocity. The angle θ_e of the cone corresponds to the direction in which the line intensity drops to $1/e$ of the peak intensities, I_{Max}:

$$\cos\theta_e \simeq (V_{exp} - \Delta V_e)/V_{exp} \quad ,$$

where ΔV_e is the line width at $1/e\ I_{Max}$ of the narrow maser spikes.

Figure 3-3 shows the 1612-MHz OH spectrum and the maps of the maser emission from the circumstellar shell of the unidentified OH/IR object, OH26.5 + 0.6, obtained with the very large array (VLA) by Baud (1981). The maps indicate that the two maser peaks arise from two compact regions at the center of the source, while the emission toward the center of the spectrum is more extended and exhibits a ring-like structure. This observational result is consistent with the model of an expanding spherical shell described above. However, this simple model does not account for some details which can be explained by large-scale nonradial motion or turbulence which may exist in the shell.

In the framework of a symmetrical model, the OH blue-shifted and red-shifted wings correspond to the front and back of the shell, respectively. Thus, the blue-shifted wing should lead the red-shifted wing to the observer. This results in a phase lag between the blue-shifted and red-shifted components. The phase lag, which corresponds to the light travel time across the entire shell, is ~1 month for a shell size ~8 $\times$ 10^{16} cm.

The determination of the phase lag, and hence the linear source size, by means of a monitoring of the OH maser emission, combined with interferometric measurements of the angular size, constitutes a powerful method to estimate the distance of the stars (Shultz, et al., 1978; Jewell et al., 1979; Booth et al., 1981; Baud, 1981; Herman, 1983). This method has been extensively used to measure the distance of unidentified OH/IR sources for which no period/luminosity relation in the visible is available.

Another interesting feature of the OH and SiO circumstellar masers is that the maser emission is correlated with the infrared and optical phases (Harvey et al., 1974; Fillit et al., 1977; Jewell et al., 1979; Hjalmarson and Olofsson, 1979). However, the SiO fluxes appear to have a phase lag with respect to the visual light curve (see Hjalmarson and Olofsson, 1979). The correlation with the infrared fluxes suggests that the maser emission is pumped by a radiative process.

The pumping by 35-μm photons emitted by circumstellar grains may be operative in the shell and gives rise to OH masers (Elitzur et al., 1976; Bujarrabal et al., 1980). It has been suggested that direct stellar radiation can pump OH masers (Cimerman and Scoville, 1980). The pumping of the SiO and SiS masers is achieved by the infrared photons emitted by the central star. Although the OH maser emission extends far from the star, at several 10^3 stellar radii (Reid et al., 1981), SiO masers occur very close to the stellar atmosphere at a few stellar radii (Elitzur, 1980; Bujarrabal and Nguyen-Q-Rieu, 1981). This is due to the fact that OH can be excited by infrared radiation from warm circumstellar dust and that SiO is pumped by the stellar radiation. Strong SiS maser spikes also arise near the stellar surface. The pumping mechanism of H_2O masers is not well

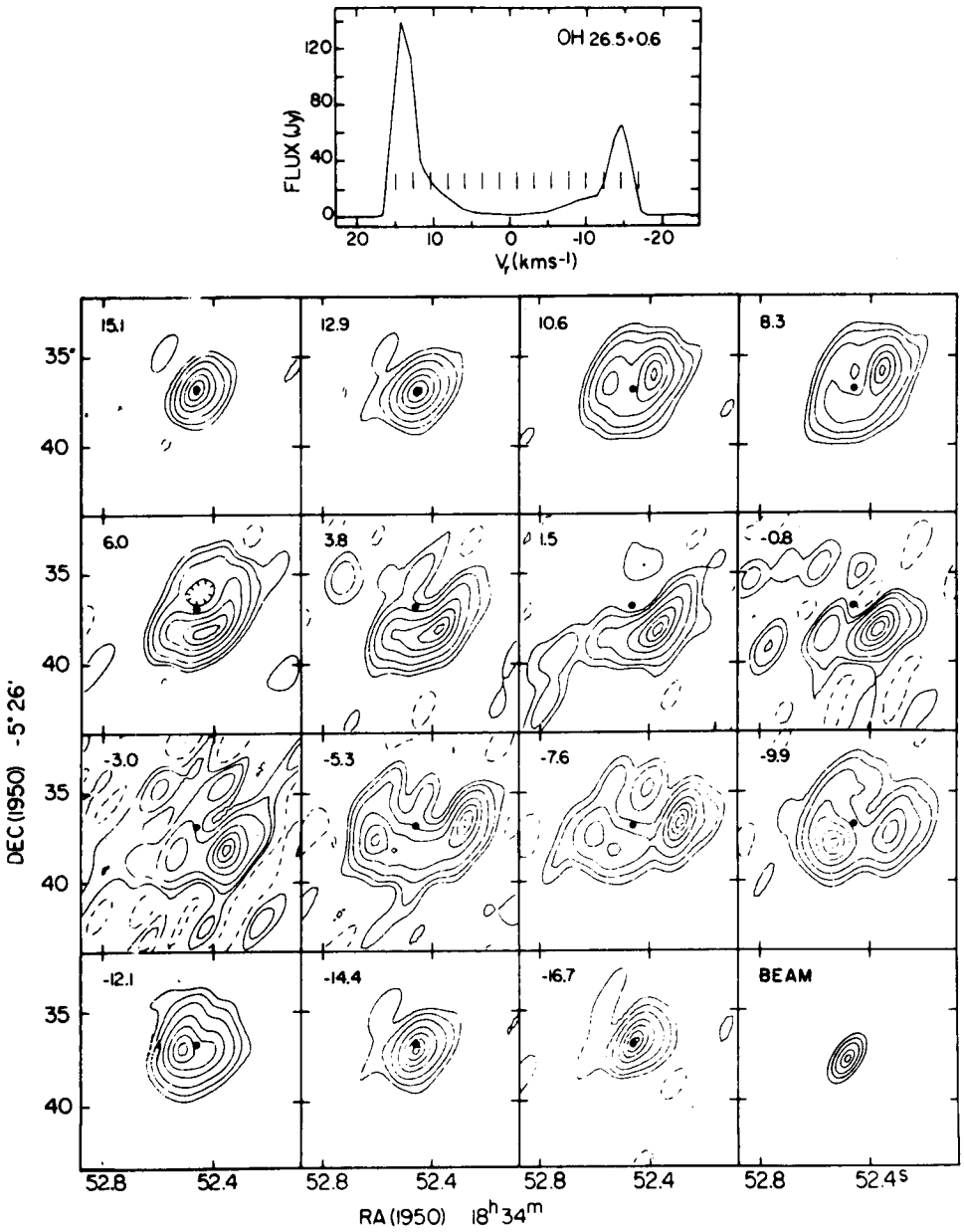


Figure 3-3. The OH spectrum (1612-MHz satellite line) (top) and the corresponding maps at different radial velocities (with respect to the stellar velocity taken equal to zero) of the OH/IR source, OH26.5 + 0.6, observed with the VLA by Baud (1981). The dot in each frame corresponds to the stellar position. Radial velocities in km s^{-1} are noted on top (left) of each frame, and the beam shape is represented in the frame at bottom right. In a spherical shell, the maps corresponding to the extreme radial velocities, 15.1 and -16.7 km s^{-1} (red-shifted and blue-shifted peaks, respectively), are associated with the part of the envelope confined within a small area in the double cone (see also Figure 3-2), where the maser amplification is maximum. The maps taken at velocities closer to the stellar velocity and corresponding to more extended areas outside the cone show a more complicated shape, in particular a ring structure (e.g., at velocities 3.8 and -5.3 km s^{-1}).

understood because of the complexity of the energy level structure.

Figure 3-4 displays the SiS maser spectrum in the ground state (v = 0, J = 1–0 at 1.65-cm wavelength of the carbon star, IRC + 10216, observed at minimum light with the 140-ft radio telescope at Green Bank together with the calculated profile (dots) derived from an excitation model of the kind described in the section *Multilevel Radiative Transfer* (Nguyen-Q-Rieu et al., 1984). The narrow maser spike at -40 km s^{-1} is likely to be produced by the amplification of the emission of the infrared core by the gas in the immediate vicinity of the core. The observations by Henkel et al. (1983) made at maximum infrared light indicate that the maser intensity is increased by ~40 percent as compared with the intensity at minimum.

The increase of the infrared flux and of the mass loss during maximum light could be responsible for the enhancement of the SiS maser emission. It is noteworthy that weak CO maser emission can exist in the circumstellar envelope (Morris, 1980).

Strong circumstellar masers are probably saturated. They are usually not subject to erratic time variation, but instead vary smoothly with the stellar phase.

OH emission is known to be polarized, up to ~60 percent (Robinson et al., 1970). Circular polarization is usually observed, but in some cases, polarization can change from circular to linear. Significant linear polarization has been detected in SiO maser spectra (Troland et al., 1979). The position angles of the polarized features vary with time. In the case of the Mira variable, R Cas, sudden changes in the position angles have been detected near the maximum of the optical light curve (Clark et al., 1982). Shock waves which can affect the gain paths and the orientation of the maser cells are believed to be responsible for this sudden variation.

THERMAL EMISSION

Thermal CO emission in the ground-state (v = 0, J = 1–0) at 2.6 mm has been discovered

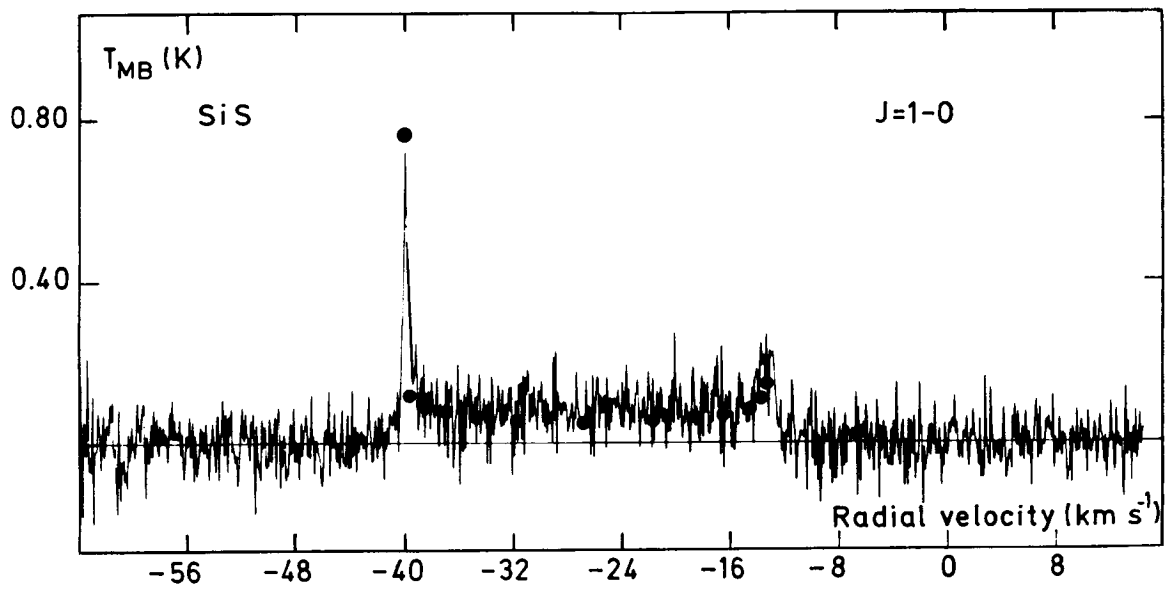


Figure 3-4. The 18155-MHz SiS (J = 1–0) spectrum of the carbon star IRC + 10216. Dots correspond to the theoretical spectrum derived from an excitation model. The blue-shifted feature at -40 km s^{-1} is the result of an amplification of the background stellar core by the SiS circumstellar maser cloud (from Nguyen-Q-Rieu et al., 1984).

in the envelope of the carbon star, IRC + 10216 (Solomon et al., 1971). Thermal emission from SiO, CO, CN, and CS (ground-state) and their isotopes was later detected in a number of oxygen-rich and carbon-rich stars, as well as in some S-type stars (Wilson et al., 1971; Zuckerman et al., 1977, 1978; Lo and Bechis, 1977; Lambert and Vanden Bout, 1978; Wannier et al., 1979; Olofsson et al., 1982a). Molecular species like HNC, HCN, HC_3N, and other linear carbon chain molecules also exist in the shell of carbon-rich stars (Jewell and Snyder, 1984; Olofsson et al., 1982b).

Figure 3-5 shows the spectra of HNC (J = 1-0), SiS (J = 5-4), and HC_3N (J = 10-9) observed simultaneously in the direction of IRC + 10216 using the millimeter Onsala radiotelescope equipped with a broadband receiver (Olofsson et al., 1982a).

Contrary to SiO masers which arise in the vicinity of the central star, thermal molecular line emission extends over the entire envelope. In this respect, thermal spectra give information on the physical parameters of the entire shell (namely, the mass loss, gas, and dust densities). For example, spatial CO mapping of the envelope of IRC + 10216 suggests that the present mass loss rate may have been higher in the past (Wannier et al., 1979). The determination of the abundance of molecules and their isotopic substitutes is useful in the understanding of the processing of matter involving the mixing mechanisms (Iben, 1981) and the photodestruction process caused by the interstellar ultraviolet radiation field (Huggins and Glassgold, 1982). Neutral/neutral reactions seem to be important in circumstellar shells, while interstellar chemistry is dominated by ion/molecule reactions. This is due to the fact that high temperatures (>100 K) allow endothermic reactions, as well as others with activation energy barriers, to proceed in the circumstellar envelope (Scalo and Slavsky, 1980; Lafont et al., 1982).

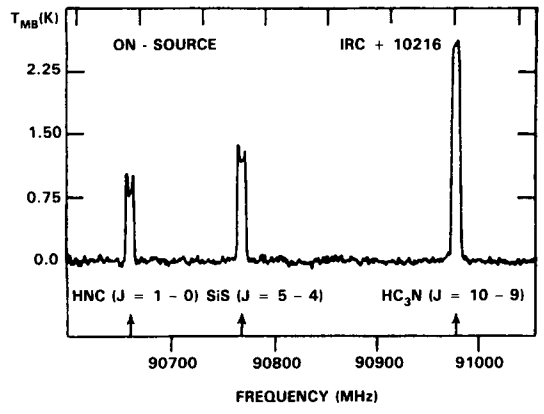


Figure 3-5. Simultaneous observations of HNC, SiS, and HC_3N lines around 91000 MHz from IRC + 10216, using a broadband receiver installed at the focus of the 20-m Onsala radio telescope (from Olofsson et al., 1982a).

Molecular Excitation and Line Profiles

The excitation of circumstellar molecules is governed by Equation (3-8) in which both collisional and radiative processes are involved. Collisions, essentially with H_2, tend to thermalize the lines. This is usually the case with CO lines in dense envelopes. Infrared radiation from the central star and dust embedded in the envelope can produce population inversion as discussed in the section *Characteristics of Circumstellar Masers.*

The main-beam brightness temperature, T_{MB}, at a radial velocity, V_r, is obtained by convolving the brightness temperature distribution, T_B (see Equation (3-15)) with the antenna main beam, which is assumed to be gaussian (Olofsson et al., 1982a):

$$T_{MB}(V) = \frac{81n2}{B^2} \int_{pmin}^{pmax} T_B(p, V_r)\, e^{-41n2\,(p/B)^2}\, pdp \quad , \tag{3-16}$$

where B is the full width at half power (FWHP) of the antenna beam and $p = r\left\{1 - (V_r/V_{exp})^2\right\}^{1/2}$ (see Figure 3-1). In Equation (3-16), we have assumed a uniformly excited

spherical shell (T_{ex} is constant throughout the shell), expanding at a constant velocity. If the mass-loss rate is constant, the total particle density is $N(r) \propto r^{-2}$. The optical depth can be expressed as (Olofsson et al., 1982a):

$$\tau(p,V_r) = \tau(B,0) \times B \left\{ p\,(1 - V_r/V_{exp})^2)^{1/2} \right\}^{-1} .$$

The diagram (Figure 3-6) which represents the line profiles T_{MB} (V_r) as a function of the optical depth, τ(B,0), and the shell size, R_e, expressed in units of beamwidth, B, is calculated using Equation (3-16).

For an unresolved optically thin shell (position 1 in the diagram), the profile is rectangular. The line shape is parabolic if the shell is optically thick (position 2) and becomes flatter when the shell size is extended with respect to the antenna beam (positions 3 and 5). The profile can exhibit a double-peaked structure for an optically thin and resolved shell (position 4). These effects can be explained by the fact that, when the source is resolved by the telescope beam, the part of the shell which is not inside the beam corresponds to low radial velocity line center. As a result, the contribution of this outer shell to the main-beam brightness temperature is not important and leads to a more or less pronounced depression at the line center. Therefore, a quick inspection of the line profiles can indicate the nature of the circumstellar shell.

Line Asymmetry and Time Variation

Figure 3-7 shows a variety of line profiles observed in the direction of IRC + 10216

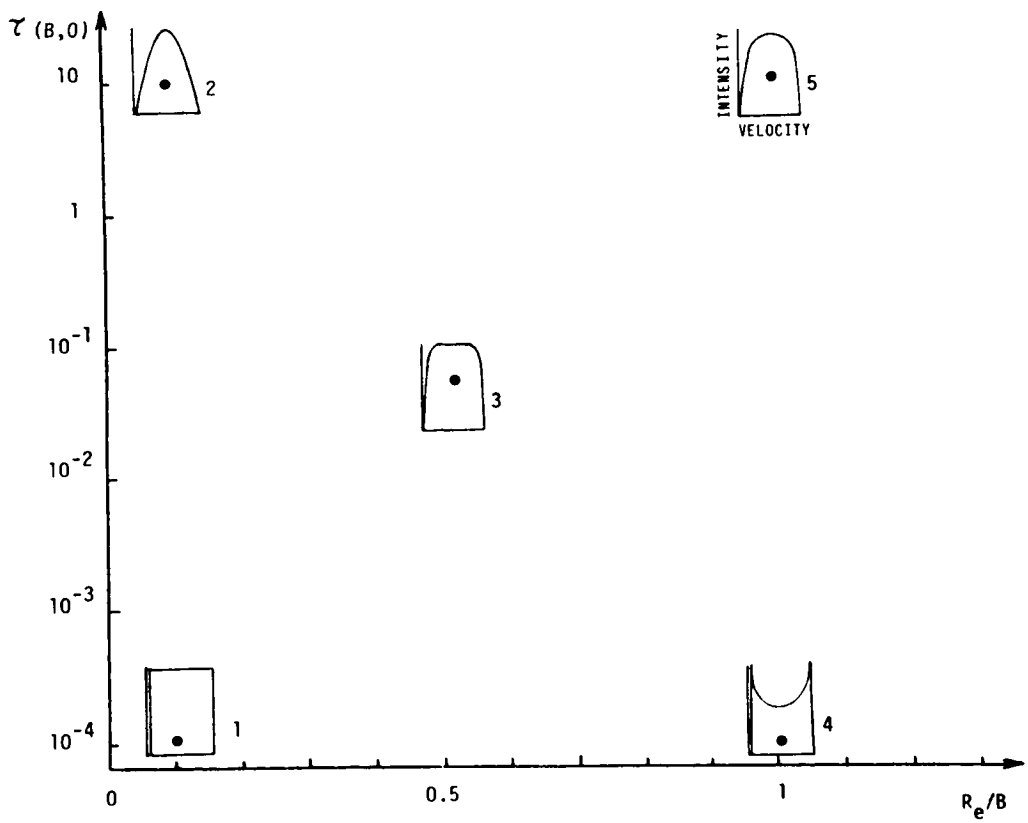


Figure 3-6. A diagram representing various line shapes as a function of optical depth (ordinate) and source size R_e in unit of beamwidth B (abscissa). Dots correspond to the points in the diagram for which the line profiles are calculated.

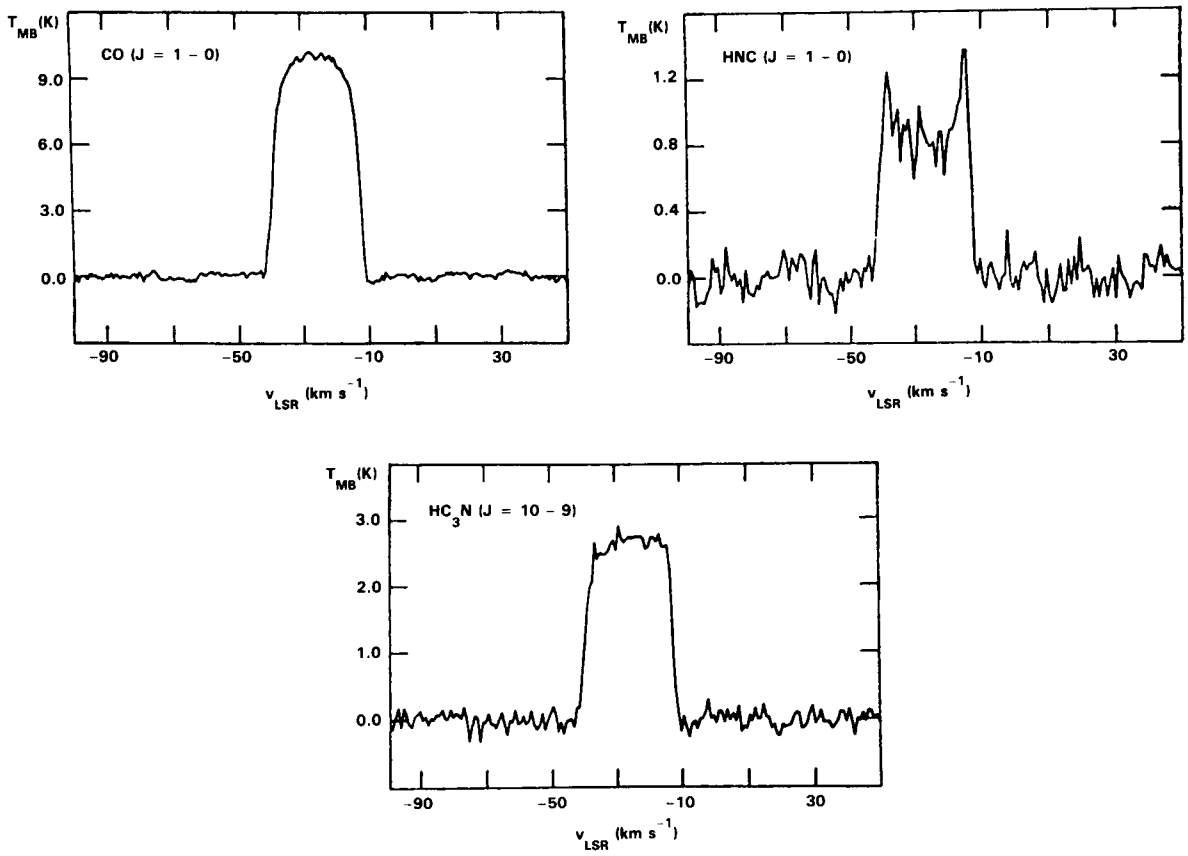


Figure 3-7. A sample of spectra (CO at 115271 MHz, HNC at 90663 MHz, and HC_3N at 90979 MHz) from IRC + 10216 obtained with a high resolution spectrometer $\nu/\Delta\nu \sim 4 \times 10^5$) (from Olofsson et al., 1982a). V_{LSR} is the radial velocity relative to the local standard of rest.

(Olofsson et al., 1982a). The spectra correspond to different line opacities and source sizes, according to the diagram shown in Figure 3-6. The CO line emanates from an optically thick extended shell. The HNC and HC_3N transitions correspond to optically thin regions. Although the HNC shell is resolved by the telescope beam, the HC_3N shell appears to be a point source. Theoretically, an estimate of the shell parameters can be derived by fitting the main-beam brightness temperature profiles, calculated by using Equation (3-16), to the observed spectra. However, the observed profiles (Figure 3-7) present some asymmetry in the sense that the blue-shifted wing is systematically weaker than the red-shifted one. This effect is most prominent in the case of ^{13}CO (Figure 3-8). It should be mentioned that in the SiS J = 1-0 profile (Figure 3-4), the depression of the blue-shifted wing is disguised by the maser action which amplifies the stellar radiation and thereby gives rise to a narrow spike at the blue wing.

In fact, the hypothesis of a constant excitation temperature throughout the circumstellar cloud cannot account for the line asymmetry. The inner shell is more excited and hotter than the outer shell. As a result, along the line of sight, outer colder material is absorbing emission from the hotter inner layers in the front hemisphere, but such absorption does not affect the back hemisphere. Similar asymmetry also seems to be observed in α Ori (Knapp et al., 1980).

In order to account for this effect, instead of using Equation (3-15), we shall calculate the

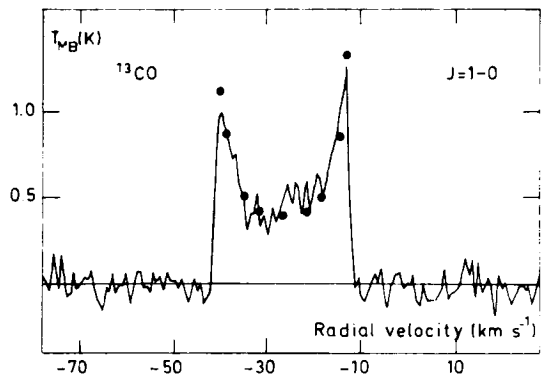


Figure 3-8. The ^{13}CO spectrum (110201 MHz) from IRC + 10216 showing the line asymmetry (blue-shifted wing weaker than red-shifted wing). Dots represent the spectrum derived from a theoretical model (Nguyen-Q-Rieu et al., 1984) which explains the asymmetry in terms of an absorption of the emission from the hot inner part of the envelope by the colder outer layers.

brightness temperature separately for the front (T_{B-}) and back (T_{B+}) hemispheres by integrating along the line of sight (see Figure 3-1):

$$T_{B-} = \int_{-\infty}^{0} (\hat{T}_{ex}(z) - \hat{T}_{bb})\, e^{-\tau_-(z)}\, \kappa(z) dz \quad . \tag{3-17}$$

$$T_{B+} = \int_{0}^{\infty} (\hat{T}_{ex}(z) - \hat{T}_{bb})\, e^{-\tau_+(z)}\, \kappa(z)\, dz \quad . \tag{3-18}$$

With

$$\tau_- = \int_{-\infty}^{z} \kappa(z')\, dz'$$

and

$$\tau_+ = \int_{0}^{z} \kappa(z')\, dz' ,$$

$\kappa(z)$ is the line absorption coefficient.

Figure 3-8 displays the observed ^{13}CO spectrum of IRC + 10216, together with the spectrum computed (dots) by Equations (3-17), (3-18), and (3-16) (Nguyen-Q-Rieu et al., 1984; see also Morris et al., 1985).

The molecular line shape is sensitive to the variation of infrared light. At the maximum of the infrared light curve, infrared photons (~ 10 μm) escaping from the central heating sources (star or infrared core) can affect the outer shell and enhance the line wings (Sahai et al., 1984). The contrast between the line wings and the line center can be higher at maximum light than at minimum. In the case of IRC + 10216, it has been shown that, at maximum, the line center and the line wings of the SiS $J = 6$–5 transition can be enhanced by ~ 20 and ~ 40 percent, respectively (Nguyen-Q-Rieu et al., 1984).

CONCLUSION AND PROSPECTS

Radio molecular lines appear to be useful probes into the stellar environment. SiO masers which are excited by stellar photons to a vibrational level as high as $v = 3$ (Scalise and Lépine, 1978), which corresponds to an energy $E/k \sim 5300$ K, provide information on the physical conditions in the immediate vicinity of the stellar photosphere. Lower vibrationally excited transitions of SiO occur in $v = 0$ and 1 ($E/k \lesssim 1800$ K) sample regions in which dust grains begin to form. The proximity of SiO masers to the pulsating stellar atmosphere implies that SiO observations can shed light on the kinematics and mass-loss process in the innermost layers. As explained in the sections *Multilevel Radiative Transfer* and *Characteristics of Circumstellar Masers*, the maser amplification and hence the line shape depend on the velocity gradient. SiO maser emission does not usually exhibit a double-peaked profile typical of OH masers, but a single feature centered at the stellar velocity. This observational difference

suggests that the velocity gradient in the inner region in which SiO occurs is higher (see Equation (3-13), where $\gamma = d\log V/d\log r$ is now $>> 1$) than in the external envelope in which OH masers are located ($\gamma << 1$). OH masers and thermal molecular emission of CO and other molecules, including cyanopolyynes, which can be excited by collisions with H_2 and by infrared radiation from circumstellar dust, can be used as probes into the physical conditions (on a larger scale) throughout the envelope. Valuable information on the physics operating in the envelope of IRC + 10216 has been recently obtained by high sensitivity observations and detailed theoretical analyses (Morris, 1975; Wannier et al., 1979; Kwan and Linke, 1982; Olofsson, et al., 1982a; Nguyen-Q-Rieu et al., 1984). However, accurate circumstellar chemistry still suffers from the lack of data on chemical processes. Chemistry is usually assumed to be frozen at its equilibrium state in the inner region and unchanging during the expansion of the envelope (McCabe et al., 1979). This is probably true for species which are not highly reactive, but not for radicals. Nonequilibrium chemistry may take place, for instance, in the regions in which molecular abundances are governed by photodissociation, which tends to produce radicals (Goldreich and Scoville, 1976; Scalo and Slavsky, 1980; Lafont et al., 1982). In this respect, mapping of the envelope of IRC + 10216 in the molecular lines emitted by some radicals and parent molecules is highly desirable. Present molecular observations of the envelopes of stars of various types (Olofsson et al., 1982b) and those with the millimeter radio telescopes of Institut de Radioastronomie Millimétrique (IRAM) may also cast some light on the problem of chemistry (see Glassgold and Huggins, this volume).

Infrared speckle interferometry in the molecular lines (Dyck et al., 1983) and in the continuum (Foy et al., 1979; Dyck et al., 1984) is helpful in the investigation of the inner region of the envelope.

The distribution of the circumstellar dust, whose emission contributes to the molecular excitation, can be determined by photometric measurements with a range of 1 to ~ 100 μm. In this respect, the preliminary results obtained with the instruments on board the Infrared Astronomical Satellite (IRAS) seem to indicate that many infrared objects associated with OH masers are extremely red and may experience mass-loss rates higher than 10^{-4} $M_\odot$ yr^{-1} (Olnon et al., 1984). High resolution spectroscopy using the Infrared Space Observatory (ISO) will also be of great importance in the detection of molecular transitions in a wide range of infrared wavelengths.

REFERENCES

Adams, W.S. 1941, *Astrophys. J.*, **93**, 11.

Baud, B. 1981, *Astrophys. J. (Letters)*, **250**, L79.

Baud, B., Habing, H.J., Matthews, H.E., and Winnberg, A. 1979a, *Astron. Astrophys. Supplement*, **35**, 179.

Baud, B., Habing, H.J., Matthews, H.E., and Winnberg, A. 1979b, *Astron. Astrophys. Supplement*, **36**, 193.

Bell, M.B., Feldman, P.A., Kwok, S., and Matthews, H.E. 1982, *Nature*, **295**, 389.

Bernat, A.P. 1981, *Astrophys. J.*, **246**, 184.

Booth, R.S., Kus, A.J., Norris, R.P., and Porter, N.D. 1981, *Nature*, **290**, 382.

Bowers, P.F. 1978, *Astron. Astrophys. Supplement*, **31**, 127.

Bujarrabal, V., Guibert, J., Nguyen-Q-Rieu, and Omont, A. 1980, *Astron. Astrophys.*, **84**, 311.

Bujarrabal, V., and Nguyen-Q-Rieu 1981, *Astron. Astrophys.*, **102**, 65.

Castor, J.I. 1970, *Mon. Not. Roy. Astr. Soc.*, **149**, 111.

Cheung, A.C., Rank, D.M., Townes, C.H., Thornton, D.D., and Welch, W.J. 1968, *Phys. Rev. Letters*, **21**, 1701.

Cheung, A.C., Rank, D.M., Townes, C.H., and Welch, W.J. 1969, *Nature*, **221**, 917.

Cimerman, M., and Scoville, N. 1980, *Astrophys. J.*, **239**, 526.

Clark, F.O., Troland, T.H., and Johnson, D.R. 1982, *Astrophys. J.*, **261**, 569.

Deguchi, S., and Iguchi, I. 1976, P.A.S.J. **28**, 307.

Dyck, H.M., Beckwith, S., and Zuckerman, B. 1983, *Astrophys. J. (Letters)*, **271** , L79.

Dyck, H.M., Zuckerman, B., Leinert, C., and Beckwith, S. 1984, *Astrophys. J.*, **287**, 801.

Elitzur, M. 1980, *Astrophys. J.*, **240**, 553.

Elitzur, M., Goldreich, P., and Scoville, N. 1976, *Astrophys. J.*, **205**, 384.

Engels, D. 1979, *Astron. Astrophys. Supplement*, **36**, 337.

Epchtein, N., and Nguyen-Q-Rieu 1982, *Astron. Astrophys.*, **107**, 229.

Evans, N.J., and Beckwith, S. 1977, *Astrophys. J.*, **217**, 729.

Fillit, R., Proust, D., and Lépine, J.R.D. 1977, *Astron. Astrophys.*, **58**, 281.

Foy, R., Chelli, A., Sibille, F., and Léna, P. 1979, *Astron. Astrophys.*, **79**, L5.

Glass, I.S. 1978, *Mon. Not. Roy. Astr. Soc.*, **182**, 93.

Goldreich, P., and Scoville, N.Z. 1976 *Astrophys. J.*, **205**, 144.

Harvey, P.M., Bechis, K.P., Wilson, W.J., and Ball, J.A. 1974, *Astrophys. J. Supplement*, **27**, 331.

Henkel, C., Matthews, H.E., and Morris, M. 1983, *Astrophys. J.*, **267**, 184.

Herman, J. 1983, Thesis, Sterrewacht Leiden.

Hjalmarson, A., and Olofsson, H. 1979, *Astrophys. J. (Letters)*, **234**, L199.

Huggins, P.J., and Glassgold, A.E. 1982, *Astron. J.*, **87**, 1828.

Iben, I., Jr. 1981, in *Physical Processes in Red Giants*, ed. I. Iben, Jr., and A. Renzini, (Dordrecht: Reidel), p. 3.

Jewell, P.R., Elitzur, M., Webber, J.C., and Snyder, L.E. 1979, *Astrophys. J. Supplement*, **41**, 191.

Jewell, P.R., and Snyder, L.E. 1984, *Astrophys. J.*, **278**, 176.

Johansson, L.E.B., Andersson, C., Goss, W.M., and Winnberg, A. 1977, *Astron. Astrophys. Supplement*, **28**, 199.

Kaifu, N., Buhl, D., and Snyder, L.E. 1975, *Astrophys. J.*, **195**, 359.

Knapp, G.R., Phillips, T.G., and Huggins, P.J. 1980, *Astrophys. J. (Letters)*, **242**, L25.

Kwan, J., and Linke, R.A. 1982, *Astrophys. J.*, **254**, 587.

Kwan, J., and Scoville, N. 1974, *Astrophys. J. (Letters)*, **194**, L97.

Knowles, S.H., Mayer, C.H., Cheung, A.C., Rank, D.M., and Townes, C.H. 1969, *Science*, **163**, 1055.

Lafont, S., Lucas, R., and Omont, A. 1982, *Astron. Astrophys.*, **106**, 201.

Lambert, D.L., and Van den Bout, P.A. 1978, *Astrophys. J.*, **221**, 854.

Litvak, M.M. 1971, *Astrophys. J.*, **170**, 71.

Litvak, M.M. 1972, *Collisional and Radiative Processes in Interstellar Molecules*, Part I, ed. A. Sume, Research Lab. of Electronics and Onsala Space Observatory.

Lo, K.Y., and Bechis, K. 1977, *Astrophys. J. (Letters)*, **281**, L27.

McCabe, E.M., Smith, R.C., and Clegg, R.E.S. 1979, *Nature*, **281**, 263.

McKellar, A. 1940, P.A.S.P. **52**, 187.

Morris, M. 1975, *Astrophys. J.*, **197**, 603.

Morris, M. 1980, *Astrophys. J.*, **236**, 823.

Morris, M., Lucas, R., and Omont, A. 1985, *Astron. Astrophys.*, **142**. 107.

Nguyen-Q-Rieu, Bujarrabal, V., Olofsson, H., Johansson, L.E.B., and Turner, B.E. 1984, *Astrophys. J.*, **286**, 276.

Nguyen-Q-Rieu, Fillit, R., and Gheudin, M. 1971, *Astron. Astrophys.*, **14**, 154.

Nguyen-Q-Rieu, Laury-Micoulaut, C., Winnberg, A., and Schultz, G.V. 1979, *Astron. Astrophys.*, **75**, 351.

Olnon, F.M., Baud, B., Habing, H., de Jong, T., Harris, S., and Pottasch, S.R. 1984, *Astrophys. J. (Letters)*, **278**, L41.

Olofsson, H., Johansson, L.E.B., Hjalmarson, A., and Nguyen-Q-Rieu. 1982a, *Astron. Astrophys.*, **107**, 128.

Olofsson, H., Johansson, L.E.B., Nguyen-Q-Rieu, Sopka, R.J., and Zuckerman, B. 1982b, Bull. Amer. Astron. Soc., **14**, 895.

Reid, M.J., Moran, J.M., and Johnston, K.J. 1981, *Astron. J.*, **86**, 897.

Ridgway, S.T. 1981, in *Physical Processes in Red Giants*, ed. I. Iben, Jr., and A. Renzini (Dordrecht: Reidel), p. 305.

Robinson, B.J., Caswell, J.L., and Goss, W.M. 1970, *Astrophys. Letters*, **7**, 79.

Robinson, B.J., Caswell, J.L., and Goss, W.M. 1971, *Astrophys. Letters*, **7**, 163.

Sahai, R., Wootten, A., and Clegg, R.E.S. 1984, *Astrophys. J.*, **284**, 144.

Scalise, E., and Lépine, J.R.D. 1978, *Astron. Astrophys.*, **65**, L7.

Scalo, J.M., and Slavsky, D.B. 1980, *Astrophys. J. (Letters)*, **239**, L73.

Schultz, G.V., Kreysa, E., and Sherwood, W.A. 1976, *Astron. Astrophys.*, **50**, 171.

Schultz, G.V., Sherwood, W.A., and Winnberg, A. 1978, *Astron. Astrophys.*, **63**, L5.

Schwartz, P.R., and Barrett, A.H. 1970, *Astrophys. J. (Letters)*, **159**, L123.

Snyder, L.E., and Buhl, D. 1974, *Astrophys. J. (Letters)*, **189**, L31.

Solomon, P., Jefferts, K.B., Penzias, A.A., and Wilson, R.W. 1971, *Astrophys. J. (Letters)*, **163**, L53.

Spencer, J.H., Winnberg, A., Olnon, F.M., Schwartz, P.R., Matthews, H.E., and Downes, D. 1981, *Astron. J.*, **86**, 392.

Swings, P., and Rosenfeld, L. 1937, *Astrophys. J.*, **86**, 483.

Thaddeus, P., Cummins, S.E., and Linke, R.A. 1984, *Astrophys. J.* (*Letters*), **283**, L45.

Troland, T.H., Heiles, C., Johnson, D.R., and Clark, F.O. 1979, *Astrophys. J.*, **232**, 143.

Wannier, P.G., Leighton, R.B., Knapp, G.R., Redman, R.O., Phillips, T.G., and Huggins, P.J. 1979, *Astrophys. J.*, **230**, 149.

Wilson, R.W., Solomon, P.M., Penzias, A.A., and Jefferts, K.B. 1971, *Astrophys. J.* (*Letters*), **169**, L35.

Wilson, W.J., and Barrett, A.H. 1972, *Astron. Astrophys*, **17**, 385.

Winnberg, A., Goss, W.M., Hoglund, B., and Johansson, L.E.B. 1973, *Astrophys. Letters*, **13**, 125.

Zuckerman, B., Palmer, P., Gilra, D.P., Turner, B.E., and Morris, M. 1978, *Astrophys. J.* (*Letters*), **220**, L53.

Zuckerman, B., Palmer, P., Morris, M., Turner, B.E., Gilra, D.P., Bowers, P.F., and Gilmore, W. 1977, *Astrophys. J.* (*Letters*), **211**, L97.

N88-11596

4

CIRCUMSTELLAR SHELLS, THE FORMATION OF GRAINS, AND RADIATION TRANSFER

Jean Lefèvre

Advances in infrared astronomy during the last decade have firmly established the presence of dust around a large number of cold giant and supergiant stars. To describe the properties of stars and to understand their evolution, it is necessary to know the nature of the grains and their influence on stellar radiation. Two questions are considered in this chapter:

- How are grains formed around cold stars?
- How is the stellar radiation modified by shell?

These questions require a highly detailed description of grain properties. The development of high angular resolution measurements that permit the spatial analysis of scattered and emitted radiation and of molecular composition of the gas will increase the importance of studies on circumstellar shells.

GRAIN FORMATION

The formation and growth of grains in the shells of cold stars has recently been discussed by several authors. The most comprehensive works are those by Draine (1979, 1981), Deguchi (1980), Yamamoto and Hasegawa (1981), and Donn (1979). A critical review of this problem was also given by Czyzak et al. (1982). The formalism generally adopted is that of the theory of homogeneous nucleation. The basic ideas and the main results of the theory are recalled without mentioning the detailed calculations. The papers quoted above and references therein give a complete description of the theory. The particular circumstances encountered in circumstellar shells and in the neighborhood of variable stars will be considered with special attention.

Nucleation

In the theory of homogeneous nucleation, the solid clusters or aggregates grow or decay atom by atom (or molecule by molecule). For clusters of each size, there is a competition between gain and loss. The formation of solid grains really occurs only if the random process is able to produce a critical size beyond which the grain grows to its final size. For a cluster, the probability of growth by collision with a particle of the gas is proportional to its surface area: it is a slowly growing function of n, the number of atoms in the solid cluster. The probability of decay is related to the cohesion forces

that keep the atoms together in the cluster. These forces are stronger when the number of atoms is higher (Gerlach, 1969). The probability of decay is then a decreasing function of n. When the partial pressure of condensing particles of the gas (monomers) equals the saturation pressure of the solid, gains and losses balance exactly for the bulk solid. When the partial pressure is lower than the saturation pressure, losses prevail over gains, whatever the size of the cluster. Finally, when the partial pressure is higher than the satuation pressure, a finite size exists for which losses and gains balance exactly. This equilibrium is unstable; any cluster can grow indefinitely if it becomes slightly larger than the critical size. It is then possible to define the critical nucleus as the smallest cluster, which, after growth by the addition of one atom, has a greater probability to grow than to decay. The rate of nucleation is the rate of the reaction leading from the critical nucleus to the next larger cluster. Thus, the existence of a critical size is a consequence of the variation of the free energy as a function of the number of atoms in the cluster. When this number is large (e.g., when the size of the cluster is about 10 Å ($n \sim 10^3$)), the variation of free energy can be related to the surface tension of the bulk material. If the critical nucleus is supposed to be spherical, its radius is then:

$$a^* = \frac{2\,\sigma\,m}{\rho\,kT \ln S} \quad , \tag{4-1}$$

where m is the mass of the monomer, p is the density of the solid, T is the temperature, and, S is the supersaturation ratio defined by:

$$S = \frac{P}{P_{sat}} \quad . \tag{4-2}$$

P is the partial pressure of the monomer, and P_{sat} is the saturation pressure of the solid at temperature T.

Actually, the condensation is effective only when the critical nucleus is very small. It is then no longer possible to use the same value for the surface tension or even to define the surface. This problem has been discussed in detail by Draine (1979). He was able to show, for graphite, that the number of atoms in the critical nucleus, n^*, is obtained with the value $\sigma/2$ when $n^* > 10$:

$$n^* = \text{integer part} \left\{ \frac{4\pi}{3} \cdot \left(\frac{m}{\rho} \right)^2 \cdot \left(\frac{\sigma}{kT \ln S} \right)^3 \right\} \quad . \tag{4-3}$$

The critical nucleus is sometimes defined as the smallest cluster for which the growth prevails. Equation (4-3) then corresponds to $n^* - 1$ (Draine, 1981; Deguchi, 1980).

The stationary nucleation rate in a dilute gas is obtained by multiplying the number of critical nuclei by the rate of collision of monomers with a nucleus:

$$J = \alpha\,\Gamma \left(\frac{m\sigma}{\pi\rho^2} \right)^{1/2} C_1^2 \exp \left\{ - \frac{n^* \ln S}{2} \right\} \quad , \tag{4-4}$$

where C_1 is the concentration of the monomer, and α is the sticking probability for an atom onto the critical nucleus. Usually known as the Lothe and Pound factor, Γ includes the translational, rotational, and vibrational partition functions of the atoms within the solid (Tabak et al., 1975; Deguchi, 1980). This point was discussed by Draine (1979), who concluded that the Lothe and Pound factor does not give the correct result when $n < 20$, at least for graphite. However, Czyzak et al. (1982) mention that a minor increase in surface energy would compensate for the effect of the Lothe and Pound factor on the nucleation rate. The question is open to discussion. Theoretically, the problem can be solved in each case by extrapolating the variation of the free energy as a function of n when n tends toward zero (Mutaftschiev, 1982).

In any case, since n^* varies as $(\ln S)^{-3}$, the argument of the exponential in the nucleation rate varies as $-(\ln S)^{-2}$. It is generally small when S is lower than 6 or 7. When S is small, the critical nucleus is large and its appearance has a low probability. Finally, the uncertainty of the value of α must be kept in mind. $\alpha = 1$ is often used, and this gives an upper limit for J. The same formulation can be saved if a new definition of the supersaturation ratio is given (Lucy, 1976; Lefèvre, 1979; Draine, 1981):

$$S = \frac{P}{P_{sat}(T_g)} \left(\frac{T_g}{T}\right)^{1/2}, \qquad (4\text{-}5)$$

where T_g is the temperature of the grains and T that of the gas. The modification may be important since P_{sat} varies rapidly with the temperature. Thus it is necessary to know the temperature of clusters containing a few atoms or several tens of atoms. A large gap exists between the quantum mechanical description of polyatomic molecules and the classical one of grains with several hundreds of atoms. The extrapolation of the results of the Mie theory toward very small dimensions is problematic. A reasonable limit probably corresponds to grains of radius greater than 10 Å, even when the modification of the refractive index due to the mean-free-path limitation of electrons is taken into account.

The attempt of Draine (1981) to solve this problem is interesting but rather risky. On one hand, the optical properties of grains of silicate are extrapolated to aggregate as small as 3 Å; on the other hand, the vibrational temperature of the molecule SiO is calculated with a simplified model. This molecule plays an important part in the kinetics of the formation of silicates. The value of the temperature obtained for the aggregates and for the molecules is the same with several gas densities. Thus, it can be hoped that the correct value is obtained in this way. The right fit, however, depends on the optical properties adopted for the silicate. Moreover, the same calculation done for small graphite grains would give a higher temperature. The fit would exist then only if the vibrational temperature of molecules C_2, C_3 ... were higher than that of SiO. The experimental and theoretical study of optical properties of very small aggregates is possible and would allow a complete description of the nucleation in a radiation field. The crux of the matter is the onset of collective phenomena when the number of atoms increases in the cluster.

What could be the influence of a chromosphere on the existence and the condensation of grains? As long as their equilibrium temperatures are radiative, grains can survive in a hot gas. For instance, near a star at 3000 K, the temperature of clean silicate grains reaches 1000 K at about 1.4 R_*. Could such grains form in the chromospheric environment? Two requirements must be satisfied. On one hand, the gas density must be sufficiently low so that the temperatures of the small aggregates are not affected by collisions. The answer again depends on the interaction of aggregates with the radiation field. If their temperatures can be obtained by extrapolation of Mie's calculations toward atomic dimensions, the preceding example requires $n < 10^{10}$ cm^{-3} if $T = 6000$ K is taken as a mean value for a chromosphere. On the other hand, the supersaturation ratio must be greater than one. Assuming in the most favorable case that Si is mainly in SiO, the nucleation of silicate near the star requires $n > 10^8$ cm^{-3}. Draine (1981) considers that the formation of clean silicate grains is possible in extended red-giant and supergiant chromospheres. A most favorable circumstance would be the presence of cold condensations in the hot gas as was proposed by Wright (1970) for 31 Cyg. Jennings and Dyck (1972) showed that the presence of circumstellar grains is accompanied by the disappearance of Ca II and Fe II chromospheric lines. Jennings (1973), studying the influence of grains on the structure of a chromosphere, found that the temperature is lowered and the chromospheric emission is quenched.

The temperature of the solid phase also plays an important part during the growth of

grains. As long as the partial pressure P is greater than $P_{sat}\,(T_g)\,\frac{T}{T_g}^{1/2}$, the radius of the grain grows as:

$$\frac{da}{dt} = \alpha \frac{P}{\rho} \left(\frac{m}{2\pi k T} \right)^{1/2} \quad . \qquad (4\text{-}6)$$

The growth is faster when n_1, the density of the monomer, is higher, but also when the gas is hot, since the rate of growth varies as $n_1 T^{1/2}$.

Similarly, the decrease of the radius by evaporation is:

$$\frac{da}{dt} = - \alpha \frac{P_{sat}\,(T_g)}{\rho} \left(\frac{m}{2\pi k T_g} \right)^{1/2} \qquad (4\text{-}7)$$

when the supersaturation ratio is much smaller than 1. The effective growth of the grain is given by the difference between the positive rate and the negative one. The equality between the two rates defines the critical radius and the final size of the grain is an asymptotic value. The number density of condensable atoms decreases due to the condensation itself and to the dilution in an expanding shell. The thermal evaporation is effective only when T_g is high (i.e., in the inner region of the shell). For instance, taking (Mukai and Mukai, 1973):

$$\begin{aligned} \mathrm{Log}\, P_{sat} &= 14.32 - \frac{38600}{T} \text{ for graphite} \quad , \\ \mathrm{Log}\, P_{sat} &= 14.72 - \frac{26300}{T} \text{ for olivine} \quad , \end{aligned} \qquad (4\text{-}8)$$

(P_{sat} is in this case the partial pressure of SiO) and with $\alpha = 1$, the lifetime is about 10^7s for a grain of radius 100 Å when $T_g = 1750$ K for graphite and $T_g = 1150$ K for olivine. The lifetime is proportional to the radius. Such grains can survive in the stellar neighborhood and grow again during subsequent ejections of matter. The opacity effects in the shell are also important; grains formed close to the star attenuate the stellar radiation and allow further nucleation and growth.

Structure of the Grains: Amorphous or Crystalline

The interpretation of photometric measurements, particularly the profile of the silicate band at 10 μ and the flux curves in the far infrared from 10 μ to the millimetric waves has favored the introduction of amorphous grains in shell models. With the help of the theory of nucleation and growth, can we decide if the grains formed in circumstellar shells are amorphous rather than crystalline?

The structure of clusters containing few atoms or several tens of atoms is not known. It is only just possible, with the help of the molecular dynamics calculations, to compare the stability of different kinds of assemblies. For argon, Farges et al. (1977) found that small clusters ($n < 50$) do not possess the geometrical shape corresponding to the subsequent growth of the crystal. Their shape is close to that of the sphere. When n increases beyond 50, a structural transition occurs. On the other hand, Barker (1977) showed that groups of atoms with a definite pattern constitute the underlying structural unit of amorphous metals. In both cases, the icosahedron appears as a privileged structure. This polyhedron, limited by twenty equilateral triangles, corresponds to a stable arrangement of atoms. Hence, it may be quite difficult to make the distinction between amorphous and crystalline for very small aggregates. The difference is rather connected to the conditions of growth, particularly the variation of the temperature. Generally speaking, a high temperature, maintained long enough, leads to the stable phase (i.e., the crystal). For circumstellar grains, a theoretical determination of the structure requires the determination of the viscosity as a function of the temperature. Seki and Hasegawa (1981), considering that the temperature of condensation is low enough to give amorphous grains, studied their probability of crystallizing during their evolution in the

shell. They found that around cold stars the grains are small ($a < 200$ Å) and have a low probability of crystallization. They must be mainly amorphous for graphite and for silicate as well. However, it is possible that the variation of the viscosity is not the same for different kinds of silicate.

Czyzak et al. (1982) critically discussed the arguments in favor of crystalline graphite. They concluded that crystals are "at best highly speculative" and emphasized the importance of a detailed description of the kinetics of growth throughout the shell. If the structure of graphite appears, order exists only at short scale, and it probably leads to highly disordered polycrystalline grains (i.e., aggregates of very small single crystals with different orientations).

Gail and Sedlmayr (1984a) give a clear analysis of the atomic processes involved in the growth of carbon grains. A grain grows as a crystal only when the sticking monomer is able to attain by migration a suitable lattice site. Then the comparison of the hopping time (i.e., the average time between two successive jumps of a monomer at the surface) and the average time between two successive captures at a given site is a good criterion. If the hopping time exceeds the capture time, the migration is not possible and the grain is amorphous. When the hopping time is just shorter than the capture time, the crystalline growth is not perfect, and a polycrystalline structure is obtained. In a cooling wind around a cold carbon star, Gail and Sedlmayr found that polycrystalline grains are produced only if their growth occurs when they are hotter than 1100 K.

The evolution of this problem has important implications in many astrophysical observations. At the moment, it is not possible to totally exclude one kind or another while the solid phase condenses. Amorphization can also be due to energetic collisions when eruptive phenomena or shock waves are produced at the stellar surface.

Time-Dependent Nucleation and Growth

The problem of the formation of grains can be solved only if the density and the temperature of the gas and the composition and the temperature of the clusters are known at every point in the shell and at each moment. The nucleation begins where the supersaturation ratio is significantly larger than 1. The grains then grow as long as $S > 1$. The saturation time scale governs the situation. The problem becomes even more difficult when the dynamical evolution of the shell is influenced by radiation pressure on the grains. In this case, the number and the size of the grains already formed determine the velocity of expansion of the shell. Conversely, the decrease in the density and temperature of the gas governs the growth of the grains. A more detailed description of these processes has been given by Deguchi (1980), Draine (1981), McCabe (1982), and Gail and Sedlmayr (1984b).

Deguchi studied shells of oxygen stars (C/O < 1) at 2000 and 2500 K, where the mass loss is caused by the radiation pressure on the grains. The shell is supposedly optically thin and $T \alpha r^{-1/2}$. The decrease of T follows the equilibrium temperature of a blackbody in a radiation field free of any adsorption and independent of the law of density of the gas in the shell. The coupled equations describing the motion of the gas and that of the grains are given without approximation, but are solved independently on each side of the sonic point. In these conditions, the nucleation of silicate (forsterite: $Mg_2\ SiO_4$) occurs in a restricted part of the shell. Grains grow to several hundreds of angstroms if the mass loss is $10^{-6}\ M_\odot$ yr^{-1} and to several thousands of angstroms if it is $10^{-5}\ M_\odot\ yr^{-1}$. Unfortunately, the temperature of the grains is not taken into account. For grains of forsterite, this temperature is lower than that of the gas. This must increase the nucleation, but can also limit the growth, due to the rapid depletion of the condensing gas.

Draine (1981) in the case of α Ori and McCabe (1982) for a carbon star take into account the temperature difference between the gas and the grains. The formation of grains is more efficient when it occurs near the star, where the density and the temperature of the

gas are higher. This is possible only with materials which absorb the stellar radiation poorly and, on the contrary, easily emit their own thermal radiation in infrared bands. Then grains are cooler than the blackbody with the same shape, and an inverse greenhouse effect occurs. It happens with pure silicate ("clean" silicate) and silicon carbide. However, the infrared emission band at 10 μ observed around many cool oxygen stars can exist only if the silicate grains absorbed energy at shorter wavelengths. Around cold stars, the ultraviolet radiation is too low to heat the grains. Thus, silicates which are more or less absorbing in the visible and near infrared must be considered "dirty" silicates. The inverse greenhouse effect no longer exists for such grains; they cannot be formed as close to the star as clean silicates. That is why Draine considers an evolution of the quality of the grains throughout the shell. This possibility was already mentioned by Weymann (1977). Very close to the star, clean silicates nucleate and, when they are driven away, become condensation nuclei for absorbing more silicates. At every point in the shell, the quantity of absorbing material is limited by an increase in the temperature that it determines. Thus the temperature of the grains is nearly constant while they grow. The optical properties of such grains are not known. In the case of α Ori, the nucleation near the star requires an ejection velocity lower than that observed in the outer part of the shell.

The scenario proposed by McCabe (1982) to explain the formation of grains in the shell of a carbon star proceeds from the same idea. Near the star, graphite grains are much hotter than the blackbody and can nucleate only with a very high partial pressure of carbon. On the other hand, silicon carbide grains are cool enough to condense. Around a star at 2230 K (IRC + 10216), SiC grains form at 1.5 R_*. If their opacity is larger than 1, the attenuation of the stellar radiation is such that the nucleation of graphite grains becomes possible at about 5 R_* and their growth up to 20 R_*. This happens only in optically thick shells. When the shell is thin, clusters or grains of SiC could also serve as condensation nuclei for graphite.

The nucleation and growth in a supersonic wind driven by dust condensation was studied by Gail et al. (1984) and Gail and Sedlmayr (1984b) around heavily obscured carbon stars. The coupled equations describing the hydrodynamics, the dust formation, the grain growth, and the chemistry have been solved numerically. For a star with T_{eff} = 2300 K, M = 1 $M_\odot$, and L = 2.10^4 $L_\odot$, the nucleation of carbon grains occurs at 3 R_*, and the average radius of the final distribution is 2.10^{-6} cm (Figure 4-1). The sharp peak in the variation of the average radius is due to the fast growth of the first grains. Then the production of a

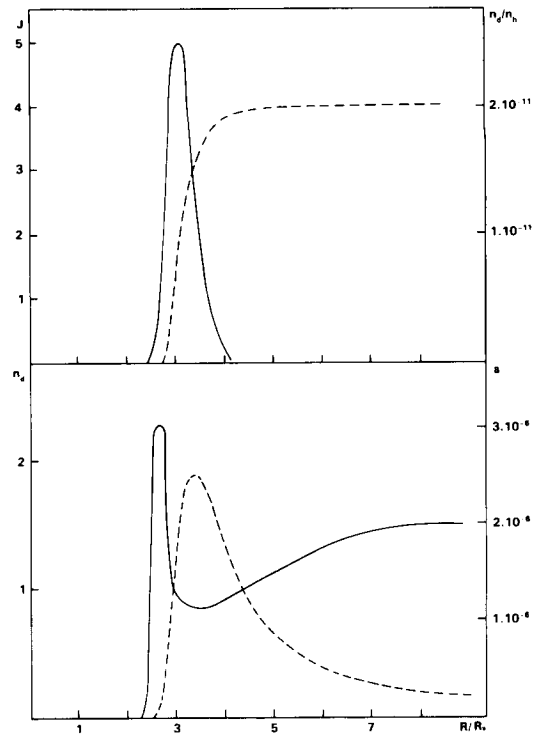


Figure 4-1. Nucleation and growth of carbon grains around a star with T_{eff} = 2300 K, M = 1 $M_\odot$, and L = 2.10^4 $L_\odot$ (from Gail and Sedlmayr, 1984b). The nucleation rate J (10^{-10} grains cm^{-3} s^{-1}) and the number of grains per hydrogen atom (top). The average grain radius a (cm) and the number density of grains (10^{-2} cm^{-3}) (bottom). These results correspond to a mass loss of 2.10^{-5} $M_\odot$ yr^{-1}.

larger number of very small grains (nucleation peak) makes the average size decrease. The grains are all formed within a thin shell.

Conclusions

The theory of homogeneous nucleation reasonably allows one to understand how grains are formed around cold stars and to locate the nucleation zone. The total number of grains, their final size, and their structure are more uncertain and are sensitive to various simplifications used in the models of the shell. The main uncertainties concern:

- The values of physical parameters of solids: the surface tension of the bulk material and of the small grains, the optical properties of very small aggregates, and the modifications of the refractive index due to impurities or defects

- Kinetics of the growth of grains in an expanding gas

The complexity of a real shell, compared with the extreme simplification of models, must be kept in mind. The gas contains a wide number of species with the ability to condense or deposit onto other grains. The outline of condensation theoretically obtained when the thermodynamical equilibrium is assumed, in absence of a strong radiation field, may be quite erroneous. The presence of molecules or radicals necessary for the nucleation works is not always obtained (Donn, 1976). The heteromolecular nucleation (i.e., the condensation of two or more different molecules) must also be considered. The nucleation of one specie is sometimes allowed only if another definite specie is present (nucleating agent); for instance, in the high terrestrial atmosphere, water nucleates in the presence of sulfuric acid.

A circumstellar shell is not an homogeneous medium. Local condensations or strong variations in the density permit the nucleation to begin, whereas the average density appears to be too low. The production of grains in definite sites makes possible an extension of the nucleation to regions of lower density or gives the entire shell condensation nuclei. Some of these complications were already considered by Salpeter (1974). When the number density of grains becomes high, coagulation works efficiently. Then the growth is faster and continues even when the supersaturation ratio is lower than 1. Coagulation is particularly efficient if every kind of turbulence is taken into account (Scalo, 1977). It could explain the existence of nonspherical grains such as those proposed by Svatos and Solc (1981) to obtain the polarization observed in Mira variable stars.

The propagation of shock waves in circumstellar shells probably influences the evolution of grains. Can they initiate the processes of growth by suddenly increasing the density or, on the contrary, destroy the grains by radiative heating? Many works exist on the propagation of shock waves in dusty gases. This mainly concerns the expansion of inhomogeneous gases in nozzle flows. Analytical methods perfected by hydrodynamicists will certainly be useful (Rudinger, 1973; Blythe and Shih, 1976). However, the problem must be stated in the frame of astrophysical conditions. The presence of a strong radiation field and unusual scale of time and dimension require special treatment.

The temperature of grains is calculated by using a well-defined photospheric stellar radius and the blackbody radiation at the effective temperature. In reality, this differs somewhat, mainly among the supergiants; the radiation at different wavelengths does not reach the same photospheric levels. The dilution factor of the radiation field should be a function of the wavelength. Schmid-Burgk and Scholz (1981) studied the possibility of forming grains inside the photosphere when the effects of sphericity are taken into account. The equilibrium temperature of grains is no longer purely radiative and is just higher than that of the gas. Schmid-Burgk and Scholz concluded that grains of Al_2O_3 can exist in the upper part of the atmosphere of low mass M giants.

Since the early fundamental works of Salpeter (1974) and Tabak et al. (1975), our

knowledge of nucleation and growth of circumstellar grains has progressed under the pressure of the fast development of infrared photometry. Further progress will probably follow new findings on molecular abundances and chemistry in the shells. It is vital to know all aspects of the shell's interior—not only the density of monomers and molecules directly implied in the growth of the grains, such as C, C_2, C_3 .... or SiO and metallic oxides, but also the density of any molecules built with C, Si, or Mg.

RADIATIVE TRANSFER IN CIRCUMSTELLAR DUST SHELLS

The absorption and the scattering of the stellar light in a circumstellar shell and the thermal infrared emission of the grains are obviously the physical consequence of the nucleation and growth of solid particles around cold giant and supergiant stars. However, it appears that most of the works on radiative transfer in circumstellar shells have been developed independently of those devoted to the formation of grains. Models of shells were built mainly to explain the results of photometry, particularly in the infrared. The constraints imposed by these results are indeed stronger, more numerous, and more accurate than those issued from the theoretical study of the nucleation and growth. For instance, the existence of silicate is indicated by their infrared bands and could not have been deduced for certain from the nucleation theory. Our knowledge on the nature and the size of the grains results from the best fit between models and observations. Studies on nucleation and growth most often attempt to justify a posteriori the existence of the grains proposed in the models. It must be hoped that this situation will evolve and that future works will include all aspects of the problem, including the dynamics of the gas and molecular equilibria.

The equation of radiative transfer must be solved in a spherical extended atmosphere—the shell—with a central source of radiation. Around cold stars, the ultraviolet radiation is too weak to ionize the gas in the shell; the grains alone are responsible for absorption, scattering, and emission. At every point in the shell, the radiation field is anisotropic. The methods of treating the radiative transfer arise directly from those perfected for stellar atmospheres, with different approximations from one author to another. After the work of Leung (1976), the most comprehensive studies devoted to the shells of cold stars are those by Jones and Merrill (1976), Mitchell and Robinson (1981), and Rowan-Robinson and Harris (1982, 1983a, 1983b).

Generally speaking, flux curves are correctly fitted to spherical models for families of stars of the same spectral class, luminosity type, and chemical composition. Some difficulties exist at long wavelengths and in the absorption bands. Moreover, the right fit is often obtained by arbitrarily adjusting the optical properties of grains. The influence of different parameters will be examined first. Then the results obtained for oxygen stars and carbon stars will be summarized. Lastly, the influence of departures from spherical symmetry will be discussed.

Resolution of the Transfer Equation in a Spherical Shell

The main goal is to obtain a correct description of the radiation field at every point in the shell. The range of wavelengths taken into consideration is necessarily very large to include the stellar radiation, the scattered light, and the thermal emission of grains. At short wavelengths, the scattering diagram of the grains, which fixes the angular repartition of the scattered light, must be carefully represented. High scattering orders—corresponding to photons scattered several times—cannot be neglected when the optical depth is larger than one. The simplifications most often concern this point; they usually give the correct result for quantities integrated over the entire spectrum when short wavelengths have a weak influence. On the other hand, the determination of the angular repartition of the radiation requires a precise description of scattering. Scattering by grains is never isotropic. When the

grains are much smaller than the wavelength, scattering is only symmetric (Rayleigh scattering). For submicronic grains, it is always possible to give a simple and accurate representation of the scattering diagram at every wavelength (White, 1979).

To define a model, it is necessary to fix the stellar characteristics (effective temperature and radius), the geometry of the shell (inner and outer radii and density), and the properties of grains (size and optical properties). The star is the only source of energy. We must know the flux it emits at every wavelength and its limb-darkening. The value of the effective temperature determines the temperature of the grains and the lower limit of the inner boundary of the shell. The photometric radius is usually used to normalize other lengths and does not appear explicitly. However, its definition is not evident for low-gravity stars. For instance, the angular diameter of Mira obtained by speckle interferometry (Bonneau et al., 1982) varies with the wavelength due to the extension of the photosphere and the wavelength dependence of the opacity.

The shell is limited by two spheres. The inner boundary of radius R_i may have different physical origins depending on other circumstances. It may be:

- The vaporization limit of the grains where they reach their maximum temperature. Closer to the star, they disappear in a time shorter than any other characteristic time of their evolution (expulsion, period of the star, etc.). For small graphite grains, it corresponds to about 1800 K, and for silicate to 1200 K.

- The region of nucleation and growth of the grains. The temperature of the hottest grains has practically the same value as the above; for a total gas density of 10^{-10} to 10^{-12} cm^3, the nucleation is possible and efficient for these values. In this situation, the density of the gas is implicitly assumed to be higher than the saturation limit. Mitchell and Robinson (1980) pointed out that the concept of inner boundary is an abstraction: the numerical density and the size of grains vary over a finite distance and what does exist is rather an "inward tail." However, the nucleation and growth has maximal efficiency in a narrow region of an expanding shell mainly because of the decrease of the density of condensable material (Draine and Salpeter, 1977). Around a variable star, for different values of the phase, the inner boundary may be alternately defined by condensation and vaporization. The temperature of hottest grains is then nearly constant, but R_i varies.

- Finally, in an expanding shell without permanent nucleation, the inner radius is determined by the dynamical evolution and is larger than in the two preceding cases.

The outer limit is less precisely defined. For a shell that is expanding with a constant velocity, it corresponds to the time of expansion. It may also be due to the interaction with the diffuse interstellar medium. In actual fact, the shell must be bounded to keep its mass and far-infrared luminosity within limits fixed by the observations and the theory. The outer radius is most often taken to obtain the correct value of the flux at the longest measured wavelength or to give the right intensity ratio for the two silicate bands at 10 and 20 μ.

The law of density is most often taken as R^{-2}, corresponding to free expansion at constant velocity. If the formation and the ejection of dust are not continuous processes (Sanner, 1976; Bernat, 1981; Goldberg, 1983), the structure of the shell may be much more complicated. The model of grain used in the model is the main source of uncertainty. The distribution of dimensions, or the average dimension, have little influence on the equilibrium temperature for submicronic particles. On the contrary, optical properties have a strong influ-

ence. Practically speaking, it was always necessary to fit the models to modify the refractive index measured on terrestrial materials. This point will be considered separately for graphite and silicates. Nevertheless, such an adaptation of an important parameter does not discredit models. It is not surprising that solid material built in circumstellar shells is somewhat different from pure species studied in the laboratory. This indicates an area for experimental and theoretical research, but it must be kept in mind that the optical properties adopted by each author are not the only possible choice.

Before models built for different kinds of stars are considered, some general results will be discussed.

Circumstellar Extinction Opacity Law. If $I(\lambda)$ is the intensity of the radiation emerging from the shell in a given direction and $I_o(\lambda)$ is the intensity emitted by the star, the effective opacity of the shell, $\tau(\lambda)$, can be defined by:

$$I(\lambda) = I_o(\lambda) \exp(-\tau(\lambda)) \quad . \qquad (4\text{-}9)$$

The function $\tau(\lambda)$ must be known in order to infer the stellar properties from the observations. Along the radial direction, the extinction opacity is:

$$\tau_{ext}(\lambda) = \int_{R_{int}}^{R_{ext}} n_{(r)}\, \pi a^2 Q_{ext}(\lambda)\, dr \quad , \qquad (4\text{-}10)$$

where $n_{(r)}$ is the number density of grains, a is their radius, and $Q_{ext}(\lambda)$ is their extinction efficiency. If a distribution of dimensions must be considered, a second integration is done over the radius. Similarly, τ_{sca} and τ_{abs} are defined with the scattering efficiency, Q_{sca}, and the absorption efficiency, Q_{abs}. These three quantities are proportional to the column density on the line of sight. They vary with λ exactly as Q's do. In the diffuse interstellar medium, any photon having an interaction with a grain (absorption of scattering) is lost for the observer. Then τ_{ext} computed along the direct trajectory from the star to the instrument gives exactly the effective opacity. The interstellar extinction curve has the shape of the variation of Q_{ext} with the wavelength. It is not the same with an unresolved circumstellar shell since photons scattered in the shell will be received by the observer. The shape of the circumstellar extinction law is consequently different from that of the interstellar extinction law at wavelengths where scattering is efficient, even if the grains have the same properties. However, τ_{ext} has a simple physical meaning: $\exp(-\tau_{ext})$ is the probability for a stellar photon to go out through the shell without absorption or scattering. Thus, the direct stellar radiation is:

$$I_d(\lambda) = I_o(\lambda) \exp(-\tau_{ext}(\lambda)) \qquad (4\text{-}11)$$

and necessarily $\tau(\lambda) < \tau_{ext}(\lambda)$. The equality occurs when the albedo is zero. When the shell is optically thin, a photon has a low probability to suffer more than one interaction. The only photons which cannot get out of the shell are those absorbed without previous scattering. The probability for a stellar photon to travel through the shell without absorption is $\exp(-\tau_{abs})$. The emerging intensity is then in the thin case:

$$I(\lambda) = I_o(\lambda) \exp(-\tau_{abs}(\lambda)) \quad , \qquad (4\text{-}12)$$

and $\tau = \tau_{abs}$. This is true only if τ_{sca} is low. When multiple scattering is significant, it effectively lengthens the path of the photon into the shell and increases its probability of absorption:

$$\tau_{abs} < \tau < \tau_{ext} \quad . \qquad (4\text{-}13)$$

Moreover, τ is not a linear function of the number density of grains. The circumstellar law of opacity has a shape different from that of the interstellar one.

Advances in high angular resolution methods, particularly in interferometry, should bring important results. When the direct stellar

radiation, $I_d(\lambda)$, and the radiation scattered by the entire shell, $I_{sca}(\lambda)$, can be unambiguously separated, for a spherical thin shell:

$$I(\lambda) = I_d(\lambda) + I_{sca}(\lambda) = I_o(\lambda) \exp(-\tau_{abs}(\lambda)) \quad , \tag{4-14}$$

and

$$I_d(\lambda) = I_o(\lambda) \exp(-\tau_{ext}(\lambda)) \quad . \tag{4-15}$$

Then

$$\tau_{sca}(\lambda) = \ln(I(\lambda)/I_d(\lambda)) \quad . \tag{4-16}$$

Measurements at different wavelengths would give the shape of the variation of Q_{sca}. If the proper radiation of the star $I_o(\lambda)$ is known, the albedo is given by:

$$\gamma = \frac{\ln(I(\lambda)/I_d(\lambda))}{\ln(I_o(\lambda)/I_d(\lambda))} \quad . \tag{4-17}$$

The condition of validity of these relations must be emphasized; τ_{sca} must be low (i.e., $I_{sca}(\lambda)$ must be lower than $I_d(\lambda)$). If it is not true, the ratio gives a lower boundary for the albedo.

Intensity Profiles. Besides the flux curve, the more complete calculations give the angular repartition of the radiation at every wavelength. Mitchell and Robinson (1978) and Rowan-Robinson (1982) have pointed out the existence of a sharp maximum of the luminance in the direction of the inner boundary of the shell. This result was also found by Yorke and Shustov (1981) for protostellar shells and by Lefèvre et al. (1982) by numerical simulation. This bright ring corresponds to the maximum of the column density of grains reached when the impact parameter is equal to the internal radius of the shell. A maximum appears even if the variation of density is not as sharp as in the models. On the other hand, the central lowering of the intensity profile is reduced by the forward scattering of grains. The maximum also exists for the scattered stellar light and the infrared thermal emission of grains. It is less and less pronounced when the opacity increases. The existence of a peak of luminance is important in the interpretation of high angular measurements. If the bright annulus can be detected, one limit of the shell is fixed with precision, and the radiative equilibrium of grains will be better understood. Preliminary results obtained by Roddier and Roddier (1983) for α Ori at $\lambda = 0.535\ \mu$ indicate a concave bright rim at about 2.5 stellar radii. If it is confirmed and is clearly attributed to scattering by dust, this implies the existence of much less-absorbing grains than those proposed in models.

A maximum of the luminance must appear for every discontinuity of quick variation of the number density of grains; the detection of rings at different distances from the star could allow one to follow the history of successive ejections of matter when the rate of grain production is not constant.

Shells Around Oxygen Stars

The main features presented by the shells of oxygen stars are the broad emission bands at 10 and 20 μ attributed to silicates. Several works are devoted to the general properties of shells and give grids of models with adjustable parameters: Jones and Merrill (1976), Mitchell and Robinson (1981), and Rowan-Robinson and Harris (1982, 1983a). Some other works were developed for a particular object: Hagen (1978) and Tsuji (1978, 1979).

Jones and Merrill (1976) made the first quantitative attempt to explain the main characteristics of the flux curve for families of cold stars. The transfer equation is solved with the help of the Eddington approximation, and the angular repartition of the radiation is not calculated. The objects studied present a wide range of opacities. The flux curve and the profile of emission bands are obtained with good precision for stars with an effective temperature of 2400 K. A valuable result of this study shows the impossibility of obtaining a good fit with

clean silicates between 0.25 and 8 μ. The model of dirty silicate ($m = 1.55 - 0.1\ i$ for $\lambda < 8\ \mu$), widely used afterward, was proposed. Clean silicates (olivine or enstatite) absorb the ultraviolet radiation but are transparent for the visible and the near infrared. Cold stars do not radiate enough energy at short wavelengths to heat the grains. The absorption of clean silicates begins beyond 9 μ; such grains cannot reemit through their near-infrared band more than they absorb and are unable to give the observed emission. Grains must absorb in the visible or the near infrared. This absorption may be due to defects or impurities. However, no detailed model of the dirty silicate absorption was given.

The profile of the emission band at 10 μ is always wide and structureless. The silicates most often used in the models—enstatite (SiO_3Mg) and forsterite (SiO_4Mg_2)—present narrower bands with several peaks when crystallized. Thus, observations imply the existence of amorphous silicates. The transfer in the bands and the influence of various parameters were studied extensively by Mitchell and Robinson (1981). For small grains of "forsterite," particularly grains with $a = 0.1\ \mu$ and $m = 1.55 - 0.01\ i$ for $\lambda < 8\ \mu$, around a star at 3000 K, they showed that the meaningful parameter is the opacity. The 10-μ band can appear either in emission or in absorption. When the opacity increases, the external regions of the shell are no longer heated by the stellar radiation. The cold grains absorb the radiation emitted by the hotter internal region. When the density varies as r^{-2}, an emission is observed at 10 μ if τ_{ext} (10 μ) < 2. If $2 < \tau_{ext}$ (10 μ) < 8, self-absorption appears at the center of the band. For instance, this is observed with NML Cyg. At last, if τ_{ext} (10 μ) > 8, the band is seen in absorption. The band at 20 μ is generally less intense and can also present this inversion. Mitchell and Robinson showed that, in every case, the determinant physical quantity is the temperature of the grains at the point where $\tau_{ext} = 1$, starting from outside.

The profile of the 10-μ band has recently been studied by Papoular and Pégourié (1983) around 23 giants and supergiants. The profile is the same for several shells and is attributed to amorphous forsterite grains with $a < 1\ \mu$. For some giants, the band is wider. This is not correlated to the spectral type of the star or the opacity, but rather to the galactic latitude. A possible explanation is a variation of the radius of grains, up to 4 μ. The increase of the size with the galactic longitude could be due to differences in the conditions of nucleation or modifications of erosion processes.

The most extended grid of models for M giants and supergiants was given by Rowan-Robinson and Harris (1982, 1983a). For 27 early M stars and 85 late M stars, a satisfactory concordance is obtained with the flux curves observed using small silicate grains similar to those of Jones and Merrill (1976) and with density varying r^{-2}. For each star, the opacity and the dimension of the shell are adjusted. The effective temperature is between 3000 and 3500 K for early-type stars and 2000 and 3000 K for late-type stars. In most of the cases, inner grains are hotter than 1000 K, but they are colder near the hottest stars when the opacity is low. Molecular bands do not sufficiently modify the total energy absorbed by the grains to have an effect on their equilibrium temperatures and the thermal radiation emitted by the shell. In most cases, scattering of an order greater than one can be safely neglected. This is the case, for instance, when the star is surrounded by small absorbing grains: most of the stellar radiation is in the near infrared where the albedo of such grains is very low. It is no longer true if the grains are large. On the whole, the observations are well explained by the grid of models with expanding spherical shells and more or less absorbing silicate grains. Moreover, VY CMa and NML Cyg must be considered separately owing to their asymmetry. For any of the objects studied, the model proposed by Rowan-Robinson and Harris is a good starting point for further adjustments.

The most often studied star is certainly α Ori. Models for its shell have been built by Hagen (1978) and Tsuji (1978, 1979). In a very detailed study, Tsuji used the method of Unno and Kondo (1976, 1977) to solve the transfer

equation. With dirty silicate grains ($k = 0.01$ and $k = 0.1$), angular dimensions compatible with the results of infrared interferometry (McCarthy and Low, 1977; Sutton et al., 1977) are obtained at different wavelengths. In this model, it is the inner boundary of the shell very close to the star: $R_i \simeq R_*$ to 3 R_*. From the total flux and the angular diameter, Tsuji deduces an effective temperature of 3900 K. Unfortunately, dirty silicate grains as considered in the model cannot survive so close to such a star; they would be hotter than 2000 K. Rowan-Robinson and Harris used $T_{\text{eff}} = 3250$ K and obtained $R_i = 10\ R_*$. The results of Roddier and Roddier (1983), already quoted, suggest $R_i \sim 2.5\ R_*$. Thus, near the star, the grains must be less absorbing than those used in the models. The value adopted for the effective temperature is the determinant. Scargle and Strecker (1979) proposed $T_{\text{eff}} = 3580$ K, using to deredden α Ori a law having the same shape as the interstellar reddening law. Further determinations of the angular repartition of the light scattered around α Ori are needed in the visible and, when possible, at 10 μ. If the existence of grains close to the star is confirmed, the model of nucleation and growth proposed by Draine (1981), with clean silicate grains at the lower part of the shell and more absorbing ones outward, would not only be a solution for the thermodynamical problem of the condensation of grains, but would also explain the angular repartition of the radiation.

Shells Around Carbon Stars

The infrared emission of shells of carbon stars do not present strong bands. An emission feature at 12 μ, attributed to silicon carbide, is always weak. In all the models, the grains responsible for the absorption and the emission into the shell are carbon grains. Silicon carbide could not produce the emission observed at large wavelengths. The thermal emission is not always clearly distinct from the stellar continuum because carbon grains can survive close to the star and can emit efficiently in the near infrared. On the whole, it is possible to obtain a good representation of the flux curve with an expanding spherical shell and small carbon grains. Jones and Merrill (1976) mention that the emission peak moves to a larger wavelength when the opacity increases as the flux curve becomes narrower. This is due to the absorption of the stellar radiation and of the near-infrared radiation of hotter inner grains. Bergeat et al. (1976), analyzing the photometry of 29 carbon stars, concluded that the thermal emission between 1.25 and 8 μ is due to graphite grains of radius greater than 1 μ. In their sample, Miras have lower effective temperatures and thicker shells of cooler grains. Large grains efficiently scatter the near-infrared radiation, and their existence could be tested by high angular resolution measurements.

The results obtained in the far infrared beyond 20 μ and, for some stars, in the millimetric waves (Fazio et al., 1980) are much more difficult to explain with crystalline graphite grains. The extinction efficiency measured for amorphous carbon grains by Koike et al. (1980) decreases as λ^{-1} and allows a better fit.

Models of shells have been presented for 41 carbon stars by Rowan-Robinson and Harris (1983b). A simplified parametric representation of the extinction efficiency of carbon grains is used. The decrease of Q_{ext} at large wavelengths must be slow, and this excludes graphite. In these models, hotter grains are at 1000 to 1300 K. The authors mentioned that the temperature "tends to be lower for larger shell optical depths."

As for silicates, the optical properties adopted for carbon grains are sometimes arbitrary, and more attention must be paid to improve the coherence of models. Optical properties of graphite grains are not always correctly described. Graphite is strongly anisotropic. For spherical grains smaller than the wavelength, the extinction efficiency is:

$$Q_{ext}(\lambda) = \frac{2}{3} Q^{\perp}_{ext}(\lambda) + \frac{1}{3} Q^{\parallel}_{ext}(\lambda) \quad , (4\text{-}18)$$

where $Q^{\perp}_{ext}$ is the extinction efficiency, the electric vector is perpendicular to the c-axis of the

crystal, and $Q_{ext}^{\parallel}$ is the extinction efficiency when it is parallel to the c-axis. The refractive index measured by Philipp (1977) allows the determination of $Q_{ext}^{\perp}$ and $Q_{ext}^{\parallel}$ is obtained from the results of Venghaus (1977). Beyond 10 μ, the variation of Q_{ext} is dominated by $Q_{ext}^{\parallel}$. This is clearly shown in the work by Mezger et al. (1982) on the origin of the diffuse galactic far-infrared and submillimetric emission. As a result, up to 100 μ Q_{ext} decreases more slowly than λ^{-2}. Moreover, a plasma resonance at 37 meV induces a secondary maximum of the extinction efficiency around 33 μ.

An excess of emission has been observed several times at 30 μ with carbon stars. Forrest et al. (1981) and Herter et al. (1982) obtained the profile of this emission for IRC + 10216. The profile of the band deduced by dividing the observed flux by a continuum varying by λ^{-1} (Herter et al.) presents a maximum at 30 μ, but this result, as mentioned by the authors, depends on the method of deconvolution. Conversely, if the observed flux is divided by the extinction efficiency of graphite grains, a smooth continuum is obtained. More precise determinations of Q_{ext} are needed for different kinds of carbon to test the validity of this hypothesis. Even if the emission band observed has nothing to do with carbon, the problem still remains: if graphite grains are responsible for the emission around carbon stars, "something" must appear at about 33 μ.

Several models have been published for the shell around IRC + 10216. However, the problem for this very interesting object is complicated. The nature of the central star is not known, and the shell is strongly asymmetrical. With a model of a spherical shell, Mitchell and Robinson (1980) nevertheless obtain a good fit with the flux curve between 1 and 100 μ. They give a very comprehensive review of the measurements and works published at this time. In their model, the shell extends from 20 to 5000 stellar radii, and the density varies by $r^{-1.3}$. The effective temperature of the star is 2000 K. The shell contains small graphite grains and a small fraction of spheroidal SiC grains necessary for obtaining the correct flux between 10 and 14 μ. The hotter graphite grains are at 600 K. A fairly similar model was proposed by Keady (1982), but with amorphous carbon in an expanding shell which corresponds to a mass loss of $1.5 \times 10^{-4} M_{\odot}$ yr^{-1}. The influence of the velocity field and the microturbulence on the profile of CO infrared lines at 2 and 4.6 μ is taken into account.

For the same object, Rowan-Robinson and Harris (1983b) found a shell extending from 5.5 to 550 stellar radii with a density proportional to r^{-2}. The hotter graphite grains are then at 850 K when $T_{\text{eff}} = 2000$ K.

Without solving the transfer equation, McCabe (1982) proposed a model to explain the molecular abundances observed throughout the shell and the nucleation and growth of grains near the star. His scenario has already been described: silicon carbide grains, responsible for the emission around 12 μ can condense at $r <$ 2 R_*. Shielding the stellar radiation at short wavelengths, they permit carbon grains to condense and grow between 5 and 20 R_*. This explains why the temperature of carbon grains is lower than the condensation temperature at the same place if the stellar radiation would not be partially absorbed. It would be interesting to confirm whether the quantity of SiC required is compatible with the strength of the emission at 12 μ.

Finally, the problems encountered in building models of shells around carbon stars are quite similar to those encountered with oxygen stars. The exact nature of the grains and the description of their optical properties require further investigation. The experimental study of amorphous carbon and polycrystalline grains, from the near infrared to the millimetric waves would be very useful.

Nonspherical Shells

Models of spherical shells necessarily give no explanation of the intrinsic polarization of stars. This polarization can be produced by elongated grains in a spherical shell, but a very

efficient mechanism of alignment is required to obtain a significant rate of polarization. The morphology of the shell is then probably also affected. The evidence of nonsphericity has been recognized in some cases; it is always associated with a strong intrinsic polarization at short wavelengths. The most striking examples are VY CMa, NML Cyg, and IRC + 10216. As for the latter, infrared interferometric measurements by McCarthy et al. (1980) indicate an asymmetry of the order of 3 to 1 for the principal directions. Models of nonspherical shells were at first mainly proposed to explain intrinsic polarization. The complete treatment of the transfer of the scattered stellar radiation in an ellipsoidal shell was realized without approximation by Daniel (1982), using numerical simulation. A shell with a constant density cannot produce a polarization higher than 12 percent. The rates of polarization observed for VY CMa—23 percent at $\lambda = 0.38\ \mu$ (Serkowski, 1973)—or IRC + 10216—24 percent at $\lambda = 0.64\ \mu$ (Dyck et al., 1971)—require a different repartition of the scattering material.

Another result highlighted by the computation is the persistence, when the opacity is modified, or a rotation of 90 degrees of the angle of polarization at a fixed wavelength. In fact, it is an individual property of grains which multiple scattering does not smooth out. Daniel (1982) obtains a relation between the index of refraction, the average radius of the grains, and the wavelength of rotation: this wavelength is shorter for smaller grains. The rotation disappears when the grains are strong absorbers, as, for instance, graphite ones. The steep variation of the angle of polarization is effectively observed for several objects, and shell models were built for ten strongly polarized stars. High rates can be obtained only if the direct stellar light is attenuated along the equatorial plane and is scattered mainly near the polar regions of the shell. For instance, the variation of the rate of polarization of VY CMa and the modification of the angle at $0.9\ \mu$ are well explained by an ellipsoidal shell with a high opacity along its equatorial plane. If the grains responsible for the scattering and the polarization are poorly absorbing silicates, their mean size is $0.26\ \mu$ (Figure 4-2). This model of bipolar nebula was also proposed by Schmidt et al. (1980) and Staude et al. (1982). More recent models by Cohen and Schmidt (1982) for three carbon stars have a similar morphology: a torus or a disc of absorbing material obscures the stellar radiation, and the scattered light comes from the polar lobes. It is interesting to note that GL 1403 (CIT6) clearly has a rotation of polarization at $0.65\ \mu$; it cannot be produced by graphite grains in an ellipsoidal shell of constant density. The rotation shows that the repartition of the materials is complex. It can also be due to silicon carbide grains.

The thermal equilibrium of grains and the transfer of infrared emitted radiation in an ellipsoidal shell has been studied by Lefèvre et al. (1983) by numerical simulation. Only the constant density case was considered. This model is certainly too simplified to represent reality, and the essential purpose was to evaluate the importance of the hypothesis of sphericity on several physical quantities. In realistic models, the law of repartition of density has a strong influence on the results and cannot be fixed arbitrarily. Density depends on the distance and at least one angular variable. The first problem to be solved is to understand the dynamics of the shell and to describe the physical mechanisms responsible for the loss of the spherical symmetry. Rotation and magnetic field are most often invoked. It is not certain that they work effectively for evolved stars with large dimensions; the rotation velocity and the magnetic field are probably low in this case. The shape of the shell can also be related to processes which induce the ejection of matter at the stellar surface, such as convection or shock waves.

In a shell of constant density, the temperature of the grains around a cold star maintains an almost spherical symmetry. As for silicate and graphite, the part taken by scattered light in the heating of grains is too weak to give significant asymmetry of the repartition of temperature. It would not be the same if the density changed according to the direction; the stellar

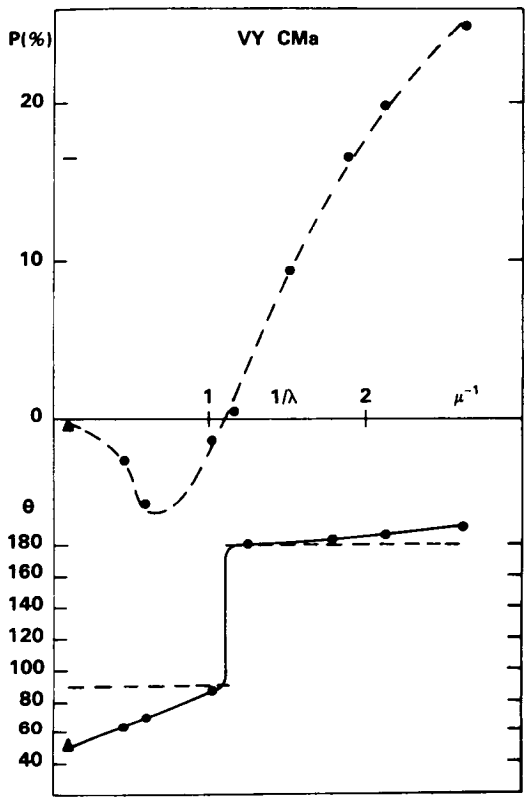


Figure 4-2. Variation of the rate of polarization p and of the angle of polarization θ for VY CMa. The dashed curves are the results obtained by numerical simulation by Daniel (1982). They are compared to the measurements of Serkowski (1973) (●) and Capps and Dyck (1972) (Δ). The negative values of p correspond to a polarization parallel to the polar axis of the shell and the positive ones to a polarization parallel to the equatorial plane. The variation of 90 degrees for θ corresponds to p = 0. The model is an ellipsoid with clean silicate grains of radius a = 0.26 μ.

radiation would be more attenuated along the equatorial plane, and the decrease in the temperature would be steeper. The radiation coming from the shell is very anisotropic due not only to the variation of opacity but also because it is strengthened by the scattered light in the polar direction. The anisotropy is low at large wavelengths and disappears when the optical depth is low in every direction. As a consequence, the flux curve depends on the shortening angle: the stellar radiation is lowered when the observer is near the equatorial plane and band profiles are modified. Since observations are possible in one direction only, the interpretation of the results with a spherical model may lead to erroneous conclusions. The thermal energy emitted by the grains is equal to the energy lost by the stellar radiation only if all the directions of space are considered. Generally, this is not true for a single direction. For the same reason, it is not possible to guess the total flux emitted by the star and its shell when the intensity is known in only one direction. The effective temperature of the star deduced from an evaluation of the flux would be different if the shell is seen pole-on or equator-on. The number of adjustable parameters used in a spherical model almost always allows it to fit the observed flux curve. Photometric and polarimetric measurements with high angular resolution are needed to set additional constraints.

Numerical simulations have shown that the spatial repartition of flux is very asymmetric at every wavelength when the opacity is low. The shape of isophotes is mainly determined by the shortening angle and do not directly reflect the true dimensions of the shell. The bright annulus observed toward the inner boundary of spherical shells is again present when the extinction on the line of sight is not too high, but differences of opacity through the shell change it into a bright arc. The first results obtained by Roddier and Roddier (1983) for α Ori at $\lambda = 0.535\mu$ showed an asymmetric shell and a bright rim over a large sector of the image. In Figure 4-3, the visibility map of fringes produced by α Ori is shown. Their analysis allowed the image reconstruction of the shell. The results also displayed many fluctuations in the luminance: the shell is certainly complex. Moreover, frequent variations of the rate and angle of polarization reflect modifications of the structure of the shell at a rather small scale.

What developments can be expected in the near future? When the spherical symmetry is lost, the complexity of computations rapidly grows; most of the physical quantities explicitly

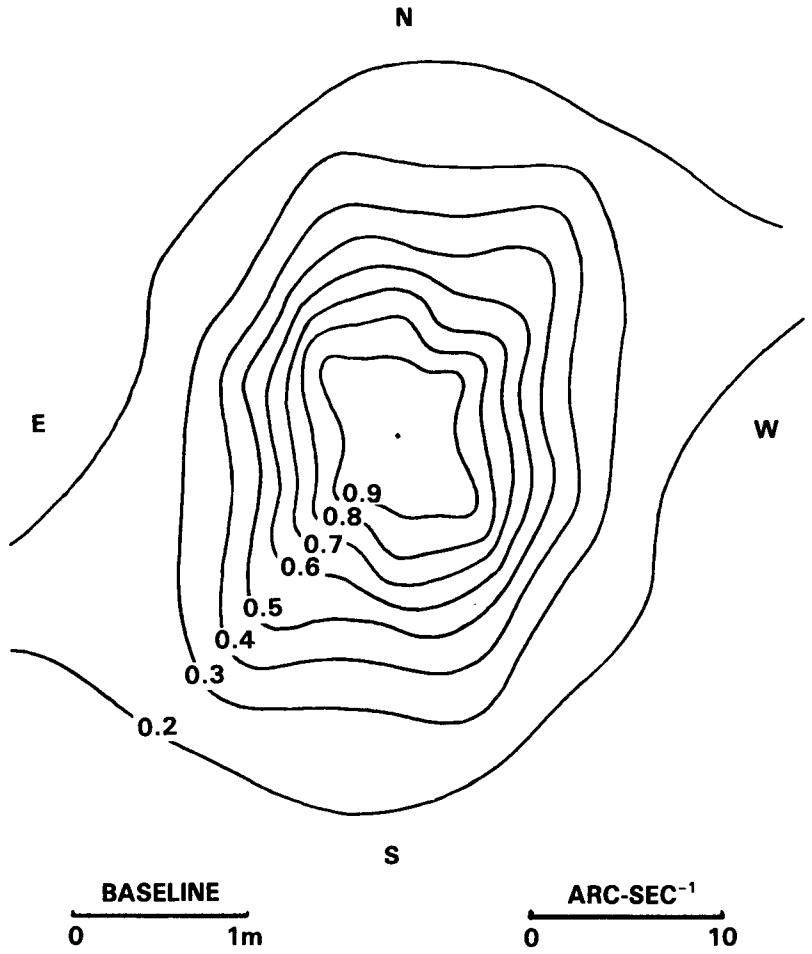


Figure 4-3. Isovisibility curves of the fringes produced by α Ori at λ = 5348 Å with the rotation shearing interferometer of Roddier and Roddier (1983). A departure from circular symmetry is clearly seen. Elongations in the visibility function are at 90 degrees from elongations in the image. Inner curves (low spatial frequencies) correspond to the shell.

involved in the resolution of the transfer equation depend on angular variables. It becomes difficult to systematically explore the influence of each parameter. Fairly simple repartitions of density can be studied by numerical simulation, but the increase of the computational time rapidly limits the possibilities. The problem of transfer must be tightly linked with the study of the dynamic evolution of the shell.

Theoretical progress in the problem of the formation of circumstellar grains and of the transfer of radiation in a shell accompany the advances of experimental methods. Spherical models of expanding homogeneous shells have thus far explained the flux curves obtained for nonresolved objects. The detailed spatial analysis of molecular abundances, polarization, luminence, etc. will consequently produce as a consequence a new generation of models, taking into account the inhomogeneities of the density, the effects of turbulence shock waves, and the temporal variations. One can but hope that the observations will not overemphasize exotic objects, but will also provide results for numerous shells with low opacity and slow variations. Significant progress in our knowledge

of the properties of circumstellar grains will follow. These observations will in themselves permit the choice between candidate materials and guide experimental research.

REFERENCES

Barker, J.A. 1977, *J. Physique Colloq.*, **38**, C2-37.

Bergeat, J., Lefèvre, J., Kandel, R., Lunel, M., and Sibille, F. 1976, *Astron. Astrophys.*, **52**, 245.

Bernat, A.P. 1981, *Astrophys. J.*, **246**, 184.

Blythe, P.A., and Shih, C.J. 1976, *J. Fluid Mech.*, **76**, 593.

Bonneau, D., Foy, R., Blazit, A., and Labeyrie, A. 1982, *Astron. Astrophys.*, **25**, 337.

Capps, R.W., and Dyck, H.M. 1972, *Astrophys. J.*, **175**, 693.

Cohen, M., and Schmidt, G.D. 1982, *Astrophys. J.*, **259**, 693.

Czyzak, S.J., Hirth, J.P., and Tabak, R.G. 1982, *Vistas in Astronomy*, **25**, 337.

Daniel, J.Y. 1982, *Astron. Astrophys.*, **111**, 58.

Deguchi, S. 1980, *Astrophys. J.* **236**, 567.

Donn, B. 1976, *Mém. Soc. Roy. Sci. Liège*, **9**, 499.

Donn, B. 1979, *Astrophys. Space Sci.*, **65**, 167.

Draine, B.T. 1979, *Astrophys. Space Sci.*, **65**, 313.

Draine, B.T. 1981, in *Physical Processes in Red Giants*, ed. I. Iben and A. Renzini (Dordrecht: Reidel), p. 317.

Draine, B.T., and Salpeter, E.E. 1977, *J. Chem. Phys.*, **67**, 2230.

Dyck, H.M., Forbes, F.F., and Shawl, S.J. 1971. *Astron. J.*, **76**, 901.

Farges, J., de Feraudy, M.F., Raoult, B., and Torchet, G. 1977, *J. Phys. Colloq.*, **38**, C2-47.

Fazio, G.G., McBreen, B., Stier, M.T., and Wright, E.L. 1980, *Astrophys. J. (Letters)*, **237**, L39.

Forrest, W.J., Houck, J.R., and McCarthy, J.F. 1981, *Astrophys. J.*, **248**, 195.

Gail, H.P., Keller, R., and Sedlmayr, E. 1984, *Astron. Astrophys.*, **133**, 320.

Gail, H.P., and Sedlmayr, E. 1984a, *Astron. Astrophys.*, **132**, 163.

Gail, H.P., and Sedlmayr, E. 1984b, preprint.

Gerlach, R.L. 1969, *J. Chem. Phys.*, **51**, 2186.

Goldberg, L. 1983, preprint.

Hagen, W. 1978, *Astrophys. J. Supplement*, **38**, 1.

Herter, T., Briotta, D.A., Gull, G.E., and Houck, J.R. 1982, *Astrophys. J. (Letters)*, **259**, L25.

Jennings, M.C. 1973, *Astrophys. J.*, **185**, 197.

Jennings, M.C., and Dyck, H.M. 1972, *Astrophys. J.*, **177**, 427.

Jones, T.W., and Merrill, K.M. 1976, *Astrophys. J.*, **209**, 509.

Keady, J.J. 1982, Ph.D. Dissertation, New Mexico State University, Las Cruces, New Mexico.

Koike, C., Hasegawa, H., and Manabe, A. 1980, *Astrophys. Space Sci.*, **67**, 495.

Lefèvre, J. 1979, *Astron. Astrophys.*, **72**, 61.

Lefèvre, J., Bergeat, J., and Daniel, J.Y. 1982, *Astron. Astrophys.*, **114**, 341.

Lefèvre, J., Daniel, J.Y., and Bergeat, J. 1983, *Astron. Astrophys.*, **121**, 51.

Leung, C.M. 1976, *J. Quart. Spectr. Rad Trans.*, **16**, 559.

Lucy, C.B. 1976, *Astrophys. J.*, **205**, 482.

McCabe, E.M. 1982, *Mon. Not. Roy. Astr. Soc.*, **196**, 801.

McCarthy, D.W., and Low, F.J. 1977, *Astrophys. J. (Letters)*, **202**, L37.

McCarthy, D.W., Howell, R., and Low, F.J. 1980, *Astrophys. J. (Letters)*, **235** L27.

Mezger, P.G., Mathis, J.S., and Panagia, N. 1982, *Astron. Astrophys.*, **105**, 372.

Mitchell, R.M., and Robinson, G. 1978, *Astrophys. J.*, **220**, 841.

Mitchell, R.M., and Robinson, G. 1980, *Mon. Not, Roy Astr. Soc.*, **190**, 669.

Mitchell, R.M., and Robinson, G. 1981, *Mon. Not. Roy. Astr. Soc.*, **196**, 801.

Mukai, T., and Mukai, S. 1973, *Pub. Astron. Soc. Japan*, **25**, 481.

Mutaftschiev, B. ed. 1982, in *Interfacial Aspects of Phase Transformations* (Dordrecht: Reidel), p. 95.

Papoular, R., and Pégourié, B. 1983, *Astron. Astrophys.*, **128**, 335.

Philipp, H.R. 1977, *Phys. Rev. B*, **16**, 2896.

Roddier, C., and Roddier, F. 1983, *Astrophys. J. (Letters)*, **270**, L23.

Rowan-Robinson, M. 1982, *Mon. Not. Roy. Astr. Soc.*, **201**, 281.

Rowan-Robinson, M., and Harris, S. 1982, *Mon. Not. Roy. Astr. Soc.*, **200**, 197.

Rowan-Robinson, M., and Harris, S. 1983a, *Mon. Not. Roy. Astr. Soc.*, **202**, 767.

Rowan-Robinson, M., and Harris, S. 1983b, *Mon. Not. Roy. Astr. Soc.*, **202**, 797.

Rudinger, G. 1973, *Appl, Mech. Rev.*, **26**, 273.

Salpeter, E.E. 1974, *Astrophys. J.*, **193**, 585.

Sanner, F. 1976, *Astrophys. J. Supplement*, **32**, 115.

Scalo, J.M. 1977 *Astron. Astrophys.*, **55**, 253.

Scargle, J.D., and Strecker, D.W. 1979, *Astrophys. J.*, **228**, 838.

Schmid-Burgk, J., and Scholz, M. 1981, *Mon. Not. Roy. Astr. Soc.*, **194**, 805.

Schmidt, G.D., Cohen, M., and Margon, B. 1980 *Astrophys. J., (Letters)*, **239**, L133.

Seki, J., and Hasegawa, H. 1981, *Prog. Theor. Phys.*, **66**, 903.

Serkowski, K. 1973. *Astrophys. J. (Letters)*, **179**, L101.

Staude, H.J., Lenzen, R., Dyck, H.M., and Schmidt, G.D. 1982, *Astrophys J.*, **255**, 95.

Sutton, E.C., Storey, J.W.V., Betz, A.L., Townes, C.H., and Spears, D.L. 1977, *Astrophys. J. (Letters)*, **217**, L97.

Svatos, J., and Solc, M. 1981, *Astrophys. Space Sci.*, **77**, 511.

Tabak, R.G., Hirth, J.P., Meyrick, G., and Roark, T.P. 1975, *Astrophys. J.*, **186**, 457.

Tsuji, T. 1978, *Pub. Astron. Soc. Japan*, **30**, 435.

Tsuji, T. 1979, *Pub. Astron. Soc. Japan*, **31**, 43.

Unno, W., and Kondo, M. 1976, *Pub. Astron. Soc. Japan*, **28**, 347.

Unno, W., and Kondo, M. 1977, *Pub. Astron. Soc. Japan*, **29**, 693.

Venghaus, H. 1977, *Phys. Stat. Sol. (b)*, **81**, 221.

Weymann, R. 1977, *Proc. IAU Colloq.* 42, ed. R. Kippenhahn, J. Rahe, and W. Strohmeier (Bamberg).

White, R.L. 1979, *Astrophys. J.*, **229**, 954.

Wright, K.O. 1970, *Vistas in Astronomy*, **12**, 147.

Yamamoto, T., and Hasegawa, H. 1981, *Prog. Theor. Phys.*, **58**, 816.

Yorke, H.W., and Shustov, B.M. 1981, *Astron. Astrophys.*, **98**, 125.

N88-11597

5

MASS LOSS

Leo Goldberg

OVERVIEW

The first observational evidence for mass loss from cool stars was the discovery by Adams and MacCormack (1935) of blue-displaced components in low-excitation lines of metals in the spectra of certain red giant stars. The first systematic study of displaced lines was made by Deutsch (1956, 1960), who demonstrated that the matter forming the blue-shifted lines was actually escaping from the M-type component of the α Her system and that the phenomenon was common to all M giants and supergiants. Deutsch derived estimates of the mass loss for these stars, in the neighborhood of $10^{-7}\ M_\odot$/yr—ten million times as great as the amount lost through the solar wind—and enough to affect the course of the late stages of stellar evolution in a major way.

Weymann (1962a) carried out a detailed spectrophotometric study of the spectrum of α Ori, the first real attempt at a quantitative analysis of the spectrum of the outflowing matter. He found that, despite variations of up to 10 km/s in the radial velocity of the photosphere, the displaced lines had not varied by as much as 2 km/s over an interval of more than 20 years, which implied a detached shell far enough away to be uncoupled from the pulsation of the photosphere. He estimated the inner radius of the shell to be at least 14 stellar radii, from which the rate of mass loss was inferred to be $4.5 \times 10^{-6}\ M_\odot$/yr. Weymann (1962b) also demonstrated that the mass loss in α Ori could not be driven by thermal gas pressure, as it is in the solar corona.

After Weymann's work and following the development of more sensitive detectors, interest shifted to the infrared region of the spectrum. Red giants were found to emit an excess of infrared radiation, as compared with a blackbody, in a broad band of wavelengths centered at about 9.7 μm. Woolf and Ney (1969) attributed the emission to dust grains in an extensive circumstellar shell and suggested that the grains were made of silicates containing metallic impurities such as Fe, Mg, and Al (e.g., $MgSiO_3$ and olivine, $(Mg,Fe)_2SiO_4$). From calculations of chemical equilibrium, Gilman (1969) showed that such molecules can condense in cool atmospheres of oxygen-rich stars (K and M stars) and identified similar

emissions at 11 μm as condensates of C in carbon-rich stars (R and N stars) and of SiC in stars with equal abundances of carbon and oxygen (S stars). Hoyle and Wickramasinghe (1962) had suggested earlier that graphite grains would condense in the outer regions of C-rich stellar atmospheres with sufficiently low temperatures. Gehrz and Woolf (1971) supposed that radiation pressure on the dust grains would propel them away from the star, dragging the gas along with it, and, using observed color excesses at 11 μm to estimate rates of mass loss for more than 50 stars, they derived values in the range 5×10^{-8} to $3 \times 10^{-5}\ M_\odot$/yr. There was still serious doubt as to whether the momentum acquired by the grains could be transmitted to the gas, in view of the very long mean free path for grain-gas collisions (Weymann, 1962b) until Gilman (1972) showed that the gas and dust are momentum-coupled and not position-coupled (i.e., primary collisions transmit momentum from dust to gas, but secondary collisions between atoms (molecules) are the principal means by which momentum is distributed through the gas). The process was shown to work for both silicate and graphite grains.

The large values of mass loss inferred from the dust emission heightened interest in mass loss from red giants as an important factor in the late stages of stellar evolution and as a major source both of the enrichment of interstellar gas by heavy elements and of the interstellar dust itself. As one result, Reimers (1975a, 1975b) undertook a systematic program of analysis of circumstellar absorption lines in the optical spectra of more than 120 K and M giants and G, K, and M supergiants. In these and later papers (see Reimers, 1981), Reimers found that the stars showing circumstellar absorption lines in their spectra, as evidence of high rates of mass loss, were confined to the upper right-hand corner of the Hertzsprung-Russell (HR) diagram and that terminal flow velocities ranged from about 5 to over 100 km/s. The wind velocity was found to increase roughly as the square of the escape velocity from the photosphere. Except in a few cases, Reimers did not publish mass-loss rates derived for individual stars, but instead presented his results in the form of an interpolation formula:

$$\dot{M} = 4 \times 10^{-13}\ L/gR\ (M_\odot/\mathrm{yr}) \quad , \quad (5\text{-}1)$$

where L is the star's luminosity, R is its radius, and g is the acceleration of gravity, all in solar units. This equation was derived from dimensional considerations, its physical significance being that the kinetic energy required to carry the escaping mass from a star to infinity is always the same fraction of the star's luminosity. The constant was evaluated by the process of fitting the formula to 4 or 5 normal points derived from the empirical mass-loss rates. Because of uncertainties in the empirical rates, as well as in L, M, and R, the proportionality constant is generally believed to be accurate only within a factor of 10. Reimers' formula has been the principal source of information on empirical rates of mass loss from red giants used in theoretical calculations of stellar evolution.

More refined methods of analysis were applied to a relatively small number of selected stars by Sanner (1976), Bernat (1977), and Hagen (1978). Hagen attempted to derive separate rates of mass loss for both the gas (from the optical lines) and the dust (from the 10-μm emission feature). The absence of reasonable agreement among the rates derived by these investigators made it apparent that far too little is known about the structure and composition of red giant atmospheres, as will become evident further on.

Observations with the International Ultraviolet Explorer (IUE) and with the High Energy Astrophysical Observatory (HEAO) have illuminated further the nature of the division in the HR diagram between stars with high and low rates of mass loss. The short-wavelength limit of observation with IUE is about 1170 Å, which reaches lines formed in the chromosphere/corona transition region, but not the coronal lines themselves. What at first appeared to be a

sharp line dividing stars with hot coronas from those with cool massive winds (Linsky and Haisch, 1979) is now seen as a gradual transition, with some stars in the boundary zone showing both types of spectra (Hartmann et al., 1980; see also Dupree, 1980; Reimers, 1981). Stars near the boundary tend to show temporal variations in the mass flows.

New techniques for observing at infrared, millimeter, and centimeter wavelengths are currently leading to dramatic advances in knowledge of the rates and evolutionary implications of mass loss from highly evolved stars. Observations with very high resolution of the vibration/rotation line spectra of CO, including both fundamental and overtone bands, have been effective in probing the structures of mass flows from red giants, especially Miras (Hall, 1980). Emission from circumstellar shells in the 1–0 and 2–1 transitions of CO at millimeter wavelengths can give direct information on stellar velocities, shell expansion velocities, shell sizes, and, with appropriate modeling, estimates of mass loss (Knapp et al., 1982; Knapp and Morris, 1984). Flux densities of radio continuum radiation measured with the very large array (VLA) may now be used to infer the temperature and extent of chromospheres in red giants. The VLA has also been used to map the α Sco system (Hjellming and Newell, 1983), in which the creation of an H II region in the expanding shell of the M star by the ultraviolet (UV) radiation of the B star permits a determination of the rate of mass loss from the M star. Finally, maser radiation emitted by H_2O, SiO, and OH has been shown in principle to yield information on the structure of various regions of late-type atmospheres and on the enormous extent of their circumstellar shells (see Elitzur, 1981). The so-called OH/IR stars offer the possibility of studying very luminous, long-period Mira variables which are not seen in visible light.

The observational study of mass loss from red giants in globular clusters was initiated by Cohen (1976), who interpreted emission associated with the Hα absorption line as arising by recombination in an expanding ionized shell of hydrogen. The same method has been extended to large numbers of stars by Mallia and Pagel (1978), Peterson (1981, 1982), and especially by Cacciari and Freeman (1981, 1983), all of whom derived rates in the neighborhood of $10^{-8}\ M_\odot$/yr. Although rates of this order of magnitude seem to satisfy the requirements of stellar evolution, there is a fundamental difficulty in the assumption that the presence of Hα emission is by itself evidence of mass loss (Reimers, 1981; Dupree, et al, 1984).

In addition to thermal gas pressure and radiation pressure on dust grains, a number of other interesting mechanisms have been proposed for both steady and episodic mass loss (e.g., wave pressure, shock waves, magnetic reconnection, dynamical and pulsational instability, and pulsational mode switching in Miras). The probability is high that the dust mechanism operates in the coolest late-type stars, but it is not at all clear which mechanisms are most relevant in other stars.

Mass loss from red giants plays a crucial role in several aspects of stellar evolution (see Renzini, 1981a; Iben, 1981b). Mass loss from stars of intermediate mass between 1 and 8 $M_\odot$ can make an important contribution to the enrichment of the interstellar medium. Moreover, in the absence of mass loss, all stars with masses exceeding 1.4 $M_\odot$ would become supernovae, but if enough mass is lost while the star is on the asymptotic giant branch (AGB) of the HR diagram, intermediate-mass stars may evolve into planetary nebulae and white dwarfs. Particularly exciting is the recognition of long-period OH/IR stars as possible progenitors of planetary nebulae. Mass loss from intermediate-mass stars may also affect the formation of interstellar dust grains, Mira variables, and carbon stars. The evolution of low-mass stars (mass less than 1.4 $M_\odot$) has been extensively studied in globular clusters. In the absence of mass loss, one finds discrepancies between the observed and calculated luminosity functions of stars on the horizontal branch (HB) and AGB, which can be removed by postulating mass losses of about 0.2 $M_\odot$ on the red-giant branch (RGB) and about 0.1 $M_\odot$ on the AGB.

EMPIRICAL RATE DETERMINATIONS

UV-Optical Spectra 0.2–5 μm

Single Stars. Figure 5-1 shows small regions of the spectra of several red giants and supergiants centered on the resonance lines of Mg +, Ca +, Na, Mn, and K. The profiles are more or less typical of the resonance lines of neutral and singly ionized metals in the visible and near-UV spectral regions of cool stars showing mass loss. Figure 5-2 shows a tracing of the R1 line of the 1–0 band of CO near 4.65 μm, which is similar in appearance to the potassium line. The cores of the Mg II and Ca II lines are strongly saturated and contaminated by chromospheric emission, but the other lines show the P Cygni profiles characteristic of resonance scattering in an extended expanding atmosphere, although distorted by the underlying, broad photospheric line. The absorption components are formed along the line of sight to the star and are displaced to the blue by the amount of the expansion velocity, whereas the emission is undisplaced relative to the center-of-mass velocity. Notice that in α Ori, the CO and K I circumstellar (CS) lines are double, with an apparent separation of about 6.5 km/s, implying the existence of two discrete shells. Curiously, in this star, the doubling is also seen in the D-lines of Na I, but not in any other lines. The absence of shell components among lines with excitation potentials greater than a few tenths of a volt has been interpreted as implying shell temperatures less than 1000 K (Weymann, 1962a).

Spectral line profiles are used for the derivation of mass-loss rates with the aid of the equation of continuity:

$$\dot{M} = 4\pi \cdot r^2 \cdot n(r) \cdot \mu \cdot m_H \cdot v(r) , \quad (5\text{-}2)$$

where r is the radius of a volume element with hydrogen number density $n(r)$ and outward velocity $v(r)$, μ is the mean molecular weight, and m_H is the mass of the H atom. This equation implies steady mass loss with spherical symmetry. In most cases, the radial dependence of velocity and density cannot be determined without additional assumptions. Since the circumstellar absorption lines appear to be relatively sharp, the velocity along the line of sight is usually assumed to be constant, which implies an inverse square law for the density. Moreover, the formation of P Cygni profiles signifies that most of the emission is occurring far from the star, and the radial velocities of the displaced components are constant even in stars with variable photospheric velocities. Therefore, the circumstellar shells are assumed to be detached from the stellar photospheres and to be far enough away to be insensible to their motions. With these two assumptions, Equation (5-2) becomes:

$$\dot{M} = 4\pi \cdot N \cdot \mu \cdot m_H \cdot R_o \cdot V , \quad (5\text{-}3)$$

where N is the column density of hydrogen gas along the line of sight, R_o is the inner radius of the detached shell, and V is the expansion velocity, assumed to be constant. The derivation of $\dot{M}$ from Equation (5-3) proceeds by steps as follows.

First, the P Cygni profile must be detached from the background photospheric line, which can be done with varying degrees of difficulty. Two quantities are extracted from the line profile: the column density of atoms or molecules in the ground level of a particular transition and the expansion velocity. The earlier work (Weymann, 1962a; Reimers, 1975a) assumed line formation in a static, plane-parallel atmosphere, but more recent work has made use of relatively exact calculations by Kunasz and Hummer (1974) of radiative transfer in an expanding spherical atmosphere and of relatively sophisticated non-LTE calculations of ionization equilibrium (Sanner, 1976; Bernat, 1977; Hagen, 1978). On the average, column densities derived by Bernat (1977) for α Ori are smaller

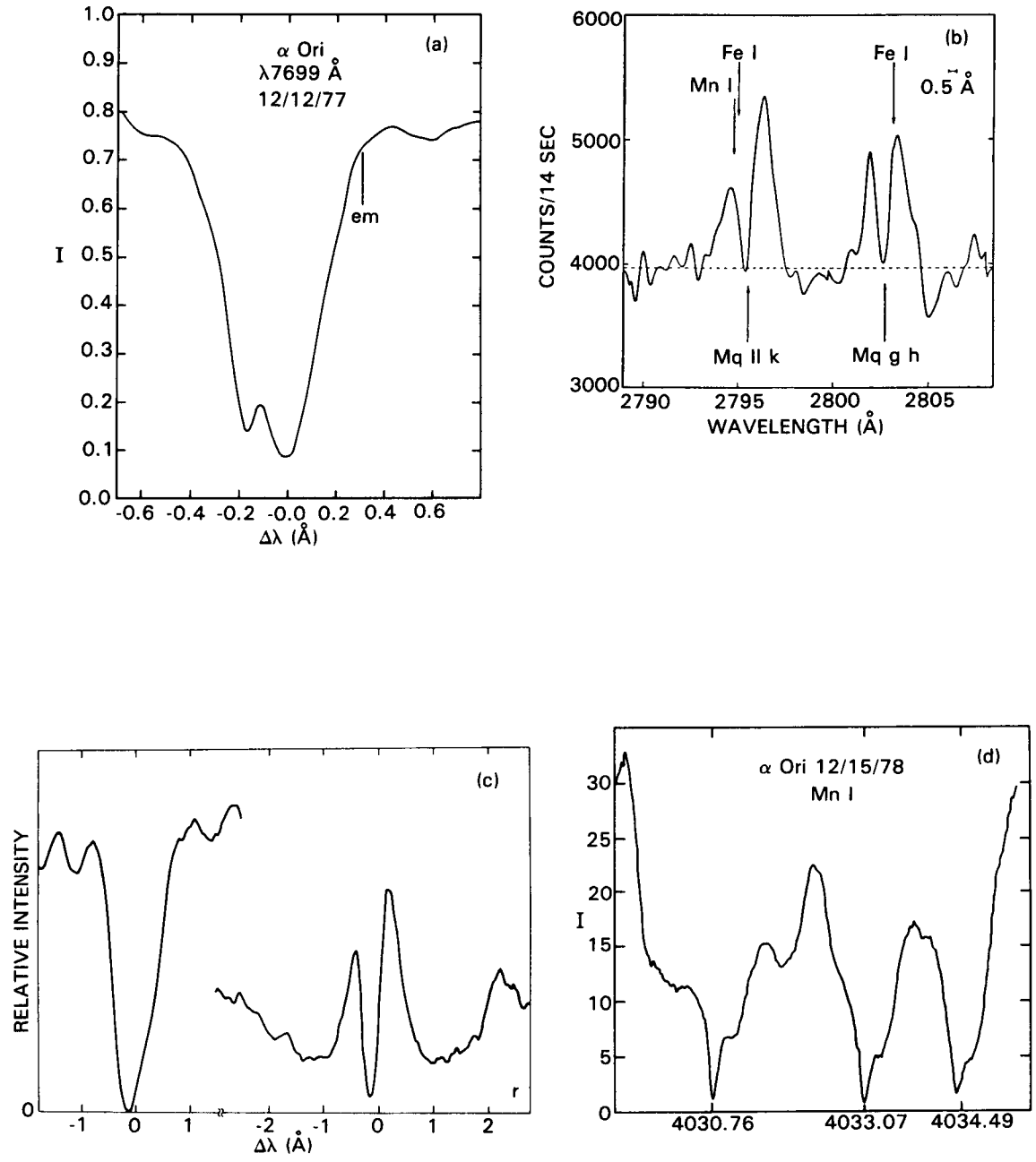


Figure 5-1. Circumstellar resonance line profiles: (a) K I in Ori; (b) Mg II in α Ori (Bernat 1976); (c) Na I 5890 Å in α Her (left); Ca II K in β Peg (Hagen, 1980) (right); (d) Mn I in α Ori. The vertical line labeled "em" in (a) marks the center of the emission component of the P Cygni profile.

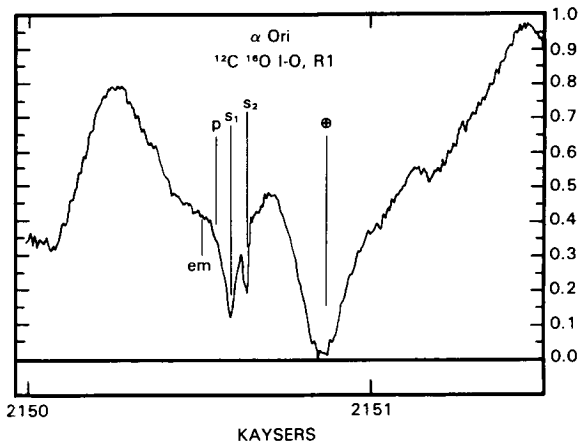


Figure 5-2. The R1 line of the 1–0 band of CO in the spectrum of α Ori. The two shell components, s_1 and s_2, are superposed on the broad photospheric line labeled p. The strong telluric component is shown to the right (Bernat et al., 1979). The vertical line labeled "em" marks the center of the emission component of the P Cygni profile.

than those of Weymann (1962a) by a factor of 3 to 4. The expansion velocity, V, is obtained by direct measurement of the displacement of the absorption line relative to neighboring photospheric lines. The emission on the redward side of the absorption line causes a spurious additional shift of the line, amounting to an error of about 25 percent (Bernat, 1976). If the velocity of the photosphere is variable, the expansion velocity is the shell velocity minus the center-of-mass velocity.

The column density of the given atom in a given stage of ionization must then be converted into, first, the column density of the element in all stages of ionization and, second, the column density of hydrogen. Most of the resonance lines seen in the visible spectrum, with the exception of those of Ca II, Sr II, and Ba II, belong to neutral metals such as Fe, Cr, Ni, Mn, and K. Since the metals are predominantly singly ionized, a theory of ionization is needed to derive the abundance of the ion. This step is omitted for Sr II and Ba II. The total column density then follows from the assumption that the abundances are solar-like, which may be reasonable for most of the metals but is questionable for Sr and Ba. The assumptions made for CO in O-rich stars are that all carbon atoms are locked up in CO, which seems reasonable, and that the C/H ratio is the same as in the Sun, which is a pure guess.

Applications of the theory of ionization have led to severe contradictions in the results. As a test of the theory, Hagen (1978) derived column densities of Sr II and Ba II in eight stars and then used solar abundances and ionization theory to predict column densities for several neutral metals. Figure 5-3 shows the logarithm of the ratio of the observed column density N(obs) to the predicted column density N(pred) plotted against the element in order of decreasing ionization potential. The discrepancy of four orders of magnitude is hard to explain. Part of it apparently results from the steep drop of the assumed blackbody radiation field below 2000 Å, and part may be caused by the depletion in grains of elements with higher ionization potentials. Figure 5-3 suggests that neutral elements of low ionization potential are much more abundant than the theory predicts and raises a question as to whether Ba and Sr are indeed predominantly singly ionized, at least in the cooler M giants.

Hagen (1978) used only the lines of Sc II, Sr II, and Ba II to derive column densities of hydrogen in eight red giants. Bernat (1977) derived hydrogen column densities in the four red supergiants—α Ori, α Sco, α Her, and μ Cep—by averaging the results obtained from 8 to 9 metallic atoms, both neutral and singly ionized. Although the scatter is large, approaching a factor of 50, there is no systematic difference between hydrogen column densities derived from neutral and ionized species, respectively. On the other hand, the column densities inferred from the Ti II lines at 3300 Å are too small relative to those from Sr II and Ba II by factors of 7 to 20, if solar relative abundances are used and if the singly ionized stage is assumed to be predominant.

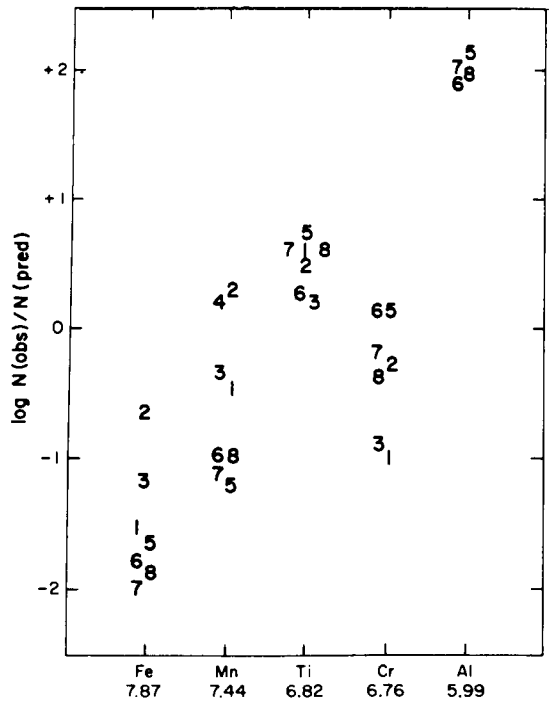


Figure 5-3. The logarithm of the ratio of the observed column density of neutral atoms to the column density predicted through the use of ionization theory and solar abundances plotted against element in order of decreasing ionization potential. The numbers refer to different stars as follows: 1 = X Her, 2 = RX Boo, 3 = HD 207076, 4 = R Leo, 5 = α Sco, 6 = α Ori, 7 = α Her, 8 = μ Cep (Hagen, 1978).

A very large error in $\dot{M}$ may arise because there is often no satisfactory method available for the determination of R_o, the inner radius of the shell; different investigators have used values differing by one or two orders of magnitude for the same star. Weymann (1962a) proposed a method for deriving the inner radius based on the idea that the cores of the infrared triplet lines of Ca II, 8542 and 8662 Å, might show small displaced absorption components formed in the expanding shell. Since the lower levels of these lines should be populated by radiative excitation, the equivalent width of the feature ought to be inversely related to the shell radius. The method has been applied to several stars by Weymann (1962a), Sanner (1976), and Bernat (1977), and although it appears to work in some stars, it leads to widely discrepant results for α Ori, for which the lines are so deep that the signal to noise tends to be relatively small at the very line center (Goldberg, 1979). Another method of estimating R_o is based on model calculations of off-limb profiles of K I emission (Bernat, 1976). When the line of sight is interior to the inner radius, the calculated profiles are asymmetric, and the observation of such asymmetries in Betelgeuse implies an inner radius of about 100 stellar radii, but the calculations are strongly model-dependent.

There is in fact some question as to whether the shell has a well-defined inner radius, as is usually assumed in mass-loss determinations. No matter what the mechanism for initiating and maintaining the flow may be, there must be a region in which the gas accelerates to its terminal velocity and in which the density is relatively high. Such a region would be difficult to identify from a P Cygni profile because, although the absorption component might be strongly asymmetrical, the asymmetry would be camouflaged by the redward-shifted emission component. The superposition of a P Cygni profile on a photospheric line would make such an asymmetry doubly difficult to detect. On the other hand, subordinate lines would not be expected to display strong redward emission, since photons absorbed in such lines tend to be reemitted in resonance lines. Such asymmetric subordinate lines are indeed observed in the spectrum of α Ori, the most prominent among them being the Fe I lines at 4140 Å and the Ca II IR triplet (Goldberg, 1979), both of which have excitation potentials of about 1.5 eV. The 8498 and 8542 Å lines of Ca II are shown in Figure 5-4, where they are plotted on a heliocentric velocity scale. Notice that the line cores are highly asymmetric in the sense that the radial velocity decreases from about 21 to 22 km/s, which is the systemic velocity of the star, in the upper part of the core, to about 13.5 km/s at the bottom of the 8542 Å line. Moreover, over a period of several years, during

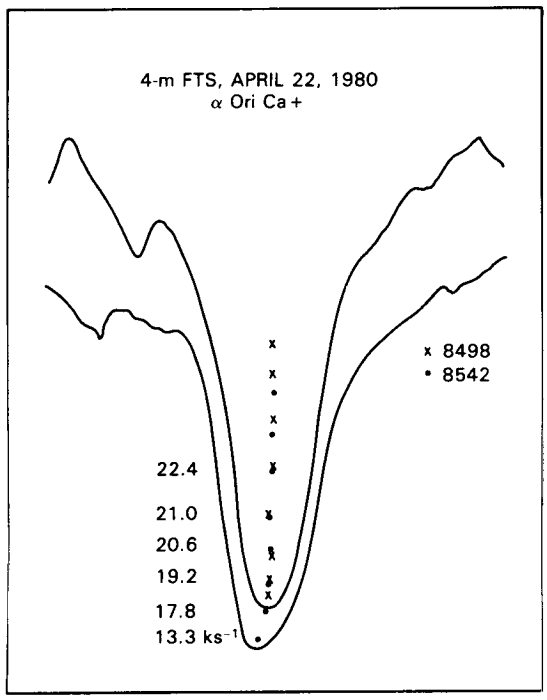


Figure 5-4. Profiles of the 8498 and 8542 Å lines of Ca II in α Ori made with the Fourier transform spectrometer of the McMath Telescope at Kitt Peak National Observatory. The lines are plotted on a velocity scale. The line bisectors are indicated by dots (8498 Å) and crosses (8542 Å), with the corresponding heliocentric velocities shown to the left.

which the mean velocity of the photosphere decreased by about 5 km/s, the velocities in these profiles remained stationary (Goldberg, 1979). The terminal velocity shown by the absorption components of the resonance lines is about 11 km/s, but if a correction is made for the spurious shift caused by their companion emission lines, the velocity would agree with that measured at the center of the 8542 Å line. Thus, the line is formed in an atmospheric region which is far enough away to be uncoupled from the motion of the photosphere, which is an argument in favor of the detached shell model. It is probable that the absorption components of the resonance lines would show the same behavior if they could be separated from their emission components.

The first high-resolution observations of circumstellar CO were made in the spectrum of α Ori by Bernat et al. (1979) with the Fourier transform spectrometer (FTS) at the Kitt Peak National Observatory (KPNO) 4-meter telescope. Numerous lines of the fundamental vibration/rotation band at 4.6 μm were observed, including several lines of the isotopic molecule, ^{13}CO. Subsequently, Bernat (1981) observed the band in nine other red giants. Figure 5-2 shows a typical CO line in the spectrum of Betelgeuse, which consists of four components: a telluric line, a broad photospheric line, and two narrow circumstellar lines with heliocentric velocities of 11.0 and 4.8 km/s, respectively. The same velocity components are observed in K I and probably also in the D-lines of Na (Goldberg et al., 1975), but in no other lines. The relative abundances $^{12}C/^{13}C$ were found to be about 6 for both components, which suggests two shells with a common origin in highly processed matter from the stellar interior and thus rules out an interstellar origin for the second component. After showing that collisional excitation dominates over radiative excitation, Bernat et al. (1979) identify the excitation temperature with the kinetic temperature, assume that the gas and dust are in thermal equilibrium, and derive distances of 150 and 2000 stellar radii, respectively, for the two shells. The further assumptions of cosmic composition and the complete association of carbon into CO lead to mass-loss rates of 5×10^{-6} and $3.2 \times 10^{-6}\ M_\odot$/yr for the near and far shells, respectively.

The results of Bernat's (1981) survey of other red giants for circumstellar CO are shown in Table 5-1. In addition to these stars, three other stars—α Boo, α Tau, and α Sco—showed no detectable CO, whereas the CO shell lines in RX Boo were found to be too strongly saturated for analysis. α Boo and α Tau are too early in spectral type to show circumstellar lines, and as Bernat points out, any CO in the shell of α Sco would be dissociated by the companion B star. Table 5-1 shows that the CO absorption features are multiple in many stars,

Table 5-1
Observations of CO in M Giants and Supergiants (Bernat, 1981)

Star	Spectral Type	Component (km/s)	T_{exc} (K)	N (CO)/v (Dop) (cm^{-2} km^{-1} s)	N (H) (cm^{-2})	N (Dust)[a] (cm^{-2})
119 Tau	M2 Iab–Ib	−9	200 ± 150	7.5 + 15	3.4 + 21[b]	—
μ Cep	M2 Ia	−8	100 ± 10	7.5 + 15	7.3 + 21[c]	—
		−13	270 ± 60	2.0 + 16	—	—
		−19	100 ± 15	1.8 + 16	—	4.0 + 21[d]
		−38	60 ± 4	1.1 + 17	—	—
		−47	100 ± 40	3.0 + 15	—	—
β Peg	M2–3II–III	−6	90 ± 30	1.3 + 16	2.7 + 20[b]	—
ϱ Per	M4 II–III	−2	90 ± 20	6.5 + 15	2.7 + 20[b]	—
α Her	M5 Ib–II+	−13	250 ± 60	4.2 + 16	6.6 + 21[d]	2.0 + 20[d]
		−25	550 ± 670	6.7 + 15	—	—
SW Vir	M7 III	−6	130 ± 20	2.9 + 16	—	—
		−9	130 ± 15	2.3 + 16	—	—
X Her	M6e	−8	110 ± 20	4.3 + 16	2.5 + 20[d]	4.0 + 21[d]
W Hya	M7–9e	−5	300 ± 90	4.8 + 16	2.5 + 20[d]	6.0 + 21[d]
		−13	120 ± 20	3.7 + 15	—	—

[a]N(Dust) is the H column density derived assuming cosmic abundances and complete condensation of silicates.
[b]Sanner (1976).
[c]Bernat (1977).
[d]Hagen (1978).

which Bernat now attributes to episodic mass loss rather than to the formation of discrete clumps by instabilities in a steady flow as was postulated for Betelgeuse (Bernat et al., 1979). Column 4 lists the excitation temperatures, interpreted as kinetic temperatures. The Doppler velocity could not be independently determined and therefore only the ratio of CO column density to Doppler velocity can be inferred, as given in column 5. Column 6 contains the hydrogen column densities derived in previous investigations of optical atomic spectra, and column 7 lists the hydrogen column density derived from the 10-μm silicate feature on the assumption that all Si atoms are condensed on grains and that the Si/H ratio has the solar value. The absence of a correlation between CO column densities and either of the two hydrogen column densities is, in Bernat's view, a major argument in favor of episodic mass loss, since the separate shells would be formed under different physical conditions.

Bernat's final conclusion is that meaningful mass-loss rates cannot be determined from observations of nonsteady mass loss unless averages are taken over several episodes. We shall come back later to the topic of episodic mass loss and comment here only that the absence of correlations between the various column densities is not unexpected in view of: (1) the large scatter of the determinations from different ions in the same star, and (2) the many sources of error in the derivation of column densities from the 10-μm emission feature.

Binary Stars. The errors introduced by uncertain knowledge of the degree of ionization and of the inner shell radius may be avoided in principle by observing circumstellar lines of elements in a predominant stage of ionization (e.g., Fe II or Ti II) in the spectrum of a hot visual companion of a red giant (Reimers, 1981). If the geometry of the binary system is known, no assumption need be made about an

inner shell radius. Stars studied in this way from the ground, from a balloon, and from IUE are α^1 Her (Reimers, 1977a) and α Sco A (Kudritzki and Reimers, 1978; van der Hucht et al., 1980; Bernat, 1982). Reimers (1977a) derived hydrogen column densities from six shell lines of Sr II (4077 Å) and Ti II (3300 Å) in the spectrum of α^2 Her (G5 III), the visual companion of α^1 Her (M5 II), and obtained a mass-loss rate of $1.1 \times 10^{-7}\ M_\odot$/yr, which is about one-sixth of Bernat's (1977) value derived from lines of neutral metals at visible wavelengths in the spectrum of α^1 Her.

The binary-star approach has been extensively applied to the α Sco system. Kudritzki and Reimers (1978) derived a rate of $7 \times 10^{-7}\ M_\odot$/yr for mass loss from α Sco A (M1.5 Iab), using the H and K lines of Ca II and the Ti II lines in the spectrum of α Sco B (B2.5 II). Van der Hucht et al. (1980) observed a variety of lines between 2000 and 3000 Å in the spectrum of α Sco B with the balloon-borne ultraviolet spectrometer (BUSS), giving greatest weight to the Zn II and Cr II lines, and obtained a rate equal to $7.1 \times 10^{-6}\ M_\odot$/yr. It is possible that the Zn II lines are primarily interstellar (Reimers, 1981). Finally, Bernat (1982) has made the most thorough investigation of mass loss from α Sco A, with the IUE satellite, by observing 90 lines of about a dozen ions in the wavelength range 1190 to 2631 Å. The result is that the column densities of hydrogen, derived from 10 different ions, predominantly singly ionized, show a spread of a factor of 30. No single explanation—observational error, shell chemistry, interstellar contributions—appears to be satisfactory. An unweighted mean over all ions gives a rate of $6.4 \times 10^{-6}\ M_\odot$/yr.

In principle, the binary-star approach may be extended to a much larger number of stars by IUE observations of spectroscopic binaries consisting of a red-giant star and a B-type companion. Observations in the ultraviolet effectively separate the two stars. The first attempts along these lines were made for 32 Cyg (Stencel et al., 1979) and ζ Aur (Chapman, 1981), but neglected to take into account the nonspherical nature of the line-transfer problem (Reimers, 1981). The angular separation of such objects is so small that radiation from both the B star and the circumstellar shell pass through the spectrograph slit, resulting in P Cygni profiles that must be analyzed in the context of a nonspherical three-dimensional line-transfer problem. The necessary theoretical framework has been developed by Hempe (1982) and applied to the analysis of a number of objects, including ζ Aur, 32 Cyg, and 31 Cyg (Che et al., 1983), δ Sge (Reimers and Schröder, 1983), and Boss 1985 (Che and Reimers, 1983). For the K supergiant, ζ Aur, Che et al. (1983) derived $\dot{M} = 0.63 \times 10^{-8}\ M_\odot$/yr and $v_{exp} = 40$ km/s, as compared with Chapman's (1981) values of $\dot{M} = 2 \times 10^{-8}\ M_\odot$/yr and $v_{exp} = 100$ km/s, respectively. For 32 Cyg, Che et al. found $\dot{M} = 2 \times 10^{-8}\ M_\odot$/yr and $v_{exp} = 60$ km/s, as compared with Stencel et al.'s (1979) $4 \times 10^{-7}\ M_\odot$/yr and 65 km/s, respectively.

Mira Stars. Optical studies of mass loss from Mira stars have benefited greatly from observations of the infrared vibration/rotation bands of CO. The star χ Cyg is a good example, in which a series of high-resolution spectra, taken with the FTS at the KPNO 4-meter telescope may have provided new insights into the mass-loss mechanism for red-giant stars (Hinkle et al., 1982). The spectra covered more than three cycles of the visible light variation and included the first and second overtone bands as well as the fundamental. Analysis has revealed four sets of lines, separated according to their velocity characteristics, and apparently arising from four different atmospheric regions: (1) a pulsating photospheric region through which a shock front passes near maximum light; (2) a cool gas ($T \sim 300$ K) expanding at 7.5 km/s relative to the center of mass, which is identified with the circumstellar shell; (3) a hotter region ($T \sim 800$ K), stationary with respect to the center of mass; and (4) a still hotter gas ($T \sim 1500$ K) falling inward at 8 km/s. The column density of the stationary layer varies on a time scale larger than the optical period of 410 days.

For example, the lines were absent in 1975, became quite pronounced 7 months later, and then weakened steadily over the next 3 years. It is conjectured that this layer contains gas ejected during particularly violent oscillations and is somehow supported by dissipated shock energy. If the stationary layer is heated by stellar photospheric radiation, its 800 K temperature implies a distance of 10 R_*, or 1.7×10^{14} cm, where dust grains can form. Roughly the same value, 10^{14} cm, was measured by infrared speckle imaging techniques (Mariotti et al., 1983). Thus, it can provide a reservoir both for the dust-driven mass loss and the infalling gas. A similar layer appears to be present in the 10 Miras which have been observed thus far by Hinkle et al. (1982), who suggest that it may also be present in most late-type stars.

Red Giants in Globular Clusters. It has been known for some time (for a summary, see Renzini, 1981a) that a mass loss of about 0.2 $M_\odot$ during the RGB (red-giant branch) phase, and an additional 0.1 $M_\odot$ during the AGB (asymptotic giant branch) phase are needed to bring the calculated distribution of stars on the HR diagrams of globular clusters into agreement with observations. In the absence of experimental evidence for mass loss from stars in globular clusters, theorists incorporated into their calculations (Fusi-Pecci and Renzini, 1976; Renzini, 1977) Reimers' (1975a, 1975b) parametric formula for mass loss, Equation (5-2), modified by an adjustable parameter, η, which is supposed to reflect the uncertainty in the empirical rates:

$$\dot{M} = -4 \times 10^{-13} \times \eta \cdot L/gR. \qquad (5\text{-}4)$$

This relationship was derived for Population I stars, and the scatter around it suggests that η lies somewhere between 0.3 and 3.0. It is therefore remarkable that, within rather close limits, the Reimers formula with $\eta = 0.40$ clears up both the HB and AGB discrepancies, despite the fact that it is based on empirical rates for relatively few Population I stars, which are themselves uncertain by a factor of 10.

Observational evidence for mass loss from red giants in globular clusters was first offered by Cohen (1976) in the form of emission associated with the Hα absorption lines in four red giants belonging to three globular clusters. Although emission has been observed on the blue wing in some cases, it has also been seen only on the red wing in other stars and on both wings in still others. Cohen's observations have been extended to a large number of stars in more than a dozen clusters by Mallia and Pagel (1978), by Peterson (1981, 1982), and especially by Cacciari and Freeman (1983). Cohen (1976) postulated that the emission arises from a circumstellar shell as a result of mass loss. As a model for estimating mass loss, Cohen took a completely ionized shell, expanding at a constant rate of 45 km/s from an inner shell radius $R_s = 2\ R_*$ to infinity. The envelope was assumed to be optically thick in the Lyman lines and optically thin in the Balmer lines. With these assumptions, the total Hα emission from the star is written as:

$$E(H\alpha) = 4\pi \cdot h\nu \cdot n_o^2 \cdot \alpha_{32}\, R_s^4 \int_{R_s}^{\infty} dr/r^2, \qquad (5\text{-}5)$$

in ergs/s, where n_o is the density of hydrogen at R_s, and α_{32} is the effective recombination coefficient for a temperature of 10000 K.

The rate of mass loss is then

$$\dot{M} = 4\pi \cdot R_s^2 \cdot m_H \cdot V_{exp} \cdot n_o, \qquad (5\text{-}6)$$

where n_o is to be substituted from Equation (5-5), and m_H is the mass of the hydrogen atom. Numerically, with the equivalent width W substituted for E(Hα), the rate of mass loss becomes (Mallia and Pagel, 1978):

$$\dot{M} = 2.76 \times 10^{-4}\, V_{exp} \cdot R_* \,(R_s \cdot W)^{1/2} \cdot \exp(-1.1/T_4) \quad . \qquad (5\text{-}7)$$

The radii are expressed in solar radii, V_{exp} is in km/s, W is in Å, T is in units of 10^4 K, and $\dot{M}$ is in $M_\odot$/yr. Note that, when expressed in terms of the observed quantity, W, the equivalent width, $\dot{M}$, is proportional to $R_*^{3/2}$, and not to $R_*^{1/2}$ as Cohen (1976) supposed.

All investigators have followed Cohen's (1976) methodology in calculating rates of mass loss. Cohen derived a minimum rate of 2×10^{-9} $M_\odot$/yr, which, when combined with a red-giant lifetime of 1×10^8 years, gave the desired loss of $0.2\ M_\odot$ on the RGB. Mallia and Pagel (1978) found much larger rates, up to 6×10^{-8} $M_\odot$/yr, principally because they used larger stellar radii, but they also believed that their results were compatible with the requirements of HB morphology. In her study of seven luminous giants in three clusters, using high spectral resolution, Peterson (1981) found that the Na D and Hα lines in some stars had blue-shifted asymmetric cores similar to those observed in M field giants and supergiants (Boesgaard and Hagen, 1979). The shifts amounted to about 6 km/s in Hα and 11 km/s in Na D. Peterson (1981) notes that emission is not usually seen in field giants with asymmetric cores. Boesgaard and Hagen (1979) find that 50 percent of stars with spectral classes M0 III to M7 III show asymmetric Hα profiles with core blue shifts of a few km/s.

In a recent extensive survey of 143 red giants in 12 globular clusters, Cacciari and Freeman (1983) detected Hα emission in about one-third of the stars brighter than $\log L = 2.9$, or $M_{bol} < -2.5$, with clear evidence of variability. Moreover, the apparent narrowing of Hα absorption in fainter stars suggests the presence of weaker emission down to $\log L = 2.3$, or $M_{bol} = -1$. Mass-loss rates calculated from Equation (5-7) are between 0.7 and 6.3 in units of 10^{-8} $M_\odot$/yr. The required total mass loss on the RGB is attained if it is assumed that the average rate of loss from $M_{bol} = -1$ to the tip of the RGB is 10^{-8} $M_\odot$/yr over an evolutionary time of 2×10^{-7} years (Sweigart and Gross, 1978).

Despite these estimates, however, the occurrence of mass loss in globular cluster stars on the RGB in an amount sufficient to satisfy evolutionary requirements is still unproven (Reimers, 1981; Dupree et al., 1984). Neither Hα emission nor the dependence of the emission on luminosity is evidence of mass loss. Model calculations of Hα line profiles in metal-deficient stars by Dupree et al. (1984) show that emission wings can arise in warm chromospheres with mass-loss rates $\ll 2 \times 10^{-9}$ $M_\odot$/yr. Moreover, chromospheric activity might well increase as stars ascend the red-giant branch. The assumption that the emission is formed in a fully ionized gas by recombination is purely arbitrary, and uncertainties in the assumed stellar radii represent another source of error, which has already led to a disagreement of an order of magnitude (Cohen, 1976; Mallia and Pagel, 1978). The observation of asymmetric blue-shifted line cores (Peterson, 1981, 1982) implies that the outer envelopes of some red giants in globular clusters are expanding, but not necessarily that matter is escaping.

Infrared Dust Emission

Emission by silicates in a broad band centered at 9.7 μm is a common occurrence in the spectra of late-type O-rich giants and supergiants. In the carbon stars, a similar but narrower band near 11 μm is probably radiated by SiC, while a third species of unknown composition contributes to the continua of some, but not all, C and S stars. The silicate feature is the most useful indicator of mass loss in the middle infrared. In the far infrared, thermal continuum emission near 400 μm by silicate and carbon grains is the most promising determinant of dust mass loss from highly evolved stars. We consider first the silicate emission at 10 μm and next the continuous emission at submillimeter wavelengths.

Emission by Silicates at 10 Microns. Figure 5-5 shows the excess emission observed in the 10-μm region of red-giant spectra, as compared with blackbody emission at the stellar

temperature. Basically, one tries to extract the optical depth of the dust grains at 10 μm from the amplitude of the excess emission, bearing in mind that the amount radiated also depends on the temperature of the dust. The dust temperature is determined by the composition of the grains and their absorbing properties at the shorter infrared wavelengths where most of the stellar radiation is concentrated. The radial optical depth τ(10 μm) is then used to calculate the column density of dust,

$$\tau(10\ \mu\text{m}) = a^2 \cdot Q(10\ \mu\text{m}) \cdot N_c\ , \qquad (5\text{-}8)$$

where a is the radius of a grain, Q is the absorption efficiency at 10 μm, and N_c is the column density of silicate grains per cm^2. If values of a and Q are known or assumed, N_c may be found from Equation (5-8). Next, the column density of hydrogen may be inferred from: (a) the assumed grain composition, (b) a judgment as to the fraction of a given element that may have condensed on the grains, and (c) an estimate of the abundance of that element relative to hydrogen. Finally, the mass-loss rate is calculated from Equation (5-3) with the aid of expansion velocities derived from optical spectra and estimates of the inner shell radius by one means or another.

The most uncertain step in the analysis is the derivation of τ(10 μm) from the observed IR emission, which requires knowledge of half a dozen other parameters, and is therefore strongly model-dependent (Hagen, 1978):

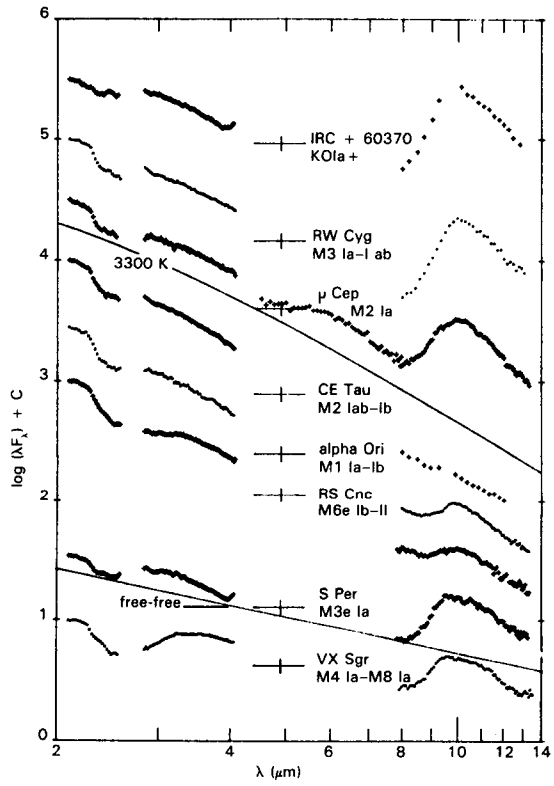


Figure 5-5. Spectral energy curves for K and M supergiants in the 2- to 3-μm region. The excess emission near 10 μm is clearly seen. For comparison, curves for a 3300 K blackbody and for free-free emission are drawn on a relative scale (Merrill, 1977).

1. The dust temperature distribution is determined by the equilibrium between the absorption of stellar radiation at wavelengths smaller than 5 μm and the emission at longer wavelengths. Knowledge of grain compositions and absorption efficiencies are of critical importance. In discussions of grain temperatures, a distinction is usually made between so-called "clean" silicates, which are relatively pure and have highly developed crystalline structures, and "dirty" silicates, which have disordered lattices (e.g., natural hydrous silicates in carbonaceous chrondrites) or are coated with impurities such as graphite. Clean silicates are transparent to short infrared wavelengths, whereas the dirty silicates are strong absorbers at these wavelengths. Jones and Merrill (1976) showed that pure silicate grains reach an equilibrium temperature that is too low to reproduce the observed 10-μm feature. The introduction of impurity (dirty silicates) raises the short-wave efficiency and warms the grains.

2. The absorption efficiencies are well known for relatively few minerals, and

although they are reasonably independent of composition at 10 μm, they differ from one mineral to another by several orders of magnitude at wavelengths less than 5 μm, where the stars radiate most of their energy. The temperature distributions are correspondingly uncertain.

3. For given optical depth, the size of the shell, particularly the inner radius, determines the flux at 10 μm.

4. The density distribution for dust grains is another important input. It is usually assumed that the density falls off as r^{-a}, where $a = 2$ for constant velocity. Hagen (1978) prefers $a = 1.5$, but nevertheless assumes constant velocity.

5. The small-grain approximation (Shawl, 1975) is usually chosen to fix the grain size, with $a = 0.05$ to 0.1 μm. In this range, $a \ll \lambda$, and $Q(\text{abs}) \propto a$. The dust temperature is independent of grain size, since both the energy absorbed per unit mass and the energy emitted are proportional to the grain volume.

6. Hagen (1978) took partial account of radiative-transfer effects by including a correction for self-absorption of starlight by the dust, but a more exact treatment is required when τ (10 μm) is greater than unity (Rowan-Robinson and Harris, 1983a).

The extensive survey of IR circumstellar emission by Gehrz and Woolf (1971) was based on IR photometry at 3.5, 8.4, and 11 μm. The color 3.5 μm - 8.4 μm was taken as a measure of silicate emission and the color 8.4 μm - 11 μm as a measure of optical depth. Gehrz and Woolf avoided many of the problems of the data analysis by adopting a model of a thin spherical shell with temperature T at a distance R from the center of the star. When the color 8.4 μm - 11 μm is plotted against the color 3.5 μm - 8.4 μm, comparison with model curves gives both $\tau(11\ \mu\text{m})$ and $(R/R_*)\ (T/T_*)^{-1/2}$. Optical depths for class Ia supergiants were found to be 0.1 to 0.2, as compared with about unity for Miras and about 0.25 for SRb variables. The adoption of a dust temperature of 900 K for all calculations led to estimates for the inner radii of shells of about 4 R_* for typical red giants and Miras and about 20 R_* for supergiants.

In a study of mass loss from nine stars, which included giants, Miras, and supergiants, Hagen (1978) computed optically thin model dust shells (Dyck and Simon, 1975) to calculate infrared fluxes, making some allowance for self-absorption. After calculating a number of emission profiles as a function of τ for assumed values of the other model parameters, Hagen chooses a value of τ by comparing the predicted and observed emission bump heights and evaluates the dust column density from Equation (5-8). The hydrogen column density then follows from the assumed grain composition. In calculating mass-loss rates from total column densities, Hagen (1978) took as inner shell radii the distances at which silicate grains condense, which vary from 1.2 R_* for a 2500 K star to 1.9 R_* for a 3600 K star. As Hagen points out, these small distances are inconsistent with the analysis of the optical line profiles, which were modeled on the assumption that the radius of the inner shell is larger than R_* by at least a factor of 3. In a more recent survey of 42 red giants and supergiants (Hagen et al., 1983), the inner shell radius is set at a uniform value of 10 R_* for all stars.

In the same paper, Hagen (1978) also derives hydrogen column densities from optical lines, using Sr II for the cooler stars later than M5 and Sr II, Ba II, and Sc II for the early M stars. Since she assumes that the same fraction of all elements is condensed into grains, the addition of the two values of N(H) gives the total column density of CS matter, and the ratio of the two is the relative proportion of metals existing as gas and dust, respectively. It is hard to understand how two elements such as Sr and Si, with fractional abundances differing by five

orders of magnitude, can be condensed on grains in the same proportions. At the very least, the investigation should be repeated, using optical observations of elements with abundances comparable to that of Si.

One of the principal conclusions from these studies is that the total quantity of CS gas derived from the Sr II 4077 Å line is uncorrelated with the quantity of CS dust implied by the strength of the 10-μm silicate feature. Such a correlation is expected from the theory of dust-driven mass loss (see Deguchi, 1980), but its absence may not be too significant in view of the many uncertainties in the derivation of dust column densities. Moreover, the use of a single line, 4077 Å of Sr II, as a measure of total gas content implies far more confidence in ionization theory and in solar-like abundances than is warranted. It appears that the fraction of metals in the form of dust and gas, respectively, are not at all well determined.

Submillimeter Dust Emission. In principle, the rate of mass loss in the form of dust may be estimated more directly from the thermal emission of the dust at submillimeter wavelengths than from the 10-μm silicate feature. Sopka et al. (1984) have reported observations of 17 evolved stars, obtained with the United Kingdom (U.K.) infrared telescope on Mauna Kea at an effective wavelength of 400 μm. At this wavelength, the dust is optically thin, and moreover, the dust emission follows the Rayleigh-Jeans law. Consequently, uncertainties in grain temperature are not as serious as at shorter wavelengths. Nine of the objects were detected, and rates of mass loss, varying in amount from about 10^{-7} to 7.6×10^{-6} $M_\odot$/yr, were estimated from the fluxes and are listed in Table 5-2. The greatest potential sources of error are the distance and $\kappa(400\ \mu\text{m})$, the cross section per unit mass of the grains. Although the composition of both carbon and silicate grains is unknown, several lines of evidence (Draine, 1981; Rowan-Robinson and Harris, 1983b; Jura, 1983a) suggest that carbon in the interstellar medium is amorphous rather than crystalline in structure and that the silicates are likely to be amorphous as well. The slopes of the far-IR to submillimeter spectra of both carbon-rich and oxygen-rich stars also support the conclusion that both carbon and silicate grains have amorphous structures. Thus, Sopka et al. (1984) adopt a common value of $\kappa = 20\ \text{cm}^2$ for both carbon-rich and oxygen-rich stars, which is estimated to be accurate to within a factor of 3, and is about an order of magnitude less for crystalline materials. The seventh column of Table 5-2 gives the ratio of mass lost in the form of gas and dust, respectively, which is seen to be consistent with the interstellar value of 100.

It is noteworthy that the largest values of $\dot{M}_d$ are found for the bipolar objects, OH 231.8 + 4.2, CRL 2688, CRL 618, the planetary nebula NGC 7027, and VY CMa, in all of which the flows are highly anisotropic. It might be believed that analysis of such objects based on spherical symmetry might give incorrect results, but Jura's (1983b) calculation of mass loss from oblate ellipsoids shows that the rates are not greatly different from values derived by assuming spherical symmetry.

Millimeter Waves

Since it was first detected a few years ago (Zuckerman et al., 1977, 1978; Lo and Bechis, 1977; Morris et al., 1979; Morris, 1980; see also Rieu, this volume, for an up-to-date review), thermal millimeter-wave radiation in rotational lines of molecules has become an increasingly important tool for studying mass loss from red giants. The CO lines have been most widely used in rate determinations. The 1–0 line has been detected in 50 stars, mostly of types M, S, and C (Knapp and Morris, 1984), and the 2–1 line in 17 of the same objects (Knapp et al., 1982). Such lines are particularly valuable for rate determinations because they are formed far from the star, where the flow is likely to have attained both its terminal velocity and spherical symmetry. One disadvantage is that they appear in emission, and hence the mass of CO in the envelope must be derived from detailed models in which the square of the distance is a free

Table 5-2
Mass-Loss Rates and Expansion Velocities of Selected Red-Giant Stars

Star	Spectral Class	$\dot{M}_g$	V_{exp} (km/s)	$\dot{M}_d$	$\dot{M}_g/\dot{M}_d$	Ref.†
ϱ Per	M4 II–III	0.012	7			2
119 Tau	M2 Ib	0.24	7			2
α Ori	M2 Iab	4	10			3,4,5
6 Gem	M1–M2 Ia–Iab	2.1	8			2
α Sco	M1.5 Iab	5.4	9			2,6
α Her	M5 Ib–II	0.11	8			2,7
δ^2 Lyr	M4 II	0.048	7			2
R Lyr	M4–5 III	0.014	5			2
μ Cep	M2 Ia	1.0	9			2,4
δ Sge	M2 II	0.02	28			8
IRC + 10011	M8	14	24	0.07	200	9,10
o Cet	M6e	0.65	4			9
NML Tau	M	5.1	28			9
S CMi	M7e	6.3	18			1
RS Cnc	M6 Ib–II	0.29	11			9
R LMi	M7e	1.0	6			1
R Leo	M8e	0.092	7			9
RX Boo	M7e	0.38	8			9
NML Cyg	M6 III	1.8	21	0.058	31	1,10
R Cas	M7e	0.66	11			1
R And	S6e	0.37	15			9
W Aql	S	9.8	20			9
χ Cyg	S7e	0.18	8			1
IC 418	PN	5.0	17			1
NGC 6543	PN	5.1	14			1
NGC 7027	PN	110	22	1.3	85	9,10
R Scl	C	31	16			9
IRC + 50096	C	6.3	18			9
CRL 618	C	77	18	0.85	90	9,10
CRL 865	C	23	14			9
IRC + 10216	C9	55	17	0.17	320	9,10
CIT 6	C4	3.0	17			9
IRC − 10236	C	47	10			9
V Hya	$C6_3e$	4.6	18			9
IRC + 20326	C	23	10			9
CRL 2155	C	17	20			9
CRL 2199	C	13	15			9
IRC + 20370	C7	10	9			9
V Cyg	C7e	25	14			1
CRL 2688	C	160	19	2.3	70	9,10
IRC + 40485	C	17	13			1
CRL 3068	C	7.3	14	0.086	85	9
IRC + 40540	C8	24	15			9
OH231.8 + 4.2		130	68	7.6	17	9,10

* $\dot{M}_g$ *and* $\dot{M}_d$ are rates derived for gas and dust, respectively, in units of $10^{-6}\ M_\odot$/yr.
† References: 1. Knapp et al. (1982); 2. Sanner (1976); 3. Bernat et al. (1979); 4. Hagen et al. (1983); 5. Mauron et al. (1984); 6. Hjellming and Newell (1983); 7. Reimers (1977); 8. Reimers and Schröder (1983); 9. Knapp and Morris (1984); 10. Sopka et al. (1984).

parameter; another is the uncertainty in the composition ratio CO/H_2, which may, in some cases, be derived indirectly from observation (see below). Circumstellar chemistry is a new field of research, which is not yet on a firm quantitative basis. (See the review by Glassgold and Huggins in this volume.)

Figure 5-6 shows typical spectra in the region of the CO J = 2–1 line for Betelgeuse and IRC + 10011. As shown by Morris (1975), the profiles of emission lines from unresolved spherical gas clouds expanding at constant velocity are flat-topped, as in Betelgeuse, when the cloud is optically thin, and parabolic, as in IRC + 10011, when the cloud is optically thick. The width of the profile at zero intensity or power is twice the expansion velocity, V_{exp}, whereas the velocity at the center of the line is the systemic, or center-of-mass velocity of the star, V_c. For Betelgeuse, the derived velocities are V_{exp} = 15.3 ± 2.5 km/s and V_c = 18.8 ± 2.5 km/s (Knapp et al., 1980), in good agreement with the optical values V_{exp} = 16.5 and 10.0 km/s (Goldberg et al., 1975; Bernat et al., 1979) and V_c = 21 km/s (Adams, 1956). The expansion velocity derived from the emission profile apparently corresponds to the larger of the two displacements observed in optical absorption spectra of α Ori. The absence of emission from the inner shell can be understood (Knapp et al., 1980) if the shell is much closer to the star than proposed by Bernat et al. (1979), 8 R_* rather than 150 R_*. Moreover, spatial mapping of the millimeter-wave emission from Betelgeuse gives a radius of about 400 R_* for the outer shell, again much smaller than the value of about 2000 R_* found by Bernat et al. (1979). Goldreich (1980) has pointed out that the gas in the circumstellar shell is heated by the drag force between gas and dust and not by the thermal dust temperature. It is therefore incorrect to equate the excitation temperature with the equilibrium temperature of the dust, at least for those objects in which the rate of mass loss and therefore the density are relatively low (Morris, 1980).

Theoretical models of circumstellar envelopes around red giants, in which rates of mass

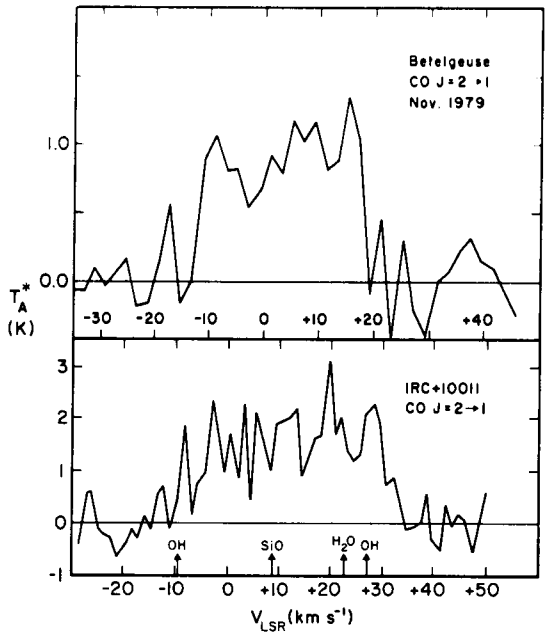


Figure 5-6. Spectra in the region of the CO J = 2–1 line at 230 GHz for α Ori (top) and IRC + 10011. Possible blends with lines of other molecules are indicated (Knapp et al., 1982).

loss and chemical compositions are parameters to be derived from molecular line observations, have been calculated by Goldreich and Scoville (1976) for OH/IR stars, by Kwan and Hill (1977) and Kwan and Linke (1982) for the carbon star, IRC + 10216, and by Morris (1980; see also Morris and Alcock, 1977) for a wide range of stellar parameters. In all of these models, mass loss is assumed to be driven by radiation pressure on dust grains in a spherically symmetric atmosphere. The gas temperature distribution is determined by the balance between heating by collisions with grains and cooling by adiabatic expansion and by the emission of H_2O in O-rich stars and of CO in carbon stars. Because most of the CO emission occurs hundreds of stellar radii from the star, Kwan and Linke (1982) assume constant outflow velocity and use the Sobolev approximation to solve the radiative-transfer problem. The solution contains three free parameters: $\dot{M}$,

the rate of mass loss, Q, the momentum transfer efficiency factor averaged over the continuum energy distribution, and $(CO)/(H_2)$, the abundance ratio carbon monoxide to molecular hydrogen. It is expected that, in the circumstellar envelopes of the cooler late-type stars, hydrogen will be predominantly in molecular form (Knapp and Bowers, 1983). The dust grains are assumed to constitute 1 percent of the mass and to have a density of 1 gm/cc. Since these quantities always enter with Q, their uncertainties are lumped together with the uncertainty in Q, which may be checked by calculating the optical depth of the dust and comparing it with that of infrared observations.

Morris (1980; see also Morris and Alcock, 1977) bases his model on temperature and velocity distributions derived from their dust model by Goldreich and Scoville (1976). For example, the velocity law is:

$$V \approx V_{Term} - 0.37 \times 10^{16}/r \ , \quad (5\text{-}9)$$

for $r > 10^{15}$ cm, equivalent to 20 R_* for Betelgeuse.

Morris solves the coupled equations of radiative transfer and statistical equilibrium to calculate the radial distribution of the populations in the lowest 11 rotational levels of both the first and second vibrational levels of CO. The processes contributing to the level excitations are:

1. The millimeter-wave radiation field, in part from the 3 K background and in part from diffused CO line radiation.

2. The 4.6-μm radiation field exciting the $v = 0$–1 transitions. The central star is assumed to be a blackbody with a temperature of 2000 K and a radius of 5×10^{13} cm, and a parameter, W, is supposed to measure the amplification of the 4.6-μm radiation by the surrounding dust. No account appears to have been taken of the weakening of the stellar radiation field by CO absorption in the photosphere.

3. The levels are also excited by collisions with H_2 molecules, the results being insensitive to the assumed temperature distribution.

Results are presented for the central intensities of the transitions $J = 1$–0, 2–1, and 3–2 as a function of $\dot{M}$ (the mass-loss rate), W (the measure of 4.6-μm luminosity), and f (the fractional abundance of CO relative to H_2), and for the beamwidths of the 11-m National Radio Astronomy Observatory telescope and the 10-m Owens Valley Radio Observatory telescope. For a completely unresolved envelope, the brightness temperature is inversely proportional to the distance squared. Actually, both of the above telescopes can resolve envelopes at distances closer than 1000 parsecs, which means that an increase in distance is partially compensated by an increase in the surface area intercepted by the beam. Therefore, the peak surface brightness falls off less rapidly than as D^{-2}.

The results show that, when the product $f \times \dot{M} < 10^{-9}$, the envelope is optically thin both in the rotational lines and in the 4.6-μm lines. The line profiles are flat for $D > 1$ kpc and become double-peaked as D decreases because the outer parts of the emitting region are no longer within the telescope beam. When $f \times \dot{M} > 2 \times 10^{-9}$, the envelope is optically thick in both rotational and vibrational lines. Increased density causes the excitation to be dominated by collisions with H_2. Finally, when $f \times \dot{M} \sim 10^{-9}$, weak maser emission may occur.

It might be believed that only the product $f \times \dot{M}$ could be derived from comparing model calculations with observations, but that is usually true only in cases in which the levels are excited purely by radiation. Otherwise, the same value of the product $f \times \dot{M}$ may produce profiles of quite different intensity and shape (double-peaked, flat, or parabolic) depending on the relative values of f and $\dot{M}$. The reason is that the value of $\dot{M}$ is a measure of the density, which controls the rate of collisions and

thus the excitation temperature. An increase in excitation temperature increases the size of the observed emitting region and therefore modifies the shape of the profile. Thus, detailed modeling of emission-line profiles can yield both the mass-loss rate and information on the chemical composition.

Another type of modeling, which seeks to combine optical and radio observations, was conceived by Jura and Morris (1981) and applied to the shell of Betelgeuse. The model is derived from observations of the 2–1 line of CO (Knapp et al., 1980) combined with measures of the surface brightness of the shell in the monochromatic radiation 7699 Å of K I at distances of 20 to 60 arc-sec from the star (Honeycutt et al., 1980). At such great distances from the star, the ionization of K is controlled entirely by the interstellar radiation field, although modified by dust extinction, or shielding, in the shell itself, and therefore the uncertainty about the stellar radiation field is avoided. The analysis has recently been repeated by Mauron et al. (1984) using new surface brightness measurements made with a Fabry-Pérot etalon and a charge-coupled device (CCD) camera. The method yields the radial density distribution of potassium and of hydrogen if the solar abundance ratio is assumed. A by-product of the analysis is the abundance ratio carbon/potassium. So far, such optical surface brightness distributions have been measured only for the star Betelgeuse.

In their survey of mass loss from 17 evolved stars, Knapp et al. (1982) avoided detailed modeling by putting the stars into two categories, those with optically thick and optically thin envelopes, respectively, and deriving simple expressions for the mass-loss rate in terms of antenna temperature, T_A^*, expansion velocity, V, and distance, D. The expressions are designed to fit the IRC + 10216 model of Kwan and Hill (1977) and Kwan and Linke (1982) as a prototype for the optically thick envelopes and the α Ori models of Bernat et al. (1979) and Jura and Morris (1981) as typical for optically thin envelopes. The models predict that the ratio of antenna temperatures of the 2–1 and 1–0 lines of CO should be about 3 in optically thick envelopes and several times larger for optically thin shells. According to this criterion, 15 of the 17 shells were shown to be optically thick, the only exceptions being Betelgeuse and Mira.

In their optically thick approximation, Knapp et al. (1982) assume that each source is a sphere of constant surface brightness, the radius being fixed by the gas density at which the CO lines are no longer thermalized. However, Jura (1983b) has shown that the outer optically thin regions of the sources cannot be neglected, since they contribute substantially to the total flux. Allowance for this effect reduces Knapp et al.'s mass-loss rates by a factor of 2 to 3. A further reduction of about 30 percent becomes necessary when the effects of dust shielding and molecular self-shielding are considered (Jura, 1983b). Jura's analysis leads to a less steep dependence of mass loss on distance, $D^{3/2}$, rather than D^2 as found by Knapp et al. (1982).

A new survey by Knapp and Morris (1984) has detected 50 sources in the 1–0 line. The analysis has been carried out with a minimum of simplifying approximations, and the results are probably more reliable than those of Knapp et al. (1982). As before, general expressions for T_A^* were derived for both optically thin and optically thick cases, respectively. For both cases, the antenna temperature is a function of $\dot{M}$, D, f, and r_m, the maximum extent of CO in the envelope. In optically thin objects, T_A^* also depends on the IR flux, W. For most objects, the model profiles are in satisfactory agreement with observations, but a few optically thin shells, including those of o Ceti and α Ori, presented problems that require further study. In view of the many free parameters in the theory, the results must still be regarded with some caution.

Microwave Emission

VLA measurements of radio emission at centimeter wavelengths from the supergiants Betelgeuse (Newell and Hjellming, 1982) and

Antares (Hjellming and Newell, 1983) are consistent with emission of an optically thick thermal radio spectrum emitted by an extended slightly ionized chromosphere extending to several stellar radii. In addition, the observations suggest that the wind from Antares is ionized by the Lyman continuum radiation of the companion B2.5 V star. Figures 5-7a and 5-7b are 4.885-GHz images of the Sco system made with the VLA, showing the unresolved M star on the left and the nebulosity surrounding the B star, the location of which is marked by a cross. Figure 5-7c is a theoretical model of the ionized portion of the Antares stellar wind, which is created by the ultraviolet flux from the B star. The agreement between theory and observation is most convincing and suggests a new method for measuring the rate of mass loss from an M supergiant. Hjellming and Newell (1983) point out that, at the ionization front between the neutral and ionized hydrogen, the number of neutral hydrogen atoms flowing per square centimeter across the ionization front must equal the attenuated Lyman continuum photon flux which ionizes the gas. Thus,

$$N_1 v_1 = L(\text{ly}) \cdot \exp(-\tau_1)/4\pi \cdot r_1^2 \quad , \quad (5\text{-}10)$$

where N_1 and v_1 are the hydrogen density and velocity of the wind at distances of R_1 and r_1 from the M and B stars, respectively; τ_1 is the optical depth for the Lyman radiation between the ionization front and the star, assumed to be unity; and L(ly) is derived from a model of the microwave radio emission from the star. Its value is proportional to the square of the stellar distance and to the $-1/6$ power of the electron temperature. Since the mass-loss rate is:

$$\dot{M} = 4\pi \cdot \varrho_1 \cdot v_1 \cdot R_1^2 \quad , \quad (5\text{-}11)$$

where ϱ is the density, the expansion velocity may be eliminated, and $\dot{M}$ is given by:

$$\dot{M} = (\varrho_1/N_1) \cdot L(\text{ly}) \cdot \exp(-\tau_1) \cdot (R_1/r_1)^2 \quad . \quad (5\text{-}12)$$

Thus, the mass-loss rate may be derived entirely from observed quantities and straightforward application of the theory of H II regions.

Because systems like α Sco are uncommon, Hjellming and Newell's (1983) method will not have wide application. Moreover, only the hottest late-type giants will have winds in which most of the hydrogen is ionized. Thus, the microwave flux from M giants and supergiants will not be useful for the determination of mass-loss rates unless there is an independent means for measuring the fraction of ionized hydrogen. α Ori is known to emit weak microwave radiation (Newell and Hjellming, 1982) from an extended warm chromosphere in which the flow is probably accelerating, but in which the fractional ionization cannot be more than 0.01 to 0.10. The same fraction has been found for α^1 Her (Drake and Linsky, 1984). Spergel et al. (1983) observed 31 evolved red giants with known high rates of mass loss with the VLA at 5 GHz and detected emission from only four stars. Upper limits of about 10^{-3} were derived for the fractional hydrogen ionization. On the other hand, the probable detection of α Boo, also with the VLA at 6 cm (Drake and Linsky, 1984), implies a mass-loss rate of $1 \times 10^{-10} M_\odot$/yr, which indicates that hydrogen in the wind is well ionized.

OH/IR Masers

The subject of red-giant masers has recently been reviewed by Elitzur (1981). Maser radiation at radio frequencies, which is usually found in oxygen-rich giants and supergiants of spectral types later than M5, is emitted by SiO, H_2O, and OH molecules. The SiO radiation is emitted by excited vibrational levels, which are pumped by collisions, and therefore must be located in the lower atmosphere of a star. The OH lines, at 1612, 1665, 1667, and 1720 MHz, originate from the ground vibrational state and

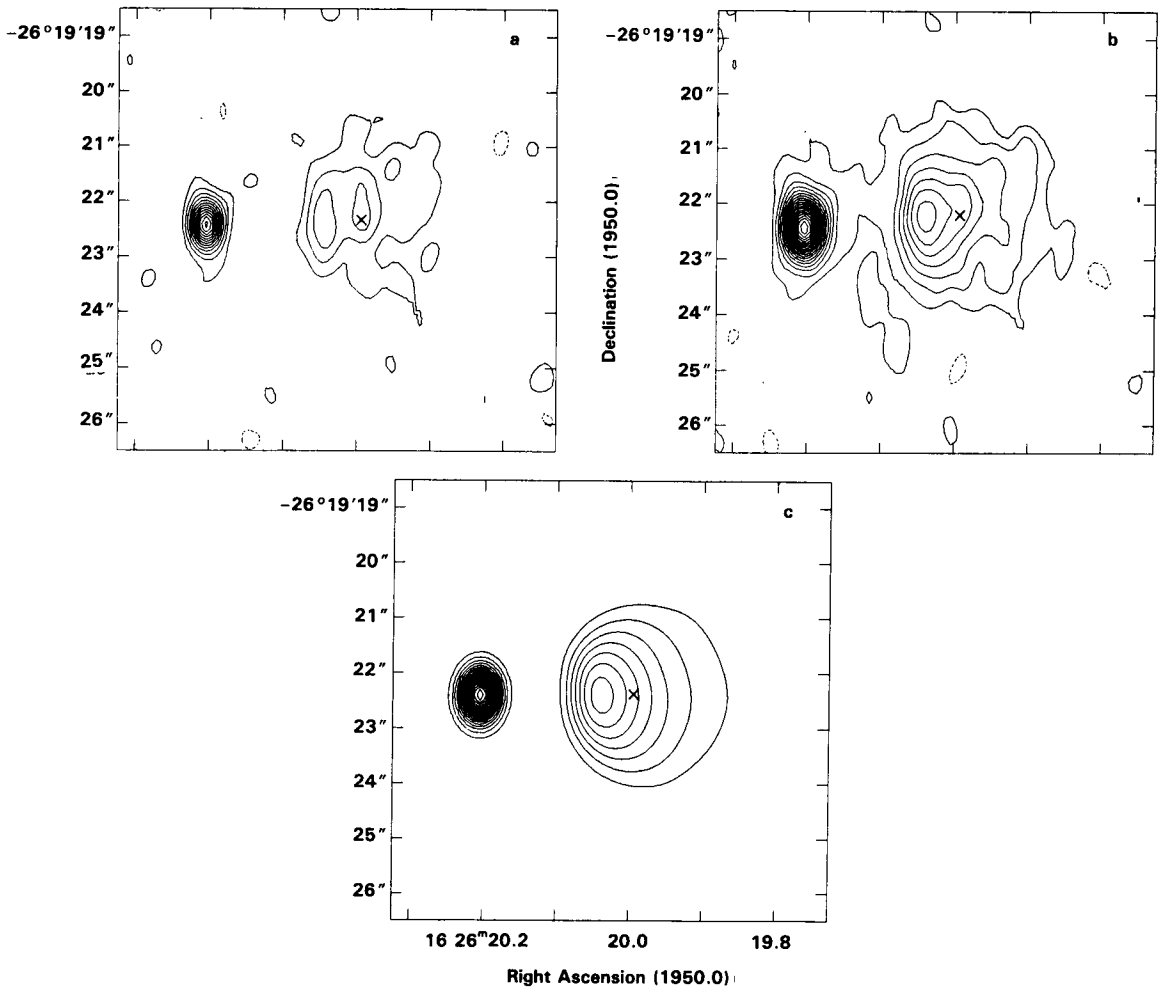


Figure 5-7. Images of the α Sco radio source made with the VLA at 4.885 GHz. The unresolved M star is at the left, and the position of the B star is marked by a cross at the right. (a) and (b) are images constructed with different methods of weighting, and (c) is a theoretical model of an H II region produced in the wind of the M star by UV photons from the B star (Hjellming and Newell, 1983).

are pumped by IR radiation, as evidenced by the variations in phase of IR and OH emission (Harvey et al., 1974). Three of these four lines have been found to emit maser radiation in late-type stars, the so-called main lines at 1665 and 1667 MHz, and the satellite line at 1612 MHz. Those stars with stronger main lines are classified as Type I and those with stronger satellite lines as Type II. We shall be concerned here only with Type II masers because model calculations show that the satellite line is emitted only by stars with very high rates of mass loss. The enormous extent of maser shells has been verified independently by different methods. Thus, Baud (1981) observed, with the VLA, extended OH emission from the source OH 26.5 + 0.6 over a diameter of 4.6×10^{16} cm. Jewell et al. (1980), making use of the phase relation between variations in the OH 1612-MHz emission originating from the front and back of the shell, derived a diameter of $(6.6 \pm 1.4) \times 10^{16}$ cm for the maser shell around IRC + 10011.

Some typical spectra in the region of the 1612-MHz line are shown in Figure 5-8. The

two peaks originate from the approaching and receding halves of the shell, respectively. Hence, the separation of the peaks measures twice the expansion velocity, and the velocity half way between the peaks is the systemic velocity of the star. Mass-loss rates are determined from these observations on the assumption that the mechanism is radiation pressure on dust grains, which is highly likely for stars with such thick dust shells. If radiation pressure on grains is much larger than all other forces, such as gravitation, it can be shown that the equation of motion, when combined with the equation of continuity and the definition of optical depth (Elitzur, 1981), reduces to:

$$\dot{M} = L \cdot \tau_D / Vc \quad , \qquad (5\text{-}13)$$

where L is the mean IR flux, V is the terminal expansion velocity, c is the velocity of light, and τ_D is the effective optical depth of the dust through the shell in response to radiation pressure. Its value is on the order of 2 for dense shells.

A second expression for the mass-loss rate may be obtained by integrating the equation of motion to obtain an expression for the terminal velocity, which, when inserted into the equation of continuity, gives (Salpeter, 1974):

$$\dot{M} = 2\pi \cdot R_o \cdot V \cdot \tau_D / \varkappa_D \cdot f \quad , \qquad (5\text{-}14)$$

where τ_D is the optical depth at a given wavelength, say, 9.7 μm, $\varkappa$ is the mass absorption coefficient at the same wavelength, f is the fraction of the total mass in the form of dust, and R_o is the radius at which dust forms. Forrest et al. (1978) have used both equations to obtain estimates of mass loss from OH26.5 + 0.6. From Equation (5-14), with $\tau > 6$, $\varkappa(9.7\ \mu\text{m}) = 3000$, $R_o/r_* > 3$, and $r_* = 6.5 \times 10^{13}$ cm, $\dot{M} > 1.5 \times 10^{-5} M_\odot$/yr. Similarly, Equation (5-13), with $L = 10^4$, which is appropriate for Miras, $V = 13$ km/s, and $\tau = 3$, gives $\dot{M}$ $> 4.5 \times 10^{-5} M_\odot$/yr. Mass-loss rates calculated for OH/IR stars with Equation (5-13) appear in Table 5-3.

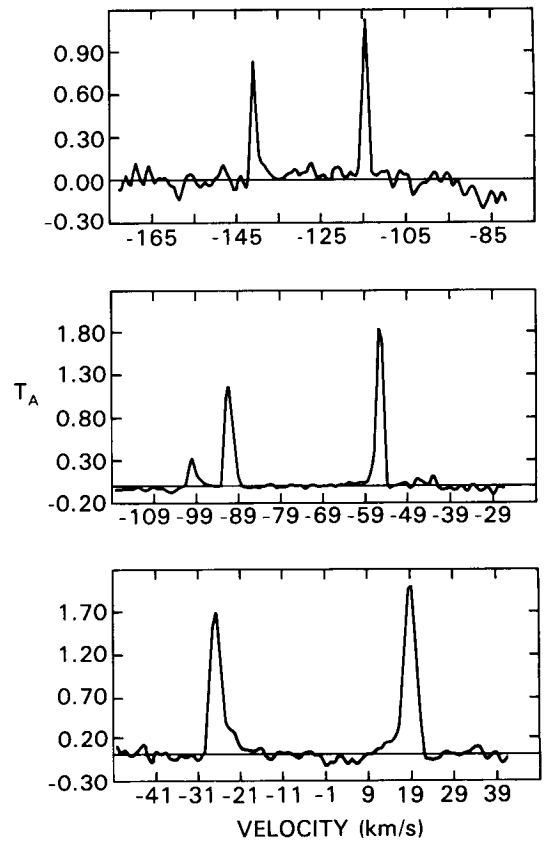


Figure 5-8. Spectra of Type II OH sources at 1612 MHz: Top: OH 1.5–0.0; middle: OH 2.2–1.7; bottom: OH 2.6–0.5. The left and right peaks arise from the approaching and receding halves of the shell, respectively (Baud et al., 1979).

Results

Compilations of mass-loss rates for late-type stars, derived by the methods described above, will be found in Gehrz and Woolf (1971), Reimers (1975a, 1975b), Sanner (1976), Bernat (1977), Hagen (1978), Werner et al. (1980), Knapp et al. (1982), Hagen et al. (1983), Jura (1983b), Baud and Habing (1983), Engels et al. (1983), Sopka et al. (1984), Pottasch (1984),

Table 5-3
Periods, Expansion Velocities, and Mass-Loss Rates of OH/IR Stars Calculated from Equation (5-13)

Star	Period (days)	V_{exp} (km s^{-1})	$\dot{M}$ (10^{-6} $M_\odot$/yr)	Ref.*
R Aql	280	6.5	0.8	1
U Ori	372	4	0.3	1
RR Aql	394	6.5	0.5	1
WX Ser	425	7.5	1	1
OH31.7 − 0.8	510	13	10.9	2
OH26.4 − 1.9	540	12	5.2	2
OH19.2 − 1.0	610	15	24	2
OH28.7 − 0.6	640	18	22.4	2
OH45.5 + 0.1	720	18	4	2,3
OH39.9 + 0.0	770	15	28.7	2
OH30.1 − 0.2	970	18	23	2,3
OH30.7 + 0.4	1140	18	8.1	2
OH26.2 − 0.6	1330	22	33.2	2
OH26.5 + 0.6	1630	14	75	2,3
OH32.8 − 0.3	1750	16	60	2,3

*References: 1. Pottasch (1984); 2. Engels et al. (1983); 3. Werner et al. (1980).

and Knapp and Morris (1984), among others. A useful tabulation of circumstellar line strengths and velocity displacements for 61 red giants is found in Boesgaard and Hagen (1979). Even for such well-studied stars as α Ori, α Sco, and IRC + 10216, published values of the mass-loss rates differ by factors of 10 to 100, and hence, it does not seem useful to present them all in tabular form. In many cases, however, discordant values can be weeded out for known reasons, and the remaining values, although still uncertain by factors of perhaps 2 to 10, serve a useful purpose in setting constraints on mechanisms and evolutionary processes.

Thus, Tables 5-2 and 5-3 are compilations of mass-loss rates of evolved stars selected, because they seemed to be relatively well determined, from among several different classes of stars. Table 5-2 contains expansion velocities and mass-loss rates for early- and late-type M stars, for carbon stars, and for a few S stars and planetary nebulae. Rates for the early M stars have been derived mainly from optical data, and the selection of the best values can be a matter of personal taste. α Ori is a case in point. Jura and Morris (1981) and Mauron et al. (1984) used exactly the same method of analysis, combining data on CO line emission with surface brightness measurements in neutral potassium, but their rates differ by a factor of 4 because the surface brightness distribution of K I emission measured by Mauron et al. (1984) differed considerably from that of Honeycutt

et al. (1980). It should be noted that the abundance ratio K/C found by Jura and Morris (1981) was 25 times larger than the solar value, but Mauron et al. (1984) reduced this discrepancy by a factor of 6. A reduction in the C/H ratio by a factor of 1 to 5 would not be unexpected for processed material. For the later spectral types and the carbon stars, the most reliable rates are probably those from rotational lines of CO. When available, the most recent values of Knapp and Morris (1984) have been adopted. The data show several clear trends:

1. Among the early M stars, rates for the supergiants exceed those for the giants by a factor of 10 or more.

2. Rates for the Miras and planetary nebulae are comparable to those for the early-type supergiants, but the value for NGC 7027 is at the extreme upper end of the range.

3. Knapp et al. (1982) found that the rates for the carbon stars were 25 times larger, on the average, than those for the O-rich stars, but this result is not borne out by the newer analysis of Knapp and Morris (1984), who allowed for the presumably higher CO abundance in C-rich stars and included the effects of excitation by stellar IR on the optically thin objects. Thus, if $f = 3 \times 10^{-4}$ for oxygen Miras and 8×10^{-4} for the carbon stars, the range of rates of mass loss found for the two groups of stars is about the same. The results of the Knapp and Morris (1984) survey are summarized in their Figure 16 in the form of histograms in which the number of stars per pc^3 is plotted against $\dot{M}$.

4. The M and S stars show considerable scatter in their expansion velocities, with values from 4 to 28 km/s, whereas among the carbon stars, v_{exp} is essentially confined between 10 and 20 km/s.

Table 5-3 is a compilation of periods, expansion velocities, and mass-loss rates of OH/IR stars, the rates having been calculated from Equation (5-13). The table contains four OH/IR objects optically identified as Miras, together with 11 unidentified OH/IR stars. The results for the OH/IR stars can be better understood in view of recent studies of these fascinating objects. About 350 OH masers are known (Engels, et al., 1981), of which less than one-third have been identified optically, most as M-type Miras but also M supergiants, semiregular variables, and some very red IRC sources. A recent survey of about 200 OH/IR stars (Engels et al., 1981) revealed that all OH/IR stars are variable, with amplitudes up to two magnitudes in the K band. At least one-half the stars have longer periods than those of Miras or IRC sources, with values up to 1600 days or more. It now seems to be well established (Baud and Habing, 1983; Engels et al., 1983) that the optically identified OH/IR stars and the unidentified sources form a continuous sequence of Mira variables extending from the optical objects with periods up to about 400 days to the unidentified sources with periods up to nearly 2000 days. As seen in Table 5-3, the expansion velocities along this sequence increase on the average from <10 km/s for optical Miras to 22 km/s. From statistical studies of velocity dispersions and galactic concentrations, Baud et al. (1981) found the expansion velocities to be correlated with age and main-sequence mass in the sense that small velocities go with small mass.

Thus, the progression with period is also one with main-sequence mass from about $0.5\,M_\odot$ for the optical Miras to $6.5\,M_\odot$ for the OH/IR sources with the longest periods. The mass-loss rates from unidentified OH/IR stars are also strikingly higher, and the increase occurs rather abruptly at periods over 400 days. There appears to be a threshold period beyond which the rate of mass loss suddenly increases by a factor of 10, and the star becomes enveloped in an opaque dust cloud.

NONSTEADY MASS LOSS

Selected Examples

Evidence is accumulating that, in some stars at least, mass loss may occur sporadically or at a variable rate. The following examples are illustrative rather than complete.

Multiple components of CS lines have been observed in the spectra of a number of red giants and supergiants, chiefly the latter (Sanner, 1976; Bernat, 1981). From a study of CO lines in the 4.6-μm band in nine red giants and supergiants, Bernat (1981) concluded that the multiple components originated in separate mass-loss episodes rather than as intermittent modulations of continuous mass loss, which is favored by Ridgway (1981). The matter is still controversial.

Reimers (1975a, 1975b) noted variability in the K-line profiles of early M giants, stars lying near the transition zone in the HR diagram between stars with low and high rates of mass loss.

Brooke et al. (1974) found evidence for large-scale motions in the atmosphere of α Ori, which appeared to be sporadic in time or position on the stellar surface.

HR 8752 and ϱ Cas, two F Ia supergiants with extensive circumstellar shells containing little dust, have undergone dramatic changes in their atomic and molecular spectra in the 2.3-μm region over a period of years (Lambert et al., 1981). During a 5-year period from 1975 to 1979, P Cygni profiles in HR 8752 were transformed into inverse P Cygni profiles, suggesting the fallback of a shell ejected in 1975. The mass-loss rate derived for ϱ Cas is very large, exceeding $10^{-3}\ M_\odot$/yr, leading Lambert et al. (1981) to propose that it is an outburst connected to a peculiar decrease in brightness observed in 1946/1947.

If the stationary atmospheric layer observed by Hinkle et al. (1982) in χ Cyg and other Miras is the source from which mass escapes, the variations in the thickness of this layer in χ Cygni may be an indication of variable mass loss.

The far-infrared (40 to 250 μm) size of IRC + 10216 (Fazio et al., 1980) suggests more dust at large distances than would be expected for an r^{-2} density distribution. This implies that, about 2000 years ago, the rate of mass loss was twice its present value. Mitchell and Robinson (1980) also derived a relatively shallow density gradient, varying as $r^{-1.3}$. On the other hand, the brightness distribution at 11 μm is consistent with r^{-2} (Sutton et al., 1979). Rowan-Robinson and Harris (1983b) conclude, however, that errors of measurement are too large to rule out the r^{-2} density law.

Optical spectropolarimetry of dust-enshrouded extreme carbon stars reveals that their circumstellar shells are highly organized (Cohen and Schmidt, 1982). In particular, GL 1403 = IRC + 30219 = CIT 6 seems to show a torus of cool dust and hot bipolar lobes, replenished by outbursts occurring after the minima of the 640-day light variation. Particularly striking were the spectral changes in 1977 through 1980 (Cohen, 1980), when the stellar photosphere nearly disappeared and the spectrum consisted of emission lines of H, He, and forbidden lines. Cohen (1980) suggests that these lines were formed when a recent episode of mass loss collided with the existing circumstellar envelope. These and similar objects may represent the evolution of high-mass carbon variables into bipolar nebulae.

VLA observations of extended OH maser emission for the envelope around OH26.5 + 0.6 show large-scale spatial asymmetries and perhaps a ring-like structure seen edge-on, indicating real density variations in the envelope.

Approximately twelve Type II OH/IR sources have been found to have dust shells of high optical depth and to display deep silicate absorption at 10 μm. Werner et al. (1980) have modeled these shells with an $r^{-1.5}$ density law, whereas Rowan-Robinson (1982) has proposed a double-shell model in which a cool star with a spherically symmetric dust shell expanding at constant velocity is surrounded by a second

shell of cold absorbing dust. The second shell is believed to represent an earlier episode of ejection. The mass of the cold dust is estimated as 4 to 15 $M_{\odot}$, which implies that the sources are very massive highly evolved stars.

Near-infrared (1.65 to 4.8 μm) speckle interferometry of IRC + 10216 (Dyck et al., 1984) shows the outer regions of the object to be circularly symmetric on scales >1.6 inch, but at intermediate distances, the brightness distribution is strongly asymmetrical, being more extended north-south than east-west, as found previously by McCarthy et al. (1980). McCarthy et al. also reported variations with time of the apparent envelope size, which have been confirmed by Dyck et al. (1984).

Evidence for Sporadic Mass Loss in α Orionis

α Ori has been relatively well observed for many years, and there is now an impressive amount of evidence for nonsteady ejections of matter at all levels of its highly extended atmosphere and circumstellar shell. At the level of the photosphere, both visible light and radial velocity vary on the average in a period of 5.78 years, apparently arising from pulsation, but these smooth variations are frequently dominated by irregular fluctuations, on a time scale of about 100 days, which often mask the variations associated with the pulsation. (For a summary, see Goldberg (1979, 1984).) Ordered changes in the linear polarization of the visible light have been observed over a number of years (Hayes, 1980, 1981, 1984; Tinbergen et al., 1981). After a lapse of nearly 50 years, systematic monitoring of the photoelectric brightness of the star was resumed in 1979 (Krisciunas, 1982; Guinan, 1983). As shown in Figure 5-9, reproduced from Guinan (1983), the amount of linear polarization and the blue magnitude are at least roughly correlated, which is consistent with asymmetric ejection of matter. Similarly, the absence of a one-to-one correlation between the short-term brightness and velocity variations (Sanford, 1933) makes it apparent that these changes are not global in nature. The wavelength dependence and time variation of the polarization are qualitatively consistent with the growth of a hotspot, or large convection cell, occupying a few percent of the area of the stellar disk (Schwarz and Clarke, 1984; Clarke and Schwarz, 1984).

The brightness distribution of emission from the inner shell of Betelgeuse within 10 stellar radii also shows pronounced asymmetries (Ricort et al., 1981; Goldberg et al., 1981; Roddier and Roddier, 1983) both in Hα light and in the continuum. The asymmetries persist to very large distance scales. Diffraction-limited images of the α Ori dust shell at 10 μm, obtained with the NASA IR telescope on Hawaii (Bloemhof et al., 1984) show a marked asymmetry in the dust distribution, with peak intensity at a distance of 0.9 arc-sec from the star.

The possible association of variability in brightness and radial velocity with mass loss suggests a look at the past behavior of α Ori for evidence of events that may have signaled the ejection of substantial amounts of matter from the photosphere (Goldberg, 1984). Observations of visual brightness and radial velocity for this star have been carried out with varying degrees of regularity and accuracy for well over 60 years, the most accurate and homogeneous set of data having been acquired in 1917 through 1931 (Stebbins, 1931; Sanford, 1933). Although short-term changes in radial velocity and brightness were found to be uncorrelated in detail, Sanford (1933) noted one or two major disturbances in which decreasing velocity was accompanied by increasing light and vice versa.

The best example of such an event took place near the time of minimum radial velocity in the 6-year cycle, at about Julian day 2424500 (December 15, 1925). As shown in Figure 5-10, a large decrease in radial velocity after day 4500 was accompanied by an initial increase in brightness, followed by rapid fading. It is as though gaseous matter were ejected from the star, then diffused outward and condensed into grains which became optically thick at visible

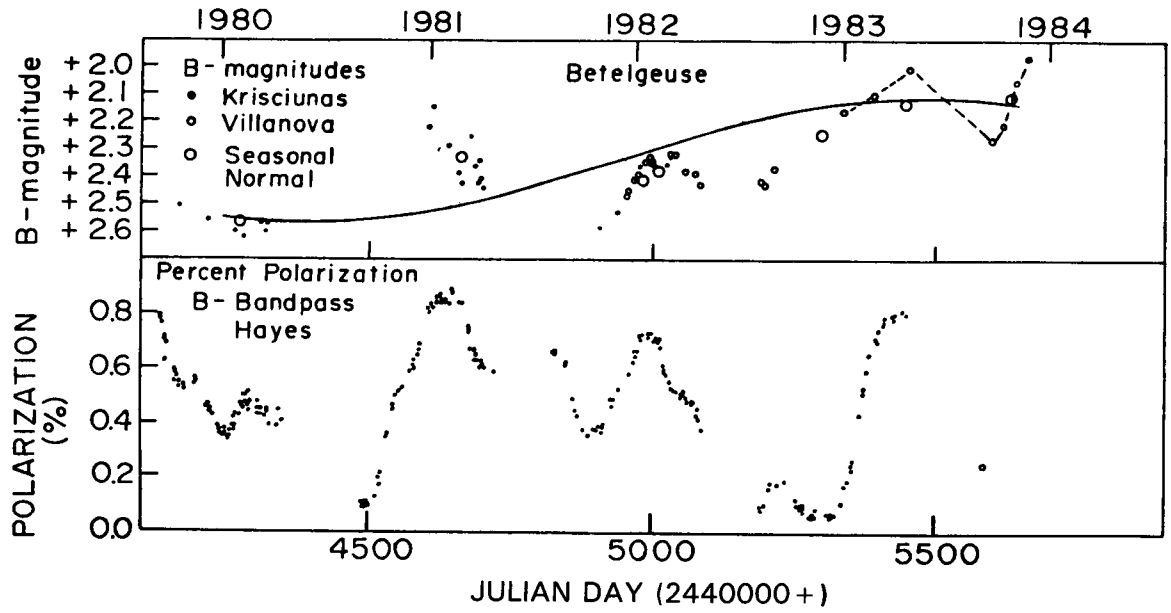


Figure 5-9. B-magnitudes and percent polarization of light from Betelgeuse. Large open circles are seasonal means, and solid curve is Stebbins' (1931) mean blue light curve (Guinan, 1983).

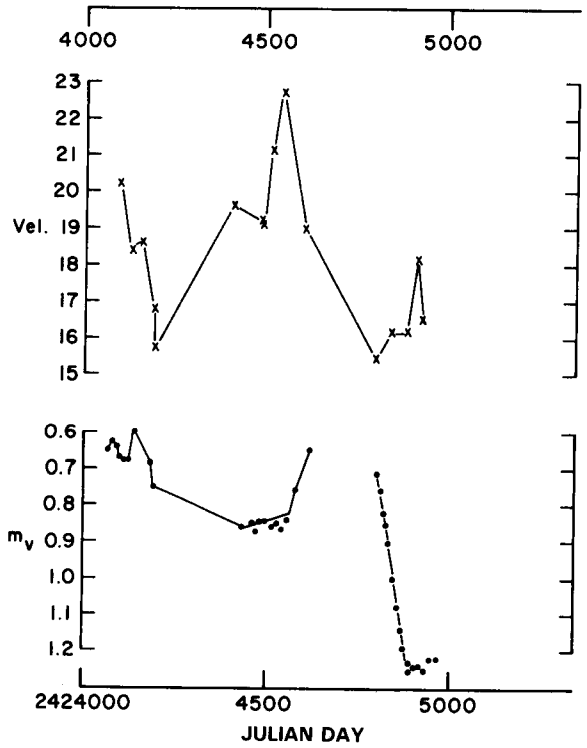


Figure 5-10. Light and velocity variations of α Ori around the time of the unusual event of December 15, 1925, when a period of decreasing radial velocity was followed by a steep decline in visual brightness (Goldberg, 1984).

wavelengths. Similar dust-forming episodes apparently occur during the development of slow novae of the DQ Herculis type (Gehrz et al., 1980) in which the visual extinction is accompanied by strongly enhanced infrared emission. Although photometric measures were not available, the records of the American Association of Variable Star Observers strongly suggest that in November 1944 (Adams, 1956) and again in 1978/1979 (Goldberg, 1979), similar events may have occurred at or soon after the minimum of the mean velocity curve.

At radial velocity minimum, a pulsating star has reached its maximum velocity of expansion and is beginning to decelerate. Given the enormous extension of a supergiant atmosphere, its motion probably lags that of the star, and the atmosphere will tend to continue accelerating outward past the minimum, as has been observed. At this time, instabilities in the atmosphere may trigger mass ejection, followed by the condensation of dust grains. In the future, systematic monitoring of α Ori with a variety of techniques before, during, and after the velocity minimum may clarify the relationship between the short-term brightness and velocity changes and the mass-loss process.

MECHANISMS

Any acceptable theory of mass-loss mechanisms must explain the location of stars showing high rates of mass loss on the HR diagram, as shown schematically in Figure 5-11. Roughly speaking, massive stellar winds, in the range 10^{-8} to 10^{-5} $M_\odot$/yr are found only among the more luminous stars lying in the upper half of the HR diagram. It is tempting to search for a single mechanism that can explain mass loss in both hot and cool stars, but this seems unlikely in view of the probable dependence of mechanisms on the environment. Thus, in the hot stars, the radiative force on atoms is optimized by the occurrence in the same wavelength region of both a strong radiation field and the resonance lines of abundant ions, whereas conditions in the low-temperature stars are favorable for mass ejection by radiation pressure on dust grains. It also does not seem probable that the same mechanism can produce terminal velocities of 10 km/s in the cool stars and 3000 km/s in the hot stars. This section will be devoted to mechanisms that seem appropriate for the late-type giants, and the reader is referred to the monographs on B stars and on O, Of, and Wolf-Rayet stars for an account of hot-star mechanisms.

Figure 5-12, from a compilation by Reimers (1977b), shows the regions in the HR diagram in which late-type stars are found to have massive winds. All G and K supergiants, the later K giants, and all M giants and supergiants show circumstellar spectral lines. The region of the diagram containing stars with circumstellar dust shells is also shown, as are the locations of maser stars and long-period variables. IUE

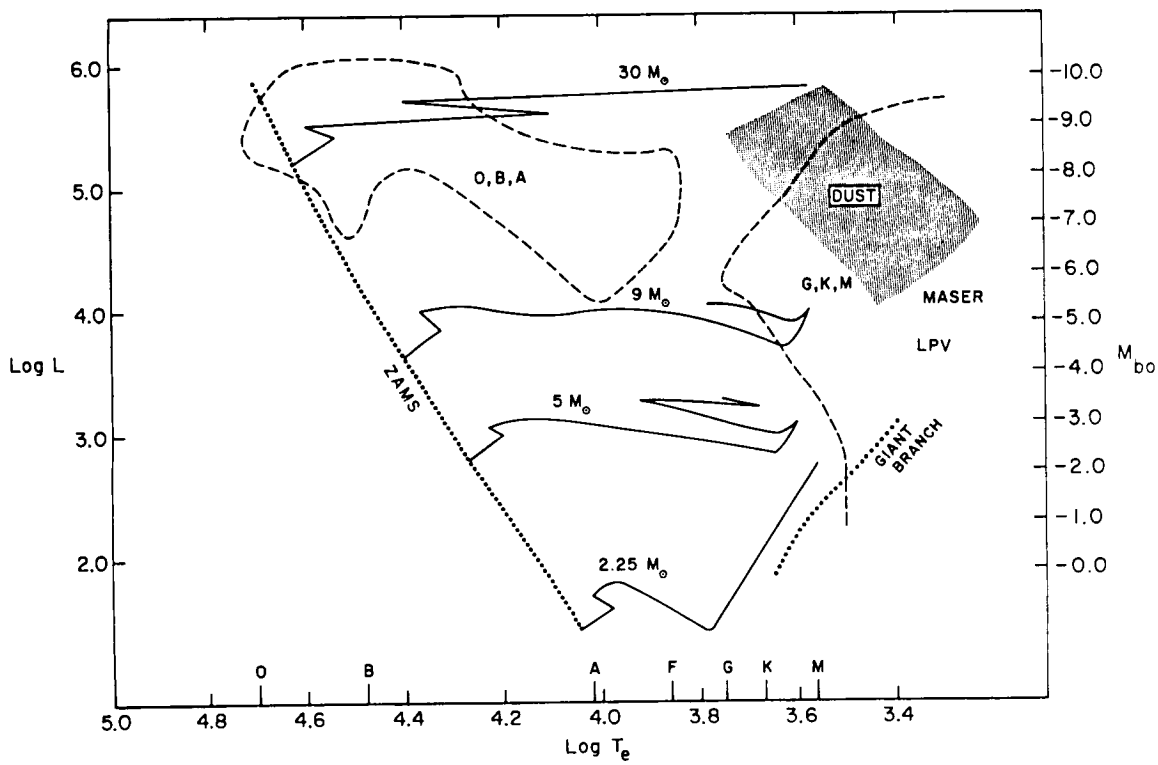


Figure 5-11. HR diagram in which dashed lines outline regions in which stars with high mass loss are found. Also shown are the zero-age main sequence (ZAMS), the giant branch, the locations of masers and long-period variables, evolutionary tracks, and the region occupied by stars showing the 10-μm dust signature (Goldberg, 1979).

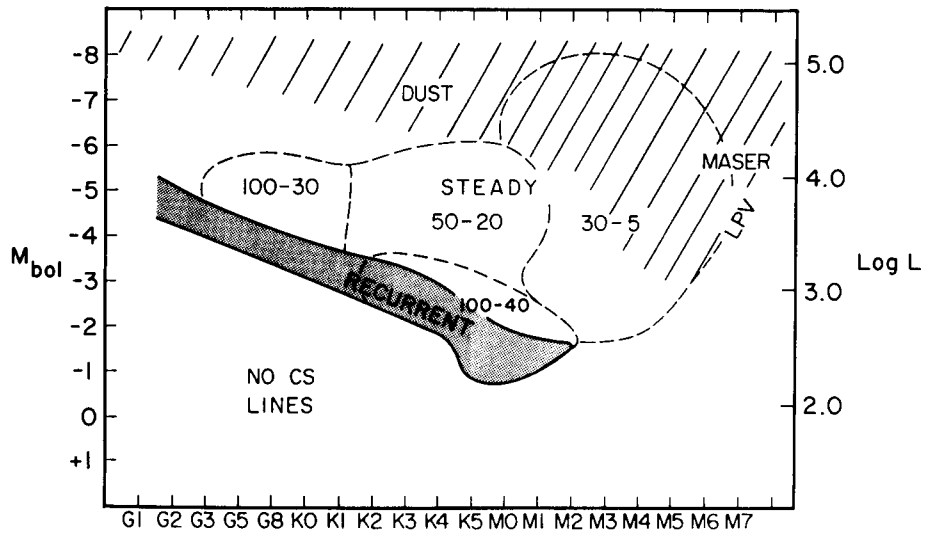


Figure 5-12. Portion of HR diagram for late-type stars, showing regions in which stars have expanding circumstellar shells. Approximate expansion velocities are shown, as well as the transition zone in which winds may be variable (Cassinelli, 1979).

and HEAO observations reveal that all late-type stars have chromospheres, but only stars with low mass loss have transition regions and high-temperature coronae (Linsky and Haisch, 1979; Vaiana et al., 1981). Linsky and Haisch (1979) first used IUE spectra to identify a boundary line in the HR diagram separating stars with coronae from those with only chromospheres.

Stars within the zone sometimes show both high-temperature lines such as C IV 1550 Å and CS lines, and the latter tend to show variability as well.

Similar boundaries, although not always coincident with one another, separate stars in which chromospheric expansion is indicated by the asymmetry of both the Ca II H and K emission (Stencel, 1978) and the Mg II h and k emission (Stencel and Mullan, 1980) and by stars with C IV line emission (Dupree, 1981) and X-ray emission (Vaiana et al., 1981). In reality, the boundary between stars with low and high mass loss is not a sharp line, but a relatively broad zone (Hartmann et al., 1980, 1981). Some stars in the boundary zone are "hybrids," so-called because their spectra show both displaced circumstellar lines and C IV line emission (Hartmann et al., 1980, 1981; Reimers, 1982). The CS lines in hybrid stars tend to show variability as well. On the average, terminal velocities increase from right to left, approaching 100 km/s near the boundary. The degree of sharpness of the boundary is still somewhat controversial (Haisch and Simon, 1982; Simon et al., 1982). The reason for the boundary is undoubtedly connected with evolutionary changes creating conditions favorable for high mass loss, but the nature of the changes is still not clear. On one side of the boundary, nonradiative energy beyond the chromosphere is dissipated into heat, and on the other side, the energy goes mainly into driving massive winds.

Several types of forces have been proposed to account for steady mass loss in red-giant stars, the principal ones being: (1) thermal gas pressure, (2) radiation pressure on dust grains, (3) shock waves, primarily those arising from pulsations in Mira stars, and (4) Alfvén waves. In addition, models of nonsteady or episodic

mass loss have been predicated on dynamical or pulsational instability, on convection, or on magnetic reconnection. Steady mass loss will be considered first.

Thermal Gas Pressure

Parker's original solar wind model has inspired numerous attempts to drive winds in late-type giants by thermal pressure, most recently by Hearn (1975), Mullan (1978), and Watanabe (1981). Basically, these models fail because the thermal energy inferred from the observed low wind temperatures is too low to overcome stellar gravity (Holzer et al., 1983). The observed mass-loss rates can be achieved only by postulating temperatures so high that the radiation emitted would far exceed that observed.

Radiation Pressure on Dust Grains

A complete theory of dust-driven mass loss should include consideration of matters such as grain formation (see Kwok, 1975; Deguchi, 1980; Draine, 1981; Lefèvre et al., 1982; Woodrow and Auman, 1982), the transfer of infrared continuum radiation (Jones and Merrill, 1976; Menietti and Fix, 1978; Rowan-Robinson, 1980), circumstellar shell chemistry (Goldreich and Scoville, 1976; Scalo and Slawsky, 1980; Huggins and Glassgold, 1982; Glassgold and Huggins, 1983 and this volume), and the dynamics of the gas and dust flow (Kwok, 1975; Goldreich and Scoville, 1976; Menietti and Fix, 1978; Tielens, 1983).

Calculations of the motion of gas in a circumstellar shell always assume a spherically symmetric atmosphere with steady flow governed by the equations of conservation of mass and momentum (Kwok, 1975):

$$\frac{d}{dr}(\rho \cdot v \cdot r^2) = 0 \ , \qquad (5\text{-}15)$$

$$\frac{d}{dr}\left(\frac{1}{2}v^2\right) = -\left(\frac{1}{\rho}\right)\left(\frac{dP}{dr}\right) - \frac{GM_*}{r^2}\left[1 - \mathfrak{F}(r)\right] \ , \qquad (5\text{-}16)$$

where v is the flow velocity, ϱ is the density, P is the gas pressure, M_* is the mass of the star, and $\mathfrak{F}(r)$ is the ratio of the radiative force to the gravitational force:

$$\mathfrak{F}(r) = \frac{\left(\dfrac{\pi a^2 \bar{Q} L n_{gr}}{4\pi c r^2}\right)}{\left(\dfrac{GM_* \rho}{r^2}\right)} \ , \qquad (5\text{-}17)$$

where $\bar{Q}$ is the flux weighted mean of the radiation pressure efficiency of the grains, n_{gr} is the number density of the grains, a is the grain radius, and L is the stellar luminosity.

These equations must be solved in conjunction with the equation of motion of the grains:

$$F_{rad} = \left(\frac{4}{3}\pi a^3 \rho_s\right)\frac{dv_{gr}}{dt} + \frac{GM_*(4/3\,\pi a^3 \rho_s}{r^2} + F_{drag} \ , \qquad (5\text{-}18)$$

where v_{gr} is the velocity of the grain, ϱ_s is its density, and F_{drag} is the drag force produced by collisions with gas molecules. It is easy to show that, for grain radii of about 0.1 μm in late-type giants, the gravitational force is much smaller than the radiative force and can therefore be neglected. It has also been found that, for α Ori for example, the terminal velocity is reached by grains in a distance on the order of one solar radius. Therefore,

$$F_{rad} = F_{drag} \ . \qquad (5\text{-}19)$$

F_{drag} is usually approximated by (Kwok, 1975):

$$F_{drag} = \alpha \cdot \pi a^2 \cdot \varrho v_d (v_T^2 + v_d^2)^{1/2} \ , \qquad (5\text{-}20)$$

where ϱ is the gas density, v_d is the drift velocity of the dust grains relative to the gas molecules, v_T is essentially the thermal velocity, and α is an elasticity factor assumed to be equal to 3/4. At this point, additional equations

must be introduced according to whatever assumptions are made about the temperature distribution, the sites of grain formation, the fraction of gas in the form of grains, and their growth and sputtering rates.

The assumptions that are made often depend on the primary goals of the models. Thus, the models of Kwan and Hill (1977), Kwan and Linke (1982), and Morris (1980), which were described in the section *Millimeter Waves*, assumed a priori that the mass loss is driven by dust and were used to calculate molecular line emission, with the rate of mass loss as an adjustable parameter to be determined from observation. In this section, we shall be concerned with models whose purpose it is to test various aspects of the dust-driven mechanism.

Following the approximate analytical expressions derived by Gehrz and Woolf (1971), Kwok (1975) made the first numerical solutions of the equations of motion, taking account of radiation pressure on grains, stellar gravity, growth and sputtering of grains, and momentum transfer from grain to gas. Kwok believed that radiative heating and cooling could be neglected and assumed the adiabatic law for the temperature variation. In their investigation of the physical properties of OH/IR stars, Goldreich and Scoville (1976) showed that collisions between gas molecules and dust grains are a significant source of heating and that the gas is cooled both by adiabatic expansion and by H_2O molecular emission. The resulting temperature distribution is markedly different from the adiabatic law. Goldreich and Scoville also considered the chemical reactions that control the abundances of OH and H_2O.

Menietti and Fix (1978) solved the equation of motion of the gas in cool luminous stars, taking account of the radiative properties of both the gas and the dust. The density, temperature, and radiative energy distributions were not assumed in advance, but were derived from the modeling process. Similarly, Rowan-Robinson (1980) has developed accurate solutions to the equation of radiative transfer for the purpose of predicting the radiative energy distributions of stars throughout the wavelength region 0.4 to 30 μm. The model consists of a blackbody of given radius and temperature at the center of a spherically symmetric dust shell. The free parameters of the model are the temperature of the central star, the condensation temperature of the grains, which is also the temperature of the inner boundary of the shell, the limiting optical depth at short wavelengths through the shell, the density gradient in the shell, the ratio of the inner and outer radii of the shell, and the interstellar extinction. The parameters are determined by fitting model calculations to the observed spectra. Models have been derived and applied to the observed spectra of 156 late-type stars, including early M stars (Rowan-Robinson and Harris, 1982), stars of type M5 and later (Rowan-Robinson and Harris, 1983a), carbon stars (Rowan-Robinson and Harris, 1983b), and OH/IR stars showing double shells (Rowan-Robinson, 1982).

The model by Deguchi (1980), of the flow in O-rich stars, focuses mainly on the process of grain formation. The theory of grain nucleation is used to calculate the number density of grains, the grain sizes, and the final amount of metals remaining in gaseous form. Woodrow and Auman (1982) construct time-dependent models of carbon-rich red giants, making use of the equations of hydrodynamics, the theory of grain nucleation and growth, and the equations describing a gray model atmosphere in LTE and radiative equilibrium.

The most recent model of dust-driven gas flow in O-rich Mira stars (Tielens, 1983) is also the most detailed and complete. The starting point of the model is the observational evidence (Hinkle, et al., 1982) that the outward motion of the pulsating photospheres of Miras generates shock waves that elevate matter to a stationary layer about 5 stellar radii above the photosphere, where the temperature is less than 1000 degrees and therefore low enough to permit dust grains to condense. The stationary layer is, in effect, a reservoir for the matter in the wind.

Some general conclusions can be drawn from these modeling investigations. Circumstellar gas shells in late-type giants and

supergiants are heated by stellar radiation and by grain/gas collisions. At least in the late-M Miras and supergiants, the gas is heated by the drag force and cooled by H_2O emission and adiabatic expansion (Goldreich and Scoville, 1976). The velocity gradient also plays an important part in the determination of the temperature structure (Tielens, 1983). When the density is high enough, photon trapping can slow radiative cooling in the absence of a velocity gradient. Thus, the temperature structure of the gas is coupled to the dynamics of the outflow.

Observed radiative energy distributions are consistent with an r^{-2} law for the density distribution (Rowan-Robinson and Harris, 1982, 1983a, 1983b). However, detailed modeling of the flow (Menietti and Fix, 1978; Tielens, 1983) shows that the density falls off much more rapidly than as r^{-2} until after the sonic point is reached. Correspondingly, in Tielens' model, the velocities increase rapidly from the stationary layer, at distance r_i, to a terminal value at about 10 r_i. An example given by Tielens (1983) shows that, if the mass-loss rate is calculated from the total mass column density by Equation (5-3) on the assumption that the velocity is constant, the rate will be overestimated by a factor of 3 to 4.

The model calculations also demonstrate that it is difficult to produce 10-μm excesses in O-rich stars with clean silicates (Jones and Merrill, 1976; Menietti and Fix, 1978; Rowan-Robinson and Harris, 1982, 1983a). In the carbon stars, amorphous carbon grains with absorption efficiency proportional to frequency give better agreement between observed and calculated energy distributions than does graphite (Rowan-Robinson and Harris, 1983b). Empirical values of the optical depth of the silicate feature at 10 μm, derived from comparison of model calculations with observation, are strongly model-dependent. For example, the values derived by Rowan-Robinson and Harris (1982, 1983a) are smaller than those of Hagen (1978), in some cases by a factor of 20 and in others by a factor of about 200. Differences in assumed grain parameters can account for a factor of 20, whereas another factor of 10 may occur in stars for which the use of an optically thin model (Hagen, 1978) may not have been justified. Until these disagreements can be resolved, it is premature to draw conclusions from dust column densities inferred from the 10-μm optical depth (Hagen, 1978; Hagen et al., 1983; Bernat, 1981).

The fraction of metals remaining in the gaseous state varies with the mass-loss rate (Deguchi, 1980) from 1 to 10 percent for $\dot{M} = 10^{-5} M_\odot$/yr, and <1 percent for $\dot{M} < 3 \times 10^{-6} M_\odot$/yr. Owing to the large drift velocity of the grains relative to the gas, the dust-to-gas ratio is not a constant with distance (Tielens, 1983). This is important in the estimation of mass-loss rates from the 10-μm feature.

We come finally to the most important question. Does radiation pressure on dust grains drive the observed mass flows in late-type giants and supergiants? The most important parameters on which the success of the mechanism depends (Kwok, 1975; Menietti and Fix, 1978) are the stellar luminosity, L, the mass, M_*, which together determine the distance of the sonic point, the effective temperature, T_{eff}, and the most critical factor, the density of gas at the condensation point, ϱ_c, which must be large enough both to ensure momentum coupling and to hold down the sputtering rate by keeping the drift velocity low. The condensation-point gas density is a function of both effective temperature, T_{eff}, which controls the distance of the condensation point from the star, and the scale height, which depends on the stellar mass, or luminosity, L. Kwok (1975) has calculated the minimum density at the condensation point required for mass ejection from stars of various luminosities and effective temperatures, and has shown that the more luminous the star, the lower the temperature at which mass loss is possible. Figure 5-13 is a plot of log L versus T_{max}, the maximum effective temperature for which dust-driven mass loss can occur. Also plotted are the positions in the diagram of four red supergiants, α Ori, α Sco,

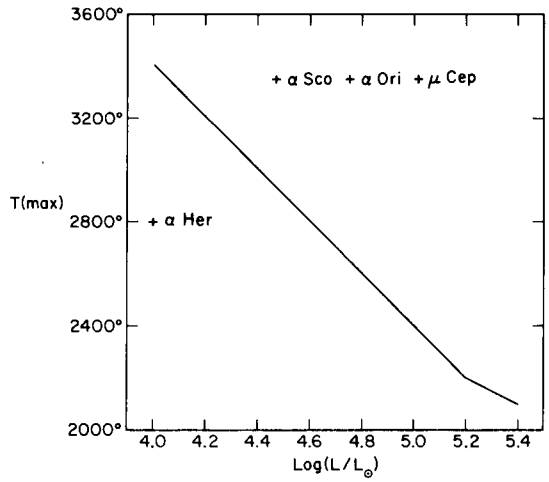


Figure 5-13. The maximum effective temperature at which dust-driven mass loss would be expected to occur, as a function of stellar luminosity according to model calculations by Kwok (1975). The positions of the four supergiants, α Ori, α Sco, α Her, and μ Cep, are indicated by crosses.

α Her, and μ Cep. Only for α Her is the temperature low enough to allow condensation at high enough gas densities. These calculations are not necessarily fatal to the dust-driven hypothesis for the hotter stars (Draine, 1981). For example, the gas density may be increased by clumping or by the ejection of discrete clouds, and "clean" grains can form relatively close to the star and gather up impurities as they move away. Note also that in α Ori, and probably in other red giants as well, the photosphere is greatly distended, its scale height being on the order of a stellar radius (Balega et al., 1982). Calculations based on plane-parallel model atmospheres give erroneously high temperatures for spherically extended atmospheres (Schmid-Burgk and Scholz, 1981). It remains to be investigated whether the temperatures are lowered sufficiently in the higher density regions to allow grain formation.

An empirical test of the dust mechanism can be made by comparing observed rates of mass loss with rates estimated on the assumption that the total energy radiated by grains in the infrared equals the energy absorbed in imparting momentum to the grains (Knapp et al., 1982). The rate of grain-driven mass loss is related to the infrared flux at the Earth by

$$M V_0/D^2 = \beta F/c , \qquad (5\text{-}21)$$

where β is a factor measuring the amount of dust in the envelope, D is the distance to the star, V_0 is the terminal velocity, and F is the bolometric flux measured at the Earth, derived by integrating the continuum spectrum inferred from published IR fluxes. On the premise that the dust mechanism works for the oxygen stars, Knapp et al. (1982) calculate β from Equation (5-21) and find it to be correlated with the color (3.5 μm) - (11 μm), which is known to measure the dust content of circumstellar envelopes. The correlation may be the best evidence to date that the dust mechanism is responsible for mass loss in the cooler O-rich stars. It is still not clear whether or not the dust mechanism is adequate to drive the mass loss in the carbon stars or whether some additional mechanism needs to be invoked.

Shock Waves

The conclusion from both theoretical and observational considerations is that radiation pressure on dust grains can drive mass loss at the observed rates in late M and S giants and supergiants, but that some additional force or forces are needed in the early M-types and especially in the carbon stars. In addition to radiation pressure on grains and thermal pressure, wave pressure has received considerable attention as an important source of momentum and energy in late-type stars, either from shock waves generated by pulsation in Mira stars (Willson and Hill, 1979; Willson, 1981; Wood, 1979, 1981) or from Alfvén waves (Hartmann and McGregor, 1980, 1982; Hartmann and Averett, 1984). Calculations of the dynamic response of model Mira atmospheres to a series of periodic shocks driven by an oscillating piston have shown that high rates of mass loss are possible in such models. Two extreme

cases have been studied. Both Willson and Hill (1979) and Wood (1979) found that isothermal shock models showed very low rates of mass loss, about $10^{-12}\ M_\odot$/yr, whereas in the adiabatic limit, the shocks give unrealistically high rates, about $10^{-2}\ M_\odot$/yr, and unacceptably large values of the terminal velocity. Thus, the critical point in the theory is whether the shocks generated by pulsation are isothermal or adiabatic. Some compromises are possible:

1. Periodic isothermal shocks can levitate the atmosphere and thereby increase grain-driven mass loss by a factor of about 40, according to Wood (1979). Another estimate by Jones et al. (1981) is that the increase in atmospheric scale height by pulsation can enhance the rate of grain-driven mass loss by several orders of magnitude.

2. In the lower atmosphere, where the emission lines originate, the shocks may be isothermal, but higher up, as the density falls, the rates of cooling diminish and the shocks may become adiabatic (Willson and Hill, 1979).

Alfvén Waves

Hartmann and McGregor (1980, 1982) have studied the response of model atmospheres of red giants and supergiants to the passage of Alfvén waves of about solar magnitude, with stellar gravity as the main parameter. They conclude that the force due to Alfvén waves can account for observed mass-loss rates and terminal velocities, provided that the waves are dissipated over a distance of the order of a stellar radius by damping arising from collisions between ions and neutral atoms. The theory is an attractive one, both because a single parameter—stellar gravity—controls the rate of mass loss and because it predicts that red giants have extended warm chromospheres as observed. However, a detailed study of Alfvén waves in stellar atmospheres (Holzer et al., 1983) concludes that cool winds driven by Alfvén waves will not exhibit both high mass loss and low terminal velocity. The basic problem with this and other stellar wind mechanisms, as Holzer et al. (1983) point out, is that energy inserted into the flow in the subsonic region increases the mass flux but not the velocity, whereas in the supersonic region, the addition of energy increases the terminal speed without affecting the mass loss. Thus, the mechanism must be such that a large fraction of the energy is dissipated in the subsonic flow region, with just the right small amount left over for the supersonic flow to overcome gravity and yet limit the terminal velocity to the observed fraction of the velocity of escape from the photosphere.

Recently, Hartmann and Averett (1984) have applied the theory to construct a model of the extended chromosphere of α Ori. Assuming that a wind of about $10^{-6}\ M_\odot$/yr is driven by dissipating Alfvén waves, they reproduce the observed free-free emission at radio wavelengths, the Hα emission observed by speckle interferometry, and the emission fluxes in a number of spectral lines. However, the model fails to reproduce the observed shapes of chromospheric line profiles, which suggests that, although the waves can heat and extend the chromosphere, the observed chromospheric expansion velocities are three times smaller than those predicted by the model. Hartmann and Averett (1984) suggest two possible ways out of this problem. Either the waves simply distend the atmosphere so that the gas density at the grain condensation point is high enough to maintain dust-driven mass loss, or spatial and temporal time variability in wave generation and damping may lead to composite emission from low- and high-velocity ejections.

If massive winds in late-type stars are driven by Alfvén waves, the stars should have extended chromospheres, which emit microwave radiation at centimeter wavelengths. Such radiation has been detected from several K and early M giants and supergiants (Drake and Linsky, 1984), but its weakness or absence in 31

evolved red giants surveyed by Spergel et al. (1983) argues against the effectiveness of the Alfvén-wave mechanism in the late M stars.

Mechanisms for Nonsteady Mass Loss

A number of mechanisms have been proposed for sporadic or nonsteady mass loss in red giants. Schwarzschild (1975) suggested that large-scale convection might trigger the ejection of a massive cloud by some process as yet unknown. Such ejections might cause both the irregular brightness variations observed in cool variable stars and the observed ordered changes in the linear polarization. Bloemhof et al. (1984) suggest that such localized and temporary phenomena are consistent with the observed asymmetric distribution of dust around α Ori. Wood (1979) has proposed that isothermal shock waves in the atmosphere of a Mira star generate mass loss by levitating the atmosphere to heights at which grains condense. Jones et al. (1981) have shown that the mass-loss rate may be enhanced by several orders of magnitude, as compared with grain-driven mass loss alone. We have already referred to the evidence that such a process may be at work in χ Cygni and in other Miras as well (Hinkle et al., 1982). In stars like α Ori, matter might be transported to the dust layer by shock waves associated with the irregular fluctuations in brightness, as suggested, for example, by Schwarzschild (1975) and by Kafatos and Michalitsianos (1979).

The region in α Ori between the photosphere and the base of the shell, which we tentatively identify as the chromosphere, may be the source of the Fe II emission lines observed by Boesgaard and Magnan (1975) and Boesgaard (1979) near 3100 Å, by van der Hucht et al. (1979) in the 2750 to 3165 Å region, and by Carpenter (1984) in the 2300 to 3000 Å region. Measurements of these lines have given conflicting results. Boesgaard and Magnan found that the motions derived from the Fe II lines were closely coupled to the photospheric motions, but indicated matter falling into the photosphere at an average speed of about 5 km/s. Conversely, van der Hucht et al.'s measurements from a balloon showed an average blue-shift of 14 km/s relative to the photosphere. From high-resolution IUE spectra, Carpenter (1984) found no evidence of strong coupling between photosphere and chromosphere and no systematic difference between the mean velocities of the photosphere and chromosphere. He interpreted the relation between line asymmetry and line strength as evidence for a schematic velocity field that is initially constant with height and then increases outward to a maximum value before decreasing to an asymptotic value. These apparently contradictory results might be resolved if the velocity fields varied with time, which might be expected if the Fe II emission is responsive to fluctuations in photospheric activity. On the other hand, Carpenter's data are more complete and of higher quality than those obtained from the ground and with balloons. Continued monitoring from IUE would be very important in resolving this question.

Burke (1972) suggested that rising shock waves ejecting matter would be expected whenever there is pulsation or a strong convection zone near the surface of a star. The mass would be ejected preferentially from the equator in the direction of rotation and would lead to loss of angular momentum without the need for magnetic fields. Kafatos and Michalitsianos (1979) have applied this mechanism to the determination of the rate of spin-down of red supergiants. The ejection of matter is predicted to form a disk or torus of silicate grains in the equatorial regions.

Mass loss is also predicted to occur from dynamically and pulsationally unstable envelopes of red-giant stars (Tuchman et al., 1978, 1979, and earlier references therein). According to Tuchman et al. (1978), dynamical instability sets in when, owing to partial ionization and/or partial dissociation, the quantity, γ, the adiabatic value of the logarithmic pressure gradient, falls below 4/3 over a sufficiently large and/or deep region. An initial expansion turns into violent oscillations in the envelope. Shocks

generated within the envelope lead to repetitive episodes of mass loss on a time scale of < 30 years, which would cause large amounts of mass to be lost during evolutionary time scales. Newer calculations by Fox and Wood (1982) show that the apparent instabilities are caused by the neglect of nonadiabatic effects in the models.

Magnetic Reconnection

A few years ago, Mullan (1978) suggested that the boundary in the HR diagram between stars with high and low mass loss is a supersonic transition locus (STL), along which the sonic points of the wind dip below the heights reached by the tops of spicules. Holzer (1980) and others have shown the STL hypothesis to be untenable, and Mullan (1982) has proposed instead that the boundary is caused by a transition in magnetic topology. (See also Mullan and Ahmad, 1982; Mullan and Steinolfson, 1983). The idea is that, since X-ray emission in the Sun is associated with closed magnetic loops and the solar wind is enhanced over coronal holes where the field is mainly open, massive winds and the absence of X rays may result when stars are unable to maintain closed magnetic field lines in the steady state. With the aid of Pneuman's (1968) model of helmet streamers, Mullan (1982) investigates the question of where in the HR diagram the transition from closed to open field configurations might occur. Pneuman (1968) found that helmet streamers would be unstable and would not exist in a steady state when the parameter,

$$\Psi = \mu \cdot G \cdot M_* \cdot m_p / R_* kT \quad , \qquad (5\text{-}22)$$

is smaller than 4. In Equation (5-22), μ is the mean molecular weight, m_p is the proton mass, M_* and R_* are the mass and radius of the star, respectively, and T is the temperature at the sonic point. Since the radius, R_s, of the sonic point is $\mu G M_* m_p / 2\ kT$, the condition that long-lived closed lines can exist is $R_s > 2\ R_*$. The locus $R_s = 2\ R_*$ on the HR diagram defines a so-called magnetic topology transition locus (MTTL) which happens to closely follow the boundary between stars with weak and strong mass loss. Once it is accepted that the onset of massive winds in red giants is associated with open field lines, the Alfvén-wave mechanism may be invoked to drive the wind. Alternatively, Mullan (1981) has speculated that after unstable emerging loops are ejected from the surface, field-line reconnection at the base of the loops furnishes the energy for accelerating them upward.

EVOLUTIONARY CONSEQUENCES OF MASS LOSS

Supernovae

The evolutionary effects of mass loss on red giants have been well reviewed, for example, by Iben (1981b) and Renzini (1981a, 1981b). The most convincing evidence comes from supernovae. In the absence of mass loss, all stars with initial masses less than 1.44 $M_\odot$ would become white dwarfs, whereas all those with larger masses would explode as supernovae of either Type I or Type II, depending on the mass. It is estimated that, without mass loss, the frequency of supernovae in a galaxy would be one per year, which is about 10 times greater than observed. Observed rates of mass loss allow one to predict that stars with initial masses as large as 5 to 8 $M_\odot$ can end up as white dwarfs. The predicted frequency of supernovae is reduced to about the observed level.

Stars in Globular Clusters

A second theoretical argument for mass loss in red giants is morphological and is based on the observed distribution of stars on the giant and horizontal branches of Population II globular clusters. Evolutionary calculations without mass loss give perfect fits to the main-sequence and red-giant branches of the HR diagram, but the tip of the asymptotic giant branch (AGB) is about 2.5 mag too bright and the horizontal branch (HB) is too short: blue

stars and RR Lyrae stars are absent. Stars embarking on the red-giant branch (RGB) are estimated to have initial masses of 0.8 to 0.9 $M_\odot$. The HB discrepancy may be removed if stars lose 0.2 $M_\odot$ solar masses during the RGB phase before helium flash, whereas the AGB problem is resolved if an additional 0.1 $M_\odot$ is lost during the AGB phase. The computed HB tracks are still too short, unless it is assumed that stars arriving at the HB have a spread in their masses of about 10 percent.

Evolutionary calculations incorporating mass loss as given by the revised Reimers formula, Equation (5-4), reproduce the observed morphology of the RGB, HB, and AGB in Population II globular clusters. It is claimed further that such morphological considerations put narrow constraints of about 10 percent on the correct values of mass-loss rates themselves. Judgment on this point must be reserved until more is known about the interior physics of stars (e.g., convection, neutrino physics, turbulent diffusion, primordial chemical composition, and meridional mixing).

Composition of Interstellar Matter

The theory of stellar evolution also predicts that red supergiants may be the most important source of interstellar grains, both from mass loss and from supernova explosions. Variations in the surface composition during the AGB phase should affect grain characteristics in the winds. At the beginning of the AGB phase, the star is type M with C/O <1, and consequently, silicate grains can form in the wind. Later, the star becomes a carbon star with C/O >1; after the third dredge-up (Iben, 1981a), O is locked up in CO, but there is an abundance of free carbon and C-rich molecules. Hence, grains in the winds will contain not silicates but ample quantities of C-rich particles such as amorphous carbon grains, graphite, and SiC grains.

Formation of Planetary Nebulae

The formation of planetary nebulae is one of the most spectacular consequences of mass loss from red giants, and in fact, observations of planetary nebulae are providing critical tests of the entire theory of the late stages of stellar evolution, in which mass loss plays a critical role. It is generally accepted that planetary nebulae are produced by asymptotic branch stars, which eject their hydrogen-rich envelopes, after which the stellar remnant evolves to a high temperature and radiates the far-UV photons needed to excite the envelope. By what mass-loss process is the envelope ejected and at what rate? Assuming with Renzini (1981b) that a typical planetary nebula has a mass of 0.2 $M_\odot$, a radius of 0.1 pc, and an expansion velocity of 20 km/s, we find that the nebula must form in about 5000 years, which requires a mass-loss rate of about 4×10^{-5} $M_\odot$/yr. Since this rate is an order of magnitude greater than that given by the Reimers formula when applied near the top of the AGB, Renzini postulated the more or less sudden onset of a "superwind" that would turn on at the end of the AGB phase and operate for a relatively short time.

Such a superwind could take one of several forms. It could occur when Mira variables switch oscillation modes from the first overtone to the fundamental (Wood, 1974, 1981; Tuchman et al., 1979; Fox and Wood, 1982) or by the onset of pulsation in Miras, which Willson (1981) believes is normally in the fundamental mode. It was once believed that the formation of planetary nebulae might be caused by dynamical instability, but detailed calculations (Tuchman et al., 1978) have shown that the relevant models should stabilize while the envelope mass is still too large ($>0.1\ M_\odot$). The mode-switching mechanism leads to a relatively sudden ejection of the stellar envelope in less than 1000 years (Tuchman et al., 1979). A different scenario which does not require sudden ejection has been proposed by Kwok et al. (1978) and has been elaborated by Kwok (1982). The steady mass loss eventually depletes the H-rich envelope, exposing the hot core and causing a sudden change in the mass-loss mechanism to one of radiation pressure on ions. The velocity of the wind increases by a factor of 100, and the snowplow effect builds up a dense

shell at the interface between the new and the old wind. In this model, the planetary nebula forms in about 3000 years. The distinction between steady and sudden ejection seems artificial, inasmuch as both mechanisms require a sudden increase in mass-loss rate, and the difference in time scales is well within the uncertainties of the calculations. Moreover, interaction is bound to occur between the old circumstellar shell and the new wind, no matter which mechanism is operative.

Recent observations of unidentified OH/IR stars (Baud et al., 1981; Engels et al., 1983) are providing considerable evidence in favor of Mira variables as progenitors of planetary nebulae, as was suggested by Wood and Cahn (1977). As stars evolve up the AGB, they lose mass steadily, and at some value of the luminosity, which depends on the mass, they begin pulsating as Mira variables in the first-overtone mode. As the luminosity increases, so do the radius and the period. Eventually, for a given stellar mass, a star reaches a value of the luminosity at which the fundamental mode becomes dominant, the envelope is ejected, and the planetary nebula forms in a matter of a few thousand years. The evolutionary model of Wood and Cahn (1977) was developed in considerable detail by Tuchman et al. (1979), but encountered several disagreements with observation, the most serious being the termination of first-overtone pulsation at much lower luminosities and shorter periods than observed, and the occurrence of dynamical instabilities at the point at which the fundamental mode takes over, which limits the observed periods to less than 600 days. It now appears that the instabilities do not in fact occur (Fox and Wood, 1982) and hence that pulsations with periods longer than 2000 days are stable.

From a study of the statistical properties of about 20 OH/IR stars, Baud and Habing (1983) were able to investigate the physical parameters that determine the OH luminosity. The OH luminosity is correlated with the size of the circumstellar shell and with the mass-loss rate. They make the basic assumption that the sequence of OH/IR stars arranged in order of increasing period and mass-loss rate (see Table 5-3) is an evolutionary sequence, and they derive a timescale of between 0.6×10^5 and 6.5×10^5 years for main-sequence masses between 0.7 to 6 $M_\odot$ for the OH maser lifetime. Of this time, 99 percent is spent as a visible Mira with low mass loss, and 1 percent is spent as a luminous OH/IR star. Comparison of the derived physical parameters of the stars with the models of Fox and Wood (1982) suggests that the OH maser turns on at about the time that the pulsation mode switches from first overtone to fundamental. The models also predict that the longest periods go with the highest mass-loss rates, as found by Engels (1982). Engels et al. (1983) also conclude that OH/IR stars are AGB variables, but that they are probably in the same evolutionary stage as Miras. They argue that, since OH/IR stars show higher concentration to the galactic plane than Miras, they must have higher masses, in the range 2 to 10 $M_\odot$. The high galactic concentration of unidentified OH/IR stars is not a problem (Baud and Habing, 1983), inasmuch as these stars represent only 1 percent of the OH/IR and are distant objects. It is less clear why there should be no low-mass OH/IR stars with high OH luminosity.

Radio continuum emission at 6 cm, which may be emitted by ionization fronts propagating into CS shells during the preplanetary nebula stage, has been detected in five of 32 cool evolved stars: NGC 7027, CRL 618, R Aqr, IRC + 10216, and O Ceti (Spergel et al., 1983). Model calculations predict that, in objects with low mass-loss rates, $M < 10^{-4}$ $M_\odot$/yr, a planetary nebula is produced in $< 10^3$ years after the hot core is exposed. In those with intermediate masses, 4 to 6 $M_\odot$, and high mass-loss rates, the ionization front moves so slowly that the shell is always ionization-bounded, and most of the mass is ejected as neutral gas and dust. NGC 7027 is an example of a recently formed planetary nebula, while CRL 618 is a protoplanetary nebula with its hot core still obscured by dust, and IRC + 10216

may or may not ever reach the planetary stage. Thus, the requirement for PN formation is a short period of very high mass loss, such as is found in long-period OH/IR sources, followed by one of reduced mass loss to allow the rapid propagation of an ionization front.

REFERENCES

Adams, W.S. 1956, *Astrophys. J.*, **123**, 189.

Adams, W.S., and MacCormack, E. 1935, *Astrophys. J.*, **81**, 119.

Balega, Y., Blazit, A., Bonneau, D., Koechlin, L., Foy, R., and Labeyrie, A. 1982, *Astron. Astrophys.*, **115**, 253.

Baud, B. 1981, *Astrophys. J. (Letters)*, **250**, L79.

Baud, B., and Habing, H.J. 1983, *Astron. Astrophys.*, **127**, 73.

Baud, B., Habing, H.J., Matthews, H.E., and Winnberg, A. 1979, *Astron. Astrophys. Supplement*, **35**, 179.

Baud, B., Habing, H.J., Matthews, H.E., and Winnberg, A. 1981, *Astron. Astrophys.*, **95**, 156.

Bernat, A.P. 1976, Thesis, University Microfilms International.

Bernat, A.P. 1977, *Astrophys. J.*, **213**, 756.

Bernat, A.P. 1981, *Astrophys. J.*, **246**, 184.

Bernat, A.P. 1982, *Astrophys. J.*, **252**, 644.

Bernat, A.P., Hall, D.N.B., and Ridgway, S.T. 1979, *Astrophys. J. (Letters)*, **233**, L135.

Bloemhof, E.E., Townes, C.H., and Vanderwyck, A.H.B. 1984, *Astrophys. J. (Letters)*, **276**, L21.

Boesgaard, A.M. 1979, *Astrophys. J.*, **232**, 485.

Boesgaard, A.M., and Hagen, W. 1979, *Astrophys. J.*, **231**, 128.

Boesgaard, A.M. and Magnan, C. 1975, *Astrophys. J.*, **198**, 369.

Brooke, A.L., Lambert, D.L., and Barnes, T.G., III. 1974, *Pub. Astron. Soc. Pacific*, **86**, 419.

Burke, J.A. 1972, *Mon. Not. Roy. Astr. Soc.*, **160**, 233.

Cacciari, C., and Freeman, K.C. 1981, in *Physical Processes in Red Giants*, ed. I. Iben and A. Renzini (Dordrecht: Reidel), p. 311.

Cacciari, C., and Freeman, K.C. 1983, *Astrophys. J.*, **268**, 185.

Carpenter, K.G. 1984, *Astrophys. J.*, **285**, 181.

Cassinelli, J.P. 1979, *Ann. Rev. Astron. Astrophys.*, **17**, 275.

Chapman, R.D. 1981, *Astrophys. J.*, **248**, 1043.

Che, A., Hempe, K., and Reimers, D. 1983, *Astron. Astrophys.*, **126**, 225.

Che, A., and Reimers, D. 1983, *Astron. Astrophys.*, **127**, 227.

Clarke, D., and Schwarz, H.E. 1984, *Astron. Astrophys.*, **132**, 375.

Cohen, J.G. 1976, *Astrophys. J. (Letters)*, **203**, L127.

Cohen, M. 1980, *Astrophys. J. (Letters)*, **238**, L81.

Cohen, M., and Schmidt, G.D. 1982, *Astrophys. J.*, **259**, 693.

Deguchi, S. 1980, *Astrophys. J.*, **236**, 567.

Deutsch, A.J. 1956, *Astrophys. J.*, **123**, 210.

Deutsch, A.J. 1960, in *Stars and Stellar Systems*, **VI**, ed. J.L. Greenstein (Chicago: Univ. Chicago Press), p. 453.

Draine, B.T. 1981, in *Physical Processes in Red Giants*, ed, I. Iben and A. Renzini (Dordrecht: Reidel), p. 317.

Drake, S.A., and Linsky, J.L. 1984, in *Proc. Third Cambridge Workshop on Cool Stars, Stellar Systems and the Sun*, ed. S.L. Baliunas and L. Hartmann (Berlin: Springer-Verlag), p. 350.

Dupree, A.K. 1980, in *Highlights of Astronomy*, **5**, IAU Montreal, p. 263.

Dupree, A.K. 1981, in *Proc. Second Cambridge Workshop on Cool Stars, Stellar Systems and the Sun*, ed. M.S. Giampapa and L. Golub, SAO Special Report 392, **II** p. 3.

Dupree, A.K., Hartmann, L., and Avrett, E.H. 1984, *Astrophys. J. (Letters)*, **281**, L37.

Dyck, H.M., and Simon, T. 1975, *Astrophys. J.*, **195**, 689.

Dyck, H.M., Zuckerman, B., Leinert, Ch., and Beckwith, S. 1984, *Astrophys. J.*, **287**, 801.

Elitzur, M. 1981, in *Physical Processes in Red Giants*, ed. I. Iben and A. Renzini (Dordrecht: Reidel), p. 363.

Engels, D. 1982, *Thesis*, Bonn.

Engels, D., Kreysa, E., Schultz, G.V., and Sherwood, W.A. 1983, *Astron. Astrophys.*, **124**, 123.

Engels, D., Schultz, G.V., and Sherwood, W.A. 1981, in *Physical Processes in Red Giants*, ed. I. Iben and A. Renzini (Dordrecht: Reidel), p. 401.

Fazio, G.G., McBreen, B., Stier, M.T., and Wright, E.L. 1980, *Astrophys. J. (Letters)*, **237** L39.

Forrest, W.J., et al. 1978, *Astrophys. J.*, **219**, 114.

Fox, M.W., and Wood, P.R. 1982, *Astrophys. J.*, **259**, 198.

Fusi-Pecci, F., and Renzini, A. 1976, *Astron. Astrophys.*, **46**, 447.

Gehrz, R.D., Grasdalen, G.L., Hackwell, J.A., and Ney, E.P. 1980, *Astrophys. J.*, **237**, 855.

Gehrz, R.D., and Woolf, N.J. 1971, *Astrophys. J.*, **165**, 285.

Gilman, R.C. 1969, *Astrophys. J. (Letters)*, **155**, L185.

Gilman, R.C. 1972, *Astrophys. J.*, **178**, 423.

Glassgold, A.E., and Huggins, P.J. 1983, *Mon. Not. Roy. Astr. Soc.*, **203**, 517.

Goldberg, L. 1979, *Quart. J. Roy. Astr. Soc.*, **20**, 361.

Goldberg, L. 1984, *Pub. Astron. Soc. Pacific*, **96**, 366.

Goldberg, L., Hege, E.K., Hubbard, E.N., Strittmatter, P.A., and Cocke, W.J. 1981, in *Proc. Second Cambridge Workshop on Cool Stars, Stellar Systems and the Sun*, ed. M.S. Giampapa and L. Golub, SAO Special Report 392. p. 131.

Goldberg, L., Ramsey, L., Testerman, L., and Carbon, D. 1975, *Astrophys. J.*, **199**, 427.

Goldreich, P. 1980, see discussion of paper by Hall (1980).

Goldreich, P., and Scoville, N.J. 1976, *Astrophys. J.*, **205**, 144.

Guinan, E.F. 1983, in *Proc. Third Cambridge Workshop on Cool Stars, Stellar Systems and the Sun*, ed. S. Baliunas and L. Hartmann (Berlin: Springer-Verlag), p. 336.

Hagen, W. 1978, *Astrophys. J. Supplement*, **38**, 1.

Hagen, W. 1980, in *Proc. First Cambridge Workshop on Cool Stars, Stellar Systems and the Sun*, ed. A.K. Dupree, SAO Special Report 389, p. 143.

Hagen, W., Stencel, R.E., and Dickinson, D.F. 1983, *Astrophys. J.*, **274**, 286.

Haisch, B.M., and Simon, T. 1982, *Astrophys. J.*, **263**, 252.

Hall, D.N.B. 1980, in *Proc. IAU Symp. 87, Interstellar Molecules* (Dordrecht: Reidel), p. 515.

Hartmann, L. and Avrett, E.H. 1984, *Astrophys J.*, **284**, 238.

Hartmann, L., Dupree, A.K., and Raymond, J.C. 1980, *Astrophys. J. (Letters)*, **236**, L143.

Hartmann, L., Dupree, A.K., and Raymond, J.C. 1981, *Astrophys. J.*, **246**, 193.

Hartmann, L., and McGregor, K.B. 1980, *Astrophys. J.*, **242**, 260.

Hartmann, L., and McGregor, K.B. 1982, *Astrophys. J.*, **257**, 264.

Harvey, P.M., Bechis, K.P., Wilson, W.J., and Ball, J.A. 1974, *Astrophys. J. Supplement*, **27**, 331.

Hayes, D.P. 1980, *Astrophys. J. (Letters)*, **241**, L165.

Hayes, D.P. 1981, *Pub. Astron. Soc. Pacific*, **93**, 752.

Hayes, D.P. 1984, *Astrophys. J. Supplement*, **55**, 179.

Hearn, A.G. 1975, *Astron. Astrophys.*, **40**, 355.

Hempe, K. 1982, *Astron. Astrophys.*, **115**, 133.

Hinkle, K.H., Hall, D.N.B., and Ridgway, S.T. 1982, *Astrophys. J.*, **252**, 697.

Hjellming, R.M., and Newell, R.T. 1983, *Astrophys. J.*, **275**, 702.

Holzer, T.E. 1980, in *Proc. First Cambridge Workshop on Cool Stars, Stellar Systems and the Sun*, ed. A.K. Dupree, SAO Special Report 389, p. 153.

Holzer, T.E., Flå, T., and Leer, E. 1983, *Astrophys. J.*, **275**, 808.

Honeycutt, R.K., Bernat, A.P., Kephart, J.E., Gow, C.E., Sandford, M.T., II, and Lambert, D.L. 1980, *Astrophys. J.*, **239**, 565.

Hoyle, F., and Wickramasinghe, N.C. 1962, *Mon. Not. Roy. Astr. Soc.*, **124**, 417.

Huggins, P.J., and Glassgold, A.E. 1982, *Astrophys. J.*, **252**, 201.

Iben, I. 1981a, in *Physical Processes in Red Giants*, ed. I. Iben and A. Renzini (Dordrecht: Reidel), p. 3.

Iben, I. 1981b, in *Proc. IAU Colloq. 59, Effects of Mass Loss on Stellar Evolution*, ed. C. Chiosi and R. Stalio (Dordrecht: Reidel), p. 373.

Jewell, P.R., Webber, J.C., and Snyder, L.E. 1980, *Astrophys. J. (Letters)*, **242**, L29.

Jones, T.W., and Merrill, K.M. 1976, *Astrophys. J.*, **209**, 509.

Jones, T.W., Ney, E.P., and Stein, W.A. 1981, *Astrophys. J.*, **250**, 324.

Jura, M. 1983a, *Astrophys. J.*, **267**, 647.

Jura, M. 1983b, *Astrophys. J.*, **275**, 683.

Jura, M., and Morris, M. 1981, *Astrophys. J.*, **251**, 189.

Kafatos, M., and Michalitsianos, A.G. 1979, *Astrophys. J. (Letters)*, **228**, L115.

Knapp, G.R., and Bowers, P.F. 1983, *Astrophys. J.*, **266**, 701.

Knapp, G.R., and Morris, M. 1985, *Astrophys. J.*, **292**, 640.

Knapp, G.R., Phillips, T.G., and Huggins, P.J. 1980, *Astrophys. J. (Letters)*, **242**, L25.

Knapp, G.R., Phillips, T.G., Leighton, R.B., Lo, K.Y., Wannier, P.G., Wooten, H.A., and Huggins, P.J. 1982, *Astrophys. J.*, **252**, 616.

Krisciunas, K. 1982, *IAU Info. Bull. Var. Stars*, No. 2104.

Krisciunas, K. 1983, *IAU Info. Bull. Var. Stars*, in press.

Kudritzki, R.P., and Reimers, D. 1978, *Astron. Astrophys.*, **70**, 227.

Kunasz, P.B., and Hummer, D.G. 1974, *Mon. Not. Roy. Astr. Soc.*, **166**, 57.

Kwan, J., and Hill, F. 1977, *Astrophys. J.*, **215**, 781.

Kwan, J., and Linke, R.A. 1982, *Astrophys. J.*, **254**, 587.

Kwok, S. 1975, *Astrophys. J.*, **198**, 583.

Kwok, S. 1982, *Astrophys. J.*, **258**, 280.

Kwok, S., Purton, C.R., and FitzGerald, P.M. 1978, *Astrophys. J. (Letters)*, **219**, L125.

Lambert, D.L., Hinkle, K.H., and Hall, D.N.B. 1981, *Astrophys. J.*, **248**, 638.

Lefévre, J., Bergeat, J., and Daniel, J.-Y. 1982, *Astron. Astrophys.*, **114**, 341.

Linsky, J.L., and Haisch, B.M. 1979, *Astrophys. J. (Letters)*, **229**, L27.

Lo, K.Y., and Bechis, K.P. 1977, *Astrophys. J. (Letters)*, **218**, L27.

Mallia, E.A., and Pagel, B.E.J. 1978, *Mon. Not. Roy. Astr. Soc.*, **184**, 55P.

Mariotti, J.M., Chelli, A., Foy, R., Lena, P., Sibille, F., and Tchountonov, G. 1983, *Astron. Astrophys.*, **120**, 237.

Mauron, N., Fort, B., Querci, F., Dreux, M., Fauconnier, T., and Lamy, P.H. 1984, *Astron. Astrophys.*, **130**, 341.

McCarthy, D.W., Howell, R.R., and Low, F.J. 1980, *Astrophys. J. (Letters)*, **235**, L27.

Menietti, J.D., and Fix, J.D. 1978, *Astrophys. J.*, **224**, 961.

Merrill, K.M. 1977, in *IAU Colloq. 42, The Interaction of Variable Stars With Their Environment*, ed. R. Kippenhahn, J. Rahe, W. Strohmeier (Bamberg: Remeis-Sternwarte), p. 46.

Mitchell, R.M., and Robinson, G. 1980, *Mon. Not. Roy. Astr. Soc.*, **190**, 669.

Morris, M. 1975, *Astrophys. J.*, **197**, 603.

Morris, M. 1980, *Astrophys. J.*, **236**, 823.

Morris, M., and Alcock, C. 1977, *Astrophys. J.*, **218**, 687.

Morris, M., Redman, R.O., Reid, M.J., and Dickinson, D.F. 1979, *Astrophys. J.*, **229**, 257.

Mullan, D.J. 1978, *Astrophys. J.*, **226**, 151.

Mullan, D.J. 1981, in *Physical Processes in Red Giants*, ed. I. Iben and A. Renzini (Dordrecht: Reidel), p. 355.

Mullan, D.J. 1982, *Astron. Astrophys.*, **108**, 279.

Mullan, D.J., and Ahmad, I.A. 1982, *Solar Phys.*, **75**, 347.

Mullan, D.J., and Steinolfson, R.S. 1983, *Astrophys. J.*, **266**, 823.

Newell, R.T., and Hjellming, R.M. 1982, *Astrophys. J. (Letters)*, **263**, L85.

Peterson, R.C. 1981, *Astrophys. J. (Letters)*, **248**, L31.

Peterson, R.C. 1982, *Astrophys. J.*, **258**, 499.

Pneuman, G.W. 1968, *Solar Phys.*, **3**, 578.

Pottasch, S.R. 1984, *Planetary Nebulae* (Dordrecht: Reidel).

Reimers, D. 1975a, *Mém. Soc. Roy. Sci. Liège*, 6th Ser. **8**, 369.

Reimers, D. 1975b, in *Problems in Stellar Atmospheres and Envelopes*, ed. B. Baschek, W.H. Kegel, and G. Traving (Berlin-Heidelberg, New York: Springer-Verlag), p. 229.

Reimers, D. 1977a, *Astron. Astrophys.*, **61**, 217. (*Erratum* **67**, 161.)

Reimers, D. 1977b, in *Proc. IAU Colloq. 42, The Interaction of Variable Stars with Their Environment*, ed. R. Kippenhahn, J. Rahe, W. Strohmeier (Bamberg: Remeis-Sternwarte).

Reimers, D. 1981, in *Physical Processes in Red Giants*, ed. I. Iben and A. Renzini (Dordrecht: Reidel), p. 269.

Reimers, D. 1982, *Astron. Astrophys.*, **107**, 292.

Reimers, D., and Schröder, K.-P. 1983, *Astron. Astrophys.*, **124**, 241.

Renzini, A. 1977, in *Advanced Stages in Stellar Evolution*, ed. P. Bouvier and A. Maeder (Geneva), p. 149.

Renzini, A. 1981a, in *Proc. IAU Colloq. 59, Effects of Mass Loss on Stellar Evolution*, ed. C. Chiosi and R. Stalio (Dordrecht: Reidel), p. 319.

Renzini, A. 1981b, in *Physical Processes in Red Giants*, ed. I. Iben and A. Renzini (Dordrecht: Reidel), p. 269.

Ricort, G., Aime, A., Vernin, J., and Kadiri, S. 1981, *Astron. Atrophys.*, **99**, 232.

Ridgway, S.T. 1981, in *Physical Processes in Red Giants*, ed. I. Iben and A. Renzini (Dordrecht: Reidel), p. 305.

Roddier, C., and Roddier, F. 1983, *Astrophys. J. (Letters)*, **270**, L23.

Rowan-Robinson, M. 1980, *Astrophys. J. Supplement*, **44**, 403.

Rowan-Robinson, M. 1982, *Mon. Not. Roy. Astr. Soc.*, **201**, 281.

Rowan-Robinson, M., and Harris, S. 1982, *Mon. Not. Roy. Astr. Soc.*, **200**, 197.

Rowan-Robinson, M., and Harris, S. 1983a, *Mon. Not. Roy. Astr. Soc.*, **202**, 767.

Rowan-Robinson, M., and Harris, S. 1983b, *Mon. Not. Roy. Astr. Soc.*, **202**, 797.

Salpeter, E.E. 1974, *Astrophys. J.*, **193**, 585.

Sanford, R.F. 1933, *Astrophys. J.*, **77**, 110.

Sanner, F. 1976, *Astrophys. J. Supplement*, **32**, 115.

Scalo, J.M., and Slawsky, O.B. 1980, *Astrophys. J. (Letters)*, **239**, L73.

Schmid-Burgk, J., and Scholz, M. 1981, in *Physical Processes in Red Giants*, ed. I. Iben and A. Renzini (Dordrecht: Reidel), p. 341.

Schwarz, H.E., and Clarke, D. 1984, *Astron. Astrophys.*, **132**, 370.

Schwarzschild, M. 1975, *Astrophys. J.*, **195**, 137.

Shawl, S.J. 1975, *Astron. J.*, **80**, 602.

Simon, T., Linsky, J.L., and Stencel, R.E. 1982, *Astrophys. J.*, **257**, 225.

Sopka, R.J., Hildebrand, R., Jaffe, D.T., Gatley, I., Roellig, T., Werner, M., Jura, M., and Zuckerman, B. 1985, *Astrophys. J. (Letters)*, **294**, 242.

Spergel, D.N., Giuliani, J.L., Jr., and Knapp, G.R. 1983, *Astrophys. J.*, **275**, 330.

Stebbins, J. 1931, *Pub. Washburn Obs., Univ. of Wisc.*, **15**, 177.

Stencel, R.E. 1978, *Astrophys. J. (Letters)*, **223**, L37.

Stencel, R.E., Kondo, Y., Bernat, A.P., and MacCluskey, G.E. 1979, *Astrophys. J.*, **233**, 621.

Stencel, R.E., and Mullan, D.J. 1980, *Astrophys. J.*, **238**, 221; **240**, 718.

Sutton, E.C., Betz, A.L., Storey, J.W.V., and Spears, D.L. 1979, *Astrophys. J. (Letters)*, **230**, L105.

Sweigart, A.V., and Gross, P.G. 1978, *Astrophys. J. Supplement*, **36**, 405.

Tielens, A.G.G.M. 1983, *Astrophys. J.*, **271**, 702.

Tinbergen, J., Greenberg, J.M., and de Jager, C. 1981, *Astron. Astrophys.*, **95**, 215.

Tuchman, Y., Sack, N., and Barkat, Z. 1978, *Astrophys. J.*, **219**, 183.

Tuchman, Y., Sack, N., and Barkat, Z. 1979, *Astrophys. J.*, **234**, 217.

Vaiana, G.S., et al. 1981, *Astrophys. J.*, **245**, 163.

van der Hucht, K.A., Bernat, A.P., and Kondo, Y. 1980, *Astron. Astrophys.*, **82**, 14.

van der Hucht, K.A., Stencel, R.E., Haisch, B.M., and Kondo, Y. 1979 *Astron. Astrophys.*, **36**, 377.

Watanabe, T. 1981, *Pub. Astr. Soc. Japan*, **33**, 679.

Werner, M.W., Beckwith, S., Gatley, I., Sellgren, K., Berriman, G., and Whiting, D.L. 1980, *Astrophys. J.*, **239**, 540.

Weymann, R.J. 1962a, *Astrophys. J.*, **136**, 844.

Weymann, R.J. 1962b, *Astrophys. J.*, **136**, 476.

Willson, L.A. 1981, in *Physical Processes in Red Giants*, ed. I. Iben and A. Renzini (Dordrecht: Reidel), p. 225.

Willson, L.A., and Hill, S.J. 1979, *Astrophys. J.*, **228**, 854.

Wood, P.R. 1974, *Astrophys. J.*, **190**, 609.

Wood, P.R. 1979, *Astrophys. J.*, **227**, 220.

Wood, P.R. 1981, in *Physical Processes in Red Giants*, ed. I. Iben and A. Renzini (Dordrecht: Reidel), p. 205.

Wood, P.R., and Cahn, J.H. 1977, *Astrophys. J.*, **211**, 499.

Woodrow, J.E.J., and Auman, J.R. 1982, *Astrophys. J.*, **257**, 247.

Woolf, N.J., and Ney, E.P. 1969, *Astrophys. J. (Letters)*, **155**, L181.

Zuckerman, B., Palmer, P., Gilra, D.P., Turner, B.E., and Morris, M. 1978, *Astrophys. J. (Letters)*, **220**, L53.

Zuckerman, B., Palmer, P., Morris, M., Turner, B.E., Gilra, D.P., Bowers, P.F., and Gilmore, W.S. 1977, *Astrophys. J. (Letters)*, **211**, L79.

N88-11598

6

CIRCUMSTELLAR CHEMISTRY

Alfred E. Glassgold and Patrick J. Huggins

INTRODUCTION

The definitive detection of circumstellar (CS) material around a cool evolved star was made by Deutsch (1956) for α Her, although the possibility had been discussed as long as 50 years ago. Weymann was one of the first to make physical models of extended envelopes, and in an early review, (Weymann, 1963) wrote "... the pages expended in reviewing the subject (of mass loss)... probably exceed the number of pages of material being reviewed." The situation has since changed dramatically as the result of new observing techniques, particularly in the infrared (IR) and millimeter wave bands. Some of the important early milestones were the observation of IR emission from CS dust, the detection of the 10-micron silicate feature (Woolf and Ney, 1969), the detection of microwave molecular emission from IRC + 10216 (Solomon et al., 1971), and the detection of IR molecular absorption lines (Geballe et al., 1972). These and many other new developments have been followed up by numerous detailed investigations, which have been reviewed previously by Zuckerman (1980).

The observational information available on a few of the closest CS envelopes is now approaching the stage at which some detailed conclusions on their physical and chemical properties can be obtained. A prime example is the carbon star, IRC + 10216, for which we have extensive data on the spatial and spectral properties of the dust and observations of over 20 molecules (not counting isotopically substituted species). The CS gas around the M supergiant, α Ori, has also been well studied; in this case, optical observations of atoms and atomic ions play an important role. Better data on more objects will become available as sensitive high-resolution observational techniques are developed.

The data on numerous atomic and molecular species make it possible to investigate the chemical nature of CS shells. Because this is a new area of research, this review must necessarily be fairly qualitative. One long-range goal of the study of CS chemistry is to obtain a sufficiently quantitative description of the constituents so that deductions can be made about the history of the wind material (e.g., the formation of dust) and the tangled problems of stellar evolution and mass loss. The relatively well-ordered gas in the outer parts of the CS envelopes also offers opportunities to understand a number of basic physical and chemical

PRECEDING PAGE BLANK NOT FILMED

PAGE 290 INTENTIONALLY BLANK

processes which have applications to the study of interstellar clouds.

After a brief introduction on the physical properties of CS envelopes (see the section *General Physical Considerations*), the bulk of this chapter is divided between a summary of the observations (see the section *Observations*) and a discussion of theoretical considerations concerning the chemistry (see the section *Chemistry*). We conclude with a short summary (see the section *Conclusions*). The literature cited is mainly to articles published before 1984, although references to the major journals for much of 1984 have been included.

GENERAL PHYSICAL CONSIDERATIONS

This section primarily concerns the massive expanding CS envelopes around the cooler M giants and supergiants, S stars, and the cooler carbon stars. Observational evidence on the physical properties of the envelopes comes from several main lines of investigation: strong continuum emission in the infrared, accompanied by spectral signatures of dust; optical absorption lines of low ionization potential atoms and ions; near-infrared absorption lines of molecules; and microwave molecular emission lines. Details can be found in the review by Zuckerman (1980); observations relevant to chemistry are summarized in the section *Observations*.

Certain basic dynamical and structural facts emerge from the observational data:

1. The terminal wind speeds are small with respect to stellar escape velocities and are typically of the order of 10 km s^{-1}.
2. The CS envelopes are large with respect to stellar sizes, ranging up to 1×10^{18} cm with corresponding ages up to 2×10^4 yr.
3. The mass-loss rates are large, in the range 10^{-7} to $10^{-4}\ M_\odot\ yr^{-1}$.

Of course, other detailed dynamical properties are of interest, such as the time dependence of the mass loss (e.g., mass loss may be episodic) and the detailed spatial variation of the wind density and velocity (e.g., angular as well as radial variations, clumpiness, and shocks). Little is known at present about these issues, but the basic framework given above should be a sufficient starting point for a discussion of the chemistry.

For purposes of simplicity, the winds are often assumed to be spherically symmetric, as well as steady. There are many envelopes which conform to this assumption, at least to first order, and many that do not; only passing reference is made to the latter cases. For the spherically symmetric case, the spatial profile of the mean density of hydrogen nuclei is:

$$n(r) = \frac{C}{r^2}\,(V/v(r)) \quad , \tag{6-1}$$

$$C = 3 \times 10^{37}\,\frac{\dot{M}_{-5}}{V_6}\ \mathrm{cm}^{-1} \quad , \tag{6-2}$$

where V is the terminal value for the velocity profile $v(r)$, and $\dot{M}_{-5}$ and V_6 measure the mass-loss rate and velocity in units of $10^{-5}\ M_\odot\ yr^{-1}$ and 10 km s^{-1}, respectively. In a typical case, the outer envelope extends from $\sim 10^{15}$ to 10^{17} or 10^{18} cm; the corresponding density range is $\sim 10^6$ to 10^3 or 10^2 cm^{-3}, roughly the range encountered in interstellar clouds. The temperature profile can also be important for chemical considerations, but little observational information is available on the gas kinetic temperature. Theoretical considerations (heating in gas/dust collisions and cooling by line radiation (Goldreich and Scoville, 1976; Kwan and Hill, 1977; Slavsky and Scalo, 1984)) suggest that the gas kinetic temperature in the outer envelope varies more slowly than the mass density. That is,

$$T(r) \propto r^{-m} \quad , \tag{6-3}$$

with $m \cong 0.7$. A typical temperature at 10^{16} cm might be of the order of 100 K. Closer to the

star the temperature may increase more rapidly than is implied by Equation (6-3), especially if there is a chromosphere.

The temperature and density distributions described above imply that different types of chemistry may dominate in different parts of the envelopes. Beginning just above the photosphere, we may expect to find the conditions for themal equilibrium to be satisfied. As material moves out into cooler and more rarefied regions, individual species will freeze out when the ratios of appropriate reaction to dynamical time scales exceed unity. Eventually, photochemistry induced by the penetration of galactic UV radiation will dissociate any molecules and ionize the heavy atoms. This qualitative picture becomes more complicated in the presence of active regions associated with a chromosphere or with shocks.

These considerations suggest that the variation in the physical conditions is enormous when we consider the chemical evolution of the wind as it travels from the stellar surface out into the interstellar medium. Furthermore, the formation of dust in the inner envelope is intimately connected with the thermal, dynamical, and chemical evolution of the wind. Not only do space limitations preclude the presentation of such a general discussion of CS chemistry, but, in fact, little research has thus far been done along these lines. Most of the difficult questions about the origin and the physical and chemical properties of the envelopes remain unanswered.

In view of the developing nature of this subject, we have chosen to emphasize the outer parts of the shells ($r > 10^{15}$ cm) because these appear to be the most accessible to quantitative study at this time. This approach avoids such difficult theoretical questions as the development of the wind and the formation of the dust, but it takes advantage of the main body of currently available observational data. Thus, we emphasize the gas-phase chemistry of the atoms, ions, and molecules outside the region of dust formation. In order to lay the foundations for this study of circumstellar chemistry, we begin by reviewing the observations.

OBSERVATIONS

This section reviews the observations of CS envelopes which are relevant to a discussion of the chemistry. Many of the observations address more directly other related issues, such as mass loss and dust (see, for example, Zuckerman, 1980; and Goldberg and Lefèvre, this volume), but the concern here is primarily with the gas-phase chemistry. As will become clear, few of the observations directly confront current theoretical ideas, but many more contribute to the development of an overall picture of the physical and chemical properties of the shells. We discuss in turn, hydrogen, the heavy molecules observed in the IR and radiowave bands, and the atoms and ions observed in the optical. Finally, we summarize some other observations which also have a bearing on the chemistry.

Hydrogen

Although hydrogen is the most abundant element in most stars, it has not yet been observed in atomic (HI) or molecular (H_2) form in the extended CS envelopes of cool stars. However, both forms are seen in more evolved objects (see below). Of course, HI is observed in absorption and emission from photospheric and chromospheric regions, but three recent searches for the 21-cm line have failed to reveal HI in the extended envelopes. The searches have been made by Zuckerman et al. (1980), Knapp and Bowers (1983), and Clegg et al. (1983b) using the Arecibo 305-m telescope, the VLA, and the WSRT, respectively. Together, they have surveyed a variety of objects, including M giants and supergiants, C stars, and protoplanetary and planetary nebulae. The Arecibo beamsize (3.2′) is comparable to the largest known CS envelope (that of IRC + 10216), whereas the two smaller interferometer beams (~15″) could, in principle, spatially resolve a number of the envelopes observed.

Interpretation of the observed upper limits on the 21-cm lines in terms of limits on the HI content of the envelopes is relatively straightforward, apart from the contamination effects of background galactic HI emission and uncertainties in the total masses of the envelopes.

Two results from these surveys deserve special mention. The first is for IRC + 10216, where < 1 percent (or less) of the envelope mass is in the form of HI (Zuckerman et al., 1980; Knapp and Bowers, 1983); the exact limit depends on the adopted total mass of the envelope and the level of significance of the flux limit used. In any event, the absence of HI means that the bulk of the hydrogen must be in molecular form. This result is, perhaps, not too surprising in view of the obvious strong association into molecules evident for other species. However, the limit begins to approach values of interest in connection both with the processes which associate hydrogen molecules in the inner envelope and with photodestruction of H_2 by the ambient galactic UV radiation field. (See the section *Photochemistry*.)

The second limit of particular interest is that for α Ori. Knapp and Bowers (1983) give a 5σ upper limit of $\dot{M}(\mathrm{HI}) < 5 \times 10^{-6}\ M_\odot\ \mathrm{yr}^{-1}$, which is essentially the same as that given by Clegg et al. (1983b). This value is comparable to many estimates of the total mass-loss rate for the star and is somewhat less than that given by the model of the envelope by Jura and Morris (1981). For an early M supergiant like α Ori, hydrogen is not expected to be strongly associated into molecules, at least on the basis of the simplest picture of the chemistry. The limits here are then tantalizingly close to confronting the simplest ideas on the HI/H_2 problem. Needless to say, the detection of HI in cool CS envelopes would be a significant contribution to the study of the chemistry.

For completeness, note that the planetary nebulae included in the above surveys also failed to yield detectable HI (see also, Pottasch et al., 1982). Recently, however, Rodriguez and Moran (1983) reported the detection of 21-cm absorption toward NGC 6302 using the VLA. The absorption is probably associated with the nebula, and they interpret it as arising from the neutral outer part of an expanding ring whose inner part is ionized and produces the thermal continuum. The mass in HI is $\sim 0.06\ M_\odot$.

Although hydrogen must be predominantly in the form of H_2 in the CS envelopes of the coolest stars, it is not observable under normal circumstances. However, IR quadrupole lines of H_2 are seen in absorption in the atmospheres of certain S and carbon Miras, but in other stars, they have generally proved to be much weaker than expected (Tsuji, 1983; Johnson et al., 1983). This possibly indicates that the theoretical atmospheric structures of cool stars are still not well determined or that effects such as chromospheric heating destroy the H_2 in the line-forming regions.

However, the presence of H_2 in CS envelopes can be seen in objects whose central stars have evolved from the cool giant phase. H_2 quadrupole lines in emission have been detected in planetaries and protoplanetaries such as CRL 2688, CRL 618, and NGC 7027 (e.g., Treffers et al., 1976; Beckwith et al., 1978), which still retain many of the CS characteristics of cool stars. Although other interpretations are possible (Black, 1983), the emission appears to be shock-excited and acts as a useful diagnostic of the processes which ionize and dissipate the neutral shell as the central star evolves. The hydrogen molecular ion, H_2^+, may also have been detected in some planetary nebulae by characteristic continuum absorption in the UV shortward of ~ 1500 Å (Heap and Stecher, 1981; Feibelman et al., 1981). However, this identification does not appear to be firmly established (see the discussion following Black, 1983).

Heavy Molecules

The detection of numerous heavy molecules in the CS envelopes of cool stars has been of major significance in understanding processes which occur during the later stages of stellar evolution. The observations yield a variety of

information on the envelope kinematics and mass loss and provide evidence of a rich chemistry. The molecules are detected at radio (mainly millimeter) wavebands in emission and in the IR in absorption. The two techniques are complementary. The IR observations measure vibration-rotation absorption along the line of sight to the continuum-forming regions, whereas the radio measurements sample lower energy (mainly rotational) transitions from the extended envelopes, although the emission is normally not spatially resolved with single antennas. Some symmetric molecules, which possess no permanent dipole moment and thus no rotational spectrum, can be readily detected in the IR.

The C/O ratio dominates the heavy molecule chemistry in stellar photospheres, and this also appears to be true for the CS envelopes. Therefore, the envelopes of C stars and M and S stars will be discussed separately below.

IRC + 10216. Because of its proximity and the richness of its spectrum, IRC + 10216 is by far the most extensively observed CS envelope, and it serves as the prototype for the study of carbon-rich systems. The molecules identified in the envelope are listed in Table 6-1. Most of them have been observed only in the radio, four only in the IR, and three in both. Because most species have been observed in several transitions and/or in isotropically substituted forms, the actual number of lines identified is quite large. There remain several unidentified lines scattered in the literature and a number of upper limits, some of significance. Notably absent are common oxygen-bearing species (e.g., Johansson et al., 1984), except for CO and trace

Table 6-1
Molecules in IRC + 10216*

$n(x)/n(CO)$	Species				References†
10^{-1}	—	—	—	—	
	C_2H_2				1
10^{-2}	HCN	—	—	—	1,2,6
				CN	3
10^{-3}	NH_3	—	—	C_4H	4,5; 6,7
	C_2H_4	CS	HC_5N	C_2H	8; 9,6; 10,6; 3,6
	CH_4	SiS	HC_3N	C_3N	1,11; 12,9,16; 13,9,6; 6
10^{-4}	—	SiC_2	HC_7N	—	17;10
	HNC	SiO	$HC_{11}N$	C_3H	6; 9,6; 14; 18,19
10^{-5}	—	SiH_4	—	—	15
	CH_3CN				6

* For comparison, the reactive radicals, the cyanopolyyne chains, and the S- and Si-bearing molecules are listed separately from the remaining species.

† References: 1. Hall and Ridgway (1978), 2. Kwan and Hill (1977), 3. Huggins et al. (1984b), 4. Betz et al. (1979), 5. Kwok et al. (1981), 6. Johansson et al. (1984) (see also Olofsson et al. (1982a), 7. Guelin et al. (1978), 8. Betz (1981), 9. Morris (1975), 10. Winnewisser and Walmsley (1978), 11. Clegg et al. (1982), 12. Henkel et al. (1983), 13. Carlson et al. (1984), 14. Bell et al. (1982), 15. Goldhaber and Betz (1984), 16. Sahai et al. (1984), 17. Thaddeus et al. (1984), 18. Johansson et al. (1984), 19. Thaddeus et al. (1985).

amounts of SiO. This is not too surprising in view of the carbon-rich environment. Also absent are the molecular ions like HCO^+ and N_2H^+ (e.g., Wannier and Linke, 1978), which are readily observable in molecular clouds where their presence is usually interpreted as evidence for a chemistry dominated by ion-molecule reactions.

The interpretation of observed lines, or indeed upper limits, in terms of abundances in the envelope is not straightforward. Because both the radio and IR measurements integrate over regions which are physically, and possibly chemically, inhomogeneous, the results must be treated with some caution.

The IR line measurements are generally interpreted with simple column density arguments, using assumed or measured excitation temperatures to determine partition functions. In some cases, column density estimates may be good to a factor of 3, but are often less accurate. For example, the column densities of C_2H_2 (Rinsland et al., 1982) and CH_4 (Clegg et al., 1982) have recently been revised down by factors of 10 from earlier determinations. The high spectral resolution now attainable with IR instrumentation (Fourier transform spectroscopy and heterodyne techniques) offers opportunities for investigating in detail the kinematics and excitation of molecules in the inner envelope (e.g., Ridgway and Hall, 1980; Betz et al., 1979), but detailed models of this region have not yet been constructed. The possibility of obtaining spatial information from the IR lines has recently been demonstrated (Dyck et al., 1983; Wannier and Sahai, 1983) and will be important for future development.

In contrast to the situation in the IR, fairly complete modeling has been carried out for some species observed in emission in the radio. Kwan and Hill (1977; see also Kwan and Linke, 1982) have shown that the CO rotational levels in IRC + 10216 are primarily excited by collisions; the CO emission is therefore coupled to the gas kinetic temperature. They have developed a thermal model for the gas (including heating by gas/grain collisions and molecular line cooling) and have computed the CO emissivity, convolved with the appropriate beams, for comparison with the observations. They deduce a mass-loss rate for IRC + 10216 of $4 \times 10^{-5}\ M_\odot\ \mathrm{yr}^{-1}$ (if its distance is 200 pc) and a CO/H_2 abundance ratio of 6×10^{-4}. Two aspects of the observations are not completely dealt with in this model: the asymmetry seen in the lines (see, for example, Olofsson et al., 1982a), which may be an effect of radiative transfer or geometry, and the great extent of the CO emission (see Kwan and Linke, 1982). However, neither of these is likely to have much effect on the inferred mass-loss rate or CO abundance.

In the same spirit, Morris (1975) analyzed the emission of high dipole moment molecules in IRC + 10216 and found that their rotational levels are primarily populated by the absorption of IR radiation, followed by rapid decay to different rotational levels of the ground vibrational state. The excitation of these species is therefore coupled to the IR continuum by the absorption-line strengths of the exciting transitions. This kind of model has now been used to analyze a number of species in IRC + 10216: SiS, SiO, CS, HC_3N, CN, C_2H, and HCN (Morris, 1975; Kwan and Hill, 1977; Henkel et al., 1983; Huggins et al., 1984b; Carlson et al., 1985; Sahai et al., 1984; Nguyen-Q-Rieu et al., 1984a). For some of these species, as well as many others not yet analyzed, the IR absorption-line strengths are not (or are poorly) known; however, these are not usually crucial parameters in the analysis. Further complications arise if the molecule has a complex hyperfine structure or if the IR lines are optically thick, but in the best cases, the resulting abundances may be good to a factor of 3. Several other abundance estimates appear in the literature and are based on simplifying assumptions (e.g., beam-averaged column densities or an arbitrarily assumed constant excitation temperature). These should be treated with some caution.

Several tables of abundances for the envelope of IRC + 10216 have been compiled. The early one of McCabe et al. (1979) is not now to be recommended. That of Lafont et al. (1982)

attempts to interpret quoted abundances from a number of different studies in a uniform way. The list of Johansson et al. (1984; see also Olofsson et al., 1982a) is restricted to those species found in the Onsala line survey of IRC + 10216 (which forms an excellent homogeneous data set), but is partially vitiated by the assumption of constant excitation temperatures in the line-forming regions. The abundances quoted for some species differ by a factor of 10 in the last two tables mentioned.

Table 6-1 indicates the approximate abundances of the species observed in IRC + 10216 relative to the CO abundance. The abundances are purposefully given only in decades (with rough ordering within each) so that the reader will not be misled. For the IR data, we use the ratios of column densities, as did Lafont et al. (1982), but with updated values. For the radio-line data, we use the results of model analyses, when available, augmented by other estimates, suitably scaled, where necessary. The references give the most recent analyses and/or primary references from which the earlier results can be found. If more accurate abundance ratios for particular species are required (and are warranted), they can be constructed from the references cited. Implicit in all of the foregoing discussion is the chemical homogeneity of the envelope, which may not be satisfied (see below).

The molecular line observations of IRC + 10216 (and other CS envelopes) are, of course, excellent sources for the determination of isotopic abundances. However, although the observed isotopic ratios are important for understanding nucleosynthesis and envelope mixing processes, they are only indirectly linked to a study of the chemistry of the envelope. Therefore, this subject lies beyond the scope of this chapter, and we refer the reader to the fairly recent reviews by Wannier (1980) and Zuckerman (1980) for further information on this aspect of the observations.

The implications of the observed abundances in IRC + 10216 are discussed in the section *Chemistry*. For convenience, some of the main points relevant to the chemistry are listed and commented on:

1. The oxygen (i.e., CO) abundance in the gas phase is not very different (a factor ~ 3) from solar.

2. In comparison with galactic molecular clouds, HCN is strongly enhanced, by a factor 100 to 1000 if the cloud analyses of Wootten et al. (1978) are used.

3. The absence of molecular ions and O-bearing species (other than CO and SiO) has already been discussed. However, Johansson et al. (1984) have pointed out that the limits on their abundances are not significantly smaller than their observed levels in molecular clouds. However, these species are highly underabundant compared to HCN.

4. The very low value of the isomeric ratio HNC/HCN ($= 4 \times 10^{-3}$, Johansson et al., 1984) compared to that in molecular clouds has been interpreted (e.g., McCabe et al., 1979; Zuckerman, 1980) as evidence for a simple freeze-out model for these species. Note that because this ratio varies widely in molecular clouds and values as low as 1.5×10^{-2} have been observed (Goldsmith et al., 1981), the argument may not be overly compelling.

5. If the observed Si- and S-bearing species are their major carriers in the gas phase, then, assuming solar abundances, these elements must be highly depleted (>95 percent) into grains. The depletion of other metals is unclear because the lines of their expected major carriers are generally inaccessible. Clegg and Wootten (1980) have searched for AlCl, and find it to be at least 20 times less abundant than would be expected on the basis of

complete association and solar abundances. Cl itself, however, is also not present in the possible alternate form of HCl (Clegg et al., 1982), and it too may be hidden in grains or in more complex molecules.

6. After CO, C_2H_2, and HCN, the highly reactive radicals CN, C_2H, C_3N, C_4H, and possibly C_3H, are as abundant as most of the other molecules observed. Their presence argues strongly against a simple freeze-out process in the inner envelope as the source of their production (Lafont et al., 1982), as discussed in the section *Chemistry*.

7. The significance of the preponderance of linear-chain polyatomics observed in the envelope is not clear. The low abundance of methyl cyanide (CH_3CN) and the limits on vinyl cyanide (CH_2CHCN) and ethyl cyanide (CH_3CH_2CN) are not particularly stringent when compared to galactic clouds like TMC-1 (cf. Johansson et al., 1984), but they are deficient relative to HCN. The falloff in abundance of the cyanopolyynes with increasing chain length is quite weak: the presence of very large molecules in considerable abundance cannot be ruled out.

We conclude our discussion of IRC + 10216 with a review of the sparse observational data on the spatial extent of the molecules in the envelope. At 100 GHz, the emitting regions of most species are barely resolved with the largest single dishes, so that the information available is very limited. Line profiles provide some information on the extent of the emission, and Olofsson et al. (1982a) have mapped a number of lines to yield characteristic sizes for the emission (e.g., SiO $\lesssim 20''$ and HCN $\simeq 40''$, FWHM). These sizes are probably determined mainly by excitation and optical depth effects and do not readily suggest evidence of spatially varying abundances. On the other hand, at higher frequencies and increased resolution ($\sim 30''$), Wootten et al. (1982) have mapped CN in the (2–1) lines and show that it is more extended than HCN, suggesting a possible spatial variation in abundances. Their limit on the absorption column density of CN in the IR is consistent with this, and their data have been shown by Huggins et al. (1984b) to be consistent with a photochemical model in which CN is photoproduced by ambient UV photons from HCN in the outer unshielded envelope. If this proves to be correct, then tables of abundances (e.g., Table 6-2) made assuming constant abundances in the envelope obviously have little meaning.

The CO emission in IRC + 10216 is observable over a much more extended region than other species. Wannier et al. (1979) have shown that the emission is roughly circularly symmetric on a scale of $\sim 1'$; on a much smaller scale in the optical and near IR, it is not. Knapp et al. (1982) have shown that the emission extends out to a radius of at least $3'$, which corresponds to a physical radius ~ 0.25 pc for an assumed distance of 290 pc. Since photodestruction must limit the size of molecular shells (e.g., Jura and Morris, 1981; Huggins and Glassgold, 1982a; Lafont et al., 1982), the large extent of the CO emission region yields useful information on this process. Unfortunately, the photodestruction rate and dissociating transitions for CO are poorly known (cf. Glassgold et al., 1985), but Morris and Jura (1983a) have shown that the large map size is consistent with CO line self-shielding.

Finally, note that the new development of interferometry at millimeter wavebands will be useful for more detailed studies of the envelope. A first interferometer map in HCN has been made by Welch et al. (1981) at a resolution of $\sim 9''$. The emission is well resolved and circularly symmetric. Jura (1983a) has argued that the limited extent of the emission implies significant photodestruction of HCN outside a radius of $30''$ (10^{17} cm), which is consistent with the photoproduction model for CN mentioned

above. Similar maps of other species, particularly the radicals, will obviously be important in refining our picture of the envelope over the next few years.

Other Carbon Stars. In contrast to the fairly extensive observational data on the envelope of IRC + 10216, the available data on other carbon-rich envelopes is very limited. Their lines are generally much weaker because they are farther away and/or have less massive envelopes, so that most of the data are of low signal-to-noise (S/N) ratio. The observations consist of detections of CO in a fair number of objects, and detections of a few other molecules in a handful of objects. Because of the scarcity of data, we are not yet in a good position to evaluate from the observational point of view how the chemistry of the envelopes depends on parameters such as mass-loss rate, spectral type, or dust content.

Surveys in the CO (1–0) and (2–1) lines (e.g., Zuckerman et al., 1978; Knapp et al., 1982; Knapp and Morris, 1985) have detected CO emission in about 50 cool CS envelopes, and about half of these are carbon stars. Thus, carbon stars are strongly represented, but the significance of this has not yet been fully evaluated. Notable among the objects detected are the protoplanetary AFGL 2688 (Lo and Bechis, 1976; Zuckerman et al., 1976) and the planetary NGC 7027 (Mufson et al., 1975), whose central stars have presumably evolved from late-type carbon stars. In any event, their envelopes appear to be carbon rich (Zuckerman et al., 1976; Zuckerman, 1982). According to Knapp et al. (1982), the CO lines in many objects are optically thick and are therefore rather insensitive to the CO abundance in the envelope. ^{13}CO lines have also been detected in several objects (e.g., Knapp and Chang, 1985), but they tell us more about the nuclear history of the material than its chemistry.

We give two examples of those objects which have been observed in lines other than CO. In CIT 6, HCN, HC_3N, CN, SiS, C_3N, and CS have been detected (Wilson et al., 1973; Jewell and Snyder, 1982, 1984; Allen and Knapp, 1978; Henkel et al., 1985; Sahai et al., 1984), and in AFGL 2688, HCN, NH_3, HC_3N, HC_7N, SiS, CS, and C_2H have been detected (Zuckerman et al., 1976; Huggins et al., 1984a; Sahai et al., 1984; Nguyen-Q-Rieu et al., 1984b). CIT 6 (IRC + 30219) is a late-type carbon star with a mass-loss rate smaller than that of IRC + 10216 by a factor ~30 (Morris, 1980; Knapp et al., 1982). AFGL 2688, on the other hand, is an F supergiant with a mass-loss rate comparable to that of IRC + 10216 (Morris, 1980; Knapp et al., 1982). Because lower limits on the $^{12}C/^{13}C$ ratio in these objects are ~20, they may not be very different from that in IRC + 10216, where $^{12}C/^{13}C$ ~35. Henkel et al. (1985) have analyzed their line observations of CIT 6 and find no significant abundance differences (< a factor of 5) between it and IRC + 10216. Although AFGL 2688 has not been analyzed, the intensities of its molecular lines, relative to CO, are not very different from those in IRC + 10216. For these two objects, therefore, we have no strong evidence for a different chemistry. Recently, however, Beichman et al. (1983) have tentatively detected neutral atomic carbon at 610 μm in emission in AFGL 2688, but not in CIT 6 or IRC + 10216. Their observations suggest that AFGL 2688 is very carbon rich, although the effect on the envelope chemistry of the early spectral type of the central star has not been investigated in detail. Obviously, many more sensitive observations of carbon stars, other than IRC + 10216, are needed to clarify the general characteristics of the chemistry of their envelopes as a group.

M and S Stars. The list of heavy molecules detected in the expanding CS envelopes of M and S stars is limited to OH, H_2O, SiO, CO, H_2S, HCN, and NH_3. There is no equivalent to IRC + 10216, showing a rich oxygen-dominated chemistry. The overall picture of the chemistry in these envelopes is therefore very incomplete.

The most extensive observations have, of course, been made in the masing transitions of OH, H_2O, and SiO. Many of these data have been tabulated by Engels (1979), and interpreta-

tions of the masing lines in circumstellar envelopes have been reviewed by Goldreich (1980) and Eliztur (1982). As yet, these observations appear to reveal little about chemical processes as such, other than that these species are present at sufficient column densities to produce the maser gain. Further general comment, therefore, is beyond the scope of this review. However, we note that the Type II OH masers may be fairly directly linked to the chemistry of the outer envelopes. Both mapping (e.g., Bowers et al., 1983) and phase-lag measurements (e.g., Herman and Habing, 1981) show that the maser emission arises in a shell of radius $\sim 10^{16}$ to 10^{17} cm. Inside this shell in optically opaque envelopes, OH is expected to be rapidly converted to H_2O by reactions with H_2, so that the presence of the OH emission requires a source of production for the radical, as discussed by Goldreich and Scoville (1976). One possibility which they suggest is the photodestruction of H_2O by ambient galactic UV photons, and further studies of this effect have been made by Deguchi (1982) and Huggins and Glassgold (1982b). The calculated sizes of the photoproduced OH shells are consistent with the observations, but they do not rule out the possibility that the OH is primarily produced by other processes.

In addition to the masers, "thermal" millimeter emission from SiO and CO has been surveyed in a number of stars (e.g., Morris et al., 1979; Zuckerman et al., 1977, 1978; Knapp et al., 1982; Knapp and Morris, 1985). HCN emission has been detected in only two S stars (Olofsson et al., 1982b), and H_2S in only OH 231.8 + 4.2 (Ukita and Morris, 1983). CO and NH_3 have been observed in a handful of stars in absorption in the IR (Bernat et al., 1979; Bernat, 1981; McLaren and Betz, 1980), and low temperature (600 K) SiO absorption has been observed in VY CMa (Geballe et al., 1979). OH and H_2O have been detected in the IR in R Leo (Hinkle and Barnes, 1979), although these appear to be kinematically associated with the upper photosphere, or inner shell, rather than with the extended envelope. One important result from the IR CO measurements is the existence of multiple velocity components, which may indicate that the mass loss is episodic (Bernat, 1981).

Specific inferences on the chemistry, based on the observations, are few. Zuckerman (1980) notes that millimeter SiS emission is not detected, implying SiS/SiO < 1, as might be expected on the basis of simple thermodynamic freeze-out in an oxygen-rich environment. Morris et al. (1979) note that, relative to CO, the thermal SiO emission is more readily observable in M and S stars than in C stars. (SiO is not detected in C stars except for IRC + 10216.) They interpret this as an abundance effect, which again is consistent with simple ideas on the different (O or C dominated) chemistries involved. However, when the SiO emission-line data are interpreted with the radiative-transfer models of Morris and Alcock (1979), Si is found to be heavily depleted (~ 99 percent) into grains in the regions sampled by the observations. As Zuckerman (1980) points out, this is unlikely to be the case in the inner regions where the SiO masers are produced, so that the bulk of the Si is condensed into grains between $r \approx 10^{14}$ and 10^{16} cm, which is at least consistent with the overall picture determined from observations of the dust.

Finally, note that the CO (2–1) observations (Knapp et al., 1980) and the KI scattering data (see below) of α Ori have been modeled in some detail by Jura and Morris (1981). They find that the small size of the CO-emitting region requires that CO is photodissociated at a relatively high rate between 10^{16} and 10^{17} cm from the star. They also find that CO is underabundant by a factor ~ 25, relative to solar abundances fully associated, and they suggest that C is deficient by this factor in α Ori. On the other hand, CO may not be fully associated. Model analysis of the CO emission in R Cas by Morris (1980) also indicates that only 10 percent of C is in CO, assuming solar abundances. Clearly, accurate CNO photospheric abundances would be very useful in refining the interpretation of observations of the circumstellar material.

Heavy Atoms

Observations of neutral atoms and ions are potentially useful in assessing the physical conditions in CS envelopes (e.g., the degree of ionization and the degree of depletion into grains); they may also play a critical role in the buildup of molecules in the inner envelope, particularly in the presence of a warm chromosphere (e.g., Clegg et al., 1983a). It is also worth remembering that atoms and ions are the likely ultimate fate of all gas-phase circumstellar material (Huggins and Glassgold, 1982a), although they reach this state in very rarefied conditions of low column density and are difficult to detect.

A number of studies of optical circumstellar atomic lines have been made, mainly for earlier M giants and supergiants (cf. Hagen et al., 1983, and references therein; Goldberg, this volume). Lines of neutral and singly ionized metals are seen in absorption against the stellar continuum and are blue-shifted relative to photospheric lines. Analysis of the lines yields column densities, although the inner radius of the actual column observed has been a point of some controversy (see, for example, the review by Castor, 1981). Most metals observed appear to be predominantly singly ionized. According to Hagen et al. (1983), there appears to be no correlation between the quantities of circumstellar dust and atomic gas, although for the thicker envelopes of cooler stars, it is evident from the CO surveys that there is some correlation between dust and molecular gas (e.g., Knapp, 1985). In α Ori, the atomic envelope has also been observed in the scattered radiation of the KI λ 7699 resonance line. The emission has been imaged by Honeycutt et al. (1980) and Mauron et al. (1984). It extends out to a radius of at least 60″ and is roughly circularly symmetric. Honeycutt et al. infer a radial power law dependence for n(KI) of slope 1.65 $\pm$ 0.2, and Mauron et al. quote 2.5 $\pm$ 0.8; both measurements are consistent with an inverse square power law. In principle, this information could be combined with the column density measurements of α Ori to constrain detailed models of the atomic envelope, but this has not yet been done. Because atomic column densities have been measured in α Ori and several other stars with molecular envelopes, the potential exists for developing a coherent understanding of these envelopes which include all components. (See the section *Photochemistry*.)

Other Observations

Although this discussion has emphasized observations of the extended expanding envelopes, the physical structure of the transition region between the photosphere and the extended envelope can affect, and may dominate, the chemistry of the wind flow. We comment briefly on two factors: chromospheres and shocks.

At least some cool giants and supergiants possess warm chromospheres, as evidenced by atomic emission lines and radio continuum emission. (See Querci and de la Reza, this volume.) The chromospheres can influence the outer envelope in at least two ways. First, the UV emission may dominate that of the central star and produce a substantial radiation field in the extended envelope. For α Ori, for example, the UV flux has been measured, and Clegg et al. (1983a) calculated photodestruction rates for a number of molecules and neutral atoms. At 2 stellar radii, these rates are typically 10^6 faster than in the general interstellar medium, so that chromospheric radiation will dominate photoprocesses throughout much of the expanding envelope.

A second effect of chromospheres is that they will change the inner boundary conditions of the extended flow. Instead of the high densities, low temperatures, and low-ionization characteristic of photospheres, the physical conditions will be completely different and should affect the processes of molecular association. Unfortunately, as yet, the observations tell us little about the structure of the outer chromosphere and the inner wind flow.

Another complication in the transition region is the observed presence of shock waves. We briefly mention two striking examples. The first concerns the late-type carbon star, CIT 6,

which Cohen (1980) has observed over a period of a few years. (See the section *Heavy Molecules*.) During that time, an optical emission-line spectrum of H, O I, O II, N II, and S II developed and then vanished, which Cohen interpreted as a shock spectrum produced in regions in which recent stellar mass loss encountered the extended envelope. Associated changes in the continuum are attributed to thermal emission from dust grains which may have condensed from gas ejected during this phase. The second example concerns the S-type Mira variable, χ Cygni, which has been extensively monitored in the IR by Hinkle et al. (1982). They find four distinct kinematic components in the CO absorption spectrum: a pulsating photosphere, a stationary 800 K shell (which they estimate to be at 10 stellar radii), an infalling component, and an outer expanding shell. Their overall picture is one in which shock waves driven through the photosphere build up the stationary layer, which in turn is the reservoir for both the expanding shell and the infalling material. These observations are a sober reminder that the physical conditions—and thereby the chemical processes—which take place in the inner regions of circumstellar envelopes may be quite complex.

CHEMISTRY

Time-Scale Considerations

An intrinsic difficulty in the theoretical study of CS envelopes is that the material lost by the star is carried through regions with widely differing physical conditions, beginning with both high density and temperature in the photosphere and ending with rarefied cool conditions in the far outer envelope. In between, several dynamical, thermal, and chemical processes are operative which would have to be treated self-consistently in order to have a proper theory of the mass loss and the associated properties of the CS envelope. The demand that a broad range of physical phenomena be included makes the theory of the envelopes challenging as well as interesting. In fact, nothing like a comprehensive theory has been attemped thus far, in part because we do not understand enough about such fundamental problems as the mechanisms for mass loss and the formation of dust. Nevertheless, some useful first steps have been made by investigating simple but general models, such as the thermal equilibrium and the photochemical models discussed below.

At this early stage in the theoretical study of CS chemistry, it has been customary to make several simplifying assumptions which serve to isolate the chemistry from other problems. In particular, one or more of the following distributions are specified a priori: density, velocity, temperature, and dust. For example, in the following, the discussion is restricted to spherically symmetric and steady flows, with the gas density following an inverse square law at large distances, as described by Equation (6-1). Likewise, with a few notable exceptions, dust and temperature profiles have been specified rather than calculated consistently together with the chemistry. Whenever possible, these distributions are based on observational information, which is rather limited at this stage.

The chemistry of CS envelopes is basically time-dependent; this follows from their small size (< 1 pc). Most chemical time scales will become larger than the dynamical time scale somewhere in the shell. We use the following definition for the dynamical time scale (always measured in seconds),

$$\tau_{dy} = r/v = 1 \times 10^9 \left(\frac{r_{15}}{v_6}\right), \qquad (6\text{-}4)$$

where r and v are measured in units of 10^{15} cm and 10^6 cm s^{-1}. For typical inner and outer radii of 10^{15} and 10^{17} cm and an expansion velocity of 10 km s^{-1}, the dynamical time scale ranges from 10^9 to 10^{11} s, or 30 to 3000 yr.

A qualitative understanding of the time-dependent nature of CS chemistry is aided by classifying reactions as one-body, two-body,

three-body, etc., according to the number p of reactants. Important examples for CS shells are:

1. Photo processes—For example,

$$h\nu + CO \rightarrow C + O \qquad (G)$$

2. Ordinary chemical reactions—For example,

$$H + OH \rightarrow O + H_2 \qquad (k)$$

$$e + H^+ \rightarrow H + h\nu \qquad (\alpha)$$

3. Three-body reactions—For example,

$$H + H + H \rightarrow H_2 + H \qquad (K)$$

$$e + e + H^+ \rightarrow e + H \qquad (\gamma)$$

The symbols in parentheses are generic rate constants. This classification is significant because the various types have very different rate constants and time scales. If we use:

$$\tau_{ch}(X) = n(X)/\frac{dn(X)}{dt}$$

as the definition of the chemical time scale for species X, $\tau_{ch}(X)$ will be proportional to $r^{2(p-1)}$. To illustrate, some examples are:

1. Photo time scale:

$$\tau_{ph} = \left[G_{IS} J(r) + G_0 K(r) \left(\frac{R_0}{r} \right)^2 \right]^{-1}. \qquad (6\text{-}5)$$

Here, G_{IS} is the asymptotic rate at the outside of the shell due to interstellar radiation, $J(r)$ is the shell attenuation factor to be discussed in the section *Photochemistry*, G_0 specifies the rate due to stellar or CS (e.g., chromospheric) radiation specified at some nominal distance R_0, and $K(r)$ gives corrections to the inverse square dilution factor, including attenuation by the shell. A characteristic value for G_{IS} is 1×10^{-10} s^{-1}, so that photodestruction times in the farthest outer envelope are of the order of 100 yr. α Ori is an example of a star with a strong UV field, and G_0 is about $10^6 \times G_{IS}$ at $R_0 = 1(14)$ cm; thus, photodestruction by chromospheric radiation dominates its CS shell out to $> 3 \times 10^{17}$ cm.

2. Two-body chemical time scale:

$$\tau_{ch} = 333\, r_{15}^2\, e^{T^*/T}\, \frac{\dot{M}_{-5}}{V_6} \times \begin{cases} 1/x' \text{ for destruction,} \\ x/x'x'' \text{ for formation.} \end{cases} \qquad (6\text{-}6)$$

The reactant abundances have been denoted by x, x', and x'', with x for the species whose time scale is of interest and x' and x'' for other species. The rate constant for the exothermic direction has been written as $k = A \exp(-T^*/T)$, where the preexponential factor usually depends weakly on temperature T. The numerical value used in Equation (6-6), $A = 4 \times 10^{-11}$ cm^3 s^{-1}, is for a relatively fast neutral reaction. There are three critical factors in this formula:

a. Expansion of the shell—The r^2 effect alone boosts the numerical factor to 25 yr at 3×10^{17} cm.

b. Activation energy—If T^* is large, the exponential makes the chemical time scale much larger than all others in the cool outer envelope (i.e., exothermic reactions with large activation energies are readily frozen out). Clearly, endothermic reactions will also be frozen out when T becomes much less than

G/K_B, where G is the free energy of the reaction.

c. Abundances—The factors $1/x'$ for destruction and $x/x'x''$ for production can also increase the time scale significantly.

Despite these obstacles, the moderately high temperatures in the dense inner regions of CS envelopes provide conditions for chemical activity which are not found in cool molecular clouds.

3. Three-body time scale:
As examples, we give the time scales for the recombination of three H atoms:

$$\tau(H_2) = 8.3 \times 10^{13}\ \mathrm{s}\ T^{3/4}\ r_{15}^4 \left(\frac{V_6^2}{\dot{M}_{-5}^2}\right), \quad (6\text{-}7)$$

and the time scale for three-body recombination of H^+ with two electrons:

$$\tau(H^+) \cong 10^{12}\ \mathrm{s}\ \frac{T r_{15}^2}{x_e^2} \left(\frac{V_6^2}{\dot{M}_{-5}^2}\right). \quad (6\text{-}8)$$

The additional factor of r^2 means that three-body reactions are only important close to the star.

The implications of the above time-scale estimates will be discussed below in the context of specific models and objects. In general, they span a large range of values, depending on the abundances and the activation energies entering into individual reactions. At this stage, it is sufficient to note, for example, that the chemical time scales will be longer than the dynamical time scales at large distances, and that photo time scales can dominate in different parts of the envelope, depending on the radiation source (stellar or interstellar) and dilution and attenuation effects. Therefore, the chemistry of CS envelopes is essentially kinetic in character, rather than steady state.

Thermal Equilibrium Models

Thermal equilibrium represents the simplest of all models because the results depend only on temperature, pressure, and elemental abundances—and not at all on the specifics of reaction mechanisms. Underlying the model is the assumption that the conditions for equilibrium are met (i.e., that all the relevant reactions are in detailed balance). Although these conditions may be expected to be satisfied inside the star, they will eventually fail as the temperature and density decrease going away from the star.

As we have seen in the section *Time-Scale Considerations*, $\tau_{ch} \ll \tau_{dy}$ for small r and $\tau_{ch} \gg \tau_{dy}$ for large r. Thus, a freeze-out position R_{FO} can be defined by the condition that $\tau_{ch} = \tau_{dy}$; R_{FO} depends sensitively on species. Less reactive species (e.g., H_2 and CO) may freeze out close to the star, whereas radicals may not freeze out until well into the envelope. Most applications of the thermal equilibirum model have been based on the premise that a *single* freeze-out location applies to all species, in contrast to the more realistic situation in which each species freezes out at a different place.

A basic limitation in applying the thermal equilibrium model is the quality of the thermochemical data. For IRC + 10216, for example, the data required to calculate the abundances for the most complicated and exotic species do not exist.

Early comparisons of observations of CS molecules in IRC + 10216 with thermal equilibrium calculations were made by Morris (1975), Ridgway et al. (1976), and Hall and Ridgway (1978). The last authors, for example, found that the relative column densities of CO, C_2H_2, HCN and CH_4 could be accounted for by a C-rich supergiant atmosphere with $T \cong 1000$ K and $n \cong 1 \times 10^{14}$ cm^{-3}. A more comprehensive application of the model to this same object was made by McCabe et al. (1979),

who did equilibrium calculations both with and without graphite formation. These authors compiled abundances of a dozen CS molecules and radicals from available observations, and they attempted to find a single set of temperature and pressure values which would give the best agreement between the thermal equilibrium model and the observations. Their best-fit parameters were $T \cong 1250$ K and $n \cong 4 \times 10^{14}$ cm^{-3} and required the omission of dust formation. They obtained a factor of 2 to 5 agreement for eight molecules (relative to CO), but four others were in serious disagreement (3 to 6 orders of magnitude): CN and NH_3 were observed to be greatly overabundant, and SiO and SiS were greatly underabundant. The very large pressure adopted for the upper atmosphere of IRC + 10216 seems to be inconsistent with our present understanding of the upper atmospheres of cool stars.

Thermal equilibrium calculations for IRC + 10216 have been repeated by Lafont et al. (1982), with improved estimates of abundances and thermochemical data. They used a broader criterion for agreement (a factor of 10), consistent with the large uncertainties in these quantities, and they worked with lower pressures. However, their overall results are similar to those of McCabe et al. (1979). Figure 6-1 gives an example of their results for C/O = 2.

We can summarize the equilibrium model for IRC + 10216 using the rough abundances given in Table 6-1 and the equilibrium calculations discussed above:

1. The simplest C,N,O molecules and hydrocarbons:

   a. The model works well for CO, C_2H_2, HCN, and CH_4.

   b. The model fails for NH_3, which is observed to be overabundant by a large factor.

2. Sulfur and silicon molecules:

   a. CS is somewhat overabundant.

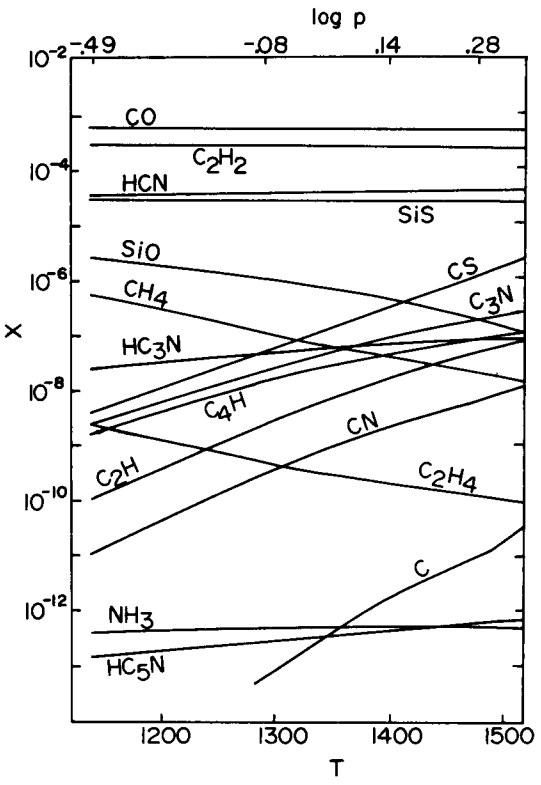


Figure 6.1. Thermal equilibrium abundances calculated for the envelope of IRC + 10216 by Lafont et al. (1982) assuming C/O = 2.

   b. SiS and SiO are underabundant by very large factors.

3. Chain molecules:

   a. HC_3N agreement is satisfactory, but HC_5N is grossly overabundant.

   b. The thermochemical data base is too weak to make definitive conclusions on the other cyanopolyyenes and related species.

4. Radicals:

   a. All radicals are overabundant by large factors.

   b. The worst cases are CN and C_2H.

C - 5

Another way of stating item 4 is that the ratios of radicals to parent molecules (i.e., CN/HCN, C_2H/C_2H_2, and C_3H/HC_3N) are much larger than expected on the basis of thermal equilibrium; this suggests that the radicals are made by some process directly from their parents. In conclusion, we find that the simple thermal equilibrium model (unique choices for T and p) is consistent with the measured abundances of only the few most abundant molecules.

Even the limited successes of the thermal equilibrium model must be viewed with some skepticism as long as dust formation has been omitted from the calculations. Although the most abundant molecules may be frozen out in the upper atmosphere, as suggested by the above fits, some of them may participate in the formation of dust. Otherwise, it is unlikely that the envelopes would be as dusty as they are. Certainly, the time scale for a gas molecule to strike a dust grain, Equation (6-10) below, is less than the dynamical time scale in the relevant regions, roughly from 10^{14} to 10^{15} cm. As our knowledge of the thermochemical quantities improves, it would be of interest to develop the equilibrium model further to include the formation of dust, as well as more complicated molecules.

The distribution of atomic and molecular hydrogen in the upper atmospheres of cool stars can be studied in detail because the relevant reactions are limited and are fairly well understood (Glassgold and Huggins, 1983). As discussed in the section *Observations*, molecular hydrogen has been detected in very cool stars, but all attempts to detect the 21-cm line of atomic hydrogen have been unsuccessful thus far. Molecular hydrogen is a good example of a molecule which freezes out close to the photosphere. Figure 6-2 shows the fraction of atomic hydrogen obtained from equilibrium calculations in which T and p profiles were specified by model atmosphere calculations (Johnson et al., 1975; Lucy, 1976; the latter having an expanding wind). The variation in the physical conditions in the upper stellar atmosphere changes the H/H_2 ratio by large amounts. The open circles in the figure indicate where freeze-out of three-body recombination occurs according to the time-scale estimate (Equation (6-7)). This freeze-out ratio provides the initial condition for calculating any changes which the hydrogen undergoes in the CS shell, as will be discussed in the following sections.

Studies of Chemical Reactions

In this section, we discuss the reactions appropriate for describing the chemical evolution of CS wind material. We consider regions in which the formation of dust has essentially ceased, but do not completely ignore the chemical activity associated with dust. Photoprocesses will be discussed in the next section. It is useful to divide the discussion of CS chemistry according to whether the environment is carbon- or oxygen-rich, and we begin with O-rich stars.

Goldreich and Scoville (1976) solved the time-dependent equations for the H_2O and OH system, using only the following reactions:

$$OH + H \rightleftharpoons H_2O + H \ ,$$

$$OH + H \rightleftharpoons O + H_2 \ .$$

They considered a 1 $M_\odot$ star with a mass-loss rate of $3 \times 10^{-5}\ M_\odot\ \mathrm{yr}^{-1}$ and a terminal velocity of 20 km s^{-1}. They found that these reactions maintained equilibrium abundances out to 2×10^{15} cm, (where $T = 500$ K and $n = 1 \times 10^7$ cm), beyond which they are frozen. Scalo and Slavsky (1980) made similar calculations without including shielding, but extending the chemistry to include silicon, and generally underscored the importance of time-dependent chemistry. These authors have recently completed a comprehensive study of the chemistry of O-rich CS envelopes (Slavsky and Scalo, 1984).

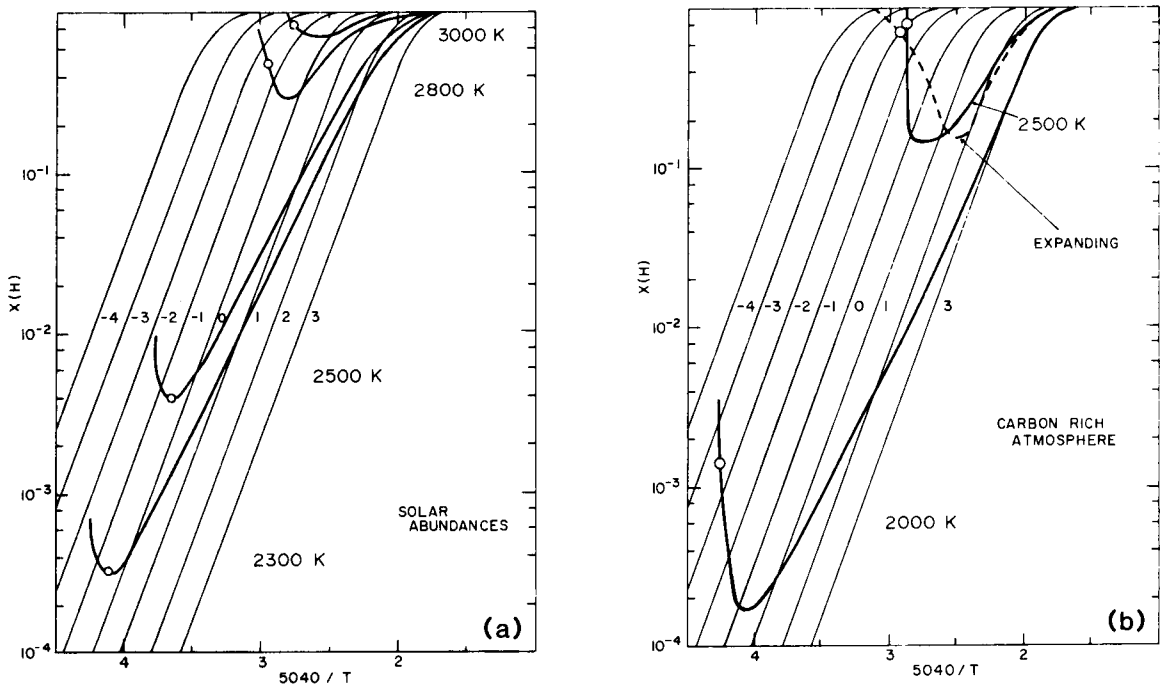


Figure 6-2. Thermal equilibrium abundance of atomic hydrogen calculated by Glassgold and Huggins (1983) for the atmospheres of (a) O-rich and (b) C-rich stars for several photospheric temperatures. The heavy lines trace the variation starting from the photosphere in the upper right; the open circles show where freeze-out occurs. The other curves are isobars labeled by log p.

A similar position was taken by Jameson and Williams (1981), who solved a restricted system of rate equations appropriate for the study of interstellar carbon and oxygen chemistry: molecules are formed by ion-molecule reactions (H^- for H_2), radiative association, and neutral reactions and are destroyed by ion-molecule reactions; the ions are produced by cosmic rays. The initial condition was that all species were dissociated and ionized; solar abundances were assumed. Jameson and Williams showed that this plasma quickly recombined and that substantial molecular synthesis occurred before freeze-out, depending on the initial density. Rather different abundances would have been obtained if the initial conditions had been appropriate for cool stars. On the other hand, such plasma might result from chromospheric conditions.

Clegg et al. (1983a) extended the chemical analysis of Scalo and Slavsky (1980) by including the H-H_2 and the C^+-C-CO systems, as well as by incorporating reactions to describe the oxygen and silicon compounds expected for O-rich envelopes. They used the density profile for an expanding wind and carried out steady-state calculations for a particular temperature profile: $T = 1000$ K for r in the range 2 to 5 R_*, and decreasing as $1/r$ for r in the range 5 to 30 R_* (the calculation is cut off at this point); dust formation is ignored. Solar abundances are used, and although the results are intended to apply to a variety of O-rich envelopes, α Ori is used as an example with $R_* = 7 \times 10^{13}$ cm, $\dot{M} = 2 \times 10^{-6} M_\odot$ yr^{-1}, and $v = 1$ km s^{-1}. Most important, Clegg et al. calculate the rates for photoionization and photodissociation by the chromospheric UV radiation field of α Ori for H^-, the heavy elements Mg, S, Na, and Ca, and oxygen- and silicon-bearing molecules. The rates are typically 10^6 larger than those familiar from the interstellar medium, and these large values are confirmed by independent calculations by Bernat (1976)

and ourselves. Such strong photodestruction greatly inhibits molecule formation, although it still occurs at a reduced level. Of course, stars without strong chromospheres will have shells which are more conducive to the formation of molecules. In the presence of a strong radiation field, the temperature profile adopted by Clegg et al. is inappropriate (i.e., chromospheric temperatures are considerably larger than 1000 K). Finally, Clegg et al. find that the use of steady abundances is justified in many cases, but an important exception is the H-H_2 system.

One of the most important questions relating to the silicon chemistry is the rather low abundance of SiO deduced from nonmaser microwave emission, as discussed in the section *Heavy Molecules*. Scalo and Slavsky (1980) suggested that destruction by chromospheric UV radiation might be an alternative to the more obvious explanation that the silicon is mainly condensed into dust. They assumed that silicon entered the CS shell of α Ori in the form of atoms, and then showed that relatively little SiO was formed by reactions with OH (produced by photodissociation of H_2O). The work of Clegg et al. (1983a) supports this, and they calculate correctly that the appropriate form for most of the gaseous silicon is Si^+. Practically nothing is known about the photodissociation of SiO, and Clegg et al. estimate that the rate is the same as that of CO (which is not well understood either). The conclusion that stars with chromospheres have low SiO abundances is fairly independent of this rate; moreover, it could be tested by observations to detect chromospheric activity.

No solutions are available for systems of chemical reactions appropriate to C-rich stars. It is generally accepted, on the basis of comparing the chemical and dynamical time scales (Equations (6-4) and (6-6)), that fast reactions with small activation energies can operate far out in the shells. Certainly radicals, which are either emitted by the star or produced by photodissociation, will participate in such chemical activity—and this holds for O-rich and C-rich shells. A general survey of chemical processes in C-rich stars has been given by Lafont et al. (1982). They pointed out that chemical reactions with radicals R of the type:

$$R + C_{2n}H_2 \rightarrow RC_{2n}H + H \ , \qquad (6\text{-}9)$$

which have recently been discussed in the context of Titan's atmosphere (Allen et al., 1980), may also be relevant for CS chemistry. The measured rate constant in the case of $R = C_2H$ and $n = 1$ (acetylene) is large ($k = 3 \times 10^{-11}$ cm^3 s^{-1}), and the activation energy is probably small. Reactions of this type provide the means for synthesizing acetylene and cyanoacetylene chains. For example, the following reactions could produce HC_3N:

$$C_2H + HCN \rightarrow HC_3N + H \ ,$$

$$CN + C_2H_2 \rightarrow HC_3N + H \ .$$

Although we are not aware of any measurement of the first reaction, the rate for the reaction of CN with acetylene into all possible channels has been measured to be 5×10^{-11} cm^3 s^{-1} (Schacke et al., 1977); branching to C_3N is likely.

We have also analyzed some of the reactions that might be operative in C-rich CS envelopes. The ion $C_2H_2^+$, produced by photoionization of acetylene, may be an important progenitor of ion-molecule hydrocarbon reactions which lead to chain molecules. Two examples of reactions in which the measured rate constants are large are:

$$C_2H_2^+ + C_2H_2 \rightarrow C_4H_2^+ + H_2 \ ,$$
$$k = 5 \times 10^{-10} \text{ cm}^3 \text{ s}^{-1} \ ,$$

$$C_2H_2^+ + HCN \rightarrow H_2C_3N^+ + H \ ,$$
$$k = 1.2 \times 10^{-10} \text{ cm}^3 \text{ s}^{-1} \ .$$

These reactions lead to C_4H and HC_3N by dissociative recombination of the ions with electrons. Thus, there are promising leads to investigate, but their analysis may not be simple.

First of all, important gaps exist in our information on rates for chemical reactions. Second, many species must be considered simultaneously, and the reaction network must include a good theory of the ionization of the shell. Finally, the chemistry must be formulated in terms of differential equations in order to follow the intrinsic time dependence of the chemistry.

Until now, we have focused on reactions in the gas phase. Even in regions in which the formation of dust has essentially ceased, the dust could be chemically active. Furthermore, there may be no sharp demarcation between regions with and without dust formation. In grain chemistry, the shortest time scale is that for collisions of atoms and molecules with dust particles, using the geometric cross section. We make a rough estimate using the properties of interstellar dust as determined from extinction studies and measuring grain cross sections in units of 10^{-21} cm^2 (the column density 2×10^{21} cm^{-2} for one magnitude of visible extinction corresponds to a cross section of 0.5×10^{-21} cm^2):

$$\tau_{gr} \simeq 3.3 \times 10^7 \, r_{15}^2 \, (U/\dot{M}_{-5} \, \sigma_{gr-21}) \ , \quad (6\text{-}10)$$

where U is the ratio of the gas expansion velocity to the gas/grain relative (or drift) velocity. For sufficiently large mass-loss rate, grain area, and relative velocity, this time scale can be smaller than the dynamical time scale in the inner part of a CS dust shell. On the other hand, Equation (6-10) indicates that any grain chemistry will freeze out in the outer envelope. (This discussion completely omits the difficult questions of the probabilities for sticking and subsequent chemical activity, whose consideration would certainly lead to time scales longer than those given by Equation (6-10).)

The collision of the gas and dust can lead to both the formation and the destruction of molecules and to the incorporation of gaseous species into the dust particles. Little is known about these processes in general, but it is almost certain that they are specific to the dust surface and incident species. Lafont et al. (1982) believe that the most likely grain reaction is the production of CH_4 and C_2H_4 following the sticking of H atoms. They also suggest that radicals such as CN and C_2H are almost certain to react on striking a dust grain. A large fraction of these particular radicals may be produced, however, by photodissociation farther out in the shell where the probability for hitting a grain is negligible.

Glassgold and Huggins (1983) discussed the possibility that the warm grains in the inner envelope catalyze the formation of H_2 following H chemisorption, whereas Lafont et al. (1982) consider it very unlikely that any strongly bound molecule can be synthesized on CS grains. In view of our ignorance about almost all physical and chemical properties of CS grains, the question of catalysis in the inner part of the envelope (but after the dust has already been formed) must be left open.

We conclude this discussion of chemical reactions with some remarks on shocks. Shock phenomena are common in the interstellar medium because there are many ways to generate supersonic velocities (e.g., supernova remnants, winds from young stellar objects, collisions between clouds, etc.). The shocks are important for the transfer of energy and momentum and for the emissivity and chemical composition of the interstellar gas. (See the reviews by McKee and Hollenbach, 1980; and Hollenbach, 1982.) If shocks are present in CS shells, they may play important analogous roles in affecting the physical properties of these envelopes.

Shocks in CS shells have been discussed primarily in the context of the origin of the mass loss (e.g., Willson, 1976; Willson and Hill, 1979; Wood, 1979). In these calculations, stellar pulsations drive shocks into the atmosphere, which leads to mass loss. The observational evidence for shocks in χ Cygni obtained by Hinkle et al. (1982) supports this general picture. However, there have been no theoretical studies of the thermal and chemical effects of shocks propagating through CS envelopes. Judging from the theory of interstellar shocks, we might

expect that the resulting enhancements in density and temperature would promote both chemical activity and the excitation of characteristic line radiation—potentially useful for diagnostic purposes. Very likely the ratio of radicals to parent molecules would be enhanced. The detailed predictions should depend on the velocity of the shock and on the density of the ambient shell (i.e., on mass-loss rate). Calculations of shocks in CS shells should prove to be quite illuminating.

Photochemistry

Photodestruction is important because it significantly affects the chemical composition of the CS wind. The radiation may be either external (e.g., the interstellar radiation field) or from the star itself. Most of this section will deal with the first situation; some effects of chromospheric radiation have already been mentioned in the foregoing section, *Studies of Chemical Reactions*.

The photodestruction process for a species in an expanding wind can be characterized by two parameters, the mean distance it travels (ignoring absorption) before being destroyed by radiation, $V\tau_{ph}$, and the absorption length, d. The simplest case is the ambient interstellar radiation field, where $\tau_{ph} = 1/G_{IS}$. Because G_{IS} ranges from 10^{-11} to 10^{-9} s^{-1}, molecules which are easily destroyed by radiation would survive only to 10^{15} cm in an unshielded shell, whereas molecules which are difficult to destroy would survive out to $\sim 10^{17}$ cm. The radial dependence of the abundance is $\exp(-rG_{IS}/V)$, but when shielding is present, the molecules survive longer and the radial dependence for thick shells becomes $\exp(-d/r)$. The shielding distance, d, depends on the molecule in question because the cross sections for dissociation and absorption are sensitive functions of wavelength.

These qualitative considerations have been investigated by solving rate equations appropriate for an expanding envelope. For a species, X, with abundance relative to the total density of hydrogen $x = n(X)/n$, the equation in a comoving frame is:

$$\frac{\partial}{\partial t} x = -G(r(t))x + P(r(t)) \quad , \qquad (6\text{-}11)$$

where $r(t)$ locates a fluid element at time t (i.e., $\dot{r}(t) = v(r(t))$ where $v(r)$ is the specified velocity profile), and G and P are destruction and production rates. The simplest example is the solution for the case P = 0 and destruction by interstellar radiation is shielded exponentially. That is,

$$G(r) = J(r)G_{IS} \quad , \qquad (6\text{-}12)$$

$$J(r) = \exp(-d/r) \quad . \qquad (6\text{-}13)$$

The exact solution (Huggins and Glassgold, 1982a) for constant $v = V$ is:

$$x(r) = x_0 \left[\exp -(rG_{IS}/V)\, E_2\, (d/r)\right] \quad , \qquad (6\text{-}14)$$

where E_2 is a standard exponential integral. It has also been possible to obtain an exact solution for a "photodissociation chain," at which the products of photodissociation are themselves destroyed by radiation (e.g., $C_2H_2 \rightarrow C_2H \rightarrow C_2 \rightarrow C \rightarrow C^+$); Figure 6-3 shows this chain as calculated for IRC + 10216. The solution (Equation (6-14)) was obtained independently by Jura and Morris (1981), using a different technique.

From the above discussion, we see that the radial distributions of progenitor and fragment species are determined by the "free" photodissociation rates for a given radiation field, such as the mean interstellar field, and by the optical properties of CS material at wavelengths at which the CS species are destroyed by radiation. It is therefore important to discuss how well these quantities are known before applying the photochemical model to observations of CS shells.

Reasonably good information is available on the photodissociation cross sections for the

most stable molecules injected into CS envelopes (e.g., H_2O, C_2H_2, HCN, and CH_4); two notable exceptions are CO and SiO. Improved far-UV absorption cross sections have recently become available for CO through the use of synchrotron radiation sources, and it seems likely that, with new instrumentation, better information on the photodissociation process will become available in the next few years. Of course, much less is known about radicals, but here the level of theoretical effort has been increasing. It should be noted that great accuracy is not required in considerations of CS photochemistry, especially for the products of molecular breakup. Certainly, at this stage we have the essential information, which is the relative values of the important rates. Thus, our position is that the unshielded rates can be considered as known relative to other uncertainties in the problem.

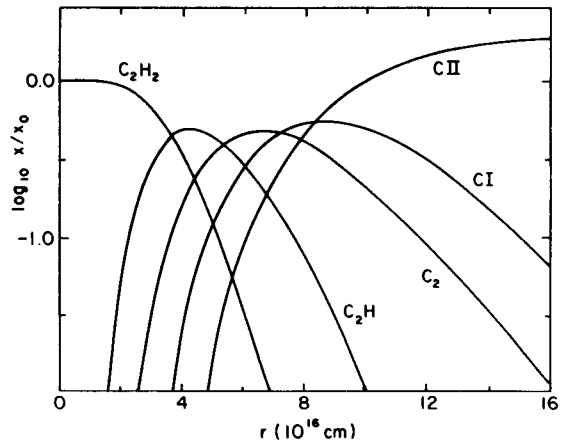


Figure 6.3. The C_2H_2 photodestruction chain calculated for envelope parameters typical of IRC + 10216 (Huggins and Glassgold, 1982a).

The situation with regard to the optical properties of CS material is just the opposite. Here, dust grains play an important role, and we know essentially nothing about the far-UV extinction and albedo of CS dust. For certain species (e.g., CO, C, and S), the wavelength region below 1100 Å is critical. We conclude that determining the optical properties of the CS dust becomes one of the objectives of studying the spatial distribution of the molecules. In order to progress, we must begin with some model for the dust, and our initial choice has been to assume that the CS dust has the same optical properties as interstellar dust. The status of this first-order assumption will be discussed below in the context of IRC + 10216 (see also Lefèvre, this volume, and Sopka et al., 1985).

The far-UV radiation is absorbed in the envelope by atoms and molecules with large absorption cross sections and abundances (i.e., H_2, C, CO (and H_2O for O-rich shells)), as well as by dust. Although a detailed discussion of these shielding problems would be inappropriate here, they do have a quantitative effect on molecular distributions, as will be discussed below for the case of CO.

When the optical properties and spatial distribution of all the absorbers have been specified, the attenuation factor in Equation (6-12) must be calculated by solving the equation of transfer. At this stage, it is appropriate to use approximate solutions (e.g., the closed forms given by Gerola and Glassgold, 1978). If dust attenuation dominates, this approximation reduces to the simple exponential form, Equation (6-13), for thick shells with the shielding length given by

$$d = C/N_{sh} \ . \qquad (6\text{-}15)$$

Here N_{sh} is the column density of hydrogen which produces unit optical depth (assuming the same dust-to-gas ratio as the interstellar medium), and C is the parameter which specified the density in Equation (6-2). This length depends on species; for CO, $d = 6 \times 10^{16}$ cm $\dot{M}_{-5}/V_6$.

The case of CO deserves special mention. First, recall that dust can provide substantial shielding of CO. Using Equations (6-13) and (6-15), we can express the attenuation factor as:

$$J(r) = \exp\,[-N_{sh}/N(r)] \ , \qquad (6\text{-}16)$$

where the outside column density, $N(r) = C/r$, is measured from infinity to position r; in this

case, $N_{sh} = 5 \times 10^{20}$ cm^{-2}. There are two kinds of self-shielding to consider, depending on whether CO photodissociation proceeds by way of line absorption followed by breakup or whether it is directly dissociated with a smoothly varying cross section. Until recently, continuum dissociation was believed to dominate, in which case Equation (6-16) would still apply, but N_{sh} would be replaced by a constant times N(CO), the column density of CO. This has the effect of steepening the rise in the CO abundance going into the envelope, because x(CO) is proportional to $1/J$. We also see that self-shielding introduces a nonlinearity into the calculation of the abundance of CO. If CO photodissociation is basically a line process, which seems likely (Glassgold et al., 1985), then the CO abundance curve is changed for the cross section, assumes larger values than in the continuum case, and the radiation transport is modified. Figure 6-4 (from Morris and Jura, 1983a) shows how the different kinds of shielding operate on the CO density profile for IRC + 10216. Curves *C* and *N* refer to no dissociation (constant abundance) and no shielding, respectively; the intermediate cases are *D* for dust only and $n = 2, 5$, and 10 lines producing self-shielding. Morris and Jura suggested that the large spatial extent of CO in IRC + 10216 might be explained by line self-shielding.

In the recent calculations with the photochemical model, recombination of ions has been included, as well as photoprocesses. For example, C^+ is the eventual dominant form of carbon toward the outside of the shell, just as in the interstellar medium. In order to obtain a quantitatively correct treatment of the transition from C to C^+ and to obtain the proper asymptotic C/C^+ ratio, recombination must be included. The other situation in which recombination is important is that in which molecular ions are produced by photoionization (i.e., both $C_2H_2^+$ and C_2H are obtained when UV photons are absorbed by acetylene). In such cases, dissociative recombination into various radicals occurs rapidly, and it is sufficient to reexpress this sequence in terms of renormalized photo rates (Huggins and Glassgold, 1982a).

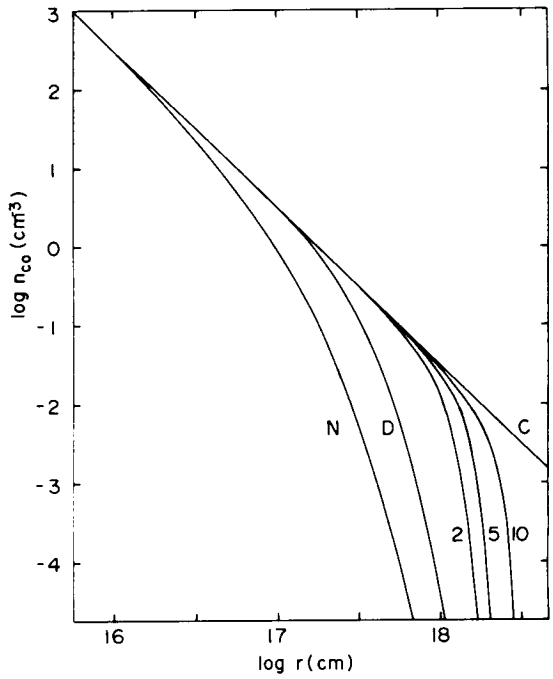


Figure 6-4. The effect of shielding on the CO density in the envelope of IRC + 10216 (Morris and Jura, 1983a). Curves C and N refer to no dissociation (constant abundance) and no shielding, respectively; the intermediate cases are D for dust only and n = 2,5,10 lines producing self-shielding.

The photodestruction of molecular hydrogen in CS envelopes has been discussed by Zuckerman et al. (1980) and Morris and Jura (1983a), as well as by Glassgold and Huggins (1983), whose treatment we follow here. As discussed in the sections *Thermal Equilibrium Models* and *Studies of Chemical Reactions*, the chemical evolution of the H/H_2 ratio can be traced from the photosphere to the outer envelope. If there is no warm grain formation of H_2 in the inner envelope, this ratio is determined by freeze-out in the upper atmosphere of the star. Present stellar atmospheres suggest that, for stars with $T_* > 2500$ K, the frozen outflowing hydrogen will be mainly atomic. For cooler stars, the question then becomes how much of the atomic H in the outer envelope is due to the low level initially frozen out and how much arises from that photodissociation. A

small amount of H is also produced by the photodestruction of the most abundant hydrocarbons in C-rich envelopes (Lafont et al., 1982) and from H_2O for O-rich shells.

The radial distribution of H has been derived from a time-dependent theory of H_2 photodissociation (by way of the Lyman band lines) appropriate for an expanding shell with dust. In the interior of the shell, the solution is similiar to that given for heavy molecules in Equation (6-14). That is,

$$f(r) = f(R_0) \times \exp\left(-a[E_{3/2}(d/r) - E_{3/2}(d/R)]\right), \quad (6\text{-}17)$$

where $a = (d\, G_{IS}(H_2)/V)\,[dM/C]^{1/2}$ and $M = 6.7 \times 10^{11}$ cm^{-2}. For $r \gg d$, the exponential in Equation (6-16) varies as $r^{3/2}$. At the edge of the shell, there is a very sharp transition to complete dissociation. The spatial distribution of atomic H is illustrated in Figure 6-5, for which the initial value was assumed to be zero.

We complete this discussion of CS photochemistry with some examples. We first consider the heavy molecules in the C-rich envelope, IRC + 10216. We begin with the idea that IRC + 10216 has no strong internal source of UV radiation, or if it does, it is well shielded from the bulk of the envelope. We use observations to specify the most abundant species entering the outer envelope and consider how they are altered by photoprocesses initiated by UV radiation penetrating from the outside. The remaining species will be similarly modified, but other chemical processes will also be important in these cases.

We consider those radicals (e.g., CN and C_2H) whose observed abundances are not reduced much from their likely progenitors (HCN and C_2H_2, respectively). Because both progenitors are observed to be abundant in the inner envelope (from IR absorption measurements), it is natural to investigate whether the radicals can be the result of photoproduction. This question can be pursued in some detail for the HCN–CN system because both species have been well observed in IRC + 10216. For C_2H_2 and C_2H, the data are less extensive, and additional processes (e.g. reactions involving $C_2H_2^+$ as mentioned in the section *Studies of Chemical Reactions*) may be operative.

The photochemical model has been applied to IRC + 10216 by a number of authors, including Wootten et al. (1982) and Jura (1983a) in the context of the HCN–CN problem and by Huggins et al. (1984b) for both the CN and C_2H problems. Figure 6-6 shows the CN N = 1–0 and N = 2–1 line shapes for the Kitt Peak (66″) and Owens Valley (30″) beams, as calculated by the last authors. The symbol C indicates calculations for the best fit to the 1–0 peak line intensity observed with the Kitt Peak beam, using a *constant* abundance of 1.3(–6). Curves with S are based on the photochemical model and thus have variable HCN and CN abundances; S stands for standard (interstellar) dust, whereas S/3 and SX3 stand for dust which gives three times less and three times more extinction. Equally acceptable fits to the 1–0 data can be obtained with both the constant and photoproduction models, but the constant abundance model fails to fit the roughly flat-topped 2 K line observed at Owens Valley. The 70″ map size observed at Owens Valley cannot be explained by a constant abundance, but a variable abundance model with an opacity 1 to 3 times standard agrees with all of the measurements.

A similar conclusion about the dust in IRC + 10216 was reached by Jura (1983a) by applying the photochemical model to the spatial distribution of HCN as measured by Olofsson et al. (1982a) and Welch et al. (1981). Thus, the observed properties of the HCN–CN system in IRC + 10216 are consistent with the photochemical model. The more limited information on C_2H can be reproduced by either a constant or variable abundance model. The above discussion suggests that important information can be obtained about CS dust by detailed fitting with the photochemical model. High-resolution studies of CS shells are also seen to be required to provide useful comparisons.

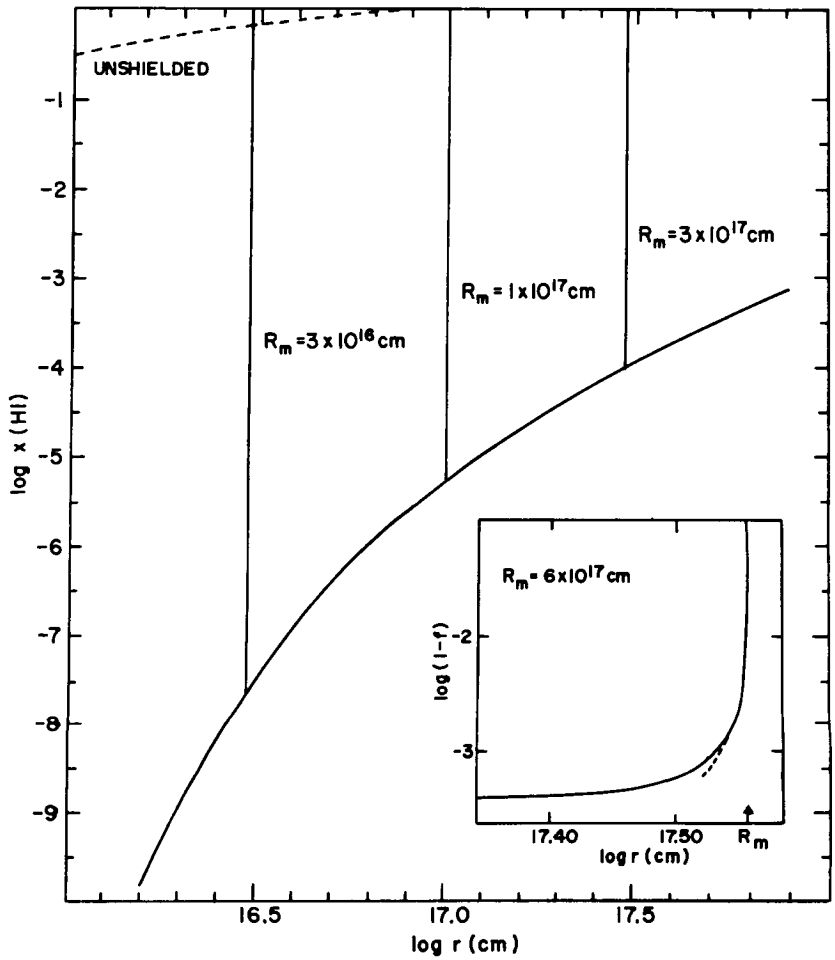


Figure 6-5. The amount of atomic hydrogen produced by the photodissociation of molecular hydrogen from the calculations of Glassgold and Huggins (1983). Three different stages of the evolution of an envelope are shown: t = 600, 1800, and 6000 yr or outer radii R_m = 0.3, 1.0, and 3.0 × 10^{17} cm. The parmeters have been chosen to correspond to IRC + 10216. The H I abundance at each stage consists of the heavy solid curve for r < R_m plus the vertical line at r = R_m. The insert shows that the transition to x(H I) = 1 at R_m is not discontinuous.

We conclude this discussion of IRC + 10216 with some brief remarks on atomic and molecular hydrogen. Molecular hydrogen has been detected by IR absorption in several very cool stars, but not in IRC + 10216. The observations are consistent with the conclusions of the discussion in the section *Thermal Equilibrium Models*, based on the variation of the H/H_2 ratio in the upper atmospheres of cool stars. A more definitive conclusion requires the calculation of the absorption-line profiles, and not just the abundances. Johnson et al. (1983) have suggested that H_2 has not been observed in some stars with effective temperatures somewhat above 2500 K because they may have chromospheres.

The fact that the 21-cm line has not yet been detected in CS shells is probably consistent with currently available sensitivity. In IRC + 10216, the upper limit in the column density of 6 ×

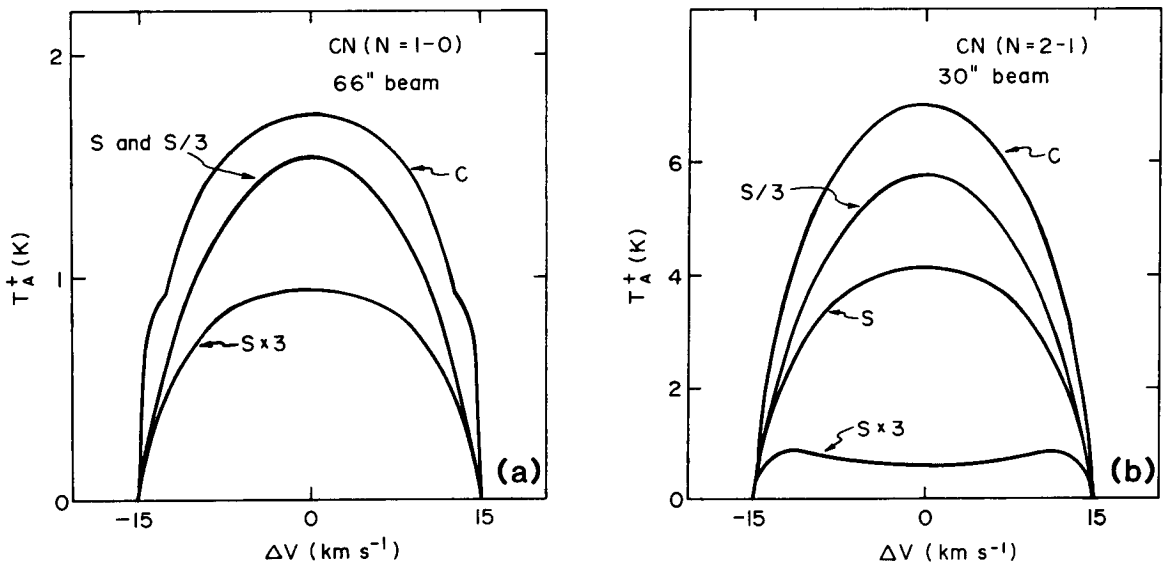


Figure 6-6. Photochemical model on-source line profiles for: (a) N = 1-0 and (b) N = 2-1 transitions for the CN radical (Huggins et al., 1984b) adapted to the Kitt Peak National Radio Astronomy Observatory and Owens Valley Radio Observatory beams, respectively. Curves C are for a constant abundance 1.3 × 10^{-6}, S for a "standard" set of model parameters, and S/3 and SX3 for dust shielding three times less and three times more effective than standard. The observations are fit best by a variable abundance model similar to the SX3 curves.

10^{18} cm^{-2} determined by Zuckerman et al. (1980) corresponds to an upper limit to the H I mass of 1.1 × 10^{31} g, using a distance of 290 pc. Table 6-2 gives the H I contributions expected from the different regions of the star and its CS shell (Glassgold and Huggins, 1983). The total amount of H I produced by photodissociation is 4 × 10^{29} g, well below the current observed upper limit. On the other hand, the small fractional abundance of atomic H injected into the envelope after freeze-out gives roughly 1 × 10^{31} g, about the observational limit. Of course, the theoretical estimate is uncertain because of the limitations in stellar atmosphere calculations, but new higher sensitivity searches for H I in IRC + 10216 are called for.

Much less is known about molecular abundances in O-rich stars. As discussed in the section *Observations*, the CO measurements have been used to determine mass-loss rates for O-rich and C-rich stars on the assumption of solar abundances. We have already discussed the significance of the low SiO abundances in the section *Studies of Chemical Reactions* (i.e., most of the silicon is probably incorporated into grains). As for detailed studies of the spatial distribution of molecules in O-rich shells, the main body of information consists of interferometer studies of the OH masing regions.

Unfortunately, the OH maser maps are not directly interpretable into abundance information because of the complexities of the maser emission mechanism. However, the maser models require a substantial OH abundance in the emitting regions. To account for this, Goldreich and Scoville (1976) have proposed that the OH is produced from the photodestruction of H_2O, and further studies of this model have been made by Deguchi (1982) and Huggins and Glassgold (1982b). Because the size of the H_2O distribution is determined by the amount of shielding and the photoproduced OH is distributed in a shell about the H_2O, the photo

Table 6-2
Sources of Atomic Hydrogen in IRC + 10216

Photosphere	2.1 (29) g
Injected into envelope	~1 (31)
H_2 photodissociation in shell interior	1.5 (29)
H_2 photodissociation at shell surface	1.9 (29)
Photodissociation of hydrocarbons	~2 (28)
Total from photodissociation	4 (29)
Upper limit of Zuckerman et al. (1980)	1.1 (31)

model predicts a specific correlation between the size of the OH shell and mass-loss rate. The observed maser map sizes correlate with mass-loss rate, as was noticed first by Bowers et al. (1981), and to that extent are supportive of the models. Deguchi has argued that destruction of H_2O molecules in collisions with grains, a possible alternative source of OH production, is probably unimportant.

Morris and Jura (1983b) have developed an interesting variation in the photochemical model for the unusual OH/IR supergiant, NML Cygnus. They explain the observed axially symmetric radio continuum emission (Habing et al., 1982) in terms of the ionizing radiation from the nearby Cyg OB association. Jura (1983b) has also considered dust and self-shielding of anisotropic molecular outflows.

The case of α Ori holds particular interest because of the large and diverse body of data which exists on its circumstellar envelope. A coherent theoretical treatment of the observations does not exist, however, and we focus on a few issues relating to the photochemistry of its outer envelope.

As discussed in the section *Observations*, CO is the only molecule detected in this CS envelope. Its IR absorption occurs at two velocities, 10 and 16 km s^{-1}; the weak 1.3 mm (J = 2–1) emission is at the higher velocity and seems to be confined to within 10″ (i.e., 3×10^{16} cm if the distance is taken to be 200 pc). On the other hand, scattered K I resonance radiation and polarized light are observed much farther out, 60″ and 90″, respectively. The dust shell, which appears to begin at about 10 R_*, or 8×10^{14} cm, appears to be rather thin, producing a weak silicate feature and no more than a few tenths of a magnitude of visual extinction. Among the various atomic lines observed in this star, the radial profile of scattered K I radiation (see the section *Heavy Atoms*) appears to have significant potential for understanding the outer shell.

Jura and Morris (1981) made the first serious attempt to utilize the information in the CO emission-line profile and the distribution of the scattered K I line radiation. They solved time-dependent rate equations for these two species, which they linked in an interesting way. In their theory, the abundance of K I is determined by photoionization by interstellar UV radiation and by radiative recombination. The electrons are assumed to come primarily from the photoionization of C, with the fractional contribution from other heavy elements restricted to be 1×10^{-6}. The photochemical model enters in that the C comes from the photodissociation of CO. Jura and Morris determined the mass-loss rate of α Ori to be $1.5 \times 10^{-5}\ M_\odot\ \mathrm{yr}^{-1}$ from the K I distribution and the assumption that the abundance of potassium is solar. From the CO emission, they determined the abundance of carbon to be 1.25×10^{-5}, assuming that all the carbon is in CO.

This attractive theory may serve as the first step in a more general approach to understanding the α Ori shell. The effects of the chromospheric radiation will have to be included because, in many cases, photo rates calculated at the photosphere are $\sim 10^6$ larger than those for the interstellar radiation field. The chemical reactions investigated by Clegg et al. (1983a) are also relevant, and time-dependent calculations are required in some cases. Consideration should also be given to the atomic column densities (e.g., as measured by Hagen, 1978; and Bernat, 1977), which provide important information on the ionization and gaseous abundances.

CONCLUSIONS

The foregoing discussion shows that the study of the outer envelopes of cool evolved stars has become an active area of research. Observations at many wavelength bands are relevant—from the ultraviolet to the radio, although infrared and millimeter-wave techniques are especially useful. Future investigations with new high-resolution methods (both spatial and spectral) should be particularly significant for understanding these small, but now resolvable, structures. Although relatively little theoretical research has been done thus far, a number of interesting initiatives have been made.

Extensive observations of specific objects should be particularly useful for the development of theoretical models, as exemplified by the case of IRC + 10216. In the future, it will be important to obtain equally detailed information for other C-rich stars and for O-rich stars as well: IRC + 10216 has attracted most of the theoretical attention thus far, but perhaps it is not as typical as usually believed.

Recent theoretical considerations show that the thermal equilibrium model is of limited use for understanding the chemistry of the outer CS envelopes. Indeed, their small sizes and moderate expansion velocities indicate that time-dependent considerations dominate this subject. At the present time, we only have the results of time-dependent chemical studies for situations in which photodestruction of atoms and molecules dominate particle reactions. One clear result of the photochemical models is that molecules cannot survive very long after they reach the outer edges of isolated CS envelopes, even if they are quite thick. In other words, interstellar molecules must be produced locally within clouds because CS molecules will be destroyed within envelopes embedded in an ultraviolet radiation field. This is in contrast to dust grains, which are able to survive passage through CS envelopes. The possibility also exists that sufficiently detailed measurements of gas-phase species in circumstellar envelopes could provide some insights into the formation of the CS dust. Finally, the theoretical modeling of the chemistry of CS envelopes provides quantitative tests of chemical concepts which have a broader interest than the envelopes themselves. In certain cases, the observations confirm the density and velocity profiles characteristic of a constant and spherically symmetric mass loss, so that the physical and chemical problems can be investigated with known flow conditions. Such situations rarely occur in the study of interstellar chemistry, so that, in a sense, CS envelopes provide a better controlled chemical laboratory than interstellar clouds.

This work has been supported in part by NASA grant NGR-33-016-196 (to A.E. Glassgold), by NSF grant AST-8216484 (to P.J. Huggins), and by an Alfred P. Sloan Fellowship (to P.J. Huggins). The authors thank A. Omont and M. Jura for permission to use illustrations from their papers for Figures 6-1 and 6-4, and M. Jura, H.R. Johnson, and B. Zuckerman for helpful comments.

NOTE ADDED IN PROOF

Since the review was completed in 1984, there have been a number of new observations and theoretical investigations of circumstellar chemistry. We mention briefly here some of the main results.

In IRC + 10216, a second ring molecule C_3H_2 has been added to the list of detected species (Matthews and Irvine, 1985; Thaddeus et al., 1986); a new free radical has also been found (Guelin et al., 1986), but the exact carrier of the lines has not been identified. Observations of CRL 2688 with the new 30-m IRAM telescope (Lucas et al., 1986) have shown that lines previously seen only in IRC + 10216 can now be detected in other CSEs so that the detailed intercomparison of the chemistry of different objects is now a real possibility. One main theoretical development of carbon-rich envelopes has been the exploration of the role of atomic and molecular ions by Nejad et al. (1984) and Glassgold et al. (1986). The latter have developed a model for the distribution of

molecular ions in IRC + 10216 which is consistent with new limits on the abundance of HCO^+ reported by Lucas et al. (1986). Jura and Morris (1985) have investigated the condensation of molecules onto the dust in the outflowing winds.

In oxygen-rich stars, both SO_2 (Lucas et al., 1986) and HCN have been detected (Deguchi and Goldsmith, 1986), so for these objects, the number of observed species is beginning to approach a level where quantitative comparison with theory becomes interesting. In the CSE of α Ori, CO in the CSE (Huggins, 1985) and C/H in the photosphere (Lambert et al., 1984) have been reevaluated: C appears to normal in the photosphere, and CO is probably underassociated in the envelope. The role of chromospheric radiation has been discussed by Glassgold and Huggins (1986), and their model gives a satisfactory account of the available KI scattering data.

It seems clear from these latest developments that rapid progress can be expected in many areas of circumstellar chemistry in the next few years.

REFERENCES

Allen, M., and Knapp, G.R. 1978, *Astrophys. J.*, **225**, 843.

Allen, M., Pinto, J.P., and Yung, Y.L. 1980, *Astrophys. J. (Letters)*, **242**, L125.

Beckwith, S., Persson, S.E., and Gatley, I. 1978, *Astrophys. J. (Letters)*, **219**, L33.

Beichman, C.A., Keene, J., Phillips. T.G., Huggins, P.J., Wootten, H.A., Masson, C., and Frerking, M.A. 1983, *Astrophys. J.*, **273**, 633.

Bell, M.B., Feldman, P.A., Kwok, S., and Matthews, H.E. 1982, *Nature*, **295**, 389.

Bernat, A.P. 1976, Ph.D. Thesis, Univ. of Texas, Austin.

Bernat, A.P. 1977, *Astrophys. J.*, **213**, 756.

Bernat, A.P. 1981, *Astrophys. J.*, **246**, 184.

Bernat, A.P., Hall, D.N.B., Hinkle, K.H., and Ridgway, S.T. 1979, *Astrophys. J. (Letters)*, **233**, L135.

Betz, A.L. 1981, *Astrophys. J. (Letters)*, **244**, L103.

Betz, A.L., McLaren, R.A., and Spears, D.L. 1979, *Astrophys. J. (Letters)*, **229**, L97.

Black, J.H. 1983, in *Proc. IAU Symp. 103, Planetary Nebulae*, ed. D.R. Flower (Dordrecht: Reidel), p. 91.

Bowers, P.F., Johnston, K.J., and Spencer, J.H. 1981, *Nature*, **291**, 382.

Bowers, P.F., Johnston, K.J., and Spencer, J.H. 1983, *Astrophys. J.*, **274**, 733.

Carlson, W.J., Huggins, P.J., and Glassgold, A.E. 1985, in preparation.

Castor, J.I. 1981, in *Physical Processes in Red Giants*, ed. I. Iben and A. Renzini (Dordrecht: Reidel), p. 285.

Clegg, R.E.S., Brinks, E., and d'Hendecourt, L.B. Le S., 1983b, *Astron. Astrophys.*, preprint.

Clegg, R.E.S., Hinkle, K.H., and Lambert, D.L. 1982, *Mon. Not. Roy. Astr. Soc.*, **201**, 95.

Clegg, R.E.S., van Ijzendoorn, L.J., and Allamandola, L.J. 1983a, *Mon. Not. Roy. Astr. Soc.*, **203**, 125.

Clegg, R.E.S., and Wootten, H.A. 1980, *Astrophys. J.*, **240**, 822.

Cohen, M. 1980, *Astrophys. J. (Letters)*, **238**, L81.

Deguchi, S. 1982, *Astrophys. J.*, **259**, 634.

Deguchi, S., and Goldsmith, P. 1985, *Nature*, in press.

Deutsch, A.J. 1956, *Astrophys. J.*, **123**, 210.

Dyck. H.M., Beckwith, S., and Zuckerman, B. 1983, *Astrophys. J. (Letters)*, **271**, L79.

Elitzur, M. 1982, *Rev. Mod. Phys.*, **54**, 1225.

Engels, D. 1979, *Astron. Astrophys. Supplement*, **36**, 337.

Feibelman, W.A., Boggess, A., McCracken, C.W., and Hobbs, R.W. 1981, *Astron. J.*, **86**, 881.

Geballe, T.R., Lacy, J.H., and Beck, S.C. 1979, *Astrophys. J. (Letters)*, **230**, L47.

Geballe, T.R., Wollmann, E.R., and Rank, D.M. 1972, *Astrophys. J. (Letters)*, **177**, L27.

Gerola, H., and Glassgold, A.E. 1978, *Astrophys. J. Supplement*, **37**, 1.

Glassgold, A.E., and Huggins, P.J. 1983, *Mon. Not. Roy. Astr. Soc.*, **203**, 517.

Glassgold, A.E., and Huggins, P.J. 1986, *Astrophys. J.*, in press.

Glassgold, A.E., Huggins, P.J., and Langer, W.D. 1985, *Astrophys. J.*, **290**, 615.

Glassgold, A.E., Lucas, R., and Omont, A. 1986, *Astron. Astrophys.*, in press.

Goldhaber, D., and Betz, A.L. 1984, *Astrophys. J. (Letters)*, **279**, L55.

Goldreich, P. 1980, in *Proc. IAU Symp. 87, Interstellar Molecules*, ed. B.H. Andrew (Dordrecht: Reidel), p. 551.

Goldreich, P., and Scoville, N.Z. 1976, *Astrophys. J.*, **205**, 144.

Goldsmith, P.F., Langer, W.D., Elldér, J., Irvine, W., and Kollberg, E. 1981, *Astrophys. J.*, **249**, 524.

Guelin, M., Cernicharo, J., Kahane, C., and Gomez-Gonzalez, J. 1986, *Astron. Astrophys*, in press.

Guelin, M., Green, S., and Thaddeus, P. 1978, *Astrophys. J. (Letters)*, **224**, L27.

Habing, H.J., Goss, W.M., and Winnberg, A. 1982, *Astron. Astrophys.*, **108**, 412.

Hagen, W. 1978, *Astrophys. J. Supplement*, **38**, 1.

Hagen, W., Stencel, R.E., and Dickinson, D.F. 1983, *Astrophys. J.*, **274**, 286.

Hall, D.N.B., and Ridgway, S.T. 1978, *Nature*, **273**, 281.

Heap, S.R., and Stecher, T.P. 1981, in *The Universe at Ultraviolet Wavelengths*, ed. R.D. Chapman, NASA CP-2171, p. 657.

Henkel, C., Matthews, H.E., and Morris, M. 1983, *Astrophys. J.*, **267**, 184.

Henkel, C., Matthews, H.E., Morris, M., Terebey, S., and Fich, M. 1984, *Astron. Astrophys.*, in press.

Herman, J., and Habing, H.J. 1981, in *Physical Processes in Red Giants*, ed. I. Iben and A. Renzini (Dordrecht: Reidel), p. 383.

Hinkle, K.H., and Barnes, T.G. 1979, *Astrophys. J.*, **227**, 923.

Hinkle, K.H., Hall, D.N.B., and Ridgway, S.T. 1982, *Astrophys. J.*, **252**, 687.

Honeycutt, R.K,. Bernat, A.P., Kephart, J.E., Gow, C.E., Sandford, M.T., and Lambert, D.L. 1980, *Astrophys. J.*, **239**, 565.

Hollenbach, D. 1982, in *Symp. on the Orion Nebula to Honor Henry Draper*, ed. A.E. Glassgold, P.J. Huggins, and E.L. Schucking, Ann. New York Acad. Sci., **395**, 242.

Huggins, P.J. 1985, in *Mass Loss from Red Giant Stars*, ed. M. Morris and B. Zuckerman (Dordrecht: Reidel), p. 161.

Huggins, P.J., Carlson, W.J., and Kinney, A.L. 1984a, *Astron. Astrophys.*, **133**, 347.

Huggins, P.J., and Glassgold, A.E. 1982a, *Astrophys. J.*, **252**, 201.

Huggins, P.J., and Glassgold, A.E. 1982b, *Astron. J.*, **87**, 1828.

Huggins, P.J., Glassgold, A.E., and Morris, M. 1984b, *Astrophys. J.*, **279**, 284.

Jameson, P., and Williams, D.A. 1981, *Astrophys. Space Sci.*, **75**, 341.

Jewell, P.R., and Snyder, L.E. 1982, *Astrophys. J. (Letters)*, **255**, L69.

Jewell, P.R., and Snyder, L.E. 1984, *Astrophys. J.*, **278**, 176.

Johansson, L.E.B., Andersson, C., Elldér, J., Friberg, P., Hjalmarson, A., Höglund, B., Irvine, W.M., Olofsson, H., and Rydbeck, G. 1984, *Astron. Astrophys.*, **130**, 227.

Johnson, H.R., Beebe, R.F., and Sneden, C. 1975, *Astrophys. J. Supplement*, **29**, 123.

Johnson, H.R., Goebel, J.H., Goorvitch, D., and Ridgway, S. 1983, *Astrophys. J. (Letters)*, **270**, L63.

Jura, M. 1983a, *Astrophys. J.*, **267**, 647.

Jura, M. 1983b, *Astrophys. J.*, **275**, 683.

Jura, M., and Morris, M. 1981, *Astrophys. J.*, **251**, 181.

Jura, M., and Morris, M. 1985, *Astrophys. J.*, **292**, 487.

Knapp, G.R. 1985, *Astrophys. J.*, **293**, 273.

Knapp, G.R., and Bowers, P.F. 1983, *Astrophys. J.*, **266**, 701.

Knapp, G.R., and Chang, K.M. 1985, *Astrophys. J.*, **293**, 281.

Knapp, G.R., and Morris, M. 1985, *Astrophys J.*, **292**, 640.

Knapp, G.R., Phillips, T.G., and Huggins, P.J. 1980, *Astrophys. J. (Letters)*, **242**, L25.

Knapp, G.R., Phillips, T.G., Leighton, R.B., Lo, K.Y., Wannier, P.G., Wootten, H.A., and Huggins, P.J. 1982, *Astrophys. J.*, **252**, 616.

Kwan, J., and Hill, F. 1977, *Astrophys. J.*, **215**, 781.

Kwan, J., and Linke, R.A. 1982, *Astrophys. J.*, **254**, 587.

Kwok, S., Bell, M.B., and Feldman, P.A. 1981, *Astrophys. J.*, **247**, 125.

Lafont, S., Lucas, R., and Omont, A. 1982, *Astron. Astrophys.*, **106**, 201.

Lambert, D.L., Brown, J.A., Hinkle, K.H., and Johnson, H.R. 1984, *Astrophys. J.*, **284**, 223.

Lo, K.Y., and Bechis, K.P. 1976, *Astrophys. J. (Letters)*, **205**, L21.

Lucas, R., Omont, A., and Guilloteau, S. 1986, *Astron. Astrophys.*, in press.

Lucy, L. 1976, *Astrophys. J.*, **205**, 482.

Matthews, H.E., and Irvine, W.M. 1985, *Astrophys. J. (Letters)*, **298**, L61.

Mauron, N., Fort, B., Querci, F., Dreux, M., Fauconnier, T., and Lamy, P. 1984, *Astron. Astrophys.*, **130**, 341.

McCabe, E.M., Smith, R.C., and Clegg, R.E.S. 1979, *Nature*, **281**, 263.

McKee, C.F., and Hollenbach, D. 1980, *Ann. Rev. Astron. Astrophys.*, **18**, 219.
McLaren, R.A., and Betz, A.L. 1980, *Astrophys. J. (Letters)*, **240**, L159.

Morris, M. 1975, *Astrophys. J.*, **197**, 603.

Morris, M. 1980, *Astrophys. J.*, **236**, 823.

Morris, M., and Alcock, C. 1979, *Astrophys. J.*, **218**, 687.

Morris, M., and Jura, M. 1983a, *Astrophys. J.*, **264**, 546.

Morris, M., and Jura, M. 1983b, *Astrophys. J.*, **267**, 179.

Morris, M., Redman, R., Reid, M.J., and Dickinson, D.F. 1979, *Astrophys. J.*, **229**, 257.

Mufson, S.L., Lyon, J., and Marionni, P.A. 1975, *Astrophys. J. (Letters)*, **201**, L85.

Nejad, L.A.M., Millar, T.J., and Freeman, A. 1984, *Astron. Astrophys.*, **134**, 129.

Nguyen-Q-Rieu, Bujarrabal, V., Olofsson, H., Johansson, L.E.B., and Turner, B.E. 1984a, *Astrophys. J.*, **286**, 276.

Nguyen-Q-Rieu, Graham, D., and Bujarrabal, V. 1984b, *Astron. Astrophys.*, **138**, L5.

Olofsson, H., Johansson, L.E.B., Hjalmarson, A., and Nguyen-Quang-Rieu. 1982a, *Astron. Astrophys.*, **107**, 128.

Olofsson, H., Johansson, L.E.B., Nguyen-Q-Rieu, Sopka, R.J., and Zuckerman, B. 1982b, *Bull. Amer. Astron. Soc.*, **14**, 895.

Pottasch, S.R., Goss, W.M., Arnal, M., and Gathier, R. 1982, *Astron. Astrophys.*, **106**, 229.

Ridgway, S.T., and Hall, D.N.B. 1980 in *Proc. IAU Symp. 87, Interstellar Molecules*, ed. B.H. Andrew (Dordrecht: Reidel), p. 509.

Ridgway, S.T., Hall, D.N.B., Kleinman, S.G., Weinberger, D.A., and Wojslaw, R.S. 1976, *Nature*, **264**, 345.

Rinsland, C.P., Baldacci, A., and Rao, N. 1982, *Astrophys. J. Supplement*, **49**, 487.

Rodriguez, L.F., and Moran, J.M. 1983, in *Proc. IAU Symp. 103, Planetary Nebulae*, ed. D.R. Flower (Dordrecht: Reidel), p. 510.

Sahai, R., Wootten, A., and Clegg, R.E.S. 1984, *Astrophys. J.*, **284**, 144.

Scalo, J., and Slavsky, D.B. 1980, *Astrophys. J. (Letters)*, **239**, L73.

Schacke, H., Wagner, H.G., and Wolfrum, J. 1977, *Berichte der Bunsen Gesellschaft*, **81**, 670.

Slavsky, D.D., and Scalo, J.M. 1984, preprint.

Solomon, P.M., Penzias, A.A., and Jefferts, K.B. 1971, *Astrophys. J. (Letters)*, **169**, L35.

Sopka, R.J., Hildebrand, R., Jaffee, D.T., Gatley, I., Roellig, T., Werner, M., Jura, M., and Zuckerman, B. 1985, *Astrophys. J.*, in press.

Thaddeus, P., Cummins, S.E., and Linke, R.A. 1984, *Astrophys. J. (Letters)*, **283**, L45.

Thaddeus, P., Gottlieb, C.A., Irvine, W.M., Friberg, P., Hjalmarson, A., Johansson, L.E.B., and Linke, R.A. 1985, preprint.

Thaddeus, P., Vrtilek, J.M., and Gottlieb, C.A. 1986, *Astrophys. J. (Letters)*, in press.

Treffers, R.R., Fink, U., Larson, H.P., and Gautier, T.N. 1976, *Astrophys. J.*, **209**, 793.

Tsuji, T. 1983, *Astron. Astrophys.*, **122**, 314.

Ukita, N., and Morris, M. 1983, *Astron. Astrophys.*, **121**, 15.

Wannier, P.G. 1980, *Ann. Rev. Astron. Astrophys.*, **18**, 399.

Wannier, P.G., Leighton, R.B., Knapp, G.R., Redman, R.O., Phillips, T.G., and Huggins, P.J. 1979, *Astrophys. J.*, **230**, 149.

Wannier, P.G., and Linke, R.A. 1978, *Astrophys. J.*, **225**, 130.

Wannier, P.G., and Sahai, R. 1983, in *Proc. IAU Symp. 103, Planetary Nebulae*, ed. D.R. Flower (Dordrecht: Reidel), p. 292.

Welch, W.J., Chapman, B., and Bieging, J.H. 1981, *Bull. Amer. Astr. Soc.*, **13**, 865.

Weymann, R.J. 1963, *Ann. Rev. Astron. Astrophys.*, **1**, 97.

Willson, L.A. 1976, *Astrophys. J.*, **205**, 172.

Willson, L.A., and Hill, S.J. 1979, *Astrophys. J.*, **228**, 854.

Wilson, W.J., Schwartz, P.R., and Epstein, E.E. 1973, *Astrophys. J.*, **183**, 871.

Winnewisser, G., and Walmsley, C.M. 1978, *Astron. Astrophys.*, **70**, L37.

Wood, P.R. 1979, *Astrophys. J.*, **227**, 220.

Woolf, N.J., and Ney, E.P. 1969, *Astrophys. J. (Letters)*, **155**, L181.

Wootten, A., Evans, N.J., Snell, R., and Vanden Bout, P. 1978, *Astrophys. J. (Letters)*, **225**, L143.

Wootten, A., Lichten, S.M., Sahai, R., and Wannier, P.G. 1982, *Astrophys. J.*, **257**, 151.

Zuckerman, B. 1980, *Ann. Rev. Astron. Astrophys.*, **18**, 263.

Zuckerman, B. 1982, in *Proc. IAU Symp. 103, Planetary Nebulae*, ed. D.R. Flower (Dordrecht: Reidel), p. 101.

Zuckerman, B., Gilra, D.P., Turner, B.E., Morris, M., and Palmer, P. 1976, *Astrophys. J. (Letters)*, **205**, L15.

Zuckerman, B., Palmer, P., Gilra, D.P., Turner, B.E., and Morris, M. 1978, *Astrophys. J. (Letters)*, **220**, L53.

Zuckerman, B., Palmer, P., Morris, M. Turner, B.E., Gilra, D.P., Bowers, P.F., and Gilmore, W. 1977, *Astrophys. J. (Letters)*, **211**, L97.

Zuckerman, B., Terzian, Y., and Silvergate, P. 1980, *Astrophys. J.*, **241**, 1014.

N88-11599

7

THERMAL ATMOSPHERIC MODELS

Hollis R. Johnson

INTRODUCTION

Makers of atmospheric models could well be intimidated by the wide variety and unusual character of the red-giant stars as revealed by the observations already described, which quite commonly include such features as emission lines, thermal emission from dust shells, maser emission, mass outflow (and inflow), polarization, variability, and rapid evolution. These phenomena present tough questions. To what extent are the atmospheres of M, S, and C stars to be understood simply as cooler examples of ordinary warmer stars? Are inhomogeneous atmospheres common among red giants and supergiants? Will discrepancies due to our present inadequate treatments of convection conceal other theoretical deficiencies? Are chromospheres permanent or transient? By what mechanisms are they produced? Where and how does grain formation and growth occur? What mechanisms are responsible for mass loss, and what are the consequences? With extended atmospheres and temperature inversions, aren't departures from local thermodynamic equilibrium (LTE) likely? Can one neatly separate atmospheres into photospheres, chromospheres, and circumstellar shells? The questions go on and on.

In spite of the uncertainties raised by these questions, atmospheric model makers have historically treated all these more exotic phenomena as secondary and have concentrated first on modeling photospheres. A photospheric model is not only a desirable first step, but it has a rather logical priority since all other structures, processes, and phenomena depend on it. In this chapter, we describe the *static thermal atmosphere* and compare its predictions to observations both to test the validity of the classic assumptions and to distinguish and describe those spectral features with diagnostic value. By thermal atmosphere, we mean an atmosphere based on hydrostatic equilibrium, radiative equilibrium, and LTE. Nonthermal atmospheric models, including nonradiative heating and departures from LTE, are treated in a succeeding chapter (de la Reza, this volume), and more exotic phenomena are described in other chapters.

Several useful reviews of the challenges of computing atmospheres for red-giant stars and using these to interpret observations have already been given. Vardya (1970) gave a broad-brush treatment of the topic from information then available, and Johnson (1972) analyzed the few theoretical models computed to that time. Although advances in modeling atmospheres of red-giant stars have come slowly, it is heartening to note the obvious progress from these early reviews to the present. Remarkably, even the recent excellent general works on stellar atmospheres (for example, Gray, 1976; Mihalas, 1978; Baschek and Scholz, 1982) contain few

applications to red-giant stars. More valuable are recent specialized reviews. Carbon (1979) gives a detailed general review of problems and techniques of computation of atmospheres of intermediate and late-type stars from the point of view of the model maker; Gustafsson (1981) writes a topical review of late-type stars from the point of view of the observer; and Johnson (1985) discusses the current availability of models for peculiar red-giant stars. Carbon (1984) examines both the opacity-distribution function and the opacity-sampling treatments of line opacities, the latter by means of a Monte Carlo technique.

PHYSICAL PRINCIPLES

For modeling red-giant atmospheres, workers have adopted the same principles and techniques used in modeling hotter main-sequence stars, for which these principles were perhaps more appropriate. The most obvious exception is in the treatment of line opacity, for which the relatively few lines in hot stars can be treated individually but the millions of lines in cooler stars must be treated collectively. The basic physical principles are hydrostatic equilibrium, radiative equilibrium, and local thermodynamic equilibrium (LTE). The solution of these equations in a plane-parallel horizontally homogeneous geometry constitutes the problem of the *classic stellar atmosphere.*

Hydrostatic equilibrium in a plane-parallel geometry is:

$$dp = -g\varrho dz \quad , \tag{7-1}$$

where the total pressure $p = p(\text{gas}) + p(\text{radiation}) + p(\text{turbulence})$, and the surface gravity $g = GM/r^2$ is held constant. Turbulent pressure is often neglected.

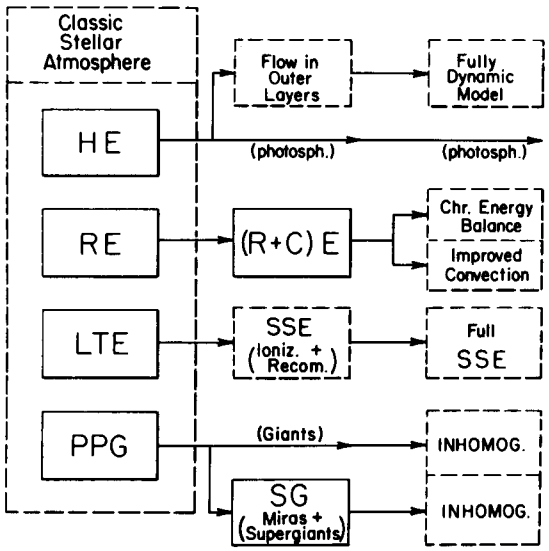
The constancy of the total energy flux is:

$$F = \sigma T_{\text{eff}}^4 \quad , \tag{7-2}$$

where F is the energy flux (erg cm^{-2} s^{-1}) and T_{eff} is the effective temperature, defined by Equation (7-2). Strict radiative equilibrium implies $\int F_\nu \, d\nu = F(\text{rad}) = F$, whereas convective energy transport is included through $F(\text{rad}) + F(\text{conv}) = F$. When included, convection has usually been treated by the usual local mixing length (LML) theory without overshoot (Böhm-Vitense, 1958; Henyey et al., 1965; Mihalas, 1978; Lester et al., 1982).

As generally used, LTE includes two key assumptions: (1) concentrations of molecules, atoms, and ions are given by the relevant equations of equilibrium statistical mechanics with the single parameter of electron temperature; and (2) the source function for all bound-bound transitions and for all continuous transitions except for pure scattering is the blackbody radiation (Planck) function, $B(\nu, T)$. Nothing in the modern treatments of bound-bound opacity (opacity distribution functions, opacity sampling (OS), or Voigt-analog/Elsassar-band model; see following section) *requires* this assumption on the line source function; they are all flexible enough to accommodate a simple mixture of pure absorption and pure scattering. (The OS has, however, a clear advantage.) The LTE assumption is made for simplicity and to test this hypothesis in the face of departures anticipated because of the observed departures of the emitted energy flux of cool stars from that of a blackbody and the low gas densities (hence collision rates) in the outer atmosphere.

We attempt to display the present situation and foreseeable developments in Figure 7-1. Principles of the classic stellar atmosphere are shown at the left. Developments or improvements currently available or on the horizon are shown in solid boxes; developments still in the future are shown in dotted boxes. Except for the addition of convective energy transport and the extension to spherical geometry, both of which are, in some form, already in use, generalizations of these classic principles may be slow in appearing. Recall that we are speaking here of stellar photospheres. Some of the improvements labeled "future" are regularly applied in studies of circumstellar (CS) envelopes and mass loss; current progress in these areas



HE = hydrostatic equilibrium
RE = radiative equilibrium
LTE = local thermodynamic equilibrium
PPG = plane-parallel geometry
SG = spherical geometry
CE = convective equilibrium
SSE = steady-state equilibrium

Figure 7-1. Overview of the physical principles underlying current theoretical research on classic thermal atmospheres of red-giant stars. Present physical principles and generalizations are enclosed with solid lines, and possible future generalizations are enclosed with dotted lines.

can be gaged from other chapters in this volume. The rate of future progress can be guessed at by the reader as it has been guessed at by others (Johnson, 1985). With the arrival of information in the ultraviolet, infrared, and radio regions and with the prospects for employing supercomputers to model the entire atmosphere, including mass flow, on the horizon, we appear to be entering an exciting era.

OPACITIES

Continuous Opacities

Many of the opacities for cool stars are similar to, or can be extrapolated from, those at higher temperatures. Throughout most of the photosphere, H^- provides the dominant continuous opacity over most of the spectrum even down to stars of T_{eff} = 2500 K and for a variety of chemical compositions (Johnson, 1982). In the coolest region of the atmosphere, hydrogen may be associated into H_2, and the H^- opacity will become so small that He^- (free-free) will become a dominant continuous opacity. This may be the case in hydrogen-deficient atmospheres as well. Bound-free continua of H I are only of minor importance, and the bound-free continua of He I are completely negligible. (These may be of importance, however, in shocks or in the hot chromospheres of cool stars.) Absorption due to bound-free continua of other neutral elements (Si, Al, Na, Mg, Ca, and Fe) are likewise of minor importance because their absorption edges lie in the ultraviolet, where the stellar flux is weak. Except for H^-, the opacity of negative ions (Vardya, 1970) does not appear to be significant. Although Rayleigh scattering from H I, H_2, and He I—with minor contributions from C I, N I, O I, and N_2—is most significant in the ultraviolet, its effect extends increasingly longward in wavelength as the temperature decreases, and it becomes of major importance in the upper photosphere. Information on cross sections for continuous opacity sources is contained in, for example, Carbon and Gingerich (1969); Kurucz (1970); Tsuji (1971); and Baschek and Scholz (1982); while references may be found in Gustafsson et al. (1975); Mihalas (1978); Kurucz (1979); Johnson et al. (1980); and Dzervitis (1983).

Dust Grains

Wherever condensation occurs in a stellar atmosphere, dust will almost certainly become a major opacity because of its very large absorption coefficient. Many cool stars, especially cool supergiants and Miras, show evidence of circumstellar dust (Lefèvre, this volume). Whether grains commonly form in the outer

stellar *photosphere* is still uncertain, despite considerable work on this important problem. Two enormous obstacles to progress in overcoming this uncertainty are the lack of knowledge of both the physical conditions in the outer photospheres (this chapter; Zuckerman; 1980; Goldberg, this volume) and the mechanism of nucleation (Deguchi, 1980; Draine, 1981; McCabe, 1982; Alexander et al., 1983; Gail and Sedlmayr, 1984). Vital to the question of grains in red-giant atmospheres is the location of the condensation point, but this is still quite uncertain (c.f. Draine, 1984). For clean silicate grains in M stars, condensation may occur at a distance (from the stellar *center*) of 3 to 4 stellar radii (Deguchi, 1980) or perhaps closer (Draine, 1981; Alexander et al., 1983). In carbon-rich atmospheres, condensation of graphite may occur at 5 stellar radii (from the stellar *center*), and SiC may condense even closer (McCabe, 1982), perhaps as close as 1.5 stellar radii (Lucy, 1976; Woodrow and Auman, 1982). Several minerals condense at about 1500 K (cf. Draine, 1981; McCabe, 1982; Alexander et al., 1983), and such temperatures might be reached in the outer photospheres of sufficiently cool stars, especially if presently unaccounted for spherical effects (Schmid-Burgk and Scholz, 1981) *lower* the temperature even further than predicted by current models. On the other hand, chromospheric heating may *raise* the temperatures in the outer layers. Clearly, the most favorable site for condensation is the outer atmosphere of a cool Mira variable star (Deguchi, 1980; Alexander et al., 1983), where grain formation may be related not only to mass loss but also to pulsation (Woodrow and Auman, 1982). At present, there is no *compelling* evidence for dust in any cool-star *photosphere* (see, for example, Chapters 3 and 7 and the foregoing references). For this reason, and for the sake of simplicity, dust is neglected in most model atmospheres. If future observations demonstrate the existence of photospheric dust grains, their inclusion will extend atmospheric modeling into a rather different opacity regime.

Spectral Line Blanketing

Before plunging into the complexities of the subject, it is worth reminding ourselves of the central role of the *atomic and molecular data* themselves. Much work lies ahead, particularly for the molecules, and we salute those who pursue this unglamorous but necessary research.

Several excellent reviews of line blanketing are available. A description of LTE line blanketing in terms of physical mechanisms is given by Carbon (1979), and a mathematical analysis is presented by Mihalas (1978). Quantitative non-LTE analyses are provided by Athay and Skumanich (1969), Mihalas and Luebke (1971), and Athay (1972). Much of this development builds on foundations laid earlier by Chandrasekhar (1935), Münch (1946), and Pecker (1951).

From the point of view of the observer, the most striking feature of a stellar spectrum is the removal of light by the spectral lines, an effect referred to as *line blocking*. Since the line represents an increase of opacity and the total flux is required to be constant in radiative equilibrium, the temperature in deeper layers must rise to drive the same flux through the increased opacity, an effect referred to as *backwarming*. In addition, the gas in the outer layers may be heated or, more frequently, cooled. Altogether, the effects are referred to as *line blanketing*.

Physical processes near the surface and their effect on the thermal structure are complex. Purely coherent scattering lines change the temperature very little because they are weakly coupled to the thermal reservoir of the atmosphere (Chandrasekhar, 1935; Münch, 1946; Mihalas, 1978). Purely absorbing lines generally act to *lower* the temperature of the outer layers if they lie on the *redward* side of the flux maximum (e.g., H_2O, CN, and CO); purely absorbing lines lying *blueward* of the flux peak (TiO and most atomic lines) tend to *raise* the temperature of the layers in which they finally become thin. These latter effects can be understood as follows (Krupp et al., 1978; Carbon, 1979; Gustafsson, 1981). Absorption of a red (low-energy) photon by an atom or molecule

and the reemission of a (higher energy) photon characteristic of the local temperature in the outer layers results in a net energy loss (i.e., a cooling). In the same way, absorption of a UV photon and reemission of a (lower energy) photon characteristic of the local temperature results in a net energy gain (i.e., a heating). This is a simplified picture of a very complex process, however, and a careful quantitative description, including the effects of departures from LTE and a proper description of the mechanism of line formation may be necessary to understand the physics involved in a particular line (Jefferies, 1968; Athay and Skumanich, 1969; Mihalas and Luebke, 1971; Athay, 1972; Mihalas, 1978). Although line formation in the general case, where LTE does not hold, properly belongs in a chapter on nonthermal phenomena (de la Reza, this volume), we mention it here because of its possible importance in treating line blanketing.

In fact, the effect of a line on the atmospheric structure depends on the line strength relative to the continuum, the variation of the line strength with depth, the wavelength of the line, and the mechanism of line formation. This last consideration is sometimes specified beforehand (e.g., pure absorption or pure scattering), which oversimplifies the actual physics of the problem. Of these effects, the blocking and backwarming depend principally on the line strength, whereas the surface cooling depends principally on the mechanism of line formation, but also on the line strength (Mihalas and Luebke, 1971). Quite generally (cf. Athay and Skumanich, 1969; Athay, 1972), the condition of radiative equilibrium requires $dH/d\tau = 0$, where H is the normalized total (integrated) flux. Although the total flux is conserved, the continuous flux is now no longer conserved but is given by:

$$\frac{dH_c}{d\tau_c} = \frac{M^{-1}}{r_o} ZS_\ell + \int (J_c - J_\nu)\, d\nu = t + c \quad , \tag{7-3}$$

where $M = \sqrt{\pi}\,\Delta\nu_D$ (for a Doppler line); $\Delta\nu_D$ is the Doppler halfwidth; $Z = 1 - J/S_\ell$ is the net radiative bracket; J is the mean intensity averaged over the absorption coefficient; and

$$r_o = \frac{d\tau_c}{d\tau_o} = \frac{d\tau_c}{d\tau_\ell(\nu_o)} \quad . \tag{7-4}$$

Here ℓ and c refer to line and continuous quantities, respectively, and ν designates total (line plus continuous) quantities. The net radiative bracket (Thomas, 1960) or escape coefficient (Athay, 1981), when multiplied by the Einstein spontaneous emission coefficient, gives the *net downward* rate of radiative transitions in a given spectral line. This equation states that the presence of a spectral line causes a net exchange of energy between the line and the continuum—an exchange which may proceed in either direction and may depend sensitively on depth. It is the *atmospheric adjustment* to the requirements that total flux be conserved which produces the changes in the thermal structure referred to as line blanketing.

The c term (Athay, 1972) is proportional to the equivalent width of the line and is defined to be positive if the line is in absorption. This term is then independent of the mechanism of line formation, at least to the first order. If an absorption line is present, it provides a sink for the continuous photons and thus tends to cool the atmosphere. This is always the case in the outer layers, and c therefore acts to cool the outer layers regardless of its position in the spectrum, strength, or depth of formation. As one proceeds into the atmosphere, the line may stay in absorption or may go into emission, depending on the wavelength, the line strength (or value of r_o), and the depth dependence of r_o. Lines in the blue part of the spectrum—blueward of the flux peak, where $J > B$—tend to stay in absorption and therefore cool (provide a sink for continuum photons) at all depths, whereas lines redward of the peak, where $J < B$, tend to go into emission (locally) deep in the

atmosphere and therefore produce the considerable backwarming observed. A rapid increase in r_0 deep in the atmosphere increases the tendency of lines to go into emission and therefore increases the backwarming.

The t term (Athay, 1972), which is proportional to Z, the net radiative bracket, tends to zero in the layers deep enough that the line is thermalized. Its principal effect appears near the surface. Although its value depends on the strength of the line and has somewhat different values for lines on the linear, flat, or damping part of the curve of growth, its value is certainly positive, so that it cools. For weak lines, c tends to exceed t and produces the cooling; for medium and strong lines, t exceeds c, often by a large amount, and is responsible for the surface cooling. Often, this cooling of outer layers is accomplished by a few very strong lines such as Na I D, Ca II H and K, Ca I 4227, Mg I b lines, and Mg II h and k lines; in other cases, the more numerous medium strong lines provide most of the cooling except in the extreme outer atmosphere.

What of the lines which *warm* the surface, such as TiO (Mould, 1975; Lengyel-Frey, 1977; Tsuji, 1978a; Krupp et al.; 1978)? Carbon (1979) explains these in a physical way based on analogy with processes in the continuum discussed by Dumont and Heidmann (1973, 1976). In these processes, a major change in opacity occurs near the surface. Such processes can be discussed quantitatively within the above framework (Athay, 1972) if r_0 decreases rapidly with optical depth. Some molecules (TiO, H_2O, and HCN) exist in highest concentration near the outermost layers, where r_0 may change appreciably. In such cases, c becomes negative, and the surface layers are heated. This occurs for both the Schuster-Schwarzschild and Milne-Eddington atmospheres and is independent of the mechanism of line formation. The warming is enhanced by a flatter temperature gradient in the outer atmosphere, a line closer to LTE (ϵ is larger), and a value of r_0 which *decreases* with depth near the surface. An illuminating example of an atmosphere with an opacity discontinuity has also been explored by Mihalas (1969).

In actual calculation of stellar atmospheres, consideration of the detailed processes of line formation is normally avoided through the assumption of pure absorption (or even stronger assumption of LTE) so that the line source is equal to the Planck function for all lines, as shown in Figure 7-1. Occasionally, scattering is included for the strongest lines. Although this assumption may be adequate for deeper layers, its use might lead to fairly serious errors in the upper photosphere. Its only justification is a currently necessary simplicity. In fact, although some progress has been made, a *thorough examination of the mechanism of line formation* and of the possible errors arising from the assumption of pure absorption *is still lacking for even the strongest lines in the red-giant stars* (Carbon, 1979; Gustafsson, 1981; de la Reza, this volume). Research on this problem can be expected to yield significant new knowledge.

Treatments of Line Opacity

Even with the assumption of pure absorption in the line-source function, accounting for the rapid, almost random variation of the bound-bound absorption coefficient with wavelength across the entire spectrum, as implicit in the carbon-star spectrum shown in Figure 7-2 (Querci and Querci, 1975b), is a formidable task, and some statistical procedure becomes necessary. The successive steps in treating such opacities form the backbone of a history of cool-star atmospheric modeling and the successful treatment of at least certain atomic and molecular opacities represents one of the significant recent triumphs in stellar atmospheres.

Intuitively, one knows that an increase of opacity in a given frequency band will inhibit the flow of radiation there, and flux constancy then requires an increase in radiative flux at neighboring frequencies. This leads naturally to the idea of a harmonic mean (HM) opacity (i.e., K^{-1} is the integral of the reciprocal of the

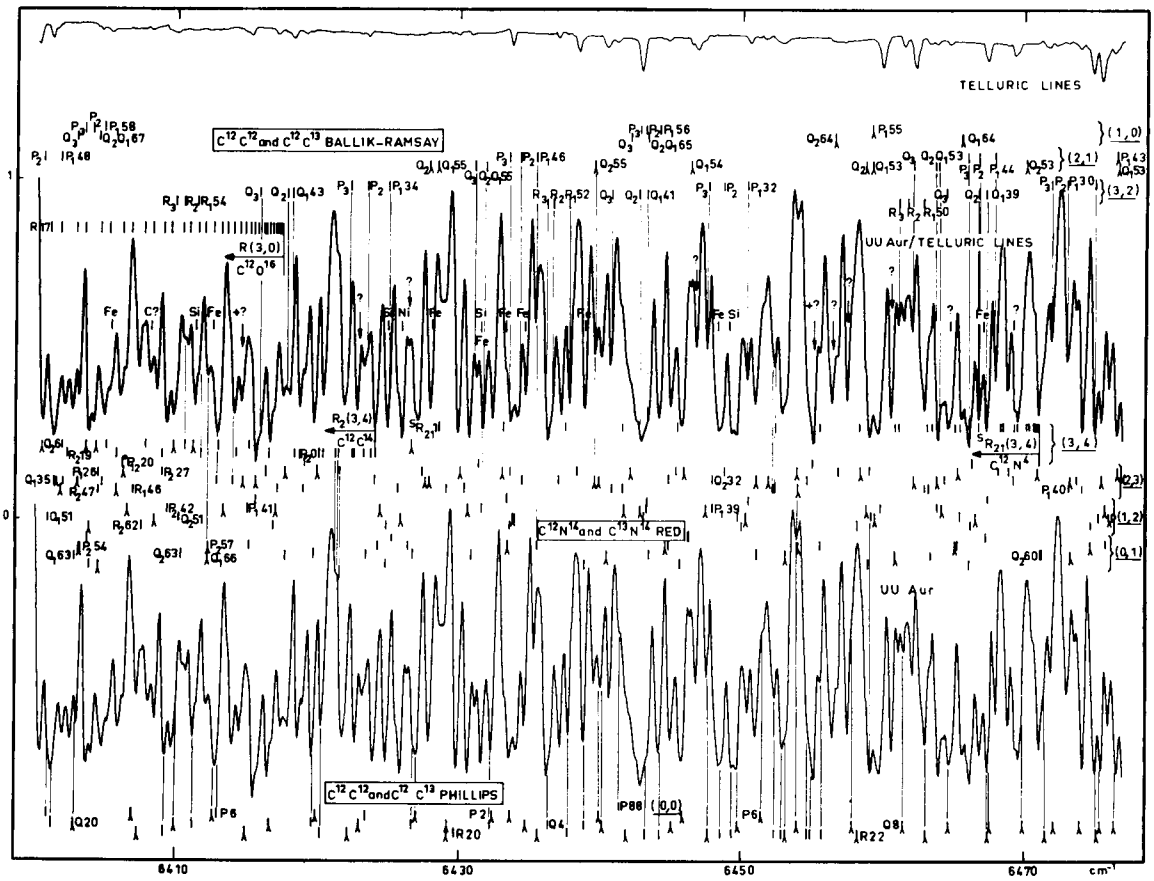


Figure 7-2: The observed spectrum of the N-type carbon star UU Aur in the region 6400 to 6480 cm^{-1} (bottom graph) and the same spectrum corrected for weak telluric lines (middle graph). Many lines of C_2 and CN are identified (from Querci and Querci, 1975b).

total absorption coefficient over a certain spectral interval divided by that interval). Unfortunately, different sources are not easily additive in an HM opacity, which makes its use cumbersome at best. Furthermore, the HM underestimates the opacity (Querci et al., 1972; Carbon, 1974, 1979; see also Figure 7-4). It has been used in only one set of models (Auman, 1969), in which H_2O was the only opacity treated.

A markedly different approach is represented by the straight mean (SM) opacity, which is simply the average integrated absorption coefficient of all lines in a spectral interval. An SM absorption coefficient (per molecule) for each species in each interval is fitted by a simple polynomial as a function of temperature, and the fitting coefficients are tabulated once for all (Alexander and Johnson, 1972; Johnson, 1974). Absorption coefficients for several absorbers are easily combined, and models are quickly calculated. The weakness of the SM is that the averaging process spreads the opacity over an entire spectral region, filling in the narrow spectral windows through which much of the radiation in reality escapes. The SM therefore overblankets the model, as has been elucidated by several studies (Querci et al., 1972; Johnson, 1974; Carbon, 1974, 1979). The accuracy of the SM obviously improves as the spectral interval over which the smoothing is done is decreased. Johnson et al. (1972) show

an example for CN. For comparable spectral intervals, the SM can be thought of as a one-picket opacity distribution function (see also Figure 7-4).

The opacity distribution function (ODF) was described by Strom and Kurucz (1966), and its modern use dates from about that time. In a given spectral interval (of, say, 50 Å), one rearranges the absorption coefficient in wavelength to obtain a monotonic ordering, the result having the appearance of one giant spectral line (Figure 7-3). This new monotonic function—termed the opacity distribution function—is then approximated by a series of pickets as shown. (Care must be taken, of course, to flip the giant line from side to side in alternate intervals and depths to avoid systematic effects (Gustafsson et al., 1975).) Various mathematical descriptions of the ODF are available (Querci et al., 1971; Carbon, 1973, 1979, 1984; Kurucz et al., 1974; Mihalas, 1978), and several applications have been made (Querci et al., 1974; Querci and Querci, 1975a; Gustafsson et al., 1975; Kurucz, 1979; Eriksson et al., 1985).

A representative ODF of CN and C_2 for conditions typical of carbon stars is shown in Figure 7-4 (Querci et al., 1971). Although the absorption of C_2 is much less than that of CN, it influences the ODF significantly. Also shown are the (constant) values for the SM and HM opacity; clearly the SM overestimates, and the HM underestimates, the true opacity. Similar comparison of SM, HM, and ODF opacities for CN in a carbon-rich model atmosphere was made by Carbon (1974).

Calculating the ODF is tedious, but construction of models proceeds rapidly when the ODF is available. If, however, the ODF is sensitive in a given wavelength region to several opacity sources, the relative strengths of which might depend on a parameter (such as chemical composition) that is not known beforehand, one could be forced to a time-consuming iterative procedure (cf. Carbon, 1979, 1984). At least some of this liability could be overcome by a two-step procedure in which ODF's are formed separately for each species and are then

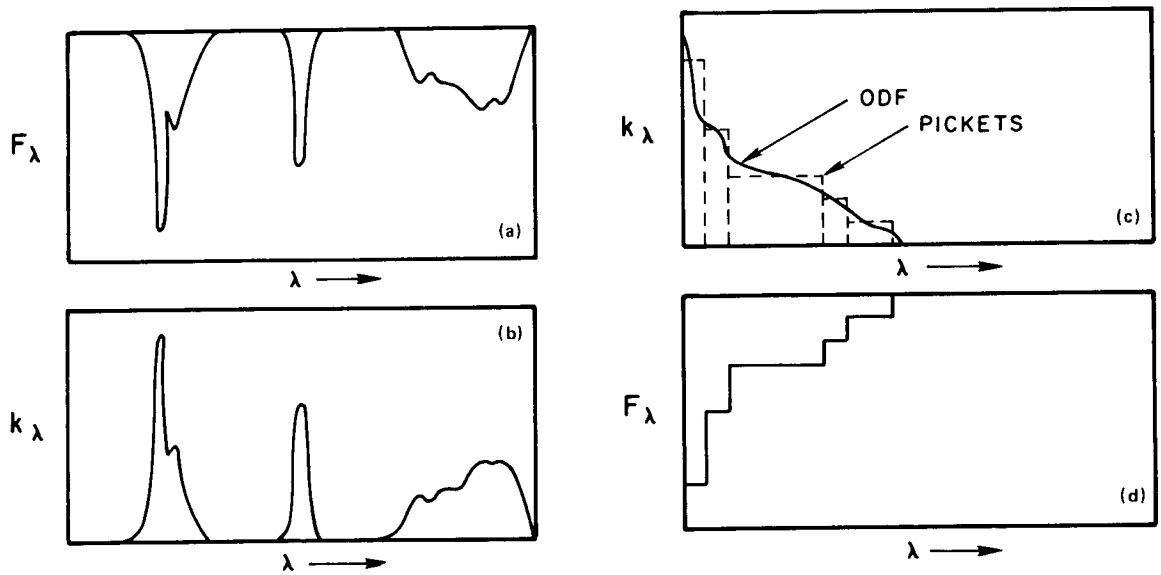


Figure 7-3. (a) Hypothetical spectrum over a spectral interval between λ_1 and λ_2. (b) Hypothetical line absorption coefficient over this interval. (c) The information in Figure 7-2b rearranged by strength of absorption to form an ODF or giant line (solid line) as described in the text. A possible six-picket representation of the giant line is shown by the dotted line. (d) The flux emitted by the picket representation of the opacities in (c).

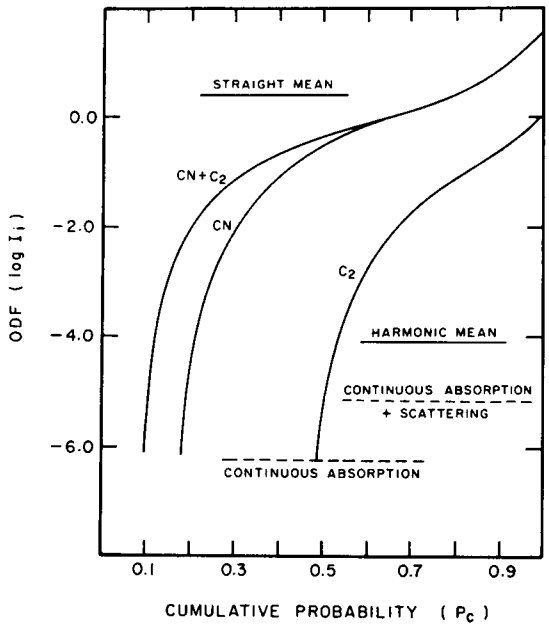


Figure 7-4. Comparison of various opacity treatments for CN and C_2 in the wave-number interval 6320 to 6420 cm^{-1}. The graph shown (from Querci et al., 1972) is for T = 2500 K, P = 1 dyne/cm^2, and microturbulent velocity VT = 5 km/s.

reshuffled to account for the changing depth dependence of the opacities (Tsuji, 1976a). Recently, in what appears to be a significant advance, the Swedish group has demonstrated the practicability of this suggestion by actual calculation and has further shown how the accuracy of the ODF can be increased by spline-fitting (Olander, 1981; Saxner and Gustafsson, 1984). This method allows the ODF to accommodate even the well-known problems of the depth-dependent combination of CN, C_2, and CO opacities in cool carbon stars.

Another drawback to the ODF arises from the rearranging of the absorption coefficient and its representation by a series of pickets; in this smoothing, all information regarding individual absorbers is lost. To ascertain the effect of a change in even one spectral line, as might arise from departures from LTE in even one atomic species, it is necessary not simply to recompute an atmosphere with this changed value, but to recalculate the ODF. It is difficult even in principle to determine how this weakness of the ODF method can be overcome (Carbon, 1984). For certain general problems, in which self-consistency between input parameters and results is necessary, the ODF may be too restrictive. For problems in which all parameters to which the absorption is sensitive can be specified beforehand, however, the ODF method is convenient and accurate. In addition, the ODF appears to be capable of describing the opacity in a differentially moving atmosphere (cf. Mihalas et al., 1976).

Suppose one begins to calculate model atmospheres without averaging the opacity in any way (i.e., suppose one were not constrained by the amount of computing time available). Under these ideal circumstances, a straightforward procedure would be to calculate the integrated flux and its depth derivatives by a direct integration over *many* monochromatic fluxes. Even though the variation of the absorption coefficient with frequency is rapidly changing, its integral can be obtained to any desired precision by taking a sufficient number of frequency points. This approach is called opacity sampling (OS), for there is no attempt to use all the opacity information; rather, one samples until one has sufficient.

How many frequency points are needed? Very favorable answers are already available; even for complex opacities, only 500 to 1000 frequency points are necessary if they are scattered over the entire spectrum and are randomly chosen with regard to opacity features (Peytremann, 1974; Johnson and Krupp, 1976). Models computed with even as few as 100 frequency points match fairly well a more exact model in the photosphere, but depart from it in the outer layers, and several models with different sets of 100 frequencies lie within a certain envelope in a T–τ diagram. As the number of frequency points is increased, the envelope narrows, and the envelope of models with 500 points has a spread which ranges from near zero deep in the photosphere to ± 50 K near the surface (Johnson and Krupp, 1976). The final model is thus "converged" in the sense that, for more

than about 500 points, *every set of points gives the same model*. Related interesting numerical experiments with an ODF and an OS calculation are reported by Gustafsson et al. (1975) and Gustafsson (private communication, 1984). Such characteristics put the OS method easily within the capabilities of current computers.

The power of the OS method arises from its simplicity and its retention of all information on all lines which influence the transfer of radiation at the selected frequencies. Everything is under the control of the investigator. New values of such factors as chemical composition, turbulent velocity, or even departures from LTE are easily accommodated. This flexibility comes at a cost, however, because the construction of each atmosphere demands much computing. Normally, the absorption of several tens of thousands of spectral lines (selected from a much larger sample) are accounted for in each calculation, making each iteration fairly time-consuming. Although some tricks (such as beginning with a small frequency set and using a larger set only for the final iterations) can save considerable computing, the OS method generally requires more machine time per model than other methods. Furthermore, even after a model is converged, the computation of the emergent flux requires the calculation of fluxes at many frequencies within each element of spectral resolution, and the fluxes are then smoothed to the desired resolution. Finally, one must be cautious of OS models in the extreme outer photosphere, in which the few strongest spectral lines which control the energy balance and the thermal structure may not be properly sampled. Quantitative investigation of this point is needed. Use of the OS method for radiative transfer in an atmosphere with a velocity gradient is also very awkward (Carbon, 1984) because of the shifting of line centers with depth.

Although the ODF and OS may appear to be competitors, they are in some sense complementary (cf. Carbon, 1984). When all parameters can be specified beforehand (e.g., in constructing a grid of stars of known composition), the ODF method is preferable because of its speed. When absorption-affecting parameters are to be varied (e.g., in constructing a sequence of stars differing in C/O or in accounting for departures from LTE), the OS is superior. (Additional insight can be gained from reading Gustafsson et al., 1975; Johnson and Krupp, 1976; Carbon, 1979; Gustafsson, 1981; and especially Carbon, 1984; and Saxner and Gustafsson, 1984). *We suspect that both the ODF and OS are capable of further development and look forward to these improvements.*

Less complicated than implied by the name (Voigt-analog/Elsasser-band model, or mercifully VAEBM), an offspring of the ODF has been developed (Tsuji, 1976a) and used with success in constructing red-giant atmospheres. The method proceeds from a generalization (Golden, 1969) to Voigt profiles of the Elsasser band model, which treats the opacity of a complex molecule by a picket-fence model consisting of an infinite set of equally spaced spectral lines of equal strength. Although real spectral lines have different strengths, shapes, and widths, one can nevertheless define average values of these quantities, adding pickets as needed. Even overlapping lines can be roughly accounted for. Restrictive as these assumptions appear, the VAEBM representation is, over a spectral interval sufficiently small that the Planck function does not vary appreciably, formally equivalent to the ODF described earlier (Tsuji, 1976a), and it has been exploited with good results. However, one can easily imagine the method failing in the case of overlapping opacities, especially with different depth dependences (Saxner and Gustafsson, 1984). In short, the VAEBM is a simple ODF, with the strengths and weaknesses of the ODF in addition to the more severe approximations by which the VAEBM gains its simplicity. On the other hand, it has the advantages of speed and the power to treat, at least crudely, even such complicated molecules as H_2O. Certain molecular VAEBM opacities have been compared to Rosseland (harmonic mean) opacities and JOLA opacities (just overlapping line approximation) in an interesting paper (Tsuji, 1971).

Like a phoenix, SM opacities never really die, and they have recently been in the news again because of their use in spherical models. A comparison of Rosseland opacities from SM and OS treatments (Scholz and Tsuji, 1984) finds good agreement for solar composition, but for a carbon-rich composition, the OS opacities are much smaller. Unfortunately, the agreement for solar composition is largely fortuitous because the OS treatment included H_2O as SM opacity (Johnson et al., 1980), and at the temperature used (T = 3000 K), the OS opacities are in fact dominated by H_2O. Accord between "OS" and "SM" is therefore simply accord between the SM of Johnson and the SM of Tsuji. Clearly, the Rosseland opacity must always be greater for SM than for OS or ODF, because the SM approximation fills in all opacity windows and acts, in a given spectral interval, exactly as an additional *continuous* opacity source.

In the following thought experiment, we imagine a continuous opacity and a superposed line opacity. Let the lines (rectangular for simplicity) cover half the spectrum and have an (equal) absorption coefficient 100 times that of the continuum. If calculated by the ODF or OS method, the Rosseland opacity is approximately *twice* that of the continuum alone since that half of the interval covered by lines is extremely opaque. If calculated by the SM, the average line opacity would be *50* times the continuous opacity, and the Rosseland opacity would also be increased by a factor of *50*. Clearly, *Rosseland opacities and SM opacities are not to be mixed.* Yet consider the absorption of a molecule with enormous numbers of weak lines, such as H_2O or HCN. If the 100000 strongest lines of HCN make little difference in an atmosphere (Tsuji, 1984), but 6 million weak lines make a large difference (Jørgensen, 1985), we understand the reason. Such an enormous number of lines fills in *all* the spectral windows, and like the SM, acts at that depth as an additional *continuous* opacity. If a molecule contributes a haze of lines (even weak ones), it may greatly increase the opacity, and such polyatomic opacities (Auman, 1969; Tsuji, 1984; Eriksson et al., 1984) must be included (laboriously) in at least the coolest red-giant atmospheres. A similarly large Rosseland opacity can be obtained by filling in the opacity windows with isotopic lines and very large microturbulant broadening (Sharp, private communication, 1984).

THEORETICAL PHOTOSPHERIC MODELS

As might be expected, the passage of time has seen a steady improvement in theoretical photospheric models, particularly in regard to the treatment of opacity. It is convenient, then, to separate models into two groups according to the opacity approximation employed: (1) first-approximation opacities (SM, HM, or similar treatment), and (2) second-approximation opacities (ODF, OS, or VAEBM treatments). *We include in this chapter only giant and supergiant models with effective temperatures below 4000 K.*

First-approximation models have already been summarized and extensively discussed (Vardya, 1970; Johnson, 1972, 1974; Kipper, 1973; Carbon, 1979; Gustafsson, 1981). Although they are now generally superseded by superior models with the same range of parameters, these earlier models were the basis of several noteworthy discoveries. Perhaps the most significant was that, contrary to common belief, convection (in the usual mixing-length formulation) was of minor importance in the photosphere itself—both for M stars (Auman, 1969) and for carbon stars (Johnson, 1972). Somewhat surprisingly, even though models with SM and HM opacities have quite different structures, computed molecular column densities agree very well (Goon and Auman, 1970; Johnson et al., 1975), indicating that these latter are rather insensitive to the details of the atmospheric structure. The large scale heights observed in stars such as ζ Aur were duplicated by theoretical models with appropriately low values of surface gravity (Johnson, 1972). The observed flux from a cool carbon star was fairly

well represented by the predicted flux from an appropriate model (Johnson, 1972), except that the model flux was too high in the blue and the CN bands were too deep. Older atmospheric models were used for several projects: (1) to examine the remarkable cooling by CO in the outer layers of stars (Johnson, 1973); (2) to interpret the infrared spectra of several carbon Mira stars in support of the hypothesis of C enrichment rather than CNO processing (Thompson, 1977); (3) to study the atmosphere of Betelgeuse (Fäy and Johnson, 1973); (4) to deduce, from IR observations, approximate effective temperatures of K and M giants and supergiants (Scargle and Strecker, 1979); and (5) to infer the ratio $^{12}C/^{13}C$ in five carbon stars (Olson and Richer, 1979). Finally, to explore the gross molecular features of S stars, Piccirillo (1980) computed 85 SM model atmospheres for $2500 \leqq T_{eff} \leqq 3500$ K and log $g = 0$ for compositions enriched in C to give ratios of C/O in the range 0.6 (solar) to 1.00. A point of interest here is his finding that the thermal structures of some of these SM models were similar to OS models. Several conclusions regarding C/O and s-process enhancements in S stars emerged from a comparison of his molecular column densities and observed band strengths—perhaps the most significant being that, in certain S stars, C/O may be nearer 0.9 than 1.0.

In considering models with *second-generation opacities*, we continue to distinguish models which are oxygen-rich (M stars) and carbon-rich (C-stars). S stars, which are intermediate, will be discussed along with C stars.

Models for M Stars

An overview of currently available models for solar composition is given in Figure 7-5 (from Johnson, 1985), where models are shown in the parameter space of effective temperature and surface gravity (log g). All published models with the assumptions of Figure 7-1 and plane-parallel geometry (PPG) and based on ODF, VAEBM, or OS opacities are shown; they are identified as BEGN (Gustafsson et al., 1975; Bell et al., 1976a). T (Tsuji, 1976a; 1978a), or JBK (Johnson et al., 1980). In each group, certain additional models with variations in parameters other than those shown as coordinates were calculated. Models of Tsuji (1976a, 1978a) are purely radiative, whereas models of Gustafsson et al. (1975), Bell et al. (1976a), and Johnson et al. (1980) also include convection. Although it may appear that this parameter space is fairly well covered by models, the coverage is sparse in places, and several principles of the classic atmosphere may be stretched rather badly toward lower temperatures. Perhaps the worst assumption is the crude treatment of H_2O opacity, but the assumption of PPG and even homogeneity may not be met in the coolest, most extended stars.

Designed to represent Population I and II giants, the grid of Gustafsson et al. (1975) and

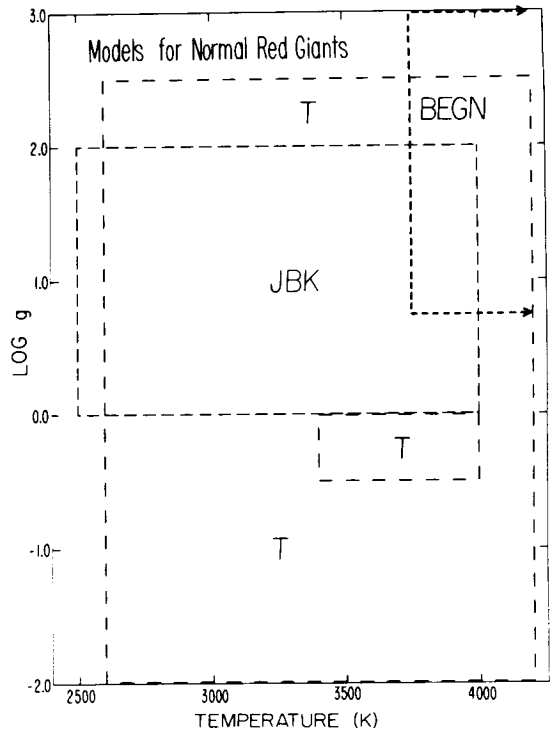


Figure 7-5. Overview of available models for normal red giants of solar composition displayed in the space defined by the surface gravity (log g) and the effective temperature. References are given in the text (from Johnson, 1985).

Bell et al. (1976a) spans the ranges 3750 K $\leqq T_{\rm eff} \leqq$ 6000, 0.75 $\leqq \log g \leqq$ 3.0, and $-3.0 \leqq$ [A/H] $\leqq$ 0.0. Altogether, 103 models based on ODF opacities for CO, CN, OH, NH, MgH, and atomic lines were computed. No TiO lines were included, which unfortunately compromises the accuracy of models with $T_{\rm eff} \leqq$ 4000 K—precisely those of interest here. Convection was treated by the mixing-length theory with a mixing length 1.5 times the pressure scale height. Although turbulent pressure was neglected, a study of the possible effects of its neglect was made. For a model from near the middle of their grid, Gustafsson et al. (1975) find that, for v(turb) = 5 km/s, P(turb) becomes an important component of P(total), but the thermal structure [$T(\tau)$] is affected only slightly except in the convection zone. The surface cooling of CO lines was confirmed quantitatively, and CN lines were shown always to backwarm the entire atmosphere. The authors conclude (Gustafsson et al., 1975) that self-consistent LTE models with as many as 10^5 wavelength points are possible, but a much smaller number of points is satisfactory for either the ODF or OS method. The temperature uncertainty due to all accumulated errors is estimated at 100 K in the outer layers, 20 to 30 K through most of the photosphere, and 100 K in the convective zone. Uncertainties due to the assumptions of LTE and homogeneity, which were not investigated, could be considerably larger. Several applications of these models to astrophysical questions are described in the section *Spectral Distribution of Energy Fluxes* (see also Gustafsson, 1981).

To find a middle ground between the crude approximations inherent in SM opacities and the tedious computations required for the usual ODF opacities, Tsuji (1976a) used the VAEBM method described earlier to treat the opacities of OH, CN, CH, TiO, MgH, SiH, CaH, CO, and H_2O (some approximated more carefully than others) and construct 11 models for supergiant stars. They range in effective temperature from 3400 to 4000 K and $\log g$ = 0.0 or −0.5. Turbulent pressure is included in the hydrostatic equilibrium equation with velocities of 3, 6, and 12 km/s, but convection is neglected. In a companion paper, Tsuji (1976b) uses these models for a specific discussion of Betelgeuse, for which he deduces a value of $T_{\rm eff} = 3900 \pm 150$ K.

A grid of 22 models for K and M giants based on these VAEBM opacities was later computed and used to define a new relation between spectral type and effective temperature (Tsuji, 1978a). Based on LTE, hydrostatic equilibrium (including radiative and turbulent pressure with a turbulent velocity of 3 km/s), and radiative equilibrium (convection was neglected), these models were computed for the ranges 2600 $\leqq T_{\rm eff} \leqq$ 4200 K and $-2.0 \leqq \log g \leqq 2.5$. Predicted fluxes were then compared to photometry of a number of cool stars to fix the relation between effective temperature (from the models) and spectral class (from the stars). Tsuji emphasizes the desirability of comparing infrared fluxes for finding best fits because of the relative insensitivity of the infrared flux to opacity variations. Yet we wonder whether a fit also to the visual region (with its much steeper slope) as well might fix the temperature of a star with greater precision. Many of these models predict substantially too much flux in the visual region (a common problem).

Based on the ATLAS computer program (Kurucz, 1970), Johnson et al. (1980) calculate 40 atmospheres with solar composition and the parameters: $T_{\rm eff}$ = 2500, 2750, 3000, 3200, 3400, 3600, 3800, and 4000 K and $\log g$ = 0.0, 0.5, 1.0, 1.5, and 2.0. Convection is included, but turbulent pressure is neglected. Atomic lines and molecular lines from CN, CO, C_2, TiO, OH, NH, CH, and MgH are treated by the OS method; H_2O is added as an SM opacity. In a sense, these results complement those of Gustafsson et al. (1975) to provide a complete set of models for cool giants and supergiants for all temperatures. Although this work is the most complete now available for very cool stars, the weakness of several assumptions should caution the reader against uncritical acceptance of every value. Treating H_2O as an SM opacity overblankets the coolest models

($T_{\rm eff} \leqq 3200$ K) (Auman, 1969; Tsuji, 1971), and this is probably the most serious defect. Neglect of grain formation in the coolest models may also be incorrect. The temperature and density in the surface layers of the supergiant ($\log g = 0.0$) models might be even lower if sphericity were included.

How well do the models agree where they overlap? A comparison of $T(\tau)$ has been made, for the particular case of (4200/2.25/solar), between a Bell et al. (1976a) (ODF) model and a Johnson et al. (1980) model (Johnson and Krupp, 1976). All opacity parameters were identical, but the opacity treatment, as well as the computer codes, was different. The excellent accord in $T(\tau)$ — within ± 30 K except in the extreme outer layers — indicates that both the ODF and OS methods are satisfactory. In the extreme outermost layers, the temperature is fixed by those few strong lines which still have some opacity (i.e., for which $\tau(\nu) \approx 1$), and these may not be accurately treated by the OS method (Carbon, 1979; Johnson et al., 1980). Departures from LTE and possible chromospheric heating are also more likely in these superficial regions. Since TiO opacity, which is important in warming the outer layers, is neglected by Gustafsson et al. (1975) and Bell et al. (1976a), their coolest models ($T_{\rm eff} < 4000$ K) are not recommended (McGregor, 1980).

A parallel comparison of a model (4000/1.5/S) with VAEBM opacities from Tsuji's grid with a similar model of Bell et al. (1976a) shows that the two agree within ± 50 over most of the atmosphere, but the former is hotter in the outer layers and cooler in the deeper layers (by up to 130 K). Emergent fluxes from the two also agree well, whereas similar fluxes from an SM model display molecular bands which are too deep (Tsuji, 1976a).

The atmospheres of Johnson et al. (1980) form a sequence parallel to that of Tsuji (1978a), and together these constitute the only models for M giant stars with realistic opacities. A comparison of the T–τ relation between models from each set has been made by Johnson et al. for the parameters 3600/0.0/S, and the agreement is excellent. This is the more impressive because the computer codes and molecular data were independent and the methods of treating the line opacities were different (VAEBM by Tsuji and OS by Johnson et al.).

Models for Carbon and S Stars

An overview of the available models for carbon and S stars (i.e., with C/O > 0.6) is provided by Figure 7-6 (Johnson, 1985), which shows the regions in the parameter space of effective temperature and the ratio of carbon to oxygen covered by various sets of models. Figure 7-6 is, of course, a two-dimensional projection of the multidimensional space whose axes are the parameters specifying these models. Be-

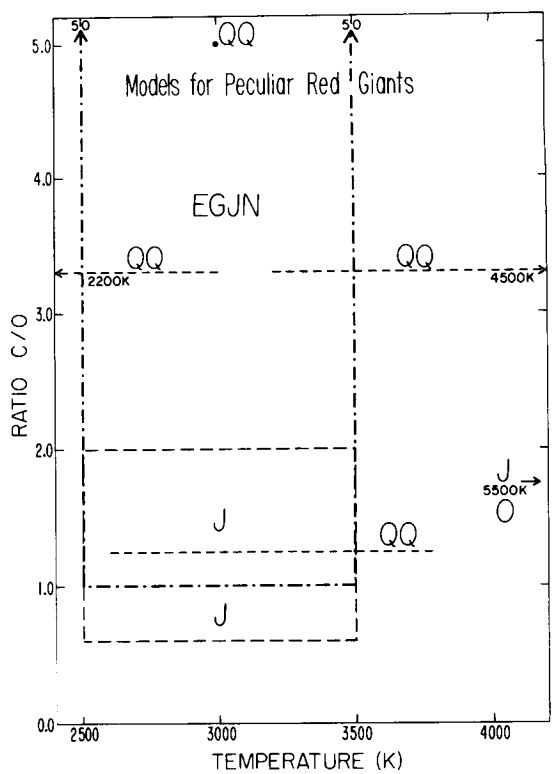


Figure 7-6. Overview of available models for peculiar red giants (M, S, R, and N-type stars) displayed in the space defined by the carbon-to-oxygen ratio and the effective temperature. References are given in the text (from Johnson, 1985).

sides surface gravity, they include the abundance of *all* significant elements, especially C, N, and O. Clearly, Figure 7-6 is a considerable simplification, and sets of models shown as lines (such as QQ) contain models varying in some parameter other than the two used as coordinates—in this case, N/H and log g.

Based on an ODF which included lines of the molecules CN, C_2, and CO, but no atomic lines, the French group (Querci et al., 1974) constructed 12 carbon-star model atmospheres with effective temperatures of 4500, 4200, 3800, and 3400 K and surface gravities of g = 0.1, 1.0, 10 cm/s^2. These were later supplemented with 9 cooler models having effective temperatures of 3000, 2600, and 2200 K (Querci and Querci, 1974). Convection was neglected, but a turbulent pressure $P(\text{turb}) = \beta\varrho v^2$ was used in the hydrostatic equation. Values of β = 1 and β = 0 and v = 5 km/s were chosen to agree with the microturbulent velocity deduced earlier from the spectrum of UU Aur. Solar abundances were used for all elements except CNO, which were fixed at H/C/N/O = 1/4.1 × 10^{-5}/1.48 × 10^{-3}/1.25 × 10^{-5} (C/O = 3.2 and N/C = 37), to represent a composition produced by CNO processing and mixing. The effect of molecule line blanketing is clearly seen in their models (Figure 7-7); for successively lower temperatures, the molecular line blanketing increasingly cools the surface layers and warms the photosphere compared to the unblanketed models. These authors found: (1) considerable surface cooling and photospheric heating due to CO, C_2, and CN; (2) good agreement in thermal structure (perhaps surprising) with certain SM models; (3) fair agreement—slightly better than with a blackbody—of predicted fluxes, except in the visual region, with wideband photometry of TX Psc for models with T_{eff} = 3000 and 3400 K. An additional set of 14 models with compositions representing both CNO cycling and triple-alpha processing were calculated, and certain molecular features characterizing each composition were noted (Querci and Querci, 1975a). Synthetic spectra from these models are discussed later.

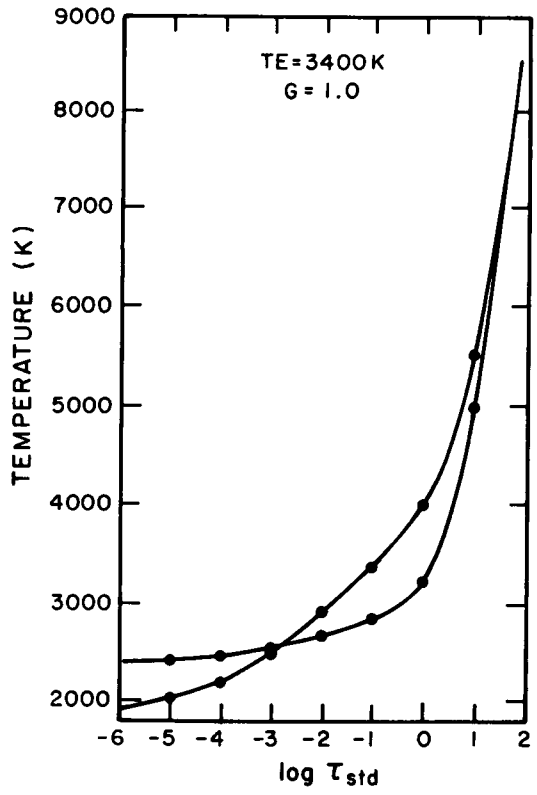


Figure 7-7. Effect of molecular line opacity. At an effective temperature of 3400 K and surface gravity of 1.0, a photospheric model for a carbon star with C_2, CN, and CO opacity is compared to an identical model without these (Querci and Querci, 1974). In each case, the blanketed model is cooler at the surface and warmer in the photosphere.

Another set of 27 models for M, S, and C stars has been produced with OS opacities for atomic lines and the molecules CH, NH, OH, MgH, CO, CN, and C_2 (Johnson, 1982). Three series of models were computed, all with log g = 0.0, at effective temperatures of 2500, 3000, and 3500 K. Beginning with a model of solar composition, carbon is added incrementally to give C/O ratios of 0.60 (approximately solar), 0.90, 0.95, 0.98, 1.00, 1.02, 1.05, 1.20, and 2.00. Convection is included in the usual mixing length formulation with ℓ/H = 1.0; turbulent pressure is neglected. The effect of C/O on the structure is illustrated in Figure 7-8,

which displays models with C/O = 0.60, 1.00, and 2.00—possibly representing a cool M supergiant, an S star, and an N-type carbon star, respectively. For comparison, a model with solar composition but *no* line blanketing (labeled 0.60*) has the expected form: a steep gradient in the photosphere and a flat outer portion with a boundary temperature T_o = 2300 K. An identical model that includes atomic and molecular opacities is warmer throughout the photosphere due to the backwarming and cooler (due mainly to CO and H_2O) in the outer layers (outside the graph shown) with T_o = 2100 K. As carbon is added and free oxygen is reduced by the formation of CO, the partial pressures and opacities of H_2O and TiO decrease. Recall that H_2O cools near the surface and backwarms the photosphere, while TiO warms the surface layers (Krupp et al., 1978; Gustafsson and Olander, 1979; Gustafsson, 1981). This decrease in backwarming as H_2O and TiO decrease in abundance causes the temperature drop noted. In the outer atmosphere, the increase in CO cooling as carbon is added more than compensates for the loss of H_2O cooling, and the outer layers continue to cool (Carbon, 1974; Heasley et al., 1978; Carbon, 1979). The remarkable resemblance between the model with C/O = 1.0 and the unblanketed model illustrates well that an S star has little molecular line opacity.

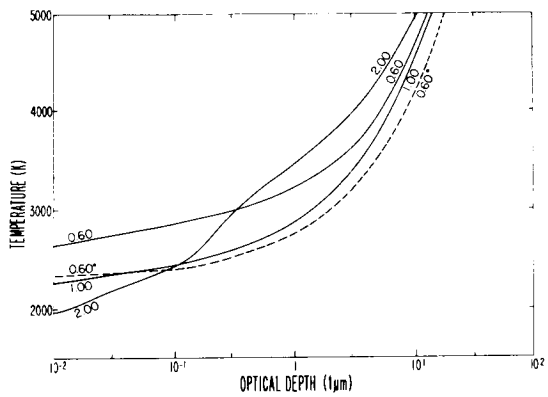


Figure 7-8. Effect of the enhancement of C on the thermal structure ($T(\tau_1)$) of a model with (3000/0.0/solar except C) (from Johnson, 1982). Optical depth is measured in the continuum at 1 μm. The parameter is C/O. A dotted line is a model with solar composition (C/O = 0.60) but without any line blanketing.

As additional carbon is added beyond C/O = 1.0, the temperature increases again throughout the photosphere due to the backwarming of CN and C_2 (Querci et al., 1972, 1974; Querci and Querci, 1975a; Sneden et al., 1976). In the outer layers, the temperature seems to decrease. In actuality, the *boundary* temperature (1400 K) does not fall, but it is reached at a larger value of optical depth as C/O increases; that is, this cool outer layer deepens as carbon is enhanced (Johnson, 1982). Figure 7-8 illustrates that, because an enhancement of carbon changes the atmospheric structure, spectral features—including those of elements other than carbon or its compounds—may also change. This point has previously been made from a study of molecular column densities (Johnson et al., 1975; Piccirillo, 1980; Johnson and Sauval, 1982), approximate band strengths (Scalo, 1973), and synthetic spectra (Querci and Querci, 1976).

Of great interest is the value of the boundary temperature and the thermal structure of the outer layers of red-giant atmospheres. In his review of model atmospheres for intermediate and late-type stars, Carbon (1979) pointed out that, in the discovery paper (Johnson, 1973), the cooling due to CO (based on SM models) was twice that found in later studies with more accurate ODF opacities (Gustafsson et al., 1975). In this present case, the cooling of the M supergiant is about 200 K, whereas that of the S star and carbon star are about 900 K. In addition, Johnson et al. (1980) list three considerations which might further *lower* the boundary temperature: (1) models may not be calculated at sufficiently small optical depths to reach the true value of T_o; (2) the OS method may fail to sample the strongest lines in the outermost layers and therefore underestimate the

cooling; and (3) neglected sphericity effects may lower T_0. A cooler surface layer will increase the chance for grain formation in the photosphere (Lucy, 1976; Menietti and Fix, 1978; Deguchi, 1980; Schmid-Burgk and Scholz, 1981; Draine, 1981; Alexander et al., 1983). On the other hand, chromospheric heating may *raise* the boundary temperature. At present, the boundary temperatures for these stars are unknown, but the value of T_{min} may be obtainable from high-resolution International Ultraviolet Explorer (IUE) observations, and such investigations are strongly encouraged.

Although the R stars, at least those of spectral class R0 to R3, correspond more closely to K than M stars, they are included in this volume because of their carbon-rich spectra and advanced evolutionary state. Models have been computed by two groups. The Swedish group published 20 models (Olander, 1981) with effective temperatures in the range 3800 to 4800 K. An interesting aspect of this project is the attempt to circumvent some of the drawbacks of the ODF (Carbon, 1979) by reshuffling the ODF's of different species. The author concludes that: (1) because of the relatively high temperatures of R stars, changes in compositions do not drastically affect the temperature structure; (2) raising the N abundance causes a slight backwarming ($\leqq$ 100 K) and surface cooling due to the increased CN opacity; (3) the effect of changes in the O abundance is very slight; and (4) raising the microturbulent velocity from 2 to 5 km/s causes a slight warming throughout the atmosphere, as was found for G and K giants by Gustafsson et al. (1975) and Bell et al. (1976a) and for cooler carbon stars by Johnson (1982). At approximately the same time, the Indiana group produced 11 models for R stars (Johnson and Yorka, 1985). These span a slightly higher temperature range (4200 to 5600 K), and surface gravity is fixed at either log g = 2.0 or 3.0. The log abundances of H/C/N/O were taken as 12.00/9.09/8.31/8.55, to give C/O = 1.74, although models were calculated for the additional values 0.60, 1.00, and 2.50 at a temperature of 4600 K. Yorka (1981) found the two sets of models to be in excellent agreement, and Dominy (1984) used them to help infer the effective temperatures of a set of warm R stars (R0 to R3).

None of the carbon-star models published to date contains polyatomic opacities (except for a few SM models by Johnson, 1974), but the importance of HCN in cool carbon stars has recently been reemphasized (Eriksson et al., 1984; Tsuji, 1984; Jørgensen, 1984). A large set of models for $2500 \leqq T_{eff} \leqq 3500$ K and $1.00 \leqq C/O \leqq 50$ which include ODF opacities of HCN and C_2H_2, as well as the usual diatomic opacities, has been calculated. We refer to these as the EGJN models (Ericksson et al., 1985) and eagerly await their publication.

Finally, we mention a set of 10 carbon-rich models with the parameters 3000/0.0/S except C; C/O = 1.05, in which the fractional abundance of H was incrementally reduced and replaced by He (Johnson et al., 1985). Interestingly, even this drastic change in composition alters the thermal structure (T–τ) only very slightly, whereas the pressure structure (P–τ) is greatly changed (equivalent to a change in gravity). The energy flux curve is also changed in the sense that, as the hydrogen abundance is decreased, the H^- flux peak at 1.67 μm is steadily reduced relative to the blackbody peak near 1.0 μm.

Again, how well do the model makers agree among themselves? A comparison of models for carbon stars is more difficult than for M stars because the extra dimensions of chemical composition mean less overlap between different sets of models. Nevertheless, in Figure 7-9 we compare, for models with the parameters 3000/0.0/solar except C; C/O = 2.00, the thermal structure ($T(\tau)$) and the pressure structure ($T(P)$) of the HJ (Johnson, 1982) models and EGJN models (Gustafsson, private communication, 1984). For models with diatomic molecular opacities only, both the thermal structure and the pressure structure are in good agreement, the differences being attributable to differences in molecular data and computer codes. When polyatomic opacities are included, the thermal structure is almost unchanged,

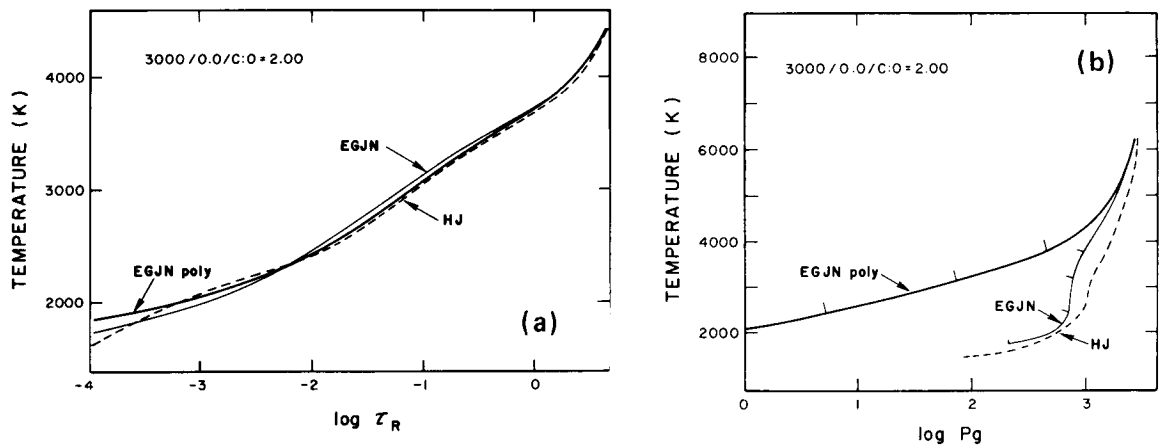


Figure 7-9. Comparison of carbon-rich models computed by the Swedish group (EGJN) and the Indiana group (HJ) and the effect of polyatomic opacities. (a) The T–τ structure of models by the two groups with (EGJN poly) and without (HJ, EGJN) HCN opacity. (b) The T–P structure of models with and without HCN opacity. (Gustafsson, private communiction, 1984; other references are given in the text.)

but the pressure is greatly reduced because of the large increase in opacity.

From this brief overview of models with carbon-rich composition, it should be apparent that the coverage of parameter space is sparce; we are barely beginning. *Before using any model atmosphere* for red-giant stars to calculate quantities, such as profiles of very strong lines, which depend sensitively on the temperatures in the extreme outer layers ($\tau \leqq 0.0001$, say), one should *contact the maker of the model* to discuss problems. (The guarantee normally covers only the photosphere!)

SPHERICAL MODELS

While calculations (Auman, 1969; Johnson, 1972; Tsuji, 1976a) confirm the adequacy of PPG for giants ($\log g = 2.0$), it may fail for low-mass supergiants and Miras. Three changes must be made in the usual equations to accommodate sphericity.

1. The equation of radiative transfer must include a curvature term:

$$\mu \frac{\partial I}{\partial r} + \frac{(1-\mu^2)}{r} \frac{\partial I}{\partial \mu} = \epsilon - \chi I \ ,$$

where $I(r,\mu,\nu)$ is the specific intensity, $\mu = \cos\theta$ as usual, $\epsilon(r,\nu)$ is the volume emissivity, and $\chi(r,\nu)$ is the linear extinction coefficient. Azimuthal symmetry and time-independence are assumed. If $(\partial I/\partial\mu) = 0$, one recovers the usual equation of PPG.

2. The surface gravity is no longer constant, but $g = GM/r^2$, and the variation of g (but not M) with r must be accounted for.

3. A third parameter, in addition to $T_{\rm eff}$ and g, is needed to specify fully the atmosphere. This is often the stellar radius, measured to some reference level, such as $\tau = 1.00$.

The complete equations for spherical geometry and methods for their solution have been available for several years (cf. Mihalas,

1978). Rather different mechanisms produce atmospheric extension in the early-type and the late-type stars. In hot stars, electron scattering produces an outward radiative force which leads to an extended atmosphere. Contrarily, red-giant atmospheres are extended only because of the very low surface gravity (unless, of course, there are outward flows; see Goldberg, this volume).

A commonly used measure of the importance of sphericity is the *extension*, or the relative thickness of the atmosphere compared to the stellar radius. More precisely, the extension is $d = (r(\text{top}) - r(\text{phot}))/r(\text{phot})$, where $r(\text{top})$ is the radius measured to the point at which $\tau = 0.0001$, say, and $r(\text{phot})$ is the stellar radius measured to $\tau = 1.00$. Authors differ slightly in employing a Rosseland optical depth or a monochromatic optical depth and in the exact value of the optical depth (10^{-5} to 10^{-3}) chosen for the top of the atmosphere.

To delineate the regions of the HR diagram in which sphericity might be important, Hundt et al. (1975) and Schmid-Burgk and Scholz (1975) computed a series of spherical models for late-type stars having gray opacities. Of interest here are two principal findings: (1) many red giants and supergiants of moderate mass ($M \approx 1\ M_\odot$) develop extended atmospheres at some epoch during their lives, usually near the peak of their RG luminosity; and (2) temperatures in the outer layers are considerably lower than in a comparable plane-parallel model.

More realistic models were obtained by Watanabe and Kodaira (1978, 1979), who included the line opacities of H_2O, CO, CN, OH — approximated with a mixture of SM, JOA (just overlapping approximation), and VAEBM. In these spherical models, the temperature was lower in the outer layers (by 150 to 200 K in the model with $T_{\text{eff}} = 3200$ K, for example) and higher in the deeper layers than in a corresponding PPG (here called compact) model. The density was also lower in the outer layers than in a corresponding PPG model. The number density of most molecular species, such as CO and CN, followed the overall decrease, but there were certain exceptions, notably those for which the increased efficiency of molecular formation due to the lower temperature overcomes the reduction in the overall density (e.g., H_2O in the model with $T_{\text{eff}} = 3200$ K). For atmospheres with extensions up to $d = 1.5$, these workers found: (1) an increase of atmospheric extent, (2) a reddening of (R–I), and (3) a decrease in the absolute visual magnitude. In addition, stellar diameters measured at wavelengths within those molecular bands formed in extreme outer layers and hence sensitive to atmospheric extension, such as H_2O and TiO, increased as much as a factor of 1.5 compared to the adjacent continuum.

Similar calculations which reinforced these tentative conclusions were carried out by Schmid-Burgk et al. (1981) and Kipper (1982) for models with solar composition. Most of the conclusions were drawn from models computed with continuous opacities and H_2O only, which is probably the dominant absorber in this temperature range. These authors document the great sensitivity of the thermal structure to the treatment of molecular opacities, the incorrect treatment of which can obscure other effects. Figure 7-10 (Schmid-Burgk et al., 1981) illustrates one of the principal effects of sphericity—a lowering of the temperature in the outer layers, where divergence of the flux is important. The temperature drop is greater in the lower gravity A models. (A slight backwarming—too small to be seen here—accompanies the surface cooling.) In the outermost layers, the temperature decrease is 300 to 500 K for a model with extension $d = 0.25$ compared to a compact model. The other principal effect of atmospheric extension—the decrease in density in the outer layers—is illustrated in Figure 7-11 (Schmid-Burgk et al., 1981). The key effect is the drop in pressure (and density as well) from A0 to A2 and B0 to B3; the lower gas density arises from the decreasing gravity, which falls as r^{-2} in these spherical models. Figure 7-11 also shows the radius (r/R) plotted against an optical depth scale ($\tau(1.2\ \mu\text{m})$); the transformation from radius to optical depth is sensitive to the details of the opacities and to the relation of H and H_2, which dominate the

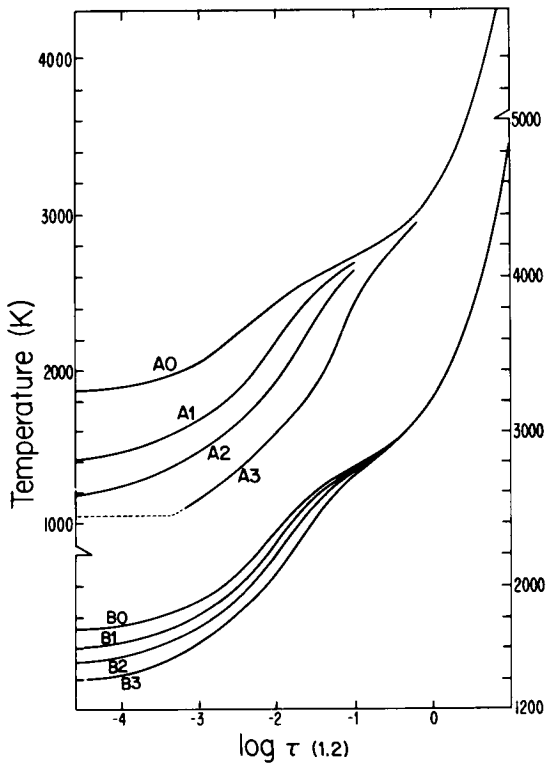


Figure 7-10. The effect of atmospheric extension on the thermal structure of a star. For each series of models, the extension of the atmosphere is increased from A0 (PPG) and B0 (PPG) to A3 (d = 1.39) and B3 (d = 0.20). Parameters of the models are: A: 3000/-1.0; B: 3000/0.0 (from Schmid-Burgk et al., 1981).

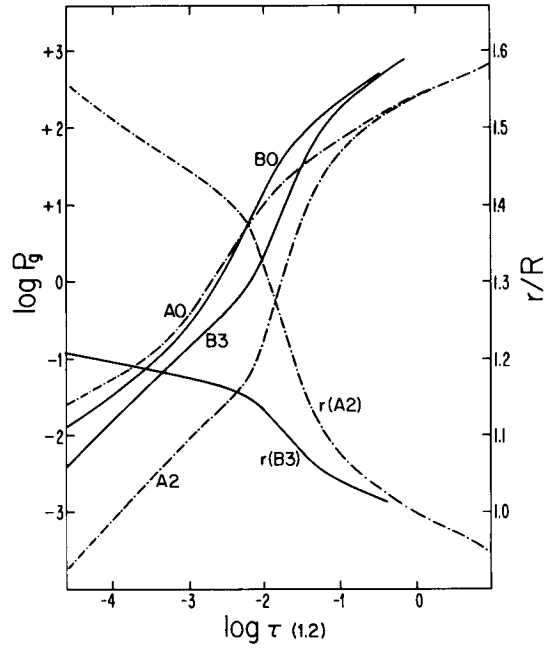


Figure 7-11. Effect of atmospheric extension on the gas pressure for the models of Figure 7-10 (from Schmid-Burgk et al., 1981). The radius (r/R) is also shown for the most extended models.

equation of state at these low temperatures (Schmid-Burgk et al., 1981). As is clear from a consideration of the two figures, the number density or partial pressure of a particular species depends rather critically on the details of the temperature/density relation in the outer atmosphere, which is not well known at this stage of research. Schmid-Burgk et al. also estimate the maximum tolerable value of the extension to be $d = 0.05$ or perhaps as large as $d = 0.10$ in certain cases. The values are exceeded, *at some epoch, in almost all M giants* with luminosities $\geqq 10^3$ solar luminosities and masses near 1 $M_\odot$ (see, for example, Scalo et al. (1978) and Scalo and Miller (1979) for an estimate of these masses).

Pursuing further the consequences of variations in the chemical composition for M supergiants, still within the framework of SM molecular opacities, Wehrse (1981) varied separately the abundances of He, the CNO group, and the metals. Lowering the metal abundance increases atmospheric extension and surface cooling, whereas introducing a hydrogen deficiency reduces sphericity effects. However, because of its interplay of various factors, separating sphericity from compositional effects appears to be extremely difficult.

To find an observational third parameter, Scholz and Wehrse (1982) computed very cool ($T_{\rm eff}$ = 2750, 3000 K) models based on SM opacities of several molecules in addition to H_2O and then calculated band strengths from these models. They find that *for their models*: (1) the 1.04–4.00 and the 2.10–4.00 μm colors can be calibrated to yield effective temperatures; (2) certain metal/ion atomic lines can yield the surface gravity; and (3) TiO lines in

the red are especially sensitive to atmospheric extension.

Again utilizing SM opacities, Scholz and Tsuji (1984) study carbon-rich spherical atmosphere. Because of the greater temperature sensitivity of the carbon-rich opacities, these atmospheres are *less extended* than oxygen-rich atmospheres. For the same reason, gas pressure and density are higher in C-rich spherical atmospheres than comparable PPG (compact) atmospheres, but oxygen-rich stars behave *oppositely*.

Spherical models will clearly come to play a major role in the study of red-giant stars—especially for supergiants and Miras—as soon as realistic opacities can be used.

CONVECTION AND INHOMOGENEITIES

Despite much research on the subject, convection is one of the more uncertain aspects of atmospheric modeling. The problem is simply that we do not understand the phenomenon; not only is convection an extremely complex hydrodynamic phenomenon, but we are without the benefit of sure terrestrial or laboratory analogs.

Envelopes of red-giant stars must be the scene of deep strong convection due to the opacity associated with hydrogen and helium ionization/recombination zones. Somewhere in the deep photosphere—near the depth where $\tau(R) = 10$, but depending on effective temperature, surface gravity, and composition—the envelope changes rapidly from a convective to a radiative regime. Photospheres lie at and immediately above this transition, and it has been shown for both M stars (Auman, 1969) and carbon stars (Johnson, 1972) that convection, if treated in the usual local mixing-length theory without overshoot, is unimportant in the photosphere (see also Gustafsson et al., 1975). Because of the rapid changeover from a convective to a radiative regime, our conclusions regarding convection may be sensitive to the details of the photospheric models, and at present, these are somewhat uncertain. Thus, although convection appears to be unimportant, this is not a robust conclusion, particularly if inhomogeneities are present.

Several authors have found it convenient to distinguish convective theories as being "local" or "nonlocal." The local theories are constructed so that, at a given position in a star, all quantities depend on local values of other variables, while nonlocal theories depend on values of variables at distant points in the atmosphere. By all odds, the most widely used treatment of convection is the local mixing-length theory (Böhm-Vitense, 1958). This theory has the advantage of ease of computation, a free parameter which can, if necessary, be adjusted to match observations, and comparability with past research. In the mixing-length theory (cf. Mihalas, 1978), the convective flux is

$$F_c = \varrho C_P \upsilon T (\nabla - \nabla_E) \ell / H , \quad (7\text{-}5)$$

where υ is the average velocity of a bubble of gas, $\nabla = d \ln T / d \ln P$ in the ambient atmosphere, ∇_E refers to the value of ∇ in the convective element, ℓ is the mixing length (the average distance traveled by a bubble before it loses all its energy), and H is the pressure scale height. The average velocity υ is found by setting the kinetic energy of the bubble to one-half the work done by the buoyant force. The other half goes to overcome friction by other bubbles. The gradients ∇ and ∇_E are calculated from considerations of the energy loss by the bubble during its lifetime and depend on assumptions regarding optical thickness of the bubble and its rate of radiation. To the present time, all significant sets of atmospheres for red-giant stars have been based on radiative equilibrium, or if convection has been included, it has been handled by the local mixing-length theory. Improvements made in or suggested for the standard mixing-length theory include taking account of the optical depth of the convective bubble (Henyey et al., 1965) and averaging the opacity across horizontal layers, rather than averaging the temperature and then calculating the opacity (Deupree, 1979).

The question of the mixing length, or the ratio of mixing length to pressure scale height (ℓ/H), has provoked considerable study. Most often one simply sets $\ell/H = 1.0$ or 1.5. For cool giant stars, surface convection is of such minor importance that ℓ/H apparently cannot be fixed from observations. (Indeed, it is not even certain whether convection can be treated by a local theory.) It is possible that the shape of the flux peak at 1.67 μm (Bell et al., 1976b) or the profile of a strong LTE line such as Ca I 6572 or CO (Carbon et al., 1976) might be a valuable diagnostic feature for temperature structure and hence convection. In a different approach toward determining the scale length of convection, Böhm-Vitense and Nelson (1976) note the near coincidence in the HR diagram of: (1) the boundary line separating convective and nonconvective stars, and (2) the red edge of the Cepheid instability strip and use this fact to fix the mixing length at H, the pressure scale height. A later study (Böhm-Vitense and Dettman, 1980) demonstrates that chromospheric emission is observed by IUE only for giants cooler than F2, and by implication, this denotes the onset of convection. A comparison of IUE fluxes with model predictions (Böhm-Vitense, 1982) appears to confirm this conclusion.

Based on scaling the quantity $(\nabla - \nabla_{ad})$, which is related to the depth of the convective zone, Schwarzschild (1975) speculated that enormous granules ($\sim 10^8$ km) might exist on Betelgeuse. Although Böhm-Vitense and Nelson (1976) found no evidence for such giant eddies, such features may not be entirely theoretical. High-resolution spectrophotometry of the Ca II K line in α Boo (Chiu et al., 1977) appears to require two states of excitation of the chromosphere. The normal state gives a mass loss $dM/dt < 10^{-9} M_\odot$/yr, whereas the excited states gives $dM/dt \sim 8 \times 10^{-9} M_\odot$/yr. The authors wonder whether the excited state arises from the appearance at the surface of a giant convective element. The argument for a two-component atmosphere is strengthened by a study of CO, which shows that no single-component atmosphere can match observations of both the wings of the Ca II infrared triplet (Ayres and Linsky, 1975) and the CO lines (Heasley et al., 1978). Of greater relevance here is Betelgeuse, whose Ca II and Mg II lines appear to require an inhomogeneous atmosphere (Basri et al., 1981). Finally, observations of a regular variation in the polarization of this object (Hayes, 1984) strongly suggest rotation of a "hot spot" (Schwarz and Clarke, 1984; Clarke and Schwarz, 1984)—perhaps a large convective cell or a magnetic complex.

Nonlocal theories of convection have not yet been widely adopted for cool star atmospheres. It may be, however, that the application of the most successful of these theories will constitute a major field of progress during the coming decade. A pioneering, nonlocal theory of convection (Spiegel, 1963) made an analogy with the equation of radiative transfer, the "source function" being chosen so that, in a uniform medium, this "generalized mixing-length" theory gave the same flux as the standard theory. In a "diffusion approximation", this theory was later applied, with gray opacities, to the Sun (Travis and Matsushima, 1973a) and to G and K dwarf stars (Travis and Matsushima, 1973b). For his study of yellow giants, Parsons (1969) introduced a nonlocal element into the standard mixing-length theory by averaging the convective velocity over the entire trail of the convective elements. Convective thermal plumes in the terrestrial atmosphere provided an analogy for a totally different nonlocal theory (Ulrich, 1970a), which was then applied to the Sun, where significant overshooting into optically thin regions was found (Ulrich, 1970b). A critical review of these theories and numerical comparison of their predictions for the Sun was made by Nordlund (1974). With a correction in the Ulrich theory, its similarity to the schemes of Parsons was demonstrated. The low value of ℓ/H required by the Travis-Matsushima formulation to match solar limb darkening was explained as a result of excessive overshoot. By a proper choice of such free parameters as the mixing length, the methods of Parsons, (modified) Ulrich, or even the simple mixing-length theory

can be made to yield similar results and may confidently be used to calculate models of the optically thin photospheres of main-sequence stars and giants down to K0. In deeper layers, in which convection is more important, the theories offer qualitatively correct but parameterized descriptions of convection.

Nonlocal theories, particularly those of Spiegel (1963) and Ulrich (1970a, 1970c), were compared by Ulrich (1976), who showed that these differ principally in the way in which the averaging is done. The length over which averages are taken—the diffusion length—thus becomes a significant parameter. The choice of a particular kernal function for the integration leads to the more tractable differential equation found by Travis and Matsushima (1973a, 1973b).

Another approach is the anelastic convective theory (Latour et al., 1976), which borrows from meteorology the idea of greatly restricting the allowed acoustic modes. Horizontal modes are also simplified to permit a more detailed examination of the large-scale vertical structure. In subsequent papers, the anelastic convective theory has been applied to convection in an A star, for which the convective zones are well separated and convection is relatively modest (Toomre et al., 1976; Latour et al., 1981).

All of the foregoing theories, whether local or nonlocal, are based on a "one-stream" model of convection in which convective elements (bubbles or plumes) move relative to a static ambient atmosphere. A more powerful, but much more complex, scheme would be a "two-stream" model. A number of such semi-empirical models have been constructed to interpret velocity and brightness inhomogeneities in the solar photosphere. A more or less deductive two-stream model of convection was derived by Ulrich (1970a, 1970c), and a fully deductive model was derived by Nordlund (1976). This latter method has been applied to convection in the Sun and cooler stars with excellent results (Nordlund, 1980, 1982). It is possible to simulate realistically photospheric granular convection and to predict reasonable values of line shifts and widths, which in turn give rise to what is called macroturbulence and microturbulence. Overshooting of convective elements into superficial radiative layers is specifically allowed, and the resulting large temperature differences (~ 10 to 10^3 K) between the two streams in visible layers of the photosphere constitute one of the most dramatic differences between these results and those of the local mixing length theory. At large depths ($\tau > 50$), the predictions of the two-component theory and those of the local mixing-length theory are quite similar. The interplay of various terms in the energy balance between the hot (ascending) components and the cool (descending) components at various heights is complex and instructive. In the outermost layers, where the radiation begins to escape directly to the surface, these temperature fluctuations are due principally to radiative terms—radiative heating from below, radiative exchange between the two components, and radiative losses to the surface—which implies that the temperature difference in the optically thin layers depends on the horizontal scale of the convecting elements and emphasizes the crucial role of that quantity (Schwarzschild, 1975, Böhm-Vitense and Nelson, 1976). Clearly, there is a hint of far-reaching potential in this two-stream theory, and we eagerly look forward to future advances (Nordlund, 1982, 1985) and applications to red-giant stars.

A fascinating study of the effect of certain improvements in the mixing-length theory and a comparison with other theories has now been made for the Sun (Lester et al., 1982). Two improvements were incorporated into the ATLAS6 treatment of convection: (1) the proper horizontally averaged opacity (Deupree, 1979) was taken, and (2) a depth-variable mixing length was employed. The results are summarized by the authors as follows, in comparing the new calculations with otherwise identical calculations for the Sun without these modifications.

1. Convection (in the improved treatment) transports a smaller fraction of the total flux.

2. The convection zone is narrower, and F_{conv}/F_{tot} is smoother.

3. The temperature is higher in the convective region.

4. The model is brighter in the region 1500 to 2000 Å.

5. Small differences arise in the visual spectrum. These differences result almost entirely from the use of the horizontally averaged opacity. Compared to other theories, there are also differences, and these result from both the horizontally averaged opacity and the variable mixing length (Deupree and Varner, 1980).

6. Compared to nonlocal mixing-length theories, the new calculation has less convection in the upper photosphere, and this leads to these models being hotter below $\tau_R = 0.6$.

7. Compared to Nordlund's (1976) two-stream model, the new results agree well above $\tau = 15$, but are much hotter below that depth.

8. Compared to empirical solar models, there is good agreement above $\log \tau = 0.4$, but the new results are too warm below that point.

The Sun is a natural testing ground for new theories, and it may be some time before better theories are applied to the red-giant stars which form the subject of interest here. At present, the entire field of convection is fragmented and in turmoil (as if convecting?), making a coherent review next to impossible (cf. Marcus et al., 1983). Worse yet, for our purposes, application of the available theoretical work is almost exclusively to the Sun, for which high-quality observations of limb darkening, granulation, and line profiles can be obtained and an empirical model is available. Improvements in convective theory for red-giant stars will likely be borrowed from applications in warmer stars. Two comments are relevant here: (1) inhomogeneities are likely to be relatively much more important in red-giant stars than in the warmer more compact stars in which convection is usually studied; and (2) because red giants are variable and thermal models are crude, the power of this combination to constrain or guide the theory of convection is weak.

In summary, we note that convection and inhomogeneities might play important roles in at least the following ways.

1. Because concentrations of certain molecules (H_2O, H_2, HCN, TiO, and CaCl) are extremely temperature-sensitive, their concentrations must increase over cooler regions of the photosphere. One can imagine a feedback mechanism through which increased molecular concentrations further cool the atmosphere (Gustafsson, 1981).

2. The subphotospheric convective zone presumably supplies the mechanical energy to produce a chromospheric temperature rise and perhaps promote mass loss (cf. Schmitz and Ulmschneider, 1981; and de la Reza and Goldberg, both this volume).

3. Grain formation might occur, or occur more readily, in or over cooler photospheric regions (Lucy, 1976; Deguchi, 1980; Draine, 1981, 1984; Woodrow and Auman, 1982; see also Lefèvre, this volume).

4. Microvelocity fields deduced from high-resolution spectra—or their interpretation—would be affected (Dravins et al., 1981; Nordlund, 1982).

5. Departures from LTE might be increased, perhaps dramatically, in an inhomogeneous atmosphere.

6. The conversion of theoretical quantities (such as $T_{\rm eff}$) to observed quantities (such as colors) might be affected, as has already been noticed for F stars (Nelson, 1980).

INTERLUDE

How well do the predictions of the theoretical models of the previous section compare with the observations of real stars? A moment's reflection suffices to remind us, of course, that these thermal models will yield only a background continuous spectra and symmetric absorption lines, and *there is no possibility that thermal models can reproduce the dazzling array of observations presently available* (as described, for example, by the Quercis in Chapters 1 and 2). Much more work is necessary before we can model, in a self-consistent fashion, such nonstatic and nonthermal phenomena as turbulence, departures from LTE, pulsation, and mass loss (see Figure 7-1). Progress toward these goals is reported in later chapters. It is only fair, however, to give the thermal models a chance to demonstrate whether they can explain even what they were *meant* to explain. In addition, we seek spectral features which are particularly sensitive to a single property of the atmosphere and may therefore help to diagnose the physical and chemical properties of the star. At the outset, we set forth our most difficult problem: how does one test the goodness of a comparison between theory and observation? As will become obvious from several examples, we will stumble over this problem again and again.

SPECTRAL DISTRIBUTION OF ENERGY FLUXES (Photometry, Spectrophotometry, and Colors)

Oxygen-Rich Stars (M and S Stars)

Although the models of Gustafsson et al. (1975) and Bell et al. (1976a) are intended for G and K giant stars, we mention them here because of their obvious implications for cooler stars and the paucity of such comparisons for M, S, and C stars. The excellent overall match of observed spectrophotometry and narrowband photometry with predicted fluxes from these models confirms that the line-blanketing and thermal structure of present models of G–K giants is essentially correct (Gustafsson and Bell, 1979). This impressive work has reached a new level of sophistication for stars of intermediate temperature. Unfortunately, the red-giant stars of interest in this volume constitute a rather different class of stars.

A persistent flux excess shortward of 4000 Å was carefully scrutinized by Gustafsson et al. (1975), who conclude that, although massive chromsopheres, temperature inhomogeneities, and departures from LTE cannot be ruled out as sources for the discrepancy, the most likely interpretation is neglected ultraviolet opacities—from either metal lines, molecular lines, or some continuous absorber. A violet discrepancy is not unique to these models, but has been noted in other models as well. For example, Peytremann (1974) found that his models produced too much flux in the violet, a feature he also suggested was due to insufficient lines there. In her models of F dwarf stars, Böhm-Vitense (1982) finds the same circumstance and suggests that it arises from either an unaccounted-for continuous opacity source or a substantially increased convective flux. A similar problem appears in the M giant models of Johnson et al. (1980). (See Steiman-Cameron and Johnson, 1985.) To investigate the possible luminosity dependence of the relative flux peak at 1.67 μm, for which there is some observational evidence, ODF spectra of CN and CO were computed and found to be in fair agreement with the observations (Bell et al., 1976b). These conclusions are only tentative until additional observations at many frequencies, as well as improved theoretical spectra including the contributions of TiO and H_2O, are available. Limb-darkening coefficients for the set of models have also been calculated (Manduca et al., 1977) for the wavelengths of the *UBV* and *uvby* bandpasses.

Based on Gustafsson et al. (1975) and Bell et al. (1976a) atmospheres with $4000 < T_{eff} < 6000$ K, Bell and Gustafsson (1980) calculate the visual surface brightness (VSB) and study theoretically its dependence on color, gravity, and metallicity. The total effects of all these factors are *smallest* for the V-R color, and the theoretical relation between VSB and V-R agrees well with the empirical relation from stars with known angular diameters (Barnes and Evans, 1976; Barnes et al., 1978; Eaton and Poe, 1984). This agreement provides additional evidence that the background continuous spectrum, including the effects of line blanketing, is well predicted by these theoretical models for G and K giants.

Spectrophotometry provides a somewhat stiffer test of models than does photometry, and the comparison of predictions from the Gustafsson et al. (1975) and Bell et al. (1976a) models with spectrophotometry of G, K, and M stars (Strecker et al., 1979) is of considerable interest. Water vapor, but not TiO, was included in the synthetic spectrum, although neither was included in the calculations of the models. Figure 7-12 shows the comparison for β And (M0 III) and β Peg (M2 II-III) (Manduca et al., 1981); the agreement over most of the range from 1.2 to 5.5 μm is better than 10 percent. (Fits for warmer models are generally even better.) The largest discrepancy in β And occurs in the first overtone bands of CO at 2.5 μm. While that particular problem could in principle be remedied by altering the CNO abundance, the ratio of the fundamental and the first overtone of CO cannot be so easily corrected. The fit for β Peg is slightly worse, but this comparison should not be pushed too far, since the authors suspect that the star may be cooler than any of their models. The authors also note that effective temperatures deduced from model fitting are in satisfactory agreement with other temperature estimates, and angular diameters inferred from fitting at 3.5 μm are in good agreement with measured values of those deduced from the VSB relation and V-R colors.

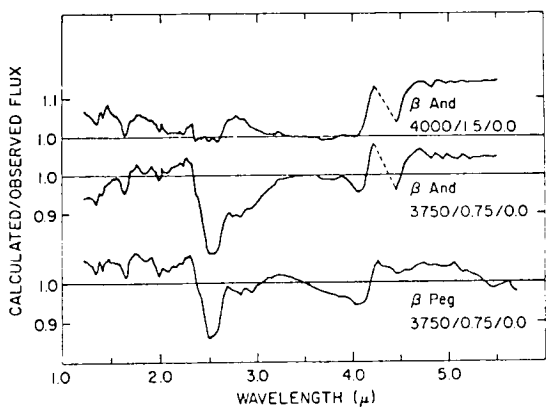


Figure 7-12. Comparison of observed spectrophotometry of early M giant stars β And and β Peg (Strecker et al., 1979) and predictions from the Gustafsson et al. (1975) and Bell et al. (1976a) models identified in the figure (from Manduca et al., 1981).

Comparison of computed fluxes from a grid of SM models (Johnson, 1974) with infrared spectrophotometry of 24 cool giant stars (K0 through M9) taken from above the Earth's atmosphere (Scargle and Strecker, 1979) furnishes some food for thought. As a matter of fact, the predicted fluxes often agree rather well with the observations. Yet some of this agreement must surely reflect the insensitivity of the fluxes to the precise structure of the models because SM models have outer photospheres that are generally too warm. More surprisingly, many of these "models" were interpolated or extrapolated where models did not exist in the original grid. Furthermore, there is a strange clustering of stars with $T_{eff} = 3500$ K, which appears to be an artifact of the available set of models, and the temperatures from several of the models are lower than those found for some of the same stars by other methods (Gustafsson, 1981). All of this is a bit disquieting because it forces us to admit that, unless the effective temperature is constrained rather carefully from other evidence, *observations, especially for variable stars, can be matched reasonably well by crude models. Better observations*, especially calibrated spectrophotometry of both the visual and infrared regions taken

at the same time, *are necessary to test even thermal models.*

Tsuji (1976b) found good agreement between infrared fluxes from his models of M supergiants and accumulated photometry and spectrophotometry of Betelgeuse. The fit was improved if the composition was taken to be C-poor and N-rich, rather than solar. (That the atmosphere of Betelgeuse is actually C-poor and N-rich has recently been determined through a careful study using spectral synthesis (Lambert et al., 1984).) A relatively high microturbulent velocity of 6 km/s was used; this was not taken as evidence for supersonic turbulence, but was attributed to deficiencies in the VAEBM method for molecular line opacities. The best fit to the infrared fluxes (1 to 5 μm) gave an effective temperature of 3900 $\pm$ 150 K for Betelgeuse (M2 Iab). The implied angular diameter of 0.40 milliarc-sec is, however, lower than most other determinations. No resolution of this discrepancy was offered, but Tsuji noted that this higher temperature resolves a problem with the K I line (Goldberg et al., 1975; see also Goldberg, 1984). (Could it be that most earlier observations detected the larger radii in TiO bands?) Subsequently, Tsuji (1978b) demonstrated that scattered light from an optically thin dust shell had negligible effect on the *colors*, but it might appreciably increase the measured *angular diameter*, which might resolve the Betelgeuse discrepancy. The strength of the TiO bands (Collins, 1974) implied by the variation of angular diameter of Betelgeuse across them appears to require a lower temperature, however, than 3900 K (Balega et al., 1982). The curious behavior of the angular diameter of Betelgeuse is quite complex and is not yet understood (Goldberg, this volume).

In a pioneering extension of model atmospheres to cooler stars, Tsuji (1978a) saw sufficient agreement between fluxes from his models and available photometry and spectrophotometry of K and M giant stars to define a new scale of effective temperature for these objects. A careful scrutiny of these comparisons reveals that, in the infrared, the slopes of the flux curves of all models are quite similiar, and most of the temperature sensitivity comes from wavelengths less than 1 μm. Here, however, none of the predicted fluxes fit well because of distortions by molecular bands. The fitting is therefore fairly subjective. Nevertheless, if R–I colors are used as a baseline, there is reasonable accord between Tsuji's scale of effective temperature and the scale deduced from the angular diameters then available. Finally, Tsuji pointed out that colors and band strengths could well be understood on the basis of this new temperature scale, but no information about variations in abundances among the CNO elements could be inferred.

As additional values of stellar angular diameters became available, especially from observations of lunar occultations, it became possible to define an empirical temperature scale for red giants from K0 to M6 (Ridgway et al., 1980b). Although the scatter among individual stars is rather high and certain large discrepancies exist even for stars for which the formal errors are small, this calibration of effective temperature against spectral class or Wing color temperature (T_c) has become the criterion against which all theoretical results are tested. From time to time, more values of angular diameters and temperatures have been obtained, but no basic alteration of the Ridgway et al. scale has been necessary.

An additional link between models and observations was forged by Tsuji (1981a), who used his atmospheres and the method of infrared photometry (IR) (Blackwell and Shallis, 1977) to define a new independent temperature scale for M giant stars. Basically, the IR method is a clever application of the relation between observed flux (f_λ), flux emitted at the stellar surface (F_λ), and the stellar angular diameter, in which the monochromatic flux from an appropriate *model* is substituted for the emitted *stellar* monochromatic flux (F_λ) and is used with the *observed* monochromatic flux (f_λ) to obtain the angular diameter. With this value of the angular diameter and the *integrated* observed flux (f), the *integrated* emitted stellar flux (F) and hence the effective temperature can be derived. The derived effec-

tive temperature depends only rather weakly on the model used. Furthermore, since the ratio of IR flux to total flux varies roughly as $T_{\rm eff}^{3}$, the method is quite powerful in determining the temperature even in the presence of imprecision in the models from missing opacities, inexact opacity treatment, or imperfect match in chemical composition. The necessary equations have been combined into an especially convenient form (Blackwell et al., 1980). From photometric measurements on 62 giant stars from spectral class K1 through M6, Tsuji (1981a) used L-band photometry for the IR fluxes to deduce effective temperatures. The resultant temperature scale agrees quite satisfactorily with that deduced from angular diameters (Ridgway et al., 1980b). A minor difference is that Tsuji found evidence for a plateau at $T_{\rm eff}$ = 3800 K for stars of spectral types M0 through M2 and speculated that, in this spectral range, luminosity might affect the spectral classification in such a way that stars of identical temperature but differing luminosities were assigned different spectral classes. (The reader may detect a minor inconsistency here, because the values of $T_{\rm eff}$ calculated from the models do not show a gravity dependence.) Although a slowing of the steady decrease of $T_{\rm eff}$ with spectral type cannot presently be excluded by angular diameter data, Keenan (1982) has demonstrated that there is a steady progression of color and spectra of Fe, Cr, and TiO lines through these spectral classes.

Another crucial issue, noted but not resolved by Tsuji (1981c), arises from the masses of the M giants inferred from various luminosity measurements and his effective temperatures. In the resultant HR diagram (Figure 12, Tsuji, 1981c) the K–M giants scatter along the theoretical evolutionary track for a star of 3 solar masses, yet present knowledge of the luminosity and initial mass function appears to establish that most of these stars must have masses near 1 solar mass (Scalo et al., 1978; Scalo and Miller, 1979).

Based on the Johnson et al. (1980) models of K and M giants described earlier, Piccirillo et al. (1981) calculated Wing color temperatures and compared the relation between T_c and $T_{\rm eff}$ with that obtained from previous work. The original calibration of T_c against $T_{\rm eff}$ is semiempirical (Ridgway et al., 1980b). As is clear from Figure 7-13, in their respective ranges of overlap, the models of Gustafsson et al. (1975) and Bell et al. (1976a), of Tsuji (1978a), and of the Indiana group (Johnson et al., 1980) agree well with the semiempirical relation. *This agreement of the three sets of theoretical models with the semiempirical relation constitutes the most convincing evidence that theoretical models of early M giants are basically correct.* Piccirillo et al. (1981) further demonstrate that the difference between T_c and $T_{\rm eff}$ is due to a multitude of weak TiO lines, unseen even at fairly high spectral resolution, which depress the stellar flux by significant amounts in the region of the short-wavelength continuum filter at 7540 Å (Wing, 1981).

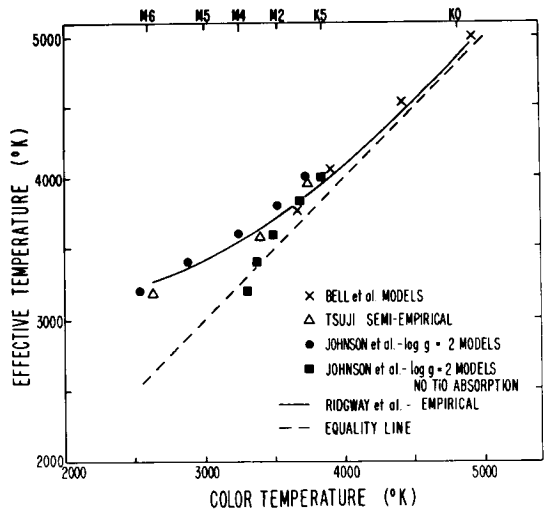


Figure 7-13. The relation between Wing color temperature and effective temperature for K and M giants. Solid line is the semiempirical relation (Ridgway et al., 1980b); symbols represent results obtained from model calculations by three different groups (Gustafsson et al., 1975, and Bell et al., 1976a; Tsuji, 1978a; Johnson et al., 1980). Note that the points calculated without TiO absorption appear to follow the equality line. References are given in the text (from Piccirillo et al., 1981).

Results from the first comprehensive comparison of colors from models of K–M giant stars and observations are also quite encouraging (Steiman-Cameron and Johnson, 1985). Magnitudes on the VRIJHKL broadband system and on the wing narrowband system have been computed for the models of Johnson et al. (1980) and compared to observations. Figure 7-14 shows a comparison of effective temperature against the TiO band strength index computed from the Johnson et al. models, compared with the relations of Ridgway et al. (1980b) and Tsuji (1981a). We note that the Ridgway et al. curve is *semiempirical* (the best fit by eye through the observed points shown), the Tsuji curve is also *semiempirical* since it uses T_{eff} deduced by the IR method and TiO measured for the corresponding spectral classes, and the Johnson et al. curve is *purely theoretical*. The agreement is quite satisfactory, certainly within the large observational scatter, down to a temperature of 3500 K, below which the theoretical TiO band strengths are too weak. Steiman-Cameron and Johnson (1985) have considered several possible effects to explain the discrepancy at lower temperatures, including dissociation of TiO by chromospheric heating, increasing effects of sphericity as the luminosity increases and the surface gravity decreases toward cooler stars, changed thermal structure due to possible carbon enhancement in the cooler stars, and a variation of radius with wavelength. (A chromospheric effect apparently exists (Steiman-Cameron et al., 1985).) In any case, the excellent accord for early M stars is reassuring.

Carbon Stars and S Stars

What of the fascinating peculiar red-giant stars—types N, S, and R? Most model calculations are so recent that time has not allowed careful comparison with observations, and such comparisons remain a pressing need. The assurance we could give earlier that predictions from classic thermal models for early M giants were in reasonable accord with observations of the continuous flux, and that reasonable values of angular diameters and temperatures could be deduced on the basis of model fitting, cannot be repeated for the cooler stars.

The French group (Querci and Querci, 1976) compare two of their triple-alpha-enriched carbon-star models with the observed broadband colors of 19 Psc and UU Aur. The fit for a model with T_{eff} = 3600 K to UU Aur is fair, and the theoretical predictions fit better than the blackbody curve, especially in the 0.8- to 1.6-μm region. The flux curve for 3000 K matches almost as well, but is disfavored by Querci and Querci because of a poor fit to the observed spectrum. All models predict excess fluxes in the blue part of the spectrum. Altogether, the comparison leaves much to be desired because the fit is only fair, and the temperature deduced from the best fit—T_{eff} = 3600 K for UU Aur for the triple-alpha composition—appears to be considerably too high (Ridgway et al., 1980a; Tsuji, 1981b). A lower temperature is obtained for a model based on CNO processing, but synthetic spectra are then in conflict with observations. One is hard pressed, as were Querci and Querci (1976), to select from a large number of choices the specific causes for the relatively poor fits—possibly including at least incorrect chemical composition, neglected opacities, and neglected convection.

In a bold extension of his earlier work on M giants, Tsuji (1981b) used the available models of carbon stars (Querci et al., 1974; Querci and Querci, 1975a) and the L-band observations of Noguchi et al. (1977) to deduce a temperature scale for N-type carbon stars by the IR photometry method described earlier. In this case, it was necessary to correct theoretically the L-band observations for molecular absorption due to HCN and CO. The resulting temperatures are in satisfactory agreement with the six obtained by lunar occultation angular diameters (Ridgway et al., 1980a). Tsuji (1981c) further demonstrates that several broadband colors of carbon stars can be understood on the basis of this effective temperature scale.

Recently, NASA/Ames Research Center spectrophotometry of 10 non-Mira S stars and

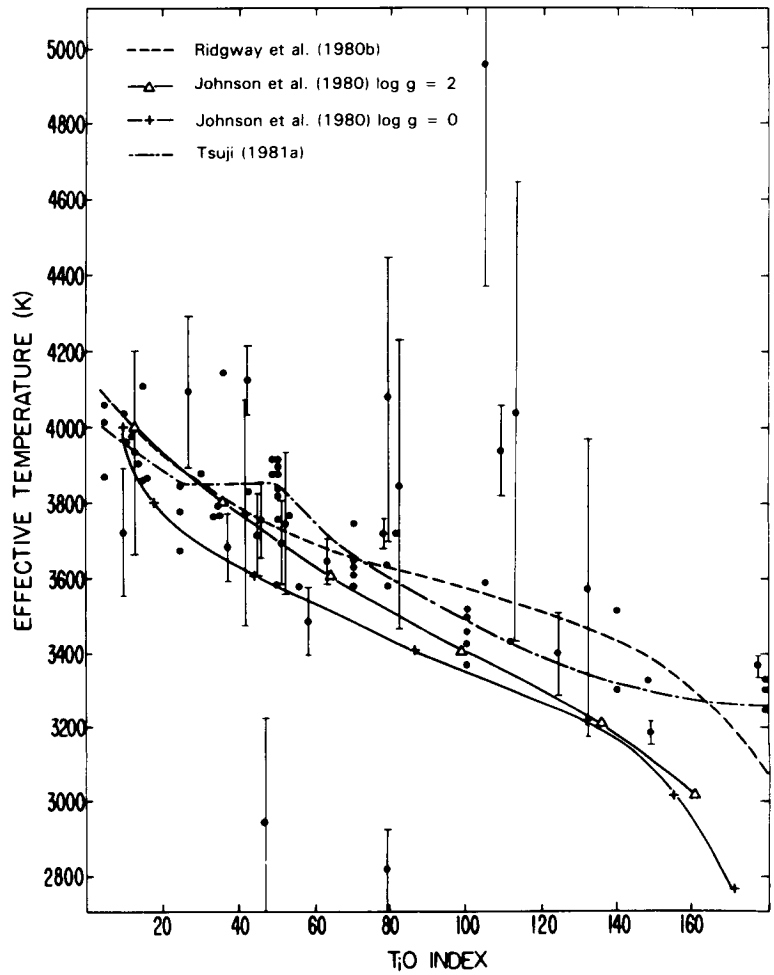


Figure 7-14. The relation between effective temperature and spectral type (TiO band strengths) for K and M giant stars. Shown are the observations, the semiempirical curve which best fits the observations (Ridgway et al., 1980b), the semiempirical relation from IR photometry (Tsuji, 1981a), and the theoretical fit by the models of Johnson et al. (1980). (From Steiman-Cameron and Johnson, 1985.)

fluxes from theoretical models (Johnson, 1982) have been compared in an attempt to calibrate a temperature scale for S stars (Augason et al., 1985). Effective temperatures have been obtained both by model fitting and by the method of IR photometry; results from the two methods are in good agreement. An example of the observed and calculated spectrophotometry for the warm S star, HD 35155, is shown in Figure 7-15. The relative strengths of the fundamental and the first overtone bands of CO do not agree well (a problem we have met before). The keen observer will also note the unusual flat-topped region near the maximum of the H^- peak at 1.67 μm, which differs strikingly in appearance in S and C stars. If the observations were extended to shorter wavelengths, an excess of flux in the visual and ultraviolet spectral regions from the model would also be noticed, and comparisons of the theoretical flux curves to the observations of cooler S stars are not as good as the fit shown. Also, ZrO is not included in these models, and ZrO bands are prominent in the comparison. Although judgment is left to the reader, it is clear that progress is being made in understanding even these complex objects by thermal models.

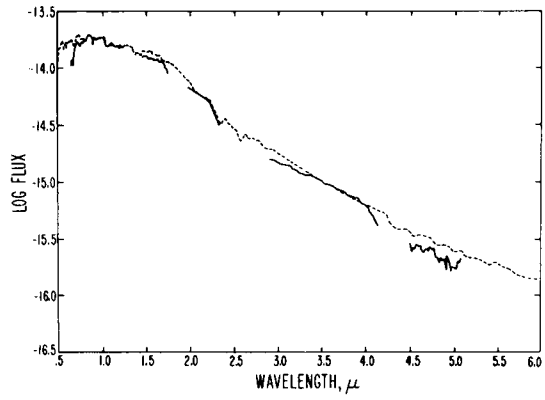


Figure 7-15. Comparison between spectrophotometry of an early S star and predicted flux from an Indiana model (from Augason et al., 1985).

A similar study has been made of the carbon star, Y CVn (C5,5), based on extensive photometry (Goebel et al., 1980). A good fit to the entire spectral range 0.5 to 5.0 μm is obtained for theoretical fluxes from models (Querci et al., 1974; Querci and Querci, 1975a). Not only is the continuous spectral energy distribution well matched, but the molecular band strengths of CN and C_2 are satisfactory. Whether the effective temperature is correct, is not yet clear, however, and one must be cautious of extrapolating general conclusions from an isolated case.

Broadband photometry, which is often the only data available on a given star, carries a minimum amount of information, and the power of observations of one star to constrain the parameters of models is very weak. The power of photometric observations of many stars with differing properties to constrain a series of models is considerably enhanced. Narrowband photometry and spectrophotometry are considerably more powerful tools. Although we await eagerly such complete spectrophotometry for a wide variety of M, S, and C stars, we must be cautious, because unlike warmer stars, essentially all stars of interest here are *variable*. Combining observations taken at random phases—sometimes of necessity—introduces a significant uncertainty into the results.

We conclude that thermal models of the classic variety are able to reproduce the continuous flux curves of giant stars of solar composition in spectral classes M0 through M5. Progress is also apparent for S stars, especially the warmer ones. Testing of C-star models is just beginning. Many further improvements on models are necessary. Continually updated opacities are needed. More molecular lines may be needed for familiar molecules (the huge numbers of weak lines), and opacities from additional molecules should be included. For cool M stars, the lack of an accurate opacity for H_2O is perhaps the single greatest impediment to further progress, but VO is also important. In S stars, ZrO may be important. In cool carbon stars, one must add HCN (Eriksson et al., 1984; Tsuji, 1984; Jørgensen, 1985), C_2H_2, and perhaps C_2H, C_3, and SiC_2. Perhaps we should look at SiO, CS, SiS, FeH, HCl, AlCl, and CaCl—the list could be long.

It is also in these coolest M, S, and N stars (especially the M stars, according to Scholz and Tsuji (1984)) that the effect of sphericity is expected to become important as the gravity decreases with the increase in radius during these late stages of stellar evolution. It is encouraging to note the progress being made by the Heidelberg group and the Japanese workers. Some of our fitting or lack of fitting could be profoundly changed as a result of sphericity. However, a gulf still exists here. The model makers who use plane-parallel models have the extensive opacity data and, understandably, continue their zealous research with these models. Surely there is much room for that. The spherical models have generally been converged with relatively crude opacities. It is time for a merging of forces—of those that have the good opacities with those that have the good spherical codes.

SPECTRAL LINES

There are at least three vital questions, the answers to which will be essential as we consider to what extent line profiles from classic

thermal models match observations of real stars. How can one judge quantitatively goodness of fit? Can one isolate the specific reason for the lack of perfect fit? What can one deduce regarding physical conditions in the stellar atmosphere from various lines? The questions are especially pertinent to red-giant stars, in which variability is known and departures from plane-parallel geometry, LTE, and homogeneity are expected. Present progress in answering these questions for K giants can be learned from the detailed review of the conference on Arcturus (Trimble and Bell, 1981). Much less work has been done on the red-giant stars. In addition, spectral lines in supergiants are remarkably broad, and considerable macroturbulence must often be invoked to match observations.

An example of attempts to deduce $^{12}C/^{13}C$ ratios in carbon stars will illustrate the problem in answering definitively the foregoing questions. Values obtained for the well-observed N-type star, V460 Cyg, from excellent high-resolution spectra by several methods make an engrossing story: (1) 100, from a pseudo-curve-of-growth and the isointensity method (Fujita and Tsuji, 1977); (2) 9, from the Minnaert semi-empirical formula (Climenhaga et al., 1977); (3) 32, from a curve of growth (Dominy et al., 1978); (4) 24, from spectral synthesis and a model atmosphere (Johnson et al., 1982); (5) 22–29, from a careful reapplication of the Minnaert formula (Little-Marenin and Little, 1984). The precise values are of less importance in this discussion than the fact that crude methods and atmospheres gave results as good (or bad) as those for better atmospheres. We are evidently in the awkward position of admitting that crude model atmospheres can sometimes both produce good fits to fine observations and permit the inference of useful quantities about the star. Apparently, fitting observed spectra is a necessary, but not sufficient, condition for accepting a thermal atmosphere! Clearly one needs tougher tests for atmospheres: broader spectral intervals, lines from several atoms, ions, and molecules and lines spanning a larger range in region of formation (hence temperature). Otherwise, in the absence of fairly strong constraints, goodness of fit to average lines is a very weak criterion for the identity of the model with a real star.

A useful illustration of the problems of deducing stellar parameters from a comparison of observed and synthetic spectra is provided by the pioneering attempt to determine H, C, N, and O ratios in UU Aur and Y CVn (Querci and Querci, 1976). Such comparisons, the best of which is illustrated for UU Aur in Figure 7-16, provide some reassurance that the models generally have a correct thermal structure, but uncertainty in other parameters do not allow a more detailed test. For example, the models shown give $T_{\rm eff} \approx 3600$ K for UU Aur, yet this is much higher than temperatures inferred for similar N-type stars (Ridgway et al., 1980a; Tsuji, 1981b). Compositions enriched in C (called PL in Figure 7-16) fit generally better than those with CNO-cycle compositions (called DE), but line and band f-values are not sufficiently well known to extract more precise information concerning H, C, N, and O abundances. Although the influence of gravity on line profiles is quite small, it increases slightly toward the lower temperatures. Its influence varies somewhat from band to band; for example, CO and CN behave oppositely, and each behaves differently for PL and DE compositions. Because only one value of the turbulence, $v = 5$ km/s, was used, little information can be deduced from it. Reasonable overall fits to observed spectra of both stars in three spectral regions could be obtained, and the lack of better matches can also be attributed to imprecision of molecular data as to deficiencies in the atmospheric models. We will find other examples of this sort of impasse.

In their comprehensive study, Gustafsson and Bell (1979) compared LTE synthetic spectra from their models for G and K giants to observed spectra for several wavelength bands; the overall fit is fairly impressive.

An attempt at a more objective approach to the comparison of synthetic and observed spectra was applied to five carbon stars (Olson and Richer, 1979) to infer the values of X(CNO), turbulent velocity, and $^{13}C/^{12}C$ by minimizing

the residuals between observed spectra and synthetic spectra based on earlier models (Johnson, 1974). Such differences depend critically on accurate values for wavelengths and other molecular parameters, and perhaps the method was pushed a bit beyond the precision of the data. Yet such methods appear to hold considerable promise for the future as better observational and molecular data become available. Our present interest centers on the goodness of the fit. The authors note that their synthetic spectra fit very well the high dispersion (13 A/mm) observations of TX Psc, Z Psc, X Cnc, UU Aur, and Y CVn in the region 7800 to 8300 A for reasonable values of the parameters. Unfortunately, however, no absolute criterion exists for judging goodness of fit. One of the parameters determined by fitting is the microvelocity. The values derived by Olson and Richer (1979) are all subsonic (Vs = 5 km/s) and significantly lower than values obtained by other workers.

We await the results of a more extensive study of $^{12}C/^{13}C$ in approximately 30 N-type carbon stars from infrared Fourier transform spectrometer spectra and synthetic spectra from unpublished atmospheres (Lambert, 1984; Eriksson et al., 1985; Gustafsson, 1985).

One of the more significant results to come from spectroscopy of peculiar red-giant stars concerns the discovery and strength of the quadrupole lines of H_2 in the infrared (cf. Lambert et al., 1973; Hall and Ridgway, 1977; Goorvitch et al., 1980; Bragg et al., 1982; Jennings et al., 1984). The 1–0 S(1) line of H_2 at 2.1 μm—the line most often studied because of its strength and its location in a clear region of

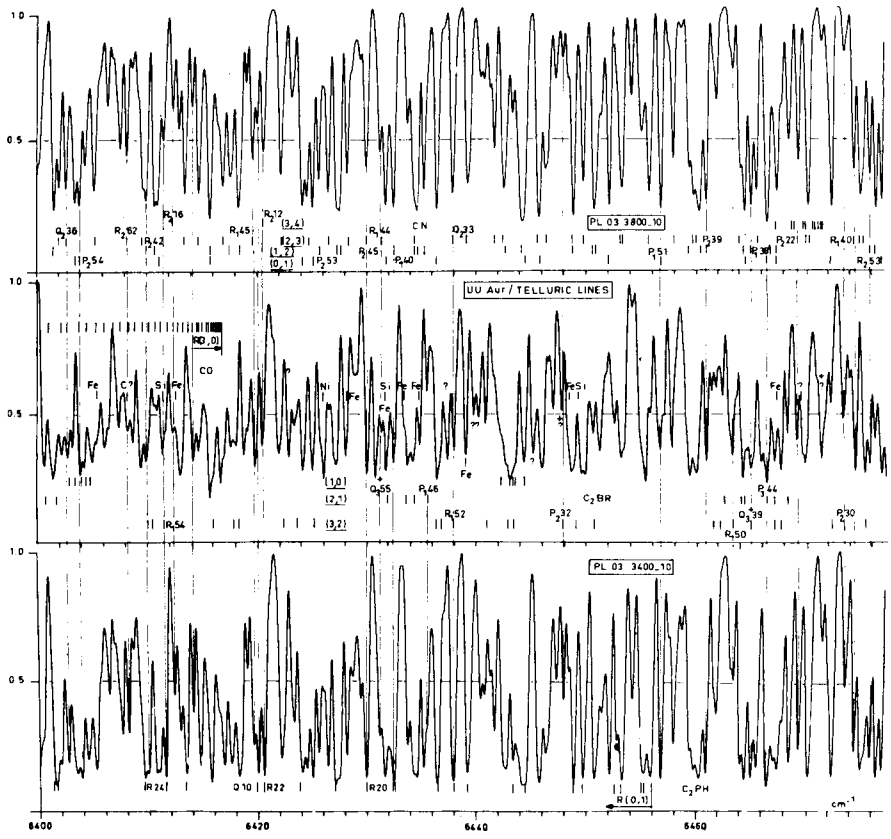


Figure 7-16. Spectra of the carbon star UU Aur and synthetic spectra from theoretical models with compositions representing triple-alpha-enriched material, by the French group (from Querci and Querci, 1976).

the spectrum—has been detected and its strength followed throughout the cycle in the two S Miras, Chi Cyg and R And (Hall and Ridgway, 1977; Hinkle, private communication, 1983). The same line has been detected in the carbon stars, V CrB, U Cyg, RZ Peg, and WZ Cas, but is not present in eight other N-type carbon stars, most of which are irregular or semiregular variables (Johnson et al., 1983). In a parallel investigation, Tsuji (1983) found no trace of this line in any M giant star, even though he studied stars as cool as RZ Ari (M6), WX Vir (M7), and RX Boo (M8). These results are even more unexpected because the line is predicted to be strong by published model atmospheres (Querci et al., 1974; Johnson, 1982; Tsuji, 1978a) in all stars of this temperature range. Several possible causes for the nonappearance of the H_2 line in carbon stars have been suggested (Johnson et al., 1983): (1) the temperature scale for carbon stars is too low by 500 to 800 K; (2) the models are inaccurate—the most important deficiencies being the assumption of a plane-parallel geometry and the neglect of the opacities of polyatomic molecules; (3) H_2 might be dissociated by chromospheric heating; (4) H_2 might be underabundant because of some nonequilibrium process; (5) non-Mira carbon stars might be hydrogen-deficient. Several of these considerations apply to the M giant star as well. At the moment, the source of the discrepancy is unclear. The claim has recently been put forward that the strength of the O–O S(1) line of H_2 is correctly predicted in N-type carbon stars by atmospheres with HCN opacities (Eriksson et al., 1984). The outer atmospheres of cool carbon stars are undoubtedly complex and variable thermodynamic regimes, and we suspect that a full understanding may entail a lot more work.

All of this is not directly relevant for testing thermal atmospheres because only the presence or absence of the line is at stake, and that alone is not a strong criterion for the goodness of the atmosphere. The H_2 quadrupole lines are excellent diagnostics for the temperature and density of the upper photosphere, however, and careful observations of these lines at various phases in several stars are urgently needed.

DIAGNOSTIC FEATURES

Having discussed in some detail the (relatively rare) comparisons of model predictions with observations, we now consider attempts to infer from observations, perhaps with the aid of model atmospheres, specific characteristics of a star. In other words, how can one infer for a particular star the value of a specified property?

An excellent general overview of the strengths and weaknesses of traditional methods of using model atmospheres to infer (or diagnose) values of effective temperatures and surface gravity for stars of all types is that of Pecker (1973). Curves of growth are frequently used, and many good discussions of these are available, including both general references (Aller, 1960; Gray, 1976; Mihalas, 1978) and specific discussions of the use of curves of growth with atmospheres. Required reading for this section is the comprehensive and sobering review of progress in determining effective temperature, surface gravity, microturbulent velocity, chemical composition, and mass for Arcturus (Trimble and Bell, 1981). Uncertain as these quantities are for Arcturus, they are far less certain for red-giant stars, for which observations are much less complete or accurate. Furthermore, red-giant stars are *variable*. Alksne and Ikaunieks (1981) have summarized some of the problems for carbon stars.

Effective Temperature

Effective temperature determinations for red-giant stars will continue to be based, into the foreseeable future, on measured angular diameters and integrated flux curves. Angular diameters are currently best obtained for the red-giant stars from lunar occultation (cf. Ridgway et al., 1980b), and this will continue to be the case for some time. However, interferometers operating in the infrared and later

in the visual—perhaps from space—will eventually be developed, leading to a new breakthrough in our knowledge of stellar atmospheres. Although the concept of effective temperature will lose some of its meaning for the coolest and most extended stars if their radii are found to depend on wavelength (Bonneau et al., 1982; Balega et al., 1982), the effective temperature will continue to be used. Because uncertainty in the temperature can mask several other problems, including bad models, its determination is a matter of prime importance. We commend those who have tirelessly pursued this research over the years and encourage them to continue their efforts, improving them when possible by observing at several wavelengths.

The uncertainties of both the *lunar-occultation method* and the reduction of such data have been carefully described (Ridgway et al., 1980a). We reiterate here a warning for the observations of red-giant stars, most of which are *variable*. Broadband colors of the cool carbon star, AQ Sgr, measured as part of a major photometric program (Walker, 1979), for example, are noticably different from remeasurements of the same star at the time of a lunar occultation (Walker et al., 1979). For determining effective temperature, therefore, the photometry for these variable stars should be obtained *at the same time as the angular diameter.*

Effective temperatures have been obtained by the method of *infrared photometry* (Blackwell and Shallis, 1977; Blackwell et al., 1980) for both M giants (Tsuji, 1981a) and cool carbon stars (Tsuji, 1981b). Values for $T_{\rm eff}$ deduced in this manner are in good agreement with those obtained from angular diameters as described earlier. As infrared spectrophotometry becomes available, temperatures can be obtained from an application of the IR method at several wavelengths, thus reducing any possible error. Such a project should be given high priority since it can be done with existing equipment and models.

A paper which calibrates the relation of the *visual surface brightness* (*VSB*) to (V–R) color and claims to extend this relation to stars of all spectral types and luminosity classes (Barnes et al., 1978) has already been noted (see also Eaton and Poe, 1984). Although primarily conceived to yield angular diameters, the method also gives effective temperatures when bolometric corrections are available. The validity of the method for the red-giant stars of this volume has not been securely established because of the paucity of angular diameters and the variability of these stars. The VSB method has been used to determine effective temperatures for R stars (Dominy, 1984) and has been reexamined for N-type carbon stars (Johnson, private communication, 1984).

While *model fitting* is commonly used for deducing effective temperatures of hot stars, its application to red-giant stars has been delayed by the scarcity of both realistic models and infrared spectrophotometry. A single published example employs the N-type carbon star, Y CVn, for which a temperature of $T_{\rm eff}$ = 2600 K was inferred by fitting fluxes from model atmospheres (Querci et al., 1974) to the observed infrared flux curve (Goebel et al., 1980). Effective temperatures for 10 non-Mira S stars—ranging from 2800 to 3600 K—have also been obtained from infrared spectrophotometry by both model fitting and IR photometry (Augason et al., 1985). As additional fluxes from (present and future) theoretical models are calculated and more extensive spectrophotometry becomes available, model fitting should prove to be a powerful tool for deducing effective temperatures.

Color temperatures, such as (R + I) – (J + K), calibrated by comparison with M giants (Mendoza and Johnson, 1965) or by blackbodies (Scalo, 1976; Walker, 1980), have been used for carbon stars, and certainly have their utility today in the absence of more fundamental calibrations. Narrowband photometric colors (cf. Baumert, 1972) may yield more precise temperatures. Additional insights on the relation of colors and effective temperatures for carbon stars is given by Alksne and Ikaumieks (1981), Tsuji (1981c), and Alksne et al. (1983). All of these authors find broadband colors to

be generally well correlated with effective temperatures deduced for cool carbon stars. An opposing view, based on studies of carbon stars in our Galaxy and the Magellanic Clouds (Cohen et al., 1981), holds that infrared broadband colors are more indicative of composition than of effective temperature. What is really needed, of course, is a calibration of either broadband or narrowband colors (Ridgway et al., 1980b; Wing, 1981) in terms of effective temperatures for *all types* of red-giant stars, so that these colors may be conveniently used to gage the effective temperature.

A comprehensive scheme for determining the atmospheric parameters necessary for an abundance analysis of G and K giant stars by spectral synthesis or by equivalent widths and a fine analysis, both depending on good model atmospheres, has been described in several papers (Luck, 1979; Luck and Bond, 1980). After a microturbulent velocity has been chosen from a curve of growth, the effective temperature is fixed at the value so that the Fe abundance derived from both Fe I and Fe II lines shows no dependence on the excitation potential of the lower level of the atom. The estimated error in the temperature determined by this means is about ± 0.05 in $\theta = 5040/T$ for early M giants, or about 150 K (Luck and Bond, 1980). No Fe II absorption lines appear in the spectra of M giants, however, and therefore the temperature determinations must be based solely on lines of Fe I. Observational evidence for departures from LTE in the K0 giant star, Pollux, has been presented by Ruland et al. (1980), and the extra precautions against using lines from low-lying levels of Fe I is described by Luck (1982).

A further instructive example is the detailed discussion of the derivation and uncertainty in effective temperature, surface gravity, abundance, and turbulent velocity for giant stars in globular clusters (Pilachowski et al., 1983), some of which are only slightly hotter than the red-giant stars of interest in this volume. The task is, of course, considerably easier in the globular cluster stars, for which a common mass ($0.8\ M_{\odot}$) can be assumed with less resultant error in surface gravity ($\Delta \log g = 0.25$) than the value deduced from ionization equilibrium ($\Delta \log g = 0.50$). Departures from LTE appear to be the probable cause of the difference in Fe abundance deduced from Fe I and Fe II. If so, the effect is an overionization of Fe I, the direction predicted theoretically (Auman and Woodrow, 1975). Observational evidence for overionization of Ca in M supergiants has been presented by Ramsey (1981).

Effective temperatures for M giants derived from lunar-occultation angular diameters (Ridgway et al., 1980b) or from IR photometry (Tsuji, 1981a) and for M supergiants derived from a variety of sources have been plotted against the unreddened V–K color, and that relation has been used to infer the effective temperature for individual stars for which the (unreddened) V–K colors can be obtained (Luck and Lambert, 1982).

Thermal Structure

Even when the effective temperature of a star is known, the thermal *structure*—$T(\tau)$, $T(P)$, or $T(r)$—is a quantity of additional interest. In the Sun, this relation is easily determined by limb-darkening measurements, but such measurements are essentially impossible in stars, except perhaps in special cases (cf. the discussion of limb darkening for Aldebaran by Ridgway et al., 1982). Possible methods for probing the structure of a stellar atmosphere are few: (1) a flux scan at a fixed wavelength across the solar or stellar disk, (2) a flux scan in wavelength from line center to wing across a strong spectral line, (3) observations at line center of different lines of a multiplet, (4) a flux scan in wavelength from the visible part of the spectrum toward shorter or longer wavelengths, and (5) the variation in angular diameter with wavelength. The fourth method probes increasingly shallower layers in the atmosphere because the opacity increases in both directions due to atomic lines and Rayleigh scattering at shorter wavelengths and increasing free-free absorption at longer wavelengths.

As far as the author is aware, no attempt has yet been made to deduce empirically, using these or any other methods, the thermal structure of even a single red-giant star. All of our knowledge comes from the opposing direction—comparing line profiles predicted from models with those observed—in which the fits can be said to be good (for example, see Querci and Querci, 1975a; Olson and Richer, 1979; Johnson et al., 1982). However, these fits are not good enough, nor is the physics of line formation sufficiently well applied, to be used for diagnostics. We can perhaps say that the models are not *badly* off in thermal structure; as we have seen, however, even crude models of atmospheric structure and line formation yield profiles in good agreement with observations.

Ramsey and Johnson (1975) attempted to find sufficiently rich and strong multiplets to apply method (3) and invert their line-center fluxes to find a run of excitation temperature with depth (Ramsey, 1977). Unfortunately, the presence of both rotation and (large) macroturbulence in real red-giant stars places severe restraints on the utility of this method (Desikachary and Gray, 1978).

A study of the strong infrared lines of the first overtone bands of CO in Arcturus (K2 III) reveals an apparently irreducible discrepancy between models deduced from CO and those deduced from Ca II K, forcing a realization that inhomogeneous atmospheres are upon us (Ayres and Linsky, 1975; Heasley et al., 1978). An investigation of these lines in red-giant stars appears to hold considerable promise for deducing thermal structures.

Of particular interest is the value of the temperature minimum. In the Sun, one sees radiation from the region of the temperature minimum in the ultraviolet (1600 Å) and infrared (130 μm) wavelength regions (cf. Vernazza et al., 1981; Avrett, 1984). We have almost no knowledge of this quantity for any red-giant star except Betelgeuse (T_{min} = 2700 K), and even this value is uncertain because of the failure of any homogeneous chromosphere to match both Ca II and Mg II line profiles (Basri et al., 1981). Although Johnson and O'Brien (1983) speculate that the spectral region near 2850 Å is formed at the temperature minimum in three N-type carbon stars, no confirmation by extensive line identification nor atmospheric modeling has yet been published. *We anxiously await the first identification of the wavelength region corresponding to the temperature minimum in any red-giant star.*

Chemical Composition

Much of the interest in red-giant stars arises from the unusual composition of their surface layers. Changes in the composition during the star's lifetime are vital clues to the processes of nucleosynthesis and mixing which have taken place. These processes have been repeatedly discussed from the point of view of the interior of the star (cf. Iben and Renzini, 1983, 1984). Our interest here is in inferring the abundances from stellar lines. In warmer stars, there is usually no problem in finding sufficient atomic and molecular lines to identify and find the abundance of numerous elements, including even those rare species. In cool stars, the problem is much worse, and one must be careful to select those lines which give a valuable diagnosis of abundance. The lines and methods are carefully described in several papers (Wallerstein, 1973; Lambert, 1985; Gustafsson, 1985) to which readers are referred.

Some of the difficulties involved in abundance analysis of the cool giants are described by Luck and Lambert (1982) in their attempt to extract the Li abundance in 31 M giants and supergiants. Even after careful calculation, including spectral synthesis of TiO lines over a 1000 Å spectral band, the level of the continuum near the Li I line remains the largest uncertainty in their analysis.

The well-known difficulties in diagnosing the chemical composition of carbon stars are dramatically illustrated by V460 Cyg (earlier called DS Peg). Repeated analyses of high-dispersion spectra by empirical pseudocurves of growth (curves of growth using central depths rather than equivalent widths) and the isointensity method led to values of $^{12}C/^{13}C$ = 100 (Fujita and Tsuji, 1977). Parallel analyses with

similarly high-resolution spectra using the line-depth method and empirical pseudocurves of growth by another group yielded $^{12}C/^{13}C = 8$ (Climenhaga et al., 1977). Later work aimed at reducing the discrepancy gave values of 32 from CN and CO (Dominy et al., 1978), of 25 from spectral synthesis of CN from the same spectra used by Climenhaga et al. (Johnson et al., 1982), and of 22 to 29 from the same method as Climenhaga et al. but with different spectra (Little-Marenin and Little, 1984). Recent work based on synthetic spectra and new model atmospheres which include polyatomic opacities will provide more reliable values of CNO abundances and isotopic ratios in N-type carbon stars (Gustafsson 1985: private communication).

Surface Gravity

Surface gravity not only is important in its own right but also is useful as a constraint on the mass, especially since stars of all masses tend to mingle in that part of the HR diagram where red giants are found. The emergent flux from a plane-parallel model is very weakly dependent on the gravity, and excellent observations for stars for which other parameters (such as chemical composition and turbulent velocity) were well known would be necessary to give any leverage on the gravity. That the gravity of such a well-observed cool giant star as Arcturus should be sufficiently controversial to justify an international conference to investigate the matter testifies eloquently of our ignorance (cf. Trimble and Bell, 1981). The uncertainty in gravity increases as the temperature decreases.

Gravities cannot be directly measured, but must be inferred from some other quantity, such as the pressure. A common method is to adopt for the gravity that value for which the abundance of a common element, such as Fe or Ti, is the same when two different stages of ionization are employed. Finding sufficient unblended lines from two such stages becomes increasingly difficult in the coolest stars.

An illustration of the methods and problems in deducing the surface gravity comes from slightly hotter stars, in which a comprehensive scheme for deducing the effective temperature, surface gravity, and microturbulent velocity for G and K giant and supergiant stars has been outlined by Luck (1979). All of these parameters must be inferred from Fe lines because only that element is represented by a sufficient number of suitable lines. The inferred abundance of Fe depends naturally on the value of all three of these parameters. One proceeds to choose that value of the microturbulent velocity for which there is no dependence on abundance for moderately strong lines ($W \leqq 200$ mÅ). That effective temperature is then chosen for which there is no dependence of the abundance on the excitation energy of the lower level of the line. That value of gravity is then chosen for which the abundance of Fe as deduced from Fe I and Fe II lines was the same. One then iterates as necessary, but this is not usually necessary. Surface gravities in K giant stars deduced by this scheme have estimated uncertainties of a factor of 2.

Unfortunately, because Fe II lines are weak or absent in the spectra of M giants and supergiants (except for the Fe II emission lines in the ultraviolet, which are probably circumstellar (Boesgaard and Boesgaard, 1976)), even the foregoing scheme is inapplicable, and to the author's knowledge, no application of the method of ionization equilibrium to red-giant stars has been made. In fact, some evidence cautions against it (Ramsey, 1981). The following procedure has therefore been adopted by some workers (Luck and Lambert, 1982; Luck, 1982; and references therein). The luminosity of the star, generally estimated from the Wilson-Bappu effect and a bolometric correction, is combined with the effective temperature and compared with theoretical evolutionary tracks on an HR diagram, from which a mass is inferred. From the mass, effective temperature, and luminosity, the surface gravity is deduced. For M stars, the uncertainty in log g is estimated to be 0.5 corresponding to a factor of 3 in surface gravity or mass.

An estimate of surface gravity can also be obtained from the pressure broadening of the wings of spectral lines—the traditional method in hotter stars. If the abundance is not accurately known (a common problem in red-giant

stars), that quantity must be determined from nearby weak lines formed in the same region of the atmosphere as the wings of the strong line to be used for gravity determination (Blackwell and Willis, 1977). The method, equivalent to finding lines on the damping portions of the curve of growth and calculating the damping constant, and hence the gravity from these, has not yet been applied to red-giant stars, but it should be useful if spectral lines meeting the necessary criteria can be found.

A new method, specifically aimed at stars with molecular features, has recently been suggested and applied to Arcturus (Bell et al., 1985). This method attempts to deduce the gravity from the pressure as the latter is manifested through molecular concentrations—in this case, MgH. Again, although this is not a cool star in the sense of the definition of this volume, the method has obvious application.

Analysis of the Ca II K line core and wings holds potential for diagnosing the thermal structure, the turbulent velocity, and perhaps the pressure of cool outer atmospheres, but it has not yet been applied to red-giant stars. The method of formation of the line cores is still a matter of some uncertainty, with several contending theories in the field (cf. Linsky, 1980): (1) the width of the emission core (W_o), measured by Wilson and Bappu (1957) and correlated with the absolute visual magnitude of the star, is formed in the Doppler core of the line and is therefore most sensitive to the turbulent velocities in the atmosphere; (2) the emission core is formed in the damping part of the profile and hence is most dependent on the column mass above the temperature minimum (cf. Ayres, 1979); (3) the line is formed in an isothermal layer (no chromosphere necessary) by the fact of a sharp drop in the source function as it changes to coherent scattering just outside the Doppler core (Basri, 1980); (4) the line is formed by a temperature rise due to an instability caused by infrared CO emission (Ayres, 1981; Kneer, 1983). Clearly the diagnostic value of the line for various parameters depends on the mechanism of line formation, and application must await further elucidation of this mechanism, which may not be the same in every star.

Is this relevant for red-giant stars? Can we expect the same processes to hold here? Several authors have derived empirical relations between the width (FWHM) for the Ca K emission and other characteristics of the star (e.g., one common formulation, based on 55 stars, is $\log W_o = -0.22 \log g + 1.65 \log T_{\rm eff} + 0.10(\rm Fe/H) - 3.69$. Other authors find quite similar expressions (Ayres et al., 1975; Engvold and Rygh, 1978; Cram et al., 1979), including some based on theoretical calculations. Sikorski (1982) has generalized somewhat the relation found by Cram et al., and Glebocki and Stawikowski (1980) have extended it to include more fully the dependence of the line width on the core emission intensity. A similar relation holds for the Mg II h and k lines (Weiler and Oegerle, 1979). Unfortunately, the dependence on surface gravity is very weak and is of little value in stars in which the line itself is weak, as it tends to be in M giants. No application of these possibilities have yet been made in our stars except for Betelgeuse. The lines were measured in a few R stars and were used to find the luminosities (Richer, 1975) and thus confirm that the R stars were giants, whereas the hydrogen-deficient R stars were supergiants. In fact, incredible as it may seem, no measurement, not even detection, of Ca K line cores has yet been made in cool carbon stars.

Turbulence

It is remarkable that, in a conference as recent and comprehensive as the IAU Colloquium 51 on *Stellar Turbulence* (Gray and Linsky, 1980), hardly a word can be found on turbulence in red-giant stars. Understandably, theories must be tested under the simplest circumstances and under conditions closer to those on the Sun, which is the standard astrophysical laboratory, but the paucity indicates our present poor knowledge of these processes in cool giants and supergiants.

Methods for deducing turbulence are the classic ones, in which an extra broadening parameter beyond the thermal broadening is added to the line-absorption coefficient to

match the stellar line profiles. These methods are described under surface gravity because the two are inferred from the same data. Among early K stars, the macroturbulent velocities appear to remain near 3 km s^{-1} for stars with a range of M_{bol} from +4 to −1, whereas for brighter stars, there is a sharp increase to about 6 km s^{-1} but with considerable scatter (Smith and Dominy, 1979). Values are in the range 2.5 ± 0.5 km s^{-1} for K and M giants (Luck and Lambert, 1982) to 4.0 ± 1.0 km s^{-1} for M supergiants (Luck, 1982). Although values for individual stars, especially some supergiants, are somewhat larger than these mean values, they are generally considerably lower than those given in the tabulation by Glebocki (1973), at least partly due to the lower value of turbulent velocity now accepted in the Sun.

In a study of the lithium abundance in 19 G and K Ib stars, microturbulent velocities of 1.9 to 2.6 km s^{-1} and macroturbulent velocities of 4.0 to 9.0 km s^{-1} were determined (Luck, 1977a, 1977b, 1978).

Very few reliable determinations of turbulent velocities in S or C stars have been carried out, but we note that, in a study of two N-type carbon stars by spectral synthesis and model atmospheres, a microturbulent velocity of 4 to 5 km s^{-1} and a weakly determined macroturbulent velocity of 5 km s^{-1} were required to match the broad lines of the CN 2–0 system in two N-type carbon stars (Johnson et al., 1982).

With values of turbulent velocities are now available for several red-giant stars, these have been derived from a variety of methods and data and are not of the same precision. Turbulent velocities from Miras vary with phase, wavelength, and excitation potential because of their formation in different regions of an extended and mass-losing atmosphere. Many of the velocities in the literature are in fact supersonic; the sound speed in a red giant of T_{eff} = 3000 K is about 5 km/s, and it varies little for the conditions described here. Certainly no claim should be advanced for supersonic turbulence on the basis of any values inferred to the present, because deficiencies of various kinds in models and line formation can manifest themselves as microturbulence. There is also a downward trend of the values as spectra of higher resolution and better models have been employed.

The turbulent pressure enters the equation of hydrostatic equilibrium through its contribution to the total pressure. In a sense, it can be thought of as a levitating force slightly reducing gravity. As far as the author is aware, no attempts have been made to deduce the effects of turbulent pressure in cool giants. Indeed, these depend on the same techniques as those for inferring the gravity and atmospheric extension, and any information on turbulent pressure must await more precise measurement of these other quantitites.

Sphericity

Although sphericity may be important in many of the coolest red-giant stars (especially in supergiants and Miras), insufficient knowledge of the influence of other factors makes it difficult to identify any observational features that are dependent primarily on extension. Lines of TiO in the red have been suggested as especially sensitive to atmospheric extension (Scholz and Wehrse, 1982). This area of research is just beginning.

Chromospheres, Nonradiative Heating, Departures from LTE, and Mass Flow

It was envisioned, when this volume was being planned, that we would now proceed to a discussion of those spectral features inexplicable by thermal models, which, therefore, were diagnostic for the nonthermal and nonstationary processes that form the main thrust of this series of books (cf. Thomas, 1983). As has become painfully clear from at least this chapter, however, *even common observations are still beyond the explicatory powers of present thermal atmospheric models.*

Quasi-thermal models, including chromospheres and departures from LTE, are analyzed in a succeeding chapter by de la Reza. As in K giant stars, the best diagnostic features for

stellar chromospheres are emission cores in the Ca II H and K lines, Fe II emission lines in the ultraviolet (Bidelman and Pyper, 1963; Boesgaard and Boesgaard, 1976), emission or exceptionally weak or strong absorption in Hα, and emission in Mg II h and k lines (cf. Linsky, 1980, 1982; Baliunas, 1984; Brown, 1984). Lines from coronal and transition regions are generally not seen in red-giant stars because these stars all lie on the "mass-loss" side of the line which divides stars with coronae from stars with mass loss (Linsky and Haisch, 1979; Ayres et al., 1981). The prime diagnostic for mass loss is the violet-shifted central absorption component in the Mg II h and k lines (Stencel and Mullen, 1980). This latter requires a high-resolution spectrum, and most types of red-giant stars are too faint for IUE.

Spectra of M giant and supergiant stars almost universally show all the foregoing indicators. However, except for the well-studied star Betelgeuse (Goldberg, 1984, and this volume), models for the upper photosphere, the region of the temperature minimum, and the chromosphere are generally yet in the future (de la Reza, this volume).

Much less is known about S stars because they have not been so intensively studied. An early study found variable Mg II h and k emission in the S-Mira, Chi Cyg (Cassetella et al., 1980), and emission in this line (h and k are blended at the low resolution needed to detect the ultraviolet emission in these cool objects) has been reported in several non-Mira S stars but with a wide range in strength (Johnson et al., 1984). No high-resolution ultraviolet spectrum has been published.

Certain N-type carbon stars have been known to show Fe II emission lines in the violet (Bidelman and Pyper, 1963), but no Ca H and K line data are available (Richer, 1975). Ultraviolet spectra taken by IUE show weak Mg II h and k lines in the few cool carbon stars that are bright enough to detect (Johnson and O'Brien, 1983). A single high-resolution spectrum of TX Psc is now available and under study. The emission lines in HD 20234 are also variable (Querci and Querci, 1985).

R stars show Ca II H and K emission cores (Richer, 1975), indicating a chromosphere, but low-resolution IUE spectra are remarkably similar to those of G and K giants. The early R stars (R0–R3) show, on low-resolution IUE spectra, Mg II and Mg I in absorption and no emission features whatever. Middle R stars (R5) show either no Mg II h and k line or faint absorption features. Late R stars (R8) show weak Mg II emission features similar to those of N-type stars (Eaton et al., 1985). Only one high-resolution IUE spectrum has been obtained (the R0 HdC star, HD 182040), and this shows only the faintest hint of any emission at h or k.

Chromospheric modeling for red-giant stars had hardly begun (cf. Avrett and Johnson, 1984) and presents a perfect illustration of a field ripe for research (de la Reza, this volume).

ACKNOWLEDGMENTS

Many scientists have contributed to this chapter through their influence on the writer. I am especially grateful to Eugene Avrett, Duane Carbon, Joel Eaton, and Leo Goldberg for many useful comments on the manuscript and references. Paula Jentgens has been a fine and patient typist. Research on the atmospheres of cool stars will surely continue to provide an exciting adventure in the years ahead!

REFERENCES

Alexander, D.R., and Johnson, H.R. 1972, *Astrophys. J.*, **176**, 629.

Alexander, D.R., Johnson, H.R., and Rypma, R.L. 1983, *Astrophys. J.*, **272**, 773.

Alksne, Z., Alksnis, A., and Dzervitis, U. 1983, in *Properties of the Carbon Stars of the Galaxy* (Riga: Zinatne), p. 162.

Alksne, Z.K., and Ikaunieks, Y.Y., 1981, in *Carbon Stars* (Tucson: Pachart), p. 57.

Aller, L.H. 1960, in *Stellar Atmospheres*, ed. J.L. Greenstein (Chicago: Univ. Chicago Press), p. 156.

Athay, R.G. 1972, *Radiation Transport in Spectral Lines* (Dordrecht: Reidel).

Athay, R.G. 1981, in *The Sun as a Star*, ed. S. Jordan, NASA SP-450, p. 85.

Athay, R.G., and Skumanich, A. 1969, *Astrophys. J.*, **155**, 273.

Augason, G.C., Bregman, J.D., Johnson, H.R., and Witteborn, F.C. 1985, *Astrophys. J.* (submitted).

Auman, J.R. 1969, *Astrophys. J.*, **157**, 799.

Auman, J.R. and Woodrow, J.E.J. 1975, *Astrophys. J.*, **197**, 163.

Avrett, E.H. 1984, in *Chromospheric Diagnostics and Modeling*, ed. B.W. Lites (National Solar Observatory).

Avrett, E.H., and Johnson, H.R. 1984, in *Cool Stars, Stellar Systems and the Sun*, ed. S.L. Baliunas and L. Hartmann (New York: Springer-Verlag), p. 330.

Ayres, T.R. 1979, *Astrophys. J.*, **228**, 509.

Ayres, T.R. 1981, *Astrophys. J.*, **244**, 1064.

Ayres, T.R., Linsky, J.L. 1975, *Astrophys. J.*, **200**, 660.

Ayres, T.R., Linsky, J.L., and Shine, R.A. 1975, *Astrophys. J. (Letters)*, **195**, L121.

Ayres, T.R., Linsky, J.L., Vaiana, G.S., Golub, L., and Rosner, R. 1981, *Astrophys. J.*, **250**, 293.

Balega, Y., Blazit, A., Bonneau, D., Koechlin, L., Foy, R., and Labeyrie, A. 1982, *Astron. Astrophys.*, **115**, 253.

Baliunas, S.L. 1984, in *Future of Ultraviolet Astronomy Based on Six Years of IUE Research*, ed. J.M. Mead, R.D. Chapman, and Y. Kondo, NASA CP-2349.

Barnes, T.G., and Evans, D.S. 1976, *Mon. Not. Roy. Astr. Soc.*, **174**, 489.

Barnes, T.G., Evans, D.S., and Moffett, T.J. 1978, *Mon. Not. Roy. Astr. Soc.*, **183**, 285.

Baschek, B., and Scholz, M. 1982, in *Landolt-Bornstein: Numerical Data and Functional Relationships in Science and Technology*, New Series, Vol. 2, Subvol. b: *Stars and Star Clusters*, ed. K. Schaifers and H.H. Voigt (New York: Springer-Verlag), p. 91.

Basri, G.S. 1980, *Astrophys. J.*, **242**, 1133.

Basri, G.S., Linsky, J.L., and Eriksson, K. 1981, *Astrophys. J.*, **251**, 162.

Baumert, J.H. 1972, Ph.D. Thesis, Ohio State University.

Bell, R.A., Edvardsson, B., and Gustafsson, B. 1985, *Mon. Not. Roy. Astr. Soc.*, **212**, 497.

Bell, R.A., Eriksson, K., Gustafsson, B., and Nordlund, Å. 1976a, *Astron. Astrophys. Supplement*, **23**, 37.

Bell, R.A., and Gustafsson, B. 1980, *Mon. Not. Roy. Astr. Soc.*, **191**, 435.

Bell, R.A., Gustafsson, B., Nordh, H.L., and Olofsson, S.G. 1976b, *Astron. Astrophys.*, **46**, 391.

Bidelman, W.P., and Pyper, D.M. 1963, *Pub. Astron. Soc. Pacific.*, **75**, 389.

Blackwell, D.E., Petford, A.D., and Shallis, M.J. 1980, *Astron. Astrophys.*, **82**, 249.

Blackwell, D.E., and Shallis, M.J. 1977, *Mon. Not. Roy. Astr. Soc.*, **180**, 177.

Blackwell, D.E., and Willis, R.B. 1977, *Mon. Not. Roy. Astr. Soc.*, **180**, 169.

Boesgaard, A.M., and Boesgaard, H. 1976, *Astrophys. J.*, **205**, 448.

Böhm-Vitense, E. 1958, *Zt. f. Ap.*, **46**, 108.

Böhm-Vitense, E. 1982, *Astrophys. J.*, **255**, 191.

Böhm-Vitense, E., and Dettman, T. 1980, *Astrophys. J.*, **236**, 560.

Böhm-Vitense, E., and Nelson, G.D. 1976, *Astrophys. J.*, **210**, 741.

Bonneau, D., Foy, R., Blazit, A., and Labeyrie, A. 1982, *Astron. Astrophys.*, **106**, 235.

Bragg, S.L., Brault, J.W., and Smith, W.H. 1982, *Astrophys. J.*, **263**, 999.

Brown, A. 1984, in *Cool Stars, Stellar Systems and the Sun*, ed. S.L. Baliunas and L. Hartmann (New York: Springer-Verlag), p. 282.

Carbon, D.F. 1973, *Astrophys. J.*, **183**, 903.

Carbon, D.F. 1974, *Astrophys. J.*, **187**, 135.

Carbon, D.F. 1979, *Ann. Rev. Astron. Astrophys.*, **17**, 513.

Carbon, D.F. 1984, in *Methods in Radiative Transfer*, ed. W. Kalkofen (Cambridge: Cambridge Univ. Press), p. 395.

Carbon, D.F., and Gingerich, O. 1969, in *Proc. Third Harvard-Smithsonian Conf. on Stellar Atmospheres, Theory and Observation of Normal Stellar Atmospheres*, ed. O. Gingerich (Cambridge: MIT Press), p. 377.

Carbon, D.F., Milkey, R.W., and Heasley, J.N. 1976, *Astrophys. J.*, **207**, 253.

Cassatella, A., Heck, A., Querci, F., Querci, M., and Strickland, D.J. 1980, in *Proc. Second European IUE Conference*, ESA SP-157, p. 243.

Chandrasekhar, S. 1935, *Mon. Not. Roy. Astr. Soc.*, **96**, 21.

Chiu, H.Y., Adams, P.S., Linsky, J.L., Basri, G.S., Maran, S.P., and Hobbs, R.W. 1977, *Astrophys. J.*, **211**, 453.

Clarke, D., and Schwartz, H.E. 1984, *Astron. Astrophys.*, **132**, 375.

Climenhaga, J.L., Harris, B.L., Holts, J.T., and Smolinski, J. 1977, *Astrophys. J.*, **215**, 836.

Cohen, J.G., Frogel, J.A., Persson, S.E., and Elias, J.H. 1981, *Astrophys J.*, **249**, 481.

Collins, J.G. 1974, Ph.D. Thesis, Indiana University.

Cram, L.E., Krikorian, R., and Jefferies, J.T. 1979, *Astron. Astrophys.*, **71**, 14.

Deguchi, S. 1980, *Astrophys. J.*, **236**, 567.

Desikachary, K., and Gray, D.F. 1978, *Astrophys. J.*, **224**, 1073.

Deupree, R.G. 1979, *Astrophys. J.*, **234**, 228.

Deupree, R.G., and Varner, T.M. 1980, *Astrophys. J.*, **237**, 558.

Dominy, J.F. 1984, *Astrophys. J. Supplement*, **55**, 27.

Dominy, J.F., Hinkle, K.H., Lambert, D.L., Hall, D.N.B., and Ridgway, S.T. 1978, *Astrophys J.*, **223**, 949.

Draine, B.T. 1981, in *Physical Processes in Red Giants*, ed. I. Iben and A. Renzini (Dordrecht: Reidel), p. 317.

Draine, B.T., 1984, in *Proc. Conf. on Mass Loss in Red Giant Stars* (Los Angeles: Univ. of California).

Dravins, D., Lindegren, L., and Nordlund, A. 1981 *Astron. Astrophys.*, **96**, 345.

Dumont, S., and Heidmann, N. 1973, *Astron. Astrophys.*, **27**, 273.

Dumont, S., and Heidmann, N. 1976, *Astron. Astrophys.*, **49**, 271.

Dzervitis, U. 1983, *Investigations of the Sun and Red Stars*, **19**, 65.

Eaton, J.A., Johnson, H.R., O'Brien, G.T., and Baumert, J.H. 1985, *Astrophys. J.*, **290**, 276.

Eaton, J.A., and Poe, C.H. 1984, *Acta Astr.*, **34**, 97.

Engvold, O., and Rygh, B.O. 1978, *Astron. Astrophys.*, **70**, 399.

Eriksson, K., and Gustafsson, B., Jørgensen, U.G., and Nordlund, Å. 1984, *Astron. Astrophys.* **132**, 37.

Eriksson, K., Gustafsson, B., Jørgensen, U.G., and Nordlund, Å. 1985 (in preparation).

Faÿ, T.D., and Johnson, H.R. 1973, *Astrophys. J.*, **181**, 851.

Fujita, Y., and Tsuji, T. 1977, *Pub. Astron. Soc. Japan*, **29**, 711.

Gail, H.-P., and Sedlmayr, E. 1984, *Astron. Astrophys.*, **132**, 163.

Glebocki, R. 1973, *Acta Astr.* **23**, 135.

Glebocki, R., and Stawikowski, A. 1980, *Acta Astr.*, **30**, 285.

Goebel, J.H., Bregman, J.D., Goorvitch, D., Strecker, D.W., Puetler, R.C., Russell, R.W., Soifer, B.T., Willner, S.P., Forrest, W.J., Houck, J.R., and McCarthy, J.F. 1980, *Astrophys. J.*, **235**, 104.

Goldberg, L. 1984, in *Cool Stars, Stellar Systems and the Sun*, ed. S.L. Baliunas and L. Hartmann (New York: Springer-Verlag), p. 333.

Goldberg, L., Ramsey, L., Testerman, L., and Carbon, D. 1975, *Astrophys. J.*, **199**, 427.

Golden, S.A. 1969, *J. Quant. Spect. Rad. Transf.*, **9**, 1067.

Goon, G., and Auman, J.R. 1970, *Astrophys. J.*, **161**, 533.

Goorvitch, D., Goebel, J.H., and Augason, G.C. 1980, *Astrophys. J.*, **240**, 588.

Gray, D.F. 1976, *The Observation and Analysis of Stellar Photospheres* (New York: John Wiley Co.).

Gray, D.F., and Linsky, J.L., ed. 1980, in *Proc. IAU Colloq. 51, Stellar Turbulence* (New York: Springer-Verlag).

Gustafsson, B. 1981, in *Physical Processes in Red Giants*, ed. I. Iben and A. Renzini (Dordrecht: Reidel), p. 25.

Gustafsson, B. 1985, *Ann. Rev. Astron. Astrophys.*, in preparation.

Gustafsson, B., and Bell, R.A. 1979, *Astron. Astrophys.*, **74**, 313.

Gustafsson, B., Bell, R.A., Eriksson, K., and Nordlund, Å. 1975, *Astron. Astrophys.*, **42**, 407.

Gustafsson, B., and Olander, N. 1979, *Phys. Scripta.*, **20**, 570.

Hall, D.N.B., and Ridgway, S.T. 1977, *Les Spectres des Molecules Simples au Laboratoire et en Astrophysique, Mém. Soc. Roy. Sci. Liège* (21^{e} Colloque Internationale d'Astrophysique de Liège), p. 243.

Hayes, D.P. 1984, *Astrophys. J. Supplement*, **55**, 179.

Heasley, J.N., Ridgway, S.T., Carbon, D.F., Milkey, R.W., and Hall, D.N.B. 1978, *Astrophys. J.*, **219**, 970.

Henyey, L., Vardya, M.S., and Bodenheimer, P. 1965, *Astrophys. J.*, **142**, 841.

Hundt, E., Kodaira, K., Schmid-Burgk, J., and Scholz, M. 1975, *Astron. Astrophys.*, **41**, 37.

Iben, I., and Renzini, A. 1983, *Ann. Rev. Astron. Astrophys.*, **21**, 271.

Iben, I., and Renzini, A. 1984, in *Physics Reports*, **105**, 329.

Jefferies, J.T. 1968, *Spectral Line Formation* (Waltham, Massachusetts: Blaisdell).

Jennings, D.E., Bragg, S.L., and Brault, J.W. 1984, *Astrophys. J. (Letters)*, **282**, L85.

Johnson, H.R. 1972, in *Proc. Conf. on Red Giant Stars*, ed. H.R. Johnson, J.P. Mutschlecner, and B.F. Peery, (Bloomington: Indiana Univ.), p. 288.

Johnson, H.R. 1973, *Astrophys. J.*, **180**, 81.

Johnson, H.R. 1974, NCAR TN STR-95 (Boulder: NCAR).

Johnson, H.R. 1982, *Astrophys. J.*, **260**, 254.

Johnson, H.R. 1985, in *Cool Stars with Excesses of Heavy Elements*, ed. M. Jaschek and P.C. Keenan (Dordrecht: Reidel), p. 271.

Johnson, H.R., Ake, T.B., and Eaton, J.A. 1985, in *Cool Stars with Excesses of Heavy Elements*, ed. M. Jaschek and P.C. Keenan (Dordrecht: Reidel), p. 53.

Johnson, H.R., Alexander, D.R., Bower, C.D., Lemke, D.A., Luttermoser, D.G., Petrakis, J.P., Reinhart, M.D., Welch, K.A., and Goebel, J.H. 1985, *Astrophys. J.*, **292**, 228.

Johnson, H.R., Beebe, R.F., and Sneden, C. 1975, *Astrophys. J. Supplement*, **29**, 123.

Johnson, H.R., Bernat, A.P., and Krupp, B.M. 1980, *Astrophys. J. Supplement*, **42**, 501.

Johnson, H.R., Goebel, J.H., Goorvitch, D., and Ridgway, S.T. 1983, *Astrophys. J. (Letters)*, **270**, L63.

Johnson, H.R., and Krupp, B.M. 1976, *Astrophys. J.*, **206**, 201.

Johnson, H.R., Marenin, I.R., and Price, S.D. 1972, *Jour. Quant. Spectr. and Rad. Transf.*, **12**, 189.

Johnson, H.R., and O'Brien, G.T., 1983, *Astrophys. J.*, **265**, 952.

Johnson, H.R., O'Brien, G.T., and Climenhaga, J.L. 1982, *Astrophys. J.*, **254**, 175.

Johnson, H.R., and Sauval, A.J. 1982, *Astron. Astrophys. Supplement*, **49**, 77.

Johnson, H.R., and Yorka, S.B. 1985, *Astrophys. J.* (in press).

Jorgensen, U.G. 1985, in *Cool Stars with Excesses of Heavy Elements*, ed. M. Jaschek and P.C. Keenan (Dordrecht: Reidel), p. 191.

Keenan, P.C. 1982, *Pub. Astron. Soc. Pacific*, **94**, 299.

Kipper, T. 1973, *Pub. Tartu Astronomical Obs.*, **41**, 63.

Kipper, T. 1982, *Model Calculations of Stellar Spectra*, Acad. Sciences, Estonian SSR, p. 3.

Kneer, F. 1983, *Astron. Astrophys.*, **128**, 311.

Krupp, B.M., Collins, J.G., and Johnson, H.R. 1978, *Astrophys. J.*, **219**, 963.

Kurucz, R.L. 1970, *Smithsonian Astrophys. Obs. Special Rpt.*, No. 309.

Kurucz, R.L. 1979, *Astrophys. J. Supplement*, **40**, 1.

Kurucz, R.L., Peytremann, E., and Avrett, E.H. 1974, *Blanketed Model Atmospheres for Early-Type Stars* (Washington: Smithsonian Institution).

Lambert, D.L. 1985, in *Cool Stars with Excesses of Heavy Elements*, ed. M. Jaschek and P.C. Keenan (Dordrecht: Reidel), p. 191.

Lambert, D.L., Brooke, A.L., and Barnes, T.G. 1973, *Astrophys. J.*, **186**, 573.

Lambert, D.L., Brown, J.A., Hinkle, K.H., and Johnson, H.R. 1984, *Astrophys. J.*, **284**, 223.

Latour, J., Spiegel, E.A., Toomre, J., and Zahn, J.-P. 1976, *Astrophys. J.*, **207**, 233.

Latour, J., Toomre, J., and Zahn, J.-P. 1981, *Astrophys. J.*, **248**, 1081.

Lengyel-Frey, 1977, Ph.D. Dissertation, University of Maryland.

Lester, J.B., Lane, M.C., and Kurucz, R.L. 1982, *Astrophys. J.*, **260**, 272.

Linsky, J.L. 1980, *Ann. Rev. Astron. Astrophys.*, **18**, 439.

Linsky, J.L. 1982, in *Advances in Ultraviolet Astronomy: Four Years of IUE Research*, ed. Y. Kondo, J.M. Mead, and R.D. Chapman, NASA CP-2238, p. 17.

Linsky, J.L., and Haisch, B.M. 1979, *Astrophys. J. (Letters)*, **229**, L27.

Little-Marenin, I.R., and Little, S.S. 1984, *Astrophys. J.*, **283**, 188.

Luck, R.E. 1977a, *Astrophys. J.*, **212**, 743.

Luck, R.E. 1977b, *Astrophys. J.*, **218**, 752.

Luck, R.E. 1978, *Astrophys. J.*, **219**, 148.

Luck, R.E. 1979, *Astrophys. J.*, **232**, 797.

Luck, R.E. 1982, *Astrophys. J.*, **263**, 215.

Luck, R.E., and Bond, H.E. 1980, *Astrophys. J.*, **241**, 218.

Luck, R.E., and Lambert, D.L. 1982, *Astrophys. J.*, **256**, 189.

Lucy, L.B. 1976, *Astrophys. J.*, **205**, 482.

Manduca, A., Bell, R.A., and Gustafsson, B. 1977, *Astron. Astrophys.*, **61**, 809.

Manduca, A., Bell, R.A., and Gustafsson, B. 1981, *Astrophys. J.*, **243**, 883.

Marcus, P.S., Press, W.H., and Teukolsky, S.A. 1983, *Astrophys. J.*, **267**, 795.

McCabe, E.M. 1982, *Mon. Not. Roy. Astr. Soc.*, **200**, 71.

McGregor, P. 1980, Ph.D. Thesis, Australian Natl. Univ., Canberra, Chapter 5.

Mendoza, V.E.E., and Johnson, H.L. 1965, *Astrophys. J.*, **141**, 161.

Menietti, J.D., and Fix, J.D. 1978, *Astrophys. J.*, **224**, 961.

Mihalas, D. 1969, *Astrophys. J.*, **157**, 1363.

Mihalas, D. 1978, *Stellar Atmospheres* (2nd edition), (San Francisco: Freeman and Co.).

Mihalas, D., and Athay, R.G. 1973, *Ann. Rev. Astron. Astrophys.*, **11**, 187.

Mihalas, D., Kunasz, P.B., and Hummer, D.G. 1976, *Astrophys. J.*, **203**, 647.

Mihalas, D., and Luebke, W.R. 1971, *Mon. Not. Roy. Astr. Soc.*, **153**, 229.

Mould, J.R. 1975, *Astron. Astrophys.*, **38**, 283.

Münch, G. 1946, *Astrophys. J.*, **104**, 87.

Nelson, G.D. 1980, *Astrophys. J.*, **238**, 659.

Noguchi, K., Maihara, T., Okuda, H., Sato, S., and Mukai, T. 1977, *Pub. Astron. Soc. Japan*, **29**, 511.

Nordlund, Å. 1974, *Astron. Astrophys.*, **32**, 407.

Nordlund, Å. 1976, *Astron. Astrophys.*, **50**, 23.

Nordlund, Å. 1980, in *Proc. IAU Colloq. 51, Stellar Turbulence*, ed. D.F. Gray and J.L. Linsky, (New York: Springer-Verlag).

Nordlund, Å. 1982, *Astron. Astrophys.*, **107**, 1.

Nordlund, Å. 1985, *Astron. Astrophys.*, (in preparation).

Olander, P.P. 1981, *Uppsala Astr. Obs. Rpt. No. 21.*

Olson, B.I., and Richer, H.B. 1979, *Astrophys. J.*, **227**, 534.

Parsons, S.B. 1969, *Astrophys. J. Supplement*, **18**, 127.

Pecker, J.C. 1951, *Ann. d'Astrophysique*, **14**, 152.

Pecker, J.C. 1973, in *Proc. IAU Symp. 54, Problems of Calibration of Absolute Magnitudes and Temperature of Stars*, ed. B. Hauck and B.E. Westerlund (Dordrecht: Reidel), p. 173.

Peytremann, E. 1974, *Astron. Astrophys.*, **33**, 203.

Piccirillo, J. 1980, *Mon. Not. Roy. Astr. Soc.*, **190**, 441.

Piccirillo, J., Bernat, A.P., and Johnson, H.R. 1981, *Astrophys. J.*, **246**, 246.

Pilachowski, C., Sneden, G., and Wallerstein, G. 1983, *Astrophys. J. Supplement*, **52**, 241.

Querci, F., and Querci, M. 1974, *Highlights of Astr.*, **3**, 341.

Querci, F., and Querci, M. 1975a, *Astron. Astrophys.*, **39**, 113.

Querci, F., Querci, M., and Kunde, V.G. 1971, *Astron. Astrophys.*, **15**, 256.

Querci, F., Querci, M., and Tsuji, T. 1972, *Mém. Soc. Roy. des Sci. de Liège, 6 Ser.*, **3**, 179.

Querci, F., Querci, M., and Tsuji, T. 1974, *Astron. Astrophys.*, **31**, 265.

Querci, M., and Querci, F. 1975b, *Astron. Astrophys.*, **42**, 329.

Querci, M., and Querci, F. 1976, *Astron. Astrophys.*, **49**, 443.

Querci, M., and Querci, F. 1985, *Astron. Astrophys.*, **147**, 121.

Ramsey, L.W., and Johnson, H.R. 1975, *Solar Phys.*, **45**, 3.

Ramsey, L.W. 1977, *Astrophys. J.*, **215**, 827.

Ramsey, L.W. 1981, *Astrophys. J.*, **245**, 984.

Richer, H.B. 1975, *Astrophys. J.*, **197**, 611.

Ridgway, S.T., Jacoby, G.H., Joyce, R.R., Siegel, M.J., and Wells, D.C. 1982, *Astron. J.*, **87**, 1044.

Ridgway S.T., Jacoby, G.H., Joyce, R.R., and Wells, D.C. 1980a, *Astron. J.*, **85**, 1496.

Ridgway, S.T., Joyce, R.R., White, N.M., and Wing, R.F. 1980b, *Astrophys. J.*, **235**, 126.

Ruland, F., Holweger, H., Griffin, R., and Biehl, D. 1980, *Astron. Astrophys.*, **92**, 70.

Saxner, M., and Gustafsson, B. 1984, *Astron. Astrophys.*, **140**, 334.

Scalo, J.M. 1973, *Astrophys. J.*, **186**, 967.

Scalo, J.M. 1976, *Astrophys. J.*, **206**, 474.

Scalo, J.M., Dominy, J.F., and Pumphrey, W.A. 1978, *Astrophys. J.*, **221**, 616.

Scalo, J.M., and Miller, G.E. 1979, *Astrophys. J.*, **233**, 596.

Scargle, J.D., and Strecker, D.W. 1979, *Astrophys. J.*, **228**, 838.

Schmid-Burgk, J., and Scholz, M. 1975, *Astron. Astrophys.*, **41**, 41.

Schmid-Burgk, J., and Scholz, M. 1981, *Mon. Not. Roy. Astr. Soc.*, **194**, 805.

Schmid-Burgk, J., Scholz, M., and Wehrse, R. 1981, *Mon. Not. Roy. Astr. Soc.*, **194**, 383.

Schmitz, F., and Ulmschneider, P. 1981, *Astron. Astrophys.*, **93**, 178.

Scholz, M., and Tsuji, T. 1984, *Astron. Astrophys.*, **130**, 11.

Scholz, M., and Wehrse, R. 1982, *Mon. Not. Roy. Astr. Soc.*, **200**, 41.

Schwartz, H.E., and Clarke, D. 1984, *Astron. Astrophys.*, **132**, 370.

Schwarzschild, M. 1975, *Astrophys. J.*, **195**, 137.

Sikorski, J. 1982, *Acta. Astr.*, **32**, 225.

Smith, M.A., and Dominy, J.F. 1979, *Astrophys. J.*, **231**, 477.

Sneden, C., Johnson, H.R., and Krupp, B.M. 1976, *Astrophys. J.*, **204**, 281.

Spiegel, E.A. 1963, *Astrophys. J.*, **138**, 216.

Steiman-Cameron, T.Y., and Johnson, H.R. 1985, *Astrophys. J.* (in press).

Steiman-Cameron, T.Y., Johnson, H.R., and Honeycutt, R.K. 1985, *Astrophys. J. (Letters)*, **291**, L51.

Stencel, R.E., and Mullan, D.J. 1980, *Astrophys. J.*, **238**, 221.

Strecker, D.W., Erickson, E.F., and Witteborn, F.C. 1979, *Astrophys. J. Supplement*, **41**, 501.

Strom, S.E., and Kurucz, R. 1966, *Jour. Quant. Spectr. and Rad. Transf.*, **6**, 591.

Thomas, R.N. 1960, *Astrophys. J.*, **131**, 429.

Thomas, R.N. 1983, *Stellar Atmospheric Structural Patterns*, NASA SP-471.

Thompson, R.I. 1977, *Astrophys. J.*, **212**, 754.

Toomre, J., Zahn, J.-P., Latour, J., and Spiegel, E.A. 1976, *Astrophys. J.*, **207**, 545.

Travis, L.D., and Matsushima, S. 1973a, *Astrophys. J.*, **180**, 975.

Travis, L.D., and Matsushima, S. 1973b, *Astrophys. J.*, **182**, 189.

Trimble, V., and Bell, R.A., 1981, *Quart. J. Roy. Astr. Soc.*, **22**, 361.

Tsuji, T. 1971, *Pub. Astron. Soc. Japan*, **23**, 553.

Tsuji, T. 1976a, *Pub. Astron. Soc. Japan*, **28**, 543.

Tsuji, T. 1976b, *Pub. Astron. Soc. Japan*, **28**, 567.

Tsuji, T. 1978a, *Astron. Astrophys.*, **62**, 29.

Tsuji, T. 1978b, *Pub. Astron. Soc. Japan*, **30**, 435.

Tsuji, T. 1981a, *Astron. Astrophys.*, **99**, 48.

Tsuji, T. 1981b, *J. Astrophys. Astron.*, **2**, 95.

Tsuji, T. 1981c, *J. Astrophys. Astron.*, **2**, 253.

Tsuji, T. 1983, *Astron. Astrophys.*, **122**, 314.

Tsuji, T., 1984, *Astron. Astrophys.*, **134**, 24.

Ulrich, R.K. 1970a, *Astrophys. Space Sci.*, **7**, 71.

Ulrich, R.K. 1970b, *Astrophys. Space Sci.*, **7**, 183.

Ulrich, R.K. 1970c, *Astrophys. Space Sci.*, **9**, 80.

Ulrich, R.K. 1976, *Astrophys. J.*, **207**, 564.

Vardya, M.S. 1970, *Ann. Rev. Astron. Astrophys.*, **8**, 87.

Vernazza, J.E., Avrett, E.H., and Loeser, R. 1981, *Astrophys. J. Supplement*, **45**, 635.

Walker, A.R. 1979, *South Africa Astr. Obs. Circ.*, **1**, p. 112.

Walker, A.R. 1980, *Mon. Not. Roy. Astr. Soc.*, **190**, 543.

Walker, A.R., Wild, P.A.T., and Byrne, P.B. 1979, *Mon. Not. Roy. Astr. Soc.*, **189**, 455.

Wallerstein, G. 1973, *Ann. Rev. Astron. Astrophys.*, **11**, 115.

Watanabe, T., and Kodaira, K. 1978, *Pub. Astron. Soc. Japan*, **30**, 21.

Watanabe, T., and Kodaira, K. 1979, *Pub. Astron. Soc. Japan*, **31**, 61.

Wehrse, R. 1981, *Mon. Not. Roy. Astr. Soc.*, **195**, 553.

Weiler, E.J., and Oegerle, W.R. 1979, *Astrophys. J. Supplement*, **39**, 537.

Wilson, O.C., and Bappu, M.K.V. 1957, *Astrophys. J.*, **125**, 661.

Wing, R.F. 1981, in *Physical Processes in Red Giants*, ed. I. Iben and A Renzini (Dordrecht: Reidel), p. 41.

Woodrow, J.E.J., and Auman, J.R. 1982, *Astrophys. J.*, **257**, 247.

Yorka, S.B. 1981, Ph.D. Thesis, Ohio State University.

Zuckerman, B. 1980, *Ann. Rev. Astron. Astrophys.*, **18**, 263.

N88-11600

8

QUASI-THERMAL MODELS

Ramiro de la Reza

INTRODUCTION

The atmospheres of giant and supergiant stars of the M-, S-, C-type appear to be intrinsically very different from the late-type dwarfs. Although M dwarfs possess a chromosphere, a transition region, and a corona that are qualitatively similar to that of the Sun, these luminous giant and supergiant objects appear to be devoid of transition regions and coronae, but to be characterized by vast amounts of circumstellar matter (Rieu, Lefèvre, and Glassgold and Huggins, this volume) and often important mass loss (Goldberg, this volume). As shown by observations of highly ionized lines in the ultraviolet with the International Ultraviolet Explorer (IUE), there are no indications that plasmas of temperatures of 10^5 K, corresponding to a transition region, exist. A recent review on late-type IUE observations is given by Baliunas (1983). The same negative results were obtained by absence of direct detections of the X-ray fluxes by means of the Einstein Observatory Satellite, indicating the absence of coronae (Vaiana et al., 1981). Indirect observations of coronae made by observing the He I line at 10830 Å (Zirin, 1982) also gave negative results. This chromospheric line can be formed by a photoionization/recombination process, produced by illumination of a coronal radiation. Moreover, no lines from high stages of ionization were seen in a short wavelength exposure with IUE of the carbon star, TX Psc, with an exposure of 7 hours (Johnson and O'Brien, 1983).

Some recent evidences show that, above the photosphere, a vast chromosphere could exist (Stencel, 1982a), at least for the early red giants and supergiants, extending to several stellar radii. These chromospheres connect the photosphere to the circumstellar regions. The important mass loss observed in these stars begins to operate somewhere in these chromospheres. If these chromospheres are extended, a new problem appears: to find the mechanism that could support them—turbulence? magnetic field? The answers are not definite.

In our discussion and construction of quasi-thermal models, we will relax the local thermodynamic equilibrium (LTE) assumption in photospheres and chromospheres. In general, hydrostatic equilibrium will be valid everywhere. Radiative equilibrium is valid in the photosphere, but this will no longer be the case in the chromosphere. Some velocity fields are, in this context, sometimes "ad-hoc" parameters, existing for empirical purposes only. In reality, our knowledge of turbulence

PRECEDING PAGE BLANK NOT FILMED

PAGE 372 INTENTIONALLY BLANK

in these stars is meager; the empirical curve-of-growth microturbulence is, in general, inconveniently supersonic in some outer layers.

The Mira characteristics (M. Querci, this volume), which will be discussed in the section *Shock-Wave Gas Dynamics and Pulsation Theory*, are more appropriate for a nonthermal concept. In this case, the velocities are no longer ad hoc parameters, and the shock-wave velocities that can exist in those stars are large enough to produce aerodynamic dissipation. In any case, the complete nonthermal models for Mira and non-Mira-type giant and supergiant cool stars will be obtained in the future when a consistent solution of the dynamic-transfer problems will be found.

Another important characteristic of the present models is that they are one-component models, and the probable existence of surface inhomogeneities is not taken into account. We know that large inhomogeneities exist in the atmospheres of the Sun and of the late-type dwarfs. Giant cells are predicted to exist in the late-type giants (Schwarzschild, 1975), but to the present time, no satisfactory observational evidences of these cells have been advanced (see, for example, Johnson, this volume). One possibility for future development of multicomponent atmospheric models can be made by a simultaneous diagnosis of the hotter and cooler components of the atmosphere, for instance, by the Mg II emission and by the CO fundamental vibration and rotation bands, respectively. (See Heasley et al., 1978, for an analogous study of Arcturus.)

Two main regions are important for these stars: the photosphere and the chromosphere. In view of the observational evidence of the absence of a high-temperature plasma, no transition regions and coronae are considered. The section *Photospheres* is devoted to the discussion of non-LTE effects in photospheres. In the section *Chromospheres*, we discuss the recent research on the chromospheres of these types of stars. In the section *Shock-Wave Gas Dynamics and Pulsation Theory*, we discuss elementary shock-wave and pulsation theories and their applications to Mira long-period variables.

PHOTOSPHERES

Our approach to the study of quasi-thermal photospheres will consist of relaxing the LTE hypothesis. In the subsection *Kinetic Equilibrium Line Formation*, we consider the non-LTE line-formation theory in photospheres. In the following subsection, we will discuss the metal ionization equilibrium and an application to a typical carbon-rich star photosphere.

Kinetic Equilibrium Line Formation

The main purpose of this subsection is to calculate a theoretical stellar spectra starting from a given atmospheric model representing the photosphere. This model consists essentially of a distribution in height of the kinetic temperature, gas and electronic pressures, and continuum opacities. The validity of the Maxwellian velocity distribution of particles provoking the collisions is assumed. Non-LTE line formation using this assumption has received the name "kinetic equilibrium" (KE) line formation (Athay, 1972).

Statistical Equilibrium. By definition, the statistical equilibrium equation relates the population numbers of different levels of the atom (n_i) to the rates causing changes in this population. Note the important assumption that $dn_i/dt = 0$. Considering an atomic model of N bound levels and a continuum (k), the statistical equilibrium equation can be written as:

$$n_i\left(\sum_{l=1}^{N} P_{il} + P_{ik}\right) = \sum_{l=1}^{N} n_l P_{li} + n_k P_{ki} \quad , \tag{8-1}$$

where $P = R + C$, and R and C are the radiative and collisional rates, respectively. The

upward rate is the excitation between two bound levels (i, l) or the ionization for a bound-free transition (i, k). The respective inverse processes are the deexcitation and recombination. The total number density of the atom is given by the particle conservation equation,

$$n_{tot} = \sum_{l=1}^{N} n_l + n_k \quad , \qquad (8\text{-}2)$$

where n_k is the number density of ionized atoms. Assuming that n_{tot} is known and that the total rates can be calculated, the equations can be solved to find the populations n_l and n_k.

The radiative photoionization and recombination rates depend on the mean intensity of radiation J_ν by the following expression:

$$R_{lk} = 4\pi \int_{\nu_{kl}}^{\infty} \frac{1}{h\nu} a_l(\nu) J_\nu d\nu \quad , \qquad (8\text{-}3)$$

where $a_l(\nu)$ is the photoionization cross section and ν_{kl} is the ionization threshold frequency.

If $J_\nu = B_\nu(T_e)$, B being the Planck function, the recombination rate can be calculated (see, for example, Mihalas, 1978) by

$$R_{kl} = \frac{n_l^*}{n_k^*} R_{lk} \quad , \qquad (8\text{-}4)$$

where n^*_l/n^*_k is given by the known Saha-Boltzmann equation. Knowing the collisional ionization rate, C_{lk}, a relation similar to (8-4) can be used to calculate the collisional recombination rate, C_{kl}. Radiative and collisional excitation rates can be calculated by classical relations using the Einstein radiative coefficients and Maxwellian distribution of level populations (see also Mihalas, 1978).

For two levels i and j, the line-source function is defined as:

$$S_L = \frac{2h\nu_{ij}^3/c^2}{\frac{g_j}{g_i}\frac{n_i}{n_j} - 1} \quad , \qquad (8\text{-}5)$$

g being the statistical weight. This last expression can always be written in the form (using relation (8-1)):

$$S_L = \frac{\int \Phi_\nu J_\nu d\nu + \epsilon B'}{1 + \epsilon} \quad , \qquad (8\text{-}6)$$

Φ_ν being the normalized absorption profile. This expression contains three fundamental physical processes: (1) the diffusion term, $\int \Phi_\nu J_\nu d\nu$, (2) the source term or creation of line photons, $\epsilon B'$, and (3) the sink term or destruction of line photons, ϵ.

Transfer Equation. In reality, S_L and J_ν are related by the equation of radiative transfer, measuring the change in distance of the intensity of radiation I_ν, making an angle θ ($\mu = \cos\theta$) with the normal to the surface:

$$\mu \frac{dI_\nu}{dz} = -k_\nu (I_\nu - S_L) \quad . \qquad (8\text{-}7)$$

If we write the line-absorption coefficient as $k_\nu^L = k_o^L \phi_\nu$, where $\phi_\nu = \Phi_\nu / \Phi_o$, we obtain the total monochromatic optical depth defined by:

$$d\tau = (\phi_\nu + r_o)\, d\tau_o \quad , \qquad (8\text{-}8)$$

where $d\tau_o = k_o^L\, dz$ and $r_o = k^C/k_o^L$. The transfer equation is then written as:

$$\mu \frac{dI_\nu}{d\tau} = I_\nu - S_t \quad , \qquad (8\text{-}9)$$

S_t being the total source function.

$$S_t = \frac{\phi_\nu S_L + r_o S_C}{\phi_\nu + r_o} \quad , \qquad (8\text{-}10)$$

where C refers to the continuum. The line-source function S_L, as written in relation (8-6), admits the validity of the complete redistribution of line photons (i.e., the emission profile is equal to the absorption profile). S_L is then not frequency-dependent. The main goal of the KE line formation consists of solving simultaneously the statistical (8-6) and transfer (8-9) equations, specifying the boundary conditions and the geometry of the medium.

Applications of KE Line Formation in LTE M–C Photospheres

Very few works have been devoted to the KE line formation in photospheres of late-type giants and supergiants of the M–C type. This is not the case of the slightly hotter stars of type G and K, which have received much more attention. Regarding the cooler types, the main work is related to the abundance determination of lithium. The importance of this element as an indicator of the internal and atmospheric evolutionary state of these stars is well known. Due to the relative ease of creation and destruction of this element, very large abundance differences can be found in these stars. These abundances vary from values smaller than the solar abundance to the extremely large values found in the "super lithium" C stars: WZ cas, WX Cyg, and T Ara. In the latter case, Li can no longer be considered as a trace element. However, abundances for these stars are not well known because they depend on solutions of the excitation/ionization problem described above, and these are not yet available.

Lithium Line Formation of M–C Giant Photospheres. Recent work on Li abundance determination in M-type photospheres has been undertaken by Luck and Lambert (1982), using improved observational data and based on model photospheres taken from the grid of Johnson et al. (1980). They used the complete linearization KE method code (Auer et al., 1972) to calculate the non-LTE abundance of Li with an atomic model of four levels plus continuum (Luck, 1977). Using an empirical solar line blanketing adapted to late-type giants, they found no non-LTE effects giving abundance differences for Li larger than 0.1 dex, suggesting that, because of the reduction of the ionizing field by line blanketing, non-LTE effects are not important in the ionization balance of Li in early M giants and supergiants. This work is based on the resonance Li I line at λ6708. It would be desirable for future Li studies to attempt to observe and use the subordinate Li I line at λ6103. This weak line has been identified by A. M. Boesgaard (Merchant, 1967) in early high-luminosity M stars.

Concerning the carbon-enriched photospheres, de la Reza and Querci (1978) performed KE calculations for the neutral lithium lines. The method they employed for solving the radiative and transfer equations is the integral flux divergence method (Athay and Skumanich, 1967; Athay, 1972). An atomic model of four levels and a continuum was also used. The photospheric LTE models were taken from the grid calculated by Querci (1972) and Querci and Querci (1975). The effective temperatures had values between 3800 and 3500 K, $g = 10$, C/O = 1.3. The photoionizing radiation field and the abundance were considered to be free parameters. The radiation field had the purpose of mimicking the effect of possible chromospheres and of simulating more or less blanketing. The main results were:

1. Li I is almost completely ionized in all models with $T_{\text{eff}} > 3500$ K.
2. The ionization is increased in KE.
3. $S_L > B_\nu(T)$ in the line-forming region, except for the case of the resonance λ6708 line with an Li abundance equal to 10^{-8}.
4. Profiles are sensitive to Li abundance and the chromospheric radiation temperatures, but not to the possible presence of graphite grains in the temperature minimum region.

5. Appreciable differences between KE and LTE were found for λ6708 only, although the Li I line at λ6103 is useful for distinguishing the effects of abundance from those of the chromospheric radiation field.

6. In LTE, to produce lines of Li I as strong as those observed in the lithium-rich C stars without enhancing the Li abundance, would require $T_{\rm eff}$ 2600 K.

Future Li abundance analysis should probably take into account aspects that have not been considered in the past: heterogeneities and spherical symmetry. Recently, Giampapa (1984) found that an enhanced chromospheric activity, such as a solar plage, can diminish the equivalent widths (W_λ) up to a factor 2 due to the increased ionization. This agrees with the observed anticorrelation found between the increase of emission of Ca II K line and the W_λ of the λ6707 Li line in the Sun. Special care must be taken when the Li I λ6707 line is compared to lines of Ca or Na as, for example, to the neighbor line of Ca I at 6717 Å. A proper KE analysis must also be made for these comparison elements.

Steenbock and Holweger (1984) investigated the ionization effect of the ultraviolet radiation field shortward of 3500 Å, which controls the ionization balance of Li. The thermalization effect of the H–Li atomic collisions was also estimated. In the case of a typical galactic disk late-type supergiant, the non-LTE effect measured by $\Delta\log\epsilon = \log\epsilon - \log\epsilon$ (LTE) can be equal to 0.57. This value is reduced by a factor of 2 if line blocking is considered. Due to the low densities involved, the thermalization collisions with H atoms have a negligible effect. For late-type halo giants of smaller metallicity, the results are similar; however, due to the larger densities, the thermalization collisions can be somewhat more important. To examine the influence of W_λ on the Li abundance, a careful comparison must be made between the works of Steenbock and Holweger (1984) and Luck and Lambert (1982). Also, spherical symmetry must be taken into account, particularly in the case of late-type supergiants.

KE Line Formation of Molecules. The KE problem of line formation for molecules in stellar spectra can be significantly more complex than that for atoms. In fact, the analysis must contain all the rates of formation and destruction of molecules. In some cases, the destruction process, such as photodissociation of molecules, can be a minor process in the statistical equilibrium (i.e., the case, for example, of the important molecules TiO and SiO in M stars and CO and CN in C stars). These molecules have large dissociation energies, and the corresponding radiation for photodissociation is located in the ultraviolet ($\lambda < 1500$ Å), which is very low in these stars, especially in the C stars.

Other considerations that limit the applicability of this analysis are the poor knowledge of the cross sections involved and the numerical intractability of the calculation of a band formed by hundreds of molecular lines. An interesting and general work on these problems is presented by Hinkle and Lambert (1975). Another work related to the formation of CO is that of Thompson (1973). The main conclusions of Hinkle and Lambert are as follows:

1. Because of the domination of the collisional process, LTE line formation ($S_L = B$) is the appropriate form for vibration/rotation transitions occurring within the ground electronic state. (These are the transitions found in the infrared spectra.)

2. The equilibrium of the excited electronic state is radiatively controlled, especially for late-type supergiants. These lines would be formed by the scattering process ($S_L = \int \Phi_\nu J_\nu d\nu$). For an optically thin absorption line, $S_L = J_\nu^c$, where J_ν^c is the local mean intensity in the continuum. (These transitions are found in

the visible and near-infrared stellar spectral regions.)

For the thin-line approximation, the equivalent widths will depend on the ratio, J_ν/B_ν, which can be very high in the outermost layers of stars. The equivalent widths will then be lower than those calculated in LTE. However, for the lines that are not optically thin, the line-source function depends on the scattering term, $\int \Phi_\nu J_\nu d\nu$, and the continuum source function. The line formation will be nonlocal in nature, and the complete KE equations must be solved. This complete KE calculation has been made by Mount et al. (1975) and Mount and Linsky (1975) for the violet CN band in the Sun and α Boo and by Carbon et al. (1976) for the fundamental bands of CO in cool stars. All these investigations found significant departures from LTE. For late-type stars, $S_L < B$ has been found. Contrary to the thin case, these results give stronger absorption lines in KE than in LTE.

The electronic bands, as is the case of CO, can be found in the ultraviolet. Ayres et al. (1981) showed evidence of the presence of fluorescent spectra of CO bands pumped by chromospheric emissions of O I at λ1380 and C I at λ1600. These bands appear as weak emissions near the C II (λ1335) and C IV (λ1550) features, which are normally indicators of the presence of a hot gas at 10^5 K. These authors then call for caution in the interpretation of these features in red giants.

Ionization Equilibrium in Photospheres

Non-LTE effects have always been suspected to exist in the atmospheres of late-type giant and supergiant stars due to their low total densities. However, rather than the total density, it is the free electron density which is important, because of its contribution to the excitation/ionization collisional process and to the continuous opacity. The goal of the study of ionization equilibrium is to determine the real distribution and effects of the electron density produced by the electron donors. In cool stellar photospheres, instead of H, which is the fundamental electron donor in chromospheres, the most abundant metals with low-ionization potentials are the principal sources of electrons. These are principally K, Na, Al, Mg, and Ca.

In this respect, very little study has been directed to these interesting problems in the photospheres. We can cite only two investigations: the theoretical work of Auman and Woodrow (1975) and the empirical work of Ramsey (1977, 1981). Ramsey compared the observed ratios of the equivalent widths of the [Ca II] λ7323 and Ca I λ6573 lines with those calculated by LTE model atmospheres of late-type supergiants. A certain discrepancy of these ratios begins to be detected for models cooler than 4250 K. This could be interpreted as evidence of non-LTE effects. However, as Luck and Lambert (1982) show, the continuum placement in these spectral regions is difficult, suggesting an inadequacy of the apparent local continuum of Ramsey. Nevertheless, we must not be far from reality, and as the theoretical work of Auman and Woodrow show, there are clear indications of non-LTE effects in high-luminosity cool stars. These authors iteratively solve the atmospheric equations with only the statistical equilibrium of the metallic electronic donors mentioned above. The simplifications are: (1) no radiative transfer is assumed, (2) the bound-bound transitions are treated in radiative detailed balance, and (3) no atomic or molecular (with the exception of H_2O) blanketing is taken into account. Even with these simplifications, their work was a fundamental step in this type of research.

To discuss the basic features of the ionization equilibrium, we consider the simplest case of a one-level atom with a continuum. The statistical equilibrium (see Equation (8-1)) is then:

$$n_l (R_{lk} + C_{lk}) = n_k (R_{kl} + C_{kl}) . \quad (8\text{-}11)$$

Using Equations (8-3) and (8-4) and the Saha-Boltzmann relation, Equation (8-11) can

be solved to give the value of the departure coefficient, b, which is given by:

$$b_l = \left(\frac{n_l}{n_l^*}\right) \Big/ \left(\frac{n_k}{n_k^*}\right) \quad . \tag{8-12}$$

When the atoms are predominately neutral, almost all atoms are at level 1; therefore:

$$b_1 \sim n_k^*/n_k \, , \tag{8-13}$$

and when atoms are strongly ionized, $n_k \sim n_k^*$, b is reduced to:

$$b_1 \sim n_1/n_1^* \, . \tag{8-14}$$

Actually, the mean intensity, J_ν, appearing in Equation (8-11) is also a function of b_1, and the expression relating J_ν to b can be found by simultaneously solving the statistical and transfer equations (KE). Since the line-absorption coefficient is also a function of n_l and b_1, an iterative process must be used to solve the equations for the values of b_1. Due to the low electron densities existing in the atmospheres of late-type giants, the value of b_1^{-1} depends exclusively on the ratio J_ν/B_ν. (For an explicit form of Equation (8-12), see Avrett and Loeser, 1969.) This ratio may be very large in the outermost regions due to the large values of the Rayleigh scattering coefficient compared to the other continuous opacities, especially in the ultraviolet. In the deeper layers, the ratio, J_ν/B_ν, converges to unity, giving a departure coefficient b_1 equal to unity.

A practical form to express the ionization equilibrium is (Auman and Woodrow, 1975):

$$\left(\frac{N^+ N_e}{N}\right)_{\text{KE}} = \frac{U^*}{U} \left(\frac{N^+ N_e}{N}\right)_{\text{LTE}} \, , \tag{8-15}$$

where N^+, N, and N_e are the ion, neutral, and electron densities. U and U^* are the partition functions assuming KE and LTE, respectively. It is easy to see that, in general, $b_1^{-1} \simeq U^*/U$. Assuming the neutrality of the plasma, the new electrons can be calculated by means of the new ion density. This "new" model can be iterated to obtain new values of J_ν which can be used again in the KE calculation. This iterative process can be used until convergence in the departure coefficients is obtained.

To illustrate the behavior of the b_1 values in model photospheres, we have calculated the KE for neutral atoms of K, Na, and Mg (for 5, 4, and 5 bound levels, respectively). These calculations consist of finding the first values of U^*/U, using the mean intensities J_ν from an LTE molecular-blanketed model photosphere. The model chosen is that of Querci (1972) and Querci and Querci (1975) corresponding to $T_{\text{eff}}/g/$ratio of C/O equal to 3400/0.1/3.26. Because no atomic line or grain blanketing was considered in those models, the J_ν values, especially in the ultraviolet, are maximum values. The U/U^* obtained, then, expresses maximum departures from LTE. It is important to mention, however, that subsequent iterations with model calculations will reduce, even more, the b_1 values. These results are presented in Figure 8-1.

We have experimented numerically to gage the sensitivity of U^*/U to the changes of J_ν values at different continua. We find that a reduction in J_ν by a certain factor for the first excited levels of all atoms produces a reduction of approximately the same factor in the values of U^*/U. These results are also sensitive to the second excited state of Mg I (as also found by Auman and Woodrow, 1975). We have examined the abundance effects by arbitrarily changing the model abundances for K and Na. Although there are no significant changes in the J_ν values of the LTE model, the KE populations of the bound levels change, giving larger departures for smaller abundances.

The converged values of Auman and Woodrow do not show significant temperature changes from the initial models. The most important changes are found in the electron density for the models: $T_{\text{eff}} = 2500$ K, $\log g = 0.0$, and $T_{\text{eff}} = 2000$ K, $\log g = -1.0$, in which

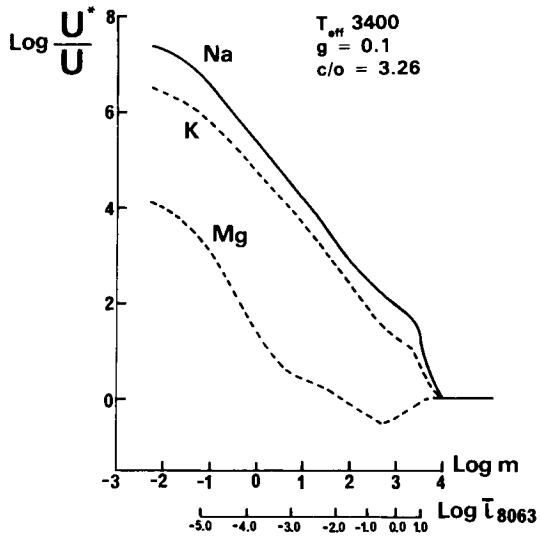


Figure 8-1. Behavior of the ratio of the initial partition functions with depth in the photospheres of a carbon-star model and for the principal electron donors, K, Na, and Mg. m is the column mass. A scale of depth for the reference wavelength, λ8063, is also shown.

the electron pressures increase in the outer layers, compared to LTE models, by factors of 14 and 60, respectively. Only slight changes are found in the continuous opacity (in general, less than 5 percent). This is due to the fact that, in the outermost layers where the non-LTE effects are larger, the continuum opacity is controlled by Rayleigh scattering by atomic and molecular hydrogen (especially in the ultraviolet), which is independent of Ne. Of course, H^- is an important source of the continuous spectra in these stars, and it depends on Ne. However, H^- appears to be important only in deeper layers in which the non-LTE effects are smaller. It is also important in this respect that a complete calculation of the H^- equilibria be performed following the suggestions of Lites and Mihalas (1984).

We conclude that non-LTE effects found for the carbon-star astmospheres shown in Figure 8-1 are large. These maximum values, however, are partial and will be reduced by iteration with the model. We hope that future models will contain blanketing by atomic lines (and grains?) to enable construction of reliable non-LTE blanketed atmospheres.

CHROMOSPHERES

The chromospheres of noncoronal stars such as M and C high-luminous stars are regions that lie immediately above the photospheres and in which a large part of the nonradiative energy available heats and expands the gas in order to produce an extended warm region. It is in these regions that the mass loss begins to take place.

Nevertheless, it is precisely in this type of star that real atmospheres seem to be much more complicated than in our simple models. That is due to the presence of a number of physical processes involved (e.g., abundance and grain effects, weak and strong shock waves, magnetohydrodynamic waves, turbulence, and possible large convection effects). Although a realistic energetic budget will be difficult to calculate under these conditions; it is the only way to understand why some stars have different kinds of chromospheres. (See Linsky, 1984a, for a recent review on chromospheres of non-Mira M and hotter G- and K-type stars.)

Hydrogen Ionization

In photospheres, ionization of abundant low-ionization metals was important, whereas in chromospheres, the ionization role is played by hydrogen. In fact, even at the modest temperatures, between 4000 and 10000 K, which exist in these zones, hydrogen will be ionized. Ionization of helium is less important, since it will be produced only at higher temperatures.

The construction of chromospheres must then calculate simultaneously the H line and continuum formation, together with the atmospheric equations using methods, for example, like those developed by Avrett (for a recent paper, see Avrett, 1985). H continua can also be treated by a method developed by O'Brien (1980) using the code (LINEAR) of Auer et al. (1972; see also Auer, 1973). This last procedure can be modified to treat H lines also.

Regarding H, another interesting problem that should be mentioned is the puzzle of the H_2 quadrupole line in M and S stars (Tsuji, 1983) and in C stars (Goorvitch et al., 1980; Johnson et al., 1983). The strongest infrared H_2 quadrupole line is not detected in non-Mira M stars, contrary to the theoretical expectation which predicts an increasing strength of this line as we go to cooler stars (Tsuji, 1983). This H_2 feature is clearly observed in S-type Mira stars (Hall and Ridgway, 1977; Tsuji, 1983). In C stars, the line is present in Mira variables.

Tsuji (1983) and Johnson et al. (1983) describe the principal physical scenarios that could explain the presence or absence of this line. Even if the problem between M and C stars appears to be similar, it is not clear whether the explanation will be the same for both types of stars.

Lower surface temperatures produce a stronger H_2 line if we consider the thermal sensitivity of the line. Spherical symmetry can produce these lower temperatures (Schmid-Burgk et al., 1981). This effect could thus explain the presence of H_2 in S stars. Tsuji (1983), however, favors the explanation of lower surface temperatures in S stars in respect to M stars (differences between 150 and 350 K), produced by the more efficient cooling effect of CO in S stars. Nevertheless, the problem concerning the non-Mira M stars remains open. Unless a general revision of the temperature scale is made, other mechanisms, such as the presence of a chromosphere, particularly on later types, could be invoked to explain the destruction of the H_2 molecules.

It is possible that the puzzle has an explanation other than thermal sensitivity for the case of C stars. Johnson (see Chapter 7) suggests the possibility of hydrogen deficiency in C stars. This suggestion is strengthened by an important characteristic of C stars (i.e., the absence of Balmer lines in N carbon stars (Yamashita, 1972, 1975)). Another fact that suggests an H deficiency is the weak observed emission peak of H^- at 1.6 μm in N stars as compared to that predicted by models (Goebel and Johnson, 1984). These authors propose that, if H deficiency is real in N carbon stars, this can be explained by an episodical ejection of an H-rich shell. That conclusion has important consequences for the evolutionary study of these objects and the chemical evolution of galaxies. It is important in this respect, however, to calculate the H^- equilibrium in the most complete way, following the treatment given by Lites and Mihalas (1984). Perhaps we could explain the absence of Balmer lines in N stars by the mechanism put forward by them, in which charge neutralization processes decrease excited H-level populations in favor of protons and H^- ions affecting the H ionization and the Balmer lines.

Bifurcated Chromospheres

The behavior of such important heating and cooling sources as H^-, CO bands, and metallic lines in stellar gases at the minimum solar temperature region, $T_{min} \simeq 4000$ K, has introduced new ideas on the structure of the solar chromosphere (Ayres, 1981). For the latest discussions, see Ayres (1985) and Avrett (1985). We think it will be interesting to check whether these concepts can be applied to future studies of detailed late-type star atmospheres.

First, let us examine the mechanisms: from one side, CO cooling is important for temperatures lower than 4000 K. For $T \gtrsim 4000$ K, the molecule dissociates, and its cooling effect diminishes. (The role of CO as a cooling source in late-type stars has been discussed initially by Johnson, 1973.) On the other hand, at this $T_{min} \simeq 4000$ K region, H^- is contrary a heating source due to photodetachment. H^- will be converted in a coolant only at higher temperatures near 5000 K. Bearing this in mind, we can now describe the principal physical idea (Ayres, 1985). For temperatures near 4000 K in a stationary atmosphere, the cooling properties of CO can act against the heating produced by H^- and the deposition of nonradiative energy, maintaining a cool gas at $T \simeq 4000$ K up to higher zones which were classically defined as belonging to the chromosphere.

However, in some supposedly restricted areas of the photosphere surface (e.g., magnetic flux tubes), the deposition of nonradiative energy can be strong enough to destroy the CO molecule and produce a temperature inversion that forms a localized chromosphere, for which the classical T_{min} concept can be applied. This stationary atmosphere will then be a two-component thermal atmosphere in which two zones—one hot, the other cold—will coexist at the same height. This type of bifurcated model can also be explained by nonstationary atmospheres (Muchmore and Ulmschneider, 1985) in which waves produced hot compressed zones and rarefied cool zones cooled further by CO radiation. Kneer (1983) has also examined the possibility that the thermal instability of optically thin infrared vibration/rotation bands of CO could produce chromospheres of late-type stars, proposing an interpretation of the known Wilson-Bappu effect (Wilson and Bappu, 1957).

One of the purposes of these bifurcated models is to reproduce the ionic emission as Ca II K simultaneously with the radiation of the CO infrared band. The empirical basis of these models is presented in Ayres (1985). Future development will depend, as Ayres explains, on a detailed treatment of non-LTE effects of CO, especially for ultraviolet electronic transitions. Metallic blanketing will be important because non-LTE effects will not only decrease the cooling effects of metals by a large factor but will also increase their effectiveness in depth by a similar factor (Kalkofen, 1985).

We would like to emphasize that it will be interesting to investigate the application of bifurcated models to late-type stars for which simultaneous observations of metallic emission lines and CO bands have been made.

Chromospheres of M-Type Stars

Observational Evidences. The research on chromospheres in M-type giants and supergiants has been based on the presence of some emission lines (see, for example, M. Querci, this volume) like the Mg II and Ca II resonant lines (Basri et al., 1981; Hagen et al., 1983) and Fe II lines (Boesgaard and Magnan, 1975; Boesgaard, 1979). Other lines also appearing in emission are the hydrogen Balmer lines (Jennings and Dyck, 1972; Hagen et al., 1983) and the Hϵ line (Wilson, 1957, 1982). However, the hydrogen lines can be explained by other mechanisms (e.g., shock waves). In the ultraviolet, research is also concentrated on the C II lines.

Dyck and Johnson (1969) and Jennings and Dyck (1972) first showed an anticorrelation between the H and K lines of Ca II and the infrared excess and polarization, characterizing the presence of dust grains in their atmospheres. This anticorrelation was interpreted by Jennings (1973) as due to a quenching effect by dust grains. These grains would radiate the nonthermal energy, preventing the formation of a chromosphere. This anticorrelation has also been found by Hagen et al. (1983) in a relatively large sample of M stars. However, the results of Hagen et al. show a difference in the sense that the real anticorrelation of Ca II emission is not with circumstellar dust, but appears to be with a dust-to-gas ratio (the degree of grain condensation). The core emission of the Ca II lines disappears in the coolest stars having strong dust-to-gas ratios. That is the case, for example, for the stars, HD 207076 (M7 III) and R Dor (M8 III). We can infer that these stars probably do not possess a chromosphere. However, any conclusion must be analyzed in detail because R Dor also shows Mg II in emission, which is normally considered as a chromospheric indication. Hagen et al. suggest a possible shock origin for this Mg line. This shock origin is also suggested for the Balmer emission lines that appear only in stars with high dust-to-gas ratios (Jennings and Dyck, 1972; Hagen et al., 1983).

Extension of the Chromospheres. Recent work based on the ultraviolet (UV) C II emission lines has permitted an empirical estimate of the temperatures, electronic densities, and geometric extensions of chromospheres of luminous stars of spectral types between G9 and

M3. The C II lines involved are the resonance triplet (UV 1) at 1335 Å and the multiplet (UV 0.01) at 2325 Å. Stencel et al. (1981) showed that, for electronic densities between $10^7 \leq N_e \leq 10^9$ cm^{-1}, the line ratios of the multiplet, UV 0.01, can be used as an indicator of N_e. The electronic temperatures are obtained by comparison of the observed ratios of the UV 1 and UV 0.01 total fluxes, together with a theoretical calibration of this ratio with N_e and T_e like that of Hayes and Nussbaumer (1984). Brown and Carpenter (1985) introduced this technique to obtain the temperatures of the C II line-emitting regions in several luminous late-type stars, assuming that the radiation arising from both multiplets came from a region of constant N_e. For M stars, the chromospheric values are $N_e \sim 10^8$ cm^{-3} and 7000 K $\leq T_e \leq$ 9000 K. The most interesting estimations are, however, those related to the sizes of these chromospheric C II emission regions. The most recent results are those of Carpenter et al. (1985), obtained by using the observed total fluxes of multiplet UV 0.01, the above-mentioned values of N_e, T_e, the photospheric radii, R_*, and the angular diameter, ϕ_*. The mean thickness of the emitting region, L, is calculated by these authors by the relation:

$$L = \frac{f_{2325}}{\Lambda E} \quad , \qquad (8\text{-}16)$$

where Λ is the solid angle subtended by the chromosphere and E is its volume emissivity given by:

$$E = \frac{1}{4} N_e N_{\mathrm{C\,II}} C_{12} h\nu_{21} \quad . \qquad (8\text{-}17)$$

The number density of C II can be calculated by:

$$N_{\mathrm{C\,II}} = \frac{N_{\mathrm{C\,II}}}{N_{\mathrm{C}}} \frac{N_{\mathrm{C}}}{N_{\mathrm{H}}} \frac{N_{\mathrm{H}}}{N_e} N_e \quad , \qquad (8\text{-}18)$$

for which the expression of fractional ionization of C and H and C abundance must be known. The solid angle is expressed in terms of the chromospheric radius, R, and the values of R_* and ϕ_*. The principal unknowns, L and R, are then related, and an iterative technique is used. These estimations, although subject to uncertainties, as values of N_e and the C abundance, clearly show that late-type giants with coronal regions (G9 and K0) have very thin chromospheres, with $R < 0.1$ percent of the photosphere. Noncoronal stars like M giants and supergiants have instead, on the average, chromospheric emission regions extending out to 2.5 photospheric radii. In the case of the M star, α Ori, for example, this method gives a chromospheric radius smaller by a factor of 2 than that found by Newell and Hjellming (1982) using radio observations. Of course, one must consider that the assumption of constant N_e is quite simplistic.

Thus it appears that these red high-luminosity stars contain a vast chromosphere extending to several stellar radii many times larger than their isothermal pressure scale heights. Mass loss is bound to be happening in these regions. Kinematically speaking, the chromospheres could, in a way, be physically detached from the photospheres (Goldberg, 1979). How can these extended chromospheres be produced? Certainly, the mechanism of thermal evaporation, which works in a hot stellar wind, will be inoperative here, due to the low temperatures and thermal pressures involved. In addition, it is not clear whether radiation pressure impinging on molecules (Maciel, 1976, 1977) or Lα radiation (Wilson, 1960; Haisch et al., 1980) could produce those extended regions by gas levitation and expansion. This will require further study. Other pressures of turbulent or magnetic origin can also be invoked. Stencel (1982b) mentioned that an rms turbulent velocity of the order of 50 km s^{-1} would be necessary to support material with a density of 10^8 cm^{-3} at 5 stellar radii. A magnetic pressure of a modest magnetic surface field could produce this support (see Goldberg, this volume).

Line Formation in Extended Atmospheres. If

chromospheres extended to several photospheric radii, spherical geometry must be taken into account in any realistic treatment of line formation. In addition, chromosphere expansion effects must be considered if mass loss is taking place somewhere in these regions. Because wind outflow velocities of the order of 10 to 50 km s^{-1} are only a factor of 2 larger than typical microturbulence values in late-type giant stars, the Sobolev approximation that is valid for strong winds will probably be of no value. Recent numerical applications solve the transfer equation in a comoving frame for a spherical atmosphere in expansion, assuming a partial redistribution (PRD) of line photons (Drake and Linsky, 1983; Drake, 1985 (differential equation method); Avrett and Loeser, 1983 (integral equation method)).

For the photospheres, Equation (8-6) admitted the validity of the complete redistribution (CRD) function, in which the emission-line profile, Ψ_ν, is equal to the absorption profile, Φ_ν. This is no longer the case in the interpretation of strong resonance chromospheric lines. Here the PRD approximation represents an intermediate situation between the coherent scattering and the CRD (in which, contrary to the coherent case, no frequency relation exists between the incoming and outcoming photons). A recent numerical solution is presented by Hubený and Heinzel (1984) on the effects of PRD on subordinated lines.

The total actual probability of a photon of frequency ν being absorbed and reemitted at ν' is:

$$R(\nu,\nu') = \gamma R_{II}(\nu,\nu') + (1-\gamma)\,\Phi(\nu)\,\Phi(\nu')\,, \tag{8-19}$$

where R_{II} is the angle averaged probability, and γ is the coherence mixing fraction given by:

$$\gamma = \frac{\Gamma_{rad} + \Gamma_I}{\Gamma_{rad} + \Gamma_I + \Gamma_E}\,, \tag{8-20}$$

where R_{II} is the angle averaged probability, and γ is the coherence mixing fraction given by: inelastic deexcitation collisions, and elastic collisions (i.e., Stark and Van der Waals collisions).

Noncoherent scattering (CRD) is valid in the Doppler core, whereas coherent scattering is important in the inner wings. Absorption by continuum processes is important in the extreme wings. The difference between PRD and CRD has been discussed by Basri (1980) in static atmospheres and by Drake and Linsky (1983) in expanding chromospheres. The results of Drake and Linsky show, for example, that the increase of flow velocity and geometrical extension gradually transforms a double peak Mg II line into an approximate P Cygni Mg II line. Drake (1985) has described and applied the PRD techniques in a semiempirical way to interpret the Mg II line in Arcturus. However, no unique atmospheric model that explains the line profile has been found. As Drake mentions, it is important to make future tests of cooler giants that show other chromospheric line indicators. Also in this respect, it is instructive to compare the results obtained with those produced by pure theoretical models. For an extensive review paper on PRD stellar applications, see Linsky (1984b).

Model Diagnosis. Two different approaches are generally made to model chromospheric temperature, density, and velocity distributions. One is to calculate the KE of important resonance lines, usually Mg II and Ca II for various assumed chromospheric models, and then select the model which best fits the observed profiles. This semiempirical method has been applied by several workers in F-, G-, and K-type stars (see, for example, Linsky, 1980, 1981). Some elements of this methodology are presented in the section *Chromospheres of Carbon Stars*. The other approach is a theoretical one that consists of predicting a chromospheric model from an adopted nonradiative heating mechanism. This theoretical treatment has also been applied in the study of F-, G-, and K-type stars (Ulmschneider, 1979; Musielak and Sikorski, 1981). An important general theoretical work on this field is that of Athay (1981).

Very few detailed chromospheric studies of M-type stars exist, and to our knowledge, only the supergiant α Orionis (M2 Iab) has received special attention. Lambert and Snell (1975) first examined whether a simple nonextended constant-temperature chromosphere could contribute to the infrared excess observed in α Ori and in the semiregular variable, W Hydrae (M7-9). This contribution would be important only at wavelengths for which the silicate dust is a poor emitter. Isothermal chromospheres of 5000 and 8000 K were proposed for α Ori and W Hya, respectively. However, this kind of approach requires a detailed knowledge of the sometimes badly known dust properties. In addition, those chromospheres must now be placed in a huge CS region in which grains exist. New problems are now emerging as to determining the real distribution of grains in space and time in those huge atmospheres. Forming dust grains near the surface of α Ori also appears to be difficult (Draine, 1981).

Another approach in the study of chromospheres of M stars has been to analyze the velocity fields in α Ori (Boesgaard and Magnan, 1975; Boesgaard, 1979) and in the M2.5 giant, β Pegasi (Boesgaard, 1981); these studies were devoted to the formation of their strong Fe II emission lines in the 3100 Å region. The transfer problems are solved in a spherical moving atmosphere covering an extended region around the photosphere of the star. The line-source function is not specifically solved, but rather, it is parameterized in order to represent a chromospheric rise of the temperature. Finally, the optical depths are adjusted, by varying the velocity fields, to fit the observed profiles. One important result for α Ori is that the Fe II lines in this model are formed in a region that shows an infall of matter. The velocity changes from 15 km s^{-1} at 1.8 R_* (R_* is the stellar radii) to 60 km s^{-1} at the photosphere. In the giant, β Peg, the Fe II emission lines show a rather uniform outflow beginning at zero velocity at the photospheric surface and attaining 25 km s^{-1} at 2 R_*.

A more direct semiempirical approach to the chromosphere of α Ori has been undertaken by Basri et al. (1981), who fit KE partial redistribution calculations with the observed profiles of Mg II and Ca II resonant lines. The computed models are nonextended chromospheres in hydrostatic equilibrium, resulting in a plane-parallel atmosphere. These authors could not find a homogeneous chromosphere for α Ori that fitted both the Ca II and Mg II profiles. This preliminary model is shown in Figure 8-2.

Zarro (1984) has recently studied the possibility that the profiles of Balmer lines, such as Hα, could be chromospheric indicators in late-type giants. However, as we will see later in the section *Shock-Wave Gas Dynamics and Pulsation Theory*, H-lines can be formed in some M giants by processes other than chromospheric ones (i.e., strong shocks). Also in this respect, in N irregular carbon-type stars, the Balmer lines are extremely weak (Yamashita, 1972, 1975).

A different approach (theoretical) has been taken by Hartmann and Avrett (1983), who construct a model for α Ori by including the Alfvénic wave pressure to produce an extended chromosphere. The momentum and energy equations of the wind are solved for a radial steady spherical symmetric flow. The temperature, density, and velocity of the flow is then later computed to attempt to reproduce some observed features in α Ori. The temperatures are those resulting from the energetic balance of wave heating, adiabatic expansion, and radiative cooling.

The principal difficulty of this mechanism stems from our limited understanding of the dissipation of these waves. The geometrical scale in which this dissipation occurs is represented by the damping length, L. Considering L to be constant, the physical situation is very sensitive to the values of $\lambda = L/R_*$. If $\lambda > 1$, the theoretical terminal velocity of the wind greatly exceeds the observed values, whereas for $\lambda < 0.85$, no mass loss occurs, Hartmann and Avrett (1983) choose an intermediate constant value $\lambda = 0.9$ for their calculations. The two computed models are shown in Figure 8-2. The "high-expansion" curve corresponds to a model giving a mass loss

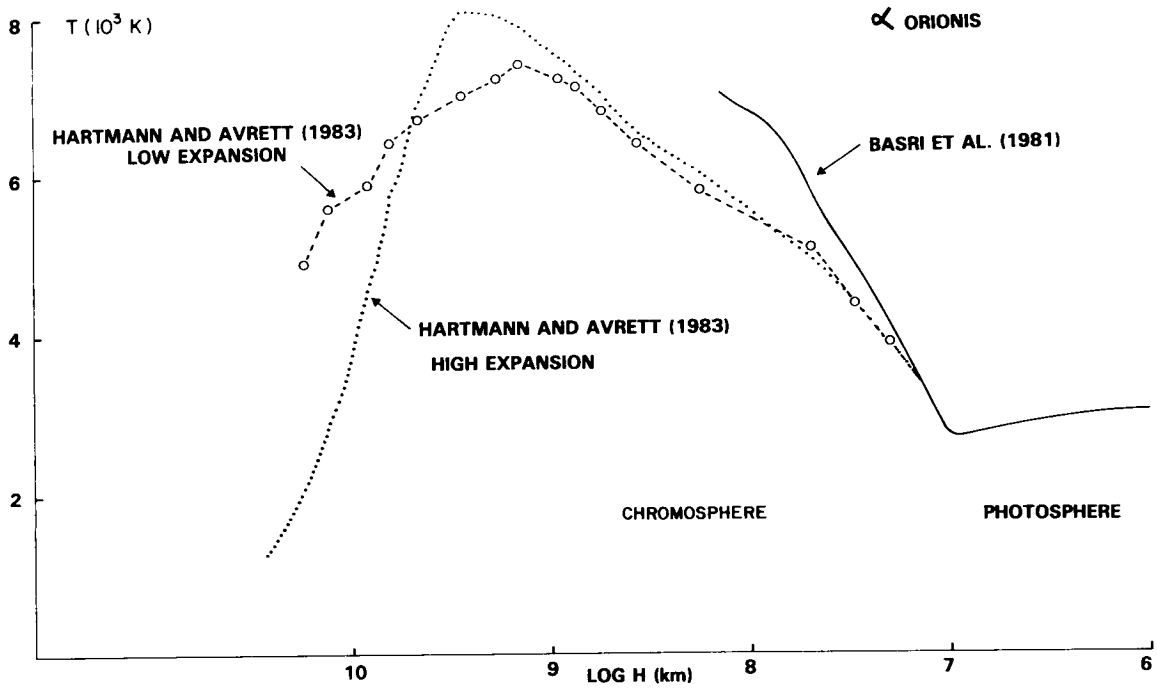


Figure 8-2. Temperature versus height chromospheric models of the supergiant M star, α Orionis. The nonextended semiempirical atmosphere of Basri et al. (1981) is shown, together with the theoretical extended models by Alfvén pressure waves (high and low expansion) of Hartmann and Avrett (1983). The photospheric zone is the same for all models.

equal to $1.4 \times 10^{-6} M_{\odot}$ yr^{-1}. The expansion velocities (V_{exp}) are of the order of 20 km s^{-1} and are larger than the turbulent velocities (V_{turb}). The other model, "low-expansion" with $V_{exp} < V_{turb}$, corresponds to a static energy equation. The photospheric model is the same as that of Basri et al. (1981). Both the high- and low-expansion models produce similar line and radio continuum emission in reasonable agreement with observations. Discrepancies with observations appear only when observed and computed profiles are compared. Theoretical profiles are much narrower than those observed. Predicted asymmetries are also too large. (The low-expansion model, however, produces nearly symmetric profiles.) In conclusion, larger V_{turb} and smaller V_{exp} by factors of 2 and 3, respectively, are necessary to match the observed data, suggesting a "quasi-static" extended chromosphere for α Ori.

Holzer et al. (1983) have criticized the use of a constant damping length. They believe that a more realistic interpretation will be one in which L is nonlinearly related to the state of the atmosphere (temperature, density, ionization, and radiative losses). They show that, if an ion-frictional damping is used in which the wave dissipation is produced by charge-transfer collisions between ions and atoms, it will give a thermal structure very different from that obtained by assuming constant L. These new temperatures are also the result of balance between heating by dissipation and cooling by radiation obtained in a self-consistent way. Holzer et al. (1983) also raise objections to the Alfvén wave mechanism as a general way to

produce cool massive low-speed winds for low-gravity stars. For them, any efficient mechanism (Alfvén waves or something else) must add the major part of the available energy in the subsonic region, without affecting the asymptotic flow speed u_∞. (u_∞ is much less than the escape velocity in low-gravity stars.) A small remaining energy will then be necessarily added to the flow in the supersonic region to guarantee the real escape of the wind.

Future modelers of α Ori must consider that time-dependent phenomena can be important input data. Although α Ori is a long-period variable (P = 2110 days), some rapid variations on a monthly scale have been observed (Goldberg, 1979). Other time-dependent phenomena could also be associated with possible large convective cells (Schwarzschild, 1975) or other mechanism, producing sporadic ejection of matter with velocities generally inferior to the escape velocity, so that infalling gas will be common, supporting perhaps the infall acceleration suggested by Boesgaard (1979). In addition, we cannot avoid the possible coexistence of hot and cool material producing an inhomogeneous multicomponent model.

Chromospheres of Carbon Stars

Although the presence of some Fe II emission lines in the violet appear to indicate the existence of chromospheres in N-type carbon stars, confirmation in certain stars (N stars) has come only recently through IUE observations of the 2200 to 3200 Å interval (Johnson and O'Brien, 1983; Querci et al.,1982; Querci and Querci, 1985), and in R stars by Eaton et al. (1985).

The stars observed by Johnson and O'Brien (1983) were all warm N-type stars, and none of them showed a strong violet depression. In fact, their ultraviolet spectra, beginning at 3200 Å, show a continuation of the photospheric spectrum with several absorption features down to wavelength λ2850, where the spectra appear to change and present emission lines. Here, two clear emission features are present that correspond to the Mg II and C II lines at λ2800 and λ2325, respectively. Because of the low resolution of IUE, the Mg II h and k lines are not resolved. The ratios f(Mg II)/f_{bol} obtained are, on the average, 100 and 25 times smaller than the respective ratios of K and early M stars. However, the ratio f(C II)/f_{bol} is only 2 to 4 times smaller than that of M giants. This difference is partially a consequence of the enhanced carbon abundance in carbon stars relative to M-type stars. The ratio f(Mg II)/f(C II) could be considered, in a way, to be independent of any superposed absorption. Even in this case, the latter ratio is 4 to 5 times smaller than that of M stars. From these results, Johnson and O'Brien suggest that chromospheres, weaker than those of M stars, must exist in these observed N-type stars.

How can the absence of light detection from other target stars be explained? Some of them have been integrated with exposure time up to 5 hours. Querci et al. (1982) explain this in two ways: one is the possible absence of a chromosphere. (This chromosphere could also be variable in time.) The other is the existence of a supplementary "ultraviolet depression." It is not clear if this supplementary opacity is or is not related to the classical violet depression that exists in some C stars and which begins at ~4200 A. At this point, it is important to note that the detection of light depends on the brightness of the star at U. Only the light of the brightest U stars like TX Psc and TW Hor were detected, whereas faint U stars such as YCVn and WZ Cas were not detected. This simple fact indicates that this is due to ultraviolet opacity of molecular and/or grain origin. (For a discussion of grains, see Lefèvre, this volume.)

Simple atmospheres can be formed by a photosphere and empirical plane-parallel ad-hoc chromosphere. When the photosphere is known, the chromosphere can be calculated using the following relations:

1. The hydrostatic equilibrium expressed by:

$$P - P_o = g(m - m_o) , \qquad (8\text{-}21)$$

where P_o and m_o are the total gas pressure and the column mass at the top of the chromosphere.

2. The total pressure given by the sum of partial pressures of the most abundant elements (in number N_{el})

$$P = n_H \sum_{l}^{N_{el}} (A_l + N_e) KT \ , \qquad (8\text{-}22)$$

where A_l is the abundance of the element l.

3. The charge neutrality,

$$N_e = N_p + N_H \sum_{l}^{N_{el}} A_l \frac{f_l}{1+f_l} \ , \qquad (8\text{-}23)$$

where N_p is the proton number, and each first stage of ionization is given by the function, f_l, between neutral elements and ions of the element, l. For H, the statistical equilibrium must be solved to obtain the departure coefficient, b_1, for the ground level. For H_e and other metals, ionization can be given by the Saha law.

We have four unknowns: N_H, P, N_e, and N_p for Equations (8-21), (8-22), and (8-23). The fourth equation must necessarily result from the energy-momentum conservation equation at any depth of the chromosphere. One way to replace it is to obtain an arbitrary relation between temperature and mass. One simple way is given by:

$$T = \alpha \log m + \beta \ , \qquad (8\text{-}24)$$

where α and β are constant coefficients determined from the boundary conditions: T_o at the top of the chromosphere and T_{min} at the minimum temperature region corresponding to the top of the photospheric model. All these equations can be solved by a rapid iterative process to produce the chromosphere.

The energy boundary conditions must be established for the fundamental variables, P and T: P_o, T_o and P_{min} and T_{min}. The choice of a smaller value of P_o will produce a more extended chromosphere for a given temperature gradient.

Using this method and keeping in mind the exploration of possible chromospheres of carbon stars, we have calculated some linear chromospheric extensions to the photospheric models of Johnson (1982). For these calculations, we have chosen two different carbon-enriched model photospheres with very different gravities and different effective temperatures. The main parameters ($T_{\rm eff}$/log g/ratio of C/O) are 3500/0.0/1.05 and 3000/2.0/1.02. For a chosen temperature distribution, the model will contain the calculated values of the column mass, the electron densities, and the departure coefficient, b_l, of the hydrogen. In the photosphere, b_l will be equal to unity. We have also calculated an ad-hoc depth-dependent microturbulence (increasing outward) by means of the following relation:

$$\xi = \alpha' \log m + \beta' \ . \qquad (8\text{-}25)$$

As boundary conditions for the top of the chromospheres, we have chosen a velocity that is somewhat smaller than the sound velocity and a zero velocity for the minimum temperature. (The published models of Johnson do not contain microturbulence velocities.)

For each photospheric model, we have calculated two linear chromospheres having different gradients. One corresponds to a "hot" model (T_o = 7000 K), and the other corresponds to a "cold" model (T_o = 4000 K). The boundary conditions are presented in Table 8-1, where P is the total pressure. The extension of the chromosphere, H_{chro}, is also contained in the table. For illustration, Figure 8-3 shows the behavior of the temperature versus column mass and the respective velocities.

KE Line Formation of the Magnesium Resonance Lines. In order to study the main

Table 8-1
Main Characteristics of the Chromospheres

Effective Temperature	Log g	P_o (dynes/cm^2)	T_o	T_{min}	H_{chro} (km)
3500	0.0	10^{-7}	7000,4000	2380	1.4×10^8
3000	2.0	10^{-5}	7000,4000	2010	9×10^5

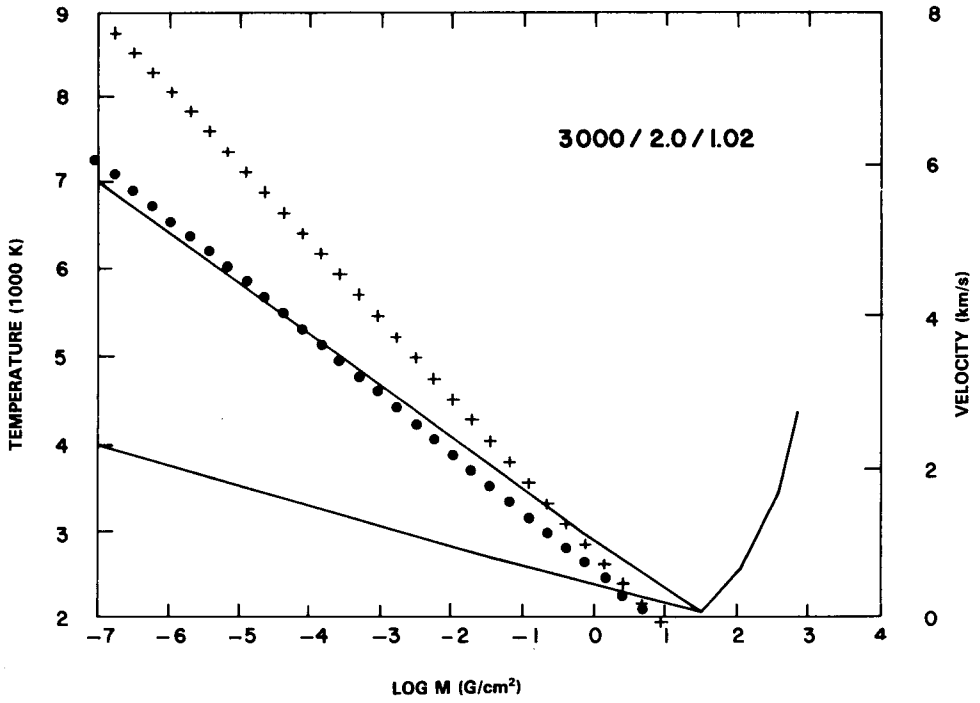


Figure 8-3. Distribution of temperature (solid lines) and velocities for the model 3000/2.0/1.02. Velocities for the hot chromosphere (T_o = 7000 K) are represented by crosses, and those for the cold chromosphere (T_o = 4000 K) by points.

characteristics of the presented atmospheric models, we have calculated the KE line formation of the resonance lines of Mg I at λ2852 and Mg II at λ2798. The latter line represents a mean of the h and k lines of Mg II. (The mentioned IUE observations do not resolve the h and k lines.) The KE calculations have been made by means of the LINEAR code indicated earlier. This code has been adapted to the condition appropriate to carbon-rich atmospheres and has been modified to use Voigt profiles.

One of the main characteristics of our KE calculations is that we assume the complete redistribution of photons. This analysis has been improved in studies considering partial redistribution. For our exploratory purposes, however, the assumption of the complete redistribution will be sufficient for the study of the core line formation. Only the indicated resonant lines are treated explicitly in the LINEAR code. All the other permitted transitions are considered as fixed. The radiation temperatures (T_{rad}) for the photoionizations and fixed transitions are equal to T_{eff} (with a

dilution factor of 1/2) in the chromospheric layers where T_e is larger than T_{eff}. In the following deeper layers, $T_{rad} = T_e$. A fixed-level atom is used for both Mg I and Mg II atoms. A solar Mg abundance is used.

A strong absorption Mg I line at 2852.1 A is observed in many late-type stars. (This can be seen, for instance, in the spectrum of the M3 III star, η Gem, in Johnson and O'Brien (1983).) This line, however, appears to be absent or weak in the spectra of the N carbon stars observed by Johnson and O'Brien. Normally, a strong absorption should be produced by the cooler photospheres of these stars, and this is not observed. Instead, a small emission feature appears at this wavelength in all the observed stars. Is this feature an indication of a "filling-in" process? Can an emission in the chromosphere produce this filling-in? All the Mg I lines obtained with these simple models are absorption profiles which show no sign of a central emission feature because of the strong photoionizing control of the line-source function.

An alternative filling-in process has been suggested by Johnson and O'Brien (1983) in which a large shell of gas could exist above this chromosphere. This shell must be sufficiently cool for Mg to be neutral and large enough to emit Mg I. The low-lying emission lines of Ti I, V I, and Zr I found by Gilra (1976) in the carbon star, UU Aur, could be formed in even larger shells because of their lower abundances. Scattering processes may also produce those emissions.

Figure 8-4 shows the resulting theoretical profiles of the resonance line of Mg II at λ2798 for the 3000/2.0/1.02 model. In both cases (hot and cold chromospheres), the line appears in emission with a central reversal. The shapes of these profiles are more or less typical of those found in late-type stars. One characteristic of this line is to be optically very thick, beginning to get thin only on the very top of the chromosphere. This line is, in all cases, formed at layers higher in the chromosphere than the Mg I line. The Mg II lines are much more controlled by collisions, indicating that very low radiation is available to photoionize from these two levels of the transition. The respective continua are at λ824 and λ1169, whereas those for Mg I are λ1621 and λ3756. For a general discussion on collisional and photoionization control processes, see Jefferies (1968) and Athay (1972).

The effects of the microturbulent velocities increasing outward are shown in Figure 8-5. The presented profiles are calculated for the same model 3000/2.0/1.02, both with and without microturbulence. The global effect of the velocity field is to broaden the line and shift the emission features, forming a broader reversal. More or less the same qualitative behavior has been found by Basri (1980) by means of a partial redistribution analysis. These turbulent effects are important in the detailed analyses of supergiants, which have much broader emission cores than those of dwarfs or giants.

The Avrett-Johnson Model. Apart from the Mg I and Mg II characteristics discussed above, any chromospheric model calculation of a warm N carbon star should take into account other important observational facts that act as constraints in the modeling construction. These are: (1) the presence of the emission line of C II at 2325 Å, (2) the notorious absence of the hydrogen Balmer lines (Yamashita, 1972, 1975), and (3) the reversal in the Ca II H and K lines observed in R stars (Richer, 1975) but not in N stars.

Avrett and Johnson (1984) recently constructed semiempirical chromospheres to fit these observational constraints (with the exception of the Ca II lines). The chromospheric model of an N star should be sufficiently cool to produce a low number density of the level 2 of hydrogen (n_2) to prevent the production of an Hα feature and should, at the same time, be sufficiently hot to produce Mg II and C II line emissions.

Their calculations are much more complete than the linear chromospheres calculated in the preceding subsections. They solved the

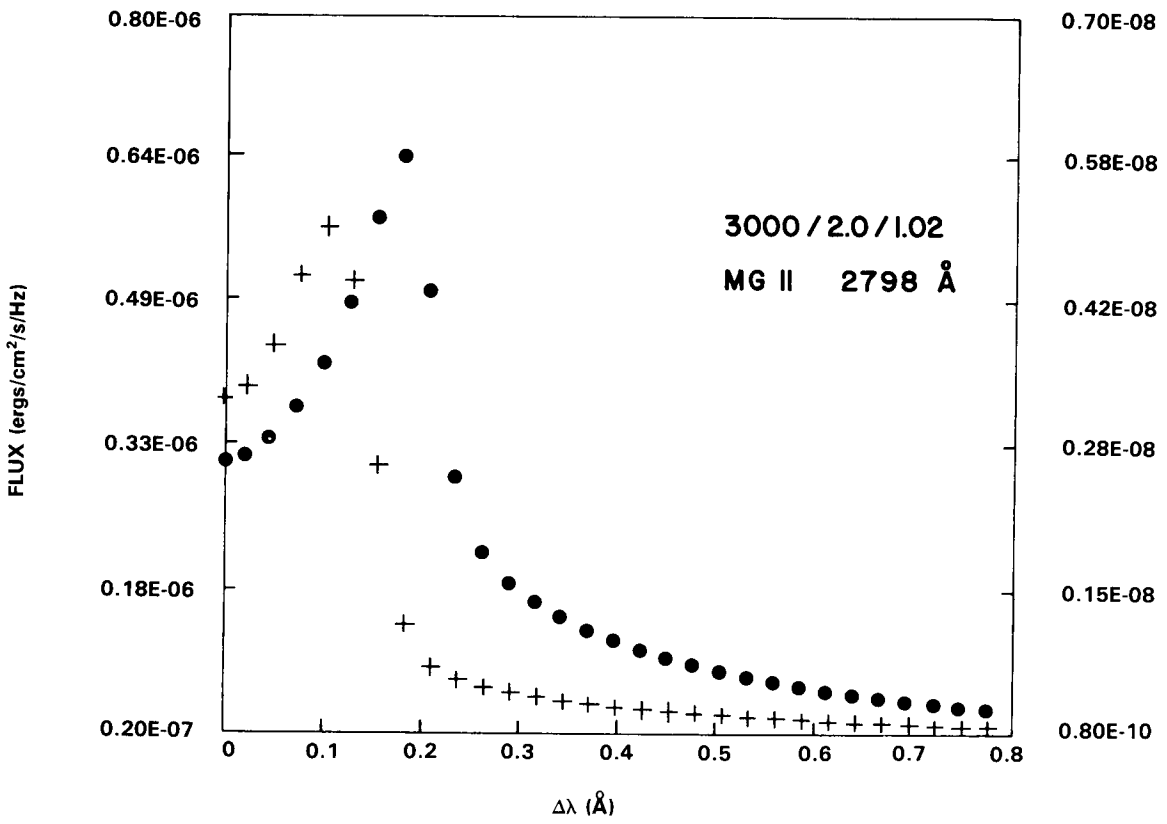


Figure 8-4. Computed profiles of the core of the resonant line of Mg II λ2798 for the model 3000/0.0/1.05. The points correspond to the hot chromosphere (flux scale on the left), and the crosses correspond to the cold chromosphere (flux scale on the right).

hydrostatic equilibria together with the KE of various elements such as H, H^-, H_2, Mg I, Mg II, C I, and C II and considered partial redistribution in the calculation of the Mg II line. The radiation temperatures used in their calculations (between 2200 and 2500 K) are smaller than those of the linear models of the subsection *Chromospheres of Carbon Stars* which have lower electron densities.

The resulting models 1 and 2 are presented in Figure 8-6, taken from the work of Avrett and Johnson (1984). The cool model 1 fills the condition of not producing the H feature; it seems, nevertheless, to be too cool to produce sufficient Mg II emission to fit the observed one. A negligible C II line is produced with this model. The hotter model 2 is also not convenient because it contains sufficient n_2 to produce an emission or absorption Hα feature, depending on whether the source function is larger or smaller than B.

In conclusion, both simple linear models and more sophisticated ones produce emission lines of Mg II. However, it is not clear whether future models will produce a C II emission feature or will maintain the H condition. (Avrett and Johnson (1984) are presently investigating hotter lower chromospheric models.) Two possible states appear to solve this problem: a high carbon abundance or a hydrogen underabundance.

Radiative Cooling and Energetic Balance. Several studies have recently appeared in the literature which treat the important problem of

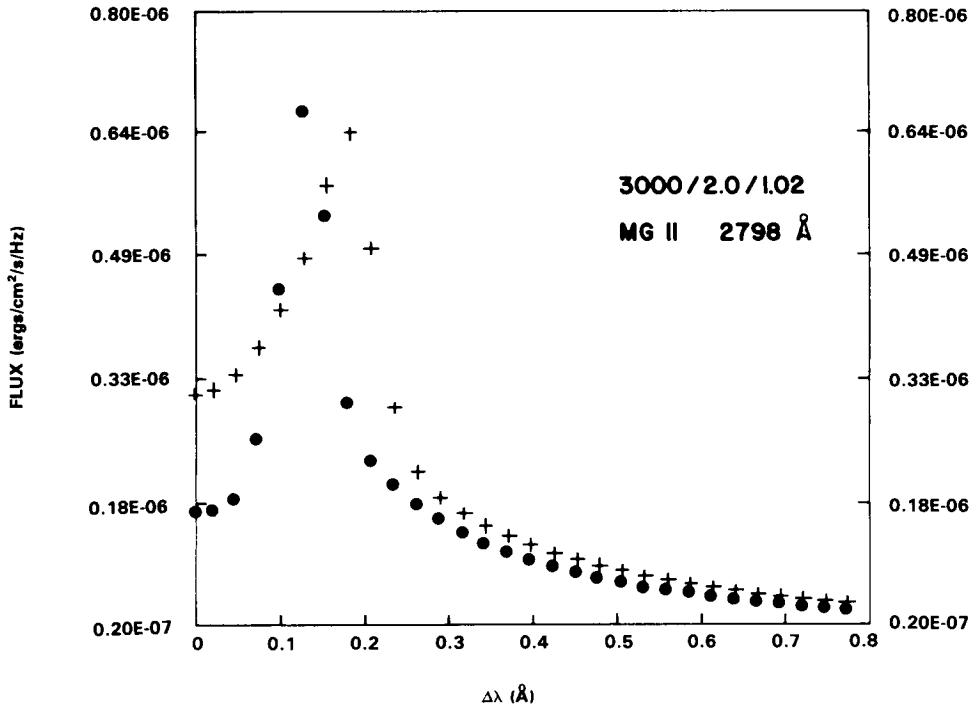


Figure 8-5. Theoretical profiles of the Mg II line for the hot model, 3000/2.0/1.02, with (crosses) and without (points) microturbulence.

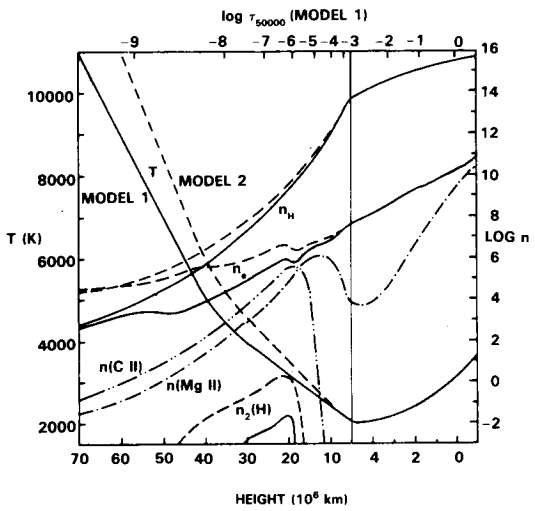


Figure 8-6. Temperature as a function of height (measured above $\tau_{5000} = 1$) for two chromospheric models and the corresponding values of the total hydrogen density, the electron density, and the level 2 hydrogen density. The τ_{5000} scale and the Mg II and C II number density for model 1 are also shown (from Avrett and Johnson, 1984).

the energetic balance in the atmospheres of the Sun and late-type stars (Linsky, 1980, 1981; Avrett, 1980). Two main processes exist in stellar atmospheres that maintain a temperature structure in equilibrium. These are the cooling and heating by radiative processes and the heating by nonradiative mechanisms. To obtain the net radiative contribution of each chemical element, the cooling and heating must be calculated for all the important bound-bound and bound-free transitions. In the chromosphere, a net radiative cooling flux results. This net cooling is a direct measure of the nonradiative (mechanical or magnetic) heating required to produce the chromosphere. In late-type giants, the lines of Ca II and Mg II are the main contribution to the net cooling, followed by H and H^-. As we go from the Sun to cooler giants, there is a growing importance of Mg II as a net cooler agent in the higher layers of the chromosphere.

For a transition between levels u (upper) and l (lower), the radiative cooling rate is (Vernazza et al., 1981):

$$\Phi'_{ul} = h\nu \, [n_u \, (A_{ul} + B_{ul} \int \Phi_\nu \, J_\nu \, d\nu) - n_l B_{lu} \int \Phi_\nu \, J_\nu \, d\nu] \, . \quad (8\text{-}26)$$

This expression can also be written using the net ϱ radiative bracket (Thomas, 1960). Note that the same symbol, Φ, is used for two different quantities:

$$\Phi'_{ul} = h\nu \, n_u \, A_{ul} \, \varrho \, , \quad (8\text{-}27)$$

where

$$\varrho = 1 - \frac{\int \Phi_\nu \, J_\nu \, d\nu}{S^L} \, . \quad (8\text{-}28)$$

Figure 8-7 presents the values of Φ'_{ul} for the resonant line of Mg II calculated for the models 3500/0.0/1.05 and 3000/2.0/1.02 with hot chromospheres. The cooling rates for the higher gravity model are found to be larger than those of the log g = 0.0 model. In fact, denser atmospheres are better radiators than diluted ones. If we can express Φ'_{ul} as a function of the geometrical depth, z, the net cooling rate can be known by calculating the integral, $\int \Phi' \, (z) \, dz$, for the positive values of Φ'_{ul}. The cooling rates shown here are presented for illustration purposes. Realistic values can be obtained by matching theoretical and observational integral fluxes.

Ultraviolet Spectra Variability. Systematic observations of ultraviolet spectral time variability are rare in S- and C-type cool giants (Cassatella et al., 1980, for the S-type star, X Cyg; Querci and Querci, 1985, for the N-type carbon star, TW Hor). Interpretation of the carbon star, TW Hor, appears to be very difficult because of the erratical behavior of emission lines such as those of Fe II at 3280 Å. As is the case in these carbon stars, several constraints must be taken into account in the atmospheric model of TW Hor, such as the absence of Balmer lines (either absorption or emission) and the absence of emission peaks of Ca II H and K lines. The Mg II emission lines appear to have a more or less normal behavior, indicating smaller variability. (For a discussion on the observations of TW Hor, see M. Querci, this volume.)

To understand the spectral characteristics of TW Hor, Querci and Querci (1985) analyzed a simple energetic budget which considers different types of physical mechanisms such as short-period acoustic waves, variable magnetic fields, and flare-like activity. The emergent picture that appears is that of a chromosphere with a flat temperature minimum and a gradual increase in higher layers. However, this increase of temperature is low enough to prevent emission peaks in Ca II H and K lines, but strong enough in higher layers to produce ionic emission features of the more abundant elements, Mg and Fe. Nevertheless, it is not clear how this chromospheric model will be able to prevent Balmer lines. The erratic behavior of the Fe II lines is, however, the most difficult aspect to understand. A variable Lα flux which induces variable Fe II emission lines (Furenlid, 1984) will not be an appropriate mechanism here because of the atypical characteristics of H in these stars. Querci and Querci (1985) state that the cause of this variability can be due to variable wave pulses (or variable magnetic field) in the chromosphere which is heated by short-period acoustic waves (Schmitz and Ulmschneider, 1981). The Mira S-type variable, X Cyg, observed by Cassatella et al. (1980) has been qualitatively interpreted using the dynamical shock-wave model of Hill and Willson (1979). (See the section *Radial Pulsation Modes.*)

SHOCK-WAVE GAS DYNAMICS AND PULSATIONAL THEORY

The preceding sections of this chapter discussed stellar photospheres and chromospheres as stationary components of static

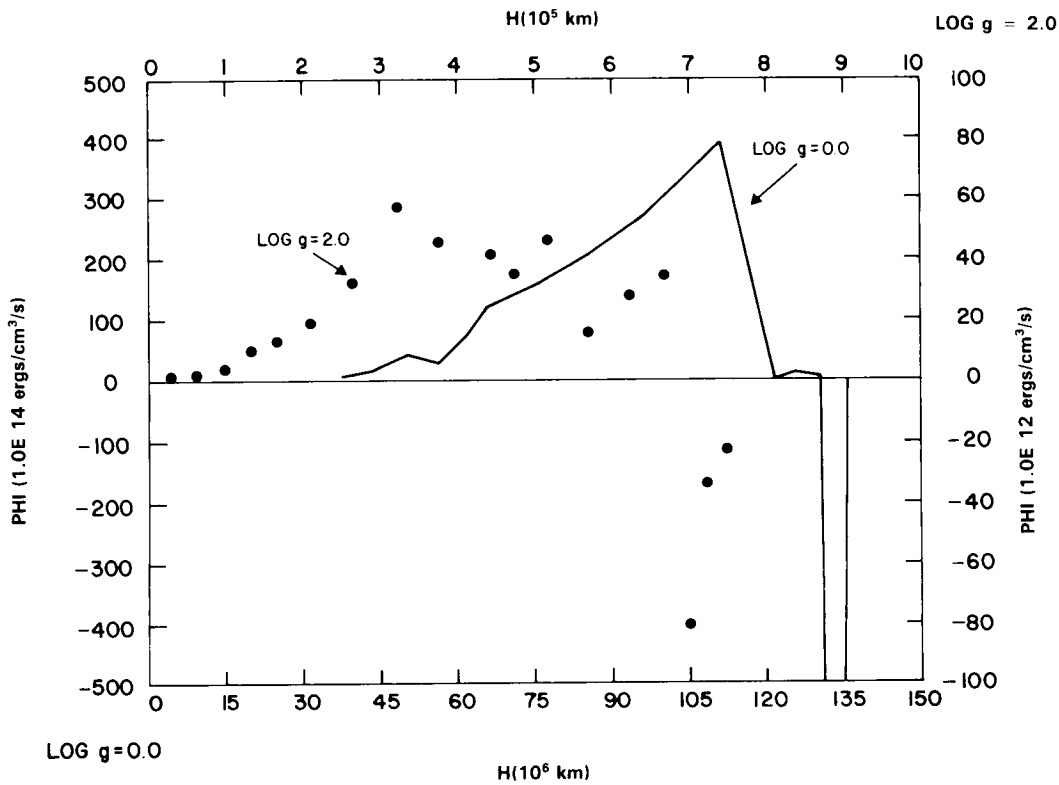


Figure 8-7. Cooling radiative functions Φ' for the Mg II line. Only the positive values contribute to the cooling. The solid line represents the hot chromosphere of the log g = 0.0 model. (The corresponding scales are on the left and on the bottom of the figure.) The points represent the hot chromosphere of the log g = 2.0 model. (The corresponding scales are on the top and right of the figure.) The top of the chromosphere is on the left.

atmospheres of single stars. However, some M and C late-type giants, as the long-period variables (Mira variables), present a complex time variability of their line spectra which requires an appropriate dynamical scenario for interpretation. Progressive shock waves are probably the principal physical mechanism that can explain this complex behavior. These shock-wave models are described by M. Querci (this volume), who focuses mainly on the observational aspects. Here we will put more emphasis on some of the basic theoretical aspects related to dynamical effects on the atmospheric structure and pulsational characteristics.

First, we will present a short discussion on the principal physical basis of the classical theory of shock waves in order to analyze the current research on this field.

Elementary Shock-Wave Theory

Gas dynamics is characterized by quantities such as velocity (v), pressure (P), density (ϱ), etc. which generally vary continuously. However, discontinuities of these quantities, which will represent shock waves, can exist. These discontinuities can move with different velocities of the gas flow itself and can be crossed by this flow of gas particles in their motion. If we consider a fixed coordinate system in which we define v_n as the gas velocity normal to the surface and v_s as the velocity of the discontinuity (shock wave), $u = v_n - v_s$ will be the velocity

of the gas relative to the discontinuity. Let us call gas 1 the one into which the discontinuity moves (preshock) and 2 the gas which follows the discontinuity (postshock). The respective velocities will be u_1 and u_2.

One of the most important theoretical tools that enable us to treat shock waves is the fact that the laws of mass, momentum, and energy conservation can be applied to those discontinuity regions. Applying these laws (see, for instance, Zeldovich and Raizer, 1966), we have the following respective equations:

$$\varrho_1 u_1 = \varrho_2 u_2 , \tag{8-29}$$

$$P_1 + \varrho_1 u_1^2 = P_2 + \varrho_2 u_2^2 , \tag{8-30}$$

$$\epsilon_1 + \frac{P_1}{\varrho_1} + \frac{u_1^2}{2} = \epsilon_2 + \frac{P_2}{\varrho_2} + \frac{u_2^2}{2} , \tag{8-31}$$

where P, ϱ, and ϵ are the pressure, density, and internal energy, respectively. Equation (8-29) reflects the existence of a continuous mass flux crossing a "zero-mass" discontinuity. Equation (8-30) represents the existence of the continuous momentum flux, meaning that the force exerted by the gases on each other across the discontinuity must be equal. If no external energy sources are considered, Equation (8-31) means that the internal energy, ϵ, of a given element is the result of the compressive work done on the element by the surrounding medium.

The Hugoniot Relations. A new important relation can be obtained from the conservation laws. Introducing the specific volumes, $V_1 = 1/\varrho_1$ and $V_2 = 1/\varrho_2$, we obtain from Equation (8-29):

$$\varrho_1 u_1 = \varrho_2 u_2 = J \tag{8-32}$$

that $u_1 = JV_1$ and $u_2 = JV_2$. Substituting in Equation (8-30), we obtain

$$J^2 = \frac{P_2 - P_1}{V_1 - V_2} . \tag{8-33}$$

Since J^2 is positive, two possibilities may arise: $P_2 > P_1$, $V_1 > V_2$ or $P_2 < P_1$, $V_1 < V_2$. In realistic shock waves, only the first case may actually occur. This corresponds to stable compression waves that result in an increase of entropy (Zeldovich and Raizer, 1966).

We can write Equation (8-31) in the following form:

$$\epsilon_1 + P_1 V_1 + \frac{1}{2} J^2 V_1^2 = \epsilon_2 + P_2 V_2 + \frac{1}{2} J^2 V_2^2 . \tag{8-34}$$

Replacing J^2 from Equation (8-33), we find finally:

$$\epsilon_2 - \epsilon_1 = \frac{1}{2} (P_1 + P_2)(V_1 - V_2) . \tag{8-35}$$

This relation is known as the *shock adiabatic* or *Hugoniot relation*. Graphically, this relation is represented in a PV-plane by Figure 8-8. An important conclusion can be obtained simply from this relation. First, we will determine the physical behavior of weak shock waves for small values of $P_2 - P_1$ and $V_2 - V_1$. Equation (8-33) can be written in first approximation as:

$$J^2 = - \frac{\partial P}{\partial V} . \tag{8-36}$$

The velocities u_1 and u_2 being equal in the same approximation, we have:

$$u_1 = u_2 = u = JV . \tag{8-37}$$

With Equation (8-36), we obtain:

$$u = \left[- V^2 \left(\frac{\partial P}{\partial V} \right) \right]^{1/2} = \left(\frac{\partial P}{\partial \varrho} \right)^{1/2} , \tag{8-38}$$

which is the velocity of sound C for that medium. We can conclude that, in the first approximation, the propagation velocity of a weak shock is equal to the velocity of sound,

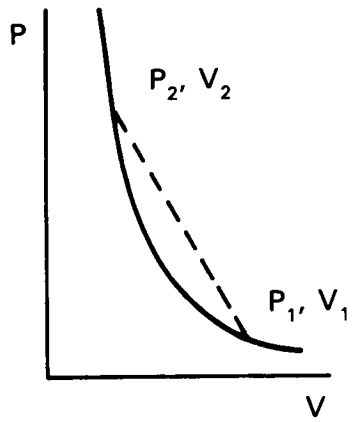


Figure 8-8. Graphical representation of the Hugoniot curve in a pressure-specific volume plane.

or in other words, the weak shock is a small perturbation that is approximately the same as a compression sound wave. Because real shock waves are compression waves, we must have $P_2 \quad P_1$. The point, 1 (P_1, V_1), must lie below the point, 2 (P_2, V_2), in Figure 8-8. Chord 12 has a slope J^2 larger than the tangent to the adiabatic at point 1:

$$J^2 > - \frac{\partial P}{\partial V_1} \tag{8-39}$$

Multiplying both sides by V_1^2, we have:

$$\begin{aligned} J^2 V_1^2 = u_1^2 &> V_1^2 \left(\frac{\partial P}{\partial V_1} \right) \\ &= \frac{\partial P}{\partial \varrho_1} = C_1^2 \quad . \end{aligned} \tag{8-40}$$

Then,

$$u_1 > C_1 \quad . \tag{8-41}$$

The gas flows into the discontinuity with a supersonic velocity. In other words, the shock wave propagates at a supersonic velocity with respect to the undisturbed gas 1. The slope of the chord being smaller than the adiabatic tangent at point 2, we obtain in the same manner as before that:

$$u_2 < C_2 \quad . \tag{8-42}$$

This means that the gas flows out of the discontinuity with a subsonic velocity, or in other words, the shock wave propagates at a subsonic velocity with respect to the compressed gas behind it. Because of the compression, $\varrho_2 > \varrho_1$, we have by means of Equation (8-29) that $u_1 > u_2$.

Shock Waves in a Perfect Gas. If we now consider the shock waves in a perfect gas with a constant ratio of specific heat, γ, we can introduce the internal energy:

$$\epsilon = \frac{PV}{\gamma - 1} \quad , \tag{8-43}$$

into the Hugoniot relation (8-35) and obtain the following relation:

$$\frac{V_2}{V_1} = \frac{(\gamma + 1) P_1 + (\gamma - 1) P_2}{(\gamma - 1) P_1 + (\gamma + 1) P_2} \quad . \tag{8-44}$$

Also, using the state equation of a perfect gas, we obtain the ratio of temperatures of the two sides of the discontinuity to be:

$$\frac{T_2}{T_1} = \frac{P_2 (\gamma + 1) P_1 + P_2 (\gamma - 1) P_2}{P_1 (\gamma - 1) P_1 + P_1 (\gamma + 1) P_2} \quad . \tag{8-45}$$

From Equations (8-29), (8-30), and (8-44), we can obtain the velocities of propagation of the shock waves relative to the preshock and postshock gases:

$$u_1^2 = \frac{1}{2} V_1 \left\{ (\gamma - 1) P_1 + (\gamma + 1) P_2 \right\} \quad , \tag{8-46}$$

$$u_2^2 = \frac{1}{2} V_1 \left\{ (\gamma + 1) P_1 + (\gamma - 1) P_2 \right\}^2 \Big/ \left\{ (\gamma - 1) P_1 + (\gamma + 1) P_2 \right\} \tag{8-47}$$

In the case of very strong shock waves for which $P_2 \gg P_1$ and $P_2 \gg (\gamma + 1)P_1/(\gamma - 1)$, we obtain the following result from Equations (8-44), (8-45), (8-46), and (8-47):

$$\frac{V_1}{V_2} = \frac{\varrho_2}{\varrho_1} = S = \frac{\gamma + 1}{\gamma - 1} , \quad (8\text{-}48)$$

$$\frac{T_2}{T_1} = \frac{\gamma - 1}{\gamma + 1} \frac{P_2}{P_1} , \quad (8\text{-}49)$$

$$u_1 = \left[\frac{1}{2} (\gamma + 1) P_2 V_1 \right]^{1/2} , \quad (8\text{-}50)$$

$$u_2 = \left[\frac{1}{2} (\gamma - 1)^2 P_2 V_1/(\gamma + 1) \right]^{1/2} . \quad (8\text{-}51)$$

These relations have important physical implications. First, the ratio, T_2/T_1, can be as large as P_2/P_1; second, the velocities, u_1 and u_2, depend on the square root of P_2. This means that T_2 and the velocities can take very large values.

This is not the case for the density, ϱ_2. In fact, the ratio of densities S will attain a constant value, depending on the value of γ: $S = 4$ for a monoatomic gas with $\gamma = 5/3$, and $S = 6$ for a diatomic gas with $\gamma = 7/5$. If full vibration/excitation is taken into account with $\gamma = 9/7$, S will be equal to 8. This ratio can be even larger if dissociation of molecules, excitations, and ionizations of the atoms or ions are taken into account.

Shock Model Applications

Three main directions characterize the work related to shock waves in the atmospheres of late-type stars: (1) the energy balance (the influence on the thermal structure), (2) the modes of pulsation which induce the shocks, and (3) shocks as a mechanism that produces mass loss. As mentioned previously, the observational evidence of the presence of shock waves, their behavior, and the models interpreting them are presented in detail in Chapter 2 (M. Querci). Here we will mention those observational aspects related to specific points of the theoretical discussion.

The motivation of the first theoretical approaches was to explain the origin of the bright hydrogen lines. Gorbatskii (1961) made one of the first theoretical studies of the ionization and radiation of zones heated by shock waves. This study, however, did not take into account the dissociation of the H_2 molecule, which is an important cooling effect. Later, Whitney and Skalafuris (1963) studied the restricted case of the behavior of the high-temperature region between 10000 to 30000 K near the shock front in a pure hydrogen atmosphere with no density gradient in front of the shock. The effects of the dissociation of the H_2 molecule have been taken into account by Slutz (1976) in his study of the acceleration of a single isolated adiabatic (with no radiative energy losses) shock wave in a photosphere having a density gradient. This study shows that, if the shock has a large amplitude, the acceleration ends in a terminal velocity smaller than 25 km s^{-1} (this value depending on the quantity of H_2). This could imply that, for stars with an escape velocity smaller than 20 km s^{-1}, an ejection of a shell of matter is possible. However, this kind of shock, called first shock, has been shown by Wood (1979) to be an atypical shock. In fact, a typical shock would be the one moving into matter falling inward, originated by a preceding shock, or matter flowing outward in a form of cool stellar wind. In addition, the proper initial conditions must be correctly established to consider the periodical nature of the problem. A sinusoidal varying pressure which simulates the star pulsation could be this initial condition.

The intrinsic pulsation nature of cool giants or supergiant variable stars (see, for example, M. Querci, this volume) could be the source of shock waves. Even the microturbulent or macroturbulent velocities, in spite of being generally ill-determined quantities, are sometimes found to be larger than the sonic velocities and

are therefore able to produce shock waves. However, it is in the interpretation of the complex spectra of Mira variables that the most powerful evidence of the presence of shock waves is found. The work of Willson (1976) is, in this respect, the most illuminating. Without considering in detail the complex behavior, doubling, and variations of absorption and emission lines (M. Querci, this volume), we mention the existence of two types of lines. The primary lines of Mg II, Ca II, Fe, and Ti II, formed in the region behind the shock (region 2) and the secondary lines of Sc I, Mn I, and Fe I (fluorescent or pumped lines) formed in front of the shock (region 1).

The main argument of Willson (1976) is that the fluorescent lines are formed by excitation of radiation emitted by the primary lines in a region of velocity discontinuity (shock wave). Each fluorescent line has its proper primary line exciting radiation approaching or receding with a characteristic velocity difference, producing an appropriate shift. Willson was able to show that, in general, the complex spectrum of typical Mira LPV atmosphere could be interpreted by a velocity discontinuity of the order of 40 to 80 km s^{-1}, thus providing strong evidence of the existence of a shock wave. Broadly speaking, the picture is the following: a moderately strong shock with a mean velocity of near 50 km s^{-1} appears at the base of the photosphere shortly after the visual light maximum. As this shock travels outward, it thermally excites the primary lines behind the shock; these lines at their turn radiatively excite (or pump) the fluorescent lines in the regions in front of the shock.

It is important to realize that the fluorescent lines permit one to determine only a velocity discontinuity (Δv), not the actual shock-wave velocity (v_s) with respect to the center of mass of the star. Positive or negative Δv indicates whether an exciting atom is approaching or receding from the region in which the excited (pumped) lines are formed. In this way, Δv 0 will mean that the compressed region 2 is moving outward. In this region, as discussed in the section *Elementary Shock-Wave Theory*, $u_2 = v_2 - v_s$, where v_2 is the gas velocity normal to the discontinuity. From relation (8-42), we see that this difference is smaller than the speed of sound, C_2, which is less than 10 km s^{-1} for a gas at $T < 10^4$ K and a typical density of 10^{-12} gr cm^{-3}. Taking into account the limited precision of the measurements, we can say that $v_2 \approx v_s$. In that condition, the velocity u_1 (velocity of the shock with respect to region 1) is a good measure of Δv obtained by the fluorescent lines: $u_1 \approx \Delta v$. If region 1 is falling toward the star, the actual shock velocity would be smaller than Δv, $v_s = v_2 = \Delta v - v_1$. On the contrary, if the material is flowing outward, the velocity of the compressed region will be larger, $v_s \approx v_2 = \Delta v + v_1$.

Influences on the Thermal Structure. The existence of a supplementary kinetical energy due to shocks produces an extension of the entire scale of the atmosphere of a late-type giant or supergiant star. This extension can be a factor 10 greater than the nonshocked atmosphere. For example, for a star with a radius equal to 10^{10} cm, this scale is similar to the stellar radius (Willson, 1976). The shock waves must then be considered as spherical shock waves which produce observable effects at greater distances from the stellar surface. In fact, shocks can persist for more than a period, and the product of the period and the shock velocity is of the order of the stellar radius.

We also expect to find structural changes in the distribution of temperature and density. However, these changes are not clearly determined at the present time because of the absence of a detailed calculation of the coupled interaction of the structure parameters and the detailed study of the shocks. A comparison between plane-parallel and the more realistic spherical isothermal atmospheres can be found in Willson (1982). The main theoretical approaches have been made using two different models: adiabatic (Wood, 1979) and isothermal (Willson and Pierce, 1982). The isothermal condition is expected to be satisfied in the lower

dense regions of the photosphere in which some absorption lines can be formed. Due to the higher density, any shock-heated material can cool more efficiently. This cooling is then produced in a small distance compared to the entire scale of the atmosphere. The isothermal condition is less valid in the outer less dense regions. We then expect a progressive change toward the adiabatic condition.

Using a pure adiabatic model, Wood (1979) found a resultant decreasing temperature distribution corresponding to a mean heating of the order of 5000 K in relation to an initial hydrostatic atmosphere. However, this adiabatic model produces an unrealistic high mass-loss rate. Using the isothermal approximation, Willson and Pierce (1982) found, in an atmosphere which suffers repeated shock passages, that the minimum temperature attained between shocks is an increasing outward function, contrary to the adiabatic case mentioned before. Due to the failure of the isothermal approximation at densities lower than $\log \varrho = -15$ (corresponding to a radius larger than $900\, R_\odot$), these authors can no longer describe the gas in the outer regions by a single temperature. In this picture we do not have a clear idea of the height at which the shocked model will attain a temperature low enough to allow the formation of dust grains. When dust grains are formed, they will produce heating by gas/grain collisions. At the same time, opposite cooling processes will appear such as rotational cooling of molecules or a simple adiabatic expansion. A recent work by Tielens (1983) has considered all these factors in a study of the flows of Mira variables driven by radiation pressure on dust grains. Tielens especially considered the direct coupling of the cooling of the gas with the velocity gradients in a two-component fluid composed by dust and gas interacting by collisions. This study is related to the existence of a stationary layer located between 5 and 10 R_* from the star, in which matter can return to the star or be pushed outward. The existence of this layer at 800 K at 10 R_* from which the maser features of SiO could originate, is proposed by Hinkle et al. (1982) and Hinkle (1983).

Detailed Structure of Shock Waves. Some studies of the detailed physical parts of stellar shocks appeared recently in the literature (Gillet and Lafon, 1983, 1984, in a strictly theoretical point of view; Fox et al., 1984, combining theory and observations). (See also the subsection *Shock-Wave Gas Dynamics of Balmer Emission Lines.*) A complete detailed analysis of the shock regions would be quite difficult, especially when the real finite shock front is considered, in which very large gradients of the physical variables have to be taken into account. Appropriate mathematical methods will then be necessary. Perhaps one promising method for future studies is the "Adaptive-Mesh Radiation Hydrodynamics" (Winkler et al., 1984). Here, an adaptive coordinate system, fixed neither to the fluid nor to the laboratory, is free to follow the evolution of the flow and the radiation field. The importance of this method is that, although the observed quantities are measured, for instance, in a comoving frame of the fluid, the radiation transport equation can be written in this adaptive frame which can move with arbitrarily high velocities. Large gradients such as shock fronts can then be treated.

As mentioned in the subsection *Shock Waves in a Perfect Gas*, the ratio $S = \varrho_2/\varrho_1$ can change if excitation and ionization are taken into account. It can be demonstrated that the increase of S for a given T depends on molecular dissociation and the internal energy of the particles (e.g., ionization) (Zeldovich and Raizer, 1966). Values larger than $S = 10$ can be obtained for high degrees of dissociation and ionization. In a medium composed of a mixture of gases, we expect to find a variable behavior of S as the strength of the shock increases.

In a medium formed by pure H, Gillet and Lafon (1984) analyze the precursor region (e.g., the immediate preshock region), putting emphasis on the importance of molecules in the weakening of the shock. For this, they considered the physical nonlinear relation between the precursor and the postshock region. In fact, before being affected by the advancing front,

the precursor is already influenced by the radiation coming from the hot postshock region. This radiation photodissociates the molecules and photoionizes the medium, producing a radiative cooling of the postshock region. This cooling is further accentuated by the thermal dissociation of molecules that cross the front.

Pulsation Theory

Radial pulsations are clearly seen in a large part of luminous M and C cool stars (see M. Querci, this volume). The aim of the theoretical research on the pulsation theory on these stars has been to answer the following fundamental and difficult questions: (1) Which is the pulsation mode? (2) Is pulsation an effective mass-loss mechanism? To answer these questions, linear (and nonlinear) adiabatic (and nonadiabatic) pulsation models have been developed in recent years. However, even with the great effort of some authors, no definite answers to these questions have been given.

Pulsations are produced in the large diluted envelopes of the stars in which the high luminosity determined by the core mass is being transported essentially by a convective process. The luminosity in these late-type stars can be so high that a net positive energy produces a dynamical instability. The pulsation provokes shock waves that locally heat and probably extend the atmosphere. This pulsational instability can relax into a steady regular pulsation such as those observed in LPV stars. However, the pulsations can also be transformed into strong relaxing oscillations in which mass loss can occur (Tuchman et al., 1978). Nevertheless, the success of this mechanism in interpreting real variable stars unfortunately depends on a badly known time-dependent convection theory. Another important theoretical input is the necessity to introduce realistic surface boundary conditions. Wood (1980) clearly shows these necessities when he discusses the uncertain results concerning the pulsational instabilities mentioned above and those of Wood (1979) and Willson and Hill (1979). In these models, not only convection is the weakest point, but also the mass loss produced. In fact, only few external zones are ejected, and the consideration of a proper external boundary, such as circumstellar material, could inhibit this mass loss. A general discussion on these aspects can be found in Wood (1982). More details concerning mass loss can be seen in Goldberg (this volume).

Nonradial Pulsations. Although pulsation has been discussed as a radial oscillation, there is a possibility of the existence of nonradial oscillations as supplementary energy-transporting mechanisms other than convection. These oscillations have been explored by linear nonadiabatic calculations in late-type models by Ando (1976). Later, Smith (1980) considered the possibility that these nonradial oscillations could be the source of what is commonly called "macroturbulence." The predicted amplitudes of this "late-type star seismology" are nevertheless very small, probably a few tenths of ms^{-1}. They would therefore be very difficult to detect. Recent observations in this direction are not yet conclusive (Smith, 1983, in α Tau and α Boo; Moon et al., 1983, in an M-S giant, ϵ Oct). Other promising candidates could be the following M semiregular giants which show short-period variations, particularly of the spectral region around the Ca I λ4227 absorption feature: R Crt (Livi and Bergmann, 1982) and L_2 Pup (Gómez Balboa and de la Reza, 1985).

Radial Pulsation Modes. One of the fundamental relations of radial pulsational stellar theory is the period-density relation (see for instance, Cox, 1980) which introduces the pulsation constant, Q, in the form:

$$Q = P(\varrho/\varrho_\odot)^{1/2} = P(M/M_\odot)^{1/2}\,(R/R_\odot)^{-3/2}\,. \qquad (8\text{-}52)$$

However, as has been shown in linear nonadiabatic models (Fox and Wood, 1982), Q is not a constant for any of the three lower order radial pulsation modes (fundamental, first and second overtone modes). Figure 8-9

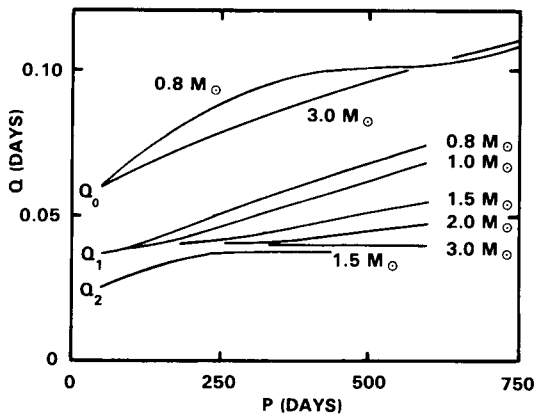


Figure 8-9. Q values for the three lowest order radial pulsation modes plotted against period (from Wood, 1982).

presents their corresponding values of Q_0, Q_1, and Q_2 against the first overtone period. If molecular opacity is introduced, Q_0 will be reduced. On the contrary, Q_1 will be somewhat larger. Another result of Fox and Wood is that, for high-luminosity stars, the nonadiabatic fundamental period, P_0, is shorter than the adiabatic, P_0. This has an important consequence because the adiabatic dynamical instabilities produced by large periods (Tuchman et al., 1978) disappear when nonadiabatic effects are included. In this linear nonadiabatic regime, the fundamental period, P_0, behaves as $P_0 \alpha R^2$ rather than $P \alpha R^{3/2}$ of the classical relation (8-52). An approximate simple relation can be found for Q_0 between definite values of M and P. No simple relation, however, can be found for the first overtone period, P, which behaves as $R^{3/2}$ for higher mass and as $R^{5/2}$ for lower mass. These results are found for typical galactic-disk long-period and semiregular variables. The L–M–R relations change when massive disk supergiants (up to 25 $M_\odot$) or other populations with different metallicities are considered.

Linear and nonlinear nonadiabatic pulsation models have also been investigated by Ostlie et al. (1982) in view of applications to typical galactic Mira stars. They obtain P–M–R relations for fundamental and first overtone pulsations, examining in particular the effect of a turbulence pressure. In the linear case, pressure effects appear to be important for the fundamental mode and lower mass. In the nonlinear models, turbulence amplifies the nonadiabatic effects.

How do Mira stars pulsate? This is a controversial subject, and no definite answers have been given. Looking back to the past, Kamijo (1963a, 1963b) concluded that Miras do not pulsate in the fundamental mode, but rather in higher modes with shorter periods. Later, the research has been based on the possibility of finding stable pulsational adiabatic static models (Keeley, 1970; Wood, 1974, 1975). The introduction of more realistic nonadiabatic models has introduced stable models which can be applied to massive LPV supergiants and pulsating carbon giant stars. These stars show secondary periods with $P \sim 2000$ to 7000 days (Leung and Stothers, 1977), which are approximately 7 times the typical primary periods of 300 to 700 days. Fox and Wood (1982) found several supergiant models in which $P_0/P_1 \sim 7$, indicating that the primary period is produced by excitation of the first overtone and the secondary period of the fundamental mode.

Let us now discuss the arguments supporting the fundamental mode pulsation of Miras. These are based on a dynamical model of shock waves (Willson and Hill, 1979; Hill and Willson, 1979; Willson et al., 1982). A general discussion can be found in Willson (1982). In particular, Hill and Willson (1979) developed a dynamical model, and in their calculations, they used the spherical symmetry and isothermality assumptions. Their model is characterized by the existence of two shocks. One lower shock emerges, with large amplitude, at the photosphere and lasts about a period. With the next period, another shock appears; two shocks can then be present: one stronger and lower and another weaker and higher. This lower shock is formed near the piston by the impact of the infalling large volume of rarefied preshock material with the rising material near the

C-6

photosphere. Because rarefied matter is falling and dense compressed material is rising, no net inward or outward motion is produced in this model.

In this model, the lower shock gives rise to the hydrogen emission lines in the postshock region, whereas the passage of the weaker upper shock model affects the absorption lines. The emission and absorption velocities then show the velocity variation across the lower and upper shock velocities, respectively.

In both these shocks, we can define $\Delta v = v_2 - v_1$, where v_1 and v_2 are the velocities defined in the section *Elementary Shock-Wave Theory*. Considering the relation (8-29), we obtain:

$$-v_2 = \frac{\Delta v}{S-1} \quad , \tag{8-53}$$

$$-v_1 = \left(\frac{S}{S-1}\right) \Delta v \quad . \tag{8-54}$$

Because $u_2 = v_2 - v_s$, where v_s is the shock velocity, it can be written as:

$$v_s = \frac{dr_s}{dt} = (1+q)\, v_2 \quad , \tag{8-55}$$

where

$$q = \frac{\Delta v / v_2}{S-1} \quad . \tag{8-56}$$

For a strong shock (higher S), $v_s \approx v_2$.

One important consequence of the model of Hill and Willson (1979) is that the ratio defined by $\beta = v_2/v_e$ is nearly constant, and equal to 0.2. v_e is the escape velocity $(2\ GM/r_o)^{1/2}$, where r_o is the radial distance of the lower shock. The value and behavior of β characterize the dynamical aspect of the model and is the basis of the interpretation of the observational results. In that case,

$$v_2(r) = \beta\, v_e(r) = v_2(r_o)\,(r/r_o)^{1/2} \quad . \tag{8-57}$$

For constant values of β and q, the solutions of Equations (8-55) and (8-57) give:

$$v_2\,(t=P) = v_2\,(t=o) \left[1 + \frac{3}{2}\,(1+q)\,\frac{v_2\,(o)\,P}{r\,(o)}\right]^{-1/3} \tag{8-58}$$

Hill and Willson (1979) place, in an M–R diagram (see their Figures 10 and 11), the values of constant velocity $v_2(o)$ and $v_2\,(P)$ for the stars R Leo and O Cet. It is possible to find a region in this diagram that is best satisfied by the observational data. Probable masses and radii are then obtained for R Leo (M = 1.8 - 4.0 $M_\odot$, R = 1.7 - 2.5 × 10^{13} cm) and for Mira ($M \approx$ 0.8 - 1.5 $M_\odot$, $R \approx$ 1.3 - 2.0 × 10^{13} cm).

Lines of constant Q values also allow one to establish the best possible pulsation modes between Q = 0.1 (fundamental mode) and Q = 0.04 (overtone mode). Both values seem a priori satisfactory; however, considering supplementary data on masses and radii, Hill and Willson (1979) preferred the fundamental mode for both stars.

The work of Hill and Willson (1979) has been criticized by Wood (1980, 1982). As mentioned previously, considerable controversy exists about this subject. Wood (1975, 1980) favors the first overtone mode. Wood derived larger radii (smaller Q) than those of Hill and Willson. Nevertheless, the principal arguments of Wood concern the dynamical and kinematical interpretations of the measured shock velocities in LPV. On the dynamical aspect, Wood (1979) found that, if a radial temperature gradient is introduced, the ratio β is no longer constant, being 0.24 for a lower shock and 0.11 for an upper shock. The other point of discussion concerns the possibility of measuring the values of the postshock velocity of the upper shock. Wood (1980, 1982) showed that, if the upper shock velocity can be measured, its low accuracy will severely compromise the results. In fact, for a dynamical shock-wave model, Q is very sensitive to the

velocity values because $Q \alpha (v_{lower}/v_{upper})^3$, and an uncertainty of ± 1 km s^{-1} will introduce an error in the determination of Q of the order of ± 0.1.

In conclusion, we can say that appropriate surface boundary conditions will help future studies. These conditions will probably affect primarily the overtone pulsations, which are more surface phenomena than those of the fundamental mode. A new approach, based on the detailed shock evolution of the Balmer emission lines, is now beginning to be explored.

Shock-Wave Gas Dynamics of Balmer Emission Lines. The observed behavior of the Balmer emission lines in different phases of Mira variables has been known since the pioneer works of Merrill (1945) and Joy (1947), but not until now have careful high spectral resolution observations of these lines been made in order to study the pulsation properties (Fox et al., 1984). A qualitative study of the dynamical evolution of Hα in the star, o Cet, has also appeared recently (Gillet et al., 1983), in which the variations of the Hα emission profile is interpreted as a spherical shock wave propagating outward from the photosphere. The shock leaves the photosphere when Hα emission appears for the first time in the cycle. Because of the occultation by the photosphere, the observer sees only the advancing part (detecting a blue-shifted emission). The emission profile appears to be mutilated by absorptions of an external molecular region. This mutilation diminishes as the shock leaves the molecular region. At that moment, the shock is quite far from the photosphere, and the observer is able to see the receding part of the always-outgoing shock, now producing a red-shifted emission. The atmosphere is then crossed from the luminosity maximum to the minimum by a single strong spherical shock wave which produces the emission lines in the hot postshock region. However, observed evidence of a second supersonic infalling shock in the same star has been detected by Ferlet and Gillet (1984) by means of an inverse P Cygni profile of Ti I. This infalling shock could be the return of nonejected upward-accelerated matter.

Fox et al. (1984) published a series of high-resolution spectral observations of the Balmer lines Hγ, Hδ, Hζ, and Hη of nine Mira stars during half cycle around maximum phase. Observations of the thermal excited line, Mg I λ4571, and the pumped line, Fe I λ4202 (pumped by the Mg II resonance line at λ2795), were also made. The Balmer emission lines present a full base width of near 80 km s^{-1} which decreases at later phases. Hδ seems to be the most indicated line for the study of evolution of emission regions because it is the least affected by superposed absorptions.

A detailed shock model to be applied to these observations is in progress (Fox and Wood, 1985). However, in advance of the presentation of this detailed model, a schematic simple shock is presented by Fox et al., (1984). This shock is shown in Figure 8-10. The precursor is formed by H and He at $T \sim 2500$ K, with an infalling velocity of 20 km s^{-1}. The hot postshock region is at $T = 34500$ K. It is in this region that the broad emission lines are formed by an important Balmer line scattering. In fact, the broadening temperature of the lines indicate temperatures of the order of 30000 K. The velocities shown in Figure 8-10 agree with those obtained from high-infrared spectroscopy of CO lines (Hinkle et al., 1984). In the shock model of Fox and Wood (1985), the far side of the outgoing shock does not contribute to the observed Balmer emission because of the total absorption of the inward Balmer radiation. This is contrary to the Hα interpretation of Gillet et al. (1983) mentioned previously. The metallic lines observed are very important in that they permit the Balmer emission variations in the cycle to be related to the velocities obtained from these metallic lines. This relation suggests a slowing down of the shock with phase. A further study is necessary to determine where the Mg I and Fe I lines mentioned are formed. Are they formed in the precursor or in the postshock region? The detailed model

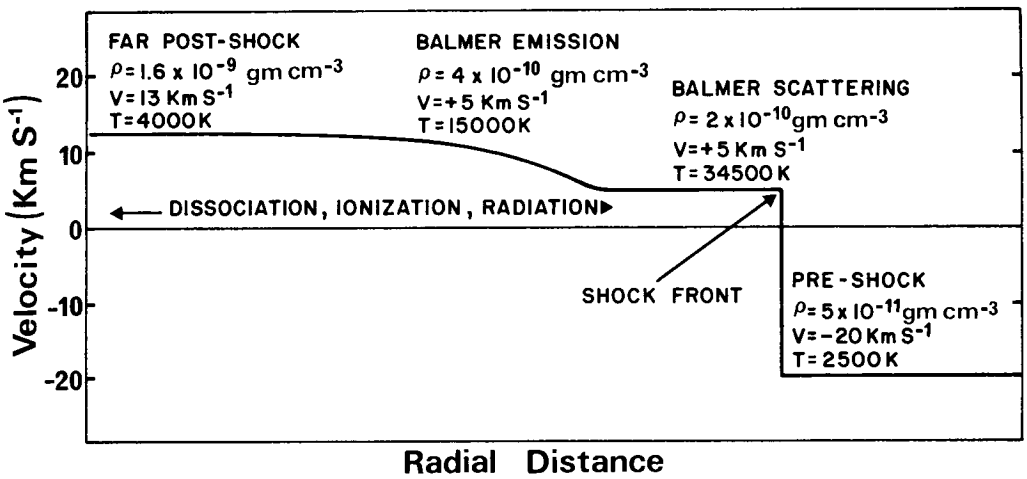


Figure 8-10. A schematic diagram of shock structure in a typical Mira variable near-maximum light. Velocities are in the rest frame of the star (from Fox et al., 1984).

of Fox and Wood will possibly give the answers and may give new information concerning the pulsation modes of the Mira stars investigated.

REFERENCES

Ando, H. 1976, *Pub. Astron. Soc. Japan*, **28**, 517.

Athay, R.G. 1972, *Radiation Transport in Spectral Lines* (Dordrecht: Reidel).

Athay, R.G. 1981, *Astrophys. J.*, **250**, 709.

Athay, R.G., and Skumanich, A. 1967, *Ann. Astrophys.* **30**, 669.

Auer, L. 1973, *Astrophys. J.* **180**, 469.

Auer, L.H., Heasley, J.R., and Milkey, R.W. 1972, *Kitt Peak Obs. Contrib. 555.*

Auman, J.R., and Woodrow, J.E.J. 1975, *Astrophys. J.* **197**, 163.

Avrett, E.H. 1980, in *Proc. Nato Adv. Inst., Solar Phenomena in Stars and Stellar Systems*, ed. A.K. Bonnet-Duppree (Bonas).

Avrett, E.H. 1985, to appear in *Proc. Sac. Peak Workshop, Chromospheric Diagnosis and Modeling*, ed. B. Lites.

Avrett, E.H., and Johnson, H.R. 1984, in *Proc. Third Cambridge Workshop, Cool Stars, Stellar Systems, and the Sun*, ed. S.L. Baliunas and L. Hartmann (Berlin-Heidelberg, New York, Tokyo: Springer-Verlag).

Avrett, E.H., and Loeser, R. 1969, *Smith. Astrophys. Obs., Special Report. 303.*

Avrett, E.H., and Loeser, R. 1983, in *Methods in Radiative Transfer*, ed. W. Kalkofen (Cambridge: Cambridge Univ. Press), p. 341.

Ayres, T.R. 1981, *Astrophys. J.*, **244**, 1064.

Ayres, T.R. 1985, to appear in *Proc. Sac. Peak Workshop, Chromospheric Diagnosis and Modeling*, ed. B. Lites.

Ayres, T.R., Moos, H.W., and Linsky, J.L. 1981, *Astrophys. J. (Letters)*, **248**. L137.

Baliunas, S. 1983, *Pub. Astron. Soc. Pacific*, **95**, 532.

Basri, G.S. 1980, *Astrophys. J.*, **242**, 1133.

Basri, G.S., Linsky, J.L., and Eriksson, K. 1981, *Astrophys. J.*, **251**, 162.

Boesgaard, A.M. 1979, *Astrophys. J.*, **232**, 485.

Boesgaard, A.M. 1981, *Astrophys. J.*, **251**, 564.

Boesgaard, A.M., and Magnan, C. 1975, *Astrophys. J.*, **198**, 369.

Brown, A., and Carpenter, K.G. 1985, JILA, University of Colorado, preprint.

Carbon, D.F., Milkey, R.W., and Heasley, J.N. 1976, *Astrophys. J..*, **207**, 253.

Carpenter, K.G., Brown, A., and Stencel, R.E. 1985, *Astrophys. J.*, **289**, 676.

Cassatella, A., Heck, A., Querci, F., Querci, M., and Stickland, D.J. 1980, in *Proc. Second European IUE Conference*, ESA SP-157.

Cox, J.P. 1980, *Theory of Stellar Pulsation* (Princeton: Princeton Univ. Press).

de la Reza, R., and Querci, F. 1978, *Astron. Astophys.*, **67**, 7.

Draine, B.T. 1981, in *Physical Processes in Red Giants*, ed. I. Iben and A. Renzini (Dordrecht: Reidel), p. 317.

Drake, S.A. 1984, *Progress in Stellar Spectral Line Formation Theory* (Trieste), ed. J.E. Beckman and L. Crivellari (Dordrecht: Reidel).

Drake, S.A., and Linsky, J.L. 1983, *Astrophys. J.*, **273**, 299.

Dyck, H.M., and Johnson, H.R. 1969, *Astrophys. J.*, **156**, 389.

Eaton, J.A., Johnson, H.R., O'Brien, G.T., and Baumert, J.H. 1985, *Astrophys. J.*, **290**, 276.

Ferlet, R., and Gillet, D. 1984, *Astron. Astrophys.*, **133**, L1.

Fox, M.W., and Wood, P.R. 1982, *Astrophys. J.*, **259**, 198.

Fox, M.W., and Wood, P.R. 1985, in preparation.

Fox, M.W., Wood, P.R., and Dopita, M.A. 1984, *Astrophys. J..*, **286**, 337.

Furenlid, I. 1984, *Astron. Astrophys.*, **140**, 49.

Giampapa, M.S. 1984, *Astrophys. J.*, **277**, 235.

Gillet, D., and Lafon, J.P.J. 1983, *Astron. Astrophys.*, **128**, 53.

Gillet, D., and Lafon, J.P.J. 1984, *Astron. Astrophys.*, **139**, 401.

Gillet, D., Maurice, E., and Baade, D. 1983, *Astron. Astrophys.*, **128**, 384.

Gilra, D.P. 1976, Mém. Soc. Roy. Sci. Liège, **9**, 77.

Goebel, J.H., and Johnson, H.R. 1984, *Astrophys. J. (Letters)*, **284**, L39.

Goldberg, L. 1979, *Quart. J. Roy. Astr. Soc.*, **20**, 361.

Gómez Balboa, A., and de la Reza, R. 1985, in preparation.

Goorvitch, D., Goebel, J.H., and Augason, G.C. 1980, *Astrophys. J.*, **240**, 588.

Gorbatskii, V.G. 1961, *Soviet Astronomy.*, **5**, 192.

Hagen, W., Stencel, R.E., and Dickinson, D.F. 1983, *Astrophys. J.*, **274**, 286.

Haisch, B.M., Linsky, J.L., and Basri, G.S. 1980, *Astrophys. J..*, **235**, 519.

Hall, D.N.B., and Ridgway, S.T. 1977, in *Proc. IAU Collog. 21, Les Spectres des Molecules Simples au Laboratoire et en Astrophysique* (Liège, Belgium: Univesité de Liège), p. 243.

Hartmann, L., and Avrett, E.H. 1983, *Astrophys. J.*, **284**, 238.

Hayes, M.A., and Nussbaumer, H. 1984, *Astron. Astrophys.*, **134**, 194.

Heasley, J.N., Ridgway, S.T., Carbon, D.F., Milkey, R.W., and Hall, D.N. 1978, *Astrophys. J.*, **219**, 970.

Hill, S.J., and Willson, L.A. 1979, *Astrophys. J.*, **229**, 1029.

Hinkle, K.H. 1983, *Pub. Astron. Soc. Pacific*, **95**, 550.

Hinkle, K.H., Hall, D.N.B., and Ridgway, S.T. 1982, *Astrophys. J.*, **252**, 697.

Hinkle, K.H., and Lambert, D.L. 1975, *Mon. Not. Roy. Astr. Soc.*, **170**, 447.

Hinkle, K.H., Scharlach, W.W.G., and Hall, D.N.B. 1984, *Astrophys. J. Supplement*, **56**, 1.

Holzer, T.E., Flå, T., and Leer, E. 1983, *Astrophys. J.*, **275**, 808.

Hubený, I., and Heinzel, P. 1984, *J. Quant. Spect. Rad. Transf.*, **32**, 159.

Jefferies, J.T. 1968, *Spectral Line Formation*, (Waltham: Blaisdell).

Jennings, M.C. 1973, *Astrophys. J.*, **185**, 197.

Jennings, M.C., and Dyck, H.M. 1972, *Astrophys. J.*, **177**, 427.

Johnson, H.R. 1973, *Astrophys. J.*, **180**, 81.

Johnson, H.R. 1982, *Astrophys. J.*, **260**, 254.

Johnson, H.R., Bernat, A.P., and Krupp, B. 1980, *Astrophys. J. Supplement*, **42**, 501.

Johnson, H.R., Goebel, J.H., Goorvitch, D., and Ridgway, S.T. 1983, *Astrophys. J. (Letters)*, **270**, L63.

Johnson, H.R., and O'Brien, G.T. 1983, *Astrophys. J.*, **265**, 952.

Joy, A.H. 1947, *Astrophys. J.*, **106**, 288.

Kalkofen, W. 1985, to appear in *Proc. Sacramento Peak Workshop, Chromospheric Diagnosis and Modeling*, ed. B. Lites.

Kamijo, F. 1963a, *Pub. Astron. Soc. Japan*, **14**, 271.

Kamijo, F. 1963b, *Pub. Astron. Soc. Japan*, **15**, 440.

Keeley, D.A. 1970, *Astrophys. J.***161**, 634.

Kneer, F. 1983, *Astron. Astrophys.*, **128**, 311.

Lambert, D. L., and Snell, R.L. 1975, *Mon. Not. Roy, Astr. Soc.*, **172**, 277.

Leung, K.C., and Stothers, S.R. 1977, *J. Brit. Astron. Assoc.*, **87**, 263.

Linsky, J.F. 1980, *Ann. Rev. Astron. Astrophys.*, **18**, 439.

Linsky, J.F. 1981, in *Physical Processes in Red Giants*, ed. I. Iben and A. Renzini (Dordrecht: Reidel), p. 247.

Linsky, J.F. 1984a, *Mass Loss from Red Giants*, (Los Angeles: Univ. California), preprint.

Linsky, J.F. 1984b, *Progress in Stellar Spectra Line Formation* (Trieste), ed. J.E. Beckman and L. Crivellari (Dordrecht: Reidel).

Lites, B., and Mihalas, D 1984, *Solar Physics*, **93**, 25.

Livi, S., and Bergmann, T. 1982, *Astron. J.*, **87**, 1783.

Luck, R.E. 1977, *Astrophys. J.*, **218**, 752.

Luck, R.E., and Lambert, D.L. 1982, *Astrophys. J.*, **256**, 189.

Maciel, W.J. 1976, *Astron. Astrophys.*, **48**, 27.

Maciel, W.J. 1977, *Astron. Astrophys.*, **57**, 273.

Merchant, A.E. 1967, *Astrophys. J.*, **147**, 587.

Merrill, P.W. 1945, *Astrophys. J.*, **102**, 347.

Mihalas, D. 1978, *Stellar Atmospheres*, 2d ed. (San Francisco: W.H. Freeman and Co.).

Moon, T.T., Coates, D.W., Innis, J.L., and Thompson, K. 1983, *Inf. Bull. Var. Stars*, p. 2394.

Mount, G.H., Ayres, T.R., and Linsky, J.L. 1975, *Astrophys. J.*, **200**, 383.

Mount, G.H., and Linsky, J.L. 1975, *Solar Phys.*, **41**, 17.

Muchmore, D., and Ulmschneider, P. 1985, *Astron. Astrophys.*,**142**, 393.

Musielak, Z., and Sikorski, J. 1981, *Acta Astronom.*, **31**, 493.

Newell, R.T., and Hjellming, R.M. 1982, *Astrophys. J., (Letters)*, **263**, L85.

O'Brien, G.T. 1980, Thesis, Univ. of Texas.

Ostlie, D.A., Cox, A.N., and Cahn, J.H. 1982, in *Pulsations in Classical and Cataclysmic Variable Stars*, ed. J.P. Cox and C.J. Hansen (Boulder: Joint Inst. for Laboratory Astrophys), reprint, p. 297.

Querci, F. 1972, Thesis, Université de Paris.

Querci, F., and Querci, M. 1975, *Astron. Astrophys.*, **39**, 113.

Querci, M., and Querci, F. 1985, *Astron. Astrophys.*, **147**, 121.

Querci, F., Querci, M., Wing, R.F., Cassatella, A., and Heck, A. 1982, *Astron. Astrophys.*, **111**, 120.

Ramsey, L.W. 1977, *Astrophys. J.*, **215**, 827.

Ramsey, L.W. 1981, *Astrophys. J.*, **245**, 984.

Richer, H.B. 1975, *Astrophys. J.*, **197**, 611.

Schmid-Burgk, J., Scholz, M., and Wehrse, R. 1981, *Mon. Not. Roy. Astr. Soc.*, **194**, 383.

Schmitz, F., and Ulmschneider, P. 1981, *Astron. Astrophys.*, **93**, 178.

Schwarzschild, M. 1975, *Astrophys. J.*, **195**, 137.

Slutz, S. 1976, *Astrophys. J.*, **210**, 750.

Smith, M.A. 1980, *Space Sci. Rev.*, **27**, 307.

Smith, M.A. 1983, *Astrophys. J.*, **265**, 325.

Steenbock, W., and Holweger, H. 1984, *Astron. Astrophys.*, **130**, 319.

Stencel, R.E. 1982a, *Second Cambridge Workshop on Cool Stars*, SAO Special Rep., **392**, 137.

Stencel, R.E. 1982b, in *IAU Symp. 102, Solar and Stellar Magnetic Fields: Origins and Coronal Effects*, ed. J.O. Stenflo (Dordrecht: Reidel).

Stencel, R.E., Linsky, J.L., Brown, A., Jordan, C., Carpenter, K.G., Wing, R.F., and Czyzak, S. 1981, *Mon. Not. Roy. Acad. Sci.*, **196**, 47.

Tielens, A.G.G.M. 1983, *Astrophys. J.*, **271**, 702.

Thomas, R.N. 1960, *Astrophys. J.*, **131**, 429.

Thompson, R.I. 1973, *Astrophys. J.*, **181**, 1039.

Tsuji, T. 1983, *Astron. Astrophys.*, **122**, 314.

Tuchman, Y., Sack, N., and Barkat, Z. 1978, *Astrophys. J.*, **219**, 183.

Ulmschneider, P. 1979, *Space Sci. Rev.*, **24**, 71.

Vaiana, G.S., et al. 1981, *Astrophys. J.*, **245**, 163.

Vernazza, J.E., Avrett, E.M., and Loeser, R. 1981, *Astrophys. J.* Supplement, **45**, 635.

Whitney, C.A., and Skalafuris, A.J. 1963, *Astrophys. J.*, **138**, 200.

Wilson, O.C. 1957, *Astrophys. J.*, **126**, 46.

Wilson, O.C. 1960, *Astrophys. J.*, **131**, 75.

Wilson, O.C. 1982, *Astrophys. J.*, **257**, 179.

Wilson, O.C., and Bappu, M.K.V. 1957, *Astrophys. J.*, **125**, 661.

Willson, L.A. 1976, *Astrophys. J.*, **205**, 172.

Willson, L.A. 1982, in *Pulsations in Classical and Cataclysmic Variable Stars*, ed. J.P. Cox and C.J. Hansen (Boulder: Joint Inst. Laboratory Astrophys.) reprint, p. 269.

Willson, L.A., and Hill, S.J. 1979, *Astrophys. J.*, **228**, 854.

Willson, L.A., and Pierce, J.N. 1982, in *Second Cambridge Workshop on Cool Stars*, ed. M.S. Giampapa and Golub, Smithsonian Astrophys. Obs. Special Report, **392**, p. 147.

Willson, L.A., Wallerstein, G., and Pilachowski, C.A. 1982, *Mon. Not. Roy. Acad. Sci.*, **198**, 483.

Winkler, K.-H.A., Norman, M.L., and Mihalas, D. 1984, *J. Quant. Spect. Rad. Transf.*, **31**, 473.

Wood, P.R. 1974, *Astrophys. J.*, **190**, 609.

Wood, P.R. 1975, *Mon. Not. Roy. Astr. Soc.*, **171**, 15.

Wood, P.R. 1979, *Astrophys. J.*, **227**, 220.

Wood, P.R. 1980, in *Physical Processes in Red Giants*, ed. I. Iben and A. Renzini (Dordrecht: Reidel) p. 205.

Wood, P.R. 1982, in *Pulsations in Classical and Cataclysmic Variable Stars*, ed. J.P. Cox and C.J. Hansen (Boulder: Joint Inst. Laboratory Astrophys.) reprint, p. 284.

Yamashita, I. 1972, *Ann. Tokyo Astr. Obs.*, **13**, 169.

Yamashita, I. 1975, *Ann. Tokyo Astr. Obs.*, **15**, 47.

Zarro, D.M. 1984, *Astrophys. J.*, **285**, 232.

Zeldovich, Y.B., and Raizer, Y.P. 1966, *Physics of Shock Waves and High-Temperature Phenomena* (New York: New York Academic Press).

Zirin, H. 1982, *Astrophys. J.*, **260**, 655.

N88-11601

9

THE ATMOSPHERES OF M DWARFS: OBSERVATIONS

Marcello Rodonò

INTRODUCTION: THE SOLAR/ STELLAR CONNECTION

Until recently, many astrophysicists have viewed the Sun as a special object separated from the stellar context. This situation has arisen mainly because solar research has benefited from high spatial, spectral, and time-resolved observations which were and, for the most part, are unreachable in the observations of ordinary stars. In fact, owing to their enormous distances, only global properties of stars can usually be obtained.

Indeed, especially before the recent opening of the new spectral domains that have been made available by spaceborne instrumentation, solar astrophysicists were regarded by their stellar colleagues as privileged people who were actually able to "see" what they were observing and interpreting. Stellar astronomers could only speculate on the surface characteristics of stars on the basis of indirect and sometimes only rather circumstantial evidence. Solar and stellar research were following increasingly diverging paths because the detailed studies of the Sun, that, usually unintentionally, built up a conceptual division between the study of solar microphenomena and of stellar global characteristics.

I do not know about the authenticity of the following sentence that pictorically reflects the mood of those days: "Solar people are probably watching the Sun too extensively and with excessively powerful instruments, like those looking at an old master painting with a microscope: they might learn a lot about painting techniques but will certainly have a hard time in trying to appreciate the value of the work of art standing in front of them."

As a matter of fact, the astronomical literature and history offer eloquent counterexamples promoting "the investigation of the Sun as a typical star in connection with the study of stellar evolution," as George E. Hale first put it in 1905 (cf. Goldberg, 1983). Nevertheless, for several decades afterwards, Hale's attitude toward what we now call the *solar/stellar connection* did not become astronomical mass culture, in spite of additional positive inputs of several leading scientists such as Eberhard, Schwarzschild, Kron, Unsold, Struve, Schatzman, and Lovell. It was not until the sixties that systematic observations of so-called "active" stars began and the problem of solar-type stellar activity was specifically addressed (cf. Schatzman,1967; Godoli, 1968, and references therein). It is of some significance that the first IAU-sponsored interdisciplinary meetings on topics related to the solar/stellar connection took place only in 1982 (Byrne and Rodonò, 1983; Stenflo, 1983).

From the observational point of view, as both solar and stellar astronomers have constantly increased their respective instrumental

capability, leaving almost unchanged the dividing gap between them. Nor will this situation change in the future, as the relative location of the Sun and the stars with respect to the Earth will remain unchanged, with all the obvious implications that differentiate solar and stellar observational capability.

What has definitely changed in the recent past is the attitude of both solar and stellar astrophysicists (as envisaged by Hale long before): the solar/stellar or stellar/solar connection has opened the *solar laboratory*, in which "stellar" phenomena can be studied in detail, to stellar astrophysics and the *stellar laboratory*, where "solar" phenomena occur in different physical environments, to solar astrophysics. A truly "two-way street" connecting solar and stellar research does not appear to be any more an elite culture and is waiting to be fully exploited in the near future.

As always, improvements bring with them an increase of the parameters to be taken into account. Specifically, a new temporal parameter, the stellar evolution time scale, will enter our problem, as well as the other global parameters specifying the physical state of the star's environment.

Recent observations and interpretation of M dwarfs, about 1000 times fainter and 10 times smaller than the Sun, have shown how scientifically fruitful their comparative study could be. Indeed, the intrinsic faintness of M dwarfs and the favorable interior physical conditions for solar-type phenomena to develop render their observation particularly suitable for solar/stellar studies. Therefore, my contribution is aimed at presenting recent observations of M dwarf atmospheres, with particular emphasis on those that relate to the stellar/solar connection (i.e., at the other side—or, perhaps, the "far" (stellar) side—of the topic with respect to the content of *The Sun as a Star* volume in this CNRS-NASA Monograph Series on Nonthermal Phenomena in Stellar Atmospheres.

M dwarf atmospheres, whose theoretical aspects are presented by D. J. Mullan in Chapter 10 of this book, are particularly useful for the purpose of establishing observational constraints on stellar activity parameters. These constraints will greatly help in narrowing the range of possible mechanisms that can give rise to the activity phenomena observed in the Sun and stars. It goes without saying that activity phenomena often announce departure from static thermodynamic equilibrium with particular nonthermal processes dominating others.

After presenting global properties of M dwarfs (*Global Properties of Quiescent M Dwarfs*), I will concentrate on the principal diagnostic of activity phenomena occurring in their atmosphere from the geometrical, energetic, and temporal points of view. Observations of starspots, plages, flares, and activity cycles will be presented in the section *Activity Signatures*. In the final section, the major sources of activity will be discussed with particular emphasis on the generation, intensification, and measurements of stellar magnetic fields.

GLOBAL PROPERTIES OF QUIESCENT M DWARFS

The intrinsic faintness of M dwarfs makes them suitable for accurate observations only within a relatively restricted volume centered on the Sun. Actually, reasonably detailed photometric and spectroscopic observations have been carried out only for M dwarfs lying within 25 parsecs of the Sun. Nevertheless, since the number density of dM stars is impressively large—0.06 parsecs^{-3} (Thé and Staller, 1974)—a sufficiently numerous sample is available for observations in the solar neighborhood. Basically, there are two distinct groups of M dwarfs: dM and dMe stars, the latter showing hydrogen Balmer lines in emission. (See the section *Effective Temperature, Radius, and Surface Gravity*.) Long-term variability and short-duration flares characterize dMe stars. (See the section *Activity Signatures*.) However, sporadic or quasi-periodic variability seems to be a common feature of a large fraction of M stars (Stokes, 1971).

Extensive and detailed works have been carried out on dMe flare stars. Their global properties are similar to those of ordinary M dwarfs and are of interest here because of the great variety of nonthermal phenomena occurring in their atmospheres.

Multiplicity and Mass

About 35 percent of late-type main-sequence stars and 60 percent of known flare stars within 25 parsecs of the Sun are members of binary systems (Rodonò, 1978). The majority are visual binaries with well-determined orbits. V 1396 Cyg (Gliese 815 A) and BY Dra (Gliese 719) are spectroscopic binaries, CM Dra (Gliese 630.1) and YY Gem (Gliese 278c) also show eclipses. The most reliable values of masses for well-studied binaries are given in Table 9-1. They range between 0.06 and 0.62 solar masses. Using empirical mass-luminosity relations (viz. Gatewood, 1976) additional determinations of masses are possible. (See the section *Effective Temperature, Radius, and Surface Gravity*.) The smallest value is 0.038 $M_\odot$ (V 1298 Aql = Gliese 752 B). However, stars with such low masses cannot be regarded as true main-sequence stars because their contraction times toward the main sequence are comparable to, or even exceed, the age of the Galaxy.

The theoretical models by Grossman et al. (1974) indicate that an increasing fraction of the stellar interior becomes convectively unstable as mass decreases. A star of about 0.2 $M_\odot$ or less (i.e., with spectral type later than M5) is already fully convective. Following Mullan

Table 9-1
Masses of dMe Flare Stars in Binary Systems

Gliese (1969) No.	Variable Star Name	Catalog	Spectral Type	Binary Type*	$M_A + M_B$ (Sun = 1)	Ref.†
473 AB	FL Vir	Wolf 424 AB	dM5.5e + dM5e	VB	0.067 + 0.064	1
234 AB	V 577 Mon	Ross 614 AB	dM4.5(A + B)	VB	0.114 + 0.062	2
					0.12 + 0.06	3
65 AB	UV Cet	L726-8 AB	dM5.5e + dM6e	VB	0.12 + 0.108	4, 5
447	FI Vir	Ross 128	dM5	VB	0.15	6, 7
860 AB	DO Cep	Kruger 60 B	dM4.5e	VB	0.16	8, 6
166 C	—	40 Eri C	dM4e	VB	0.16	9
630.1	CM Dra	LP101 - 15/16	dM4e + dM4e	EB, SB	0.238 + 0.207	10
15 AB	GQ And	Groom 34 AB	dM1e + dM6e	VB	0.29 + 0.15	6
815 A	V 1396 Cyg	AC + 30 1214 - 608	dM3e + ?	SB	0.2 + 0.3 + ?	11
22	—	BD + 66 34 AA'	dM2.5e + ?	AB	(0.4) + 0.13	6, 12
799 AB	AT Mic	LDS 720 BC	dM4e + dM4e	VB	0.39 + 0.30	13
725 AB	—	BD + 59 1915 AB	dM4 + dM5	VB	0.41 + 0,41	14
644	V 1054 Oph	BD - 8 4352 AB	dM3.5e (A + B)	VB	0.46 + 0.45	6
719	BY Dra	HDE 234677	dM0e + dM0e	SB	0.58 + 0.60	15
278 C	YY Gem	BD + 32 1582	dM1 + dM1	EB, SB	0.62 + 0.57	16

*Binary type: AB = astrometric, EB = eclipsing, SB = spectroscopic, VB = visual.

†References: 1. Heintz (1972), 2. Lippincott and Hershey (1972), 3. Probst (1977), 4. Worley and Behall (1973), 5. Harrington and Behall (1973), 6. Gatewood (1976), 7. Lippincott (1978), 8. Lippincott (1953), 9. Heintz (1974), 10. Lacy (1977a), 11. Fekel et al. (1978), 12. van de Kamp (1968), 13. De Freitas Mourão (1976), 14. van de Kamp (1971), 15. Bopp and Evans (1973), 16. Leung and Schneider (1978).

(1976), it is tempting to relate the onset of complete convection with the appearance of hydrogen emission lines in almost all dwarfs with spectral type later than M5.

The high fraction of active M dwarfs in binary systems seems to be linked to their ability in preventing rotational breaking with age, a consequence of forced synchronization between rotation and orbital motion (Bopp and Fekel, 1977; Bopp and Espenak, 1977). Rather than duplicity, their higher than normal rotational velocity and deep convection zones appear to be necessary conditions for activity phenomena to develop in late-type stars. On the other hand, that enhanced activity results from triggering effects due to their proximity is not supported by the present observations of flare events in binaries (Rodonò, 1978).

Galactic Density, Motion, and Age

M dwarfs account for about 73 percent of all main-sequence stars in the solar neighborhood or about 66 percent of the total number of stars in our Galaxy (Allen, 1973; Arakelian, 1969). Hence, as the histograms in Figure 9-1 show, although their individual masses are very low (bottom panel), their huge number (middle panel) makes them the largest single contributors to the stellar mass of our Galaxy. Assuming that the mass and space distribution of neighborhood stars are representative of the entire Galaxy, the upper panel in Figure 9-1 shows that M dwarfs account for about 50 percent of the total mass of main-sequence stars.

From the relative abundance of dMe and dM stars versus the absolute magnitude given by Joy and Abt (1974) and the luminosity function in Allen (1973), the number of dMe is about 75 percent of dM stars (i.e., they have a number density in the solar neighborhood of about 0.04 stars pc^{-3}). Hence, assuming: (1) all dMe to be flare stars, (2) the density in the solar neighborhood to be representative for the entire Galaxy, and (3) a conventional volume of the Galaxy of 10^{12} pc^3, the number of flare stars amounts to the impressive number 3.8×10^{10} stars. An even higher estimation is given

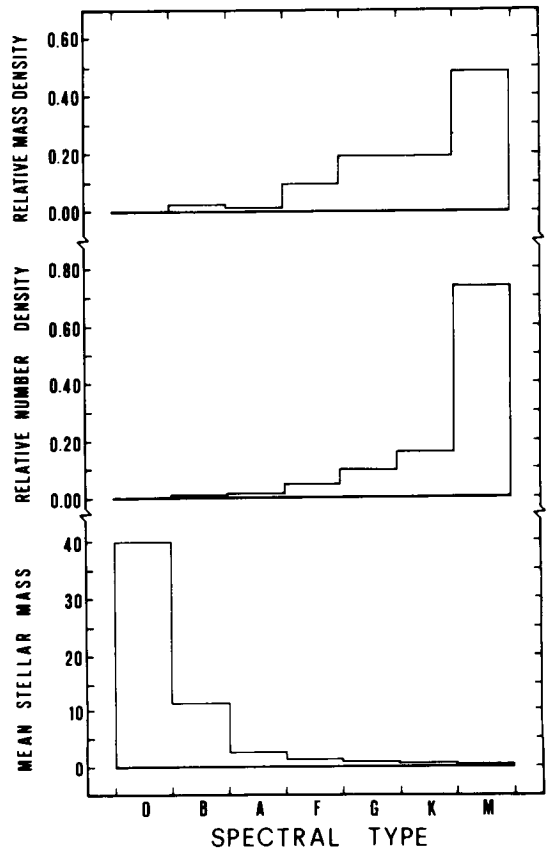


Figure 9-1. Distribution of mean mass versus spectral type for main-sequence stars (bottom histogram), their relative number (middle histogram), and mass density (upper histogram) in the solar neighborhood. Assuming that these distributions are representative of the entire Galaxy, the low-mass M dwarfs appear to be the largest single contributor to the stellar mass in our Galaxy.

by Coleman and Worden (1976): 1.0 to 8.6×10^{11} stars. They have also suggested that a large fraction of stellar mass loss may arise from dMe active stars during the course of flare events with important consequences on the physics and composition of the interstellar medium. (See also Staller, 1976; Gershberg and Shakovskaya, 1976; and Mullan, 1979.) Even assuming our lower estimate of the total number and mass of flare stars, the mass loss due to flares from dMe stars might constitute an important fraction of the total mass loss

from stars, especially if a quasi-steady solar-type wind is also present.

The mass density of M dwarfs is 0.025 $M_\odot$ pc^{-3} (Allen, 1973), accounting for about 19 percent of the total mass of our Galaxy as given by Oort from z velocity (Allen, 1973). Therefore, dMe flare stars alone constitute a sizable mass component of the Galaxy ($\sim$15 percent).

The relative maximum in the luminosity function at about M_V = 15 (Luyten, 1968; Arakelian, 1969) is almost entirely due to emission-line dwarfs. This leads Arakelian (1969) to suggest the existence of a relatively young group of physically related stars in the solar neighborhood. Moreover, since dMe stars have lower dispersion velocity and higher vertex deviation than dM stars (Einasto, 1954, 1955; Vyssotsky and Dyer, 1957; Gliese, 1958), flare stars have been generally considered young objects. However, Greenstein and Arp (1969) first detected flare activity on a kinematically old star (Wolf 359 = CN Leo). Moreover, considering the space motions of the 22 flare stars which were known at that time, Lippincott (1971) found their mean velocity (21 km s^{-1}) to be comparable to the average (23 km s^{-1}) for 202 M dwarfs in the Gliese (1969) catalog. Hence, Lippincott (1971) questioned the younger age of flare stars relative to other M dwarfs.

On the other hand, Chugainov (1972) and Kunkel (1972) gave evidence for the existence of both young and old flare stars and for higher activity levels on younger stars. Recent investigations on the space motions of 646 red dwarfs (Shakhovskaya, 1975) have confirmed that the most active UV Cet type variable stars are indeed young; however, less active stars belong to the old disk population and at least one case is known (CF UMa = Gliese 451B) with both kinematic and chemical (Tomkin, 1972) halo population characteristics. In addition, the short-period spectroscopic and eclipsing binary system, CM Dra (Gliese 630.1), which shows a light curve distortion outside eclipses attributable to starspots such as for BY Dra, has Population II kinematical motion (Lacy, 1977a).

Other examples of old flare stars are presented by Veeder (1974a), who found 14 of 31 single or double flare stars to have space motions typical of old disk population. Updating his flare list, 18 of 38 single or double flare stars included in Veeder's (1974b) list of M dwarfs have old disk motions. This high fraction of old flare stars (47 percent) can be biased by observational selection since most of them originally came from lists of large proper motion stars. Actually, Iwanowska (1972) has found that only about 13 percent of dM and 11 percent of dMe stars belong to Population II. The relatively large fraction of old stars in Lippincott's (1971) flare star sample can explain her negative result on the younger age of flare stars relative to other dM dwarfs. This is certainly true on the average, as demonstrated by the larger number and earlier spectral type of flare stars in young clusters and associations and by their rather strong emission lines, which are an index of youth as suggested by Wilson (1963) and demonstrated by Wielen (1974) and Upgren (1978).

The existence of old flare stars is not completely consistent with the widespread idea on the fading of flare activity with age. For instance, the suggestion that the dMe or the flare star, which forms a binary system with another dM, is always the less evolved member has not been confirmed. Several brighter components of such systems do show flare activity (see Rodonò, 1978). The most recently reported case is that of Gliese 867A (Byrne, 1979; Butler et al., 1981). Moreover, contrary to previous evidence, Veeder (1974a) has shown that, in the M_{bol}-(V-K) diagram, some UV Cet type flare stars lie below the main sequence by as much as one magnitude.

In conclusion, although youth can be considered a sufficient condition for low-mass stars to show flare activity, the existing evidence also suggests that some mechanism, such as enforced rotation in binary systems, is capable of

prolonging considerably the active phase on a large fraction of stars.

Effective Temperature, Radius, and Surface Gravity

The most reliable values of surface gravity are those obtained from the radii and masses of the spectroscopic and eclipsing binaries, CM Dra (Lacy, 1977a) and YY Gem (Bopp, 1974a; Leung and Schneider, 1978). We must rely on indirect methods for additional data.

Pettersen (1983a) has critically reviewed the existing data on global properties of active M dwarfs in their quiescent state. The resulting empirical relations involving effective temperature (T_e), bolometric correction (BC), absolute visual magnitude (M_v), and color indices B-V, V-R, R-I, and V-K are presented in Table 9-2. Given the well-defined correlation between T_e and V-K, the HR diagram (M_{bol} versus log T_e) in Figure 9-2 has been calibrated to show the M_{bol} versus V-K correlation also.

Since well-observed dM stars are very near the Sun, their trigonometric parallaxes are quite reliable, and absolute visual magnitudes can be determined. Hence, by using the bolometric correction (Gatewood, 1976) or the bolometric magnitude and the effective temperature derived from their spectral energy distribution (Veeder, 1974a), masses and radii can be computed. Assuming the mass-luminosity relation and the effective temperature/(V-K) color relation given by Veeder (1974b), we have:

$$\log R/R_\odot = 0.92 - 0.20\, M_{bol} + 0.104\,(V\text{-}K) \quad . \tag{9-1}$$

Another method of determining stellar radii has been adopted by Lacy (1977b). He has estimated the radii of nearby stars with known distance using the Barnes-Evans relation (Barnes and Evans, 1976; Barnes et al., 1976):

$$F_v = A - B\,(V\text{-}R)_o \quad , \tag{9-2}$$

where A and B are constant within given ranges of the V-R color index. The quantity F_v is the so-called "visual surface brightness parameter," which is related to the stellar surface flux, and is given by the relation,

$$F_v = 4.2207 - 0.1\, V_o - 0.5 \log \phi' \quad , \tag{9-3}$$

Table 9-2
Empirical Correlations Between Global Parameters of M Dwarfs from Various Sources (see text)

$BC = -0.379\, M_V + 2.386$	(± 0.27)
$BC = -4.816\,(B\text{-}V) + 5.430$	(± 0.36)
$BC = -2.267\,(V\text{-}R) + 1.689$	(± 0.13)
$BC = -2.124\,(R\text{-}I) + 0.874$	(± 0.13)
$BC = -0.816\,(V\text{-}K) + 1.709$	(± 0.07)
$T_e = -1510\,(B\text{-}V) + 5738$ K	(± 156)
$T_e = -645\,(V\text{-}R) + 4469$ K	(± 112)
$T_e = -648\,(R\text{-}I) + 4311$ K	(± 79)
$T_e = -264\,(V\text{-}K) + 4624$ K	(± 120)
$\log (R/R_\odot) = 0.92 - 0.20\, M_{bol} + 0.104\,(V\text{-}K)$	(Eq. (9-1))
$\log (M/M_\odot) = 1.82 - 0.25\, M_{bol}$ $(M_{bol} > 7.8)$	(Eq. (9-6))
$\log (M/M_\odot) = 0.45 - 0.09\, M_{bol}$ $(M_{bol} < 7.8)$	(Eq. (9-7))
$\log T_e = 3.77 - 0.052\,(V\text{-}K)$	(Eq. (9-8))

where V_o is the unreddened visual magnitude and ϕ' is the stellar angular diameter in milliarcsec. Combining relation (9-3) and the relationship between ϕ', the stellar radius (R) and distance (d), in the form:

$$R/R_\odot = 0.1074 \times (\phi'\text{m-arcsec}) \times d\,(\text{pc}), \quad (9\text{-}4)$$

Lacy (1977b) derived the relation,

$$\log R/R_\odot = 7.4724 - 0.2\,V_o - 2\,F_v\,(V\text{-}R) + \log d\,(\text{pc})\,. \quad (9\text{-}5)$$

This method is a powerful one because it is free from assumptions about spectral classification, luminosity class, effective temperature, and bolometric correction. Its application is particularly useful for statistical purposes. A systematic difference between the radii computed using Equation (9-1) and Veeder's (1974b) data and those computed by Lacy (1977b) is apparent in Figure 9-3. Lacy (1977b) has not considered this difference to be significant. However, because Lacy's data are consistent with independent estimates obtained by Gray (1967, 1968) following an observational/theoretical approach, it would be interesting to check whether the above discrepancy is due to a systematic overestimation of the effective temperature with increasing M_{bol} in the (V-K) - T_e calibration by Veeder.

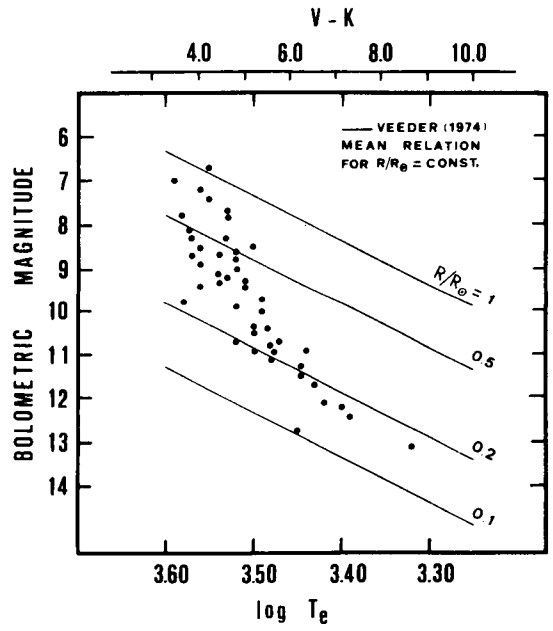


Figure 9-2. Bolometric magnitude versus effective temperature for M dwarfs. The upper scale (V-K) has been calibrated using Equation (9-8). Continuous lines indicate Veeder's (1974b) relation for constant $R/R_\odot$ values (Eq. (9-1)).

Lacy (1977b) and Sienkiewicz (1982) have confirmed the result already found by Hoxie (1973) that theoretical radii for the solar composition zero-age main sequence by Copeland et al. (1970) are about 30 to 15 percent smaller than those derived from observations. A systematic overestimation of effective temperature for theoretical models of very late main-sequence stars or inadequate treatment of the opacity sources in their atmospheres can cause these discrepancies.

Bolometric magnitude, V-K color, mass, effective temperature, radius, and surface gravity are given in Table 9-3. The bolometric magnitudes and V-K colors (Veeder, 1974b), which are given in the first two columns, were used to calculate the remaining parameters by means of the empirical relation (9-1) and the following ones:

$$\log (M/M_o) = 1.82 - 0.25\,M_{bol} \quad (M_{bol} > 7.8)\,, \quad (9\text{-}6)$$

$$\log (M/M_o) = 0.45 - 0.91\,M_{bol} \quad (M_{bol} < 7.8)\,, \quad (9\text{-}7)$$

$$\log T_e = 3.77 - 0.052\,(V\text{-}K)\,. \quad (9\text{-}8)$$

The above relations are from Gatewood (1976), Cester (1965), and Veeder (1974b), respectively. Independently determined more recent data (e.g., the masses and the T_e values) computed by Veeder (1974b) by fitting a blackbody curve to broadband magnitudes, which

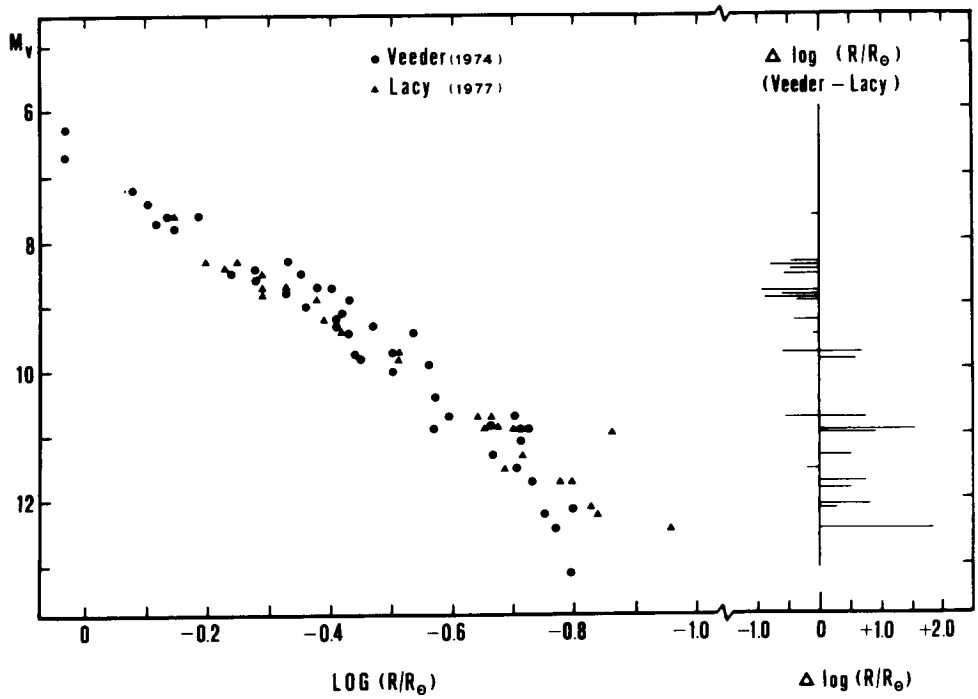


Figure 9-3. Absolute visual magnitude versus log ($R/R_\odot$) for M dwarfs. The comparison between the radii computed using Equation (9-1) and Veeder's (1974b) data and those given by Lacy (1977b) shows a systematically increasing deviation, which is probably due to a systematic overestimation of the effective temperature in the (V-K) - T_e calibration by Veeder.

are listed in Table 9-1, are preceded by the symbol, Λ. The surface gravity, $g/g_\odot$ was computed from the values of mass and radius given in Table 9-1.

The radius of well-studied dMe stars ranges from about 1 $R_\odot$ for CR Dra (Gliese 612.2) and FF And (Gliese 29.1) to 0.16 $R_\odot$ for UV Cet (Gliese 65B), G 51-15, and V 1298 Aql (Gliese 752B); the surface gravity ranges from less than the solar value for CR Dra to 5.2 $g_\odot$ for Gliese 725B; and the effective temperature ranges from 3800 K for the primary component of YY Gem (Gliese 278C) to 2100 K for V 1298 Aql. For the two components of the spectroscopic binary YY Gem, Leung and Schneider (1978) give 3806 ± 182 and 3742 ± 214 K, respectively. Given the listed values of mass and radius, the mean density of dM stars is higher, up to more than 20 times, than the solar value. V 1298 Agl (Gliese 752B) is the faintest and coolest dM star which is known.

Quiescent Optical Spectra and Abundances

As already noted at the beginning of this chapter, the global characteristics of dM and dMe stars are similar. Due to their low temperature (2100 to 3800 K), the optical spectra are dominated by strong molecular bands of TiO (4590, 4630, 4670, 4810, 5010, 5175, 5450, 5850, and 6520 Å) and of CaOH (5500 to 5560 Å blended with the TiO band at 5450 Å). The most intense absorption line is due to CaI at 4226 Å. In addition, other faint absorption features due to CO, OH, MgH (4845, 5210, and 5620 Å), CrI (between 4200 and 4300 Å), and CaH (6389 Å) are usually visible in low dispersion spectra (100 to 200 Å mm^{-1}).

Table 9-3
Bolometric Magnitude (M_{bol}), $V-K$ Color, Mass ($M/M_\odot$), Effective Temperature (T_e), Radius ($R/R_\odot$), and Surface Gravity ($g/g_\odot$) for UV Cet and BY Dra-Type Dwarfs

Gliese No.	Variable Star Name	Spectral Type	M_{bol}	$V-K$	$M/M_\odot$	log T_e	$R/R_\odot$	$g/g_\odot$	Notes*
15 A	GQ And a	M2.5e V	8.9	4.0	Λ0.29	3.56	0.36	2.24	—
15 B	GQ And b	M4.5e V	10.9	5.1	Λ0.15	Λ3.498	0.19	4.16	—
29.1	FF And	dM0e	7.2	4.1	0.62	3.56	0.81	0.94	SB
48	—	dM3.5e	8.3	4.0	0.56	Λ3.532	0.55	1.85	—
51	V 358 Cas	dM7e	10.7	6.0	0.14	Λ3.470	0.25	2.24	—
65 A	UV Cet a	dM6e	11.7	6.6	Λ0.12	Λ3.431	0.18	3.70	—
65 B	UV Cet b	dM4e	12.1	6.7	Λ0.11	3.42	0.16	4.30	—
83.1	TX Ari	dM5e	11.1	5.6	0.11	3.48	0.19	3.05	—
109	—	dM4e	9.2	4.6	0.33	3.53	0.36	2.55	—
207.1	V 371 Ori	dM3e	8.6	4.9	0.47	3.52	0.51	1.81	—
234 A	V 577 Mon	dM4e	10.4	5.6	Λ0.12	Λ3.484	0.26	1.78	VC
268	—	dM5e	9.8	5.6	0.23	3.58	0.35	1.89	—
277 A	—	dM3e	7.7	4.7	0.56	3.53	0.74	1.02	SB
277 B	—	dM4.5e	8.5	5.1	0.50	3.50	0.56	1.59	—
278 C1	YY Gem a	M1e V	7.8	3.8	Λ0.62	Λ3.580	Λ0.66	1.42	EB
278 C2	YY Gem b	M4.5e V	8.1	3.8	Λ0.57	Λ3.573	Λ0.58	1.69	EB
285	YZ CMi	dM4.5e	9.7	5.5	0.25	Λ3.491	0.36	1.93	—
—	G51-15	dMe	12.4	7.6	0.05	Λ3.389	0.17	1.73	—
388	AD Leo	M4.5e V	8.8	4.8	0.42	3.52	0.46	1.98	—
406	CN Leo	dM6e	12.2	7.4	0.06	Λ3.398	0.18	1.85	—
412 B	WX UMa	dM5e	12.7	6.1	0.04	3.45	0.10	4.00	—
424	SZ UMa	M1 V	8.3	3.8	0.56	3.57	0.45	2.77	—
447	FI Vir	dM5	10.8	5.5	Λ0.15	3.48	0.21	3.40	—
473 AB	FL Vir	dM5.5e	11.5	6.4	Λ0.07	Λ3.447	0.19	1.94	MC
494	DT Vir	dM2e	7.4	4.2	0.60	3.55	0.75	1.07	—
516 A	VW Com	dM4e	9.1	4.5	0.35	3.54	0.37	2.56	—
526	—	M4e V	8.5	4.0	0.50	3.56	0.43	2.70	—
551	V 645 Cen	dM5e	11.7	6.6	0.08	Λ3.431	0.18	2.47	—
616.2	CR Dra	M1e	6.7	4.2	0.69	3.55	1.04	0.64	—
630.1A	CM Dra a	M4e	10.4	—	Λ0.24	Λ3.498	Λ0.25	Λ3.48	EB
630.1B	CM Dra b	—	10.5	—	Λ0.21	Λ3.498	Λ0.23	Λ3.97	EB
644 AB	V 1054 Oph	dM4.5e	8.7	4.6	Λ0.46	Λ3.538	0.46	2.17	MC
669 A	V 639 Her a	dM4e	9.0	4.9	0.37	Λ3.518	0.43	2.00	—
669 B	V 639 Her b	dM5e	10.0	5.5	0.21	Λ3.491	0.31	2.19	—
719	BY Dra	M0e V	7.0	3.4	Λ0.60	3.59	0.75	1.07	SB
725 A	—	dM4	9.3	4.4	Λ0.41	Λ3.538	0.33	3.76	—
725 B	—	dM5	9.9	4.7	Λ0.41	Λ3.519	0.27	5.62	—
729	V 1216 Sgr	dM4.5e	10.9	5.2	0.12	Λ3.477	0.19	3.32	—
735	V 1285 Aql	M2e	7.8	4.6	0.55	3.53	0.69	1.16	—
752 B	V 1298 Aql	dM3.5e V	13.1	8.7	0.04	3.32	0.16	1.56	—
781	—	dM3e	9.4	4.0	0.30	3.56	0.29	3.57	SB
860 B	DO Cep	dM4.5e	10.7	4.9	Λ0.16	3.52	0.19	4.43	—
866	—	dM6e	10.9	6.6	0.12	Λ3.439	0.27	1.65	—
867 B	—	dM4e	9.3	5.0	0.31	3.51	0.38	2.15	—
873	EV Lac	dM4.5e	9.4	5.0	0.30	3.51	0.36	2.31	—
905	—	dM6e	11.3	6.4	0.10	Λ3.447	0.21	2.27	—
908	—	M2e V	8.7	3.9	0.44	3.57	0.39	2.89	—

*Notes: EB = eclipsing binary component; MC = mean component of visual double; SB = mean component of spectroscopic binary; VC = corrected for visual companion; Λ = parameter obtained independently, not from empirical relations (see text).

For temperatures lower than 3500 K, H_2O rotational lines appear. The relation of molecular line strength to effective temperature is shown in Figure 9-4 from Pettersen (1983a). For further detail, refer to the standard dM star spectra by Abt et al. (1968) and Keenan and McNeil (1976).

Another common feature of dM and dMe spectra is the occurrence of chromospheric Ca II H and K resonance lines in emission, which characterize all dwarf stars with spectral types cooler than F5 (Wilson, 1973; Linsky et al., 1979; Giampapa et al., 1981; Linsky et al., 1982).

The spectral feature that differentiates dMe from dM stars is the hydrogen Hα emission line (Joy and Abt, 1974). Most dMe stars also show other emission lines, such as the higher Balmer lines up to H8–9, the He I (5876 and 6678 Å) and Na D lines (5890 to 5896 Å) (Giampapa et al., 1978; Worden et al., 1981).

A distinctive characteristic of Hα and other higher Balmer lines in emission is the central reversal that is apparent in spectra with resolution of the order of 0.1 Å (Kulapova and Shakhovskaya, 1973; Worden and Peterson, 1976; Pettersen and Coleman, 1981; Worden et al., 1981; Linsky et al., 1982). Repeated observations of the same star, although nonsystematic, clearly show that this feature is variable. Hα reversal does not appear in the spectra of dMe spectroscopic binaries, probably because it is smeared by rotational broadening.

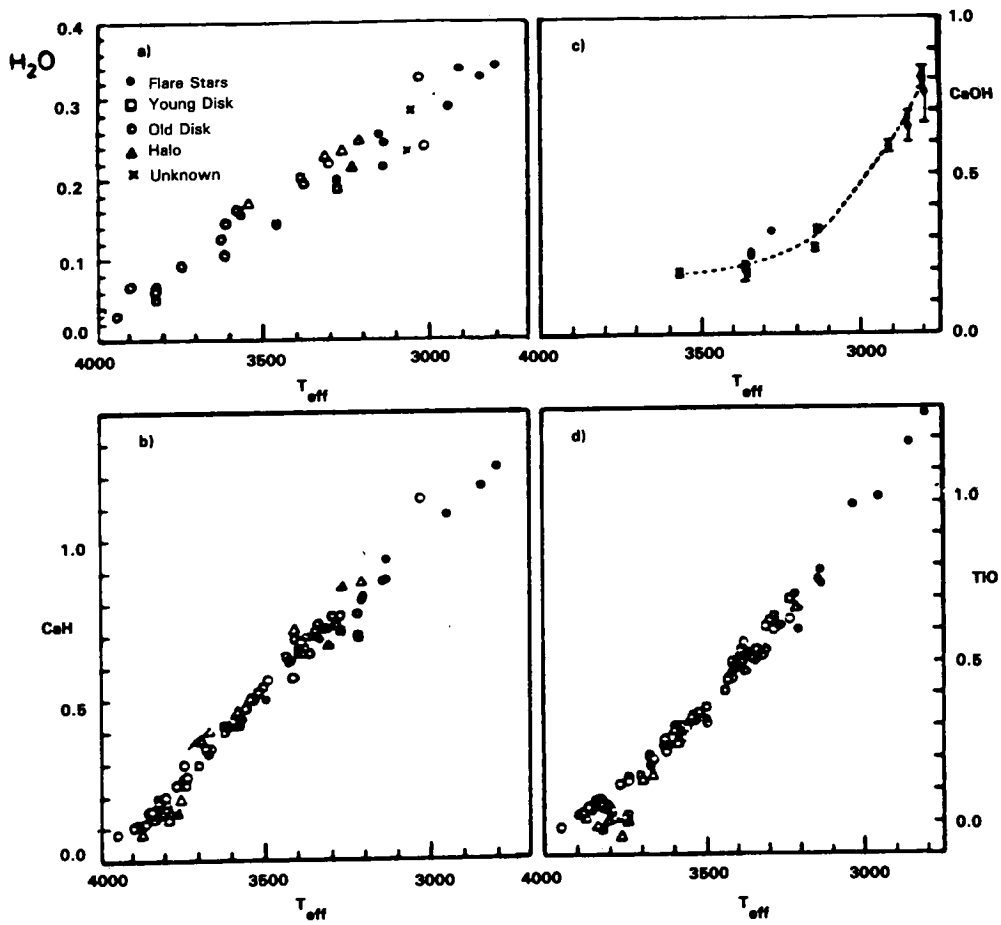


Figure 9-4. Empirical correlations between effective temperature and strengths of molecular features in red-dwarf stars (from Pettersen, 1983a).

Several interpretations of Hα reversal are possible. However, following Worden and Peterson (1976) and Worden et al. (1981), optically thick emitting regions in the Hα emission-line core—similar to solar active regions such as plages, spicules, and prominences—seem to be likely candidates. A selection of line profiles of Ca II H and K, Hα, and Na D is presented in Figures 9-5, 9-6, and 9-7.

From comparative study of high-resolution Ca II H and K lines in dM and dK5-Me stars, Giampapa et al. (1981) have shown that surface fluxes and radiation temperatures are systematically higher in the latter. They have also confirmed that, for both emission and nonemission dwarfs, the ratio of surface flux in the H and K lines to the bolometric one, $R_{HK} = [F'(H_1) = F'(K_1)]/(\sigma T_e)$, is comparable to or larger than that for supergiants and definitely larger than that for giants (Blanco et al., 1974; Linsky et al., 1979).

The fraction of dMe stars among all M dwarfs increases with advancing spectral subclass to nearly 100 percent at M5. However, Liebert et al. (1979) and Giampapa (1983a) have found several non-emission-line stars among M dwarfs with $M_v > 15$. The occurrence of such emission lines in only a fraction of late K and M dwarfs indicates that different outer atmospheric regimes can be set up in stars that have similar global physical properties. In emission-line dwarfs, excess nonradiative energy deposition leads to chromospheric temperature gradients steeper than in non-emission-line dwarfs so that, as shown by Kelch et al. (1979) and Cram and Mullan (1979), Balmer lines develop emission cores. They have found that successful modeling of Balmer-line absorption in dwarfs also requires some degree of nonradiative chromospheric heating. A solar analogy is particularly useful in this context in predicting a possible origin for the enhanced chromospheric emissions. As shown by Shine and Linsky (1974), Basri et al. (1979), and Vernazza et al. (1981), the strong emission lines from solar chromospheric plages require temperature or pressure gradients steeper than those of adjacent quiescent regions.

Since solar plages are characterized by enhanced magnetic flux, nonradiative heating in closed magnetic structures is likely to produce the required steep temperature gradient and the observed enhanced emission. This analogy suggests that dMe star chromospheric structures are dominated by closed magnetic fields. Some debate has occurred on how the magnetic fields might be generated (cf. Worden, 1974; Mullan, 1975a). This topic will be discussed at some length in the section *Nonthermal Energy Sources of Activity and Conclusions*, together with other indirect evidence and actual measurements of magnetic field strength in dMe stars. (See also the section *Activity Signatures*.) Here, it is worth mentioning that a self-excited α–ω dynamo in the convection zone appears to be the basic mechanism for magnetic field production in active stars (cf. Belvedere, 1983). The interaction of convection and rotation leads to a regime of differential rotation, which is required by the dynamo mechanism. Since dM and dMe stars have comparable masses and the theoretical models indicate that they are highly convective, the parameter that triggers emission-line characteristics and activity should be the higher than normal rotational velocity of dMe stars with respect to M stars. The high incidence of late K–M emission-line active stars in close binary systems, in which synchronization between orbital motion and rotation enforces high stellar rotation, is consistent with the foregoing scenario of magnetic field generation.

In Table 9-4, typical parameters for emission lines in late K–M dwarfs and the observed range of variability are presented. In fact, one must bear in mind that sporadic variability of the emission-line intensity frequently occurs. From the very beginning of systematic spectroscopy of dMe flare stars at the Crimea and McDonald Observatories, independent evidence of sporadic emission-line variability on time scales of the order of 1 hour, other than during flare events, was collected (cf. Gershberg, 1977). Even a transient, almost complete gradual disappearance of H I and Ca II emission lines has been observed on YZ CMi (Bopp,

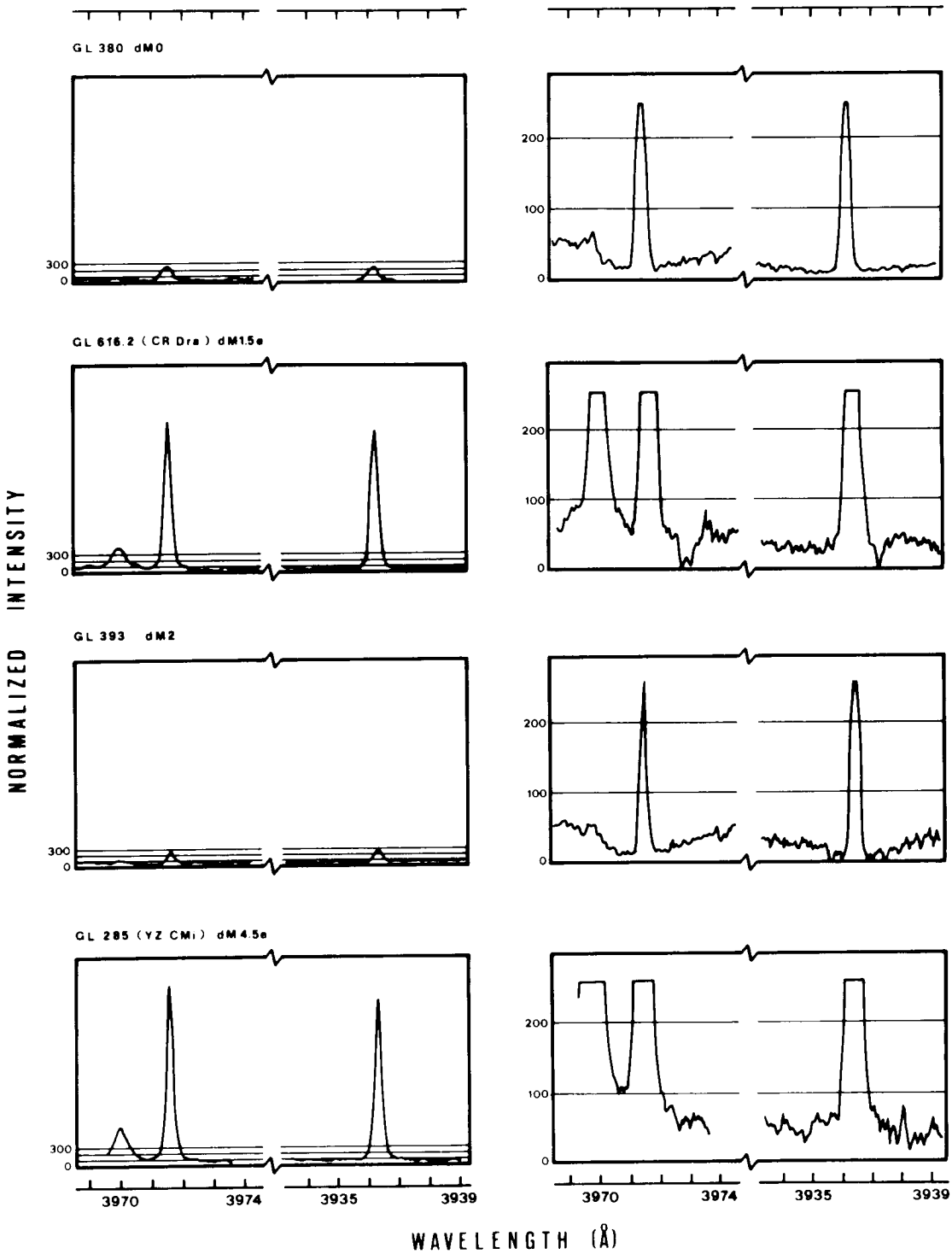


Figure 9-5. High-resolution Ca II H and K line profiles in dM and dMe stars (from Giampapa et al., 1981). The vertical axes are scaled so that 100 corresponds to the maximum surface flux between the H and K lines. Each star is plotted twice on two different scales (left and right panels). The vertical scales on the right panels have been enlarged with respect to those on the left for the same star to show the line core profiles.

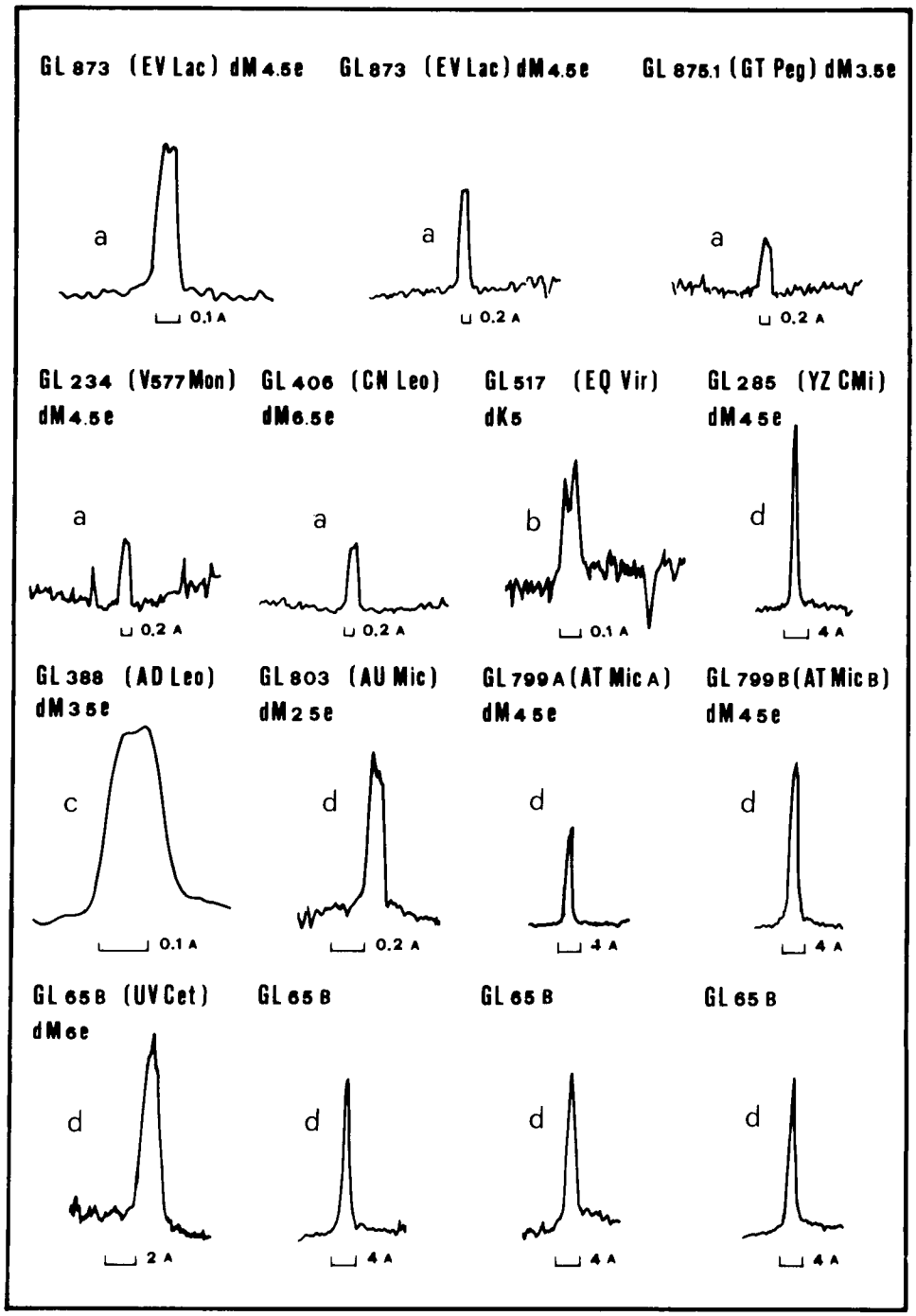


Figure 9-6. High-resolution neutral hydrogen Hα line profiles from various sources. Repeated observations of the same star have shown that the Hα central reversal, which probably arises from solar-type optically thick active regions, is a variable spectral feature. From (a) Worden and Peterson (1976), (b) Hartmann and Anderson (1977), (c) Giampapa et al. (1978), and (d) Linsky et al. (1982).

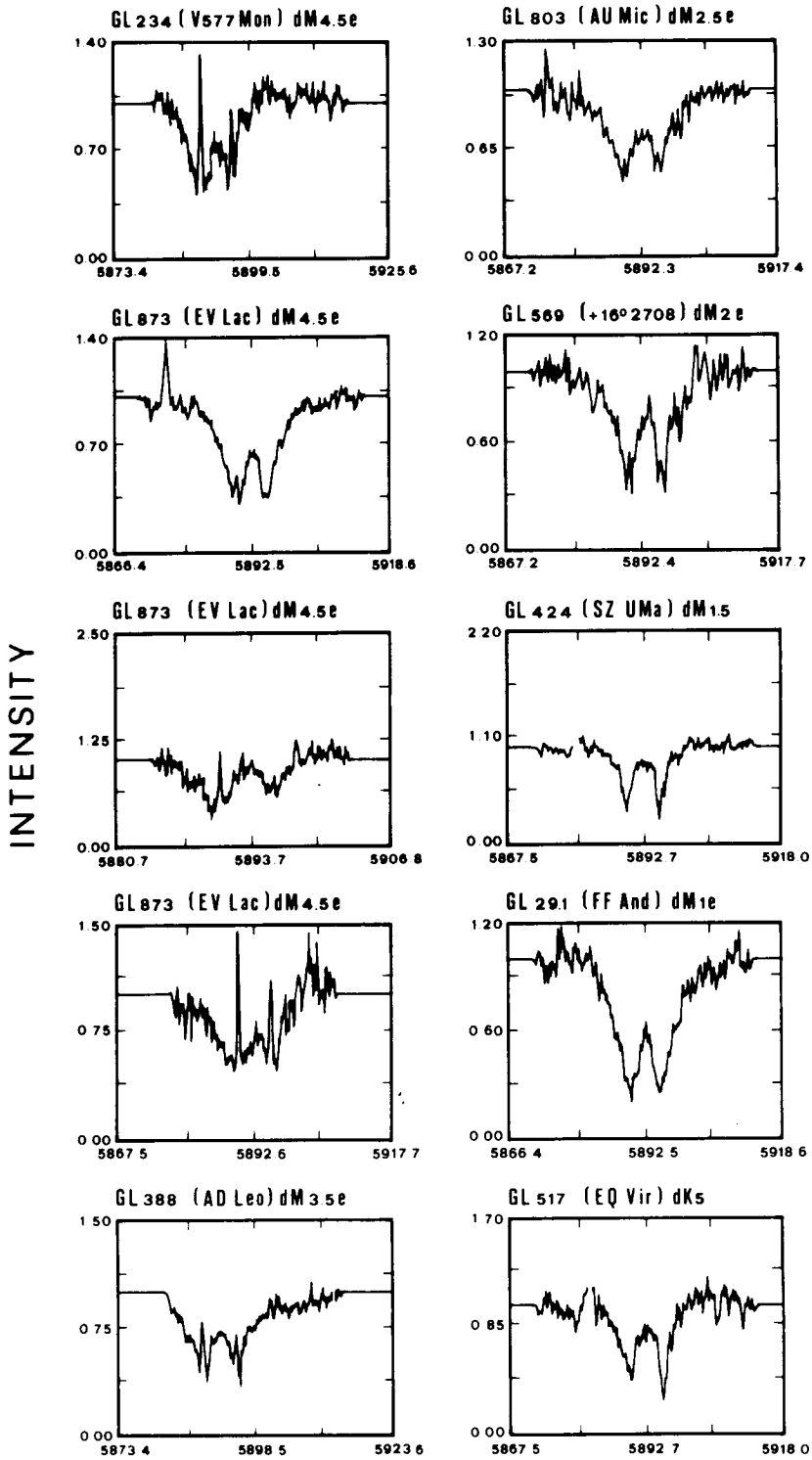


Figure 9-7. High-resolution profiles of Na D lines in M dwarfs (from Worden et al., 1981).

Table 9-4

Surface Flux (F) in the Principal Ultraviolet Emission Lines for the Sun and Active Late-Type K–M Dwarfs and Assumed Ratio of Surface Flux to Observed Flux at Earth ($F/f_\oplus$)

Star (spectral type)	T_e	$F/f_\oplus$	λ(A): 1240 Ion: NV T_{max}(K:) 2(5)	1304 O I, S I 9(3)? (fluor)	1335 C II 2(4)	1400 b1 Si IV, O IV 8.3(4)	1549 C IV 1.3(5)	1640 He II 2(4)? (recomb)	1657 C I 6.(3)	1812 b1 Si II, S I 6.5(3)	2610 b1 Fe II	2800 b1 Mg II 6.5(3)	3960 + 3990 Ca II H+K 6.(3)	6563 H I (H α – Hk) 6.(3)	Ref.†
Quiet Sun (G2V)	5770	–	6.4(2)(a)*	5.6(3)	6.7(3)	3.6(3)	6.6(3)	1.2(3)	8.4(3)	2.4(4)	abs.	1.3(6)	5.0(5)	–	1
Solar Active Region	–	–	5.8(3)	2.2(4)	3.0(4)	1.5(4)	2.9(4)	1.9(4)	1.7(4)	5.0(4)	–	–	–	–	2
Solar Very Act. Region	–	–	8.1(3)	3.0(4)	4.7(4)	2.1(4)	2.6(4)	2.7(4)	2.4(4)	7.4(4)	–	–	–	–	2
α Cen B (K1V)	5225	4.02(15)	8. (2)	5.3(3)	5.0(3)	3.4(3)	6.4(3)	8. (2)	–	2.0(4)	–	9.5(5)	–	–	3
II Peg–Quiet (K2V)	(4700)	3.52(17)	1.4(4)	1.2(5)	1.4(5)	3.5(4)	2.7(5)	1.9(5)	1.4(5)	1.4(5)	–	3.1(6)		–	4
II Peg–Plage	(4700)		1.2(5)	3.9(5)	5.6(5)	5.1(5)	1.6(6)	5.0(5)	4.5(5)	3.3(5)	–	4.4(6)		–	4
ε Eri (K2V)	5010	3.25(16)	5.9(3)	1.8(4)	2.2(4)	1.1(4)	3.3(4)	1.8(4)	1.6(4)	6.4(4)	–	2.4(6)	1.5(6)	–	3
ε Ind (K5V)	4400	4.22(16)	–	4.4(3)	5.5(3)	–	<1.9(3)	–	5.3(3)	1.4(4)	–	5.9(5)	–	–	5
EQ Vir (dK5e)	4400	1.50(18)	8.1(4)	<3 (4)	1.2(5)	~1.1(5)	1.4(5)	~1.2(5)	4.8(4)	~7.5(4)	2.4	2.0(6)	1.9(6)	–	1
61 Cyg B(K7V)	4130	4.31(16)	1.2(3)	2.1(3)	1.4(3)	–	3.5(3)	9.1(2)	2.4(3)	6.9(3)	1.2(5)	2.7(5)	1.2(5)	–	1
HD 88230 (K7V)	4100	5.87(16)	–	5.0(3)	6.5(3)	–	3.5(3)	1.8(3)	~5. (3)	8.8(3)	2.0(4)	>5.1(5)	1.3(5)	–	1
HD 1326A (M1.3V)	3780	1.37(17)	1.5(4)	–	<5. (3)	–	<7. (3)	–	3.2(3)	1.0(4)	–	5.5(5)	–	–	1
AU Mic (M1.6eV)	3730	2.17(17)	3.5(4)	4.1(4)	4.8(4)	~5. (4)	1.3(5)	6.3(4)	5.2(4)	5.2(4)	6.7(5)	8.9(5)	1.5(6)	4.5(6)	1
	–	–	4.1(4)	2.6(4)	3.7(4)		6.2(4)	6.5(4)		1.3(4)	1.7(5)	5.6(5)	–	–	6
AU Mic – Quiet	–	–	1.4(4)	2.8(4)	2.6(4)	1.1(4)	5.6(4)	2.8(4)	2.0(4)	2.2(4)	2.8(5)	5.6(5)	–	–	4
– Plage	–	–	1.6(4)	2.4(4)	4.0(4)	2.6(4)	9.6(4)	5.4(4)	2.1(4)	3.7(4)	3.0(5)	8.0(5)	–	–	4
– Flare	–	–	3.0(4)	–	3.9(4)	2.2(4)	1.2(4)	5.0(4)	2.4(4)	3.1(4)	–	–	–	–	7
HD 95735 (M1.0V)	3720	5.88(16)	–	1.3(3)	<1. (3)	–	<2. (3)	5. (3)?	<3. (3)	4.7(3)	2.1(4)	4.6(4)	1.1(4)	–	1
EQ Peg A (M3.5eV)(b)*	3510	2.88(17)	2.1(4)	2.0(4)	5.5(4)	3.2(4)	1.1(5)	2.7(4)	2.9(4)	3.5(4)	–	–	–	–	1
B (M4.5eV)															
AT Mic A (M4.5eV)	3430	2.73(17)	2.0(4)	4.1(4)	6.6(4)	3.5(4)	1.7(5)	4.6(4)	3.8(4)	5.5(4)	3.5(5)	3.9(5)	–	–	1
B (M4.5eV)															
EV Lac (M4.5eV)	3430	3.05(17)	–	–	–	–	–	–	–	–	–	–	6.9(5)	5.2(5)	1
YZ CMi (M4.3eV)	3380	6.60(17)	8.6(4)	1.1(4)	7.3(4)	~2.4(4)	1.8(5)	3.6(4)	9.2(4)	5.0(4)	4.8(5)	8.6(5)	5.5(5)	3.9(6)	1
V 645 Cen (M5.5eV)	3200	1.16(16)	9 (3)	6 (3)	1.0(4)	–	1.9(4)	6. (3)	–	6. (3)	–	1.0(5)	–	–	1
(Prox Cen)															
UV Cet (M6e V+M6eV)	3200	2.80(17)	1.4(4)	1.2(4)	1.7(4)	1.8(4)	5.9(4)	1.0(4)	1.8(4)	1.1(4)	7.3(4)	1.4(5)	6.7(4)	2.4(6)	1

*Notes: (a) 6.4(2) = 6.4×10^2, (b) computed from observed fluxes by Hartmann et al. (1982) and $F/f_\oplus$ ratio (= 2.88×10^{17}) by Linsky et al. (1982).

†Reference: 1. Linsky et al. (1982), 2. quoted by Hartmann et al. (1979a), 3. Ayres et al. (1981b), 4. unpublished data from coordinated SERC-NASA-ESA observations with IUE by the Armagh, Boulder, and Catania groups, 5. Hartmann et al. (1982), 6. from observed fluxes by Hartmann et al. (1982) and $F/f_\oplus$. ratio by Linsky et al. (1982), 7. Butler et al. (1981).

ORIGINAL PAGE IS
OF POOR QUALITY

1974b). This type of short-term sporadic variability—if not due to fading flares or rotational modulation of active region visibility—suggests actual transient changes in the physical conditions underlying the emitting region; these are conceivably due to nonthermal instabilities. Baliunas et al. (1981) have also detected periodic variability of the emission cores of Ca II H and K lines in ϵ Eri (K2 V) similar to those seen in solar oscillations.

Stellar model chromospheres developed at the Joint Institute for Laboratory Astrophysics by J.L. Linsky and his collaborators in a recent series of papers, most of which are quoted in this section, have corroborated the suggestion first outlined by Gershberg (1970, 1974) about the qualitative similarity of solar and stellar chromospheres. However, the latter are less extended, hotter, denser and show larger surface inhomogeneities than those of the Sun (cf. 3.2). (See the section *Surface Inhomogeneities in the Outer Atmosphere.*)

From the width of hydrogen lines, an upper limit of 14000 K for the chromospheric electron temperature can be predicted. However, the centrally reversed Hα profiles have a half-width of $\sim$1 Å, implying a temperature of 4×10^4 K for an optically thick emitting region with electron density lower than 10^{13} cm^{-3}. The intensity ratio of triplet to singlet He I emission lines, I(5876)/I(6678), is 3.7 (i.e., similar to that in active solar prominences). These He I lines are probably excited by collision from ground state in the chromospheric region with $T = 2$–5×10^5 K and column density $n_e \times \ell \sim 6 \times 10^{18}$ cm^{-2}, implying that the chromospheric regions for $n_e = 10^{10}$ to 10^{12} cm^{-3} are thin. Even thinner chromosphere could result if, according to Kunkel (1970) and Gershberg (1974), $n_e = 10^{12}$ to 10^{14} cm^{-3}.

In addition to age, abundance is believed to be responsible for the large spread of M dwarfs in the HR diagram. However, Hartmann and Anderson (1977) did not find appreciable abundance differences between emission and non-emission K7–M1 dwarfs. They made a curve of growth analysis of high-dispersion echelle spectra of six old disk stars obtained at the Kitt Peak 4-meter telescope in the region of 5900 to 6600 Å with 0.1 to 0.15 Å resolution. The derived abundances were similar to the solar ones to 0.2 dex.

From high-resolution Fourier transform infrared (1.5 to 2.5 μ) spectra of six K7–M5 dwarfs and subdwarfs obtained with the same Kitt Peak telescope, Mould (1978) concluded that subdwarfs are metal poor ([M/H] $\simeq -0.3$), whereas the one star in his sample which was above the main sequence is metal rich ([M/H] = 0.5). He also gave an upper limit of 0.2 magnitude to the dispersion in the HR diagram attributable to abundance effects.

A search for the lithium line at 6707 Å (Bopp, 1974c) in 14 flare stars showed no detectable lithium (EW $<$ 50 mA), but on Gliese 182 = V 1005 Ori (EW $\sim$ 200 mA). De la Reza et al. (1981) have confirmed this detection and obtained a ratio [Li/H] close to the interstellar value.

Essentially, none of the studied late K–M emission-line dwarfs differ from field K–M stars in their lithium content (Herbig, 1965). This is consistent with their highly convective structures, implying severe pre-main-sequence lithium depletion (Bodenheimer, 1965). The only BY Dra flare star with high lithium abundance is the K4 Ve dwarf, BD-10 4662AB (FK Ser). However, it is not clear whether it is in a post T Tauri phase (Herbig, 1973) or, according to its infrared colors, is a low-active T Tauri star (Zappala, 1974). Actually, its infrared excess is one order of magnitude lower than a *bona fide* T Tauri star (Hackwell et al., 1974).

Pettersen (1983a) notes that much caution should be exercised in deriving metal-to-hydrogen ratios for active stars from the photometric metallicity index. As demonstrated by Giampapa et al. (1979) for the solar case, active region photometry in the Strömgren system leads to apparent lower metal abundance than for the quiet Sun. Therefore, photometrically determined metal abundance for dMe stars will be systematically lower than for dM stars because of the integrated effect of their huge active regions with filling factors up to 100 percent.

Ultraviolet, X-Ray, and Radio Data

The optical spectra of dM and dMe stars show the signatures of powerful solar-type chromospheres (i.e., of atmospheric regions in which the temperature gradient dT/dh, which is negative in the photosphere, becomes positive, and nonradiative heating dominates the energy balance). However, the temperature regime of chromospheres (4300 to 25000 K) and of the overlying shallow transition regions (25000 to 1×10^6 K) and the coronae (1 to 3×10^6 K), together with the monotonic decrease of matter density, allow the formation of numerous low to high excitation emission lines and continua, which fall into the ultraviolet and X-ray domains. The International Ultraviolet Explorer (IUE) and Einstein satellites, which became operative in 1978, have greatly contributed to the impressive progress in the study of the outer atmospheres, particularly for red-dwarf stars. Their faint or nonexistent ultraviolet background continua make it possible to detect and analyze important spectral features, such as Mg II h and k (2803 and 2796 Å), O I (1305 and 1355 Å), C I (1657 Å), Si II (1808 and 1812 Å), the Fe II multiplet (~2610 Å), Si II (1335 Å), Si III (1892 Å), C III (1175 and 1909 Å) Si IV (1394 and 1403 Å), C IV (1548 and 1551 Å), N V (1238 and 1242 Å), and O V (1371 Å). Soft X-ray emission is essentially ubiquitous among red-dwarfs, with dMe stars having the largest ratios of L_x/L_{bol} (cf. Linsky, 1980a, 1980b; Vaiana, 1981; Vaiana et al., 1981). These are powerful diagnostics for nonradiative heating processes in the outer stellar atmospheres.

A few representative LWR* and SWP† spectra of quiescent dMe stars obtained with IUE are presented in Figures 9-8 and 9-9, respectively.

The recent insight into the physics of red-dwarf atmospheres needs to be viewed in the general context of stellar outer atmospheres. The major observational results include the following:

1. The radiative loss in the Ca II H and K emission lines alone, which accounts for only a fraction of the total chromospheric energy loss in red dwarfs (Linsky et al., 1982), cannot be accounted for by the dissipation of acoustic fluxes based on the Lighthill-Proudman theory (cf. Stein, 1967; Renzini et al., 1977) as first shown by Blanco et al. (1974). Refined calculations by Bohn (1983) now seem to overcome this difficulty also at the coronal level.

2. The Mg II fluxes (Linsky and Ayres, 1978; Basri and Linsky, 1979; Linsky et al., 1982) and the coronal soft X-ray emissions (Vaiana et al., 1981; Ayres et al., 1981b) are independent of gravity and effective temperatures, contrary to what is expected if heating by acoustic-wave dissipation dominates. Slow mode magnetohydrodynamics (MHD) waves in flux tubes have been subsequently proposed to overcome this difficulty (Ulmschneider and Bohn, 1981).

3. A plot of emission-line surface fluxes versus temperature of line formation in quiescent G–M dwarfs shows a qualitative trend similar to that of the quiet Sun, but in M dwarfs, the emission lines are fainter by a factor of 3. Instead, active and dMe star surface fluxes in chromospheric lines are comparable to, or up to one order of magnitude larger than, those of solar very active regions (VAR's). The enhanced emissions in dMe stars get progressively larger than the solar one, up to two orders of magnitude, at higher temperatures of formation (i.e., at transition region and coronal levels (Ayres et al., 1981b; Oranje et al., 1982; Rodonò, 1983; Linsky et al.,

*Long-wavelength redundant (camera).
†Short-wavelength primary (camera).

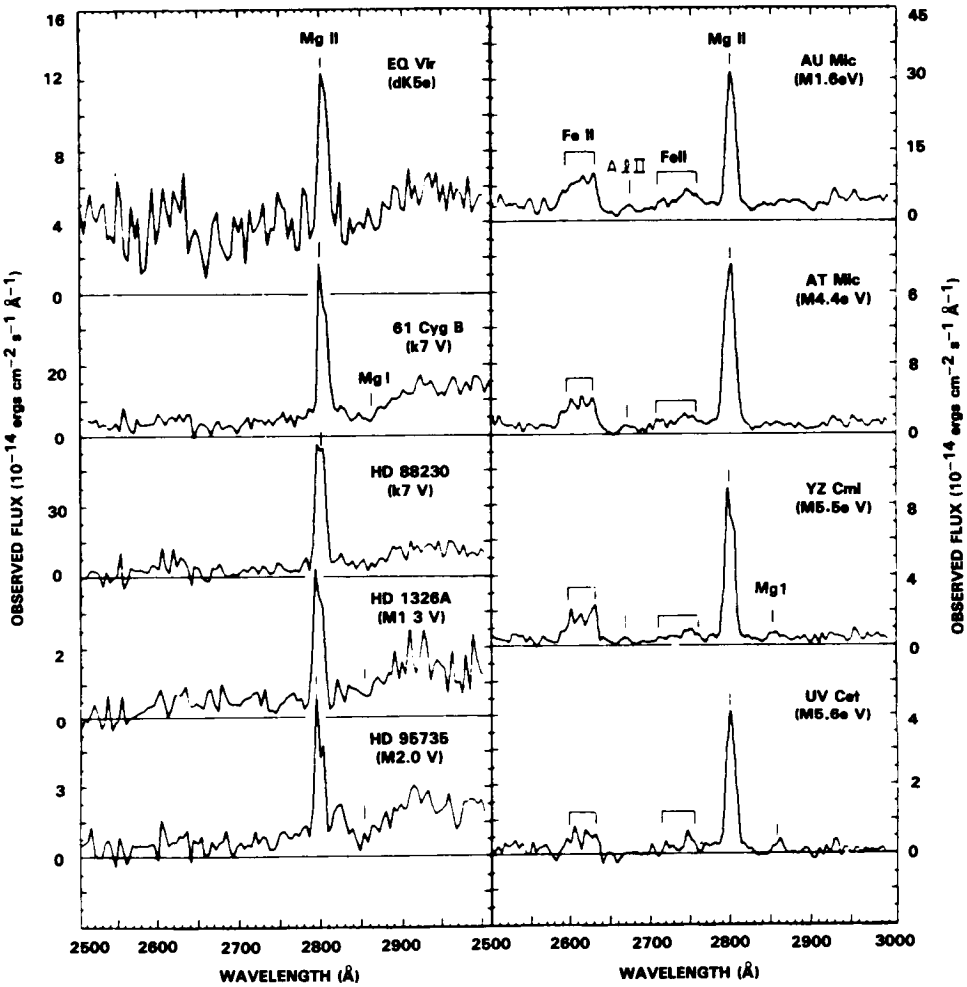


Figure 9-8. Typical Mg II h and k emission lines and Fe II line blend (2610 Å) in low-resolution ultraviolet spectra of M dwarfs obtained with the LWR (2000 to 3200 Å) camera of IUE. The line flux increases by several units during active phases (from Linsky et al., 1982).

1982)). A plot of surface fluxes in UV emission lines versus temperature of formation for several representative sources (Figure 9-10) clearly shows that the heating rate of transition regions and coronae is much higher or efficient than at chromospheric levels. The correlation plots in Figure 9-11 between chromospheric, transition region, and coronal flux ratios for cool giants and dwarfs (Ayres et al., 1981a) indicate linear logarithmic correlations, whose slopes increase in passing from chromospheric to coronal diagnostics.

4. Stars with chromosphere-corona transition regions appear to be located in definite areas of the HR diagram (Linsky and Haisch, 1979; Ayres et al., 1981b; Simon et al., 1982), areas in which solar-type hot coronae are observed (F–M dwarfs and late F–K giants), whereas cool stellar winds or hybrid-spectra (Hartmann et al., 1980; Hartmann, 1983) characterize

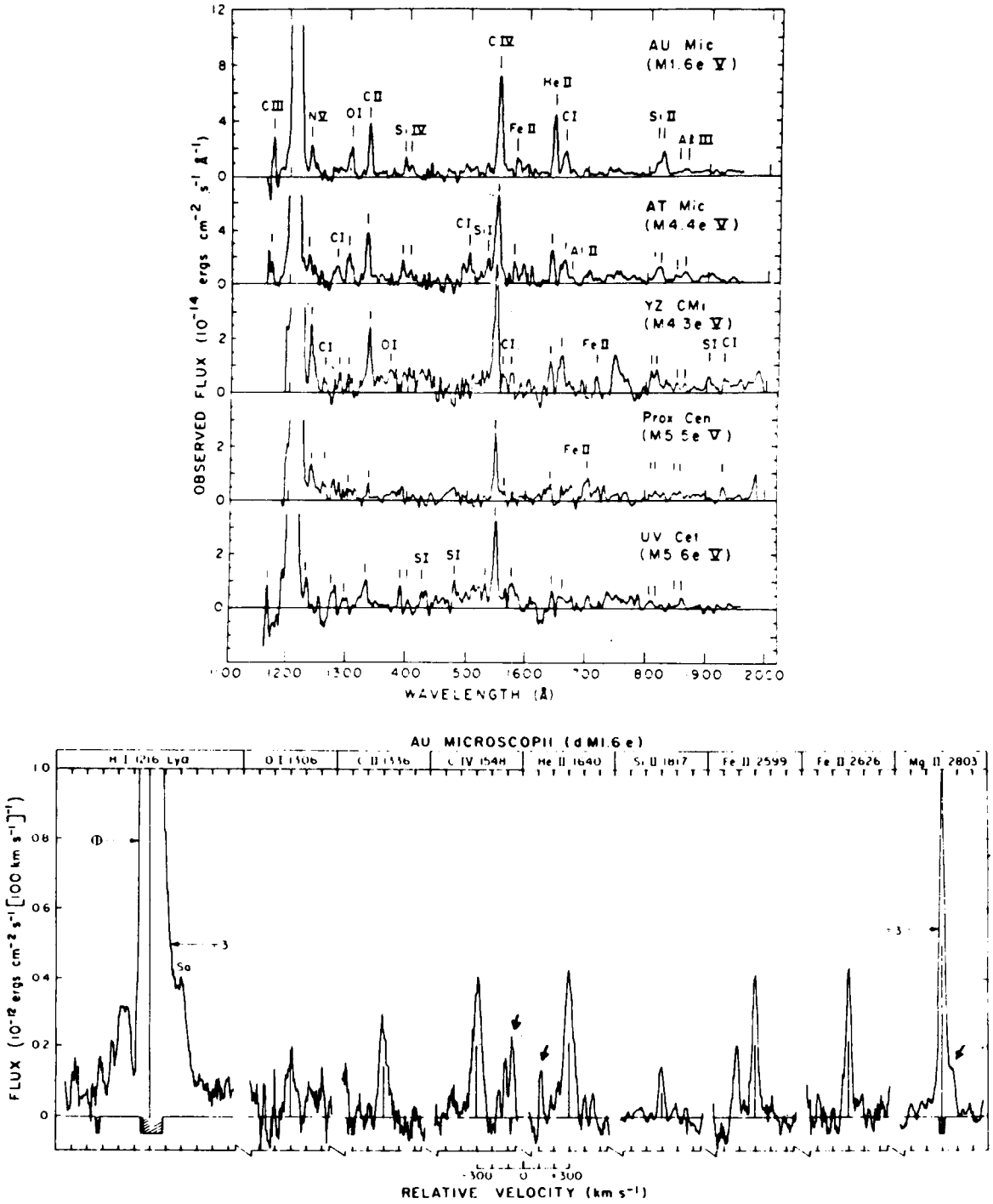


Figure 9-9. Upper panel: Chromospheric and transition-region emission lines in low-resolution ultraviolet spectra of M dwarfs obtained with the SWP (1150 to 2000 A) camera of IUE (from Linsky et al., 1982). The temperature of line formation ranges from a few thousands (C I, O I) to more than 200000 K (C IV, N V). Lower panel: High-resolution profiles of major UV lines from deeply exposed SWP and LWR spectra of the flare star, AU Mic (M1.5e), obtained by Ayres et al. (1983). The wavelength scale is calibrated in relative velocity. Arrows designate prominent particle radiation events or blemishes (from Ayres et al., 1983).

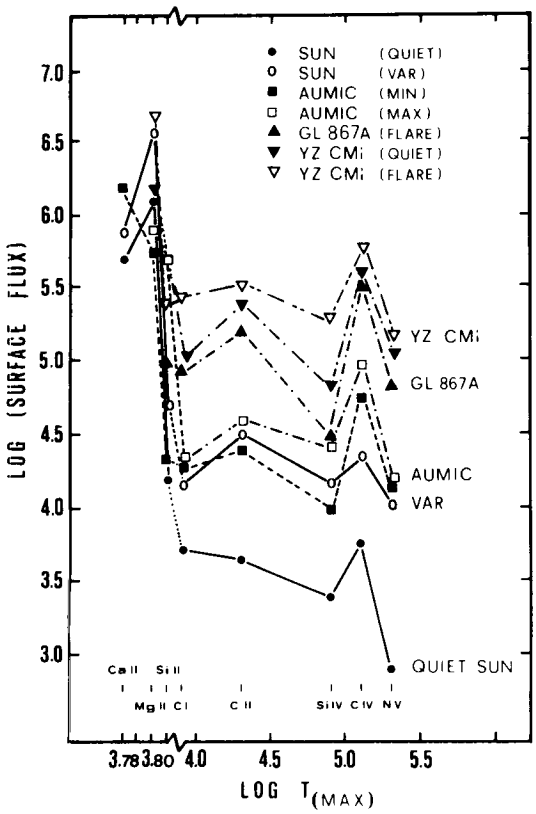


Figure 9-10. Surface fluxes in UV emission lines versus maximum temperature of formation (T_{max}) for M stars at quiescent and active phases compared with the qualitatively similar trends for the quiet Sun and a solar very active region (VAR) (from Rodonò, 1983).

brighter red giants and supergiants (Stencel, 1978; Stencel and Mullan, 1980; Haisch and Simon, 1982). As suggested by Linsky (1983a, 1983b), among others, what differentiates cool dwarfs with transition regions and hot coronae from supergiants with cool winds is the structure of magnetic fields that dominate in their outer atmospheres; *closed flux tubes* enhance the energy deposition and prevent the outflow of plasma across the field lines, whereas *open magnetic structures* lead to strong stellar winds. The evidence for closed magnetic loops from observed activity phenomena in red dwarfs will be presented in the section *Activity Signatures*. As in the best known active star—the Sun—closed and open magnetic structures may well exist at the same time. What differentiates dMe from dM stars is that, in the former, closed magnetic loops dominate over open structures so that the energy deposition in the outer atmosphere is enhanced, giving rise to surface inhomogeneities like plages. (See the section *Surface Inhomogeneities in the Outer Atmosphere*.) On the other hand, open structures and possibly slow mass loss may dominate in dM stars, making them observationally less remarkable than active dMe stars.

5. The well-known increase of chromospheric radiative losses with rotationl velocity and inverse square root of age (Skulmanich, 1972, and references therein) also apply to chromospheric UV, transition region, and coronal fluxes (Ayres and Linsky, 1980; Pallavicini et al., 1981; Walter, 1982; Golub, 1983, references therein). Several of these functional relations have been critically analyzed by Catalano and Marilli (1983). They conclude that the various empirical relations between chromospheric and coronal diagnostics with stellar rotation and age for main-sequence stars arise because the rotation period depends *only* on stellar mass (m) and age (t). They found the following exponential correlations:

$$L_K\,(M/M_\odot\,,\,t) \sim L_K\,(1,0)$$
$$\times\,(M/M_\odot)^{5.1} \times 10^{-1.5 \times 10^5 \sqrt{t}}\ ,$$

$$L_X \sim L_K^{2.6}\ .$$

These empirical relations are fundamental for the purpose of establishing firm observational constraints on theories of stellar activity, such as the α–ω dynamo

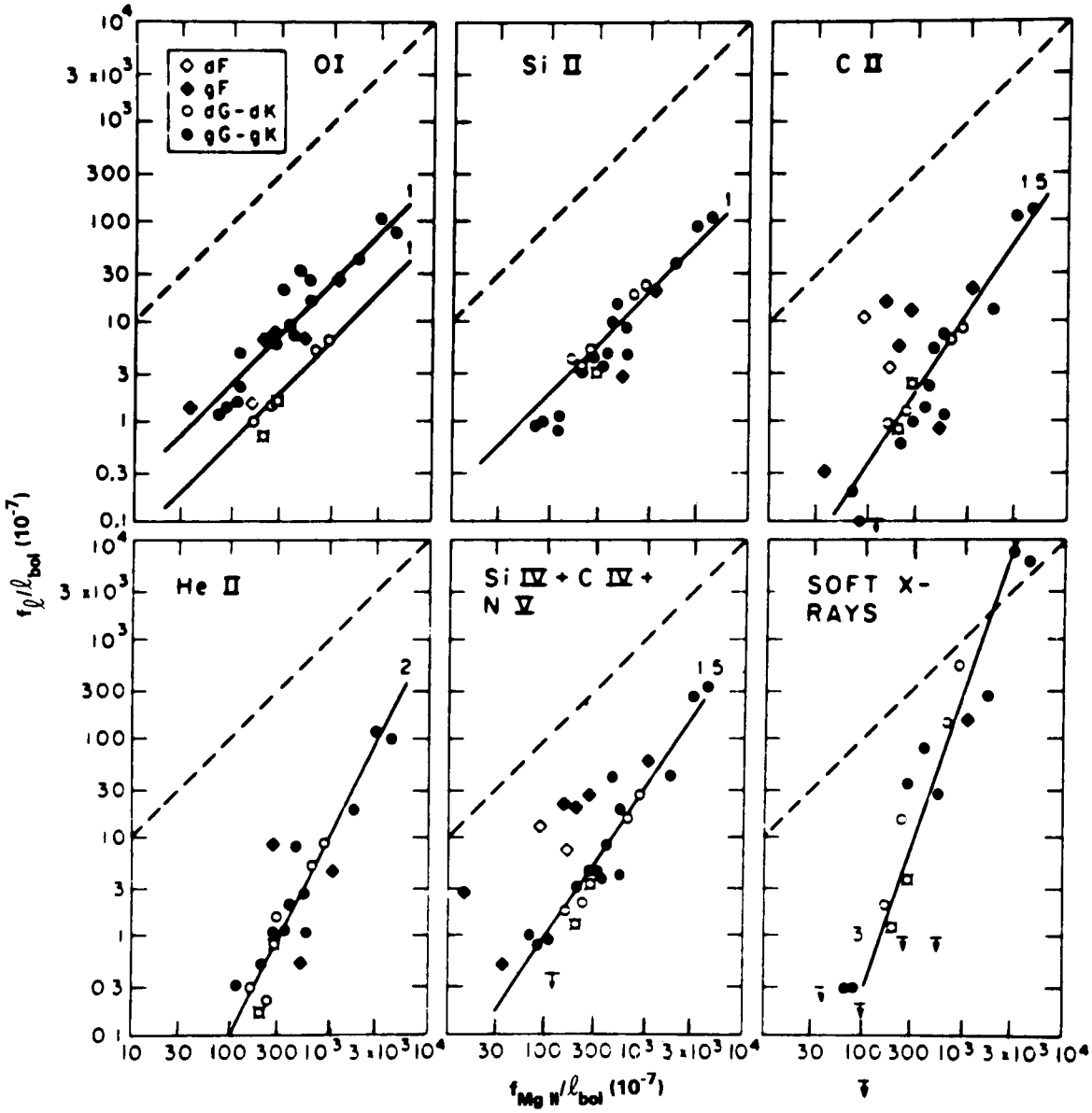


Figure 9-11. Correlation plots showing the power-law dependence of chromospheric, transition region, and coronal fluxes from Mg II line relative flux (from Ayres et al., 1981b).

(cf. reviews by Rosner, 1983; Belvedere, 1983), that can account for the generation and emergence of magnetic field on the stellar atmospheres (Belvedere et al., 1980; Durney et al., 1981).

6. Soft X-ray luminosities in the range 10^{26} to 10^{30} erg s^{-1} have been determined for about 40 dM stars (cf. Golub, 1983; Johnson, 1983). They show a large luminosity spread and variability. Quiescent emission coronal temperatures lie in the restricted range log T = 6.4 to 6.9, except for the very active stars, BY Dra and Cr Dra, whose coronal temperatures exceed 10^7 K. Soft X-ray luminosities versus coronal temperatures are plotted in Figure 9-12 (from Serio et al., 1985).

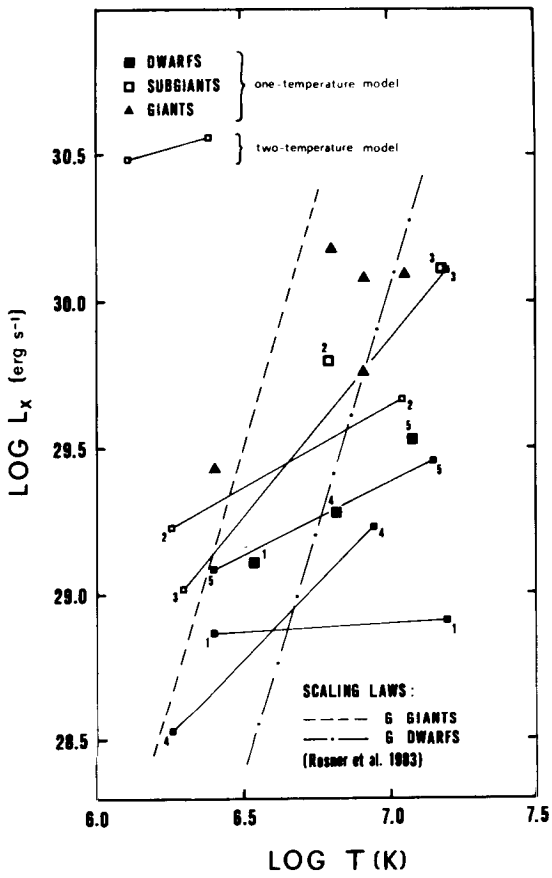


Figure 9-12. Soft X-ray luminosity of late-type stars, including M dwarfs, versus coronal temperature from observations with the image proportional counter (IPC) of the Einstein Observatory. The IPC spectra of dwarfs and subgiants, except one subgiant, suggest two coronal components at temperatures of about 2.1 × 10^6 and 1.3 × 10^7 K (from Serio et al., 1985).

It is apparent that X-ray emission is positively correlated with coronal temperature for main-sequence stars and negatively correlated with stellar surface gravity, in fairly good agreement with the Rosner et al. (1983) model for the formation and maintenance of magnetically confined hot coronal plasma. All of the X-ray spectra of cool dwarfs and subgiants, except one subgiant, in Serio et al. (1985) indicate two-temperature coronal components. The temperatures differ up to one order of magnitude and do not appear to be correlated with X-ray luminosity.

7. After several negative results and unsuccessful attempts (Altenhoff et al., 1976; Johnson and Cash, 1980), quiescent microwave emission at the 1 to 2 mJy level has been detected with very large array (VLA) from the active dMe stars chosen because of their strong X-ray coronal emission and/or other activity indicators (Gary and Linsky, 1981; Topka and Marsh, 1982; Fischer and Gibson, 1982; Gary et al., 1982; Linsky and Gary, 1983). Only upper limits were obtained for all dwarfs earlier than M except χ^1 Ori (GO V). In Table 9-5, quiescent radio and X-ray data for dMe stars are presented. The detected microwave fluxes exceed by 1 to 2 orders of magnitude those predicted by assuming optically thin thermal bremsstrahlung consistent with the flat radio spectra unless implausibly large and relatively cold (~5 × 10^6 K) coronae are postulated, which is inconsistent with X-ray observations. Linsky and Gary (1983) conclude that gyrosynchrotron emission from a more confined nonthermal electron component is the likely emission mechanism. Occasionally, they observed both right- and left-hand circular polarization up to 50 percent.

There are now sufficient arguments suggesting that, as in the Sun, the atmospheric structures of dM and, especially, of dMe stars are controlled, even in their "quiescent" phases, by the magnetic field strength and topology (Vaiana and Rosner, 1978; Linsky, 1980a, 1983a, 1983b). The long-lasting efforts to detect those important but elusive fields are now paying their dividends; successful detection is being reported at an ever increasing rate. (See the section *Nonthermal Energy Sources of Activity and Conclusions.*)

Table 9-5
X-Ray and Microwave Luminosities of Active M Dwarfs from the Einstein IPC and VLA 6-cm Fluxes, Respectively*

Gliese (1969) No.	Star Name	Spectral Type	log L_x (erg s^{-1})	Ref.†	log L_R (erg s^{-1} Hz^{-1})	Ref.†
15 AB	GQ And	dM2.5e + dM4.5e	27.1	1		
65 AB	UV Cet	dM5.5e + dM5.5e	27.3–27.6	1	13.04–13.36(B)	2
83.1	TX Ari	dM5e	27.6			
166 C	40 Eri C	dM4.5e	27.8	1		
206	V 998 Ori	dM4e	29.1	3		
229	HD 42581	dM2.5e	28.8	4		
234 AB	V 577 Mon	dM7e	26.9	4		
268	Ross 986	dM7e	27.5	4		
278 C1	YY Gem	dM1 + dM1e	29.6	1	14.36–14.66	2
285	YZ CMi	dM5e	28.6	5		
388	AD Leo	dM4.5e	29.0	4		
406	CN Leo	dM8e	26.6–27.1	1, 4		
412 AB	WX UMa	dM2e + dM8e	27.5–28.5	4		
477	FI Vir	dM5	26.6	3		
490 AB	DM + 36 2322	dM0e + dM4e	28.9	1		
551	V 645 Cen	dM5e	26.6–27.4	4		
612	CR Dra	dM1.5e	29.1	6		
644 AB	V 1054 Oph	dM3.5e	29.3	1	13.40–13.83	2
644 C	Wolf 630 C	dM5e	26.4	4		
719	BY Dra	dM0e + dM2e	29.5	6		
752 AB	V 1298 Aql	dM3.5 + dM5e	27.1	1		
799 A	AT Mic	dM4.5e + dM4.5e	29.3	4		
803	AU Mic	dM2.5e	29.9	4		
852 AB	Wolf 1561	dM4.5 + dM5e	29.5	4		
860 AB	DO Cep	dM3 + dM4.5e	27.4	1		
866	L 789-6	dM7e	26.9–27.0	3, 4		
867 AB	HD 214479	dM2e + dM4e	29.0	4		
896 AB	EQ Peg AB	dM4e + dM5.5e	28.8	1		
905	HH And	dM6e	26.3	3		
—	HD 202560	dM0e	27.2	4		
—	DM + 01 2684	dM0e	28.2	4		

*When several measurements are available, the range of variability is given.
† References: 1. Vaiana et al. (1981), 2. Linsky and Gary (1983), 3. Johnson (1983), 4. Golub (1983) and references therein, 5. Kahler et al. (1982), 6. Serio et al. (1985).

ACTIVITY SIGNATURES

Having discussed at some length the global characteristics of late-type dwarfs and, in particular, of dM–dMe stars in their quiescent phases, we can now turn our attention to their active phases. Variability on time scales from a few seconds to several months seems to be a peculiar characteristic of some dM and of all dMe stars.

This variability arises from nonstationary activity phenomena occurring in their atmospheres from atmospheric to coronal levels. Assuming the solar activity as a valid guideline, the stellar phenomena we expect to detect and study are transient atmospheric inhomogeneities (such as spots, plages, and coronal structures), flare events, and activity cycles.

Surface Inhomogeneities in the Photosphere

Periodic, or quasi-periodic, low-amplitude wideband photometric variations are observed in several nearby K–M emission-line dwarfs and subgiants. Most of them are members of binary systems. The observed light curve shape is almost sinusoidal, so that it is widely referred to as the *photometric wave* or *distortion wave*, the latter to emphasize its distortion effects on eclipsing binary light curves. The peak-to-peak "wave" amplitudes are of the order of 0.1 magnitude and the photometric periods are typically a few days. Both the wave amplitude and period undergo striking changes. Systematic observations have shown that notable asymmetric or double-wave structures often develop, and at other times, essentially no variability is detected. Generally, after a period of apparently irregular changes, a sinusoidal wave is restored. These variations are acompanied by small ($\sim$0.01 mag), if any, $U-B$ and $B-V$ color changes, so that, following Kron's (1950, 1952) suggestion, they are attributed to unevenly distributed cool photospheric spots, whose visibility is modulated by the star's rotation.

The discrepancy between the spectroscopically determined 5.97599d orbital period for the double dM0 close binary, BY Dra (Bopp and Evans, 1973), and the 3.836d photometric period (Chugainov, 1966; Rodonò et al., 1983), which is identified as the active component's rotational period, has substantiated the spotted-star hypothesis or the so-called *BY Dra syndrome* (Kunkel, 1975). Typical synoptic light curves are shown in Figure 9-13. In Table 9-5, the most relevant data on the photometric wave in BY Dra stars are given. Most of the stars listed in Table 9-6 are also known UV Ceti type flare stars. (See the section *Stellar Flares*.) This makes it manifestly questionable to separate BY

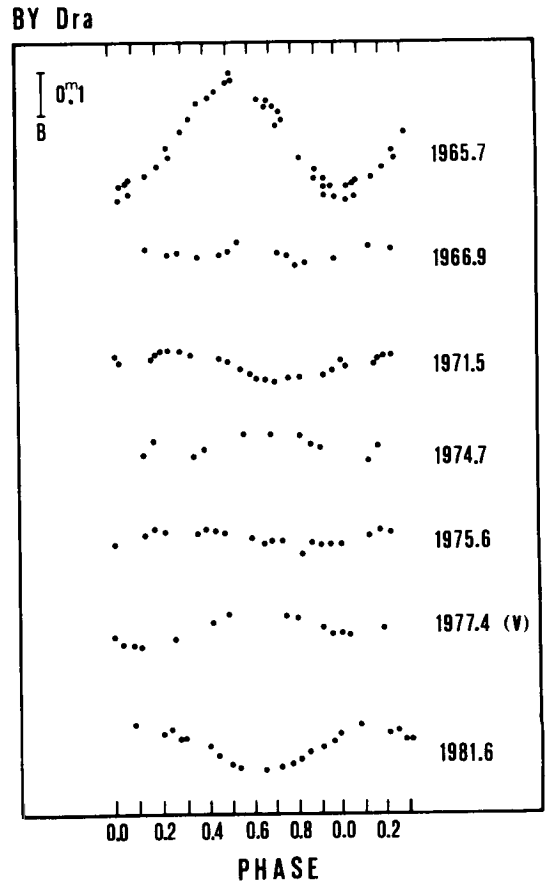


Figure 9-13. Synoptic light curves of BY Dra from observations obtained at several places (from Rodonò, 1983). The highly variable photometric wave is attributed to surface spots, whose visibility is modulated by the star's rotation.

Table 9-6
Relevant Properties of the Best Known BY Dra Type Stars
(Most are also known UV Ceti type flare stars)

Gliese (1969) or Woolley et al. (1970) No.	Variable Name	Catalog No.	Spectral Type	M_V	V	Δm	P_{phot}	Duplicity*	P_{orb}	Notes†	Ref.‡
29.1	FF And	BD + 34 106	dM0e	8.7	10.38	0.06	2.162	SB 25	2.1730	(a)	1, 2
103	CC Eri	HD 16157	K7e V	8.5	8.85	0.30	1.56	SB 89	1.56145	(a)	3, 4
113.1	VY Ari	HD 17433	G9	5.2	6.87	0.10	7.85	RV Var		(a)	5, 6
182	V 1005 Ori	Yale 1121	dM1e	9.3	10.14	0.08	1.96 ?			(a)	7
278 C	YY Gem	BD + 32 1582	M1 Ve	8.2	9.08	0.04	0.816	EB	0.81679	(a)	8, 9
285	YZ CMi	Ross 882	dM4.5e	12.3	11.20	0.15	2.770			(a)	10, 21
9369 A	–	BD + 48 1958A	dM0e	8.4	10.14	0.05 ?	–	SB 436	1.03382		7, 11
494	DT Vir	BD + 13 2618	dM2e	9.1	9.76	0.05 ?	–			(a)	7
517	EQ Vir	HD 118100	dK5e	7.8	9.36	0.1	3.96			(a)	7, 12
566 A	ξ Boo	HD 131156	G8e V	5.53	4.68	0.03	10.15	VD		(d)	12
566 B	ξ Boo	HD 131156	K4e V	7.69	6.84	–	–	VD		(d)	12
630.1	CM Dra	G 225-67	dM4e	12.90	12.90	0.01	1.27	EB	1.26796		13
–	FK Ser	BD – 10 4662	dK5e	–	10.51	0.10	5.20	VD		(a)	10
719	BY Dra	HDE 234677	M0 Ve	7.4	8.44	0.25	3.836	SB 695	5.97599	(a)	14, 15
799	AT Mic	HD 196982	dM4e	11.1	10.55	0.07	–	VD		(a)	4, 16
803	AU Mic	HD 197481	M0e V	8.9	8.75	0.30	4.85	SB ?		(a)	4, 17
815 AB	V 1396 Cyg	AC + 39 57322	dM3e	9.5	10.13	0.006	–	VD	28.25 y	(a)	18
								A: SB	3.276		1, 7, 19, 20
867 A	FK Aqr	HD 214479	dM2e	9.3	9.10	0.06	4.08 ?	SB 992	4.08322	(a)	7
873	EV Lac	BD + 43 4305	dM4.4e	11.5	10.2	0.03	4.375	AB ?		(a)	21
875.1	GT Peg	AC + 31 70565	dM3.5e	9.8	11.66	0.15	1.641			(a)	1, 10, 19
879	TW PsA	HD 216803	K5 Ve	7.03	6.49	0.04	10.3	SB ?		(a)	4, 16
–	–	HD 218738	dK2	–	7.98	0.08	3.0	SB 952	3.03287	(b)	7
905	–	Ross 248	dM6e	14.80	12.29	0.06	115	WP ?			8
–	II Peg	HD 224085	K2 V	5.1	7.4	0.30	6.63 ?	SB	6.72	(c)	5, 22
–	–	HDE 319139	dK5e	7.4	10.4	0.06	1.7				4

* Duplicity: AB = astrometric binary, EB = eclipsing binary, SB = spectroscopic binary, VD = visual binary, WP = wide pair.

† Notes: (a) flare stars, (b) B component of a wide VD with HD 218739, (c) uncertain variable-type, probably a transition prototype between RS CVn and BY Dra variables, (d) The Δm and P_{phot} data refer to the joint system.

‡ References: 1. Krzeminski (1969), 2. Bopp and Fekel (1977b) and Bopp et al. (1978), 3. Evans (1971), 4. Busko and Torres (1978), 5. Chugainov (1976a), 6. Chugainov (1976b), 7. Bopp and Espenak (1977), 8. Kron (1950), 9. Leung and Schneider (1978), 10. Chugainov (1974), 11. Bopp and Fekel (1974), 12. Ferraz Mello and Torres (1971), 13. Lacy (1977a), 14. Chugainov (1971), 15. Bopp and Evans (1973), 16. Torres and Ferraz Mello (1973), 17. Torres et al. (1972), 18. Lippincott (1975), 19. Chugainov (1973), 20. Fekel et al. (1978), 21. Pettersen (1983a), 22. Rucinski (1977), 23. Rodono et al. (1983).

Dra stars as a distinct group of variables relative to the UV Ceti type stars (Gershberg and Shakhovskaya, 1974; Rodonò, 1980).

Similar low-amplitude *photometric waves* have been found on several Pleiades dwarfs (Robinson and Kraft, 1974; van Leeuwen and Alphenaar, 1983) and on G-K subgiants, notably pre-main-sequence T Tau stars (Rydgren and Vrba, 1983) and mainly post-main-sequence components of RS CVn binaries (cf. Hall, 1981; Rodonò, 1981; Catalano, 1983).

Useful information on the physical characteristics and surface distribution of starspots can be inferred from spot modeling methods first developed by Torres and Ferraz Mello (1973). Basically, analytical light curves, which are produced by a rotating spotted-star model, are computed (cf. Bopp and Evans, 1973; Friedmann and Gurtler, 1975; Vogt, 1975, 1981a, 1981b) and compared with observations. However, due to the large number of free parameters—the inclination of the stellar rotation axis, the light level of the unspotted star, the spot location on the stellar surface, the spot extent and temperature difference with respect to the unperturbed photosphere—unique solutions are not possible unless some of the required parameters are obtained independently and accurate color variations are available (cf. Vogt's 1983 review and references therein). Although modeling a given light curve may be questionable or even meaningless, independent modeling of synoptic light curves spanning many years are of value for the purpose of investigating average characteristic and temporal behavior of spots.

Typically, spotted areas covering 10 to 40 percent of the projected stellar disk and spot temperatures cooler than the surrounding photosphere by about 400 to 1500 degrees have been inferred. Of particular value is the study of photometric period variations because it might reflect the migration of the spotted area photocenter on the surface of a differentially rotating star (Oskanian et al., 1977). The resulting lower limits obtained for binary star components are comparable to or smaller than the solar differential rotation in the 5 to 35 degree latitude range (Blanco et al., 1982; Bartolini et al., 1983; Rodonò et al., 1983; Busso et al., 1984).

This result is somewhat surprising because the huge starspots, inferred from light-curve modeling, would require powerful and efficient dynamos (i.e., higher than solar differential rotation rates). However, in addition to the circumstance that only lower limits of stellar differential rotation of binary system components have been determined, tidal coupling torques in binary systems might strongly affect the differential rotation regime of the individual components (Scharlemann, 1981, 1982; Rodonò, 1982; Catalano, 1983). This suggests that active systems experience a continuous competition between magnetohydrodynamic forces and dynamical orbital coupling, whose relative effects on stellar activity and orbital motion are at present unknown. It would be interesting to consider possible implications of this dynamical "struggle" in determining the duration and amplitude of activity cycles.

Typical characteristics of sunspots and starspots are presented in Table 9-7. A comparison of the listed parameters is valuable as long as the fundamental difference between solar and stellar observations is not overlooked: sunspot parameters are obtained from direct spatially resolved observations of active regions, whereas starspot parameters are inferred from the integrated surface properties of stellar photospheres.

Standard spot models assume either bright or dark spots to have no effect on the surrounding photosphere (i.e., no spatial redistribution of the missing flux is postulated). This is consistent with the available observations because, as noted by Hartmann and Rosner (1979), the missing flux in the large spotted area required by the observed light variations, if spatially redistributed, should produce color changes larger than those observed. Mullan (1975b) has suggested that a fraction of the missing energy in starspots could energize stellar flares. A

Table 9-7
Typical Characteristics of Spots on the Sun and Active Stars

Parameter	Sun	Stars
Spectral type	G2V	K0–M5 V–IV
Equatorial surface velocity (km s^{-1})	2.03	5–40
Differential rotation (rad s^{-1} $degree^{-1}$) (latitude range for the Sun: 35–5 degrees)	6.0×10^{-9}	$< 2 \times 10^{-10}$ (RS CVn) $< 3 \times 10^{-10}$ (BY Dra)
Area (in unit of disk, sunspot number = 100)	2×10^{-5} – 2×10^{-3}	0.1 – 0.4
Effective temperature (K):		
Umbra	4250	3500 ± 400
Penumbra	5680	
Temperature difference:		
Photosphere-umbra	1800	600 ± 1200
Photosphere-penumbra	400	
Temperature ratio:		
Umbra/photosphere	0.70	0.75 – 0.85
Penumbra/photosphere	0.94	
Brightness ratio (V-band):		
Umbra/photosphere	0.24	0.30 – 0.50
Penumbra/photosphere	0.78	
Variability due to rotational modulation of spots at maximum (%)	< 0.03	10 – 40
B_0 (kilogauss)	1–4	3 – 10*
Lifetime of large groups (months)	< 1.5	0.3 – 10
Spot cycle (years)	11.04	5 – 60

*From theoretical estimates (see Mullan, 1983).

similar qualitative mechanism has been proposed by Gershberg (1983) to explain a variety of phenomena, including flare activity and the irregular light variations of T Tau stars.

Hence, in the photospheres of active late K–M emission dwarfs, strong departures from static thermal equilibrium, similar to conditions in the vicinity of a sunspot group, occur. Taking into account that the theoretical studies of the role of magnetic fields in affecting the efficiency of convective energy transport are at present inconclusive, we may conclude that, following Gershberg (1983) and Phillips and Hartmann (1978), qualitative models cannot be worked out in detail. Moreover, additional time-resolved spectroscopic and photometric data on BY Dra type variability are needed to establish firm observational constraints on theoretical models (cf. Mullan, 1983).

Surface Inhomogeneities in the Outer Atmosphere

Pursuing the solar/stellar analogy toward the outer atmosphere, enhanced emission at chromospheric and transition region levels should occur in the so-called plages—large areas of enhanced emission that generally overlie sunspots. Their large extent is consistent with the upward divergence of magnetic field lines originating in sunspots. The most prominent chromospheric lines show variable flux correlated with both the solar cycle (Wilson, 1978; White and Livingstone, 1981) and the solar rotation phase (Bumba and Ruzickova-Topolova, 1967; Bappu and Sivaraman, 1971). The latter was detected near the minimum of the solar cycle, when the reduced number of localized plages allowed the detection of a few percent modulation of Ca II H and K line fluxes induced by the solar rotation. Oranje (1983a, 1983b) has recently shown the effect of plages on the Ca II K line intensity and profile integrated over the full solar disk (i.e., when the Sun is observed as a star). He concludes that the Ca II K variations with the solar activity cycle are largely due to plage extension and intensity variations, the chromospheric network contribution (< 8 percent) remaining unchanged.

Wilson's (1978) pioneering stellar work on Ca II H and K line fluxes has demonstrated the existence of cyclical variability on time scales close to 10 years and irregular changes on time scales from 1 day to several months on several tens of late-type main-sequence stars. A periodicity analysis of Wilson's data allowed Stimets and Giles (1980) to discover rotational modulation on 10 stars. This is a remarkable and indicative result because Wilson's sampling schedule for acquiring the data was not devised for rotational modulation studies. At present, several programs for searching for variability of stellar chromospheric lines are being carried out successfully (Baliunas and Dupree, 1979; Baliunas et al., 1981, 1983; Vaughan et al., 1981; Vaughan, 1983).

The orbital motion of binary systems offers a useful timing reference for the rotational phase of active components (i.e., for the passage of active areas across the visible hemisphere) so that it is possible to map their location and extent by monitoring the intensity of chromospheric lines (Bopp, 1974a; Ferland and Bopp, 1976; Kodaira and Ichimura, 1980, 1982). Typically, stellar plages produce variation of Ca II emission-line flux of about 10 to 30 percent. Cyclical variability is not generally observed at high flux levels, probably because the emission arises from large plages evenly distributed in longitude so that any rotational modulation is smoothed out, as at solar maximum.

The IUE is now offering an outstanding opportunity for studying stellar plages from chromospheric to transition region levels by monitoring the numerous diagnostic lines in the wavelength region 1200 to 3200 Å. (See the section *Quiescent Optical Spectra and Abundances*.) Earlier, however, marginal evidence of rotationally modulated ultraviolet emission-line fluxes was obtained by Weiler et al. (1979), Rodonò et al. (1980), Hallam and Wolff (1981), and Baliunas and Dupree (1982). Since 1980, internationally coordinated programs of simultaneous IUE and ground-based observations have clearly shown that chromospheric and transition region plages are correlated with photospheric spots (cf. Rodonò, 1983; Linsky, 1983a, and references therein). Figure 9-14 clearly shows the antiphase correlated variation of the UV emission flux in several UV chromospheric and transition region lines and of V magnitudes versus rotational phase for II Peg. Generally, the antiphase correlation of photospheric and upper atmosphere diagnostics is at best marginal for dMe stars, such as BY Dra. It is likely that microflaring activity or high plage filling factors on dMe stars make it more difficult to detect rotational modulation of plages than on K stars. Pure plage UV spectra obtained by subtracting the average quiescent spectra from those at active phases, show transition region line fluxes enhanced by a factor of 5 and chromospheric fluxes by only a factor of 2, relative to quiescent flux. The observed

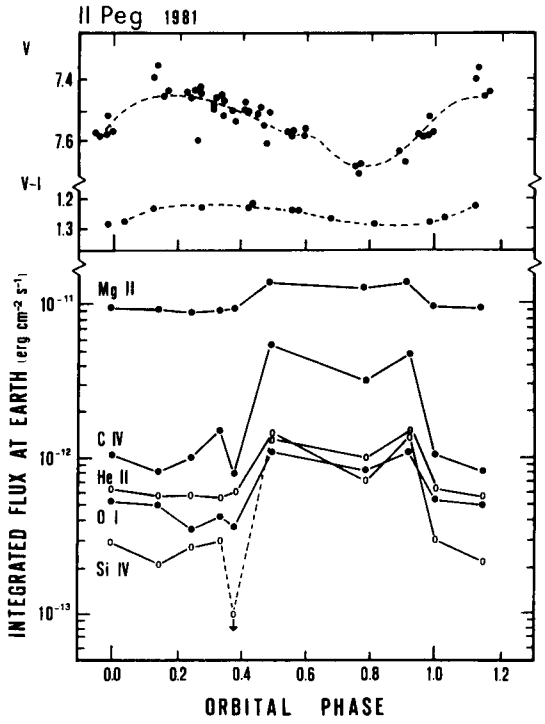


Figure 9-14. Top: V-band photometry from ground-based observations (closed circles) and from IUE fine error sensor (FES) counts (open circles) and V–I color index. A two-spot modeling of the V light curve is also shown (dashed line). Bottom: Integrated flux in major UV lines versus photometric phases. It is evident that the photometric wave attributable to photospheric spots is anticorrelated with the line-flux variability attributable to chromopheric and transition region plages (from Rodonò et al., 1985).

increase of line enhancement with the temperature of formation is also typical of solar plages and suggests that nonradiative energy dissipation plays an increasingly important role as temperature increases (i.e., in the outermost atmospheric layers). A quantitative comparison of solar and stellar behavior (cf. Figure 9-10) shows that, even at "quiescent" phases, the surface flux from active stars is larger than that from very active solar regions (VAR's) and becomes increasingly larger as the atmospheric level increases. Clearly, active star surfaces are covered by intense and extensive solar-like plages that affect even their "quiescent" hemisphere.

X-ray and radio observations have provided definite evidence of quiescent coronae in late-type stars and, particularly, in M dwarf flare stars and RS CVn systems. (See the section *Ultraviolet, X-Ray, and Radio Data.*) As in the Sun, highly structured coronae are expected. Again, rotational modulation of the observed X-ray flux is able to disclose such structures, as demonstrated by recent observations of YZ CMi in quiescent phases (Pettersen et al., 1980) and of the RS CVn system, AR Lac (Walter et al., 1983). Further progress requires systematic dedicated programs to be carried out with spaceborne instrumentation. Allocation of observation time for long-term programs on available X-ray satellites is not usually favored by present selection committees. Apparently, repentance does not always work in science: when Olin Wilson first applied to the U.S. National Science Foundation for a grant to carry on his pioneering and fundamental research work on stellar activity cycles, his proposal was rejected because one referee considered it not particularly motivating.

Stellar Flares

The most prominent phenomena of stellar activity are short-lived flare events which occur in the atmosphere of K–M dwarfs and subgiants. Sudden and unpredictable enhancement of continuum and line fluxes in the optical and UV spectral domains, and of X-ray and radio emission fluxes, may occur on time scales as short as a few hundredths of seconds. Even moderately time-resolved (10 s) photometry of stellar flares indicates that, usually, complex multipeaked events, probably resulting from successive inputs of energy into the atmosphere, are observed (cf. Byrne, 1983, and references therein). Moreover, the incidence of rapidly following flares, higher than predicted by Poisson statistics (Lacy et al., 1976; Pazzani and Rodonò, 1981), suggests that sympathetic flares can occur almost simultaneously in the same

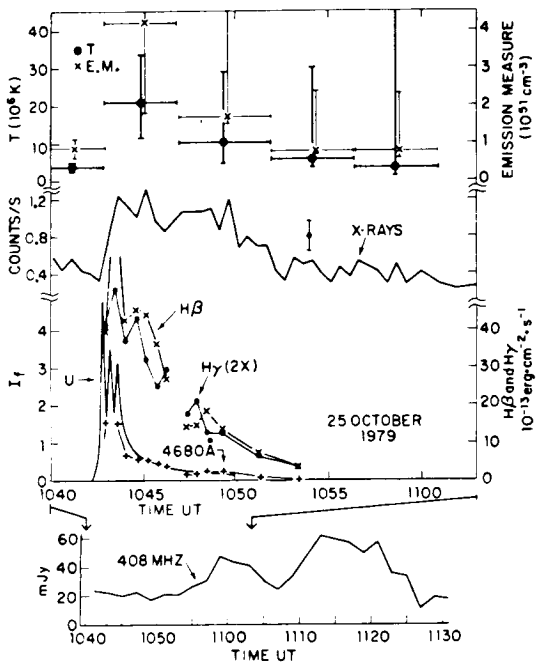


Figure 9-15. Simultaneous optical, radio, and X-ray observations of a flare on YZ CMi (from Kahler et al., 1982).

star (Moffett, 1972; Rodonò, 1976), like the solar flares, or in both components of a binary system (Rodonò, 1978; Fischer and Gibson, 1982). In Figure 9-15, a typical flare U-band light curve is shown, together with simultaneous X-ray and radio observations from Kahler et al. (1982). Generally, the flare color temperature is above 10000 K, so that the relative flare enhancement, normalized to the quiescent star level, increases toward shorter wavelengths because of the increasing contrast between the high-temperature flare radiation and the cool photospheric background of M dwarfs. For this reason, wideband photometry usually fails to detect flares in intrinsically bright stars due to their high photospheric background. However, in limited spectral regions or lines and at radio and X-ray wavelengths, the flare to background flux ratio is higher than in the optical region, so that flare or flare-like events have also been observed occasionally in RS CVn type K subgiants or even in earlier type stars (cf. Kunkel, 1975; Bakos, 1983), but this topic is beyond the scope of this review.

Detailed comparative studies of flares in the Sun and dM stars (Mullan, 1977; Gershberg, 1977) suggest that, also in the latter, the likely physical process underlying flaring phenomena is the storage and explosive release of magnetic energy, even though the energy involved in stellar flares is sometimes up to 2 to 3 orders of magnitude higher than in the Sun.

At present, only integrated characteristics over the entire flare region can be obtained from stellar observations. Typical parameters of stellar flares, obtained from wideband photometry of red dwarfs, are presented in Table 9-8.

Only in the optical domain have a statistically significant number of events been observed. Several statistical investigations have concluded that, with the exception of the above-mentioned possible sympathetic flares, the time intervals between flares follow Poisson statistics. Small "precursor" flares, both positive and negative, as well as overall enhancements of the quiescent flux, are observed before major flares (Rodonò et al., 1979; Cristaldi et al., 1980). However, no correlation between flare intensity and time elapsed with respect to adjacent flares is apparent (Lacy et al., 1976). The recent thorough statistical study by Shakhovskaya (1979), including 1500 flares observed mainly at the Catania, Crimea, and McDonald Observatories in 7000-hr photoelectric patrolling of 21 dMe stars, has quantitatively assessed several qualitative or preliminary results. A tendency is apparent for slow (rise time >1 min) and more energetic (>10 erg^{33}) flares to occur on intrinsically brighter stars. The time-integrated energy release in U- and B-bands ranges from 10^{28} to a few 10^{35} erg. The cumulative flare frequency ν ($E_f > E_o$) (i.e., the average occurrence of flares with total energy release $E_f > E_o$) follows the linear equation $\log \tilde{\nu}\ (h^{-1}) = a - b \log E$, where a depends on the star considered and b ranges from 0.4 to 1.4, being systematically larger for intrinsically fainter stars and equal for the B- and U-bands. The time-averaged power due to flares decreases from a little more than 10^{29}

Table 9-8
Typical Parameters of Stellar Flares from Wideband Photometry

Rise time (min)	0.1 – 10*	
Rise/decay time (sometimes > 1)	1. – 10^{-2}	
Log (peak power) erg s^{-1}	26.5 – 31.5 (B)	27. – 32. (U)
Log (time-averaged power, L_f) erg s^{-1}	25.5 – 28.0 (B)*	25.8 – 28.3 (U)*
Log (total energy, E_t) erg	27.5 – 33.8 (B)*	27.6 – 34.0 (U)*
Log ($L_f / L_{quiet\ star}$)	(–1.9) – (–3.4) (B)	
Mean colors at maximum:		
$U-B$	+0.3 ± 0.4	
$B-V$	–0.9 ± 0.3	
Spectral index of occurrence rate (b) $[N(E_{\Delta t} > E) = E^{-b}\ (h^{-1})]$	0.4 – 1.1 (B)†	0.3 – 1.4 (U)†
Time distribution	Poisson-type with strong deviation within Δt < 10 minutes.	

*Systematically larger values for more luminous stars.
†Systematically smaller values for more luminous stars.

erg s^{-1} to less than 10^{27} erg s^{-1} for stars with absolute magnitude M_v equal to 7 and 16, respectively. This implies that, in intrinsically fainter dMe stars, the time-averaged energy dissipation through flares relative to the global energy budget of the star is about 2 orders of magnitude more important than in brighter stars and accounts for about 1 percent of the energy release of the optical region.

Optical spectroscopy of flares (cf. Figure 9-16) indicates that there is strong intensification of the H I, Ca II, He I, and occasionally He II (4686 Å) emission lines (cf. Gershberg, 1977; Worden, 1983; Giampapa, 1983b). The equivalent width of Hα (~2 Å) can increase by more than one order of magnitude during intense flares, and inverse Balmer decrements and large Balmer jumps (J ≃ 4-6) are sometimes observed. Line broadening and red asymmetry, indicating random motion of 10^7 to 10^8 cm s^{-1} and mass inflow at speeds of up to 1000 km s^{-1}, respectively, have also been observed but not in all cases (Bopp and Moffett, 1973; Worden et al., 1983). The line enhancement of the different species takes place on different time scales and can last 10 to 100 times longer than the continuum flare. The relative contribution of line emission to the continuum reaches a minimum at flare maximum (10 to 15 percent) and increases up to more than 40 percent in B-light as the flare decays. The optical flare plasma is characterized by electron densities ($N_e \approx 10^{12}$ to 10^{14} cm^{-3}) and temperatures ($T_e \approx 1.5$ to 2.0×10^4 K) ranging from solar values to much higher ones, depending on the model adopted. Typical emission measures and flare volume are 10^{52} cm^{-3} and 10^{26} cm^3, respectively. The relative timing of line and continuum enhancements investigated by Bopp and Moffett (1973) by simultaneous photometry and time-resolved spectroscopy, and more recently by Pettersen (1983b) using narrow filters centered at hydrogen Hα and Hβ emission lines and broadband U, B, V, and R filters, indicates that the emission lines peak a few minutes after the continuum and remain enhanced for several minutes or even hours, after the continuum has decayed to its preflare level.

UV spectra of stellar flares on dMe stars have recently been obtained with IUE (cf. Worden, 1983; Giampapa, 1983b, and references therein). More extended and systematic observations are now being collected. However, some interesting properties have already been found: (1) a strong UV continuum—normally absent—was detected on Gliese 867A (Butler

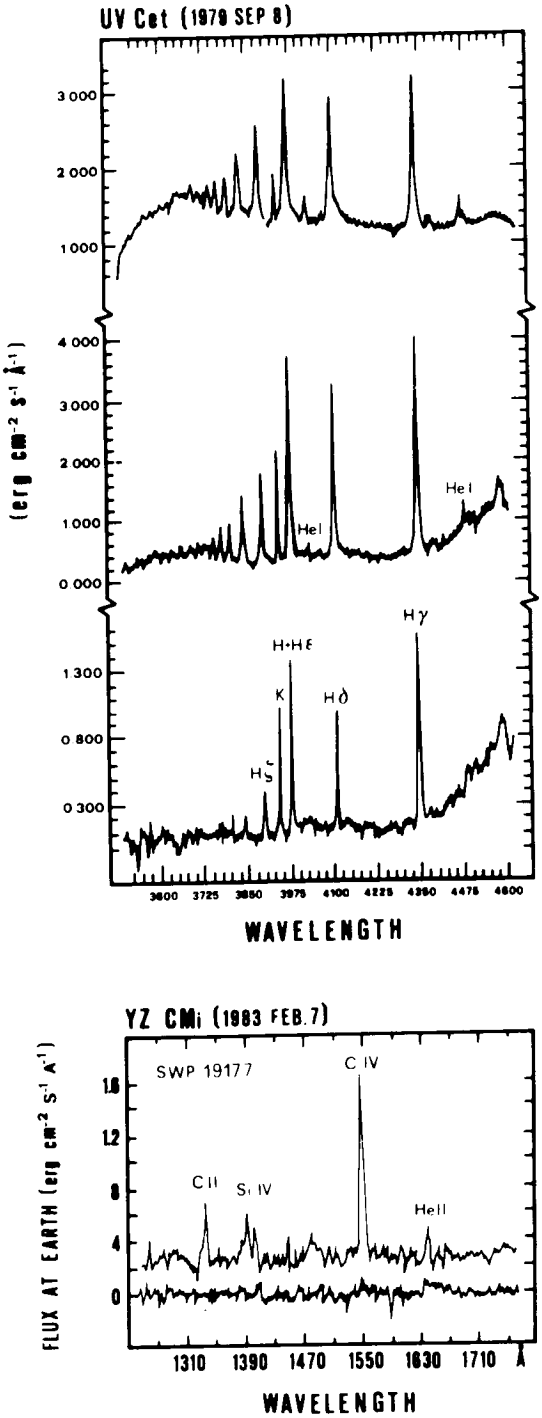


Figure 9-16. Flare and quiescent spectra of the dMe stars in the optical (Giampapa et al., unpublished) and UV spectral domains (unpublished data from coordinated observations made by the Armagh, Catania, and Boulder groups).

et al., 1981), YZ CMi (Figure 9-16), and Gliese 182 (unpublished data from coordinated observations by the Armagh, Boulder, and Catania groups); (2) the relative enhancement of transition region lines for flares and plages (as seen in disk-averaged fluxes) are comparable; (3) the relative emission enhancement is larger for transition region lines than for lower temperature chromospheric lines; (4) the line surface fluxes at the time of stellar flares, or from plages, can be up to more than one order of magnitude larger than those from very active regions on the Sun (Figure 9-10).

After occasional detection of *stellar X-ray flares*, several coordinated X-ray optical, and radio observations of flare and RS CVn stars have been carried out (cf. Haisch, 1983; Golub, 1983, and references therein). Comprehensive observations of a flaring event in YZ CMi (Figure 9-15) have clearly shown that the long-suspected similarity between solar and stellar flares is considerable (Kahler et al., 1982). A gradual and impulsive phase, an X-ray coronal temperature of about 10^7 K, and the appearance of a 408-MHz burst delayed by 17 minutes from the flare onset, are similar to the corresponding typical values for type IV solar bursts. Therefore, high-energy electrons might be produced in stellar flares in the same way as in the solar flares. Due to the high sensitivity and time resolution of these Einstein observations, much better than had ever been available before, it was possible to measure simultaneously the monotonic decay of the X-ray and optical flares and the variable but ever-increasing ratio between the soft X-ray and optical fluxes (L_x/L_c) for most of the flare decay phase. The average ratio over the entire event was 1.5. Coupled with the observed decay time of the X-ray flux, this suggested that radiation was the predominant mechanism for cooling the coronal plasma. However, previous estimates of the L_x/L_c ratio cover a wide range: from a few hundredths up to 50. Therefore, radiative cooling is not always predominant (i.e., different physical situations can develop in different flare events). Typical emission measures and densities $\sim 2 \times 10^{51}$

and 3×10^{11} cm^{-3}, respectively—suggest that the flare volume at coronal level is two orders of magnitude larger than that in the chromosphere.

Radio observations of flares on dMe stars have shown highly polarized radiation in the meter and cm wavelengths at brightness temperatures up to 10^{15} K in coincidence with several optical flares (Lovell, 1971; Spangler and Moffett, 1976; Melrose and Dulk, 1982; Gibson, 1983, and references therein). Basically, two types of flares have been observed: (1) impulsive events lasting from a few seconds to a few minutes, and (2) long-duration enhancement of the radio power lasting more than 10 minutes. Lang et al. (1983) have recently reported a rapid sequence of 100-percent left-hand circularly polarized spikes with rise times < 0.2 s during the gradual rise of a long-duration event on AD Leo. They derived lower limits for the linear size of the emitting region ($L > 6 \times 10^9$ cm) and of the brightness temperature ($T_B > 10^{13}$ K). These observations were explained by Lang et al. in terms of maser emission at the gyrofrequency $2.8 \times 10^6 \times H_\ell$ Hz, implying a longitudinal magnetic field $H_\ell \sim 250$ gauss. Typically, observed amplitudes for flares on nearby dwarfs range from detection limit to several tens of mJy. Although spectral indices are mainly strongly nonthermal (-2 to -10), positive spectral indices have also been reported (Gibson, 1983). The flare radio emission does not appear to be broadband, as in the quiescent phase, suggesting that the flare emission is due to coherent rather than incoherent synchrotron radiation. This is especially true for flares with brightness temperatures > 10^{12} K that are not compatible with incoherent emission mechanisms. The typical ratios of the optical and X-ray fluxes to the radio flux are 10^4 to 10^5 and < 10^3, respectively. Bearing in mind the moderate time-coincidence of flare peaks and evolution at the various wavelengths, any conclusion would be hazardous. Actually, no systematic correlation of flare amplitudes, morphology, and time of occurrence is apparent from simultaneous multiband observations. The most extended optical-radio coverage (Spangler and Moffett, 1976) indicates only a moderate tendency for radio and optical flares to be associated within ± 10 minutes. Most likely, as suggested by Spangler and Moffett (1976), highly beamed coherent synchrotron radio emissions imply severe geometrical constraints on the detection of radio flares. Moreover, the high occurrence rate of optical flares might hinder time-coincidence studies.

Activity Cycles

The observations of solar-type activity phenomena in late K–M dwarfs have naturally suggested that activity cycles might occur in the stars as in the Sun. Actually, as already anticipated in the section *Surface Inhomogeneities in the Photosphere*, Wilson's (1978) Ca II H and K emission-line observations have demonstrated the existence of activity cycles at the chromospheric level with time scales of 7 to 14 years. Hartmann and collaborators (cf. Hartmann, 1981, and references therein), by using the Harvard archival plate collection, have found evidence of possible cyclic photometric variations in a few well-known active dwarfs. These light variations are suggestive of starspot cycles with time scales of about 50 years. One of the red dwarfs which they studied (BD + 26° 730) is seen almost pole-on, so that its cyclic light variation can be entirely attributed to the variation of the total area covered by spots, as no rotational modulation of spot visibility can occur. For II Peg (Figure 9-17), they also found the analog of a Maunder minimum, the period of almost null solar activity, that occurred from 1645 to 1715.

Long-term cyclic suppression of convection by magnetic fields might give rise to the observed variability on time scales of the order of 10 years. Hartmann and Rosner (1979) argue that, other than spatial and spectral redistribution of the flux missing in the observed huge spotted areas, the present observations suggest that temporal redistribution of flux is more likely; the flux is temporarily stored beneath the photosphere and released when spots decay.

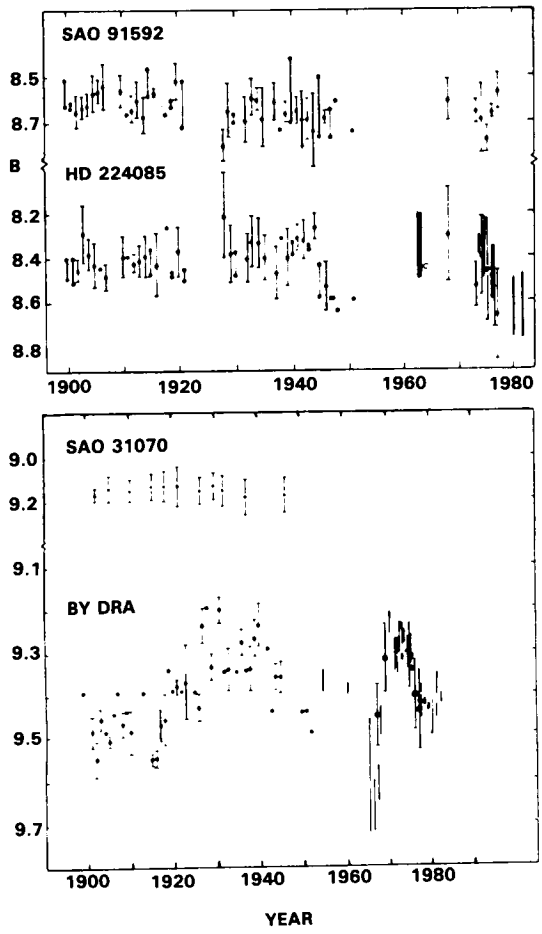


Figure 9-17. Long-term variability of II Peg (HD 224085) and BY Dra from Harvard archival plates (Hartmann et al., 1979b; Phillips and Hartmann, 1978) and from recent photoelectric photometry (Rodonò et al., 1983, and references therein). Dots denote Harvard plates and heavy bars denote range of season variability from photoelectric photometry. BY Dra shows a clear flux modulation with a possible cycle of about 50 years. II Peg was fairly constant from 1900 to 1945, when a definite light decrease occurred. The systematic light decrease from 1970 to 1982 suggests an ever-increasing degree of spottedness. This photometric behavior suggests that II Peg has become active after a relatively quiescent interval (1900–1945), which is reminiscent of the solar Maunder minimum.

The flare activity level on the Sun closely follows the activity cycle. Although all flare stars show significant variations of their seasonal activity level, no evidence of activity cycles has been obtained (Rodonò, 1980; Mavridis et al., 1982). Actually, the presently available data are not sufficiently extensive and systematically collected to reveal flare activity cycles. Incompleteness of data will remain serious as the short duration and random occurrence of flares make detection more dependent on observation methods and scheduling than is the case with relatively "permanent" spots. Moreover, theoretical models of activity cycles in late-type stars, particularly in M dwarfs, show that successive cycles overlap each other (Belvedere et al., 1980; Belvedere, 1984) so that any cycle-dependent variability is smoothed out. This is consistent with the decreasing number of stars showing evidence of activity cycles with advancing spectral type, although the level of activity increases, as suggested by their X-ray luminosity.

NONTHERMAL ENERGY SOURCES OF ACTIVITY AND CONCLUSIONS

As already mentioned in the preceding sections, activity signatures and transient variability phenomena on late-type dwarfs, particularly on dMe stars, indicate that their atmospheres are controlled by energy fluxes which are nonthermal or have a nonthermal origin. In fact, the solar analogy has suggested that the whole panoply of stellar activity phenomena is directly, or at least indirectly, linked to the intensity and structure of surface magnetic fields. Consequently, the manner in which stellar magnetic fields are usually generated and strengthened has called attention to such nonthermal energy sources as *convection, velocity fields, turbulence*, and *rotation*.

Stellar structure models (e.g., Grossman et al., 1974; Cox et al., 1981) have already shown that red dwarfs later than spectral types M4–M5 are fully convective, with perhaps a tiny radiative core.

Due to the faintness of M dwarfs and the fact that their spectra are overcrowded by molecular bands, spectroscopic studies of *turbulence* and *velocity fields* are scanty. The principal aim of line-profile fittings has been that of determining the stellar-projected rotational velocity, v sin i (Anderson et al., 1977; Vogt and Fekel, 1979; Vogt et al., 1983), rather than turbulence. Cross-correlation techniques based on the comparison of observed profiles with a reference mask also appear to be very promising (Lucke and Mayor, 1980). Most of the presently available *rotational velocity* data have been obtained from the study of periodic modulation of continuum and line fluxes which are attributed to photospheric spots and chromospheric/transition region plages, respectively, whose visibility is modulated by the star rotation (cf. reviews by Rodonò, 1983; Catalano, 1983; Pettersen, 1983a; Vaughan, 1983). The rotational velocity data of BY Dra stars indicate that active stars tend to be fast rotators (v sin i > 5 km s^{-1}). Whether fast rotation is a sufficient condition for spot formation is still an open question. The present evidence suggests that, when both rapid rotation and deep convection occur, the consequent differential rotation is a sufficient condition for stellar activity to occur. Actually, as predicted by the so-called α-ω dynamo (cf. Belvedere, 1983, and references therein), differential rotation generates a toroidal field (ω effect), and the twisting of field structures by the Coriolis force in a rotating star regenerates the poloidal field (α effect).

An indirect method of estimating stellar *differential rotation* is offered by photometric studies of active stars. Assuming starspots as tracers of stellar rotation, the variation of the "photometric wave" period as spots or the latitude of spot formation migrate on the stellar surface, together with topological data on the spot location from light-curve modeling, offers a potentially powerful method of estimating the stellar differential rotation (cf. Rodonò et al., 1983; Busso et al., 1984). Preliminary data have already been obtained and are included in Table 9-7. This approach will greatly benefit from space observations, as uninterrupted data extending over many rotations would permit, at least in principle, accurate estimations of differential rotation.

Several attempts have been made to find correlations between activity indicators such as data on Ca II, C IV, and X-ray fluxes, and rotation. (See the section *Ultraviolet, X-Ray, and Radio Data.*) Different authors have found different empirical correlations, which appear to be somewhat in conflict (Ayres and Linsky, 1980; Pallavicini et al., 1981; Ayres et al., 1981a; Catalano and Marilli, 1983; Noyes, 1983). Recently, Marilli and Catalano (1984) have rediscussed this matter by analyzing most of the available data on main-sequence stars. They were able to show that, irrespective of spectral types, the emission luminosities (L) in the K Ca II and C IV lines and in the soft X-ray domain are exponentially related to the stellar rotational period (P): $L = a\ 10^{-P/b}$, where a and b are numerical constants. This implies the important conclusion that the heating rates at chromospheric, transition region, and coronal levels are related. Moreover, the emission luminosities show a functional dependence on only the stellar angular velocity, as required by the α-ω dynamo theory. Mangeney and Praderie (1983) have carried out independently a similar investigation by studying the dependence of the X-ray to convective flux ratio (F_x/F_c) on an effective Rossby number defined as $R_o = V_m/(\alpha\omega\ell_c)$, where V_m is the maximum convective velocity, ω is the angular velocity, and ℓ_c is the depth of the convection zone. Again, an exponential correlation between these two parameters appears to be valid over a wide range of spectral types. However, for late F- to M-type dwarfs, the result by Mangeney and Praderie (1983) indicates a dependence also on the depth of convection zone (i.e., on the spectral type), in contrast to Marilli and Catalano's (1984) result. Only more extended and statistically complete data sets, together with progress on nonlinear α-ω dynamo theory calculations, can throw light on this matter.

Until recently, the missing piece of the increasingly coherent scenario of stellar activity

was the detection of surface *magnetic fields*. Robinson (1980) has employed the technique of comparing the profiles of magnetic sensitive and insensitive lines to measure the excess broadening due to the components of the Zeeman triplet originating in a magnetic field. The Robinson technique also allows us to estimate the ratio of magnetic-to-nonmagnetic areas (filling factor) from the relative enhancement of the central component with respect to the outer components (Figure 9-18). About 20 G-K dwarfs have detected magnetic fields in the range 500 to 3000 gauss with area filling factors ranging from 20 to 80 percent (Marcy, 1983; Giampapa and Worden, 1983). These data imply magnetic fluxes 2 to 3 orders of magnitude greater than the solar flux, which is consistent with the huge activity phenomena observed in these stars. Although the data are meager, they suggest some interesting qualitative conclusions: (1) the ratio of soft X-ray flux to bolometric flux increases as the photospheric magnetic area coverage increases (i.e., the photospheric magnetic fields control the stellar atmospheres up to coronal level); (2) the magnetic field flux increases toward later spectral types and with increasing rotational velocity, in qualitative agreement with the two basic requirements of the α–ω dynamo theory (Belvedere et al., 1981).

An additional indirect evidence that active star atmospheres are controlled by magnetic structures has recently been presented by Musielak and Bielicz (1982, 1983). From theoretical models of intense magnetic flux tubes (Bielicz and Musielak, 1982), they have shown that in active stars the atmospheric level of temperature minimum rises and the average magnetic field is higher than in nonactive stars. These models were used to compute the Ca II K line width (W_o) for both types of stars for the purpose of interpreting the corrected Wilson-Bappu effect, which takes into account the dependence of W_o on the intensity of the K line itself (Glebocki and Stawikowski, 1980). As already suggested by Zwaan (1977), the line width W_o is a powerful quantitative diagnostic

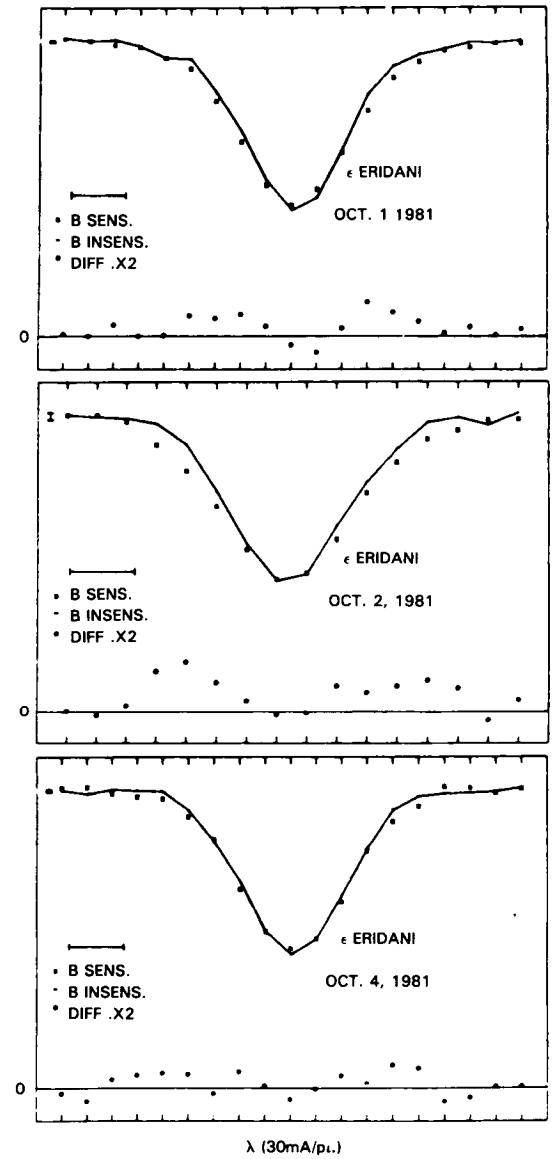


Figure 9-18. Comparison between the observed line profiles of the Zeeman sensitive line (6173.34 Å) and the insensitive line (6240.65 Å) of Fe I, represented by the dots and the continuous line, respectively. The bottom curve on each panel shows the difference between the two profiles, multiplied by 2. Observed changes in the difference profile suggest that the magnetic field on ε Eridanii changes on a time scale of 1 day (from Marcy, 1983).

of the average properties of the discrete magnetic flux tubes which permeate the atmospheres of active stars.

The observations reviewed in this chapter clearly indicate that a basic solar-type scenario underlies the nonthermal activity phenomena which occur in the atmospheres of late-type main-sequence stars, particularly late K-M emission-line dwarfs. This returns us to the fundamental concept presented in the introductory section on the scientific value of the two-way street connecting solar and stellar research in the study of nonthermal activity phenomena occurring in their atmospheres.

ACKNOWLEDGMENTS

I am grateful to several colleagues for stimulating and inspiring discussion and for permission to quote unpublished results, in particular to D. M. Gibson, J. L. Linsky, S. Catalano, G. Belvedere, L. Paterno, G. Cutispoto, and V. Pazzani. The last two colleagues also greatly assisted in the collection of data. I should like to thank A. Cali for drawing some of the illustrations and Mrs. M. G. Nastasi for accurately typing several drafts of this chapter.

The IUE and Einstein Observatory staffs deserve special mention for the sterling work done in assisting guest investigators, including myself, in the collection and reduction of UV and X-ray data.

Finally, I should like to acknowledge financial support from the *Ministero della Pubblica Istruzione* to the *Institute of Astronomy, Catania University,* and from the *Consiglio Nazionale delle Ricerche (Gruppo Nazionale di Astronomia)* to the *Osservatorio Astrofisico di Catania.*

REFERENCES

Abt, H.A., Meinel, A.B., Morgan, W.W., and Tapscott, J.M. 1968, *An Atlas of Low-Dispersion Grating Spectra* (Tucson: Kitt Peak National Obs.).

Allen, C.W. 1973, *Astrophysical Quantities* (London: Univ. of London, The Athlone Press).

Altenhoff, W.J., Braes, L.L.E., Olnon, F.F., and Wendker, H.J. 1976, *Astron. Astrophys.*, **46**, 11.

Anderson, C.M., Schiffer, F.M., and Bopp, B.W. 1977, *Astrophys. J.*, **216**, 42.

Arakelian, M.A. 1969, in *Proc. IVth IAU Colloq. on Variable Stars, Non-Periodic Phenomena in Variable Stars*, ed. L. Detre (Budapest: Academic Press), p. 161.

Ayres, T.R., Eriksson, K., Linsky, J.L., and Stencel, R.E. 1983, *Astrophys. J. (Letters)*, **270**, L17.

Ayres, T.R., and Linsky, J.L. 1980, *Astrophys. J.*, **241**, 279.

Ayres, T.R., Linsky, J.L., Vaiana, G.S., and Rosner, R. 1981a, *Astrophys. J.*, **250**, 293.

Ayres, T.R., Marstad, N.C., and Linsky, J.L. 1981b, *Astrophys. J.*, **247**, 545.

Bakos, G.A. 1983, *Astron. J.*, **88**, 674.

Baliunas, S.L., and Dupree, A.K. 1979, *Astrophys. J.*, **227**, 870.

Baliunas, S.L., and Dupree, A.K. 1982, *Astrophys. J.*, **252**, 668.

Baliunas, S.L., Hartmann, L., Vaughan, A.H., Liller, W., and Dupree, A.K. 1981, *Astrophys. J.*, **246**, 473.

Baliunas, S.L., Vaughan, A.H., Hartmann, L., Middelkoop, F., Mihalas, D., Noyes, R.W., Preston, W., Frazer, J., and Lanning, H. 1983, *Astrophys. J.*, **275**, 752.

Bappu, M.K.V., and Sivaraman, K.R. 1971, *Solar Phys.*, **17**, 316.

Barnes, T.J., and Evans, D.S. 1976, *Mon. Not. Roy. Astr. Soc.*, **174**, 316.

Barnes, T.J., Evans, D.S., and Parson, S.B. 1976, *Mon. Not. Roy. Astr. Soc.*, **174**, 503.

Bartolini, C., et al. 1983, *Astron. Astrophys.*, **117**, 149.

Basri, G.S., and Linsky, J.L. 1979, *Astrophys. J.*, **243**, 1023.

Basri, G.S., Linsky, J.L., Bartoe, J.-D.F., Brueckner, G., and Van Hooster, M.E. 1979, *Astrophys. J.*, **230**, 924.

Belvedere, G. 1983, in *Proc. IAU Colloq. 71, Activity in Red-Dwarf Stars*, ed. P.B. Byrne and M. Rodonò (Dordrecht: Reidel), p. 579.

Belvedere, G. 1984, *Astron. Nach.*, **305**, 237.

Belvedere, G., Chiuderi, C., and Paternó, L. 1981, *Astron. Astrophys.*, **96**, 369.

Belvedere, G., Paternó, L., and Stix, M. 1980, *Astron. Astrophys.*, **91**, 328.

Bielicz, E., and Musielak, Z. 1982, *Acta Astron.*, **32**, 251.

Blanco, C., Catalano, S., Marilli, E., and Rodonò, M. 1974, *Astron. Astrophys.*, **33**, 257.

Blanco, C., Catalano, S., Marilli, E., and Rodonò, M. 1982, *Astron. Astrophys.*, **106**, 301.

Bodenheimer, P. 1965, *Astrophys. J.*, **142**, 451.

Bohn, H.U. 1983, in *Proc. IAU Colloq. 71, Activity in Red-Dwarf Stars*, ed. P.B. Byrne and M. Rodonò (Dordrecht: Reidel), p. 605.

Bopp, B.W. 1974a, *Astrophys. J.*, **193**, 389.

Bopp, B.W. 1974b, *Mon. Not. Roy. Astr. Soc.*, **166**, 79.

Bopp, B.W. 1974c, *Pub. Astron. Soc. Pacific*, **86**, 281.

Bopp, B.W., and Espenak, F. 1977, *Astron. J.*, **82**, 916.

Bopp, B.W., and Evans, D.S. 1973, *Mon. Not. Roy. Astr. Soc.*, **164**, 343.

Bopp, B.W., and Fekel, F. 1974, *Pub. Astron. Soc. Pacific*, **86**, 978.

Bopp, B.W., and Fekel, F. 1977a, *Astron. J.*, **82**, 490.

Bopp, B.W., and Fekel, F. 1977b, *Pub. Astron. Soc. Pacific*, **89**, 65.

Bopp, B.W., and Moffett, T.J. 1973, *Astrophys. J.*, **185**, 239.

Bopp, B.W., Torres, C.A.O., Busko, I.C., and Quast, G.R. 1978, *Comm. 27 IAU, Inf. Bull. Var. Stars*, No. 1443.

Bumba, V., and Ruzickova-Topolova, B. 1967, *Solar Phys.*, **1**, 216.

Busko, I.C., and Torres, C.A.O. 1978, *Astron. Astrophys.*, **64**, 153.

Busso, M., Scaltriti, F., Blanco, C., Catalano, S., Marilli, E., Pazzani, V., and Rodonò, M. 1984, *Astron. Astrophys.*, **135**, 255.

Butler, C.J., Byrne, P.B., Andrews, A.D., and Doyle, J.G. 1981, *Mon. Not. Roy. Astr. Soc.*, **197**, 815.

Byrne, P.B. 1979, *Mon. Not. Roy. Astr. Soc.*, **187**, 153.

Byrne, P.B. 1983, in *Proc. IAU Colloq. 71, Activity in Red-Dwarf Stars*, ed. P.B. Byrne and M. Rodonò (Dordrecht: Reidel), p. 139.

Byrne, P.B., and Rodonò, M., ed. 1983, *Proc. IAU Colloq. 71, Activity in Red-Dwarf Stars* (Dordrecht: Reidel).

Catalano, S. 1983, in *Proc. IAU Colloq. 71, Activity in Red-Dwarf Stars*, ed. P.B. Byrne and M. Rodonò (Dordrecht: Reidel), p. 343.

Catalano, S., and Marilli, E. 1983, *Astron. Astrophys.*, **121**, 190.

Cester, B. 1965, *Mem. Soc. Astron. Ital.*, **36**, 215.

Chugainov, P.F. 1966, *Comm. 27 IAU, Inf. Bull. Var. Stars*, No. 122.

Chugainov, P.F. 1971, *Comm. 27 IAU, Inf. Bull. Var. Stars*, No. 520.

Chugainov, P.F. 1972, *Izv. Krim. Astrofiz. Obs.*, **46**, 14.

Chugainov, P.F. 1973, *Izv. Krim. Astrofiz. Obs.*, **48**, 3.

Chugainov, P.F. 1974, *Izv. Krim. Astrofiz. Obs.*, **52**, 3.

Chugainov, P.F. 1976a, *Izv. Krim. Astrofiz. Obs.*, **54**, 89.

Chugainov, P.F. 1976b, *Izv. Krim. Astrofiz. Obs.*, **55**, 85.

Coleman, G.D., and Worden, S.P. 1976, *Astrophys. J.*, **205**, 475.

Copeland, H., Jensen, J.O., and Jorgensen, H.E. 1970, *Astron. Astrophys.*, **5**, 12.

Cox, A.N., Shaviv, G., and Hodson, S.W. 1981, *Astrophys. J., (Letters)*, **245**, L37.

Cram, L.E., and Mullan, D.J. 1979, *Astrophys. J.*, **234**, 579.

Cristaldi, S., Gershberg, R.E., and Rodonò, M. 1980, *Astron. Astrophys.*, **89**, 123.

De Freitas Mourão, R.R. 1976, Astrophys. Letters, **18**, 37.

de la Reza, R., Torres, C.A.O., and Busko, I.C. 1981, *Mon. Not. Roy. Astr. Soc.*, **194**, 829.

Durney, B.R., Mihalas, D., and Robinson, R.D. 1981, *Pub. Astron. Soc. Pacific*, **93**, 537.

Einasto, J. 1954, *Pub. Tartu Astron. Obs.*, **32**, 37.

Einasto, J. 1955, *Pub. Tartu Astron. Obs.*, **33**, 57.

Evans, D.S. 1971, *Mon. Not. Roy. Astr. Soc.*, **154**, 329.

Fekel, F., Bopp, B.W., and Lacy, C.H. 1978, *Astron. J.*, **83**, 1445.

Ferland, G., and Bopp, B.W. 1976, *Pub. Astron. Soc. Pacific*, **88**, 451.

Ferraz Mello, S., and Torres, C.A.O. 1971, *Comm. 27 IAU, Inf. Bull. Var. Stars*, No. 577.

Fischer, P.L., and Gibson, D.M. 1982, in *Cool Stars, Stellar Systems and the Sun*, ed. M.S. Giampapa and L. Golub, SAO-SR 392, p. 109.

Friedmann, C., and Gürtler, J. 1975, *Astron. Nachr.*, **296**, 125.

Gary, D.E., and Linsky, J.L. 1981, *Astrophys. J.*, **250**, 284.

Gary, D.E., Linsky, J.L., and Dulk, G.A. 1982, *Astrophys. J. (Letters)*, **263**, L79.

Gatewood, G. 1976, *Icarus*, **27**, 1.

Gershberg, R.E. 1970, *Astrophysics*, **6**, 92.

Gershberg, R.E. 1974, *Sov. Astron.*, **18**, 326.

Gershberg, R.E. 1977, *Astrophysics*, **13**, 310.

Gershberg, R.E. 1983, in *Proc. IAU Colloq. 71, Activity in Red-Dwarf Stars*, ed. P.B. Byrne and M. Rodonò (Dordrecht: Reidel), p. 487.

Gershberg, R.E., and Shakhovskaya, N.I. 1974, *Izv. Krim. Astrofiz. Obs.*, **49**, 73.

Gershberg, R.E., and Shakhovskaya, N.I. 1976, *Astrophys. Space Sci.*, **44**, 463.

Giampapa, M.S. 1983a. in *Proc. IAU Symp. 102, Solar and Stellar Magnetic Fields: Origin and Coronal Effects*, ed. J.O. Stenflo (Dordrecht: Reidel), p. 187.

Giampapa, M.S. 1983b, in *Proc. IAU Colloq. 71, Activity in Red-Dwarf Stars*, ed. P.B. Byrne and M. Rodonò (Dordrecht: Reidel), p. 223.

Giampapa, M.S., Linsky, J.L., Schneeberger, T.J., and Worden, S.P. 1978, *Astrophys. J.*, **226**, 144.

Giampapa, M.S., and Worden, S.P. 1983, in *Proc. IAU Symp. 102, Solar and Stellar Magnetic Fields: Origins and Coronal Effects*, ed. J.O. Stenflo (Dordrecht: Reidel), p. 29.

Giampapa, M.S., Worden, S.P., and Gilliam, L.B. 1979, *Astrophys. J.*, **229**, 1143.

Giampapa, M.S., Worden, S.P., Schneeberger, T.J., and Cram, L.E. 1981, *Astrophys. J.*, **246**, 502.

Gibson, D.M. 1983, in *Proc. IAU Colloq. 71, Activity in Red-Dwarf Stars*, ed. P.B. Byrne and M. Rodonò (Dordrecht: Reidel), p. 273.

Glebocki, R., and Stawikowski, A. 1980, *Acta Astron.*, **30**, 285.

Gliese, W. 1958, *Z. Astrophys.*, **45**, 293.

Gliese, W. 1969, *Catalogue of Nearby Stars* (Heidelberg: Veroff. Astron. Rechen-Inst.), No. 22.

Golub, L. 1983, in *Proc. IAU Colloq. 71, Activity in Red-Dwarf Stars*, ed. P.B. Byrne and M. Rodonò (Dordrecht: Reidel), p. 83.

Gray, D.F. 1967, *Astrophys. J.*, **149**, 317.

Gray, D.F. 1968, *Astron. J.*, **73**, 769.

Greenstein, J.L., and Arp, H. 1969, *Astrophys. Letters*, **3**, 149.

Grossman, A.S., Hays, D., and Graboske, H.C., Jr. 1974, *Astron. Astrophys.*, **30**, 95.

Hackwell, J.A., Bopp, B.W., and Gehrz, R.D. 1974, *Astrophys. J. (Letters)*, **192**, L79.

Haisch, B.M. 1983, in *Proc. IAU Colloq. 71, Activity in Red-Dwarf Stars*, ed. P.B. Byrne and M. Rodonò (Dordrecht: Reidel), p. 255.

Haisch, B.M., and Simon, T. 1982, *Astrophys. J.*, **263**, 252.

Hall, D.S. 1981, in *Solar Phenomena in Stars and Stellar Systems*, ed. R.M. Bonnet and A.K. Dupree (Dordrecht: Reidel), p. 431.

Hallam, K.L., and Wolff, C.L. 1981, *Astrophys. J. (Letters)*, **248**, L73.

Harrington, R.S., and Behall, A.L. 1973, *Astron. J.*, **78**, 1096.

Hartmann, L. 1981, in *Solar Phenomena in Stars and Stellar Systems*, ed. R.M. Bonnet and A.K. Dupree (Dordrecht: Reidel), p. 487.

Hartmann, L. 1983, in *Achievements in Space Astrophysics*, ed. H.S. Hudson, A.K. Dupree, and J.L. Linsky, *Adv. Space Res.*, **2**, No. 9, 29.

Hartmann, L., and Anderson, C.M. 1977, *Astrophys. J.*, **215**, 188.

Hartmann, L., Davis, R., Dupree, A.K., Raymond, J., Schmidtke, P.C., and Wing, R.F. 1979a, *Astrophys. J. (Letters)*, **233**, L69.

Hartmann, L., Dupree, A.K., and Raymond, J.C. 1980, *Astrophys. J. (Letters)*, **236**, L143.

Hartmann, L., Dupree, A.K., and Raymond, J.C. 1982, *Astrophys. J.*, **252**, 214.

Hartmann, L., Londoño, C., and Phillips, M.J. 1979b, *Astrophys. J.*, **229**, 183.

Hartmann, L., and Rosner, R. 1979, *Astrophys. J.*, **230**, 802.

Heintz, W.D. 1972, *Astron. J.*, **77**, 160.

Heintz, W.D. 1974, *Astron J.*, **79**, 819.

Herbig, G. 1965, *Astrophys. J.*, **141**, 588.

Herbig, G. 1973, *Astrophys J.*, **182**, 129.

Hoxie, D.T. 1973, *Astron. Astrophys.*, **26**, 437.

Iwanowska, W. 1972, *Studia Soc. Sci. Torunensis*, **5**, 1.

Johnson, H.M. 1983, in *Proc. IAU Colloq. 71, Activity in Red-Dwarf Stars*, ed. P.B. Byrne and M. Rodonò (Dordrecht: Reidel), p. 109.

Johnson, H.M., and Cash, W.C., Jr. 1980, in *Cool Stars, Stellar Systems and the Sun*, ed. A.K. Dupree, SAO-SR 389, p. 137.

Joy, A.H., and Abt, H.A. 1974, *Astrophys. J.* Supplement, **28**, 1.

Kahler, S., et al. 1982, *Astrophys. J.*, **252**, 239.

Keenan, P.C., and McNeil, R.C. 1976, *An Atlas of Spectra of the Cooler Stars* (Chicago: Ohio Univ. Press).

Kelch, W.L., Linsky, J.L., and Worden, S.P. 1979, *Astrophys. J.*, **229**, 700.

Kodaira, K., and Ichimura, K. 1980, *Pub. Astron. Soc. Japan*, **32**, 451.

Kodaira, K., and Ichimura, K. 1982, *Pub. Astron. Soc. Japan*, **34**, 21.

Kron, G.E. 1950, *Astron. J.*, **55**, 69.

Kron, G.E. 1952, *Astrophys. J.*, **115**, 301.

Krzeminski, W. 1969, in *Low-Luminosity Stars*, ed. S.S. Kumar (New York: Gordon and Breach), p. 57.

Kulapova, A.N., and Shakhovskaya, N.I. 1973, *Izv. Krim. Astrofiz. Obs.*, **48**, 31.

Kunkel, W.E. 1970, *Astrophys. J.*, **161**, 503.

Kunkel, W.E. 1972, *Comm. 27 IAU, Inf. Bull. Var. Stars*, No. 748.

Kunkel, W.E. 1975, in *Proc. IAU Symp. 67, Variable Stars and Stellar Evolution*, ed. V.E. Sherwood and L. Plaut (Dordrecht; Reidel), p. 15.

Lacy, C.M. 1977a, *Astrophys. J.*, **218**, 444.

Lacy, C.M. 1977b, *Astrophys. J. Supplement*, **34**, 479.

Lacy, C.M., Moffett, T.J., and Evans, D.S. 1976, *Astrophys. J. Supplement*, **30**, 85.

Lang, K.R., Bookbinder, J., Golub, L., and Davis, M.M. 1983, *Astrophys. J. (Letters)*, **272**, L15.

Leung, K.C., and Schneider, D.P. 1978, *Astron. J.*, **83**, 618.

Liebert, J., Dahn, C.C., Gresham, M., and Strittmatter, P.A., 1979, *Astrophys. J.*, **233**, 226.

Linsky, J.L. 1980a, *Ann. Rev. Astron. Astrophys.*, **18**, 439.

Linsky, J.L. 1980b, in *Cool Stars, Stellar Systems and the Sun*, ed. A.K. Dupree, SAO-SR 389, p. 217.

Linsky, J.L. 1983a, in *Proc. IAU Colloq. 71, Activity in Red-Dwarf Stars*, ed. P.B. Byrne and M. Rodonò (Dordrecht: Reidel), p. 39.

Linsky, J.L. 1983b in *Proc. IAU Symp. 102, Solar and Stellar Magnetic Fields: Origin and Coronal Effects*, ed. J.O. Stenflo (Dordrecht: Reidel), p. 313.

Linsky, J.L., and Ayres, T.R. 1978, *Astrophys. J.*, **220**, 619.

Linsky, J.L., Bornmann, P.L., Carpenter, K.G., Wing, R.F., Giampapa, M.S., and Worden, S.P. 1982, *Astrophys. J.*, **260**, 670.

Linsky, J.L., and Gary, D.E. 1983, *Astrophys. J.*, **274**, 776.

Linsky, J.L., and Haisch, B.M. 1979, *Astrophys. J. Supplement*, **229**, 27.

Linsky, J.L., Worden, S.P., McClintock, W., and Robertson, R.M. 1979, *Astrophys. J. Supplement*, **41**, 47.

Lippincott, S.L. 1953, *Astron. J.*, **58**, 135.

Lippincott, S.L. 1971, in *Proc. IAU Colloq. 15, New Directions and New Frontiers in Variable Stars Research* (Bamberg: Veroff Remeis-Sternwarte), Band IX, Nr. 100, p. 109.

Lippincott, S.L. 1975, *Astron. J.*, **80**, 831.

Lippincott, S.L. 1978, *Space Sci. Rev.*, **22**, 153.

Lippincott, S.L., and Hershey, J.L. 1972, *Astron. J.*, **77**, 679.

Lovell, B. 1971, *Quart. J. Roy. Astr. Soc.*, **12**, 98.

Lucke, P.B., and Mayor, M. 1980, *Astron. Astrophys.*, **92**, 182.

Luyten, W.J. 1968, *Mon. Not. Roy. Astr. Soc.*, **139**, 221.

Mangeney, A., and Praderie, F. 1983, in *Proc. Japan-France Seminar, Active Phenomena in the Outer Atmospheres of the Sun and Stars*, ed. J.C. Pecker and Y. Uchida (Paris: CNRS-Obs. Paris), p. 96.

Marcy, G.W. 1983, in *Proc. IAU Symp. 102 Solar and Stellar Magnetic Fields: Origin and Coronal Effects*, ed. J.O. Stenflo (Dordrecht: Reidel), p. 3.

Marilli, E., and Catalano, S. 1984, *Astron. Astrophys.*, **133**, 57.

Mavridis, L.N., Asteriadis, G., and Mahmoud, F.M. 1982, in *Compendium in Astronomy*, ed. E.G. Mariopoloulos, T.S. Theocaris, and L. Mavridis (Dordrecht: Reidel), p. 253.

Melrose, D.B., and Dulk, G.A. 1982, *Astrophys. J.*, **259**, 844.

Moffett, T.J. 1972, *Nature Phys. Sci.*, **240**, 41.

Mould, J.R. 1978, *Astrophys. J.*, **276**, 923.

Mullan, D.J. 1975a, *Pub. Astron. Soc. Pacific*, **87**, 455.

Mullan, D.J. 1975b, *Astrophys. J.*, **200**, 641.

Mullan, D.J. 1976, *Irish Astron. J.*, **12**, 641.

Mullan, D.J. 1977, *Solar Phys.*, **54**, 183.

Mullan, D.J. 1979, *Astrophys. J.*, **234**, 558.

Mullan, D.J. 1983, in *Proc. IAU Colloq. 71, Activity in Red-Dwarf Stars*, ed. P.B. Byrne and M. Rodonò (Dordrecht: Reidel), p. 527.

Musielak, Z. and Bielicz, E. 1982, *Acta Astron.*, **32**, 263.

Musielak, Z., and Bielicz, E. 1983, in *Proc. IAU Symp. 102, Solar and Stellar Magnetic Fields: Origin and Coronal Effects*, ed. J.O. Stenflo (Dordrecht: Reidel), p. 413.

Noyes, R.W. 1983, in *Proc. IAU Symp. 102, Solar and Stellar Magnetic Fields: Origin and Coronal Effects*, ed. J.O. Stenflo (Dordrecht: Reidel), p. 133.

Oranje, B.J. 1983a, *Astron. Astrophys.*, **122**, 88.

Oranje, B.J. 1983b, *Astron. Astrophys.*, **124**, 43.

Oranje, B.J., Zwaan, C., and Middelkoop, F. 1982, *Astron. Astrophys.*, **110**, 30.

Oskanyan, V.S., Evans, D.S., Lacy, C.M., and McMillan, R.S. 1977, *Astrophys. J.*, **214**, 430.

Pallavicini, R., Golub, L., Rosner, R., Vaiana, G.S., Ayres, T., and Linsky, J.L. 1981, *Astrophys. J.*, **248**, 279.

Pazzani, V., and Rodonò, M. 1981, *Astrophys. Space Sci.*, **27**, 347.

Pettersen, B.R. 1983a, in *Proc. IAU Colloq. 71, Activity in Red-Dwarf Stars*, ed. P.B. Byrne and M. Rodonò (Dordrecht: Reidel), p. 17.

Pettersen, B.R. 1983b, in *Proc. IAU Colloq. 71, Activity in Red-Dwarf Stars*, ed. P.B. Byrne and M. Rodonò (Dordrecht: Reidel), p. 239.

Pettersen, B.R., and Coleman, L.A. 1981, *Astrophys. J.*, **251**, 571.

Pettersen, B.R., Kahler, S., Golub, L., and Vaiana, G.S. 1980, in *Cool Stars, Stellar Systems and the Sun*, ed. A.K. Dupree, SAO-SR 389, p. 113.

Pettersen, B.R., Kern, G.A., and Evans, D.S. 1983, *Astron. Astrophys.*, **123**, 184.

Phillips, M.J., and Hartmann, L. 1978, *Astrophys. J.*, **224**, 182.

Probst, R.G. 1977, *Astron. J.*, **82**, 656.

Renzini, A., Cacciari, C., Ulmschneider, P., and Schmitz, F., 1977, *Astron. Astrophys.*, **61**, 39.

Robinson, R.D. 1980, *Astrophys. J.*, **239**, 961.

Robinson, E.L., and Kraft, R.D. 1974, *Astron. J.*, **79**, 698.

Rodonò, M. 1976, in *Proc. IAU Symp. 71, Basic Mechanisms of Solar Activity*, ed. V. Bumba (Dordrecht: Reidel), p. 475.

Rodonò, M. 1978, *Astron. Astrophys.*, **66**, 175.

Rodonò, M. 1980, *Mem. Soc. Astron. Ital.*, **51**, 623.

Rodonò, M. 1981, in *Photometric and Spectroscopic Binary Systems*, ed. E.B. Carling and Z. Kopal (Dordrecht: Reidel), p. 285.

Rodonò, M. 1983, in *Achievements in Space Astrophysics*, ed. H.S. Hudson, A.K. Dupree, and J.L. Linsky, *Adv. Space. Res.*, **2**, No. 9, 225.

Rodonò, M., Catalano, S., Byrne, P.B., Doyle, J.G., Andrews, A.D., Butler, C.J., Linsky, J.L., Marstad, N., Simon, T., and Neff, J. 1985, in progress.

Rodonò, M., Pazzani, V., and Cutispoto, G. 1983, in *Proc. IAU Colloq. 71, Activity in Red-Dwarf Stars*, ed. P.B. Byrne and M. Rodonò (Dordrecht: Reidel), p. 179.

Rodonò, M., Pucillo, M., Sedmak, G., and de Biase, G.A. 1979, *Astron. Astrophys.*, **76**, 242.

Rodonò, M., Romeo, G., and Strazzulla, G. 1980, in *Proc. Second European IUE Conference*, ESA SP-157, p. 55.

Rosner, R. 1983, in *Proc. IAU Colloq. 71, Activity in Red-Dwarf Stars*, ed. P.B. Byrne and M. Rodonò (Dordrecht: Reidel), p. 5.

Rosner, R., Golub, L., and Vaiana, G.S. 1983, Center for Astrophys., Preprint 1719, in press.

Rucinski, S.M. 1977, *Pub. Astron. Soc. Pacific*, **89**, 280.

Rydgren, A.E., and Vrba, F.J. 1983, *Astrophys. J.*, **267**, 191.

Scharlemann, E.T. 1981, *Astrophys. J.*, **246**, 305.

Scharlemann, E.T. 1982, *Astrophys. J.*, **253**, 298.

Serio, S., Vaiana, G.S., Blanco, C., Catalano, S., Marilli, E., and Rodonò, M. 1985, *Astrophys. J.* (submitted).

Shakhovskaya, N.I. 1975, *Izv. Krim. Astrofiz. Obs.*, **53**, 165.

Shakhovskaya, N.I. 1979, *Bull. Crimean Astrophys. Obs.*, **60**, 10.

Shine, R.A., and Linsky, J.L. 1974, *Solar Phys.*, **39**, 49.

Sienkiewicz, R. 1982, *Acta Astron.*, **32**, 275.

Simon, T., Linsky, J.L., and Stencel, R.E. 1982, *Astrophys. J.*, **257**, 225.

Skumanich, R. 1972, *Astrophys. J.*, **171**, 565.

Spangler, S.R., and Moffett, T.J. 1976, *Astrophys. J.*, **203**, 497.

Staller, R.F.A. 1976, *Astron. Astrophys.*, **50**, 159.

Stein, R.F. 1967, *Solar Phys.*, **2**, 385.

Stencel, R.E. 1978, *Astrophys. J. (Letters)*, **223**, L37.

Stencel, R.E., and Mullan, D.J. 1980, *Astrophys. J.*, **238**, 221.

Stenflo, J.O., ed. 1983, *Proc. IAU Symp. 102, Solar and Stellar Magnetic Fields: Origin and Coronal Effects* (Dordrecht: Reidel).

Stimets, R.W., and Giles, R.H. 1980, *Astrophys. J. (Letters)*, **242**, L37.

Stokes, R.N. 1971, *Mon. Not. Roy. Astr. Soc.*, **152**, 165.

Thé, P.S., and Staller, R.F.A. 1974, *Astron. Astrophys.*, **36**, 155.

Tomkin, J. 1972, *Mon. Not. Roy. Astr. Soc.*, **156**, 349.

Topka, K., and Marsh, K.A. 1982, *Astrophys. J.*, **254**, 641.

Torres, C.A.O., and Ferraz Mello, S. 1973, *Astron. Astrophys.*, **27**, 231.

Torres, C.A.O., Ferraz Mello, S., and Quast, G.R. 1972, *Astrophys. Letters*, **11**, 3.

Ulmschneider, P., and Bohn, H.U. 1981, *Astron. Astrophys.*, **254**, 173.

Upgren, A.R. 1978, *Astron. J.*, **83**, 626.

Vaiana, G.S. 1981, Institute of Space and Astronautical Science, Report No. 597, Japan.

Vaiana, G.S., et al. 1981, *Astrophys. J.*, **245**, 163.

Vaiana, G.S., and Rosner, R. 1978, *Ann. Rev. Astron. Astrophys.*, **16**, 393.

van de Kamp, P. 1968, *Am. Soc. Pacific Leaflets*, No. 470.

van de Kamp, P. 1971, *Ann. Rev. Astron. Astrophys.*, **9**, 103.

van Leeuwen, F., and Alphenaar, P. 1983, in *Proc. IAU Colloq. 71, Activity in Red-Dwarf Stars*, ed. P.B. Byrne and M. Rodonò (Dordrecht: Reidel), p. 189.

Vaughan, A.H. 1983, in *Proc. IAU Symp. 102, Solar and Stellar Magnetic Fields: Origin and Coronal Effects*, ed. J.O. Stenflo (Dordrecht: Reidel), p. 113.

Vaughan, A.H., Baliunas, S.L., Middelkoop, F., Hartmann, L.W., Mihalas, D., Noyes, R.W., and Preston, G.W. 1981, *Astrophys. J.*, **250**, 276.

Veeder, G.J. 1974a, *Astron. J.*, **79**, 702.

Veeder, G.J. 1974b, *Astron. J.*, **79**, 1056.

Vernazza, J.E., Avrett, E.H., and Loeser, R. 1981, *Astrophys. J. Supplement*, **45**, 635.

Vogt, S.S. 1975, *Astrophys. J.*, **199**, 418.

Vogt, S.S. 1981a, *Astrophys. J.*, **247**, 975.

Vogt, S.S. 1981b, *Astrophys. J.*, **250**, 327.

Vogt, S.S. 1983, in *Proc. IAU Colloq. 71, Activity in Red-Dwarf Stars*, ed. P.B. Byrne and M. Rodonò (Dordrecht: Reidel), p. 137.

Vogt, S.S., and Fekel, F. 1979, *Astrophys. J.*, **234**, 958.

Vogt, S.S., Soderblom, D.R., and Penrod, G.D. 1983, *Lick Obs. Bull.*, Preprint.

Vyssotsky, A.N., and Dyer, E.R. 1957, *Astrophys. J.*, **125**, 297.

Walter, F.M. 1982, *Astrophys. J.*, **253**, 745.

Walter, F.M., Gibson, D.M., and Basri, G.S. 1983, *Astrophys. J.*, **267**, 665.

Weiler, E.J., Owen, F.N., Bopp, B.W., Schmitz, M., Hall, D.S., Fraquelli, D.A., Piirola, V., Ryle, M., and Gibson, D.M. 1979, *Astrophys. J.*, **225**, 919.

White, O.R., and Livingston, W.C. 1981, *Astrophys. J.*, **249**, 798.

Wielen, R. 1974, in *Highlights of Astronomy*, **3**, 395.

Wilson, O.C. 1963, *Astrophys. J.*, **138**, 832.

Wilson, O.C. 1973, in *Proc. IAU Colloq. 19, Stellar Chromospheres*, ed. S.D. Jordan and E.H. Avrett, NASA SP-317, p. 305.

Wilson, O.C. 1978, *Astrophys. J.*, **226**, 379.

Wooley, R., Epps, E.A., Penston, M.J., and Pocock, S.B., 1970, *Catalogue of Stars Within Twenty-Five Parsecs of the Sun*, Roy. Obs. Ann., No. 5.

Worden, S.P. 1974, *Pub. Astron. Soc. Pacific*, **86**, 595.

Worden, S.P. 1983, in *Proc. IAU Colloq. 71, Activity in Red-Dwarf Stars*, ed. P.B. Byrne and M. Rodonò (Dordrecht: Reidel), p. 207.

Worden, S.P., and Peterson, B.M. 1976, *Astrophys. J. (Letters)*, **206**, L145.

Worden, S.P., Schneeberger, T.J., and Giampapa, M.S. 1981, *Astrophys. J. Supplement*, **46**, 159.

Worden, S.P., Schneeberger, T.J., Giampapa, M.S., Deluca, E.E., and Cram, L.E. 1983, *Astrophys. J.*, **276**, 270.

Worley, C.E., and Behall, A.L. 1973, *Astron. J.*, **78**, 650.

Zappala, R.R. 1974, *Astrophys. J.*, **187**, 257.

Zwaan, C. 1977, *Mem. Soc. Astron. Ital.*, **48**, 525.

N88-11602

10

M DWARFS: THEORETICAL WORK

Dermott J. Mullan

MODEL PHOTOSPHERES

Theoretical work on the atmospheres of M dwarfs has progressed along lines parallel to those followed in the study of other classes of stars. The earliest work was aimed solely at constructing models of the photosphere, in which the only relevant energy fluxes were considered to be thermal (radiative plus convective). Such models have become increasingly sophisticated as improvements in opacities, in the equation of state, and in the treatment of convection have been incorporated during the last 15 to 20 years. As a result, spectrophotometric data on M dwarfs can now be fitted rather well by current models. The section *Thermal Model Atmospheres of Normal M Dwarfs* summarizes the various attempts at modeling M dwarf photospheres in purely thermal terms. Some extensions of these models to include (in an ad hoc manner) the effects of microturbulence and magnetic inhomogeneities are summarized in the sections *Quasi-Thermal Model Photospheres of dM Stars* and *Quasi-Thermal Model Photospheres of dMe Stars*. The thermal models can be constrained not only by predictions of *emergent* radiation, but also by carrying the integrations *inward* and constructing credible models of the entire star. In this regard, the M dwarfs are in a somewhat unique position because they bracket the mass range in which main-sequence stars are believed to become completely convective. Slight errors in surface parameters and in modeling techniques can lead to large uncertainties in the interior structure (because one picks out the wrong adiabat near the surface). Thus, M dwarfs may allow one to check the constitutive thermal physics which enter into the study of all stars. These points are summarized in the section *Thermal Models of Internal Structure*, which is aimed at placing atmospheric studies in perspective. The chromospheric and coronal phenomena have dominated the literature on M dwarfs so much in recent years that one is tempted to lose sight of the ultimate origin of the energy which makes these phenomena possible: nuclear processes in the deep interior. Although the interior processes are believed to be entirely thermal in nature and therefore supposedly readily amenable to modeling, it appears that significant uncertainties still persist in our knowledge of the internal structure of M dwarfs. Thus, even the thermal models of M dwarfs require further study.

Despite the successes which the thermal models have had, nonthermal processes also make a contribution to the physics of M dwarf atmospheres. The first flare (in continuum light) in an M dwarf was recognized some 60 years ago, and as data were accumulated on such events, an increasing amount of attention was paid to the similarities between these events and transient brightenings (in chromospheric

PRECEDING PAGE BLANK NOT FILMED

PAGE 454 INTENTIONALLY BLANK

lines) in the Sun. The latter represent the most spectacular form of nonthermal energy release in the Sun. Of course, other evidence for the presence of nonthermal energy in the solar atmosphere is provided by the presence of a corona and chromosphere even outside flares. In fact, the question of where one draws a dividing line between flares and coronal heating in the Sun has received much attention recently (Lin et al., 1984; Porter et al., 1984), and no definitive answer is presently available. Precisely the same question arises in the M dwarfs (Doyle and Butler, 1985; Butler and Rodonò, 1985): their prominent flare activity is not the only evidence of nonthermal processes in the atmosphere. During even the earliest years of stellar spectroscopic classification, certain M dwarfs distinguished themselves from most other cool stars by the presence of prominent emission lines of hydrogen. (Emission in the cores of the calcium lines was also known, but this is an almost ubiquitous feature of cool stars.) The Balmer emission lines provided the first clear sign that modeling the atmospheres of all M dwarfs in terms of purely thermal energy fluxes would be inadequate; at least a chromosphere would have to be provided to account for the hydrogen emission. In order to model the nonthermal processes, the first step is to determine the requirements of nonthermal energy fluxes in the chromosphere; this process has gotten under way in the last few years. (See the section *Semiempirical Chromospheric Models.*) The second step is harder: to identify the source of the nonthermal energy and model it in physically realistic ways. This step has not yet been solved, although a surprising recent development is of major interest in this regard. X-ray data from the Einstein satellite have indicated that many M dwarfs emit large fluxes of X rays; in fact, when expressed as fractions of the bolometric flux, the M dwarfs emit more X rays than any other cool stars. (See the section *Semiempirical Transition Region and Coronal Models.*) In fact, the *corona* in an M dwarf may be supplied with even more nonthermal energy than the chromosphere in that star. Astronomers who are interested in bolometric magnitudes with an accuracy of 0.01 magnitude must now include the X-ray emission from the corona if they are to achieve such precision in the case of many M dwarfs. (See the section *Nonthermal Models of M Dwarf Atmospheres.*) The strong coronae in M dwarfs, in which flaring activity is also pronounced, have once again raised the question of whether or not a dividing line exists between coronal heating and flaring (Mullan, 1979; Doyle and Butler, 1985; Butler and Rodonò, 1985). Models for flares in M dwarfs are presently available only in outline form. (See the section *Semiempirical Flare Models.*)

Thermal Model Atmospheres of Normal M Dwarfs

The combination of high gravity and low effective temperatures in red dwarfs ensures copious molecular formation. By "copious," we mean that the number density of molecules (eg., H_2) becomes a significant fraction of the atomic number density (e.g., H), or even exceeds it at certain levels in the atmosphere (see Figure 10-1). With the new degree of freedom associated with the molecules, the equation of state is altered. Thus, as well as the well-known convective instability associated with the ionization of abundant *atomic* species deep in the photosphere ($\tau_{5000} \gtrsim 1$), dissociation of abundant *molecules* (especially H_2) creates a new convective instability at rather high levels of the photosphere ($\tau_{5000} < 0.1$). Historically, model atmospheres of M dwarfs have evolved in the direction of attempting to incorporate the double complexities of molecule formation and optically thin convection with increasing realism. Dust may also form in the coolest stars if no chromosphere is present. Molecules and dust have an especially serious effect in the opacities, increasing them by up to 10^5 relative to the purely atomic values (Bohn, 1981).

The earliest thermal model atmosphere of an M dwarf (Tsuji, 1966) ignored convection altogether, but included opacities due to H_2O, H_2, and CO. Vardya (1966) treated convection, using the mixing-length formalism of

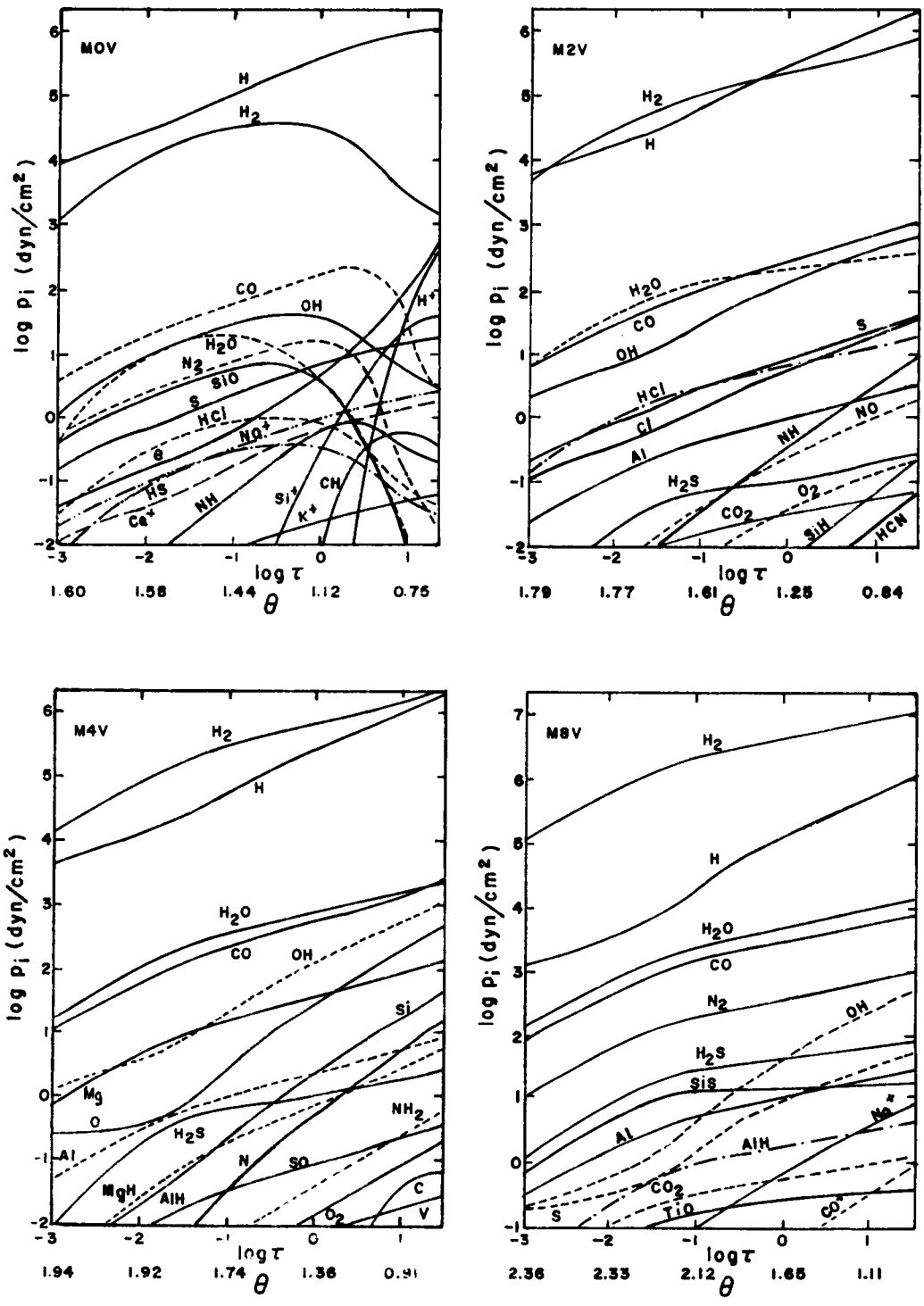


Figure 10-1. Variation of relative abundances of molecules as a function of depth in the model atmospheres of Vardya (1966). Abscissa scales are log (continuum optical depth) and θ = 5040/T. Ordinates are partial pressures of various species. Results for M0, M2, M4, and M8 dwarfs are shown for selected molecular species.

Henyey et al. (1965), and derived thermal models in which the molecular equilibrium of 160 species (including TiO, CaH, MgH) were subsequently evaluated (see Figure 10-1). Vardya felt that it would be premature to attempt to iterate the convective/molecular equations (including molecular opacities) because of deficiencies in, for example, the convection treatment and in "missing opacity" (Vardya and Böhm, 1965). Heavy line blanketing by overlapping lines is difficult to incorporate when so many different molecular species are present in the atmosphere. Thus, it is almost inevitable that one misses some important sources of opacity. Nevertheless, Vardya's results are important in that they suggest that molecular hydrogen is the dominant species throughout the atmosphere (rather than atomic hydrogen) at spectral types M4 and later ($T_{eff} < 3230$ K).

Kandel (1967a, 1967b) included even more molecular species than Vardya (1966). Kandel was concerned about the presence of a density inversion in some earlier model photospheres: he thought this might be attributed to deficiencies in the standard mixing-length formalism of convection (in which the mixing-length parameter $\alpha = L/H_p$ is kept constant at all depths). He therefore devised a modified mixing-length formalism in which the parameter α is allowed to vary with depth in such a way that the density inversion is just eliminated. (This is Kandel's "minimum convection condition.") He found that α must vary greatly with depth (by factors of 10^4). Radiative fluxes from the models were found to fit R–I colors well, but predicted colors at shorter and longer wavelengths became increasingly poor, presumably due to lack of major sources of line opacity. In recent years, it has become apparent that the presence of a density inversion in a model may have little or nothing to do with errors in the mixing-length theory: a detailed 2-D treatment of the Navier-Stokes equation shows that a density inversion is a natural feature of a convection zone where hydrogen is ionizing, at least in the warmer stars, A5 and F0 (Chan and Sofia, 1984).

A better treatment of H_2O line opacity (due to Auman) allowed Hershey (1968) to obtain more realistic emergent flux distributions from his models: Hershey's predicted continua show radical departures from Planck behavior around $\lambda = 1\ \mu$. To obtain flux-constant models, Hershey used the Avrett-Krook temperature correction method, but with the important addition of convection (with constant $\alpha = 1$). Inclusion of convection had the computational effect that convergence to flux constancy was considerably more difficult to achieve than in the purely radiative case. In the coolest models ($T_{eff} = 3200$ K), convection was found to carry 10 percent of the flux already at very high levels in the photosphere ($\tau = 0.05$). Hershey concluded that, because of the efficiency of convection even in the high photosphere, it is not permissible to scale the $T(\tau)$ relation from the Sun to the stars with $T_{eff} < 4000$ K. Hershey used his models to compute the wings of strong lines (Ca I 4226, Na D, Hα, Mg Ib, Ca H+K) and was successful with Hα and Na D. (Notice that only the wings can be computed reliably by these purely photospheric models.) However, he also found (cf. Vardya and Böhm, 1965) that, at λ4226 Å, there must be "missing opacity" which is several times larger than the known continuous opacity.

Auman (1969) applied his extensive H_2O opacity calculations to cool stars. He devised a method of replacing a large number of closely spaced lines by a representative mean opacity; this was an important step forward in modeling the thermal photospheres of cool dwarfs. Auman found that, in dwarfs, H_2O is the dominant source of opacity at $T_{eff} < 2520$ K. In the equation of state, Auman calculated molecular equilibria for 58 species (not including TiO, although bands of TiO are prominent in M dwarf spectra (cf. Figure 10-2)). In the presence of H_2O, the surface temperatures fall below the values which would occur (in a star of given T_{eff}) without H_2O; this occurs because H_2O opacity reaches its maximum on the redward side of the Planck peak in these stars. Auman commented on the difficulties of

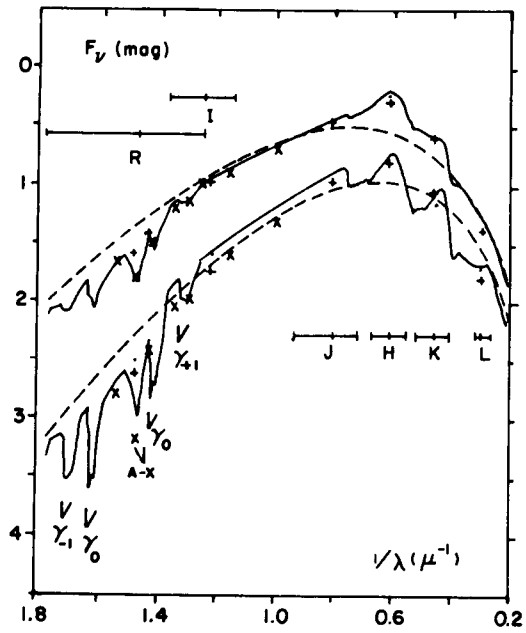


Figure 10-2. Emergent fluxes from models with T_{eff} = 3750 and 3250 K are shown by solid lines (Mould, 1976). Broadband photometry and scans of two stars, Yale 4794 and Yale 3501, are denoted by + and x, Yale 4794 being above. Half-power bandpasses of broadband filters are shown. Also shown are bands of TiO (γ and γ' systems ΔV = 0 and 1) and CaH. Dashed curves are from blackbody radiators of equal total flux.

applying his model predictions to observed fluxes. The predicted emergent fluxes have been determined to be sensitive to the way in which one derives a mean opacity (i.e., whether one uses a straight mean or a harmonic mean of the $\sim 10^6$ lines in Auman's case). Moreover, the wavelength dependence of the dominant absorbers (H^- and H_2O) are different, and the predicted spectral shape depends on where the opacities "cross over." In turn, the latter depends on the metal abundances (controlling free electrons) and on the competition of C, Si, and H for the oxygen atoms. Since metal abundances in M dwarfs may differ from solar by 2 to 3 (Mould, 1978), these can affect the atmospheric structure by several hundred degrees (Carbon, 1979). Lack of TiO in these models makes Auman's colors less accurate in the visible region.

Mould (1976) computed an extensive grid of models combining Tsuji's molecular equilibria (including even more molecular species than Vardya did) with the ATLAS model atmosphere code. By allowing for atomic and molecular line blanketing (which redistributes emergent flux across the spectrum), Mould obtained emergent spectra which could be fitted rather well to RIJHKL filter data for several M dwarfs (see Figure 10-2). In particular, note that the strong TiO bands and H_2O bands appear prominently in the emergent fluxes from Mould's models. By matching many colors of each star to the colors predicted by the models according to certain weighting functions (determined by temperature sensitivity), Mould and Hyland (1976) exploited information contained in many bandpasses, distributed across a broad spectral range, to derive T_{eff} values for 20 M dwarfs with an accuracy of ± 100 K at 4000 K and ± 200 K at 2850 K. These represent substantial improvements in accuracy compared to deriving T_{eff} by fitting a single observed color, say R–I, to the predicted color of a model. A striking colorimetric feature which emerged from Mould's work is shown in Figure 10-3: the J–H color of dwarfs is *not* a monotonic function of the H–K color. Mould showed that this behavior is due to the onset of efficient convection in the upper atmosphere when H_2 molecules form. (Giants do not show the effect because convection is not efficient enough; radiative leakage between hot and cool streams is more serious in the lower density gas of a giant atmosphere.) The peak J–H color in Figure 10-3 is a measure of metal abundance and gravity. The major source of uncertainty in Mould's models is probably his treatment of water vapor opacities; his values appear to be underestimates of the true opacities (Mould, 1980).

Norlund (1976) applied his two-stream convection model to red dwarfs (T_{eff} = 3750 and 4250 K) and found that the high gas densities result in temperature differences between hot and cold streams which are much less than in

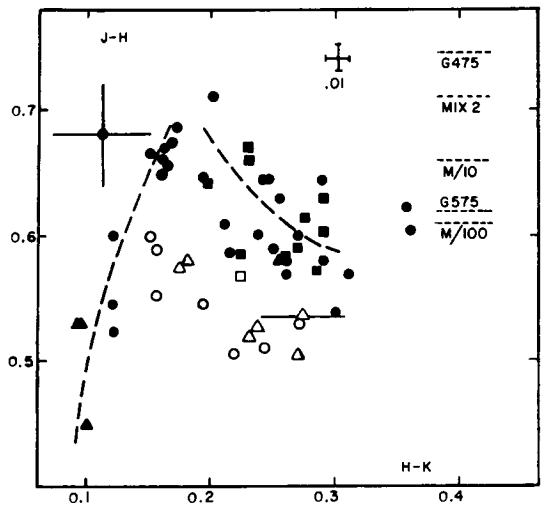


Figure 10-3. Two-color diagram (J-H, H-K) for red dwarfs in halo and disk populations. Theoretical maximum J-H values for various models are indicated by horizontal dashed lines at upper right. Models differ in log g, mixing length, and metal abundances. Solid circles = old disk stars; solid squares = young disk stars; open symbols = halo stars; solid triangles = K dwarfs.

the solar case. As a result, predictions of standard mixing-length theories in red dwarfs might be expected to be more reliable than those in the Sun.

Quasi-Thermal Model Photospheres of dM Stars

In some of the foregoing models (Auman, Mould), the authors incorporated a nonthermal line broadening (microturbulence) of ξ = 2 km s^{-1}. The reason for this choice is the observed line broadening in red dwarfs (0.9 to 2.6 km s^{-1}; Bonsack and Culver, 1966). Presumably, microturbulence has something to do with convective flows. However, convective velocities, v_c, in, for example, Auman's models turned out to be quite small ($\sim$0.3 km s^{-1}). The relation between v_c and ξ in red dwarfs is therefore obscure. In the Sun, Cloutman (1979) has suggested that the solar granules are not true convective cells, but are bubbles which break away from a density inversion below the surface. If the same is true in dwarfs (cf. Kandel's (1967a) discussion of density inversions), perhaps this is the source of the discrepancy between v_c and ξ. However, it would then become necessary to incorporate turbulent pressure gradients in all hitherto calculated model atmospheres.

A further aspect of the microturbulence is its height dependence: in the Sun, ξ = 1 to 2 km s^{-1} in the photosphere, but it increases rapidly upward (reaching $\sim$10 km s^{-1} in the chromosphere). On the other hand, in dM and dMe stars, it appears that ξ remains small ($<$ 2 km s^{-1}) even in the chromosphere (Giampapa et al., 1982b). This may be due to stronger magnetic fields in the M dwarf chromospheres which restrict the motion of ionized gas.

Uncertainties in understanding the origin of microturbulence have a serious effect when one wishes to predict the acoustic fluxes emitted by a convection zone. (These fluxes may be important in heating chromospheres and/or coronae; see below.) Which velocity parameter, v_c or ξ, should be used in the Lighthill-Proudman acoustic formula? Uncertainties of 3 to 10 in the velocity parameter create errors of 10^4 to 10^8 in the predicted acoustic flux which might heat the chromosphere. Discussions of chromospheric heating along the the main sequence have not included these uncertainties (e.g., Bohn, 1981).

Quasi-Thermal Model Photospheres of dMe Stars

This section summarizes work which has been done on inhomogeneities and on the modeling of magnetic effects.

Dark spots exist on the surface of certain dMe stars, especially those which rotate faster than a critical velocity ($\sim$5 km/s; Bopp and Espenak, 1977). The spots are cooler than the photosphere by at least several hundred degrees (ensuring quite different molecular equilibria in the spot atmosphere than outside). The spot areas may be >10 percent of the disk area. The problem of energy transport through the star in the presence of such a gross inhomogeneity

is one of great interest (Spruit, 1982): part of the normal energy flux may be trapped beneath the surface, reducing the bolometric luminosity of the star. (This occurs in the solar case; much of the missing flux of large sunspots essentially disappears from the solar "constant." See Willson et al., 1981.) However, some of the missing starspot energy in red dwarfs may be finding its way into the corona (Gershberg, 1983).

Active region areas on the surfaces of dMe stars may contribute to the differences between dM and dMe spectroscopic properties. With this assumption, Giampapa (1980) has estimated area coverage factors for several M dwarfs; in the most active dMe stars, coverage may be much more extensive than that in dM stars.

By analogy with the Sun, spots and active regions on M dwarfs are believed to be of magnetic origin. The surest evidence for magnetic fields in flare stars is the presence of large circular polarization in radio emission (Gibson, 1983), particularly when the maximum radio emission coincides with maximum visibility of a starspot (Linksy and Gary, 1983). The degree of circular polarization can be especially high during flares—essentially 100 percent (e.g., Lang et al., 1983). Indirect estimates of magnetic field strengths |B| based on interpretation of radio and X-ray properties (with guidance from solar analogs) have yielded values of |B| of at least 210 to 2960 gauss in a group of five M dwarfs (Golub, 1983), 1000 to 2000 gauss for UV Ceti (Linsky and Gary, 1983), and > 9000 gauss for YZ CMi (Haisch, 1983). Although these results are model-dependent, they suggest that fields of many kilogauss may exist on the surfaces of M dwarfs (cf. Mullan, 1984a). Direct measurements of field strength and areal coverage in M dwarfs by the Robinson (1980) technique have not yet been made.

Magnetic fields of kilogauss strength certainly interfere with convective flow patterns in M dwarfs. A steady-state model for a vertical flux tube in the umbra of a sunspot or starspot can be constructed by quantifying the magnetic reduction in convective efficiency, allowing for finite electrical conductivity (Mullan, 1974a, 1974b). The missing thermal flux is converted into Alfvén waves, and a self-consistent depth-dependent model of a spot can be derived. The surface cooling can be severe ($\sim$2000 K on a red dwarf with surface field of $\sim$20 kilogauss). (See also Staude, 1978.) In normal conditions, the Alfvén waves are trapped beneath the surface of the spot by reflection at the steep photospheric density gradient. However, in exceptional conditions (during large flares), the Alfvén waves may be able to leak upward into the corona and escape from the star. Waves which have all of the properties predicted for such umbral Alfven waves in sunspots have been detected recently in the solar wind following a large flare (Mullan and Owens, 1984), but there seems to be little likelihood of detecting umbral Alfvén waves in spots on M dwarfs.

The time-dependent behavior of magnetic flux tubes in red-dwarf convection zones may be more complex than in the solar case (because spot sizes on red dwarfs are much larger fractions of the stellar radius), and some of the solar analogs may therefore be invalid. For example, long-lived sunspots with well-developed penumbrae may owe their quasi-stability to the particular radial profile of differential rotation, $\partial\Omega/\partial r$, beneath the Sun's visible surface (Meyer et al., 1977). In the case of red dwarfs, $\partial\Omega/\partial r$ may be quite different, and flux tubes may never achieve even a quasi-stable state; in that case, the assumption of a solar-like (umbral and penumbral) single spot may be irrelevant (Mullan, 1983; Vogt, 1983).

However, from the scale sizes of inhomogeneities on M dwarfs (both dark and bright; cf. Bopp, 1974a, 1974b), the magnetic flux ropes must be very large, of the order of a stellar radius, R_s, in diameter. Some measure of interference between magnetic fields and red-dwarf luminosity seems therefore likely. Bolometric variability due to such interference has been discussed by Hartmann and Rosner (1979) and by Gershberg (1978, 1983). It is not yet clear whether it is the total magnetic flux

in a tube which controls the variability, or the field strength.

Parenthetically, we note that, if a flux rope intersects the stellar surface over a length scale of $\sim R_s$, then the flux loops in the rope must arch up to heights which cannot be much less than $\sim R_s$ above the photosphere. (In the solar case, coronal X-ray loops typically extend upward to less than $\sim 0.1\ R_s$.) This quantitative feature should be borne in mind when one considers coronal heating in M dwarfs and flare visiblity beyond the limb.

Thermal Models of Internal Structure

Although the internal structure of a star is not the main topic of interest in this series of monographs, ultimately the most stringent test of a model atmosphere is: can it be matched with a sensible model of the *interior* of the star which it is supposed to represent? In other words, can complete stellar models be found which reproduce the observed mass-luminosity (M–L) relationship and the observed mass-radius (M–R) relationship on the lower main sequence? Several research groups have investigated these questions for stars of all spectral types along the main sequence. For present purposes, the most interesting result of these works is the prediction that a main-sequence star becomes completely convective if its mass is less than about $0.3\ M_\odot$. (For a summary of this work, see Neece, 1984.) Because stars of such mass are predicted to have spectral type of middle M, the passage to complete convection is relevant to us here.

One of the parameters which characterizes convection in the thermal models described above (see the section *Thermal Model Atmosphere of Normal M Dwarfs*) is the mixing length, $\alpha = L/H_p$. The best-fitting models required $\alpha \approx 1$. However, Cox et al. (1981) attempted to integrate inward to the center of a star for which the surface parameters were fairly well known (60 Kruger A, mass $0.27\ M_\odot$, luminosity 3.81×10^{31} ergs s^{-1}, $T_{eff} = 3100$ K). The only free parameter in the integration is the value of α: the requirement for a sensible model is that the integration must reach the center of the star with the proper mass. The star chosen by Cox et al. is particularly interesting because its mass falls close to the boundary where stars are expected to become completely convective. Thus, it might provide a rather stringent test of the convection theory. Surprisingly, Cox et al. found that, to obtain a sensible model, they had to assume $\alpha = 0.07$ to 0.17 in regions in which the local temperature lay below 9000 K. (The range of values of α corresponds to a variety of compositions and opacities.) These values of α are much smaller than those used by the atmospheric modelers (Hershey, Mould, etc.), and they had the effect of making the convection zone quite shallow. The interior model of 60 Kruger A turned out to have an appreciable radiative core, with a mass of as much as $0.62\ M_*$ in one model. Of course, for a small enough mass, the models of Cox et al. would eventually have found a completely convective star. But the difference from earlier models of a nearly convective star was striking.

Cox et al. proposed the following explanation for small α: magnetic fields in the envelope are expected to reduce the efficiency of convection on a global scale (see the section *Quasi-Thermal Model Photospheres of dMe Stars*), and the mixing-length formalism responds to this by reducing α. Cox et al. (1981) claimed that the differences between their models and earlier ones are due to improved opacities and improved allowance for particle interactions (including electrostatic corrections) in the equation of state. Cox et al. claimed that their models were in better agreement with the M–L and M–R relationships than other models.

However, Neece (1984) subsequently used the same opacities and an improved equation of a state to derive models of lower main-sequence stars and found acceptable fits to the observed M–L and M–R relationships by assuming a conventional value for α, $\alpha = 1$. Neece found that complete convection sets in for stars with masses between 0.25 and 0.3 $M_\odot$. In the somewhat more massive stars, 0.4

to 0.55 $M_\odot$, Neece found that a small convective core appeared within the radiative interior. The major difference between the equation of state used by Cox et al. (1981) and by Neece occurs in Neece's inclusion of interactions between neutral particles and all other species (including molecules), rather than simply the electrostatic corrections. If this is really the only difference between the two modeling efforts, it suggests that the equation of state will have to be known with extraordinary precision if we are to obtain credible models of M dwarfs. On the other hand, VandenBerg et al. (1983) were able to reproduce the lower main sequence without having to assume a complicated equation of state.

Refinements of the equation of state have recently become a matter of pressing interest in solar physics in attempts to fit the rich spectrum of eigenmodes detected in solar oscillation studies. For example, electrostatic corrections to the equation of state increase the local gas pressure by up to 7 percent in models of the convection zone, push the base of the model convection zone deeper, and shift the model eigenfrequencies by amounts which are larger than the current error bars (Shibahashi et al., 1983). Cox et al. (1981) admitted that even the Coulomb corrections to the pressure in M dwarfs are very uncertain. Shibahashi et al. claim that the major unsolved problem in the solar model at present is how to calculate the internal partition functions for partially ionized constituents: these functions affect the degree of ionization of the gas by an amount which is serious enough that no known solar convection model satisfies all the constraints imposed by the observed eigenmode spectrum. If such problems exist in constraining solar models, the achievement of successful interior models of M dwarfs (in which partially ionized constituents are more abundant than in the Sun) is probably a matter of many years hence, even with purely thermal models.

In fact, Neece (1984) is sufficiently pessimistic about current uncertainties in the surface parameters of M dwarfs (implying large uncertainties in interior structure) that he suggests we can no longer rely on data from single M dwarfs to improve our knowledge of the inner structure. Neece proposes that a more fruitful avenue of research may center on the cataclysmic variables (CV's); i.e., binaries in which an M dwarf is losing mass to a compact companion. The evolution of such a system depends on the way in which the M dwarf radius evolves with respect to the Roche lobe. It is interesting to note that, during mass loss, a convective star tends to expand, whereas a radiative star tends to contract. (This may be relevant to an understanding of the "gap" which exists in the CV period distribution between 2.0 and 3.0 hours: Robinson et al., 1981.) Thus, if a reliable evolutionary model of CV secondaries could be derived from the available CV data, it might lend some credibility to the interior models of M dwarfs.

However, even if thermal models can be derived with reliability, it will still be necessary to pick the surface boundary condition with care in order to get onto the correct adiabat. The extent to which this boundary condition depends on the overlying chromosphere and corona has not yet been determined. (In fitting the solar oscillation data, a rather realistic model chromosphere must be incorporated because the eigenmodes are standing waves in a cavity, one boundary of which is the chromosphere/corona.) As has been the case with the solar/stellar connection in the past, improvements in the equation of state in the solar context are expected to be beneficial to modelers of M dwarfs.

In regard to the oscillations, it is currently unknown to what extent energy transport in either g-modes or p-modes affects the internal structure of the Sun. In M dwarfs, the same problem exists except that, in the latest M dwarfs in which the radiative core presumably disappears, the g-modes will no longer contribute to the problem.

NONPHOTOSPHERIC MODELS OF M DWARF ATMOSPHERES

All of the model atmospheres described previously are strictly photospheric: their emergent fluxes are adequate to account for the observed continua, plus the major molecular absorption features. The $T(\tau)$ relations in all cases are monotonic. However, these models are incapable of accounting for the most characteristic feature of dMe spectra—the profiles of *emission* lines of hydrogen (and calcium). In fact, the profiles of even some of the strong atomic *absorption* lines such as Hα cannot be reproduced satisfactorily, particularly in the cores of the lines. Because the *wings* of Hα in the warmer M dwarfs have a contribution from the photosphere, purely photospheric models can achieve a measure of success in accounting for the wings of M dwarfs with $T_{\rm eff} \gtrsim 4000$ K (see Hershey, 1968). However, in the cooler M dwarfs in which photospheric contributions to Hα are expected to become vanishingly small, there is a major difficulty in explaining the presence of strong Hα absorption in such stars.

The first step in remedying these deficiences has been to construct semiempirical chromospheres in which a temperature rise is superimposed above the photosphere and the temperature is adjusted until a satisfactory fit to some spectral feature is achieved. This approach is summarized for the nonflaring chromosphere in the section *Semiempirical Chromospheric Models*, for nonflaring transition regions in the section *Semiempirical Transition Region and Coronal Models*, and for flares in the section *Semiempirical Flare Models*.

A more fundamental approach seeks to predict mechanical fluxes from first principles and to use these predictions to compute chromospheric and coronal temperatures *ab initio*. (See the section *Nonthermal Models of M Dwarf Atmospheres*.) This approach would also be ultimately desirable for flares, but no such work has yet been published.

Semiempirical Chromospheric Models

Kandel (1967b) studied a chromosphere with two temperature plateaus: the cooler (T_e = 3750 K) radiates mainly in H^-, while the hotter radiates mainly by means of H atoms. Two parameters characterize a model: N_c, the electron column density above the base of the hot plateau (i.e., the chromosphere), and T_c, the temperature of the hot plateau. In each model, a two-level Ca atom was used to compute total emission fluxes in the K core. Comparing with available data, only a very restricted portion of (T_c, N_c) space is acceptable: thus, if $T_c = 2 \times 10^4$ K, log N_c must lie in the range 18.9 to 19.1. Kandel's discussion of Balmer line emission, although inadequate (as he himself admitted), was important in stressing that, in red dwarfs, collisional processes might dominate over photoionization in the source function (contrary to the solar case).

This point was discussed in more detail by Fosbury (1974) in the context of an isothermal chromosphere. He found that, in an M dwarf with $T_{\rm eff}$ = 3500 K, collisional control becomes strong enough to drive Hα into emission if $N_e > 10^{11}$ cm $^{-3}$. Fosbury suggested that a breakdown in the observed correlation between $T_{\rm eff}$ and Hα - width at $T_{\rm eff} \sim 3000$ K (Spinrad, 1973) can be interpreted in terms of a transition from photoelectric control to collisional control in the Hα source function. Thus, if chromospheric heating rates remain unchanged along the main sequence, the Balmer lines would inevitably go into emission at the coolest $T_{\rm eff}$. This is consistent with the early work of Joy and Abt (1974), who found that, among M dwarfs, the fraction of stars classified as dMe (indicating Balmer emission) increases toward later types, reaching almost 100 percent at M5.5. Some exceptions to this rule may now exist (Giampapa, 1983), indicating that chromospheric heating may not in all cases remain unchanged in the coolest dwarfs. In the M dwarfs, irradiation by the overlying corona may dominate the heating of the chromosphere (Cram, 1982). The presence of weak X rays in

the coolest M dwarfs (Golub, 1983) undoubtedly contributes to weakening of Balmer emission there (Mullan, 1984b). However, even if Hα never goes into emission in certain cool dwarfs, remaining always an absorption line, this may still require significant chromospheric heating (Cram and Mullan, 1979).

Gershberg (1974) used a thick slab isothermal chromospheric model to interpret Balmer decrements in flare stars. The Sobolev method was used to determine the population of 30 levels in hydrogen. Only collisional processes were included; no photospheric radiation was included. A three-parameter family of models was considered: T_e, n_e, and β_0 (the photon escape probability at the center of Lyman-α). Ratios of Hα/Hβ intensities are shown in Figure 10-4. The decrement may be either normal or inverted; both types of decrements are observed in flare stars. In quiescent conditions, Gershberg found best fits to 17 spectrograms of nine flare stars with $n_e = (1\text{–}4) \times 10^{12}$ cm^{-3}, $T_e = 10^4$ K, and $\beta_0 = (1\text{–}2) \times 10^{-6}$. Such escape probabilities can be understood if there are velocity fields in the stars of the order of 10 to 30 km/s.

Subsequently, Grinin (1979) extended Gerschberg's (1974) work to include the photospheric radiation field. Although this did not change the level populations by much (cf. Fosbury, 1974), so that the n_e and T_e values remained almost the same as above, the existence of the background radiation allowed Grinin to derive the fractional area of the disk covered by Hα emitting regions; he found 6 to 7 percent (AD Leo) and 14 percent (EQ PegA). Similar coverage was deduced by Greenstein (1977) in another flare star. Active region coverages of a few percent (< 6 percent) have also been derived for Proxima Centauri on the basis of a static-loop analysis of the X rays in the quiescent corona (Haisch et al., 1983). Extreme inversions in the Balmer decrement may indicate highly inhomogeneous physical conditions in the atmosphere (Grinin, 1980).

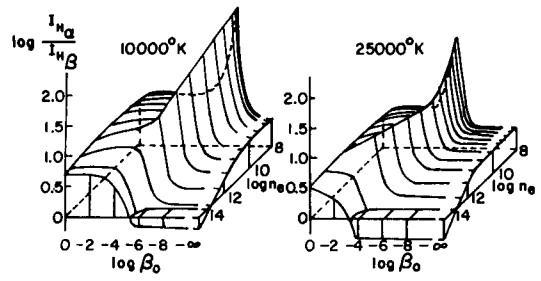


Figure 10-4. Relative intensities of Hα and Hβ in isothermal gas of temperature T_e and electron density n_e. Escape probability of a photon at the center of Lyman-α is denoted by β_0 (Gershberg and Shnol', 1974).

Kelch et al. (1979) modeled Ca K emission-line profiles in two cool dwarfs (61 Cyg B and EQ Vir) in terms of a chromospheric temperature profile, $dT/d \log m = C_i$ (m is mass column density; C_i are constants, and $i = 1,2...$). Several segments of chromosphere are adopted to fit various parts of the profile. Thus, the deepest part begins at $\log m = +0.3$ (61 Cyg B) and -0.2 (EQ Vir), where the temperature is allowed to depart from radiative equilibrium (RE), falling off less slowly with increasing height than in an RE model. At a certain point ($\log m = -1.4$, both stars), the temperature is allowed to pass through a minimum ($T_{min} = 0.8\ T_{eff}$). Above T_{min}, T rises to 8000 K at the "top" of the chromosphere (m_0). Above m_0, T jumps abruptly to coronal values. In this structure, the radiative transfer code for a three-level Ca^+ atom is solved until a best-fit profile is obtained.

The Ca^+ data constrain the model mainly in the region close to T_{min}; above T_{min}, in EQ Vir, for example, the best model has γ ($= dT/d \log m$) = 1800 to 1900 K. This is much steeper than in the quiet Sun (γ = 900 to 1000 K), but is comparable to active regions and flares (γ = 1600 K). In less active stars, (e.g., 61 Cyg, B), γ is closer to solar values. Kelch et al. suggest that dMe stars may differ from dM stars (i.e., have larger γ) because of stronger magnetic fields (cf. also Mullan, 1975). The "best" models of Kelch et al. require chromospheric mechanical fluxes F_{chr} such that $\phi_{chr} = F_{chr}/\sigma T_{eff}^4$ is 6×10^{-5} in the "quiet" star (61 Cyg B) and 2×10^{-4} in the active star (EQ

Vir). (These ratios were estimated by summing over the strongest emission lines.) Although the models of Kelch et al. (1979) are subject to nonuniqueness problems, they had significant success in "predicting" that Hα is in absorption in 61 Cyg B but in emission in EQ Vir, in qualitative agreement with observations. Although the Hα profiles did not fit the data to better than a factor of 2, the work of Kelch et al. represented a start in studying nonlocal thermodynamic equilibrium (NLTE) radiative transfer in a realistic hydrogen atom, in cool dwarfs.

Independently, Cram and Mullan (1979) undertook a parametric study of Balmer line formation in the quiescent spectrum of cool dwarfs. A temperature rise of the form $dT/d \log m = C_{1,2}$ in two segments (from T_{min} to T_0 and T_0 to T_1) was superimposed on Mould's (1976) photospheres. An H atom with five bound levels plus continuum was used, allowing the radiative-transfer problem to be solved in the Lyman continuum and in Hα, Hβ, and Hγ. The parameter space of the study is listed in Table 10-1, and representative Hα profiles are shown in Figure 10-5. In the absence of a chromosphere (Model 1), Hα would be only a weak absorption line in a star with $T_{eff} = 3500$ K. As T_0 increases and the chromosphere "builds up," Hα first goes more deeply into *absorption*, reaching a maximum equivalent width (EW) of -0.66 Å: interestingly, 61 Cyg B, which has T_{eff} close to 3500 K, has Hα in absorption with EW of just this order (Kelch et al., 1979). The implication is that, in cool dwarfs, even if Hα is observed to be in *absorption*, there may be a well-developed chromosphere requiring significant mechanical energy deposition, and such stars may even be flare stars (e.g., SZ UMa; see Worden et al., 1981). In view of this, one should not conclude *solely on the basis of Hα emission or absorption* that division of M dwarfs into dMe and dM is *necessarily* a division into "chromospheric" and "nonchromospheric" stars.

Cram and Mullan (1979) found that further buildup of the superposed chromosphere drives Hα into emission, first in the wings and subsequently in the integrated profile. (A central dip in the Hα emission is caused by optical depth effects; early observational interpretations of such dips in terms of Zeeman splitting have not been confirmed.) For $T_0 > 9700$ K, Cram and Mullan found that integrated Hα is in emission (with $\tau > 1$) for $n_e (m_o) > 10^{11}$ cm^{-3}, in good agreement with Fosbury's (1974) conclusion. Young et al. (1984) have used the results of Cram and Mullan to argue that the chromospheres in dM stars are systematically less dense than those in dMe stars. (For a two-component model, this conclusion is equivalent to varying areal coverage by active regions.) The Hα profile is sensitive mainly to atmospheric behavior between temperatures of ~5000 and ~30000 K. Near the temperature minimum, the radiation field from the photosphere dominates the source function, and as a result, Hα contains essentially no information about such regions. Thus, Hα can serve as a useful complement to Ca K emission as a diagnostic of chromospheric structure in red dwarfs. In general, Mg h and k emission is most sensitive to conditions around 8000 K (i.e., around m_o; see Kelch et al., 1979).

Recently, Linsky et al. (1982) have quantified some properties of dM and dMe chromospheres and have estimated mechanical energy fluxes, F_{chr}, in M dwarfs. They find that the fraction, ϕ_{chr}, remains roughly constant among the main-sequence dM stars ($\phi_{chr} \approx 2 \times 10^{-5}$), but in dMe stars, ϕ_{chr} is about 5 times larger than in dM stars ($\phi_{chr} \approx 10^{-4}$). However, the important point is that the dM stars *need* a finite amount of mechanical energy to create the chromosphere which gives rise to their Hα lines in absorption; thus, one *cannot* conclude that chromospheres are entirely absent from dM stars. (The value of ϕ_{chr} in the dM stars is close to the value in the quiet Sun.) Furthermore, whereas Mg II emission is the dominant line for chromospheric radiative losses in solar-type stars (and also in dM stars), in the dMe stars, emissions in Ca II and Fe II become comparable to Mg II, and Balmer line emission is several times stronger than Mg II. Optical depth in Hα is certainly larger than

Table 10-1
Some Properties of Model dM Stellar Chromospheres*

Model	T_0	log m_0	log m_1	log N_e	$\tau_{H\alpha}$	$EW_{H\alpha}$	$EW_{H\beta}$	$EW_{H\gamma}$
1	- - - isothermal - - -			10.0	10	−0.08	−0.07	−0.07
2	5000	−5.5	−7.0	10.3	5	−0.60	−0.24	−0.13
3	7000	−5.5	−7.0	10.5	8	−0.66	−0.30	−0.16
4	9000	−5.5	−7.0	10.6	40	−0.62	−0.38	−0.26
5	9500	−5.5	−7.0	11.0	70	−0.22	−0.23	−0.16
6	10000	−5.5	−7.0	11.2	120	0.69	0.36	0.34
7	10500	−5.5	−7.0	11.5	200	3.68	1.76	1.74
8	9000	−5.0	−7.0	11.0	96	0.38	0.18	0.19
9	9000	−4.75	−7.0	11.3	140	2.24	1.14	1.17
10	9000	−4.5	−7.0	11.6	210	6.66	3.55	3.76
11	9000	−4.25	−7.0	11.9	290	15.18	8.34	9.34
12	9000	−5.0	−6.5	11.0	96	0.54	0.26	0.26
13	9000	−5.0	−5.5	11.1	85	0.73	0.42	0.42
14	9000	−5.0	−7.0	11.3	180	1.43	0.80	0.80
15	9000	−5.0	−7.0	11.2	150	1.58	0.86	0.87
16	9000	−5.0	−7.0	11.5	110	−0.08	−0.20	−0.17

*Notes:

Models 1 to 14 are based on Mould's (1976) model with T_{eff} = 3500 K, log g = 4.75, and "old disk" abundances.

In model 14, the temperature minimum has been moved deeper, to T_{min} = 3081 K and log M_{min} = 0.56. In models, 1 to 13, the corresponding values are T_{min} = 1659 and log m_{min} = −0.65.

Model 15 is based on the same T_{eff} and log g as above, but the relative abundances have been reduced by a factor of 5.

Model 16 has T_{eff} = 4200 K, log g = 4.75, and "old disk" abundances.

The value of T_1 is always 30000 K.

N_e is the maximum chromospheric electron density (cm^{-3}).

EW is the equivalent width, negative for absorption lines. Units are in Å.

unity in dMe stars (Petterson, 1984). Hydrogen atom emissions are the dominant coolants of dMe chromospheres, although the calcium infrared triplet is also important in the most active stars (Petterson, 1984).

Semiempirical Transition Region and Coronal Models

The work of Linsky et al. (1982) also attempts to model the transition region (TR) between chromosphere and corona. They find that the fraction ϕ_{TR} of σT_{eff}^4 which heats the TR in dMe stars is as large as 2×10^{-5} in active stars, which is ~100 times larger than ϕ_{TR} in solar plages. X-ray data (Golub, 1983) can be interpreted to show that the coronal heating fraction in M dwarfs, ϕ_{cor}, may also rise to a maximum of >100 times larger than that in the Sun; in the strongest emitters (of spectral type M1-M2), the X-ray luminosity is ~1 percent of the bolometric luminosity (i.e., ϕ_{cor} = 0.01). This is the maximum value of ϕ_{cor} reported for any single star of late spectral type. (In the Sun, the maximum value of ϕ_{cor} in active regions is $\sim 10^{-4}$ (Withbroe and Noyes,

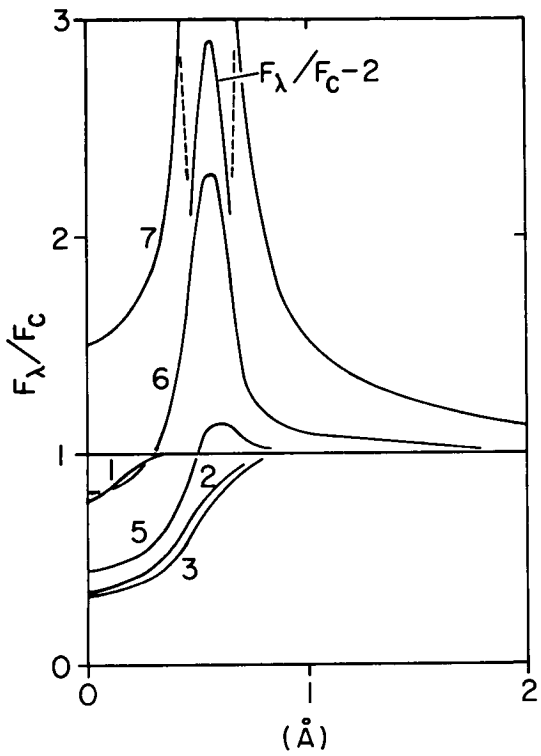


Figure 10-5. Relative flux profiles for the Hα line emitted by a grid of dM star chromospheres. The number associated with each profile refers to a model in Table 10-1. Note that only one half of each profile is shown (Cram and Mullan, 1979).

1977).) It is remarkable that, in M dwarfs, the nonthermal processes have an efficiency as large as 1 percent. The value of ϕ_{cor} falls off rather steeply in the later M dwarfs (Mullan, 1984b). Now, in the quiet Sun, $\phi_{chr} \sim 10\,\phi_{cor}$, whereas in active regions, $\phi_{chr} \sim 2\,\phi_{cor}$ (Withbroe and Noyes, 1977). Hence, the *chromospheric* heating problem to be solved by solar theorists is more exacting than the *coronal* heating problem. However, in certain M1–M2 dwarfs, it appears that $\phi_{cor} > \phi_{chr}$ by a factor which may be as large as ~100, and the heating problem is qualitatively reversed. (At some spectral types, the X-ray luminosity, L_x, spans a range of up to 3 orders of magnitude, with no clear correlation with kinematic grouping; it seems unlikely that rotation differences alone can explain the large range in L_x (Johnson, 1983).) In dMe stars, *the principal problem is to explain how the corona of certain M1–M2 dwarfs can be heated so efficiently* (Mullan, 1984b). When this problem is solved, the chromospheric heating may actually be understood simply in terms of absorption of X rays from the overlying corona (Cram, 1982).

Why should coronal heating be so efficient in dMe stars? Gershberg (1983) has pointed out that, in certain flare stars, ϕ_{cor} is comparable to the "missing flux" in starspots. He postulates that dMe stars are somehow efficient at transferring the "missing flux" into coronal heating (unlike the Sun). We will return to a quantitative discussion of this point in the section *Nonthermal Models of M Dwarf Atmospheres.*

Semiempirical Flare Models

In the same spirit as the foregoing discussion, flare models have been proposed in which it is assumed that an abrupt energy release from an unspecified source causes local heating; the aim is then to reproduce flare light curves and colors as a time-dependent problem.

Gershberg (1970) has summarized the "nebular" model, in which a single impulse heats a region of the atmosphere to "chromospheric" temperatures (i.e., (10–20) × 10^3 K). (These temperatures are constrained by the observed Balmer jumps.) Hydrogen recombination is assumed to be the source of flare light. As the flare volume expands, an analytic expression can be derived for the decaying branch of the flare light curve. Observed light curves were fitted quite well in many cases, and from the decay time, initial densities were derived: $n_0 = 10^9$ to 10^{11} cm^{-3}. Subsequently, these estimates were found to be too small on two counts: they would require the flare volume to be extremely large (covering the entire stellar disk), and they would yield incorrect Balmer decrements (Gershberg, 1978). Apparently, flare decay is not due to recombination, but is controlled by some other slower process (Gershberg, 1975); Gershberg did not identify what that slower process might be.

A further argument against recombination as the source of flare light is based on the colors ($U-B$, $B-V$) of flare light; during flare decay, the predicted colors have a trajectory in the two-color diagram which is inconsistent with observations. However, it must be admitted that arguments based on the two-color diagram are not especially forceful; the observed colors are scattered over a wide area of the diagram, and many different interpretations of such colors are now known to be admissible. For example, Gershberg (1978, his Figure 2) shows how the observed $U-B$, $B-V$ colors in a large sample of flares (at maximum light) are spread over such a large area of the two-color diagram that individual events can be found which are consistent with one or more of seven different emission mechanisms:

1. H^- emission at $T = (5\text{–}10) \times 10^3$ K
2. Nonthermal bremsstrahlung
3. Inverse Compton scattering of photospheric radiation
4. Synchrotron emission with spectral index 0–2
5. Optically thin plasma at $T > 8 \times 10^4$ K
6. Blackbody with $T > 4000$ K
7. Hydrogen plasma, optically thick in Balmer lines, with $T = (15\text{–}25) \times 10^3$ K

The flare material considered by Gershberg is strictly "chromospheric," with no attempt to link it with the overlying corona or underlying photosphere. Kunkel (1970) proposed that the chromopsheric flare would irradiate the photosphere and "burn" it to a state of a few hundred degrees hotter than the undisturbed photosphere. Kunkel suggested that the "burn" might help to interpret flare colors during the late stages of flare decay. That a flare can cause excess heating even in the photosphere has been established in the case of the Sun: $\Delta T \sim 100$ K at $\tau \sim 0.1$ during certain flares (Machado and Linsky, 1975).

The most detailed discussion of the photospheric "burn" has been given by Grinin (1973, 1976) in his treatment of time-dependent radiative transfer in the presence of an external source of radiation. Scattering and diffusion of a δ-function source causes the reflected signal to have a well-defined form with a time scale of the order of radiative relaxation time, τ_r. If the flare light has a particular time variation (e.g., $L(t) \sim (1 + t/B)^{-2}$, as the "nebular" model predicts), the reflected light can be derived by convolution. For conditions in M dwarfs, $\tau_r \sim 3$ to 5 minutes. Since this is comparable to observed flare decay times, Grinin concludes that the reflected signal may indeed contribute detectably to flare light.

An interesting feature which emerges from Grinin's work concerns the temperature sensitivity of the opacity in the photosphere. Depending on the atmospheric composition (especially the metal abundance) when the photosphere is "burned," the opacity may increase momentarily so much that the "burn" actually blocks off the radiation emerging from inside the star. Grinin (1976) proposes that "negative" flares may be due to this effect (i.e., dips in the star's light below the nonflaring level) occurring during a flare. Although many features of "negative" flares can apparently be accounted for in this context, Grinin pointed out that the model cannot explain "negative" dips which occur *before* the optical flare itself, unless there is some other source of radiation (other than optical flare light) to cause the prior "burn." Grinin did not specify such a source. However, his analysis of the evolution of flare colors during decay has already led him to conclude that the "burn"must be much hotter than the photosphere (by several thousand degrees); he realized that this would be almost impossible if "nebular" gas alone were the source of the "burn." Something hotter would be required. Subsequently, Grinin (1980) proposed a different explanation of "negative" flares in which preflare changes in magnetic fields reduce the active region emission. A different

interpretation of "negative" flares is provided by Giampapa et al. (1982a); they suggest that a flare occurs when a prominence is destabilized and deposits its material on the surface of the star. They suggest that, before hitting the surface, the prominence material obscures part of the surface, thereby causing a "negative" precursor to the main flare outburst.

A further indication of the important role which deep-seated gas has on stellar flares emerged from the work of Grinin and Sobolev (1977). They placed the optical flare-emitting gas in the photosphere/chromosphere boundary region ($N = 10^{15}$ to 10^{17} cm^{-3}) and considered H^- emission as well as opacity beyond the Balmer jump. This model successfully accounted for the *UBV* colors of flare light, the correlation with *U–B* color, and the Balmer jump. Solar "white" light flare emission may also emerge from analogously deep parts of the atmosphere. Nevertheless, the relaxation time scales associated with deep gas are difficult to reconcile with observed light curves, and the necessity of an externally imposed time scale again emerges if such light curves are to be understood. Gershberg (1978) has argued that, since flare luminosity L on many different flare stars (with quite different photospheric properties) obeys a "universal" relation near maximum $(d \log L/dt)_{max} \sim L^{-1/4}$ (Shakhovskaya, 1974a, 1974b), this in itself is not compatible with significant photospheric contributions to flare light near maximum. Gershberg believes that a "universal" relation is more likely to be an indication that very hot gas is contributing to flares at maximum. (See also Mullan, 1976a, 1976b.)

Cram and Woods (1982) have reported a systematic study of semiempirical flare models along similar lines to those used by Cram and Mullan (1979) for quiescent chromospheres. (The models were chosen to represent various proposed heating mechanisms; an analogous study of solar flares has recently been reported by Canfield et al. (1984).) In the flare case, however, as well as computing Balmer line profiles, the broadband continuum was also computed. A general conclusion is that the flaring chromosphere has higher pressures and temperatures than the quiescent chromosphere. In regards to high pressures in solar flares, Canfield et al. (1984) have shown that flares which show Hα in emission without any central reversal must have $P \gtrsim 100$ dyn/cm^2 (i.e., 10^2 to 10^3 times the quiet Sun value). On the other hand, flares which show broad Stark wings in Hα cannot be understood in terms of high pressure alone; they require large fluxes of energetic electrons $> 10^{10}$ erg/cm^2/sec in electrons with $E > 20$ keV. Empirical evidence for high pressure in line-forming regions of stellar flares indeed emerges from a study of the broadening of the various lines in the Balmer series; in six flares on YZ CMi, the data yield electron densities in a rather well-constrained range: 10^{13} to 10^{14} cm^{-3} (Worden et al., 1984). If $T = 10^4$ K in the Balmer line-forming region, this indicates pressures of 30 to 300 dyn/cm^2 in these flares. A significant conclusion which emerges from the work of Cram and Woods is that, in order to produce strong narrow Balmer lines with an inverted decrement but at the same time show no very strong Balmer jump (such as flare data suggest), it is necessary to have the line-emitting region cover at least 10 to 20 percent of the stellar surface (i.e., much larger than previous estimates of flare area). If the area of the flare decreases with time, while leaving pressures and temperatures high, the observed time dependence of the Balmer decrement can be explained. On the other hand, the flare *continuum* (as opposed to lines) appears to emerge from much smaller areas (~ 1 percent of the surface). (Mochnacki and Zirin (1980) derived flare areas in YZ CMi and UV Cet which are equivalent to < 0.2 percent areal coverage of the surface in continuum emission; these estimates are uncertain because of the assumption that the flare radiates as a blackbody.) Cram and Woods mention the analog of solar flares in which compact "kernels" of continuum emission involve deep atmospheric heating in a few isolated patches under the Hα flare. The areas of Hα flare emission proposed by Cram

and Woods (1982) are reminiscent of the areal coverage of starspots on red dwarfs. If the spots are indeed magnetic flux tubes, it appears that the entire tube must participate in the release of magnetic energy when a flare occurs.

As was mentioned above, the Hα line profile is sensitive to conditions even at rather high temperatures (30000 K or even more; cf. Dame and Cram, 1981). Other arguments (Gershberg, 1970; Grinin, 1976) also suggest that, in order to obtain a correct interpretation of flare light, it is important to consider the effects of very hot gas (i.e., much hotter than "nebular").

Andrews (1965) was the first to model flare light curves by free-free emission (implying very hot gas, $T > 10^7$ K). This emission gives way to recombination as the temperature drops, and Andrews successfully modeled observed light curves by this two-stage process. At the time of Andrew's work, there were no data to prove the existence of hot gas in stellar flares. Since 1975, abundant evidence has accumulated from various satellites (Astronomical Netherlands Satellite, Small Astronomy Satellite C, High Energy Astronomy Satellite 1, and Einstein) to confirm Andrews' assumption of gas at $T\sim$ few times 10^7 K (cf. Haisch, 1983).

Mullan (1976b) investigated the effects of inserting a plasma at $T = 10^7$ K into a flare star atmosphere. The flare plasma establishes a thermal structure which, if steady state is achieved, has one of two universal forms, depending on whether the density is constant or the pressure is constant (Shmeleva and Syrovatskii, 1973). The constant density limit is relevant in "spike" flares, in which energy is released so rapidly ($\ll 1$ minute) that pressure equalization is not immediately possible. In such cases, continuum emission would dominate the flare spectrum as observed (Moffett, 1973). The U–B, B–V colors of free-free continuum are consistent with flare colors. In M dwarfs, the background photosphere is not bright enough to mask the plasma continuum, although in the solar case, this would not in general be true. If stellar flare light is indeed free-free emission from coronal plasma, the bolometric corrections to UBV flare luminosities may be as large as $\sim 5^m$ (cf. also Kodaira, 1977); this is the major source of uncertainty in our current knowledge of stellar flare energetics. (Of course, the bolometric corrections to the photospheric radiation of a flare star is also large, up to 5^m in the latest M dwarfs (Petterson, 1983), but these bolometric corrections are easier to determine because of the nontransient nature of the emission.)

Eventually, the flare plasma reaches pressure equalization, and then the thermal structure of the flare atmosphere switches to the second universal form described by Shmeleva and Syrovatskii (1973). The result is two-fold: the flare emission falls dramatically (by a factor of 10^2 to 10^3), and the continuum gives way to emission lines. Flares in which the energy release is slow should evolve entirely via the constant pressure structure and should show predominantly line emission throughout, rather than in the decay state only; this is consistent with data (Moffett, 1973).

Hot plasma loses energy by radiation, conduction, and expansion. Estimates (Mullan, 1976a) suggested that conductive time scales would be the most rapid in stellar flares. Thus, a flare light curve would be the response of the atmosphere heated from above mainly by conduction. This led to the prediction that the optical flare light curve decays on a time scale which is associated with conduction from the flare plasma. Thus, the unidentified "slowly decaying agent" which Gershberg (1975) invoked to account for optical flare light curves was attributed to conduction. This conclusion is model-dependent because of uncertainties in the length scales associated with conduction. Note that, in his analysis of X-ray data, Haisch (1983) assumes that flare plasma cools not only by conduction but also by radiation, with equal cooling rates in both modes.

Flare plasma irradiates the photosphere with X rays which, as they propagate through the

denser gas in the lower atmosphere, become degraded into optical photons (Mullan and Tarter, 1977). These optical photons, in conjunction with the direct emission from the flare plasma, may help to explain the evolution of flare light in the U–B, B–V plane. Also, the fact that X rays can reach the photosphere essentially instantaneously, whereas conductive heating requires a finite time scale, may help to explain why "negative" flares in Grinin's (1976) scenario can occur prior to the optical flare.

An idealized time-dependent model of flare plasma, including energy losses by radiation, conduction, and expansion, was calculated by Mullan (1977). Nonmonotonic light curves, including preflares and still-stands, can be reproduced in this model. In subsequent applications of these calculations to flares on AD Leo, temperatures of (20–30) $\times$ 10^6 K were derived, with coronal densities of (0.35–1) $\times$ 10^{12} cm^{-3} (Schneeberger et al., 1979); in the case of a flare on YZ CMi, the derived temperatures were 13 $\times$ 10^6 K, with densities of 0.07 $\times$ 10^{12} cm^3 (Worden et al., 1984). The flare temperatures derived by this method are quite consistent with those derived in other flares by more direct methods (Haisch, 1983), whereas the densities are not grossly different from those derived by Gershberg (1978) in his "nebular" model.

Kodaira (1977) incorporated very hot gas into his "reservoir-emitter" model of a very large stellar flare on EV Lac. The hottest gas ($T \sim 10^8$ K) in the magnetic flux-tube reservoir emits X rays, whereas optical flare light comes from "emitter" gas at the foot points of the flux tube ($T \sim 10^5$ K). To contain the reservoir, $B = 200$ gauss is required, corresponding to 2 kilogauss at the foot points. The latter cover $\sim$10 percent of the stellar hemisphere, comparable to what Cram and Woods (1982) also require. The "reservoir" flux tube extends to great heights; Kodaira finds that its scale length is comparable to the radius of the star. This conclusion is consistent with the point noted above: if starspots and active regions occupying $\sim$10 to 20 percent of the disk area are magnetic flux tubes, then these tubes must extend upward to great heights ($\sim R_s$) above the photosphere. Flux-tube lengths of up to (0.5–1) R_s have also been inferred in the case of a flare on Proxima Cen and a giant flare in a Hyades star (Haisch, 1983).

In view of the possibility that magnetic fields in red dwarfs may be considerably stronger than those in the Sun, we may ask why the flare temperatures in the red dwarfs are essentially identical to solar flare temperatures. One possibility is to hypothesize that the atmospheric densities scale as $n \sim B^2$ (Mullan, 1975): if a flare involves magnetic reconnection in which the final plasma has a beta ($= P_{gas}/P_{mag}$) of order unity (Moore and Datlowe, 1975), the flare temperatures would be relatively constant if $n \sim B^2$. Is it reasonable to expect such a scaling? To answer that, we note that, in the solar corona, static loops of length L and pressure p have temperatures T which scale as $T \sim (pL)^{1/3}$ (Rosner et al., 1978). Observed loop temperatures are confined within a fairly narrow range so that, to a first approximation, we can adopt $T \approx$ constant. Hence, the densities n scale as L^{-1}. Now, the vertical field strength, B_z, in a coronal loop has been found to scale as follows: $p \sim B_z^{3/2} L^{-1/4}$ (Golub et al., 1982). If T = constant, this reduces to $n \sim B_z^2$. This can be considered as providing some support for Mullan's (1975) hypothesis.

The most detailed study to date of the hydrodynamics of a stellar flare is that of Livshits et al. (1981). A beam of nonthermal electrons is supposed to be created (in an unspecified manner) in the atmosphere, and a one-dimensional numerical code is used to follow the effects. When the electrons deposit their energy, a region of high pressure is formed: shocks propagate upward and downward. Radiative losses are especially severe in the downward shock, and as a result, that shock may have a very large density jump ($\varrho_2/\varrho_1 \sim 100$). Because of the greater densities and shorter scale heights in red-dwarf atmospheres, the region of shock compression may become optically thick even in the visible continuum ($\tau_{4500} \sim 1$)

for a short time. The authors ascribe the short-lived continuum in red-dwarf flares to this process. This treatment of a shock in a stellar atmosphere is more realistic than an earlier discussion by Korovyakovskaya (1972); in the latter case, although flare light curves could be reproduced, there were difficulties with the energetics.

Nonthermal electrons also play an essential role in the "fast-electron hypothesis" of stellar flares (Gurzadyan, 1973). There, flare light is supposed to be the result of an inverse Compton scattering of photospheric photons off a large number of 1- to 10-MeV electrons. However, there are many serious difficulties with this hypothesis (Kodaira, 1977; Gershberg, 1978). For example, to explain a total flare energy of 10^{34} ergs, allowing for the inefficiency of Compton scattering ($\sim 10^{-5}$), Gurzadyan's model requires that the total energy in fast electrons must be 10^{39} ergs. If each electron has an energy of ~ 1 MeV, this requires a total number of 10^{45} electrons. With a flare duration of $\sim 10^2$ seconds and even supposing the electron beam is spread out over the maximum possible area (πR_s^2, where R_s is the stellar radius), the current density would still be so large that a magnetic field of $\sim 10^{13}$ gauss would be induced by the beam. (Note that there is no reverse current to cancel the outward-streaming electrons.) The back-reaction of such a field on the star would be enormous. These numbers are so large that his hypothesis must be rejected.

Nonthermal Models of M Dwarf Atmospheres

Kuperus (1965) and de Loore (1970) discussed the generation of acoustic waves in convection zones, followed by their dissipation in the atmosphere. However, neither of these authors considered stars as cool as M dwarfs. Renzini et al. (1977) extended the earlier work to M dwarfs. They estimated that, at $T_{\rm eff}$ = 3200 K and log g = 5, the acoustic flux F_{ac} = 140 ergs cm^{-2} s^{-1} (i.e., some 10^5 times less than solar). Bohn (1981) discusses various corrections to this estimate and finds that F_{ac} may be 10^2 to 10^3 times larger than Renzini et al. found. However, even this correction is not large enough to avoid the prediction that F_{ac} in red dwarfs should be *less* than in the Sun: the data do not support this. Thus, the flux of chromospheric mechanical energy, F_{chr}, alone in the dMe stars is about equal to the solar value (Linsky et al., 1982), whereas the coronal radiative losses, ϕ_{cor} in certain dMe stars is > 100 times the solar value (Mullan, 1984b). To these, the effects of the mechanical energy required to power the winds from the stars should be added for completeness. Therefore, if acoustic waves are to provide for the sum total of mechanical energy deposition in the atmosphere, we must have $F_{ac} = F_{tot}$, where $F_{tot} = F_{chr} + F_{cor} + F_{wind}$. However, in the solar corona, even in coronal holes, where F_{wind} is maximum, F_{chr} dominates F_{wind} by a factor of almost 10. In solar active regions, F_{wind} contributes less than 1 percent to F_{tot}. (See, for example, Withbroe and Noyes, 1977.) Hence, in the solar case, neglect of F_{wind} appears to be permissible in estimating F_{tot}.

What can we say about M dwarfs? It would seem that F_{wind} will also be rather unimportant for two reasons: (1) the gravitational potential well of an M dwarf is deeper than solar, thereby impeding steady wind flow; and (2) strong coronal radiation from M dwarfs suggests that their surfaces are almost entirely covered with active regions (Mullan, 1984b), and from these, steady wind flow is also inhibited by closed magnetic field lines. We cannot exclude the possibility that transient mass ejections occur during flares (Coleman and Worden, 1976; Shlosman et al., 1979). It seems acceptable to discuss F_{tot} outside flares as the sum of only two terms, F_{chr} and F_{cor}. If we then attempt to equate F_{tot} with F_{ac}, we find that the predicted behavior of convective acoustic power along the lower main sequence is not even qualitatively in agreement with the observed properties of chromospheres/coronae. Adding the possible effects of transient mass ejections during flares makes the disagreement even worse. Therefore,

either acoustic heating is unimportant or perhaps the wrong velocity has been used in estimating acoustic power. (See the section *Quasi-Thermal Model Photospheres of dM Stars.*)

Ulmschneider and his colleagues have devoted considerable attention to the propagation and dissipation of acoustic waves in stellar atmospheres. On the basis of this, Ulmschneider et al. (1977a, 1977b) have found that, in a red dwarf with $T_{\rm eff} = 4000$ K, $\log g = 4$, a shock should form (and presumably lead to a temperature minimum) at a mass loading $m_s \sim 10^{-3}$ gm cm^{-2}. However, empirically, the temperature minimum in such a star is observed to occur much deeper, at $m_s = 0.05$ gm cm^{-2} (Cram and Ulmschneider, 1978; Kelch et al., 1979). Again, the acoustic theory does not appear to apply well to red dwarfs.

The deficiency of acoustic heating has led several investigators to consider how magnetic effects might enter into the mechanical heating of red-dwarf atmospheres. Katsova (1973) considered the dissipation of slow-mode waves in a stratified atmosphere. With a prescribed flux at the bottom of the atmosphere, and allowing the dissipation to be balanced locally at each height by radiative losses, Katsova obtained the run of temperature with density (i.e., height). The magnetic field was set to a constant value (20 gauss). Two quasi-plateaus appear in the atmosphere at $\sim 10^4$ K and at $\sim 5 \times 10^4$ K. The calculations were carried up to a maximum temperature of 2×10^6 K. At that level, Katsova found that the density in the red dwarf was ~ 10 times larger than in the solar model at the same temperature. Glebocki et al. (1974) extended Katsova's work to somewhat warmer stars. For semiquantitative arguments in support of magnetic heating of the chromospheres/coronae of cool dwarfs, see Mullan (1975). For a discussion of propagation and dissipation of magnetohydrodynamic waves in stellar atmospheres in general, see Leibacher and Stein (1981) and Ulmschneider and Stein (1982); on the basis of the latter work, Marcy (1984) has argued that chromospheric/coronal heating in G and K dwarfs can be understood in terms of slow and Alfvén modes. However, this argument has not yet been extended to M dwarfs, where serious line blending has so far prevented meaningful application of Marcy's observing technique.

Much detailed research has been carried out in the post-Skylab era in an attempt to put magnetic heating in the solar corona on a sound footing. The incentive for this is the obvious dominance of magnetic loops in the solar corona. Current dissipation and heating by Alfvén waves have received the most attention. However, thus far, none of these ideas have been applied in detail to red dwarfs, apart from the application of certain scaling relations between loop lengths, pressures, temperatures, field strengths, etc. (Golub, 1983; Haisch, 1983). Even in the absence of detailed application, some points can already be made. For example, if the densities in red-dwarf chromospheres/coronae are indeed $\gtrsim 10$ times solar (cf. Gershberg, 1970; Katsova, 1973; Mullan, 1975), then the critical current, $j_c = nev_{th}$, where anomalous current dissipation sets in (i.e., when the drift velocity equals the thermal speed) is >10 times larger in red dwarfs than in the Sun. As a result, the critical Joule dissipation rate, $\sim j_c^2/\sigma$, is >100 times greater than solar. If the onset of rapid Joule heating when the current goes supercritical acts as a flare initiator, then this result may help to explain why many stellar flares have a very rapid rise to maximum light, particularly the so-called "spike" flares (Moffett, 1973), in which rise times are < 1 second.

As a second example, we may consider the heating of coronal magnetic loops by waves. The waves are presumably generated over a certain spectrum of frequencies in the convection zone. There is no a priori reason why the wave spectrum in the convection zone should be well matched to resonance periods of atmospheric loops. In the Sun, the convective wave periods are in the region of $\tau_c \sim 500$ seconds (Ionson, 1982), whereas typical loop resonance periods may be of order $\tau_A = 5$ seconds (Mullan, 1984b). Thus, in the Sun, impedance matching between the source of the waves and their sink is not particularly good, and the electrodynamic

coupling efficiency, ϵ, between convection zone and corona ($\sim \tau_A/\tau_c$ when $\tau_A < \tau_c$; Ionson, 1984) is small, of the order of 1 percent. As a result, the mechanical energy deposited in solar coronal loops is quite small (typically no more than 10^{-4} of the radiant energy flux).

However, consider how these arguments are affected in the case of red dwarfs. Their convection time scales, $\tau_c \sim T/\mu g v_c$ (where T is the temperature, μ is molecular weight, g is gravity, and v_c is convective velocity), are certainly *shorter* than solar time scales (see Figure 10-6). Estimates of τ_A in red dwarfs are difficult to make, but the observational evidence which is currently available (Mullan, 1984b) indicates values of τ_A as shown in Figure 10-6 (i.e.,tending toward *greater* values in later spectral types). The possibility of a "crossover point," where $\tau_c = \tau_A$, in Figure 10-6 is of great interest. If such a crossover were to exist, the coupling efficiency, ϵ, would approach unity (i.e., $\sim 10^2$ times larger than in the Sun). In fact, M1–M2 dwarfs are observed to have coronal heating efficiencies which are $\gtrsim 10^2$ times solar (Mullan, 1984b). The crossover depicted schematically in Figure 10-6 is meant to suggest that spectral types of M1–M2 ($T_{\rm eff} \simeq 4000$ K) are in fact a reasonable location for $\tau_c \simeq \tau_A$. Moreover, at spectral types later than M1–M2, impedance matching once more breaks down, and the coupling efficiency, ϵ, should fall off rapidly; this agrees with the behavior of the observed X-ray fluxes.

The question of magnetic heating of even quiescent atmospheres of red dwarfs requires much more work to be put on a quantitative basis. *A fortiori*, the relationship of magnetic heating to stellar flares is even more complicated, and no work has apparently been done on this topic. It may be that, if "normal" heating can be accounted for, then some flares can be considered as simply an extreme version of coronal heating or vice versa (cf. Mullan, 1979; Doyle and Butler, 1985; Butler and Rodonò, 1985). (Where does one draw the boundary between a small flare and a bright active region loop, for example?) On the other hand, the impulsive phase of flares may require a qualitatively distinct process, perhaps arising from an explosive instability. In this regard, we note that, in flare star coronae, the electron densities derived from the conductive interpretation of flare light curves (Mullan, 1976a) are apparently low enough that certain plasma instabilities should indeed proceed explosively (Spicer, 1975) rather than "slowly."

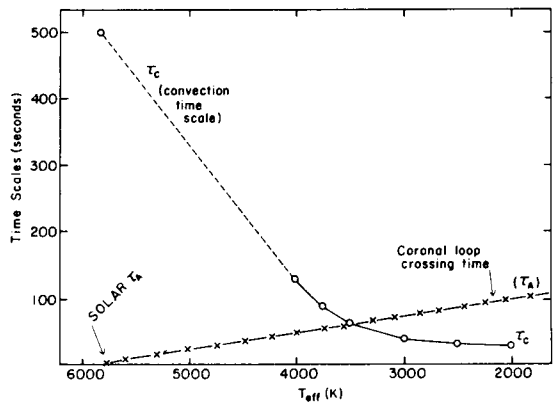


Figure 10-6. Time scales that enter into Ionson's (1984) discussion of coronal heating: τ_c = convection time; τ_A = Alfvén crossing time in a loop. Note that τ_c decreases at later spectral types, while τ_A may increase. At the crossover ($\tau_c = \tau_A$), coronal heating is maximally efficient (Mullan, 1984b).

REFERENCES

Andrews, A.D. 1965, *Irish Astron. J.*, **7**, 20.

Auman, J.R. 1969, *Astrophys. J.*, **157**, 799.

Bohn, H.U. 1981, in *Second Cambridge Workshop on Cool Stars, Stellar Systems, and the Sun*, ed. M. Giampapa and L. Golub, SAO Special Report 391, Vol. 1, p. 67.

Bonsack, W.K., and Culver, R.B. 1966, *Astrophys. J.*, **145**, 767.

Bopp, B.W. 1974a, *Mon. Not. Roy. Astr. Soc.*, **166**, 79.

Bopp, B.W. 1974b, *Mon. Not. Roy. Astr. Soc.*, **168**, 255.

Bopp, B.W., and Espenak, F. 1977, *Astron. J.*, **82**, 916.

Butler, C.J., and Rodono, M. 1985, Armagh Observatory Preprint, No. 9.

Canfield, R.C., Gunkler, T.A., and Ricchiazzi, P.J. 1984, *Astrophys. J.*, **282**, 296.

Carbon, D.F. 1979, *Ann. Rev. Astron. Astrophys.*, **17**, 513.

Chan, K., and Sofia, S. 1984, *Astrophys. J.*, **282**, 550.

Cloutman, L.D. 1979, *Astrophys. J.*, **227**, 614.

Coleman, G.D., and Worden, S.P. 1976, *Astrophys. J.*, **205**, 475.

Cox, A.N., Shaviv, G., and Hodson, S.W. 1981, *Astrophys. J. (Letters)*, **245**, L37.

Cram, L.E. 1982, *Astrophys. J.*, **153**, 768.

Cram, L.E., and Mullan, D.J. 1979, *Astrophys. J.*, **234**, 579.

Cram, L.E., and Ulmschneider, P. 1978, *Astron. Astrophys.*, **62**, 239.

Cram, L.E., and Woods, T.D. 1982, *Astrophys. J.*, **257**, 269.

Dame, L., and Cram, L.E. 1981, *Bull. Amer. Astron. Soc.*, **13**, 820.

de Loore, C. 1970, *Astrophys. Space Sci.*, **6**, 60.

Doyle, J.G., and Butler, C.J. 1985, *Nature*, **313**, 378.

Fosbury, R.A.E. 1974, *Mon. Not. Roy. Astr. Soc.*, **169**, 147.

Gershberg, R.E. 1970, *Flares on Red Dwarf Stars*, in Russian (Moscow: Nauka), English translation by D.J. Mullan (Armagh Observatory).

Gershberg, R.E. 1974, *Soviet Astron. AJ*, **18**, 326.

Gershberg, R.E. 1975, in *Proc. IAU Symp. 67, Variable Stars and Stellar Evolution*, ed. V.E. Sherwood and L. Plaut (Dordrecht: Reidel), p. 47.

Gershberg, R.E. 1977, *Peremennye Zvezdy*, **20**, 283.

Gershberg, R.E. 1978, *Low Mass Flare Stars*, in Russian (Moscow: Nauka).

Gershberg, R.E. 1983, in *Proc. IAU Colloq. 71, Activity in Red Dwarf Stars*, ed. P.B. Byrne and M. Rodonò (Dordrecht: Reidel), p. 493.

Gershberg, R.E., and Shnol', E.E. 1974, *Izv. Krim. Astrofiz. Obs.*, **50**, 122.

Giampapa, M.S. 1980, in *Cool Stars, Stellar Systems and the Sun*, ed. A.K. Dupree, SAO Special Report 389, p. 119.

Giampapa, M.S. 1983, in *Proc. IAU Symp. 102, Solar and Stellar Magnetic Fields: Origins and Coronal Effects*, ed. J.O. Stenflo (Dordrecht: Reidel), p. 187.

Giampapa, M.S., Africano, J.L., Klimke, A., Parks, J., Quigley, R.J., Robinson, R.D., and Worden, S.P. 1982a, *Astrophys. J. (Letters)*, **252**, L39.

Giampapa, M.S., Worden, S.P., and Linsky, J.L. 1982b, *Astrophys. J.*, **258**, 740.

Gibson, D.M. 1983, in *Proc. IAU Colloq. 71, Activity in Red Dwarf Stars*, ed. P.B. Byrne and M. Rodonò (Dordrecht: Reidel), p. 273.

Glebocki, R., Sikorski, J., and Barylko, J. 1974, *Acta Astron.*, **24**, 343.

Golub, L. 1983, in *Proc. IAU Colloq. 71, Activity in Red Dwarf Stars*, ed. P.B. Byrne and M. Rodonò (Dordrecht: Reidel), p. 83.

Golub, L., Noci, G., Poletto, G., and Vaiana, G.S. 1982, *Astrophys. J.*, **259**, 359.

Greenstein, J.L. 1977, *Pub. Astron. Soc. Pacific*, **89**, 304.

Grinin, V.P. 1973, *Izv. Krim. Astrofiz. Obs.*, **48**, 58.

Grinin, V.P. 1976, *Izv. Krim. Astrofiz. Obs.*, **55**, 179.

Grinin, V.P. 1979, *Izv. Krim. Astrofiz. Obs.*, **59**, 154.

Grinin, V.P. 1980, in *Flare Stars, FUORS, and Herbig-Haro Objects* (in Russian), ed. L.V. Mirzoyan (Byurakan Ap. Obs.), p. 23.

Grinin, V.P., and Sobolev, V.V. 1977, *Astrofizika*, **13**, 587.

Gurzadyan, G.A. 1973, *Flare Stars*, in Russian (Moscow: Nauka).

Haisch, B.M. 1983, in *Proc. IAU Colloq. 71, Activity in Red Dwarf Stars*, ed. P.B. Byrne and M. Rodonò (Dordrecht: Reidel), p. 155.

Hartmann, L., and Rosner, R. 1979, *Astrophys. J.*, **230**, 802.

Henyey, L.G., Vardya, M.S., and Bodenheimer, P. 1965, *Astrophys. J.*, **142**, 841.

Hershey, J.L. 1968, *Ph.D. Dissertation* (Charlottesville: Univ. of Virginia).

Ionson, J. 1982, *Astrophys. J.*, **254**, 318.

Ionson, J. 1984, *Astrophys. J.*, **276**, 357.

Johnson, H.M. 1983, *Astrophys. J.*, **273**, 702.

Joy, A.H., and Abt, H.A. 1974, *Astrophys. J. Supplement*, **28**, 1.

Kandel, R. 1967a, *Annales d'Astrophys.*, **30**, 439.

Kandel, R. 1967b, *Annales d'Astrophys.*, **30**, 999.

Katsova, M.M. 1973, *Astron. Zh.*, **50**, 774 (*Soviet Astron. AJ*, **17**, 492).

Kelch, W.L., Linsky, J.L., and Worden, S.P. 1979, *Astrophys. J.*, **229**, 700.

Kodaira, K. 1977, *Astron. Astrophys.*, **61**, 625.

Korovyakovskaya, A.A. 1972, *Astrofizika*, **8**, 247.

Kunkel, W.E. 1970, *Astrophys. J.*, **161**, 503.

Kuperus, M. 1965, *Recherches Astr. Obs. Utrecht*, **17**, 1.

Lang, K.R., Bookbinder, J., Golub, L., and Davis, M.M. 1983, *Astrophys. J. (Letters)*, **272**, L15.

Leibacher, J., and Stein, R. 1981, in *Second Cambridge Workshop on Cool Stars, Stellar Systems, and the Sun*, ed. M. Giampapa and L. Golub, SAO Special Report 392, Vol. 1, p. 23.

Lin, R.P., Schwartz, R.A., Kane, S.R., Pelling, R.M., and Hurley, K.C. 1984, *Astrophys. J.*, **283**, 421.

Linsky, J.L., Bornmann, P.L., Carpenter, K.G., Wing, R.F., Giampapa, M.S., Worden, S.P., and Hege, E.K. 1982, *Astrophys. J.*, **260**, 670.

Linsky, J.L., and Gary, D. 1983, *Astrophys. J.*, **274**, 776.

Livshits, M.A., Badalyan, O.G., Kosovichev, A.G., and Katsova, M.M. 1981, *Solar Phys.*, **73**, 269.

Machado, M.E., and Linsky, J.L. 1975, *Solar Phys.*, **42**, 395.

Marcy, G. 1984, *Astrophys. J.*, **276**, 286.

Meyer, F., Schmidt, H.U., and Weiss, N.O. 1977, *Mon. Not. Roy. Astr. Soc.*, **179**, 741.

Mochnacki, S., and Zirin, H. 1980, *Astrophys. J. (Letters)*, **239**, L27.

Moffett, T.J. 1973, *Bull. Amer. Astron. Soc.*, **5**, 399.

Moore, R.L., and Datlowe, D. 1975, *Solar Phys.*, **43**, 189.

Mould, J.R. 1976, *Astron. Astrophys.*, **48**, 443.

Mould, J.R. 1978, *Astrophys. J.*, **226**, 923.

Mould, J.R. 1980, private communication, quoted by VandenBerg et al., 1983.

Mould, J.R., and Hyland, A.R. 1976, *Astrophys. J.*, **208**, 399.

Mullan, D.J. 1974a, *Astrophys. J.*, **187**, 621.

Mullan, D.J. 1974b, *Astrophys. J.*, **192**, 149.

Mullan, D.J. 1975, *Astron. Astrophys.*, **40**, 41.

Mullan, D.J. 1976a, *Astrophys. J.*, **207**, 289.

Mullan, D.J. 1976b, *Astrophys. J.*, **210**, 702.

Mullan, D.J. 1977, *Astrophys J.*, **212**, 171.

Mullan, D.J. 1979, *Irish Astron. J.*, **14**, 73.

Mullan, D.J. 1983, in *Proc. IAU Colloq. 71, Activity in Red Dwarf Stars*, ed. P.B. Byrne and M. Rodonò (Dordrecht: Reidel), p. 527.

Mullan, D.J. 1984a, *Astrophys. J.*, **279**, 767.

Mullan, D.J. 1984b, *Astrophys. J.*, **282**, 603.

Mullan, D.J., and Owens, A.J. 1984, *Astrophys. J.*, **280**, 346.

Mullan, D.J., and Tarter, C.R. 1977, *Astrophys. J.*, **212**, 179.

Neece, G.D. 1984, *Astrophys. J.*, **277**, 742.

Nordlund A. 1976, *Astron. Astrophys.*, **50**, 23.

Petterson, B.R. 1983, in *Proc. IAU Colloq. 71, Activity in Red Dwarf Stars*, ed. P.B. Byrne and M. Rodonò (Dordrecht: Reidel), p. 19.

Petterson, B.R. 1984, *Astrophys. J.*, **282**, 214.

Porter, J.G., Toomre, J., and Gebbie, K.R. 1984, *Astrophys. J.*, **283**, 879.

Renzini, A., Cacciari, C., Ulmschneider, P., and Schmitz, F. 1977, *Astron. Astrophys.*, **61**, 39.

Robinson, R.D. 1980, *Astrophys. J.*, **239**, 961.

Robinson, E.L., Barker, E.S., Cochran, W.N., and Nather, R.F. 1981, *Astrophys. J.*, **251**, 611.

Rosner, R., Tucker, W.H., and Vaiana, G. 1978, *Astrophys. J.*, **220**, 643.

Schneeberger, T.J., Linsky, J.L., McClintock, W., and Worden, S.P. 1979, *Astrophys. J.*, **231**, 148.

Shakhovskaya, N.I. 1974a, *Izv. Krim. Astrofiz. Obs.*, **50**, 84.

Shakhovskaya, N.I. 1974b, *Izv. Krim. Astrofiz. Obs.*, **51**, 92.

Shibahashi, H., Noels, A., and Gabriel, M. 1983, *Astron. Astrophys.*, **123**, 283.

Shlosman, I., Kozlovsky, B.Z., and Shaviv, G. 1979, *Astron. Astrophys.*, **73**, 358.

Shmeleva, O.P., and Syrovatskii, S.I. 1973, *Solar Phys.*, **33**, 341.

Spicer, D.S. 1975, *Bull. Amer. Astron. Soc.*, **7**, 397.

Spinrad, H. 1973, *Astrophys. J.*, **183**, 923.

Spruit, H.C. 1982, *Astron. Astrophys.*, **108**, 348.

Staude, J. 1978, *Bull. Astron. Inst. Czecho.*, **29**, 71.

Tsuji, T. 1966, in *Colloq on Late Type Stars*, ed. M. Hack (Trieste: Osservatorio Astronomico di Trieste).

Ulmschneider, P., Kalkofen, W., Nowak, T., and Bohn, U. 1977a, *Astron. Astrophys.*, **54**, 61.

Ulmschneider, P., Schmitz, F., Renzini, A., Caccari, C., Kalkofen, W., and Kurucz, R. 1977b, *Astron. Astrophys.*, **61**, 515.

Ulmschneider, P., and Stein, R. 1982, *Astron. Astrophys.*, **106**, 9.

VandenBerg, D.A., Hartwick, F.D.A., Dawson, P., and Alexander, D.R. 1983, *Astrophys. J.*, **266**, 747.

Vardya, M.S. 1966, *Mon. Not. Roy. Astr. Soc.*, **134**, 347.

Vardya, M.S., and Böhm, K.-H. 1965, *Mon. Not. Roy. Astr. Soc.*, **131**, 89.

Vogt, S.S. 1983, in *Proc. IAU Colloq. 71, Activity in Red Dwarf Stars*, ed. P.B. Byrne and M. Rodonò (Dordrecht: Reidel), p. 137.

Willson, R.C., Gulkis, S., Jannsen, M., Hudson, H.S., and Chapman, G.A. 1981, *Science*, **211**, 700.

Withbroe, G.W., and Noyes, R.W. 1977, *Ann. Rev. Astron. Astrophys.*, **15**, 363.

Worden, S.P., Schneeberger, T.J., and Giampapa, M.S. 1981, *Astrophys. J. Supplement*, **46** , 159.

Worden, S.P., Schneeberger, T.J., Giampapa, M.S., Deluca, E.E., and Cram, L.E. 1984, *Astrophys. J.*, **276**, 270.

Young, A., Skumanich, A., and Harlan, E. 1984, *Astrophys. J.*, **282**, 683.

SUBJECT INDEX

absorption lines (photospheric)
in Miras 116–119, 121
in SR and L 146
change in strengths with phase
in Miras 115
in RCB stars 67–68
change in radial velocities with phase in Miras 116–119
doubling
in Miras 118–120, 122, 125
in semiregulars 123, 125
weakening of 62

abundances (*see* composition)

accretion disk 81, 194

acoustic heating (*see* heating nonradiative)

acoustic waves (*see* waves)

ages of red giants 19

Alfvén waves (*see also* heating, nonradiative)
exciting chromospheres 148, 474
driving mass-loss outflow 273

atmosphere (*see also* separate parts of atmosphere: chromosphere, circumstellar envelopes, corona, photosphere)
definition 114
morphology 146, 148, 165–166, 187, 188

Ba II stars (*see* barium stars)

Balmer lines (*see* hydrogen lines)

barium stars (*see also* binary stars)
characteristics 9
color indices 13
composition 3, 9, 20
evolutionary status 3, 10
luminosity 3, 9, 20, 21, 22, 23
mass 9, 10, 18, 21, 22
spectra 3, 9, 15, 21
temperature 9

binarity (*see also* binary stars) 1, 13, 14, 15, 79–81, 85
correlation with shell extension and geometry, 151, 194
in α Ori 67, 147, 148–149, 186–187, 191–192
in R stars 3
in CH stars 9

binary stars
barium stars 3, 9, 22
light curves of 58, 62
mass loss in 81, 253–254

broadband photometry (*see* photometry)

Ca II H and K lines 15, 20, 22, 67, 79, 85, 86, 126, 133–136, 144–147, 152–153, 155–157, 160–162, 165–166, 174, 267–268, 382, 418, 419, 420, 424, 464–466

carbon (C) stars (*see also* irregular stars; Mira variables; N-type carbon stars; R stars; SR stars; separate topics; stars, individual)
chromospheres of 387–393
color indices 7
evolutionary status 7, 10
mass loss in 246
photospheric models of 336–338
spectra 6, 7
temperature 6
variability in (*see also* variability in red-giant stars) 30, 58, 61, 63
circumstellar chemistry in (*see* circumstellar chemistry)

CH stars
CH-like stars 8
characteristics 8
composition 4, 8
evolutionary status 9
luminosity 21, 22
spectra 8

PRECEDING PAGE BLANK NOT FILMED

PAGE 480 INTENTIONALLY BLANK

subgiant CH stars 9
weak G band stars 8

changes in spectrum (*see* variability)

chromospheres (*see also* circumstellar envelopes; moving atmospheres; spectra)
as boundary conditions for mass flow 301, 302
definition of 144, 146, 147, 148, 149
and dividing lines in HR diagram 14, 246, 269
extension of 17, 138, 144, 148-149
heating of (*see* heating, nonradiative)
models for M-dwarf stars 464-467
models for M-giant stars 144, 147, 148, 362-363, 373-374, 392-393
microwave emission from 263-264
minimum temperature of 147, 357, 358
of N-type carbon stars 62, 362-363, 387-391
observations of 362-363, 373-374, 419-429
of R stars 362-363
of S stars 362-363
radiative losses 147
temperature and density of 14, 15, 138, 139, 144, 148, 382-383

circumstellar (CS) chemistry
chemical processes and reactions in 217, 219-220, 302-304, 308-317
in carbon-rich envelopes 294-300, 315-316
of hydrogen 293-294, 304-306, 308-310
in oxygen-rich envelopes 300-302, 315-316
photochemistry in 310-316
time scales of 302-304

circumstellar (CS) envelopes (*see also* chromosphere; circumstellar lines; dust; IR emission; mass loss; nebula; radio emission)
changes in 265-266
chemistry of (*see* circumstellar chemistry)
clumpy 63, 70, 174, 177, 184, 188
column densities 163-164, 168, 177
components of 301, 302
dust (*see also* dust) 256-259, 266
expansion velocities 70, 152, 156, 159, 160, 161, 162-165, 167-168, 177, 266-267
geometrical extension of (*see also* binarity; diameter, angular) 26, 70, 152, 162, 165, 166-167, 169, 190-193, 209
geometrical shape 16-17, 161, 166, 177
mapping, radio, IR (*see* infrared observations)
optical 78
UV 83
models of 259-263, 266-267, 296
molecules identified (*see also* molecular emission; molecules) 295, 296
observational evidence of 57, 61, 63, 67, 70, 119, 139, 143, 148, 149, 151, 154, 209
radius of 251, 258
stationary layer 119, 125, 135, 146, 154, 166, 167-168, 188, 251, 265
temperature of 70, 119, 121, 149, 159, 160, 161, 162, 164, 166-167

circumstellar lines (*see also* line profiles, P Cygni; circumstellar envelopes, molecules identified)
changes in radial velocities 152-153, 153-154
modeling 156, 161-162
multiple components in (*see* velocity, radial)

classification (stellar) 1, 4-10, 11
barium stars 22
C stars 6-7
Keenan-Morgan (KM) 6
M stars 4, 5-6
N-type stars 11
R-type stars 6, 11
RCB stars 7

CN-strong stars 8

CO
causing bifurcated chromospheres 381-382
in CS envelopes 296-300, 308, 316
infrared observations of 113, 116-121, 123, 130, 159-160, 161, 164, 167, 169, 174, 193, 246, 247, 252, 281, 302
millimetric of 5, 113, 123, 160, 165, 167, 209, 216, 218, 219, 247, 259, 261
radio excitation of 217

color indices
in barium stars 13
in M-giant stars 7, 11, 25
in N-type stars 7, 10, 11, 21, 25-26, 43, 89
in nonvariable stars 42, 43, 55
in R-type stars 13, 21
in red giants 11, 12, 13
in RCB stars 21, 69, 71, 73, 75
in S stars 8
relation with effective temperature in red giants 10, 26, 43
and type of variability 43
variation in Mira stars 41-43, 49
variation in semiregular stars 57, 61
variation with spectral class 10, 42

color temperature 25, 26

comparison of model predictions and observations
broadband observations 347-353
spectral lines 353-356

composition, chemical
$^{12}C/^{13}C$ ratio 6, 7, 20, 252
C/O ratio 4, 7, 8, 20, 26
$^{6}Li/^{7}Li$ ratio 9, 20
and classification 4, 6
in CS shells 252, 263, 294-298
of barium stars 3, 9, 20
of CH stars 4, 8
of HdC stars 4, 7
of helium stars 8
of M giants 4, 5, 6, 7, 20
of M dwarfs 424
of MS stars 20

of N-type stars 4, 6, 8, 20
of nonvariable HdC stars 8
of R stars 7, 20
of RCB stars 7
of S stars 4, 8, 20
of SC stars 20
s-process elements 2, 3, 6, 7, 8, 9, 20
of red-giant photospheres 1, 359–360, 362
technicium 8

continuous spectrum
observed infrared 11, 49, 89
observed UV 13, 14, 15, 17, 21, 63, 69, 86
observed radio 17

convection
coupling with pulsation 29
in M-dwarf atmospheres 456, 458–460, 462–463
and mass loss 70, 344, 345
local mixing-length theory of 343–345, 456, 458, 462–463
nonlocal theories of 345–347
two-stream models 345–347, 459–460

corona in M-dwarf stars 425–430, 474–475

CS stars 9, 19

D-line stars (*see* SC stars)

departures from LTE (*see also* statistical equilibrium)
for CO in CS envelopes 167, 261–263
effects of, in line blanketing 327–329
in photospheres of red-giant stars 373–376
ionization equilibrium in CS envelopes 250, 257–258, 261

diagnostic features of thermal models
effective temperatures 356–358
thermal structure 358–359
chemical composition 359–360
surface gravity 360–361
turbulence 361–362
sphericity 362
chromospheres 362–363
mass flow 362–363
nonradiative heating (*see also* heating, nonradiative) 362–363

diameter, angular (*see also* CS envelopes, geometrical extension of; dust-shell radius; radius)
in connection with effective temperature determination 23–25
of N-type stars 24–25
of R stars 24
techniques for finding 23–24, 190
variability of 190–191

distribution, space (*see* space distribution of red giants)

dust (*see also* circumstellar (CS) envelopes; grains; infrared (IR) excess; polarization; radio emission)
and chromospheres 228
column densities 168, 171, 172
composition of CS 69, 80, 168, 169, 171, 227
and polarization 177
dust-shell model 74, 166, 168, 171, 172, 173, 186, 191–192, 232–233
for oxygen stars 235–237
for carbon stars 237–238
of nonspherical shells 238–242
dust-shell radius 70, 174, 177, 189, 190, 191, 192, 193–194, 233, 237
dust-shell geometry 191–195, 239
grain formation 225–228, 245, 271
in RCB stars 68
in stellar atmospheres 245, 270, 271
interaction with CS gas 174, 246, 301, 311–312
mass loss by radiation pressure on 68, 74, 167, 168, 173, 188, 192–193, 229, 246, 274–277
observational evidence of 168, 169, 175, 235–240
optical depth in CS 172, 174, 256–257
polarization due to circumstellar (*see also* polarization) 382
properties of CS 257–258
temperature of 168, 174, 187, 227–231, 236–238, 257
thermal reemission from (*see also* IR observations, IR excess) 50, 256–259
thermosphere 50

effective temperature (*see also* color temperature; stars, individual; stars, properties of)
as a function of intrinsic color 25
of barium stars 9
of carbon stars 6
of helium stars 8
of M giants 24, 25
of Mira variables 26
of N-type stars 24, 25
of OH-IR stars 5, 24
of R-type stars 6, 24
of RCB stars 7, 8, 26
of S stars 24, 26
methods for finding 22–24, 356–358
variability of, in Miras 32

Einstein satellite (*see* X rays)

ejection (*see* mass loss, nonsteady; steady)

emission, maser (*see* masers)

emission (thermal) (*see also* CO; infrared (IR) excess; SiO)
excitation of 217
radio detection 52, 216
radio extension of 216–217
weakening of 169, 171

emission (free-free) 16, 61, 172

emission lines (*see also* name of line; ultraviolet spectra)

change in strengths with phase
in Miras 125, 126;
in RCB stars 67–68;
in semiregulars 126–128, 148
changes in radial velocities with phase in Miras 128–130, 140–141, 142–143
fluorescent 128, 130, 139, 141, 143, 148
Mg (*see also* Mg II h and k) 362–363
in Miras 10, 125, 140–143
presence of polarization and 176, 177
in semiregular and irregular variables 10
in α Ori 132–133, 134, 136, 138, 144–147, 148, 149

energy budget (*see also* chromosphere, radiative losses) 147, 148, 391–393, 464–467

eruptive stars (*see also* RCB stars)
in parallel with pulsating stars 8, 29

escape velocity (*see* velocity, radial)

evolution of stars (*see* stellar evolution)

extended atmosphere (*see* chromosphere, circumstellar envelopes, corona)

Fe II lines 13, 15, 55, 63, 67, 79, 126, 128, 132–133, 135, 141–142, 144–145, 147, 148

flare (*see also* chromosphere)
in giants and supergiants 48, 65, 172, 174, 187, 189
semiempirical models of, for M dwarfs 437–441, 468–473

flare stars 412–414

fluorescent lines (*see* emission lines)

flux (*see also* continuous spectrum; light curves; radio emission)
bolometric 14, 23, 26
correlation with SiO maser flux 52
color-color diagram in UV 15, 21
correlation between IR and radio fluxes 50, 51, 52, 58, 90, 215, 219
correlation between radio and optical fluxes 51, 58
infrared (*see also* IR observations, IR excess) 10, 26, 55, 70
violet-deficiency in N-type stars (*see also* ultraviolet) 6, 11, 43

forbidden lines 126, 138

globular clusters
mass loss in 255–256, 280–281
mode of pulsation of stars in 54

grains (*see also* dust)
critical nucleus of 226, 228
extinction opacity law 234–235
growth of 69–70, 225–226, 228–231, 238
influence of grains on stellar radiation 229–231
nucleation 225–231, 238
structure of 228–229, 237
supersaturation ratio 226–227, 229, 231

granulation (*see* convection; inhomogeneities)

gravity
generalities 27
input parameter 324
determination of, in stars 360–361
in helium stars 8
in RCB stars 8

greenhouse effect 171, 230

heating, nonradiative (*see also* Alfvén waves; shock waves)
by acoustic waves 55, 63, 125, 130, 147–148, 149, 474
in flares 468–473
in M-dwarf atmospheres 442–445, 473–475
by magnetic acoustic waves 48, 148, 189
by magnetic fields 442–445, 473–475

helium (He) lines 7, 14, 67–68, 80, 138–139, 148

helium (He) stars
characteristics 7, 77
composition 8
evolutionary status 8
gravity 8
link to RCB stars 67, 74
luminosity 22
nonvariable 8
period of pulsation 8
spectra 8
temperature 8

Hipparcos spacecraft, observations with 90, 91

HR (Hertzsprung-Russell) diagram
coronal (or X-ray) dividing line for giants in 13
mass-loss dividing line for giants in 14
observational 22
M dwarfs in 414–416, 424–426
red-giants (RG) stars in 2, 4, 5, 9, 22, 26, 31, 56, 62, 75
regions with winds from late-type giants in 246, 268, 426, 428
temperature dividing line for giants in 13, 14

hydrogen-deficient carbon (HdC) stars
characteristics 7
composition 4, 7
evolutionary status 7
nonvariable (*see also* R supergiant stars) 7
properties 21
spectral irreversible variations 87–88

hydrogen lines (*see also* circumstellar envelopes)
in CS shells 253–254, 256, 293–294, 303–304,

313–316
H_2 293–294, 303, 314–315, 354–355, 381
in irregular stars 62
in main-sequence stars 418–419, 421, 424, 464–467, 470
in Miras 79, 125–126, 128, 130, 138, 140–141, 142, 143, 403–404
and maser activity 53
polarization and 176, 177, 178, 180, 182, 184, 186
in semiregular stars 55, 57, 131, 132, 143, 147, 148, 154–155, 158

hypergiant stars 16, 22, 91

indices, color (*see* color indices)

infrared (IR) observations (*see also* CO; flux; photometry; SiO; spectra)
IR excess, observation of 5, 6, 16, 32, 62, 69, 73, 74, 80, 167, 169–172, 232, 237, 245–246, 256–259, 291–292; change with time of 66, 172–174; correlation with polarization 177; correlation with period in Miras 49–50
IR mapping (*see also* dust-shell radius) 16, 190, 191, 192
IRAS data 6, 15–16, 70, 169, 220
ISO project 15, 220
in molecular lines 5, 6, 245
optical depth of 256–259
radio mapping 79, 81, 82, 217

infrared (IR) photometry (*see* photometry)

infrared (IR) spectra (*see* spectra)

inhomogeneities (*see also* convection)
in dwarf atmospheres 460–462
in giant atmospheres 144–145, 343–346

intermediate-band photometry (*see* photometry)

ionization equilibrium (*see* statistical equilibrium)

IRAS data (*see also* infrared observations) 6, 90

irregular (Lb, Lc) stars
brightness changes 63–64; relation with line radial-velocity variation 66
of carbon type 30
chaotic process, randomness process (*see* variability of red giants)
characteristics 10, 29, 61
evolutionary status 62
light curves 29, 61
period changes 63, 64
spectral classes 62
spectral irreversible variations in 84–87
superposition of periods 65
variation in light-curve amplitude with time 62

IUE spectra (*see also* ultraviolet spectra) 90

jet 78–79, 81–83, 84

Large Magellanic Cloud (*see* Magellanic Clouds, red giants/supergiants in)

light curves (*see* Mira variables; semiregular stars; irregular stars; RCB stars; OH/IR stars)

line blanketing
correlation with light-curve shape 39, 41
description of 326–328
in M dwarfs 458–459
mathematical treatments of 328–333
opacity distribution function (ODF), description of 330–333
opacity sampling (OS), description of 331–333
straight-mean-opacity, description of 328–330, 333–334

line profiles (*see also* absorption lines; emission lines)
effects of outflow and inflow (*see also* moving atmospheres) 246–247
P Cygni (*see also* circumstellar lines) 68, 79, 128, 138, 139, 149, 151, 152, 159, 162, 248–250; inverse P Cygni 139
quadrupole lines of H_2 (*see* hydrogen lines)
radio 218, 259, 261–264
variations in (*see* absorption lines; emission lines; name of lines)

line formation (*see also* departures from LTE)
by complete redistribution 374–375
effect of mechanisms of, in line blanketing 327–328
for molecules 377–378
in Li I 376–377

lines, individual (*see* name of line)

lithium-rich stars (LRS) 9

local thermodynamic equilibrium (LTE)
assumed in model atmospheres 324
departures from (*see* separate entry)

long-period variables (*see also* Mira variables) 27, 28, 53, 54

luminosity in (*see also* individual stars)
Barium stars 3, 9, 20, 21, 22
CH stars 21, 22
CS stars 19
He stars 22
M-giant stars 20, 22
Mira variables 5, 22
MS stars 19, 20
N-type carbon stars 19, 20, 21
nonvariable HdC stars 21, 22
OH/IR stars 5
R stars 3, 20

RCB stars 21, 22
red giants 10, 11, 12, 19
S stars 19, 20
SC stars 20

M-dwarf (dM and dMe) stars
activity cycles in 432–435, 441–442
chromospheres of 418, 425–429, 464–467
coronas of 467–468
flares in 412–414, 437–441, 455–456
nonthermal photospheric models of 460–462, 469–470
properties of 410–431
thermal photosphere models of 456, 458–460
transitions regions of 467–468

M-giant stars (*see also* stars, individual; stars, properties of; separate topics)
chromospheres of 362–363, 385–387
circumstellar envelopes of 299–300
classification 4, 5
color indices 7, 11, 25
composition 4, 5, 6, 7, 20
evolutionary status (*see* stellar evolution)
luminosity 20, 22
masses 20
models of 333–346
nonvariable 5, 77
spectra 5, 14, 20
temperatures 24, 25

macroturbulence (*see* inhomogeneities)

Magellanic Clouds, red giants/supergiants in
classification 10
distribution 18–19
evolutionary status 27–29
infrared colors for C stars 26
infrared photometry 27
luminosity 22
modes of pulsation of RG in 53, 54
physical properties 28

magnetic fields (*see also* flares; polarization, sources of asymmetries for; starspots)
and atmospheric structure 419, 432–437, 442–445, 474–475
in giants and supergiants 63, 65, 148, 186, 187, 188–189
magnetic flux tubes 419, 430, 436–437, 442–445, 474–475
magnetic reconnection driving mass loss 280
in starspots 460–462

magnitude (*see* luminosity; flux)

masers (*see also* CO; pumping mechanisms; OH-IR stars; radio emission) 5, 210, 214–216
behavior with phase 35
H_2O 34, 35, 51, 58, 62, 264, 299–300
OH (*see* separate entry)
masing region extension/mass-loss rate relation 53
and polarization 177, 189, 210, 216
SiO (*see* separate entry)
SiS 33
time variation in 17, 58, 216, 218

mass loss (*see also* circumstellar (CS) envelopes; dust; stars, individual; infrared emission)
binary stars, value of, in determining rates of 80, 253–254
equations for 246, 248, 255, 264, 266, 292
evolutionary consequences of 2, 246–247, 280–283
from Miras (*see also* moving atmospheres) 49, 53–54, 254–255
in globular cluster stars (*see* globular clusters)
mechanisms for 246, 272–280
methods for estimating rate of 246, 254, 255–256, 263–264, 266
nonsteady 57, 67, 153, 161, 166, 167, 168, 192, 269–271, 279–280
observational evidence of 14, 66, 68, 151, 245–247, 248–271, 293–301, 362–363, 383, 394, 428
rates of 52–53, 194, 217, 220, 245–247, 248–256, 262, 266, 269, 292, 294
steady 56
by superwind 2, 281–282
uncertainty in rates of 250–253, 255, 256, 264

masses (*see also* stars, properties; stars, individual)
barium stars 9, 18, 20, 22
correlation with pulsation constant 53
generalities 1, 2, 19
M, MS, N, R, S, and SC stars 20
OH-IR stars 5, 6

metal-deficient stars (*see* CH stars; HdC stars)

Mg II h and k lines 14, 15, 21, 63, 68, 126–128, 136, 143, 144–145, 147, 248, 273, 362–363, 388–390, 425
effective temperature/flux in relation 21

microturbulence 144–145

microwave emission (*see* radio emission)

Mie scattering 186, 187, 227

Mira variables (*see also* M-giant stars; N-type carbon stars; S stars)
of carbon type 31
characteristics 5–6, 10, 29, 31–32
connections with OH-IR stars (*see* OH-IR stars)
connection with planetary nebulae (*see also* planetary nebulae) 281–283
evolutionary status 5, 27, 29
light curves 29, 32, 38–41, 46
light curve shape/period relation 48
luminosity 22

masers in (*see also* separate entry) 25, 31, 264–266
mass loss from (*see also* separate entry) 254–255, 268, 273, 275, 279, 281–283
modes of pulsation 53, 54
OH types 33
periods, superposition of 46–47
period changes 43–46
period of pulsation 22, 32, 39, 41, 48; and spectral type variations 43, 49
period/color indices relation 49, 50
period/expansion velocity relation 51
period/metal abundance relation 48–49
period/population relation 48
phase lags between light curves 32, 33–35, 36, 215
pulsation of (*see also* moving atmospheres) 119–121, 125, 128, 140, 144, 148, 401–403
spectral irreversible variations 78–84
variability, line (*see also* absorption lines; emission lines; velocity, radial) 114, 115, 116, 122
variation in light-curve amplitude with wavelength, with time 35–37, 41, 48; with period 49

model photospheres
comparison with observation, photometry 347–353, spectroscopy 353–356
diagnostic features of (*see* diagnostic features)
geometry 324–325
nonthermal (*see* nonthermal models)
of carbon and S stars 336–340, 351–353
of M-dwarf stars 455–462
of M-giant stars 46–54, 334–336, 343–347
opacities in (*see* opacities)
physical principles, of classic 324–325
spherical 340–343, 362
thermal structure of 358–359

molecular emission
in optical range 67, 126
in radio range (*see also* radio emission) 6, 209, 210, 214, 216

molecules (*see also* circumstellar envelopes, molecules identified)
abundances in C-rich CS shells 295–299
abundances in O-rich CS shells 299–301
carbon chain 6, 209, 216
infrared observations of (*see also* spectra) 259
line blanketing due to 328–331
radio observations (*see* radio emission)

motion, in space, of red giants (*see* space motion)

moving atmospheres (*see also* Mira variable stars, pulsation of; shock waves; mass loss)
discussion 120, 121, 125
evidence 122–123, 125, 132–133, 134–135, 136, 144, 145–146, 148–149, 151, 153, 158

MS stars
characteristics 9
composition 20
evolutionary status 3
luminosity 19, 20
masses 20
spectra 20

narrowband photometry (*see* photometry)

N-type carbon stars
characteristics 6
chromospheres of (*see also* chromospheres; heating, nonradiative) 87, 147, 148, 149, 362–363, 387–393
color indices 7, 10, 11, 21
composition 4, 6, 20
evolutionary status 2, 27
and light-variation classification 10
luminosity 19, 20, 21
masses 20
model atmospheres of 58–62, 336–340, 341, 351–353, 353–356
spectra 6, 14, 15, 20, 85–87
temperatures 24, 25, 26
ultraviolet observations of (*see also* ultraviolet) 362–363, 387–393
variability of (*see* variability in red-giant stars)

nebulae (*see also* circumstellar envelopes, mappings; planetary nebulas)
nebular lines 79, 80
observations of 78–81, 84, 85
physical properties 80, 81, 84, 85
structures in (*see also* jet) 82–84

non-LTE (*see* departures from LTE)

nonradiative heating (*see* heating, nonradiative)

nonthermal models (*see also* chromospheres)
of M-dwarf atmospheres 473–475
of RG stars 385–391

nonvariable stars 5, 7, 8, 21, 22, 75–78

OH
maser emission of 5, 31, 32, 33, 36, 49, 50, 51, 62, 210, 214–215, 216, 219, 220, 264–266, 299–300
relation with OH-IR stars 5

OH-IR sources 215
dust-to-gas ratio 174
evolutionary status 28
extension 27
infrared/radio fluxes relation 50
luminosity 5
masses 5
mass loss in 6, 52, 264–268, 275
mode of pulsation 28
nature of 5, 6, 264–265

period of pulsation 5, 6, 28
phase lags in light curves 34
relation to Miras 5, 10, 16, 268
relation to planetary nebulae 6, 194, 195, 282–283
temperature 5
variability 36

opacities
continuous 325
dust grains (*see also* dust; grains) 325–326
spectral lines (*see* line blanketing)

period (*see also* Mira variables; semiregular stars; irregular stars; stellar types)
correlation with pulsation constant 53

photometry (*see also* color indices; magnitudes; light curves; stars, properties of; spectrophotometry; X rays) 10–17
broadband 10, 11, 12, 23, 41, 55, 58, 63, 65, 71, 89
and classification 4, 6, 11
far-UV (*see also* ultraviolet) 13
infrared (*see also* infrared observations, IR excess) 10, 25, 31, 39, 55, 89, 169, 171, 172, 232, 235, 237; method of (Blackwell-Shallis) 24, 25, 348–350, 355–356
intermediate band (DDO, Geneva, Strömgren, Vilnius systems) 11
M-giant stars 11, 31
Mira variables 11
narrowband 11, 41, 65, 71, 78, 89
N-type carbon stars 11, 31, 55, 88, 89
nonvariable HdC stars 75
R stars 11
RCB stars 71
S stars 11, 31
and space motion and space distribution 17
UBV standard stars 78
Wing system 11

photosphere
definition 146
models of M giants (*see* model photospheres)
models of S and C stars (*see* model photospheres)
pulsating 119, 121, 125, 146, 148
theory of 324–325, 333–340

planetary nebulae (*see also* OH-IR sources; nebulae)
bipolar 193, 195, 239–242
characteristics of 91, 168, 171
evolutionary link with red giants 1, 2, 27, 28, 31, 67, 70, 171–172, 193, 195
observational evidence of 80, 85
X rays 13

polarization (*see also* emission lines; hydrogen lines; magnetic fields in giants and supergiants)
circular 177, 216
correlation with CS dust amount 177
correlation with IR excess emission 177
correlation with stellar light changes 175
in maser emission 216
observaton of 145, 175
origin of 184; due to dust 269; across absorption spectral features 185–186; in *o* Cet 186–187; in α Ori 186–187
sources of asymmetries for 184, 185, 186, 187, 188, 193, 195, 239–240
variability with time of 57, 65, 66, 67, 69, 175, 176, 177–178, 179, 181, 184, 186, 269, 270
wavelength dependence of percentage and rotation angle of 175, 177, 178, 180; correlation with grain properties 240

Populations I and II stars 1, 2, 3, 8, 17, 19, 22, 48, 50, 62

population inversion (*see* pumping mechanisms)

pulsating stars (*see* Mira variables; semiregular stars; irregular stars)

pulsation (*see also* Mira variables; shock waves)
effects on line profiles 403–404
effects on light curves 66
mode of 28, 47, 53–54, 59, 64, 87
models of 54
parameters of pulsating models 400–403
period of (*see also* period)
in OH-IR stars 5, 6
in helium stars 8
in RCB stars (*see* separate entry)
in Mira variables (*see* separate entry)
and shock waves 400–403

pumping mechanisms 50, 51, 210, 211–215

R (ordinary) stars (otherwise called R stars) 363
characteristics 6, 77
classification 6
color indices 13
composition 7, 20
evolutionary status 3
luminosity 3, 20, 21
masses 20
spectra 6, 15, 20
temperature 6, 24

R supergiant stars (*see also* HdC stars, nonvariable)
characteristics 7, 75–76
color indices 76
composition 8
correlation hydrogen deficiency/spatial distribution 17
correlation with RCB stars 69
infrared excess 76
luminosity 21, 22

radiation (*see also* radiative equilibrium; radiative transfer)
radiative pressure on dust grains (*see also* dust,

mass loss by radiation pressure on) 274–277

radiative equilibrium 324–325

radiative transfer
plane-parallel layers 324–325
spherical atmosphere 232–238, 340–343
in circumstellar envelopes 213–214, 217, 232–242, 261, 262

radio emission (*see also* emission, thermal; emission, maser; flux)
from flares 17, 437–438, 440–441
from M dwarfs 430
millimetric observations of molecules (*see also* molecular emission in radio range) 6, 245–246, 259–263
submillimetric dust emission 173, 259
variability in 33

radius (*see also* circumstellar envelopes, geometrical extension of; diameter, angular; dust)
correlation with pulsation constant 53
generalities 1, 26, 41
photospheric 120
technique for evaluating 26, 53–54

rate of mass loss (*see* mass loss)

RCB stars
bimodal distribution 70
characteristics 7, 29, 67
classification 7
color indices 21, 67, 71, 73, 74, 75
composition 7
connection with helium stars 74
connection with nonvariable HdC stars 69
connection with planetary nebulae 70
eruptive stars 8, 29
evolutionary status 8
flux 70
gravity 8
infrared excess 69, 74
light curves 8, 30, 67, 70–71, 74
line radial-velocity/brightness relation 74
luminosity 21, 22, 69
modeling 68–69, 74
oscillations on light curves 71–74
period changes 87, 88
period of pulsation 8, 21, 71, 87
spectra 7, 67–68
spectral irreversible variations 87–88
spectral-type variation 67
temperatures 7, 8, 26

rotation 185, 189, 239

S stars
characteristics 8
color indices 8
composition 4, 8, 20
evolutionary status 2, 3, 8, 29
luminosity 20
masses 20
spectra 8, 15, 20
temperatures 26

SC stars 9, 20

semiregular (SRa, SRb, and SRc) stars
chaotic process, randomness process (*see* variability in red giants)
characteristics 10, 29, 53
cycle (= period) of pulsation 53, 55, 58, 59
distribution among red giants 53
light curves 29, 53, 55, 56, 58
light variations/line radial-velocity variation relation 51
luminosity/spectral-type relation 58
multiperiods 59, 61
period changes 55, 61
period/color indices relation 58
period/luminosity relation 58, 59
spectral irreversible variations in 84–87
superposition of periods 61
variation in light-curve amplitude with time, with spectral class 56, 58, 61

shell (*see* circumstellar envelopes)

shock waves (*see also* moving atmospheres)
in chromospheres 301–302, 309–310, 393–404
and color-index variations 43
and dust grains 229, 231
and dust irradiation energy 186, 188
and masers in Miras 33, 216
and Mira light curves 39, 41, 48
in Mira variables 48, 119, 122, 123–125, 130, 140, 141–143, 148, 149, 254–255, 398, 399, 401–404
mass loss driven by 273, 277–278, 279, 309–310, 400–403
in semiregulars 63, 122–123, 125, 131, 143–144, 145, 146, 147, 148, 149
theory of 143, 393–397

SiO
maser emission 5, 17, 33, 34, 47, 51, 52, 58, 160, 168, 209, 210, 215, 216, 219, 247, 264–266, 299–300, 308
thermal emission 53, 113, 123, 216

solar/stellar connection 409–410

sound waves (*see* heating, nonradiative)

space distribution of red giants 17–19, 20

space motion of red giants 17–19

Space Telescope, observations with 84, 90–91

spectra
and classification 4
double-lined 118, 119, 120, 122
infrared (IR) (*see also* CO; infrared observations; radio emission; SiO) 5, 11, 121, 140, 171, 172–173
of barium stars 3, 9, 15, 20
of CH stars 8
of helium stars 8
of M stars 5, 14, 20
of MS stars 20
of N-type carbon stars 6, 14, 15, 20, 85–87
of R stars 6, 15, 20
of RCB stars 7, 67–68
of red giants (*see also* name of stellar type) 4
of S stars 8, 15, 20
of SC stars 20
violet (in C stars) 6, 7, 11, 171, 172
visible, source of 121, 168
ultraviolet (IUE) (*see* separate entry)

spectral lines (*see* absorption lines; emission lines; line profiles; lines, individual)
sensitive to non-LTE (*see* departure from LTE)

spectrophotometry (*see also* photometry)
comparison with model predictions 347–353
in connection with bolometric flux determination 23
in connection with color-index variation 41
infrared (*see also* infrared observations, infrared excess) 55, 69, 169, 171,189
and classification 6
ultraviolet (*see* ultraviolet spectra)
visible 73

super-supergiant stars (*see* hypergiant stars)

stars, individual (*see* Star Index)

stars, properties of (*see also* stars, individual; separate entries)
barium stars 3, 9, 20, 21, 22
carbon-star cepheids 30
CH stars 4, 8, 9, 21, 22
CN-strong stars 8
CS stars 10, 19
HdC stars 4, 7, 21
helium stars 8, 22
Isb stars 30
lithium-rich stars (LRS) 9
M-dwarf stars 410–431
M-giant stars, 4, 5–6, 7, 10, 20, 22
Mira variables 22
MS stars 3, 19, 20
N-type carbon stars 2, 4, 6, 10, 19, 20, 21
nonvariable HdC stars 8, 21, 22, 77
OH-IR stars 5, 6, 10
R stars 3, 6, 7, 20, 21
RCB stars 7, 8, 21, 22, 68, 69
RVa stars 30
S stars 2, 4, 8, 19, 20
SC stars 10, 20

starspots (*see also* magnetic fields)
observations of
in M dwarfs 432–435, 460–462
in giants and supergiants 184, 185, 186

statistical equilibrium (*see also* departures from LTE)
for CO in CS envelopes 259, 261
ionization equilibrium
in CS envelopes 248, 250, 264
in photospheres 378–380
of hydrogen in chromospheres 380–381
in photochemical reactions 295–299, 302–304
of molecules in CS shells 295–299, 302–304
theory of 374–375

stellar evolution (*see also* HR diagram)
AGB 1, 2, 4, 6, 9, 18, 19, 27, 88, 247, 255, 280–281
barium stars 3, 9
CH stars 9
CS stars 10
effect of mass loss (*see* mass loss, evolutionary consequences of)
generalities 1, 2, 3, 4, 19
HdC stars 7, 87
helium (He)-shell flash 2, 7, 22, 27, 28, 45
helium stars 8
irregular variables 62
M stars 10
N stars 7, 27
nonvariable M stars 5
OH-IR stars 5, 6, 10, 28
planetary nebulae (*see also* separate entry) 281–283
R stars 3, 7
RCB stars 8
red giants in Magellanic Clouds 27–29
RGB 2, 22, 247, 255, 281
S stars 3, 8, 28
SC stars 10
semiregular (SRc) variables 56

temperature (*see also* chromosphere; circumstellar envelopes; color indices; dust)
color temperature (*see* separate entry)
effective temperature (*see* separate entry)
far-UV radiation temperatures of M giants 14
of flares 439, 441, 468–469, 471–472
of red-giant photospheres 1, 191, 356–358
of line-forming region 119, 121, 138, 139

thermal equilibrium
in CS envelopes 304–306

thermal models (*see* model atmospheres)

time scale, short, variations on
in lines 47–48, 55, 56, 57, 71–73, 128, 131
in light curves 31, 46, 64, 66, 77
in colors 55, 66

time scale, long, variations on 56, 57, 59, 73, 88

transition region (*see also* chromosphere, corona) 425–428, 467–468

turbulence (*see also* convection; microturbulence)
in M-dwarf models 456, 458–460
in M-dwarf stars 443
in red-giant photospheres 361–362

ultraviolet (*see also* continuous spectrum; spectra, violet)
deficiency, in carbon stars (*see also* flux) 6–7, 11, 86, 387–388
spectra
IUE (*see also* name of lines) 13–15, 63, 68, 69, 77, 80, 84, 126–128, 133, 136, 138, 144, 147, 362–363, 425–429, 436, 439–440
other satellites (BUSS, OAO) 13, 132, 136, 149
radiation field 153

variability in red-giant (RG) stars (*see also* Miras; SR; L; RCB stars; OH-IR stars; pulsation; stars, individual; time scale, variations on)
chaotic process 59, 61, 63, 65, 66
distribution of the types of 30
line profile (*see also* emission lines; absorption lines) 63, 68
origin 29
radial velocity (*see* separate entry)
in radio flux 33
randomness process 59, 63, 65–66
of spectral class with time 56, 57
spectral irreversible changes 78–88
and stellar classification 4
types of 29
ultraviolet (*see also* ultraviolet, spectra) 393

velocity, radial (*see also* circumstellar lines; name of lines)
of center-of-mass of stars 113–114, 128
changes with phase (absorption lines) 116, 118, 121; (emission lines) 128–130
dependence on the excitation potential 115, 123, 130
dependence of the ionization potential 116, 123
of expansion 113
fields 161 in α Ori 385–387
fluid 144, 145, 168
gradients 15, 116, 130, 133, 142, 145, 156, 158, 165–166
histograms in Miras 123–124, 141
of mass outflow 266–267; correlation with period 51
multiple components 118, 119, 123; in circumstellar lines 152–154, 159–161, 162, 165, 167, 168, 175
photospheric 42, 114, 152–154
S-shaped velocity curves
in Miras 118, 121, 122, 125, 130
in semiregulars 122–123, 125
systemic 113

waves (acoustic) (*see* heating, nonradiative, shock waves)

weak G-band stars (*see* CH stars)

Wilson-Bappu effect
in Mg II lines 136
in Ca II lines 21, 22

winds (*see also* mass loss)
observations of 246, 268–269

Wing photometry (*see* photometry, Wing system)

X rays 11, 13, 14, 90, 429–431, 437–438, 456, 467–473

Zeeman effect (*see also* magnetic fields)
in giants and supergiants 189

STAR INDEX

β And, 6, 13, 78, 136, 155, *158*, 161, 348, *348*

FF And, 416, *417*, *422*, *433*

GQ And, *411*, *417*, *431*

HH And, *431*

R And, 31, 44, 45, 46, 115, 132, 138, 179, *260*, 356

RU And, 55

SV And, 46

UR And, 64

W And, 44

Antares (see α Sco)

S Aps, 7, 71, 76, 87, 88, *88*

HS Aql, 45

RR Aql, *267*

R Aql, 17, 31, 33, 34, 35, 36, 38, 45, 48, 51, 171, 172, 189, *267*

S Aql, 32, 55

V Aql, 29, *62*, 63

W Aql, *260*

V374 Aql, 30

V1285 Aql, *417*

V1298 Aql, *411*, 416, *417*, *431*

FK Aqr, 433

R Aqr, 13, 31, 39, 79–85, *82*, *83*, 90, 282

RS Aqr, 13

V Aqr, 55

Z Aqr, 46, 55

T Ara, 9, 376

Arcturus, 26, 359, 360, 361, 374

RZ Ari, 356, 391

TX Ari, *417*, *431*

VY Ari, *433*

ζ Aur, 254, 333

π Aur, 77

DY Aur, 30

NV Aur, *170*

R Aur, 44

RV Aur, 61

S Aur, 64

UU Aur, 55, 87, 139, 169, *170*, *329*, 337, 351, 354, 355, *355*, 390

UV Aur, *123*

Betelgeuse (see α Ori

α Boo, 252, 264, 344, 378, 400

ε Boo, *433*

R Boo, 179, 181

RX Boo, 43, *43*, 55, 58, 62, *164*, *251*, 252, *260*, 356

PAGE 492 INTENTIONALLY BLANK

U Boo, 32, 45

V Boo, 55

R Cae, 31

R Cam, 34, 41

RU Cam = BD +69°417, 30, 77

S Cam, 61

TX Cam, 170

U Cam, 61

UV Cam, 61

XX Cam, 7-8, 30, 69, 70, 71, 73, *73*, 77

μ Cap, 253

ξ Cap, 22

Z Cap, 39

R Car, 32, 46, 181

S Car, 39, 116, 136, 140, *140*, 141

ϱ Cas, 22, 30, 57, *58*, 269

R Cas, 32, 34, 39, 51, 52, 62, *170*, 172, *173*, 216, *260*, 300

T Cas, 32, 36, *38*, 41, 46, *47*

TZ Cas, 30

UV Cas, 67, 69, 70

UX Cas, 30

V Cas, 45

V358 Cas, *417*

W Cas, 39

WZ Cas, 9, 30, 55, 132, 356, 376, 387

XY Cas, 41

Y Cas, 34

Z Cas, 39

α Cen, 423

Proxima Centauri, *427*, 465, 472

R Cen, 31, 39, *40*, 44, 45, 181

RS Cen, 38, 45

RT Cen, 38, 39

RV Cen, 126

T Cen, 55

UW Cen, 72, 73, 75, 88

V Cen, 38

V545 Cen, 46

V645 Cen, *417*, *423*, *431*

W Cen, *42*

μ Cep, 22, 26, 54, 55, 63, *63*, 65, 66, 80, 131, 138, 143, 144, 149, 158, 159, 162, 164, *164*, 166, 169, *170*, 172, *173*, 175, *176*, 182-184, 185, 186, 250, *251*, *253*, *257*, *260*, 277, *277*

DO Cep, *411*, *417*, *431*

RW Cep, 139

T Cep, 39, 41, *41*, 45, 46, 48

VV Cep, 63, *63*

α Cet, 78, 189

o Cet = o Ceti = Mira, 17, 29, 31, 32, 34, 35, 36, *36*, 37, 38, *38*, 39, *43*, *44*, 46, 47, 48, 80, 91, 115, 116, 126, 127, 129, *130*, 131, 134, 139, 140-141, 142, 143, 149, 152, 153, 159, *160*, *161*, 168, *170*, 172, *173*, 175, 176, *176*, 177-181, *178*, *179*, *180*, 181, 185, 186, 187, *188*, *260*, 263, 282, 402, 403

R Cet, 38

U Cet, 39

UV Cet, *411*, 413, 416, *417*, *421*, *423*, *426*, *427*, *431*, 432, *433*, 434, *440*, 461, 470

X Cet, 39

R Cha, 41

δ CMa, 57

σ CMa, 158

S CMa, *58*

VY CMa, 33, 55, 63, *63*, 64, 236, 239, *240*, 259, 300

W CMa, 63

S CMi, 35, *36*, 37, 38, 39, *40*, *260*

U CMi, 39

W CMi, 64

YZ CMi, *417*, 419, *420*, *421*, *423*, *426*, *427*, *428*, *431*, *433*, 437, *438*, 440, *440*, 461, 470, 472

R Cnc, 44, 45

RS Cnc, 55, *170*, *257*, *260*

T Cnc, 55, 122, *123*, 131

V Cnc, 44

X Cnc, 25, 55, 61, 62, 355

T Col, 39

VW Com *417*

R CrB, 7, 8, 20, 30, 66–68, 69, 70, 71, 72, 73, 74, 77, 91, 127, 138, 175

S CrB, 34, 35, *35*, 46, 50, *176*

V CrB, 122, *123*, *176*, 356

R Crt, 55, 58, 400

γ Cru, 136

BH Cru, 44

R Crv, 39

RS CVn, 434, *435*, 437, 438, 440

TT CVn, 65

V CVn, 171, 175, *176*, 181, *181*, 185, 188

Y CVn, 55, 58, 139, 353, 354, 355, 357, 387

χ Cyg, 2, 11, *12*, 26, 29, 31, 32, 34, 36, *37*, 39, *40*, 41, *43*, 44, 48, 116, 117, *118*, *119*, 120, 121, 125, 126, 127, 129, *130*, 136, 137, 138, *138*, 140, 143, 152, 154, *161*, 167, 168, 254, *260*, 269, 279, 302, 309, 356, 363, 393

31 Cyg, 227, 254

32 Cyg, 254

61 Cyg, *423*, *426*, 465, 466

AD Cyg, 63

BC Cyg, *12*

CO Cyg, 30

CH Cyg, 13

LW Cyg, 43

NML Cyg, 33, 58, 236, 239, *260*, 316

P Cyg, 12, 31

R Cyg, 31, 32, 39, 126, 135

RS Cyg, 55

RT Cyg, 39, *40*, 124, 141–142, *142*

RW Cyg, 55, *170*, *257*

SV Cyg, 64

TT Cyg, 55, 62

TU Cyg, 45

U Cyg, *12*, 31, 122, *123*, 136, 356

V Cyg, 17, 31, 48, 169, 172, 189, *260*

V460 Cyg, 63, 359

V462 Cyg, 45

V734 Cyg, 45

V1016 Cyg, 13, 31, 85, 91

V1396 Cyg, 411, *411*, *433*

V1489 Cyg, *170*

WX Cyg, 9, 376

Z Cyg, 45

R Dor, 55, 62, 382

R Dra, 39

BY Dra, 24, 411, *411*, 413, *417*, 424, 429, *431*, *432*, *433*, 435, *435*, 436, *442*, 443

CM Dra, 411, *411*, 413, 414, *417*, *433*

CR Dra, 416, *417*, 429, *431*

RY Dra, 55

T Dra, 31

UX Dra, 55, 59

ϵ Eri, *423*, 424, *444*

γ Eri, 136

CC Eri, *433*

RT Eri, 46

40 Eri C, *431*

R For, 39

η Gem, 390

μ Gem, 78, 136

6 Gem, *260*,

BM Gem, 64

R Gem, 39, *40*, 138, 172

RS Gem, 55, 59, *60*

TV Gem, 55

YY Gem, 411, *411*, 414, 416, *417*, *431*, *433*

T Gru, 38, 47, *42*

α Her, 54, 63, 132, 136, 138, *148*, 152, 153, 159, 164, *164*, 166, 245, *249*, 250, *251*, *253*, 254, *260*, 264, 277, *277*, 291

AC Her, 30

g Her, 189

DQ Her, 271

RR Her, 122, *123*, 131, 149

RU Her, 179

SS Her, 38, 39

U Her, 33, 34, 35, 39, *43*, 45, 51, *170*, *176*, 179, 181

V 639 Her, *417*

W Her, 45

X Her, *164*, *251*, *253*

R Hor, *42*

T Hor, 39

TW Hor, 56, *56*, 127, *128*, 132, 133, *134*, 143, 144, 147–148, *148*, 149, 387, 393

R Hya, 31, 34, 39, 45, 46, 129, *130*, 138, 179

RT Hya, *30*

RV Hya, 33

T Hya, 41

U Hya, 63

V Hya, *12*, 46–47, 63, 122, *123*, 131, 149, *260*

W Hya, 35, 45, *164*, *253*, 385

SY Hyi, 22

ϵ Ind, 423

R Ind, 41

T Ind, 55, 132, *148*

AR Lac, 437

EV Lac, *417*, *421*, *422*, 465, 472

72 Leo, *148*

AD Leo, *417*, *421*, *422*, *431*, 441, 465, 472

CN Leo, 413, *417*, 421, *431*

CW Leo (see IRC +10216)

R Leo, 33, 34, 48, 115, 116, 121, 125, 129, *130*, 131, 134, 139, 140, 152, *164*, 167, 169, *170*, 188, 189, *251*, *260*, 300, 402

VY Leo = 56 Leo, 55, 59

R Lep, 29, 31, 39, 122, *123*, 169, *170*, 179, 181

RX Lep, 64

S Lep, 182, 185

σ Lib, *158*

X Lib, 45

R LMi, *12*, 34, *170*, *260*

R Lup, 46

α Lyn, 161

R Lyn, 34

Y Lyn, 55, 64

δ^2 Lyr, *260*

HO Lyr, 45

R Lyr, 55, *134*, 154, *260*

T Lyr, 63, 161

W Men, 22

AT Mic, *411*, *421*, *423*, *426*, *427*, *431*, *433*

AU Mic, *421*, *422*, *423*, *426*, *427*, *428*, *431*, 433

Mira (see *o* Cet)

SU Mon, 63

U Mon, 179

V Mon, 41

V577 Mon, *411*, *417*, *421*, *422*, *431*

CR Mus, 39

R Nor, 39

T Nor, 41

ϵ Oct, 400

R Oct, *42*

S Oct, *42*

δ Oph, *153*

TW Oph, 25

V Oph, 39, 122, *123*

V1054 Oph, *411*, *417*, *431*

X Oph, 122

α Ori = Betelgeuse, 2, 11, *12*, 13, 14, 15, 17, 26, 54, 55, 57, 63, 65–67, 90, 91, 122, 127, 132, 133, 135, 136, *137*, 138, 143, 144–147, *145*, 148, *148*, 149, 150, *151*, 152, 153, *153*, 154, 155, *155*, *156*, 158, 159, 160, 161, *161*, 162, 163, 164, *164*, 165, 166, 167, 168, 169, *170*, 172, 177, 182–184, *183*, 186–187, 189, 190–193, *192*, *193*, 219, 229, 230, 235, 237, 240, *241*, 245, 248, *249*, 250, *250*, 251, *251*, 252, *252*, 253, *257*, *260*, 261, *261*, 262, 263, 264, 267, 269, 270–271, *271*, 274, 276, 277, *277*, 278, 279, 291, 294, 300, 301, 307, 308, 316, 318, 344, 349, 359, 361, 383, 385, 386, *386*, 387

χ Ori, 430

BL Ori, 63, *148*

S Ori, *30*

U Ori, 31, 33, 34, 35, 39, 51, 115, 126, *170*, *267*

V352 Ori, *30*

V371 Ori, *417*

V998 Ori, *431*

V1005 Ori, *417*, 424, 433

W Ori, 55

R Pav, 39

S Pav, 37, *42*

II Peg, *423*, *433*, 436, *437*, 441, *442*

β Peg, 13, 30, 144, 145, *148*, 149, 154, *158*, *249*, *253*, 348, *348*, 385

ψ Peg, 78

EQ Peg, *423*, *431*, 465

GT Peg, 421, 433

RZ Peg, 136, 356

χ Per, 64

ϱ Per, 30, 55, *253*, *260*

S Per, 30, 34, 55, 58, *60*, 63, *63*, 64, *170*, *257*

U Per, 46

UZ Per, 59

V384 Per, *170*

Y Per, 46

T Phe, 46

TW PsA, *433*

χ Psc, 387

TX Psc, 11, *12*, 25, 63, 64, 116, 132, 138, 148, *148*, 150, 337, 355, 363, 373, 387

Z Psc, 355

19 Psc, 351

L_2 Pup, 55, 175, 176, 182, 185, 400

SU Pup, 126

W Pup, 39

Ross 986, *431*

R Sci, *260*

α Sco = Antares, 13, 57, 63, 65, 90, 132, 136, *151*, 152, 154, *154*, 159, *160*, 161, 163–164, *164*, 166, 247, 250, *251*, 252, 254, *260*, 264, *265*, *267*, 276, *277*

AH Sco, *134*

RS Sco, *42*

S Sct, 55

S Ser, 45

FK Ser, 16, *433*

WX Ser, 51, *267*

δ Sge, 254, *260*

HM Sge, 13, 31, 91

AQ Sgr, 25, 356

GU Sgr, 72

MV Sgr, 8, 22, 26, 45, 70

RT Sgr, 41

RU Sgr, 39

RY Sgr, 7, 8, 30, 67–68, 69, 70, 71, 72, *72*, 74, 75, *75*, *76*, 77, 87

SZ Sgr, 25

T Sgr, 9, 39

WX Sgr, 33

V348 Sgr, 26

V1216 Sgr, *417*

V1280 Sgr, 46

VX Sgr, 22, 55, 58, 63, *63*, 64, *170*, 257

α Tau, 66, 252, 400

119 Tau, 78, 153, *253*, *260*

CE Tau, *170*, *257*

IK Tau, *170*

NML Tau, 33, *43*, 51, *176*, *260*

RV Tau, 179

SU Tau, 30, 67, 70, 71

T Tauri, 424

W Tau, 45

Y Tau, 25

RR Tel, 13

RS Tel, 25

T Tuc, 39

U Tuc, 46

R Tri, 39, *41*, 43, 44

83 UMa, 78

CF UMa, 413

R UMa, 32, 39, *40*

S UMa, 32, 39, *40*

SZ UMa, *417*, *422*, 466

VY UMa, 63

WX UMa, *417*, *431*

R UMi, 55

U UMi, 39

δ Vir, 78, 91

DT Vir, *417*, *433*

EQ Vir, *421*, *422*, *423*, *426*, *433*, 465, 466

FI Vir, *411*, *417*

FL Vir, *411*, *417*, *431*

R Vir, 38, 39, *41*, 46

RS Vir, 34

SS Vir, 31, 39, *40*, 44

SW Vir, 55, *253*

W Vir, 142

WX Vir, 356

S Vol, 39

α Vul, 161

Wolf 630 C, *431*

Wolf 1561, *431*

AF GL 2688, 299

AGL 809, *170*

AGL 865, *170*

AGL 2136, *170*

AGL 2205, *170*

AGL 2290, *170*

AGL 2885, *170*

AGL 3099, *170*

BD −17°4889, *78*

BD +02°3326, 78

BD +10°2179, 8, 77

BD +13°3224, 8, 77

BD +19°3109, 78

BD +20°5071, 77

BD +26°730, 441

BD +37°442, 77

BD +56°595, 155, 157

BD +57°2161, 78

BD +69°417 (*see* RU Cam)

CIT 6 = GL 1403, *176*, 195, 239, *260*, 269, 299, 301

CRL 2155, *260*

CRL 2199, *260*

CRL 2688, *260*, 317

CRL 3068, *260*

DM + 01 2684, *431*

DM + 36 2322, *431*

G 51-15, 416, *417*

GL 867A, *428*

HD 1326A, *423*, *426*

HD 6860, 13

HD 20234, 363

HD 35155, 352

HD 37212, *148*

HD 42581, *431*

HD 44179, 80

HD 52432, *148*

HD 59643, 31, 85, 86, *86*, 91

HD 80943, 87

HD 88230, 423, 426

HD 95735, 423, 426

HD 95950, 134

HD 100029, 13

HD 100764, 7, 18

HD 124448, 8, 77

HD 137613, 8, 22, 77

HD 148839, 8

HD 156074, 7, 20

HD 160641, 77, *78*

HD 168476, 8, 77, 88

HD 173409, 8, 22

HD 175893, 8

HD 182040, 7, 8, 18, 20, 22, 77, 88, 363

HD 202560, 431

HD 207076, *164*, *251*, 382

HD 216131, 13

HD 214479, *431*

HD 217906, 14

HD 224085, 442

HD 264111, 77

HR 8714, 9

HR 8752, 269

HV 5637, 7, 22

HV 12842, 22

Hyades, 472

IC 418, *260*

IRC −10236, *260*

IRC −10529, 33

IRC +10011, 33, 51, *260*, 261, *261*, 265

IRC +10216 = CW Leo, 2, 33, 159, *161*, 167, 168, *170*, 171, 172, 175, 190, 193–195, *194*, 209, 210, 216, *216*, 217, *217*, 218, 219, 220, *220*, 221, 230, 238, 239, *260*, 261, 263, 267, 269, 270, 282, 291, 293, 294, *295*, 295–299, 300, 304, 305, *305*, 310, 311, *311*, 312, *312*, 313, 314, *314*, 315, *316*, 317, 318

IRC −10236, *260*

IRC +20326, *260*

IRC +20370, *260*

IRC +40485, *260*

IRC +40540, *260*

IRC +50137, 33

IRC +50096, *260*

IRC +50357, *170*

IRC +60370, *170*, *257*

L 789-6, *431*

NGC 6543, *260*

NGC 7027, *260*, 299

OH 1.5 - 0.0, *266*

OH 2.2 - 1.7, *266*

OH 2.6 - 0.5, *266*

OH 17.7 - 2.0, 17

OH 19.2 - 1.0, *267*

OH 26.2 - 0.6, *267*

OH 26.4 - 1.9, *267*

OH 26.5 + 0.6, 17, 265, 266, 267, 269

OH 28.7 - 0.6, *267*

OH 30.1 - 0.2, *267*

OH 30.7 + 0.4, *267*

OH 31.7 - 0.8, *267*

OH 32.8 - 0.3, *267*

OH 39.9 + 0.0, *267*

OH 45.5 + 0.1, *267*

OH 231.8 + 4.2, *260*, 300

SAO 31070, *442*

SAO 91592, *442*

Yale 4794, *459*

Yale 3501, *459*

LIST OF CONTRIBUTING AUTHORS

Leo Goldberg
Kitt Peak National Observatory
P.O. Box 26732
Tucson, AZ 85726

Alfred E. Glassgold
Physics Department
New York University
New York, NY 10003

Patrick J. Huggins
Physics Department
New York University
New York, NY 10003

Hollis R. Johnson
Astronomy Department
Indiana University
Bloomington, IN 47405

Jean LeFèvre
Observatoire de Nice
BP 139
F-06003 Nice, France

Dermott J. Mullan
Bartol Research Foundation
University of Delaware
Newark, DE 19711

François R. Querci
Observatoire du Pic-du-Midi
et de Toulouse
14 Ave. Edouard Belin
F-31400 Toulouse, France

Monique Querci
Observatoire du Pic-du-Midi
et de Toulouse
14 Ave. Edouard Belin
F-31400 Toulouse, France

Ramiro de la Reza
Conselho Nacional de Desenvolvimento
Cientifico E. Technologico
Rua General Bruce, 586
Rio De Janeiro, Brazil

Nguyen-Quang-Rieu *Observatoire da Paris*
Section d'Astrophysique
5, Place Jules Janssen
92195 - Meudon, France

Marcello Rodonò *Instituo Di Astronomia*
Universita Degli Studi
Citta Universitaria, Viale A, Doria 6
1 95125 Catania, Italy